Transactions of the ASME

Technical Editor, L. B. FREUND

Division of Engineering
Brown University
Providence, R.I. 02912

APPLIED MECHANICS DIVISION

Chairman, J. R. RICE
Secretary, THOMAS L. GEERS
Associate Editors,
D. B. BOGY
R. M. CHRISTENSEN
R. J. CLIFTON
THOMAS J. R. HUGHES
W. D. IWAN
W. G. KNAUSS
F. A. LECKIE
J. T. C. LIU
FRANCIS C. MOON
J. W. NUNZIATO
R. H. PLAUT
J. G. SIMMONDS
K. R. SREENIVASAN
Z. WARHAFT
L. T. WHEELER
S. E. WIDNALL

BOARD ON COMMUNICATIONS
Chairman and Vice-President
K. N. REID, JR.

Members-at-Large
W. BEGELL
J. T. COKONIS
M. FRANKE
W. G. GOTTENBERG
M. KUTZ
F. LANDIS
J. R. LLOYD
T. C. MIN
R. E. NICKELL
R. E. REDER
F. W. SCHMIDT

President, N. D. FITZROY
Exec. Dir.
PAUL ALLMENDINGER
Treasurer, ROBERT A. BENNETT

PUBLISHING STAFF
Mng. Dir., Pub., J. J. FREY
Dep. Mng. Dir., Pub.
JOS. SANSONE
Managing Editor,
CORNELIA MONAHAN
Production Editor, REMO SALTA
Prod. Asst., MARISOL ANDINO

Transactions of the ASME, Journal of Applied Mechanics (ISSN 0021-8936) is published quarterly (Mar., June, Sept., Dec.) for $105 per year by The American Society of Mechanical Engineers, 345 East 47th Street, New York, NY 10017. Second class postage paid at New York, NY and additional mailing offices. POSTMASTER: Send address changes to The Journal of Applied Mechanics, c/o THE AMERICAN SOCIETY OF MECHANICAL ENGINEERS, 22 Law Drive, Box 2300, Fairfield, NJ 07007-2300.
CHANGES OF ADDRESS must be received at Society headquarters seven weeks before they are to be effective. Please send old label and new address.

PRICES: To members, $24.00, annually; to nonmembers, $105.00. Add $6.00 for postage to countries outside the United States and Canada.

STATEMENT from By-Laws. The Society shall not be responsible for statements or opinions advanced in papers or . . . printed in its publications (B7.1, Par. 3).

COPYRIGHT © 1987 by the American Society of Mechanical Engineers. Reprints from this publication may be made on condition that full credit be given the TRANSACTIONS OF THE ASME, JOURNAL OF APPLIED MECHANICS, and the author, and date of publication be stated.

INDEXED by the Engineering Information

Journal of Applied Mechanics

Published Quarterly by The American Society of Mechanical Engineers

VOLUME 54 • NUMBER 1 • MARCH 1987

TECHNICAL PAPERS

1 **Cumulative Plastic Flow in Rolling and Sliding Line Contact**
A. D. Hearle and K. L. Johnson

8 **The Stress Field Induced by Normal Contact Between Dissimilar Spheres**
D. A. Hills and A. Sackfield

15 **A Rate-Independent Constitutive Theory for Finite Inelastic Deformation**
M. M. Carroll

22 **Remaining at Yield During Unloading and Other Unconventional Elastic-Plastic Response**
D. C. Drucker and Devo Seereeram

27 **Balance Laws and Constitutive Relations for Plane Flows of a Dense, Binary Mixture of Smooth, Nearly Elastic, Circular Disks**
J. T. Jenkins and F. Mancini

35 **The Modified Mixture Theory for Fluid-Filled Porous Materials: Theory** (87-APM-7)
N. Katsube and M. M. Carroll

41 **The Modified Mixture Theory for Fluid-Filled Porous Materials: Applications** (87-APM-8)
N. Katsube and M. M. Carroll

47 **A Simple Kinetic Theory for Granular Flow of Rough, Inelastic, Spherical Particles**
C. K. K. Lun and S. B. Savage

54 **A Continuum Theory of Crack Shielding in Ceramics** (87-APM-9)
M. Ortiz

59 **A Complex-Variable Method for Two-Dimensional Internal Stress Problems and Its Applications to Crack Growth in Nonelastic Materials: Part I – Theory** (87-APM-10)
K. C. Wu and C. Y. Hui

65 **A Complex-Variable Method for Two-Dimensional Internal Stress Problems and Its Applications to Crack Growth in Nonelastic Materials: Part II – Applications** (87-APM-11)
K. C. Wu and C. Y. Hui

72 **On the Characterization of the Transient Stress Field Near the Tip of a Crack**
K. Ravi-Chandar and W. G. Knauss

79 **Asymptotic Analysis of a Mode I Crack Propagating Steadily in a Deformation Theory Material**
P. Ponte Castañeda

87 **A Semi-Infinite Crack Partially Penetrating a Circular Inclusion**
P. S. Steif

93 **The Interface Crack in a Tension Field**
A. K. Gautesen and J. Dundurs

99 **On the Numerical Boundary Integral Equation Method for Three-Dimensional Dynamic Shear Crack Problems**
S. Das and B. V. Kostrov

105 **Boundary Element Method by Dislocation Distribution** (87-APM-14)
C. F. Sheng

110 **On the Distribution of Hoop Stresses Around Circular Holes in Elastic Sheets**
R. Kienzler and Duan Zhuping

115 **Three-Dimensional Vibration Analysis of a Truncated Quadrangular Pyramid**
T. Irie, G. Yamada, and Y. Tagawa

121 **Asymmetric Wave Propagation in an Elastic Half-Space by a Method of Potentials** (87-APM-4)
R. Y. S. Pak

127 **An Acoustoelastic Theory for Surface Waves in Anisotropic Media** (87-APM-6)
G. Thomas Mase and G. C. Johnson

136 **An Experimental Study of the Reflection and Transmission of Flexural Waves at an Arbitrary T-Joint**
J. F. Doyle and S. Kamle

141 **On the Initiation of Necking Modes in Layered Plastic Solids**
P. S. Steif

147 **The Reverse Spaghetti Problem: Drooping Motion of an Elastica Issuing from a Horizontal Guide**
L. Mansfield and J. G. Simmonds

151 **Ray Solutions on Surfaces of Revolution** (87-APM-13)
L. S. Chien and C. R. Steele

159 **Crushing of an Elastic-Perfectly Plastic Ring or Tube Between Two Planes** (87-APM-3)
C. Y. Wang

165 **Asymptotic Solutions for Warping and Distortion of Thin-Walled Box Beams** (87-APM-15)
C. D. Balch and C. R. Steele

174 **Initial Postbuckling Behavior of Imperfect, Antisymmetric Cross-Ply Cylindrical Shells Under Torsion** (87-APM-12)
David Hui and I. H. Y. Du

(Contents continued on Inside Back Cover)

Downloaded 04 May 2010 to 171.66.16.49. Redistribution subject to ASME license or copyright; see http://www.asme.org/terms/Terms_Use.cfm

CONTENTS (CONTINUED)

181 **A Composite Plate Theory for Arbitrary Laminate Configurations**
A. Toledano and H. Murakami

190 **Axisymmetric Motion of a Viscous Fluid Inside a Slender Surface of Revolution** (87-APM-1)
D. A. Caulk and P. M. Naghdi

197 **Turbulent Boundary Layers With Mass Transfer by the Dorodnitsyn Finite Element Method**
C. A. J. Fletcher and R. W. Fleet

203 **Transient Stokes Flow in a Wedge** (87-APM-2)
Bohou Xu and E. B. Hansen

209 **Frequency Response of a Nonlinear Pneumatic System** (87-APM-5)
Ying-Tsai Wang and Rajendra Singh

215 **Transfer Function of a Class of Nonlinear Multidegree of Freedom Oscillators**
L. E. Galhoud, S. F. Masri, and J. C. Anderson

BRIEF NOTES

Torsion of an Elasto-Plastic Bar Via a Dislocation Method — 226
D. A. Sotiropoulos and T. Mura

Energy Release Rate in an Idealized Nonlinear DCB Specimen — 227
L. B. Mannion

Dynamic Inelastic Response of Beams and Plates Under Combined Loading — 228
S. S. Rao and K. S. Raghavan

Perforation of Aluminum Plates With Conical-Nosed Rods — 230
M. J. Forrestal, Z. Rosenberg, V. K. Luk, and S. J. Bless

Approximate Solution of Differential Equations Governing the Orientation of a Rigid Body in a Reference Frame — 232
T. R. Kane and D. A. Levinson

234 The Cracked Semi-Infinite Cylinder Under Internal Pressure
J. A. Alabi

235 A Method of Eliminating Lagrangian Multipliers from the Equation of Motion of Interconnected Mechanical Systems
S. Vlase

237 Surface Microextensometry by Means of Moire Interferometry With a Scanning Electron Microscope
Marc-Henri Ambroise, T. Bretheau, P. Viaris de Lesegno

239 Impact With an Impulsive Frictional Moment
Joseph B. Keller

240 Perturbation Solutions on J-Integral for Nonlinear Crack Problems
Ming-Yuan He

DISCUSSION

243 **Discussion on a previously published paper by J. F. Wilson and G. Orgill**

243 **Discussion on a previously published paper by D. R. Otis**

244 **Discussion on a previously published paper by J. F. Wilson and G. Orgill**

245 **Discussion on a previously published paper by T. Kundu**

245 **Discussion on a previously published paper by J. Brindley, L. Elliott, and J. T. McKay**

246 **Discussion on a previously published paper by H. D. van der Zande and J. H. Grootenboer**

247 **Discussion on a previously published paper by P. A. Dashner**

BOOK REVIEWS

249 ***The Behavior of Structures Composed of Composite Materials by*** **J. R. Vinson and R. L. Sierakowski** . . . Reviewed by **C. W. Bert**

249 ***Dynamic Fracture edited by*** **M. L. Williams and W. G. Knauss** . . . Reviewed by **F. Erdogan**

250 ***Hydrodynamic Stability Theory by*** **A. Georgescu** . . . Reviewed by **J. T. Stuart**

250 ***Nonlinear Oscillations in Physical Systems by*** **Chihiro Hayashi** . . . Reviewed by **D. T. Mook**

251 ***Sound and Structural Vibration: Radiation, Transmission and Response by*** **Frank Fahy** . . . Reviewed by **D. G. Crighton**

252 Books Received by the Office of the Technical Editor

7, 26, 34, 254 Worldwide Mechanics Meeting List

64 17th International Congress of Theoretical and Applied Mechanics

78 Proposals to Host a IUTAM Symposium

135 Symposium on Three-Dimensional Fracture Processes

150 IUTAM Symposium on Advanced Boundary Element Methods

248 Change of Address Form

58, 92, 104, 120, 126 189, 208, 214, 225, 242 Applied Mechanics Symposium Proceedings

Downloaded 04 May 2010 to 171.66.16.49. Redistribution subject to ASME license or copyright; see http://www.asme.org/terms/Terms_Use.cfm

A. D. Hearle

K. L. Johnson

University Engineering Department,
Cambridge University,
Cambridge, England CB2 1PZ

Cumulative Plastic Flow in Rolling and Sliding Line Contact

Rollers loaded above their shakedown limit are known to undergo cumulative plastic shearing of their surface layers. An approximate analysis of this deformation by Merwin and Johnson (1963) was in good accord with experiments, but a recent finite-element calculation by Bhargava et al. (1984) predicted much larger deformations. This paper investigates the discrepancy and presents an alternative analysis which supports that by finite-elements.

1 Introduction

It has long been known that rollers loaded above their elastic limit, even in pure rolling, undergo a cumulative plastic deformation in which surface layers are progressively sheared relative to the subsurface material in the direction of motion of the surface. This phenomenon was first reported by Crook (1957). Since the surface advances ahead of the bulk of the roller, it was referred to as "forward flow" (see Fig. 1). A further experimental investigation was carried out by Hamilton (1963), and many similar observations have been reported since, e.g., Shima et al. (1981). A theoretical study of the phenomenon led to the realization that it posed a "shakedown problem" in the theory of elastic-perfectly plastic solids. If the maximum Hertz pressure p_o exceeds 3.1 k (by the von Mises criterion) yield will first occur at a point $0.7a$ below the surface, where a is the semicontact width and k is the yield stress in shear. For contact stresses in the range $3.1k < p_o \leqq 4.0k$, Johnson (1962) used the statical shakedown theorem due to Melan to show that residual stresses introduced during early cycles of rolling load lead, in the steady-state, to "elastic shakedown" in which the elastic limit of the material is no longer exceeded. More recently Belyakov (1980) used the kinematical shakedown theorem due to Koiter to show that if p_o exceeds $4.0k$, repeated plastic flow will take place with every passage of the load. $p_o = 4.0k$ is therefore an exact elastic shakedown limit for line-contact in pure rolling. The shakedown theory was extended to tractive rolling and sliding contact by Johnson and Jefferis (1963) who showed that when the coefficient of friction f (= tangential force T/normal force N) exceeds 0.3, shakedown is controlled by surface rather than subsurface stresses.

A rigorous analysis of the progressive plastic deformation which takes place with repeated rolling/sliding at a load above the shakedown limit is not trivial. Merwin and Johnson (1963) used the *elastic* strain field as a kinematically admissible field to calculate the history of plastic stress for elements passing through the loaded region. Conditions of equilibrium were not satisfied during this process, but equilibrium was restored in the residually stressed state, which enabled the residual strains and hence the permanent "forward flow" to be estimated. These estimates were well supported by experiment in the case of pure rolling (Merwin and Johnson, 1963), but not so well under sliding conditions (Johnson and Jefferis, 1963) (see Figs. 6, 7, and 8).

There has been a revival of interest in this problem recently when Bhargava, Hahn, and Rubin (1985) sought to remove the approximations from the Merwin and Johnson approach by carrying out an elastic-plastic finite-element analysis of repeated rolling contact. This method has the advantage of satisfying (within the finite-element approximations) the conditions of both compatibility and equilibrium, and also offers the possibility of taking into account more realistic cyclic-strain behavior of the material, but the computing effort is considerable. The steady-state must be approached by following the loading history from the first passage of the load. The results of these computations were in general qualitative agreement with Merwin and Johnson: shakedown took place for a load of $3.5k$; similar distributions of compressive residual stress built up to the subsurface layers and progressive forward flow of the surface was found above $4.0k$. However, the

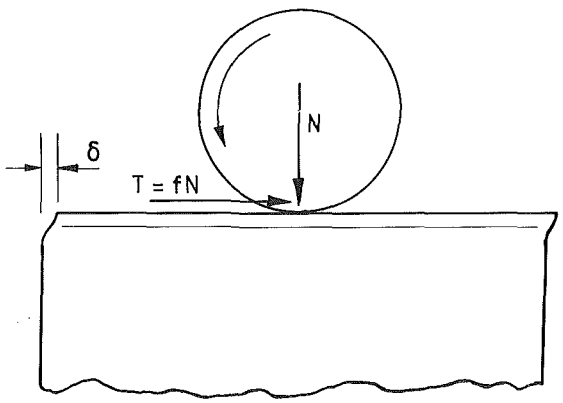


Fig. 1 Forward flow in rolling and sliding contact

Contributed by the Applied Mechanics Division for publication in the JOURNAL OF APPLIED MECHANICS.

Discussion on this paper should be addressed to the Editorial Department, ASME, United Engineering Center, 345 East 47th Street, New York, N.Y. 10017, and will be accepted until two months after final publication of the paper itself in the JOURNAL OF APPLIED MECHANICS. Manuscript received by ASME Applied Mechanics Division, December 26, 1985; final revision, August 11, 1986.

Copyright © 1987 by ASME
Downloaded 03 May 2010 to 171.66.16.27. Redistribution subject to ASME license or copyright; see http://www.asme.org/terms/Terms_Use.cfm

magnitude of the surface displacement per cycle at the maximum load ($p_o = 5.0k$) was about 5 times that predicted by Merwin and Johnson. This discrepancy called for further investigation.

Merwin, in his dissertation (1962), likened the mechanism of forward flow to an edge dislocation moving through the solid in a plane parallel to the surface and suggested how plastic shearing on that plane might be modelled by a distribution of dislocations lying in the plane of maximum orthogonal shear stress. The same technique has been used recently (Chang, et al. 1983) to analyze the micro-slip motion of a tire which is shrink-fitted to the periphery of a solid roller. In rolling contact, the tire is observed to advance progressively relative to the core, through the action of micro-slip at the tire-core interface, in a manner very similar to plastic "forward flow".

Merwin's suggestion has been taken up in the present paper to produce an alternative analysis of progressive plastic deformation in rolling and sliding contact. The conditions of the problem demand that, in the steady-state, the only permissible *residual* plastic strain component is the shear strain γ^p_{zx}, but small variations in the other components of strain ϵ^p_{xx}, ϵ^p_{yz}, and ϵ^p_{zz} are possible during the deformation cycle. Our method is approximate since it assumes that the shear component γ^p_{zx} is the only plastic strain occurring throughout the cycle. However, it removes the more serious assumptions and approximations of the Merwin and Johnson method. Compared with the use of finite-elements it is particularly economical in computing time since (*a*) it goes straight to the steady-state and (*b*) numerical analysis is confined to the small contained zones of plastic deformation.

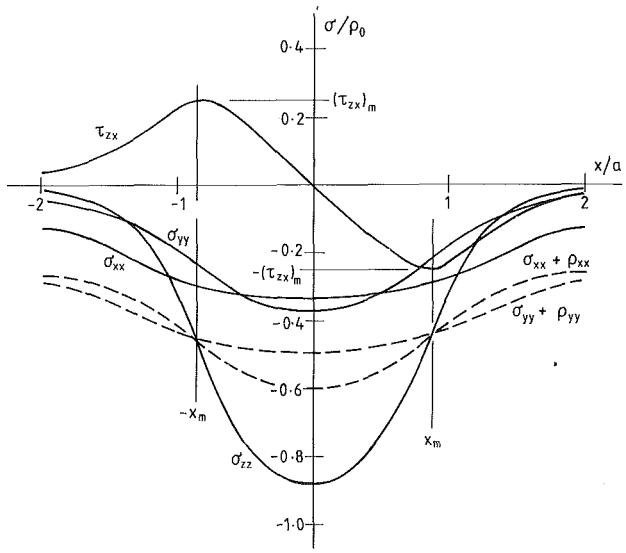


Fig. 2 The shakedown state in pure rolling ($f = 0$). Residual stresses ρ_{xx} and ρ_{yy} make the direct stresses equal at the points $\pm x_m$ where τ_{zx} is a maximum.

2 The Dislocation Model

2.1 Shakedown State. The two-dimensional stress field due to a rolling cylinder in line contact (without traction) is shown in Fig. 2. Shakedown is controlled by the maximum orthogonal shear stresses $\pm (\tau_{zx})_m = 0.25\, p_o$ at the points $x_m = \mp 0.87a$, $z_m = 0.50a$, respectively (Johnson, 1962). In the shakedown state residual stresses ρ_{xx} and ρ_{yy} have developed such that the deviatoric stresses at these two points are zero, i.e.,

$$\sigma_{xx} + \rho_{xx} = \sigma_{yy} + \rho_{yy} = \sigma_{zz}. \tag{1}$$

Since no residual orthogonal shear stress can exist, the shakedown limit will be exceeded if $(\tau_{zx})_m$ exceeds k, i.e., if p_o exceeds $4.0k$. If traction is also applied to the contact area one of these peak values of τ_{zx} is increased and the other reduced. The shakedown limit is then given by

$$|\tau_{zx}|_m = k \tag{2}$$

and the residual stresses satisfy equation (1) at the (single) point of $|\tau_{zx}|_m$.

2.2 Shear Band. We now imagine the contact load to be increased by dp_o. In view of the stress state expressed by equations (1) and (2), it follows from the von Mises flow rule that the only *plastic* strain component is the orthogonal shear $d\gamma^p_{zx}$. This may be visualized as a small contained shear band, parallel to the surface, in the location of the point of $|\tau_{zx}|_m$. This plastic shear band may be modelled by a distribution of edge dislocations lying along the band, which glide parallel to the surface with the motion of the load. The strength and distribution of the dislocations $\beta(x)$ (where β is the Burgers' vector) is such that the shear stress $\tau^*_{zx}(x)$ which they generate, when added to the shear stress due to the load $\tau_{zx}(x)$, do not exceed yield. Thus, within the band

$$|\tau_{zx}(x) + \tau^*_{zx}(x)| = k \tag{3a}$$

and outside the band

$$|\tau_{zx}(x) + \tau^*_{zx}(x)| < k \tag{3b}$$

Within a band, where plastic flow is taking place, $\beta(x)$ must be nonzero and of sign such as to correspond to positive

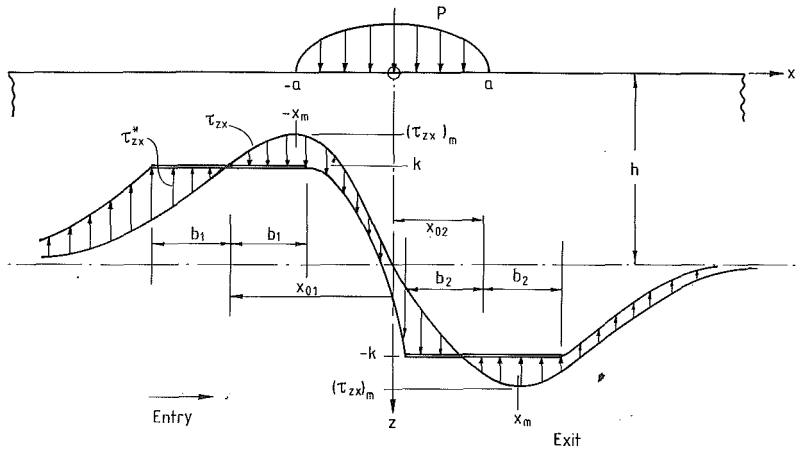


Fig. 3 Orthogonal shear stresses in pure rolling at depth h: τ_{zx} due to the contact stress and τ^*_{zx} due to the distribution of dislocations in the shear bands at entry ($x_{o1} - b_1 \leq x \leq x_{o1} + b_1$) and at exit ($x_{o2} - b_2 \leq x \leq x_{o2} + b_2$). Note the asymmetry.

Downloaded 03 May 2010 to 171.66.16.27. Redistribution subject to ASME license or copyright; see http://www.asme.org/terms/Terms_Use.cfm

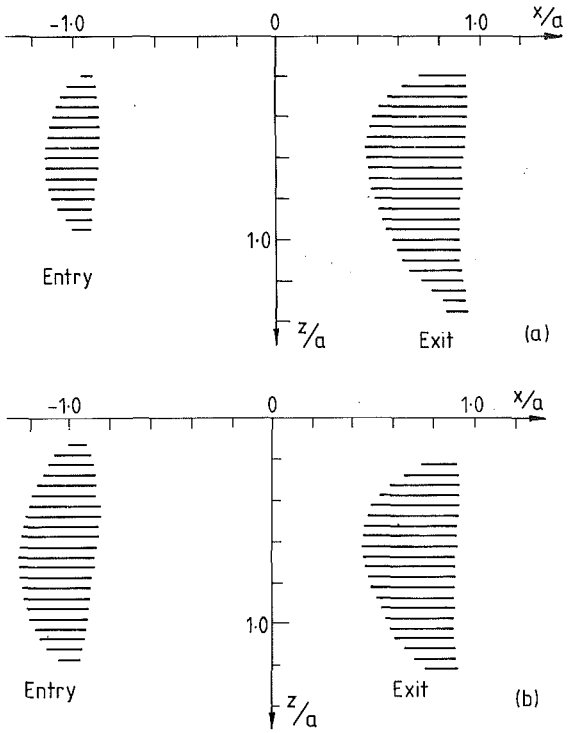


Fig. 4 Zones of plasticity at entry and exit due to $p_o/k = 4.76$ represented by multiple dislocation bands: (a) Pure rolling ($f = 0$); (b) Backward traction ($f = -0.05$)

plastic work. The shear stress along the line of the band is related to $\beta(x)$ by (Cottrell, 1953)

$$\tau^*_{zx}(x) = -\frac{G}{2\pi(1-\nu)}\int_L \frac{\beta(s)}{x-s}\,ds \tag{4}$$

where L is the length of the band. The net displacement δ of the material above the band relative to that below it (forward or backward flow) is then given by

$$\delta = -\int_L \beta(x)dx \tag{5}$$

This model is illustrated in Fig. 3 for the case of pure rolling where the peak values of orthogonal shear stress $(\tau_{zx})_m$ are equal and opposite at entry ($x < 0$) and exit ($x > 0$). The shear bands have length $2b_1$ at entry and $2b_2$ at exit and the shear stress τ^*_{zx} due to the dislocations is shown shaded. Note that the net shear stress is constant $= +k$ in the band at entry and constant $= -k$ in the band at exit. For positive plastic work this requires the dislocation distribution $\beta(x)$ to be positive in the band at entry and negative in the band at exit. By equation (5) the displacement δ is therefore backwards ($-ve$) at entry and forwards ($+ve$) at exit. Two further aspects of the problem can be appreciated from Fig. 3. Firstly, for the net stress to maintain the same sign within the band and not to exceed yield just outside the trailing edge of the band, it follows that the gradient of τ^*_{zx}, $d\tau^*_{zx}/dx$, must be continuous at the trailing edge. This gives rise to the unsymmetrical form of the distribution of τ_{zx} at entry and exit. Secondly, the stress field $\tau^*_{zx}(x, z)$ extends outside the band itself, so that the bands at entry and exit will interact with each other. This interaction is also unsymmetrical. The shear stress at entry due to dislocation band at exit is of negative sign, thereby reducing the tendency to yield at entry; the shear stress at exit due to the dislocation band at entry is also of negative sign, thereby increasing the tendency to yield. Therefore, the intensity of dislocations in the band at exit to maintain the net stress at yield is greater than that in the band at entry. In consequence, the forward displacement produced by the band at exit outweighs the backward displacement at entry, giving a net forward flow.[1]

The above argument is based on the concept of representing the plastic flow by shear bands at one depth only, but this simple model would clearly lead to the yield condition being violated above and below the band. To model the plastic zones more realistically an array of parallel dislocation bands is introduced as shown in Fig. 4. Clearly the interaction between the bands at different depths, as well as at entry and exit, must then be taken into account.

2.3 Solution Technique. As a start we consider dislocation bands at one depth only and assume that the variation of τ_{zx} in the neighborhood of its maximum value $(\tau_{zx})_m$ can be represented by a *parabolic* variation with x.

i.e., $$\tau_{zx}(x) = (\tau_{zx})_m - c(x-x_m)^2 \tag{6}$$

Further the presence of the free surface ($z = 0$) will be neglected in the first instance. It is shown in the Appendix that the distribution of dislocations in an infinite solid which gives rise to a shear stress $\tau^*_{zx}(x)$ which satisfies the conditions discussed above is given by

$$\beta(x) = \beta_o(1-\xi)(1-\xi^2)^{1/2} \tag{7}$$

where x_o is the midpoint of the band, $2b$ is the length of the band, and $\xi = (x - x_o)/b$. The shear stress in the band from equation (4) is then

$$\tau^*_{zx} = \frac{G\beta_o}{2\pi(1-\nu)}\left\{\xi^2 - \xi - \frac{1}{2}\right\} \tag{8}$$

The maximum value, $(\tau^*_{zx})_m = 3G\beta_o/8\pi(1-\nu)$, occurs at $\xi = 1/4$ (see Fig. 8(*b*)). The displacement across the band, given by equation (5), is

$$\delta = -\frac{1}{2}\pi\beta_o b \tag{9}$$

Fitting a positive distribution $\beta_1(x)$ of the form given by equation (7) to the peak at entry and a negative distribution $\beta_2(x)$ to the peak at exit results in the shear stress distribution shown in Fig. 3. Due to the interaction between the bands at entry and exit it is shown in the Appendix that the size and strength of the band at exit exceeds that at entry, leading to a net forward displacement.

$$\delta = \delta_1 + \delta_2 = \frac{1}{2}\pi(\beta_{o2}b_2 - \beta_{o1}b_1) \tag{10}$$

The approximate analysis presented above and in the Appendix clearly illustrates the mechanism of forward flow. It applies equally to the situation where traction is present and the values of $(\tau_{zx})_m$ at entry and exit are unequal. However, the values of δ predicted by equation (10) are in serious error due to the assumption of shear on one plane only and to the neglect of the free surface. To overcome these deficiencies a numerical technique was developed which makes use of the stress field caused by a dislocation band of length $2b$, parallel to and at a depth h beneath a free surface given by Dundurs (1964 and 1969), viz:

$$\tau^*_{zx}(\xi,\zeta) = A\int_{-1}^{+1} g(\xi',\zeta)\beta(\xi')(\xi-\xi')d\xi' \tag{11}$$

where,

$$g(\xi',\zeta) = \frac{1}{\rho_1^2}\left[\frac{2\zeta_1^2}{\rho_1^2} - 1\right] + \frac{1}{\rho_2^2} + \frac{1}{\rho_2^4}(4\lambda^2 - 4\lambda\zeta_2 - 2\zeta_2^2) + \frac{16\lambda\zeta_2^2}{\rho_2^6}(\zeta_2 - \lambda)$$

[1] A valuable discussion of this point with J. R. Barber and M. Comninou is acknowledged.

Downloaded 03 May 2010 to 171.66.16.27. Redistribution subject to ASME license or copyright; see http://www.asme.org/terms/Terms_Use.cfm

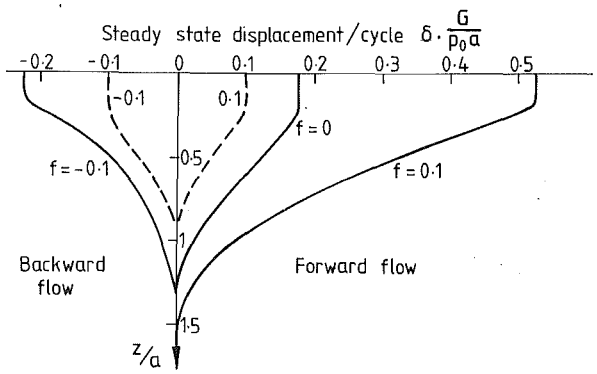


Fig. 5 Distribution with depth z of the forward displacement δ; (-----) $p_o/k = 4.0$; (———) $p_o/k = 4.76$

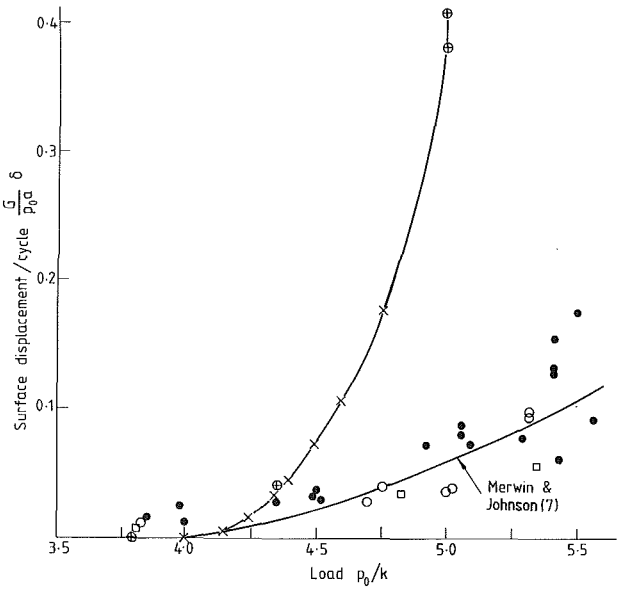


Fig. 6 Steady-state surface displacement per cycle in pure rolling. x = Present method; ⊕ = Finite-element method, Bhagava et al. (1985); compared with Merwin and Johnson theory and experimental results; o = copper; □ = duraluminium (Merwin, 1962); • = copper (Hamilton (1963).

$$\zeta_1 = \zeta - \lambda,\ \zeta_2 = \zeta + \lambda,\ \rho_1^2 = \zeta_1^2 + (\xi - \xi')^2,$$

$$\rho_2^2 = \zeta_2^2 + (\xi - \xi')^2,\ \xi = x/b,\ \lambda = h/b.$$

In this analysis, the zones of plastic deformation were represented by parallel bands of dislocations, as shown in Fig. 4. The distribution of dislocation strength in each band was assumed to have the form given by equation (7), which has been shown in the Appendix to give rise to the required parabolic distribution of shear stress. To effect a solution it is required to find for each (ith) band the locations of its center x_{oi}, its width $2b_i$, and its strength β_{oi}. However, the bands interact: the dislocations in one band affect the shear stress in all the others, so that the final solution has been obtained iteratively.

At the depth of each band h_i, equation (6) was fitted to the positive elastic stress peak at entry to fix values of x_{mi}, $(\tau_{zx})_{mi}$, and c_i. Equation (8) was then used to find the values of x_{oi}, $2b_i$, and β_{oi} such that

$$\tau_{zx} + \tau^*_{zx} \begin{cases} = k & \text{within the band} \\ < k & \text{outside the band} \end{cases}$$

The dislocation distribution $\beta_i(x)$ so found introduces shear stresses at exit and at all other depths according to equation (11) which must be added to the elastic stresses due to the load. This whole procedure is now repeated, first for the negative τ_{zx} peak at the same depth at exit and then for the shear bands at other depths, proceeding in sequence from the higher stresses to the lower. Due to the continuous modification of stresses at any given depth by the introduction of dislocations at other depths, it was necessary to make between 4 and 10 iterations of the whole system to obtain a satisfactory result. The spacing of the bands influences the final result. When the spacing Δz was reduced below $a/40$ no further change was found.

3 Results

The calculations yield the net forward displacement per cycle $\Delta\delta$ of the material above each of the dislocation bands show in Fig. 4 relative to the material below it. Summations of these displacements from the deepest to the shallowest band give the displacement δ at the surface. If the band spacing is Δz, the ratio $\Delta\delta/\Delta z$ gives the plastic shear strain increment per cycle $\Delta\gamma^p_{zx}$.

The distribution of displacement with depth is shown in Fig. 5 for a few of the conditions examined. The results in broken lines in Fig. 5 are for a load $p_o/k = 4.0$, which is the shakedown limit in pure rolling. No forward flow then takes place in the steady-state; the peak values of shear stress $(\tau_{zx})_m$ at entry and exit are equal and just within yield ($= k$). The addition of a traction force $Q = \pm 0.1P$ violates the shakedown limit. One of the peak stresses exceeds k but the other falls below k. There is then only a single plastic zone, at exit if Q is positive and at entry if Q is negative. The plastic displacements in each case are of identical magnitude but opposite in sign since the bias towards flow arises from the interaction between the *two* plastic zones.

The results for a higher load, $p_o/k = 4.76$, are shown by full lines in Fig. 4. In this case there are two plastic zones and the shakedown limit is exceeded at all values of f ($= Q/P$). A forward displacement is found in pure rolling ($f = 0$) and the forward displacement for $f = +0.1$ is double the backward displacement for $f = -0.1$. All these results are qualitatively in agreement with Merwin and Johnson (1963) and Johnson and Jefferis (1963), but the magnitudes are significantly different.

The forward flow in pure rolling, calculated by the present method, is plotted against load in Fig. 6 where it is compared with the approximate analysis of Merwin and Johnson, the finite element analysis of Bhagava et al. (1985) and with experiments. It is immediately clear that the present method gives results which are very close to those obtained by finite elements and much in excess of both the predictions of Merwin and Johnson and of the measurements. The possible reasons for this discrepancy will be discussed later.

The results of calculation with sliding traction are presented in Fig. 7 for a load $p_o/k = 4.0$ and in Fig. 8 for $p_o/k = 4.76$, where they are compared with the theory of Johnson and Jefferis (1963) and also with Jefferis' experiments (1985). The predictions of the present theory are again considerably greater than those of the earlier analysis but the experimental measurements of forward flow lie between the two theories and, in the case of copper rollers, lie closer to the present theory. Finite-element calculations are not currently available for rolling with traction.

4 Discussion and Conclusions

The very good agreement between the predictions of forward flow by the present method and by the finite-element

Downloaded 03 May 2010 to 171.66.16.27. Redistribution subject to ASME license or copyright; see http://www.asme.org/terms/Terms_Use.cfm

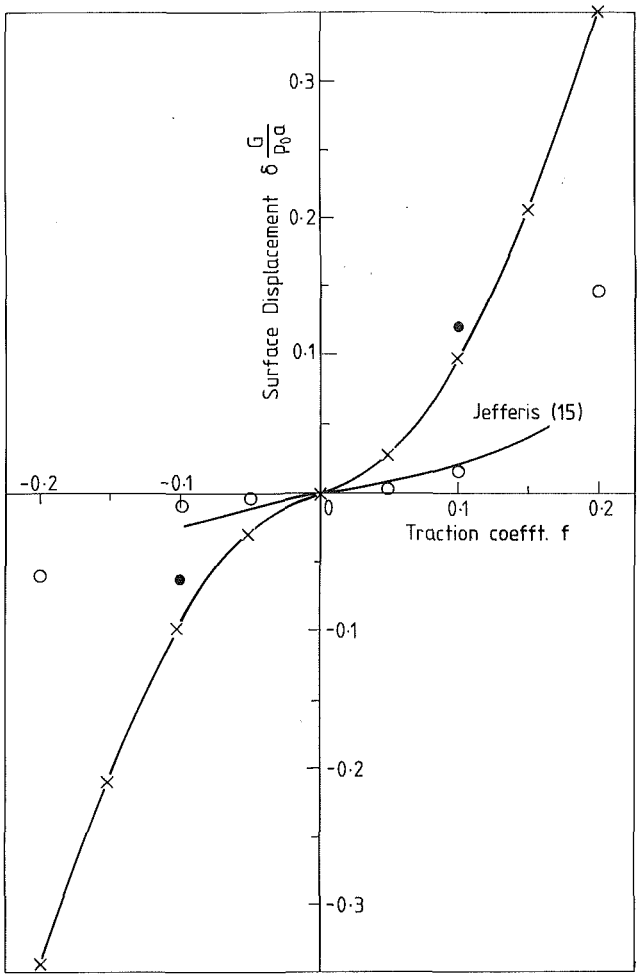


Fig. 7 Variation of steady-state surface displacement with traction: p_o/k = 4.0

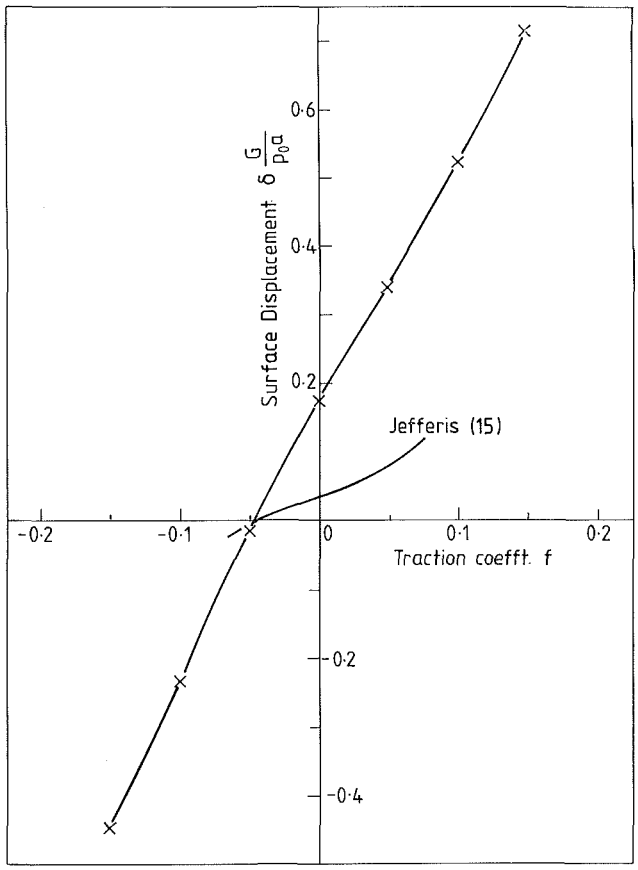


Fig. 8 Variation of steady-state surface displacement with traction: p_o/k = 4.76

analysis of Bhagava et al. (1985) provides encouraging support for both. Although the finite-element method satisfies in principle all the equations of continuum mechanics, the finite size of the mesh in relation to a stress field with large stress gradients gives cause for concern. The present method satisfies the field equations of equilibrium and compatibility, but only satisfies the plastic stress-strain relations at one point in each dislocation band. At other points in the band the deviatoric direct stresses, though small, are not zero, so that small plastic strains ϵ^p_{xx}, ϵ^p_{yy}, and ϵ^p_{zz} of alternating sign will, in fact, occur, though they are neglected in the analysis. The errors involved in this approximation are likely to be very small and the method is judged to be far more reliable than that of Merwin and Johnson for the prediction of forward flow, although the work of Bhagava et al. (1985) has shown that the prediction of residual stresses by Merwin and Johnson to be in very reasonable agreement with finite elements.

We view the finite element method and the present dislocation method as complementary. Accepting the approximation in the dislocation method, it has the practical advantage of going directly to the steady state and restricting the discretization of the stress field to the relatively small contained zones of plastic deformation. The saving in computing effort is considerable. Bhagava et al. (1985) quote 7 to 24 hours on a VAX 11/780 computer for a single contact sequence; the present method takes 1 to 15 minutes on an IBM 3081 computer for the same result.

Turning now to the discrepancy between the new theories and experiment, there would seem to be two possible causes: (*i*) departure in the experiment from plane strain conditions and (*ii*) variation in the experimental materials from ideal elastic-perfectly plastic behavior.

In the experiments reported here the rolling track did not extend across the full width of the rollers. It was necessary to provide unloaded shoulders at each side of the track to prevent lateral plastic flow. A recent study of rolling point contacts by Ponter et al. (1985) has shown that in these circumstances residual shear stresses develop which inhibit the steady-state forward flow and may prevent it entirely. In effect, the unloaded material at each side of the track holds back the loaded material in the center of the track. In the experiments of Merwin (1963) and of Jefferis (1966) it was observed that the edges of the rolling track, even in line contact, did not move forward as much as the center.

All analyses of this problem show that the observed forward flow, particularly under pure rolling conditions, arises from a relatively small difference between forward shear in the plastic zone at exit and the backward shear at entry. Thus a small difference in the yield points of the material at entry and exit would have a marked effect on the net flow. We see from Fig. 8 that a traction coefficient of -0.05 reduces the net forward flow to zero. A traction coefficient of this magnitude increases the maximum shear stress at entry $(\tau_{zx})_{m1}$ and reduces it at exit $(\tau_{zx})_{m2}$, so that they differ by about 12 percent. The same effect could be achieved in pure rolling, where $(\tau_{zx})_{m1} = (\tau_{zx})_{m2}$, by making the yield stress at exit 12 percent greater than at entry. The plastic behavior of materials under cyclic loading is very complex and there are few firm rules. However, most metals display some degree of kinematic hardening in which the yield locus is displaced in the sense of the maximum plastic strain occurring in the cycle. This

Downloaded 03 May 2010 to 171.66.16.27. Redistribution subject to ASME license or copyright; see http://www.asme.org/terms/Terms_Use.cfm

behavior would suggest a displacement of the yield locus during the early cycles of load in the sense of the plastic strain at exit which exceeds the strain at entry. The yield stress at exit would thereby be increased compared with that at entry with a corresponding reduction in the net forward flow.

In conclusion, therefore, we can say that a method of analysis of the progressive plastic shearing of surfaces under the action of rolling contact loads, in which the plastic flow is modelled by parallel bands of distributed dislocations, shows good agreement (where results are available) with a complete finite element analysis. The new method is thought to be an improvement on the approximate analysis of Merwin and Johnson (1963) which, while qualitatively correct, has been shown to underestimate the accumulated deformation by a significant factor. Existing measurements of progressive deformation are also much less than the new theories predict. This discrepancy is thought to be due to a combination of non-plane-strain conditions in the experiments and strain hardening properties of the materials in cyclic loading.

References

Belyakov, see Gokhfeld, D.A., and Cherniavski, O. F., 1980, *Limit Analysis of Structures at Thermal Cycling*, Sijthoff and Noordhoff, Groningen.

Bhagava, V., Hahn, G. T., and Rubin, C. A., 1985, "An Elastic-Plastic Finite-Element Model of Rolling Contact. Part I: Single Contacts, Part II: Repeated Contacts," ASME JOURNAL OF APPLIED MECHANICS, Vol. 52, Ser. E, pp. 66–74, pp. 75–82.

Chang, F. K., Comninou, M., and Barber, J. R., 1983, "Slip Between a Layer and a Substrate Caused by a Normal Force Moving Steadily Over the Surface," *Int. J. Mech. Sci.*, Vol. 25, pp. 803–809.

Crook, A. W., 1957, "Simulated Gear-Tooth Contacts: Some Experiments on Their Lubrication and Sub-Surface Deformation," *Proc. Inst. Mech. Engrs.*, Vol. 171, pp. 187–196.

Dundurs, J., and Mura, T., 1964, "Interaction Between an Edge Dislocation and a Circular Inclusion," *J. Mech. Phys. Solids*, Vol. 12, pp. 177–189.

Dundurs, J., 1969, "Elastic Interaction of Dislocations and Inhomogeneities," In *Math. Theory of Dislocations*, Mura, ed., p. 70.

Hamilton, G. M., 1963, "Plastic Flow of Rollers Loaded Above Their Yield Point," *Proc. Inst. Mech. Engrs.*, Vol. 177, pp. 667–675.

Johnson, K. L., 1962, "A Shakedown Limit in Rolling Contact," *Proc. 4th US Nat. Congress of Appl. Mech.*, Berkeley, CA, pp. 971–975.

Johnson, K. L., 1985, *Contact Mechanics*, CUP, Cambridge, England.

Johnson, K. L., and Jefferis, J. A., 1963, "Plastic Flow and Residual Stresses in Rolling and Sliding Contact," *Proc. Inst. Mech. Engrs. Symp. on Rolling Contact Fatigue*, London, England, pp. 50–61.

Merwin, J. E., 1962, "Plastic Deformation of Surfaces in Rolling," Ph.D. dissertation, Cambridge University, Cambridge, England.

Merwin, J. E., and Johnson, K. L., 1963, "An Analysis of Plastic Deformation in Rolling Contact," *Proc. Inst. Mech. Engrs.*, Vol. 177, pp. 676–685.

Ponter, A. R. S., Hearle, A. D., and Johnson, K. L., 1985, "Application of the Kinematical Shakedown Theorem to Rolling and Sliding Point Contacts," *J. Mech. Phys. Solids*, Vol. 33, pp. 339–362.

Shima, M., Okada, K., Kimura, Y., and Yamamoto, T., 1981, "Measurements of Subsurface Plastic Flow in Rolling Contact," *Jl. Japan Soc. Lub. Engrs.*, Int. Ed., Vol. 2, pp. 75–80.

APPENDIX

A band of edge dislocations, distributed along the line $-b \leqq x \leqq +b$ with intensity of Burger's vectors $\beta(x)$ per unit length, gives rise to a shear stress along the x axis given by (Cottrell, 1953)

$$\tau^*_{zx}(x) = -A\int_{-b}^{+b} \frac{\beta(s)}{x-s}\,ds$$

$$= -A\int_{-1}^{+1} \frac{\beta(\xi')}{\xi-\xi'}\,d\xi' \qquad (4)$$

where $\xi = x/b$, $\xi' = s/b$, and $A = G/2\pi(1-\nu)$, G = elastic shear modulus and ν = Poisson's ratio. We seek a distribution of dislocations $\beta(\xi)$ which satisfies the following conditions:

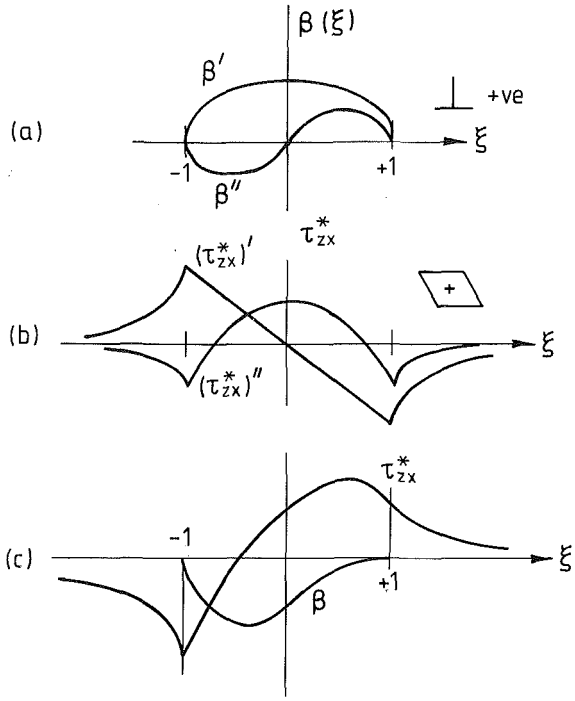


Fig. 9 (a) Distribution of dislocations $\beta'(\xi)$ and $\beta''(\xi)$; (b) Resulting shear stress distribution $\tau^*_{zx}(\xi)$; (c) Combination of $\beta'(\xi)$ and $\beta''(\xi)$ such that $\beta(\xi)$ does not change sign and $d\tau^*_{zx}/d\xi$ is continuous at $\xi = 1$

(*i*) $\beta(\xi)$ is uni-directional;
(*ii*) $\tau^*_{zx}(\xi)$ is second order in x;
(*iii*) $\tau^*_{zx}(\xi)$ is continuous at $\xi = +1$.

Inserting condition (*ii*) into equation (4) gives a singular integral equation for $\beta(\xi)$ of a type familiar in contact stress analysis (see Johnson, 1985). Possible solutions are

$$\beta'(\xi) = \beta'_o(1-\xi^2)^{1/2} \qquad (A1)$$

$$\beta''(\xi) = \beta''_o\xi(1-\xi^2)^{1/2} \qquad (A2)$$

Substituting in equation (4) above, gives

$$(\tau^*_{zx})' = -A\beta'_o\xi, \qquad |\xi| \leqq 1 \qquad (A3a)$$

$$-A\beta'_o\{\xi \mp (\xi^2-1)^{1/2}\}, \qquad |\xi| \geqq 1 \qquad (A3b)$$

$$(\tau^*_{zx})'' = -A\beta''_o(\xi^2-1/2), \qquad |\xi| \leqq 1 \qquad (A4a)$$

$$-A\beta''_o\{\xi^2 \mp \xi(\xi^2-1)^{1/2} - 1/2\}, \qquad |\xi| > 1 \qquad (A4b)$$

Conditions (*i*) and (*iii*) above are satisfied if we take $\beta'_o = -\beta''_o = \beta_o$ and superpose the two distributions as shown in Fig. 9, so that

$$\beta(\xi) = \beta_o(1-\xi)(1-\xi^2)^{1/2} \qquad (A5)$$

and $$\tau^*_{zx}(\xi) = A\beta_o\{\xi^2-\xi-1/2\}, \qquad |\xi| \leqq 1 \qquad (A6)$$

The minimum value is

$$(\tau^*_{zx})_m = 3A\beta_o/4$$

and occurs at $\xi = 1/2$.

At large values $|\xi| \gg 1$, i.e., $|x| \gg b$,

$$\tau^*_{zx}(x) \simeq -A\beta_o b/2x \qquad (A7)$$

The shear stress due to the contact load in the vicinity of its maximum is approximated by equation (6) which may be written

$$\tau_{zx}(\xi) = (\tau_{zx})_m - cb(\xi-\xi_o)^2 \qquad (A8)$$

We now superpose the traction due to the dislocations given

Downloaded 03 May 2010 to 171.66.16.27. Redistribution subject to ASME license or copyright; see http://www.asme.org/terms/Terms_Use.cfm

by (A1) and (A2). If we put $A\beta_o = cb$ and $\xi_o = 1/2$,

$$\tau_{zx} + \tau^*_{zx} = (\tau_{zx})_m - 3A\beta_o/4 \tag{A9}$$

We now consider the interaction between the positive peak at entry and the negative peak at exit, denoted by sufficies 1 and 2, respectively. To a first approximation the interaction stress is given by equation (A7) in which x is replaced by ℓ, the distance between the peak stresses at entry and exit. Substituting from (A7) into equation (3), we find, at entry,

$$(\tau_{zx})_{m1} - 3A\beta_{o1}/4 + A\beta_{o2}b/2\ell = k \tag{A10a}$$

and at exit

$$(\tau_{zx})_{m2} - 3A\beta_{o2}/4 - A\beta_{o1}b/2\ell = -k \tag{A10b}$$

where $A\beta_{o1} = c_1 b_1$ and $A\beta_{o2} = c_2 b_2$.
$(\tau_{zx})_{m1}$, $(\tau_{zx})_{m2}$, c_1, c_2, and ℓ are obtained from the elastic stress field, whereupon the above equations can be solved simultaneously for b_1, b_2, β_{o1}, and β_{o2}. The net forward flow is then given by

$$\delta = \delta_1 + \delta_2 = 1/2\pi\,(\beta_{o2} b_2 - \beta_{o1} b_1) \tag{A11}$$

Downloaded 03 May 2010 to 171.66.16.27. Redistribution subject to ASME license or copyright; see http://www.asme.org/terms/Terms_Use.cfm

D. A. Hills
Department of Engineering Science,
University of Oxford,
Oxford, England OX1 3PJ

A. Sackfield
Department of Mathematics,
Trent Polytechnic,
Nottingham, England NG1 4BU

The Stress Field Induced by Normal Contact Between Dissimilar Spheres

The stress field induced by the mutual compression of two spheres having dissimilar elastic constants is deduced. Solutions are found assuming full slip, full stick, and partial slip at the interface, but coupling between the shear traction and vertical displacement of the surfaces is neglected. It is shown that significant modifications to the Hertzian stress field occur at the surface, and that these decay rapidly with depth.

Introduction

When an elastic sphere is pressed into the flat surface of a large elastic body, a circular contact patch results and intense stresses develop locally. If the contacting surfaces are frictionless, or if the elastic constants of the two bodies are identical, no interfacial shear stresses develop. If, further, the applied load is modest, so that the radius of contact is much less than that of the sphere, it is admissible to approximate the shape of the sphere by a paraboloid of equivalent local curvature, and a classical Hertzian contact results (Johnson, 1985). Normally, the assumptions cited above are not restrictive, and an analysis of the stress field developed is not appreciably in error. However, one instance where a neglect of the interfacial shear tractions due to differing elastic constants may produce appreciable discrepancies is in ring and cone crack experiments.

Quasi-static indentation of a glass block by a steel ball results in the sudden formation of a crack, whose surface approximates the frustum of a cone (Lawn and Wilshaw, 1975). The test is of considerable fundamental interest, and should enable the fracture toughness of a highly brittle material to be found rapidly. Approximate solutions for the crack-tip stress intensity for this configuration have been found (Frank and Lawn, 1967) but our understanding of the bulk stress field present in the glass block, and an explanation of the characteristic cone angle are incomplete. Johnson et al. (1973) have made careful measurements of the cone crack, and noted that it usually originates in the surface just outside the contact disk. They have investigated the influence of the difference between the elastic constants of steel and glass on the surface stress field, and noted that the crack originates at a point where the radial stress is most tensile. It is the purpose of this paper to develop the analysis presented in Johnson et al. (1973) and enable a more complete picture of the stress field induced to be found.

Statement of Problem

The effect of a difference in the elastic constants may be appreciated from a consideration of the frictionless Hertz contact problem. Particles in the surface have an inwards radial displacement proportional to $(1 - 2\nu)/\mu$ where ν is Poisson's ratio and μ is the modulus of rigidity. Hence, if the contacting bodies have different values of this parameter, the one having the greater compliance (larger value of $(1 - 2\nu)/\mu$) will suffer a larger displacement: frictional forces will tend to oppose relative motion and therefore give rise to an outwards radial tangential traction on the surface of the more compliant body.

The problem was studied by Goodman (1962), who assumed that the coefficient of friction was sufficiently high to prevent slip at all points within the contact. Furthermore, he neglected the effect of all tangential tractions on the z-direction displacement of the contacting surfaces, Fig. 1, so that the direct traction remains Hertzian. The resulting surface shear traction is:

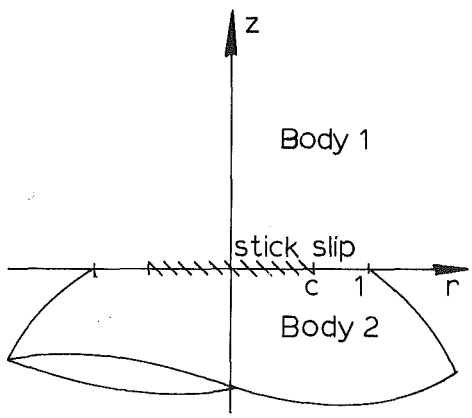


Fig. 1 Geometry of contact

Contributed by the Applied Mechanics Division for publication in the JOURNAL OF APPLIED MECHANICS.
Discussion on this paper should be addressed to the Editorial Department, ASME, United Engineering Center, 345 East 47th Street, New York, N.Y. 10017, and will be accepted until two months after final publication of the paper itself in the JOURNAL OF APPLIED MECHANICS. Manuscript received by ASME Applied Mechanics Division, March 13, 1986; final revision June 10, 1986.

Copyright © 1987 by ASME
Downloaded 03 May 2010 to 171.66.16.27. Redistribution subject to ASME license or copyright; see http://www.asme.org/terms/Terms_Use.cfm

$$\frac{\tau_{rz}}{\beta p_o} \equiv \frac{q}{\beta p_o} = r\int_0^{\sqrt{1-r^2}} \frac{\ln x}{(1-x^2)^2}\,dx \qquad 0<r<1 \tag{1}$$

where we adopt coordinates normalized with respect to contact radius (Fig. 1), and β is Dundurs' constant, defined by:

$$\beta = \frac{(1-2\nu_1)/\mu_1 - (1-2\nu_2)/\mu_2}{(1-\nu_1)/\mu_1 + (1-\nu_2)/\mu_2} \tag{2}$$

While the value of τ_{rz} is finite at all radii ($r \le 1$, $z = 0$) the ratio $\tau_{rz}/p(r)$, where p is the Hertzian contact pressure, becomes infinite as $r \to 1$. It is clear, therefore, that an annulus of slip must exist at the edge of contact.

An alternative approximation, more appropriate if the coefficient of friction, f, is small, is to assume that slip persists throughout the contact region, so that a boundary value problem of the first kind may be written down directly. Again, neglecting coupling of direct and shear tractions, we may write:

$$\frac{q}{fp_0} = \sqrt{1-r^2}\,\mathrm{sgn}(\beta) \qquad 0<r<1 \tag{3}$$

Detailed considerations of the nature of the interfacial shear tractions where the slip annulus is of finite size have been carried out by Spence in a series of articles (Spence 1968, 1973, 1975). The last is of direct significance to the present work, since again it enables us to write down the surface tractions as a boundary value problem of the first kind. Spence tackles the problem of coupling between the direct and shear traction effects by successive approximation, choosing for his first approximation to neglect the effect. In keeping with the above, we shall restrict ourselves to a solution based on this first approximation. However, Spence solves primarily the problem of frictional indentation by a flat-ended rigid punch, and uses a transformation to solve the corresponding Hertzian indentation. In the following the subscript B is used to denote the solution to the Boussinesq punch problem:

$$q_B = \frac{fp_0}{2\sqrt{1-r^2}}(1-\Psi(r,c))\,\mathrm{sgn}(\beta) \qquad 0<r<1 \tag{4}$$

where $\Psi(r,c)$

$$= \frac{2}{\pi}\left[wr\int_0^{\pi/2} \frac{d\theta}{(1-(1-r^2)\sin^2\theta)\sqrt{1-c'^2\sin^2\theta}} - \frac{cK(c')}{r} \times \right.$$

$$\left. \times \left\{\frac{w}{c} - \frac{Q_0(w)}{Q_0(c)}\right\}\right] \qquad 0 \le r \le c \tag{5}$$

$$= 0 \qquad c \le r \le 1$$

$$w^2 = \frac{c^2 - r^2}{1-r^2}$$

$$c'^2 = 1 - c^2$$

$$Q_0(x) = \frac{1}{2}\ln\left[\frac{1+x}{1-x}\right]$$

$K(c)$ is a complete elliptic integral of the first kind, p_0 is the peak *Hertzian* contact pressure and c is the radius of the stick slip interface. The surface shear traction for the Hertz problem is:

$$q = 2r\int_r^1 \frac{q_B(t)\,dt}{t^2} \tag{6}$$

and the radius of the stick/slip interface is obtained by demanding a smooth transition from stick to slip regions, yielding;

$$\frac{f}{\beta} = \frac{Q_0(c)}{cK(c')} \tag{7}$$

Since the direct traction distribution remains Hertzian we shall consider here only shear tractions, and superpose the stresses induced by pressure, which are well known (see, e.g., Huber, 1904). Therefore, closed form solutions will be obtained for the interior and surface stress fields within a half-space due to each of the above three boundary conditions, i.e., equations (1) or (3) or (6) in conjunction with the following, on $z = 0$:

$$\sigma_{zz} = \tau_{z\theta} = 0 \qquad 0 \le r \le \infty \tag{8}$$
$$\tau_{rz} = 0 \qquad 1 < r \le \infty$$

General Theory

For axisymmetric problems in the half-space a convenient solution is provided by the method of Green and Collins (Barber, 1983). Choose a potential ψ defined by:

$$\psi = Im\int_0^1 g(t)\log\{r^2 + (z+it)^2)^{1/2} + (z+it)\}\,dt \tag{9}$$

i.e.,

$$\phi \equiv \frac{\partial\psi}{\partial z} = Im\int_0^1 \frac{g(t)\,dt}{\sqrt{r^2 + (z+it)^2}} \tag{10}$$

The corresponding stress field is given by Green and Zerna (1968) as:

$$\sigma_{rr} = 2\psi_{rr} + 2\nu\frac{\psi_r}{r} + z\psi_{rrz} \tag{11}$$

$$\sigma_{\theta\theta} = -2\nu\psi_{zz} + 2(1-\nu)\frac{\psi_r}{r} + \frac{z}{r}\psi_{rz} \tag{12}$$

$$\sigma_{zz} = z\psi_{zzz} \tag{13}$$

$$\tau_{rz} = \psi_{rz} + z\psi_{zzr} \tag{14}$$

where subscripts to the potential ψ denote derivatives. From equations (10) and (14) we see that the value of τ_{rz} on the surface is given by

$$q(r) = \frac{\partial\phi}{\partial r} = -\frac{d}{dr}\left\{\int_r^1 \frac{g(t)\,dt}{\sqrt{t^2 - r^2}}\right\} \tag{15}$$

This Abel integral may be inverted (Barber, 1983, Table 2) to give

$$\frac{g(x)}{x} = \frac{2}{\pi}\int_x^1 \frac{q(r)\,dr}{\sqrt{r^2 - x^2}} \tag{16}$$

When $g(x)$ is established ψ and its derivatives may be found from equation (9) and substituted into equations (11)–(14). These general equations for the stress components are tabulated in Appendix A.

Of particular interest in this problem, as with many contact geometries, are the values of the stress components within the surface, since the severest state of stress quite often occurs there, and it is a favored site for crack initiation. In the present problem, the only remaining surface stress components not specified by the surface tractions (equations (1, 3, 6, 8)) are σ_{rr} and $\sigma_{\theta\theta}$, since $\tau_{r\theta}$ is clearly zero from a consideration of symmetry. The equations for the derivatives of ψ take on particularly simple forms for $z = 0$, and, after some algebra, the following expressions result;

$$\sigma_{rr} = \frac{2(1-\nu)}{r^2} I - \frac{2}{r}\frac{dI}{dr} \tag{17}$$

$$\sigma_{\theta\theta} = \frac{2(1-\nu)}{r^2} I - \frac{2\nu}{r}\frac{dI}{dr}$$

where

$$I = \int_0^s \frac{tg(t)\,dt}{\sqrt{r^2 - t^2}} \qquad \frac{dI}{dr} = r\int_0^s \frac{g'(t)\,dt}{\sqrt{r^2 - t^2}} \tag{18}$$

$$s = r \quad \text{if} \quad r \le 1$$

$$s = 1 \quad \text{if} \quad r \ge 1$$

Downloaded 03 May 2010 to 171.66.16.27. Redistribution subject to ASME license or copyright; see http://www.asme.org/terms/Terms_Use.cfm

Table A

Material Pair	β
Aluminum/Steel	0.234
Steel/Cast Iron	0.240
Steel/Glass	0.408
Aluminum/Glass	0.138
Alumina/Glass	0.460
Steel/Brass	0.314
Steel/Lead	0.151
Steel/PMMA	0.291

Full Stick Solution

Substituting equation (1) into (16) and carrying out the integration eventually leads to the following expression;

$$\frac{g(t)}{\beta p_0} = \frac{1-t}{\pi}\left\{t - \frac{(1+t)}{2}\log\left[\frac{1-t}{1+t}\right]\right\} \tag{19}$$

Values of Dundurs' constant are given in Table A for various pairs of materials in frequent engineering use. As will be noted, the combination of steel and glass gives rise to one of the largest values, and in figures illustrating the stress field, we shall take $|\beta| = 0.4$. Of primary interest in the cone crack problem is the magnitude of the more positive principal stress in the $r-z$ plane. This is shown for both surfaces, together with the frictionless case, for comparison, in Fig. 2. The stress field used is a superposition of that due to frictional tractions described in detail above, together with that due to frictionless Hertzian indentation (Huber, 1904; Sackfield and Hills, 1983). Except where stated otherwise, Poisson's ratio is taken to be 0.3.

It is clear that the effect of the surface shear traction does not persist to any depth, and is confined principally to the periphery of the contact. In the less compliant body the radial tension found under frictionless conditions is augmented, while in the more compliant material, it is suppressed. In the case of indentation of a glass block by a steel ball glass is the more compliant material, and it may be seen that the effect of the frictional tractions is to push the critical contour separating tension and compression radially outwards slightly, near the surface, as noted by Johnson et al. (1973).

Full Slip Solution

Substituting equation (3) into (16) and carrying out the integration gives:

$$\frac{g(t)}{fp_0} = \frac{2t}{\pi}\{K(t') - E(t')\}\,\mathrm{sgn}(\beta) \tag{20}$$

where $t'^2 = 1 - t^2$, and $K(t')$, $E(t')$ are complete elliptic integrals of the first kind.

Since a coefficient of friction of about 0.4 is the largest which is easily achieved in practice, this is used in the figures. The effect of friction on the more positive principal stress in the $r-z$ plane is shown in Fig. 3, and it will be noted that the effect is qualitatively similar to that found under full stick conditions. Values near the origin should be disregarded since this constitutes a singularity, and it is not physically reasonable to expect that slip will persist as $r \to 0$, since the radial displacement also vanishes.

Partial Slip Solution

Determination of the function $g(t)$ for partial slip conditions follows essentially the same recipe as that detailed in the two previous sections. Further steps are needed, however. First equation (4) is substituted into equation (6) giving the surface shear traction present in the Hertz problem, i.e.,

$$\frac{q(r)}{fp_0}\,\mathrm{sgn}(\beta) = \sqrt{1-r^2} - rH(c-r)\int_r^c \frac{\Psi(t,c)\,dt}{t^2\sqrt{1-t^2}} \quad 0<r<1 \tag{21}$$

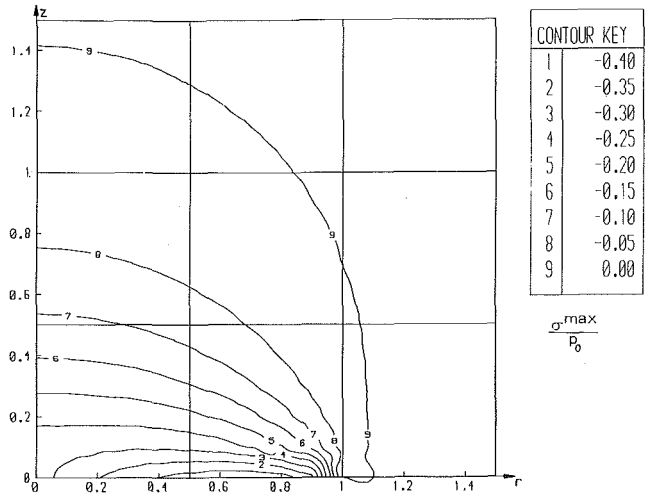


Fig. 2(a) More compliant surface

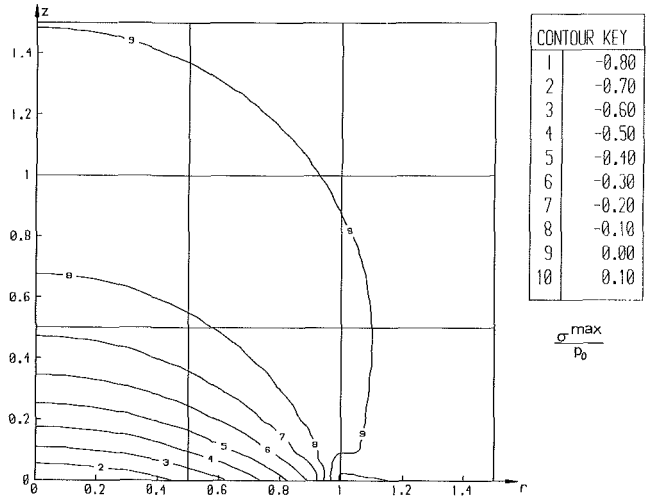


Fig. 2(b) Frictionless, i.e., Hertzian contact

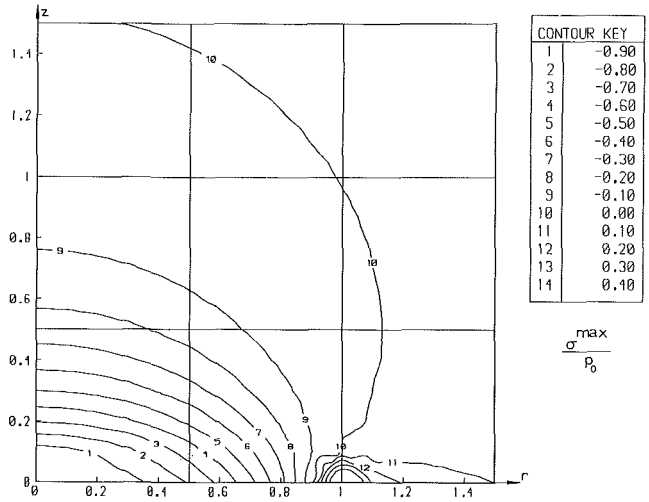


Fig. 2(c) Less compliant surface

Fig. 2 Contours of more positive principal stress in $r-z$ plane, assuming full stick $|\beta| = 0.4$

Downloaded 03 May 2010 to 171.66.16.27. Redistribution subject to ASME license or copyright; see http://www.asme.org/terms/Terms_Use.cfm

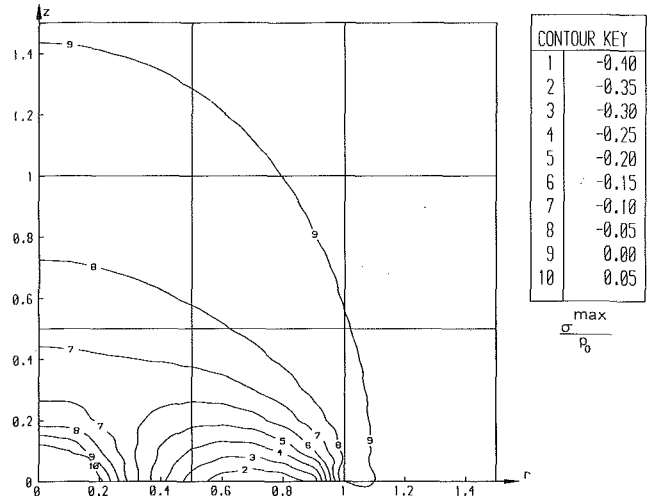


Fig. 3(*a*) More compliant surface

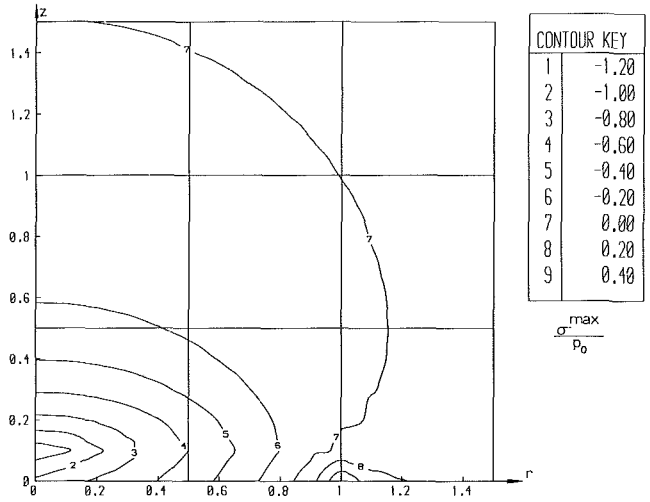


Fig. 3(*b*) Less compliant surface

Fig. 3 Contours of more positive principal stress in $r-z$ plane, assuming full slip, $f = 0.4$

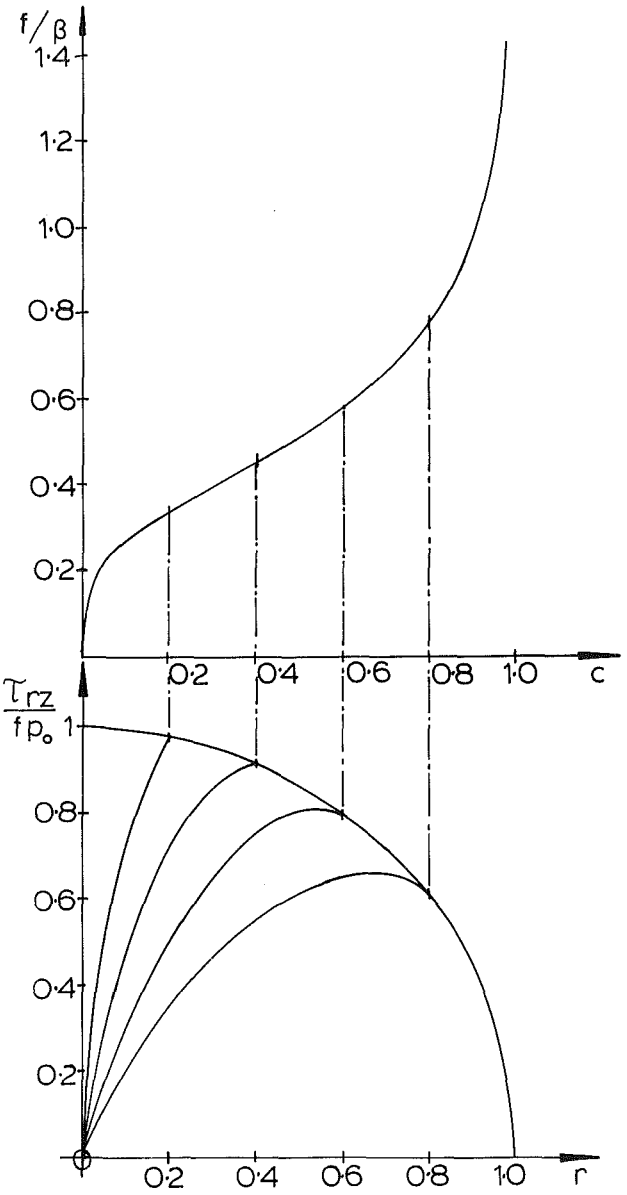


Fig. 4 Variation of position of stick/slip boundary, c, with ratio f/β; (*b*) surface radial shear traction for full and partial slip cases

where $H(r)$ is Heaviside's step function. The first term on the right-hand side is readily identified as being the full slip surface traction, for which the corresponding function $g(t)$ has already been solved (equation (20)). Attention is, therefore, focussed on the second "corrective" term, which corresponds to abatement of the shear traction within the stick zone, and giving (from equation (16)):

$$\frac{g_c(t)}{fp_0 t}\,\mathrm{sgn}(\beta) = -\frac{2}{\pi}\int_r^c \frac{r}{\sqrt{r^2-t^2}}\int_t^c \frac{\Psi(u,c)}{u^2\sqrt{1-u^2}}\,du.dr$$

$$= -\frac{2}{\pi}\int_t^c \frac{\Psi(u,c)}{u^2}\sqrt{\frac{u^2-t^2}{1-u^2}}\,du \qquad (22)$$

After considerable manipulation this yields;

$$\frac{g_c(t)\pi}{2fp_0 t}\,\mathrm{sgn}(\beta) = K(c')\left\{\frac{t}{2c}(1+c^2) + \frac{t'}{2Q_0(c)}\left[\frac{ct'}{t}\,Q_0(t) + \frac{c-t}{t'}\right]\right\}$$

$$-\frac{t}{c}\,E(c') - K(t') + E(t') \qquad (23)$$

where E is an elliptical integral of the first kind, and

$$c'^2 = 1 - c^2$$

The surface shear traction corresponding to equation (21) is shown in Fig. 4, together with a plot of equation (7), indicating the position of the stick/slip boundary as a function of f/β. It may be noted, that, unlike the partial slip problems involving an externally imposed shear, i.e., the problems of Mindlin and Deresiewicz (Johnson, 1985, pp. 222, pp. 232), the surface shear traction may be higher over part of the stick zone than within the slip annulus.

Contour plots of the move positive principal stress in the $r-z$ plane are shown in Fig. 5, for $f = 0.4$ and $c = 0.8$.

Surface Stresses

It will have become apparent that, while the complete stress-field induced by normal contact is appreciably affected by frictional tractions, it is at the surface where the influence dominates. In view of the experimental observation that many cracks propelled by contact loads originate there, and the

Downloaded 03 May 2010 to 171.66.16.27. Redistribution subject to ASME license or copyright; see http://www.asme.org/terms/Terms_Use.cfm

economies in calculating stress components which may be effected, further detailed consideration will be given.

First, considering the full stick case, it is found that $I(r)$ may be found from the first of equations (18) in closed form, and dI/dr obtained by direct differentiation. The stress components given by equation (17) transpire to be:

$$\left.\begin{aligned}\frac{\sigma_{rr}}{\beta r_0} &= \frac{2}{3}(2+\nu)\frac{r}{\pi} - p + \frac{(1-\nu)}{3r^2}(1-p^3) \qquad (24)\\ \frac{\sigma_{\theta\theta}}{\beta p_0} &= \frac{2}{3}(1+2\nu)\frac{r}{\pi} - \nu p - \frac{(1-\nu)}{3r^2}(1-p^3) \qquad (25)\\ p^2 &= 1-r^2\end{aligned}\right\} r \le 1$$

which have previously been found by Johnson et al. (1973) and

$$\left.\begin{aligned}\frac{3\pi\sigma_{rr}}{2\beta p_0} &= (1-\nu)\frac{\alpha}{r^2} - (2+\nu)(q-r)\\ &\quad - \frac{q}{r^2}\log\left[\frac{r}{q}\right][1-\nu+r^2(2+\nu)] \qquad (26)\\ \frac{3\pi\sigma_{\theta\theta}}{2\beta p_0} &= -(1-\nu)\frac{\alpha}{r^2} - (1+2\nu)(q-r)\\ &\quad + \frac{q}{r^2}\log\left[\frac{r}{q}\right][1-\nu-r^2(1+2\nu)] \qquad (27)\\ q^2 &= r^2-1\end{aligned}\right\} r \ge 1$$

$$\tan\alpha = 1/q$$

In particular, the stresses at the edge of contact take on a simple form, viz;

$$\left.\begin{aligned}\frac{3\pi\sigma_{rr}}{\beta p_0} &= \frac{2(2+\nu)}{\pi} + 1 - \nu \qquad (28)\\ \frac{3\pi\sigma_{rr}}{\beta p_0} &= \frac{2(1+2\nu)}{\pi} - 1 - \nu \qquad (29)\end{aligned}\right\} r = 1$$

while at the origin;

$$\frac{\sigma_{rr}}{\beta p_0} = \frac{\sigma_{\theta\theta}}{\beta p_0} = -\frac{(1+\nu)}{2} \qquad r = 0 \qquad (30)$$

Surface stresses for full stick, equations (1) and (24)–(27) are shown in Fig. 6.

For the case of full slip integrals, equations (18) may not be evaluated in closed form. However, it is useful to note that the derivative of $g(t)$ for this case is given by;

$$g'(t) = \frac{2}{\pi}\{K(t') - 2E(t')\} \qquad (31)$$

Furthermore, integrals (18) are proper and well behaved if $r > 1$, but singular if $r \le 1$, and hence appropriately evaluated by Gauss-Chebyshev quadrature.

Surprisingly, it turns out to be possible to express some of the surface stresses for the partial slip case in closed, albeit lengthy, form. Owing to their complexity, we quote values of $I(r)$ and dI/dr for substitution into equations (17). Within the stick zone

$$\left.\begin{aligned}\frac{3\pi I}{2\beta p_0} &= \frac{1-p^3}{2} + Mr^3 \qquad (32)\\ \frac{1}{\beta p_0}\frac{dI}{dr} &= pr + \frac{4}{\pi}Mr^2 \qquad (33)\end{aligned}\right\} 0 \le r \le c$$

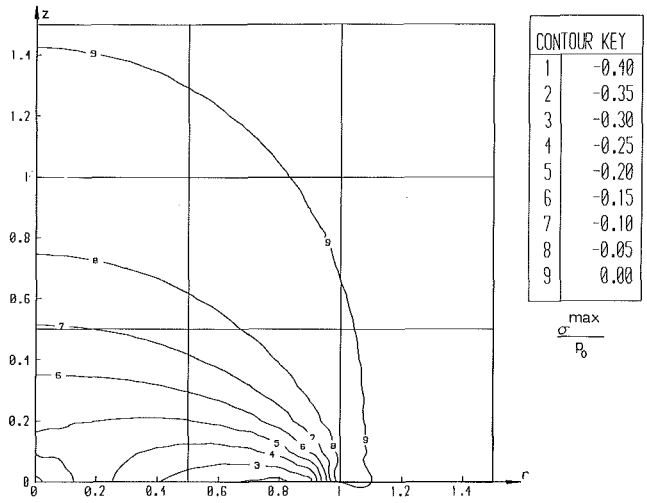


Fig. 5(a) More compliant surface

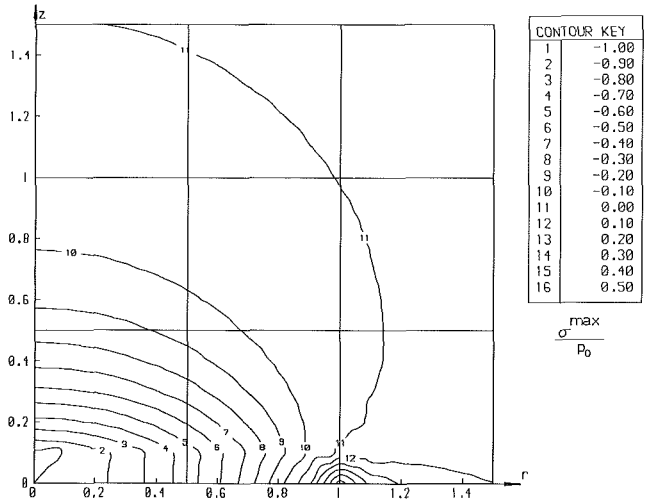


Fig. 5(b) Less compliant surface

Fig. 5 Contours of more positive principal stress in $r-z$ plane, for partial slip case, $f = 0.4$, $c = 0.8$

where $M = \dfrac{1+c^2}{2c^2}Q_0(c) - \dfrac{1}{2c} - \dfrac{E(c')Q_0(c)}{c^2K(c')}$

and in particular, at the origin, the same stresses found under full stick conditions (equation (30)) obtain. Within the slip annulus:

$$\frac{3\pi I}{2p_0} = \beta\left[\lambda - p^2\tan^{-1}\left\{\frac{pc}{v}\right\}\right] + 3f\int_c^r \frac{t^2}{\sqrt{r^2-t^2}}\left\{K(t') - E(t')\right\}dt \qquad (34)$$

$$c \le r \le 1$$

$$\frac{\pi}{2p_0}\frac{dI}{dr} = \beta\left[pr\tan^{-1}\left\{\frac{pc}{v}\right\} + rvQ_0(c) + 2r(r-v)M\right] + fr\int_c^r \frac{K(t') - 2E(t')}{\sqrt{r^2-t^2}}\,dt \qquad (35)$$

$$c \le r \le 1$$

Downloaded 03 May 2010 to 171.66.16.27. Redistribution subject to ASME license or copyright; see http://www.asme.org/terms/Terms_Use.cfm

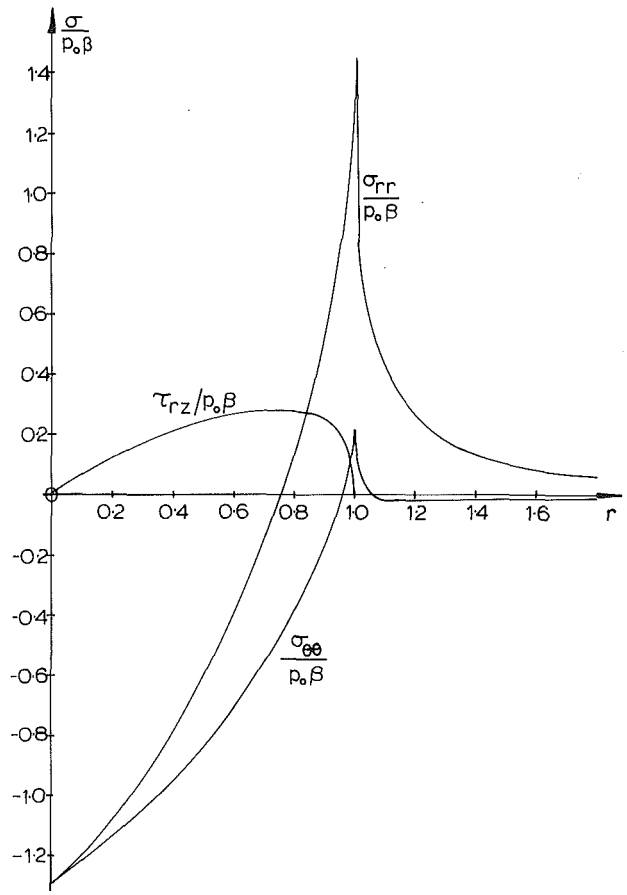


Fig. 6 Surface stresses due to shear tractions under conditions of full-stick

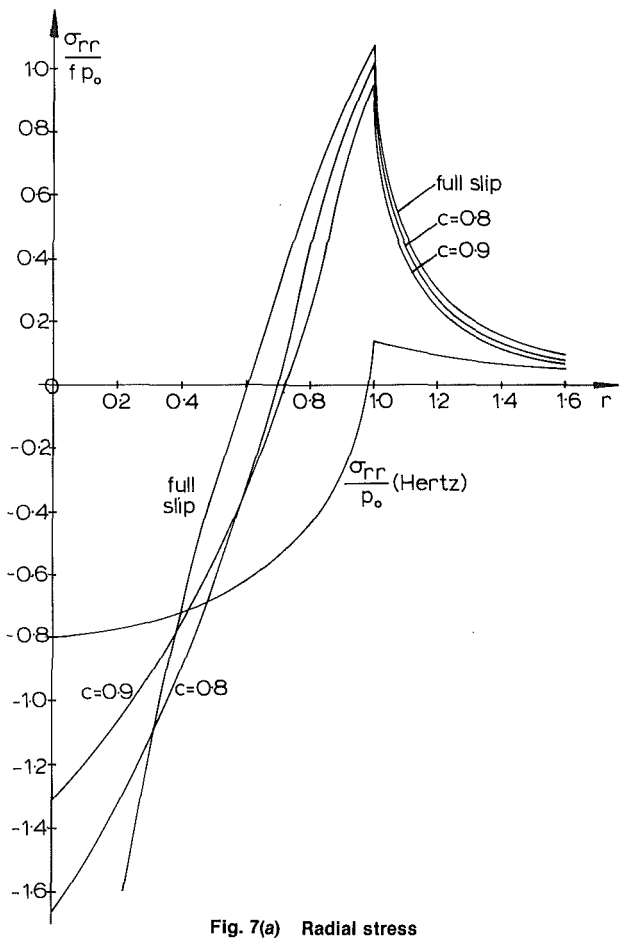


Fig. 7(*a*) Radial stress

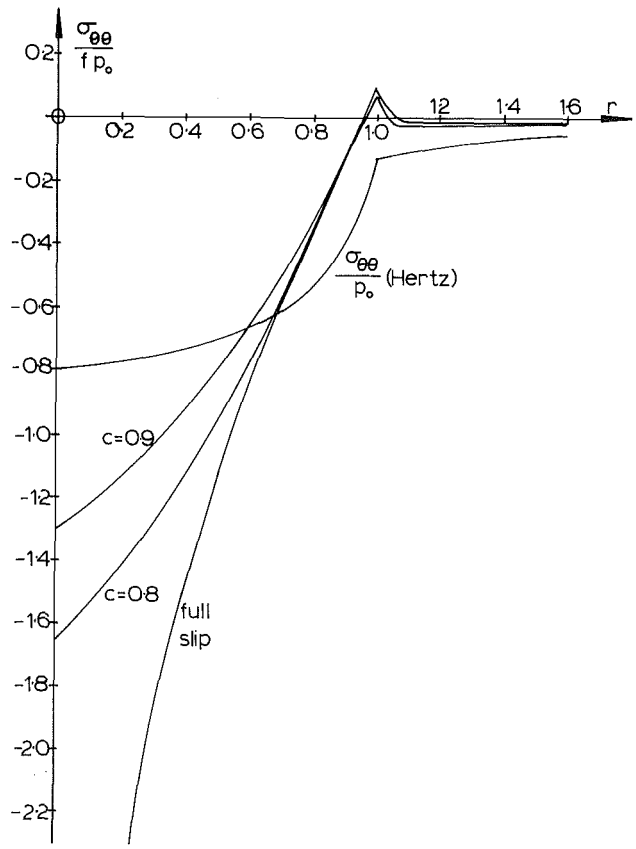


Fig. 7(*b*) Circumferential stress, less compliant body shown

Fig. 7 Surface stresses under partial and full slip conditions

where $\lambda=\theta+M.\,(2r^3+v^3-3vr^2-\frac{v}{2}\,(3-c^2-2r^2)Q_0\,(c)-\frac{vc}{2}$

$$v^2=r^2-c^2$$

$$\sin\theta=c/r$$

and it may be noted that normalization may be made entirely with respect to β or f by making use of equation (7). Lastly, exterior to the contact we have;

$$\frac{3\pi I}{2p_0}=\beta\left[\lambda-q^3Q_0\left\{\frac{cq}{v}\right\}\right]$$

$$+3f\int_c^1\frac{t^2}{\sqrt{r^2-t^2}}\left\{K(t')-E(t')\right\}dt \qquad r>1$$

$$\frac{\pi}{2p_0}\,\frac{dI}{dr}=\beta\left[-\frac{c}{3rv}+M\left(2r^2-\frac{r^3}{v}-vr\right)\right.$$

$$-\frac{Q_0\,(c)}{6}\left\{\frac{r}{v}(3-c^2-2r^2)-4rv\right\}-$$

$$-\frac{rc}{6v}-qrQ_0\left\{\frac{cq}{v}\right\}-\frac{cq^2}{3rv}+ \qquad (36)$$

$$+fr\left[\frac{c}{v}\left\{K(c')-E(c')\right\}\right.$$

$$\left.+\int_c^1\frac{K(t')-2E(t')}{\sqrt{r^2-t^2}}\,dt\right]$$

$$r>1$$

Downloaded 03 May 2010 to 171.66.16.27. Redistribution subject to ASME license or copyright; see http://www.asme.org/terms/Terms_Use.cfm

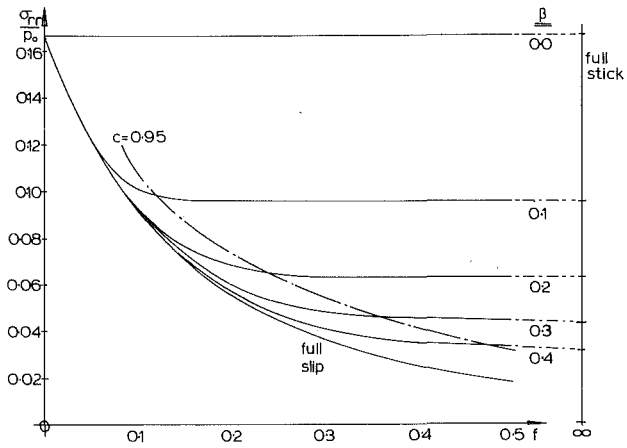


Fig. 8 Maximum radial stress due to both Hertzian and frictional loads, in more compliant body; $\nu = 0.25$

Surface direct stresses under full and partial slip conditions, together with the corresponding Hertzian values, are shown in Fig. 7. It is apparent that the circumferential stress, Fig. 7(*b*), which is of significance in understanding the radial cracks appearing in rock indentation tests, is only marginally influenced at the periphery of contact, although significant additional compression arises near the center, in the less compliant body. Turning to the radial stress, Fig. 7(*a*) shows that the effect of surface shear is significant both at the edge of contact, where the radial tension is augmented, and at the center, where significant additional compression arises. Again the figure relates to the less compliant body, and it may be noted that in the *more* compliant mating body a significant tension might arise near the center of contact.

Summary

The entire stress field arising when two spheres having dissimilar constants are pressed together, is found. Simplified formulae relating to the limiting cases of stick everywhere ($f \to \infty$) and slip everywhere ($f \to 0$, but remaining finite) are derived, and particular attention is focused on the surface, where more easily managed expressions obtain. It has been shown that the effect of friction is most significant near the surface, and near the contact disk, which might be expected since the traction field is self-equilibrating, and therefore has no far-field resultant. However, a thorough quantitative understanding of the stresses thought to be responsible for the nucleation and propagation of surface flaws is essential, as was demonstrated by Johnson et al. (1983). Their model successfully explains the experimental observation that cone cracks originate outside the contact disk, but appeals to the asymptotic solutions of full-slip and full stick. We are now in a position to derive the maximum surface radial stress under partial slip conditions, Fig. 8, where $\nu = 0.25$. Comparison with Fig. 3 of Johnson et al. shows that their estimated curve was well-judged.

Acknowledgment

The authors wish to thank Alison Dygnas for her help in typing this paper.

References

Barber, J. R., 1983, "The Solution of Elasticity Problems for the Half-Space by the Method of Green and Collins," *Applied Scientific Research*, Vol. 40, pp. 135–157.

Frank, F. C., and Lawn, B. R., 1967, "On the Theory of Hertzian Fracture," *Proc. Roy. Soc. London*, Vol. A.299, pp. 291–306.

Goodman, L. E., 1962, "Contact Stress Analysis of Rough Spheres," ASME JOURNAL OF APPLIED MECHANICS, Vol. 84, pp. 515–522.

Green, A. E., and Zerna, W., 1968, *Theoretical Elasticity*, 2nd Ed., O.U.P.

Huber, M. T., 1904, "Zur Theorie der Beruhrung Fester Elasticher Korper," *Ann. der Phys.*, Vol. 14, pp. 153–163.

Johnson, K. L., O'Connor, J. J., and Woodward, A. C., 1973, "The Effect of Indentor Elasticity on the Hertzian Fracture of Brittle Materials," *Proc. Roy. Socl. Lond.*, Vol. A.334, pp. 95–117.

Johnson, K. L., 1985, *Contact Mechanics*, Cambridge University Press.

Lawn, B. R., and Wilshaw, T. R., 1975, *Fracture of Brittle Solids*, Cambridge University Press, pp. 62–64.

Sackfield, A., and Hills, D. A., 1983, "A Note on the Hertz Contact Problem: A Correlation of Standard Formulae," *Jnl. Strain Anal.*, Vol. 18, pp. 195–197.

Spence, D. A., 1968, "Self-Similar Solutions to Adhesive Contact Problems with Incremental Loading," *Proc. Roy. Soc.*, Vol. A305, pp. 55–80.

Spence, D. A., 1973, "An Eigenvalue Problem for Elastic Contact with Finite Friction," *Proc. Camb. Phil. Soc.*, Vol. 73, pp. 249–268.

Spence, D. A., 1975, "The Hertz Contact Problem with Finite Elasticity," *Jnl. Elasticity*, Vol. 5, pp. 297–319.

APPENDIX A

$$\frac{\psi_r}{r} = -\int_0^1 \frac{g(t)\{\rho\sin\alpha + z\sin(\alpha/2) + t\cos(\alpha/2)\}dt}{\rho\{(\rho\cos(\alpha/2)+z)^2 + (\rho\sin(\alpha/2)+t)^2\}}$$

$$\psi_{zz} = \int_0^1 \frac{g(t)\{z\sin(3\alpha/2) - t\cos(3\alpha/2)\}dt}{\rho^3}$$

$$\frac{\psi_{rz}}{r} = \int_0^1 \frac{g(t)\sin(3\alpha/2)dt}{\rho^3}$$

$$\psi_{zzr} = -3r\int_0^1 \frac{g(t)\{z\sin(5\alpha/2) - t\cos(5\alpha/2)\}dt}{\rho^5}$$

$$\psi_{zzz} = -\int_0^1 \frac{g(t)\{(2z^2 - 2t^2 - r^2)\sin(5\alpha/2) - 4zt\cos(5\alpha/2)\}dt}{\rho^5}$$

where

$$\left.\begin{aligned} \rho^2\cos\alpha &= r^2 + z^2 - t^2 \\ \rho^2\sin\alpha &= 2zt \end{aligned}\right\} \quad \begin{aligned} &\rho > 0 \\ &0 < \alpha < \pi \end{aligned}$$

and

$$\sigma_{rr} + \sigma_{\theta\theta} + \sigma_{zz} = -2(1+\nu)\psi_{zz}$$

$$\psi_{rr} = -\frac{\psi_r}{r} - \psi_{zz}$$

Downloaded 03 May 2010 to 171.66.16.27. Redistribution subject to ASME license or copyright; see http://www.asme.org/terms/Terms_Use.cfm

A Rate-Independent Constitutive Theory for Finite Inelastic Deformation

M. M. Carroll
Department of Mechanical Engineering,
University of California,
Berkeley, CA 94720
Fellow ASME

A rate-independent constitutive theory for finite inelastic deformation is formulated in terms of the symmetric Piola-Kirchhoff stress, the Lagrangian strain, and a kinematic tensor which describes inelastic or microstructural effects. Assumptions of (a) *continuity in the transition from loading to neutral loading,* (b) *consistency, and* (c) *nonnegative work in closed cycles of deformation, lead to simplification of the theory. The response is described by two scalar functions—a stress potential and a loading function. The theory can describe isotropic or anisotropic response, and allows for hardening, softening, or ideal behavior. It may also be appropriate to describe the response of porous materials, such as metals, rocks and ceramics, and also the evolution of damage.*

1 Introduction

The development of constitutive theories to describe the mechanical response of inelastic solids undergoing finite deformations is a topic of considerable current interest and, indeed, of controversy. Here we present such a theory, which is properly invariant, which can describe both isotropic and anisotropic response, which is stable in the sense that the external work needed to carry a body through any closed cycle of deformation is nonnegative, and which has the additional virtue that the constitutive description may be relatively simple.

One approach to the description of finite strain elastic-plastic response has been developed in a series of papers by Naghdi and coworkers. These include the initial formulation of the theory by Green and Naghdi (1965, 1966) and the strain space formulation of the theory, the introduction of the above-mentioned work assumption, and an investigation of its consequences by Naghdi and Trapp (1975a, b). These developments and some additional results, including a detailed treatment of hardening, softening, and ideal behavior, are summarized in a recent paper by Casey and Naghdi (1984).

The development of the present theory closely parallels that presented in this latter paper. The primitive variables here are the symmetric Piola-Kirchhoff stress tensor $\mathbf{S}$, the Lagrangian strain tensor $\mathbf{E}$ and a symmetric second order tensor $\mathbf{K}$. This tensor has the same invariance properties as $\mathbf{E}$ but it is otherwise left undefined. The starting point of the constitutive theory is the statement of a stress response equation, a loading and yield criterion, and an evolution equation for $\mathbf{K}$, and these involve three response functions; one scalar, one second order tensor, and one fourth order tensor. We show that the assumption of continuity of the evolution equation in the transition from loading to neutral loading, the consistency condition, and the work assumption, lead to a simplification of the theory to the point where the response is characterized by two scalar response functions, namely, a stress potential $\psi(\mathbf{E}, \mathbf{K})$ and a loading function $g(\mathbf{E}, \mathbf{K})$.

This simplification of the constitutive theory is described in Section 2. The mathematical structure of the present theory is a special case of that presented by Casey and Naghdi (1984), obtained by reducing the set of independent variables $\mathfrak{U} = (\mathbf{E}, \mathbf{E}^p, \kappa)$ to the set $(\mathbf{E}, \mathbf{K})$, i.e., by omitting dependence on the hardening parameter κ and by not identifying $\mathbf{K}$ as the plastic strain. Thus, all of the previous results are already available to us. The reduction of the constitutive description to the specification of two scalar functions ψ and g requires that a certain linear transformation involving a fourth order tensor $\mathfrak{D}$ be invertible. The key point in effecting this reduction is the omission of κ from the stress response law. Thus, a more general theory to describe strain hardening or work hardening may be obtained by specifying a stress potential $\psi(\mathbf{E}, \mathbf{K})$ and a loading function $g(\mathbf{E}, \mathbf{K}, \kappa)$, where κ is defined in terms of the prior history.

The situation that arises when $\mathfrak{D}$ is singular is discussed in Section 3. This occurs, for example, as a consequence of the assumption that the inelastic deformation preserves volume.

An interesting aspect of the present theory is that the work assumption gives rise to a normality condition, even though plastic strain or strain rate tensors are not defined. The inelastic contribution to the stress rate $\dot{\mathbf{S}}$ is directed parallel to the inward normal to the strain space yield surface or, equivalently, the inelastic contribution to the strain rate $\dot{\mathbf{E}}$ is directed parallel to the outward normal to the stress space yield surface. In general, neither of these contributions is the time derivative of a tensor function. Inversion of the normality condition gives a condition on $\dot{\mathbf{K}}$ but, in general, this is not a normality condition.

The relationship of the present theory to that described by

Contributed by the Applied Mechanics Division for publication in the JOURNAL OF APPLIED MECHANICS.
Discussion on this paper should be addressed to the Editorial Department, ASME, United Engineering Center, 345 East 47th Street, New York, N.Y. 10017, and will be accepted until two months after final publication of the paper itself in the JOURNAL OF APPLIED MECHANICS. Manuscript received by ASME Applied Mechanics Division, December 18, 1985.

Copyright © 1987 by ASME
Downloaded 03 May 2010 to 171.66.16.27. Redistribution subject to ASME license or copyright; see http://www.asme.org/terms/Terms_Use.cfm

Casey and Naghdi (1984), as well as the work assumption of Naghdi and Trapp (1975b), *vis a vis* Il'Yushin's (1961) postulate and the investigation of its consequences by Hill and Rice (1973), are discussed in Section 4.

The present paper treats the general structure of the theory, but specific constitutive response functions to describe particular types of material behavior are not presented. The original motivation for this work was the development of a constitutive theory to describe the response of porous rocks. However, the theory should have much wider application to metals, ceramics, granular materials, materials undergoing damage, etc. Each application will, of course, require an identification of the tensor $\mathbf{K}$. Our main result is that assuming that the external work in closed strain cycles must be nonnegative reduces the constitutive description in such theories to the specification of a stress potential and a loading function.

We use script capitals to denote fourth order tensors and boldface capitals to denote symmetric second order tensors. The fourth order tensors are assumed to have symmetries

$$\mathfrak{D}_{ijk\ell}=\mathfrak{D}_{jik\ell} \text{ and } \mathfrak{D}_{ijk\ell}=\mathfrak{D}_{k\ell ij}. \tag{1.1}$$

We also use the notation $\mathbf{V}\cdot\mathbf{W}$ for the scalar $V_{ij}W_{ij}$, $\mathfrak{D}\mathbf{V}$ for the second order tensor with components $\mathfrak{D}_{ijk\ell}V_{k\ell}$, and $\mathbf{V}\otimes\mathbf{W}$ and $\mathfrak{D}\mathfrak{G}$ for fourth order tensors with components $V_{ij}W_{k\ell}$ and $\mathfrak{D}_{ijk\ell}\mathfrak{G}_{k\ell mn}$, respectively.

2 Constitutive Equations

Our development of the constitutive equations for finite inelastic deformation parallels that of Naghdi and coworkers for elastic-plastic materials, as presented by Casey and Naghdi (1984), but with the modifications described in the Introduction. We begin with a stress response equation, a yield condition, and an evolution equation.

The Stress Response Law. We assume that the symmetric Piola-Kirchhoff stress tensor $\mathbf{S}$ is a function of the Lagrangian strain tensor $\mathbf{E}$ and a tensor $\mathbf{K}$ which, in some way, describes the inelastic state of the material, thus[1]

$$\mathbf{S}=\mathbf{S}(\mathbf{E},\mathbf{K}). \tag{2.1}$$

We leave the exact nature of $\mathbf{K}$ unspecified, except that it is a symmetric second order tensor with the same invariance property as $\mathbf{E}$, i.e., it is unaltered if the body is at any time subjected to a rigid body translation and rotation. The response equation (2.1) is then properly invariant. Equation (2.1) may describe isotropic or anisotropic response, depending on the form of the response function. We also assume that equation (2.1) can be inverted[2] to give a strain response law

$$\mathbf{E}=\mathbf{E}(\mathbf{S},\mathbf{K}). \tag{2.2}$$

The Yield Criterion. We assume that there is a loading function g which is nonpositive for all admissible states

$$g(\mathbf{E},\mathbf{K})\le 0, \tag{2.3}$$

and which, for each value $\mathbf{K}$, defines an open region e: $g<0$ of six-dimensional strain space (called the elastic region), with boundary ∂e: $g=0$ (called the yield surface). States $(\mathbf{E},\mathbf{K})$ with $g<0$ are elastic. States with $g=0$ are plastic, and the function $\hat{g}$, defined by

$$\hat{g}=\frac{\partial g}{\partial \mathbf{E}}\cdot\dot{\mathbf{E}}, \tag{2.4}$$

affords definition of unloading ($\hat{g}<0$), neutral loading ($\hat{g}=0$), and loading ($\hat{g}>0$) from a plastic state, at a regular point of the yield surface. It is evident from equation (2.4) that these various conditions prevail depending on whether the strain rate $\dot{\mathbf{E}}$ is directed into, tangent to, or out of the yield surface $g=0$.

Use of equations (2.2) and (2.3) leads to the definition of a nonpositive loading function f, so that

$$f(\mathbf{S},\mathbf{K})\le 0; \quad f(\mathbf{S},\mathbf{K})=g(\mathbf{E}(\mathbf{S},\mathbf{K}),\mathbf{K}). \tag{2.5}$$

This defines an elastic region e: $f<0$ and a yield surface ∂e: $f=0$ in stress space. The sign of the function $\hat{f}$, defined by

$$\hat{f}=\frac{\partial f}{\partial \mathbf{S}}\cdot\dot{\mathbf{S}}, \tag{2.6}$$

establishes the orientation of the stress rate $\dot{\mathbf{S}}$ relative to the tangent plane to the yield surface in stress space. It is important to bear in mind, however, that the definitions of unloading, neutral loading, and loading have been established in terms of $\hat{g}$. During loading ($g=0$, $\hat{g}>0$), the function $\hat{f}$ may be positive (if the material is hardening), zero (if the material is behaving ideally), or negative (if the material is softening), so that these three conditions are characterized by $\hat{f}/\hat{g}>0$, $\hat{f}/\hat{g}=0$, and $\hat{f}/\hat{g}<0$, respectively. This implies some ambiguity in a stress space formation; for instance, a situation with $f=0$, $\hat{f}<0$ may represent unloading, or it may represent loading while the material is softening.

The Evolution Equation. We assume that the evolution of the tensor quantity $\mathbf{K}$ is described by

$$\dot{\mathbf{K}}=\begin{cases}\mathfrak{A}(\mathbf{E},\mathbf{K})\dot{\mathbf{E}} & (g=0,\ \hat{g}>0)\\ \mathbf{0} & \text{(otherwise)},\end{cases} \tag{2.7}$$

where $\mathfrak{A}$ is a fourth order tensor. Thus, the tensor $\mathbf{K}$ changes only during loading, so that $\mathbf{K}$ provides a measure of the inelastic state.

At this stage of development, the problem of describing realistic inelastic response appears to be a formidable one, requiring specification of a scalar function g, a second order tensor function $\mathbf{S}$, and a fourth order tensor function $\mathfrak{A}$.

Continuity. We assume that $\dot{\mathbf{K}}$ is continuous in the transition from loading to neutral loading. Equation $(2.7)_1$ must hold at any point on the yield surface and for all $\dot{\mathbf{E}}$ satisfying $\hat{g}>0$. Tending to the limit as $\dot{\mathbf{E}}$ approaches the tangent plane, i.e., as we approach neutral loading ($\hat{g}=0$), we conclude that $\mathfrak{A}\dot{\mathbf{E}}=\mathbf{0}$ for all $\dot{\mathbf{E}}$ for which $\hat{g}=0$, i.e., for which $\dot{\mathbf{E}}$ is orthogonal to the normal $\partial g/\partial \mathbf{E}$[3]. It follows that the tensor $\mathfrak{A}$ has the form

$$\mathfrak{A}=\mathbf{A}\otimes\frac{\partial g}{\partial \mathbf{E}}. \tag{2.8}$$

(The symmetric second order tensor $\mathbf{A}(\mathbf{E},\mathbf{K})$ enters as a Lagrange multiplier in the derivation of equation (2.8) (see Green and Naghdi, 1965). Substituting from equation (2.8) in (2.7) leads to the reduced evolution equation

$$\dot{\mathbf{K}}=\begin{cases}\hat{g}\mathbf{A} & (g=0,\ \hat{g}\ge 0)\\ \mathbf{0} & \text{(otherwise)}.\end{cases} \tag{2.9}$$

Consistency. In an elastic state ($g<0$) the function $\dot{g}$ may be positive, negative, or zero. In a plastic state ($g=0$), the inequality (2.3) requires that $\dot{g}$ be negative (unloading) or zero (neutral loading or loading). This leads to the consistency condition

[1] For simplicity sake, we use the same symbol for functions and their values.

[2] Actually, we need only assume this invertibility for the range defined by the inequality (2.3).

[3] It is useful to consider symmetric second order tensors as vectors in a six dimensional vector space, with the trace operator defining the inner product.

Downloaded 03 May 2010 to 171.66.16.27. Redistribution subject to ASME license or copyright; see http://www.asme.org/terms/Terms_Use.cfm

$$\hat{g}+\frac{\partial g}{\partial \mathbf{K}}\cdot\dot{\mathbf{K}}=0 \quad (g=0,\ \hat{g}\geq 0) \tag{2.10}$$

or, in view of equation (2.9),

$$1+\frac{\partial g}{\partial \mathbf{K}}\cdot\mathbf{A}=0 \quad (g=0). \tag{2.11}$$

The corresponding condition on the stress space loading function is, from equation $(2.5)_2$,

$$\hat{f}/\hat{g}+\frac{\partial f}{\partial \mathbf{K}}\cdot\mathbf{A}=0 \quad (g=0). \tag{2.12}$$

The Work Assumption. The work assumption of Naghdi and Trapp (1975b) is that the external work in any homogeneous cycle of deformation is nonnegative. This leads to the condition[4]

$$\int_{t_1}^{t_2}\mathbf{S}\cdot\dot{\mathbf{E}}dt\geq 0 \tag{2.13}$$

for any such cycle occurring in the time interval $[t_1, t_2]$. We adopt this assumption and we set down two important consequences.

(*a*) *The Stress Potential.* Imposing the condition (2.13) for cycles of elastic deformation establishes the existence of a stress potential $\psi(\mathbf{E},\mathbf{K})$, so that

$$\mathbf{S}=\partial\psi/\partial\mathbf{E}. \tag{2.14}$$

A Legendre transformation $\psi+\Psi=\mathbf{E}\cdot\mathbf{S}$ leads to the strain potential $\Psi(\mathbf{S},\mathbf{K})$, with

$$\mathbf{E}=\partial\Psi/\partial\mathbf{S}. \tag{2.15}$$

Before proceeding to examine the second consequence of the work assumption, we compute the stress rate $\dot{\mathbf{S}}$ and the strain rate $\dot{\mathbf{E}}$ from equations (2.1) and (2.2), or equations (2.14) and (2.15), as

$$\dot{\mathbf{S}}=\mathcal{C}\dot{\mathbf{E}}+\mathcal{D}\dot{\mathbf{K}}; \quad \dot{\mathbf{E}}=\mathcal{C}^{-1}\dot{\mathbf{S}}+\mathcal{E}\dot{\mathbf{K}}, \tag{2.16}$$

where the fourth order tensors $\mathcal{C}$, $\mathcal{D}$, $\mathcal{C}^{-1}$, and $\mathcal{E}$ are defined by

$$\mathcal{C}=\frac{\partial\mathbf{S}}{\partial\mathbf{E}}=\frac{\partial^2\psi}{\partial\mathbf{E}\partial\mathbf{E}}; \quad \mathcal{D}=\frac{\partial\mathbf{S}}{\partial\mathbf{K}}=\frac{\partial^2\psi}{\partial\mathbf{E}\partial\mathbf{K}} \tag{2.17}$$

and

$$\mathcal{C}^{-1}=\frac{\partial\mathbf{E}}{\partial\mathbf{S}}=\frac{\partial^2\Psi}{\partial\mathbf{S}\partial\mathbf{S}}; \quad \mathcal{E}=\frac{\partial\mathbf{E}}{\partial\mathbf{K}}=\frac{\partial^2\Psi}{\partial\mathbf{S}\partial\mathbf{K}}. \tag{2.18}$$

Clearly, $\mathcal{C}(\mathbf{E},\mathbf{K})$ is the instantaneous elastic tangent modulus tensor and $\mathcal{C}^{-1}(\mathbf{S},\mathbf{K})$ is the corresponding compliance tensor. The tensor $\mathcal{D}\dot{\mathbf{K}}$ represents the inelastic contribution to the stress rate and $\mathcal{E}\dot{\mathbf{K}}$ represents the inelastic contribution to the strain rate. It follows from equations (2.17) and (2.18) that the tensors $\mathcal{C}$, $\mathcal{C}^{-1}$, $\mathcal{D}$, and $\mathcal{E}$ have the symmetries (1.1). By writing equation (2.1) in the form

$$\mathbf{S}=\mathbf{S}(\mathbf{E}(\mathbf{S},\mathbf{K}),\mathbf{K}) \tag{2.19}$$

and taking the partial derivative with respect to $\mathbf{K}$, we obtain

$$\mathcal{O}=\mathcal{C}\mathcal{E}+\mathcal{D}, \tag{2.20}$$

where $\mathcal{O}$ is the null fourth order tensor. This gives

$$\mathcal{D}\dot{\mathbf{K}}=-\mathcal{C}(\mathcal{E}\dot{\mathbf{K}}). \tag{2.21}$$

Also, the chain rule for partial differentiation, and the fact that $\mathcal{C}$ is symmetric, give

$$\partial g/\partial\mathbf{E}=\mathcal{C}\frac{\partial f}{\partial\mathbf{S}}. \tag{2.22}$$

Thus, the inelastic contributions to the stress rate and the strain rate are related through the linear transformation $-\mathcal{C}$, and the normals to the yield surfaces in strain space and stress space are related through $\mathcal{C}$.

(*b*) *Normality.* Naghdi and Trapp (1975b), by considering a special sequence of elastic-plastic cycles of deformation, obtained normality conditions from the work inequality (2.13). In the present instance, this analysis gives

$$\dot{\mathbf{E}}\cdot(\mathcal{D}\dot{\mathbf{K}})\leq 0 \quad (g=0,\ \hat{g}>0). \tag{2.23}$$

This condition must be met for all strain rates for which $\hat{g}>0$, and this leads to the normality condition

$$\mathcal{D}\dot{\mathbf{K}}=-\gamma\frac{\partial g}{\partial\mathbf{E}} \quad (g=0, \quad \hat{g}\geq 0), \tag{2.24}$$

where γ is some nonnegative scalar. The condition (2.24) is that *the inelastic contribution to the stress rate is directed parallel to the inward normal to the strain space yield surface* $g=0$. Equations (2.21), (2.22), and (2.24) give the equivalent normality condition

$$\mathcal{E}\dot{\mathbf{K}}=\gamma\frac{\partial f}{\partial\mathbf{S}} \quad (g=0, \quad \hat{g}\geq 0), \tag{2.25}$$

i.e., *the inelastic contribution to the strain rate is directed parallel to the outward normal to the stress space yield surface* $f=0$.

The Regular Case: $\det\mathcal{D}\neq 0$. We now assume that the fourth order tensor $\mathcal{D}$ is nonsingular ($\det\mathcal{D}\neq 0$). In view of equation (2.20), this implies that $\mathcal{E}$ is also nonsingular.

With this assumption, equations (2.24) and (2.25) can be inverted to give

$$\dot{\mathbf{K}}=-\gamma\mathcal{D}^{-1}\frac{\partial g}{\partial\mathbf{E}} \quad (g=0, \quad \hat{g}\geq 0) \tag{2.26}$$

and

$$\dot{\mathbf{K}}=\gamma\mathcal{E}^{-1}\frac{\partial f}{\partial\mathbf{S}} \quad (g=0, \quad \hat{g}\geq 0). \tag{2.27}$$

Substitution from equations (2.26) in the consistency condition (2.11), and use of equation $(2.9)_1$, gives

$$\hat{g}/\gamma=\frac{\partial g}{\partial\mathbf{K}}\cdot\mathcal{D}^{-1}\frac{\partial g}{\partial\mathbf{E}}, \tag{2.28}$$

and hence

$$\dot{\mathbf{K}}=\begin{cases}-\hat{g}\mathcal{D}^{-1}\dfrac{\partial g}{\partial\mathbf{E}}\Big/\dfrac{\partial g}{\partial\mathbf{K}}\cdot\mathcal{D}^{-1}\dfrac{\partial g}{\partial\mathbf{E}} & (g=0,\ \hat{g}\geq 0)\\ \mathbf{0} & \text{(otherwise).}\end{cases} \tag{2.29}$$

Similarly, equations (2.9), (2.12), and (2.27) lead to

$$\dot{\mathbf{K}}=\begin{cases}-\hat{f}\mathcal{E}^{-1}\dfrac{\partial f}{\partial\mathbf{S}}\Big/\dfrac{\partial f}{\partial\mathbf{K}}\cdot\mathcal{E}^{-1}\dfrac{\partial f}{\partial\mathbf{S}} & (g=0,\ \hat{g}>0;\ \ \hat{f}\neq 0)\\ \mathbf{0} & (g<0 \text{ or } g=0,\ \hat{g}\leq 0).\end{cases} \tag{2.30}$$

It is important to bear in mind that the stress-space form (2.30) is not valid when the material is behaving ideally.

The constitutive equations have now been reduced to the stress response equation (2.14) and the evolution equation (2.29), or to the strain response equation (2.15) and the evolution equation (2.30). The restrictions imposed by continuity,

[4]The condition (2.13) is derived from the condition of nonnegative external work by making use of the equation of motion, the condition that the deformation is homogeneous, and the fact that the kinetic energy returns to its initial value on completion of the closed cycle.

Downloaded 03 May 2010 to 171.66.16.27. Redistribution subject to ASME license or copyright; see http://www.asme.org/terms/Terms_Use.cfm

consistency, and the work assumption have simplified the description of inelastic response to the specification of two scalar functions ψ and g, or Ψ and f.

Generalization. The possibility of inverting the normality condition (2.24) to obtain the evolution equation (2.29) resulted from our not including dependence on a scalar hardening parameter κ in the stress response equation (2.1). This simplification is not lost if we include dependence on κ in the loading function and the evolution equation. Thus, if we specify $\psi(\mathbf{E},\mathbf{K})$ and $g(\mathbf{E},\mathbf{K},\kappa)\leq 0$, the constitutive response is described by equation (2.14) and a modified form of equation (2.29);

$$\dot{\mathbf{K}}=\begin{cases}-(\hat{g}+\dot{\kappa}\,\partial g/\partial\kappa)\mathfrak{D}^{-1}\dfrac{\partial g}{\partial \mathbf{E}}\Big/\dfrac{\partial g}{\partial \mathbf{K}}\bullet\mathfrak{D}^{-1}\dfrac{\partial g}{\partial \mathbf{E}} & (g=0,\ \hat{g}\geq 0)\\ \\ \mathbf{0} & (\text{otherwise}).\end{cases}\tag{2.31}$$

The corresponding description in the stress space formulation is furnished by equation (2.15) and

$$\dot{\mathbf{K}}=\begin{cases}-(\hat{f}+\dot{\kappa}\partial f/\partial\kappa)\mathfrak{E}^{-1}\dfrac{\partial f}{\partial \mathbf{S}}\Big/\dfrac{\partial f}{\partial \mathbf{K}}\bullet\mathfrak{E}^{-1}\dfrac{\partial f}{\partial \mathbf{S}} & (g=0,\quad \hat{g}>0;\ \hat{f}\neq 0)\\ \\ \mathbf{0} & (g<0 \text{ or } g=0,\ \hat{g}\leq 0).\end{cases}\tag{2.32}$$

The hardening parameter κ may be defined in terms of the prior history, for example, analogously to the plastic work ($\kappa=\int_o^t \mathbf{S}\bullet\dot{\mathbf{K}}dt$) or the equivalent plastic strain

$$\left(\kappa=\int_o^t\sqrt{\frac{2}{3}\dot{\mathbf{K}}\bullet\dot{\mathbf{K}}}dt\right).$$

Alternatively, the evolution of κ may be described by an equation

$$\dot{\kappa}=\begin{cases}\hat{g}\lambda(\mathbf{E},\mathbf{K},\kappa) & (g=0,\ \hat{g}\geq 0)\\ 0 & (\text{otherwise}),\end{cases}\tag{2.33}$$

in which case the description of the elastic-plastic response requires specification of three scalar functions ψ, g, and λ.

Hardening, Softening, and Ideal Behavior. Previous results on hardening, softening, and ideal behavior (Casey and Naghdi, 1981, 1984) are readily adapted to the present theory. As mentioned earlier, loading is defined by the strain space condition $g=0$, $\hat{g}>0$, and the material may be hardening, behaving ideally, or softening, depending on the sign of the function $\Phi=\hat{f}/\hat{g}$. It is obviously desirable to have an expression for Φ which does not depend on the rates $\dot{\mathbf{E}}$ and $\dot{\mathbf{S}}$. It is convenient to rewrite equations $(2.29)_1$ and $(2.30)_1$ as

$$\dot{\mathbf{K}}=-\hat{g}\zeta\mathfrak{D}^{-1}\frac{\partial g}{\partial \mathbf{E}};\quad 1/\zeta=\frac{\partial g}{\partial \mathbf{K}}\bullet\mathfrak{D}^{-1}\frac{\partial g}{\partial \mathbf{E}}\tag{2.34}$$

and

$$\dot{\mathbf{K}}=-\hat{f}\xi\mathfrak{E}^{-1}\frac{\partial f}{\partial \mathbf{S}};\quad 1/\xi=\frac{\partial f}{\partial \mathbf{K}}\bullet\mathfrak{E}^{-1}\frac{\partial f}{\partial \mathbf{S}}.\tag{2.35}$$

In view of equation (2.22), these two equations give

$$\Phi=-\xi/\zeta.\tag{2.36}$$

An alternative expression for Φ is obtained by substituting from equation $(2.16)_1$ in (2.6), to obtain

$$\hat{f}=\frac{\partial f}{\partial \mathbf{S}}\bullet(\mathcal{C}\dot{\mathbf{E}}+\mathfrak{D}\dot{\mathbf{K}}).\tag{2.37}$$

Use of equations (2.4), (2.22), and $(2.34)_1$ gives

$$\Phi=1-\zeta\frac{\partial g}{\partial \mathbf{E}}\bullet\frac{\partial f}{\partial \mathbf{S}}.\tag{2.38}$$

Equations (2.4) and $(2.16)_1$ give

$$\dot{\mathbf{S}}=\left(\mathcal{C}-\zeta\frac{\partial g}{\partial \mathbf{E}}\otimes\frac{\partial g}{\partial \mathbf{E}}\right)\dot{\mathbf{E}}\quad (g=0,\ g\geq 0).\tag{2.39}$$

In view of equation (2.22), this linear relationship may also be written as

$$\dot{\mathbf{S}}=\mathcal{K}\mathcal{C}\dot{\mathbf{E}};\quad \mathcal{K}=\mathcal{I}-\zeta\frac{\partial g}{\partial \mathbf{E}}\otimes\frac{\partial f}{\partial \mathbf{S}},\tag{2.40}$$

where $\mathcal{I}$ is the unit fourth order tensor (with appropriate symmetry). Because of the dyadic structure of the second term on the right in equation $(2.40)_2$ it is evident that this equation and equation (2.38) give

$$\det\,\mathcal{K}=\Phi.\tag{2.41}$$

Thus, the linear relationship between $\dot{\mathbf{S}}$ and $\dot{\mathbf{E}}$ during plastic deformation is invertible except when the material is behaving ideally ($\Phi=0$).

3 The Singular Case: $\det\mathfrak{D}=0$

The flow rules (2.29) and (2.30) were obtained from the normality conditions (2.24) and (2.25), and the consistency condition, by assuming that the tensor $\mathfrak{D}$ (and hence also $\mathfrak{E}$) is nonsingular. At first it may appear that this must be the case, since otherwise equation (2.16) admits the possibility of nonzero values of $\dot{\mathbf{K}}$ corresponding to $\dot{\mathbf{S}}=\mathbf{0}$ and $\dot{\mathbf{E}}=\mathbf{0}$. Inelastic change at constant stress and strain is not acceptable in a rate-independent and time-independent theory. However, this argument is spurious, since the evolution equation (2.9) does not admit such nonzero values of $\dot{\mathbf{K}}$. Thus, we must consider the possibility $\det\mathfrak{D}=0$. This singularity may be persistent, i.e., $\mathfrak{D}(\mathbf{E},\mathbf{K})$ may be singular for all $\mathbf{E}$ and $\mathbf{K}$, or it may only occur for special values of $\mathbf{E}$ and $\mathbf{K}$.

When $\mathfrak{D}$ is singular, solutions $\dot{\mathbf{K}}$ of equations (2.24) exist provided $\partial g/\partial\mathbf{E}$ is orthogonal to the null space of $\mathfrak{D}$, and these solutions are nonunique to within an arbitrary additive tensor in the null space of $\mathfrak{D}$. Thus

$$\frac{\partial g}{\partial \mathbf{E}}\bullet\mathbf{W}=0\ \text{ whenever }\ \mathfrak{D}\mathbf{W}=\mathbf{0}\tag{3.1}$$

and

$$\dot{\mathbf{K}}=\mathbf{V}_1+\mathbf{V};\ \ \mathfrak{D}\mathbf{V}=\mathbf{0},\tag{3.2}$$

where $\mathbf{V}_1$ is determinate and $\mathbf{V}$ is arbitrary subject to equation $(3.2)_2$. We observe, from equation $(3.1)_1$, that singularity of $\mathfrak{D}$ (and hence of $\mathfrak{E}$) imposes a condition on the loading function. For example, if $\mathfrak{D}$ has rank 5 and if $\mathbf{W}$ is a constant tensor, then the yield surface in strain space is always a hypercylinder with generators parallel to $\mathbf{W}$. The indeterminacy in $\dot{\mathbf{K}}$ does not affect the stress and strain rates $\dot{\mathbf{S}}$ and $\dot{\mathbf{E}}$ (see equations (2.16) and (2.20)) and, since γ is evaluated from the consisten-

Downloaded 03 May 2010 to 171.66.16.27. Redistribution subject to ASME license or copyright; see http://www.asme.org/terms/Terms_Use.cfm

cy condition, it does not affect the evolution of the yield surface. Thus, we might make $\dot{\mathbf{K}}$ determinate by requiring that it be orthogonal to the null space of $\mathfrak{D}$, so that

$$\dot{\mathbf{K}}\cdot\mathbf{V}=0 \text{ whenever } \mathfrak{D}\mathbf{V}=\mathbf{0}. \tag{3.3}$$

An interesting example of a persistent singularity is the common assumption that the inelastic deformation preserves volume. The Jacobian $J=\det\mathbf{F}=\sqrt{\det\mathbf{C}}$ provides a measure of local volume change in a finite deformation. Here $\mathbf{F}$ is the deformation gradient tensor, and the deformation tensor $\mathbf{C}$ is related to the Lagrangian strain tensor $\mathbf{E}$ through

$$\mathbf{C}=\mathbf{1}+2\mathbf{E}=\mathbf{C}(\mathbf{S},\mathbf{K}), \tag{3.4}$$

where $\mathbf{1}$ is the unit tensor. The condition that there be no inelastic contribution to the rate of change of volume becomes

$$\frac{\partial}{\partial\mathbf{K}}(\det\mathbf{C})=\mathbf{0} \tag{3.5}$$

which, with equations $(2.18)_2$ and (3.4), leads to

$$2(\det\mathbf{C})\mathcal{E}\mathbf{C}^{-1}=\mathbf{0}. \tag{3.6}$$

Thus, $\mathcal{E}$ has a null tensor $\mathbf{C}^{-1}$, and so the assumption of inelastic incompressibility introduces a persistent singularity in the theory. In view of equation (3.6), the existence of solutions $\dot{\mathbf{K}}$ of the normality equation (2.25) requires that

$$\frac{\partial f}{\partial\mathbf{S}}\cdot\mathbf{C}^{-1}=0. \tag{3.7}$$

We recall that

$$\mathbf{S}=J\mathbf{F}^{-1}\mathbf{T}(\mathbf{F}^{-1})^T=J\mathbf{F}^{-1}(-p\mathbf{I}+\mathbf{T}')(\mathbf{F}^{-1})^T=-pJ\mathbf{C}^{-1}+\mathbf{S}', \tag{3.8}$$

where $\mathbf{T}$ is the Cauchy stress, $\mathbf{T}'$ is its deviatoric part and p is the pressure. Thus, the hydrostatic part of $\mathbf{S}$ is directed parallel to $\mathbf{C}^{-1}$, and the condition (3.7) is simply that this must lie in the tangent plane to the yield surface $f=0$ in stress space.

The purpose of this section is not to carry out a thorough investigation of constraints in finite strain plasticity. Rather, we wish to point out that while the assumption $\det\mathfrak{D}\neq 0$ is not always a valid one, the theory can be adapted to cope with exceptions. Similar remarks apply to other constraints such as overall incompressibility ($\det\mathbf{C}=1$).

We remark that, while the choice of variables $\mathbf{S}$ and $\mathbf{E}$ leads to a simple definition of a properly invariant stress rate ($\dot{\mathbf{S}}$) and facilitates the treatment of anisotropic response, it leads to a rather cumbersome treatment of constraints such as incompressibility. For example, the direction of hydrostatic loading in $\mathbf{S}$-space is the varying direction of $\mathbf{C}^{-1}$, while the corresponding direction in $\mathbf{T}$-space is that of the constant tensor $\mathbf{1}$.

4 Comparison with Other Theories

We now describe the relationship between the theory developed in the previous Sections and the elastic-plastic theory developed by Naghdi and coworkers in the papers cited in the Introduction. We also discuss the definition of plastic strain.

Comparison With the Elastic-Plastic Theory. In terms of its mathematical structure, the present theory is a special case of the earlier-plastic theory which is summarized by Casey and Naghdi (1984). Indeed, the two developments are identical up through equation (2.25), if we regard $\mathbf{S}$ and $\mathbf{E}$ as 6-vectors and $\mathbf{K}$ as the 7-vector $(\mathbf{E}^p,\kappa)$. The tensors $\mathcal{C}$ and $\mathcal{C}^{-1}$ are then represented by 6×6 matrices and $\mathfrak{D}$ and $\mathcal{E}$ by 6×7 matrices.

If we identify $\mathbf{K}$ with plastic strain $\mathbf{E}^p$ then our theory becomes an elastic-plastic theory in which the hardening parameter does not affect the stress response. However, the fact that $\mathbf{K}$ is not necessarily identified as plastic strain broadens the range of potential applicability of the theory. In different applications of the theory $\mathbf{K}$ might be a damage tensor, a fabric tensor, a crack density tensor, and so on.

We remark that the normality condition analogous to equation (2.24), i.e., equation (4.10) of Casey and Naghdi (1984), can be solved for $\dot{\mathbf{E}}^p$ if the tensor $\partial\mathbf{S}/\partial\mathbf{E}^p$ is nonsingular. This equation may be written as

$$\frac{\partial\mathbf{S}}{\partial\mathbf{E}^p}\dot{\mathbf{E}}^p+\frac{\partial\mathbf{S}}{\partial\kappa}\dot{\kappa}=-\gamma\frac{\partial g}{\partial\mathbf{E}}. \tag{4.1}$$

if $\det(\partial\mathbf{S}/\partial\mathbf{E}^p)\neq 0$, this leads to

$$\dot{\mathbf{E}}^p=-\left(\frac{\partial\mathbf{S}}{\partial\mathbf{E}^p}\right)^{-1}\cdot\left(\gamma\frac{\partial g}{\partial\mathbf{E}}+\dot{\kappa}\frac{\partial\mathbf{S}}{\partial\kappa}\right). \tag{4.2}$$

The scaler function γ is given by the consistency condition

$$\hat{g}+\frac{\partial g}{\partial\mathbf{E}^p}\cdot\dot{\mathbf{E}}^p+\frac{\partial g}{\partial\kappa}\dot{\kappa}=0 \tag{4.3}$$

as

$$\gamma=\left\{\hat{g}+\dot{\kappa}\left[\frac{\partial g}{\partial\kappa}-\frac{\partial g}{\partial\mathbf{E}^p}\cdot\left(\frac{\partial\mathbf{S}}{\partial\mathbf{E}^p}\right)^{-1}\frac{\partial\mathbf{S}}{\partial\kappa}\right]\right\}\Big/\frac{\partial g}{\partial\mathbf{E}^p}\cdot\left(\frac{\partial\mathbf{S}}{\partial\mathbf{E}^p}\right)^{-1}\frac{\partial g}{\partial\mathbf{E}}. \tag{4.4}$$

Thus, the constitutive description reduces to the specification of three scalar functions of the set of variables $\mathfrak{U}=(\mathbf{E},\mathbf{E}^p,\kappa)$, namely, the stress potential ψ, the loading function g, and a function λ which describes the evolution of the hardening parameter κ.

Definition of the Plastic Strain. We are certainly free to identify $\mathbf{K}$ with the plastic strain, when this can be defined. For instance, the residual strain $\mathbf{E}^r$ which is obtained by unloading to zero stress (assuming that $f(\mathbf{0},\mathbf{K})\leq 0$) is given by

$$\mathbf{E}^r=\mathbf{E}(\mathbf{0},\mathbf{K}) \tag{4.5}$$

and this equation relates $\mathbf{K}$ to the residual strain. We observe from equation $(2.16)_2$, i.e.,

$$\dot{\mathbf{E}}=\mathcal{C}^{-1}(\mathbf{S},\mathbf{K})\dot{\mathbf{S}}+\mathcal{E}(S,K)\dot{\mathbf{K}}, \tag{4.6}$$

that the inelastic contribution to the strain rate is not the time derivative of a tensor function, except in the special case when elastic and inelastic effects in the strain response are not coupled, i.e., when

$$\mathbf{E}(\mathbf{S},\mathbf{K})=\mathbf{E}_1(\mathbf{S})+\mathbf{E}_2(\mathbf{K}). \tag{4.7}$$

This may give rise to some difficulty in defining the plastic strain and it raises some question as to its usefulness as a kinematic variable, especially when kinematic hardening leads to a situation where $\mathbf{S}=\mathbf{0}$ is outside of the yield surface.

A Special Class of Materials. Naghdi and Trapp (1975) indicated that a considerable simplification of the elastic-plastic theory results from the assumption that the stress depends only on the strain difference $\mathbf{E}-\mathbf{E}^p$. A corresponding specialization of equation (1) to

$$\mathbf{S}=\mathbf{S}(\mathbf{E}-\mathbf{K}) \tag{4.8}$$

leads to a similar simplification. The tensors $\mathfrak{D}$ and $\mathcal{E}$ in equations (2.17) and (2.18) reduce to

$$\mathfrak{D}=-\mathcal{C};\quad \mathcal{E}=\mathcal{I}. \tag{4.9}$$

In particular, equation (2.25) becomes a normality condition on $\dot{\mathbf{K}}$. A further simplification results from the assumption that the stress response relation (4.8) is linear, so that $\mathcal{C}$ is a constant tensor.

5 The Work Assumption and Normality

The work assumption of Naghdi and Trapp (1975b) seems a

Downloaded 03 May 2010 to 171.66.16.27. Redistribution subject to ASME license or copyright; see http://www.asme.org/terms/Terms_Use.cfm

very plausible one. In view of the importance of the resulting normality conditions (2.24) or (2.25) in simplifying our constitutive theory, it seems worthwhile to examine the assumption further. It also seems worthwhile to discuss the assumption and its consequences *vis a vis* the postulate of Il'Yushin (1961) and the discussion of its implications for finite strain elastic-plastic deformations by Hill and Rice (1973).

For simplicity sake, we consider a cycle of deformation, which starts at $(\mathbf{E}_o,\mathbf{K}_o)$ inside the yield surface at time t_o, reaches the yield surface at $(\mathbf{E}_*,\mathbf{K}_o)$ at time $t*$, continues to load inelastically to $(\hat{\mathbf{E}},\hat{\mathbf{K}})$ at time t, and returns elastically to $(\mathbf{E}_o, \hat{\mathbf{K}})$ at time $\bar{t}$. It follows from equations (2.9) and (2.14) that

$$\int_{t_o}^{\bar{t}} \mathbf{S}\cdot\dot{\mathbf{E}}dt=\int_{t_o}^{\bar{t}} \dot{\psi}dt-\int_{t*}^{\hat{t}} \frac{\partial\psi}{\partial\mathbf{K}}\cdot\dot{\mathbf{K}}dt \tag{5.1}$$

or

$$\int_{t_o}^{\bar{t}} \mathbf{S}\cdot\dot{\mathbf{E}}dt=\psi(\mathbf{E}_o,\hat{\mathbf{K}})-\psi(\mathbf{E}_o,\mathbf{K}_o)-\int_{t_*}^{\hat{t}} \frac{\partial\psi}{\partial\mathbf{K}}\cdot\dot{\mathbf{K}}dt. \tag{5.2}$$

In general, the work by the external forces gives rise to changes in kinetic and internal energies and to dissipation. If the definition of a closed cycle of deformation includes the proviso that the initial velocity is resumed on completing the cycle, so that there is no net change in kinetic energy, then equation (5.2) describes the effect of the external work in changing the internal energy and in dissipation.

The thermodynamic condition of nonnegative dissipation $(\partial\psi/\partial\mathbf{K}\cdot\dot{\mathbf{K}}\le 0)$ would lead to

$$\int_{t_o}^{\bar{t}} \mathbf{S}\cdot\dot{\mathbf{E}}dt\ge\psi(\mathbf{E}_o,\hat{\mathbf{K}})-\psi(\mathbf{E}_o,\mathbf{K}_o), \tag{5.3}$$

i.e., the external work in a closed cycle cannot be less than the net change in the internal energy. This is clearly different from the work assumption (2.13), which requires that

$$-\int_{t^*}^{\hat{t}} \frac{\partial\psi}{\partial\mathbf{K}}\cdot\dot{\mathbf{K}}dt\ge\psi(\mathbf{E}_o,\hat{\mathbf{K}})-\psi(\mathbf{E}_o,\mathbf{K}_o). \tag{5.4}$$

We remark that requiring both conditions (5.3) and (5.4) does not determine the sign of the net change in internal energy.

Il'Yushin (1961) proposed a requirement similar to the condition (2.13) of Naghdi and Trapp (1975b), in the context of the static, small strain theory; he required that the condition (2.13) be met for all closed cycles of (infinitesimal) deformation, with strict inequality when the cycle involves plastic deformation. Hill and Rice (1973) discussed some implications of Il'Yushin's postulate for finite elastic-plastic deformations, and they also discussed normality conditions of the form (2.24) and (2.25). Their discussion has apparently created a mistaken impression that they have derived the normality conditions as a consequence of the Il'Yushin postulate for finite deformations (c.f. the survey papers by Asaro, 1983, and Nemat-Nasser, 1983), although this claim is not made in the paper by Hill and Rice (1973).

The treatment of Hill and Rice may be adapted to the present theory by assuming that their conjugate stress and strain measures are $\mathbf{S}$ and $\mathbf{E}$ and that their descriptor of the inelastic state is a symmetric second order tensor $\mathbf{K}$. Their examination of the condition (2.13) is by consideration of the following strain cycle: (*a*) an elastic path from $\mathbf{E}_o$ to $\mathbf{E}_*$ on the yield surface, (*b*) inelastic loading from $\mathbf{E}_*$ to $\mathbf{E}_*+\Delta\mathbf{E}_*$ and elastic unloading back to $\mathbf{E}_*$, and (*c*) retracing the original path elastically to $\mathbf{E}_o$. The inelastic portion of the cycle is small and brings about a small change in $\mathbf{K}_o$ to the new value $\mathbf{K}_o+\Delta\mathbf{K}$. They argue that segment (*b*) contributes a term of second order to the work so that, to first order,

$$\oint\mathbf{S}\cdot d\mathbf{E}=\int_{\mathbf{E}_o}^{\mathbf{E}_*}\{\mathbf{S}(\mathbf{E},\mathbf{K}_o)-\mathbf{S}(\mathbf{E},\mathbf{K}_o+\Delta\mathbf{K})\}\cdot d\mathbf{E}. \tag{5.5}$$

This leads to the condition

$$\left\{\int_{\mathbf{E}_o}^{\mathbf{E}_*} d\mathbf{E}\cdot\mathfrak{D}(\mathbf{E},\mathbf{K}_o)\right\}\cdot\Delta\mathbf{K}\le 0 \tag{5.6}$$

and, in view of equation $(2.17)_2$, to the interesting result

$$\frac{\partial}{\partial\mathbf{K}}\{\psi(\mathbf{E}_*,\mathbf{K}_o)-\psi(\mathbf{E}_o,\mathbf{K}_o)\}\cdot\Delta\mathbf{K}\le 0. \tag{5.7}$$

Hill and Rice also pointed out that a local form of the condition (5.7) is equivalent to the normality conditions (2.24) or (2.25). This local form may be obtained by setting $\mathbf{E}_o=\mathbf{E}_*-\Delta\mathbf{E}$, i.e., by starting the cycle close to the yield surface. Then equation (5.7) reduces to

$$\Delta\mathbf{E}\cdot\mathfrak{D}(\mathbf{E}_*,\mathbf{K}_o)\Delta\mathbf{K}\le 0, \tag{5.8}$$

which is similar to (2.23). However, in this localization the contribution from segments (*a*) and (*c*) of the strain cycle has now become of second order, so that one must reconsider the neglect of comparable terms in the contribution from segment (*b*). Thus, the analysis of Hill and Rice, which treats only the first-order contribution to the external work in the cycle of deformation (*a*), (*b*), and (*c*), does not provide a proof of the normality condition.

By writing the integrand in equation (2.13) as $\mathbf{S}\cdot\overline{(\mathbf{E}-\mathbf{E}_*)}$ and integrating by parts, we see that the second order *inelastic* contribution from segment (*b*) is

$$\Delta W_p=-\frac{1}{2}\Delta\mathbf{E}_*\cdot\mathfrak{D}(\mathbf{E}_*,\mathbf{K}_o)\Delta\mathbf{K}. \tag{5.9}$$

Naghdi and Trapp considered a sequence of strain cycles for which the elastic and inelastic contributions are comparable. Naghdi (1984) gave a simpler derivation of the condition (5.8), for rate-dependent materials.

The consequences of the work postulate of Naghdi and Trapp have also been examined by Naghdi (1984), for rate-dependent materials, and by Casey (1984) and Casey and Tseng (1984). In the latter paper, for instance, consideration of strain cycles starting on the yield surface leads to a condition analogous to equation (2.23) and hence to normality conditions analogous to equations (2.24) and (2.25). Consideration of strain cycles starting inside the yield surface leads to complementary conditions which, in the present context, have the rate-independent form

$$\frac{\partial}{\partial\mathbf{K}}\{\psi(\mathbf{E},\mathbf{K})-\psi(\mathbf{E}_o,\mathbf{K})\}\cdot\mathbf{A}(\mathbf{E},\mathbf{K})\le 0;$$
$$g(\mathbf{E},\mathbf{K})=0,\ g(\mathbf{E}_o,\mathbf{K})<0 \tag{5.10}$$

and

$$\frac{\partial}{\partial\mathbf{K}}\{\Psi(\mathbf{S},\mathbf{K})-\Psi(\mathbf{S}_o,\mathbf{K})\}\cdot\tilde{\mathbf{A}}(\mathbf{S},\mathbf{K})\ge 0;$$
$$f(\mathbf{S},\mathbf{K})=0,\ f(\mathbf{S}_o,\mathbf{K})<0, \tag{5.11}$$

where $\mathbf{A}$ is the response tensor in the evolution equation (2.9) and $\tilde{\mathbf{A}}$ is the corresponding function obtained with the change of variable (2.2). The inequality equation (5.10) is similar to equation (5.7) and it may be written as a condition on the rate of dissipation

$$-\frac{\partial}{\partial\mathbf{K}}\psi(\mathbf{E},\mathbf{K})\cdot\dot{\mathbf{K}}\ge-\frac{\partial}{\partial\mathbf{K}}\psi(\mathbf{E}_o,\mathbf{K})\cdot\dot{\mathbf{K}}. \tag{5.12}$$

For the special class of materials with stress response (4.11), these conditions imply convexity of the yield surface $f=0$ in stress space. When the stress response is also linear, the yield surface $g=0$ in strain space is also convex.

6 Discussion

We have presented a constitutive theory to describe finite

Downloaded 03 May 2010 to 171.66.16.27. Redistribution subject to ASME license or copyright; see http://www.asme.org/terms/Terms_Use.cfm

strain inelastic response. The primitive variables in the theory are the symmetric Piola-Kirchhoff stress $\mathbf{S}$, the Lagrangian strain $\mathbf{E}$, and an unidentified tensor $\mathbf{K}$ to describe the inelastic state. The constitutive theory is simplified greatly by a continuity assumption, the consistency condition, and the very plausible assumption that the external work in smooth closed cycles of deformation is nonnegative. This latter assumption, in particular, gives rise to normality conditions on the inelastic contributions to the stress rate $\dot{\mathbf{S}}$ and strain rate $\dot{\mathbf{E}}$, even though plastic strain and plastic strain rate are not defined. With the assumption that the fourth order tensor $\mathfrak{D} = \partial \mathbf{S}/\partial \mathbf{K}$ is nonsingular, the normality condition can be solved for $\dot{\mathbf{K}}$. The inelastic response is then described by two equations, (2.14) and (2.29), involving two scalar functions $\psi(\mathbf{E},\mathbf{K})$ and $g(\mathbf{E},\mathbf{K})$. The corresponding equations, in the stress space formulation, are (2.15) and (2.30). The theory may be generalized to allow for dependence of the loading functions f or g on a history dependent hardening parameter κ. The situation that arises when $\det \mathfrak{D} = 0$ is also discussed.

We have been concerned primarily with the structure of the constitutive theory, and so we have not presented specific response functions to describe particular classes of material behavior. Such developments will, in particular, require some definition of the tensor $\mathbf{K}$. There are various candidates in the literature, such as fabric tensors and damage tensors, in addition to the plastic strain tensor. The simple structure of the theory and its ability to describe isotropy, anisotropy, hardening, ideal behavior, or softening, etc., suggest that it may prove useful in a variety of applications.

In this regard, it is worth taking note of Nemat-Nasser's (1983) comment that the associative flow rule, i.e., a normality condition such as equations (2.24) or (2.25), involving normality to the yield surface and not to some "nonassociated" plastic potential surface, is not appropriate for dilatant frictional or pressure sensitive materials. This suggestion seems to be based on the requirement $\partial\tau/\partial p > 0$ on the yield surface, where τ is a measure of deviatoric stress and p is the pressure. While $\partial\tau/\partial p$ should be positive on a *failure* surface, there does not seem to be any firm basis for requiring that it be positive on the yield surface. Indeed, it is negative on the compactive portion (and positive on the dilatant portion) of the yield surface in the Cam-Clay critical state model for soils (c.f. Schofield and Wroth, 1968), and it is also negative on the cap portion of the yield surface in the CAP model for rocks (c.f. DiMaggio and Sandler, 1971). It should be clear that the present theory does not in any way preclude description of dilatancy, internal friction, or pressure sensitivity.

Acknowledgment

This work was supported in part by a contribution from the Shell Companies Foundation in support of a Shell Distinguished Chair at the University of California, Berkeley, and in part by a Grant No. MEA-820534 from the National Science Foundation (Solid Mechanics Program) to the University of California, Berkeley. I am grateful for this support.

References

Il'Yushin, A. A., 1961, "On a Postulate of Plasticity," *Prikl. Mat. Meh.*, Vol. 25, pp. 503–507.

Green, A. E., and Naghdi, P. M., 1965, "A General Theory of an Elastic-Plastic Continuum," *Arch. Ration. Mech. Analysis*, Vol. 18, pp. 251–281.

Green, A. E., and Naghdi, P. M., 1966, "A Thermodynamic Development of Elastic-Plastic Continua," *Proc. IUTAM Symp. on Irreversible Aspects of Continuum Mechanics and Transfer of Physical Characteristics in Moving Fluids*, Parkus, H., and Sedov, L. I., Springer-Verlag, pp. 117–131.

Schofield, A. N., and Wroth, P., 1968, *Critical State Soil Mechanics*, McGraw-Hill, London.

DiMaggio, F. L., and Sandler, I. S., 1971, "Material Model for Granular Soils," *ASCE Journal of the Engineering Mechanics Division*, Vol. 97, pp. 935–950.

Hill, R., and Rice, J. R., 1973, "Elastic Potentials and the Structure of Inelastic Constitutive Laws," *SIAM J. Appl. Math.*, Vol. 25, pp. 448–461.

Naghdi, P. M., and Trapp, J. A., 1975a, "The Significance of Formulating Plasticity Theory With Reference to Loading Surfaces in Strain Space," *Int. J. Engng. Sci.*, Vol. 13, pp. 785–797.

Naghdi, P. M., and Trapp, J. A., 1975b, "Restrictions on Constitutive Equations of Finitely Deformed Elastic-Plastic Materials," *Q. J. Mech. Appl. Math.*, Vol. 28, pp. 25–46.

Casey, J., and Naghdi, P. M., 1981, "On the Characterization of Strain-Hardening in Plasticity," ASME JOURNAL OF APPLIED MECHANICS, Vol. 48, pp. 285–296.

Asaro, R. J., 1983, "Crystal Plasticity," ASME JOURNAL OF APPLIED MECHANICS (50th Anniversary Issue), Vol. 50, pp. 921–934.

Nemat-Nasser, S., 1983, "On Finite Plastic Flow of Crystalline Solids and Geomaterials," ASME JOURNAL OF APPLIED MECHANICS (50th Anniversary Issue), Vol. 50, pp. 1114–1126.

Casey, J., 1984, "A Simple Proof of a Result in Finite Plasticity," *Q. Appl. Math.*, Vol. 42, pp. 61–71.

Casey, J., and Naghdi, P. M., 1984, "Further Constitutive Results in Finite Plasticity," *Q. J. Mech. Appl. Math.*, Vol. 37, pp. 231–259.

Casey, J., and Tseng, M., 1984, "A Constitutive Restriction Related to Convexity of Yield Surfaces in Plasticity," *J. Appl. Math. and Phys.* (ZAMP), Vol. 35, pp. 478–496.

Naghdi, P. M., 1984, "Constitutive Restrictions for Idealized Elastic-Viscoplastic Materials," ASME JOURNAL OF APPLIED MECHANICS, Vol. 51, pp. 93–101.

Downloaded 03 May 2010 to 171.66.16.27. Redistribution subject to ASME license or copyright; see http://www.asme.org/terms/Terms_Use.cfm

Remaining at Yield During Unloading and Other Unconventional Elastic-Plastic Response[1]

D. C. Drucker
Graduate Research Professor of Engineering Sciences, University of Florida, Gainesville, FL 32611
Honorary Mem. of ASME

Devo Seereeram[2]
Research Assistant in Civil Engineering, University of Florida, Gainesville, FL 32611

A rather special time-independent or elastic-plastic response is proposed in which, although there is elastic response to unloading, the material remains at yield for all or a significant portion of the unloading path following plastic deformation. In the most elementary form, the material exhibits no memory of prior plastic deformation; the current state of the material is given solely *by the current state of stress. A simple but unconventional field of plastic moduli then can be chosen to produce a limit surface that cuts through a nested set of yield surfaces and to model critical aspects of the behavior of sand.*

A Material Remaining At Yield During Unloading

At each state of stress, suppose, as in conventional plasticity theory, there is a local surface passing through the stress point which, for any small stress increment vector, separates the domain of purely elastic response from the domain of plastic (actually elastic-plastic) response (Fig. 1(*a*)). These local surfaces are further supposed to join to form a set of continuous surfaces in stress space. A nested set of these surfaces (Fig. 1(*b*)) then resembles a sequence of successive yield surfaces or loading surfaces for a stress-hardening plasticity theory, analogous to but very different from the Mises or J_2 isotropic hardening idealization. As in the conventional formulation, when the stress point moves about on one of these surfaces in stress space (neutral loading), purely elastic deformation takes place. Any motion of the stress point directed toward the outside will produce plastic as well as elastic deformation. A move directed inward gives purely elastic response.

However, a move inward has very different consequences in conventional plasticity and in the special formulation proposed here. Conventional plasticity does appropriately idealize the macroscopic behavior of metals and alloys at temperatures that are a small fraction of their melting point. The current yield or loading surface remains unchanged as the stress point moves inside it. Plastic deformation will not take place again until the stress point reaches and then penetrates the yield surface established by the prior history of loading (Fig. 2(*a*)). In the proposed formulation, there may or may not

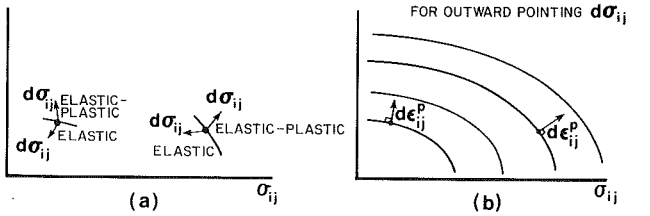


Fig. 1 The current yield surface passes through the current stress point and locally separates the domain of purely elastic response from the domain of elastic-plastic response

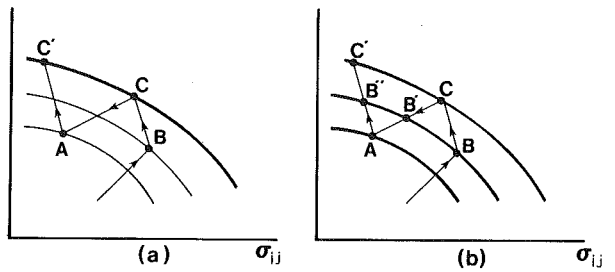


Fig. 2 In conventional plasticity (2a) path CAC′ is purely elastic, in the proposed formulation (2b) path CB′A is elastic but AB″C′ is elastic-plastic

be a purely elastic domain of stress. Outside of that domain, if one is postulated, or throughout the entire stress space if one is not, the current yield surface always passes through the current stress point, whether the motion of the stress point represents loading or unloading (Fig. 2(*b*)). Inelastic deformation occurs immediately when the stress point once again moves outward.

For the simplest form of no purely elastic domain and no history dependence or memory of prior plastic deformation, there is no change in either the family of yield surfaces or the

[1]Presented at the Tenth U.S. National Congress of Applied Mechanics, Austin, Texas, June 16-20, 1986.

[2]Presently at Seereeram Bros. Ltd., Chaguanas, Trinidad.

Contributed by the Applied Mechanics Division for publication in the JOURNAL OF APPLIED MECHANICS.

Discussion on this paper should be addressed to the Editorial Department, ASME, United Engineering Center, 345 East 47th Street, New York, N.Y. 10017, and will be accepted until two months after final publication of the paper itself in the JOURNAL OF APPLIED MECHANICS. Manuscript received by ASME Applied Mechanics Division, December 20, 1985; final revision July 21, 1986.

Copyright © 1987 by ASME
Downloaded 03 May 2010 to 171.66.16.27. Redistribution subject to ASME license or copyright; see http://www.asme.org/terms/Terms_Use.cfm

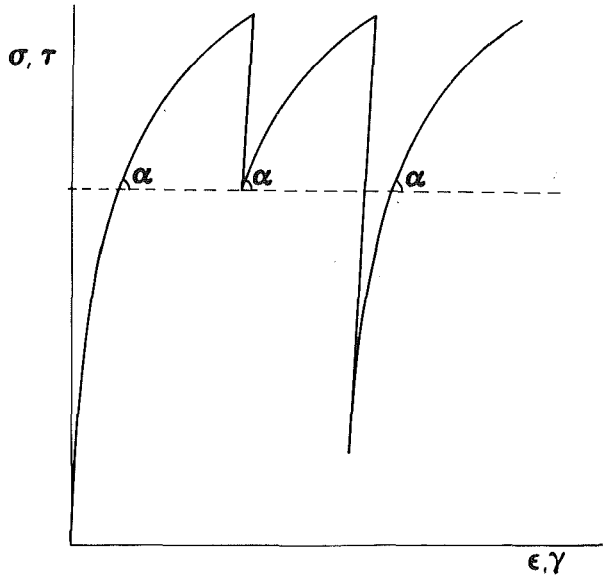


Fig. 3 Successive stress-strain curves for uniaxial stress or shear are the initial curve translated along the strain axis in the simplest model

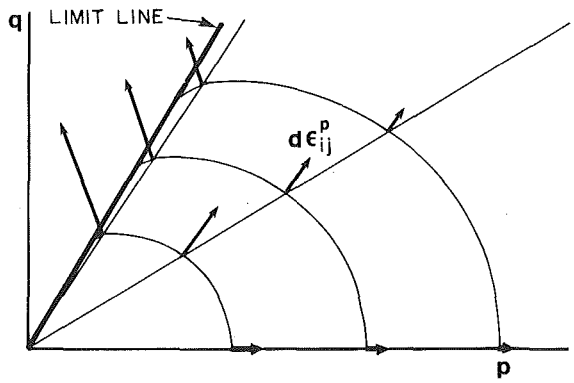


Fig. 4 Pictorial representation for sand of the nested set of yield surfaces, the limit line, and the field of plastic moduli (shown by the $d\epsilon_{ij}^p$ associated with a constant value of $n_{pq}d\sigma_{pq}$)

field of plastic moduli. In one dimension (simple tension or simple shear), as shown in Fig. 3, the slope of the stress-strain curve for reloading at each stress level is the same as for the initial loading. Each reloading curve is simply the original loading curve translated along the strain axis.

The representation resembles in part the proposal by Drucker and Palgen (1981) for the stable cyclic behavior of metals, without either kinematic hardening or isotropic workhardening or softening (see their Fig. 3). Other earlier proposals, such as those by Eisenberg and Phillips (1971), Dafalias and Popov (1975), and Hashiguchi (1980) also have some of the features of this one with plastic deformation occurring inside of or on surfaces labeled as bounding surfaces or loading surfaces, respectively, both of which are distinguished from yield surfaces enclosing an elastic domain. These earlier idealizations were developed to simulate the behavior termed *metarecovery* by Cherian, Pietrokowsky, and Dorn (1949) in their study of commercially pure aluminum. For uniaxial stress, the reloading curve is asymptotic to what would have been the uninterrupted virgin loading curve. The simple form of the idealization proposed here is a special case of what they termed orthorecovery; the reloading curve is parallel to the original curve (Fig. 3).

As illustrated, each yield surface in stress space will be taken to be convex and the material to be stable in the small in the forward sense (positive elastic and positive plastic moduli). Yet both an instability in the small for a cycle of unloading followed by reloading, and an instability in the large, are present in the sense of Drucker (1951). Work can be extracted from the material and the system of forces or stresses acting upon it in a cycle of stress, or equally well in a cycle of strain, a characteristic shared with metarecovery idealizations. Consequently, neither the comforting equivalent of the shakedown theorem nor the lower bound theorem of perfect plasticity holds. Inelastic deformation will continue to grow indefinitely with constant increments as the stress level is oscillated between fixed limits. Such continual deformation is associated with a simple frictional system, as a block subjected to fluctuating tangential and normal forces that cause it to be alternatively at and just above incipient sliding on a rough surface, or a fully or partially continuously annealing metal or alloy, but not with a metallic system well below its annealing temperature.

The possible value of so overly simple and yet unconventional an idealization for metals or for granular media remains to be demonstrated. The reader is urged to both withhold judgment until a few illustrative examples are explored and to expect no greater generality of response than from any simple idealization of inelastic behavior.

The Stress-Strain Relation

The behavior of the material at each state of stress is supposed to be stable in the small in the forward sense for an outward motion of the stress point and for a cycle of elastic return. Then, at a smooth point on the yield surface, the plastic strain increment vector $d\epsilon_{ij}^p$ produced by the outward stress increment vector $d\sigma_{ij}$ is normal to the current yield surface, F = constant:

$$d\epsilon_{ij}^p = \lambda \frac{\partial F}{\partial \sigma_{ij}} \tag{1}$$

or

$$d\epsilon_{ij}^p = G \frac{\partial F}{\partial \sigma_{ij}} \left(\frac{\partial F}{\partial \sigma_{pq}} d\sigma_{pq} \right) \tag{2}$$

where in the simplest formulation both G and F are functions of stress only.

In a more transparent form for loading ($n_{pq}d\sigma_{pq} > 0$),

$$d\epsilon_{ij}^p = \frac{1}{K_p} n_{ij} (n_{pq} d\sigma_{pq}) \tag{3}$$

where n_{ij} is the unit normal $\partial F/\partial \sigma_{ij} \,/\, \sqrt{[(\partial F/\partial \sigma_{rs})\ (\partial F/\partial \sigma_{rs})]}$, $n_{pq}d\sigma_{pq}$ is the normal component of the stress increment vector $d\sigma_{pq}$, and the plastic modulus K_p is a scalar function of the current stress only.

$$\frac{1}{K_p} = \left(\frac{\partial F}{\partial \sigma_{rs}} \frac{\partial F}{\partial \sigma_{rs}} \right) G \tag{4}$$

The field of plastic moduli, K_p, remains fixed throughout stress space in this simplest version of the proposed behavior. More elaborate formulations, which take one or more aspects of the history of deformation into account, are easily devised. It seems premature at this stage to go much beyond the exploration of the possible value of the simple version.

Modeling the Behavior of Sand

Consider a material subjected to shear stress q and hydrostatic pressure p having a set of nested yield surfaces in $q-p$ space as shown in Fig. 4. The surfaces are chosen so that the normal to each is constant in direction along a radial line from the origin. The modulus K_p is taken to increase with

Downloaded 03 May 2010 to 171.66.16.27. Redistribution subject to ASME license or copyright; see http://www.asme.org/terms/Terms_Use.cfm

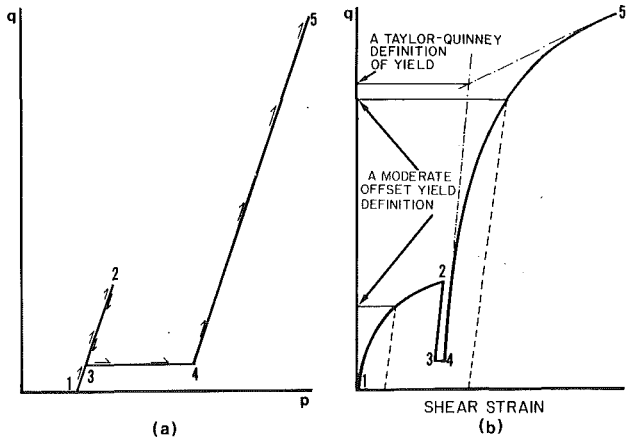


Fig. 5 (a) Type "A" loading-unloading-reloading stress path and (b) corresponding stress-strain curve

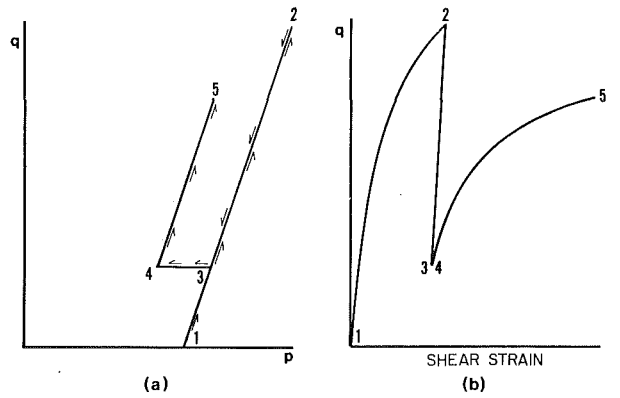


Fig. 6 (a) Type "B" loading-unloading-reloading stress path and (b) corresponding stress-strain curve

radial distance from the origin in accord with the stiffening of the response of sand with increase in hydrostatic pressure. The modulus is taken to decrease with increase in the angle of inclination of the radius to hydrostatic pressure axis, slowly at first and more and more rapidly later. K_p goes to zero at a limiting line, which is beyond the zero dilation line, in accord with the failure condition for sand. This inelastic response is indicated schematically in Fig. 4 by the direction and relative length of the plastic strain-increment vectors produced by the same normal increment of stress $n_{pq}d\sigma_{pq}$ at each and every point. It is worth noting that because F and G are purely stress dependent, satisfaction of the consistency condition is automatically assured in contrast to the more difficult approach commonly adopted for isotropic hardening soil models (see Mroz, 1984, for a survey of current approaches).

The proposed choices, motivated by the observed behavior of sand, are instructive because they are so very different in so many ways from the familiar behavior of metals and their customary idealizations as elastic-plastic. Note that the limiting line from the origin, taken as straight and radial for simplicity, intersects the successive yield surfaces at an appreciable angle and is not a yield surface itself. However, if the plastic moduli are comparable to the elastic until the limiting line is approached, and if a large strain offset definition of yield is employed, instead of the infinitesimal plastic strain definition, the initial "yield" surface so defined would be rather close to the limit line. More generally, for the model of sand as described, initial and subsequent "yield" surfaces determined by a moderate plastic strain offset or a Taylor-Quinney (1931) definition so suitable for metals, have entirely different shapes from the nested set of yield surfaces that generate them. Figures 5 and 6 each show a loading-unloading-reloading path and the corresponding stress-strain curves that the representation gives. Figure 7 indicates schematically the shape of the surface that would be defined as a "yield" surface with either a moderate (but constant) offset definition or with a Taylor-Quinney definition.

Comments on the Correspondence to Reality

Too much should not be expected from any simple model, especially one that is unconventional and so by definition will not give the traditional results that have served so well for so long for the plastic deformation of metals and alloys. Certainly this representation, unlike conventional plasticity, is not intended to capture the essence of the response of most structural metals to a generally outward path of loading in stress space followed by a full or partial unloading and then reloading. However, it is worth noting that the behavior of cyclically stabilized metals and alloys between two fixed limits

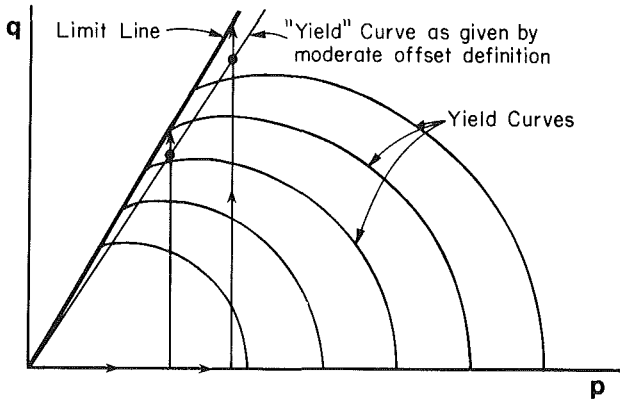


Fig. 7 The "yield" surface as defined in Fig. 5(b) by a moderate offset definition cuts across the nested set of yield surfaces that generates Fig. 5(b)

of strain can be given reasonably well by such a simple formulation. Ratcheting will be predicted for oscillation between two unsymmetric stress limits of opposite sign: too much ratcheting for a large number of cycles, but not so bad an approximation for just a few cycles.

It is by no means clear that such a representation is adequate for sand, despite the qualitative agreement of the stress-strain curves of Figs. 5 and 6 with experimental results. However, the concept of the yield surface following the stress point for unloading as well as loading has some physical appeal. The response of a granular medium to shear at a given void ratio does depend upon the hydrostatic pressure. Furthermore, the void ratio does not change appreciably with inelastic shear deformation until the deformation becomes quite large. At any given void ratio, a reduction in hydrostatic pressure surely will lower the shear stress level required for any given ratio of incremental inelastic shear to volumetric strain; an increase will raise the shear stress required. If it makes sense to think of yield surfaces in stress space for sand (and that's a very big *if*), then it is not unreasonable to associate a fixed ratio of shear stress to hydrostatic pressure with a corresponding ratio of inelastic strain increments as sketched in Fig. 4. It is also not unreasonable for the current yield surface to go through the current stress point for an unloading as well as a loading path. Inelastic deformation would be observed at a point O in Fig. 8 for each of the outward paths drawn through that stress point, even though the operative segment DO of path CDO is well inside the largest yield surface reached earlier and so its extension beyond O would be thought of as elastic in conventional plasticity.

In a sequence of careful experiments by Poorooshasb,

Downloaded 03 May 2010 to 171.66.16.27. Redistribution subject to ASME license or copyright; see http://www.asme.org/terms/Terms_Use.cfm

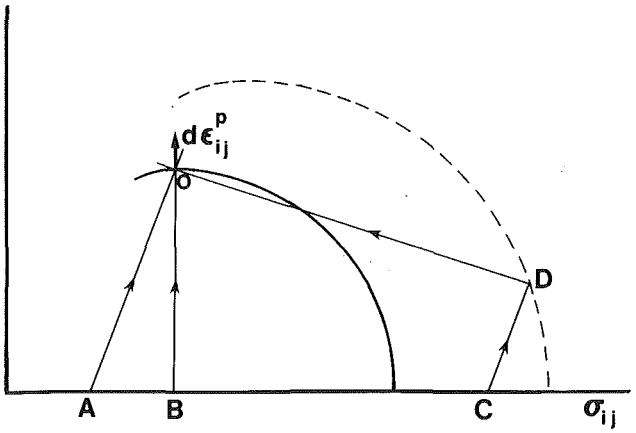


Fig. 8 Plastic deformation at O for the extension of path CDO as well as of AO and BO

Holubec, and Sherbourne (1966, 1967), the direction of the plastic strain increment vector at O was observed to be independent of the direction of the path of loading through O. It was, in fact, these experimental observations and those of Tatsuoka and Ishihara (1974a, 1974b) which suggested that the combination of the yield curve following the stress point on unloading, a fixed field of plastic moduli, and nested surfaces might provide a suitable first approximation for sand. As stated by Tatsuoka and Ishihara (1974a), "the sample behaves as if it were in a virgin state when the mobilization of shear stress is reversed in direction".

Modifications of the Proposal to Exhibit More Complex Behavior

As mentioned earlier, a domain of purely elastic response can be postulated that is fixed in stress space or that expands or contracts in accord with the inelastic history of the material. In the most convenient but not necessarily appropriate form, the elastic domain will be bounded by one of the nested yield surfaces. If desired, the elastic domain can be taken to expand as the stress paths repeatedly penetrate successive yield surfaces. Should hardening of the material occur within any surface, such as the farthest out yield surface reached in prior loading, the plastic modulus K_p at interior points can be taken to increase. The increase may be chosen to depend upon the distance from the interior stress point to a conjugate point on that surface, or the number of times the interior yield surfaces have been crossed in an outward direction, or the extent of the prior plastic deformation, or the decrease in void ratio, or any other measures believed important separately or in combination. Similarly, if softening of the material takes place as a result of significant dilation or the accumulation of plastic distortion, the plastic modulus can be decreased appropriately.

Another complexity that can be added if needed to improve agreement with experiment is the alteration of the limiting line in $q-p$ space, or the limiting surface in a more general stress space to follow any large change in void ratio or fabric. Also, the limiting line need not be taken as straight or to pass through the origin.

Concluding Remarks

Two entirely independent special modes of elastic-plastic response have been described within the framework of stability in the small in the forward sense. The first is a rather radical departure from the conventional formulation of plasticity theory. In the proposed formulation, the current yield surface continues to pass through the current stress point, whether the motion of the stress point represents loading or unloading. Inelastic deformation occurs immediately when the stress point once again begins to move outward. Experimental results on sand provided the motivation for this basic assumption which leads to instability in the large for some important paths of loading as well as instability in the small for an unloading-reloading cycle. One of the unpleasant aspects of this instability is that the response to imposed loads of a body under an inhomogeneous state of stress can be highly dependent upon the initial state of stress, even when the subsequent inelastic strain becomes quite large. However, granular and frictional media do exhibit such instability in the large and corresponding sensitivity to initial stress. Although metallic systems rarely do, the formulation is of some use for metals that self anneal or have been stabilized under cyclic loading.

The second major departure from conventional plasticity theory does in principle lie within the scope of the general theory for fully stable workhardening materials. A limit line or surface is produced by choosing the plastic modulus as approaching zero as the stress point moves outward toward the limit surface. However, in contrast with the traditional approach, the limit surface chosen here cuts across and is not one of the family of initial or subsequent yield or loading surfaces. For a workhardening metal or alloy, such a choice of a field of plastic moduli also would exhibit the same selected limit surface for generally outward loading. It would not, however, for loading appreciably in any one direction that does not intersect the limit surface in stress space, then unloading to a state of pure hydrostatic pressure and reloading in another direction that does. The subsequent outward loading path could reach and cross the limit surface as a purely elastic path and the supposed limiting surface would not limit.

It is the combination, a yield surface following the stress point for unloading as well as loading and a limiting surface in stress space established by the approach to zero of the plastic modulus on a very different surface from the set of yield surfaces, that provides the promise of a useful consistent model for the response of sand and other granular media. The limit surface then is a surface in stress space that will not be passed by the stress point on reloading following loading and unloading to a state of pure hydrostatic stress. All is not quite as it should be in this simple formulation because the limit surface can be penetrated by a neutral or a somewhat unusual inward loading path starting near the limit surface. Further development is needed to circumvent this difficulty and to include other significant aspects of material behavior as needed.

The final point to emphasize is that definitions of yield are arbitrary and can be misleading. The calculated curves, Figs. 5 and 6, for elastic-plastic response of the simple model, with its fixed nested set of yield surfaces in stress space, Fig. 4, match the results of the usual triaxial tests on sand very well. Consequently, they do give the customarily reported set of moderate or large offset yield surfaces, Fig. 7, which bear no resemblance at all to the (infinitesimal offset) yield surfaces that generated these quite differently defined "yield" surfaces. The conclusions an observer is likely to draw from the calculated data, treated as though they were experimental, is that the inelastic stress-strain relation does not obey normality to the current yield surface, i.e., it is nonassociated. Of course, the fact that an associated flow rule gives data that could reasonably be interpreted as nonassociated does not demonstrate that nonassociated flow rules are simply artifacts of interpretation. The associated flow rule results do, however, provide some food for thought as well as a stabilizing option for computation.

Acknowledgments

Daniel C. Drucker gratefully acknowledges the support of

Downloaded 03 May 2010 to 171.66.16.27. Redistribution subject to ASME license or copyright; see http://www.asme.org/terms/Terms_Use.cfm

the National Science Foundation under Grant MSM-8604812. Devo Seereeram gratefully acknowledges the support of the United States Air Force Office of Scientific Research under Grant No. AFOSR-84-0108 to the Civil Engineering Department, University of Florida (M.C. McVay, Principal Investigator).

References

Cherian, T. V., Pietrokowsky, P., and Dorn, J. E., 1949, "Some Observations on the Recovery of Cold Worked Aluminium," *Trans. AIME*, Vol. 185, pp. 948–956.

Dafalias, Y. F., and Popov, E. P., 1975, "A Model of Nonlinearly Hardening Materials for Complex Loading," *Acta Mechanica*, Vol. 21, pp. 173–192.

Drucker, D. C., 1951, "A More Fundamental Approach to Stress-Strain Relations," *Proceedings of the First U.S. National Congress of Applied Mechanics*, ASME, pp. 487–491.

Drucker, D. C., and Palgen, L., 1981, "On Stress-Strain Relations Suitable for Cyclic and Other Loading," ASME JOURNAL OF APPLIED MECHANICS, Vol. 48, pp. 479–485.

Eisenberg, M. A., and Phillips, A., 1971, "A Theory of Plasticity With Noncoincident Yield and Loading Surfaces," *Acta Mechanica*, Vol. 11, pp. 247–260.

Hashiguchi, K., 1980, "Constitutive Equations of Elastoplastic Materials With Elastic-Plastic Transition," ASME JOURNAL OF APPLIED MECHANICS, Vol. 47, pp. 266–272.

Mroz, Z., 1984, "On Isotropic Hardening Constitutive Models in Soil Mechanics," *Results of the International Workshop on Constitutive Relations for Soils*, Gudehus, G., Darve, F., and Vardoulakis, I., eds., A. A. Balkema, Netherlands, pp. 463–469.

Poorooshasb, H. B., Holubec, I., and Sherbourne, A. N., 1966, "Yielding and Flow of Sand in Triaxial Compression, Part I," *Canadian Geotechnical Journal*, Vol. III, No. 4, pp. 179–190.

Poorooshasb, H. B., Holubec, I., and Sherbourne, A. N., 1967, "Yielding and Flow of Sand in Triaxial Compression, Part II and III," *Canadian Geotechnical Journal*, Vol. IV, No. 4, pp. 376–397.

Tatsuoka, F., and Ishihara, K., 1974a, "Yielding of Sand in Triaxial Compression," *Soils and Foundations*, Vol. 14, No. 2, pp. 63–76.

Tatsuoka, F., and Ishihara, K., 1974b, "Drained Deformation of Sand under Cyclic Stresses Reversing Direction," *Soils and Foundations*, Vol. 14, No. 3, pp. 51–65.

Taylor, G. I., and Quinney, H., 1931, "The Plastic Distortion of Metals," *Philosophical Transactions of the Royal Society*, Ser. A, Vol. 230, London, pp. 323–362.

Downloaded 03 May 2010 to 171.66.16.27. Redistribution subject to ASME license or copyright; see http://www.asme.org/terms/Terms_Use.cfm

Balance Laws and Constitutive Relations for Plane Flows of a Dense, Binary Mixture of Smooth, Nearly Elastic, Circular Disks

J. T. Jenkins
Mem. ASME

F. Mancini

Department of Theoretical and Applied Mechanics, Cornell University, Ithaca, NY 14853

We derive balance laws and constitutive relations for plane flows of a dense, binary mixture of smooth, nearly elastic, circular disks. The disks may differ in size and mass and in the coefficients of restitution characterizing the energy lost in collisions between like and unlike pairs. We focus attention on those parts of the fluxes and sources of momentum and energy that are due to collisions. To calculate them, we suppose that the complete pair distribution function for two colliding disks is the product of Maxwellian velocity distributions for each disk and a factor that incorporates the effects of excluded area and collisional shielding. In an Appendix we provide constitutive relations calculated in a similar way for a dense, binary mixture of smooth, nearly elastic, spheres.

Introduction

Methods from the kinetic theory of dense gases have recently been employed to derive balance laws and constitutive relations for idealized granular materials experiencing rapid deformations. The main difference between the granular material and a molecular gas is that energy is lost in collisions between grains. However, it is relatively easy to take this into account and to derive kinetic theories that apply at least when the energy dissipated in collisions is small. Such theories have been obtained for identical, smooth, nearly elastic spheres by Lun, Savage, Jeffrey, and Chepurniy (1984) and Jenkins and Richman (1985a) and for plane flows of identical, rough, inelastic disks by Jenkins and Richman (1985b).

The interest in formulating a similar theory for granular mixtures stems from the observations of particle separation by size in shearing flows and the desire to predict the apparent viscosity of a rapidly sheared granular mass consisting of different types of particles.

Numerical simulations of the detailed dynamics of identical, circular disks moving in a plane and interacting through collisions have been carried out by Campbell and Brennen (1982), Campbell and Gong (1985), and Walton and Braun (1986) for steady shearing flow and by Campbell and Brennen (1985) for flow down an incline. Such numerical simulations are presently being extended to binary mixtures. Air table experiments in progress at Clarkson University will provide information on shearing flows maintained by the relative motion of parallel boundaries and gravity driven flows between fixed parallel walls. Consequently, the theory developed for plane flows of disks can be checked against the results of numerical simulations and experiments.

Here we use methods from the kinetic theory to derive balance laws and constitutive relations for plane flows of a dense, binary mixture of smooth, nearly elastic, circular disks. The disks may have different radii and masses and the coefficients of restitution, characterizing the energy lost in collisions between like and unlike pairs, may all be different. Following Dahler and Sather (1963) and Condiff, Lu, and Dahler (1965), we derive the balance laws for mass, momentum, and energy for the individual species and for the mixture. The collisional fluxes and sources of momentum and energy that appear in these involve the complete pair distribution functions for colliding pairs of like and unlike disks. We suppose first that these distribution functions can be expressed as the product of the single particle velocity distribution functions for each disk and a factor that accounts for the effects of excluded area and collisional shielding. Then, rather than determining the single particle velocity distribution functions as approximate solutions to the kinetic equations governing their evolution, we simply suppose that they are Maxwellian. Jenkins and Savage (1983) do essentially the same in deriving constitutive relations for identical, smooth, nearly elastic, spheres and Longuet-Higgins, Pople, and Valleau (1956) make the identical assumption when calculating expressions for the energy flux and the particle fluxes in a dense, binary mixture of elastic spheres with equal radii. For a binary mixture of inealstic spheres, Shen (1984) uses an even simpler method of averaging to calculate the shear stress, normal stress, and rate of dissipation in steady simple shear.

Upon employing the resulting collisional pair distribution functions and supposing that the spatial gradients of the mean fields and the perturbations to the mixture velocity and mixture temperature are small, we calculate the sources of

Contributed by the Applied Mechanics Division for publication in the JOURNAL OF APPLIED MECHANICS.

Discussion on this paper should be addressed to the Editorial Department, ASME, United Engineering Center, 345 East 47th Street, New York, N.Y. 10017, and will be accepted until two months after final publication of the paper itself in the JOURNAL OF APPLIED MECHANICS. Manuscript received by ASME Applied Mechanics Division, June 5, 1985; final revision May 29, 1986.

Copyright © 1987 by ASME
Downloaded 03 May 2010 to 171.66.16.27. Redistribution subject to ASME license or copyright; see http://www.asme.org/terms/Terms_Use.cfm

momentum and energy for each species and the collisional contributions to each species' pressure tensor and energy flux. We then use the constitutive relations in the balance laws to obtain approximate expressions for the velocity of diffusion and the difference in the temperature perturbations. The resulting theory is applied to a steady, rectilinear, shearing flow.

In an Appendix, we extend the calculations of Longuet-Higgins, Pople, and Valleau (1956) to nearly elastic spheres with different radii and, in addition, provide expressions for the pressure tensors and energy sources.

Binary Collisions

We treat particles of two different species, A and B. Particles of each species are smooth, homogeneous, circular disks. Those of A have radius σ_A and mass m_A; those of B have radius σ_B and mass m_B.

Consider a collision between particle number 1 of species i and particle number 2 of species k, where i and k may be either A or B. Let $\mathbf{c}_1$ and $\mathbf{c}_1'$ be, respectively, the velocity of particle number 1 immediately before and immediately after a collision. Let $\mathbf{c}_2$ and $\mathbf{c}_2'$ be defined in the same way for particle number 2. Then the relative velocities $\mathbf{c}_{21}$ and $\mathbf{c}_{21}'$ before and after a collision are

$$\mathbf{c}_{21} \equiv \mathbf{c}_2 - \mathbf{c}_1 \text{ and } \mathbf{c}_{21}' \equiv \mathbf{c}_2' - \mathbf{c}_1'. \tag{1}$$

If $\mathbf{k}$ is the unit vector directed from the center of particle 2 to the center of particle 1 at collision, the components of the relative velocities in the direction of $\mathbf{k}$ before and after a collision are assumed to be related by

$$\mathbf{k}\cdot\mathbf{c}_{21}' = -e_{ik}(\mathbf{k}\cdot\mathbf{c}_{21}), \tag{2}$$

where e_{ik} is the coefficient of restitution for a collision between a particle of i and a particle of k. Clearly, $e_{ik} = e_{ki}$ and, as usual, $0 \le e_{ik} \le 1$.

Let $m_{ik} \equiv m_i + m_k$, and $M_i \equiv m_i/m_{ik}$; note that for collisions between particles of the same species, $M_i = M_k = 1/2$. Then the mass-center velocity $\mathbf{G}_{ik}$ is

$$\mathbf{G}_{ik} \equiv M_k\mathbf{c}_2 + M_i\mathbf{c}_1 = M_k\mathbf{c}_2' + M_i\mathbf{c}_1'. \tag{3}$$

So, for example,

$$\mathbf{c}_1' = \mathbf{G}_{ik} - M_k\mathbf{c}_{21}' \text{ and } \mathbf{c}_1 = \mathbf{G}_{ik} - M_k\mathbf{c}_{21}. \tag{4}$$

Consequently,

$$\mathbf{c}_1' - \mathbf{c}_1 = M_k(\mathbf{c}_{21} - \mathbf{c}_{21}'), \tag{5}$$

or, because the particles are smooth,

$$\mathbf{c}_1' - \mathbf{c}_1 = M_k(1 + e_{ik})(\mathbf{k}\cdot\mathbf{c}_{21})\mathbf{k}. \tag{6}$$

A similar calculation for particle 2 leads to

$$m_k(\mathbf{c}_2' - \mathbf{c}_2) = -m_i(\mathbf{c}_1' - \mathbf{c}_1). \tag{7}$$

Given any particle property $\psi_i = \psi_i(\mathbf{c})$ of species i, we may use equation (6) to calculate its change, $\psi_i' - \psi_i$, in a collision. As an example, consider the energy, $\psi_i \equiv m_i c^2/2$, where $c^2 \equiv \mathbf{c}\cdot\mathbf{c}$:

$$\frac{1}{2}m_i(c_1'^2 - c_1^2) = \frac{1}{2}m_i\Big[2M_k(1+e_{ik})(\mathbf{k}\cdot\mathbf{c}_{21})(\mathbf{k}\cdot\mathbf{G}_{ik}) - M_k^2(1-e_{ik}^2)(\mathbf{k}\cdot\mathbf{c}_{21})^2\Big]. \tag{8}$$

Because energy is not conserved in a collision,

$$\frac{1}{2}m_k(c_2'^2 - c_2^2) \neq -\frac{1}{2}m_i(c_1'^2 - c_1^2). \tag{9}$$

Mean Values

Mean values are calculated in terms of the single particle velocity distribution function $f^{(1)}(\mathbf{c},\mathbf{r},t)$ for the species of interest. Here, for example, $f_i^{(1)}(\mathbf{c},\mathbf{r},t)$ **dc dr** is the number of particles of i at time t with velocities in the interval **dc** centered at **c** that are located in the area element **dr** at **r**. Consequently, the number density $n_i(\mathbf{r},t)$ of species i is given by

$$n_i(\mathbf{r},t) = \int f_i^{(1)}(\mathbf{c},\mathbf{r},t)\mathbf{dc}, \tag{10}$$

where the integration is over all **c**. The mass density ρ_i is the product of m_i and n_i.

The total number density n is the sum over both species,

$$n = n_A + n_B. \tag{11}$$

Likewise, the mixture mass density ρ is

$$\rho = \rho_A + \rho_B = m_A n_A + m_B n_B. \tag{12}$$

Given a typical property $\psi_i = \psi_i(\mathbf{c})$ of particle i, its mean $\langle\psi_i\rangle$ is defined by

$$\langle\psi_i\rangle \equiv \frac{1}{n_i}\int\psi_i(\mathbf{c})f_i(\mathbf{c})\mathbf{dc}, \tag{13}$$

where the dependence of the mean upon **r** and t is to be understood. For example, the mean velocity $\mathbf{u}_i$ of species i is $\langle\mathbf{c}_i\rangle$. Then the mass average, or barycentric velocity, **u** of the mixtures is defined by

$$\mathbf{u} = \rho^{-1}(\rho_A\mathbf{u}_A + \rho_B\mathbf{u}_B). \tag{14}$$

The peculiar velocity $\mathbf{C}_i$ of an i particle is its velocity relative to the barycentric,

$$\mathbf{C}_i \equiv \mathbf{c}_i - \mathbf{u}; \tag{15}$$

while the diffusion velocity $\mathbf{v}_i$ of species i is its relative mean motion,

$$\mathbf{v}_i \equiv \mathbf{u}_i - \mathbf{u}. \tag{16}$$

We note that $\mathbf{v}_i$ is $\langle\mathbf{C}_i\rangle$ and

$$\rho_A\mathbf{v}_A + \rho_B\mathbf{v}_B = 0. \tag{17}$$

The temperature T_i of species i is defined by

$$T_i \equiv \frac{1}{2}m_i\langle C_i^2\rangle, \tag{18}$$

where $C_i^2 \equiv \mathbf{C}_i\cdot\mathbf{C}_i$. It is the mean of the kinetic energy of the fluctuations from the barycentric velocity. The mixture temperature T is given in terms of the number densities and the species temperatures by

$$T \equiv n^{-1}(n_A T_A + n_B T_B). \tag{19}$$

Note that the mixture temperature is a number average of the two species temperatures, while the barycentric velocity is a mass average of the two species velocities.

Balance Laws

Consider a particle property ψ_i that is a function of $\mathbf{c}_i$. The time rate of change of the total amount $\langle n_i\psi_i\rangle\mathbf{dr}$ of this property in a fixed area element **dr** is the sum of the means of the net influx to the element of particles bearing ψ_i, the intrinsic rate of change of ψ_i within the element due to the variation of $\mathbf{c}_i$ with time, and the rate at which collisions within the element produce ψ_i. Let $\mathcal{C}_{ik}(\psi_i)$ be the rate of production of ψ_i per unit area in collisions with particles of species k and $\mathbf{F}_i$ be the external force experienced by a particle of i, then the balance law for the particle property ψ_i of species i has the form,

$$\frac{\partial}{\partial t}\langle n_i\psi_i\rangle + \nabla\cdot\langle n_i\mathbf{c}_i\psi_i\rangle - \left\langle n_i\frac{d\mathbf{c}_i}{dt}\cdot\frac{\partial\psi_i}{\partial\mathbf{c}_i}\right\rangle = \sum_{k=A,B}\mathcal{C}_{ik}(\psi_i), \tag{20}$$

where the particle acceleration is equal to $\mathbf{F}_i/m_i$.

Downloaded 03 May 2010 to 171.66.16.27. Redistribution subject to ASME license or copyright; see http://www.asme.org/terms/Terms_Use.cfm

The collisional rate of production, $\mathcal{C}_{ik}(\psi_i)$, is given in terms of the complete pair distribution function $f_{ik}^{(2)}(\mathbf{c}_1,\mathbf{r}_1,\mathbf{c}_2,\mathbf{r}_2,t)$ defined so that, at time t, $f_{ik}^{(2)}(\mathbf{c}_1,\mathbf{r}_1,\mathbf{c}_2,\mathbf{r}_2)\mathbf{dc}_1\mathbf{dr}_1\mathbf{dc}_2\mathbf{dr}_2$ is the number of pairs of particles such that particle i is located in the area element $\mathbf{dr}_1$ centered at $\mathbf{r}_1$ with its velocity in the interval $\mathbf{dc}_1$ centered at $\mathbf{c}_1$ while particle k is located within $\mathbf{dr}_2$ at $\mathbf{r}_2$ with its velocity in the interval $\mathbf{dc}_2$ at $\mathbf{c}_2$. Suppose that at time t particle i is located in $\mathbf{dr}$ at $\mathbf{r}$ with its velocity in $\mathbf{dc}_1$ at $\mathbf{c}_1$; then, in an increment of time dt, the number of particles with velocities in $\mathbf{dc}_2$ at $\mathbf{c}_2$ that will collide with it over that part of its boundary within the angle dk at $\mathbf{k}$ is

$$f_{ik}^{(2)}(\mathbf{c}_1,\mathbf{r},\mathbf{c}_2,\mathbf{r}-\sigma_{ik}\mathbf{k})\sigma_{ik}(\mathbf{k}\cdot\mathbf{c}_{21})dk\mathbf{dc}_1\mathbf{dc}_2\mathbf{dr}dt, \tag{21}$$

where $\sigma_{ik} \equiv \sigma_i + \sigma_k$ and, for impending collisions, $\mathbf{k}\cdot\mathbf{c}_{21}$ must be positive. The factor $\sigma_{ik}(\mathbf{k}\cdot\mathbf{c}_{21})dkdt$ is the area of the parallelopiped in which the centers of the particles of species k must reside in order for such a collision to occur. Then the collisional rate of production $\mathcal{C}_{ik}(\psi_i)$ per unit area at $\mathbf{r}$ is given by

$$\mathcal{C}_{ik}(\psi) = \sigma_{ik}\int\int\int\Big[\psi_i(\mathbf{c}_1')-\psi_i(\mathbf{c}_1)\Big]f_{ik}^{(2)}(\mathbf{c}_1,\mathbf{r},\mathbf{c}_2,\mathbf{r}-\sigma_{ik}\mathbf{k}) \times(\mathbf{k}\cdot\mathbf{c}_{21})dkd\mathbf{c}_1\mathbf{dc}_2. \tag{22}$$

where the integrations are to be carried out over all values of the variables for which a collision is impending, $\mathbf{k}\cdot\mathbf{c}_{21} > 0$.

Following Dahler and Sather (1963), we decompose $\mathcal{C}_{ik}(\psi_i)$ into two parts:

$$\mathcal{C}_{ik}(\psi_i) = \mathfrak{N}_{ik}(\psi_i) + \Delta_{ik}(\psi_i), \tag{23}$$

where

$$\mathfrak{N}_{ik}(\psi_i) \equiv \frac{1}{2}\sigma_{ik}\int\int\int(\psi_i'-\psi_i)(\mathbf{k}\cdot\mathbf{c}_{21})\Big[f_{ik}^{(2)}(\mathbf{c}_1,\mathbf{r},\mathbf{c}_2,\mathbf{r}-\sigma_{ik}\mathbf{k}) + f_{ki}^{(2)}(\mathbf{c}_2,\mathbf{r},\mathbf{c}_1,\mathbf{r}+\sigma_{ik}\mathbf{k})\Big]dk\mathbf{dc}_1\mathbf{dc}_2, \tag{24}$$

and

$$\Delta_{ik}(\psi_i) \equiv \frac{1}{2}\sigma_{ik}\int\int\int(\psi_i'-\psi_i)(\mathbf{k}\cdot\mathbf{c}_{21})\Big[f_{ik}^{(2)}(\mathbf{c}_1,\mathbf{r},\mathbf{c}_2,\mathbf{r}-\sigma_{ik}\mathbf{k}) - f_{ki}^{(2)}(\mathbf{c}_2,\mathbf{r},\mathbf{c}_1,\mathbf{r}+\sigma_{ik}\mathbf{k})\Big]dk\mathbf{dc}_1\mathbf{dc}_2, \tag{25}$$

for $\mathbf{k}\cdot\mathbf{c}_{21} > 0$. If the particle property ψ is conserved in a collision,

$$\psi_i' + \psi_k' = \psi_i + \psi_k; \tag{26}$$

then

$$\mathfrak{N}_{ik}(\psi_i) = -\mathfrak{N}_{ki}(\psi_k) \text{ and } \Delta_{ik}(\psi_i) = \Delta_{ki}(\psi_k). \tag{27}$$

In the integrals (24) and (25) we employ the Taylor series expansions for $f_{ik}^{(2)}(\mathbf{c}_1,\mathbf{r},\mathbf{c}_2,\mathbf{r}-\sigma_{ik}\mathbf{k})$ at $\mathbf{r}+(1/2)\ \sigma_{ik}\mathbf{k}$ and $f_{ki}^{(2)}(\mathbf{c}_2,\mathbf{r},\mathbf{c}_1,\mathbf{r}+\sigma_{ik}\mathbf{k})$ at $\mathbf{r}-(1/2)\ \sigma_{ik}\mathbf{k}$ to obtain

$$\mathfrak{N}_{ik}(\psi_i) = \sigma_{ik}\int\int\int(\psi_i'-\psi_i)(\mathbf{k}\cdot\mathbf{c}_{21}) \times\Big[1+(1/2!2^2)\sigma_{ik}^2(\mathbf{k}\cdot\nabla)^2+\ldots\Big] \times f_{ik}^{(2)}\Big(\mathbf{c}_1,\mathbf{r}+\frac{1}{2}\sigma_{ik}\mathbf{k},\mathbf{c}_2,\mathbf{r}-\frac{1}{2}\sigma_{ik}\mathbf{k}\Big)dk\mathbf{dc}_1\mathbf{dc}_2, \tag{28}$$

and

$$\Delta_{ik}(\psi_i) = -\nabla\cdot\Big[\boldsymbol{\Theta}_{ik}(\psi_i)\Big], \tag{29}$$

where, when $\psi_i = \psi_i(\mathbf{c}_i)$,

$$\boldsymbol{\Theta}_{ik}(\psi_i) = \frac{1}{2}\sigma_{ik}^2\int\int\int\mathbf{k}(\psi_i'-\psi_i)(\mathbf{k}\cdot\mathbf{c}_{21}) \times\Big[1+(1/3!2^2)\sigma_{ik}^2(\mathbf{k}\cdot\nabla)^2+\ldots\Big] \times f_{ik}^{(2)}\Big(\mathbf{c}_1,\mathbf{r}+\frac{1}{2}\sigma_{ik}\mathbf{k},\mathbf{c}_2,\mathbf{r}-\frac{1}{2}\sigma_{ik}\mathbf{k}\Big)dk\mathbf{dc}_1\mathbf{dc}_2, \tag{30}$$

for $\mathbf{k}\cdot\mathbf{c}_{21} > 0$.

Note, however, that if $\psi_i = \psi_i(\mathbf{C}_i)$, then, because $\mathbf{u}$ depends upon $\mathbf{r}$, there is an additional term in the expression for $\Delta_{ik}(\psi_i)$,

$$\Delta_{ik}(\psi_i) = -\nabla\cdot[\boldsymbol{\Theta}_{ik}(\psi_i)] - tr\Big[\boldsymbol{\Theta}_{ik}\Big(\frac{\partial\psi_i}{\partial\mathbf{C}_i}\Big)\nabla\mathbf{u}\Big]. \tag{31}$$

Here tr denotes the trace and, in terms of Cartesian components, $(\nabla\mathbf{u})_{\alpha\beta} \equiv u_{\alpha,\beta}$; so, for example, $tr[\boldsymbol{\Theta}(\mathbf{C})\nabla\mathbf{u}] = \Theta_\alpha(C_\beta)u_{\beta,\alpha}$, where Greek indices take the values 1 and 2 and the summation convention has been employed.

The balance law (20) for a particle property $\psi_i = \psi_i(\mathbf{c}_i)$ of species i may now be written in the form

$$\frac{\partial}{\partial t}\langle n_i\psi_i\rangle + \nabla\cdot\Big[\langle n_i\mathbf{c}_i\psi_i\rangle + \sum_{k=A,B}\boldsymbol{\Theta}_{ik}(\psi_i)\Big] - n_i\frac{\mathbf{F}_i}{m_i}\cdot\Big\langle\frac{\partial\psi_i}{\partial\mathbf{c}_i}\Big\rangle = \sum_{k=A,B}\chi_{ik}(\psi_i), \tag{32}$$

where i is A or B.

For example, when $\psi_i = m_i$, the mass balance for species i results:

$$\frac{\partial\rho_i}{\partial t} + \nabla\cdot(\rho_i\mathbf{u}_i) = 0. \tag{33}$$

If we sum the individual mass balances and employ the definition (14) of the barycentric velocity, we may write the mixture mass balance as

$$\dot{\rho} + \rho\nabla\cdot\mathbf{u} = 0, \tag{34}$$

where the overdot indicates a time derivative calculated with respect to the barycentric motion.

If $\psi_i = m_i\mathbf{c}_i$ in equation (32), the balance of linear momentum for species i is obtained:

$$\frac{\partial}{\partial t}(\rho_i\mathbf{u}_i) + \nabla\cdot(\rho_i\mathbf{u}_i\mathbf{u}_i + \boldsymbol{\pi}_i) - n_i\mathbf{F}_i = \boldsymbol{\phi}_i. \tag{35}$$

In this, the species pressure tensor $\boldsymbol{\pi}_i$ is the sum of diffusional, transport, and collisional contributions:

$$\boldsymbol{\pi}_i \equiv -\rho_i\mathbf{v}_i\mathbf{v}_i + \langle\rho_i\mathbf{C}_i\mathbf{C}_i\rangle + \sum_{k=A,B}\mathbf{P}_{ik}, \tag{36}$$

where

$$\mathbf{P}_{ik} \equiv \boldsymbol{\Theta}_{ik}(m_i\mathbf{c}_i); \tag{37}$$

and

$$\boldsymbol{\phi}_i \equiv \chi_{ik}(m_i\mathbf{c}_i), \text{ for } i \neq k. \tag{38}$$

As a consequence of equation (6), the collisional pressure tensors $\mathbf{P}_{ik}$ are symmetric and, because linear momentum is conserved in a collision, the momentum source $\boldsymbol{\phi}_i$ results only from collisions between unlike particles.

Upon summing the individual linear momentum balances, recalling the definitions and properties of the various velocities, and employing the mixture mass balance (34), we may write the balance of linear momentum for the mixture as

$$\rho\dot{\mathbf{u}} = -\nabla\cdot\mathbf{P} + n\mathbf{F}, \tag{39}$$

where the total pressure tensor $\mathbf{P}$ is the sum of the conductive pressure tensors $\mathbf{P}_i$ of each species.

$$\mathbf{P}_i \equiv \boldsymbol{\pi}_i + \rho_i\mathbf{v}_i\mathbf{v}_i = \langle\rho_i\mathbf{C}_i\mathbf{C}_i\rangle + \sum_{k=A,B}\mathbf{P}_{ik}; \tag{40}$$

Downloaded 03 May 2010 to 171.66.16.27. Redistribution subject to ASME license or copyright; see http://www.asme.org/terms/Terms_Use.cfm

$$n\mathbf{F} \equiv n_A \mathbf{F}_A + n_B \mathbf{F}_B; \tag{41}$$

and we have used

$$\phi_A \equiv \chi_{AB}(m_A \mathbf{c}_A) = -\chi_{BA}(m_B \mathbf{c}_B) \equiv -\phi_B. \tag{42}$$

When the particle property ψ_i is a function of $\mathbf{C}_i$ rather than $\mathbf{c}_i$, the form of the balance law is more complicated. In this case, the intrinsic change in ψ_i is due to both the change in $\mathbf{c}_i$ and to the variation in $\mathbf{u}$ following the particle, and the additional term in the decomposition of the collisional production must be employed:

$$\frac{\partial}{\partial t}\langle n_i \psi_i \rangle + \nabla \cdot \left[\langle n_i \mathbf{c}_i \psi_i \rangle + \sum_{k=A,B} \boldsymbol{\Theta}_{ik}(\psi_i) \right] + \sum_{k=A,B} tr\left[\boldsymbol{\Theta}_{ik} \left(\frac{\partial \psi_i}{\partial \mathbf{C}_i} \right) \nabla \mathbf{u} \right] - \left\langle n_i \frac{d\mathbf{C}_i}{dt} \cdot \frac{\partial \psi_i}{\partial \mathbf{C}_i} \right\rangle = \sum_{k=A,B} \chi_{ik}(\psi_i), \tag{43}$$

where

$$\frac{d\mathbf{C}_i}{dt} = \frac{\mathbf{F}_i}{m_i} - \frac{\partial \mathbf{u}}{\partial t} - (\mathbf{c}_i \cdot \nabla)\mathbf{u}, \tag{44}$$

or, with equation (39),

$$\frac{d\mathbf{C}_i}{dt} = \frac{\mathbf{F}_i}{m_i} - (\mathbf{C}_i \cdot \nabla)\mathbf{u} + \frac{1}{\rho}(\nabla \cdot \mathbf{P} - n\mathbf{F}). \tag{45}$$

Then, for example, if $\psi = m_i C_i^2/2$, the balance of fluctuation energy for species i results:

$$\frac{\partial}{\partial t}(n_i T_i) + \nabla \cdot (n_i \mathbf{u}_i T_i + \mathbf{Q}_i) + tr(\mathbf{P}_i \nabla \mathbf{u}) - n_i \mathbf{F}_i \cdot \mathbf{v}_i - \frac{\rho_i}{\rho} \mathbf{v}_i \cdot (\nabla \cdot \mathbf{P} - n\mathbf{F}) = \gamma_i. \tag{46}$$

Here $\mathbf{Q}_i$ is the species energy flux,

$$\mathbf{Q}_i \equiv -n_i \mathbf{v}_i T_i + \frac{1}{2}\langle \rho_i \mathbf{C}_i C_i^2 \rangle + \sum_{k=A,B} \mathbf{q}_{ik}, \tag{47}$$

where

$$\mathbf{q}_{ik} \equiv \boldsymbol{\Theta}_{ik}(m_i C_i^2/2); \tag{48}$$

and γ_i is the collisional energy source,

$$\gamma_i \equiv \sum_{k=A,B} \chi_{ik}(m_i C_i^2/2). \tag{49}$$

If we sum the energy balances (46), we obtain, after some familiar manipulations, the balance of fluctuation energy for the mixture

$$n\dot{T} - T\nabla \cdot \mathbf{j} = -\nabla \cdot \mathbf{q} - tr(\mathbf{P}\nabla \mathbf{u}) + \sum_{i=A,B} \mathbf{F}_i \cdot \mathbf{j} - \gamma. \tag{50}$$

In this, $\mathbf{j}$ is the particle flux,

$$\mathbf{j} \equiv n_A \mathbf{v}_A + n_B \mathbf{v}_B; \tag{51}$$

the mixture energy flux $\mathbf{q}$ is the sum of the conductive energy fluxes $\mathbf{q}_i$,

$$\mathbf{q}_i \equiv \mathbf{Q}_i + n_i \mathbf{v}_i T_i = \frac{1}{2}\langle \rho_i \mathbf{C}_i C_i^2 \rangle + \sum_{k=A,B} \mathbf{q}_{ik}; \tag{52}$$

and the rate of dissipation γ is negative of the sum of the collisional energy sources γ_i.

Finally, if we take $\psi_i = m_i \mathbf{C}_i$ in equation (31), we obtain the balance law for the diffusion velocity $\mathbf{v}_i$ which, after employing several of the balance laws already derived, we may write as

$$\frac{\partial \mathbf{v}_i}{\partial t} + (\mathbf{u}_i \cdot \nabla)\mathbf{v}_i = -(\mathbf{v}_i \cdot \nabla)\mathbf{u} + \frac{1}{\rho}(\nabla \cdot \mathbf{P} - n\mathbf{F}) - \frac{1}{\rho_i} \nabla \cdot \pi_i + \frac{1}{m_i} \mathbf{F}_i + \frac{1}{\rho_i} \phi_i. \tag{53}$$

Alternatively, this equation may be obtained directly from the balance law (35).

Constitutive Relations

In order to calculate the collisional fluxes $\mathbf{P}_{ik}$ and $\mathbf{q}_{ik}$ and the collisional sources ϕ_i and γ_i, we must have definite forms for the complete pair distribution functions $f_{ik}^{(2)}(\mathbf{c}_1, \mathbf{r} + 1/2\,\sigma_{ik}\mathbf{k}, \mathbf{c}_2, \mathbf{r} - 1/2\,\sigma_{ik}\mathbf{k})$ at contact.

We ignore any correlation in the velocities of a pair of disks just prior to their collision and employ Enkog's method of accounting for the correlations in the positions of the pair. Then the complete pair distribution functions at collision may be written as the product of the single particle velocity distribution functions of each disk and a factor that accounts for the fact that the area of the disks is a significant fraction of the area occupied by the granular material:

$$f_{ik}^{(2)}(\mathbf{c}_1, \mathbf{r} + \frac{1}{2}\sigma_{ik}\mathbf{k}, \mathbf{c}_2, \mathbf{r} - \frac{1}{2}\sigma_{ik}\mathbf{k}) = g_{ik}(\mathbf{r}) f_i^{(1)}(\mathbf{c}_1, \mathbf{r} + \frac{1}{2}\sigma_{ik}\mathbf{k}) f_k^{(1)}(\mathbf{c}_2, \mathbf{r} - \frac{1}{2}\sigma_{ik}\mathbf{k}). \tag{54}$$

The factors g_{ik} incorporate the effects of excluded area and particle shielding on the spatial distribution of colliding pairs. They are the local equilibrium values of the radial distribution functions, assumed here to be evaluated at the midpoint of the line of centers of a colliding pair. We obtain these as functions of the radii and the number densities in a way similar to that employed by Mansoori et al. (1971) for mixtures of spheres. They generate them from the contact radial distribution function for identical spheres proposed by Carnahan and Starling (1969). The corresponding generalization of Verlet and Levesque's (1982) contact radial distribution function for identical disks is

$$g_{ik} = \frac{1}{1-\nu} + \frac{9}{8} \frac{\sigma_i \sigma_k}{(\sigma_i + \sigma_k)} \frac{\zeta}{(1-\nu)^2}, \tag{55}$$

where ν is the total area fraction, given as the sum of the species area fractions $\nu_i \equiv n_i \pi \sigma_i^2$, and $\zeta \equiv \pi(n_A \sigma_A + n_B \sigma_B)$. We find that mixture pressures (given later in equation (78)) based upon equation (55) are in excellent agreement with the results of numerical simulations carried out by Dickinson (1977).

We must next specify the form of the single particle velocity distribution functions $f_i^{(1)}(\mathbf{c}, \mathbf{r}, t)$. Here, rather than attempt to determine them as solutions to the appropriate form of Boltzmann's equation, we simply suppose that they are Maxwellian:

$$f_i^{(1)}(\mathbf{c}, \mathbf{r}, t) = \frac{n_i m_i}{2\pi T_i} \exp\left[\frac{-m_i (\mathbf{c} - \mathbf{u}_i)^2}{2T_i} \right], \tag{56}$$

where $(\mathbf{c} - \mathbf{u}_i)^2 \equiv (\mathbf{c} - \mathbf{u}_i) \cdot (\mathbf{c} - \mathbf{u}_i)$. The mean fields n_i, T_i, and $\mathbf{u}_i$ are to be evaluated at the position $\mathbf{r}$ of the center of the disk of species i at time t. In distinguishing between the positions of the centers of a pair of colliding disks in equation (54), we retain the possibility of calculating collisional fluxes of particle properties for even the Maxwellian distributions. These could be improved upon, at the expense of much more elaborate computations, by determining the perturbations to the Maxwellians using the procedure of Chapman and Enskog.

The velocity distributions will be nearly Maxwellian if the spatial gradients of the mean fields are small and the disks are

Downloaded 03 May 2010 to 171.66.16.27. Redistribution subject to ASME license or copyright; see http://www.asme.org/terms/Terms_Use.cfm

nearly elastic. Consequently, we restrict our attention to such situations. We further suppose that the diffusion velocities $\mathbf{v}_i$ are small and that the species temperatures T_i differ by small quantities θ_i from the mixture temperature T:

$$T_i = T + \theta_i, \text{ with } n_A\theta_A + n_B\theta_B = 0. \tag{57}$$

In this event the complete pair distribution function (54) can be expanded as a Taylor series about $\mathbf{r}$ and expressed in terms of $\mathbf{v}_i$ and θ_i with an error that is quadratic in small quantities:

$$f_{ik}^{(2)}\left(\mathbf{c}_1,\mathbf{r}+\frac{1}{2}\sigma_{ik}\mathbf{k},\mathbf{c}_2,\mathbf{r}-\frac{1}{2}\sigma_{ik}\mathbf{k}\right)$$
$$= g_{ik}\frac{n_in_km_im_k}{(2\pi T)^2}\Big\{1+\frac{1}{2}\sigma_{ik}(\mathbf{k}\cdot\nabla)\left(\ell n\frac{n_i}{n_k}\right)$$
$$+\frac{1}{2}\sigma_{ik}\Big[\frac{m_i}{2T^2}(\mathbf{V}_{ik}+M_k\mathbf{c}_{21})^2-\frac{m_k}{2T^2}(\mathbf{V}_{ik}$$
$$-M_i\mathbf{c}_{21})^2\Big](\mathbf{k}\cdot\nabla)T$$
$$+\frac{1}{2}\sigma_{ik}\Big[\frac{m_i}{T}(\mathbf{V}_{ik}+M_k\mathbf{c}_{21})-\frac{m_k}{T}(\mathbf{V}_{ik}$$
$$-M_i\mathbf{c}_{21})\Big]\cdot\Big[(\mathbf{k}\cdot\nabla)\mathbf{u}\Big]$$
$$+\frac{m_i}{T}(\mathbf{V}_{ik}+M_k\mathbf{c}_{21})\cdot\mathbf{v}_i+\frac{m_k}{T}(\mathbf{V}_{ik}-M_i\mathbf{c}_{21})\cdot\mathbf{v}_k$$
$$+\frac{m_i}{2T^2}(\mathbf{V}_{ik}+M_k\mathbf{c}_{21})^2\theta_i+\frac{m_k}{2T^2}(\mathbf{V}_{ik}-M_i\mathbf{c}_{21})^2\theta_k$$
$$-\frac{1}{T}(\theta_i+\theta_k)\Big\}\exp\left(-\frac{m_{ik}}{2T}V_{ik}^2-\frac{m_im_k}{2m_{ik}T}c_{21}^2\right), \tag{58}$$

where we recall that $M_i = m_i/m_{ik}$,

$$\mathbf{V}_{ik}\equiv\mathbf{G}_{ik}-\mathbf{u}=M_i\mathbf{c}_1+M_k\mathbf{c}_2-\mathbf{u}, \tag{59}$$

and the mean fields and their spatial derivatives are evaluated at the midpoint $\mathbf{r}$ of the line of centers.

In the general expression for the collisional source (28) and the collisional flux (30), we retain only the first term in the Taylor series expansion. Then, upon employing the definitions (37), (38), (48), and (49) and making use of the integral tables provided by Jenkins and Richman (1985b), we may carry out the integrations for $\mathbf{P}_{ik}$, $\boldsymbol{\phi}_i$, $\mathbf{q}_{ik}$, and γ_i. The results are:

$$\mathbf{P}_{ik}=\frac{\pi}{4}g_{ik}\sigma_{ik}^2n_in_k(1+e_{ik})\Big\{\Big(T+\frac{m_i\theta_k+m_k\theta_i}{m_{ik}}\Big)\mathbf{1}$$
$$-\sigma_{ik}\left(\frac{2m_im_kT}{\pi m_{ik}}\right)^{1/2}\left[\mathbf{D}+\frac{1}{2}(tr\mathbf{D})\mathbf{1}\right]\Big\}, \tag{60}$$

where $\mathbf{1}$ is the unit tensor and $\mathbf{D}$ is the symmetric part of the velocity gradients,

$$2\mathbf{D}\equiv\nabla\mathbf{u}+(\nabla\mathbf{u})^T, \tag{61}$$

with the superscript T indicating the transpose:

$$\boldsymbol{\phi}_i=\frac{\pi}{4}g_{ik}\sigma_{ik}^2n_in_k(1+e_{ik})T\Big[\Big(\frac{m_k-m_i}{m_{ik}}\Big)\nabla\ell nT$$
$$+\nabla\ell n\frac{n_i}{n_k}+\frac{4}{\sigma_{ik}}\left(\frac{2m_im_k}{\pi m_{ik}T}\right)^{1/2}(\mathbf{v}_k-\mathbf{v}_i)\Big], \tag{62}$$

for $i \neq k$;

$$\mathbf{q}_{ik}=g_{ik}\sigma_{ik}^2\frac{n_in_k}{m_{ik}}(1+e_{ik})T\Big\{\Big[-\frac{1}{2}\sigma_{ik}\left(\frac{2\pi m_im_kT}{m_{ik}}\right)^{1/2}\nabla\ell nT$$
$$+\frac{\pi}{4}(m_i\mathbf{v}_i+m_k\mathbf{v}_k)\Big]$$
$$-\frac{m_k}{m_{ik}}(1-e_{ik})\Big[\frac{3}{16}\sigma_{ik}(m_k-m_i)\left(\frac{2\pi m_{ik}T}{m_im_k}\right)^{1/2}\nabla\ell nT$$
$$+\frac{1}{8}\sigma_{ik}\left(\frac{2\pi m_{ik}^3T}{m_im_k}\right)^{1/2}\nabla\ell n\frac{n_i}{n_k}+\frac{3\pi}{8}m_{ik}(\mathbf{v}_k-\mathbf{v}_i)\Big]\Big\}; \tag{63}$$

and

$$\gamma_i=\sum_{k=A,B}2g_{ik}\sigma_{ik}n_in_k(1+e_{ik})T\Big\{\frac{\pi}{8}\sigma_{ik}\left(\frac{m_i-m_k}{m_{ik}}\right)(tr\mathbf{D})$$
$$-\left(\frac{2\pi m_im_kT}{m_{ik}}\right)^{1/2}\left(\frac{\theta_i-\theta_k}{m_{ik}T}\right)$$
$$-\frac{m_k}{m_{ik}}(1-e_{ik})\Big[\frac{1}{2}\left(\frac{2\pi m_{ik}T}{m_im_k}\right)^{1/2}-\frac{3\pi}{8}\sigma_{ik}(tr\mathbf{D})$$
$$+\frac{3}{4}\left(\frac{2\pi m_{ik}T}{m_im_k}\right)^{1/2}\left(\frac{m_i\theta_k+m_k\theta_i}{m_{ik}T}\right)\Big]\Big\}. \tag{64}$$

For nearly elastic disks the constitutive relations may be simplified further. In this case the $(1 - e_{ik})$ are small quantities so, to the order of the approximation, we may replace $(1 + e_{ik})$ by two and ignore products of $(1 - e_{ik})$ with the spatial gradients or the perturbations θ_i and $\mathbf{v}_i$.

With the single particle velocity distribution function (56) we may also calculate the transport fluxes of momentum energy. These are

$$\rho_i\langle\mathbf{C}_i\mathbf{C}_i\rangle = n_i(T+\theta_i)\mathbf{1}, \tag{65}$$

and

$$\rho_i\langle\mathbf{C}_iC_i^2\rangle/2 = 2n_iT\,\mathbf{v}_i, \tag{66}$$

respectively.

We next indicate how the "constitutive relation" corresponding to Fick's law is obtained from the balance law (53) for the species i diffusion velocity. We ignore the inertia associated with diffusion and the nonlinear term $(\mathbf{v}_i\cdot\nabla)\mathbf{u}$ and subtract the resulting equation for species B from that for species A:

$$0=-\frac{1}{\rho_A}\nabla\cdot\pi_A+\frac{1}{\rho_B}\nabla\cdot\pi_B+\frac{1}{m_A}\mathbf{F}_A$$
$$-\frac{1}{m_B}\mathbf{F}_B+\frac{1}{\rho_A}\boldsymbol{\phi}_A-\frac{1}{\rho_B}\boldsymbol{\phi}_B. \tag{67}$$

In this we suppose that the species pressure tensors π_i are approximated by their lowest order, isotropic parts:

$$\pi_i=\Big(n_i+\sum_{k=A,B}\frac{\pi}{2}g_{ik}\sigma_{ik}^2n_in_k\Big)T\,\mathbf{1}. \tag{68}$$

Then, upon employing the constitutive relation (62), we obtain the desired expression for the velocity of diffusion $\mathbf{v}_A - \mathbf{v}_B$,

$$\mathbf{v}_A-\mathbf{v}_B=-\frac{n^2}{n_An_B}D_{AB}\Big\{\frac{\rho_A\rho_B}{\rho nT}\left(\frac{\mathbf{F}_B}{m_B}-\frac{\mathbf{F}_A}{m_A}\right)$$
$$+\frac{\rho_B}{\rho nT}\nabla\Big[n_AT(1+b_A\rho_Ag_{AA}+b_B'\rho_Bg_{AB})\Big]$$
$$-\frac{\rho_A}{\rho nT}\nabla\Big[n_BT(1+b_B\rho_Bg_{BB}+b_A'\rho_Ag_{AB})\Big]$$
$$+\frac{\pi}{2}\frac{n_An_B}{n}\sigma_{AB}^2g_{AB}\Big[\Big(\frac{m_A-m_B}{m_{AB}}\Big)\nabla\ell nT$$
$$+\nabla\ell n\frac{n_B}{n_A}\Big]\Big\} \tag{69}$$

where the diffusion coefficient D_{AB} is given by

Downloaded 03 May 2010 to 171.66.16.27. Redistribution subject to ASME license or copyright; see http://www.asme.org/terms/Terms_Use.cfm

$$D_{AB}=\frac{1}{2n\sigma_{AB}g_{AB}}\left(\frac{m_{AB}T}{2\pi m_A m_B}\right)^{1/2}, \tag{70}$$

and

$$b_A\rho_A\equiv 2\pi n_A\sigma_A^2,\ b'_B\rho_B\equiv\frac{\pi}{2}\,n_B\sigma_{AB}^2,$$

$$b_B\rho_B\equiv 2\pi n_B\sigma_B^2,\ b'_A\rho_A\equiv\frac{\pi}{2}\,n_A\sigma_{AB}^2. \tag{71}$$

For a binary mixture of elastic spheres, Chapman and Cowling (1970, Sec. 16.6) provide the corresponding but slightly more elaborate expression that results from Enskog's method of solution of the Boltzmann equation.

Finally, we obtain an expression, analogous to equation (69), for the difference in the temperature perturbations by dividing the species energy equations (46) by their respective densities, subtracting, and ignoring the time derivatives and terms quadratic in small quantities:

$$\begin{aligned}\theta_B-\theta_A=\frac{nm_{AB}}{2\rho}\,D_{AB}\Big\{\Big[&m_B(1+b_A\rho_A g_{AA})\\&+2(m_B^2b'_B\rho_B-m_A^2b'_A\rho_A)\frac{g_{AB}}{m_{AB}}\\&-m_A(1+b_B\rho_B g_{BB})\Big]tr\mathbf{D}+2\Big[(1-e_{AA})m_Bb_A\rho_A\,\frac{g_{AA}}{\sigma_A m_A^{1/2}}\\&+2\sqrt{2}(1-e_{AB})\,(m_B^2b'_B\rho_B\\&-m_A^2b'_A\rho_A)\frac{g_{AB}}{\sigma_{AB}(m_Am_Bm_{AB})^{1/2}}\\&-(1-e_{BB})m_Ab_B\rho_B\,\frac{g_{BB}}{\sigma_B m_B^{1/2}}\Big]\left(\frac{T}{\pi}\right)^{1/2}\\&+\frac{1}{\rho T}(m_A\mathbf{F}_B-m_B\mathbf{F}_A)\cdot(\rho_A\mathbf{v}_B+\rho_B\mathbf{v}_A)\Big\}.\end{aligned} \tag{72}$$

Shear Flow

We illustrate the use of the theory by applying it to a steady rectilinear shearing flow, supposed to be maintained in the absence of external forces by the relative motion of parallel boundaries. We employ rectangular Cartesian coordinates x and z and assume that the x component u of the barycentric velocity, the mixture temperature T, the perturbations θ_i, and the number densities n_i are functions of z alone. In this steady flow, the diffusion velocities $\mathbf{v}_i$ are zero and both species move with the barycentric velocity.

In this event, the x and z components of the mixture momentum balance (39) reduce to

$$P'_{zx}=0 \text{ and } P'_{zz}=0, \tag{73}$$

where a prime denotes a derivative with respect to z. In these

$$P_{zx}=-\mu u', \tag{74}$$

where the mixture viscosity μ is given by

$$\mu=\left[\frac{K_{AA}}{\sigma_A}\,m_A^{1/2}+4\,\frac{K_{AB}}{\sigma_{AB}}\left(\frac{2m_Am_B}{m_{AB}}\right)^{1/2}+\frac{K_{BB}}{\sigma_B}\,m_B^{1/2}\right]\left(\frac{T}{\pi}\right)^{1/2}, \tag{75}$$

with

$$K_{ij}=\frac{\pi}{8}\,n_in_j\sigma_{ij}{}^4g_{ij}, \tag{76}$$

and

$$P_{zz}=-p, \tag{77}$$

where the mixture pressure p is, to lowest order,

$$p=\left(n+\frac{K_{AA}}{\sigma_A^2}+8\,\frac{K_{AB}}{\sigma_{AB}^2}+\frac{K_{BB}}{\sigma_B^2}\right)T. \tag{78}$$

Upon integration of equations (73), we obtain

$$\mu u'=S \text{ and } -p=N, \tag{79}$$

where S and N are, respectively, the constant values of the shear and normal stress.

The mixture energy equation (50) is, for this flow,

$$-Q'_z+Su'-\gamma=0, \tag{80}$$

where

$$Q_z=-\kappa T', \tag{81}$$

with

$$\kappa\equiv 2\left[\frac{K_{AA}}{\sigma_Am_A}\,m_A^{1/2}+8\,\frac{K_{AB}}{\sigma_{AB}m_{AB}}\left(\frac{2m_Am_B}{m_{AB}}\right)^{1/2}+\frac{K_{BB}}{\sigma_Bm_B}\,m_B^{1/2}\right]\left(\frac{T}{\pi}\right)^{1/2}; \tag{82}$$

and

$$\begin{aligned}\gamma=2\Big[&(1-e_{AA})\frac{K_{AA}}{\sigma_A^3m_A}\,m_A^{1/2}\\&+8(1-e_{AB})\frac{K_{AB}m_{AB}}{\sigma_{AB}^3m_Am_B}\left(\frac{2m_Am_B}{m_{AB}}\right)^{1/2}\\&+(1-e_{BB})\frac{K_{BB}}{\sigma_B^3m_B}\,m_B^{1/2}\Big]\left(\frac{T^3}{\pi}\right)^{1/2}.\end{aligned} \tag{83}$$

Upon employing the first of equations (79) and (81), we may write the energy equation (80) as

$$(\kappa T')'+\mu^{-1}S^2-\gamma=0. \tag{84}$$

This and the second of equations (79) are two of the three equations governing n_A, n_B, and T.

The third equation is obtained from the expression (69) for the diffusion velocities. For the flow under consideration this may be written as

$$\frac{1}{T}\left[\left(n_A+\frac{K_{AA}}{\sigma_A^2}+4\,\frac{K_{AB}}{\sigma_{AB}^2}\right)T\right]'+4\,\frac{K_{AB}}{\sigma_{AB}^2}\left[\left(\frac{m_A-m_B}{m_{AB}}\right)(\ell nT)'+\left(\ell n\,\frac{n_B}{n_A}\right)'\right]=0, \tag{85}$$

where we have used the fact that the mixture pressure is constant to conclude that

$$\left[\left(n_B+\frac{K_{BB}}{\sigma_B^2}+4\,\frac{K_{AB}}{\sigma_{AB}^2}\right)T\right]'=-\left[\left(n_A+\frac{K_{AA}}{\sigma_A^2}+\frac{4K_{AB}}{\sigma_{AB}^2}\right)T\right]'. \tag{86}$$

The constants associated with the integrations that have been carried out are determined by employing suitable boundary conditions—for example the appropriate generalizations of those derived by Jenkins and Richman (1985c). We defer the integration of the remaining equations and the application of such boundary conditions to a sequel to this paper. However we note that, if there exist boundaries on which $T'=0$, then T, n_A, n_B, and u' can all be uniform throughout the flow. In this event, the simplification of the energy equation (84) used with equation $(79)_2$ yields

$$\left(\frac{S}{N}\right)^2=\frac{\mu\gamma}{p^2}, \tag{87}$$

or

$$\frac{\sigma_{AB}^2(u')^2}{T}=\frac{\sigma_{AB}^2\gamma}{T\mu}, \tag{88}$$

Downloaded 03 May 2010 to 171.66.16.27. Redistribution subject to ASME license or copyright; see http://www.asme.org/terms/Terms_Use.cfm

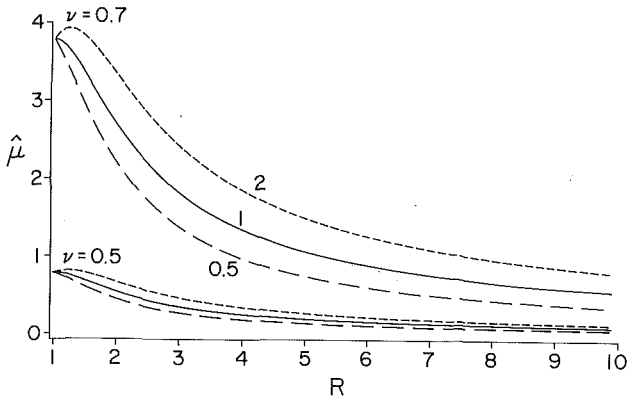


Fig. 1 Nondimensional viscosity versus radii ratio for three area ratios at two total area fractions

where the right-hand side of either is independent of T. The relations (87) and (88) are the analogs of those provided by Jenkins and Savage (1983, equations (62) and (63)) for identical, smooth, nearly elastic spheres.

As an example, we consider the homogeneous shearing of disks made of the same material. Then $e_{ik} = e$ and $m_A/m_B = (\sigma_A/\sigma_B)^2$. We use equation (88) to determine T and employ the result in the definition (75) of the mixture viscosity. We may then express the nondimensional mixture viscosity $\hat{\mu} \equiv \mu[2\pi^3(1-e)]^{1/2}/m_{AB}u'$ as a function of the area fractions ν_A and ν_B and the radii ratio $R \equiv \sigma_A/\sigma_B$:

$$\hat{\mu} = \frac{\nu_B^2 R^2}{(1+R^2)} \frac{[2(\nu_A/\nu_B)^2 g_{AA} + 2g_{BB} + \sqrt{2}(\nu_A/\nu_B) g_{AB}(1+R)^3/2R(1+R^2)^{1/2}]^{3/2}}{[2(\nu_A/\nu_B)^2 g_{AA} + 2R^4 g_{BB} + \sqrt{2}(\nu_A/\nu_B) g_{AB} R(1+R)(1+R^2)^{1/2}]^{1/2}} \tag{89}$$

where

$$g_{AA} = \frac{1}{(1-\nu)} + \frac{9}{16}\frac{\nu_A + \nu_B R}{(1-\nu)^2}, \tag{90}$$

$$g_{BB} = \frac{1}{(1-\nu)} + \frac{9}{16}\frac{\nu_A + \nu_B R}{R(1-\nu)^2}, \tag{91}$$

and

$$g_{AB} = \frac{1}{(1-\nu)} + \frac{9}{8}\frac{\nu_A + \nu_B R}{(1+R)(1-\nu)^2}. \tag{92}$$

In Fig. 1 we plot $\hat{\mu}$ versus R for two values of the total area fraction, $\nu = 0.5$ and 0.7. In each case we display curves for three values of the area ratio, $(\nu_A/\nu_B) = 0.5$, 1, and 2. The corresponding ratio of number densities is given in terms of R and the area ratio by

$$\frac{n_A}{n_B} = \frac{1}{R^2}\frac{\nu_A}{\nu_B}. \tag{93}$$

As might be expected, the nondimensional viscosity is always greater in the system with larger total area fraction. When the area fraction of the smaller disks is greater than that of the larger, this viscosity decreases as the difference in their radii increases. However, when the area fraction of the smaller disks is less than that of the larger, this viscosity initially increases to a maximum before decreasing. When the radii of the disks are much different, the assumption that the velocities of a colliding pair of disks are uncorrelated ceases to be valid and the representation (54) of the complete pair distribution function breaks down (see, for example, Sung and Stell (1982)). Consequently, values of the nondimensional viscosity around and beyond $R = 5$ should be regarded with suspicion.

Acknowledgment

We are grateful to M. W. Richman for his technical assistance and valuable discussions. This work was supported by a grant from the Geotechnical Engineering Division of the US National Science Foundation.

References

Carnahan, N. F., and Starling, K. E., 1969, "Equations of State of Nonattracting Rigid Spheres," *J. Chem. Phys.*, Vol. 51, pp. 635–636.

Campbell, C. S., and Brennen, C. E., 1982, "Computer Simulations of Shear Flow of Granular Materials," In *Mechanical of Granular Materials: New Models and Constitutive Relations*, Jenkins, J. T., and Satake, M., eds., Elsevier, Amsterdam, pp. 313–326.

Campbell, C. S., and Brennen, C. E., 1985, "Chute Flows of Granular Material: Some Computer Simulations," *J. Appl. Mech.*, Vol. 52, pp. 172–178.

Campbell, C. S., and Gong, A., 1985, "The Stress Tensor in a Two-Dimensional Granular Shear Flow," *J. Fluid Mech.*, Vol. 164, pp. 107–125.

Chapman, S., and Cowling, T. G., 1970, *The Mathematical Theory of Non-Uniform Gases*, Third Ed., University Press, Cambridge.

Condiff, D. W., Lu, W.-K., and Dahler, J. S., 1965, "Transport Properties of Polyatomic Fluids, a Dilute Gas of Perfectly Rough Spheres," *J. Chem. Physics*, Vol. 42, pp. 3445–3475.

Dahler, J. S., and Sather, N. F., 1963, "Kinetic Theory of Loaded Spheres," *J. Chem. Physics*, Vol. 38, pp. 2363–2382.

Dickinson, E., 1977, "Molecular Dynamics Simulation of Hard-Disk Mixtures. The Equation of State," *Mol. Phys.*, Vol. 33, pp. 1463–1478.

Jenkins, J. T., and Savage, S. B., 1983, "A Theory for the Rapid Flow of Identical, Smooth, Nearly Elastic, Spherical Particles," *J. Fluid Mech.*, Vol. 130, pp. 187–202.

Jenkins, J. T., and Richman, M. W., 1985a, "Grad's 13-Moment System for a Dense Gas of Inelastic Spheres," *Arch. Rat'l Mech. Anal.*, Vol. 87, pp. 355–377.

Jenkins, J. T., and Richman, M. W., 1985b, "Kinetic Theory for Plane Flows of a Dense Gas of Identical, Rough, Inelastic, Circular Disks," *Physics of Fluids*, Vol. 28, pp. 3485–3494.

Jenkins, J. T., and Richman, M. W., 1985c, "Boundary Conditions for Plane Flows of Smooth, Nearly Elastic, Circular Disks," *J. Fluid Mech.*, Vol. 171, pp. 53–69.

Longuet-Higgins, H. C., Pople, J. A., and Valleau, J. P., 1956, "The Transport of Energy and Matter in a Dense Two-Component Mixture of Hard Spheres," In *Transport Processes in Statistical Mechanics*, Prigogine, I., ed., Interscience, New York, pp. 73–96.

Lopez de Haro, M., Cohen, E. G. D., Kincaid, J. M., 1983, "The Enskog Theory for Multicomponent Mixtures. I. Linear Transport Theory," *J. Chem. Phys.*, Vol. 78, pp. 2746–2759.

Lun, C. K. K., Savage, S. B., Jeffrey, D. J., and Chepurniy, N., 1984, "Kinetic Theories for Granular Flow: Inelastic Particles in Couette Flow and Slightly Inelastic Particles in a General Flow Field," *J. Fluid Mech.*, Vol. 140, pp. 223–256.

Mansoori, G. A., Carnahan, N. F., Starling, K. E., and Leland, T. W., Jr., 1971, "Equilibrium Thermodynamic Properties of the Mixture of Hard Spheres," *J. Chem. Phys.*, Vol. 54, pp. 1523–1525.

Reed, T. M., and Gubbins, K. E., 1973, *Applied Statistical Mechanics*, McGraw-Hill, New York.

Shen, H. H., 1984, "Stress in Rapid Deformations of Spherical Solids with Nonuniform Sizes," *J. Particulate Sci. and Tech.*, Vol. 2, pp. 37–56.

Sung, W., and Stell, G., 1982, "Transport Theory of Binary Mixture with One Trace Component of Disparate Mass," *J. Chem. Phys.*, Vol. 77, pp. 4636–4649.

Tham, M. K., and Gubbins, K. E., 1971, "Kinetic Theory of Multicomponent Dense Fluid Mixtures of Rigid Spheres," *J. Chem. Phys.*, Vol. 55, pp. 268–279.

Verlet, L., and Levesque, D., 1982, "Integral Equations for Classical Fluids: III—The Hard Disks System," *Mol. Phys.*, Vol. 46, pp. 969–980.

Walton, O. R., and Braun, R. L., 1986, "Viscosity, Granular-Temperature and Stress Calculations for Shearing Assemblies of Inelastic, Frictional Disks," *J. Rheol.*, Vol. 30, pp. 949–980.

APPENDIX

Binary Mixtures of Spheres

In terms of the obvious extension of our notation from two to three dimensions, the expressions for the source and flux for colliding spheres may be obtained from equations (28) and (30) by multiplying the integral in each by an additional factor of σ_{ik} and regarding dk as an element of solid angle (Condiff, Lu, and Dahler, 1965, Appendix E). Then, upon employing the simplifications analogous to equations (54) and (56) and an expansion corresponding to equation (58), we find, with

Downloaded 03 May 2010 to 171.66.16.27. Redistribution subject to ASME license or copyright; see http://www.asme.org/terms/Terms_Use.cfm

the help of integral tables provided by Jenkins and Savage (1983) and Jenkins and Richman (1985a), that:

$$\mathbf{P}_{ik}=\frac{\pi}{3}\,g_{ik}\sigma_{ik}^3 n_i n_k(1+e_{ik})\left\{\left[T+\frac{m_i\theta_k+m_k\theta_i}{m_{ik}}\right]\mathbf{1}\right.$$
$$\left.-\frac{4}{5}\,\sigma_{ik}\left(\frac{2m_i m_k T}{\pi m_{ik}}\right)^{1/2}\left[\mathbf{D}+\frac{1}{2}(tr\mathbf{D})\mathbf{1}\right]\right\} \qquad (A1)$$

$$\boldsymbol{\phi}_i=\frac{\pi}{3}\,g_{ik}\sigma_{ik}^3 n_i n_k(1+e_{ik})T\left[\left(\frac{m_k-m_i}{m_{ik}}\right)\nabla \ell nT\right.$$
$$\left.+\nabla \ell n\,\frac{n_i}{n_k}+\frac{4}{\sigma_{ik}}\left(\frac{2m_i m_k}{\pi m_{ik}T}\right)^{1/2}(\mathbf{v}_k-\mathbf{v}_i)\right], \qquad (A2)$$

for $i \neq k$;

$$\mathbf{q}_{ik}=g_{ik}\sigma_{ik}^3\,\frac{n_i n_k}{m_{ik}}(1+e_{ik})T\left\{-\frac{2}{3}\,\sigma_{ik}\left(\frac{2\pi m_i m_k T}{m_{ik}}\right)^{1/2}\nabla \ell nT\right.$$
$$+\frac{\pi}{3}(m_i\mathbf{v}_i+m_k\mathbf{v}_k)$$
$$-\frac{m_k}{m_{ik}}(1-e_{ik})\left[\frac{1}{4}\,\sigma_{ik}(m_k-m_i)\left(\frac{2\pi m_{ik}T}{m_i m_k}\right)^{1/2}\nabla \ell nT\right.$$
$$+\frac{1}{6}\,\sigma_{ik}\left(\frac{2\pi m_{ik}^3 T}{m_i m_k}\right)^{1/2}\nabla \ell n\,\frac{n_i}{n_k} \qquad (A3)$$
$$\left.\left.+\frac{\pi}{2}\,m_{ik}(\mathbf{v}_k-\mathbf{v}_i)\right]\right\};$$

and

$$\gamma_i=\sum_{k=A,B}2g_{ik}\sigma_{ik}^2 n_i n_k(1+e_{ik})T\left\{\frac{\pi}{6}\,\sigma_{ik}\left(\frac{m_i-m_k}{m_{ik}}\right)(tr\mathbf{D})\right.$$
$$+2\left(\frac{2\pi m_i m_k T}{m_{ik}}\right)^{1/2}\left(\frac{\theta_k-\theta_i}{m_{ik}T}\right)$$
$$-\frac{m_k}{m_{ik}}(1-e_{ik})\left[\left(\frac{2\pi m_{ik}T}{m_i m_k}\right)^{1/2}-\frac{\pi}{2}\,\sigma_{ik}(tr\mathbf{D})\right.$$
$$\left.\left.+\frac{3}{2}\left(\frac{2\pi m_{ik}T}{m_i m_k}\right)^{1/2}\left(\frac{m_i\theta_k+m_k\theta_i}{m_{ik}T}\right)\right]\right\}. \qquad (A4)$$

In three-dimensions the temperature of a species is defined as two-thirds the mean of the kinetic energy of its velocity fluctuations; so the appropriate generalizations of equations (46), (47), and (50) have T replace by $3T/2$. The radial distribution functions at contact as determined by Mansoori et al. (1971) are given, for example, by Reed and Gubbins (1973, Chapter 9). In our notation they are

$$g_{ik}=\frac{1}{1-\nu}+\frac{6\sigma_i\sigma_k}{(\sigma_i+\sigma_k)}\,\frac{\xi}{(1-\nu)^2}+8\left(\frac{\sigma_i\sigma_k}{\sigma_i+\sigma_k}\right)^2\frac{\xi^2}{(1-\nu)^3} \qquad (A5)$$

where

$$\nu=\frac{4}{3}\,\pi(n_A\sigma_A{}^3+n_B\sigma_B{}^3) \qquad (A6)$$

and

$$\xi=\frac{2}{3}\,\pi(n_A\sigma_A{}^2+n_B\sigma_B{}^2). \qquad (A7)$$

For elastic spheres of equal radii, the expressions (A2) and (A3) for $\boldsymbol{\phi}_i$ and $\mathbf{q}_{ik}$ reduce to those calculated in a similar fashion by Longuet-Higgins, Pople, and Valleau (1970, Section V and VI).

Tham and Gubbins (1971) and Lopez de Haro et al. (1983) have employed Chapman and Enskog's methods to determine more exact constitutive relations for a dense, multicomponent mixture of elastic spheres with different masses and radii. These may be employed with the expression (A4) for the rate of energy dissipation in order to obtain what is likely the best possible constitutive theory for binary mixtures of smooth, nearly elastic, spheres.

Downloaded 03 May 2010 to 171.66.16.27. Redistribution subject to ASME license or copyright; see http://www.asme.org/terms/Terms_Use.cfm

The Modified Mixture Theory for Fluid-Filled Porous Materials: Theory

N. Katsube
Assistant Professor,
Department of Engineering Mechanics,
The Ohio State University,
Columbus, Ohio 43210
Assoc. Mem. ASME

M. M. Carroll
Professor,
Department of Mechanical Engineering,
The University of California,
Berkeley, Calif. 94720
Fellow ASME

The mixture theory by Green and Naghdi is modified and applied to the problems of flow-through porous materials. By introducing porosity, we make clear that two constituents occupying the same point in the original mixture theory are an equivalent homogeneous solid and an equivalent homogeneous fluid which, respectively, represent a porous solid and a porous fluid in the actual sample. The micro-mechanical response studied by Carroll and Katsube is introduced and detailed deformation and flow mechanisms are provided at each point of the mixture. The resulting theory is compared with Biot's theory and in fact reduces to Biot's theory when the fluid velocity gradient terms are ignored.

1 Introduction

From a continuum mechanics point of view, theories have been developed for mixtures, where each point of the continuum is co-occupied by two or more different constituents. Truesdell and Toupin [1] and Trusdell and Noll [2] originated the formulation of this basic theoretical framework in the context of modern continuum mechanics. By taking a different approach, Green and Naghdi [3] later established their mixture theory. Goodman and Cowin [4], Passman [5], and Nunziato and Walsh [6] have in turn applied mixture theories to the problems of granular material. An extensive review of mixture theories and applications is given by Atkin and Craine [7, 8].

Since mixture theories provide a fundamental description of the interaction of the constituents, attempts have been made to apply mixture theories to the problems of fluid flow through porous material (for example, Green and Steel [9], Crochet and Naghdi [10]). The conventional mixture theories, however, exhibit some difficulties in the application of fluid-filled porous materials. The mixture theories have been built on the basic assumption that particles of each constituent occupy the same point at time t. Because of this assumption, when fluid is removed, a solid material is left instead of a dry porous solid skeleton. While the conventional mixture theories can be successfully applied to the filtration processes where the porosity is very small, some modifications are necessary to the problems of fluid flow through highly porous materials. In an attempt to provide detailed constitutie relations in mixture theories, Morland [11] postulated that "the effective deformation," defined by a simple multiplicate decomposition of the deformation gradient, is related to effective stress through the constitutive law for each component as a single continuum. Garg [12–14] applied Morland's theory to various wave propagation problems. Although it is certainly acceptable to define effective deformations and effective stresses in any way, there is no guarantee that those two are actually related through the constitutive law for each component. More recently Bowen [15] included porosity as an internal state variable at each point of the mixture, assuming a constitutive equation of rate type. While the notion of introducing the porosity into the mixture theories is certainly innovative, the micro-mechanical responses of the constituents are not included in Bowen's theory, so that the shortcoming of the mixture theories previously discussed has not yet been overcome.

Apart from the development of mixture theories, some phenomenological approaches have been developed. Biot proposed his three-dimensional phenomenological theory in 1941 [16] and improved his theory through a series of papers [17–21]. His theory is based on the classical theory of linear elasticity and Darcy's law. Although Biot's theory was developed almost forty years ago, it still remains highly recognized. For example, Rice and Cleary [22] reformulated his theory and obtained stress diffusion solutions. In recent years, the constitutive relations for poroelastic solids have been investigated from viewpoints somewhat different from Biot. Nur and Byerlee [23] have obtained the expression of the effective stress law based on isotropic linear elasticity. Motivated by their work, Carroll [24] and Carroll and Katsube [25] have shown that the deformation of fluid-filled poroelastic solids can be separated into the three distinct deformation mechanisms, i.e., solid deformation, fluid compaction, and relative pore geometry change. Most recently Katsube [26, 27] has shown that the constitutive theory for the deformation of the solid and the compaction of fluid by Carroll and Katsube is identical to those proposed by Biot and has

Contributed by the Applied Mechanics Division for presentation at the 1987 Applied Mechanics, Biomechanics, and Fluids Engineering Conference, Cincinnati, OH, June 14–17, 1987, of the American Society of Mechanical Engineers.
Discussion of this paper should be addressed to the Editorial Department, ASME, United Engineering Center, 345 East 47th Street, New York, N.Y. 10017, and will be accepted until two months after final publication of the paper itself in the JOURNAL OF APPLIED MECHANICS. Manuscript received by ASME Applied Mechanics Division, June 15, 1984; final revision, June 24, 1986.
Paper No. 87-APM-7.

Copyright © 1987 by ASME
Downloaded 03 May 2010 to 171.66.16.27. Redistribution subject to ASME license or copyright; see http://www.asme.org/terms/Terms_Use.cfm

employed the same methods to investigate the fluid flow mechanisms, taking into account the stress due to fluid viscosity, which has not been included in Biot's constitutive theory.

The purpose of this present work is to possibly clarify the longtime discussion of the validity of the mixture theories in their application to the problems of fluid-filled porous material versus Biot's well-established theory. We start with the same assumptions as Biot: the solid matrix is linearly elastic, the fluid inside the pores is Newtonian viscous, the pores are all interconnected and fully saturated with a fluid, and the volumetric porosity of a porous material is initially uniform throughout the region. Introducing the micromechanical constitutive equations developed by Katsube [26], together with a new kinematical quantity, porosity, into the formulation of the mixture theory, we make it clear that a porous solid material and a porous fluid material in an actual sample are idealized as an equivalent homogeneous solid and equivalent homogeneous fluid, respectively, within the theoretical framework of the mixture theory. The kinetical and kinematical quantities of a solid and a fluid (without pores) which are related to those of a porous solid material and a porous fluid material, are introduced and the material constants which appear in the constitutive equations in the original mixture theory are expressed in terms of more physically meaningful material constants. Due to this modification, the difficulties associated with the recovery of a solid material without pores in the absence of a fluid in the original mixture theories are overcome. The resulting theory is found to be more general than Biot's theory since the shear interaction between the solid and the fluid is properly considered within the structure of the mixture theory and thus reduces to Biot's theory if the velocity gradient effect is suppressed. For example, examination of the equations of motion in the modified mixture theory reveals that Darcy's law is merely a special form of the equation of motion for an equivalent homogeneous fluid, in which the velocity gradient effect is ignored. In Katsube [27], the general features of the resulting theory are discussed through simple steady boundary value problems and the successfully approximated nature of Biot's theory are pointed out.

2 Constitutive Theory

We will first summarize the constitive equations obtained in Katsube [26]. We consider the response of a representative sample of an anisotropic fluid-filled porous material under the confining stress t_{ij}. This representative sample should be large enough to contain the detail of the micro-structure (e.g., several pores or grains) and small enough so that the average response is representative of the local response of the porous material idealized as a continuum. Introducing the total volume average stress t_{ij}, fluid volume average stress t^f_{ij}, solid volume average stress t^s_{ij}, and the volumetric porosity $\phi = V(R_f)/V(R)$ of this representative volume element, we have the following equations:

$$t_{ij} = \phi t^f_{ij} + (1-\phi)t^s_{ij} = t'_{ij} + t''_{ij} \tag{1}$$

$$t'_{ij} = -\phi P_f \delta_{ij} + (1-\phi)t^s_{ij} \tag{2}$$

$$t''_{ij} = \phi(t^f_{ij} + P_f \delta_{ij}) \tag{3}$$

While Equation $(1)_1$ is derived for volume averages, it has the appropriate form to describe the manner in which the total stress t_{ij} on a surface element with areal porosity ϕ in the porous material is shared by the fluid and the solid. In Equation $(1)_2$, the total stress is separated into the stress due to the deformation of the porous solid material with the effect of the hydrostatic fluid pressure, and the stress due to the viscous flow of the porous fluid material. The effect of pointwise stress distribution on the pore walls, on the overall deformation of the porous solid material, compared to that of the average hydraulic fluid pressure, is assumed to be negligible.

Focusing our attention on the deformation of the porous solid material, we represent the volume average infinitesimal strains of the porous solid material and the solid matrix by $e^{(1)}_{ij}$ and e^s_{ij}, respectively. Making use of the average strain theorem, which states that the volume average infinitesimal strain is determined by the geometry and the displacements of the boundary surface, we introdouce the infinitesimal strain of the pore space $e^{p(1)}_{ij}$. From their definitions of the volume averages, $e^{(1)}_{ij}$, e^s_{ij}, and $e^{p(1)}_{ij}$ are related by equation (4) and can be rewritten as equations (5):

$$e^{(1)}_{ij} = (1-\phi)e^s_{ij} + \phi e^{p(1)}_{ij} \tag{4}$$

$$e^{(1)}_{ij} = e^s_{ij} + e^{*(1)}_{ij}, e^{*(1)}_{ij} = \phi(e^{p(1)}_{ij} - e^s_{ij}). \tag{5}$$

Equation (5), which resolves the total strain of the porous solid material into a component due to solid volume strain and one due to change in relative pore geometry, is of importance because it identifies the two distinct physical processes of solid deformation and relative pore geometry change. If we remove the solid from the fluid-filled porous material, we will recover the porous fluid material in which the hydrostatic compaction should be investigated. Corresponding to $e^{(1)}_{ij}$, e^s_{ij}, and $e^{p(1)}_{ij}$ for the porous solid material, we introduce the average infinitesimal volumetric strain of the porous fluid material, the fluid, and the pore (of the porous fluid material), denoted by $e^{(2)}_{mm}$, e^f_{mm}, and $e^{p(2)}_{mm}$, respectively.

$$e^{(2)}_{mm} = \phi e^f_{mm} + (1-\phi)e^{p(2)}_{mm} \tag{6}$$

$$e^{(2)}_{mm} = e^f_{mm} + e^{*(2)}_{mm}, e^{*(2)}_{mm} = (1-\phi)(e^{p(2)}_{mm} - e^f_{mm}) \tag{7}$$

Equations (6) and (7) are the fluid counterpart of equations (4) and (5). The superscripts (1) and (2) indicate the association with the porous solid material and the porous fluid material, respectively. Limiting our attention to the hydrostatic case, the porosity change of the porous solid material $e^{*(1)}_{mm}$ and the porosity change of the porous fluid material $e^{*(2)}_{mm}$ are shown to be related to each other because a porous material is fully saturated with fluid after the deformation occurs:

$$(1-\phi)e^{*(1)}_{mm} = -\phi e^{*(2)}_{mm} \tag{8}$$

The constitutive relations for the linear deformation are given by

$$t^s_{ij} = M^s_{ijk\ell} e^s_{k\ell}, e^s_{ij} = C^s_{ijk\ell} t^s_{k\ell} \tag{9}$$

$$t'_{ij} + P_f \delta_{ij} = M^{*(1)}_{ijk\ell} e^{*(1)}_{k\ell}, e^{*(1)}_{ij} = C^{*(1)}_{ijk\ell}(t'_{k\ell} + P_f \delta_{k\ell}) \tag{10}$$

$$P_f = -K_f e^f_{kk} \tag{11}$$

Since in the linear response range the relation between the average stress and average strain is the same as the local relation, $M^s_{ijk\ell}$ and K_f are the elastic moduli of the solid matrix and the bulk modulus of the fluid, respectively. The derivation of equation (10), in which Terzaghi effective stress is related to the total strain due to change in relative pore geometry $e^{*(1)}_{ij}$, is shown in Carroll and Katsube [25]. The material constants $M^{*(1)}_{ijk\ell}$ can be calculated from the following equation of compliance:

$$C^{*(1)}_{ijk\ell} = C^{(1)}_{ijk\ell} - \frac{1}{1-\phi} C^s_{ijk\ell} \tag{12}$$

where $C^{(1)}_{ijk\ell}$ is the effective elastic compliance for porous solid material. The constitutive relations (9), (10), and (11) can be rewritten by using the different kinematical quantities as follows:

Downloaded 03 May 2010 to 171.66.16.27. Redistribution subject to ASME license or copyright; see http://www.asme.org/terms/Terms_Use.cfm

$$t^s_{ij} = M^s_{ijk\ell}\left[\frac{1}{2}(\delta_{km}\delta_{\ell n} + \delta_{kn}\delta_{\ell m}) - (1-\phi)C^a_{k\ell rs}M^s_{rsmn}\right]e^{(1)}_{mn} + (1-\phi)K_f M^s_{ijk\ell}C^a_{k\ell rr}e^{(2)}_{ss} \tag{13}$$

$$P_f = -\frac{(1-\phi)^2}{\phi}K_f M^s_{rsk\ell}C^a_{k\ell ii}e^{(1)}_{rs} - K_f\left[1 - \frac{(1-\phi)}{\phi}C^a_{iinn}K_f\right]e^{(2)}_{mm} \tag{14}$$

where

$$M^a_{ijk\ell} = M^{*(1)}_{ijk\ell} + (1-\phi)M^s_{ijk\ell} + \frac{(1-\phi)^2}{\phi}K_f\delta_{ij}\delta_{k\ell}$$

$$C^a_{ijk\ell}M^a_{k\ell rs} = \frac{1}{2}(\delta_{ir}\delta_{js} + \delta_{is}\delta_{jr}) \tag{15}$$

When the fluid is incompressible, the constitutive relations corresponding to equations (13) and (14) are given by

$$t^s_{ij} = M^s_{ijk\ell}C^b_{k\ell mn}\left[M^{*(1)}_{mnrs} + \frac{(1-\phi)\delta_{mn}C^b_{ppqt}M^s_{qtrs}}{C^b_{uuvv}}\right]e^{(1)}_{rs} + \frac{\phi M^s_{ijk\ell}C^b_{k\ell mm}}{(1-\phi)C^b_{uuvv}}e^{(2)}_{ss} \tag{16}$$

$$P_f = -\frac{M^s_{ijk\ell}C^b_{k\ell mm}}{C^b_{uuvv}}e^{(1)}_{ij} - \frac{\phi}{(1-\phi)^2C^b_{uuvv}}e^{(2)}_{ss} \tag{17}$$

where

$$M^b_{ijk\ell} = M^{*(1)}_{ijk\ell} + (1-\phi)M^s_{ijkl}$$

$$C^b_{ijk\ell}M^b_{k\ell rs} = \frac{1}{2}(\delta_{ir}\delta_{js} + \delta_{is}\delta_{jr}) \tag{18}$$

In the isotropic case, equations (13) and (14) become identical to the Biot's constitutive relations.

By applying the methods of the construction of constitutive equations for the deformation of the porous solid material to the flow of the porous material, we obtain equations (19) as the dynamic counterpart of Equations (13) and (14).

$$t''_{ij} = M^{(2)}_{ijk\ell}d^{(2)}_{k\ell}\ ,\ \ d^{(2)}_{ij} = C^{(2)}_{ijk\ell}t''_{k\ell} \tag{19}$$

where $d^{(2)}_{ij}$ are the volume average strain rates of the porous fluid material and can be calculated by taking the material derivative of $e^{(2)}_{ij}$. In general, the viscosity moduli $M^{(2)}_{ijk\ell}$ of the porous fluid material is anisotropic due to the anisotropy of pore structures.

3 The Mixture Theory

As it is discussed in the extensive review of mixture theories by Atkin and Craine [7, 8], the basic governing equations in mixture theories have reached an agreement among various researchers. In this paper, we will follow the notation used by Green and Naghdi [3], which is summarized as follows: a mixture of two continua s_1 and s_2 which are in relative motion to each other, where each point of the mixture at time t is occupied simultaneously by s_1 and s_2, is considered. Thus an energy balance at time t for a fixed volume V with a closed surface A is postulated in the following equation:

$$\frac{\partial}{\partial t}\int_v\left[(\rho_1+\rho_2)U + \frac{1}{2}\rho_1\mathbf{v}^{(1)}\cdot\mathbf{v}^{(1)} + \frac{1}{2}\rho_2\mathbf{v}^{(2)}\cdot\mathbf{v}^{(2)}\right]dV + \int_A\left[\mathbf{n}\cdot(\rho_1\mathbf{v}^{(1)}+\rho_2\mathbf{v}^{(2)})U + \frac{1}{2}\rho_1(\mathbf{n}\cdot\mathbf{v}^{(1)})(\mathbf{v}^{(1)}\cdot\mathbf{v}^{(1)}) + \frac{1}{2}\rho_2(\mathbf{n}\cdot\mathbf{v}^{(2)})(\mathbf{v}^{(2)}\cdot\mathbf{v}^{(2)})\right]dA$$

$$= \int_V(\rho\gamma + \rho_1\mathbf{b}^{(1)}\cdot\mathbf{v}^{(1)} + \rho_2\mathbf{b}^{(2)}\cdot\mathbf{v}^{(2)})dV + \int_A(\mathbf{t}\cdot\mathbf{v}^{(1)} + \mathbf{p}\cdot\mathbf{v}^{(2)})dA - \int_A h dA \tag{20}$$

where the scalars U, h, and r comprise the internal energy, the heat flux, and the heat supply per unit mass of the mixture, respectively. $\mathbf{v}^{(1)}$ and $\mathbf{v}^{(2)}$, ρ_1 and ρ_2, $\mathbf{t}$ and $\mathbf{p}$, and $\mathbf{b}^{(1)}$ and $\mathbf{b}^{(2)}$ are the velocities, the mass densities, and surface force vectors per unit area, and the body force of s_1 and s_2, respectively. Using the above energy balance together with invariance conditions under superposed rigid body motions, the basic governing equations were obtained. The partial stress for s_1 and s_2, denoted by σ_{ki} and π_{ki} respectively, are not in general symmetric and the antisymmetric part of σ_{ki} is equal to the negative of the antisymmetric part of π_{ki}. The continuity equations, equations of motion, and the local energy equation for purely mechanical case are given as follows:

$$\frac{\partial\rho_\alpha}{\partial t} + \text{grad}(\rho_\alpha\mathbf{v}^{(\alpha)}) = 0 (^\alpha = 1,2;\ \text{no summation over } ^\alpha) \tag{21}$$

$$\left.\begin{aligned}&\text{div}P^{(1)} + \text{div}\psi - \pi = \rho_1(\dot{\mathbf{v}}^{(1)} - \mathbf{b}^{(2)})\\ &\text{div}P^{(2)} - \text{div}\psi + \pi = \rho_2(\dot{\mathbf{v}}^{(2)} - \mathbf{b}^{(2)})\end{aligned}\right\} \tag{22}$$

$$-\rho\frac{DU}{Dt} + \text{tr}\{P^{(1)}L^{(1)}\} + \text{tr}\{P^{(2)}L^{(2)}\} + \text{tr}\{\psi\Lambda\} + \pi\cdot v = 0 \tag{23}$$

where

$$P^{(1)} = \{\sigma_{(ki)}\},\ P^{(2)} = \{\pi_{(ki)}\},\ \psi = \{\alpha_{[ki]} = -\pi_{[ki]}\}$$

$$\mathbf{v} = \mathbf{v}^{(1)} - \mathbf{v}^{(2)},\ L^{(\alpha)} = \{v^{(\alpha)}_{i,j}\}$$

$$\Lambda = \Gamma^{(1)} - \Gamma^{(2)}, \Gamma^{(\alpha)} = \left\{\frac{1}{2}(v^{(\alpha)}_{i,j} - v^{(\alpha)}_{j,i})\right\} \tag{24}$$

The linear constitutive equations for flow of fluid through an elastic solid for anisotropic case are obtained in the same manner that Green and Naghdi [3] obtained the linear constitutive equations for isotropic case. Limiting our attention to the isothermal case and introducing the infinitesimal strain of the solid $e_{ij} = 1/2(u_{i,j} + u_{j,i})$ where u_i are the infinitesimal displacements of the solid, we have

$$\sigma_{ij} = \sigma'_{ij} + \sigma''_{ij},\ \ \pi_{ij} = \pi'_{ij} + \pi''_{ij},\ \ \pi_i = \pi'_i + \pi''_i \tag{25}$$

$$\left.\begin{aligned}&\sigma'_{(ij)} = A_{ijk\ell}e_{k\ell} - D_{ij}\left(\frac{\rho_2 - \rho_{2o}}{\rho_{2o}}\right)\\ &\pi'_{(ij)} = \left[-\lambda_7\left(\frac{\rho_2-\rho_{2o}}{\rho_{2o}}\right) + D_{mn}e_{mn}\right]\delta_{ij}\\ &\pi'_i = 0,\quad \sigma'_{[ij]} = \pi'_{[ij]} = 0.\end{aligned}\right\} \tag{26}$$

$$\left.\begin{aligned}\sigma''_{(ij)} &= G_{ijk\ell}d^{(1)}_{k\ell} + H_{ijk\ell}d^{(2)}_{k\ell}\\ \pi''_{(ij)} &= J_{ijk\ell}d^{(1)}_{k\ell} + L_{ijk\ell}d^{(2)}_{k\ell}\end{aligned}\right\} \tag{27}$$

$$\pi''_i = Q_{ij}v_j + R_{ijk}\Lambda_{jk},\ \ \sigma''_{[ij]} = -\pi''_{[ij]} = -S_{ijk\ell}\Lambda_{k\ell} + T_{ijk}v_k \tag{28}$$

4 The Modified Mixture Theory

The conventional mixture theory has some difficulties in the application to fluid saturated porous materials. The mixture theory has been built on the basic assumption that particles of each constituent occupy the same point at time t. Because of this assumption, where fluid is removed, one is left with a solid material instead of a dry porous solid skeleton. Let ρ_2

Downloaded 03 May 2010 to 171.66.16.27. Redistribution subject to ASME license or copyright; see http://www.asme.org/terms/Terms_Use.cfm

approach zero in equation (20), then since $\mathbf{b}^{(2)} \to 0$ and $\mathbf{p} \to 0$, we recover the energy balance for a single continuum. Also there are some conceptual difficulties associated with partial stresses. The total stress is the sum of the partial stresses and there is no explicit accounting for areal porosity. The above two difficulties, one associated with recovery of a solid material in the absence of fluid, the other with partial stresses, are actually interrelated, and come from the lack of a clear notion of what the two different constituents occupying the same point are.

In obtaining the constitutive equations for the porous solid material with the effect of the hydrostatic fluid pressure and the porous fluid material in Katsube [26], a dry porous solid skeleton and an empty porous fluid skeleton were replaced by an equivalent homogeneous solid and an equivalent homogeneous fluid. The equivalent homogeneous solid and equivalent homogeneous fluid, can be identified as two distinct homogeneous continua occupying the same point, which appear in the mixture theory. In order to emphasize this identification within the structure of the mixture theory, and to provide more detailed information on deformation and flow mechanism at each point in the mixture, we introduce a new kinematical quantity, i.e., porosity ϕ, which appeared in the phenomenological study, into the mixture theory. We recall that ρ_1 and ρ_2 in the mixture theory are the solid mass and the fluid mass per unit overall representative volume, respectively. Thus, with the help of volumetric porosity ϕ,

$$\rho_1 = (1-\phi)\rho_s, \quad \rho_2 = \phi\rho_f \tag{29}$$

where ρ_s and ρ_f are the densities of the solid matrix and the fluid, respectively. The displacements or the velocities of constituents s_1 and s_2, i.e., $u_i^{(1)}$ or $v_i^{(1)}$ and $u_i^{(2)}$ or $v_i^{(2)}$ are those of an equivalent homogeneous solid and an equivalent homogeneous fluid, respectively. e_{ij} in equation (26) in the mixture theory, for example, is identified as the strain tensor of an equivalent homogeneous solid $e^{(1)}$. Similarly,

$$-\frac{\rho_2 - \rho_{20}}{\rho_{20}}$$

in equation (26) can be approximated by e_{mm} within the infinitesimal theory.

We assume that the pores are randomly distributed in location but not necessarily in orientation. Then even if the pore structure is anisotropic, the areal porosity is independent of the direction of the cross section and is the same as the volumetric porosity. Within the assumption of the infinitesimal deformation, this holds even after the deformation, and therefore there is no distinction between volumetric porosity and areal porosity. Introducing the areal porosity, we have

$$t_i = (1-\phi)t_i^s, \quad p_i = \phi p_i^f \tag{30}$$

$$\sigma_{(ki)} = (1-\phi)t_{ki}^s, \quad \pi_{(ki)} = \phi t_{ki}^f \tag{31}$$

where t_i^s and p_i^f are the solid surface force per unit solid area and the fluid surface force per unit fluid area, respectively. While the skew-symmetric part of the stress tensor σ_{ki} and π_{ki} are beyond the scope of usual single continuum theory, the symmetric part of σ_{ki} and π_{ki}, which are the solid and fluid surface force, respectively, in the x_i direction per unit area of the mixture perpendicular to the x_k axis, are related to the solid and fluid stress tensors t_{ij}^s and t_{ij}^f in the study of representative volume element by equation (31).

With the above modification the energy equation can be rewritten in terms of ϕ, ρ_f, ρ_s, $\mathbf{t}^s$, and $\mathbf{p}^f$, where, if we let ϕ approach one, then we recover the energy balance for a fluid without pores. Similarly, if we let ϕ approach zero, we recover the energy balance for solid material without pores. Also, we can see immediately from equation (30) that the total surface force vector is related to the weighted sum of solid stress and fluid stress.

We compare the static constitutive equations in the mixture theory with those in the study of representative volume element. Using equation (31), we multiply equation (13) by $(1-\phi)$ and compare it with equation (26), also multiplying equation (14) by $-\phi$ and comparing it with equation $(26)_2$. These comparisons lead to:

$$\begin{aligned} A_{ijk\ell} &= (1-\phi)M_{ijmn}^s\left[\frac{1}{2}(\delta_{mk}\delta_{n\ell}+\delta_{m\ell}\delta_{nk}) - (1-\phi)C_{mnrs}^a M_{rsk\ell}^s\right] \\ D_{ij} &= (1-\phi)^2 K_f M_{ijk\ell}^s C_{k\ell nn}^a \\ \lambda_7 &= K_f\{\phi - (1-\phi)^2 C_{ssnn}^a K_f\} \end{aligned} \tag{32}$$

When the fluid is incompressible, we compare equations (16) and (17) with equations (26) to obtain

$$\begin{aligned} A_{ijk\ell} &= (1-\phi)M_{ijmn}^s C_{mnrs}^b\left[M_{rsk\ell}^{*(1)} + \frac{(1-\phi)\delta_{rs}C_{ppgt}^b M_{gtk\ell}^s}{C_{uuvv}^b}\right] \\ D_{ij} &= \frac{\phi M_{ijk\ell}^s C_{k\ell mm}^b}{C_{rrtt}^b} \\ \lambda_7 &= \frac{\phi^2}{(1-\phi)^2 C_{rrtt}^b} \end{aligned} \tag{33}$$

It is worth noting that the equations (33) can also be obtained by considering the limit case $K_f \to \infty$ in equation (32). This one-to-one correspondence between the static constitutive equations of the mixture theory and those in the study of the small representative volume element, indicated in equations (32) and (33), makes it possible to experimentally determine material constants $A_{ijk\ell}$, D_{ij}, and λ_7 in the mixture theory. In addition, the comparison of equations (32) and (33) allows us to distinguish between the compressible fluid and incompressible fluid.

Next, we compare the dynamic constitutive equations in the mixture theory with those in the study of the representative volume element. From the study of the small representative volume element in Katsube [26], there is no dynamic solid stress and the dynamic fluid stress depends only on the strain rate of an equivalent homogeneous fluid. As a result, equations (19) and (27) lead to

$$G_{ijk\ell} = H_{ijk\ell} = J_{ijk\ell} = 0, \quad L_{ijk\ell} = M_{ijk\ell}^{(2)} \tag{34}$$

No matter how slowly the fluid is flowing through the porous material, there exists a pointwise stress distribution on the pore walls. In the study of the small representative volume element, these interactions between fluid and solid were not considered. However, the mixture theory by Crochet and Naghdi [10] provides us a way to consider these shear interactions. Due to the basic assumption that two distinct particles occupy the same point, skew symmetric part-of-stress tensors $\psi = \psi(\mathbf{x},t)$ as well as the resistance to diffusion π, occur naturally in addition to the usual symmetric part of solid stress tensor and that of fluid stress tensor in their formulation. When we consider the equilibrium of forces acting on the equivalent homogeneous solid, equations $(22)_1$, the skew-symmetric part of the solid stress tensor ψ is related to the moment exerted on the solid by the fluid, while the resistance to diffusion, $-\pi$, can be considered as the force exerted on the solid by the fluid. The constitutive equations of these two new kinetical quantities, which are related to the shear interactions between fluid and solid, are expressed in equations (28).

5 Comparison With the Phenomenological Theory of Biot

Let us first compare the continuity equations which appear

Downloaded 03 May 2010 to 171.66.16.27. Redistribution subject to ASME license or copyright; see http://www.asme.org/terms/Terms_Use.cfm

in the modified mixture theory with the continuity equation in the phenomenological theory. Assuming the infinitesimal deformation of the porous solid material, the fluid mass expelled per unit volume of the porous solid material, Δm, may be expressed in terms of mass densities in the mixture theory as follows:

$$\Delta m = \rho_{2o}\left(-\frac{\rho_1-\rho_{1o}}{\rho_{1o}}+\frac{\rho_2-\rho_{2o}}{\rho_{2o}}\right) \tag{35}$$

The linear combination of two continuity equations (21) in the mixture theory and equation (35), together with the assumption of homogeneous initial conditions, lead to

$$\frac{\partial m}{\partial t}+\frac{\partial m}{\partial x_k}v_k^{(1)}+\frac{\partial \rho_2}{\partial x_k}(v_k^{(2)}-v_k^{(1)}) + \rho_{2o}\left(\frac{\rho_2}{\rho_{2o}}v_{k,k}^{(2)}-\frac{\rho_1}{\rho_{1o}}v_{k,k}^{(1)}\right)=0 \tag{36}$$

If the porous solid skeleton is stationary, i.e., $v_k^{(1)}=0$, equation (36) reduces to

$$\frac{\partial m}{\partial t}+q_{i,i}=0 \tag{37}$$

where the fluid mass flow rate in the x_i direction per unit area of the sample $q_i=\rho_2 v_i^{(2)}$ is used. In equation (37), we have recovered the usual form of continuity equation which appears in the phenomenological theories. In obtaining equation (37) from the continuity equations in the mixture theory, it is important to note that we did not make any assumption on the magnitude of q_i so that equation (37) holds for large fluid mass flow rate.

Secondly, we compare the equations of motion in the mixture with those in the phenomenological theory. Introducing the body force per unit mass of the mixture **b** as follows:

$$\rho\mathbf{b}=\rho_1\mathbf{b}^{(1)}+\rho_2\mathbf{b}^{(2)} \tag{38}$$

and adding two equations of motion (22) in the mixture theory, we have

$$t_{ki,k}=\rho_1\dot{v}_i^{(1)}+\rho_2\dot{v}_i^{(2)}-\rho b_i \tag{39}$$

which, in quasi-static case, becomes identical to the usual form of equation of motion in the phenomenological theory. Using $\pi'_{(ij)}=-\phi P_f\delta_{ij}$ and constitutive equations $(27)_2$ and (28) with (34), and assuming the infinitesimal deformation for porous material as well as uniform porosity, the equation of motion for porous fluid material $(22)_2$ can be expressed by the following equation:

$$-\phi P_f,\ i+\Gamma_{kijl}^{(2)}d_{jl,k}^{(2)}-S_{kijl}\Lambda_{jl,k}-T_{kij}v_{j,k}+Q_{ij}v_j+R_{ijk}\Lambda_{jk} = \rho_2(\dot{v}_i^{(2)}-b_i^{(2)}) \tag{40}$$

Restricting our attention to the quasi-static case, the case of equal body force for solid and fluid, and the stationary porous solid material, and simply ignoring the velocity gradient terms, equation (40) further reduces to

$$-P_{f,i}+P_f b_i=\frac{Q_{ij}}{\phi^2\rho_f}q_j \tag{41}$$

where a generalized form of Darcy's law for an anisotropic material in the phenomenological theories is recovered.

From the comparison between the modified mixture theory and the phenomenological theory in their equations of motion, we have found that the equation of motion for an equivalent fluid can be reduced to an equation which is similar to Dracy's law but with some extra terms. While Dracy's law fits the global experimental results for simple steady state boundary value problems, there is no guarantee that Darcy's law holds locally, especially in the region closer to boundaries where the velocity gradient is not small.

Darcy's law is often compared with Fourier's heat conduction equation because of the similarity in the form of equations. However, the mixture theory demonstrates that Darcy's law is nothing but a reduced form of the equation of motion for an equivalent homogeneous fluid, while Fourier's heat conduction equation is a constitutive relation. While Darcy's law takes the same form of equation with Fourier's heat conduction equation, the nature of these two equations are quite different, and this similarity in the form of equations may be deceptive.

Thirdly, we compare the energy equation in the mixture theory with the energy consideration in Biot's theory. The local energy equation (23) in the mixture theory indicates that the rate of change of the internal energy of the mixture is the sum of the rate of work done to an equivalent homogeneous fluid in the usual single continuum sense and the rate of work done to the mixture through the interaction force and the interaction moment. The second and the third terms in equation (23) can be rewritten in component forms as follows:

$$\sigma_{(ki)}d_{ik}^{(1)}+\pi_{(ki)}d_{ik}^{(2)}=t'_{ki}d_{ik}^{(1)}+\phi P_f(d_{mm}^{(1)}-d_{mm}^{(2)})+t''_{ki}d_{ik}^{(2)}. \tag{42}$$

In the above equation, the rate of work done to an equivalent homogeneous solid and an equivalent homogeneous fluid is equal to the rate of work done to the porous solid through the confining static stress t'_{ki}, $t'_{ki}d_{ik}^{(1)}$, the rate of work necessary to push fluid into the pores of the porous solid $\phi P_f(d_{mm}^{(1)}-d_{mm}^{(2)})$ and the rate of work done to a dynamical equivalent homogeneous fluid, $t''_{ki}d_{ik}^{(2)}$.

Even though Biot did not have an expression of energy balance in the mixture, he considered the elastic potential energy and the rate of dissipation energy separately. He obtained the expression for the elastic potential energy corresponding to the first and the second terms in the right-hand side of equation (42). Ignoring the velocity gradient in the constitutive equation (28), and assuming the stationary porous solid material, the fifth term in equation (23) corresponds to the equation of rate of dissipation energy by Biot. Although a notion of kinetical quantities such as interaction force, interaction moment and fluid stress caused by viscosity are missing in the phenomenological theory by Biot, we see that it is parallel to the limited version of our modified mixture theory from this comparison in the energy consideration.

6 Summary

The modified mixture theory for the fluid-filled porous material was obtained by introducing the micro-mechanical constitutive theory by Katsube [26] into the conventional mixture theory. The resulting theory is based on the same material assumptions as the phenomenological theory by Biot. The governing equations, however, are found to be more general than Biot's theory and the resulting theory reduces to Biot's theory when the fluid velocity gradient terms are ignored. As in the phenomenological theory, the effect of point wise stress distribution throughout the pore walls on the deformation of the porous solid material is approximated to that of the average hydrostatic fluid pressure. However, the interaction force and torque between the fluid and the solid constituents were considered within the framework of the mixture theory. Also, in addition to the stress due to infinitesimal solid deformation, the stress due to viscous flow was also considered.

Currently, further attempts are underway to elucidate the physical meanings of the interaction terms ψ and π from a micro-mechanical point of view and the assumptions involved in bridging the two theories.

In the phenomenological theory, we have six independent equations – three equations of motion and three equations of Darcy's law – to solve for six independent kinematical variables comprising three displacement components of solid and three velocity components of fluid. However, we eliminate the fluid mass flow rate q_i from the equation of

Downloaded 03 May 2010 to 171.66.16.27. Redistribution subject to ASME license or copyright; see http://www.asme.org/terms/Terms_Use.cfm

Darcy's law and the continuity equation and as a result the number of independent equations are reduced from six to four. We solve four independent equations for four unknowns, i.e., three displacement components of solid and the fluid content or hydrostatic fluid pressure. After solving the boundary value problems, we find the fluid velocity components from Darcy's law. This reduction in the number of independent variables as well as the number of independent equations restrict the freedom of specifying the fluid velocity components in the phenomenological theory.

Despite some limitations, the phenomenological theory by Biot is a remarkably successful one. It is shown in Katsube [27] that the velocity gradient effects, which are ignored in the phenomenological theory, do not play an important role in most practical applications by solving simple steady state boundary value problems. This is due to the fact that the interaction force, which is proportional to the relative velocity in the absence of velocity gradient effects, comes into the structure of the phenomenological theory through the fluid mass flow rate in Darcy's law and the continuity equation. While there is no kinetical quantity corresponding to the interaction force, the most important shear interaction effects due to fluid viscosity is actually taken into account within the structure of the phenomenological theory.

Acknowledgment

This work was supported in part by Grant No. MEA 80-20216 from the National Science Foundation (Solid Mechanics Program) to the University of California, Berkeley. N. Katsube was also supported by an Amelia Earhart Fellowship from Zonta International.

References

1 Truesdell, C., and Toupin, R. A., "The Classical Field Theories," *Handbuch der Physik*, Flugge, S., ed., Vol. III/1, Springer-Verlag, 1965.

2 Truesdell, C., and Noll, W., "The Non-Linear Field Theories of Mechanics," *Handbuch der Physik*, Flugge, S., ed., Vol. III/3, Springer-Verlag.

3 Green, A. E., and Nagdi, P. M., "A Dynamical Theory of Interacting Continua," *International Journal of Engineering Science*, Vol. 3, 1965, pp. 231–241.

4 Goodman, M. A., and Cowin, S. C., "A Continuum Theory for Granular Materials," Archive for Rational Mechanics and Analysis, Vol. 44, 1971, pp. 249–265.

5 Passman, S. L., "Mixtures of Granular Materials," *International Journal of Engineering Science*, Vol. 15, 1977, pp. 117–129.

6 Nunziato, J. W., and Walsh, E. K., "On the Influence of Void Compaction and Material Non-uniformity on the Propagation of One-dimensional Acceleration Waves in Granular Materials," *Archive for Rational Mechanics and Analysis*, Vol. 64, 1977, pp. 299–316.

7 Atkin, R. J., and Craine, R. E., "Continuum Theories of Mixtures: Basic Theory and Historical Development," *Quarterly Journal of Mechanics and Applied Mathematics*, Vol. 29, 1976, pp. 209–244.

8 Atkin, R. J., and Craine, R. E., "Continuum Theories of Mixtures: Applications," *Journal of Institute of Mathematics and Applications*, Vol. 17, 1976, pp. 153–207.

9 Green, A. E., and Steel, T. R., "Constitutive Equations for Interacting Continua," *International Journal of Engineering Science*, Vol. 4, 1966, pp. 483–500.

10 Crochet, N. J., and Naghdi, P. M., "On Constitutive Equations for Flow of Fluid Through an Elastic Solid," *International Journal of Engineering Science*, Vol. 4, 1966, pp. 383–401.

11 Morland, L. W., "A Simple Constitutive Theory for a Fluid-Saturated Porous Solid," *Journal of Geophysical Research*, Vol. 77, 1971, pp. 890–900.

12 Garg, S. K., "Wave Propagation Effects in a Fluid-Saturated Porous Solid," *Journal of Geophysical Research*, Vol. 76, 1971, pp. 7947–7962.

13 Garg, S. K., Nayfeh, A. H., and Good, A. J., "Compressional Waves in Fluid-Saturated Elastic Porous Media," *Journal of Applied Physics*, Vol. 45, 1974, pp. 1968–1974.

14 Garg, S. K., Brownell, D. H., Jr., Pritchett, J. W., and Herrman, R. G., "Shock-Wave Propagation in Fluid-Saturated Porous Media," *Journal of Applied Physics*, Vol. 46, 1975, pp. 702–713.

15 Bowen, R. M., "Compressible Porous Models by Use of the Theory of Mixtures," *International Journal of Engineering Science*, Vol. 20, 1982, pp. 697–735.

16 Biot, M. A., "General Theory of Three-Dimensional Consolidation," *Journal of Applied Physics*, Vol. 12, 1941, pp. 155–164.

17 Biot, M. A., "Theory of Elasticity and Consolidation for a Porous Anisotropic Solid," *Journal of Applied Physics*, Vol. 26, 1955, pp. 182–185.

18 Biot, M. A., General Solutions of the Equations of Elasticity and Consolidation for a Porous Material," *Journal of Applied Physics*, Vol. 78, 1956, pp. 91–96.

19 Biot, M. A., "Theory of Propagation of Elastic Waves in a Fluid-Saturated Porous Solid. I. Low Frequency Range," *Journal of Acoustical Society of America*, Vol. 28, 1956, pp. 168–178.

20 Biot, M. A., "Theory of Propagation of Elastic Waves in a Fluid-Saturated Porous Solid. II. High Frequency Range," *Journal of Acoustical Society of America*, Vol. 28, 1956, pp. 179–191.

21 Biot, M. A., and Willis, D. G., "The Elastic Coefficients of the Theory of Consolidation," ASME JOURNAL OF APPLIED MECHANICS, Vol. 24, 1957, pp. 594–601.

22 Rice, J. R., and Cleary, M. P., "Some Basic Stress Diffusion Solutions for Fluid-Saturated Elastic Porous Media with Compressible Constituents," *Reviews of Geophysics and Space Physics*, Vol. 14, 1976, pp. 227–241.

23 Nur, A., and Byerlee, J. D., "An Exact Effectie Stress Law for Elastic Deformation of Rock with Fluids," *Journal of Geophysical Research*, Vol. 76, 1971, pp. 6414–6419.

24 Carroll, M. A., "Mechanical Response of Fluid-Saturated Porous Materials," *Proceedings of 15th International Congress of Theoretical and Applied Mechanics*, Rimrott, F. P. J., and Tabarrok, B., eds., North-Holland, New York, 1980.

25 Carroll, M. M., and Katsube, N., "The Role of Terzaghi Effective Stress in Linearly Elastic Deformation," *ASME Journal of Energy Resources Technology*, Vol. 105, pp. 509–511.

26 Katsube, N., "The Constitutive Theory for Fluid-Filled Porous Materials," ASME JOURNAL OF APPLIED MECHANICS, Vol. 52, 1985, pp. 185–189.

27 Katsube, N., "Mechanical Response of Fluid-Filled Poroelastic Solids," Ph.D. Dissertation, University of California-Berkeley, 1982.

Downloaded 03 May 2010 to 171.66.16.27. Redistribution subject to ASME license or copyright; see http://www.asme.org/terms/Terms_Use.cfm

N. Katsube
Assistant Professor,
Department of Engineering Mechanics,
The Ohio State University,
Columbus, Ohio 43210
Assoc. Mem. ASME

M. M. Carroll
Professor,
Department of Mechanical Engineering,
The University of California,
Berkeley, Calif. 94720
Fellow ASME

The Modified Mixture Theory for Fluid-Filled Porous Materials: Applications

The recently established modified mixture theory for fluid-filled porous materials is applied to two steady state boundary value problems; also, how the newly developed theory provides more general solution than Biot's theory is examined. The velocity profiles in steady state boundary value problems are found to depend on the ratio of a characteristic length of the microstructure to a characteristic length defined by the boundary conditions. As opposed to Biot's theory, the zero fluid velocity condition on the boundary are satisfied and the existence of a non-Darcy flow closer to the boundary are shown.

1 Introduction

For problems of fluid-saturated porous material, the theory developed by Biot [1–4] more than thirty years ago is the one still most widely accepted. It is assumed that the model consists of linearly elastic solid and Newtonian viscous fluid, and the pores are all interconnected and randomly distributed. His governing equations are based on classical linear elasticity and Darcy's law. One of the well-cited references is the work by Rice and Cleary [5], where some basic stress diffusions were obtained by reinterpreting Biot's theory. Deresiewicz [6], Geertsma and Smit [7], Hajra and Mukhopadhyay [8], and many others applied Biot's theory to problems of wave phenomena.

Some attempts have been made to obtain a more general theory than Biot's by approaching the same problems from different points of view. Burridge and Keller [9] tried the two-space method of homogenization. From a continuum mechanics point of view, Morland [10] tried to provide detailed constitutive relations to the continuum theory of mixtures. More recently, Bowen [11] included porosity as an internal state variable at each point of the mixture. These attempts to establish a theory beyond Biot's from different points of view are of great importance. However, the attempts made so far do not appear yet quite complete because even though it is shown how a new set of equations in a general theory can be reduced to those in Biot by neglecting certain terms, it has not yet been shown how a newly developed theory can provide more general solutions to particular boundary value problems than Biot's does.

Contributed by the Applied Mechanics Division for presentation at the 1987 Applied Mechanics, Biomechanics, and Fluids Engineering Conference, Cincinnati, OH, June 14–17, 1987, of the American Society of Mechanical Engineers.
Discussion of this paper should be addressed to the Editorial Department, ASME, United Engineering Center, 345 East 47th Street, New York, N.Y. 10017, and will be accepted until two months after final publication of the paper itself in the JOURNAL OF APPLIED MECHANICS. Manuscript received by ASME Applied Mechanics Division, June 15, 1984; final revision, June 24, 1986.
Paper No. 87-APM-8.

Recently, Katsube and Carroll [12] obtained the modified mixture theory for fluid-filled porous materials where a detailed micromechanical constitutive theory by Katsube [13] and Carroll [14, 15] was introduced into the mixture theory by Green and Naghdi [16] and Crochet and Naghdi [17]. With the introduction of a new kinematical quantity—porosity—in the original mixture theory, a porous solid material and a porous fluid material, which an actual sample consists of, are idealized as an equivalent homogeneous solid and an equivalent homogeneous fluid, respectivley, and are identified as two different constituents occupying the same point in the original mixture theory. The obtained theory is more general than Biot's phenomenological theory in the sense that the shear interactions between fluid and solid are properly considered within the structure of the mixture theory and reduces to Biot's theory if fluid velocity gradient effects are suppressed.

In this work we will apply this modified mixture theory to some simple steady state boundary value problems and examine how this recently established modified mixture theory provides more general solutions than Biot's theory. First, we will solve the steady state flow between two infinite plates discussed in Crochet and Naghdi [17]. The obtained velocity profile is found to depend on the characteritic length of the microstructure relative to a characteristic length of the boundary condition. Given the width between two infinite plates, the smaller the grain size, the sharper the square of the velocity profile and the local fluid mass flow rate can be approximated by the conventional Darcy's law for most of the region. In any fluid flow, however, in contrast to the phenomenological theory, the zero fluid velocity condition on the walls are satisfied and there exists a non-Darcy fluid flow closer to the boundary. Secondly, by solving the axisymmetric steady state flow in a circulr cylindrical fluid-filled porous material, we obtain results similar to steady state flow between two infinite plates, i.e., the dependence of the velocity profile on the ratio of a characteristic length of the microstructure to a characteristic length defined by the boundary conditions and the existence of a non-Darcy flow close to the boundary.

Copyright © 1987 by ASME
Downloaded 03 May 2010 to 171.66.16.27. Redistribution subject to ASME license or copyright; see http://www.asme.org/terms/Terms_Use.cfm

2 Summary of the Modified Mixture Theory

The basic governing equations of the modified mixture theory are identical to those of the conventional mixture theory except that the micromechanical deformation and flow mechanism are provided at each point of the mixture with the introduction of the new kinematical quantity, porosity. Following the notations in the original mixture theory, Crochet and Naghdi [17], the continuity equations and the equations of motion are given as follows:

$$\frac{\partial \rho_\alpha}{\partial t} + \text{grad}(\rho_\alpha \mathbf{v}^{(\alpha)}) = 0$$
$$(\alpha = 1,2; \text{ no summation over } \alpha) \tag{1}$$

$$\left.\begin{aligned} &\text{div } P^{(1)} + \text{div } \psi - \pi = \rho_1 (\dot{\mathbf{v}}^{(1)} - \mathbf{b}^{(2)}) \\ &\text{div } P^{(2)} - \text{div } \psi + \pi = \rho_2 (\dot{\mathbf{v}}^{(2)} - \mathbf{b}^{(2)}) \end{aligned}\right\} \tag{2}$$

where

$$P^{(1)} = \{\sigma_{(ki)}\},\ P^{(2)} = \{\pi_{(ki)}\},\ \psi = \{\sigma_{[ki]} = -\pi_{[ki]}\} \tag{3}$$

The superscripts (1) and (2) indicate the solid and the fluid constituents, respectively. The stress tensors, σ_{ki} and π_{ki}, are i component of the stresses on the surface perpendicular to x_k axis for solid and fluid constituents, respectively. The skew symmetric part of the solid stress tensor is equal to the negative of the skew symmetric fluid tensor and is related to the moment exerted on the solid by the fluid at each point of the mixture through shear interaction between fluid and solid, while the resistance to diffusion $-\pi_i$ is related to the force exerted on the solid by the fluid. ρ_1, $\mathbf{u}^{(1)}$, $\mathbf{b}^{(1)}$ and ρ_2, $\mathbf{u}^{(2)}$, $\mathbf{b}^{(2)}$ represent, respectively, the mass density, the displacement vector and the body force of the solid and those of the fluid. When the solid matrix as well as the pore structure are isotropic, the constitutive equations for the deformation of fluid-filled porous material are summarized as follows:

$$\begin{aligned} &\sigma'_{(ij)} = (1-\phi) t^s_{ij} = \lambda_1 e^{(1)}_{kk} \delta_{ij} + 2\mu_1 e^{(1)}_{ij} + \lambda_6 e^{(2)}_{mm} \delta_{ij} \\ &\pi'_{(ij)} = (-\phi P_f)\delta_{ij} = (\lambda_7 e^{(2)}_{mm} + \lambda_6 e^{(1)}_{mm})\delta_{ij} \\ &\pi'_i = 0, \quad \sigma'_{[ij]} = \pi'_{[ij]} = 0 \end{aligned} \tag{4}$$

where

$$\lambda_1 + \frac{2}{3}\mu_1 = k_1 = \frac{(1-\phi)k^s\{\phi k^{*(1)} + (1-\phi)^2 K_f\}}{\phi k^{*(1)} + \phi(1-\phi)k^s + (1-\phi)^2 K_f}$$

$$\lambda_6 = \frac{\phi(1-\phi)^2 k^s K_f}{\phi k^{*(1)} + \phi(1-\phi)k^s + (1-\phi)^2 K_f}$$

$$\lambda_7 = \frac{\phi K_f\{\phi k^{*(1)} + \phi(1-\phi)k^s\}}{\phi k^{*(1)} + \phi(1-\phi)k^s + (1-\phi)^2 K_f} \tag{5}$$

$$\mu_1 = \frac{(1-\phi)\mu^s \mu^{*(1)}}{\mu^{*(1)} + (1-\phi)\mu^s} = \mu^{(1)}$$

t^s_{ij} are components of the solid stress tensor corresponding to the solid surface force per unit solid area of the mixture with porosity ϕ and P_f is the hydrostatic fluid pressure. $e^{(1)}_{ij}$, $e^{(1)}_{mm}$, and ϕ are the components of the infinitesimal solid strain tensor, the fluid volumetric strain and the porosity, respectively. λ_1, μ_1, λ_6, and λ_7 are material constants of fluid-filled porous materials and can be expressed in terms of more physically meaningful material constants, i.e., the bulk and shear modulus of the solid material (without pores) k^s and μ^s, the bulk modulus of the fluid (without pores) K_f, the bulk modulus of the porosity change $k^{*(1)}$, and the shear modulus of the relative pore shape changes of porous material $\mu^{*(1)}$.

When the fluid is incompressible, the constitutive equations corresponding to equations $(3)_{1,2}$ are

$$\begin{aligned} \sigma'_{(ij)} &= (1-\phi) t^s_{ij} = \left((1-\phi)k^s - \frac{2}{3}\mu_1\right) e^{(1)}_{kk}\delta_{ij} \\ &\quad + 2\mu_1 e^{(1)}_{ij} + \phi k^s e^{(2)}_{mm}\delta_{ij} \end{aligned} \tag{6}$$

$$\pi'_{(ij)} = -\phi P_f \delta_{ij} = \left[\frac{\phi^2(k^{*(1)} + k^s(1-\phi))}{(1-\phi)^2} e^{(2)}_{mm} + \phi k^s e^{(1)}_{mm}\right]\delta_{ij}.$$

For the isotropic porous material, the constitutive equations for the fluid flow are summarized as follows:

$$\begin{aligned} &\sigma''_{(ij)} = (1-\phi) t^s_{ij} = 0 \\ &\pi''_{(ij)} = \phi(t^f_{ij} + P_f \delta_{ij}) = \lambda_2 d^{(2)}_{mm}\delta_{ij} + 2\mu_2 d^{(2)}_{ij} \\ &\sigma''_{[ij]} = -\pi''_{[ij]} = -2\mu_{11}\Lambda_{ij}, \quad \pi''_i = \lambda_9 v_i. \end{aligned} \tag{7}$$

where

$$\begin{aligned} &\Lambda_{ij} = \Gamma^{(1)}_{ij} - \Gamma^{(2)}_{ij} \\ &\Gamma^{(\alpha)}_{ij} = \tfrac{1}{2}(v^{(\alpha)}_{i,j} - v^{(\alpha)}_{j,i})\ (\alpha = 1,2), d^{(2)}_{ij} = \tfrac{1}{2}(v^{(2)}_{i,j} + v^{(2)}_{j,i}) \\ &v_i = v^{(1)}_i - v^{(2)}_i \end{aligned} \tag{8}$$

t^f_{ij} are the components of the fluid stress tensor corresponding to the fluid surface per unit area of the fluid. $d^{(2)}_{ij}$ are the components of the rate of deformation tensor of the equivalent homogeneous fluid material. λ_2 and μ_2 are the viscosities of the equivalent homogeneous fluid material. The material constant μ_{11} relates the interacting moment between fluid and solid due to the shear stress distribution on the pore boundaries to the relative velocity tensor. The material constant λ_9 relates the diffusive force between fluid and solid to the relative velocity.

3 Steady State Flow Between Two Infinite Plates

Consider a layer of porous medium in the $x_1 - x_2$ plane bounded by two planes of impermeable material at $x_2 = \pm L$. We assume the displacement components of the solid and the velocity of the fluid in the form

$$\begin{aligned} &u^{(1)}_1 = \bar{u}(x_2),\ u^{(1)}_2 = u^{(1)}_3 = 0 \\ &v^{(2)}_1 = \bar{v}(x_2),\ v^{(2)}_2 = v^{(2)}_3 = 0 \end{aligned} \tag{9}$$

and require that

$$\bar{u}(\pm L) = 0,\ \bar{v}(\pm L) = 0 \tag{10}$$

We also assume that the deformation of a porous material is infinitesimal and the fluid inside the pores is incompressible, i.e., $\rho_f = \rho_{fo}$. The constitutive equations (6) and (7) with the assumption (9) lead to

$$\begin{aligned} &\sigma'_{11} = \sigma'_{22} = \sigma'_{33} = \phi k^s e^{(2)}_{mm},\ \sigma'_{(12)} = \mu_1 \bar{u}_{,2} \\ &\pi'_{11} = \pi'_{22} = \pi'_{33} = \frac{\phi^2(k^{*(1)} + (1-\phi)k^s)}{(1-\phi)^2} e^{(2)}_{mm},\ \pi''_{12} = \mu_2 \bar{v}_{,2} \\ &\sigma''_{[12]} = -\pi''_{[12]} = \mu_{11}\bar{v}_{,2},\ \pi''_1 = -\lambda_9 \bar{v}. \end{aligned} \tag{11}$$

Using the constitutive relations (11), nontrivial equations of motion (2) in the absence of body force are

$$\begin{aligned} &\phi k^s e^{(1)}_{mm,1} + \mu_1 \bar{u}_{,22} - \mu_{11}\bar{v}_{,22} + \lambda_9 \bar{v} = 0 \\ &\frac{\phi^2(k^{*(1)} + (1-\phi)k^s)}{(1-\phi)^2} e^{(2)}_{mm,1} + (\mu_2 + \mu_{11})\bar{v}_{,22} - \lambda_9 \bar{v} = 0 \\ &\phi k^s e^{(2)}_{mm,2} = 0 \\ &\frac{\phi^2(k^{*(1)} + (1-\phi)k^s)}{(1-\phi)^2} e^{(2)}_{mm,2} = 0. \end{aligned} \tag{12}$$

Assuming that ϕ is a constant ϕ_o prior to the deformation, ϕ in equations (12) may be replaced by ϕ_o within the infinitesimal deformation assumption. From equations $(12)_{3,4}$ we know that $e^{(2)}_{mm}$ is a function of x_1 only, and equation $(12)_2$ leads to

Downloaded 03 May 2010 to 171.66.16.27. Redistribution subject to ASME license or copyright; see http://www.asme.org/terms/Terms_Use.cfm

$$(\mu_2+\mu_{11})\bar{v}_{,22}-\lambda_9\bar{v}=-\frac{\phi^2(k^{*(1)}+(1-\phi)k^s)}{(1-\phi)^2}\frac{de^{(2)}_{mm}}{dx_1}. \tag{13}$$

In equation (13) the right-hand side is a function of x_1 only while the left-hand side is a function of x_2 only so that we must have

$$\frac{de^{(2)}_{mm}}{dx_1}=M \tag{14}$$

where M is a constant. The equation obtained by summing equations $(12)_1$ and $(12)_2$

$$\frac{\phi^2k^{*(1)}+\phi(1-\phi)k^s}{(1-\phi)^2}M+\mu_1\bar{u}_{,22}+\mu_2\bar{v}_{,22}=0 \tag{15}$$

and equation $(12)_2$

$$\frac{\phi^2(k^{*(1)}+(1-\phi)k^s)}{(1-\phi)^2}M+(\mu_2+\mu_{11})\bar{v}_{,22}-\lambda_9\bar{v}=0 \tag{16}$$

together with equation (14) are a simplified set of equations of motion (12). In addition to the equations of motion, the following continuity equation for an equivalent homogeneous fluid must be satisfied:

$$\frac{\partial\rho_2}{\partial t}+\rho_{2,i}v^{(2)}_i+\rho_2v^{(2)}_{i,i}=0 \tag{17}$$

Equation (17) can be rewritten by using $\rho_2=\phi\rho_f$. The incompressible condition $\rho_f=\rho_{f0}$ and the velocity field assumptions $(9)_{3,4}$ lead to

$$\frac{\partial\phi}{\partial t}+\phi_{,1}\bar{v}=0. \tag{18}$$

Introducing the dimensionless variables X_1, X_2, U, V, T

$$X_1=\frac{x_1}{L},\ X_2=\frac{x_2}{L},\ U=\frac{\bar{u}}{L},\ V=\frac{L\lambda_9\bar{v}}{(k^{*(1)}+(1-\phi)k^s)},$$
$$T=\frac{(k^{*(1)}+(1-\phi)k^s)t}{\lambda_9L^2} \tag{19}$$

into the governing equations (15), (16), (18), and (10), we obtain the following set of nondimensionalized equations and the nondimensionalized boundary conditions

$$\frac{\{\phi^2k^{*(1)}+\phi(1-\phi)k^s\}ML}{(1-\phi)^2\mu_1}+\frac{d^2U}{dx_2^2}+\frac{\mu_2(k^{*(1)}+(1-\phi)k^s)}{L^2\lambda_9\mu_1}\frac{d^2V}{dX_2^2}=0$$
$$\frac{\phi^2LM}{(1-\phi)^2}+\frac{a^2}{L^2}\frac{d^2V}{dX_2^2}-V=0 \tag{20}$$
$$\frac{\partial\phi}{\partial T}+\frac{\partial\phi}{\partial X_1}V=0$$

where

$$a^2=\frac{\mu_2+\mu_{11}}{\lambda_9} \tag{21}$$

$$U(\pm1)=0,\ V(\pm1)=0 \tag{22}$$

Since $\partial\phi/\partial X_1$ is of the order ϵ due to the infinitesimal deformation assumption, if we further assume that the nondimensionalized velocity V is of order ϵ, then the continuity equation $(20)_3$ is automatically satisfied. It is worth noting that we did not make any assumption on the order of velocity gradient.[1] The solution of equations $(20)_{1,2}$ which satisfies equation (22) can be obtained as follows:

$$V=\frac{\phi^2LM}{(1-\phi)^2}\left[1-\frac{\cosh\frac{LX_2}{a}}{\cosh\frac{L}{a}}\right]$$

$$U=\frac{\mu_2(k^{*(1)}+(1-\phi)k^s)M\phi^2}{\mu_1\lambda_9L(1-\phi)^2}\left[\frac{\cosh\frac{LX_2}{a}}{\cosh\frac{L}{a}}-1\right]$$
$$-\frac{L(\phi^2k^{*(1)}+\phi(1-\phi)k^s)M}{2\mu_1(1-\phi)^2}(X_2^2-1) \tag{23}$$

Rewriting equation $(23)_1$ by using the fluid mass flow rate in X_1 direction per unit area of the sample, $q_1=\phi\rho_f v^{(2)}_1$,

$$q_1=\frac{\rho_f\phi^3(k^{*(1)}+(1-\phi)k^s)M}{(1-\phi)^2\lambda_9}\left[1-\frac{\cosh\frac{LX_2}{a}}{\cosh\frac{L}{a}}\right] \tag{24}$$

Integrating equation (24)

$$Q_1=\frac{1}{2L}\int_{-L}^{L}q_1dx_2$$
$$=\frac{\rho_f\phi^3(k^{*(1)}+(1-\phi)k^s)M}{(1-\phi)^2\lambda_9}\left[1-\frac{a}{L}\tanh\left(\frac{L}{a}\right)\right] \tag{25}$$

where Q_1 indicates the average fluid mass flow rate in X_1 direction per unit area, which we actually measure in the laboratory.

We note that the nondimensionalized velocity profile (23) depends on the constant $A=a/L$. We assign two values to the constant A and plot the nondimensionalized velocity profile in Fig. 1. The constants μ_2, μ_{11}, and λ_9 depend on the microscopic structure of the porous solid material and the fluid viscosity. Therefore, the constant

$$a=\sqrt{\frac{\mu_2+\mu_{11}}{\lambda_9}},$$

which has a dimension of the length, also depends on the

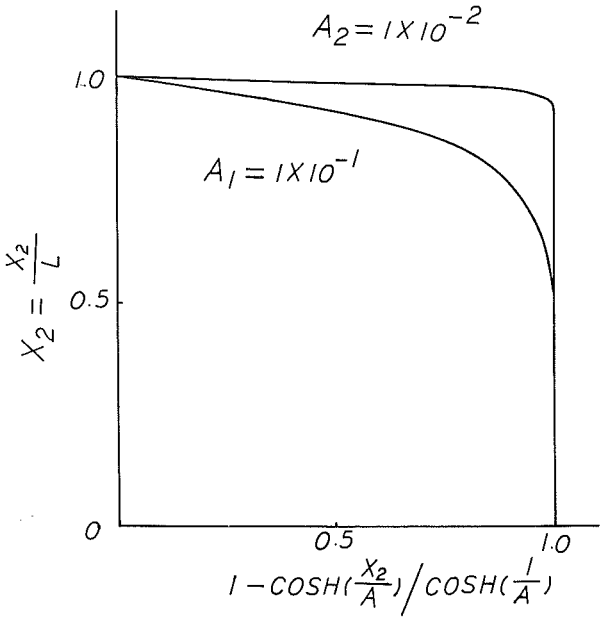


Fig. 1 Velocity profile of steady state flow between two infinite plates

[1] In Crochet and Naghdi [17], the velocity as well as the velocity gradient were assumed to be of infinitesimal order, which basically prohibits us from considering the flow near the wall.

Downloaded 03 May 2010 to 171.66.16.27. Redistribution subject to ASME license or copyright; see http://www.asme.org/terms/Terms_Use.cfm

microscopic structure of the porous solid material and the fluid viscosity. For example, if we choose grain shape to be sphere and also determine the way of packing as well as the fluid viscosity, then we expect that the constant a is proportional to the diameter of the spherical grain. Hence, in general, constant a can be considered as a characteristic length of microscopic structure of fluid saturated porous material and the constant $A = a/L$ can be considered as a measure of the characteristic length of microstructure relative to a characteristic length of the body. Given the width between two infinite plates, the constant A assumes a smaller value if the grain diameter is smaller. The plotted velocity profile with two different values of A shows us that the smaller the grain diameter, the sharper the square of the velocity profile.

When $A = 1\times10^{-2}$, Q_1 in equation (25) can be approximated by

$$Q_1 \simeq \frac{\rho_f \phi^3 (k^{*(1)} + (1-\phi)k^s)M}{(1-\phi)^2 \lambda_9},$$

which may be rewritten as

$$Q_1 \simeq -\frac{\phi^2 \rho_f}{\lambda_9} \frac{dP_f}{dx_1}$$

by using equations $(6)_2$, $(9)_{1,2}$, and (14), within 1 percent error, and q_1 in equation (24) can be approximated by the same quantity for region $x_2 < 0.95L$ within 1 percent error. This implies that when $A = a/L$ is small, 1×10^{-2} for example, then the local fluid mass flow rate can be approximated by the conventional Darcy's law for most of the region, i.e., $Q_1 = q_1$. However, as we can observe in the plotted velocity profile, in any fluid flow, there exists a non-Darcy fluid flow closer to the boundary.

In the nondimensionalized equation of motion for an equivalent homogeneous fluid $(20)_2$, V and LM are of the order ϵ. If $a^2/L^2\, d^2V/dX_2^2$ is of the order ϵ^2, it can be omitted and equation $(20)_2$ may be rewritten as follows.

$$q_1 = \frac{\rho_f \phi^3 (k^{*(1)} + (1-\phi)k^s)}{(1-\phi)^2 \lambda_9} M = -\frac{\phi^2 \rho_f}{\lambda_9} P_{f,1} \tag{26}$$

Using the Kozeny-Carman equation for the permeability, the conventional Darcy's law can be expressed as

$$q_1 = -\frac{\phi^3}{(1-\phi)^2} \frac{\rho_f}{k_o S^2 \mu_f} P_{f,1} \tag{27}$$

where k_o and S are a factor depending on pore shape and geometry, and a specific surface area, respectively. The comparison between equation (26) and (27) indicates that the equation $(20)_2$ reduces to the Darcy's law (27) when

$$\frac{a^2}{L^2} \frac{d^2V}{dX_2}$$

is omitted. Furthermore, the material constant λ_9 in the modified mixture theory may be expressed as

$$\lambda_9 = \frac{(1-\phi)^2}{\phi} \mu_f k_o S^2 \tag{28}$$

which is in agreement with our physical sense since it indicates that, given the same fluid flow rate, the diffusive force is larger if the viscosity of the fluid and the specific surface area are larger.

The equation of motion for an equivalent homogeneous solid (15) can be nondimensionalized as follows:

$$\frac{L}{\mu_1} \frac{(\phi^2 k^{*(1)} + \phi(1-\phi)k^s)}{(1-\phi)^2} M + \frac{d^2\bar{U}}{dX_2^2} + \frac{d^2V}{dX_2^2} = 0 \tag{29}$$

where

$$\bar{V} = \frac{\mu_2}{\mu_1} \frac{\bar{v}}{L},\ U = \frac{\bar{u}}{L},\ X_2 = \frac{x_2}{L} \tag{30}$$

When the third term in equation (29), $\bar{V}_{22}$, is much smaller than the first and the second term in equation (30), equation (29) reduces to

$$\frac{\phi^2 k^{*(1)} + \phi(1-\phi)k^s}{(1-\phi)^2} M + \mu_1 \bar{u}_{,22} = 0 \tag{31}$$

In the phenomenological theory where the fluid velocity gradient terms, i.e., constitutive equations $(11)_{3,4}$, are missing in their formulation, the usual form of quasi-static equations of motion in the absence of body forces takes the form of equation (31) for this boundary value problem. Hence the equation of motion (29) reduces to the usual form of equation of motion of the phenomenological theory when $\bar{V}_{,22}$ is of the order ϵ^2.

It is important to note that in these reductions, we did not use the fluid incompressibility and therefore we can recover the governing equations of motion of the conventional theory even when the fluid is compressible. In the phenomenological theory, the equation of fluid flow takes a reduced form "Darcy's law", where no velocity gradient appears, and only the fluid mass flow rate per unit section q_i appears in the equation of motion. Since the continuity equation in the phenomenological theory,

$$\frac{\partial q_i}{\partial x_i} + \frac{\partial m}{\partial t} = 0, \tag{32}$$

holds whether the fluid is incompressible or compressible, it makes it possible to solve this simple example even when the fluid is compressible while in the modified mixture theory, we need fluid incompressibility to satisfy the continuity equation automatically. This simple example points out various features of the phenomenological theory due to the suppression of the fluid velocity gradient effect. It is important to know, however, that despite the defects pointed out here, the phenomenological theory is a good approximate theory for most practical applications since the non-Darcy flow is confined to the vicinity of the boundary. In Crochet and Naghdi [18], the confining hydrostatic pressure gradient, instead of the fluid hydrostatic pressure gradient, is related to fluid mass flow rate in their expression of Darcy's law. In our development of the modified mixture theory, the introduction of the porosity leads to the identification of total pressure, fluid pressure, and solid pressure. Furthermore, it is the fluid pressure which appears in Darcy's law.

4 Axisymmetric Steady State Flow

We consider the steady state flow in a circular cylindrical fluid-filled porous material. We assume the displacement components of the solid and the velocity components of the fluid in the form

$$\begin{aligned} u_r^{(1)} = u_\theta^{(1)} = 0,\ u_z^{(1)} = \bar{u}(r) \\ v_r^{(2)} = v_\theta^{(2)} = 0,\ v_z^{(2)} = \bar{v}(r) \end{aligned} \tag{33}$$

and require that

$$\bar{u}(r_o) = 0,\ \bar{v}(r_o) = 0. \tag{34}$$

We also assume that the deformation of the porous material is infinitesimal and that the fluid inside the pores is incompressible, i.e., $\rho_f = \rho_{fo}$.

In the axisymmetric case, the strain rates components, vorticity components, and strain components on cylindrical coordinates are as follows:

$$d_{rr}^{(\alpha)} = \frac{\partial v_r^{(\alpha)}}{\partial r},\ d_{\theta\theta}^{(\alpha)} = \frac{v_r^{(\alpha)}}{r},\ d_{zz}^{(\alpha)} = \frac{\partial v_z^{(\alpha)}}{\partial z}$$

$$d_{rz}^{(\alpha)} = \frac{1}{2}\left(\frac{\partial v_z^{(\alpha)}}{\partial r} + \frac{\partial v_r^{(\alpha)}}{\partial z}\right),\ \Gamma_{rz}^{(\alpha)} = \frac{1}{2}\left(\frac{\partial v_r^{(\alpha)}}{\partial z} - \frac{\partial v_z^{(\alpha)}}{\partial r}\right)$$

Downloaded 03 May 2010 to 171.66.16.27. Redistribution subject to ASME license or copyright; see http://www.asme.org/terms/Terms_Use.cfm

$$e_{rr}^{(\alpha)}=\frac{\partial u_r^{(\alpha)}}{\partial r},\ e_{\theta\theta}^{(\alpha)}=\frac{u_r^{(\alpha)}}{r},\ e_{zz}^{(\alpha)}=\frac{\partial u_z^{(\alpha)}}{\partial z} \tag{35}$$

$$e_{rz}^{(\alpha)}=\frac{1}{2}\left(\frac{\partial u_z^{(\alpha)}}{\partial r}+\frac{\partial u_r^{(\alpha)}}{\partial z}\right)$$

Also the nontrivial equations of motion are

$$\begin{gathered}\frac{\partial \sigma_{rr}}{\partial r}+\frac{\partial \sigma_{zr}}{\partial z}+\frac{\sigma_{rr}-\sigma_{\theta\theta}}{r}-\pi_r=\rho_1(\dot{v}_r^{(1)}-b_r^{(1)})\\ \frac{\partial \sigma_{rz}}{\partial r}+\frac{\partial \sigma_{zz}}{\partial z}+\frac{\sigma_{rz}}{r}-\pi_z=\rho_1(\dot{v}_z^{(1)}-b_z^{(1)})\\ \frac{\partial \pi_{rr}}{\partial r}+\frac{\partial \pi_{zr}}{\partial z}+\frac{\pi_{rr}-\pi_{\theta\theta}}{r}+\pi_r=\rho_2(\dot{v}_r^{(2)}-b_r^{(2)})\\ \frac{\partial \pi_{rz}}{\partial r}+\frac{\partial \pi_{zz}}{\partial z}+\frac{\pi_{rz}}{r}+\pi_z=\rho_2(\dot{v}_z^{(2)}-b_z^{(2)})\end{gathered} \tag{36}$$

The constitutive equations (6) and (7) with the assumption (33) lead to

$$\sigma'_{rr}=\sigma'_{\theta\theta}=\sigma'_{zz}=\phi k^s e_{mm}^{(2)},\ \sigma'_{(rz)}=\mu_1\frac{d\bar{u}}{dr}$$

$$\pi'_{rr}=\pi'_{\theta\theta}=\pi'_{zz}=\frac{\phi^2(k^{*(1)}+(1-\phi)k^s)}{(1-\phi)^2}e_{mm}^{(2)},\ \pi''_{(rz)}=\mu_2\frac{d\bar{v}}{dr}$$

$$\sigma''_{[rz]}=-\pi''_{[rz]}=-\mu_{11}\frac{d\bar{v}}{dr},\ \pi''_z=-\lambda_9\bar{v} \tag{37}$$

Using the constitutive equations (37), equations of motion for the steady state case in the absence of body force are

$$\begin{gathered}\phi k^s\frac{\partial e_{mm}^{(2)}}{\partial r}=0\\ \mu_1\left(\frac{d^2u}{dr^2}+\frac{1}{r}\frac{d\bar{u}}{dr}\right)-\mu_{11}\left(\frac{d^2\bar{v}}{dr^2}+\frac{1}{r}\frac{d\bar{v}}{dr}\right)\\ +\phi k^s\frac{\partial e_{mm}^{(2)}}{\partial z}+\lambda_9\bar{v}=0\\ \frac{\phi^2(k^{*(1)}+(1-\phi)k^s)}{(1-\phi)^2}\frac{\partial e_{mm}^{(2)}}{\partial r}=0\\ (\mu_2+\mu_{11})\left(\frac{d^2\bar{v}}{dr^2}+\frac{1}{r}\frac{d\bar{v}}{dr}\right)\\ +\frac{\phi^2(k^{*(1)}+(1-\phi)k^s)}{(1-\phi)^2}\frac{\partial e_{mm}^{(2)}}{\partial z}-\lambda_9\bar{v}=0\end{gathered} \tag{38}$$

From equations $(38)_{1,3}$, we know that $e_{mm}^{(2)}$ is a function of z only so that the equation $(38)_4$ can be rewritten

$$(\mu_2+\mu_{11})\left(\frac{d^2\bar{v}}{dr^2}+\frac{1}{r}\frac{d\bar{v}}{dr}\right)-\lambda_9\bar{v}=-\frac{\phi^2(k^{*(1)}+(1-\phi)k^s)}{(1-\phi)^2}\frac{de_{mm}^{(2)}}{dz}. \tag{39}$$

Since the left-hand side is a function of r only, while the right-hand side is a function of z only in equation (39), we must have

$$\frac{de_{mm}^{(2)}}{dz}=M \tag{40}$$

where M is a constant. The equation obtained by summing equations $(38)_2$ and $(38)_4$,

$$\mu_1\left(\frac{d^2\bar{u}}{dr^2}+\frac{1}{r}\frac{d\bar{u}}{dr}\right)+\mu_2\left(\frac{d^2\bar{v}}{dr^2}+\frac{1}{r}\frac{d\bar{v}}{dr}\right)=-\frac{\phi(1-\phi)k^s+\phi^2k^{*(1)}}{(1-\phi)^2}M, \tag{41}$$

and equation $(38)_4$,

$$(\mu_2+\mu_{11})\left(\frac{d^2\bar{v}}{dr^2}+\frac{1}{r}\frac{d\bar{v}}{dr}\right)-\lambda_9\bar{v}=-\frac{\phi^2(k^{*(1)}+(1-\phi)k^s)}{(1-\phi)^2}M, \tag{42}$$

together with equation (40), are a simplified set of equations of motion (38). In addition to the equations of motion, the following continuity equation for an equivalent homogeneous fluid must be satisfied.

$$\frac{\partial \rho_2}{\partial t}+\frac{\partial \rho_2}{\partial r}v_r+\frac{\partial \rho_2}{\partial z}v_z+\rho_2\left(\frac{\partial v_r}{\partial r}+\frac{v_r}{r}+\frac{\partial v_z}{\partial z}\right)=0 \tag{43}$$

Equation (43) can be rewritten by using $\rho_2=\phi\rho_f$, the incompressible condition $\rho_f=\rho_{fo}$ and the velocity field assumption $(33)_{3,4}$ as follows:

$$\frac{\partial \phi}{\partial t}+\frac{\partial \phi}{\partial z}\bar{v}=0 \tag{44}$$

Introducing the dimensionless variable R, Z, U, V, and T,

$$R=\frac{r}{r_o},\ Z=\frac{z}{r_o},\ U=\frac{\bar{u}}{r_o},\ V=\frac{r_o\lambda_9\bar{v}}{k^{*(1)}+(1-\phi)k^s},\ T=\frac{(k^{*(1)}+(1-\phi)k^s)t}{\lambda_9 r_o^2}, \tag{45}$$

into the governing equations (41), (42), and (44), we obtain the following set of nondimensionalized equations and the nondimensionalized boundary conditions:

$$\begin{gathered}\frac{d^2\bar{U}}{dR^2}+\frac{1}{R}\frac{d\bar{U}}{dR}+\frac{\mu_2(k^{*(1)}+(1-\phi)k^s)}{\lambda_9\mu_1 r_o^2}\left(\frac{d^2V}{dR^2}+\frac{1}{R}\frac{dV}{dR}\right)+\frac{r_o\{\phi(1-\phi)k^s+\phi^2k^{*(1)}\}}{\mu_1(1-\phi)^2}M=0\\ \frac{a^2}{r_o^2}\left(\frac{d^2V}{dR^2}+\frac{1}{R}\frac{dV}{dR}\right)-V+\frac{\phi^2r_oM}{(1-\phi)^2}=0\\ \frac{\partial \phi}{\partial T}+\frac{\partial \phi}{\partial z}V=0\end{gathered} \tag{46}$$

where

$$a^2=\frac{\mu_2+\mu_{11}}{\lambda_9} \tag{47}$$

$$U(1)=0,\ V(1)=0 \tag{48}$$

Since $\partial\phi/\partial Z$ is of order ϵ due to the infinitesimal deformation assumption, if we further assume that the nondimensionalized velocity V is of the infinitesimal order, then the continuity equation $(45)_3$ is automatically satisfied. The general solution of differential equation $(46)_2$ is given by

$$V=GI_0\left(\frac{r_oR}{a}\right)+BK_0\left(\frac{r_oR}{a}\right)+\frac{\phi^2r_oM}{(1-\phi)^2} \tag{49}$$

Since $K_0(r_oR/a)$ is unbounded when R approaches zero, the integration constant B in equation (49) is zero. This leads to the integration of equation $(46)_1$ as follows:

Downloaded 03 May 2010 to 171.66.16.27. Redistribution subject to ASME license or copyright; see http://www.asme.org/terms/Terms_Use.cfm

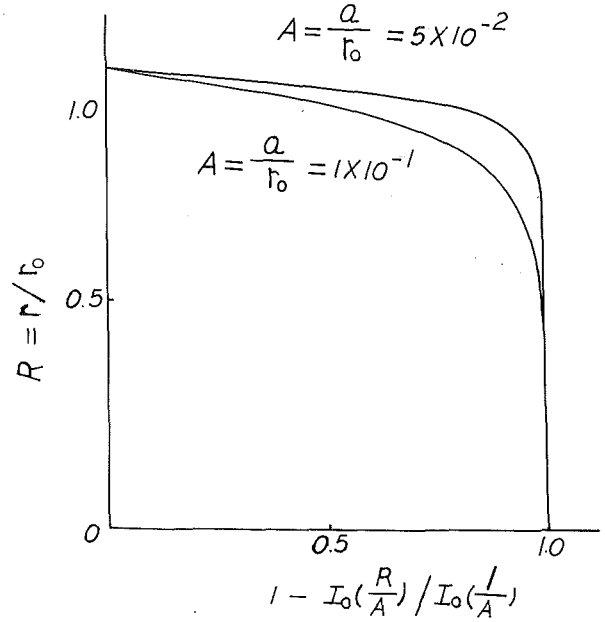


Fig. 2 Velocity profile of axisymmetric steady state flow

$$U=-\frac{\mu_2(k^{*(1)}+(1-\phi)k^s)G}{\mu_1\lambda_9 r_o^2}I_o\left(\frac{r_oR}{a}\right)$$

$$-\frac{r_o\{\phi(1-\phi)k^s+\phi^2k^{*(1)}\}M}{4\mu_1(1-\phi)^2}R^2+E\ln R+F \tag{50}$$

Since $\ln R$ is unbounded when R approaches zero, the integration constant E in equation (50) is zero.

Determining the constants G and F from the boundary conditions (48), the solution of equations $(46)_{1,2}$ which satisfy (48) are obtained as follows:

$$V=\frac{\phi^2r_oM}{(1-\phi)^2}\left[1-\frac{I_o\left(\frac{r_oR}{a}\right)}{I_o\left(\frac{r_o}{a}\right)}\right]$$

$$U=\frac{\mu_2(k^{*(1)}+(1-\phi)k^s)M\phi^2}{\mu_1\lambda_9 r_o(1-\phi)^2}\left(\frac{I_o\left(\frac{r_oR}{a}\right)}{I_o\left(\frac{r_o}{a}\right)}-1\right)$$

$$-\frac{r_o\{\phi(1-\phi)k^s+\phi^2k^{*(1)}\}M}{4\mu_1(1-\phi)^2}(R^2-1) \tag{51}$$

The velocity profiles for different values of $A = a/r_o$ were obtained in Fig. 2 by numerically solving equation (51) via a fifth order Runge-Kutta Scheme. As we might expect from the results in the previous section, the smaller the grain size, the sharper the velocity profile.

Acknowledgment

This work was supported in part by Grant No. MEA 80-20216 from the National Science Foundation (Solid Mechanics Program) to the University of California, Berkeley. N. Katsube was also supported by an Amelia Earhart Fellowship from Zonta International.

References

1 Biot, M. A., "General Theory of Three-Dimensional Consolidation," *Journal of Applied Physics*, Vol. 12, 1941, pp. 155–164.

2 Biot, M. A., "Theory of Elasticity and Consolidation for a Porous Anisotropic Solid," *Journal of Applied Physics*, Vol. 26, 1955, pp. 182–185.

3 Biot, M. A., "General Solutions of the Equations of Elasticity and Consolidation for a Porous Material," *Journal of Applied Physics*, Vol. 78, 1956, pp. 91–96.

4 Biot, M. A., and Willis, D. G., "The Elastic Coefficients of the Theory of Consolidation," ASME JOURNAL OF APPLIED MECHANICS, Vol. 24, 1957, pp. 594–601.

5 Rice, J. R., and Cleary, M. P., "Some Basic Stress Diffusion Solutions for Fluid-Saturated Elastic Porous Media with Compressible Constituents," *Reviews of Geophysics and Space Physics*, Vol. 14, 1976, pp. 227–241.

6 Deresiewicz, H., "The Effect of Boundaries on Wave Propagation in a Liquid-Filled Porous Solid," *Bulletin of the Seismological Society of America*, Vol. 50, 1960, pp. 599–607.

7 Geertsma, J., and Smit, D. C., "Some Aspects of Elastic Wave Propagation in Fluid-Saturated Porous Solids," *Geophysics*, Vol. 26, 1961, pp. 169–181.

8 Hajra, S., and Mukhopadhyay, A., "Reflection and Refraction of Seismic Waves Incident Obliquely at the Boundary of a Liquid-Saturated Porous Solid," *Bulletin of the Seismological Society of America*, Vol. 72, 1982, pp. 1509–1533.

9 Burridge, R., and Keller, J. B., "Poroelasticity Equations Derived from Microstructure," *Journal of Acoustic Society of America*, Vol. 70, 1981, pp. 1140–1146.

10 Morland, L. W., "A Simple Constitutive Theory for a Fluid-Saturated Porous Solid," *Journal of Geophysical Research*, Vol. 77, 1971, pp. 890–900.

11 Bowen, R. M., "Compressible Porous Models by Use of the Theory of Mixtures," *International Journal of Engineering Science*, Vol. 20, 1982, pp. 697–735.

12 Katsube, N., and Carroll, M. M., "The Modified Mixture Theory for Fluid-Filled Porous Materials, Theory," to appear in ASME JOURNAL OF APPLIED MECHANICS.

13 Katsube, N., "The Constitutive Theory for Fluid-Filled Porous Materials," ASME JOURNAL OF APPLIED MECHANICS, Vol. 52, 1985, pp. 185–189.

14 Carroll, M. M., "Mechanical Response of Fluid-Saturated Porous Materials," *Proceedings of 15th International Congress of Theoretical and Applied Mechanics*, Rimrott, F. P. J., and Tabarrok, B., eds., 1980, North-Holland, New York.

15 Carroll, M. M., and Katsube, N., "The Role of Terzaghi Effective Stress in Linearly Elastic Deformation," *ASME Journal of Energy Resources Technology*, Vol. 105, 1983, pp. 509–511.

16 Green, A. E., and Naghdi, P. M., "A Dynamical Theory of Interacting Continua," *International Journal of Engineering Science*, Vol. 3, 1965, pp. 231–241.

17 Crochet, N. J., and Naghdi, P. M., "On Constitutive Equations for Flow of Fluid Through an Elastic Solid," *International Journal of Engineering Science*, Vol. 4, 1966, pp. 383–401.

Downloaded 03 May 2010 to 171.66.16.27. Redistribution subject to ASME license or copyright; see http://www.asme.org/terms/Terms_Use.cfm

A Simple Kinetic Theory for Granular Flow of Rough, Inelastic, Spherical Particles

C. K. K. Lun

S. B. Savage

Department of Civil Engineering
and Applied Mechanics,
McGill University,
Montreal, Canada H3A 2K6

Using statistical methods analogous to those used in the kinetic theory of dense gases, conservation equations and constitutive equations are derived for the flow of an idealized granular material consisting of uniform, rough, inelastic spherical particles. Simple forms for the singlet and pair velocity distribution functions are employed to study the effects of particle rotary inertia in the specific case of Couette flow of such materials. A constant coefficient of restitution e *is used to characterize the inelasticity of the particles and a roughness coefficient* β *is adopted to characterize the effects of surface friction in collisions between particles.*

During collisions, surface friction causes particle rotational velocity fluctuations. As a result of particle rotary inertia, the stress tensor is found to be asymmetric during general deformations. However, for the special case of steady Couette flow which is studied in detail, the stress tensor remains symmetric. The partition of fluctuation kinetic energy between the translational and rotational modes is examined; equipartition is achieved only for the case of perfectly rough particles. In agreement with previous investigations, the stresses are found to decrease with decreasing e. *Except for the case of almost perfectly rough particles, the effects of rotary inertia generally reduce the stresses. However, the normal stresses are reduced more than the shear stresses, and the predicted ratio of shear to normal stress (the dynamic friction angle) is higher for rough particles than for smooth ones. The inclusion of roughness in the analysis yields shear to normal stress ratios that agree more closely with experimental measurements.*

Introduction

Recently, a number of authors have developed theories to predict, from considerations at the microstructural level, the constitutive equations for quantities such as stress, energy flux, and energy dissipation that are generated during rapid flows of granular materials [1–8]. Campbell and Brennen [9, 10] and Walton [11, 12] have devised computer simulations for idealized granular materials consisting of disk-like particles and have used these to provide information about the constitutive behavior. Except for the computer simulations, all of the above work has neglected the rotary inertia of the particles, the possibility of transfer of the particles' kinetic energy between the translational and rotational modes and the effects these might have upon the form of the constitutive equations. Furthermore, the model of particle collisions used by Campbell and Brennen [9, 10] was a special case in which the effects of particle surface friction were such that the postcollision *tangential velocities* of the particles at contact were equal.

Contributed by the Applied Mechanics Division for publication in the JOURNAL OF APPLIED MECHANICS.

Discussion on this paper should be addressed to the Editorial Department, ASME, United Engineering Center, 345 East 47th Street, New York, N.Y. 10017, and will be accepted until two months after final publication of the paper itself in the JOURNAL OF APPLIED MECHANICS. Manuscript received by ASME Applied Mechanics Division, November 28, 1983; final revision, July 10, 1986.

The calculations of Campbell and Brennen [9, 10] showed that, at least for their collision model, a sizeable fraction of the particles' fluctuation kinetic energy was in the rotational mode. It is thus pertinent to investigate the importance of the particles' rotary inertia which has been neglected in all of the analytical theories. In the present paper we address this problem by using a relatively simple approach. We follow the general framework of the kinetic theory of granular flow developed by Savage and Jeffrey [2], Jenkins and Savage [6], and Lun et al. [7], and extend it to include the effects of particle surface friction and rotary inertia. The specific problem of Couette flow of granular material comprised of uniform, rough, inelastic spherical particles is examined in detail. Results are presented in a manner that illustrates the significance of particle surface roughness upon the bulk stresses.

Transport Equations and Constitutive Integrals

A general equation of change for the mean value of a dynamical quantity $\langle\psi\rangle$ during the flow of granular materials was presented previously by Jenkins and Savage [6] and was given in somewhat more precise form by Lun et al. [7]. Here we adopt the latter formulation to consider the flow of uniform spherical particles which are inelastic and rough. We

Copyright © 1987 by ASME
Downloaded 03 May 2010 to 171.66.16.27. Redistribution subject to ASME license or copyright; see http://www.asme.org/terms/Terms_Use.cfm

consider a fixed volume element $d\mathbf{r}$ centered at $\mathbf{r}$ and define the ensemble average of the single particle quantity ψ as

$$\langle\psi\rangle = \frac{1}{n}\int \psi f^{(1)}(\mathbf{r},\mathbf{c},\omega;t)\,d\mathbf{c}\,d\omega \tag{1}$$

where n is the local number density of the particles and $f^{(1)}(\mathbf{r},\mathbf{c},\omega;t)$ is the usual single particle velocity distribution function defined such that $f^{(1)}(\mathbf{r},\mathbf{c},\omega;t)\ \delta\mathbf{c}\ \delta\omega$ is the differential number of particles per unit volume with translational velocities within the range $\mathbf{c}$ and $\mathbf{c} + \delta\mathbf{c}$ and with angular velocities within the range ω and $\omega + \delta\omega$. The rate of change of $\langle n\psi\rangle$ is

$$\frac{\partial}{\partial t}\langle n\psi\rangle = n\langle D\psi\rangle - \nabla\cdot\langle n\mathbf{c}\psi\rangle - \nabla\cdot\vartheta + \chi \tag{2}$$

$$\text{where } D\psi = \mathbf{b}\cdot\frac{\partial\psi}{\partial\mathbf{c}} \tag{3}$$

and $\mathbf{b}$ is the body force per unit mass. The last two terms in equation (2) comprise the collisional rate of increase of the mean of ψ per unit volume. They involve a collisional transfer term

$$\vartheta = -\frac{\sigma^3}{2}\int_{\mathbf{c}_{12}\cdot\mathbf{k}>0} (\psi_1' - \psi_1)(\mathbf{c}_{12}\cdot\mathbf{k})\mathbf{k}\, f^{(2)}\left(\mathbf{r} - \frac{1}{2}\sigma\mathbf{k},\mathbf{c}_1,\omega_1;\mathbf{r} + \frac{1}{2}\sigma\mathbf{k},\mathbf{c}_2,\omega_2;t\right) d\mathbf{k}\,d\mathbf{c}_1\,d\mathbf{c}_2\,d\omega_1\,d\omega_2 \tag{4}$$

and a collisional "source-like" contribution

$$\chi = \frac{\sigma^2}{2}\int_{\mathbf{c}_{12}\cdot\mathbf{k}>0} (\psi_2' + \psi_1' - \psi_2 - \psi_1)(\mathbf{c}_{12}\cdot\mathbf{k}) f^{(2)}(\mathbf{r} - \sigma\mathbf{k}, \mathbf{c}_1, \omega_1; \mathbf{r}, \mathbf{c}_2, \omega_2; t)\,d\mathbf{k}\,d\mathbf{c}_1\,d\mathbf{c}_2\,d\omega_1\,d\omega_2 \tag{5}$$

where $\mathbf{c}_{12} = \mathbf{c}_1 - \mathbf{c}_2$, σ is the particle diameter, and $\mathbf{k}$ is the unit vector along the line of centers from particle 1 to particle 2 at contact. The pair distribution function $f^{(2)}(\mathbf{r}_1,\mathbf{c}_1,\omega_1;\mathbf{r}_2,\mathbf{c}_2,\omega_2;t)$ is defined such that $f^{(2)}(\mathbf{r}_1,\mathbf{c}_1,\omega_1;\mathbf{r}_2,\mathbf{c}_2,\omega_2;t)\ \delta\mathbf{r}_1\delta\mathbf{r}_2\delta\mathbf{c}_1\delta\mathbf{c}_2\delta\omega_1\delta\omega_2$ is the probability of finding a pair of particles in the volume element $\delta\mathbf{r}_1$, $\delta\mathbf{r}_2$ centered on the points $\mathbf{r}_1$, $\mathbf{r}_2$ and having translational velocities within the ranges $\mathbf{c}_1$ and $\mathbf{c}_1 + \delta\mathbf{c}_1$, $\mathbf{c}_2$ and $\mathbf{c}_2 + \delta\mathbf{c}_2$, and angular velocities within the ranges ω_1 and $\omega_1 + \delta\omega_1$, ω_2 and $\omega_2 + \delta\omega_2$. Following the development of (1)–(5) by Lun et al. [7], we define the particles 1 and 2 to be centered at $\mathbf{r} - \sigma\mathbf{k}$ and $\mathbf{r}$, respectively.

By taking ψ to be the mass m, linear momentum $m\mathbf{c}$, angular momentum $I\omega$, translational kinetic energy $mc^2/2$, rotational kinetic energy $I\omega^2/2$ in equation (2), we obtain the conservation equations for mass, linear momentum, mean particle spin, and particle translational and rotational fluctuation kinetic energy

$$\frac{d\rho}{dt} = \rho\nabla\cdot\mathbf{u}, \tag{6}$$

$$\rho\frac{d\mathbf{u}}{dt} = \rho\mathbf{b} - \nabla\cdot\mathbf{p}, \tag{7}$$

$$nI\frac{d\omega_o}{dt} = -\nabla\cdot\mathbf{L} + \chi(I\omega), \tag{8}$$

$$\frac{3}{2}\rho\frac{dT_t}{dt} = -\boldsymbol{\rho}:\nabla\mathbf{u} - \nabla\cdot\mathbf{q}_t - \chi_t, \tag{9}$$

$$\frac{3}{2}\rho\frac{dT_r}{dt} = -\mathbf{L}:\nabla\omega_o - \nabla\cdot\mathbf{q}_r - \chi_r - \omega_o\cdot\chi(I\omega) \tag{10}$$

In these equations $\rho = mn = \nu\rho_p$ is the bulk mass density, ν is the bulk solids fraction, ρ_p is the mass density of a particle, $\mathbf{u} = \langle\mathbf{c}\rangle$ is the bulk velocity, and $\omega_o = \langle\omega\rangle$ is the mean particle spin velocity. Furthermore, $3/2\ m\ T_t = 1/2\ m\ \langle C^2\rangle$ is the translational fluctuation kinetic energy where $\mathbf{C} = \mathbf{c} - \mathbf{u}$, and $3/2\ m\ T_r = 1/2\ I\ \langle W^2\rangle$ is the rotational fluctuation kinetic energy where $\mathbf{W} = \omega - \omega_o$. The pressure tensor p, the angular momentum flux $\mathbf{L}$, the translational energy flux $\mathbf{q}_t$ and the rotational energy flux $\mathbf{q}_r$ are each made up of the sum of a kinetic part and a collisional transfer part denoted by subscripts k and c respectively, thus

$$\mathbf{p}_k = \rho\langle\mathbf{CC}\rangle, \tag{11}$$

$$\mathbf{p}_c = \vartheta(m\mathbf{C}), \tag{12}$$

$$\mathbf{L}_k = nI\langle\mathbf{CW}\rangle, \tag{13}$$

$$\mathbf{L}_c = \vartheta(I\mathbf{W}), \tag{14}$$

$$\mathbf{q}_{t_k} = \frac{\rho}{2}\langle\mathbf{C}C^2\rangle, \tag{15}$$

$$\mathbf{q}_{t_c} = \vartheta\left(\frac{1}{2}mC^2\right), \tag{16}$$

$$\mathbf{q}_{r_k} = \frac{nI}{2}\langle\mathbf{C}W^2\rangle, \tag{17}$$

$$\mathbf{q}_{r_c} = \vartheta\left(\frac{1}{2}IW^2\right). \tag{18}$$

In the previous studies of Jenkins and Savage [6] and Lun et al. [7] dealing with smooth particles, the difference between the translation kinetic energy of the particle pair after and before a collision was due solely to the inelasticity of the particles and $-\chi(1/2\ mc^2)$ was equal to the *rate of energy dissipation* per unit volume, part of the kinetic energy of the particles being converted into thermal energy of the molecules making up each grain.

In the present more general case, there exists the possibility that, during a collision, translational kinetic energy may be dissipated, and in addition that an exchange between translational and rotational kinetic energy may occur. Thus we define the rate of translational kinetic energy interchange per unit volume as

$$\chi_t = -\chi\left(\frac{1}{2}mc^2\right) \tag{19}$$

and the rate of rotational kinetic energy interchange per unit volume as

$$\chi_r = -\chi\left(\frac{1}{2}I\omega^2\right) \tag{20}$$

The above equations have been derived in essentially the same form by using slightly different arguments by Condiff, Lu, and Dahler [13] in the context of a kinetic theory for a gas comprised of perfectly rough spheres.

Analysis

Velocity Distribution Functions. Probably it is possible to solve for the single particle distribution function $f^{(1)}$ by making use of moment equations constructed from equation (2) in a manner similar to that developed in Lun et al. [7]. However, for the general case considered here, this would be extremely complicated and in the present paper we shall follow a much simpler approach to obtain the constitutive equations. In their comparisons of various granular flow theories, Lun et al. [7] found that the simple ad hoc assumption for the distribution functions $f^{(1)}$ and $f^{(2)}$ assumed by Savage and Jeffrey [2] and Jenkins and Savage [6] not only predicted most of the general trends of the more complete analysis which explicitly determined $f^{(1)}$ and $f^{(2)}$ but also gave surprisingly close quantitative

Downloaded 03 May 2010 to 171.66.16.27. Redistribution subject to ASME license or copyright; see http://www.asme.org/terms/Terms_Use.cfm

results, at least for the case of simple shear. Encouraged by the relative simplicity and success of the approach of Jenkins and Savage [6] we shall assume forms for the distribution functions analogous to those assumed by Jenkins and Savage and use them to calculate the required constitutive relations. Thus while we obtain approximate results which may miss out some of the details, we hope to extract the essential effects resulting from particle rotary inertia in the simplest possible way. Detailed results will be calculated for the special case of a simple shear flow. Almost all of the previously mentioned theories have either been developed specifically for this flow or have examined it as a particular flow example. Thus, they are available for comparison with the present predictions.

Two of the molecular models commonly used in the kinetic theories of fluids are perfectly smooth, perfectly elastic spheres and perfectly rough, perfectly elastic spheres [13, 14]. In the latter case the spheres "grip" each other during a collision such that the relative velocity at the point of contact is reversed. No energy dissipation occurs in either model, but in the latter, interchanges between translational and rotational kinetic energies can occur. The equilibrium single particle velocity distribution functions for both models have the form of local Maxwellians. In the present paper we wish to consider particles which are imperfectly rough such that some slip can occur during a collision and energy dissipation results from frictional slip as well as from inelastic deformation. Following the general approach of Savage and Jeffrey [2] and Jenkins and Savage [6] we approximate the single particle velocity distribution *during shear* by a local Maxwellian of the form

$$f^{(1)}(\mathbf{r},\mathbf{c},\omega;t) \simeq \frac{n}{(2\pi T_t)^{3/2}(2\pi m T_r/I)^{3/2}} \exp\left(-\frac{(\mathbf{c}-\mathbf{u})^2}{2\,T_t}\right)\exp\left(-\frac{I(\omega-\omega_o)^2}{2mT_r}\right). \tag{21}$$

Notice that this is slightly different from the form of the equilibrium distribution functions given by Chapman and Cowling [14] and Condiff et al. [13] for the case of perfectly rough spheres. In those cases there was equipartition of the mean peculiar translational and rotational kinetic energies. Here we consider different degrees of slip such that in general this kind of energy equipartition is not realized. The form of (21) which is written explicitly in terms of the translational and rotational granular temperatures allows for varying degrees of slip and different ratios of translational to rotational peculiar kinetic energies. Binary collisions are assumed and the pair distribution function $f^{(2)}$ is approximated by

$$\begin{aligned} &f^{(2)}\left(\mathbf{r}-\frac{1}{2}\,\sigma\mathbf{k},\mathbf{c}_1,\omega_1;\mathbf{r}+\frac{1}{2}\,\sigma\mathbf{k},\mathbf{c}_2,\omega_2;t\right)\\ &\simeq g_o(\sigma;\nu) f^{(1)}\left(\mathbf{r}-\frac{1}{2}\,\sigma\mathbf{k},\mathbf{c}_1,\omega_1;t\right) f^{(1)}\left(\mathbf{r}+\frac{1}{2}\,\sigma\mathbf{k},\mathbf{c}_2,\omega_2;t\right)\\ &= g_o(\sigma;\nu) f^{(1)}(\mathbf{r},\mathbf{c}_1,\omega_1;t) f^{(1)}(\mathbf{r},\mathbf{c}_2,\omega_2;t)\\ &\times\left\{1+\frac{1}{2}\,\sigma\mathbf{k}\cdot\nabla \ln[f^{(1)}(\mathbf{r},\mathbf{c}_2,\omega_2;t)/f^{(1)}(\mathbf{r},\mathbf{c}_1,\omega_1;t)]+\ldots.\right\} \end{aligned} \tag{22}$$

where $g_o(\sigma;\nu)$ is the equilibrium radial distribution function at contact. Taking the $f^{(1)}$'s in equation (22) to be given by equation (21), the approximation for $f^{(2)}$ is simpler in form than that used by Savage and Jeffrey [2] but is a generalization of the approximation proposed and used with success by Longuet-Higgins and Pople [15] for a dense fluid of smooth hard spheres. Savage and Jeffrey [2] and Jenkins and Savage [6] used Carnahan and Starling's [16] expression for the radial distribution function at contact

$$g_o(\sigma;\nu) = \frac{1}{(1-\nu)} + \frac{3\nu}{2(1-\nu)^2} + \frac{\nu^2}{2(1-\nu)^3} = \frac{(2-\nu)}{2(1-\nu)^3} \tag{23}$$

Savage [8] has suggested that the expression given by Ogawa et al. [1],

$$g_o(\nu) = [1-(\nu/\nu_M)^{1/3}]^{-1} \tag{24}$$

may be more appropriate for use in the expression for $f^{(2)}$ at high concentrations during shearing than equation (23). In equation (24) ν_M is the maxmium value of the solids fraction; it was proposed that a suitable value of ν_M is about 0.64 corresponding to a random close packing.

Collisional Model. Consider a collision between two rough, inelastic spherical particles 1 and 2 each of diameter σ and having translational velocities $\mathbf{c}_1$ and $\mathbf{c}_2$, angular velocities ω_1 and ω_2, respectively. The total relative velocty at contact point $\mathbf{g}_{12}$ just prior to the collision

$$\mathbf{g}_{12} = \mathbf{c}_{12} - \frac{\sigma\mathbf{k}}{2}\times\Omega \tag{25}$$

where $\mathbf{c}_{12} = \mathbf{c}_1 - \mathbf{c}_2$ and $\Omega = \omega_1 + \omega_2$. During a collision the components of $\mathbf{g}_{12}$ are changed such that

$$(\mathbf{k}\cdot\mathbf{g}'_{12}) = -e(\mathbf{k}\cdot\mathbf{g}_{12}) \tag{26}$$

and

$$(\mathbf{k}\times\mathbf{g}'_{12}) = -\beta(\mathbf{k}\times\mathbf{g}_{12}) \tag{27}$$

where $\mathbf{k}$ is the unit vector along the center line and primed quantities denote values after the collision. We have defined two *constant* coefficients e and β to characterize the collision process. Although the usual normal coefficient of restitution e is often taken to be constant, from physical considerations of the plastic deformations that occur during a collision as well as from experimental data [17] it is apparent that e for a given particle is dependent upon impact velocity. Thus e is merely a phenomenological coefficient suitable for particles of a particular size and material and which *in effect* has been averaged over particle impact velocities and hence is suitable for a particular translational granular temperature.

The roughness coefficient β, which is somewhat analogous to the coefficient of restitution, models the rotational aspect of the collision in a more approximate way than the coefficient of restitution models the linear velocity changes. The dynamics of the collision are in general more complicated than that given by equation (27) with β = constant. In an actual collision between two spheres, normal and tangential impulsive forces are generated at the contact surface. The final postcollisional velocities of the spheres are governed by the coefficient of surface friction and the inelasticities in both the normal and tangential components. Hence, the ratio of postcollisional to precollisional relative tangential velocities would depend upon the surface friction coefficient and the normal impulsive forces as well as the tangential inelasticity of the principles (Johnson [18]). Thus the constant roughness coefficient β is in effect a value which should be associated with a suitable averaging over various precollisional impact conditions.

We note that the case of smooth perfectly elastic particles corresponds to $\beta = -1$. This means that the tangential component of the relative velocity at the contact point is unchanged by the collision. From a physical point of view, as the two particles collide, the smooth particle surface slip over one another. There is neither loss of kinetic energy in the rotational mode nor interchange of energy between the translational and the rotational modes.

The case of perfectly rough and perfectly elastic particles corresponds to $\beta = 1$. This means that the tangential component of the relative velocity would have the same magnitude

Downloaded 03 May 2010 to 171.66.16.27. Redistribution subject to ASME license or copyright; see http://www.asme.org/terms/Terms_Use.cfm

but opposite direction before and after the collision. During such a collision, the particle surfaces are so rough that they grip one another and then rebound in an elastic manner. All the kinetic energy is transfered into elastic strain energy through the deformation in each grain. As the particles recover to their original shapes just prior to separation, all the strain energy is converted back into translational and rotational energy such that the relative velocities in both the normal and tangential directions are reversed but retain the same magnitudes as that prior to the collision. As a result, no kinetic energy is lost. It is worth noting that the perfectly rough, perfectly smooth, uniform sphere ($\beta = 1$) model was initially proposed in 1894 by Bryan [19] and has since been used as standard model in the kinetic theories of gases and dense fluids to study rotary inertia effects of complex molecules in a simple way (see, for example [14], [20–23]).

Cases for which $0 < \beta < 1$ correspond to situations in which the tangential relative velocity component is not only reduced in magnitude but is reversed in direction following the collision. This rather surprising phenomenon of spin reversal can be readily demonstrated with a child's toy called a "superball". (A superball is a small rubber ball having the combined properties of a high coefficient of restitution and a high surface friction coefficient.) Garwin [24] has described and analyzed the bizarre behavior that can be generated during the impact of a superball with rough flat surfaces. More detailed experiments of Maw et al. [25] and Johnson [18] involving steel disks, rubber disks and superballs colliding with plane walls show spin reversal. Reducing their data to obtain values for β yields positive values as large as 0.8. Johnson [18] has also pointed out that a collision analysis assuming "rigid" bodies yields no spin reversal, whereas one which accounts for elastic tangential deformations can predict $\beta > 0$. Negative values of β correspond to a reduction in the tangential relative velocity but no change in its direction following a collision.

The case of $\beta = 0$ corresponds to the model used in the computer simulations of Campbell and Brennen [9, 10] in which surface friction and inelasticity are sufficient to eliminate the postcollisional tangential relative velocities.

Using equations (26) and (27) in (25) the relationship between the pre and post-collisional velocities can be shown to be

$$\mathbf{c}_1' - \mathbf{c}_1 = -\eta_2 \mathbf{c}_{12} - (\eta_1 - \eta_2)\mathbf{k}(\mathbf{k}\cdot\mathbf{c}_{12}) + \eta_2 \frac{\sigma}{2}\,\mathbf{k}\times\boldsymbol{\Omega} \tag{28}$$

$$\mathbf{c}_2' - \mathbf{c}_2 = \eta_2 \mathbf{c}_{12} + (\eta_1 - \eta_2)\mathbf{k}(\mathbf{k}\cdot\mathbf{c}_{12}) - \eta_2 \frac{\sigma}{2}\,\mathbf{k}\times\boldsymbol{\Omega} \tag{29}$$

and

$$\omega_1' - \omega_1 = \omega_2' - \omega_2 = -\frac{\sigma m}{4I}\,\eta_2(\mathbf{k}\times\mathbf{c}_{12}) + \frac{\sigma^2 m}{4I}\,\eta_2(\mathbf{k}\cdot\boldsymbol{\Omega})\mathbf{k} - \frac{\sigma^2 m}{4I}\,\eta_2\boldsymbol{\Omega} \tag{30}$$

$$\text{where} \quad \eta_1 = \frac{(1+e)}{2} \tag{31}$$

$$\eta_2 = \left(\frac{1+\beta}{2}\right)\left(\frac{K}{1+K}\right) \tag{32}$$

and $K = \dfrac{4I}{m\sigma^2}$

$\left(K = \dfrac{2}{5}\right.$ for the uniform sphere considered here$\left.\right)$.

Couette Flow. We now consider the case of a simple shear flow (constant shear rate) $\mathbf{u} = u(y)\mathbf{e}_x$ having a uniform bulk density ρ, uniform trnaslational granular temperature T_t and uniform rotational granular temperature T_r. The solids fraction ν and shear rates are taken to be sufficiently high so that in equations (11) to (18) the kinetic contributions resulting from free particle diffusion are negligible compared to the collisional contributions to the fluxes of linear and angular momentum, and translational and rotational kinetic energy.

The theory of Lun et al. [7] and the recent three-dimensional computer simulation of smooth, inelastic spheres performed by Walton and Braun [26] have shown that for the case of simple shear flow, the collisional contributions for stress are dominant for solids concentrations greater than about 0.15. On the other hand, for concentrations near the closest random solids packing of the flow system, the assumption of binary collisions breaks down. The stresses predicted by the computer simulations of Walton and Braun [26] began to deviate from that predicted by the theory of Lun et al. [7] (which assumes binary collisions) when the solids fraction was greater than about 0.5.

Implicit in the analysis that follows is the assumption that the energy dissipation is small such that the nondimensional parameter defined by Savage and Jeffrey [2] as the ratio of the characteristic mean shear velocity to the r.m.s. of the particle translational fluctuation velocity, $R_t = (\sigma\, du/dy)/\langle C^2\rangle^{1/2}$ is small. This implies that ω_o which is of the same order as du/dy is also small, hence we may neglect second and higher order terms, e.g., $(du/dy)^2$, ω_o^2. As a result, the form of the velocity distributions from equations (21) and (22) can be written as

$$f^{(1)}(\mathbf{r},\mathbf{c},\omega;t) \simeq \frac{n\left(1+\dfrac{I\omega_o\cdot\omega}{mT_r}\right)}{(2\pi T_t)^{3/2}(2\pi m T_r/I)^{3/2}} \exp\left(-\frac{(\mathbf{c}-\mathbf{u})^2}{2T_t} - \frac{I\omega^2}{2mT_r}\right) \tag{33}$$

$$f^{(2)}\left(\mathbf{r}-\frac{1}{2}\,\sigma\mathbf{k},\mathbf{c}_1,\omega_1;\mathbf{r}+\frac{1}{2}\,\sigma\mathbf{k},\mathbf{c}_2,\omega_2;t\right) \simeq \frac{n^2 g_o(\sigma;\nu)}{(2\pi T_t)^3(2\pi m T_r/I)^3}\left(1+\frac{I\omega_o\cdot(\omega_1+\omega_2)}{mT_r} - \frac{\sigma(\mathbf{k}\cdot\nabla u)\cdot(\mathbf{c}_1-\mathbf{c}_2)}{2T_t}\right) \cdot\exp\left(-\frac{(\mathbf{c}_1-\mathbf{u})^2+(\mathbf{c}_2-\mathbf{u})^2}{2T_t} - \frac{I(\omega_1^2+\omega_2^2)}{2mT_r}\right) \tag{34}$$

where ω_o and $\mathbf{u}$ in the right-hand side of (34) are evaluated at the point $\mathbf{r}$. With the above assumptions, the mean spin equation (8), and the energy equations (9) and (10) reduce to

$$\chi(I\omega) = 0 \tag{35}$$

$$p_{yx}\frac{du}{dy} + \chi_t = 0 \tag{36}$$

and

$$\chi_r = 0 \tag{37}$$

in which equation (35) is the conservation of the rate of angular momentum transfer, equation (36) is simply a balance between the shear work and the rate of translational kinetic energy interchange and equation (37) states that the rate of rotational kinetic energy interchange is zero. Energy is supplied to the mean flow to maintain the translational and rotational velocity fluctuations.

By using the assumed form for the pair distribution function (34) in the collisional integral (12) for the stress tensor under general deformation we obtain

$$\mathbf{p} = (4\eta_1\rho_p\nu^2 g_o T_t - \mu_b\nabla\cdot\mathbf{u})\mathbf{I} - 2\mu\mathbf{S} - \zeta\mathbf{I}\times(2\omega_o - \text{curl }\mathbf{u}) \tag{38}$$

Downloaded 03 May 2010 to 171.66.16.27. Redistribution subject to ASME license or copyright; see http://www.asme.org/terms/Terms_Use.cfm

where $\mathbf{S} = 1/2\,(u_{i,j}+u_{j,i}) - 1/3\,u_{n,n}\delta_{ij}$, $\mathbf{I}$ or δ_{ij} is the unit tensor. The bulk viscosity μ_b, shear viscosity μ and the spin viscosity ζ are given as

$$\mu_b = \frac{8}{3}\,\eta_1\rho_p\sigma\nu^2 g_o\,(T_t/\pi)^{1/2} \tag{39}$$

$$\mu = \frac{2}{5}\,(4\eta_1+3\eta_2)\rho_p\sigma\nu^2 g_o\,(T_t/\pi)^{1/2} \tag{40}$$

$$\zeta = 2\eta_2\rho_p\sigma\nu^2 g_o\,(T_t/\pi)^{1/2} \tag{41}$$

It is interesting to note that as a result of the consideration of rough particles with rotary inertia, the stress tensor is asymmetric. Similar expressions for the stresses had been obtained by Sather and Dahler [27] for the case of dense polyatomic molecules with impulsive forces of repulsion. From equations (5), (30), and (34), the term $\chi(I\omega)$ is found to be the collisional rate of transfer of angular momentum due to the difference between the mean spin of the particles and the rotational deformation of the bulk materials

$$\chi(I\omega) = -2\zeta(2\omega_o - \text{curl }\mathbf{u}) \tag{42}$$

In the case of simple shear flow, the angular momentum equation (8) reduces to equation (35), $\chi(I\omega) = 0$, hence the mean spin equals the rotational bulk deformation

$$\omega_o = \frac{1}{2}\,\text{curl }\mathbf{u} \tag{43}$$

As a result, the stress tensor remains symmetric in this particular case, i.e.,

$$\mathbf{p} = 4\eta_1\rho_p\nu^2 g_o T_t\mathbf{I} - \frac{2(4\eta_1+3\eta_2)}{5\,\pi^{1/2}}\,\rho_p\nu^2 g_o T_t^{1/2}\sigma\,\frac{du}{dy}\begin{bmatrix}0&1&0\\1&0&0\\0&0&0\end{bmatrix} \tag{44}$$

Similarly, from equations (19), (5), and (34) we find the rate of translational kinetic energy interchange

$$\chi_t = \frac{48}{\pi^{1/2}}\,\rho_p\,\frac{\nu^2}{\sigma}\,g_o T_t^{1/2}\{[\eta_1(1-\eta_1) + \eta_2(1-\eta_2)]T_t - \eta_2^2 K^{-1}T_r\} \tag{45}$$

From equations (20), (5), and (34) we obtain the rate of rotational kinetic energy interchange

$$\chi_r = -\frac{48}{\pi^{1/2}}\,\rho_p\,\frac{\nu^2 g_o\eta_2}{\sigma k}\,T_t^{1/2}[\eta_2 T_t - (1-\eta_2 k^{-1})T_r] \tag{46}$$

We note that χ_t and χ_r involve both the translational and rotational granular temperatures T_t and T_r, and dissipation from inelasticity as well as surface friction (associated with the coefficients e and β).

Since by equation (37) $\chi_r = 0$, the ratio of the rotational to translational fluctuation kinetic energy is given by equation (46) as

$$\frac{T_r}{T_t} = \frac{\eta_2}{(1-\eta_2 K^{-1})} \tag{47}$$

and the ratio of rotational to the total fluctuation kinetic energy is

$$\frac{T_r}{T_r+T_t} = \frac{\eta_2}{(1+\eta_2-\eta_2 K^{-1})} \tag{48}$$

Both of these ratios, which are independent of e, are shown as functions of the roughness coefficient β in Fig. 1. The value of $\beta = -1$, corresponds to smooth particles and all of the fluctuation energy is in the translational mode. With increasing β the roughness of the particles increases the frictional dissipation and the energy exchange between the rotational and translational modes. For $\beta > 0$, the roughness and the tangential elasticity of particles increase; "spring back", tending to reverse the relative tangential velocities at contact occurs. For $\beta = 1$, the particles are perfectly rough, perfectly elastic, and no energy dissipation occurs. Equipartition of fluctuation kinetic energy between the translational and rotational modes then results.

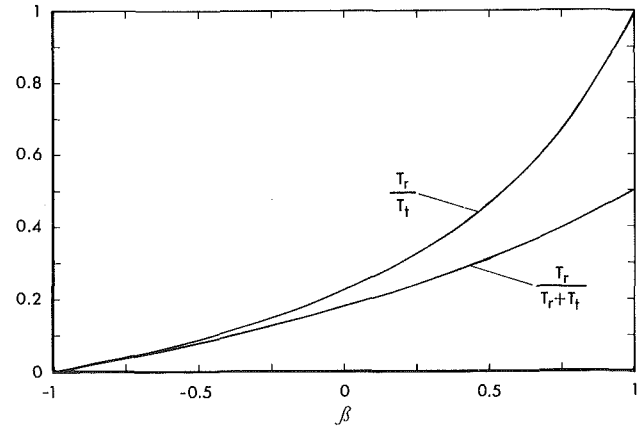


Fig. 1 Variation of specific kinetic energy ratios, T_r/T_t and $T_r/(T_r+T_t)$, with roughness coefficient β

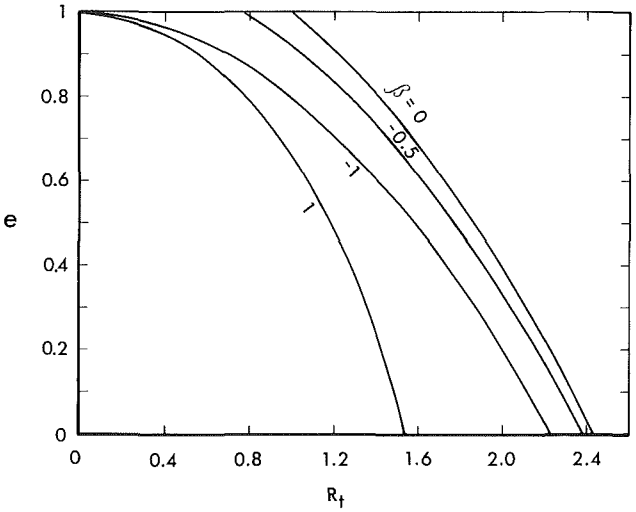


Fig. 2 Variation of coefficient of restitution e with the ratio of characteristic mean shear to the r.m.s. of the translational velocity fluctuations R_t for different values of roughness coefficient β

From equation (36) we can calculate the relationship between the ratio of characteristic mean shear to the r.m.s. of the translational velocity fluctuations and the material coefficients e and β, thus

$$R_t = \frac{\sigma(du/dy)}{\langle C^2\rangle^{1/2}} = \left\{\frac{40[\eta_1(1-\eta_1)+\eta_2(1-\eta_2)-\eta_2^3(K-\eta_2)^{-1}]}{(4\eta_1+3\eta_2)}\right\}^{1/2} \tag{49}$$

Figure 2 shows R_t plotted versus e for various values of β. For perfectly smooth ($\beta = -1$) or perfectly rough particles ($\beta = +1$), $R_t \to 0$ for $e \to 1$, corresponding to perfectly elastic dissipationless collisions. For $-1 < \beta < 1$ $R_t \neq 0$ at $e = 1$, since energy dissipation is possible through surface frictional slip or "tangential inelasticity". The general shape of the R_t versus e curves are much the same as those found from the various theories compared by Lun et al. [7], all of which neglected the effects of rotary inertia.

Downloaded 03 May 2010 to 171.66.16.27. Redistribution subject to ASME license or copyright; see http://www.asme.org/terms/Terms_Use.cfm

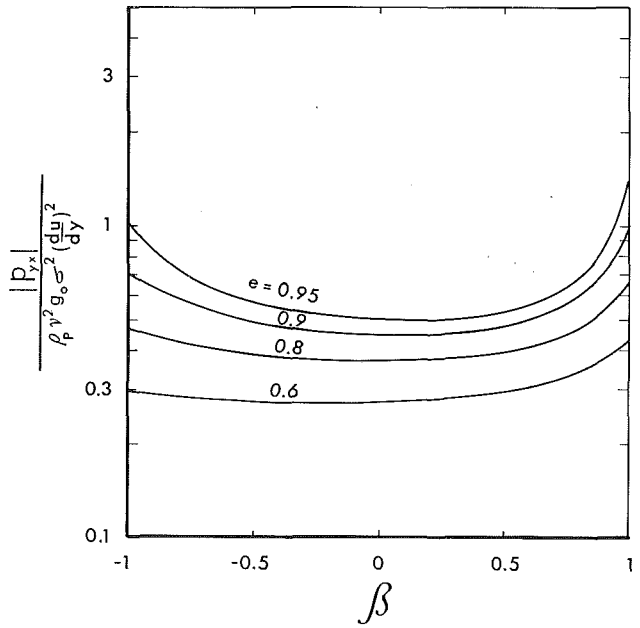


Fig. 3 Variation of nondimensional shear stress with roughness coefficient β for different values of coefficient of restitution e

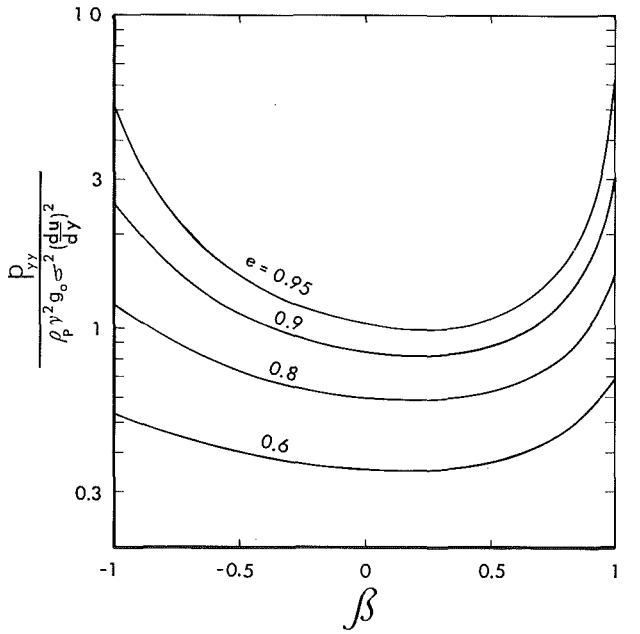


Fig. 4 Variation of nondimensional normal stress with roughness coefficient β for different values of coefficient of restitution e

As mentioned earlier, the assumption implicit in the present theory is that R_t is small compared to unity. According to the calculations shown in Fig. 2, R_t (which depends upon the roughness coefficient β) is not necessarily small compared with unity for most cases. The theory is expected to be valid and applicable only for cases of β close to -1 and $+1$, and e close to unity. However, Campbell and Gong [28] recently obtained stresses using their computer simulation code for the case of simple shear flow of frictional, inelastic disks. Their model for frictional particles corresponds to particles with infinite surface friction, i.e., $\beta = 0$. In spite of the use of a rather crude transformation to convert the three-dimensional concentration to an "equivalent" two-dimensional concentration, the predictions of the present theory were shown to agree reasonably well with the computed stresses even for the case of e as low as 0.6.

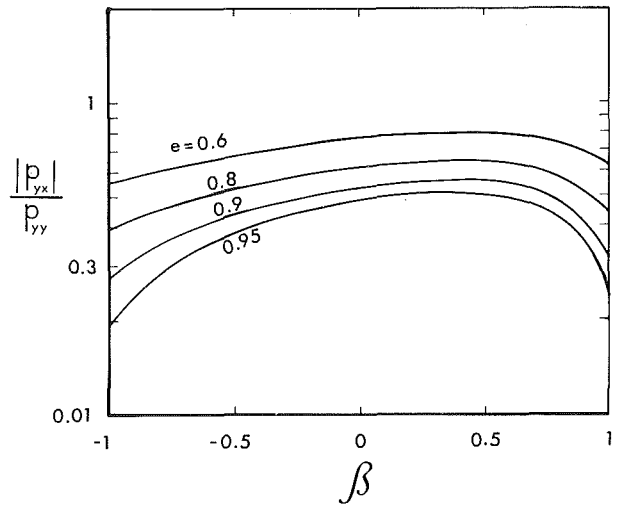


Fig. 5 Variation of the ratio of shear stress to normal stress with roughness coefficient β for different values of coefficient of restitution e

Using the definitions for T_t and equation (49), the expression for the stress tensor (44) can be rewritten in nondimensional form as

$$\frac{\mathbf{p}}{\rho_p \nu^2 g_o \sigma^2 (du/dy)^2} = \frac{4\eta_1}{3R_t^2}\mathbf{I} - \frac{2(4\eta_1 + 3\eta_2)}{5(3\pi)^{1/2}R_t}\begin{bmatrix} 0 & 1 & 0 \\ 1 & 0 & 0 \\ 0 & 0 & 0 \end{bmatrix} \tag{50}$$

Similarly, the nondimensional rate of translational energy interchange is

$$\frac{\chi_t}{\rho_p \nu^2 g_o \sigma^2 (du/dy)^3} = \frac{16}{(3\pi)^{1/2}R_t^3}[\eta_1(1-\eta_1) + \eta_2(1-\eta_2) - \eta_2^3(K-\eta_2)^{-1}] \tag{51}$$

Figure 3 shows the nondimensional shear stress $p_{yx}/\{\rho_o \nu^2 g_o \sigma^2 (du/dy)^2\}$ plotted versus the roughness coefficient β for various values of the coefficient of restitution e. We note that by equation (36), $p_{yx}/\{\rho_p \nu^2 g_o \sigma^2 (du/dy)^2\}$ equals the negative of the nondimensional rate of translational kinetic energy interchange. At the higher values of e, the stress first decreases as β increases from the smooth sphere value of -1, reaches a minimum and then increases again as β increases to the value of $+1$ corresponding to perfectly rough spheres. In such instances the increase in dissipation due to surface friction and tangential inelasticity allows the translational granular temperature to decrease, resulting in lower shear stresses.

From equation (44) it is seen that the normal stresses are isotropic. Figure 4 shows the nondimensional normal stress $p_{yy}/\{\rho_p \nu^2 g_o \sigma^2 (du/dy)^2\}$ plotted versus β for various values of e. All curves show minima and higher values for perfectly rough spheres ($\beta = 1$) than for perfectly smooth spheres ($\beta = -1$).

We can also determine the ratio of the shear to normal stresses from equation (44) as follows:

$$\frac{p_{xy}}{p_{yy}} = \frac{3(4\eta_1 + 3\eta_2)}{10(3\pi)^{1/2}\eta_1} R_t \tag{52}$$

The stress ratio given by (52) is plotted as a function of β for various values of e in Fig. 5. The curves have maxima but the stress ratios for $\beta > -1$ are all greater than the smooth surface values corresponding to $\beta = -1$. This is an interesting result since the comparisons made by Lun et al. [7] of the various smooth sphere theories with the experiments of Savage and Sayed [29], [30] showed that the predictions of the stress

Downloaded 03 May 2010 to 171.66.16.27. Redistribution subject to ASME license or copyright; see http://www.asme.org/terms/Terms_Use.cfm

ratios were too low. The inclusion of rotary inertia effects has the effect of bringing the predictions closer to the measurements.

Concluding Remarks

In this paper, we have presented a kinetic theory for the rapid flows of rough, inelastic spherical granular material and examined in detail the case of Couette flow at moderately high solids concentration. By using simple ad hoc assumptions for the singlet and pair velocity distribution functions similar in form to those used successfully by Savage and Jeffrey [2], Jenkins and Savage [6], and Lun et al. [7], the essential effects of particle rotary inertia upon the stresses, translational and rotational fluctuation kinetic energy were extracted.

The present theory can be extended by solving for the complete velocity distribution functions in a manner similar to the moment method used by Lun et al. [7]. This more exact theory would incorporate the collisional as well as the kinetic contributions to the constitutive equations and would be applicable over a wide range of solids concentration. At very high concentrations close to the value for a dense random packing, the rate-independent part of the stresses due to enduring frictional contacts between particles will become important. Such stresses have been ignored in the present as well as all other studies mentioned in the present paper. This problem as well as the question of the boundary conditions which should be used next to solid boundaries and free surfaces require further investigation.

References

1 Ogawa, S., Umemura, A., and Oshima, N., "On the Equations of Fully Fluidized Granular Materials," *Journal of Applied Mathematics and Physics (ZAMP)*, Vol. 31, 1980, pp. 483–493.

2 Savage, S. B., and Jeffrey, D. J., "The Stress Tensor in a Granular Flow at High Shear Rates," *Journal of Fluid Mechanics*, Vol. 110, 1981, pp. 255–272.

3 Shen, H., and Ackermann, N. L., "Constitutive Relationships for Fluid-Solid Mixtures," *Journal of Engineering Mechanics Division A.S.C.E.*, Vol. 108, 1982, pp. 748–763.

4 Ackermann, N. L., and Shen, H., "Stresses in Rapidly Sheared Fluid-Solid Mixtures," *Journal of Engineering Mechanics Division of A.S.C.E.*, Vol. 108, 1982, pp. 95–113.

5 Haff, P. K., "Grain Flow as a Fluid Mechanical Phenomenon," *Journal of Fluid Mechanics*, Vol. 134, 1983, pp. 401–430.

6 Jenkins, J. T., and Savage, S. B., "A Theory for the Rapid Flow of Identical, Smooth, Nearly Elastic, Spherical Particles," *Journal of Fluid Mechanics*, Vol. 130, 1983, pp. 187–202.

7 Lun, C. K. K., Savage, S. B., Jeffrey, D. J., and Chepurniy, N., "Kinetic Theories for Granular Flow: Inelastic Particles in Couette Flow and Slightly Inelastic Particles in a General Flow Field," *Journal of Fluid Mechanics*, Vol. 140, 1984, pp. 223–256.

8 Savage, S. B., "Streaming Motions in a Bed of Vibrationally-Fluidized Dry Granular Material," submitted to *Journal of Fluid Mechanics*.

9 Campbell, C. S., and Brennen, C. E., "Computer Simulation of Shear Flows of Granular Material," in *Mechanics of Granular Materials: New Models and Constitutive Relations*, Jenkins, J. T., and Satake, M., eds., Elsevier, 1983, pp. 313–326.

10 Campbell, C. S., and Brennen, C. E., "Computer Simulations of Chute Flows of Granular Materials," in *Proceedings of IUTAM Symposium on Deformation and Failure of Granular Materials*, Delft, 1983.

11 Walton, O. R., "Particle Dynamics Modelling of Geological Materials," Lawrence Livermore Laboratory Rept. UCRL-52915, University of California, 1980.

12 Walton, O. R., "Particle Dynamics Calculations of Shear Flow," in *Mechanics of Granular Materials: New Models and Constitutive Relations*, Jenkins, J. T., and Satake, M., eds., Elsevier, 1983, pp. 327–338.

13 Condiff, D. W., Lu, W. K., and Dahler, J. S., "Transport Properties of Polyatomic Fluids, A Dilute Gas of Perfectly Rough Spheres," *Journal of Chemical Physics*, Vol. 42, 1965, pp. 3445–3475.

14 Chapman, S., and Cowling, T. G., *The Mathematical Theory of Non-Uniform Gases*, 3rd Edn., Cambridge University Press, 1970.

15 Longuet-Higgins, H. C., and Pople, J. A., "Transport Properties of a Dense Fluid of Hard Spheres," *Journal of Chemical Physics*, Vol. 25, No. 5, 1956, pp. 884–889.

16 Carnahan, N. F., and Starling, K. E., "Equations of State for Non-Attracting Rigid Spheres," *Journal of Chemical Physics*, Vol. 51, 1969, pp. 635–636.

17 Goldsmith, W., *Impact: The Theory and Physical Behavior of Colliding Solids*, E. Arnold, 1960.

18 Johnson, K. L., "One Hundred Years of Hertz Contact," *Proc. Instn. Mech. Engrs.*, Vol. 196, 1982, pp. 363–378.

19 Bryan, G. H., "Report of the Present State of Our Knowledge of Thermodynamics," *Brit. Assoc. Reports*, 1894, pp. 64–106.

20 Ferziger, J. H., and Kaper, H. G., *Mathematical Theory of Transport Processes in Gases*, Chapter 11, Elsevier, 1972.

21 Bird, G. A., *Molecular Gas Dynamics*, Oxford, 1976.

22 Dahler, J. S., and Theodosopulu, M., "The Kinetic Theory of Dense Polyatomic Fluids," *Advances in Chem. Phys.*, Vol. 31, 1975, pp. 155–229.

23 Davis, H. T., "Kinetic Theory of Dense Fluids and Liquids," *Advances in Chem. Phys.*, Vol. 24, 1973, pp. 257–343.

24 Garwin, R. L., "Kinematics of an Ultraelastic Rough Ball," *American Journal of Physics*, Vol. 37, No. 1, 1969, pp. 88–92.

25 Maw, N., Baber, J. R., and Fawcett, J. N., "The Role of Elastic Tangential Compliance in Oblique Impact," *Transaction ASME Journal of Lubrication Technology*, Vol. 103, 1981, pp. 74–80.

26 Walton, O. R., and Braun, R. L., "Stress Calculations for Assemblies of Inelastic Spheres in Uniform Shear," Submitted to *ACTA Mechanica*.

27 Sather, N. F., and Dahler, J. S., "Approximate Theory of Viscosity and Thermal Conductivity in Dense Polyatomic Fluids," *The Physics of Fluids*, Vol. 5, No. 7, 1962, pp. 754–768.

28 Campbell, C. S., and Gong, A., "The Stress Tensor in a Two-Dimensional Granular Shear Flow," *Journal of Fluid Mechanics*, Vol. 164, 1986, pp. 107–125.

29 Savage, S. B., and Sayed, M., "Experiments on Dry Cohesionless Materials in an Annular Shear Cell at High Strain Rates," presented at the EUROMECH 133-Statics and Dynamics of Granular Materials, Oxford University, 1980.

30 Savage, S. B., and Sayed, M., "Stresses Developed by Dry Cohesionless Granular Materials Sheared in an Annular Shear Cell," *Journal of Fluid Mechanics*, Vol. 142, 1984, pp. 391–430.

Downloaded 03 May 2010 to 171.66.16.27. Redistribution subject to ASME license or copyright; see http://www.asme.org/terms/Terms_Use.cfm

A Continuum Theory of Crack Shielding in Ceramics

M. Ortiz
Division of Engineering,
Brown University,
Providence, RI 02912

A phenomenological constitutive model is proposed which aims at describing the overall effect of microfracture in ceramics. Based on this model, the asymptotic stress, strain, and displacement fields at the tip of a stationary macroscopic crack are determined in closed form. The near-tip stress-intensity factor is computed and observed to be significantly smaller than the applied stress-intensity factor even for moderate amounts of damage.

1 Introduction

Certain classes of ceramics are known to undergo extensive microcracking confined to a process zone surrounding macrocrack tips (Hoagland et al., 1973; Claussen, 1976; Wu et al., 1978). Under these conditions, the processes at the crack tip are screened from the remote loads by the intervening microcracks and a fracture toughness enhancement results (Evans, 1984). Microcracks develop at grain boundary facets mainly as a result of residual stresses generated during cooling and of applied tensile stresses (Fu, 1983). The net effect of the microcracks is to render the material more compliant. Under increasing loads, the microcracks already present in the material remain confined to their respective facets and their size is essentially unaltered. Thus, further elastic degradation comes about as a result of increasing microcrack density and not microcrack growth. Eventually, the number of available nucleation sites which are favorably oriented with respect to the applied tensile loads is exhausted and a saturation stage is reached in which the material does not undergo further damage.

A first attempt at quantifying the crack shielding effect has relied on computer simulation (Hoagland and Embury, 1980). However, an analytical treatment of the problem has proven elusive in part due to lack of adequate material characterization. In this study it is assumed that the length scale over which the singular fields dominate is large compared with the characteristic microcrack size and the mean distance between the microcracks, so that an asymptotic analysis can be based on the effective overall properties of the continuum. Ideally, one would like to have a description of the effective behavior based on micromechanics and a detailed knowledge of its dependence on relevant micromechanical parameters, such as grain size. However, this entails the determination of the aggregate effect of dense populations of strongly interacting microcracks, possibly with preferred orientations, distributed over a three-dimensional heterogeneous elastic medium. Even under strong simplifying assumptions, this problem poses consideration difficulties (Horii and Nemat-Nasser, 1983; Kachanov, 1985). Thus, to make progress one has to resort to phenomenological models. In Section 2, one such model is proposed which aims at describing the effective behavior of a material undergoing progressive distributed damage and exhibiting a saturation stage. The possibility of a strong damage-induced elastic anisotropy is taken into consideration. Some of the ideas involved have been taken from constitutive models proposed for other progressively fracturing materials such as concrete (Ortiz, 1985).

In Section 3 the near-tip singular fields for a stationary crack are determined in closed form. Then, Rice's J-integral (Rice, 1968) is used to relate the stress-intensity factor at the crack tip to the amplitude of the remote K field. It is found that small amounts of damage can result in a substantial reduction of the stress intensity factor and thereby bring about a toughening of the material. This situation is in sharp contrast to transformation toughening which only comes into effect for a growing crack (Budiansky et al., 1983).

2 Effective Constitutive Behavior of Progessively Fracturing Materials

A phenomenological constitutive model is presented below which aims at describing the overall effect of microfracture in ceramics. In this work, processes resulting in permanent strains as well as rate effects are neglected. The model is predicated upon the following assumptions. Stresses and strains are assumed to be linearly related according to

$$\epsilon_{ij} = C_{ijkl}\sigma_{kl} \tag{1}$$

where the elastic compliances C_{ijkl} are regarded as internal variables which evolve as a result of damage processes taking place at a microstructural level. A threshold is postulated below which no further damage can occur. For the class of materials under consideration, the onset of damage is assumed to occur when the maximum tensile stress σ_1 reaches a critical value $\sigma_c \geq 0$, i.e.,

Contributed by the Applied Mechanics Division for presentation at the 1987 Applied Mechanics, Biomechanics, and Fluids Engineering Conference, Cincinnati, OH, June 14–17, 1987, of the American Society of Mechanical Engineers.
Discussion of this paper should be addressed to the Editorial Department, ASME, United Engineering Center, 345 East 47th Street, New York, N.Y. 10017, and will be accepted until two months after final publication of the paper itself in the JOURNAL OF APPLIED MECHANICS. Manuscript received by ASME Applied Mechanics Division, February 12, 1986; final revision, May 22, 1986.
Paper No. 87-APM-9.

Copyright © 1987 by ASME
Downloaded 03 May 2010 to 171.66.16.27. Redistribution subject to ASME license or copyright; see http://www.asme.org/terms/Terms_Use.cfm

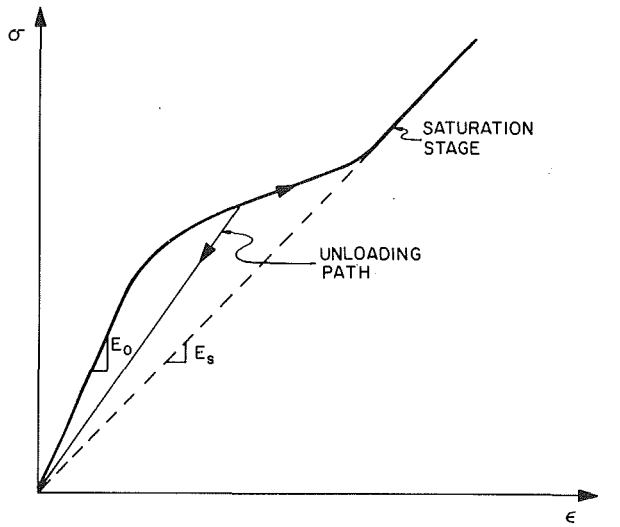


Fig. 1 Uniaxial tension stress-strain curve showing an initial elastic range and a saturation stage

$$\phi(\sigma,\sigma_c) \equiv \sigma_1 - \sigma_c = 0 \tag{2}$$

The direction of incremental damage is given by a damage rule

$$\dot{C}_{ijkl} = \dot{\lambda} n_i n_j n_k n_l \tag{3}$$

where $\mathbf{n}$, $\sqrt{n_i n_i} = 1$, is the direction of maximum tensile stress and the multiplier λ can be regarded as an effective added flexibility due to damage. Implicit in equation (3) is the assumption that the newly nucleated microcracks tend to be preferentially oriented normal to the direction of maximum tensile stress and thus most loss of stiffness occurs in that direction. Similar ideas were used by Hutchinson (1983) to estimate the macroscopic steady creep-rate of a material exhibiting power-law creep and simultaneously undergoing creep-constrained grain boundary cavitation.

The evolution of the critical stress σ_c is assumed to be governed by a damage rule of the type

$$\dot{\sigma}_c = h(\sigma_c)\dot{\lambda} \tag{4}$$

for some modulus $h(\sigma_c)$. In this simple model the dependence of h on σ_c can be determined from the uniaxial tension stress-strain curve alone. Finally, the damage and loading-unloading criteria can be expressed in Kuhn-Tucker form as the requirement that the constraints

$$\phi \le 0, \quad \dot{\lambda} \ge 0, \quad \phi\dot{\lambda} = 0 \tag{5}$$

be simultaneously satisfied at all times.

It is interesting to note that the above constitutive model shares a common structure with other rate-independent theories such as classical plasticity. In this latter case, a principal objective of the theory is to predict the evolution of the plastic strains while, in the case at hand, interest is focused on the evolution of the effective elastic moduli. In spite of these similarities, certain aspects of the behavior of materials undergoing microcracking do not have a counterpart in plasticity. The effect of closure of microcracks under load reversal falls within that category. By this mechanism microcracks can become inactive and cease to contribute to the flexibility of the material. Consideration of this effect requires adding further structure to the model. Microcrack closure can be modelled within a phenomenological theory as a unilateral constraint which requires that the deformation contributed by the microcracks be always tensile in all directions (Ortiz, 1985). In the present study attention is confined to monotonic loading processes for which microcrack closure is of no concern.

For the purpose of the asymptotic analysis that follows it proves more convenient to employ a deformation type constitutive theory rather than the incremental model introduced above. A deformation theory of damage can be readily obtained by integrating the incremental constitutive equations along proportional stress paths. This results in the following stress-strain relation

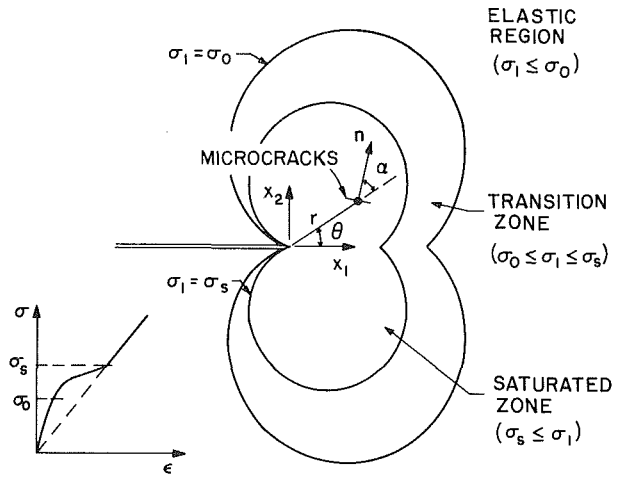


Fig. 2 Small scale microcracking problem for stationary crack

$$\epsilon_{ij} = (C^o_{ijkl} + \lambda(\sigma_1) n_i n_j n_k n_l)\sigma_{kl} \tag{6}$$

where C^o_{ijkl} are the isotropic elastic moduli of the uncracked material, $\mathbf{n}$ is the direction of maximum tensile stress and the function $\lambda(\sigma_1)$ can be determined directly from the uniaxial tension test. A typical uniaxial tension stress-strain curve is shown in Fig. 1 (Fu, 1983). It is seen that the material initially exhibits an elastic domain after which damage starts to accumulate. Eventually, a saturation stage is reached wherein no further damage takes places. In this saturation stage equation (6) simplifies to

$$\epsilon_{ij} = (C^o_{ijkl} + \lambda_s n_i n_j n_k n_l)\sigma_{kl} = C^o_{ijkl}\sigma_{kl} + \lambda_s \sigma_1 n_i n_j \tag{7}$$

where λ_s is a constant of value

$$\lambda_s = \frac{1}{E_s} - \frac{1}{E_o} \tag{8}$$

Here, E_o is the initial Young's modulus of the material and E_s is the slope of the uniaxial tension stress-strain curve in the saturation range.

The stress-strain relation (6) has a hyperelastic structure

$$\epsilon_{ij} = \frac{\partial \chi(\sigma)}{\partial \sigma_{ij}} \tag{9}$$

where the complementary energy potential $\chi(\sigma)$ takes the form

$$\chi(\sigma) = \frac{1}{2} C^o_{ijkl}\sigma_{ij}\sigma_{kl} + f(\sigma_1) \tag{10}$$

The functions $f(\sigma_1)$ and $\lambda(\sigma_1)$ are related by $f' = \lambda$. In the saturation stage equation (6) reduces to (7) and $f(\sigma_1)$ to $\lambda_s\sigma_1^2/2$, which renders the complementary energy potential (10) a homogeneous function of degree two of the stress tensor. Therefore, the strain energy potential $W(\epsilon)$ is also a homogeneous function of degree two and satisfies the identity

$$W(\epsilon) = \chi(\sigma) = \frac{1}{2}\sigma_{ij}\epsilon_{ij}, \quad \textit{when} \quad \epsilon_{ij} = \frac{\partial \chi(\sigma)}{\partial \sigma_j} \tag{11}$$

i.e., the strain and complementary energy potentials take the same numerical value when evaluated at stresses and strains which satisfy the stress-strain relations (9).

3 Asymptotic Fields for a Stationary Crack

Throughout this work it is assumed that the region around

Downloaded 03 May 2010 to 171.66.16.27. Redistribution subject to ASME license or copyright; see http://www.asme.org/terms/Terms_Use.cfm

the crack tip to which microcracking is confined is small compared with the length of the crack but orders of magnitude larger than the characteristic size of the microcracks and their mean separation. Under the first condition an asymptotic problem can be formulated for a semi-infinite crack as shown in Fig. 2. The second condition is needed for the constitutive model presented above to apply. In this paper attention is confined to plane strain conditions and Mode I loading, i.e., applied loads which result in stress fields which are symmetric with respect to the plane of the crack.

Three well-differentiated regions surrounding the crack tip can be identified, Fig. 2. In the innermost region the strains are large enough so that the material can be assumed to be in the saturation stage. On the other hand, at points far away from the crack tip the material behavior is linear isotropic elastic and the state of stress is given by

$$\sigma_{ij}(r,\theta)=\frac{K_\infty}{\sqrt{2\pi r}}\tilde{\sigma}^o_{ij}(\theta) \tag{12}$$

where K_∞ is the remote stress-intensity factor and the universal angular distributions $\tilde{\sigma}^o_{ij}(\theta)$ for a linear isotropic elastic material are given by

$$\begin{Bmatrix}\tilde{\sigma}^o_{rr}(\theta)\\ \tilde{\sigma}^o_{\theta\theta}(\theta)\\ \tilde{\sigma}^o_{r\theta}(\theta)\end{Bmatrix}=\begin{Bmatrix}(5/4)\cos(\theta/2)-(1/4)\cos(3\theta/2)\\ (3/4)\cos(\theta/2)+(1/4)\cos(3\theta/2)\\ (1/4)\sin(\theta/2)+(1/4)\sin(3\theta/2)\end{Bmatrix} \tag{13}$$

The value of K_∞ depends upon the particular geometry of the cracked specimen and represents the influence of the applied loading. In between the inner and outer field lies a transition zone in which the material is partially saturated.

The behavior of the material surrounding the crack tip is assumed to be described by the stress-strain law (6). Since these relations derive from a complementary energy potential which is homogeneous of degree two, a classical argument (see, e.g., Rice 1968) shows that the leading term in the asymptotic expansion of the stress field has to be of the form

$$\sigma_{ij}(r,\theta)=\frac{K_t}{\sqrt{2\pi r}}\tilde{\sigma}_{ij}(\theta) \tag{14}$$

where K_t is the local stress-intensity factor of the near-tip fields and the angular distributions $\tilde{\sigma}_{ij}(\theta)$ are to be determined. In general K_t is different from K_∞ because the crack tip is shielded from the remote loads by the intervening microcracks. Assuming that crack growth is controlled by the value of K_t it becomes of primary interest to determine the relation between K_t and K_∞.

In view of the fact that the constitutive behavior of the material surrounding the crack tip is nonlinear and strongly anisotropic one would expect singular stress fields which substantially depart from the linear isotropic solution. It is shown next that this is not the case. In fact, the linear isotropic stress field provides the exact asymptotic solution of the problem, i.e.,

$$\tilde{\sigma}_{ij}(\theta)=\tilde{\sigma}^o_{ij}(\theta) \tag{15}$$

Under certain circumstances, a similar situation is encountered in materials exhibiting linear creep and grain boundary cavitation (Hutchinson, 1983). On the basis of this observation, Hutchinson (1983) anticipated the result stated above, namely, that constitutive relation (7) implies the same angular distribution of stresses as in the linear elastic solution.

To prove equation (15) we start by noting that the stress field (14), (15) satisfies equilibrium and traction-free boundary conditions on the crack faces. Thus, it only remains to be shown that the corresponding strains satisfy compatibility. With reference to Fig. 2, the direction of maximum tensile stress is computed to be

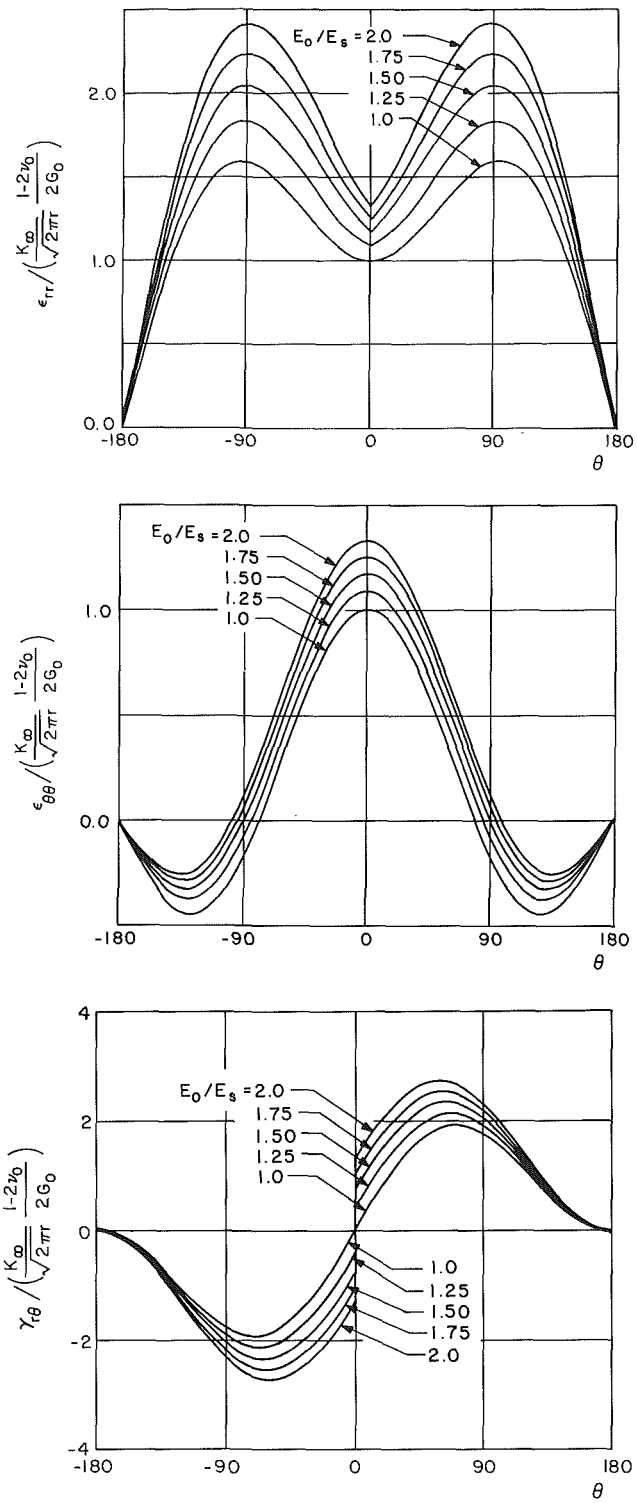


Fig. 3 Angular variations of the near-tip strain field ($\nu_0 = 0.25$)

$$\mathbf{n}=(\cos\alpha,\ \sin\alpha),\qquad \alpha=\begin{cases}\pi/4-\theta/4, & 0<\theta\le\pi;\\ -\pi/4-\theta/4, & -\pi\le\theta<0;\end{cases} \tag{16}$$

Thus, the angle α made by $\mathbf{n}$ and the radial direction varies linearly with the polar angle θ from a value of $\alpha=45°$ at $\theta=0^+$ to $\alpha=0$ on the crack face $\theta=\pi$. The vector $\mathbf{n}$ can be regarded as giving an indication of the preferred orientation of the microcracks. In this light, it is interesting to note that for $\theta=0$ one has $\tilde{\sigma}_{rr}=\tilde{\sigma}_{\theta\theta}$ and $\tilde{\sigma}_{r\theta}=0$. This would appear to render α in-

Downloaded 03 May 2010 to 171.66.16.27. Redistribution subject to ASME license or copyright; see http://www.asme.org/terms/Terms_Use.cfm

determinate on the plane of the crack. However, this indeterminacy can be resolved by computing the limiting values of α as the plane $\theta=0$ is approached from above and below. This operation yields two values of $\alpha=\pm 45°$, respectively. Thus, the model predicts two families of perpendicular microcracks at $\theta=0$ symmetrically distributed with respect to the plane of the crack.

Substituting (16) into (7) the asymptotic strain field is computed to be

$$\begin{Bmatrix} \epsilon_{rr}(r,\theta) \\ \epsilon_{\theta\theta}(r,\theta) \\ \gamma_{r\theta}(r,\theta) \end{Bmatrix} = \frac{K_t}{\sqrt{2\pi r}} \frac{1}{2G_o} \begin{Bmatrix} (5/4-2\nu_o)\cos(\theta/2)-(1/4)\cos(3\theta/2) \\ (3/4-2\nu_o)\cos(\theta/2)+(1/4)\cos(3\theta/2) \\ (1/2)\sin(\theta/2)+(1/2)\sin(3\theta/2) \end{Bmatrix} + \frac{K_t}{\sqrt{2\pi r}}\lambda_s\left(\cos\frac{\theta}{2}+\frac{1}{2}\sin\theta\right) \begin{Bmatrix} (1+\sin(\theta/2))/2 \\ (1-\sin(\theta/2))/2 \\ \cos(\theta/2) \end{Bmatrix}, \quad 0<\theta\le\pi \tag{17}$$

where E_o, ν_o, and $G_o=E_o/2(1+\nu_o)$ are the initial Young's modulus, Poisson's ratio, and shear modulus of the uncracked material. It is noted that the first term is the isotropic linear elastic solution corresponding to a stress intensity factor K_t. The second term represents the effect of damage and vanishes identically for $\lambda_s=0$, i.e., $E_s=E_o$. The strains in the lower half plane $-\pi\le\theta<0$ are obtained from the symmetry conditions

$$\epsilon_{rr}(r,-\theta)=\epsilon_{rr}(r,\theta), \quad \epsilon_{\theta\theta}(r,-\theta)=\epsilon_{\theta\theta}(r,\theta), \quad \gamma_{r\theta}(r,-\theta)=-\gamma_{r\theta}(r,\theta) \tag{18}$$

The computed angular distributions of the strain components are shown in Fig. 3 as function of the material parameters involved. A noteworthy feature of the solution is that the shearing strain $\gamma_{r\theta}$ exhibits a jump across the plane of the crack.

Lengthy but straightforward algebra shows that the strain field (17) identically satisfies the compatibility equation. Hence, equations (14), (15) do indeed provide a closed form asymptotic solution of the problem. The displacement field can be computed from the strain-displacement relations to obtain

$$\begin{Bmatrix} u_r(r,\theta) \\ u_\theta(r,\theta) \end{Bmatrix} = \frac{K_t}{4G_o}\sqrt{\frac{r}{2\pi}} \begin{Bmatrix} (2\kappa_o-1)\cos(\theta/2)-\cos(3\theta/2) \\ -(2\kappa_o+1)\sin(\theta/2)+\sin(3\theta/2) \end{Bmatrix} + K_t\lambda_s\sqrt{\frac{r}{2\pi}} \begin{Bmatrix} (\cos(\theta/2)+(1/2)\sin\theta)(1+\sin(\theta/2)) \\ \cos\theta-\sin(\theta/2)-\sin^3(\theta/2)-1 \end{Bmatrix}, \quad 0<\theta\le\pi \tag{19}$$

where $\kappa_o=3-4\nu_o$. The displacements in the lower half plane follow from the symmetry conditions

$$u_r(r,-\theta)=u_r(r,\theta), \quad u_\theta(r,-\theta)=-u_\theta(r,\theta) \tag{20}$$

Of particular interest is the crack opening profile

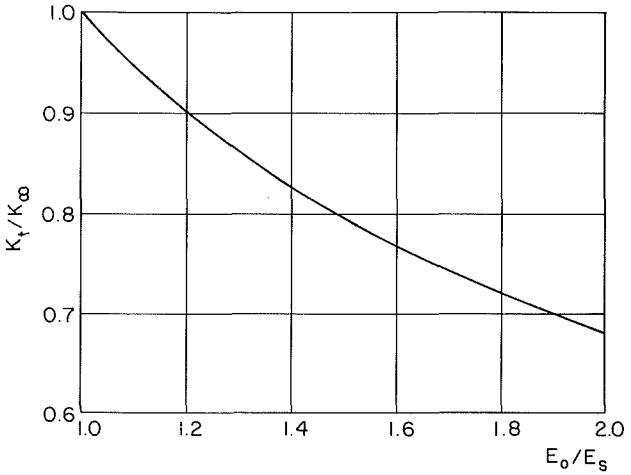


Fig. 4 Near-tip stress-intensity factor as a function of the extent of elastic degradation ($\nu_o=0.25$)

$$\delta(r)=-u_\theta(r,-\pi)+u_\theta(r,-\pi)=8K_t\left(\frac{1-\nu_o^2}{E_o}+\lambda_s\right)\sqrt{\frac{r}{2\pi}} \tag{21}$$

As can be seen, the opening profile is parabolic as in the linear elastic solution.

The asymptotic analysis presented above has been based on the deformation theory of damage given in Section 2. However, since the stress field about the crack tip is identical to the stress field in the outer undamaged region except for an amplitude factor it can be concluded that the stress paths at all material points are nearly proportional and the solution given above is consistent with the incremental constitutive model as well. A similar situation was encountered by Hutchinson (1968) and Rice and Rosengren (1968) who based their analysis on a deformation theory of plasticity to find a posteriori that their solution satisfies the incremental constitutive equations as well.

4 Crack Tip Stress-Intensity Factor: Application of the *J*-Integral

To have a complete asymptotic solution of the problem under consideration, it remains to determine the value of the crack tip stress-intensity factor K_t as a function of the amplitude K_∞ of the applied K field. This relation follows simply from an application of the J-integral of Rice (Rice, 1968). It has been shown above that under monotonic loading the stress path at all points is nearly proportional and the response of the material is indistinguishable from that of a small strain, nonlinear elastic solid with complementary energy potential (10). Under these conditions, the formalism of the J-integral applies. Let us recall that

$$J=\int_\Gamma [W(\epsilon)m_1-\sigma_{ij}m_j u_{i,1}]ds \tag{22}$$

Here, **m** signifies the outer normal to the contour Γ encircling the crack tip. If the contour is chosen to lie entirely within the remote field, J reduces to the classical expression

$$J_\infty=\frac{1-\nu_o^2}{E_o}K_\infty^2 \tag{23}$$

For a contour shrunk down to the crack tip (22) can be evaluated from equations (14), (15), and (19). For the particular material model under consideration the strain and complementary energy potentials coincide in numerical value and $W(\epsilon)$ in equation (22) can be replaced by $\chi(\sigma)$ as computed from (7), (14), and (15). A lengthy but straightforward computation yields

Downloaded 03 May 2010 to 171.66.16.27. Redistribution subject to ASME license or copyright; see http://www.asme.org/terms/Terms_Use.cfm

$$J_t = \frac{1-\nu_o^2}{E_o} K_I^2 + \beta \lambda_s K_I^2 \tag{24}$$

where the numerical constant β takes the value $\beta = 1.0942$. The path-independence of J necessitates

$$J_t = J_\infty \tag{25}$$

from where one finds

$$\frac{K_I}{K_\infty} = \frac{1}{\sqrt{1 + \frac{\beta}{1-\nu_o^2}(E_o/E_s - 1)}} \tag{26}$$

The dependence of K_I/K_∞ on E_o/E_s is shown in Fig. 4. A substantial reduction in K is observed even for moderate deviations from elastic behavior.

5 Discussion

The analysis presented above has been based on a model of damage in which permanent strains and rate effects are assumed to be negligible. The model incorporates some of the complexities that are encountered in most progressively fracturing materials such as a strong damage-induced elastic anisotropy. However, the constitutive framework is simple enough that a closed form analytical solution for the asymptotic problem can be obtained.

The computed results are indicative of a significant reduction in the crack tip stress-intensity factor from the remote K. Unfortunately, the net toughness enhancement cannot be expected to be as substantial as Fig. 4 would tend to suggest due to the fact that the microcracks created ahead of the main crack degrade the crack extension resistance of the material (Evans, 1984). The main microstructural mechanism underlying this latter effect is microcrack coalescence, a process which is poorly understood at present. Thus, it would appear that a detailed understanding of the toughness properties of ceramics will inevitably require further experimental and analytical research.

Acknowledgments

The author is indebted to helpful and stimulating conversations with C. F. Shih and J. W. Hutchinson. The support of the Office of Naval Research through grant N00014-85-K-0720 is gratefully acknowledged.

References

Budiansky, B., Hutchinson, J. W., and Lambropoulos, J. C., 1983, "Continuum Theory of Dilatant Transformation Toughening in Ceramics," *Int. J. Solids Structures*, Vol. 19, pp. 337–355.

Claussen, N., 1976, "Fracture Toughness of Al_2O_3 with an Unstabilized ZrO_2 Dispersed Phase," *J. Am. Ceram. Soc.*, Vol. 59, pp. 49–51.

Evans, A. G., 1984, "Aspects of the Reliability of Ceramics," *Defect Properties and Processing of High-Technology Monmetallic Materials*, Crawford, J. H., Chen, Y., and Sibley, W. A., eds., North-Holland, pp. 63–80.

Fu, Y., 1983, "Mechanics of Microcrack Toughening in Ceramics," Ph.D. Thesis, University of California, Berkeley, Calif.

Hoagland, R. G., Hahn, G. T., and Rosenfield, A. R., 1973, "Influence of Microstructure on the Fracture Propagation in Rock," *Roc. Mech.*, Vol. 5, pp. 77–106.

Hoagland, R. G., and Embury, J. D., 1980, "A Treatment of Inelastic Deformation Around a Crack Tip Due to Microcracking," *J. Am. Ceram. Soc.*, Vol. 63, pp. 404–410.

Horii, H., and Nemat-Nasser, S., 1983, "Overall Moduli of Solids with Microcracks: Load-Induced Anisotropy," *J. Mech. Phys. Solids*, Vol. 31, pp. 155–171.

Hutchinson, J. W., 1968, "Singular Behavior at the End of a Tensile Crack in a Hardening Material," *J. Mech. Phys. Solids*, Vol. 16, pp. 13–31.

Hutchinson, J. W., 1983, "Constitutive Behavior and Crack Tip Fields for Materials Undergoing Creep-Constrained Grain Boundary Cavitation," *Acta Metall.*, Vol. 31, No. 7, pp. 1079–1088.

Kachanov, M., 1985, "A Simple Technique of Stress Analysis in Elastic Solids with Many Cracks," *Int. J. Fracture*, Vol. 28, pp. 11–19.

Ortiz, M., 1985, "A Constitutive Theory for the Inelastic Behavior of Concrete," *Mechanics of Materials*, Vol. 4, pp. 67–93.

Rice, J. R., 1968, "Mathematical Analysis in the Mechanics of Fracture," *Fracture*, Liebowitz, H., ed., Vol. 2, Academic Press, pp. 191–311.

Rice, J. R., and Rosengren, G. F., 1968, "Plane Strain Deformation Near a Crack Tip in a Power Law Hardening Material," *J. Mech. Phys. Solids*, Vol. 16, pp. 1–12.

Wu, C. C., Freiman, S. W., Rice, R. W., and Mecholsky, J. J., 1978, "Microstructural Aspects of Crack Propagation in Ceramics," *J. Mater. Sci.*, Vol. 13, pp. 2659–2670.

Downloaded 03 May 2010 to 171.66.16.27. Redistribution subject to ASME license or copyright; see http://www.asme.org/terms/Terms_Use.cfm

A Complex-Variable Method for Two-Dimensional Internal Stress Problems and Its Applications to Crack Growth in Nonelastic Materials: Part I—Theory

K. C. Wu[1]
Post-Doctoral Fellow.

C. Y. Hui
Assistant Professor.

Theoretical and Applied Mechanics,
Kimball Hall,
Cornell University,
Ithaca, New York 14863

In Part I of this work, a systematic method based on a nonanalytic complex calculus is developed for two-dimensional internal stress problems. The method is employed to derive the internal stress due to a field of nonelastic strain, which can be nonzero at infinity, in an infinite uncracked or cracked body.

1 Introduction

The aim of this work is to develop a systematic method to determine the internal stress in a linear elastic body. A new mathematical technique, using generalized analytic functions, is employed in the development of this method. Our analysis is based on the usual small strain, small displacement theory of continuum mechanics.

Internal stress in an elastic body arises because of the presence of an incompatible strain ϵ. The incompatible strain ϵ induces an elastic strain ϵ^e so that the sum of the ϵ^e and ϵ can be associated with a continuous displacement field $\mathbf{u}$, i.e.,

$$\epsilon^t = \epsilon^e + \epsilon,$$

where

$$\epsilon^t = \frac{1}{2}\,(\nabla\mathbf{u} + (\nabla\mathbf{u})^T).$$

and $(\nabla\mathbf{u})^T$ is the transpose of $\nabla\mathbf{u}$.

The internal stress is related to the induced elastic strain through Hooke's law. Examples of ϵ are:

(*a*) inelastic strain given by the inelastic constitutive model of the material;
(*b*) stress-free transformation strain ϵ^T;
(*c*) thermal strain given by

$$\epsilon = \alpha T\mathbf{I}.$$

where α is the coefficient of thermal expansion. T is the temperature, and $\mathbf{I}$ is the unity tensor. In this work we shall use "nonelastic strain" as a general term to denote ϵ.

Assuming that the nonelastic strain ϵ is given, the internal stress induced in the linear elastic body can be determined by the method of fictitious body force suggested originally by Eshelby (1957). Details of this method are given in Section 2. This method allows the self-stresses to be calculated from the solution of a linear elasticity problem with body forces completely determined by ϵ and the elastic moduli. Consequently the problem of finding the self-stress in an elastic body can be reduced to the problem of determining the deformation field of an elastic body with body force loading. This idea of simulating the self-stress by an elastic field due to body forces has been employed by many investigators in the study of elastic-plastic fracture, e.g., Hutchison (1974). Vitek (1966), Rice (1966), Freund and Sills (1980). Tirosh and Mclintock (1978), M. Denda (1980). However, a unified and systematic approach to the general two-dimensional self-stress problem does not seem to appear. As we shall see later, such an approach is possible using a theory of nonanalytical functions.

The theory of generalized analytic functions is not entirely new in mechanics literature. Expositions of this theory can be found in monographs such as Vekua (1962). Recent progress has been made in the development of a method based on this theory by the work of Wu and Hart (1986) and Wu (1985) on steady state crack growth problems. This method, however, is still considerably unfamiliar in mechanics as compared to the analytic function method of Muskhelishvili (1962). A well-known result in Muskhelishvili's method states that, in the absence of body forces, the stresses in an elastic body can be represented by one analytical function for antiplane strain and two for plane strain or plane stress. In the presence of body forces, a particular solution must be sought so that, via the principle of superposition, the problem can be reduced to finding the stresses in an elastic body with no body forces provided that the boundary conditions are suitably modified. Since

[1]Currently Associate Professor of the Institute of Applied Mechanics, National Taiwan University, Taipei, Taiwan.

Contributed by the Applied Mechanics Division for presentation at the 1987 Applied Mechanics, Biomechanics, and Fluids Engineering Conference, Cincinnati, OH, June 14–17, 1987, of the American Society of Mechancial Engineers.
Discussion of this paper should be addressed to the Editorial Department, ASME, United Engineering Center, 345 East 47th Street, New York, N.Y. 10017, and will be accepted until two months after final publication of the paper itself in the JOURNAL OF APPLIED MECHANICS. Manuscript received by ASME Applied Mechanics Division, April 10, 1986; final revision, July 28, 1986.
Paper No. 87-APM-10.

Copyright © 1987 by ASME
Downloaded 03 May 2010 to 171.66.16.27. Redistribution subject to ASME license or copyright; see http://www.asme.org/terms/Terms_Use.cfm

particular solution is nonunique, the choice of an optimal particular solution in a given problem is often difficult to determine. We will later show that the theory of generalized analytic functions can be used to extend Muskhelishvili's method to include body forces. The stresses are now uniquely determined by two nonanalytic functions which reduce to the Muskhelishvili analytic functions if body forces are absent.

The nonanalytic complex calculus greatly facilitates the transformation of governing equations from differential forms to integral forms. Integral formulation is preferred in our method since boundary conditions can be explicitly incorporated. For a given field of nonelastic strain, the integral formulation give exact solutions to the internal stress. For cases where the nonelastic strain is a function of stress (e.g., a crack growing in a viscoplastic material), this formulation provides integral equations for the stress and can be solved simultaneously with the constitutive equations describing the inelastic behavior of the material.

2 Method of Fictitious Force

Let A be a homogenous body with traction $\mathbf{T}$ applied on the part of its boundary ∂A_T and with displacement $\mathbf{U}$ prescribed on the rest of the boundary $\partial A_U \equiv \partial A - \partial A_T$. The region A is assumed to be free of body forces. The total deformation in A can be decomposed into

$$\epsilon^t = \epsilon^e + \epsilon. \tag{2.1}$$

where ϵ^e, ϵ are the elastic and the nonelastic strains, respectively. The total strain ϵ^t is given by

$$\epsilon^t = \frac{1}{2}\left(\nabla \mathbf{u} + (\nabla \mathbf{u})^T\right) \tag{2.2}$$

where $\mathbf{u}$ is the displacement vector and the superscript T denotes the transpose of $\nabla \mathbf{u}$.

The stress in A is given by

$$\begin{aligned}\sigma &= \mathbf{C}\epsilon^e \\ &= \mathbf{C}\epsilon^t - \mathbf{C}\epsilon,\end{aligned} \tag{2.3}$$

where $\mathbf{C}$ is the elastic modulus tensor. If we define a fictitious stress σ^f by

$$\sigma^f \equiv \mathbf{C}\epsilon^t, \tag{2.4}$$

equation (2.3) can be written as

$$\sigma = \sigma^f - \mathbf{C}\epsilon. \tag{2.5}$$

Imposing equilibrium condition on σ, we have

$$\begin{aligned}\nabla \cdot \sigma &= \nabla \cdot \sigma^f - \mathbf{C}\nabla \cdot \epsilon \\ &= 0.\end{aligned} \tag{2.6}$$

Identifying

$$-\mathbf{C}\nabla \cdot \epsilon \tag{2.7}$$

with a fictitious body force $\mathbf{f}$, equation (2.6) can be expressed as

$$\nabla \cdot \sigma^f + \mathbf{f} = 0. \tag{2.8}$$

If ϵ is known a priori, σ^f can be solved as if the body were purely elastic and were subjected to a body force $\mathbf{f}$. This is because σ^f is derived from ϵ^t which is compatible. The corresponding boundary conditions for equation (2.8) are

$$\sigma^f \cdot \mathbf{n} = \mathbf{T} + (\mathbf{C}\epsilon)\cdot \mathbf{n} \qquad \text{on } \partial A_T \tag{2.9a}$$

$$\mathbf{u} = \mathbf{U} \qquad \text{on } \partial A_U \tag{2.9b}$$

Once σ^f is obtained, σ can be calculated by equation (2.5).

In the rest of this paper the material is assumed to be isotropic, for which case $\mathbf{f}$ reduces to, in Cartesian coordinates,

$$f_i = -(2G\epsilon_{ij,j} + \lambda \epsilon_{kk,i}), \tag{2.10}$$

where all indexes run from 1 to 3 and the usual summation convention over repeated indexes is adopted.

It is noted that if ϵ is homogeneous in a finite region, the method is exactly the same as Eshelby's treatment for stress-free strain transformation (Eshelby (1957)). We shall exploit a complex calculus for nonanalytic functions due to Vekua (1962) to expedite the application of the method of fictitious body force to antiplane strain and plane-strain/plane-stress problems. In the next section a general review of the complex calculus is given.

3 Mathamatical Preliminaries

Throughout the paper z will denote the complex variable $x + iy$. With respect to a Cartesian coordinate system, z can be identified by the point (x, y). All functions are defined on a simply-connected open domain A, which may be bounded or unbounded. The boundary of A, ∂A, is assumed to be piecewise continuous. The closure of A, $A \cup \partial A$, is denoted by $\bar{A}$. The complement of any set D is denoted by D^c. It is understood that the complex function $f(z)$ is used to denote $f(x, y) = u(x, y) + iv(x, y)$ and $f(\bar{z}) = u(x, -y) + iv(x, -y)$, where u and v are real-valued functions. The complex conjugate of $f(z)$ is denoted by $\overline{f(z)}$ or $\bar{f}$. This must not be confused with the usual notation $\bar{f}(z) = f(\bar{z})$. In this paper, we denote $\overline{f(\bar{z})}$ by $\tilde{f}(z)$. Partial differentiations of f with respect to x and y are denoted $f_{,x}$ and $f_{,y}$. We shall denote by $C^k(A)$ the set of functions which have all possible continuous derivatives up to order k in A.

Let us define the following complex differential operators

$$\partial_{\bar{z}} f \equiv \frac{1}{2}(f_{,x} + if_{,y}), \tag{3.1a}$$

$$\partial_z f \equiv \frac{1}{2}(f_{,x} - if_{,y}), \tag{3.1b}$$

Some immediate consequences of the above definitions are

$$f_{,y} = -i(2\partial_{\bar{z}} f - f_{,x}), \tag{3.2a}$$

$$\overline{\partial_z f} = \partial_{\bar{z}} \bar{f}. \tag{3.2b}$$

It can be shown that usual rules of differentiation apply to the operators $\partial_{\bar{z}}$ and ∂_z, e.g.,

$$\partial_{\bar{z}}(fg) = f\partial_{\bar{z}} g + g\partial_{\bar{z}} f, \tag{3.3a}$$

$$\partial_{\bar{z}}(af + bg) = a\partial_{\bar{z}} f + b\partial_{\bar{z}} g \tag{3.3b}$$

where a, b are complex numbers and f, g are complex functions. Equation (3.3b) implies that $\partial_{\bar{z}}$ is a linear operator. The Cauchy-Riemann equations for analytic functions state that $f \in C^1(A)$ is analytic in A if

$$\partial_{\bar{z}} f = 0, \forall z \in A. \tag{3.4}$$

Using equation (3.4), equation (3.3a) can be simplified if one of the functions, say f, is analytic. In that case

$$\partial_{\bar{z}}(fg) = f\partial_{\bar{z}} g. \tag{3.5}$$

Defining a two-dimensional vectorial function $\mathbf{f} \equiv u\mathbf{i} + v\mathbf{j}$, $\mathbf{i}$ and $\mathbf{j}$ being the unit vectors in x and y directions, respectively, it can be shown that

$$\partial_{\bar{z}} \bar{f} = \frac{1}{2}(\nabla \cdot \mathbf{f}) - i\frac{1}{2}|(\nabla \times \mathbf{f})|. \tag{3.6}$$

where $\bar{f} \equiv u - iv$ is the complex function associated with $\mathbf{f}$. For future reference, the general solution of $\nabla \cdot \mathbf{f} = \partial_{\bar{z}} \bar{f} + \partial_z f = 0$ is given by

Downloaded 03 May 2010 to 171.66.16.27. Redistribution subject to ASME license or copyright; see http://www.asme.org/terms/Terms_Use.cfm

$$u = h_{,y}$$

$$v = -h_{,x}, \tag{3.7a}$$

where h is a real function. In complex notation, equation (3.7a) can be written as

$$\bar{f} = 2i\partial_z h. \tag{3.7b}$$

By means of the well-known Green's formula, it is easy to verify

$$\int_A \partial_{\bar{z}} f dA = \frac{1}{2i} \oint_{\partial A} f dz, \tag{3.8a}$$

$$\int_A \partial_z f dA = -\frac{1}{2i} \oint_{\partial A} f d\bar{z}, \tag{3.8b}$$

where $dA = dxdy$, $dz = dx + idy$, $d\bar{z} = dx - idy$. All contour integrals in this work are performed in the usual counterclockwise sense. By equations (3.5) and (3.8a) it can be shown that the general solution of the equation (Vekua, (1962))

$$\partial_{\bar{z}} f = g, \; z \in A \tag{3.9}$$

is given by

$$f(z) = \frac{1}{2\pi i} \int_{\partial A} \frac{f(z')dz'}{z'-z} - \frac{1}{\pi} \int_A \frac{g(z')}{z'-z} dA'. \tag{3.10}$$

Note that if f satisfies the analyticity condition of equation (3.4), equation (3.10) is simply the well-known Cauchy integral formula for analytic functions. Thus equation (3.10) is a generalization of the Cauchy integral formula for nonanalytic functions. If A is unbounded and $f(z) \to z^{-\alpha}$, where $0 < \mathrm{Re}\alpha$, as $z \to \infty$, the boundary term vanishes and equation (3.10) becomes

$$f(z) = -\frac{1}{\pi} \int_E \frac{g(z')}{z'-z} dA', \tag{3.11}$$

where E is the whole plane. In the following sections we are interested in g that is expressible as $g = \phi_{,x}$, where ϕ is a complex function. In particular we are interested in cases where $\phi \equiv 0$ in $\bar{B}^C$ for some region B in E. The function ϕ can be conveniently expressed as (Dewit, (1973))

$$\phi = \Phi H(B), \tag{3.12}$$

where $H(B)$ is a two-dimensional Heaviside function defined by

$$H(B) = \int_B \delta(r'-r)dA', \tag{3.13}$$

where δ is the usual Dirac delta function. The function $H(B)$ has the property that $H(z) = 1$ if $z \in B$ and $= 0$ otherwise.

Taking the derivative of equation (3.12) with respect to x results in

$$\phi_{,x} = \Phi_{,x} H(B) + \Phi H_{,x}(B). \tag{3.14}$$

With equation (3.14), the following equation can be established

$$\int_E \phi_{,x'} G(z',z)dA' = \int_B \Phi_{,x'} G(z',z)dA' - \int_{\partial B} G(z',z)dy'. \tag{3.15}$$

Identifying $G(z', z)$ with $1/(z'-z)$ and g with $\phi_{,x}$ in equation (3.11), we obtain

$$f(z) = -\frac{1}{\pi} \int_B \frac{\Phi_{,x'}}{z'-z} dA' + \frac{1}{\pi} \int_{\partial B} \frac{\Phi dy'}{(z'-z)}. \tag{3.16}$$

In particular, if Φ is constant in B, equation (16) can be simplified to

$$f(z) = \frac{\Phi}{\pi} \int_{\partial B} \frac{dy'}{z'-z}. \tag{3.17}$$

A more rigorous justification of these results can be found in Schwartz (1966).

4 Anti-Plane Strain Problems

4.1 Internal Stress Due to Nonelastic Strain for an Infinitely Extended Isotropic and Homogeneous Body. Anti-plane strain deformation is characterized by one nonvanishing displacement component $u_3 = u_3(x, y)$. The nonzero stress and strain components are $\tau_i = \sigma_{3i}$ and $\gamma_i = 2\epsilon_{3i}$, $i = 1, 2$, respectively. From equation (3.6a), the equilibrium equation for the fictitious stress $\bar{\tau}^f$ can be written as

$$\partial_{\bar{z}} \bar{\tau}^f = \frac{1}{2} (\nabla \cdot \tau^f) - \frac{i}{2} | \nabla x \tau^f | = -\frac{1}{2} f_3, \tag{4.1}$$

where $\bar{\tau}^f = \tau_x^f - i\tau_y^f$. The imaginary part of equation (4.1) vanishes due to the compatibility of the total strain. By some algebraic manipulations, f_3 can be expressed in terms of the nonelastic strains γ_i by (2.10), i.e.,

$$f_3 = -G(\gamma_{,x} - 2i\partial_{\bar{z}}\gamma_y), \tag{4.2}$$

where $\gamma \equiv \gamma_x + i\gamma_y$. The reason for adopting the particular form for f_3 will become clear later. Substitution of equation (4.2) into equation (4.1) and rearrangement of the terms leads to

$$\partial_{\bar{z}} (\bar{\tau}^f + iG\gamma_y) = \frac{G}{2} \gamma_{,x}. \tag{4.3}$$

Equation (4.3) can be transformed into an integral form by using equation (3.11). The result is

$$\bar{\tau}^f + iG\gamma_y = -\frac{G}{2\pi} \int_E \frac{\gamma_{,x'}}{z'-z} dA', \tag{4.4}$$

provided that $\gamma_{,x}$ approaches zero faster than $1/z$ as $z \to \infty$. From equation (2.5), the internal stress $\bar{\tau}$ as given by

$$\bar{\tau} = \bar{\tau}^f - G\bar{\gamma} = -\frac{G}{2\pi} \int_E \frac{\gamma_{,x'}}{z'-z} dA' - G\gamma_x. \tag{4.5}$$

It is interesting to note that if the distribution of the nonelastic strain is uniform in x, i.e., $\gamma = \gamma(y)$, the interal stress field is simply given by

$$\tau_x = -G\gamma_x(y) \tag{4.6a}$$

$$\tau_y = 0. \tag{4.6b}$$

The displacement field corresponding to the above stress field is given by

$$u_3 = \int_{-\infty}^{y} \gamma_y(y)dy, \tag{4.6c}$$

which is also uniform in x.

4.2 Internal Stress Due to Nonelastic Strain in an Infinite Body Containing a Semi-Infinite Stationary Crack. The stress given by equation (4.5) is for an uncracked body. We shall now modify the stress field to account for the presence of a semi-infinite crack in the body coinciding with the negative x axis. With the introduction of the crack, the stress field represented by equation (4.5) is left undisturbed if the following tractions are applied to the opposing crack faces:

$$T = \tau_y^{(u)}(-|x|,0) = \frac{G}{2\pi} Im\left[\int \frac{\gamma_{,x'}}{z'+|x|} dA'\right], \tag{4.7}$$

Downloaded 03 May 2010 to 171.66.16.27. Redistribution subject to ASME license or copyright; see http://www.asme.org/terms/Terms_Use.cfm

where $Im[\ ]$ stands for the imaginary part of the quantity in the brackets and we have used the superscript u to denote quantities for the uncracked body. For simplicity, the following symmetry conditions are specified for the nonelastic strains

$$\gamma_x(x,-y) = -\gamma_x(x,y), \tag{4.8}$$

$$\gamma_y(x,-y) = \gamma_y(x,y). \tag{4.9}$$

It can be shown that under the symmetry conditions, the integral in equation (4.7) is purely imaginary. Thus

$$T = \frac{G}{2\pi i}\int \frac{\gamma,x'}{z'+|x|}\,dA'. \tag{4.10}$$

The traction free boundary conditions in the crack forces are obtained by the removal of the unwanted tractions which results in an image stress field $\bar{\tau}^I$. The image stress field is calculated by the well-known Cauchy integral (Muskhelishvili, (1962)):

$$\bar{\tau}^I = -\frac{1}{\pi}\frac{1}{\sqrt{z}}\int_{-\infty}^{0}\frac{T(s)\sqrt{s}}{z-s}\,ds$$

$$= -\frac{G}{2\pi}\frac{1}{\sqrt{z}}\int dA'\,\frac{\gamma,_{x'}}{\sqrt{z'}+\sqrt{z}}. \tag{4.11}$$

The desired stress field for the cracked body is obtained by adding equation (4.11) to equation (4.5). The resulting stress is

$$\bar{\tau} = -\frac{G}{2\pi}\frac{1}{\sqrt{z}}\int\frac{\sqrt{z'}\gamma,_{x'}}{z'-z}\,dA' - G\gamma_x. \tag{4.12}$$

Using the algebraic identity

$$\frac{\sqrt{z'}}{\sqrt{z}}\frac{1}{z'-z} = \frac{1}{\sqrt{z}\sqrt{z'}} + \frac{\sqrt{z}}{\sqrt{z'}}\frac{1}{z'-z}, \tag{4.13}$$

equation (4.12) can be written as

$$\bar{\tau} = \frac{K^P_{\mathrm{III}}}{i\sqrt{2\pi z}} - \frac{G\sqrt{z}}{2\pi}\int\frac{\gamma,_{x'}}{\sqrt{z'}(z'-z)}\,dA' - G\gamma_x \tag{4.14}$$

where K^P_{III} is

$$K^P_{\mathrm{III}} = -\frac{Gi}{\sqrt{2\pi}}\int dA\,\frac{\gamma,_x}{\sqrt{z}}. \tag{4.15}$$

The quantity K^P_{III} is the Mode III stress intensity factor induced by the nonelastic strain. Equations (4.14) and (4.15) are applicable to stationary cracks and quasi-statistically growing cracks.

5 Complex Potentials for Stresses Due to a Body Force Field in an Elastic Body Under Plane Strain or Plane Stress Conditions

In the following discussions, equations for plane strain will be presented. The corresponding equations for plane stress can be obtained by replacing ν with $\nu/(1+\nu)$. It is convenient to introduce the functions:

$$\theta = \frac{1}{2}(\sigma_{xx}+\sigma_{yy}), \tag{5.1a}$$

$$\Lambda = \frac{1}{2}(\sigma_{yy}-\sigma_{xx}+2i\sigma_{xy}), \tag{5.1b}$$

which uniquely determine all the inplane stress components. In terms of θ and Λ, the equilibrium equations can be put into the compact form:

$$\partial_z\theta - \partial_{\bar{z}}\Lambda = \frac{-\bar{f}}{2}, \tag{5.2}$$

where f is the complex body force defined by

$$f \equiv f_x + if_y, \tag{5.3}$$

The compatibility equation for plane strain deformation, $\nabla^2\theta = -f_{i,i}/2(1-\nu)$, can also be expressed in complex notation as

$$\partial_z\partial_{\bar{z}}\theta = -\frac{1}{8(1-\nu)}(\partial_z f + \partial_{\bar{z}}\bar{f}). \tag{5.4}$$

Since θ is real (equation (5.1a)), it can be written as

$$\theta = \Phi + \bar{\Phi}, \tag{5.5}$$

where Φ is a complex function. Note that Φ is only unique up to an imaginary function. Substituting equation (5.5) into equation (5.4) yields

$$\partial_z g + \partial_{\bar{z}}\bar{g} = 0, \tag{5.6}$$

where

$$g \equiv \partial_{\bar{z}}\Phi + \frac{f}{8(1-\nu)}. \tag{5.7}$$

By equation (3.7b), the general solution to equation (5.6) is

$$g = i\partial_{\bar{z}}h, \tag{5.8}$$

where h is a real-valued function. Equating equations (5.7) and (5.8) leads to

$$\partial_{\bar{z}}(\Phi - ih) = -\frac{f}{8(1-\nu)}. \tag{5.9}$$

Since the addition of the imaginary function $-ih$ to Φ does not affect the value of θ, we will formally set $h \equiv 0$. Thus equation (5.9) becomes

$$\partial_{\bar{z}}\Phi = \frac{-f}{8(1-\nu)}. \tag{5.10}$$

Using equations (5.5) and (5.10), equation (5.2) can be written as

$$\partial_{\bar{z}}\Lambda = \partial_z\Phi + \frac{3-4\nu}{8(1-\nu)}\bar{f}. \tag{5.11}$$

Furthermore, if we let

$$\Lambda = \bar{z}\partial_z\Phi + \Psi, \tag{5.12}$$

then Ψ is determined by

$$\partial_{\bar{z}}\Psi = \frac{1}{8(1-\nu)}\partial_z(\bar{z}f) + \frac{3-4\nu}{8(1-\nu)}\bar{f}. \tag{5.13}$$

Equations (5.5), (5.12), (5.10), and (5.13) imply that if f is identically zero, then Φ and Ψ are the analytical complex potentials defined by Muskhelishvili (1962). Equations (5.10) and (5.13), therefore, are an extension of Muskhelishvili's method for an elastic body with a body force field. The advantage of equations (5.10) and (5.13) is that they are decoupled, i.e., given f, Φ and Ψ can be determined separately. They will now be used for the fictitious body force method in the next section.

5.1 Internal Stress Due to Nonelastic Strain for an Infinite Body. Similar to the treatment for antiplane strain, f can be expressed as

$$f = 2G\left[\left(\epsilon_{yy}-\epsilon_{xx}-2i\epsilon_{xy}\right),_x - 2\partial_{\bar{z}}\left(\frac{\nu\epsilon_{\ell\ell}}{1-2\nu}+\epsilon_{yy}-i\epsilon_{xy}\right)\right], \tag{5.14}$$

where $\epsilon_{\ell\ell} = \epsilon_{xx} + \epsilon_{yy} + \epsilon_{zz}$.

Substitution of equation (5.14) into equation (5.10) leads to

$$\partial_{\bar{z}}\left[\Phi^f - \frac{G}{2(1-\nu)}\left(\frac{\nu\epsilon_{\ell\ell}}{1-2\nu}+\epsilon_{yy}-i\epsilon_{xy}\right)\right]$$

$$= -\frac{G}{4(1-\nu)}\left(\epsilon_{yy}-\epsilon_{xx}-2i\epsilon_{xy}\right),_x \tag{5.15}$$

Downloaded 03 May 2010 to 171.66.16.27. Redistribution subject to ASME license or copyright; see http://www.asme.org/terms/Terms_Use.cfm

where Φ^f is the complex potential for the fictitious stress σ^f. Application of equation (3.11) to equation (5.15) yields

$$\Phi^f = \frac{G}{2(1-\nu)}\left(\frac{\nu\epsilon_{\ell\ell}}{1-2\nu} + \epsilon_{yy} - i\epsilon_{xy}\right)$$

$$+ \frac{G}{4\pi(1-\nu)}\int dA' \frac{(\epsilon_{yy}-\epsilon_{xx}-2i\epsilon_{xy})_{,x'}}{z'-z}. \quad (5.16)$$

To obtain the other potential Ψ^f, $\bar{f}$ is written as

$$\bar{f} = 2G\left[\left(\epsilon_{zz} - \frac{\epsilon_{\ell\ell}}{1-2\nu}\right)_{,x} + 2\partial_{\bar{z}}\left(\frac{\nu\epsilon_{\ell\ell}}{1-2\nu} + \epsilon_{yy} + i\epsilon_{xy}\right)\right]. \quad (5.17)$$

Substituting equations (5.17) and (5.14) into equation (5.13) and applying equation (3.11), Ψ^f is given by

$$\Psi^f = -\frac{G}{2(1-\nu)}\left[\bar{z}\partial_z\left(\frac{\nu\epsilon_{\ell\ell}}{1-2\nu} + \epsilon_{yy} - i\epsilon_{xy}\right)\right.$$

$$\left. - 2(1-2\nu)\epsilon_{yy} - 2\nu\epsilon_{\ell\ell} - 4i(1-\nu)\epsilon_{xy}\right]$$

$$- \frac{G}{4\pi(1-\nu)}\int dA'(\epsilon_{yy}-\epsilon_{xx}-2i\epsilon_{xy})_{,x'}\left(\frac{\bar{z}'}{(z'-z)^2} + \frac{1}{z'-z}\right)$$

$$- \frac{G}{2\pi(1-\nu)}\int dA'((1-2\nu)\epsilon_{zz}-\epsilon_{\ell\ell})_{,x'}\frac{1}{z'-z}. \quad (5.18)$$

With equations (5.16) and (5.18), the fictitious stresses are determined as

$$\theta^f = \frac{G}{1-\nu}\left(\frac{\nu\epsilon_{\ell\ell}}{1-2\nu} + \epsilon_{yy}\right)$$

$$+ \frac{G}{2\pi(1-\nu)}\,\mathrm{Re}\left[\int dA' \frac{(\epsilon_{yy}-\epsilon_{xx}-2i\epsilon_{xy})_{,x'}}{z'-z}\right] \quad (5.19)$$

$$\Lambda^f = \frac{(1-2\nu)G}{1-\nu}\left[\frac{\nu}{1-2\nu}\epsilon_{\ell\ell} + \epsilon_{yy}\right] + 2iG\epsilon_{xy}$$

$$- \frac{G}{4\pi(1-\nu)}\int dA'(\epsilon_{yy}-\epsilon_{xx}-2i\epsilon_{xy})_{,x'}\left(\frac{\bar{z}'-\bar{z}}{(z'-z)^2} + \frac{1}{z'-z}\right)$$

$$- \frac{G}{2\pi(1-\nu)}\int dA'((1-2\nu)\epsilon_{zz}-\epsilon_{\ell\ell})_{,x'}\frac{1}{z'-z}. \quad (5.20)$$

The internal stress in the infinite body is given by, from equation (2.5).

$$\theta = \theta^f - G\left(\frac{2\nu\epsilon_{\ell\ell}}{1-2\nu} + \epsilon_{xx} + \epsilon_{yy}\right)$$

$$\theta = -\frac{G}{1-\nu}(\epsilon_{xx} + \nu\epsilon_{zz})$$

$$+ \frac{G}{2\pi(1-\nu)}\,\mathrm{Re}\left[\int dA' \frac{(\epsilon_{yy}-\epsilon_{xx}-2i\epsilon_{xy})_{,x'}}{z'-z}\right] \quad (5.21)$$

and

$$\Lambda = \Lambda^f - G(\epsilon_{yy}-\epsilon_{xx}+2i\epsilon_{xy})$$

$$= \frac{G}{1-\nu}(\epsilon_{xx}+\nu\epsilon_{zz}) - \frac{G}{4\pi(1-\nu)}\int dA'(\epsilon_{yy}-\epsilon_{xx}$$

$$- 2i\epsilon_{xy})_{,x'}\left(\frac{\bar{z}'-\bar{z}}{(z'-z)^2} + \frac{1}{z'-z}\right)$$

$$- \frac{G}{2\pi(1-\nu)}\int dA'[(1-2\nu)\epsilon_{zz}-\epsilon_{\ell\ell}]_{,x'}\frac{1}{z'-z}. \quad (5.22)$$

If ϵ is uniform in the x-direction (i.e., $\epsilon = \epsilon(y)$), it can be shown that

$$\sigma_{xx} = -\frac{2G}{1-\nu}(\epsilon_{xx}(y) + \nu\epsilon_{zz}(y))$$

$$\sigma_{zz} = -\frac{2G}{1-\nu}(\epsilon_{zz}(y) + \nu\epsilon_{xx}(y))$$

$$\sigma_{yy} = \sigma_{xy} = 0, \quad (5.23)$$

and the resulting displacements are given by

$$u(y) = 2\int_{-\infty}^{y}\epsilon_{xy}\,dy$$

$$v(y) = \int_{-\infty}^{y}(\epsilon_{yy} + \frac{\nu}{1-\nu}(\epsilon_{xx}+\epsilon_{zz}))dy \quad (5.24)$$

5.2 Internal Stress for an Infinite Body with a Semi-Infinite Crack. Let a semi-infinite crack along the negative x axis be introduced to the infinite body discussed in the last section. The introduction of this crack induces an image stress so that the sum of the stress for the uncracked body and the image stress renders the traction-free condition on the crack faces. For simplicity, the nonelastic strains are assumed to possess the following symmetries

$$\epsilon_{xx}(x,-y) = \epsilon_{xx}(x,y),$$
$$\epsilon_{yy}(x,-y) = \epsilon_{yy}(x,y),$$
$$\epsilon_{xy}(x,-y) = -\epsilon_{xy}(x,y), \quad (5.25)$$

Plane strain Mode I is enforced by these symmetry conditions. Applying Muskhelishvili's method, the image stress can be expressed in terms of a single analytic function $\phi(z)$ as

$$\frac{1}{2}(\sigma^I_{xx} + \sigma^I_{yy}) = \phi(z) + \phi(\bar{z}), \quad (5.26)$$

$$\frac{1}{2}(\sigma^I_{yy} - \sigma^I_{xx} + 2i\sigma^I_{xy}) = -(z-\bar{z})\frac{d\phi(z)}{dz}. \quad (5.27)$$

By a similar procedure used for Mode III cracks, $\phi(z)$ can be shown to be

$$\phi(z) = -\frac{G}{8\pi(1-\nu)}\frac{1}{\sqrt{z}}\left[2\int dA'[(1-2\nu)\epsilon_{zz}-\epsilon_{\ell\ell}]_{,x'}/(\sqrt{z'}+\sqrt{z})\right.$$

$$\left. + \int dA'(\epsilon_{yy}-\epsilon_{xx}-2i\epsilon_{xy})_{,x'}(z'-\bar{z}')\partial_{z'}\left(\frac{1}{\sqrt{z'}+\sqrt{z}}\right)\right]. \quad (5.28)$$

Using the algebraic identity

$$\frac{1}{\sqrt{z'}+\sqrt{z}} = \frac{1}{\sqrt{z'}} - \left[\frac{z}{z'}\right]^{1/2}\frac{1}{\sqrt{z'}+\sqrt{z}},$$

equation (5.40) can be rewritten as

$$\phi(z) = \frac{K^P_I}{2\sqrt{2\pi z}} + \frac{G}{8(1-\nu)}\left[2\int dA'[(1-2\nu)\epsilon_{zz}\right.$$

$$- \epsilon_{\ell\ell}]_{,x'}/(\sqrt{z'}(\sqrt{z'}+\sqrt{z}))$$

$$\left. + \int dA'(\epsilon_{yy}-\epsilon_{xx}-2i\epsilon_{xy})(z'-\bar{z}')\partial_{z'}\right.$$

$$\left.\left(\frac{1}{\sqrt{z'}(\sqrt{z'}+\sqrt{z})}\right)\right], \quad (5.29)$$

where K^P_I is the stress intensity factor induced by the nonelastic strain. It is defined by

$$K^P_I \equiv -\frac{G}{2\sqrt{2\pi}(1-\nu)}\left[2\int dA[(1-2\nu)\epsilon_{zz}-\epsilon_{\ell\ell}]_{,x}/\sqrt{z}\right.$$

$$\left. - \int dA(\epsilon_{yy}-\epsilon_{xx}-2i\epsilon_{xy})_{,x}\frac{z-\bar{z}}{2z^{3/2}}\right]. \quad (5.30)$$

Downloaded 03 May 2010 to 171.66.16.27. Redistribution subject to ASME license or copyright; see http://www.asme.org/terms/Terms_Use.cfm

Summary

This paper is concerned with the derivation of the self-stresses due to a field of nonelastic strain in a linear elastic body. Specific results are obtained for an infinite uncracked or cracked body. The derivation is based on a generalized analytic function theory. Although other methods (such as those given in references [2–7]) could be used to obtain the same results, it is felt that the method adopted in this work provides a more unified approach to the internal stress problem.

In an accompanying paper Wu and Hui (19865), there is a sequence of examples illustrating the applications of the results of this paper.

Acknowledgments

This work is supported by the National Science Foundation Grant No. NSF 84-00766. The authors would like to thank John Hutchinson, Ben Freund, James Rice, Edward Hart, Paul Steif, and Vicki Bergman for editorial comments.

References

Denda, M., 1983, "A Dislocation Approach to Steady Crack Growth," Ph.H. Thesis, Harvard University, 1983.

Dewit, R., 1973, "Theory of Dislocations. III Continuous and Discrete Disclinations in Anisotropic Elasticity," *J. of Research of the National Bureau of Standards—A. Physics and Chemistry*, Vol. 77A, No. 3, pp. 359–368.

Eshelby, J. D., 1957, "The Determination to the Elastic Field of an Ellipsoidal Inclusion, and Related Problems," *Proc. Roy. Soc. Lond.*, A241, pp. 376–396.

Freund, L. B., 1980, "The Line Plastic Zone Model for Steady Mode III Crack Growth in and Elastic-Plastic Material," *J. Mech. Phys. Solids*, Vol. 28, pp. 49–57.

Hutchinson, J. W., 1974, "On Steady Quasi-Static Growth," Harvard University, Divison of Applied Science, DEAP S-8.

Muskhelishvili, N. I., 1962, *Some Basic Problems in the Mathematical Theory of Elasticity*, Radok, J. R. M., trauns., Noordhoff, Groningen, Holland.

Rice, J. R., 1966, "Mechanics of Crack Tip Deformation and Extension by Fatigue," ASTM STP 415, pp. 257–310.

Schwartz, 1966, *Mathematics for the Physical Sciences*, Addison Wesley Publishing Co.

Tirosh, and Mclintick, F. A., 1978, "Applications of Numerical Method to Forming Processes," *Proc. of an Int. Conf. on Numerical Methods in Fracture Mechanics*, ASME AMD Vol. 28, Swausea, Wales.

Vekua, I. N., 1962, *Generalized Analytic Functions*, Addison Wesley Publishing Co.

Vitek, V., 1976, "Yielding of Inclined Planes at the Tip of a Crack Loaded in Uniform Tension," *J. Mech. Phys. Solids*, Vol. 24, pp. 263–275.

Wu, K. C., 1985, "Steady State Crack Propagation in Ductile Materials," Ph.D. thesis, Cornell University.

Wu, K. C., and Hart, E. W., 1986, "Steady State Crack Growth in Elastic-Plastic Materials," *Intl. J. Fracture*, to appear.

Wu, K. C., and Hui, C. Y., 1986, "A Complex-Variable Method for Two-Dimensional Internal Stress Problems, and its Applications to Crack Growth in Nonelastic Materials: Part II—Applications," ASME JOURNAL OF APPLIED MECHANICS.

Downloaded 03 May 2010 to 171.66.16.27. Redistribution subject to ASME license or copyright; see http://www.asme.org/terms/Terms_Use.cfm

A Complex-Variable Method for Two-Dimensional Internal Stress Problems and Its Applications to Crack Growth in Nonelastic Materials: Part II—Applications

K. C. Wu[1]
Post-Doctoral Fellow.

C. Y. Hui
Assistant Professor.

Theoretical and Applied Mechanics,
Kimball Hall,
Cornell University,
Ithaca, New York 14853

In Part I of this work the internal stress due to a field of nonelastic strain in an infinite uncracked or cracked elastic body is derived for the case of antiplane shear, plane strain and plane stress. We will apply these results to solve a variety of self-stress problems in this paper. Exact solutions are obtained for a homogeneous distribution of nonelastic strain in a circular or polygonal region for an uncracked body. For a cracked body, closed form solutions are found for homogeneous nonelastic strain in two circular or polygonal regions symmetrically located with respect to the crack line. These results can also be applied to study internal stresses due to a homogeneous stress-free strain transformation or a uniform temperature distribution in the regions considered. Integral equations of stress are derived for stationary cracks and quasi-static growing cracks imbedded in nonelastic materials under small scale yielding condition. An integral equation for steady state dynamic Mode III crack growth is also given. It is shown that for steady-state crack growth problem, the presence of the trailing deformation wake introduces a residual stress that invalidates the dominance of the K field in the wake. Numerical implementation of the proposed method for inelasticity problems is discussed.

1 Introduction

In Part I of this work, a complex calculus is used to obtain the self-stress due to a distribution of nonelastic strain in an infinitely extended, isotropic, homogeneous elastic body with or without a semi-infinite crack. We now apply these results to investigate two types of self-stress problems. Specifically, they are:

I) The internal stress generated by a nonelastic strain distribution, which was called "homogeneous stress-free strain transformation" by Eshelby (1957) if the nonelastic strain is spatially uniform.

II) Quasi-static crack growth (steady state or transient) in rate sensitive or rate independent materials under "small scale yielding" conditions (s.s.y.).

Closed form solutions are obtained for homogeneous strain transformation in a circular cylinder and a polygonal cylinder, respectively, for the uncracked body under antiplane strain or plane strain deformation. For the cracked body, the strain transformation is assumed to take place inside two n-sided polygons or two circles which are located symmetrically with respect to the crack line. The crack is assumed to be traction free. Closed form solutions are obtained for the case of Mode III and plane strain Mode I crack. In type II problems, integral equations in terms of nonelastic strain-rate for Mode I and Mode III cracks are presented. Quasi-static crack growth in a nonelastic material can be studied by coupling the integral equations with the constitutive equations for the material. As we shall see later, the effects on stress of the deformation wake are explicitly included in the integral equations.

The following notation will be used throughout this paper. Reference to equations in Part I of this work will be prefixed by I. For example, equation (I2.4) refers to equation four of section two in part one of this work.

Results for antiplane shear will be presented first, followed by results for plane strain and plane stress.

2 Antiplane Shear Results

2.1 Homogeneous Strain Transformation in a Region

[1]Currently Associate Professor of the Institute of Applied Mechanics, National Taiwan University, Taipei, Taiwan.

Contributed by the Applied Mechanics Division for presentation at the 1987 Applied Mechanics, Biomechanics, and Fluids Engineering Conference, Cincinnati, OH, June 14–17, 1987, of the American Society of Mechanical Engineers.

Discussion of this paper should be addressed to the Editorial Department, ASME, United Engineering Center, 345 East 47th Street, New York, N.Y. 10017, and will be accepted until two months after final publication of the paper itself in the JOURNAL OF APPLIED MECHANICS. Manuscript received by ASME Applied Mechanics Division, April 10, 1986; final revision, July 28, 1986.

Paper No. 87-APM-11.

Copyright © 1987 by ASME
Downloaded 03 May 2010 to 171.66.16.27. Redistribution subject to ASME license or copyright; see http://www.asme.org/terms/Terms_Use.cfm

Bounded by a Curve C. Equation (I4.5) can be used to investigate the internal stress due to a homogeneous strain transformation in a bounded region B, i.e.,

$$\gamma(z)=\gamma H(B) \quad \forall z$$

where γ in the right-hand side of the above equation is to be regarded as a complex constant and H is the Heavyside function defined in equation (I3.12). Using equations (I3.12) and (I3.17), equation (I4.5) can be simplified to

$$\bar{\tau}=\frac{G\gamma}{2\pi}\int_C \frac{dy'}{z'-z}-G\gamma_x H(B),$$

$$=\frac{G\gamma}{2\pi}I_c(z)-G\gamma_x H(B) \tag{2.1a}$$

where

$$I_c(z)=\int_C \frac{dy'}{z'-z}, \tag{2.1b}$$

and C is the boundary of the transformation zone. Equation (2.1) implies that the stresses at distances large compared to the dimensions of the transformation zone do not depend on the actual geometry of the transformation zone. This is because, for large z,

$$I_c(z)\sim -\frac{1}{z^2}\int_C x'dy'=-\frac{A}{z^2}, \tag{2.2}$$

where A is the area of the transformation zone. Equation (2.1) will now be applied to two special cases where C is a circle and a polygon, respectively.

2.1.1 Homogeneous Strain Transformation in a Circular Region. Let C be a circle centered at $z=z_o$ with radius R. The contour integral in equation (2.1) can be evaluated using the calculus of residues. The results are

$$I_c(z)=\pi \qquad \text{for } |z-z_o|<R, \tag{2.2a}$$

$$=-\frac{\pi R^2}{(z-z_o)^2} \qquad \text{for } |z-z_o|>R. \tag{2.2b}$$

The internal stresses inside and outside the transformation zone are

$$\bar{\tau}=-\frac{G}{2}\bar{\gamma} \qquad \text{for } |z-z_o|<R \tag{2.3a}$$

$$=-\frac{G\gamma}{2\pi}\frac{\pi R^2}{(z-z_o)^2} \qquad \text{for } |z-z_o|>R. \tag{2.3b}$$

Equation (2.3a) agrees with the result obtained by using Eshelby's formula for an ellipsoidal inclusion (Eshelby, 1957). As noted by Eshelby, the stress inside the circular region is homogeneous. It can be shown that across the boundary the traction is continuous while the tangential stress τ_t suffers a jump given by

$$\Delta\tau_t=G(\gamma_x t_x+\gamma_y t_y), \tag{2.4}$$

where (t_x, t_y) is the tangential unit vector.

2.1.2 Homogeneous Strain Transformation in a Polygon. Let C be the boundary of an n-sided polygon B with n vertices located at $z_1, \ldots, z_n$. The vertices are labeled in a counterclockwise order. The n sides of a polygon are denoted by $C_1, \ldots, C_n$ such that

$$C=\bigcup_{j=1}^{n} C_j.$$

For the polygon, equation (2.1) becomes

$$\bar{\tau}=\frac{G\gamma}{2\pi}\sum_{\gamma=1}^{n} I_{c_j}(z)-G\gamma_x H(B). \tag{2.5}$$

A direct evaluation of I_{c_j} gives

$$I_{c_j}(z)=\frac{y_{j+1}-y_j}{z_{j+1}-z_j}\,ln\,\frac{z-z_{j+1}}{z-z_j}. \tag{2.6}$$

The branch cut for the logarithmic function is chosen to be the line segment C_j as we expect the stress to be discontinuous across the boundary. With this choice of the branch cut, it can be shown that the discontinuity of the tangential stress across the boundary is again given by equation (2.4). For the polygon, the stress in the polygon is no longer homogeneous in contrast to the case for a circle. In the special case of a rectangle, equation (2.5) takes the simple form:

$$\bar{\tau}=\frac{G\gamma}{2\pi i}\left\{ln\left[\frac{z-z_2}{z-z_1}\right]+ln\left[\frac{z-z_4}{z-z_3}\right]\right\}-G\gamma_x H(B). \tag{2.7}$$

2.2 Homogeneous Strain Transformation in an Infinite Elastic Body with a Semi-Infinite Crack. Equation (I4.14) will now be used to investigate the internal stress field generated by a homogeneous strain transformation in a cracked infinite body. The transformation is assumed to occur in two regions symmetrically located with respect to the crack line. The distribution of the stress-free strains is assumed to be consistent with the symmetry conditions given by equations (I4.8) and (I4.9). Because of the symmetry conditions, equation (I4.14) for the problem becomes

$$\bar{\tau}=\frac{K^P_{\mathrm{III}}}{i\sqrt{2\pi z}}+\frac{\sqrt{z}}{2\pi}G(U_C(z)\gamma-\tilde{U}_C(z)\bar{\gamma})-G\gamma_x H(B), \tag{2.8}$$

where

$$U_C(z)=\int_C dy'\frac{1}{\sqrt{z'}(z'-z)}, \tag{2.9}$$

and C is the boundary of the transformation zone B in the upper half plane. Using equation (I3.16), and (I4.15) K^P_{III} can be expressed as

$$K^P_{\mathrm{III}}=-\sqrt{2/\pi}G\ Im\left[\gamma\int_C \frac{dy}{\sqrt{z}}\right]. \tag{2.10}$$

The case where B is a circle will be considered first, followed by the case where B is a polygon.

2.2.1 Homogeneous Strain Transformation in Two Circular Regions Symmetric With Respect to the Crack Line. Let B be the circle centered at z_o with radius R. K^P_{III} for this case becomes

$$K^P_{\mathrm{III}}=-\sqrt{\pi/2}\frac{GR^2}{r_o^{3/2}}\left(-\gamma_x\sin\frac{3}{2}\theta_o+\gamma_y\cos\frac{3}{2}\theta_o\right), \tag{2.11}$$

where

$$r_o\equiv\sqrt{x_o^2+y_o^2} \text{ and } \theta_o\equiv\tan^{-1}\frac{y_o}{x_o}.$$

Equation (2.11) can be simplified further by introducing

$$\gamma_x=\gamma_e\cos\alpha, \tag{2.12a}$$

$$\gamma_y=\gamma_e\sin\alpha, \tag{2.12b}$$

where

$$\gamma_e\equiv\sqrt{\gamma_x^2+\gamma_y^2} \quad \text{and} \quad \alpha=\tan^{-1}\frac{\gamma_y}{\gamma_x}.$$

Substituting equations (2.12a) and (2.12b) into equation (2.11) yields

$$K^P_{\mathrm{III}}=-\sqrt{\pi/2}\frac{GR^2\gamma_e}{r_o^{3/2}}\sin\left(\frac{3}{2}\theta_o-\alpha\right). \tag{2.13}$$

An interesting result is that for

$$\theta_o=\frac{2}{3}\alpha \text{ or } \theta_o=\frac{2}{3}(\alpha+\pi),$$

Downloaded 03 May 2010 to 171.66.16.27. Redistribution subject to ASME license or copyright; see http://www.asme.org/terms/Terms_Use.cfm

K^P_{III} is identically zero and the stress is finite at the crack tip. Using the calculus of residues, $U_C(z)$ is evaluated to be

$$U_C(z)=\frac{\pi R^2}{(z-z_o)\sqrt{z_o}}\left(\frac{1}{2}\frac{1}{z_o}-\frac{1}{z-z_o}\right)+\frac{\pi}{\sqrt{z}}\left(1+\left(\frac{R}{z-z_o}\right)^2\right) \tag{2.14}$$

for $|z-z_o|<R$ and

$$U_C(z)=\frac{\pi R^2}{(z-z_o)\sqrt{z_o}}\left(\frac{1}{2}\frac{1}{z_o}-\frac{1}{z-z_o}\right) \tag{2.15}$$

for $|z-z_o|>R$. Since $|\tilde{z}-z_o|>R$, $\tilde{U}_C(z)$ is given by

$$\tilde{U}_C(z)=\frac{\pi R^2}{(z-\tilde{z}_o)\sqrt{\tilde{z}_o}}\left(\frac{1}{2}\frac{1}{\tilde{z}_o}-\frac{1}{z-\tilde{z}_o}\right). \tag{2.16}$$

The internal stress field for the problem is obtained by substituting equations (2.14)-(2.16) into equation (2.8).

2.2.2 Homogeneous Strain Transformation in a Polygon in a Cracked Body. Let C be the same polygon as considered in Section 2.1.2. K^P_{III} for the polygon is given by (2.10) and is evaluated to be

$$K^P_{III}=-\frac{4G}{\sqrt{2\pi}}\sum_{j=1}^{n}(y_{j+1}-y_j)Im\left[\frac{\gamma}{\sqrt{z_{j+1}}+\sqrt{z_j}}\right]. \tag{2.17}$$

For the special case of a rectangle, equation (2.17) can be simplified to

$$K^P_{III}=\frac{4G}{\sqrt{2\pi}}\sum_{j=1}^{4}(-1)^j\mathrm{Re}[\gamma\sqrt{z_j}], \tag{2.18}$$

where Re stands for "the real part of".

$U_C(z)$ is computed to be

$$U_C(z)=\frac{1}{\sqrt{z}}\sum_{j=1}^{n}\left(\frac{y_{j+1}-y_j}{z_{j+1}-z_j}\right)\left[ln\frac{\sqrt{z_{j+1}}-\sqrt{z}}{\sqrt{z_{j+1}}+\sqrt{z}}-ln\frac{\sqrt{z_j}-\sqrt{z}}{\sqrt{z_j}+\sqrt{z}}\right]. \tag{2.19}$$

and

$$\tilde{U}_C(z)=\frac{1}{\sqrt{z}}\sum_{j=1}^{n}\left[\frac{y_{j+1}-y_j}{\tilde{z}_{j+1}-\tilde{z}_j}\right]\left[ln\frac{\sqrt{\tilde{z}_{j+1}}-\sqrt{z}}{\sqrt{\tilde{z}_{j+1}}+\sqrt{z}}-ln\frac{\sqrt{\tilde{z}_j}-\sqrt{z}}{\sqrt{\tilde{z}_j}+\sqrt{z}}\right]. \tag{2.20}$$

2.3 Quasi-Static Crack Growth Under Small Scale Yielding Conditions. Equations (I4.14) and (I4.15) are also valid for a quasi-statically growing crack. If the crack is moving with a velocity $\dot{a}(t)$ along the x axis, the coordinate system must now be fixed at the moving crack tip. With respect to the moving coordinate system,

$$\gamma_{,x}=(\gamma_{,t}-\dot{\gamma})/\dot{a}(t), \tag{2.21}$$

where $\gamma_{,t}$ is to be taken in the moving system and $\dot{\gamma}$ is the nonelastic strain rate at a fix material point. In particular, for steady-state crack growth, $\gamma_{,t}=0$ and $\dot{a}(t)=\dot{a}_{ss}=$ const., equation (2.21) becomes

$$\gamma_{,x}=-\dot{\gamma}/\dot{a}_{ss} \tag{2.22}$$

Substitution of equation (2.22) into equations (I4.14) and (I4.15) results in

$$\bar{\tau}=\frac{K^P_{III}}{i\sqrt{2\pi z}}+\frac{G\sqrt{z}}{2\pi\dot{a}_{ss}}\int\frac{\dot{\gamma}}{\sqrt{z'}\,(z'-z)}dA'-G\gamma_x, \tag{2.23}$$

where

$$K^P_{III}=\frac{Gi}{\sqrt{2\pi}\dot{a}_{ss}}\int dA\frac{\dot{\gamma}}{\sqrt{z}}, \tag{2.24}$$

and

$$\gamma_x=\frac{1}{\dot{a}_{ss}}\int_x^\infty\dot{\gamma}_x(s,y)ds. \tag{2.25}$$

Equation (2.23) is the internal stress in an infinite elastic body with a steadily growing semi-infinite crack due to the nonelastic strain rate. If, in addition, the body is subjected to some external loading, the stress due to the applied loading must be added to the internal stress to obtain the total stress. Under the small scale yielding conditions, the applied stress $\bar{\tau}^A$ is represented by the elastic singular solution:

$$\bar{\tau}^A=\frac{K^A_{III}}{i\sqrt{2\pi z}}, \tag{2.26}$$

where K^A_{III} is the applied stress intensity factor calculated from the external loading and the crack geometry assuming the body were free of nonelastic deformation. Due to the linearity of the stress equilibrium equations, the total stress is obtained by adding equations (2.23) and (2.26), i.e.,

$$\bar{\tau}=\frac{K_{III}}{i\sqrt{2\pi z}}+\frac{G\sqrt{z}}{2\pi\dot{a}_{ss}}\int\frac{\dot{\gamma}}{\sqrt{z'}\,(z'-z)}dA'-G\gamma_x, \tag{2.27a}$$

where

$$K_{III}\equiv K^A_{III}+K^P_{III}, \tag{2.27b}$$

is the local stress intensity factor. Equation (2.27) was first derived by Wu and Hart (1986), but similar equations were derived earlier by Hart (1980) for the case of an elastic-plastic material. The corresponding equation of energy balance per unit crack extension was also given by them to be

$$\frac{(K^A_{III})^2}{2G}=\frac{(K_{III})^2}{2G}+\frac{1}{\dot{a}_{ss}}\int dA\sigma_i\dot{\gamma}_i+G\int_o^\infty dy(\gamma_x)^2, \tag{2.28}$$

where the last integral is evaluated at $x=-\infty$. The term on the last left-hand side represents the energy flow to the crack tip if nonelastic deformation is absent. In the presence of nonelastic deformation, the energy that is actually available to drive the crack is given by the first term on the right-hand side of equation (2.28). The remaining energy is either dissipated by the plastic deformation or is stored as residual strain energy in the wake as represented by the second and the third terms, respectively.

Equations (2.27) and (2.28) can be used for rate-independent or rate sensitive materials. For rate-independent materials ($\dot{}$) must be interpreted as differentiation with respect to any monotonically increasing quantity; if the crack length is chosen to be such a quantity, we can formally set $\dot{a}_{ss}=1$. Equations (2.27a) can be considered as an integral equation for the stress with the introduction of the constitutive equations of the material. Two classes of constitutive equations of practical interest are:

(i) rate sensitive materials:

$$\dot{\gamma}_i=f(\tau_e)\tau_i, \tag{2.29}$$

where $\tau_e=\sqrt{\tau_x^2+\tau_y^2}$ and f is an increasing function of τ_e. For power-law creeping materials,

$$f(\tau_e)=\frac{\dot{\gamma}_o}{\tau_e}\left(\frac{\tau_e}{\tau_o}\right)^n. \tag{2.30}$$

for viscoplastic materials,

$$\left.\begin{aligned} f(\tau_e)&=\frac{\dot{\gamma}_o}{\tau_e}\left(\left(\frac{\tau_e}{\tau_o}\right)^n-1\right) && \text{for } \tau_e\geq\tau_o,\\ &=0 && \text{for } \tau_e\leq\tau_o,\end{aligned}\right\} \tag{2.31}$$

In equations (2.30) and (2.31), n, $\dot{\gamma}_o$, and τ_o are material parameters.

Downloaded 03 May 2010 to 171.66.16.27. Redistribution subject to ASME license or copyright; see http://www.asme.org/terms/Terms_Use.cfm

(*ii*) rate independent plasticity:

$$\left.\begin{aligned}\dot{\gamma}_i &= f(\tau_e)\dot{\tau}_e\tau_i && \dot{\tau}_e \geq 0\\ &= 0 && \dot{\tau}_e < 0\end{aligned}\right\} \quad (2.32a)$$

The case of instantaneous power-law hardening plasticity is given by

$$f(\tau_e) = \alpha\tau_e^{n-2} \quad (2.32b)$$

The stress state near the moving crack tip in a material described by the above constitutive equations can be investigated by taking $z \to 0$ in equation (2.23). If K_{III} is nonzero, the near-tip stress is given by

$$\bar{\tau} = \frac{K_{III}}{i\sqrt{2\pi z}} \quad (2.33)$$

and the stress singularity is not altered by the nonelastic deformation. Since all terms of equation (2.28) are positive, $K_{III} \leq K_{III}^A$. Thus the effect of nonelastic deformation reduces K_{III}^A to K_{III} in this case. For materials satisfying constitutive relations of the form (2.29), Hart (1980) and Hui and Riedel (1981) have shown that the condition for nonvanishing K_{III} is $n < 3$ as $\tau_e \to \infty$ (or $[f(\tau_e)/\tau_e^3] \to 0$ as $\tau_e \to \infty$). If $n > 3$, it can be shown that K_{III} is identically zero and a lower stress singularity than $r^{-1/2}$ develops. Hui and Riedel showed that for constitutive models of equations (2.30) and (2.31), the new singularity is given by $r^{-1/(n-1)}$. As a result of zero K_{III}, there is no energy flow at the crack tip. Equation (2.27*a*) and (I4.12) implies that as $z \to \infty$ the asymptotic stress is given by

$$\bar{\tau} = \frac{K_{III}}{i\sqrt{2\pi z}} - G\gamma_x, \quad (2.34)$$

if $\dot{\gamma}$ decays sufficiently fast. In the elastic region where γ_x vanishes, the elastic solution governed by K_{III} is not perturbed. In the trailing deformation wake, however, the accumulation of γ_x invalidates the dominance of the K field. Thus the usual small scale yielding assumption which assumes that the K field prevails everywhere far removed from the crack tip must be modified to equation (2.24) for steady state crack growth. The fact was noted by Freund (1979), Denda (1983), and Wu and Hart (1986).

In deriving equation (2.27*a*), it was assumed that the crack growth was quasi-static. The removal of this restriction only requires a minor modification of equation (2.27*a*) for the special case of steady state dynamic crack growth. If we define

$$\beta \equiv (1 - (\dot{a}_{ss}/c_s)^2))^{1/2}, \quad (2.35)$$

where c_s is the shear wave velocity, then the integral equation governing dynamic steady state crack growth is given by

$$\bar{\tau} = \frac{K_{III}}{i\sqrt{2\pi\zeta}} + \frac{G\sqrt{\zeta}}{2\pi\dot{a}_{ss}}\int \frac{\dot{\gamma}}{\sqrt{\xi'}(\xi' - \xi)} dA' - \beta G\gamma_x, \quad (2.36)$$

where

$$\begin{aligned}\bar{\tau} &\equiv \beta\tau_x - i\tau_y,\\ \dot{\gamma} &\equiv \frac{1}{\beta}\dot{\gamma}_x + i\dot{\gamma}_y,\\ \zeta &\equiv x + i\beta y.\end{aligned} \quad (2.37)$$

For small values of $\dot{a}_{ss}/c_s$, $\beta \to 1$, and equation (2.36) reduces to equation (2.27*a*) for quasi-static growth.

3 Plane Strain and Plane Stress Results

The case of antiplane shear considered in previous sections will be repeated for the cases of plane strain and plane stress below. We will first present results for an uncracked infinite body. Those for an infinite body with a semi-infinite crack will be given next.

For a homogeneous strain distribution in a region bounded by B, equations (I5.21) and (I5.22) become

$$\theta = -\frac{G}{1-\nu}(\epsilon_{xx} + \nu\epsilon_{zz}) - \frac{G}{2\pi(1-\nu)} \mathrm{Re}[(\epsilon_{yy} - \epsilon_{xx} - 2i\epsilon_{xy})I_c(z)], \quad (3.1)$$

$$\Lambda = \frac{G}{1-\nu}(\epsilon_{xx} + \nu\epsilon_{zz}) + \frac{G}{4\pi(1-\nu)}[(\epsilon_{yy} - \epsilon_{xx} - 2i\epsilon_{xy})(L_c(z) + I_c(z)) + 2((1-2\nu)\epsilon_{zz} - \epsilon_{\ell\ell})I_c(z)], \quad (3.2)$$

where I_c is defined by equation (2.1*b*) and L_c is defined as

$$L_c(z) = \int_C dy' \frac{\bar{z}' - \bar{z}}{(z' - z)^2}. \quad (3.3)$$

Let us first examine the far field stress of equations (3.1) and (3.2). The asymptotic expression of $L_c(z)$ for large $|z|$ compared to the dimensions of the transformation zone is given by

$$L_c(z) \sim \frac{1}{z^2}\left(1 - 2\frac{\bar{z}}{z}\right)A + \text{ higher order terms}, \quad (3.4)$$

where A is the area of the transformation zone. The asymptotic far field stress for arbitrary transformation zone is obtained by substituting equations (2.1) and (3.4) into equations (3.1) and (3.2) and the resulting stress in cylindrical coordinates is

$$\begin{aligned}\sigma_{rr} &= -\frac{GA}{2\pi(1-\nu)r^2}(3\epsilon_{rr} - \epsilon_{\theta\theta} + 2\nu\epsilon_{zz}),\\ \sigma_{\theta\theta} &= \frac{GA}{2\pi(1-\nu)r^2}(\epsilon_{rr} + \epsilon_{\theta\theta} + 2\nu\epsilon_{zz}),\\ \sigma_{r\theta} &= \frac{GA}{\pi(1-\nu)r^2}\epsilon_{r\theta},\end{aligned} \quad (3.5)$$

as $r \to \infty$. As in the case of antiplane strain, the far field stress under plane strain conditions is also characterized by A/r^2 and is independent of the detailed geometry of the transformation zone.

We will now consider the cases treated previously for antiplane strain deformation. Since the integral $I_c(z)$ has been derived for these cases, only $L_c(z)$ need be evaluated to determine the internal stress fields.

3.1 Circular Regions. It can be shown that if C is a circle centered at $z = z_o$ with radius R, the integral L_c is given by

$$L_c(z) = 0 \quad \text{for} \quad |z - z_o| < R, \quad (3.6a)$$

$$= \pi\left(\frac{R^2}{(z-z_o)^2} - 2\frac{R^2(\bar{z} - \bar{z}_o)}{(z-z_o)^3} + \frac{3R^4}{(z-z_o)^4}\right), \quad \text{for} \quad |z - z_o| > R. \quad (3.6b)$$

With equation (2.2*a*) and equation (3.6*a*), the internal stress inside the transformation zone is determined as

$$\begin{aligned}\sigma_{xx} &= -\frac{G}{4(1-\nu)}(3\epsilon_{xx} + \epsilon_{yy} + 4\nu\epsilon_{zz}),\\ \sigma_{yy} &= -\frac{G}{4(1-\nu)}(\epsilon_{xx} + 3\epsilon_{yy} + 4\nu\epsilon_{zz}),\\ \sigma_{xy} &= -\frac{G}{2(1-\nu)}\epsilon_{xy},\end{aligned} \quad (3.7)$$

in agreement with Eshelby's results for an ellipsoidal inclusion (Eshelby, 1957). Using equation (2.2*b*) and equation (3.6*b*), the internal stress outside the transformation zone is given by

Downloaded 03 May 2010 to 171.66.16.27. Redistribution subject to ASME license or copyright; see http://www.asme.org/terms/Terms_Use.cfm

$$\sigma_{rr} = -\frac{G}{2(1-\nu)}\left[(3\epsilon_{rr} - \epsilon_{\theta\theta} + 2\nu\epsilon_{zz})\left(\frac{R}{r}\right)^2 + \frac{3}{2}(\epsilon_{\theta\theta} - \epsilon_{rr})\left(\frac{R}{r}\right)^4\right],$$

$$\sigma_{\theta\theta} = \frac{G}{2(1-\nu)}\left[(\epsilon_{rr} + \epsilon_{\theta\theta} + 2\nu\epsilon_{zz})\left(\frac{R}{r}\right)^2 + \frac{3}{2}(\epsilon_{\theta\theta} - \epsilon_{rr})\left(\frac{R}{r}\right)^4\right],$$

$$\sigma_{r\theta} = \frac{G\epsilon_{r\theta}}{1-\nu}\left(\left(\frac{R}{r}\right)^2 - \frac{3}{2}\left(\frac{R}{r}\right)^4\right), \tag{3.8}$$

where $r = |z - z_o|$. It is readily verified that across the boundary the tractions, σ_{rr} and $\sigma_{r\theta}$, are continuous while $\sigma_{\theta\theta}$ and σ_{zz} attain jumps given by

$$\Delta\sigma_{\theta\theta} = \frac{2G}{1-\nu}(\epsilon_{\theta\theta} + \nu\epsilon_{zz}),$$

$$\Delta\sigma_{zz} = \frac{2G}{1-\nu}(\epsilon_{zz} + \nu\epsilon_{\theta\theta}). \tag{3.9}$$

3.2 Polygonal Regions. A direct integration of the integral $L_{c_j}(z)$ along the side C_j of the polygon described in Section (3.1.2) yields

$$L_{c_j}(z) = \frac{y_{j+1} - y_j}{z_{j+1} - z_j}\left\{\frac{\bar{z}_{j+1} - \bar{z}_j}{z_{j+1} - z_j}\, ln\left(\frac{z - z_{j+1}}{z - z_j}\right) + 2iIm[(\bar{z}_{j+1} - \bar{z}_j)(z - z_j)]\frac{1}{(z - z_j)(z - z_{j+1})}\right\}. \tag{3.10}$$

The integral $L_c(z)$ is given by the summation of $L_{c_j}(z)$, i.e.,

$$L_c(z) = \sum_{j=1}^{n} L_{c_j}(z). \tag{3.11}$$

The internal stress field is obtained by substituting equations (2.6), (3.10), and (3.11) into equations (3.1) and (3.2). Timoshenko and Goodier's result (1970) for a uniform temperature T in a rectangular region under plane stress conditions can be recovered by setting $\nu = \nu/1 + \nu$, $\epsilon_{xx} = \epsilon_{yy} = \alpha_T$, α_T being the coefficient of thermal expansion, and $\epsilon_{zz} = \epsilon_{xy} = 0$ in equations (3.1) and (3.2). Similar to the previous case of circular regions, it can be shown that the tractions σ_{nn} and σ_{ns} are continuous across the boundary whereas the tangential stress σ_{ss} and the out-of-plane stress σ_{zz} experience jumps given by

$$\Delta\sigma_{ss} = \frac{2G}{1-\nu}(\epsilon_{ss} + \nu\epsilon_{zz}),$$

$$\Delta\sigma_{zz} = \frac{2G}{1-\nu}(\epsilon_{zz} + \nu\epsilon_{ss}), \tag{3.12}$$

where ϵ_{ss} is the component of the homogeneous strain tangential to the boundary. The subscripts n and s denote the normal and tangent directions to the boundary. Together, n and s form a local right-handed coordinate system.

3.3 Homogeneous Strain Transformation in a Semi-Infinite Elastic Body with a Semi-Infinite Crack. For a homogeneous strain transformation in two regions symmetrical with respect to the crack line and with the symmetry conditions described by equation (I5.25), the internal stress is given by

$$\theta = \frac{1}{2}(\epsilon_{xx} + \nu\epsilon_{zz}) - \frac{G}{2\pi(1-\nu)}[(\epsilon_{yy} - \epsilon_{xx} - 2i\epsilon_{xy})I_c(z) + (\epsilon_{yy} - \epsilon_{xx} + 2i\epsilon_{xy})\tilde{I}_c(z)] + \phi(z) + \phi(\bar{z}), \tag{3.13}$$

$$\Lambda = -\frac{1}{2}(\epsilon_{xx} + \nu\epsilon_{zz}) + \frac{G}{4\pi(1-\nu)}[(\epsilon_{yy} - \epsilon_{xx} - 2i\epsilon_{xy})(L_c(z) + I_c(z)) + (\epsilon_{yy} - \epsilon_{xx} + 2i\epsilon_{xy})(\tilde{L}_c(z) + \tilde{I}_c(z)) + 2((1-2\nu)\epsilon_{zz} - \epsilon_{\theta\theta})(I_c(z) + \tilde{I}_c(z)) - (z - \bar{z})\frac{d\phi(z)}{dz}, \tag{3.14}$$

where the subscript C indicates that the integrals are evaluated along the boundary of the region in the upper half plane. The complex function $\phi(z)$ for the case can be expressed as

$$\phi(z) = \frac{K_I^P}{2\sqrt{2\pi z}} - \frac{G}{8(1-\nu)}[2((1-2\nu)\epsilon_{zz} - \epsilon_{\theta\theta})(P_c(z) + \tilde{P}_c(z)) + (\epsilon_{yy} - \epsilon_{xx} - 2i\epsilon_{xy})Q_c(z) + (\epsilon_{yy} - \epsilon_{xx} + 2i\epsilon_{xy})\tilde{Q}_c(z)], \tag{3.15}$$

where

$$P_c(z) \equiv \int_C dy' \frac{1}{\sqrt{z'}(\sqrt{z'} + \sqrt{z})} = I_c(z) - \sqrt{z}U_c(z), \tag{3.16}$$

$$Q_c(z) \equiv \int_C dy'(z' - \bar{z}')\partial_{z'}\left(\frac{1}{\sqrt{z'}(\sqrt{z'} + \sqrt{z})}\right) \tag{3.17}$$

and

$$K_I^P = \frac{G}{\sqrt{2\pi}(1-\nu)}\mathrm{Re}\left[2((1-2\nu)\epsilon_{zz} - \epsilon_{\theta\theta})\int_C dy\frac{1}{\sqrt{z}} - (\epsilon_{yy} - \epsilon_{xx} - 2i\epsilon_{xy})\int_c dy\frac{z - \bar{z}}{2z^{3/2}}\right]$$

$$= \frac{G}{\sqrt{2\pi}(1-\nu)}\mathrm{Re}[2((1-2\nu)\epsilon_{zz} - \epsilon_{\theta\theta})\lim_{z\to\infty}\sqrt{z}P_c(z) + (\epsilon_{yy} - \epsilon_{xx} - 2i\epsilon_{xy})\lim_{z\to\infty}\sqrt{z}Q_c(z)]. \tag{3.18}$$

In equation (3.16) $I_c(z)$ and $U_c(z)$ are defined by equation (2.1*b*) and equation (2.9), respectively. It can be shown that $P_c(z)$ and $Q_c(z)$ are continuous across the boundary.

3.3.1 Two Symmetrical Circular Regions in a Cracked Body. The circular region is assumed to be centered at $z = z_o$ with a radius R. From equation (2.2*a*) and equation (2.14), $P_c(z)$ is given by

$$P_c(z) = -\pi R^2\left[\frac{1}{(z - z_o)^2} + \sqrt{z/z_o}\frac{1}{z - z_o}\left(\frac{1}{2}\frac{1}{z_o} - \frac{1}{z - z_o}\right)\right] = \pi R^2\partial_{z_o}\left(\frac{1}{\sqrt{z_o}(\sqrt{z_o} + \sqrt{z})}\right). \tag{3.19}$$

The integral $Q_c(z)$ can be evaluated by the calculus of residue and the result is

$$Q_c(z) = -\frac{\pi R^4}{2}\partial^3{}_{z_o}\left(\frac{1}{\sqrt{z_o}(\sqrt{z_o} + \sqrt{z})}\right) + \pi(z_o - \bar{z}_o)R^2\partial^2{}_{z_o}\left(\frac{1}{\sqrt{z_o}(\sqrt{z_o} + \sqrt{z})}\right). \tag{3.20}$$

Substituting equations (3.19) and (3.20) into equation (3.18), K_I becomes

$$K_I^P = \frac{\sqrt{\pi}GR^2}{\sqrt{2}(1-\nu)r_o^{3/2}}\left\{[(1-2\nu)\epsilon_{zz} - \epsilon_{\theta\theta}]\cos\frac{3}{2}\theta_o - \gamma_{\max}\left[\left(\frac{15}{16}\frac{R^2}{r_o^2} - \frac{3}{4}\right)\sin\left(2\alpha - \frac{7}{2}\theta_o\right) + \frac{3}{4}\sin\left(2\alpha - \frac{3}{2}\theta_o\right)\right]\right\}, \tag{3.21}$$

Downloaded 03 May 2010 to 171.66.16.27. Redistribution subject to ASME license or copyright; see http://www.asme.org/terms/Terms_Use.cfm

where

$$\gamma_{\max}=\sqrt{(\epsilon_{yy}-\epsilon_{xx})^2+4\epsilon_{xy}^2}$$

and α is the direction of the slip line.

For dilatational transformation (i.e., $\epsilon_{xx}=\epsilon_{yy}=\epsilon_{zz}=\epsilon_o$ and $\epsilon_{xy}=0$, $\epsilon_{zz}\neq 0$ in plane strain since ϵ_{ij} denote the components of the inelastic strain tensor). Equation (3.21) is simplified to

$$K_{\mathrm{I}}^P=-\sqrt{2\pi}\left(\frac{1+\nu}{1-\nu}\right)GR^2\epsilon_o\frac{\cos\frac{3}{2}\theta_o}{r_o^{3/2}}. \tag{3.22}$$

Equations (3.21) and (3.22) agree with an earlier result of Hutchinson (1974).

3.3.2 Polygonal Regions in a Cracked Body. Substituting equations (2.6) and (2.14) into equation (3.16), P_c is given by

$$P_c(z)=2\sum_{j=1}^{n}\frac{y_{j+1}-y_j}{z_{j+1}-z_j}ln\left(\frac{\sqrt{z}+\sqrt{z_{j+1}}}{\sqrt{z}+\sqrt{z_j}}\right). \tag{3.23}$$

The integral $Q_c(z)$ is evaluated to be

$$Q_c(z)=2i\sum_{j=1}^{n}\left(\frac{y_{j+1}-y_j}{z_{j+1}-z_j}\right)\left[\left(\frac{y_{j+1}}{\sqrt{z_{j+1}}(\sqrt{z_{j+1}}+\sqrt{z})}\right.\right.$$

$$\left.-\frac{y_j}{\sqrt{z_j}(\sqrt{z_j}+\sqrt{z})}\right)-2\left(\frac{y_{j+1}-y_j}{z_{j+1}-z_j}\right)ln\frac{\sqrt{z}+\sqrt{z_{j+1}}}{\sqrt{z}+\sqrt{z_j}}\Bigg]. \tag{3.24}$$

With equations (3.23) and (3.24), K_{I}^P is

$$K_{\mathrm{I}}^P=\sqrt{2/\pi}\frac{G}{1-\nu}\sum_{j=1}^{n}\mathrm{Re}\Bigg[2((1-2\nu)\epsilon_{zz}-\epsilon_{\ell\ell})\frac{y_{j+1}-y_j}{\sqrt{z_{j+1}}+\sqrt{z_j}}$$

$$+i(\epsilon_{yy}-\epsilon_{xx}-2i\epsilon_{xy})\left(\frac{y_{j+1}-y_j}{z_{j+1}-z_j}\right)\left(\frac{y_{j+1}}{\sqrt{z_{j+1}}}\right.$$

$$\left.\left.-\frac{y_j}{\sqrt{z_j}}-2\frac{y_{j+1}-y_j}{\sqrt{z_{j+1}}+\sqrt{z_j}}\right)\right]. \tag{3.25}$$

3.4 Quasi-Static Crack Growth in Mode I. The discussions in Section 2.3 for Mode III crack growth can be directly carried over to Mode I crack growth. We shall not repeat the same discussions and will only present the integral equations for steady Mode I crack growth here. The equations are obtained by replacing $(\,)_{,x}$ by $-(\dot{})/\dot{a}_{ss}$ in equations (I5.21), (I5.22), (I5.28), and (I5.30). The resulting equations are (Wu and Hart, 1985):

$$\theta=-\frac{G}{1-\nu}(\epsilon_{xx}+\nu\epsilon_{zz})-\frac{G}{2\pi(1-\nu)\dot{a}_{ss}}$$

$$\mathrm{Re}\left[\int dA'\frac{(\dot{\epsilon}_{yy}-\dot{\epsilon}_{xx}-2i\dot{\epsilon}_{xy})}{z'-z}\right]+\phi(z)+\phi(\bar{z}), \tag{3.26}$$

$$\Lambda=\frac{G}{1-\nu}(\epsilon_{xx}+\nu\epsilon_{zz})+\frac{G}{4\pi(1-\nu)\dot{a}_{ss}}\left[\int dA\,(\dot{\epsilon}_{yy}-\dot{\epsilon}_{xx}\right.$$

$$-2i\dot{\epsilon}_{xy})\left(\frac{1}{z'-z}+\frac{\bar{z}'-\bar{z}}{(z'-z)}\right)+2\int dA'[(1-2\nu)\dot{\epsilon}_{zz}$$

$$\left.-\dot{\epsilon}_{\ell\ell}]\frac{1}{z'-z}\right]-(z-\bar{z})\frac{d\phi(z)}{dz}, \tag{3.27}$$

where

$$\phi(z)=\frac{K_I}{2\sqrt{2\pi z}}-\frac{G}{8(1-\nu)}\frac{1}{\dot{a}_{ss}}\left[\int dA'[(1-2\nu)\dot{\epsilon}_{zz}\right.$$

$$-\dot{\epsilon}_{\ell\ell}]\frac{1}{\sqrt{z'}(\sqrt{z'}+\sqrt{z})}+\int dA'(\dot{\epsilon}_{yy}-\dot{\epsilon}_{xx}-2i\dot{\epsilon}_{xy})(z'$$

$$\left.-\bar{z}')\partial_{z'}\left(\frac{1}{\sqrt{z'}(\sqrt{z'}+\sqrt{z})}\right)\right], \tag{3.28}$$

and K_{I} is given by

$$K_{\mathrm{I}}=K_{\mathrm{I}}^A+K_{\mathrm{I}}^P$$

$$=K_{\mathrm{I}}^A+\frac{G}{2\sqrt{2\pi}(1-\nu)\dot{a}_{ss}}\left[2\int dA[(1-2\nu)\dot{\epsilon}_{zz}-\dot{\epsilon}_{\ell\ell}]\frac{1}{\sqrt{z}},\right.$$

$$\left.-\int dA\,(\dot{\epsilon}_{yy}-\dot{\epsilon}_{xx}-2i\dot{\epsilon}_{xy})\frac{z-\bar{z}}{2z^{3/2}}\right]. \tag{3.29}$$

The corresponding equation of energy balance is given by

$$\frac{(1-\nu)}{2G}(K_{\mathrm{I}}^A)^2=\frac{1-\nu}{2G}(K_{\mathrm{I}})^2+\frac{1}{\dot{a}_{ss}}\int dA\,\sigma_{ij}\dot{\epsilon}_{ij}$$

$$+\frac{2G}{1-\nu}\int_o^{\infty}dy[(\epsilon_{xx})^2+(\epsilon_{zz})^2+2\nu\epsilon_{xx}\epsilon_{zz}], \tag{3.30}$$

where the last integral is evaluated at $x=-\infty$.

Similar energy balance for steady dynamic crack growth was independently derived by Freund and Hutchinson (1985). For $\dot{a}_{ss}<0.3C_r$, C_r being the Rayleigh wave speed, the inertial effects are insignificant and equation (3.30) can be used for all practical purposes.

4 Discussions

A numerical formulation can be constructed for steady state crack growth in nonelastic materials on the basis of equations (2.27*a*) for Mode III and (3.26)–(3.27) for Mode I. These equations imply that σ is completely determined by $\dot{\epsilon}$ in the creep zone (or active plastic zone), where $\dot{\epsilon}$ is nonzero. In the following discussions, we shall denote this region of nonvanishing $\dot{\epsilon}$ by D. If the nonelastic behavior of the material can be described by $\dot{\epsilon}$ as a function of the local stress, equations (2.27*a*) and (3.26)–(3.27) can be considered as the equations for $\dot{\epsilon}$ (or σ) in D. We can now divide D into N area elements D_j's such that

$$\sum_{j=1}^{N}D_j=D.$$

Assuming that $\dot{\epsilon}^{(J)}$ in D_j is constant, the integral equations can be simplified to yield a set of algebraic equations

$$\sigma^{(i)}=\mathbf{A}^{(i)}+\mathbf{B}^{(ij)}\dot{\epsilon}^{(J)}, \tag{4.1}$$

where $\sigma^{(i)}$ and $\mathbf{A}^{(i)}$ are the total and the applied stress evaluated at a representative point in D_i (e.g., if D_i is a rectangle, the representative point can be chosen as the center of the rectangle); $\mathbf{B}^{(ij)}$ is a tensorial function that is determined by the representative point in D_i and the area element D_j. Equation (4.1) can be solved in conjunction with the nonelastic constitutive equations for the material. Equation (4.1) for Mode I crack growth in an elastic-perfectly plastic material was derived and solved by Denda (1983). The derivation of Denda is different from the one presented in this work, the resulting equations, however, are the same as those obtained by specializing equations (3.26)–(3.27) to perfectly plastic materials. Wu and Hart (1986) have also solved equation (4.1) to investigate the reduction of the stress intensity factor for visco-plastic materials described by equation (2.31).

Possible advantages of the proposed numerical formulation over the finite element method (F.E.M.) approach are:

(1) It is only necessary to discretize a region slightly larger than the creep zone in the proposed method. In F.E.M., a sufficiently large elastic region must be included so that the elastic K field can be applied on the boundary. The existence of the

Downloaded 03 May 2010 to 171.66.16.27. Redistribution subject to ASME license or copyright; see http://www.asme.org/terms/Terms_Use.cfm

deformation wake also requires a constant modification of the applied tractions in the wake in the iterative solution process for the F.E.M.

(2) σ and $\dot{\epsilon}$ are directly calculated in the proposed method and no numerical differentiations, which lower the accuracy of the solution, need be performed. Furthermore, the proposed method incorporates the global effect (σ in one element is related to $\dot{\epsilon}$ in all elements) as opposed to the local effect in the F.E.M. As a result, it is expected that a solution with the same order of accuracy as that of the F.E.M. will be obtained with a much coarser mesh. As noted by Denda (1983), Dean and Hutchinson (1980), in their finite element analysis of the same problem studied by Denda, employed a mesh finer than that used by Denda and still could not show the existence of the elastic unloading zone as Denda did.

(3) Equation (4.1) can be easily extended to transient quasi-static crack growth by formulating the problems in terms of $\epsilon_{,x}$ instead of $\dot{\epsilon}$. The resulting set of equations is of the form:

$$\sigma^{(i)}(t) = \mathbf{A}^{(i)}(t) + \mathbf{C}^{(ij)}(\epsilon^{(j)}(t))_{,x}, \tag{4.2}$$

where t denotes time. In the moving frame attached to the crack tip the time evolution of $\epsilon^{(j)}(t)$ is given by

$$(\epsilon^{(j)}(t))_{,t} = \dot{\epsilon}^{(j)}(t) + \dot{a}(t)(\epsilon^{(j)}(t))_{,x}, \tag{4.3}$$

for a given history of crack growth $\dot{a}(t)$. Equations (4.2) and (4.3) can be solved with the constitutive equations to determine the histories of σ and ϵ. The case of a stationary crack is obtained by setting $\dot{a}(t) = 0$. Note that in the above formulation the crack tip stays stationary in the moving frame (it always coincides with the origin) and no remeshing is required. In contrast, in F.E.M. the crack tip motion is usually achieved by node-releasing techniques and proper remeshing must be effected to ensure the accuracy of the solution.

The approach presented here is applicable to general two-dimensional inelasticity problems in which $\epsilon^t = \epsilon + \epsilon^e$ and $\epsilon^e \neq 0$. Let A be a region with boundary ∂A. Let ∂A_T be the part of ∂A that is subjected to tractions $\mathbf{T}$ and ∂A_U be the remaining part of ∂A that is subjected to displacements $\mathbf{U}$. The total stress in A can be expressed as

$$\sigma = \sigma^A + \sigma^D + \sigma^I \tag{4.4}$$

where σ^A is the elastic solution with corresponding displacement $\mathbf{u}^A$ for which

$$\left.\begin{aligned} \sigma^A \mathbf{n} &= \mathbf{T} \quad \text{on} \quad \partial A_T, \\ \mathbf{u}^A &= \mathbf{U} \quad \text{on} \quad \partial A_U; \end{aligned}\right\} \tag{4.5}$$

σ^D is the internal stress due to ϵ for an infinite body, which has been derived in the previous sections, and σ^I is the image stress obtained by solving an elasticity problem with the boundary conditions

$$\left.\begin{aligned} \sigma^I \mathbf{n} &= -\sigma^D \mathbf{n} \quad \text{on} \quad \partial A_T, \\ \mathbf{u}^I &= -\mathbf{u}^D \quad \text{on} \quad \partial A_U. \end{aligned}\right\} \tag{4.6}$$

From equations (4.5) and (4.6), it is evident that σ satisfies the boundary conditions. A proper mesh is introduced in a region that contains the nonelastic zone. For a stationary problem, we can formulate the problem by assuming a constant nonelastic strain distribution in an element in the mesh. For a quasi-static growth problem as the crack problem we have discussed, it is more convenient to base the formulation on assuming $(\epsilon_{,x})$ to be constant in an element. The resulting system of nonlinear equations is basically of the same form as the one given by equation (4.1) and can be solved simultaneously with the constitutive equations describing the nonelastic behavior of the material.

In conclusion, the complex calculus introduced in Part I of this work allows considerable simplification in the formulation of some self-stress problems. One advantage is that the nonelastic strains in the formulation can arise from a wide variety of sources. For example, using this method, many of the analytic results in recent works on ceramic fracture (McMeeking and Evans, 1982; Budiansky et al., 1983) can be reproduced with little difficulty. Indeed, the complex calculus technique allows us not only to reproduce all the analytical results of McMeeking and Evans (1982) but also obtain an exact formula for their R-resistance curve. The agreement between our analytic expression and their numerical results is within 1 percent error.

Acknowledgments

This work is supported by the National Science Foundation Grant No. NSF 84-00766. The authors would like to thank John Hutchinson, Ben Freund, James Rice, Edward Hart, Paul Steif, and Vicki Bergman for editorial comments.

References

Budiansky, B., Hutchinson, J. W., and Lambropoulos, J. C., 1983, "Continuum Theory of Dilatant Transformation in Ceramics," *Int. J. Solids Structure*, Vol. 19, pp. 337–355.

Denda, M., 1983, "A Dislocation Approach to Steady Crack Growth," Ph.D. Thesis, Harvard University, 1983.

Dean, R. H., and Hutchinson, J. W., 1985, "Quasi-Static Steady Crack Growth in Small Scale Yielding," *Fracture Mechanics*, ASTM-STP 700, pp. 383–405.

Eshelby, J. D., 1957, "The Determination to the Elastic Field of an Ellipsoidal Inclusion, and Related Problems," *Proc. Roy. Soc. Lond.*, Vol. A241, pp. 376–396.

Freund, L. B., 1979, "The Line Plastic Zone Model for Growth of An Antiplane Shear Crack, Non-linear and Dynamic Fracture Mechanics," AMD-Vol. 35, ASME, New York, pp. 171–183.

Freund, L. B., and Hutchinson, J. W., 1985, "High Strain-Rate Crack Growth in Rate-Dependent Plastic Solids," *J. Mech. Phys. Solids*, Vol. 33, No. 2, pp. 169–191.

Hart, E. W., 1980, "A Theory for Stable Crack Extension Rates in Ductile Materials," *Int. J. Solids and Structures*, Vol. 16, pp. 807–823.

Hui, C. Y., and Riedel, H., 1981, "The Asymptoic Stress and Strain Rate Field Near the Tip of a Growing Crack Under Creep Conditions," *Int. J. Fracture*, Vol. 17, No. 4, pp. 409–425.

McMeeking, R. M., and Evans, A. G., 1982, "Mechanics of Transformation Toughening in Brittle Solids," *J. Am. Ceram. Soc.*, Vol. 65, pp. 242–246.

Timoshenko, S. P., and Goodier, P. N., 1970, *Theory of Elasticity*, McGraw-Hill Book Company, New York.

Wu, K. C., and Hart, E. W., 1986, "Steady State Crack Growth in Elastic-Plastic Material," accepted by *Int. J. Fracture*.

Downloaded 03 May 2010 to 171.66.16.27. Redistribution subject to ASME license or copyright; see http://www.asme.org/terms/Terms_Use.cfm

K. Ravi-Chandar
Assistant Professor,
Department of Mechanical Engineering,
University of Houston,
Houston, TX 77004
Assoc. Mem. ASME

W. G. Knauss
Professor of Aeronautics
and Applied Mechanics,
California Institute of Technology,
Pasadena, CA 91125
Mem. ASME

On the Characterization of the Transient Stress Field Near the Tip of a Crack

The dynamic stress field near a propagating crack tip is usually characterized in terms of one parameter, namely, the dynamic stress intensity factor. While analytically this is an exact representation at the crack tip itself, under transient conditions, the domain of dominance of the stress intensity factor varies as discussed by Ma and Freund (1986). In this paper, we present experimental results which show that while the stress intensity factor may dominate the near tip stress field under transient conditions as long as the crack velocity is small, it may not be dominant over an appreciable region under other transient conditions of crack tip motion, thus making it difficult to determine this quantity experimentally.

1 Introduction

Analyses of dynamic crack problems started with the idealized problem of Yoffe (1951). It was soon established that the stress field near the tip of a propagating crack can be represented in terms of a dynamic stress intensity factor analogous to that for a static crack. Dynamic stress intensity factor solutions to cracks growing rectilinearly in infinite domains under arbitrary time dependent tractions are now available in closed form for semi-infinite and center cracks (Freund, 1972–1974; Rose, 1976). Finite element codes have also been used to calculate dynamic stress intensity factors for finite sized specimens (S. Mall et al., 1978). One should note that these solutions represent a set of admissible solutions for arbitrary values of the crack speed. From this set the appropriate stress intensity factor solution is extracted by imposing a failure criterion. The correct fracture criterion to be imposed is still under active debate (see for example Knauss et al., 1983).

As experimental techniques for stress field determination became available, the dynamic fracture problem was also explored experimentally in increasing detail. Dynamic photoelasticity, the dynamic shadow spot or caustic method and wire gages are today the major tools of investigation. The goal of experiments is to determine the appropriate fracture criterion. Experimental results are available for glass and polymers such as Homalite-100, plexiglass, polycarbonate and Araldite B representing a class of brittle materials and 4340 and A533B steels representing ductile materials (see Knauss et al., 1983). It is not our purpose here to review all these results. Instead, the aim here is to address a fundamental question regarding the characterization of the crack tip stress field through a comparison of analytical and experimental results. To this end, we first summarize the key analytical results in Section 2, then outline the experimental techniques of photoelasiticty and shadowspot in Section 3. In Section 4 experimental and analytical results are compared with respect to the stress intensity factor histories. Some of the new analytical results of Ma and Freund (1986) which address the deviation between analysis and experiment are then reviewed in Section 5. Additional developments derived from experiments, specially designed in light of the analysis of Ma and Freund, are discussed in Section 6, and important conclusions regarding the dynamic stress field are then extracted from these results.

2 The Dynamic Stress Field

Consider a semi-infinite crack in an unbounded elastic plane. Let a Cartesian coordinate system be centered at the tip of the crack which moves along the x axis with speed v. The Cartesian components of the stress field near the crack tip under symmetric loading are given by

$$\sigma_{\alpha\beta} = \frac{K_I(t,v)}{\sqrt{2\pi r}} f_{\alpha\beta}(\theta, v) \quad \begin{matrix} \alpha, \beta = 1, 2 \\ r \to 0 \end{matrix} \tag{1}$$

where r and θ are the local polar coordinates centered at the tip of the moving crack, $f_{\alpha\beta}(\theta, v)$ is the angular distribution of the stresses that reduces to the appropriate static field when v goes to zero. $K(t,v)$ is the dynamic stress intensity factor which depends on the applied loading and is determined by solving the equations of linear elastodynamics for a particular domain. In general, the solution for the motion of the crack, i.e., the speed and the path, depends on the fracture criterion and is therefore material dependent. But, by assuming loads such that rectilinear crack growth occurs with an arbitrary speed, the fracture criterion is uncoupled. One then generates a set of dynamically admissible stress intensity factors from which the appropriate stress intensity factor solution is determined by in-

Contributed by the Applied Mechanics Division for publication in the JOURNAL OF APPLIED MECHANICS.

Discussion on this paper should be addressed to the Editorial Department, ASME, United Engineering Center, 345 East 47th Street, New York, N.Y. 10017, and will be accepted until two months after final publication of the paper itself in the JOURNAL OF APPLIED MECHANICS. Manuscript received by ASME Applied Mechanics Division, October 29, 1985; final revision April 23, 1986.

Copyright © 1987 by ASME
Downloaded 03 May 2010 to 171.66.16.27. Redistribution subject to ASME license or copyright; see http://www.asme.org/terms/Terms_Use.cfm

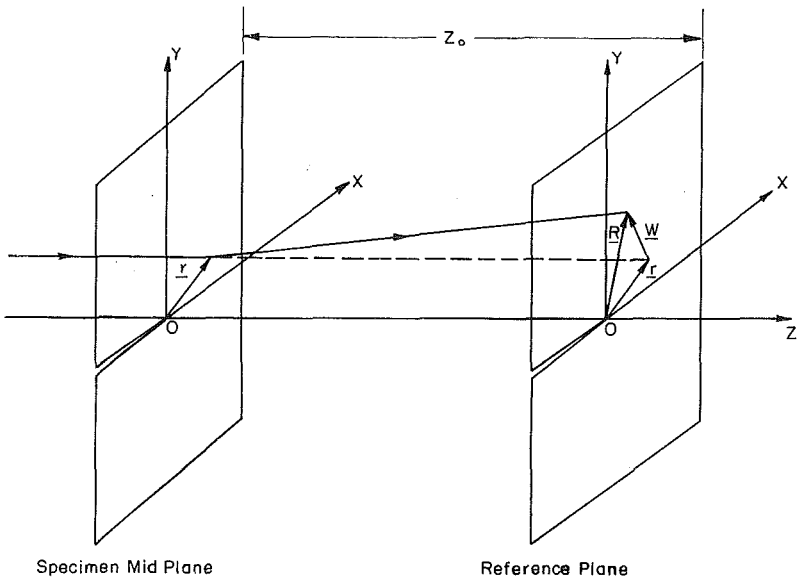


Fig. 1 Optical configuration for the method of caustics. Definition of plane separation Z_o

voking a fracture criterion. Once the dynamic stress intensity factor history is known, it is assumed that the crack tip stress field is completely determined, since in analogy with quasi-static fracture, the singular field is expected to dominate the crack tip stress field at least in a small neighborhood around the crack tip. The extent of this region of K dominance, however, is not well established particularly under transient conditions. It is essential that this size scale be known since the dynamic stress intensity factor is determined experimentally from measurements covering a finite region around the crack tip and one must be assured that a "K-field" does indeed exist within and beyond this region.

3 Experimental Determination of the Dynamic Stress Intensity

Today, the main techniques employed to determine the dynamic stress intensity factors are the photoelastic and shadow-spot methods used in conjunction with high speed framing cameras. In order to facilitate later discussions these two techniques are briefly outlined below.

3.1. Photoelasticity. Dynamic photoelasticity does not differ from traditional two-dimensional photoelasticity except for the fact that usually only isochromatic fringe patterns are recorded. A high speed framing camera is focussed onto a birefringent specimen placed in a circular polariscope. The crack tip isochromatic fringe patterns are thus recorded by the camera as a function of time. Assuming that a dynamic stress intensity field extends to some distance from the crack tip, shear stress contours corresponding to the stress field in equation (1) are fitted to the experimentally obtained isochromatic fringes by adjusting the stress intensity factor. The early work on this topic utilized the static asymptotic stress field in determining the shear stress contours, rather than the dynamic one. To be precise, one would have to know and fit to experimental data the stress history appropriate for dynamic conditions, such as those that accompany crack motion with variable speed. This is a difficult task, in general.

Typically, the fitting of the theoretical and experimental isochromatics is performed at some distance away from the crack tip since the fringe pattern is not very well defined very close to the tip. This distance varies from millimeters to centimeters. However, the consequences of making measurements over various distances from the crack tip are not yet well established or understood. Rossmanith (1983) evaluated isochromatics at different distances from the crack tip and the corresponding stress intensity factors were indeed different. To circumvent this difficulty, "higher order terms" in the asymptotic expansion *appropriate to steady crack motion* have been included in order to improve the *fit* of the analytically determined fringes to the experimental ones (Dally et al., 1985) but to date no comparison between analytical and photoelastic data has been effected. More importantly, there exists an open question as to how well the stress field for a crack moving with a constant velocity represents the transient stress field at the tip of a crack moving with changing velocities.

3.2 Shadow-Spot. The basis of the shadow-spot method is that a light beam passing near a crack tip is deviated from its straight path partly due to the thickness variation and partly due to the change in refractive index caused by the stress optic effect to form a singular curve called variously "stress corona," "shadow spot," or "caustic" on a reference plane some distance away from the specimen. The size of the shadow spot is related to the stress intensity factor corresponding to the caustic curve on the screen; there is defined an "initial curve" on the specimen plane and the radius of this initial curve depends on the optical and geometrical configuration used to obtain the caustic curve as well as on the stress intensity factor. Light rays from the outside of this initial curve fall outside the caustic curve in the screen; light rays from this initial curve fall on the caustic curve and light rays from the interior of this initial curve also fall on the outside of the caustic curve. Therefore, by making measurements of the caustic curve, one is essentially obtaining information about the crack tip stress state at a distance from the crack tip equal to the radius of the initial curve. In view of the discussion in Section 2, one must adjust the geometrical configuration of the experimental set-up such that the initial curve is in a region near the crack tip where the singular K field dominates. If the stress intensity factor were constant, the initial curve radius could be adjusted by changing the distance z_o between the specimen and the reference plane; see Fig. 1. However, if the stress intensity factor varied as in a dynamic experiment, one does not have close control over the radius of the initial curve other than limiting its variation through a judicious choice of the screen distance Z_o.

The problem then is to determine the extent of the validity

Downloaded 03 May 2010 to 171.66.16.27. Redistribution subject to ASME license or copyright; see http://www.asme.org/terms/Terms_Use.cfm

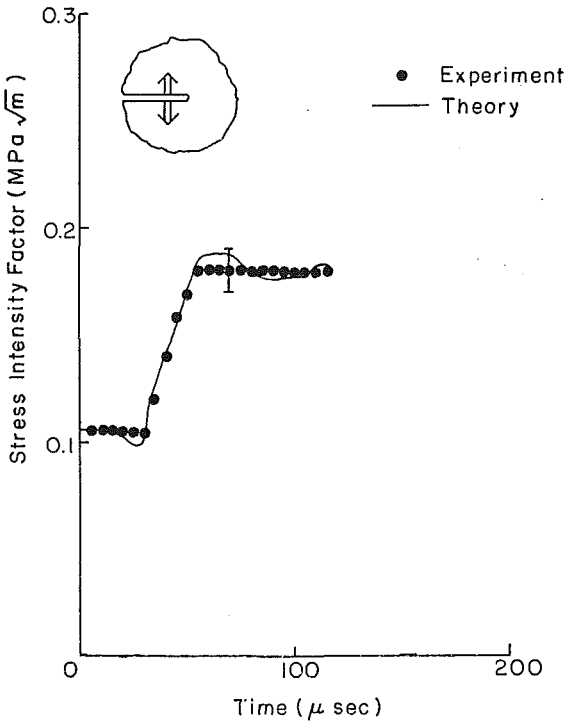


Fig. 2 Stress intensity factor history

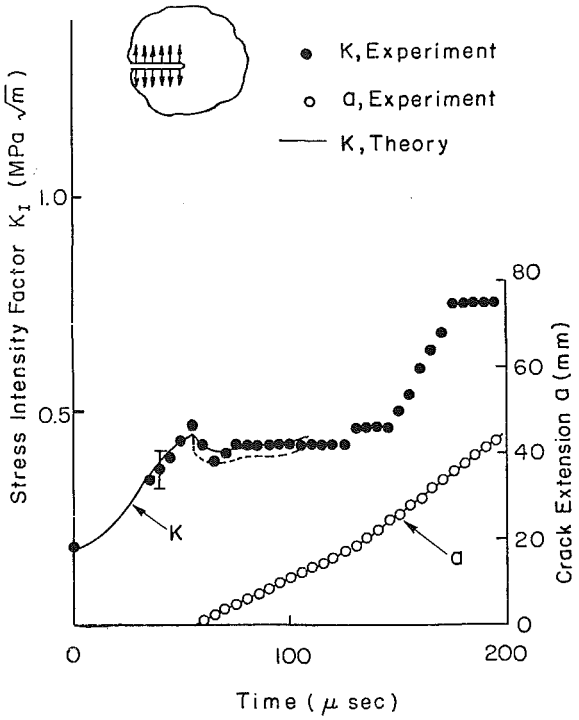


Fig. 3 Stress intensity factor and crack extension histories

of the asymptotic stress field in equation (1) so that the geometry of the shadow spot scheme can be adjusted in order that stress intensity factor measurements are made in the appropriate region with acceptable accuracy.

4 Comparison of Analytical and Experimental Results

Since, in general, the extent of the K field is uncertain in any experiment involving transient motion and stress, it is imperative that experiments be performed to compare measured stress intensity factors with well formed analytical predictions. These experiments have to be carefully designed in order to simulate the physical conditions which the analytical model assumes. In the following we shall compare experimental measurements, obtained using shadow spots, with analytical results. The details of the experimental scheme can be found in Ravi-Chandar and Knauss (1982). We consider a semi-infinite pressure loaded crack in an unbounded elastic plate of thickness d.

The shadow-spot method was implemented with a high speed camera to record the crack tip stress intensity factor at intervals of 5 μs. In Fig. 2, the result for a semi-infinite crack with pressure loading over only a length of 5 mm at about 25 mm from the crack tip is shown. We deal here with a problem of a stationary crack under dynamic loading. The analytical solution for this case may be derived from the Green's function solution by Freund (1974) and this solution is also displayed in Fig. 2. The radius of the initial curve in this experiment normalized by the plate thickness ($d=4.76$ mm) varied from 0.26 to 0.32. In Fig. 3, the results for a semi-infinite, pressure loaded crack are shown. The stress intensity factor increases till about 55 μs when K reaches a critical value and crack growth begins. The comparison between the theory and experiment as demonstrated in this figure is also very good. Upon initiation, the crack was found to grow with a constant velocity. Using this constant value of velocity (240 m/s), the stress intensity factor variation with time was computed analytically for the propagating crack. (For the cause of the preload and its effect subsequent to crack growth, see Ravi-Chandar and Knauss, 1982.) Once again, within the error of experimental measurement, the agreement between the theoretical and experimental stress intensity factor variation with time is seen to be good. The normalized initial curves for this experiment varied from 0.32 to 0.47.

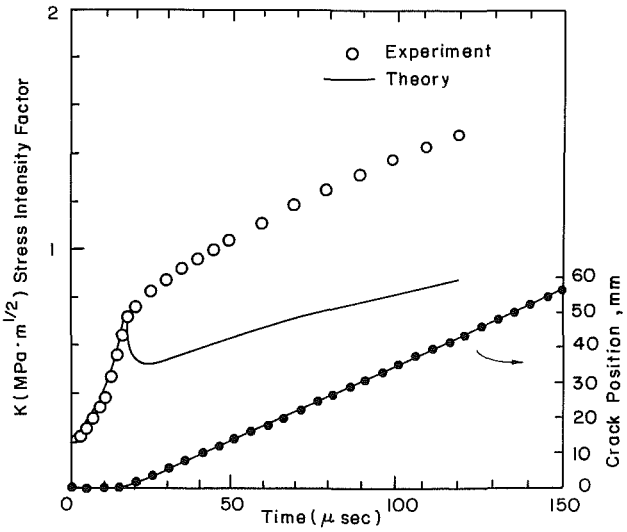


Fig. 4 Stress intensity factor history

The agreement between theory and experiment demonstrated thus far might lead one to conclude that at a distance of about 0.4 of the plate thickness from the crack tip, the stress field is indeed dominated by the dynamic stress intensity factor. Such a conclusion would certainly be valid under the conditions just described above. However, in experiments using the same configuration as indicated in Fig. 3, but with a higher loading rate, it was found that the stress intensity factor history did not resemble that shown in Fig. 3. Figure 4 displays the stress intensity factor and crack growth histories when the rate of loading was higher: First note that upon crack growth initiation, the stress intensity factor did not drop as suggested by analysis and confirmed by the ex-

Downloaded 03 May 2010 to 171.66.16.27. Redistribution subject to ASME license or copyright; see http://www.asme.org/terms/Terms_Use.cfm

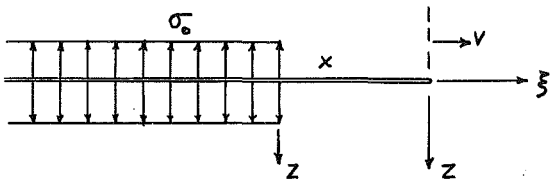


Fig. 5 Semi-infinite crack geometry

periments at low loading rates, but instead seems to continue to increase with time, albeit at a reduced rate. The analytically predicted variation of the stress intensity factor for this experimental scenario as calculated by Ma and Freund[1] (1986) is also displayed in Fig. 4.

The part of the measured stress intensity factor history for the stationary crack agrees well with the analysis, but for the growing crack, the "measured" stress intensity factors exceed the computed values. The radii of the initial curves (normalized by the plate thickness) for this case varied from 0.55 at crack growth initiation to 0.76 just prior to crack branching. This estimate is based on the experimentally determined values of K. It appears, therefore, that under transient conditions, a K-dominant field may not be established at such distances from the crack tip. This deviation between the analytical predictions based on linear elastodynamic theory and experimental observations at higher loading rates prompted a reinvestigation of the analysis of running crack problems by Ma and Freund (1986) and their results are discussed in the next section.

According to our present thinking this discrepancy may have one of two sources: First, it may be true that at these high stress levels the material no longer behaves according to the laws of linear elasticity either through intrinsically nonlinear behavior or through development of multiple microfractures; second, the transient nature of the local stress and deformation field is such that out to the presumed radius of the initial curve the stress field was not "dominated" by the singular expansion underlying a "K-field" analysis. Of the two possible sources for this discrepancy it turns out that the second is much easier to examine; in fact the first is very different to pinpoint experimentally. For this reason the transient stress analysis for illustrating this point was attempted first in collaboration with B. Freund and C. Ma. The subsequent sections are devoted to this examination.

5 Extent of the K Field Under Transient Conditions

The lack of agreement between theory and experiment as illustrated in Fig. 4 led Ma and Freund (1986) to reexamine their analytical predictions. They considered a semi-infinite crack in an unbounded elastic solid (c.f. Fig. 5). At $t=0$, a uniform normal pressure σ_o begins to act on the crack faces. At some time $t=\tau$ later, the crack tip begins to grow at a contant velocity v along the x axis and the loading continues to act only over the original crack faces. These conditions are exactly those prescribed – and observed – in our experiments.

From the solution for a semi-infinite crack (Freund, 1972–1974) two pieces of information were extracted. First, the exact and full variation of the stress $\sigma_{zz}(\xi,0,t)$ along the crack line was obtained in the form of an integral. Secondly, the asymptotic behavior of this integral was used to evaluate the stress intensity factor $K(t,v)$ and the elasto-dynamic stress field ahead of the crack tip was derived from the singular term alone. If the singular term were to be dominant at a fixed distance ξ from the moving crack tip, then the stress at that distance as calculated from the exact stress variation should be equal to that obtained from the singular term alone. Such a

[1] In these calculations the experimentally determined crack velocity was used.

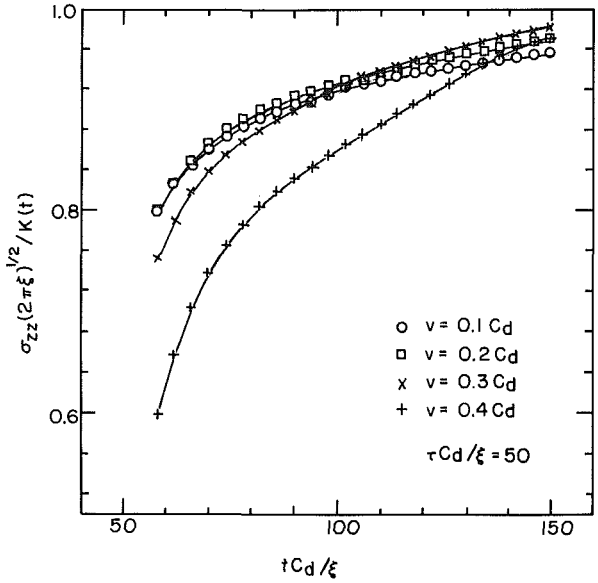


Fig. 6 Comparison of the exact stresses and the K field (from Ma and Freund, 1986)

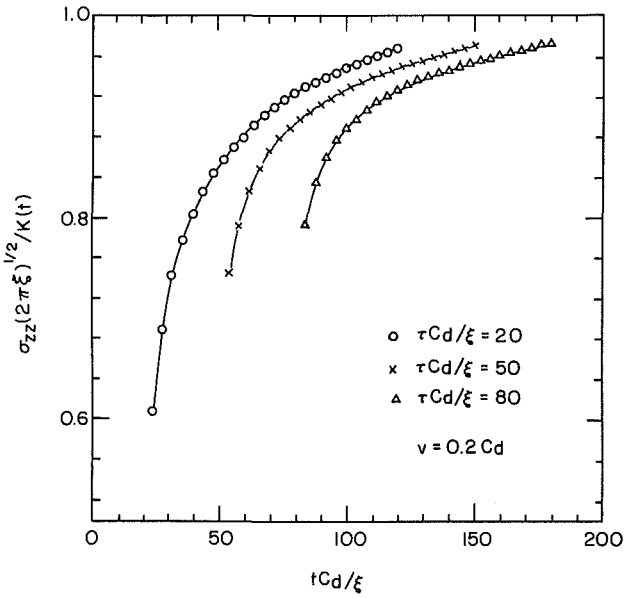


Fig. 7 Comparison of the exact stresses and the K field (from Ma and Freund, 1986)

comparison is shown in Figs. 6 and 7, where the ratio of the exact stress along the crack line $\sigma_{zz}(\xi,0,t)$ and the singular stress term $K(t)/\sqrt{2\pi\xi}$ is plotted as a function of time. The comparison is effected for an arbitrary distance ξ from the crack tip. The delay time for crack initiation τ is normalized with respect to the observation ditance ξ and the speed of dilatational waves C_d. Hence the nondimensional parameter $\eta=\tau C_d/\xi$ plays an important role in determining the comparison between the full stress field and the instantaneous asymptotic expansion.

It is seen from Figs. 6 and 7 that the stress estimated from the singular term is larger than the actual stress, and as time increases the singular field approaches the exact field. For example, since the dilational wave speed of Homalite is $\approx$ 2000 m/s the normalized time τ may be directly interpreted in μs if one considers ξ to be $\approx$ 2 mm. It is then seen from Fig. 6 that for a delay time of $\tau=20/\mu$s and a crack speed of 0.2 C_d, (approximately or closely equal to our experimental result

Downloaded 03 May 2010 to 171.66.16.27. Redistribution subject to ASME license or copyright; see http://www.asme.org/terms/Terms_Use.cfm

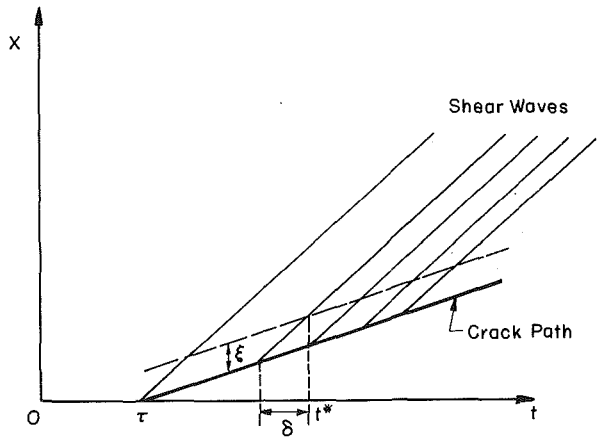


Fig. 8 x-t diagram

displayed in Fig. 4) the time taken for the singular K field to approach the exact stress field is on the order of 80 ds. Most of the fracture events of interest occur on this time scale. When the delay time for crack initiation τ is longer, the singular K field is established earlier at the same location ξ.

Clearly, the parameter of interest in these comparisons is the nondimensional delay time η. From Fig. 7 it is thus obvious that a K field dominates the crack tip region when η becomes large, say on the order of 100. For a given material this condition may be achieved either by letting the time for crack initiation τ be large, or by permitting the distance from the crack tip, ξ to be small. Let us interpret the results embodied in Figs. 3 and 4 in terms of the parameter η.

We note that the data in Fig. 3 which corresponds well with the calculations involves $\tau = 56\mu$s, crack speed $v = 0.1C_d$, $2.1 < \xi < 2.2$ mm. Thus $50 < \eta < 51$ and one sees from Fig. 7 that the ratio $\sigma_{zz}\sqrt{2\pi\xi}/K(t)$ equals approximately 0.8 at initiation and reaches 0.9 within the following 30 μs. Considering the ± 10 percent accuracy of the experimental results, one realizes that within this time frame the analytical computations should agree well with the experimental records.

Next, consider the data in Fig. 4, for which the following values are appropriate just after crack growth initiation: $\tau = 18\mu$s, $v = 0.2C_d$, and $\xi = 2.6$mm. These values render $\eta = 20$ so that the stress ratio $\sigma_{zz}\sqrt{2\pi\xi}/K(t)$ equals about 0.7 from Fig. 6. Thus one could expect the experimentally derived stress intensity factor to be about 40 percent larger than the true value. This observation agrees with the discrepancy between computed and "measured" stress intensity factor in Fig. 4. Moreover, one observes that because the value of ξ increases during the subsequent rise of the stress intensity (see Section 3) the value of η decreases further and thus accentuates the discrepancy.

One may also arrive at the above conclusion through a simple argument based on the time taken for stress waves to propagate. Consider the same semi-infinite crack problem discussed above and let the crack start to grow at a time $t = \gamma$ with a constant velocity v. In the x-t diagram in Fig. 8, this history is represented by the bold line. A typical system of dilatational, distortional, and surface waves are diffracted from the crack tip at each instant. In Fig. 8 only the distortional wave front is shown in the x-t diagram, since it has been shown that this wave carries most of the information from the crack tip. In experiments, measurements are made at a fixed distance ξ from the moving crack tip and the motion of this point is shown in the x-t diagram by a dotted line parallel to the crack path. Recalling that information flows essentially only along the shear wave characteristics, it is seen that at any time t^*, at a distance ξ from the crack tip, the stress field information corresponding to a crack tip location at $t = t^* - \delta$ is

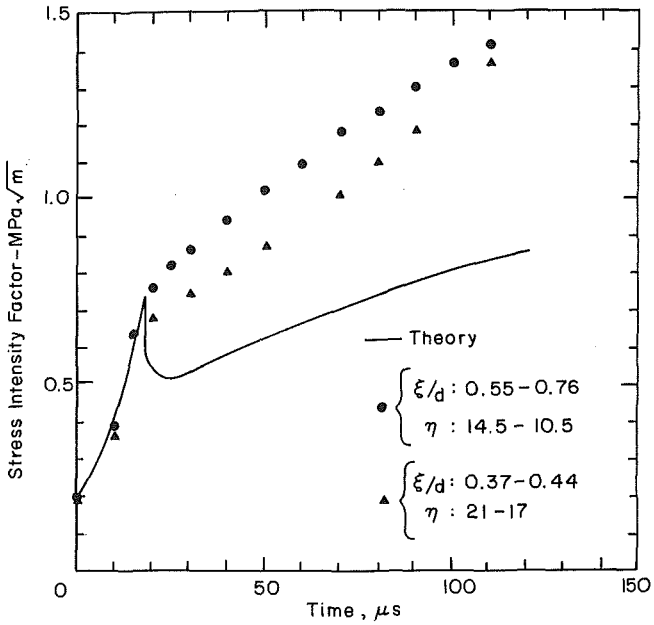


Fig. 9 Stress intensity factor history

obtained. If the information is to reflect the true stress field at time $t = t^*$, then δ has to be small compared to other significant time scales. For a transient problem, this time scale is the elapsed time from the beginning of the transient event. Hence, δ must be small compared to $t^* - \tau$. From the $x-t$ diagram, it is readily seen that $\delta = \xi/(C_s - v)$. Therefore $\delta << t^* - \tau$ can be rewritten as

$$(t^* - \tau)(C_s - v)/\xi >> 1. \tag{7}$$

This condition may be satisfied at very small distances ξ from the crack tip, for small crack velocities and at a long times after crack initiation.

Since the range of validity of the K field has now been established, it appears reasonable to attempt experiments for which the distance ξ is adjusted so as to obtain large values of η. Accordingly, experiments that repeated the loading conditions of the experiments underlying the results in Fig. 4 were performed to explore this idea further; these developments are discussed in the next section.

6 Experimental Determination of the Dynamic Stress Intensity Factor; Effect of Observation Distance from Crack Tip

The experimental configuration of a semi-infinite, pressure loaded crack was again used. The conditions of the experiment shown in Fig. 4 were repeated except for the position of measurement. Recall from Section 3 that, by adjusting the location of the reference plane Z_o, one can change the radius of the initial curve r. If the same experiment is repeated, that is one maintains the time variation for K to be the same, then a change of Z_o in different experiments is equivalent to determining the stress intensity factor at different distances from the crack tip. If the value of ξ were small enough to make η large, say ≥ 50, then, the experimentally determined stress intensity factor should be very close to the analytical prediction.

This scheme was attempted by using screen distances of $Z_o = 168$,64, 51, 21, and 13 cm (66, 25, 20, 10, and 5 in.) from the specimen plane. It was estimated that this Z_o variation would yield normalized initial curve radii in the range of 0.76 to 0.10. The results of the experiments are displayed in Fig. 9 for two cases. The radii ξ of the initial curves and the values of

Downloaded 03 May 2010 to 171.66.16.27. Redistribution subject to ASME license or copyright; see http://www.asme.org/terms/Terms_Use.cfm

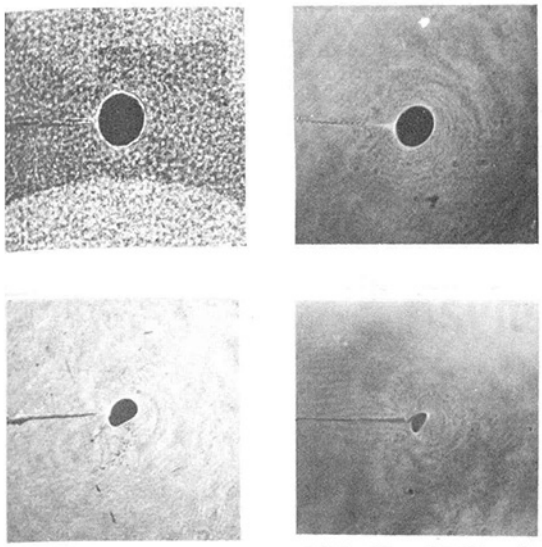


Fig. 10 Variation of caustic patterns with Z_o. (Z_o = 168, 64 cm top left and right; z_o = 21, 13 cm bottom left and right, respectively.)

the parameter η are identified in the figures for each curve. The corresponding analytical values for the stress intensity factor K are also included in the same figure. One deduces from Fig. 9 that when the radius of the initial curve is $\approx$ 0.36 to 0.42, there exists at least a tendency for the experimental stress intensity factors to approach the analytically predicted values. Note, however, that the value of η is only 17–20, and still far from 50 or even 100.

In order to attain larger values for η one must make the radius of the initial curve even smaller. Attempts at doing precisely this, by setting Z_o values of 21 and 13 cm, failed since the shadow spot patterns traditionally associated with crack tips could no longer be observed. Figure 10 shows the shadow spot patterns observed when Z was 168, 64, 21, and 13 cm (66, 25, 10, and 5 in.) respectively, taken at nearly the same instant in the crack growth history. The distortion of the shadow spot pattern suggests that the stress field at this distance from the crack tip (less than $\approx$ 1 mm) does not resemble the idealized two-dimensional singular stress field which one usually associates with a crack tip.

It is known that three-dimensional effects play a very strong role in this region. For example, in the case of a static crack, Rosakis and Ravi-Chandar (1986) showed that the stress intensity factor could not be measured accurately with shadowspot measurements derived from distances from the crack tip of less than one half the plate thickness. For a dynamic crack in Homalite-100, Ravi-Chandar and Knauss (1984) have shown that the crack tip is surrounded by a number of microcracks, and (quantitatively) evaluated the size of the process zone to be on the order of 100 μm. Hence, when the process zone size is large, (usually associated with higher loads) the processes in this zone have considerable effect in Homalite-100 on the stress field at distances of $\approx$ 1 mm. The conclusion is thus at hand that one is not able to make meaningful measurements at very small distances from the crack tip where the stress field is significantly altered by the process zone for the determination of a dynamic stress intensity factor.

Our observations, based both on the analytical results of Ma and Freund (1986) and the present experimental evidence may thus be summarized as follows: Due to the dynamic nature of the problem, the dynamic K field is established under transient conditions within a radius r from the crack tip where

$$r << (t^* - \tau)(C_s - v) \equiv \xi_o. \tag{8}$$

Due to the nonideal nature of the fracture process, the process zone affects the stress field at a distance from the crack tip $r < r_p$. Hence a K-dominated stress field exists near a crack tip at a distance r from the crack tip if

$$\xi_o > r > r_p. \tag{9}$$

In a material like Homalite-100 high loading rates cause the stress intensity factor for initiation to increase as well as the corresponding velocity of propagation. Thus the size of the process zone increases with increasing K while the K-dominated region ξ_o decreases with increasing velocity. Hence under these conditions, it may be impossible to satisfy the constraint (9) and thus an annular, K-dominated region may not exist. These results are not material specific since crack tips in all real materials possess a process zone and the crack speeds are usually about the same fraction of the corresponding wave speeds. The use of higher order terms in the asymptotic expansion of the dynamic stress field may not resolve this problem since it is not at all clear that a power series approximation is admissible near the crack tip under transient conditions. Therefore, we believe that these conclusions indicate a real need to re-examine the dynamic stress field characterizations at crack tips both experimentally and analytically.

7 Conclusion

The dynamic stress field near a transient crack tip has been explored experimentally and the following conclusions were obtained:

(1) When the transient crack motion involves small crack velocities, the dynamic stress intensity factor dominates over a substantial region near the crack tip so that it may be measured either by caustics or by photoelasticity provided such measurements are made within the K-dominated region.

(2) When the crack propagates at "high" speeds, the domain of dominance of the stress intensity factor field is small and the fracture process zone grows larger with the result that there may be no annular zone around the crack tip from which the dynamic stress intensity factor can be determined.

Further work is thus necessary to determine the proper parameters to characterize the dynamic stress field.

Acknowledgments

The work reported here has been supported by a grant from the National Science Foundation (MEA-8215438). We are grateful to Dr. C. C. Ma and Professor L. B. Freund for providing us with their analytical results (shown in Figs. 4, 6, and 7) prior to publication and for many discussions.

8 References

Dally, J. W., Fourney, W. L., and Irwin, G. R., 1985, "On the Uniqueness of the Stress Intensity Factor – Crack Velocity Relationship," *International Journal of Fracture*, Vol. 27, pp. 159–168.

Freund, L. B., 1972–1974, "Crack Propagation in an Elastic Solid Subjected to General Loading," in four parts, *Journal of the Mechanics and Physics of Solids*, Part I: 20, pp. 129–140; Part II: 20, pp. 141–152; Part III: 21, pp. 47–61; Part IV: 22, pp. 137–146.

Freund, L. B., 1974, "The Stress Intensity Factor Due to Normal Impact Loading on the Faces of a Crack," *International Journal of Engineering Science*, Vol. 12, pp. 179–189.

Knauss, W. G., Ravi-Chandar, K., and Rosakis, A. J., 1983, *Proceedings, NSF-ARO Workshop on Dynamic Fracture*, California Institute of Technology, Pasadena.

Ma, C. C., and Freund, L. B., 1986, "The Extent of the Stress Intensity Factor During Crack Growth Under Dynamic Loading Conditions," ASME JOURNAL OF APPLIED MECHANICS, 53, pp. 303–310.

Mall, S., Kobayashi, A. S., and Urabe, Y., 1978, "Dynamic Photoelastic and Dynamic Finite Element Analyses of Dynamic-Tear-Test Specimens," *Experimental Mechanics*, Vol. 18, pp. 449–456.

Ravi-Chandar, K., and Knauss, W. G., 1982, "Dynamic Crack-Tip Stresses Under Stress Wave Loading – A Comparison of Theory and Experiment," *International Journal of Fracture*, Vol. 29, pp. 209–222.

Downloaded 03 May 2010 to 171.66.16.27. Redistribution subject to ASME license or copyright; see http://www.asme.org/terms/Terms_Use.cfm

Ravi-Chandar, K., and Knauss, W. G., 1984, "An Experimental Investigation into Dynamic Fracture," in four parts, *International Journal of Fracture*, Part I: 25, pp. 247–262, Prat II: 26, pp. 65–80; Part III: 26, pp. 141–154; Part IV: 26, pp. 189–200.

Rosakis, A. J., and Ravi-Chandar, K., 1986, "On Crack Tip Stress State: An Experimental Evaluation of Three Dimensional Effects," *International Journal of Solids and Structures*, Vol. 22, pp. 121–134.

Rose, L. R. F., 1976, "On the Initial Motion of a Griffith Crack," *International Journal of Fracture*, Vol. 12, pp. 829–841.

Rossmanith, H. P., 1983, "How 'Mixed' is Dynamic Mixed-Mode Crack Propagation – A Dynamic Photoelastic Study," *Journal of the Mechanics and Physics of Solids*, Vol. 31, pp. 251–260.

Yoffe, E. H., 1951, "The Moving Griffith Crack," *Philosophical Magazine*, Vol. 42, pp. 739–750.

Downloaded 03 May 2010 to 171.66.16.27. Redistribution subject to ASME license or copyright; see http://www.asme.org/terms/Terms_Use.cfm

Asymptotic Analysis of a Mode I Crack Propagating Steadily in a Deformation Theory Material

P. Ponte Castañeda[1]
Division of Applied Sciences,
Harvard University,
Cambridge, Mass. 02138
Assoc. Mem. ASME

The near-tip asymptotic stress and deformation fields of a crack propagating steadily and quasi-statically into an elastic-plastic material are presented. The material is characterised by J_2-deformation theory, suitably modified to account for unloading and reloading, together with linear strain-hardening. The cases of plane strain and plane stress Mode I are considered. The governing equations are integrated analytically with the assistance of Muskhelishvili's complex variable formulation. The boundary and continuity conditions then lead to a set of nonlinear algebraic equations in the coefficients of the stress functions to be solved numerically. Explicit results are given for the strength of the singularity, and for the distribution of stress in the plastic loading, elastic unloading, and plastic reloading regions, as functions of the strain-hardening parameter.

1 Introduction

Knowledge of the stress and deformation fields near the tip of an advancing crack is central to the continued development of engineering fracture mechanics, and important advances have been made in recent years. Under the assumption of quasi-static growth and small-strain ideal elasto-plasticity, asymptotic solutions have been found in anti-plane strain by Chitaley and McClintock (1971); in plane strain by Slepyan (1974), Gao (1980), Rice *et al.* (1980), and Drugan *et al.* (1982); and in plane-stress Mode II by Ponte Castañeda (1986). In addition, a general discussion of the subject can be found in Rice (1982).

The corresponding work for hardening elastic-plastic solids is at a less developed stage. Slepyan (1973) provided the near-tip fields of a Mode III crack propagating steadily in a linear-hardening material using a modified J_2-deformation theory. Also for linear-hardening materials, Amazigo and Hutchinson (1977) produced steady-state asymptotic solutions for Modes I (plane strain and plane stress) and III using J_2-flow theory. These latter solutions, however, neglected the possibility of reverse plastic flow on the crack flanks which is known to occur in the elastic perfectly-plastic solutions mentioned above. Zhang *et al.* (1983) included reloading (as well as a Bauschinger effect) in their solution of the plane-strain Mode I problem. More recently, Ponte Castañeda (1987) provided a complete set of solutions including reloading for Modes I (plane strain and plane stress), II (plane strain and plane stress), and III.

Further work on the hardening elastic-plastic steadily moving crack include publications by Lo and Pierce (1981) who considered a Mode III crack moving in a linear-hardening corner-theory material, and Gao *et al.* (1983) who investigated a Mode III crack propagating in a power-hardening J_2-flow theory material.

Even though deformation theory is unreliable for non-proportional loading histories such as that which a near-tip particle experiences as it moves past a crack tip, it is found by comparing the solutions of Slepyan (1973) and Amazigo and Hutchinson (1977) for the Mode III case that the deformation theory solution presents the same general features as the flow theory solution. In fact, some of the detailed results such as the dependence of the strength of the singularity on the hardening parameter are in remarkably close agreement. The main reason for the agreement is that Slepyan's modified deformation theory properly accounts for elastic unloading, thus eliminating the main source of criticism of classical deformation theories. Furthermore, strain-hardening allows for the possibility of a more proportional loading history in the *plastic* sectors, since the yield surface is allowed to expand with the loading point, thus making it possible for the two theories to be in partial agreement. Finally, it should be emphasized, as was done by Budiansky (1959), that as long as the loading is not too severely nonproportional, deformation theory should be considered a respectable competitor to flow theory; only experiment can determine the accuracy of the predictions.

In this work we propose to solve the plane-stress and plane-strain Mode I asymptotic problems using J_2-deformation theory with linear strain-hardening, and to compare the results to the corresponding flow theory results. We will make use of

[1]Currently at the Department of Mechanical Engineering, The Johns Hopkins University, Baltimore, Maryland 21218.

Contributed by the Applied Mechanics Division for publication in the JOURNAL OF APPLIED MECHANICS.

Discussion on this paper should be addressed to the Editorial Department, ASME, United Engineering Center, 345 East 47th Street, New York. N.Y. 10017, and will be accepted until two months after final publication of the paper itself in the JOURNAL OF APPLIED MECHANICS. Manuscript received by ASME Applied Mechanics Division, December 6, 1985; final revision August 11, 1986.

Copyright © 1987 by ASME
Downloaded 03 May 2010 to 171.66.16.27. Redistribution subject to ASME license or copyright; see http://www.asme.org/terms/Terms_Use.cfm

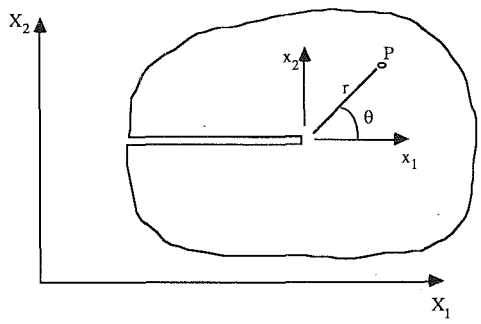


Fig. 2.1 Crack-tip geometry

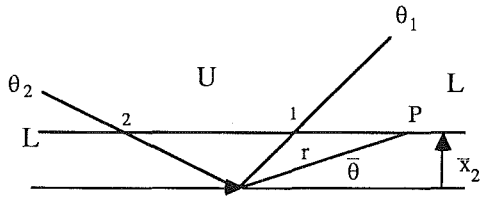


Fig. 2.2 Loading history

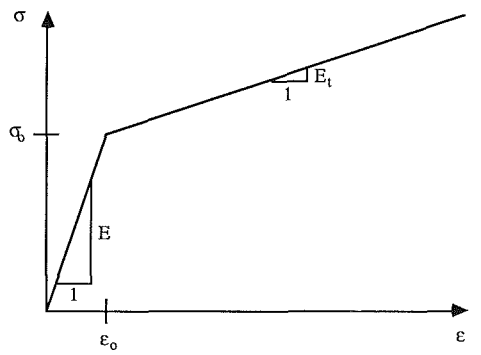


Fig. 2.3 Uniaxial stress-strain relation

concise complex-variable formulations that will yield straightforward analytical solutions for the near-tip fields.

2 Formulation

With reference to Fig. 2.1, let $x_i (i=1,2,3)$ be a Cartesian coordinate system of fixed orientation travelling with the crack tip such that the x_3 axis coincides with the straight crack front. Also let $\mathbf{e}_i$ be the unit vector corresponding to the x_i direction. Similarly, let r, θ be polar coordinates corresponding to x_α ($\alpha=1,2$), and $\mathbf{e}_r$, $\mathbf{e}_\theta$ be the corresponding unit vectors. The crack tip moves with velocity $\mathbf{V}=V\mathbf{e}_1$ with respect to the stationary coordinate system X_i. In our steady-state analysis the crack tip speed V is constant so that the material derivative is given by

$$\dot{(\ )} = -V(\ )_{,1} \tag{2.1}$$

For Mode I loading of an isotropic material with the given geometry we have that the only nonzero components of the stress tensor are $\sigma_{\alpha\beta}$ ($\alpha,\beta=1,2$) (and σ_{33} for plane strain). Then, neglecting inertia, the equilibrium equations are

$$\sigma_{\alpha\beta,\alpha}=0 \tag{2.2}$$

The only nonzero components of the strain tensor are $\epsilon_{\alpha\beta}$ (and ϵ_{33} for plane stress). The equations of compatibility are

$$e_{\alpha\beta}e_{\lambda\mu}\epsilon_{\alpha\lambda,\beta\mu}=0 \tag{2.3}$$

where $e_{\alpha\beta}$ is the two-dimensional permutation symbol ($e_{11}=e_{22}=0$, $e_{12}=-e_{21}=1$).

The constitutive relations are

$$\epsilon_{ij}=\epsilon_{ij}^{el}+\epsilon_{ij}^{pl} \tag{2.4}$$

where the components of the elastic strain tensor are given by

$$\epsilon_{ij}^{el}=(1/E)[(1+\nu)\sigma_{ij}-\nu\sigma_{kk}\delta_{ij}] \tag{2.5}$$

and the plastic strain is given by a deformation theory of plasticity modified to account for unloading and reloading. From previous work we expect to have three different types of sectors in the neighborhood of the crack tip. As depicted in Fig. 2.2, we expect to have a plastic loading sector ahead of the crack ($0<\theta<\theta_1$), followed by an elastic unloading sector ($\theta_1<\theta<\theta_2$), followed, in certain cases, by a plastic reloading sector ($\theta_2<\theta<\pi$).

Thus, when the material particle P is loading ahead of the crack, the components of its plastic strain tensor are given by

$$\epsilon_{ij}^{pl}=(3/2)(1/E_s-1/E)s_{ij} \tag{2.6}$$

where s_{ij} are the components of the stress-deviator tensor, and $E_s=E_s(\sigma_e)$ is the secant modulus, which is a function of the effective stress $\sigma_e=[(3/2)s_{ij}s_{ij}]^{1/2}$. For a bilinear material with uniaxial stress-strain behavior as depicted in Fig. 2.3, equation (2.6) reduces to

$$\epsilon_{ij}^{pl}=(3/2)(1/E)(1/\alpha-1)(1-\sigma_o/\sigma_e)s_{ij} \tag{2.7}$$

where σ_o is the yield stress in tension, and α is the ratio of the tangent modulus, E_t, to the elastic modulus, E.

Note that for $|\sigma_o/\sigma_e|<<1$, equation (2.7) simplifies to

$$\epsilon_{ij}^{pl}=(3/2)(1/E)(1/\alpha-1)s_{ij} \tag{2.8}$$

Observing that for small nondimensional $\underline{r}=r/R$, where R is some measure of the plastic zone size, we expect $\sigma_e/\sigma_o=O(\underline{r}^s)$ (where $-1/2\le s<0$ for $0<\alpha\le 1$), and therefore it follows that, sufficiently close to the crack tip ($0<\underline{r}<<e^{-1/|s|}$), and provided that $\sigma_e\neq 0$, equation (2.8) is a valid approximation to equation (2.7). Note that the approximation breaks down as $\alpha\to 0$. We conclude that for $0<\alpha\le 1$

$$\epsilon_{ij}=(1/E^*)[(1+\nu^*)\sigma_{ij}-\nu^*\sigma_{kk}\delta_{ij}] \tag{2.9}$$

where $E^*=\alpha E$ and $\nu^*=\alpha(2\nu-1)/2+1/2$.

When the particle unloads elastically at location 1 in Fig. 2.2, its plastic strain is assumed to be continuous across the boundary. As it moves through the elastic sector, its plastic strain remains constant. Thus the plastic strain in the elastic unloading sector is specified by

$$\epsilon_{ij}^{pl}=[\epsilon_{ij}^{pl}]^1 \tag{2.10}$$

Note that $[\epsilon_{ij}^{pl}]^1$ is a function of x_2 only, and is evaluated for a given particle by letting $x_1=\bar{x}_2/\tan\theta_1$ in equation (2.8).

When the particle reloads plastically at location 2 in Fig. 2.2, its plastic strain is again assumed to be continuous across the boundary, and hence is the same as the plastic strain that it had just before it unloaded. Thus the plastic strain in the plastic reloading sector is given by

$$\epsilon_{ij}^{pl}=(3/2)(1/E)(1/\alpha-1)s_{ij}-[\epsilon_{ij}^{pl}]^2+[\epsilon_{ij}^{pl}]^1 \tag{2.11}$$

where $[\epsilon_{ij}^{pl}]^2$ is evaluated for a given particle by letting $x_1=\bar{x}_2/\tan\theta_2$ in equation (2.8). Note that any further unloading/reloading can be modeled in a similar manner.

Equations (2.2), (2.3), and (2.4) together with equations (2.5) and either (2.8), (2.10), or (2.11) (depending on whether loading, unloading, or reloading occurs, respectively) are the governing equations in each sector.

We solve these equations in any given sector by first introducing a stress function f to satisfy equilibrium so that

$$\sigma_{\alpha\beta}=e_{\alpha\lambda}e_{\beta\mu}f_{,\lambda\mu} \tag{2.12}$$

Next note that in the plastic loading sector we effectively have an elastic problem with modified elastic constants E^* and ν^*, and compatibility yields

$$\nabla^4 f=0 \tag{2.13}$$

where we have used the fact that for plane stress $\sigma_{33}=0$, and

Downloaded 03 May 2010 to 171.66.16.27. Redistribution subject to ASME license or copyright; see http://www.asme.org/terms/Terms_Use.cfm

for plane strain $\epsilon_{33}=0$ (which implies $\sigma_{33}=\nu^*\sigma_{\alpha\alpha}$). The solution of equation (2.13) can be expressed as

$$f=\mathrm{Re}\{\bar{z}\,\phi(z)+\chi(z)\} \tag{2.14}$$

where ϕ and χ are analytic functions of $z=re^{i\theta}$ in the sector. Since we are interested in asymptotic results we will assume the following forms for ϕ and χ

$$\phi(z)=a\,z^{s+1} \qquad \psi(z)=\chi'(z)=b\,z^{s+1} \tag{2.15}$$

where a and b are undetermined complex constants. The stress components $\sigma_{\alpha\beta}$ can then be found in terms of a, b, and s by means of the Muskhelishvili complex variable relations given in Appendix A.

In the elastic unloading sector compatibility and either the plane stress or plane strain condition lead to

$$(1-\nu^2)\nabla^4 f=-E\{[\epsilon_{11}^{pl}]^1+\nu[\epsilon_{33}^{pl}]^1\}_{,22} \tag{2.16}$$

where $\nu=0$ for plane stress, or $\nu=\nu$ for plane strain. The solution to this P.D.E. can be written as

$$f=f^h+f^{pa} \tag{2.17}$$

where f^{pa} is any particular solution of the P.D.E., and the homogeneous solution f^h is given by an expression similar to equation (2.14) with new functions ϕ and χ (analytic in the sector) which are of the form of equation (2.15) but with different complex coefficients c and d. It follows that we can write

$$\sigma_{\alpha\beta}=\sigma^h_{\alpha\beta}+\sigma^{pa}_{\alpha\beta} \tag{2.18}$$

where the $\sigma^h_{\alpha\beta}$ can be expressed through f^h in terms of the new ϕ and ψ, and f^{pa} can be chosen such that

$$\begin{aligned}\sigma^{pa}_{11} &= -[E/(1-\nu^2)]\{[\epsilon^{pl}_{11}]^1+\nu[\epsilon^{pl}_{33}]^1\} \\ \sigma^{pa}_{12} &= \sigma^{pa}_{22}=0\end{aligned} \tag{2.19}$$

In the plastic reloading sector compatibility and either the plane stress or plane strain condition lead to

$$\begin{aligned}[1-(\nu^*)^2]\nabla^4 f=E^*\{&[\epsilon^{pl}_{11}]^2-[\epsilon^{pl}_{11}]^1 \\ &+\nu^*([\epsilon^{pl}_{33}]^2-[\epsilon^{pl}_{33}]^1)\}_{,22}\end{aligned} \tag{2.20}$$

This equation is of the same form as equation (2.16), and can be solved in the same manner. Equation (2.18) applies with new constants e and f for the functions ϕ and ψ in the expressions for the homogeneous stresses, and equations similar to (2.19) for the particular stresses.

Noting that the inhomogeneous terms in equations (2.16) and (2.20) are functions of x_2 only, it pays to consider the material derivatives of these equations (and also of equation (2.13) for consistency). Thus we find that the same homogeneous equation governs in all three sectors

$$\nabla^4\mathcal{J}=0 \tag{2.21}$$

where $\mathcal{J}=\dot{f}$ is the stress-rate function. The solution to equation (2.21) is given by

$$\mathcal{J}=\mathrm{Re}\{\bar{z}\,\Phi(z)+X(z)\} \tag{2.22}$$

where Φ and X are analytic in each sector. For consistency, in the plastic loading sector we take

$$\Phi(z)=A\,z^s \qquad \Psi(z)=X'(z)=B\,z^s \tag{2.23}$$

where A and B are undetermined complex constants, but are related to a and b through

$$A=-(s+1)Va \qquad B=-(s+1)V(a+b) \tag{2.24}$$

Note that even though it will turn out that it is most convenient to use the stress-rate function coefficients A and B in the formulation of the problem, with this simple conversion we can always go back to our original expressions above to find the stress components. Expressions analogous to equations (2.23) and (2.24) apply in the elastic unloading and plastic reloading sectors, but with complex coefficients pairs C, D, and E, F, respectively.

Later we will need expressions for the traction-rate force $\mathbf{F}$ and the velocity vector $\mathbf{v}$ in terms of the Muskhelishvili rate functions, and these are also given in Appendix A.

It is clear from the formulation in terms of the stress function that this is a fourth order problem. Given the variable-separable nature of the solution ($z=re^{i\theta}$), we need to impose four boundary conditions in θ. Mode I symmetry requires

$$u_2(r,0)=\sigma_{12}(r,0)=0 \tag{2.25}$$

and the traction-free condition on the crack faces requires

$$\sigma_{12}(r,\pi)=\sigma_{22}(r,\pi)=0 \tag{2.26}$$

Note that these four conditions are homogeneous, and lead to an eigenvalue problem for s as a function of α (and ν). Thus we expect to determine the stress and deformation distributions only up to an arbitrary amplitude factor analogous to the stress intensity factor in the elastic problem.

Next we need to connect the solutions in the different sectors through some appropriate continuity conditions. Thus we impose four conditions at each unloading and reloading boundary. Let [ ] denote the jump in a quantity as θ increases infinitesimally; then the traction components of the stress must be continuous

$$[\sigma_{r\theta}]=[\sigma_{\theta\theta}]=0 \tag{2.27}$$

and the displacement field must also be continuous

$$[u_r]=[u_\theta]=0 \tag{2.28}$$

Note that in the previous development we imposed continuity of the plastic strains, but these should not be regarded as conditions independent of equations (2.27) and (2.28); they are simply consistent with the constitutive model.

The boundary and continuity conditions described above when expressed in terms of stress functions are cumbersome due to the so-called particular terms. It is then useful to rewrite these conditions in terms of rate quantities. Thus the boundary conditions (2.25) and (2.26) take the form

$$v_2(r,0)=\Sigma_{12}(r,0)=0 \tag{2.29}$$

$$\Sigma_{12}(r,\pi)=\Sigma_{22}(r,\pi)=0 \tag{2.30}$$

where $\Sigma=\dot{\sigma}$, and $\mathbf{v}=\dot{\mathbf{u}}$. The last of these two sets of conditions can be rewritten further in terms of the traction-rate force

$$F_1(r,\pi)=F_2(r,\pi)=0 \tag{2.31}$$

Given conditions (2.27), (2.28) and the assumed continuity of the plastic strains across each elastic-plastic boundary, it can be shown that the stress tensor must in fact be fully continuous. It then follows from the equilibrium equations that the traction components of the stress-rate tensor must also be continuous

$$[\Sigma_{r\theta}]=[\Sigma_{\theta\theta}]=0 \tag{2.32}$$

This in turn implies continuity of the traction-rate force vector

$$[F_1]=[F_2]=0 \tag{2.33}$$

Similarly, it can be shown that under the given assumptions the velocity vector must also be continuous

$$[v_1]=[v_2]=0 \tag{2.34}$$

Thus conditions (2.33) and (2.34) will be used instead of the more primitive conditions (2.27) and (2.28) to connect the fields in the different sectors.

Finally, we need to characterise the onsets of unloading and reloading. For flow theory, $\dot{\sigma}_e$ is continuous across the unloading boundary, and the unloading angle, θ_1, is uniquely determined by the condition

$$\dot{\sigma}_e(r,\theta_1)=0 \tag{2.35}$$

For deformation theory, however, $\dot{\sigma}_e$ is, in general, not continuous. This is due to the fact that the component of the plastic strain-rate tensor, D^{pl}_{rr}, does not necessarily vanish

Downloaded 03 May 2010 to 171.66.16.27. Redistribution subject to ASME license or copyright; see http://www.asme.org/terms/Terms_Use.cfm

on the plastic side of the unloading boundary (as is the case for flow theory). Consequently, there may be a discontinuity in Σ_{rr}, and therefore in $\dot{\sigma}_e$.

Because of this, the choice of the unloading condition in our deformation theory is not unique as is the case in flow theory. Of the many possible choices, there are two with special significance. The unloading condition

$$\dot{\sigma}_e(r,\theta_1^-)=0 \tag{2.36a}$$

makes most sense from a physical point of view since it implies that the effective plastic strain-rate vanishes at the onset of unloading. Alternatively, the condition

$$\dot{\sigma}_e(r,\theta_1^+)=0 \tag{2.36b}$$

was chosen by Slepyan (1973) because it gives the most conservative estimate for the strength of the singularity. Here we will use condition (2.36*a*), but we will also explore the use of condition (2.36*b*).

The reloading angle, θ_2, is determined by the condition that the material particle regain the effective stress level it had when it unloaded

$$\sigma_e(\tilde{x}_2/\tan\theta_1,\tilde{x}_2)=\sigma_e(\tilde{x}_2/\tan\theta_2,\tilde{x}_2) \tag{2.37}$$

Note that unlike the boundary and continuity conditions, the unloading and reloading conditions (2.36) and (2.37) must include particular terms since they involve non-rate quantities, and cannot be simplified any further.

Conditions (2.29), (2.31), (2.33), (2.34), (2.36*a*), and (2.37) are expressed in Appendix B in terms of the eigenvalue (s), the complex coefficients of Φ and Ψ (A, B, C, D, . . .), and the unloading and reloading angles (θ_1 and θ_2) for both the two-region problem (no reloading occurs) and the three-region problem (if reloading occurs). Note that for plane stress these conditions are independent of Poisson's ratio (ν), but not so for plane strain. The solution procedures used to obtain the unknowns s, θ_1, θ_2, A, B, C, D, . . . are also sketched in this appendix. Once these are found, the stress distribution in the different sectors is determined using the expressions for the stresses determined previously.

3 Results and Discussion

3.1 Plane Stress. The results for this case are summarized in Figs. 3.1 to 3.4 and in Table 3.1. Figure 3.1 shows plots of the strength of the singularity, s, versus the square root of the hardening parameter, α, for two deformation theory materials satisfying the two extreme unloading conditions given by conditions (2.36*a*) and (2.36*b*) in the formulation section, and also for the flow theory material (Ponte Castañeda, 1987). It is found, as Slepyan (1973) observed for the Mode III problem, that the deformation theory with unloading condition (2.36*b*) results in a stronger singularity (and smaller angular extent of the plastic zone) than its counterpart with unloading condition (2.36*a*), and that deformation theory in general produces a stronger singularity than flow theory. It is also observed that s vanishes as $\alpha\to 0$.

Table 3.1 presents values of s, θ_1 and θ_2 for several values of α ranging between zero and unity for the two deformation theories, and for flow theory. It is seen that the singularities agree very well for the deformation and flow theories, especially for large strain-hardening. For the less singular deformation theory material (corresponding to condition (2.36*a*)) the unloading angle θ_1 increases from the elastic value to a maximum value of 90 deg as $\alpha\to 0$. The opposite behavior is observed for the more singular material, and θ_1 gets progressively smaller as $\alpha\to 0$. The flow theory material shows an intermediate behavior: θ_1 first increases as α decreases, and then decreases as $\alpha\to 0$. Reloading occurs for the less singular deformation theory material at the value of the hardening parameter $\alpha^*=0.215$, it never occurs for the more singular material, and takes place at $\alpha^*\sim 0.01$ for the flow theory material. The actual size of the reloading sector is considerable for the less singular deformation theory material (up to 20°), and very small for the flow theory material (less than 0.001 deg).

Table 3.1 Plane Stress Mode I

α	s(1)	s(2)	s(3)	$\theta_1(1)$	$\theta_1(2)$	$\theta_1(3)$	$\theta_2(1)$	$\theta_2(2)$	$\theta_2(3)$
1.	-0.5	-0.5	-0.5	79.92	79.92	79.92	-	-	-
0.75	-0.469	-0.469	-0.468	81.11	73.10	80.78	-	-	-
0.667	-0.456	-0.456	-0.455	81.58	70.52	80.90	-	-	-
0.5	-0.422	-0.423	-0.420	82.63	64.92	80.76	-	-	-
0.25	-0.340	-	-0.335	84.52	-	78.55	-	-	-
0.1	-0.241	-0.255	-0.237	86.10	46.75	73.65	178.7	-	-
0.01	-0.0896	-0.107	-0.0863	88.28	32.94	61.09	168.8	-	180.0
0.001	-0.0310	-0.0423	-0.0287	89.29	22.61	53.20	160.9	-	180.0

(1) Deformation theory with unloading condition $\sigma_e^{\cdot}(r,\theta_1-)=0$

(2) Deformation theory with unloading condition $\sigma_e^{\cdot}(r,\theta_1+)=0$

(3) Flow theory with unloading condition $\sigma_e^{\cdot}(r,\theta_1)=0$

Table 3.2 Plane Strain Mode I ($\nu=1/3$)

α	s(1)	s(2)	$\theta_1(1)$	$\theta_1(2)$	$\theta_2(1)$	$\theta_2(2)$	$\theta_3(1)$	$\theta_4(1)$
1.	-0.5	-0.5	88.62	88.62	-	-	-	-
0.75	-0.478	-0.478	89.19	91.91	-	-	-	-
0.67	-0.468	-0.469	89.34	93.65	-	-	-	-
0.5	-0.441	-0.442	89.61	98.40	-	-	-	-
0.2	-0.343	-0.300	89.94	113.88	174.8	179.7	-	-
0.1	-0.274	-0.197	89.99	123.35	166.0	173.6	-	-
0.05	-0.269	-0.142	89.99	130.61	139.3	161.0	103.78	137.38

(1) Deformation theory with unloading condition $\sigma_e^{\cdot}(r,\theta_1-)=0$

(2) Flow theory with unloading condition $\sigma_e^{\cdot}(r,\theta_1)=0$

Figure 3.2 shows plots of the particle (fixed x_2) effective stress for several values of α, and corresponds to the less singular material. By comparison to the elastic result, plasticity introduces two new features: unloading with a discontinuous slope $[\dot{\sigma}_e]<0$, and the production of residual stress on the wake of the crack. These phenomena become more significant for smaller α, and in fact the need for the reloading sector becomes evident for small enough α. We also note that this material has two local minima in the elastic unloading sector, whereas the flow theory material has only one. Finally, note that for very small α the effective stress level in the plastic zones approaches a constant value, thus approximating a flat variation as expected.

Figure 3.3 shows plots similar to Fig. 3.2 but correspond to the more singular material. It presents the same general features as the previous material except for the fact that reloading never occurs, and that the behavior in the elastic unloading zone resembles more closely that of the flow theory material.

Figure 3.4 shows plots of the angular (fixed r) variations of the stresses for large and moderate strain-hardening for the deformation material with unloading condition (2.36*a*). The

Downloaded 03 May 2010 to 171.66.16.27. Redistribution subject to ASME license or copyright; see http://www.asme.org/terms/Terms_Use.cfm

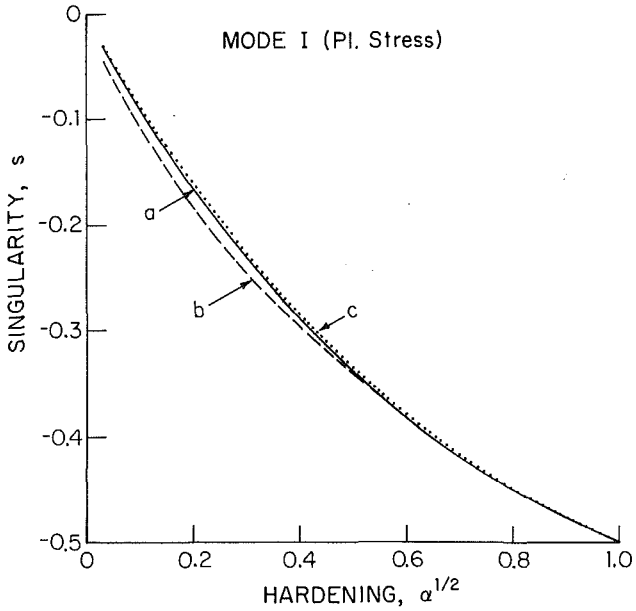


Fig. 3.1 Strength of the singularity in plane stress for: (*a*) deformation theory with unloading condition (2.36a), (*b*) deformation theory with unloading condition (2.36*b*), and (*c*) flow theory

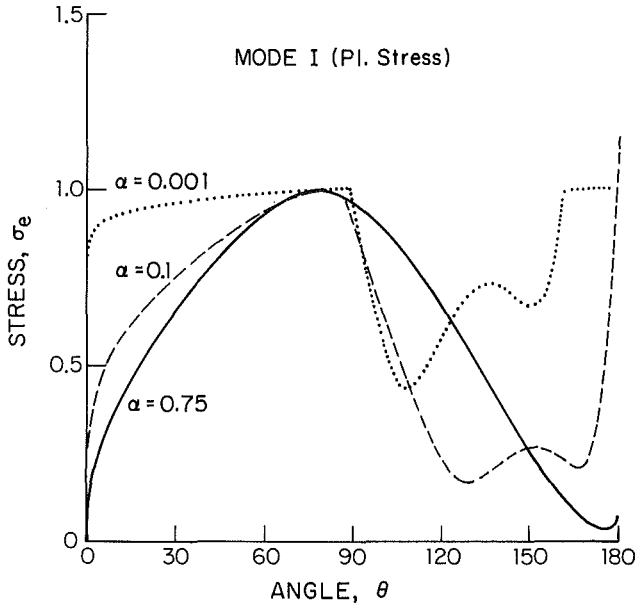


Fig. 3.2 Particle (x_2 fixed) effective stress distribution in plane stress for deformation theory with unloading condition (2.36a), normalized such that $\sigma_e(r,\theta_1)=1$

stress distributions are close to the corresponding flow theory distributions for large strain-hardening, but get progressively farther away from the flow theory distributions as $\alpha \to 0$. The main qualitative differences are the jumps in the slopes of σ_{rr} and σ_e, and the fact that all the components of the stress tensor approach $\theta=\pi$ with slopes opposite in sign to their flow theory counterparts. This effect is most noticeable for σ_{rr} which becomes positively unbounded near $\theta=\pi$, whereas it becomes negatively unbounded for flow theory.

3.2 Plane Strain. As it was pointed out in the formulation section, the results for this case are dependent on Poisson's ratio (ν). Here we chose not to investigate this dependence, and all the results presented in this section are for $\nu=1/3$. These results are summarised in Figs. 3.5 to 3.7, and in Table 3.2.

Figure 3.5 shows plots of s versus $\alpha^{1/2}$ for the deformation theory material with unloading condition (2.36*a*), and for the flow theory material. (The unloading condition (2.36*b*) did not lead to a consistent solution, even for large strain-hardening). For large strain-hardening the two plots are coincident, but as α becomes smaller the two diverge with the deformation theory material showing the stronger singularity. For very small α, the results are unexpected for both materials: the deformation theory material has a discontinuous s versus α curve, and the flow theory material has a nonvanishing s as $\alpha \to 0$ (see Ponte Castañeda, 1987).

Table 3.2 presents values of s, θ_1 and θ_2 for several values of α for the two materials mentioned above. It also presents the values of θ_3 and θ_4 corresponding to the beginning and end of an isolated plastic sector appearing inside the original elastic unloading sector of the deformation theory material for small values of α. The deformation theory material is found to reload (on the crack flank) at a higher level of hardening ($\alpha^* = 0.391$) than the flow theory material ($\alpha^* \sim 0.2$). Further, the three-region solution becomes inconsistent for the deformation theory material for $0<\alpha<\alpha^+$ ($\alpha^+ = 0.057$) due to the fact that the material particle reloads inside the elastic unloading sector, thus requiring a five region solution for $0<\alpha<\alpha^+$. The transition from the three-region solution to the five-region solution is not smooth because the (discontinuous) unloading constraint produces a redistribution of the stress and deformation fields, and it accounts for the discontinuous s versus α curve. Note that appropriate changes and additions to the formulation presented above are needed to treat the five-region problem, but they are quite messy and are not presented here. The unloading angle θ_1 is seen to increase as $\alpha \to 0$ for both materials; however, for deformation theory it has a maximum value of 90 deg, whereas for flow theory it reaches much larger values. This fact might account for the necessity of the extra plastic loading sector for deformation theory as $\alpha \to 0$. The reloading angle θ_2 is found to be of comparable magnitude for both cases.

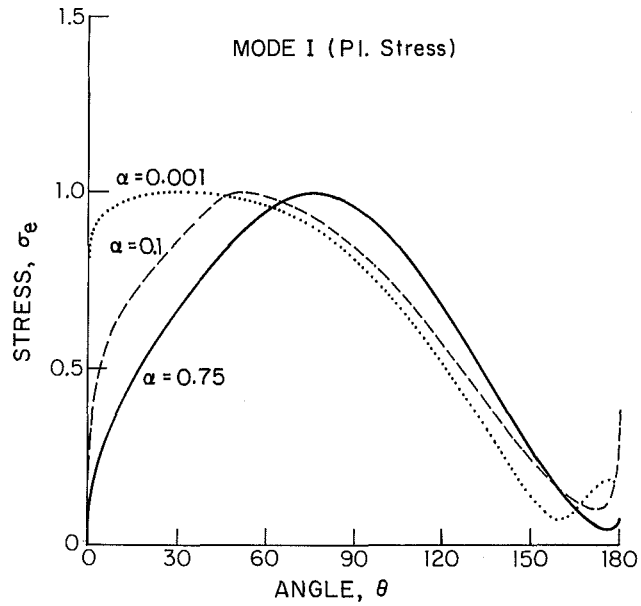


Fig. 3.3 Particle (x_2 fixed) effective stress distribution in plane stress for deformation theory with unloading condition (2.36*b*), normalized such that $\sigma_e(r,\theta_1)=1$

Figure 3.6 depicts plots of the particle effective stress for several values of α. Unloading is observed, and reloading on the crack flanks takes place at an intermediate value of α. Note that the unloading sector develops a bump which gets

Downloaded 03 May 2010 to 171.66.16.27. Redistribution subject to ASME license or copyright; see http://www.asme.org/terms/Terms_Use.cfm

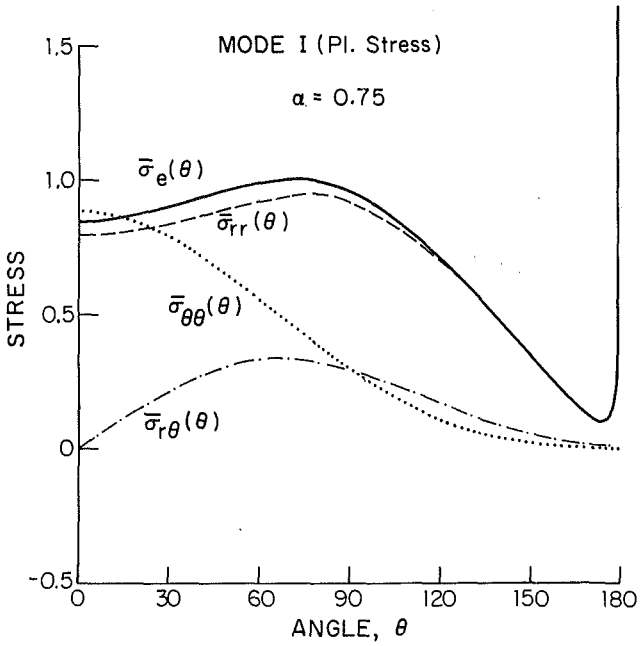


Fig. 3.4(*a*) Angular stress distribution in plane stress for deformation theory with unloading condition (2.36*a*) for large strain-hardening, normalized such that $\bar{\sigma}_e(r,\theta_1)=1$

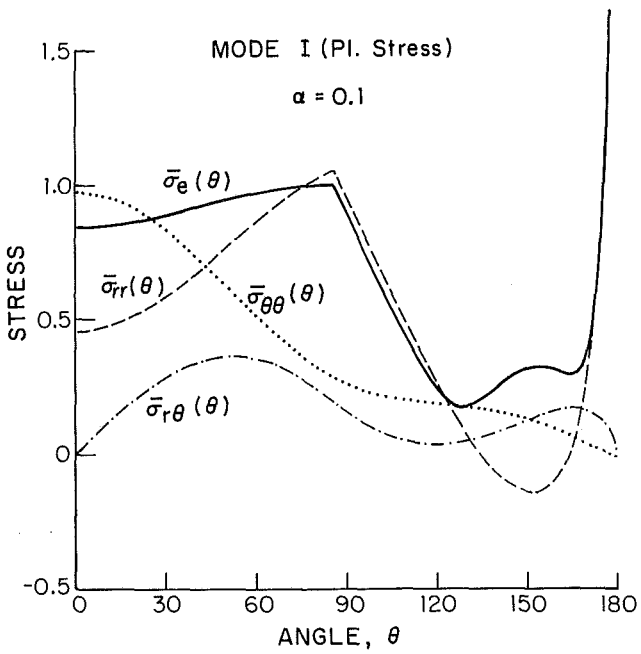


Fig. 3.4(*b*) Angular stress distribution in plane stress for deformation theory with unloading condition (2.36a) for moderate hardening, normalized such that $\bar{\sigma}_e(r,\theta_1)=1$

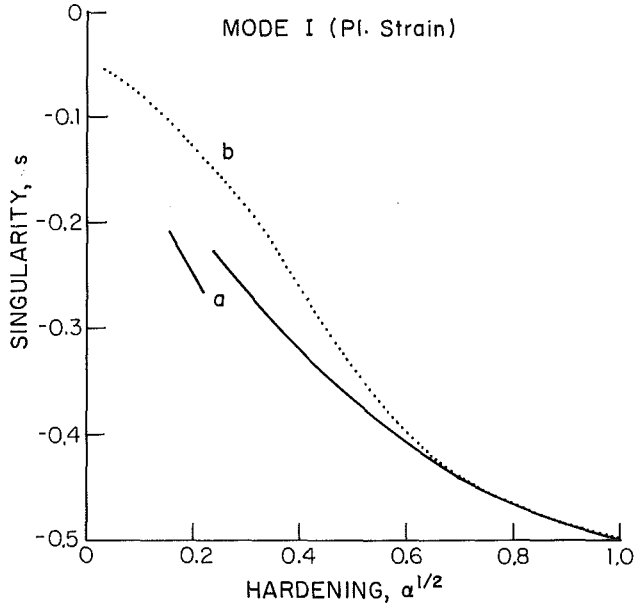


Fig. 3.5 Strength of the singularity in plane strain ($\nu=1/3$) for: (*a*) deformation theory with unloading condition (2.36*a*), (*b*) flow theory

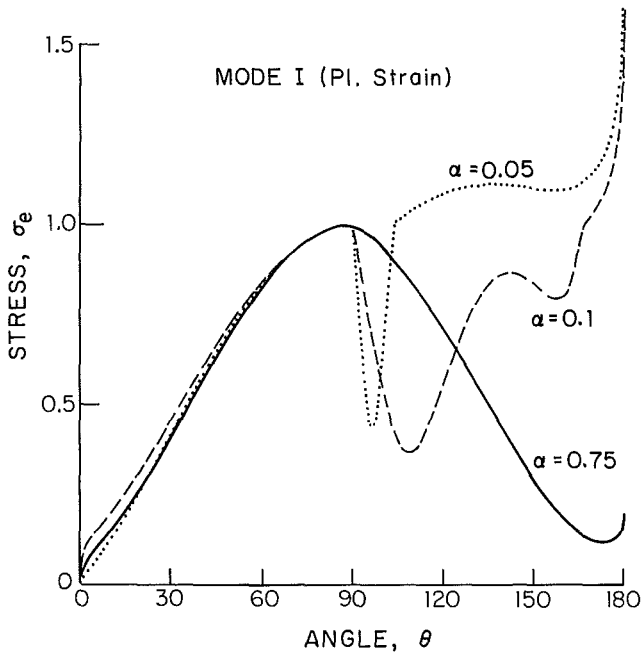


Fig. 3.6 Particle effective stress distribution in plane strain ($\nu=1/3$) for deformation theory with unloading condition (2.36*a*), normalized such that $\sigma_e(r,\theta_1)=1$

higher as α decreases, and for the critical value of $\alpha=\alpha^+$ the three-region solution gives way to the five-region solution. For very small α, and ignoring the sharp unloading sector, this curve resembles the curve corresponding to the flow theory material.

Figure 3.7 shows plots of the angular variations of the stresses for large and moderate strain-hardening. We observe discontinuities in the slopes of σ_{rr}, σ_{33}, and σ_e at both the unloading and reloading boundaries. By comparison to the stress distributions of the flow theory material we find that the distributions look roughly similar near the crack faces, but become quite different ahead of the crack as α decreases. Also the deformation theory material does not show as high a level of triaxiality as the flow theory material.

4 Conclusions

For a linear-hardening material, a deformation theory of plasticity, adequately modified to take into account unloading and reloading, yields an approximate closed-form solution for the stress and velocity fields near the tip of a steadily propagating crack. Inside a region which vanishes in size in the ideally-plastic limit, the constitutive relations can be linearized to yield modified linear elasticity problems in the different sec-

Downloaded 03 May 2010 to 171.66.16.27. Redistribution subject to ASME license or copyright; see http://www.asme.org/terms/Terms_Use.cfm

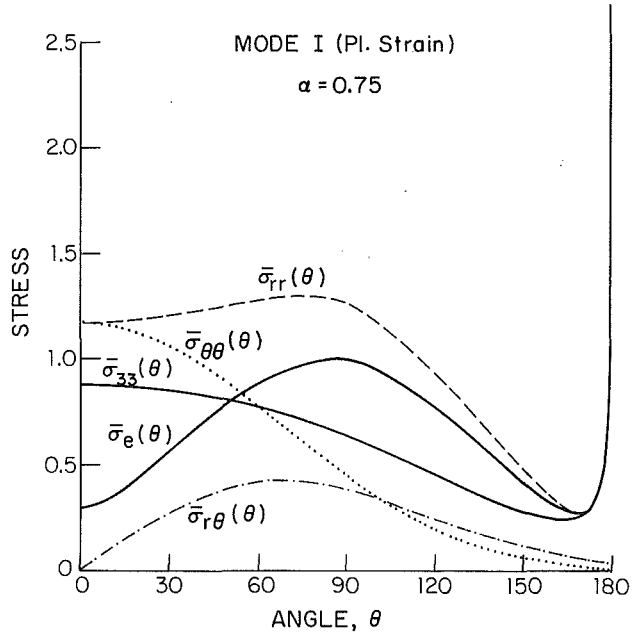


Fig. 3.7(a) Angular stress distribution in plane strain for deformation theory with unloading condition (2.36a) for large strain-hardening, normalized such that $\bar{\sigma}_e(r,\theta_1)=1$

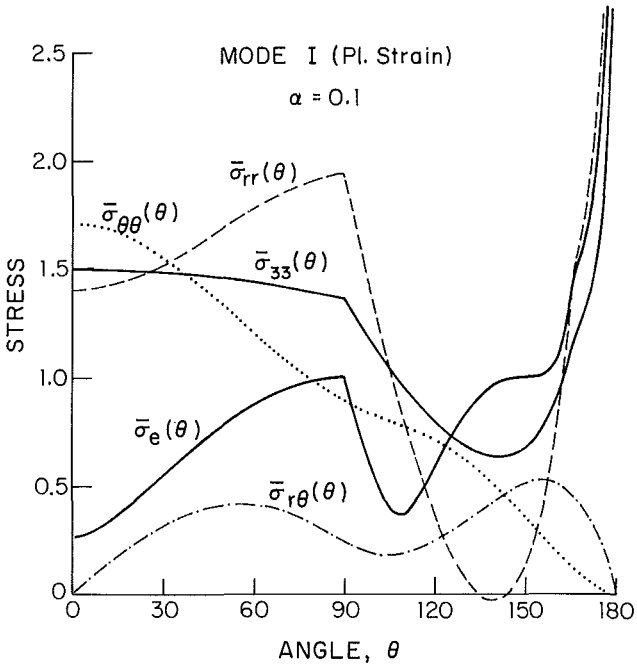


Fig. 3.7(b) Angular stress distribution in plane strain for deformation theory with unloading condition (2.36a) for moderate hardening, normalized such that $\bar{\sigma}_e(r,\theta_1)=1$

tors that can be solved analytically using concise complex-variable methods.

The results of our deformation theory for large strain-hardening ($0.5<\alpha<1$) are in very good agreement with the results of flow theory. This is not altogether unexpected since strain-hardening can contribute to making the overall loading history of a particle in a plastic sector more proportional. As the amount of available strain-hardening decreases, the loading path becomes more severely nonproportional, and the differences between the two theories becomes more marked, with deformation theory in general predicting a stronger singularity strength than flow theory. However, for plane stress, just like for antiplane strain, the predictions of deformation theory for the singularity strength remain in good agreement with the flow theory predictions, even for small strain-hardening. For plane strain, this is not the case, and in fact both theories lead to insensible results for small α. The reason for the better agreement for plane stress and antiplane strain is probably related to the fact that in these cases, the size of the plastic loading and reloading sectors is smaller than for plane strain, where for small enough α there is hardly any elastic unloading.

In general, it is found that deformation theory, appropriately modified to account for unloading and reloading, performs fairly well given the simplicity of the model. This is no doubt related to the fact that elastic unloading (whether using flow theory or deformation theory) is a key feature of elastic-plastic crack growth.

Acknowledgments

This work was supported in part by the Office of Naval Research under Contract N00014-84-K-0510, and by the Division of Applied Sciences, Harvard University. The author is grateful to B. Budiansky for suggesting and supervising this project.

References

Amazigo, J. C., and Hutchinson, J. W., 1977, "Crack-tip Fields in Steady Crack Growth with Linear Strain-Hardening," *J. Mech. Phys. Solids*, Vol. 25, pp. 81–97.

Budiansky, B., 1959, "A Reassessment of Deformation Theories of Plasticity", ASME Journal Applied Mechanics, Vol. 26, pp. 259–264.

Chitaley, A. D., and McClintock, F. A., 1971, "Elastic-Plastic Mechanics of Steady Crack Growth Under Anti-Plane Shear," *J. Mech. Phys. Solids*, Vol. 19, pp. 147–163.

Drugan, W. J., Rice, J. R, and Sham, T. L., 1982, "Asymptotic Analysis of Growing Plane Strain Tensile Cracks in Elastic-Ideally Plastic Solids," *J. Mech. Phys. Solids*, Vol. 30, pp. 447–473.

Gao, Y.-C., 1980, "Elastic-Plastic Field at the Tip of a Crack Growing Steadily in Perfectly-Plastic Medium," (in Chinese), *Acta Mechanica Sinica*, Vol. 1, pp. 48–56.

Gao, Y., Zhang, X., and Hwang, K., 1983, "The Asymptotic Near-Tip Solution for Mode III Crack in Steady Growth in Power Hardening Media," *Int. J. of Fract.*, Vol. 21, pp. 301–317.

Lo, K. K., and Pierce, D., 1981, "Effect of a Yield Surface Vertex on Crack-Tip Fields in Mode III," *J. Mech. Phys. Solids*, Vol. 29, No. 2, pp. 143–152.

Ponte Castañeda, P., 1986, "Asymptotic Fields of a Perfectly-Plastic, Plane-Stress Mode II Growing Crack," ASME Journal of Applied Mechanics, Vol. 53, pp. 831–833.

Ponte Castañeda, P., 1987, "Asymptotic Fields in Steady Crack Growth with Linear Strain-Hardening," *J. Mech. Phys. Solids*, Vol. 35.

Rice, J. R., Drugan, W. J., and Sham, T. L., 1980, "Elastic-Plastic Analysis of Growing Cracks," *Fracture Mechanics: Twelfth Conference*, ASTM-STP 700, pp. 189–219.

Rice, J. R., "Elastic-Plastic Crack Growth," 1982, *Mechanics of Solids: The Rodney Hill 60th Anniversary Volume*, Hopkins, H. G., and Sewell, M. J., eds., Pergamon Press, Oxford, pp. 539–562.

Slepyan, L. I., 1973, "Deformation at the Edge of a Growing Crack," *Mekhanika Tverdogo Tela*, Vol. 8, pp. 139–148.

Slepyan, L. I., 1974, "Growing Crack During Plane Deformation of an Elastic-Plastic Body," *Mekhanika Tverdogo Tela*, Vol. 9, pp. 57–67.

Zhang, R., Zhang, X., and Hwang, K., 1983, "Near-Tip Fields for Plane Strain Mode I Steady Crack Growth in Linear-Hardening Material with Bauschinger Effect," *Proceedings of ICF International Symposium on Fracture Mechanics*, Hwang, K., Liu, C., and He, Q., eds., Science Press, Beijing.

APPENDIX A

Muskhelishvili Formulation

Stress. Given the Muskhelishvili functions ϕ and ψ, we can express the stress components corresponding to a homogeneous elastic problem in the following fashion

$$\sigma_{11}+\sigma_{22}=2[\phi'(z)+\bar{\phi}'(\bar{z})]$$
$$\sigma_{22}-\sigma_{11}+2i\sigma_{12}=2[\bar{z}\,\phi''(z)+\psi'(z)] \qquad (A.1)$$

Traction-Rate Force. The traction-rate force on a boundary C with fixed origin z_o and variable endpoint z is given by

Downloaded 03 May 2010 to 171.66.16.27. Redistribution subject to ASME license or copyright; see http://www.asme.org/terms/Terms_Use.cfm

$$F_1 + iF_2 = \int_C [T_1(s) + iT_2(s)]ds \qquad (A.2)$$

where s is the arc length measure along C, $T_\alpha = \Sigma_{\alpha\beta} n_\beta$ are the traction stress-rates and n_β define the unit normal to C.

The integral in $(A.2)$ is path-independent, and it can be shown that $F_1 + iF_2 = -i(\mathcal{J}_{,1} + i\mathcal{J}_{,2})$ $(A.3)$

Velocity. The velocity expressions depend on the sector

(*i*) Elastic unloading sector

$$2G\,(v_1 - iv_2) = \kappa\,\bar{\Phi}(\bar{z}) - \bar{z}\,\Phi'(z) - \Psi(z) \qquad (A.4a)$$

where $\kappa = (3-\nu)/(1+\nu)$ for plane stress, or $\kappa = 3-4\nu$ for plane strain.

(*ii*) Plastic loading sectors

$$2G^*(v_1 - iv_2) = \kappa^*\bar{\Phi}(\bar{z}) - \bar{z}\,\Phi'(z) - \Psi(z) \qquad (A.4b)$$

where $\kappa^* = (3-\nu^*)/(1+\nu^*)$ for plane stress, or $\kappa^* = 3-4\nu^*$ for plane strain.

APPENDIX B

The Governing Conditions in Terms of the Unknown Constants

Two-region problem ($\alpha^* < \alpha < 1$). In this problem we have six unknowns: two real (s and θ_1), and four complex (A, B, C, D) for a total of ten real unknowns. The boundary and continuity conditions reduce to

Symmetry ($\theta = 0$)

$$\bar{A} = A \quad \bar{B} = B \qquad (B.1)$$

Vanishing traction-rates ($\theta = \pi$)

$$s\bar{C} + e^{i2s\pi}C + \bar{D} = 0 \qquad (B.2)$$

Continuity of traction-rates ($\theta = \theta_1$)

$$s\,e^{i2\theta_1}(\bar{C} - \bar{A}) + e^{i2s\theta_1}(C - A) + (\bar{D} - \bar{B}) = 0 \qquad (B.3)$$

Continuity of velocities ($\theta = \theta_1$)

$$(1+\nu^*)(1+\kappa^*)\bar{A} - \alpha(1+\nu)(1+\kappa)\bar{C} + (3/2)(\alpha-1)[A + se^{i2(s-1)\theta_1}A + e^{i2s\theta_1}B] = 0 \qquad (B.4)$$

The unloading condition ($\dot{\sigma}_e(r, \theta_1^-) = 0$) implies

$$[(4/3)\gamma^*\cos(s\theta_1)\cos(s-1)\theta_1]A^2 + \cos\theta_1\{(s-1)[s+3-4\cos^2\theta_1]A^2 + (s-1)(4\cos^2\theta_1 - 2)BA + B^2\} = 0 \qquad (B.5)$$

where $\gamma^* = 1$ for plane stress, or $\gamma^* = 1 + 4\nu^*(\nu^* - 1)$ for plane strain.

Given s, θ_1 and equations $(B.1)$, equations (B.2) to (B.4) can be viewed as a system of six linear homogeneous equations in the six unknowns A, B, C, $\bar{C}$, D, and $\bar{D}$. The condition for a nontrivial solution is that the determinant of the system matrix be zero, or

$$s^2[(1-\cos2\theta_1)\sin2\theta_1]s^3 + [(1-\delta)(1-\cos2\theta_1)\sin(2s\theta_1)] + s\{(1/2)\omega(\delta-\omega) + (1+\omega)[\cos(2s\theta_1) - 1]\}\sin(2\theta_1) + \{(1-\delta)(1+\omega)[\cos2s(\theta_1 - \pi) - 1]\sin(2s\theta_1) - (1/2)\omega(\delta+\omega)\sin(2s\theta_1) + (1/2)\omega\delta\sin[2s(2\theta_1 - \pi)]\} = 0 \qquad (B.6)$$

where $\omega = (2/3)\alpha(1+\nu)(1+\kappa)/(1-\alpha)$ and $\delta = (2/3)(1+\nu^*)(1+\kappa^*)/(1-\alpha)$.

We can next use any five of the six linear equations to solve for B, C, and D in terms of A. Given these we can look at equation $(B.5)$ as a nonlinear relation between s and θ_1, which together with equation $(B.6)$ provides a system of two nonlinear algebraic equations in s and θ_1 to be solved numerically for a given α (and ν). It is observed, however, that equations (B.1) to (B.6) are independent of ν for the plane stress case. Hence, for plane stress s, θ_1 and the stress distribution are all independent of ν.

Three-region problem ($\alpha^+ < \alpha < \alpha^*$). Here we have nine unknowns: three real (s, θ_1, θ_2) and six complex (A, B, C, D, E, F) for a total of fifteen real unknowns. The boundary and continuity conditions include equations $(B.1)$ to $(B.4)$ plus two more equations of the type of $(B.3)$ and $(B.4)$ applied to the reloading boundary ($\theta = \theta_2$). The same unloading condition $(B.5)$ applies, but we must also include a reloading condition which for brevity will not be stated here. In principle, however, given s, θ_1, θ_2, and $(B.1)$, we can identify a system of ten homogeneous linear equations in the ten unknowns (B, $\bar{B}$, C, $\bar{C}$, D, $\bar{D}$, E, $\bar{E}$, F, $\bar{F}$). The zero determinant condition, and the unloading and reloading conditions then provide three nonlinear algebraic equations in s, θ_1, and θ_2 which can be solved numerically for given α (and ν). Again it is noted that for plane stress s, θ_1 and the stress distributions are independent of ν.

Downloaded 03 May 2010 to 171.66.16.27. Redistribution subject to ASME license or copyright; see http://www.asme.org/terms/Terms_Use.cfm

A Semi-Infinite Crack Partially Penetrating a Circular Inclusion

P. S. Steif
Department of Mechanical Engineering,
Carnegie-Mellon University,
Pittsburgh, PA 15213

When a crack is lodged in an inclusion, differences between the moduli of the inclusion and the bulk material can cause the near-tip stress intensity factor to be greater or less than that prevailing in a homogeneous body. To study the influence of such moduli differences, we solve the problem of a semi-infinite crack half-way penetrating a circular inclusion. The field equations are automatically satisfied by choosing appropriate series expansions for the complex stress potentials; a doubly-infinite system of linear algebraic equations for the series coefficients then enforces continuity of traction and displacement at the inclusion boundary. Results for the reduction (or enhancement) of the stress intensity factor are given for the entire range of material parameters.

1 Introduction

With the increasing use of composite materials and the accompanying need to understand in more detail their fracture behavior, there has come an interest in crack problems involving bodies of spatially varying (often piece-wise constant) material properties. One effect peculiar to cracked, inhomogeneous elastic bodies is the possible alteration in the stress intensity factor (SIF) from its apparent value, due to the crack tip being lodged in a region with elastic moduli differing from the bulk. This composite effect, of potential importance in a variety of contexts, is studied here directly by solving the problem of a homogeneous, isotropic elastic body containing a bonded, circular inclusion which is halfway penetrated by a semi-infinite crack.

Relevant to our investigation is the work by Erdogan and Gupta (1975), who considered among other problems a finite crack with one crack tip lodged in a circular zone of stiffer material. (Their goal was to study a crack partially penetrating a fiber.) Similar situations ought to arise during the fracture of rocks as well, with mineral constituents of very different properties coexisting side-by-side. An additional motivation for studying this problem is the so-called crack-tip shielding effect (Evans and Faber, 1984), in which local damage near the crack tip (e.g., microcracking) may alter the apparent moduli and thereby the SIF. Though the shielding depends rather sensitively on the precise shape of the microcracking zone (Hutchinson, 1985), the problem considered here is fundamental to the crack-tip shielding question, and it reveals a number of effects that may also be relevant to situations involving more irregularly-shaped crack-tip zones. However, a shielding problem is not fully treated here insofar as the sources of the modulus change near the crack tip are not identified.

The simplified version of Erdogan and Gupta's (1975) problem considered here has the radius of the circular crack-tip zone as the only length scale in the problem: the local SIF, proportional to the far-field (applied) SIF, then depends only on the various elastic moduli. Therefore, the influence of the moduli differences can be focused on, without concern for various geometric parameters. Results for the local SIF are presented for the full range of moduli, and some limitations of the present model in understanding the shielding process are discussed.

2 Analysis

The boundary value problem to be solved, that of an infinite, inhomogeneous plane containing a semi-infinite crack, is shown schematically in Fig. 1. Cartesian and polar coordinate systems have been erected with their origins at the crack tip such that the crack lies along the negative x axis. Throughout the plane, the material is taken to be linear elastic

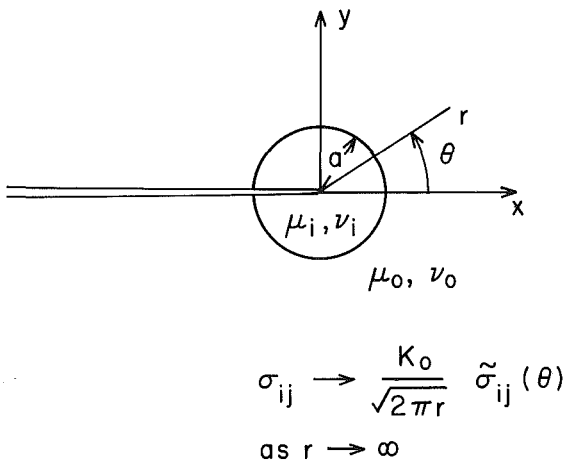


Fig. 1 Schematic of a semi-infinite crack penetrating a circular inclusion

Contributed by the Applied Mechanics Division for publication in the JOURNAL OF APPLIED MECHANICS.
Discussion on this paper should be addressed to the Editorial Department, ASME, United Engineering Center, 345 East 47th Street, New York, N.Y. 10017, and will be accepted until two months after final publication of the paper itself in the JOURNAL OF APPLIED MECHANICS. Manuscript received by ASME Applied Mechanics Division, August 1, 1985; final revision January 20, 1986.

Copyright © 1987 by ASME
Downloaded 03 May 2010 to 171.66.16.27. Redistribution subject to ASME license or copyright; see http://www.asme.org/terms/Terms_Use.cfm

and isotropic. The shear modulus and Poisson's ratio are, respectively, μ_i, ν_i in the region $0<r<a$ and μ_o, ν_o in $a<r<\infty$. At $r=a$ the materials are perfectly bonded. The composite body is constrained to undergo inplane deformations, and the crack flanks remain traction free.

Far from the crack tip, the stress field approaches the Mode I elastic singular field with SIF K_o. This problem is analogous to the small scale-yielding problem of elastic-plastic fracture mechanics. We are treating the case in which the zone of altered elastic moduli is sufficiently small compared with the actual crack length and other relevant dimensions that the near-tip elastic singular field, which would prevail in the absence of the altered zone, still provides a good approximation to the stress field at intermediate distances from the crack tip, i.e., in the range $a \ll r \ll$ crack length. In a specific problem, the applied SIF would need to be evaluated independently. Since the materials are linear, the near-tip SIF, K_i, is linearly related to K_o. Below, we determine K_i/K_o as a function of μ_i, μ_o, ν_i, and ν_o.

The solution is arrived at by developing general forms for the stress and displacement fields in the regions $0<r<a$ and $a<r<\infty$ and, then, matching those fields appropriately at $r=a$. These general forms involve combinations of Williams' (1952) crack-tip eigenfunctions. Extending a method given by Rice (1968) for deducing crack-tip fields, we reproduce the eigenfunctions in a form which allows the matching at $r=a$ to be done in a straightforward manner. For this purpose, we employ the Muskhelishvili (1953) complex potentials, $\phi(z)$ and $\psi(z)$, related to the Cartesian components of stress and displacement by

$$\sigma_{xx}+\sigma_{yy}=2[\phi'(z)+\overline{\phi'(z)}] \tag{1a}$$

$$\sigma_{yy}-\sigma_{xx}+2i\sigma_{xy}=2[\bar{z}\phi''(z)+\psi'(z)] \tag{1b}$$

$$2\mu(u_x+iu_y)=\kappa\phi(z)-z\overline{\phi'(z)}-\overline{\psi(z)} \tag{1c}$$

and we define the auxiliary potential $\Omega(z)$

$$\Omega(z)=z\phi'(z)+\psi(z) \tag{2}$$

where $z=x+iy=re^{i\theta}$, $\overline{\ }$ denotes complex conjugate, $'$ denotes differentiation with respect to z, and $\kappa=3-4\nu$ in plane strain. The functions $\phi(z)$, $\psi(z)$ and $\Omega(z)$ are analytic within the cut disk $0<r<a$ and within the cut annulus $a<r<\infty$.

The traction-free conditions on the upper and lower crack flanks may be expressed in terms of $\phi(z)$ and $\Omega(z)$ as

$$(\sigma_{yy}-i\sigma_{xy})_+=\phi'_+(x)+\bar{\Omega}'_-(x)=0 \quad (-\infty<x<0) \tag{3a}$$

$$(\sigma_{yy}-i\sigma_{xy})_-=\phi'_-(x)+\bar{\Omega}'_+(x)=0 \quad (-\infty<x<0) \tag{3b}$$

where $(\ )_+$ and $(\ )_-$ denote limits as $y\to 0$ from above and below, and $\bar{\Omega}(z)\equiv\overline{\Omega(\bar{z})}$

Adding and subtracting equations (3) leads to the conditions

$$(\phi'+\bar{\Omega}')+(\phi'+\bar{\Omega}')_-=0 \quad (-\infty<x<0)$$

$$(\phi'-\bar{\Omega}')_+-(\phi'-\bar{\Omega}')_-=0 \quad (-\infty<x<0)$$

General solutions to this pair of Hilbert equations in the two regions are

$$\phi'(z)=\begin{cases}\dfrac{h(z)}{\sqrt{z}}+m(z) & 0<r<a \qquad (4a)\\[2ex] \dfrac{f(z)}{\sqrt{z}}+g(z) & a<r<\infty \qquad (4b)\end{cases}$$

$$\bar{\Omega}'(z)=\begin{cases}\dfrac{h(z)}{\sqrt{z}}-m(z) & 0<r<a \qquad (4c)\\[2ex] \dfrac{f(z)}{\sqrt{z}}-g(z) & a<r<\infty \qquad (4d)\end{cases}$$

where $h(z)$ and $m(z)$ are analytic in the disk $0<r<a$, and $f(z)$ and $g(z)$ are bounded and analytic in the annulus $a<r<\infty$. (We have invoked the boundedness of displacements as $r\to 0$ and stresses as $r\to\infty$.)

Functions $h(z)$, $m(z)$, $f(z)$, and $g(z)$ will be chosen to satisfy continuity of tractions σ_{rr} and $\sigma_{r\theta}$ and displacements u_r and u_θ at the bimaterial interface $r=a$. In terms of the potentials $\phi(z)$ and $\Omega(z)$, these continuity conditions imply that the quantities

$$\phi'(z)+\overline{\phi'(z)}-e^{-2i\theta}[(z-\bar{z})\overline{\phi''(z)}+\bar{\Omega}'(\bar{z})-\overline{\phi'(z)}] \tag{5a}$$

and

$$\frac{1}{\mu}\{\kappa\phi'(z)-\overline{\phi'(z)}+e^{-2i\theta}[(z-\bar{z})\overline{\phi''(z)}+\bar{\Omega}'(\bar{z})-\overline{\phi'(z)}]\} \tag{5b}$$

be continuous as one approaches $r=a$ from above and below for all θ.

A solution to the above equations may be found by noting that the analyticity of functions f, g, h, and m in their respective regions implies the following Laurent expansions

$$h(z)=\sigma_o\sqrt{a}\sum_{n=0}^{\infty}h_n\left(\frac{z}{a}\right)^n \qquad m(z)=\sigma_o\sum_{n=0}^{\infty}m_n\left(\frac{z}{a}\right)^n$$

$$f(z)=\sigma_o\sqrt{a}\sum_{n=0}^{\infty}f_n\left(\frac{a}{z}\right)^n \qquad g(z)=\sigma_o\sum_{n=0}^{\infty}g_n\left(\frac{a}{z}\right)^n$$

where

$$\sigma_o f_o=\frac{K_o}{2\sqrt{2\pi a}} \text{ and } \frac{h_o}{f_o}=\frac{K_i}{K_o}$$

In the Laurent expansion for $g(z)$ we have set $g_1=0$, since no net force is applied to the body. Also, the term g_o, corresponding to a uniform tension (or compression) parallel to the crack, has been set equal to zero. (g_o and f_o are the only portions of the stress field which may be prescribed.) A tension or compression parallel to the crack can induce a nonzero SIF at the crack tip when the inclusion moduli differ from the moduli in the region exterior to the inclusion; the corresponding SIF is proportional to the square root of the *inclusion radius*. On the other hand, K_o, which is supposedly due to a remote tension normal to the crack, is generally proportional to the square root of the *crack length*. (Clearly, one can construct counter-examples, such as a crack wedged open by loads.) Thus, for many situations of practical interest, the near-tip SIF due to tension (σ_{xx}) parallel to the crack is small compared to that due to tension (σ_{yy}) normal to the crack when small scale shielding conditions prevail.

With the above forms for $\phi(z)$ and $\Omega(z)$, continuity of the quantities (5*a*) and 5(*b*) leads to two infinite sets of linear algebraic equations for the coefficients h_n, m_n, f_n, and g_n. The symmetry of the boundary value problem chosen implies that only a Mode I K_i is produced by applying a Mode I K_o, and that all the coefficients h_n, m_n, f_n, and g_n are real.

From the continuity of (5*a*) one may deduce the equation

$$\sum_{n=-\infty}^{\infty}a_n e^{in\theta}+\sum_{k=-\infty}^{\infty}b_k e^{i(k+1/2)\theta}=0 \tag{6}$$

where the a_n and b_k are given in terms of f_n, g_n, h_n, and m_n in the Appendix. Similarly, continuity of (5*b*) implies the equation

$$\sum_{n=-\infty}^{\infty}c_n e^{in\theta}+\sum_{k=-\infty}^{\infty}d_k e^{i(k+1/2)\theta}=0 \tag{7}$$

Expanding $e^{i(k+1/2)}$ in a Fourier series, one finds that

$$e^{i(k+1/2)}=\sum_{n=-\infty}^{\infty}A_{nk}e^{in\theta}$$

where

Downloaded 03 May 2010 to 171.66.16.27. Redistribution subject to ASME license or copyright; see http://www.asme.org/terms/Terms_Use.cfm

Table 1 Convergence of results for $\mu_i/\mu_o = 0.1$, $\nu_i = \nu_o = 0.2$

p	10	20	40
$(K_i/K_o)_p$	0.17819	0.17808	0.17806

$$A_{nk} = \frac{1}{\pi}\left[\frac{(-1)^{k+n}}{k+1/2-n}\right]$$

After exchanging the order of summation, equation (6) may be put in the form

$$\sum_{n=-\infty}^{\infty}\left[a_n + \sum_{k=-\infty}^{\infty} b_k A_{nk}\right]e^{in\theta} = 0$$

for all θ on $-\pi < \theta < \pi$ and, hence,

$$a_n + \sum_{k=-\infty}^{\infty} b_k A_{nk} = 0 \quad (n = 0, \pm 1, \pm 2, \ldots) \tag{8}$$

An equation similar to (8) emerges from equation (7), namely

$$c_n + \sum_{k=-\infty}^{\infty} d_k A_{nk} = 0 \quad (n = 0, \pm 1, \pm 2, \ldots) \tag{9}$$

Stress intensity factors for μ_i/μ_o very large and very small compared with one may be obtained directly as follows.[1] A relatively rigid crack-tip zone ($\mu_i/\mu_o \gg 1$) essentially sets a zero displacement condition at $r = a$. One may then determine the solution in the region $a < r < \infty$ and, in particular, the tractions acting on the interface (they depend only on ν_o). With the same tractions applied to the disk occupying $0 < r < a$ and the traction-free condition on the crack flanks, the stresses within the disk may be determined (independently of the moduli). In practice, equations (9) are solved for f_n and g_n with $h_n \mu_o/\mu_i$ m_n μ_o/μ_i set equal to zero. These values for f_n and g_n are substituted into equations (8) from which h_n and m_n are deduced, the results depending only on κ_o.

A relatively soft crack-tip zone ($\mu_i/\mu_o \ll 1$) sets a zero traction condition at $r = a$, though the displacements in the crack-tip zone, proportional to h_n μ_o/μ_i and m_n μ_o/μ_i, are finite and nonzero. With these boundary conditions at $r = a$, the displacements in $a < r < \infty$ may be determined. They depend on ν_o and are inversely proportional to μ_o. One then determines the stresses in the crack-tip zone when the displacements just calculated are applied at $r = a$ and the crack flanks remain traction-free. The stresses, and the corresponding SIF, depend on ν_i and are proportional to μ_i. This procedure is carried out by solving equations (8) for f_n and g_n with h_n and m_n set equal to zero and substituting the results into equations (9) from which h_n μ_o/μ_i and m_n μ_o/μ_i can be extracted. The SIF obtained is thus proportional to μ_i/μ_o and depends on κ_o and κ_i.

An approximate solution to the infinite system of equations was obtained by isolating a finite system containing the same number of unknowns as equations, and following the results as the size of the finite system is increased. We isolated a finite system by truncating equations (8) and (9) so that $-p < n < p$ and $-p+1 < k < p-2$: a set of $4p+2$ equations for as many unknowns results. The quantity $h_o/f_o = (K_i/K_o)_p$ is shown in Table 1 for several values of p, with $\mu_i/\mu_o = 0.1$ and $\nu_i = \nu_o = 0.2$.

Convergence like that shown in Table 1 was found to occur whenever ν_i and ν_o were equal. The results emerging from the procedure used here were independently verified (for several choices of the material parameters) by comparison with results based on a special finite element procedure for cracks in inhomogeneous domains (Steif, 1985). On the other hand, convergence was very slow in regions of the parameter space where ν_i and ν_o are very different and K_i/K_o is near 1.0. In

[1] I am indebted to A. Ruina for a discussion which motivated the extraction of these limiting cases.

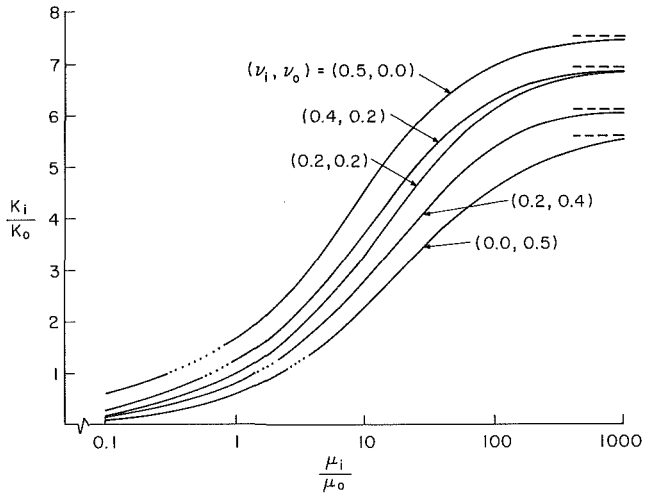


Fig. 2 Near-tip stress intensity factor K_i/K_o for an extended range of shear modulus ratio μ_i/μ_o. (. . . ~ interpolated values in range of slow convergence, _ _ _ _ ~ asymptotic K_i/K_o as $\mu_i/\mu_o \to \infty$.)

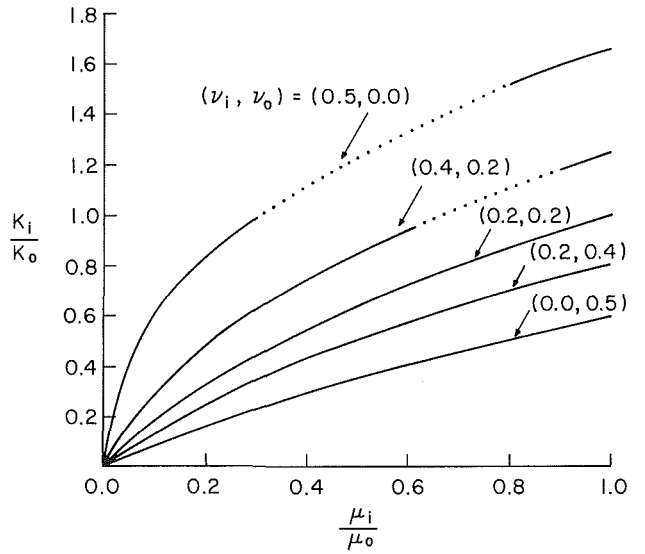


Fig. 3 Near-tip stress intensity factor K_i/K_o versus μ_i/μ_o for $o < \mu_i/\mu_o < 1$. (. . . ~ interpolated values in range of slow convergence.)

Fig. 2 discussed below, the values of K_i/K_o in the regions of slow convergence have been interpolated with a dotted curve. The procedure outlined by Steif (1985) was applied to one set of parameters in the omitted range, and it gave a result lying on a smoothly interpolated curve.

Finally, we note that there is, in general, a stress singularity at $r = 1$, $\theta = \pm\pi$ (see Bogy, 1971). The method of solution employed here, while designed specifically for deducing the magnitude of the singularity at the crack tip, is unable to resolve the singularity at $r = 1$, $\theta = \pm\pi$. We are tacitly assuming that a more careful account of this neglected singularity would alter the crack-tip singularity an insignificant amount.

3 Results and Discussion

The relative crack-tip SIF, K_i/K_o, as it depends on the shear modulus ratio, μ_i/μ_o, is shown in Figs. 2 and 3. As mentioned above, slow convergence was observed over limited ranges of μ_i/μ_o when ν_i and ν_o were different. We have interpolated a smooth dotted curve between the regions of good convergence. One obvious feature of interest is the considerable dependence on the Poisson's ratios. Particularly strong is the dependence when ν_i and ν_o are very different. In fact, the

Downloaded 03 May 2010 to 171.66.16.27. Redistribution subject to ASME license or copyright; see http://www.asme.org/terms/Terms_Use.cfm

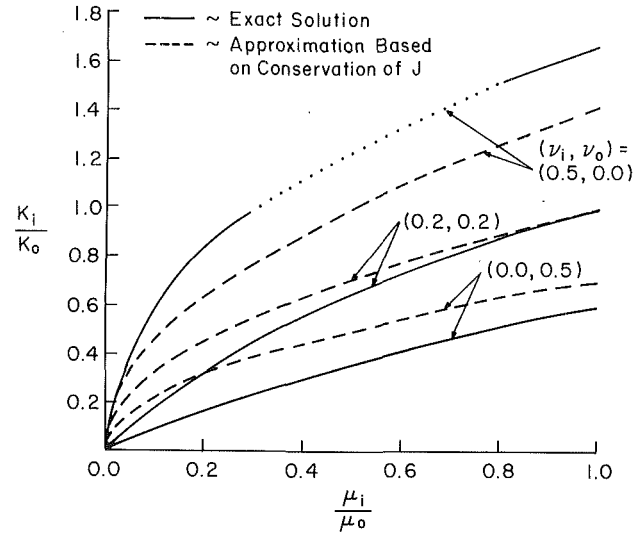


Fig. 4 Comparison of computed near-tip stress intensity factor (solid curves) and approximate near-tip stress intensity factor based on conservation of *J* integral (dashed curves)

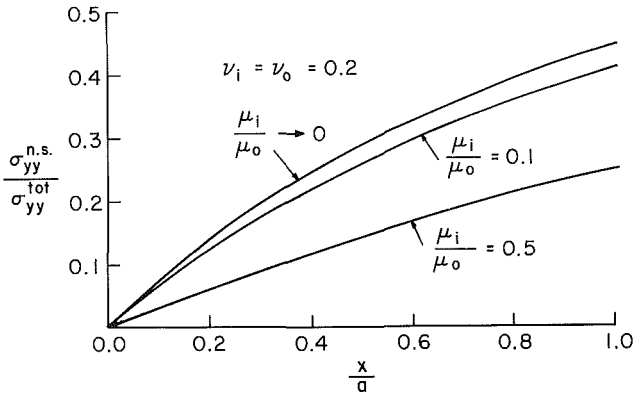


Fig. 5 Fraction fo the tensile stress ahead of the crack tip attributable to nonsingular terms, showing dominance of the singular part when inclusion is relatively compliant

curves corresponding to $\nu_i = 0.5$, $\nu_o = 0.0$ and $\nu_i = 0.0$, $\nu_o = 0.5$ bound all other curves above and below, respectively. (One can rationalize the Poisson's ratio dependence by contemplating the terms $-\gamma\kappa_i h_o + \kappa_o f_o$ in the coefficient d_{-1}.) On the other hand, fixing ν_i equal to ν_o and then varying both produces relatively little change.

One may derive an approximate expression for K_i/K_o by assuming that the *J* integral takes on equal values on opposite sides of the inclusion boundary. Since *J* is path independent for all contours lying within each homogeneous region, one obtains (for plane strain)

$$\frac{K_i}{K_o} = \sqrt{\frac{\mu_i(1-\nu_o)}{\mu_o(1-\nu_i)}}$$

For comparison, this approximate result has been plotted as dashed curves in Fig. 4 along with some of the computed results appearing in Fig. 3. Though the agreement is only fair, the trends with regard to the Poisson's ratios are similar.

We make brief contact with Erdogan and Gupta (1975) in order to show the effect of crack length. They give extensive results for a variety of crack problems with $\mu_i/\mu_o = 23.077$, $\kappa_i = 1.8$, and $\kappa_o = 1.6$ (an epoxy matrix and an aluminum inclusion). Relevant to the present work is the portion of Table 6 in Erdogan and Gupta (1975) in which $a_2/a = 0$. The quantity identical to our K_i/K_o is their quantity $k(a_2)/\sigma_o c^{1/2}$. As the crack length ranges from 1.1 to 3.0 times the inclusion radius,

Table 2 $\frac{K_i}{K_o}$ as $\frac{\mu_i}{d_o} \to \infty$ (rigid inclusion)

ν_o	0.0	0.1	0.2	0.3	0.4	0.5
K_i/K_o	7.5	7.3	6.9	6.5	6.1	5.6

Table 3 $\frac{\mu_o}{\mu_i}\frac{K_i}{K_o}$ as $\frac{\mu_i}{\mu_o} \to 0$ (complaint inclusion)

$(\nu_i$ \ (ν_o)	0.0	0.1	0.2	0.3	0.4	0.5
0.0	1.87	2.12	2.50	3.13	4.53	11.8
0.1	1.68	1.91	2.25	2.82	4.07	10.7
0.2	1.49	1.70	2.00	2.51	3.62	9.47
0.3	1.31	1.49	1.75	2.19	3.17	8.29
0.4	1.12	1.27	1.50	1.88	2.72	7.11
0.5	0.93	1.06	1.25	1.57	2.26	5.93

$k(a_2)/\sigma_o c^{1/2}$ ranges from 3.564 to 3.996. For a semi-infinite crack, we find $K_i/K_o = 4.27$. From this, one can see that the crack length must be significantly greater than the inclusion radius in order that the small-scale shielding results be valid.

Results for the limiting cases of very stiff and very compliant inclusions are tabulated in Tables 2 and 3, respectively. The variation with ν_o in the case of a rigid inclusion is relatively small, whereas for a very soft inclusion the limiting behavior can be altered significantly by suitable changes in ν_i and ν_o. Here it can be seen why there is so little variation in K_i/K_o when the Poisson's ratios are held equal while varied. At $\mu_i/\mu_o = 1$, K_i/K_o remains equal to 1 for all $\nu_i = \nu_o$; as $\mu_i/\mu_o \to \infty$ the variation is within 35 percent; and, as $\mu_i/\mu_o \to 0$ the variation is within 45 percent, except when $\nu_i = \nu_o = 0.5$. Also interesting is the rate at which the limiting cases are approached. As shown in Fig. 2, the rigid limit is approached only when μ_i/μ_o is greatly in excess of 1, on the order of 1000. However, the compliant limit provides a good approximation to K_i/K_o with only modest reduction in the modulus, say $\mu_i/\mu_o = 0.1$.

The solution method employed here also enables one to calculate the entire stress field. One can, therefore, deduce the region near the crack tip in which the singular field provides a reasonable approximation to the actual stress field. This has been done, in particular, for the stress component σ_{yy} directly ahead of the crack tip. For convenience, we define the quantity η by

$$\eta = \frac{\sigma_{yy}^{n.s.}}{\sigma_{yy}^{tot}}$$

where $\sigma_{yy}^{n.s.}$ is the nonsingular part of σ_{yy} ahead of the crack tip, and σ_{yy}^{tot} is the total σ_{yy}.

In Fig. 5, η is plotted as a function of position ahead of the crack tip for several values of μ_i/μ_o, with $\nu_i = \nu_o = 0.2$. Even for the most severe modulus difference, $\mu_i/\mu_o \to 0$, the singular field accounts for 80 percent of the stress field at $x/a = 0.3$. This is to be contrasted with the stiff inclusion case (Fig. 6), in which the nonsingular terms are substantial even close to the crack tip. In fact, the stress σ_{yy} is compressive over more than half of the inclusion. The use of a stress intensity factor in hard inclusion cases may therefore be dubious, whereas it appears acceptable in soft-inclusion cases, which are more relevant to the shielding problem.

Clearly, crack-tip shielding due to microcracking is a far more complicated phenomenon than the homogeneous inclusion model would imply. A more realistic model would have the moduli varying smoothly with distance from the crack tip until the uncracked moduli are reached. As a preliminary assessment of the effect of spatially-varying moduli, we consider the highly idealized problem of a Mode III (antiplane

Downloaded 03 May 2010 to 171.66.16.27. Redistribution subject to ASME license or copyright; see http://www.asme.org/terms/Terms_Use.cfm

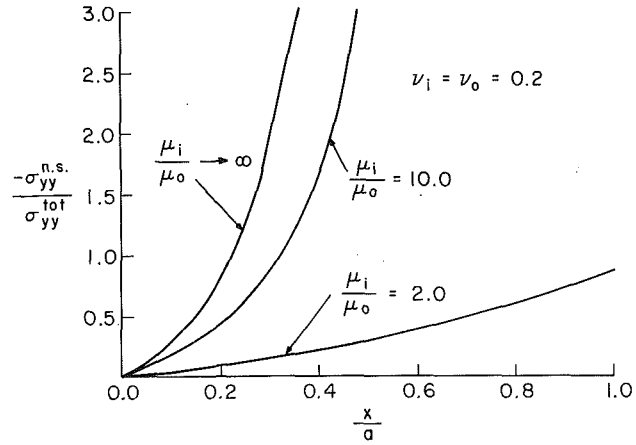


Fig. 6 Fraction of the tensile stress ahead of the crack tip attributable to nonsingular terms, showing importance of nonsingular terms when inclusion is relatively rigid

shear) crack with a circular zone centered at the crack-tip, in which the shear modulus depends on the radial coordinate alone.

The out-of-plane displacement, w, satisfies

$$\nabla^2 w = 0$$

outside the crack-tip zone and, as $r \to \infty$,

$$w \to \frac{2K_o}{\mu_o}\sqrt{\frac{r}{2\pi}}\sin\frac{\theta}{2}$$

In the region in which μ varies with r, w satisfies

$$\nabla^2 w + \frac{1}{\mu(r)}\frac{d\mu(r)}{dr}\frac{\partial w}{\partial r} = 0 \tag{10}$$

Separated solutions to equation (10) of the form $w = f(\xi)g(\theta)$ may be found, where

$$\xi^2\frac{d^2f}{d\xi^2} + \xi(1+\xi q)\frac{df}{d\xi} - \beta^2 f = 0 \tag{11}$$

$$\frac{d^2g}{d\theta^2} + \beta^2 g = 0 \tag{12}$$

and

$$\xi \equiv \frac{r}{a} \quad q(\xi) = \frac{1}{\mu(\xi)}\frac{d\mu(\xi)}{d\xi}$$

If $q(\xi)$ can be expanded in a power series in ξ about $\xi = 0$, then $\xi = 0$ is a regular singular point of equation (11). Since there is no variation of μ with θ, the exact solution (satisfying continuity of displacement and traction at $\xi = 1$) is of the form $w = f(\xi)\sin(\theta/2)$, i.e., only terms involving $\beta = 1/2$ are necessary. The solution in $1 < \xi < \infty$ is then

$$w = \left[\frac{2K_o}{\mu_o}\sqrt{\frac{a\xi}{2\pi}} + \frac{B}{\sqrt{\xi}}\right]\sin\frac{\theta}{2}$$

where B is to be determined. In $0 < \xi \le 1$, the function $f(\xi)$ is given by

$$f(\xi) = \sqrt{\xi}\sum_{n=0}^{\infty} f_n \xi^n$$

with $f_n (n \ge 1)$ defined by the recursive relation

$$f_n = -\left[\frac{(1/2)q_{n-1}f_o + (3/2)q_{n-2}f_1 + \ldots + (n-1/2)q_o f_{n-1}}{(n+1/2)^2 - 1/4}\right] \tag{13}$$

where

$$q(\xi) = \sum_{n=0}^{\infty} q_n \xi^n$$

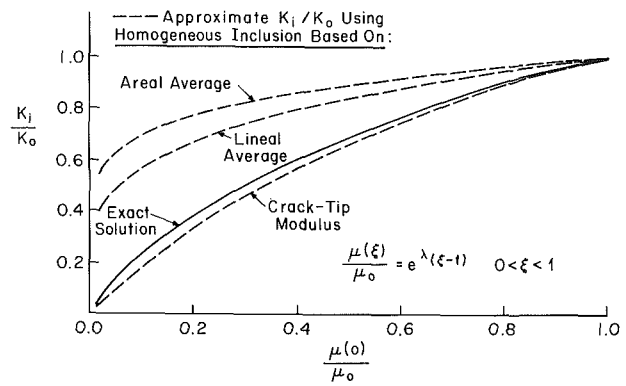


Fig. 7 Comparison of exact solution for Mode III K_i/K_o with spatially varying inclusion modulus and approximate calculations based on constant inclusion modulus

The unknowns f_o and B are found by matching w and σ_{rz} at $\xi = 1$ (recall both vary as $\sin(\theta/2)$ throughout the plane); these conditions imply that f and $df/d\xi$ are continuous at $\xi = 1$, provided μ is continuous there. Defining $\alpha_n = f_n/f_o$, one may obtain the α_n from equation (13), for a given $q(\xi)$. The quantity of interest, K_i/K_o, is then given by

$$\frac{K_i}{K_o} = \frac{\mu(0)}{\mu_o}\left[\frac{1}{\sum_{n=0}^{\infty}(n+1)\alpha_n}\right]$$

Specific calculations were carried out for

$$\frac{\mu(\xi)}{\mu_o} = \exp[\lambda(\xi - 1)] \tag{14}$$

which implies

$$q(\xi) = \lambda \text{ and } \mu(0)/\mu_o = e^{-\lambda}$$

The reduced SIF, K_i/K_o, is plotted in Fig. 7 as a function of μ_i/μ_o.

Several other curves are provided in Fig. 7 for comparison. Each involves using the Mode III version of the central problem of this study, namely, a homogeneous crack-tip zone with moduli μ_i. For Mode III, one can find simply that

$$\frac{K_i}{K_o} = \frac{2\mu_i}{\mu_i + \mu_o} \tag{15}$$

We have taken the modulus distribution (14) and averaged it in two ways to calculate an effective inclusion modulus μ_i.

lineal average: $$\frac{\mu_i}{\mu_o} \equiv \int_0^1 \frac{\mu(\xi)}{\mu_o}\,d\xi$$

areal average: $$\frac{\mu_i}{\mu_o} \equiv 2\int_0^1 \frac{\mu(\xi)}{\mu_o}\,\xi d\xi$$

The averaged moduli were substituted into equation (15) and the resulting values for K_i/K_o were plotted as dashed curves in Fig. 7 as a function of $\mu(0)/\mu_o$. Also, $\mu(0)/\mu_o$ was substituted directly into equation (15) and the result was plotted in Fig. 7. (This dashed curve is labelled "Crack-Tip Modulus.") Thus, the different curves in Fig. 7 correspond to different methods of determining K_i/K_o for the same inclusion.

Clearly, both of the averaging schemes severely underestimate the amount of shielding (SIF reduction). On the other hand, assuming the modulus right at the crack tip prevails throughout the inclusion leads to a fairly good prediction of the degree of shielding. One might argue, however, that the true SIF (as $r \to 0$) is not a proper measure of stressing intensity for such an inhomogeneous body. In fact, for the

Downloaded 03 May 2010 to 171.66.16.27. Redistribution subject to ASME license or copyright; see http://www.asme.org/terms/Terms_Use.cfm

modulus variation considered here, the singular field based on the true SIF is a relatively poor approximation to the actual stress field when $\mu(0)/\mu_o \ll 1$. Nevertheless, this plot indicates some potential pitfalls in applying the homogeneous inclusion results to a crack-tip shielding problem.

Acknowledgments

I am grateful to Mr. Steven Hoysan and Ms. Sylvia Konczol for carrying out the computations. This work has been supported by the National Science Foundation under Grant MEA-8403887 and by the Department of Mechanical Engineering, Carnegie-Mellon University.

References

Bogy, D. B., 1971, "Two Edge-Bonded Elastic Wedges of Different Materials and Wedge Angles Under Surface Tractions," ASME JOURNAL OF APPLIED MECHANICS, Vol. 38, pp. 377–386.

Erdogan, F., and Gupta, G. D., 1975, "The Inclusion Problem with a Crack Crossing the Boundary," *International Journal of Fracture*, Vol. 11, No. 1, pp. 13–27.

Evans, A. G., and Faber, K. T., 1984, "Crack-Growth Resistance of Microcracking Brittle Materials," *Journal of the American Ceramic Society*, Vol. 67, No. 7, pp. 255–260.

Hutchinson, J. W., 1985, Private Communication.

Muskhelishvili, N. L., 1953, *Some Basic Problems of Mathematical Theory of Elasticity*, P. Noordhoof, The Netherlands.

Rice, J. R., 1968, "Mathematical Analysis in the Mechanics of Fracture," *Fracture*, Vol. 11, Liebowitz, H., Ed., Academic Press, New York.

Steif, P. S., 1985, "A Superposition Procedure for Computing Stress Intensity Factors in Cracked Elastic Composites," *International Journal of Fracture*, Vol. 29, pp. 223–233.

Williams, M. L., 1952, "Stress Singularities Resulting from Various Boundary Conditions in Angular Corners of Plates in Extension," ASME JOURNAL OF APPLIED MECHANICS, Vol. 19, pp. 526–528.

APPENDIX

The following are the equations which relate the coefficients f_n, g_n, h_n and m_n to the quantities a_n, b_n, c_n, and d_n appearing in equations (8) and (9).

$$
\begin{aligned}
a_o &= -2m_o \\
a_1 &= -g_3 - m_1 \\
a_n &= (n+1)g_n - ng_{n+2} - m_n && n \geq 2 \\
a_{-1} &= 0 \\
a_{-n} &= g_n + (n-1)m_n - n\, m_{n-2} && n \geq 2 \\
b_0 &= -(5/2)f_2 - h_1 - (3/2)h_o + (3/2)f_o \\
b_n &= (n+3/2)f_n - (n+5/2)f_{n+2} - h_{n+1} && n \geq 1 \\
b_{-1} &= -(3/2)f_1 - (1/2)h_1 - h_o + f_o \\
b_{-2} &= f_1 + (1/2)h_2 + (1/2)h_o - (1/2)f_o \\
b_{-n} &= f_{n-1} + (n-3/2)h_n - (n-5/2)h_{n-2} && n \geq 3
\end{aligned}
$$

$$
\begin{aligned}
c_o &= -(\kappa_i - 1)\gamma m_o \\
c_1 &= g_3 - \kappa_i \gamma m_1 \\
c_n &= -(n+1)g_n + ng_{n+2} - \kappa_i \gamma m_n && n \geq 2 \\
c_{-1} &= 0 \\
c_{-n} &= \kappa_o g_n + \gamma[nm_{n-2} - (n-1)m_n] && n \geq 2 \\
d_o &= (5/2)f_2 + \gamma[(3/2)h_o - \kappa_i h_1] - (3/2)f_o \\
d_n &= -(n+3/2)f_n + (n+5/2)f_{n+2} - \kappa_i \gamma h_{n+1} && n \geq 1 \\
d_{-1} &= (3/2)f_1 + \gamma[(1/2)h_1 - \kappa_i h_o] + \kappa_o f_o \\
d_{-2} &= \kappa_o f_1 - \gamma[(1/2)h_2 + (1/2)h_o] + (1/2)f_o \\
d_{-n} &= \kappa_o f_{n-1} + \gamma[(n-5/2)h_{n-2} - (n-3/2)h_n] && n \geq 3
\end{aligned}
$$

where $\gamma \equiv \mu_o/\mu_i$.

Downloaded 03 May 2010 to 171.66.16.27. Redistribution subject to ASME license or copyright; see http://www.asme.org/terms/Terms_Use.cfm

The Interface Crack in a Tension Field

A. K. Gautesen
Department of Mathematics and Ames Laboratory, Iowa State University, Ames, Iowa 50011

J. Dundurs
Department of Civil Engineering, Northwestern University, Evanston, Ill. 60201

The correct formulation of the interface crack must incorporate contact between the crack faces, because the tips of an interface crack are closed for all applied loads. A numerical solution of the resulting integral equation for an interface crack in a tension field was considered by Comninou several years ago. The present paper shows how to solve the integral equation exactly. The solution is found in the form of a slowly convergent series involving elliptic functions and it is demonstrated how to convert the results into a rapidly convergent series. Specifically, we give simple formulae valid over the entire range of the physical parameters for (1) the length of the contact zones, (2) the Mode II stress intensity factor, and (3) the finite but very large normal stress at the tip of the interface crack.

1 Introduction

The elasticity solutions of the interface crack have an interesting history: The early solutions dating back to 1963 and 1965 (Erdogan, 1963; England, 1965; Rice and Sih, 1965; Erdogan, 1965) were based on the conventional assumption that the tips of the interface crack are open, or, in other words, that there is a direct transition from the bond between the two materials to free crack faces. In consequence they contained the oscillatory singularity discovered by Williams (1959). It was pointed out by England (1965) and Malyshev and Salganik (1965), however, that these solutions are contradictory because the gap between the crack faces is negative on parts of the crack. The zones over which the solution predicts overlapping of material are very small in comparison with the length of the crack for tensile loading, but Willis (1972) found later that overlapping is predicted over a large part of the crack for shear loading.

This longstanding dilemma was resolved in the late seventies by Comninou (1977, 1978, 1979) who showed that the solutions for the interface crack must allow for contact zones at the crack tips. The Comninou formulation is nothing but a recognition that all crack problems are inherently unilateral (involving inequalities), as it is generally not known at the outset whether the crack faces make contact or not. In the unilateral formulation contact between crack faces is allowed, while requiring that the contact tractions be compressive and the gap between the crack faces be positive. The interface crack constitutes an extreme case, in that there must be some contact at the tips regardless of what the applied loads are. This should be obvious without any calculations, as there are only two possibilities: either the tips are open, which leads to the oscillatory singularities and overlapping of material

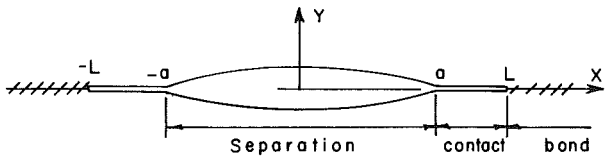


Fig. 1 Geometry of the interface crack

whether or not detached contact zones also exist, or the tips are closed. In dealing with the interface crack in a tension field, Comninou (1977) reduced the problem to a singular integral equation of the first kind and proceeded to solve it by a direct numerical method due to Erdogan and Gupta (1971). However, numerical difficulties were encountered because of the extremely small size of the contact zones at the tips, and results could be obtained only for some extreme mismatches in the elastic constants of the two materials. This problem also was taken up more recently by Atkinson (1982a, 1982b), who used a Mellin transform formulation, but at the end of the calculation had to make certain approximations whose accuracy is difficult to judge. We reconsider this problem because of its very fundamental nature, and show that the Comninou integral equation can be solved analytically. Moreover, we take advantage of the very fact that the contact zones are small to derive sharp one-term approximations which cover the whole range in the mismatch between the elastic constants.

2 Mathematical Preliminaries

The most direct formulation of the problem is achieved by using the results for a distribution of edge dislocations on the interface (Dundurs and Sendeckyj, 1965; Dundurs, 1969; Comninou, 1977). Denoting by $B_x(x)$ the density of the glide array and by $B_y(x)$ that of the climb array, the normal and shear tractions at the interface induced by the dislocations are

$$N(x)=\sigma_{yy}(x,0)=-C\left\{\beta B_x(x)+\frac{1}{\pi}\int_{-\infty}^{\infty}\frac{B_y(\xi)d\xi}{\xi-x}\right\} \qquad (2.1)$$

Contributed by the Applied Mechanics Division for publication in the JOURNAL OF APPLIED MECHANICS.

Discussion on this paper should be addressed to the Editorial Department, ASME, United Engineering Center, 345 East 47th Street, New York, N.Y. 10017, and will be accepted until two months after final publication of the paper itself in the JOURNAL OF APPLIED MECHANICS. Manuscript received by ASME Applied Mechanics Division, April 2, 1985; final revision July 26, 1986.

Copyright © 1987 by ASME
Downloaded 03 May 2010 to 171.66.16.27. Redistribution subject to ASME license or copyright; see http://www.asme.org/terms/Terms_Use.cfm

$$S(x)=\sigma_{xy}(x,0)=-C\left\{-\beta B_y(x)+\frac{1}{\pi}\int_{-\infty}^{\infty}\frac{B_x(\xi)d\xi}{\xi-x}\right\} \quad (2.2)$$

where

$$C=\frac{2\mu_1(1+\alpha)}{(1-\beta^2)(\kappa_1+1)}=\frac{2\mu_2(1-\alpha)}{(1-\beta^2)(\kappa_2+1)} \quad (2.3)$$

$$\alpha=\frac{\mu_2(\kappa_1+1)-\mu_1(\kappa_2+1)}{\mu_2(\kappa_1+1)+\mu_1(\kappa_2+1)} \quad (2.4)$$

$$\beta=\frac{\mu_2(\kappa_1-1)-\mu_1(\kappa_2-1)}{\mu_2(\kappa_1+1)+\mu_1(\kappa_2+1)} \quad (2.5)$$

and $\kappa = 3 - \nu$ for plane strain, with μ and ν denoting shear modulus and Poisson's ratio. Moreover, the dislocation arrays lead to the gap

$$g(x)=u_y(x,0^+)-u_y(x,0^-)=-\int_{-\infty}^{x}B_y(\xi)d\xi \quad (2.6)$$

and tangential shift

$$h(x)=u_x(x,0^+)-u_x(x,0^-)=-\int_{-\infty}^{x}B_x(\xi)d\xi \quad (2.7)$$

between the surfaces of the two solids. Therefore,

$$B_x(x)=-\frac{dh(x)}{dx},\quad B_y(x)=-\frac{dg(x)}{dx} \quad (2.8)$$

The geometry of the problem is shown in Fig. 1. The requirement that the dislocation arrays cancel the applied tension T on the open part of the crack $|x| < a$, and give vanishing shear tractions on the whole crack $|x| < L$, yields immediately on the basis of equations (2.1) and (2.2) the pair of integral equations

$$\beta B_x(x)+\frac{1}{\pi}\int_{-a}^{a}\frac{B_y(\xi)d\xi}{\xi-x}=-\frac{T}{C},\quad |x|<a \quad (2.9)$$

$$\beta[H(x+a)-H(x-a)]B_y(x)-\frac{1}{\pi}\int_{-L}^{L}\frac{B_x(\xi)d\xi}{\xi-x}=0,\quad |x|<L \quad (2.10)$$

where $H(x)$ is the Heaviside step function. Since the gap and tangential shift must not exist outside the intervals $|x| < a$ and $|x| < L$, respectively, the dislocation densities must also satisfy the auxiliary conditions

$$\int_{-L}^{L}B_x(x)dx=0,\quad \int_{-a}^{a}B_y(x)dx=0 \quad (2.11)$$

In addition, the following inequalities must be obeyed:

$$g(x)>0,\quad |x|<a \quad (2.12)$$

$$N(x)<0,\quad a<|x|<L \quad (2.13)$$

It is important to note that the inequalities applied to the vicinity of $|x| = a$, where the transition from contact to separation takes place, require that the density of the climb array vanishes, or $B_y(\pm a) = 0$ (Dundurs and Comninou, 1979). Symmetry about the y axis implies also that $B_x(x)$ is even and $B_y(x)$ is odd in x.

As shown by Comninou (1977), the fact that $B_y(x)$ is bounded can be used to reduce the problem essentially to the single integral equation

$$\int_{-\gamma}^{\gamma}\frac{B_y(r)}{r-s}\left\{1-\beta^2\left(\frac{1-r^2}{1-s^2}\right)^{1/2}\right\}dr=\frac{\pi T}{C},\quad |s|<\gamma=a/L \quad (2.14)$$

where

$$(x,\xi)=L(s,r) \quad (2.15)$$

We shall consider in lieu of equation (2.14), the integral equation

$$\int_E\frac{u(y)}{x-y}\{1-\beta^2\mathrm{sgn}(xy)\}dy=\frac{\pi T}{C}x,\quad x\in E \quad (2.16)$$

where

$$E=\{x:k<|x|<1\},\quad k=(1-\gamma^2)^{1/2} \quad (2.17)$$

$$u(-y)=u(y) \quad (2.18)$$

$$u(\pm 1)=u(\pm k)=0 \quad (2.19)$$

We begin by showing that the integral equations (2.16) and (2.14) are equivalent.

In equation (2.16) we multiply the integrand by $(x+y)/(x+y)$ and use property (2.18) of u being an even function to achieve

$$2\int_k^1\frac{u(y)}{x^2-y^2}\left\{1-\frac{\beta^2 y}{x}\right\}dy=\frac{\pi T}{C},\quad k<x<1 \quad (2.20)$$

Then the substitutions

$$x=(1-s^2)^{1/2},\quad y=(1-r^2)^{1/2} \quad (2.21)$$

$$u(y)=(1-r^2)^{1/2}B_y(r),\quad 0<r<\gamma \quad (2.22)$$

in equation (2.20) yield

$$2\int_0^{\gamma}\frac{rB_y(r)}{r^2-s^2}\left\{1-\beta^2\left(\frac{1-r^2}{1-s^2}\right)^{1/2}\right\}dr=\frac{\pi T}{C},\quad 0<s<\gamma \quad (2.23)$$

Using the property that $B_y(r)$ is an odd function, we can easily show that equation (2.14) reduces to (2.23). Since $B_y(0) = B_y(\gamma) = 0$, we see that equation (2.19) is satisfied.

3 Exact Solution of the Integral Equation

In this section, we give the exact solution to equation (2.16). From the integral identities (A.1) and (A.3) listed in Appendix A, we have

$$\int_E\frac{\sin[n\pi\psi(x)]}{x-y}\{1-\beta^2\mathrm{sgn}(xy)\}dy=-\mathrm{sgn}(x)\left\{\frac{\pi\Delta(n)\cos[n\pi\psi(x)]}{\sinh(n\lambda_o)\cosh(n\lambda_o)}+\frac{(-1)^n\pi\beta^2}{\sinh(n\lambda_o)}\right\},\quad x\in E \quad (3.1)$$

where

$$\psi(x)=F(x)/F(1) \quad (3.2)$$

$$F(x)=\int_k^{|x|}[(1-s^2)(s^2-k^2)]^{-1/2}ds \quad (3.3)$$

$$\Delta(n)=\sinh^2(n\lambda_o)-\beta^2\cosh^2(n\lambda_o) \quad (3.4)$$

$$\lambda_o=\lambda\,\phi_o(k) \quad (3.5)$$

$$\lambda=\pi^2/[2F(1)] \quad (3.6)$$

$$\phi_o(x)=\frac{2}{\pi}\int_o^x[(1-s^2)(k^2-s^2)]^{-1/2}ds \quad (3.7)$$

Comparison of equations (2.16) and (3.1) suggests expanding x in terms of the set of functions $\{\cos[n\pi\psi(x)]\}$ which are complete for $k < x < 1$. Thus,

$$x=\left\{\frac{1}{2}a_o+\sum_{n=1}^{\infty}a_n\cos[n\pi\psi(x)]\right\}\mathrm{sgn}(x),\quad x\in E \quad (3.8)$$

where

$$a_n=2\int_k^1 x\cos[n\pi\psi(x)]\psi'(x)dx=-\frac{2}{n\pi}\int_k^1\sin[n\pi\psi(x)]dx=\frac{(-1)^n 2\lambda}{\pi\cosh(n\lambda_o)} \quad (3.9)$$

Downloaded 03 May 2010 to 171.66.16.27. Redistribution subject to ASME license or copyright; see http://www.asme.org/terms/Terms_Use.cfm

Here, ψ' denotes $d\psi/dx$, and we have substituted from equation (A.5) for the last integral.

We now expand $u(x)$ in the complete set of functions $\{\sin[n\pi\psi(x)]\}$ which also have the properties (2.18) and (2.19). From equations (2.16), (3.1), and (3.8), we find that

$$u(x) = -\frac{2\lambda T}{\pi C}\sum_{n=1}^{\infty}\frac{(-1)^n}{\Delta(n)}\sinh(n\lambda_o)\sin[n\pi\psi(x)] \tag{3.10}$$

will be a solution to equation (2.16) provided that

$$-\beta^{-2} + 2\sum_{n=1}^{\infty}[1/\Delta(n)] = 0 \tag{3.11}$$

The left side of equation (3.11) is basically the coefficient of the term containing $\mathrm{sgn}(x)$ when equations (3.10) and (3.8) are substituted into (2.16). Since there is no solution to

$$\int_E \frac{u(y)}{x-y}\{1-\beta^2\mathrm{sgn}(xy)\}dy = \mathrm{sgn}(x), \quad x\in E \tag{3.12}$$

which satisfies equation (2.19), it is necessary that equation (3.11) be satisfied. Thus, equation (3.11) determines the relationship between β and $\gamma = a/L$.

4 Physical Quantities

Equation (3.11) can be solved to any desired accuracy by Newton's iteration. It is possible, however, to derive a simple and a highly accurate expression which relates k and β explicity. For this purpose, we observe that equation (3.11) can be expressed as $S_1(\pi) = 0$, where

$$S_1(w) = \sum_{n=-\infty}^{\infty}(-1)^n\cos(nw)/\Delta(n) \tag{4.1}$$

From equation (B.12), we have

$$S_1(\pi) \approx -(\pi/\beta\lambda_o)\{\cot[\pi\beta_o/(2\lambda_o)] + \beta_o/\pi\} = 0 \tag{4.2}$$

with

$$\beta_o = \log[(1+\beta)/(1-\beta)] \tag{4.3}$$

The physically correct solution to equation (4.2) is

$$\pi\beta_o/(2\lambda_o) = \tan^{-1}(\beta_o/\pi) + \pi/2 \tag{4.4}$$

and from the results of Appendix C,

$$\lambda_o \approx \lambda \approx \pi^2/[2\log(4/k)] \tag{4.5}$$

Then after substituting (4.5) into (4.4) and solving for k, we find

$$k^2 = 1-(a/L)^2 = 16\exp\{-(\pi^2/\beta_o)[(2/\pi)\tan^{-1}(\beta_o/\pi)+1)\} \tag{4.6}$$

The error in the approximation (4.2) is $0(k^4)$ and the error in (4.5) is $0(k^2/\log k)$. Thus, the approximation (4.6) will be accurate to at least 4 significant figures over the range $0 < \beta < 1/2$.

Equation (4.2) also has the solutions

$$\pi\beta_o/(2\lambda_o) = \tan^{-1}(\beta_o\pi) + \pi(n+1/2), \quad n=1,2,3,\ldots \tag{4.7}$$

We show in Appendix D that these solutions produce a negative gap, which confirms the conclusion by Shield (1982) that the interface crack in the Comninou formulation has a unique solution.

We now compute the stresses $\sigma_{xy}(s,0)$ and $\sigma_{yy}(s,0)$. From the paper by Comninou (1977),

$$\sigma_{xy}(s,0) = -C\beta(\pi t)^{-1}I_1\mathrm{sgn}(s), \quad |s|>1 \tag{4.8}$$

$$\sigma_{yy}(s,0) = \begin{cases} T + C\pi^{-1}\{\beta^2 I_1/t - I_o\}, & \gamma<|s|<1 \\ T - CI_o/\pi, & |s|>1 \end{cases} \tag{4.9}$$

where

$$I_j = \int_{-\gamma}^{\gamma}(1-r^2)^{j/2}B_y(r)/(r-s)ds, \quad j=0,1 \tag{4.10}$$

$$t = |1-s^2|^{1/2} \tag{4.11}$$

Since B_y is an odd function of r, equation (4.10) can also be expressed as

$$I_j = 2\int_0^{\gamma}(1-r^2)^{j/2}r\,B_y(r)/(r^2-s^2)dr \tag{4.12}$$

Making the change of integration variables (2.24) and substituting from equation (2.25) yields

$$I_j = 2\int_k^1 y^j u(y)/(1-s^2-y^2)dy \tag{4.13}$$

Finally upon substitution for u from equation (3.10) in (4.13) we find

$$I_j = \frac{4\lambda T}{\pi C}\sum_{n=1}^{\infty}(-1)^{n+1}[\Delta(n)]^{-1}\sinh(n\lambda_o)\int_k^1\{y^j\sin[n\pi\psi(y)]/(1-s^2-y^2)\}dy \tag{4.14}$$

The integrals in (4.14) are given by (A.1)–(A.4). Also, note that (4.14) remains unchanged if we divide the right side by 2 and change the lower limit of summation to $-\infty$. The results are

$$I_o = \frac{\lambda T}{Ct}\begin{cases} S_4[\lambda\phi_o(t)], & \gamma\le|s|\le 1 \\ S_3[\lambda q_o(t)], & 1<|s| \end{cases} \tag{4.15}$$

$$I_1 = \frac{\lambda T}{C}\begin{cases} S_5[\lambda\phi_o(t)] - S_1(\pi), & \gamma\le|s|\le 1 \\ S_1[\lambda q_o(t)] - S_1(\pi), & 1<|s| \end{cases} \tag{4.16}$$

where

$$S_3(w) = \sum_{n=-\infty}^{\infty}(-1)^n\tanh(n\lambda_o)\sin(nw)/\Delta(n) \tag{4.17}$$

$$S_4(w) = \sum_{n=-\infty}^{\infty}(-1)^n\tanh(n\lambda_o)\sinh(nw)/\Delta(n) \tag{4.18}$$

$$S_5(w) = \sum_{n=-\infty}^{\infty}(-1)^n\cosh(nw)/\Delta(n) \tag{4.19}$$

$$q_o(t) = \frac{2}{\pi}\int_0^t[(1+s^2)(k^2+s^2)]^{-1/2}ds \tag{4.20}$$

and λ_o, λ, and ϕ_o are given by (3.5)–(3.7). In equation (4.16), $S_1(\pi) = 0$.

When equations (4.15) and (4.16) are substituted into equations (4.8) and (4.9), we obtain exact expressions for σ_{xy} and σ_{yy}. We now give small k approximations to all quantities. From Appendix C, we have

$$\phi_o(x) = (2/\pi)\sin^{-1}(x/k) + 0(k^2) \tag{4.21}$$

$$q_o(x) = \frac{2}{\pi}\log\left\{\frac{2[x+(x^2+k^2)^{1/2}}{k[1+(x^2+1)^{1/2}]}\right\} + 0(k^2\log k), \; x>0 \tag{4.22}$$

The small k approximations to λ and λ_o given by equation (4.5) become, upon substitution from equation (4.6)

$$\lambda_o = \lambda = \pi\beta_o/[\pi + 2\tan^{-1}(\beta_o/\pi)] \tag{4.23}$$

Small k approximations for S_1, S_3, S_4, and S_5 are given by equations (B.11), (B.16), (B.17), and (B.18). The results are:

$$t\sigma_{yy}(s,0)/T = t + (1+\beta_o^2/\pi^2)^{1/2}(\sinh w_1 - \beta\cosh w_1) - k\sin[\pi\phi_o(t)/2], \quad \gamma<|s|<1 \tag{4.24}$$

Downloaded 03 May 2010 to 171.66.16.27. Redistribution subject to ASME license or copyright; see http://www.asme.org/terms/Terms_Use.cfm

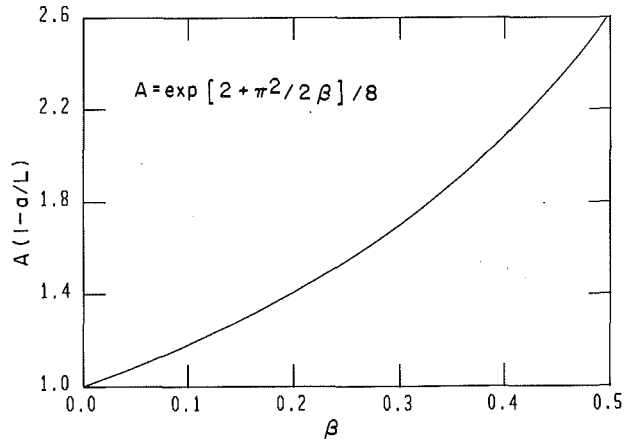


Fig. 2 Extent of contact

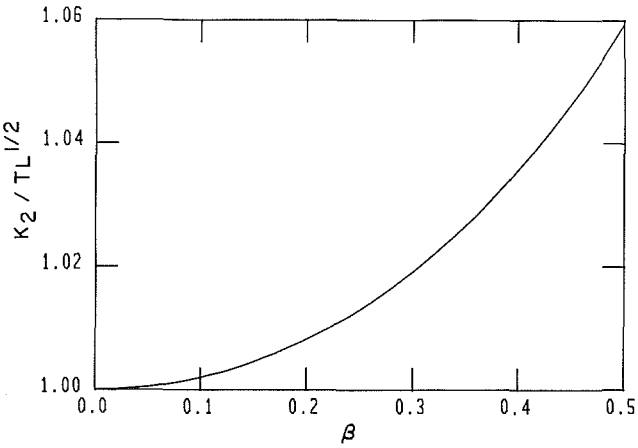


Fig. 3 Mode II stress intensity factor

$$t\sigma_{yy}(s,0)/T = t + (1+\beta_o^2/\pi^2)^{1/2}\sin w_2 + \hat{S}_3(w) - \hat{S}_3(-w), \quad |s|>1 \tag{4.25}$$

$$t\sigma_{xy}(s,0)\mathrm{sgn}(s)/T = (1+\beta_o^2/\pi^2)^{1/2}\cos w_2 + \hat{S}_1(w) + \hat{S}_1(-w), \quad |s|>1 \tag{4.26}$$

where

$$w = \lambda q_o(t) \tag{4.27}$$

$$w_1 = \beta_o \phi_o(t)/2 \tag{4.28}$$

$$w_2 = \beta_o q_o(t)/2 \tag{4.29}$$

$$\hat{S}_1(w) = 2\sin[\beta_o(\pi - w)/(2\lambda)]E_o(w)/[1-E_o(w)] \tag{4.30}$$

$$\hat{S}_3(w) = 2E_o(w)\{\cos[\beta_o(\pi-w)/(2\lambda)] - E_o^{-1/2}(w)\}/[1-E_o(w)] \tag{4.31}$$

$$E_o(w) = \exp[-\pi(\pi - w)/\lambda] \tag{4.32}$$

The error in the right sides of (4.24)-(4.26) is $0(k^2)$.

The stress intensity factor K_2 is defined by

$$K_2 = L^{1/2}\lim_{s\to 1^+}[t\sigma_{xy}(s,0)] \tag{4.33}$$

From equation (4.26), we find

$$K_2 = L^{1/2}T[(1+\beta_o^2/\pi^2)^{1/2} + 0(k^2)] \tag{4.34}$$

Moreover, from equation (4.25),

$$\sigma_{yy}(1^+,0) = (T\beta_o/\pi k)(1+\beta_o^2/\pi^2)^{1/2}[1+0(k^2)] \tag{4.35}$$

From equation (4.24), it follows that

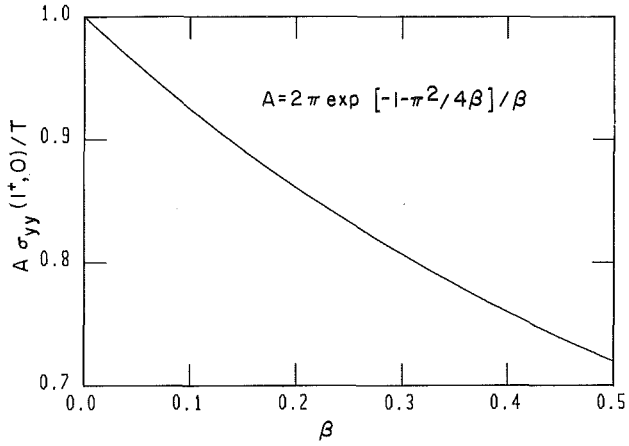


Fig. 4 Tension in the bonded region at the tip of the crack

$$\sigma_{yy}(s,0) < 0, \ \gamma < |s| < 1 \tag{4.36}$$

and that

$$\lim_{s\to 1^-}[t\sigma_{yy}(s,0)] = -\beta K_2/L^{1/2} \tag{4.37}$$

which agrees with the result observed by Comninou (1977).

5 Results and Discussion

As the contact zones are very short in comparison to the length of the crack, the one-term approximations in Section 4 give sufficiently accurate results over the whole physical range of $0 < \beta \leq 1/2$. The results, using the normalizing factors shown on the graphs, are plotted in Figs. 2, 3, and 4.

The extent of contact computed from equation (4.6) is shown in Fig. 2. This quantity also was computed exactly using the series, but no significant difference was detected. Noting the normalizing factor used, it is seen from Fig. 2 that the extent of contact vanishes as $\beta \to 0$.

The Mode II stress intensity factor from equation (4.34) is plotted versus β in Fig. 3. As already found by Comninou (1977), the variation with β is very small. The limit for $\beta = 0$, however, is singular, and K_2 on the graph does not approach zero.

The finite, but very large, tension in the bonded region near the crack tip given by equation (4.35) is plotted in Fig. 4. It is seen from the normalizing factor used that this tension grows exponentially as $\beta \to 0$.

The only numerical results reported previously in the literature are for $\beta = 0.4854$. Comninou (1977) found $1-a/L = 10^{-4}$ and $\sigma_{yy}(L^+, 0) = 23.36\mathrm{T}$, while Atkinson (1982b) gave $(0.9484)10^{-4}$ and $25.85\mathrm{T}$, respectively. Our results are $1-a/L = (1.0517)\ 10^{-4}$ and $\sigma_{yy}(L^+, 0) = 24.54\mathrm{T}$. For $1-a/L = 10^{-7}$, Comninou reported $\beta = 0.4239$, but we find $\beta = 0.2952$.

Acknowledgment

This work was supported in part by the Applied Mathematical Sciences subprogram of the Office of Energy Research, US Department of Energy, under Contract No. W-7405-ENG-82.

References

Atkinson, C., 1982, "The Interface Crack With a Contact Zone (An Analytical Treatment)," *International Journal of Fracture*, Vol. 18, pp. 161-177.

Atkinson, C., 1982, "The Interface Crack With a Contact Zone (The Crack of Finite Length)," *International Journal of Fracture*, Vol. 19, pp. 131-138.

Comninou, M., 1977a, "A Property of Interface Dislocations," *Philosophical Magazine*, Vol. 36, pp. 1281-1283.

Downloaded 03 May 2010 to 171.66.16.27. Redistribution subject to ASME license or copyright; see http://www.asme.org/terms/Terms_Use.cfm

Comninou, M., 1977b, "The Interface Crack," ASME JOURNAL OF APPLIED MECHANICS, Vol. 44, pp. 631–636.
Comninou, M., 1978, "The Interface Crack in a Shear Field," ASME JOURNAL OF APPLIED MECHANICS, Vol. 45, pp. 287–290.
Comninou, M., and Schmueser, D., 1979, "The Interface Crack in a Combined Tension-Compression and Shear Field," ASME JOURNAL OF APPLIED MECHANICS, Vol. 46, pp. 345–348.
Comninou, M., and Dundurs, J., 1980, "On the Behavior of Interface Cracks," *Res Mechanica*, Vol. 1, pp. 249–264.
Dundurs, J., and Sendeckyj, G. P., 1965, "Behavior of an Edge Dislocation Near a Bimetallic Interface," *Journal of Applied Physics*, Vol. 36, pp. 3353–3354.
Dundurs, J., 1969, "Elastic Interaction of Dislocations With Inhomogeneities," in *Mathematical Theory of Dislocations*, Mura, T., ed., pp. 70–115, American Society of Mechanical Engineers, New York.
Dundurs, J., and Comninou, M., 1979, "Some Consequences of the Inequality Conditions in Contact and Crack Problems," *Journal of Elasticity*, Vol. 9, pp. 71–82.
England, A. H., 1965, "A Crack Between Dissimilar Media," ASME JOURNAL OF APPLIED MECHANICS, Vol. 32, pp. 400–402.
Erdogan, F., 1963, "Stress Distribution in a Nonhomogeneous Elastic Plane With Cracks," ASME JOURNAL OF APPLIED MECHANICS, Vol. 30, pp. 232–237.
Erdogan, F., 1965, "Stress Distribution in Bonded Dissimilar Materials With Cracks," ASME JOURNAL OF APPLIED MECHANICS, Vol. 32, pp. 403–410.
Erdogan, F., and Gupta, G., 1972, "On the Numerical Solution of Singular Integral Equations," *Quarterly of Applied Mathematics*, Vol. 29, pp. 525–539.
Gautesen, A. K., and Dundurs, J., 1987, "On the Solution to a Cauchy Principal Value Integral Equation Which Arises in Fracture Mechanics," *SIAM Journal on Applied Mathematics*, in press.
Malyshev, B. M., and Salganik, R. L., 1965, "The Strength of Adhesive Joints Using the Theory of Fracture," *International Journal of Fracture Mechanics*, Vol. 1, pp. 114–128.
Rice, J. R., and Sih, G. C., 1965, "Plane Problems of Cracks in Dissimilar Media," ASME JOURNAL OF APPLIED MECHANICS, Vol. 32, pp. 418–423.
Shield, R. T., 1982, "Uniqueness for Elastic Crack and Punch Problems," ASME JOURNAL OF APPLIED MECHANICS, Vol. 49, pp. 516–518.
Williams, M. L., 1959, "The Stresses Around a Fault or Crack in Dissimilar Media," *Bulletin of the Seismological Society of America*, Vol. 49, pp. 199–204.
Willis, J. R., 1972, "The Penny-Shaped Crack on an Interface," *Quarterly Journal of Mechanics and Applied Mathematics*, Vol. 25, pp. 367–385.

APPENDIX A

In this Appendix, we list the following integral identities derived by Gautesen and Dundurs (1987):

$$\int_E \frac{\sin[n\pi\psi(y)]}{x-y}\,dy = 2x\int_k^1 \frac{\sin[n\pi\psi(y)]}{x^2-y^2}\,dy$$
$$= G_n\begin{cases}\cos[n\pi\psi(x)]\mathrm{sgn}(x), & x\in E\\ \sinh[n\lambda\phi_o(x)]/\sinh(n\lambda_o), & 0\le|x|\le k\end{cases} \quad (A.1)$$

$$\int_k^1 \frac{\sin[n\pi\psi(y)]}{\tau^2+y^2}\,dy = -\frac{G_n}{2\tau}\sin[n\lambda q_o(\tau)]/\sinh(n\lambda_o), \quad |\tau|<\infty \quad (A.2)$$

$$\int_E \frac{\mathrm{sgn}(y)\sin[n\pi\psi(y)]}{x-y}\,dy = 2\int_k^1 \frac{y\sin[n\pi\psi(y)]}{x^2-y^2}\,dy$$
$$= H_n\begin{cases}\dfrac{(-1)^{n+1}}{\cosh(n\lambda_o)}+\cos[n\pi\psi(x)], & x\in E\\ [(-1)^{n+1}+\cosh[n\lambda\phi_o(x)]/\cosh(n\lambda_o), & 0\le|x|\le k\end{cases} \quad (A.3)$$

$$\int_k^1 \frac{y\sin[n\pi\psi(y)]}{\tau^2+y^2}\,dy = -\frac{H_n}{2\cosh(n\lambda_o)}\{(-1)^{n-1}+\cos[n\lambda q_o(\tau)]\}, \quad |\tau|<\infty \quad (A.4)$$

$$b_n = \int_k^1 \sin[n\pi\psi(y)]dy = (-1)^{n+1}\lambda n/\cosh(n\lambda_o) \quad (A.5)$$

$$c_n = \int_k^1 y\sin[n\pi\psi(y)]dy = (-1)^{n+1}\pi^{-1}(\lambda n)^2/\sinh(n\lambda_o) \quad (A.6)$$

Here, ψ, λ, λ_o, ϕ_o, and q_o are defined by equations (3.2), (3.5)–(3.7), and (4.20), respectively. Moreover,

$$G_n = -\pi\tanh(n\lambda_o) \quad (A.7)$$

$$H_n = -\pi\coth(n\lambda_o) \quad (A.8)$$

APPENDIX B

In this Appendix we convert three slowly convergent series into rapidly convergent forms.

We begin with the series $S_1(w)$ defined by

$$S_1(w) = \sum_{n=-\infty}^{\infty}(-1)^n[\Delta(n)]^{-1}\cos(nw) \quad (B.1)$$

where $\Delta(n)$ is defined by equation (3.4). Consider the integral in the complex plane:

$$I = \frac{1}{2i}\int_{C_\infty}\cos(zw)/[\Delta(z)\sin(\pi z)]dz, \quad |w|<\pi \quad (B.2)$$

where C_∞ is a large circle. Near infinity, the integrand has exponential decay. Thus, $I = 0$. The integrand has simple poles at

$$z = n,\ \pm(\sigma+i\tau_n),\quad n=0,\ \pm1,\ \pm2,\ \ldots \quad (B.3)$$

where

$$\sigma = (2\lambda_o)^{-1}\log[(1+\beta)/(1-\beta)] = \beta_o/(2\lambda_o) \quad (B.4)$$

$$\tau_n = n\pi/\lambda_o \quad (B.5)$$

Thus we can also evaluate the integral I by summing the residues. The result is

$$0 = S_1(w) + \frac{\pi}{\beta\lambda_o}\Bigg\{\frac{\cos(\sigma w)}{\sin(\sigma\pi)} + 2\sum_{n=1}^{\infty}\{\sin[\sigma(\pi-w)]\cosh[\tau_n(\pi+w)] + \sin[\sigma(\pi+w)]\cosh[\tau_n(\pi-w)]\}/[\cosh(2\pi\tau_n)-\cos(2\pi\sigma)]\Bigg\} \quad (B.6)$$

which is an alternate form of $S_1(w)$. To improve the convergence of the series in equation (B.6) for $|w|$ near π, we add and subtract the term $\hat{S}_1(w) + \hat{S}_1(-w)]$ where

$$\hat{S}_1(w)/\sin[\sigma(\pi-w)] = 2e^{-\tau_1(\pi-w)}/[1-e^{-\tau_1(\pi-w)}]$$
$$= 2\sum_{n=1}^{\infty}e^{-\tau_n(\pi-w)} \quad (B.7)$$

The result is

$$S_1(w) = -\frac{\pi}{\beta\lambda_o}\Bigg\{\frac{\cos(\sigma w)}{\sin(\sigma\pi)} + \hat{S}_1(w) + \hat{S}_1(-w) + \sin[\sigma(\pi-w)]\bar{S}_1(w) + \sin[\sigma(\pi+w)]\bar{S}_1(-w)\Bigg\} \quad (B.8)$$

with

$$\bar{S}_1(w) = 2\sum_{n=1}^{\infty}e^{-2\pi\tau_n}\{\sinh[\tau_n(\pi-w)] + \cos(2\pi\sigma)e^{\tau_n(\pi+w)}\}/[\cosh(2\pi\tau_n)-\cos(2\pi\sigma)] \quad (B.9)$$

We note that for $|w| \le \pi$, $\bar{S}_1(w) = 0(E^2)$ where

$$E = e^{-\pi\tau_1} = e^{-\pi^2/\lambda_o} \quad (B.10)$$

The value of E is about 10^{-5} for $\beta = 0.5$, and E decreases exponentially with decreasing β. Thus equation (B.8) becomes

$$S_1(w) = -\frac{\pi}{\beta\lambda_o}\Bigg\{\frac{\cos(\sigma w)}{\sin(\sigma\pi)} + \hat{S}_1(w) + \hat{S}_1(-w) + 0(k^4)\Bigg\} \quad (B.11)$$

Downloaded 03 May 2010 to 171.66.16.27. Redistribution subject to ASME license or copyright; see http://www.asme.org/terms/Terms_Use.cfm

Here, we have written $0(k^4)$ for $0(E^2)$, since it follows from equations (B.10), (4.6), and (4.4) that $E \approx k^2/16$. At $w = \pi$, we have

$$S_1(\pi) = -\frac{\pi}{\beta\lambda_o}\left\{\cot(\sigma\pi) + \frac{1}{\pi}\log\left(\frac{1+\beta}{1-\beta}\right) + 0(k^4)\right\} \quad (B.12)$$

Proceeding in the same manner, we can show that the series

$$S_2(w) = \sum_{n=-\infty}^{\infty} (-1)^n [\Delta(n)]^{-1} \sinh(n\lambda_o)\sin(nw) \quad (B.13)$$

can be approximated by

$$S_2(w) = -\frac{\pi}{\lambda_o(1-\beta^2)^{1/2}}\left\{\frac{\sin(\sigma w)}{\sin(\sigma\pi)} - \hat{S}_2(w) + 0(k^2)\right\}, \quad 0 \le w \le \pi \quad (B.14)$$

where

$$\hat{S}_2(w) = 2\cos[\sigma(\pi - w)]e^{-\tau_1(\pi-w)}/[1 + e^{-\tau_1(\pi-w)}] \quad (B.15)$$

For $w \geq 0$, $\hat{S}_2(-w)$ is $0(k^2)$.

Likewise, it can be shown that the series defined by equations (4.18)–(4.20) can be approximated by

$$S_3(w) = -\frac{\pi}{\lambda_o}\left\{\frac{\sin(w\sigma)}{\sin(\pi\sigma)} + \hat{S}_3(w) - \hat{S}_3(-w) + 0(k^2)\right\} \quad (B.16)$$

$$S_4(w) = -iS_3(iw) = -\frac{\pi}{\lambda_o}\left\{\frac{\sinh(w\sigma)}{\sin(\sigma\pi)} - 4e^{-\pi\tau_1/2}\sin(w\tau_1/2) + 0(k^2)\right\} \quad (B.17)$$

$$S_5(w) = S_1(iw) = -\frac{\pi}{\lambda_o\beta}\left\{\frac{\cosh(\sigma w)}{\sin(\sigma\pi)} + 0(k^2)\right\} \quad (B.18)$$

where $\hat{S}_3(w)$ is given by equation (4.31).

APPENDIX C

In this Appendix, we give small k approximations to $F(1)$, λ, $\phi_o(x)$, λ_o, and $q_o(t)$.

We begin with $F(1)$ and λ defined by equations (3.3) and (3.6). We note the identity:

$$\frac{1}{[P(s)]^{1/2}} - \frac{1}{s(1-s^2)^{1/2}} - \frac{1}{(s^2-k^2)^{1/2}} + \frac{1}{s} = \frac{k^2}{[P(s)]^{1/2}} \frac{s}{[1+(1-s^2)^{1/2}][s+(s^2-k^2)^{1/2}]} \quad (C.1)$$

where $P(x) = (1-x^2)(x^2-k^2)$. The maximum value of the term inside the braces is about 0.5. Operation on equation (C.1) with $\int_k^1 ds$ yields

$$F(1) \approx \log\{[1+(1-k^2)^{1/2}]^2/k\} \approx \log(4/k) + 0(k^2\log k) \quad (C.2)$$

From equation (3.6), we obtain

$$\lambda = \pi^2/[2\log(4/k)] + 0(k^2/\log k) \quad (C.3)$$

Next, we consider $\phi_o(x)$ and λ_o. In equation (3.7), we make the change of integration variables $s = kt$ followed by $(1-k^2t^2) \approx 1 + 0(k^2)$ to achieve equation (4.21). Then substitution from equations (4.21) and (C.3) into equation (3.5) yields equation (4.5).

By a computation similar to that used to approximate $F(1)$, we can show that $q_o(x)$ can be approximated by equation (4.22).

APPENDIX D

We show in this Appendix that the extraneous solutions defined by equation (4.7) violate equation (2.12). The gap $g(s)$ can be expressed as

$$g(s) = \int_s^\gamma B_y(r)dr, \quad 0 \le s \le \gamma \quad (D.1)$$

Upon substitution from equations (2.21) and (2.22), we find that

$$\bar{g}(x) = \int_k^x u(y)(1-y^2)^{-1/2}dy, \quad k \le x \le 1 \quad (D.2)$$

where $\bar{g}(x) = g(s)$. In the expression (3.10) for u, the series is given by $S_2[\pi\psi(x)]/2$, where S_2 is defined by equation (B.13). The small k approximation to S_2 is given by equation (B.14). Since $\exp(-\pi\tau_1) = \exp(-\pi^2/\lambda_o) \approx k^2/16$ we can ignore the term $\hat{S}_2(w)$ (defined by equation (B.15)) because we are not interested in values of w near π. Then upon substitution of this approximation into equation (3.10), we find that equation (D.2) becomes

$$\bar{g}(x) = b\int_k^x (1-y^2)^{-1/2}\sin[\sigma\pi\psi(y)]dy, \quad k \le x \le 1 \quad (D.3)$$

where σ follows from equations (B.4) and (4.7) as

$$\sigma = n + 1/2 + \tan^{-1}(\beta_o\pi)/\pi \quad (D.4)$$

and

$$b = \lambda T/[\lambda_o C(1-\beta^2)^{1/2}\sin(\sigma\pi)] \quad (D.5)$$

If n is an odd integer, $b < 0$ because $\sin(\sigma\pi) < 0$. Since $\psi(y)$ increases from 0 to 1 as y increases from k to 1, we see from equation (D.5) that the gap will be negative for x sufficiently close to k. Thus n is an even integer.

We now eliminate this possibility. When n is an even integer, $b > 0$ since $\sin\sigma\pi > 0$. We shall only be interested in the case where

$$x = \bar{x} \equiv k\cosh[1.5\log(4/k)\sigma] = 0(k^{1-1.5/\sigma}) \quad (D.6)$$

For $n = 2,4,6, \ldots, 1 - 1.5/\sigma > 0$. Thus in (D.3), we approximate $(1-y^2)^{-1/2}$ by 1. To obtain a small k approximation to $\psi(x)$, we make a similar approximation in equation (3.3). Then from equations (3.2) and (C.2), we find that

$$\psi(y) = \log[\{y + (y^2-k^2)^{1/2}\}/k]/\log[4/k], \quad k \le y \le \bar{x} \quad (D.7)$$

Upon substitution of equations (D.7) and (D.6) into equation (D.3) and making the change of integration variable $y = k\cosh t$, we obtain

$$\bar{g}(\bar{x}) = bk\int_o^{1.5\pi/b_1} \sin(b_1 t)\sinh t\, dt \quad (D.8)$$

where $b_1 = \sigma\pi/\log(4/k)$. After performing the integration in equation (D.8), we find

$$\bar{g}(\bar{x}) = -bk(1+b_1^2)^{-1}\cosh(1.5\pi/b_1) < 0 \quad (D.9)$$

Thus, if n is an even positive integer, the gap is also negative. We remark that this demonstration fails when $n = 0$, because in this case both b and $\sin[\sigma\pi\psi(y)]$ are positive in equation (D.3).

Downloaded 03 May 2010 to 171.66.16.27. Redistribution subject to ASME license or copyright; see http://www.asme.org/terms/Terms_Use.cfm

On the Numerical Boundary Integral Equation Method for Three-Dimensional Dynamic Shear Crack Problems

S. Das
Lamont-Doherty Geological Observatory
of Columbia University,
Palisades, NY 10964

B. V. Kostrov
Institute of Physics of the Earth,
Academy of Sciences,
Moscow, USSR

The numerical boundary integral equation method for the solution of dynamic shear crack problems is discussed in detail, including the questions of the numerical approximation, stability, and efficiency. In particular, the necessary conditions for stability are developed. In addition to a discussion of the original algorithm proposed by Das (1980), a new version is proposed which is more efficient for some important particular cases, due to the fact that the domain of integration for the necessary convolutions is limited only to the slipping part of the crack plane instead of the entire disturbed area of the crack plane.

Introduction

In the last two decades, significant progress has been made in understanding the process of fracture at the source of an earthquake and the resulting ground motions by modelling earthquakes as dynamic shear cracks. The main goal of such forward problems is to gain insight into the possible speed of fracturing of earthquake faults and the slip history and distribution on the fault. In the early 1960's, simple problems were studied analytically by modelling earthquakes as two and three-dimensional self-similar shear cracks, usually propagating at some known velocity. Later, spontaneous shear cracks, in which a fracture criterion was used to determine the fracture process, were introduced. The solution of some very useful self-similar problems during the 1960's (e.g., Kostrov, 1964, 1966) provided an understanding of how the slip on a fault initiates and propagates during earthquakes. Very special techniques had to be used for the solution of these problems and new methods had to be developed for the solution of each particular problem. Moreover, since cracks in the earth are finite and eventually come to a stop, the self-similar solutions were limited in their applicability. On the other hand, it was impossible to write down the necessary solutions in closed form for finite cracks and so numerical algorithms had to be introduced. Numerical methods have the advantage that the same algorithm can be applied to many particular cases. The first numerical solution for finite shear cracks was developed by Burridge (1969) for two-dimensional shear crack problems. Madariaga (1976), Day (1979, 1982), Das (1980, 1981), and Virieux and Madariaga (1982) developed numerical solutions for three-dimensional shear crack problems. The introduction of numerical algorithms allowed the solution of problems which could not be approached analytically and resulted in solution of problems of shear cracks propagating on planes having variable strength and frictional properties.

The numerical methods being used at present to study shear crack problems can be divided into two groups – the finite difference (Madariaga, 1976; Virieux and Madariaga, 1982; Andrews, 1976a, b) and finite element (Day, 1979, 1982) methods on the one hand and the boundary-integral methods (Burridge, 1969; Das and Aki, 1977; Das, 1980, 1981, 1985; Burridge and Moon, 1981; Andrews, 1985) on the other.

The finite difference/element methods are very flexible and permit the introduction of inhomogeneous properties of the medium and the study of nonplanar shear cracks, though these have not yet been done. The boundary-integral methods (c.f. Cruse and Rizzo, 1975; Kupradze, 1963, for general discussion of the boundary integral methods in elastodynamics) are far less flexible in this context, but, on the other hand, for the problem of planar cracks in a medium that is homogeneous everywhere off the crack plane, it is more efficient for many problems of major interest in seismology.

In this paper, we first discuss some details of the boundary-integral method developed by Das (1980) for the study of three-dimensinal dynamic shear crack propagation, including the questions of its stability and efficiency. Then, motivated by the approach of Burridge (1969) and Burridge and Moon (1981), we propose a new method which is more efficient for the solution of some particularly important problems.

Formulation of the Problem

Consider an unbounded medium containing a plane shear crack. The medium is taken as homogeneous, isotropic and linearly elastic everywhere off the crack plane. Let the crack plane be the plane $x_3 = 0$ in the Cartesian coordinate system

Contributed by the Applied Mechanics Division for publication in the JOURNAL OF APPLIED MECHANICS.
Discussion on this paper should be addressed to the Editorial Department, ASME, United Engineering Center, 345 East 47th Street, New York, N.Y. 10017, and will be accepted until two months after final publication of the paper itself in the JOURNAL OF APPLIED MECHANICS. Manuscript received by ASME Applied Mechanics Division, December 3, 1985; final revision July 11, 1986.

Copyright © 1987 by ASME
Downloaded 03 May 2010 to 171.66.16.27. Redistribution subject to ASME license or copyright; see http://www.asme.org/terms/Terms_Use.cfm

$0x_1x_2x_3$ (Fig. 1). At an initial instant of time ($t=0$), let the medium be in equilibrium under an initial stress distribution $\sigma^0{}_{ij}(\mathbf{x})$, where $\mathbf{x}$ denotes the point (x_1, x_2, x_3). In what follows, bold letters denote vectors, Latin subscripts take values 1, 2, 3 and Greek ones the values 1, 2, the Einstein summation convention being assumed. Let us assume that the body forces (if present) are time-independent. Then the displacement vector $u_i(\mathbf{x},t)$and the stress perturbation tensor

$$\tau_{ij}(\mathbf{x},t)=\sigma_{ij}(\mathbf{x},t)-\sigma^0{}_{ij}(\mathbf{x}) \tag{1}$$

will satisfy the homogeneous governing equations of linear elastodynamics and the initial conditions

$$u_i=0,\tau_{ij}=0 \text{ at } t=0 \tag{2}$$

Let us denote the crack area as $\Sigma(t)$, the initial crack area being $\Sigma(0)$. Outside the crack surface, the medium is continuous (i.e., u_i and τ_{ij} are continuous across the plane $x_3=0$).

$$[u_i]\equiv u_i\,|_{x_3=+0}-u_i\,|_{x_3=-0}=0$$
$$\text{on } \bar{\Sigma}(t) \tag{3}$$
$$[\tau_{ij}]\equiv \tau_{ij}\,|_{x_3=+0}-\tau_{ij}\,|_{x_3=-0}=0$$

where $\bar{\Sigma}(t)$ denotes the complement of $\Sigma(t)$ on the entire plane $x_3=0$.

For shear cracks, the normal component of displacement must be continuous across the crack surface. Because no external forces are assumed to act on the crack surface, the tractions τ_{i3} must also be continuous. An obvious feature of the problem is that u_3, τ_{13}, and τ_{23} are even functions of x_3 while u_1, u_2, and τ_{33} are odd functions of x_3. Consequently,

$$\tau_{33}=0 \text{ everywhere at } x_3=0$$
$$u_1=0,\ u_2=0 \text{ on } \bar{\Sigma}(t) \tag{4}$$

Moreover, the slip

$$[u_i]\equiv u_i\,|_{x_3=+0}-u_i\,|_{x_3=-0}=2u_i\,|_{x_3=+0}.$$

On the crack surface $\Sigma(t)$, some governing conditions for slip must be assumed. In the simplest case, the tractions τ_{13} and τ_{23} are assumed to be known. In this paper, we shall assume that two independent relations between displacement components (u_1, u_2), displacement rate components ($\dot{u}_1$, $\dot{u}_2$) and traction components (σ_{13}, σ_{23}, σ_{33}) are given. In terms of the traction perturbations, these relations may be written as

$$S_1(u_1,u_2,\dot{u}_1,\dot{u}_2,\tau_{13},\tau_{23})=0$$
$$\text{on } \Sigma(t) \tag{5}$$
$$S_2(u_1,u_2,\dot{u}_1,\dot{u}_2,\tau_{13},\tau_{23})=0$$

where dots denote time derivatives. The traction perturbation has only tangential components since the normal component of traction remains undisturbed for plane shear cracks. Obviously, the functions S_1 and S_2 also depend on the initial tractions $\sigma_{i3}{}^0$. Equation (5) includes such cases as dry or viscous friction, slip-weakening, etc. In general, the functions S_1 and S_2 are nonlinear and may be time and position dependent. Equations (4) and (5) comprise mixed boundary conditions at $x_3=0$.

To complete the formulation of the problem, an edge condition at the border of $\Sigma(t)$ is necessary for uniqueness of the solution. A sufficient condition is that the displacement components u_1, u_2 must be continuous functions of x_1 and x_2 (and, consequently, must vanish at the edge). In general, the crack area $\Sigma(t)$ is unknown and must be found from a fracture criterion, which is usually formulated in terms of the stress intensity factor at the crack edge. In a numerical method, the stress singularity is "smeared out" and adequate discrete representation of the fracture criterion is a difficult problem. Some approaches to this problem were undertaken in numerical schemes for studying tension crack problems. We refer to the review paper of Atluri and Nishioka (1985) for a complete bibliography and summary of this. In this paper, we

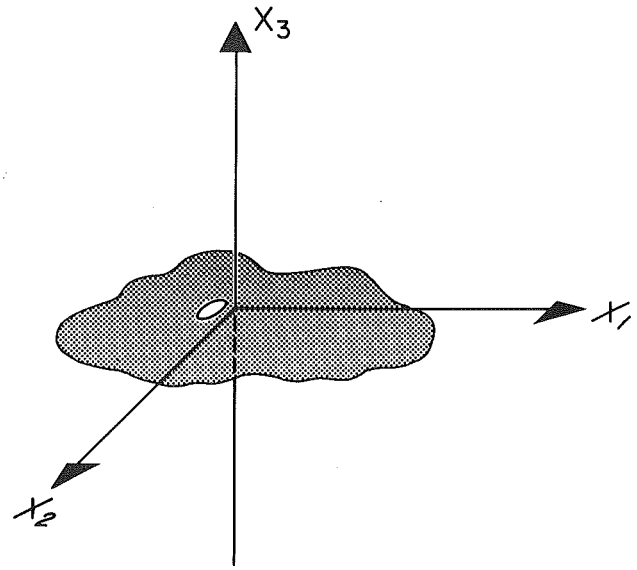


Fig. 1 Geometry of the problem and axes of coordinates. The crack spreads out areally over the (x_1-x_2) plane.

shall adopt an imperfectly brittle body model, i.e., require the stress to be finite at the crack edge and assume that some cohesive forces act in its vicinity. Then the fracture criterion can be included in the conditions (5), the functions S_1 and S_2 having a different form in the vicinity of the edge. Consequently, the edge conditions will be:

$$\tau_{13} \text{ and } \tau_{23} \text{ are finite everywhere on } x_3=0 \tag{6}$$

Finally, the problem consists of finding $u_i(\mathbf{x}, t)$, $\tau_{ij}(\mathbf{x}, t)$ and $\Sigma(t)$, solving the differential equations of linear elastodynamics subject to initial conditions (2), boundary conditions (4) and (5) and edge condition (6). Obviously, it is sufficient to solve the problem for the half-space $x_3\geq 0$.

The solution for $x_3>0$ can be easily expressed in terms of slip distribution (u_1, u_2) or traction distribution (τ_{13}, τ_{23}) on the surface $x_3=0$ by using the representation theorems of elasticity. If the traction distribution on $x_3=0$ is already known, then the displacement at some arbitrary instant t and any point $\mathbf{x}$ in the half-space $x_3>0$ will be given by

$$u_i(\mathbf{x},t)=\int_0^t d\tau\int_{-\infty}^{\infty}\int_{-\infty}^{\infty} G_{i\alpha}(\mathbf{x}-\xi,t-\tau)\tau_{\alpha 3}(\xi,\tau)d\xi_1 d\xi_2 \tag{7}$$

where $\mathbf{G}_{ij}(\mathbf{x},t)$ is the fundamental solution for $x_3>0$ satisfying the homogeneous initial conditions and the boundary conditions

$$\tau_{\alpha 3}=\delta_{i\alpha}\delta(x_1)\delta(x_2)\delta(t) \text{ at } x_3=0 \tag{8}$$

(Lamb's solution).

Alternatively, if the slip distribution

$$[u_i]\equiv u_i\,\Big|_{x_3=-0}^{x_3=+0}$$

is known, the displacement at an arbitrary point in the upper half space $x_3>0$ will be given by

$$u_i(\mathbf{x},t) = \int_0^t d\tau\iint_{-\infty}^{\infty} D_{i\alpha}(\mathbf{x}-\xi,t-\tau)[u_\alpha(\xi,\tau)]d\xi_1 d\xi_2$$
$$= 2\int_0^t d\tau\iint_{-\infty}^{\infty} D_{i\alpha}(\mathbf{x}-\xi,t-\tau)u_\alpha(\xi,\tau)d\xi_1 d\xi_2 \tag{9}$$

where $D_{i\alpha}$ is the fundamental solution corresponding to the boundary conditions

$$[u_\beta] = \delta_{\alpha\beta}\delta(x_1)\delta(x_2)\delta(t) \text{ at } x_3=+0 \tag{10}$$
$$\tau_{\alpha 3} = 0$$

Downloaded 03 May 2010 to 171.66.16.27. Redistribution subject to ASME license or copyright; see http://www.asme.org/terms/Terms_Use.cfm

(Nabarro's solution for a concentrated instantaneous dislocation, obtained from by differentation of Stokes' solution) Both G_{ij} and D_{ij} are well-known classical solutions.

The stress perturbation tensor τ_{ij} at some arbitrary point is easily obtained from equations (7) or (9) by differentation and using Hooke's law. In particular, the components $\tau_{\alpha 3}$ are obtained from equations (9) as follows:

$$\tau_{\alpha 3}(\mathbf{x},t)=\int_0^t d\tau\int_{-\infty}^{\infty}\int T_{\alpha\beta}(\mathbf{x}-\xi,t-\tau)+u_\beta(\xi,\tau)+d\xi_1 d\xi_2 \qquad (11)$$

where

$$T_{\alpha\beta}(\mathbf{x},t)=2\mu\left(\frac{\partial D_{\alpha\beta}}{\partial x_3}+\frac{\partial D_{3\beta}}{\partial x_\alpha}\right), \qquad (12)$$

where μ is the shear modulus.

Now putting $x_3=+0$ in equations (7) and (11), we obtain

$$u_\alpha(\mathbf{x},t)=\int_0^t d\tau\int_{-\infty}^{\infty}\int G_{\alpha\beta}(\mathbf{x}-\xi,t-\tau)\tau_{\alpha 3}(\xi,\tau)d\xi_1 d\xi_2 \text{ at } x_3=0 \qquad (13)$$

$$\tau_{\alpha 3}(\mathbf{x},t)=\int_0^t d\tau\int_{-\infty}^{\infty}\int T_{\alpha\beta}(\mathbf{x}-\xi,t-\tau)u_\beta(\xi,\tau)d\xi_1 d\xi_2 \text{ at } x_3=0 \qquad (14)$$

These equations are mutually inverse integral transforms relating displacement on the crack to the traction distribution on the crack plane. To solve for displacement and tractions, either one of these two relations can be used together with the boundary conditions (4) and (5). Consequently, the problem under consideration is reduced to solving the set of constrained integral equations

$$u_\alpha(\mathbf{x},t)-\int_0^t d\tau\int_{-\infty}^{\infty}\int G_{\alpha\beta}(\mathbf{x}-\xi,t-\tau)\tau_\alpha(\xi,\tau)d\xi_1 d\xi_2=0$$

$$\text{for } -\infty<\xi_1,\xi_2<\infty$$

$$S_\alpha(\mathbf{u},\dot{\mathbf{u}},\tau)=0 \text{ for } \xi\epsilon\Sigma(t) \qquad (15)$$

$$u_\alpha=0 \text{ for } \xi\epsilon\bar{\Sigma}(t)$$

or, alternatively, the set

$$\tau_\alpha(\mathbf{x},t)-\int_0^t d\tau\int\int_{\Sigma(\tau)} T_{\alpha\beta}(\mathbf{x}-\xi,t-\tau)u_\alpha(\xi,\tau)d\xi_1 d\xi_2=0$$

$$\text{at } \Sigma(t) \qquad (16)$$

$$S_\alpha(\mathbf{u},\dot{\mathbf{u}},\tau)=0$$

Here we write τ_α instead of $\tau_{\alpha 3}$ and denote by $\mathbf{u}$, etc., two-dimensional vectors (u_1, u_2), etc. The additional condition (6) is automatically fulfilled by the solution of the system (15) if τ_α is assumed to be integrable, because the kernel $G_{\alpha\beta}$ only has a weak singularity so that u_α is a smooth function. In contrast, $T_{\alpha\beta}$ is a singular kernel and with integrable u_α, $\tau_{\alpha\beta}$ obtained from equation (14) may be nonintegrable. Accordingly, the set (16) must be supplemented by the additional condition that u_α must be continuously differentiable.

In the system (16), the variables $\mathbf{x}$ and ξ are confined to $\Sigma(t)$ because the slip vanishes outside the crack. On the other hand, the system (15) is to be solved for a larger domain covering all points influenced by disturbances which propagate with the compressional wave velocity (the crack speed being assumed to be less than the compressional wave speed of the medium). The domains of integration for the systems (15) and (16) are shown (in cross section) in Fig. 2 for two particular cases. Of course the integration domains for the systems (15) and (16) coincide if the crack propagates at the P-wave velocity and never stops. The first equation of (16) is essentially the same as the integral equation developed in Budiansky and Rice (1979). Burridge (1969) used the two-dimensional form of the first equation of (16) to study dynamic crack problems and

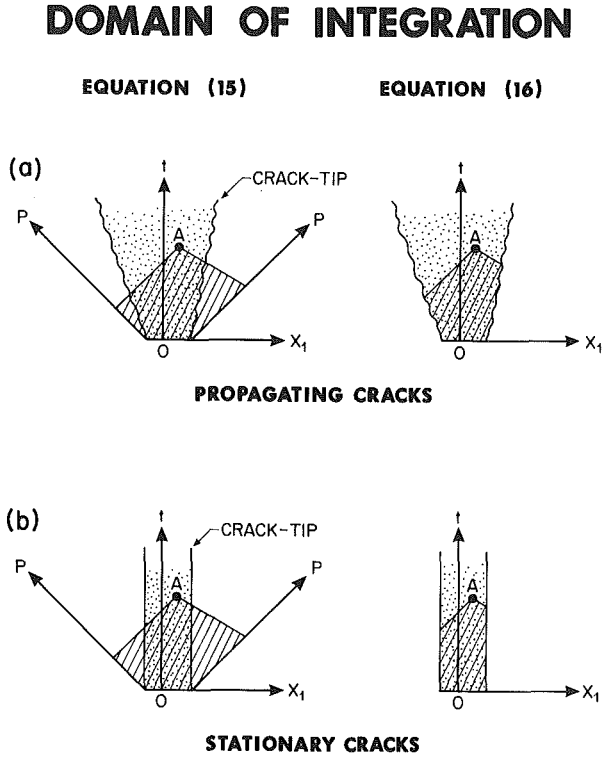


Fig. 2 Domains of integration shown in cross section for the system (15)—Das (1980)—and system (16), developed here. (*a*) For propagating cracks. (*b*) For stationary cracks. The stippled areas are the cracked areas and the hatched areas are the domains of integration for determining the slip at some representative point, say *A*.

Burridge and Moon (1981) used its scalar analog in three dimensions.

In general, neither the system (15) nor (16) can be solved analytically. In Das (1980), a numerical method for solving the system (15) was developed. In the next section, we develop the numerical counterpart of the system (16) after outlining the original method of Das.

The Numerical Algorithm

To solve the system (15) numerically, we introduce a regular network of grids centered at the points

$$\begin{aligned} x_1 &= i\Delta x, \qquad i=-\infty,\ldots\ldots-1,0,1,\ldots\ldots\infty \\ x_2 &= j\Delta x, \qquad j=-\infty,\ldots\ldots-1,0,1,\ldots\ldots\infty \\ t &= (k+1/2)\Delta t, \quad k=0,1,\ldots\ldots\infty \end{aligned} \qquad (17)$$

In each element of the network, we represent the tractions by average values

$$\tau_{\alpha ijk}=\frac{1}{\Delta t\Delta x^2}\int_o^{\Delta t} d\tau\int_{-\Delta x/2}^{\Delta x/2}\int_{-\Delta x/2}^{\Delta x/2}\tau_\alpha(i\Delta x+\xi_1,j\Delta x+\xi_2,k\Delta t+\tau)d\xi_1 d\xi_2 \qquad (18)$$

and the displacement u_α by its value at a point within the grid

$$u_{\alpha ijk}=u_\alpha(i\Delta x,j\Delta x,k\Delta t+\delta t) \qquad (19)$$

where $0\le\delta t\le\Delta t$.

Due to condition (6), the value of τ at any point within the element (i,j,k) is

$$\tau_\alpha(\mathbf{x},t)=\tau_{\alpha ijk}+o(1) \qquad (20)$$

when $\Delta x\to 0$ and $\Delta t/\Delta x$ is fixed. The approximation error term can be estimated only for a particular choice of boundary conditions (5), but usually it is of the order $(\Delta x)^\lambda$, $\lambda>0$. Next, we replace the integral in (15) by the sum of the interals over grid elements and substitute the expression (20) into the integrals to obtain

Downloaded 03 May 2010 to 171.66.16.27. Redistribution subject to ASME license or copyright; see http://www.asme.org/terms/Terms_Use.cfm

$$u_{\alpha ijk} = -\sum_{k'=0}^{k}\sum_{i'=-\infty}^{\infty}\sum_{j'=-\infty}^{\infty} F_{\alpha\beta}(i-i', j-j', k-k')\tau_{\alpha i'j'k'}$$

$$+ \text{approximation error} \tag{21}$$

where the approximation error can be estimated to be $0(\Delta x)$, and the discrete Green function $F_{\alpha\beta}$ is given by

$$F_{\alpha\beta}(i,j,k) = -\int_o^{\Delta t} d_\tau \int_{-\Delta x/2}^{\Delta x/2}\int_{-\Delta x/2}^{\Delta x/2} G_{\alpha\beta}(i\Delta x + \xi_1, j\Delta x + \xi_2, k\Delta t + \delta t - \tau)d\xi_1 d\xi_2 \tag{22}$$

Let us briefly describe the properties of $F_{\alpha\beta}$. The tensor $G_{\alpha\beta}$ is a homogeneous function in x_1, x_2 and t of the order -2 and vanishes for $t<0$. It follows then that $F_{\alpha\beta}(i,j,k)$ vanishes for $k<0$. More previsely, $G_{\alpha\beta}$ vanishes outside the cone $v_p{}^2t^2 > x_1{}^2 + x_2{}^2$, (the P-cone) where v_p is the P-wave velocity. Correspondingly, $F_{\alpha\beta}$ vanishes for all elements not intersecting the P cone. In particular, asuming that $v_p(\Delta t - \delta t) \le \Delta x/2$, $F_{\alpha\beta}(i,j,0)$ will be nonvanishing only for $i=0$, $j=0$. The value of this tip element is

$$F_{\alpha\beta}(0,0,0) = -\int_0^{\delta t} d\tau \int_{-\infty}^{\infty}\int_{-\infty}^{\infty} G_{\alpha\beta}(\xi_1,\xi_2,\tau)d\xi_1 d\xi_2,$$

or, taking into account the homogeneity and symmetry properties of $G_{\alpha\beta}$,

$$F_{\alpha\beta}(0,0,0) = \delta t F_0 \delta_{\alpha\beta} \tag{23}$$

where

$$F_0 = -\int_0^1 d\tau \int_{-\infty}^{\infty}\int_{-\infty}^{\infty} G_{11}(\xi_1,\xi_2,\tau)d\xi_1 d\xi_2 \tag{24}$$

is a positive constant independent of grid size and $\delta_{\alpha\beta}$ is the Kronecker delta. $F_{\alpha\beta}(0,0,0)$ is the maximum element of $F_{\alpha\beta}$. The minus signs in equations (21) through (24) were introduced to make F_0 positive.

Similarly, the sum of $F_{\alpha\beta}(i,j,k)$ for a fixed $k>0$ over all values of i and j is equal to $\Delta t F_0 \delta_{\alpha\beta}$:

$$\sum_{i=-\infty}^{\infty}\sum_{j=-\infty}^{\infty} F_{\alpha\beta}(i,j,k) = \Delta t \cdot F_0 \cdot \delta_{\alpha\beta} \tag{25}$$

Due to the finiteness of the grids, some grids centered outside the P cone intersect it and the corresponding elements of $F_{\alpha\beta}$ are nonvanishing. Due to this, it can be seen that the expression (21) produces disturbances which propagate at speeds greater than v_p, for some choices of $v_p\Delta t/\Delta x$. This problem can be avoided in the following manner. The expression (21) is not the only possible approximation to the integral (7). A few additional terms can be added to it provided their sum tends to zero as $\Delta x \to 0$. Now, from condition (6) the u_α's are smooth functions, so that the difference

$$u_{\alpha ijk} - u_{\alpha ij(k-1)}$$

is of the order of Δx. Consequently, if k in the right-hand side of (21) is replaced by $(k-n)$, where n is independent of the grid size, the order of approximation will remain unchanged. Next, adding n terms of the form $\Delta t F_0 \tau_{\alpha ijk}$, where $k-n<k'\le k$, we obtain, instead of (21), with the same order of accuracy of approximation,

$$u_{\alpha ijk} = -\sum_{k'=0}^{k}\sum_{i'=-\infty}^{\infty}\sum_{j'=-\infty}^{\infty} F^*_{\alpha\beta}(i-i', j-j', k-k')\tau_{\beta i'j'k'}$$

where

$$\begin{aligned} F^*_{\alpha\beta}(i,j,k) &= F_{\alpha\beta}(i,j,k-n) && \text{for } k>n \\ &= \Delta t F_0 \delta_{\alpha\beta} && \text{for } 0\le k\le n \end{aligned} \tag{26}$$

Selecting sufficiently large n, we can thus shift all nonvanishing elements of $F^*_{\alpha\beta}$ into the P cone. The minimum necessary value of n depends, obviously, on the ratio $v_p\Delta t/\Delta x$.

Note that the tip value $F^*_{\alpha\beta}$ (0,0,0) differs from equation (23) in that it contains the factor Δt instead of δt. For $\delta t < \Delta t$, this difference is of the order of Δt and is negligible from the point of view of approximation accuracy. In general, this element can be multiplied by any constant factor. This possibility will be important when analyzing the stability of the algorithm. From the above discussion, it follows that whatever the disturbances that may appear outside the P cone when using the approximation (21), they will be of the order of the approximation error. Consequently, the replacement of $F_{\alpha\beta}$ by $F^*_{\alpha\beta}$ is optional. In what follows, we shall use $F_{\alpha\beta}$ to denote either of these two quantities.

To discretize the boundary conditions (5), we replace the time-derivates, if present, by a finite difference. Then, instead of equation (5), we have

$$S_1(\tau_{ijk}, \mathbf{u}_{ijk}, \mathbf{u}_{ij(k-1)}) = 0$$
$$S_2(\tau_{ijk}, \mathbf{u}_{ijk}, \mathbf{u}_{ij(k-1)}) = 0$$

In some particular cases, e.g., viscous friction or slip weakening, this set of simultaneous equations can be solved for $u_{\alpha ijk}$ giving

$$u_{\alpha ijk} = U_\alpha(\tau_{ijk}, \mathbf{u}_{ij(k-1)})$$

and in other cases, e.g., the case of Coulomb friction, etc., it can be solved for τ_{ijk} to have the form

$$\tau_{\alpha ijk} = T_\alpha(\mathbf{u}_{ijk}, u_{ij(k-1)})$$

where U_α and T_α are some known functions.

Finally, we come to the complete formulation of the discrete problem:

$$u_{\alpha ijk} + \Delta t G_0 \tau_{\alpha ijk} = -\sum_{k'=0}^{k-1}\sum_{i'j'\epsilon\Sigma^P_{k'}} F_{\alpha\beta}(i-i', j-j', k-k')\tau_{\beta i'j'k'} \text{ for } i, j\epsilon\Sigma^P_k \tag{27}$$

$$S_\alpha(\tau_{ijk}, \mathbf{u}_{ijk}, \mathbf{u}_{ijk(k-1)}) = 0 \text{ for } i,j\epsilon\Sigma^P_k \tag{28}$$

where Σ^P_k is the union of all grids influenced by disturbances at the time $k\Delta t$, and G_0 is a positive constant to be chosen based on stability considerations. For a given k, the right-hand side of equation (27) depends only on the solution at previous times ($k'<k$), and we obtain an explicit one-step method. To find $u_{\alpha ijk}$ and $\tau_{\alpha ijk}$ one needs only to solve four (in general, nonlinear) simultaneous equations (27) and (28).

Note that equation (28) includes the fracture criterion, i.e., for unbroken grids, we have $U_\alpha = 0$. This algorithm is appropriate not only for crack problems (stress drop specified on the crack and slip to be determined) but for dislocation problems as well, where U_α will be known functions of i, j, and k.

A detailed investigation of the stability conditions for this algorithm is a very difficult task. We consider here only a necessary condition, that is the algorithm must be stable when applied to a very simple particle problem. Namely, the problem when at $x_3 = 0$ the known slip is proportional to time and independent of x_1 and x_2, i.e.,

$$\begin{aligned} u_1 &= At \qquad \text{for } x_3 = 0,\ -\infty < x_1, x_2 < \infty \\ u_2 &= 0 \end{aligned}$$

This problem has a trivial solution in the form of a plane shear wave

$$u_\alpha(\mathbf{x},t) = \delta_{\alpha 1} \cdot A \cdot (t - x_3/v_s) \tag{29}$$

where v_s is the shear-wave velocity. The tractions at $x_3 = 0$ will be

$$\tau_\alpha = -\mu A/v_s \text{ at } x_3 = 0 \tag{30}$$

independent of x_1, x_2, and t.

Now, assign $U_\alpha = \delta_{\alpha 1} \cdot A \cdot (k\Delta t + \delta t)$ and apply the algorithm (27), (28). Obviously, $u_{\alpha ijk}$ and $\tau_{\alpha ijk}$ will not depend on i and j.

Downloaded 03 May 2010 to 171.66.16.27. Redistribution subject to ASME license or copyright; see http://www.asme.org/terms/Terms_Use.cfm

Let us denote them by $u_{\alpha k}$ and $\tau_{\alpha k}$. From equation (28), we have

$$u_{\alpha k} = \delta_{\alpha 1} \cdot A \cdot (k\Delta t + \delta t) \tag{31}$$

and substituting into equation (27), we obtain

$$\tau_{\alpha k} = -\frac{F_0}{G_0} \sum_{k'=0}^{k-1} \tau_{\alpha k'} - \frac{\delta_{\alpha 1}}{G_0 \Delta t} A(k\Delta t + \delta t) \tag{32}$$

where the property (25) is used. For $k=0$ and $k=1$, we obtain

$$\tau_{\alpha 0} = -\delta_{\alpha 1} \cdot \delta t \cdot A/(G_0 \Delta t) \tag{33}$$

$$\tau_{\alpha 1} = -\frac{\delta_{\alpha 1} \cdot A}{G_0}\left(1 + \frac{\delta t}{\Delta t}\left(1 - \frac{F_0}{G_0}\right)\right) \tag{34}$$

For $k>0$, we subtract from equation (32) the equation obtained from it by substituting $(k-1)$ instead of k, to obtain

$$\tau_{\alpha k} - \left(1 - \frac{F_0}{G_0}\right)\tau_{\alpha(k-1)} = -\delta_{\alpha 1}\frac{A}{G_0}$$

which is a linear finite difference equation of first order with constant coefficients. Solving it with the initial condition (33), we get

$$\tau_{\alpha k} = -\frac{\delta_{\alpha 1} A}{F_0}\left[1 - \left(1 - \frac{\delta t}{\Delta t}\frac{F_o}{G_0}\right)\left(1 - \frac{F_0}{G_0}\right)\right]^k \quad \text{for } k \geq 1 \tag{35}$$

This solution is unstable (grows exponentially) if

$$|1 - F_0/G_0| > 1$$

This gives the necessary condition for stability in the form

$$0 < \frac{F_0}{G_0} < 2 \tag{36}$$

The solution is most stable (constant) when G_0 is chosen equal to F_0. In this case, we obtain

$$\begin{aligned} \tau_{\alpha 0} &= -\delta_{\alpha 1} \cdot A \cdot \delta t/(F_0 \Delta t) \quad \text{for } k \geq 1 \\ \tau_{\alpha k} &= -\delta_{\alpha 1} \cdot A/F_0 \end{aligned} \tag{37}$$

Substituting the exact solution (29) and (30) into equation (13) and using the defintion (24) we obtain

$$F_0 = +v_s/\mu$$

which is a positive constant, as expected from our earlier considerations. It is seen that the solution (37) coincides with the exact solution (30) for $k \geq 1$.

Application of this method to particular crack problems (Das, 1980) showed appreciable stability and the results were in good agreement with available analytical solutions.

If the entire slip and traction fields are of interest, the algorithm just described is very suitable. If a particular problem of a fault on which the area of traction perturbation is limited to some finite region is under study, i.e., some "exterior" crack problems (e.g., Das and Kostrov, 1983) this algorithm is the most efficient. However, in most problems of modelling earthquake faulting, one is usually interested in the slip distribution on a finite fault ("interior" crack) and in the far-field pulse-shape which can be easily expressed in terms of slip using the asymptotic form of equations (9). The traction distribution outside the crack is in this context of interest at most in the vicinity of the crack edge. Moreover, the crack propagation speed is often less than the shear wave speed and the final crack size is limited. Consequently, the number of grid values of interest at a fixed time step is proportional to the crack area whereas the number of traction values involved in the algorithm (27), (28) is proportional to the square of time. The number of arithmetic operations necessary to obtain the solution at the kth time step is of the order k^6 and the necessary storage is of the order k^3. So every doubling of the number of time-steps requires 8 times more storage and 64 times longer computation time. Note that these requirements are independent of the particular problem under consideration. On the other hand, for the stationary crack the number of slip values is proprtional to k. If one could express the current slip and traction values in terms of previous slip only, for a stationary crack one would require on the order of k^2 arithmetic operations and on the order of k storage. Such an algorithm would be k^4 times faster and require k^2 less storage for a stationary crack. An obvious idea consists in direct discretization of the equations (16) by a procedure analogous to the one described above for (15). However, the integral in equations (16) is a principal value and cannot be discretized by replacing u_α by its average value over a grid. A method of successful discretization of equations (16) is unknown to the authors.

Therefore, we proceed instead to produce a numerical counterpart of equations (16). Namely, let us choose U_α in the form

$$U_\alpha = \delta_{\alpha\beta}\delta_{ii''}\delta_{jj''}\delta_{kk''}$$

Obviously, $\tau_{\alpha ijk}$ obtained by solving equation (27) will depend on the differences $i-i''$, $j-j''$, $k-k''$, so it is necessary to solve the problem only once for $i''=j''=k''=0$. Let us denote this solution by $S_{\alpha\beta}(i,j,k)$. Then equation (27) can be rewritten in the following form

$$\sum_{k'=0}^{k}\sum_{i'=-\infty}^{\infty}\sum_{j'=-\infty}^{\infty} F_{\alpha\beta}(i-i',j-j',k-k')S_{\beta\gamma}(i-i'', j-j'',k-k'') = \delta_{\alpha\beta}\delta_{ii''}\delta_{jj''}\delta_{kk''} \tag{38}$$

Taking into account that $F_{\alpha\beta}$ is symmetric in α and β, we see that $F_{\alpha\beta}(i,j,k)$ and $S_{\alpha\beta}(i,j,k)$ are kernels of mutually inverse discrete operators, so that $S_{\alpha\beta}$ can easily be determined from equation (38) if $F_{\alpha\beta}$ is known. In other words, we solve the original integral equation system (15) of Das (1980) for a unit, concentrated, instantaneous dislocation (slip) applied at the tip of the P cone and the resulting stress-field is $S_{\alpha\beta}$. Note that $S_{\alpha\beta}$ can be obtained explicitly by stepping in time and one does not actually need to invert a very large matrix. Now, instead of equations (27) and (28), we obtain the discrete problem

$$\begin{aligned} \tau_{\alpha ijk} + S_o u_{\alpha ijk} &= -\sum_{k'=0}^{k-1}\sum_{i',j' \in \Sigma_{k'}} S_{\alpha\beta}(i-i', j-j', k-k')u_{\beta i'j'k'} \\ &\quad \text{for } i, j \in \Sigma_k \\ u_{\alpha ijk} - U_\alpha(\tau_{ijk}, \mathbf{u}_{ij(k-1)}) &= 0 \end{aligned} \tag{39}$$

Here Σ_k is the discrete crack area, i.e., the union of all grids with nonvanishing slip and $S_0 = S_{11}$ (0,0,0). S_0 is equal to $1/(\Delta t G_0)$ and is obviously a positive constant.

It is important to note that the system (39) is exactly equivalent to the system (27), (28) so that the solution using this algorithm must coincide with the solution of the system (27), (28), apart from different rounding error accumulation.

The general properties of the kernel $S_{\alpha\beta}$ are the same as those of $F_{\alpha\beta}$. In particular, S_0 is the maximum element of $S_{\alpha\beta}$. The elements of $F_{\alpha\beta}$ are zero for grids situated totally within the Rayleigh wave cone $v_R^2 t^2 \leq x_1^2 + x_2^2$, where v_R is the Rayleigh wave velocity of the medium. The analytical kernel $T_{\alpha\beta}$ vanishes in the even wider S-wave cone $v_S^2 t^2 \leq x_1^2 + x_2^2$. This property is not conserved in its discrete counterpart $S_{\alpha\beta}$. For a given k, the maximum values of it are observed at or near the axis $i=0=j$. In general, $S_{\alpha\beta}$ does not approximate the dislocation kernel $T_{\alpha\beta}$. This is due to the strong singularity in $T_{\alpha\beta}$. In fact, the integral operator in equations (9) is a degenerate one and can be inverted only under additional conditions, as was mentioned in the previous section, while $S_{\alpha\beta}$ is as well defined a matrix as $F_{\alpha\beta}$ is and can be inverted without any reservations.

Downloaded 03 May 2010 to 171.66.16.27. Redistribution subject to ASME license or copyright; see http://www.asme.org/terms/Terms_Use.cfm

Discussion and Conclusions

To test whether the system (27), (28), and (39) do indeed give identical results we applied both methods to the problem of determining the slip distribution due to a self-similar circular shear crack propagating with a speed of $v_p/2$. The results are found to be identical, except at the last (seventh) decimal place (due to different rounding errors) and cannot be distinguished on a plot. The reader is referred to the corresponding figure in Das (1980; 1985) where the results using equation (27) were compared with the analytical solution (Kostrov, 1964) and shown to agree well.

Thus, we have presented two forms of the boundary integral method, each appropriate for certain particular cases and analyzed the numerical algorithm in detail. The new method proposed here is very efficient for the study of "interior" crack propagation problems. The methods can be applied *mutatis mutandis* to dynamic tensile crack problems as well.

Acknowledgments

This work is part of a joint program in earthquake prediction under Area IX of the US-USSR Agreement in the Field of Environmental Protection. The paper was reviewed at Lamont-Doherty by Art Lerner-Lam and Chris Scholz, and we thank them for their comments. We also wish to thank Dr. J. Andrews at Menlo Park for his comments. The American part of the work was supported by the National Science Foundation under NSF grant EAR 83-18935 and the US Geological Survey under contract USGS-14-08-00001-G-947. Lamont-Doherty Geological Observatory Contribution Number 4082.

References

Andrews, D. J., 1976a, "Rupture Velocity of Plane Strain Shear Cracks," *J. Geophys. Res.*, Vol. 81, pp. 5679–5687.

Andrews, D. J., 1976b, "Rupture Propagation with Finite Stress in Antiplane Strain," *J. Geophys. Res.*, Vol. 81, pp. 3575–3582.

Andrews, D. J., 1985, "Dynamic Plane-Strain Shear Rupture with a Slip-Weaking Friction Law Calculated by a Boundary Integral Method, *Bull. Seismol. Soc. Am.*, Vol. 75, pp. 1–21.

Atluri, S. N., and Nishioka, T., 1985, "Numerical Studies in Dynamic Fracture Mechanics, *Intl. J. Frac.*, Vol. 27, pp. 245–261.

Budiansky, B., and Rice, J. R., 1979, "An Integral Equation for Dynamic Elastic Response of an Isolated 3-D Crack," *Wave Motion*, Vol. 1, pp. 187–192.

Burridge, R., 1969, "The Numerical Solution of Certain Integral Equations with Non-Integrable Kernels Arising in the Theory of Crack Propagation and Elastic Wave Diffraction," *Phil. Trans. Roy. Soc. Lond.*, Vol. A265, pp. 353–381.

Burridge, R. B., and Moon, R., 1981, "Slipping on a Frictional Fault Plane in Three Dimensions: A Numerical Simulation of a Scalar Analog, *Geophys. J. R. Astron. Soc.*, Vol. 67, pp. 325–342.

Cruse, T. A., and Rizzo, F., 1975, "Boundary Integral Equation Method: Computational Application in Applied Mechanics, *AM. Soc. Mech. Engrs.*, AMD, Vol. 11, New York.

Das, S., 1980, "A Numerical Method for Determination of Source Time Functions for General Three-Dimensional Rupture Propagation," *Geophys. J. R. Astron. Soc.*, Vol. 62, pp. 591–604.

Das, S., 1981, "Three-Dimensional Rupture Propagation and Implications for the Earthquake Source Mechanism," *Geophys. J. R. Astron. Soc.*, Vol. 67, pp. 373–393.

Das, S., 1985, "Application of Dynamic Shear Crack Models to the Study of the Earthquake Faulting Process," *Intl. J. Frac.*, Vol. 27, pp. 263–276.

Das, S., and Aki, K., 1977, "A Numerical Study of Two-Dimensional Spontaneous Rupture Propagation," *Geophys. J. R. Astron. Soc.*, Vol. 50, pp. 643–668.

Das, S., and Kostrov, B. V., 1983, "Breaking of a Single Asperity: Rupture Process and Seismic Radiation," *J. Geophys. Res.*, Vol. 88, pp. 4277–4288.

Day, S. M., 1979, "Three Dimensional Finite Difference Simulation of Fault Dynamics," *Final Report SSS-R-80-4295*, S-Cubed, La Jolla, CA.

Day, S. M., 1982, "Three Dimensional Finite Difference Simulation of Fault Dynamics: Rectangular Faults with Fixed Rupture Velocity, *Bull. Seismol. Soc. Am.*, Vol. 72, pp. 705–727.

Kostrov, B. V., 1964, "Selfsimilar Problems of Propagation of Shear Cracks," *J. Appl. Math. Mech.*, Vol. 28, pp. 1077–1087.

Kostrov, B. V., 1966, "Unsteady Propagation of Longitudinal Shear Cracks," *J. Appl. Math. Mech.*, Vol. 30, pp. 1241–1248.

Kupradze, V. D., 1963, *Dynamical Problems in Elasticity*, North-Holland, Amsterdam, pp. 86.

Madariaga, R., 1976, "Dynamics of an Expanding Circular Fault," *Bull. Seismol. Soc. Am.*, Vol. 66, pp. 639–666.

Virieux, J., and Madariaga, R., 1982, "Dynamic Faulting Studied by a Finite Difference Method," *Bull. Seismol. Soc. Am.*, Vol. 72, pp. 345–369.

Downloaded 03 May 2010 to 171.66.16.27. Redistribution subject to ASME license or copyright; see http://www.asme.org/terms/Terms_Use.cfm

Boundary Element Method by Dislocation Distribution

C. F. Sheng
Senior Staff Engineer,
Perkin-Elmer Corporation,
Military Systems Division,
Danbury, CT 06810
Assoc. Mem. ASME

The method of dislocation distribution has been applied extensively to crack related problems by many people in the last fifteen years. It has been proved to be very successful in terms of accuracy and versatility. However, the potential of applicability of this method has not been fully explored. This paper shows a way to apply this method to plane stress problems with any geometry and loading conditions. The method of dislocation distribution is similar to the Boundary Element Method in spirit, but has the advantage of enjoying the fully developed numerical schemes in solving the formulated system of singular integral equations. Without extensive investigation, it is hard to tell whether this new approach will produce better results than the traditional BIE method. However, as demonstrated by the excellent results from the numerical examples, this method should be competitive and have the potential to become one of the best candidates for the type of elasticity problems where local stress evaluation is needed.

Introduction

The method of dislocation distribution has been used in Fracture Mechanics to evaluate stress intensity factors for cracks in an infinite medium by many researchers such as Bilby et al. (1968), Erdogan et al. (1974), Theocaris (1977a), and Sheng and Wheeler (1981). In this process, a continuous distribution of dislocation of unknown density is assumed to exist along the crack locus as illustrated in Fig. 1. Here we designate it as Prob. I.

Its conjugate problem – Problem II – is defined as one with prescribed loading (for example, uniaxial loading at infinty) but without crack and distribution of dislocations. The dislocation-induced surface tractions along the crack locus in Prob. I are then set to be equal in magnitude and opposite in sign to those along the corresponding locus in the conjugate problem (Prob. II). Adding these two problems, we end up with one with the same loadings but with crack surfaces which are now traction free. Since Prob. II does not involve any stress singularity, what we get from Prob. I about stress intensity factors should also be representative of the combined problem.

Normally, formulation of Prob. I leads to a system of singular integral equations, which can be easily solved by the numerical method proposed by Theocaris et al. (1977b) or that by Erdogan et al. (1973) depending upon the strength of singularity at the two crack ends. The extension of this method to 2-D traction boundary value problems with arbitrary geometry is obvious: Since crack locus in an infinite domain (Prob. I) is nothing but an imaginary line with distribution of dislocations, there is no reason why we cannot let one end of this line go around a finite domain and meet the other end of the line, as Fig. 2 illustrates. Also shown there are surface tractions along the crack locus. They are induced, of course, by the continuous distribution of dislocations along the contour. Once the surface tractions are known, we can introduce a cut along the entire contour and replace the problem illustrated in Fig. 2 by two problems with their boundary loadings equivalent to those tractions specified in Fig. 2. This process, shown schematically in Fig. 3, establishes the basis of this paper. The current approach is somewhat similar to the displacement discontinuity method described in Crouch and Starfield's book (1983). These two are different from the traditional boundary integral equation (BIE) method by Rizzo (1967) or Cruse (1969) in the sense that they treat boundary value problems with finite domain as problems with infinite domain using a process described above, whereas Cruse's formulation concerns the finite domain only.

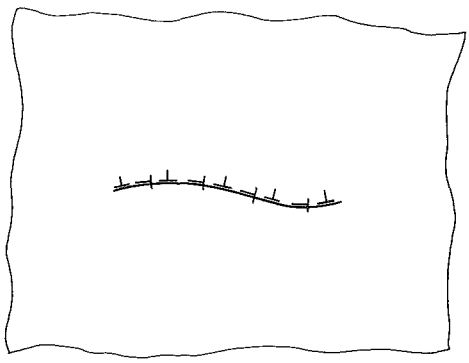


Fig. 1 Continuous distribution of dislocations along a crack locus in an infinite medium

Contributed by the Applied Mechanics Division for presentation at the 1987 Applied Mechanics, Biomechanics, and Fluids Engineering Conference, Cincinnati, OH, June 14–17, 1987, of the American Society of Mechanical Engineers.
Discussion of this paper should be addressed to the Editorial Department, ASME, United Engineering Center, 345 East 47th Street, New York, N.Y. 10017, and will be accepted until two months after final publication of the paper itself in the JOURNAL OF APPLIED MECHANICS. Manuscript received by ASME Applied Mechanics Division, August 26, 1985; final revision, June 9, 1986.
Paper No. 87-APM-14.

Copyright © 1987 by ASME
Downloaded 03 May 2010 to 171.66.16.27. Redistribution subject to ASME license or copyright; see http://www.asme.org/terms/Terms_Use.cfm

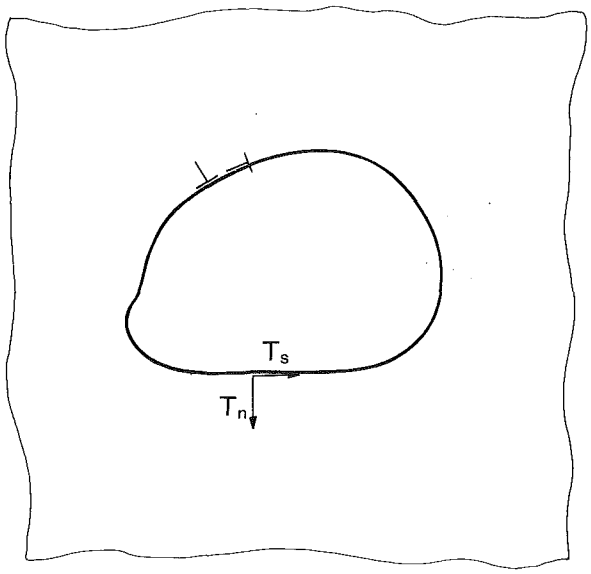


Fig. 2 Crack locus form a closed loop in an infinite medium

Formulation

In this section, formulation of the dislocation method in the form of the boundary element approach will be given. But for the sake of simplicity, only the 2-D traction boundary value problem will be dealt with here. An example is shown in Fig. 4, where the geometry is chosen arbitrarily for the sake of easy demonstration. We will also introduce, at appropriate places, some key equations of the other two methods so that we can see the differences among all three approaches.

The boundary of the domain shown in Fig. 4 can be viewed as an imaginary contour in an infinite medium. Each line segment, straight or circular, has continuous distribution of dislocations with Burgers vectors in t and w directions at every point along the contour.

Surface tractions $T_t(s)$ and $T_w(s)$ in the t and w directions at point s along the contour can be expressed as:

$$T_t(s) = \sum_{i=1}^{N} \left[\int_{s_{1i}}^{s_{2i}} K_{11i}(s,s') f_{1i}(s') ds' + \int_{s_{1i}}^{s_{2i}} K_{12i}(s,s') f_{2i}(s') ds' \right]$$

$$T_w(s) = \sum_{i=1}^{N} \left[\int_{s_{1i}}^{s_{2i}} K_{21i}(s,s') f_{1i}(s') ds' + \int_{s_{1i}}^{s_{2i}} K_{22i}(s,s') f_{2i}(s') ds' \right] \quad (1)$$

Where $f_{1i}(S')$ and $f_{2i}(S')$ stand for dislocation density functions along the ith boundary segment; K_{11i}, K_{12i}, K_{21i} and K_{22i}, having both singular and regular parts are influence coefficients representing contributions to the surface tractions due to those dislocations. The symbols S_{1i}, S_{2i} are obviously end points for segment i, and N is the total number of line segments. Since the tedious algebraic manipulations leading to the formulas for K_{11i}, K_{12i}, K_{21i}, and K_{22i} ($i = 1, \ldots, N$) can be obtained by referring to the paper by Erdogan et al. (1974), they will not be elaborated on here.

With the tractions T_t and T_w along the entire boundary known, the only unknowns remained to be determined are those dislocation density functions f_{1i} and f_{2i} ($i = 1, \ldots, N$). Once they are determined, the dislocation density functions along the entire boundary can be integrated to obtain the stress state at any interior or exterior point in the domain through the following equations:

$$T_t(p) = \sum_{i=1}^{N} \left[\int_{s_{1i}}^{s_{2i}} K_{11i}(p,s') f_{1i}(s') ds' + \int_{s_{1i}}^{s_{2i}} K_{12i}(p,s') f_{2i}(s') ds' \right]$$

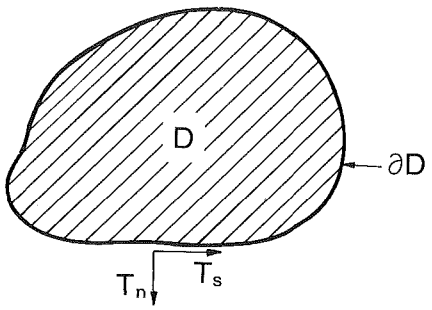


Fig. 3(a) 2-D traction boundary value problem from Fig. 2

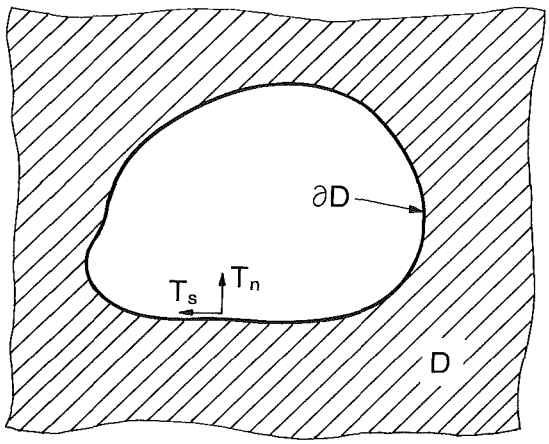


Fig. 3(b) 2-D exterior boundary value problem from Fig. 2

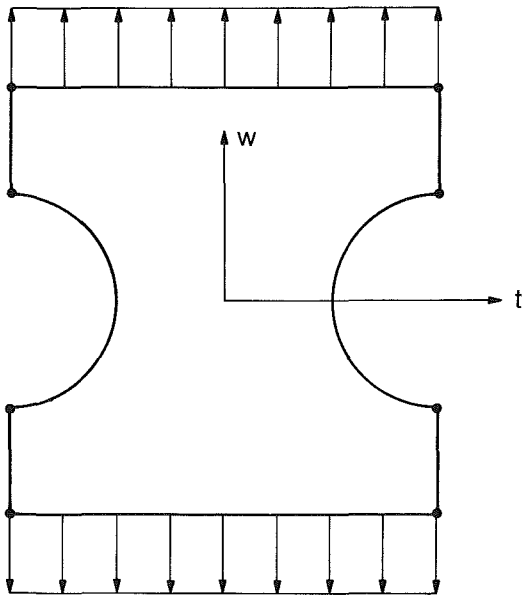


Fig. 4 A typical example for applying boundary element method

Downloaded 03 May 2010 to 171.66.16.27. Redistribution subject to ASME license or copyright; see http://www.asme.org/terms/Terms_Use.cfm

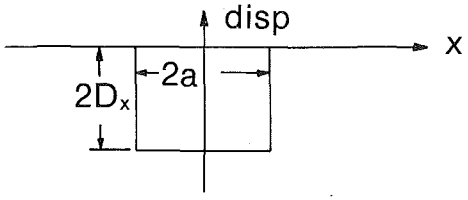


Fig. 5(a)

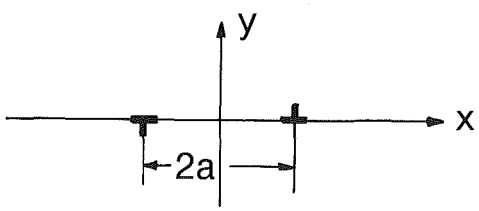


Fig. 5(b)

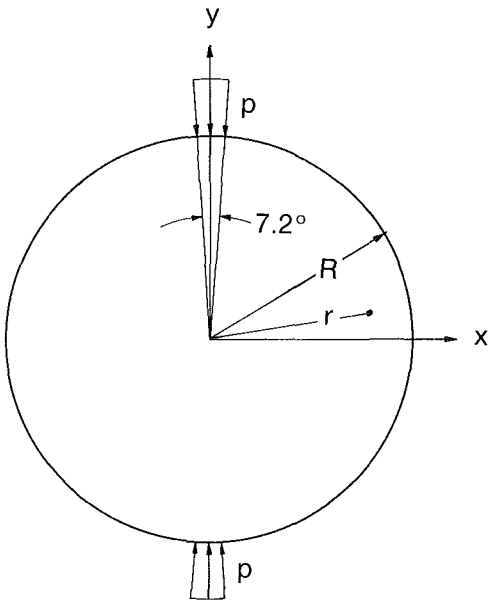


Fig. 6 Schematic representation of example 1

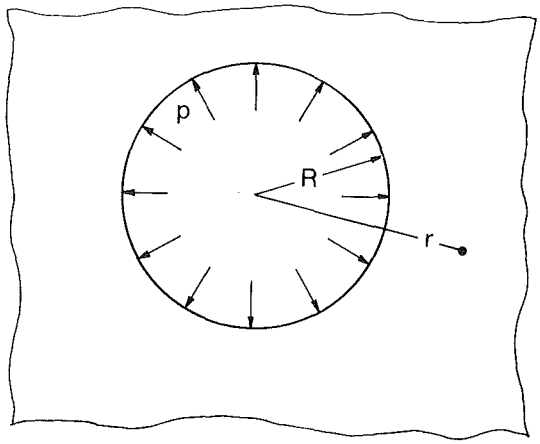


Fig. 7 Schematic representation of example 2

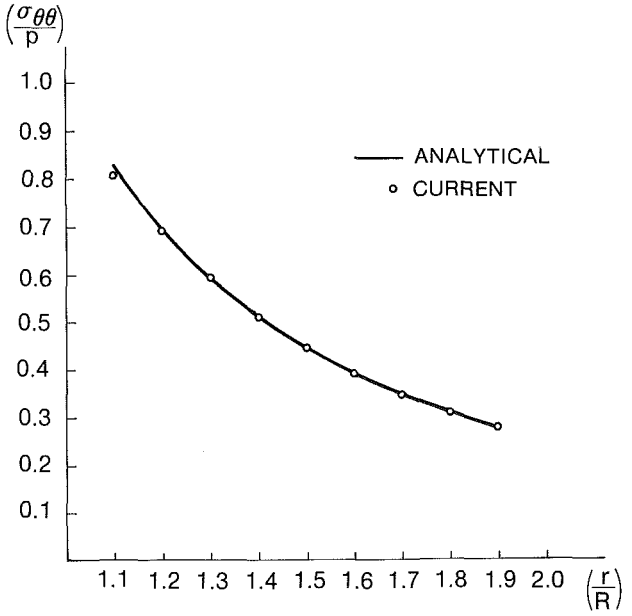


Fig. 8 Comparison of results form analytical and current approaches

$$T_w(p) = \sum_{i=1}^{N} \left[\int_{s_{1i}}^{s_{2i}} K_{21i}(p,s') f_{1i}(s')\,ds' + \int_{s_{1i}}^{s_{2i}} K_{22i}(p,s') f_{2i}(s')\,ds' \right] \tag{2}$$

Where p denotes any interior point at which the stresses are to be determined. It should be noted that the same equation can be applied to any point regardless whether this point is at the boundary, in the interior, or in the exterior. Unlike this approach, the direct potential method of Cruse (1969) gave different equations for points at the boundary and in the interior. Using our notation, the key BIE equations for a mixed boundary value problem take the following forms:

$$\tfrac{1}{2} u_j(s) + \int T_{ji}(s,s') u_i(s')\,ds' = \int U_{ji}(s,s') t_i(s')\,ds' \tag{3}$$

for any point s located at the smooth part of the boundary, and

$$u_j(p) = -\int T_{ji}(p,s') u_i(s')\,ds' + \int U_{ji}(p,s') t_i(s')\,ds'$$
$$\sigma_{ij}(p) = -\int S_{kij}(p,s') u_k(s')\,ds' + \int D_{kij}(p,s') t_k(s')\,ds' \tag{4}$$

for any interior point p.

The variables $t_i(S')$ and $u_i(S')$ are boundary tractions and displacements. The expressions for U_{ji}, T_{ji}, D_{kij}, and S_{kij} are available and can be found in Cruse's work (1969).

When equation (3) is applied to a traction boundary value problem, the unknowns are displacements along the boundary. But if equation (1) is used instead in the current approach, the unknowns are dislocation density functions along the boundary. Although both methods take advantage of the solution to Kelvin's problem which can be found in Love's book (1944), it is not straightforward to relate equations (1) to (3) mathematically. However, a direct relationship can be

Downloaded 03 May 2010 to 171.66.16.27. Redistribution subject to ASME license or copyright; see http://www.asme.org/terms/Terms_Use.cfm

established between the current approach and Crouch's (1983) displacement discontinuity method.

Physically, a "displacement discontinuity" of length $2a$ in an infinite solid (Fig. 5(*a*)) is simply a result of superposition of two dislocations as shown in Fig. 5(*b*): one is located at $x=a$, another one of equal strength but opposite sign is located at $x=-a$. Their equivalence can be verified by plotting their displacement along the x axis graphically and evaluating their stresses mathematically. Therefore, displacement discontinuity method, which from another point of view is simply discrete distribution of dislocation pairs along the boundary, can be considered as a special case of the current approach.

Numerical Method

For an ordinary crack problem, either the Gauss-Chebyshev method proposed by Erdogan et al. (1973) or the Lobatto-Chebyshev integration formula proposed by Theocaries et al. (1977) can be used to reduce equation (1) (without the summation sign, of course) to a system of linear algebraic equations. The second method is better in the sense that both crack ends are among the collocation points where the unknown dislocation density functions are to be determined. As a result, the stress intensity factors at the ends can be extracted directly from the numerical solution without extrapolation. This method should apply as well to a traction boundary value problem by simulating the boundary as a closed crack locus.

After normalizing the integration interval (S_{1i}, S_{2i}) in equation (1) to $(-1, 1)$, the Lobatto-Chebyshev formula can be readily applied. The numerical counterpart of (1) is:

$$[T_t(\xi_k)]_i = \sum_{i=1}^{N}\left[\sum_{j=1}^{M_i} W_i(\xi_k, \xi_j')K_{11i}(\xi_k, \xi_j')h_{1i}(\xi_j') + \sum_{j=1}^{M_i} W_i(\xi_k, \xi_j')K_{12i}(\xi_k, \xi_j')h_{2i}(\xi_j')\right]$$

$$[T_w(\xi_k)]_i = \sum_{i=1}^{N}\left[\sum_{j=1}^{M_i} W_i(\xi_k, \xi_j')K_{21i}(\xi_k, \xi_j')h_{1i}(\xi_j') + \sum_{j=1}^{M_i} W_i(\xi_k, \xi_j')K_{22i}(\xi_k, \xi_j')h_{2i}(\xi_j')\right] \quad (5)$$

where M_i is the number of collocation points for segment i and W_i (S_k, S_j) is the weighting function for numerical integration. The functions h_{1i} (ξ) and h_{2i} (ξ), being another form of the dislocation density functions, are related to f_{1i} (ξ) and f_{2i} (ξ) by:

$$h_{1i}(\xi) = 2f_{1i}(\xi)(1+\xi)^{1/2}(1-\xi)^{1/2}$$
$$h_{2i}(\xi) = 2f_{2i}(\xi)(1+\xi)^{1/2}(1-\xi)^{1/2} \quad (6)$$

According to the Lobatto-Chebyshev method, each element (or segment) i has $2M_i$ unknowns but only $2(M_i-1)$ equations can be generated for that element. Therefore, two more equations for each element have to be found.

Equation (6) suggests implicitly that the dislocation density function $f_{1i}(\xi)$, $f_{2i}(\xi)$, should have singularities of strength $-1/2$ at both ends for all line segments. This is not true in most cases. For example, although all the ends in Fig. 4 have singularities, none of them are of strength $-1/2$. In fact, they are all weaker than $-1/2$ as demonstrated by Williams (1952). This inconsistency can be amended by imposing the following end conditions:

$$h_{1i}(-1) = h_{1i}(1) = 0$$
$$(i = 1, \ldots\ldots, M_i) \quad (7)$$
$$h_{2i}(-1) = h_{2i}(1) = 0$$

Table 1 $\sigma_{\theta\theta}$ **along** x **axis of the disk** (N = 25 **for a quarter of the boundary**)

	x/R	0.1	0.2	0.3	0.4	0.5	0.6	0.7	0.8	0.9
$\frac{\sigma_{\theta\theta}}{p}$	Fictitious stress	−0.1172	−0.1085	−0.0955	−0.0801	−0.0639	−0.0483	−0.0341	−0.0217	−0.0111
	Displacement discontinuity	−0.1147	−0.1063	−0.0937	−0.0786	−0.0628	−0.0474	−0.0334	−0.0212	−0.0107
	Analytical	−0.1167	−0.1078	−0.0946	−0.0789	−0.0624	−0.0465	−0.0321	−0.0195	−0.0089
	Present	−0.1150	−0.1077	−0.0945	−0.0788	−0.0624	−0.0465	−0.0321	−0.0195	−0.0080

Downloaded 03 May 2010 to 171.66.16.27. Redistribution subject to ASME license or copyright; see http://www.asme.org/terms/Terms_Use.cfm

These combined with equations (5), gives $2(M_i+1)$ equations with $2M_i$ knowns.

This system of equations can be solved by minimizing the error of the solution in the least square sense. But we prefer to use the much simpler method by dropping two relatively insensitive equations for each element so that the total number of unknowns are equal to the total number of equations. This was the approach the author used in a previous publication (1981), which proved to be very successful. Using the same argument, we choose the following two equations out from (7)

$$h_{1i}(-1)=0$$

$$(i=1,\ldots\ldots,M_i)$$

$$h_{2i}(-1)=0$$

and subsequently complete the formulation of this problem.

Results and Discussion

Two examples are selected to demonstrate the effectiveness of this method. The first one shown in Fig. 6 is a problem with a ciruclar domain and a self-equilibrium uniform radial pressure with a 7.2 deg span. This problem is chosen from Crouch's book (1983) not just because its analytical solution is available, but also because the results obtained by applying the boundary element method based on several different formulations are also available. They are tabulated along with results from our approach in Table 1.

It is clear that the current method gives much better results than those generated by the fictitious stress and the displacement discontinuity methods as evidenced by the numbers presented in Table 1. Although examples are not given to compare the accuracy of results from the traditional BIE approach and the current approach, the former one should have the same accuracy as the latter one if a comparable numerical scheme is used in the BIE approach. This is because no approximation has been made in arriving at equations (1) and (3).

The second example shown in Fig. 7 is a problem with a pressurized circular hole in an infinite domain. The analytical solution for the circumferential stress is

$$\sigma_{\theta\theta}=p\frac{r^2}{R^2} \tag{8}$$

which can be found in any elasticity book. Figure 8 shows results from this equation and those from our formulation. Again, good agreement is found. In fact, except for the first point, which has an error of 2.6 percent, the rest of the data points from this formulation are identical to those from equation (8).

Someone may wonder why we did not report stress results on the boundary. This is because an unpolished BEM CODE has the deficiency of giving poor results on the boundary as shown in Crouch's book (1983). The current method is, of course, not an exception. However, it seems to be clear that, if the same numerical skills used elsewhere to extrapolate and obtain good results on the boundary are also incorporated in this method, this formulation should produce better results.

Another important finding is that this method is not sensitive to the assumption that element ends have stress singularities. This statement is justified by the good results of example 1. In fact, we break the boundary in example 1 into two elements. The one with load has five collocation points, the one without load has twenty collocation points. It is evident that all element ends do not have slope discontinuities and therefore should have no stress singularities. This feature increases the applicability of this method even further.

Conclusion

The method of dislocation distribution used extensively in fracture mechanics has been extended to an area unexplored before to solve 2-D elastostatics problems with a closed boundary. In this process the "crack locus" is allowed to form a close contour of arbitrary shape. Since the nature of this formulation is very similar to the spirit of BEM, the author would consider it as yet another approach for this recently revived method.

Based on the limited results, it appears that the dislocation formulation gives the same level or better accuracy than most BEMS for 2-D elastostatics. Consequently, this method provides a potential alternative for 2-D elasticity problems where local stress evaluation is of great concern.

However, it should be emphasized that the major purpose of this investigation is not to present another formulation for the boundary element method but to point out the fact that by closing the "crack locus," the popular dislocation distribution method frequently used in fracture mechanics can be extended and becomes another approach for the boundary element method. It is interesting to note that three different analytical methods of different physical interpretations originated from the same source (Kelvin's problem), developed independently without referring to one another for many years, finally approached the boundary element problems.

References

Bilby, B. A., and Eshelby, J. D., 1968, *Fracture*, Vol. I, Liebowitz, H., ed., Academic Press, pp. 99–182.

Crouch, S. L., and Starfield, A. M., 1983, *Boundary Element Method in Solid Mechanics with Application in Rock Mechanics and Geological Engineering*, George Allen & Unwin, London.

Cruse, T. A., 1969, "Numerical Solutions in Three Dimensional Elastostatics," *International Journal of Solids and Structures*, Vol. 5, pp. 1259–1274.

Erdogan, F., Gupta, G. D., and Ratwani, M., 1974, "Interaction Between a Circular Inclusion and an Arbitrarily Oriented Crack," ASME JOURNAL OF APPLIED MECHANICS, Vol. 41, pp. 1007–1013.

Erdogan, F., Gupta, F. D., and Cook, T. S., 1973, "Numerical Solution of Singular Integral Equations," *Methods of Analysis and Solutions of Crack Problems*, Sih, G. C., ed., Noordhoff, Leyden, The Netherlands, Chapter 7, pp. 368–425.

Rizzo, F. J., 1967, "An Integral Equation Approach to Boundary Value Problems of Classical Elastostatics," *Quarterly of Applied Mathematics*, Vol. 25, pp. 83–95.

Sheng, C. F., and Wheeler, L., 1981, "Crack Path Prediction for a Kinked Crack in the Neighborhood of a Circular Inclusion in an Infinite Medium," ASME JOURNAL OF APPLIED MECHANICS, Vol. 48, pp. 313–319.

Theocaris, P. S., 1977a, "Asymmetric Branching of Cracks," ASME JOURNAL OF APPLIED MECHANICS, Vol. 44, pp. 611–618.

Theocaris, P. S., and Ioakimidis, N. I., 1977b, "Numerical Integration Methods for the Solution of Singular Integral Equations," *Quarterly of Applied Mathematics*, Vol. 35, pp. 173–183.

Williams, M. L., 1952, "Stress Singularities Resulting from Various Boundary Conditions in Angular Corners of Plates in Extention," ASME JOURNAL OF APPLIED MECHANICS, Vol. 19, pp. 526–528.

Downloaded 03 May 2010 to 171.66.16.27. Redistribution subject to ASME license or copyright; see http://www.asme.org/terms/Terms_Use.cfm

R. Kienzler[1]
Duan Zhuping[2]

Visiting Scholars,
Division of Applied Mechanics,
Stanford University,
Stanford, Ca. 94305

On the Distribution of Hoop Stresses Around Circular Holes in Elastic Sheets

By means of well-known solutions of linear plane elasticity in polar coordinates, a remarkably simple formula is derived to calculate the distribution of hoop stresses at the boundary of a circular hole in an infinite sheet subjected to arbitrary (in plane) loads. The application of the formula is demonstrated with several examples.

1 Introduction

Holes in plane sheets cause stress concentrations since the original stress fields in the plate without holes are modified. The ratio of a selected stress norm as measured in the plate with discontinuities (plate with hole) to the same norm in the plate in the absence of the discontinuities (plate without hole) is the stress concentration factor or "Kerbziffer" (Neuber, 1958).

By using well-known solutions of linear plane elasticity in polar coordinates, a remarkably simple formula is derived in the next section to calculate hoop stresses at a circular hole in an infinite sheet subjected to arbitrary loading. The application of this formula is shown in Section 3 by several examples.

Once the hoop stresses at the boundary of a hole are known, not only can the stress-concentration factors be calculated immediately, but it is also possible to compute energy-release rates or "forces on defects" (Peach and Koehler, 1950), if dislocations or other defects are present in the neighborhood of the hole.

2 Derivation of the Formula

In the context of linear plane elasticity, we assume that the stress fields are known in an infinite medium subjected to arbitrary (in-plane) loads (point forces, distributed loads, stresses prescribed at infinity or dislocations, Fig. 1). On a circle of radius r_o the plate is supposed to be free of external loads and the stress state should have no singularities. Inside this circle no forces are applied.

Keeping the applied load unchanged we remove the material inside of the circle and create a sheet with a traction-free circular hole. We are interested in the distribution of the hoop stress at the circular boundary. The idea to solve the problem under consideration is rather classic, as illustrated in Fig. 2.

Since the overall stress state in the plate without the hole is known, the stresses on the circle can be expressed in polar coordinates (r, ϕ) in particular

$$\sigma_{rr}^{(o)}(\phi) = \sigma_{rr}(r_o, \phi),$$
$$\sigma_{r\phi}^{(o)}(\phi) = \sigma_{r\phi}(r_o, \phi),$$
$$\sigma_{\phi\phi}^{(o)}(\phi) = \sigma_{\phi\phi}(r_o, \phi).$$

We make a cut along the circle and superimpose a stress field $\sigma_{ij}^{(1)}(\phi)$ of a sheet with circular hole loaded by $-\sigma_{rr}^{(0)}(\phi)$ and $-\sigma_{r\phi}^{(o)}(\phi)$ at the boundary. It is appropriate, obviously, to expand the known stresses in Fourier-series

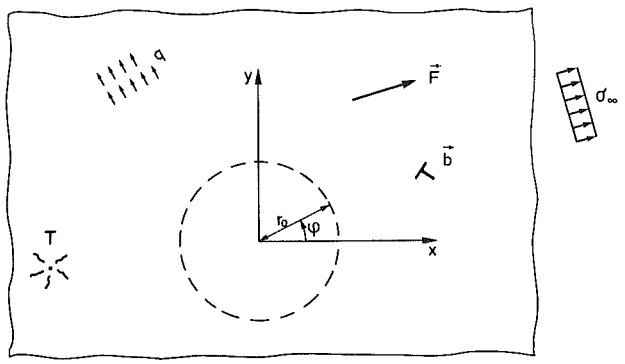


Fig. 1 Infinite sheet subjected to arbitrary loads

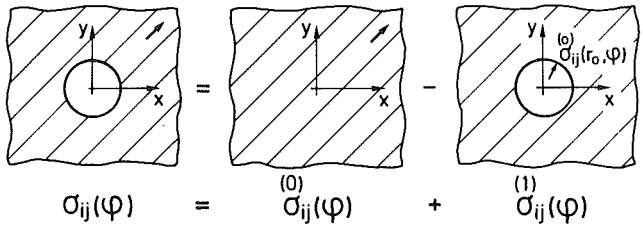


Fig. 2 Solution by superposition

[1]Now at Fraunhofer-Institut für Werkstoffmechanik, Wöhlerstr. 11, D-7800 Freiburg, FR Germany.

[2]On leave from Institute of Mechanics, Chinese Academy of Sciences, Beijing, China.

Contributed by the Applied Mechanics Division for publication in the JOURNAL OF APPLIED MECHANICS.

Discussion on this paper should be addressed to the Editorial Department, ASME, United Engineering Center, 345 East 47th Street, New York, N.Y. 10017, and will be accepted until two months after final publication of the paper itself in the JOURNAL OF APPLIED MECHANICS. Manuscript received by ASME Applied Mechanics Division, July 2, 1985; final revision May 22, 1986.

Copyright © 1987 by ASME
Downloaded 03 May 2010 to 171.66.16.27. Redistribution subject to ASME license or copyright; see http://www.asme.org/terms/Terms_Use.cfm

$$\sigma_{rr}^{(o)}(\phi)=\frac{A_o}{2}+\sum_{n=1}^{\infty}(A_n\cos n\phi+B_n\sin n\phi),$$

$$\sigma_{r\phi}^{(o)}(\phi)=\frac{C_o}{2}+\sum_{n=1}^{\infty}(C_n\cos n\phi+D_n\sin n\phi), \tag{1}$$

$$\sigma_{\phi\phi}^{(o)}(\phi)=\frac{E_o}{2}+\sum_{n=1}^{\infty}(E_n\cos n\phi+F_n\sin n\phi).$$

The constants A_n-F_n are the standard Fourier-coefficients, e.g.,

$$A_n=\frac{1}{\pi}\int_o^{2\pi}\sigma_{rr}^{(o)}(\phi)\cos n\phi\,d\phi,$$

$$B_n=\frac{1}{\pi}\int_o^{2\pi}\sigma_{rr}^{(o)}(\phi)\sin n\phi\,d\phi,\ \ldots \tag{2}$$

By making use of the basic solutions of linear plane elasticity for an infinite sheet with a circular hole (Timoshenko and Goodier, 1951) subjected to boundary loads $-\sigma_{rr}^{(o)}(\phi)$ and $-\sigma_{r\phi}^{(o)}(\phi)$ (1), the boundary hoop stress $\sigma_{\phi\phi}^{(1)}(\phi)$ is easily calculated as

$$\sigma_{\phi\phi}^{(1)}(\phi)=\frac{A_o}{2}+\left(\frac{1-\nu}{2}A_1+\frac{1+\nu}{2}D_1\right)\cos\phi$$

$$+\left(\frac{1-\nu}{2}B_1-\frac{1+\nu}{2}C_1\right)\sin\phi+\sum_{n=2}^{\infty}[(-A_n+2D_n)\cos n\phi$$

$$+(-B_n-2C_n)\sin n\phi]. \tag{3a}$$

where ν is Poisson's ratio.

Adding and subtracting equal terms and the use of equations (1) leads to an alternative representation of (3*a*) as

$$\sigma_{\phi\phi}^{(1)}(\phi)=\frac{A_o+E_o}{2}-2\sigma_{rr}^{(o)}(\phi)+\sigma_{\phi\phi}^{(o)}(\phi)$$

$$+A_o-E_o+\frac{1}{2}(5A_1+D_1-2E_1-\nu(A_1-D_1))\cos\phi$$

$$+\frac{1}{2}(5B_1-C_1-2F_1-\nu(B_1+C_1))\sin\phi \tag{3b}$$

$$+\sum_{n=2}^{\infty}[(A_n+2D_n-E_n)\cos n\phi+(B_n-2C_n-F_n)\sin n\phi].$$

In order to simplify equation (3*b*) we recall that the circular disk we cut out is subjected to self-equilibrated boundary loads $+\sigma_{rr}^{(o)}(\phi)$ and $+\sigma_{r\phi}^{(o)}(\phi)$ only, since tractions inside the circle were not admitted. Therefore, the Fourier-coefficients A_n-F_n are not independent of each other. To establish the relations between these constants we apply the basic solutions of linear plane elasticity (Timoshenko and Goodier, 1951) again, but now for a circular disk subjected to boundary loads $+\sigma_{rr}^{(o)}(\phi)$ and $+\sigma_{r\phi}^{(o)}(\phi)$, to calculate the boundary hoop stress $\sigma_{\phi\phi}^{(o)}(\phi)$

$$\sigma_{\phi\phi}^{(o)}=\frac{A_o}{2}+3A_1\cos\phi+3B_1\sin\phi$$

$$+\sum_{n=2}^{\infty}[(A_n+2D_n)\cos n\phi+(B_n-2C_n)\sin n\phi]. \tag{4}$$

In order to render the boundary loads self-equilibrated it is necessary that

$$\left.\begin{aligned}&C_o=0 && \text{(no resulting moment)}\\ &A_1=D_1\\ &B_1=-C_1\end{aligned}\right\}\ \text{(no resulting force)} \tag{5}$$

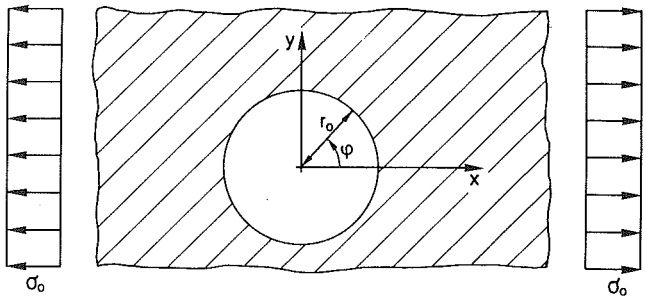


Fig. 3 Infinite sheet with circular hole subjected to uniaxial tension

Comparing coefficients of equal order of cos $n\phi$ and sin $n\phi$ in equations (1.3) and (4) we find with equations (5)

$$\begin{aligned}&A_o-E_o=0,\\ &A_1-D_1=0,\\ &B_1+C_1=0,\\ &5A_1+D_1-2E_1=0,\\ &5B_1-C_1-2F_1=0,\\ &A_n+2D_n-E_n=0,\\ &B_n-2C_n-F_n=0.\end{aligned} \tag{6}$$

With these relations equations (3*b*) is simplified considerably to

$$\sigma_{\phi\phi}^{(1)}(\phi)=\frac{A_o+E_o}{2}-2\sigma_{rr}^{(o)}+\sigma_{\phi\phi}^{(o)}(\phi). \tag{7}$$

The hoop stress at the boundary of the circular hole is obtained by adding $\sigma_{\phi\phi}^{(o)}$ and $\sigma_{\phi\phi}^{(1)}$ as

$$\sigma_{\phi\phi}(\phi)=K+2(\sigma_{\phi\phi}^{(o)}(\phi)-\sigma_{rr}^{(o)}(\phi)), \tag{8}$$

where the constant K following from equations (2) and (7)

$$K=\frac{1}{2\pi}\int_o^{2\pi}(\sigma_{rr}^{(o)}(\phi)+\sigma_{\phi\phi}^{(o)}(\phi))d\phi$$

is the integral over the first invariant of the stress tensor, i.e., its average value.

With equation (8) a remarkably simple formula is found to calculate the distribution of hoop stresses at the boundary of a circular hole in an infinite elastic sheet subjected to arbitrary loads. To the best of the authors' knowledge this relation has not been known before. Formula (8) will be applied to some problems in the following section.

3 Application of the Formula

3.1 Sheet with Circular Hole Subjected to Uniaxial Tension (Kirsch, 1898). Consider an infinite sheet (in the x, y plane) with a circular hole subjected to uniaxial tension in x direction (Fig. 3). The rather trivial solution for the plate without hole is

$$\begin{aligned}&\sigma_x=\sigma_0=\text{const.},\\ &\sigma_y=\sigma_{xy}=0,\end{aligned} \tag{9a}$$

or in polar coordinates (r, ϕ)

$$\begin{aligned}&\sigma_{rr}^{(o)}=\frac{\sigma_o}{2}(1+\cos 2\phi),\\ &\sigma_{\phi\phi}^{(o)}=\frac{\sigma_o}{2}(1-\cos 2\phi).\end{aligned} \tag{9b}$$

The constant K in equation (8) is evaluated as

Downloaded 03 May 2010 to 171.66.16.27. Redistribution subject to ASME license or copyright; see http://www.asme.org/terms/Terms_Use.cfm

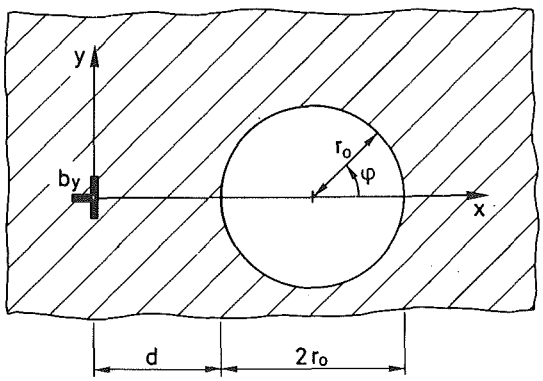


Fig. 4 Interaction between dislocation and circular hole

$$K=\frac{1}{2\pi}\,\sigma_o\int_o^{2\pi} d\phi=\sigma_o$$

and (10)

$$2(\sigma_{\phi\phi}^{(o)}-\sigma_{rr}^{(o)})=-2\sigma_o\cos 2\phi.$$

Inserting equations (10) into (8) we obtain immediately the well-known formula for the hoop stress (Kirsch, 1898)

$$\sigma_{\phi\phi}(\phi)=\sigma_o(1-2\cos 2\phi). \tag{11}$$

The stress concentration factor is three at $\phi = \pm \pi/2$. At $\phi = 0$ and $\phi = \pi$ the maximum compressive stress is $-\sigma_o$.

3.2 Interaction Between a Circular Hole and Edge Dislocation (Dundurs and Mura, 1964). Consider a plate in the x, y plane with a dislocation at the origin (burgers vector b_y in the y direction) and a circular hole (radius r_o) centered at $x = d + r_o$, $y = 0$ (Fig. 4). The stress field in the sheet without hole is due to Volterra (1907)

$$\sigma_{xx}=N\frac{r_o x(x^2-y^2)}{(x^2+y^2)^2},$$

$$\sigma_{yy}=N\frac{r_o x(x^2+3y^2)}{(x^2+y^2)^2},\quad N=\frac{2b_y G}{r_o\pi(\kappa+1)}. \tag{12}$$

$$\sigma_{xy}=N\frac{r_o y(x^2-y^2)}{(x^2+y^2)^2},$$

(G = shear modulus, $\kappa = 3-\nu/1+\nu$ for plane stress and $\kappa = 3-4\nu$ for plane strain). We introduce polar coordinates with respect to the circular boundary

$$x=r_o(1+\epsilon+\cos\phi),$$
$$y=r_o\sin\phi, \tag{13}$$
$$\epsilon=\frac{d}{r_o},$$

and transform the stress state to polar coordinates. After lengthy algebra we arrive at

$$\frac{1}{2}(\sigma_{rr}^{(o)}+\sigma_{\phi\phi}^{(o)}) = N\frac{1+\epsilon+\cos\phi}{2(1+\epsilon)(1+\cos\phi)+\epsilon^2},$$

$$2(\sigma_{rr}^{(o)}-\sigma_{\phi\phi}^{(o)}) = 8N(1+\epsilon)\frac{\sin^2\phi[1+(1+\epsilon)\cos\phi]}{[2(1+\epsilon)(1+\cos\phi)+\epsilon^2]^2}. \tag{14}$$

Integrating equation (14.1) with respect to ϕ the desired constant K is calculated to be

$$K=\frac{2N}{1+\epsilon}. \tag{15}$$

We insert equations (14) and (15) into (8) and arrive at

$$\sigma_{\phi\phi}(\phi)=\frac{2N}{1+\epsilon}-8N(1+\epsilon)\frac{\sin^2\phi[1+(1+\epsilon)\cos\phi]}{[2(1+\epsilon)(1+\cos\phi)+\epsilon^2]^2}. \tag{16}$$

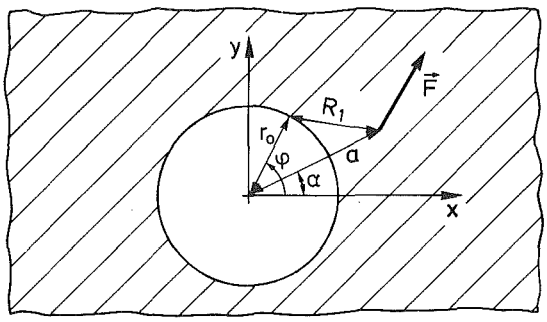


Fig. 5 Circular hole and point force

It is interesting to note that $\sigma_{\phi\phi}(\phi)$ remains finite for every ϕ even when ϵ tends to zero. Equation (16) may be used to model a crack near a hole by its dislocation density.

Dundurs and Mura (1964) studied the interaction between a dislocation and a circular inclusion. The special case of an inclusion with vanishing stiffness is, of course, included and confirms our result (16).

We want to use equation (16) further to calculate the "force on the defect." Instead of computing the Peach Köhler-force (1950) acting on the dislocation directly, we calculate (via actio = reactio) the material force on the hole by the by-now famous J integral or energy-release-rate-integral (Rice, 1968; Eshelby, 1961; Günther, 1962; Knowles and Sternberg, 1972). The general form of the ith component of the J integral vector in a coordinate invariant tensor formulation is given by

$$J_i=\oint_S(W\delta_{ij}-\sigma_{kj}u_{k,i})n_j ds. \tag{17}$$

(S is the closed contour around the "defect" with arc length s and unit outward normal $\vec{n}$, W is the strain-energy-density, δ_{ij} Kronecker's symbol, $u_{k,j} = \partial u_k/\partial x_j$ the displacement gradient, summation convention is implied for repeated indices).

By shrinking the contour of the integral so that it coincides with the boundary of the hole the x component of J reads

$$J_x=\frac{\kappa+1}{16G}\,r_o\int_o^{2\pi}\sigma_{\phi\phi}^2(\phi)\cos\phi\,d\phi. \tag{18}$$

With equation (16) J_x is evaluated by virtue of standard integral tables (e.g., Bronstein and Semendjajew, 1969) resulting in

$$J_x=-Nb_y\frac{1}{\epsilon(1+\epsilon)(2+\epsilon)}. \tag{19}$$

Dundurs and Mura showed in their paper that under certain circumstances (stiffness ratio of inclusion and matrix material, distance between inclusion and dislocation) there exists a position of equilibrium ($J_x = 0$) between inclusion and dislocation. From equation (19) it is obvious that such an equilibrium position will never exist (except if ϵ tends to infinity) between a hole and a dislocation. If the dislocation can move, it will move, namely towards the hole.

3.3 Circular Hole and Point Force (Sen, 1945). Consider an infinite plate with a circular hole (radius r_o) centered at the origin subjected to a point force at x_o, y_o with components F_x and F_y (Fig. 5). The solution for the plate without hole is (Love, 1927)

$$\sigma_{xx}=\frac{F_x}{4\pi}\frac{(x-x_o)[-(3+\nu)(x-x_o)^2-(1-\nu)(y-y_o)^2]}{[(x-x_o)^2+(y-y_o)^2]^2}$$
$$+\frac{F_y}{4\pi}\frac{(y-y_o)[-(1+3\nu)(x-x_o)^2+(1-\nu)(y-y_o)^2]}{[(x-x_o)^2+(y-y_o)^2]^2},$$

$$\sigma_{yy}=\frac{F_x}{4\pi}\frac{(x-x_o)[+(1-\nu)(x-x_o)^2-(1+3\nu)(y-y_o)^2]}{[(x-x_o)^2+(y-y_o)^2]^2}$$

Downloaded 03 May 2010 to 171.66.16.27. Redistribution subject to ASME license or copyright; see http://www.asme.org/terms/Terms_Use.cfm

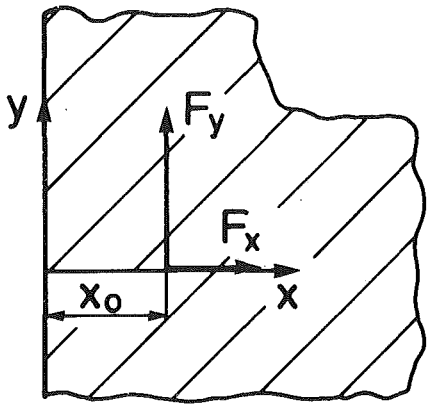


Fig. 6 Point force acting inside of half plane

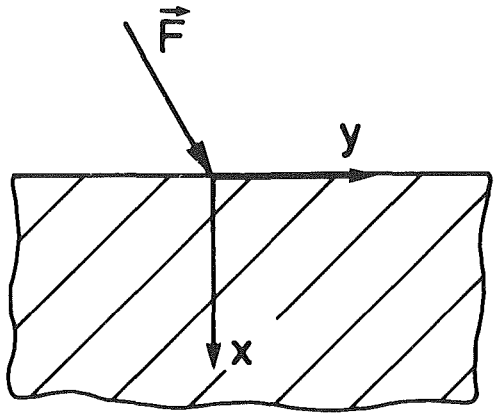


Fig. 7 Point force acting at the boundary of a half plane

$$+\frac{F_y}{4\pi}\frac{(y-y_o)[-(1-\nu)(x-x_o)^2-(3+\nu)(y-y_o)^2]}{[(x-x_o)^2+(y-y_o)^2]^2},$$

$$\sigma_{xy}=\frac{F_x}{4\pi}\frac{(y-y_o)[-(3+\nu)(x-x_o)^2-(1-\nu)(y-y_o)^2]}{[(x-x_o)^2+(y-y_o)^2]^2}$$

$$+\frac{F_y}{4\pi}\frac{(x-x_o)[-(1-\nu)(x-x_o)^2-(3+\nu)(y-y_o)^2]}{[(x-x_o)^2+(y-y_o)^2]^2}. \tag{20}$$

We introduce polar coordinates (Fig. 5)

$$\begin{aligned} x&=r_o\cos\phi,\\ y&=r_o\sin\phi,\\ x_o&=a\cos\alpha,\\ y_o&=a\sin\alpha, \end{aligned} \tag{21}$$

and make use of the abbreviations

$$\frac{a}{r_o}=1+\epsilon,$$

$$\rho^2=\frac{R_1^2}{r_o^2}=2(1+\epsilon)(1-\cos(\phi-\alpha))+\epsilon^2. \tag{22}$$

We decompose F_x and F_y in a radial and a tangential force F_r and F_ϕ, respectively,

$$\begin{aligned} F_x&=F_r\cos\alpha-F_\phi\sin\alpha,\\ F_y&=F_r\sin\alpha+F_\phi\cos\alpha. \end{aligned} \tag{23}$$

Transforming the stresses σ_{xx}, σ_{xy}, and σ_{yy} into σ_{rr}, $\sigma_{r\phi}$, and $\sigma_{\phi\phi}$ we obtain from equations (20)–(23) after some cumbersome but inevitable algebra the following expressions

$$\sigma_{rr}^{(o)}=\frac{F_r}{4\pi r_o\rho^2}\Big[(3+\nu)(1+\epsilon)-\cos(\phi-\alpha))$$
$$-2(1+\epsilon)\sin^2(\phi-\alpha)\Big(1-\nu$$
$$+(1+\nu)\frac{(1+\epsilon)(1+\epsilon-\cos(\phi-\alpha))}{\rho^2}\Big)\Big]$$
$$+\frac{F_\phi\sin(\phi-\alpha)}{4\pi r_o\rho^2}[-(3+\nu)+2(1-\nu)(1+\epsilon)\cos(\phi-\alpha)$$
$$+2(1+\nu)\frac{(1+\epsilon)^2\sin^2(\phi-\alpha)}{\rho^2}\Big],$$

$$\sigma_{\phi\phi}^{(o)}=\frac{F_r}{4\pi r_o\rho^2}\Big[-(1-\nu)(1+\epsilon-\cos(\phi-\alpha))$$
$$+2(1+\epsilon)\sin^2(\phi-\alpha)\Big(1-\nu$$
$$+(1+\nu)\frac{(1+\epsilon)(1+\epsilon-\cos(\phi-\alpha))}{\rho^2}\Big)\Big]$$
$$+\frac{F_\phi\sin(\phi-\alpha)}{4\pi r_o\rho^2}[(1-\nu)-2(1-\nu)(1+\epsilon)\cos(\phi-\alpha)$$
$$-2(1+\nu)\frac{(1+\epsilon)^2\sin^2(\phi-\alpha)}{\rho^2}\Big]. \tag{24}$$

From equations (24) and (8) the constant K is found to be

$$K=\frac{1+\nu}{2\pi(1+\epsilon)}F_r \tag{25}$$

and the formula (8) for the hoop stress distribution at the hole yields, finally, the expression

$$\sigma_{\phi\phi}(\phi)=\frac{F_r}{4\pi r_o(1+\epsilon)}\Big\{4+2(1+\epsilon)(3-\nu)\cos(\phi-\alpha)$$
$$+2(1-\nu)\epsilon(2+\epsilon)$$
$$-\frac{\epsilon(2+\epsilon)(\epsilon-\nu(4+6\epsilon+3\epsilon^2))}{\rho^2}$$
$$-\frac{(1+\nu)\epsilon^3(2+\epsilon)^3}{\rho^4}\Big\}$$
$$+\frac{F_\phi\sin(\phi-\alpha)}{2\pi r_o}\Big\{(3-\nu)-\frac{4(1+\epsilon)^2}{\rho^2}+\frac{(1+\nu)\epsilon^2(2+\epsilon)^2}{\rho^4}\Big\}. \tag{26}$$

This formula is verified by the general solution of this problem given by Sen (1945). Equation (26) may serve as a Green's function for the boundary-hoop-stress, if the sheet is subjected to distributed inplane forces (line forces, or forces per unit area).

We make use of equation (26) to study three special cases:

i Point Force Acting at the Boundary of the Hole. When ϵ approaches zero, equation (26) is simplified considerably. We arrive at

$$\sigma_{\phi\phi}(\phi)=\frac{F_r}{4\pi r_o}(4+2(3-\nu)\cos(\phi-\alpha))$$
$$+\frac{F_\phi\sin(\phi-\alpha)}{2\pi r_o}(3-\nu-\frac{2}{1-\cos(\phi-\alpha)}). \tag{27}$$

Equation (27) is confirmed by the general solution of this problem which is due to Bickley (1928).

Downloaded 03 May 2010 to 171.66.16.27. Redistribution subject to ASME license or copyright; see http://www.asme.org/terms/Terms_Use.cfm

ii Point Force Acting in a Half Plane. We introduce

$$\alpha = 0$$

$$x_o = a - r_o$$

and let r_o tend to infinity while

$$r_o \to \infty: \begin{cases} F_r \to F_x, \\ F_\phi \to F_y, \\ \sigma_{\phi\phi}(\phi) \to \sigma_{yy}(y), \\ a + r_o \to 2r_o, \\ \rho^2 \to \dfrac{x_0^2 + y^2}{r_o^2}, \\ r_o \sin(\phi - \alpha) \to y. \end{cases}$$

We derive from equation (26) the stress distribution at the boundary ($x = o$) of the half plane $x > o$ subjected to a point force acting at $x = x_o$, $y = o$ (Fig. 6)

$$\sigma_{yy}(y) = -\frac{2F_x x_o}{\pi(x_o^2 + y^2)^2}(x_o^2 - \nu y^2) - \frac{2F_y y}{\pi(x_o^2 + y^2)^2}(y^2 - \nu x_o^2). \tag{28}$$

Equation (28) is confirmed by the general solution of this problem given by Melan (1932) with a correction given by Kurshin (1959).

iii Point Force Acting at the Boundary of a Half Plane. If x_o approaches zero in equation (28) we obtain the stress distribution at the boundary of a half plane caused by a point force acting at x, $y = 0$ (Fig. 7)

$$\sigma_{yy}(y) = -\frac{2F_y}{\pi y}. \tag{29}$$

Equation (29) is readily verified by the Flammant-Boussinesq solution from 1892 (Timoshenko and Goodier, 1951).

4 Acknowledgment

This work was made possible by a fellowship of the Deutsche Forschungsgemeinschaft to Dr.-Ing. R. Kienzler, and has been sponsored in part by a grant of the Department of Energy under Contract No. DE-AT03-82ER12040 to Stanford University. This financial support is gratefully acknowledged.

5 References

Bickley, W. G., 1928, "The Distribution of Stress Round a Circular Hole in a Plate," *Philosophical Transactions of the Royal Society of London*, Ser. A, Vol. 227, pp. 383–415.

Bronstein, I. N., and Semendjajew, V. A., 1969, *Taschenbuch der Mathematik*, Teubner Verlagsgesellschaft, Leipzig.

Dundurs, J., and Mura, T., 1964, "Interaction Between an Edge Dislocation and a Circular Inclusion," *Journal of the Mechanics and Physics of Solids*, Vol. 12, pp. 177–189.

Eshelby, J. D., 1961, "Elastic Inclusions and Inhomogeneities," *Progress in Solid Mechanics*, Sneddon, I. N., and Hill, R., eds., Vol. 2, Chapter 3, North-Holland, Amsterdam, Holland.

Günther, W., 1962, "Über einige Randintegrale der Elastomechanik," *Abhandlungen der Braunschweigischen Wissenschaftlichen Gesellschaft*, Vol. 14, pp. 53–72.

Kirsch, G., 1898, "Die Theorie der Elastizität und die Bedürfnisse der Festigkeitslehre," *Verlag des Vereins Deutscher Ingenieure*, Vol. 42, pp. 797–807.

Knowles, J. K., and Sternberg, E., 1972, "On a Class of Conservation Laws in Linearized and Finite Elastostatics," *Archive for Rational Mechanics and Analysis*, Vol. 44, pp. 187–211.

Kurshin, L. M., 1959, "Mixed Plane Boundary Value Problem of the Theory of Elasticity for a Quadrant," *Prikladnaya Matematika i Mekhanika*, Vol. 23, pp. 981–984.

Love, A. E. H., 1927, *A Treatise on the Mathematical Theory of Elasticity*, Cambridge University Press, Cambridge.

Melan, E., 1932, "Der Spannungszustand der durch eine Einzelkraft im Innern beanspruchten Halbscheibe," *Zeitschrift für Angewandte Mathematik und Mechanik*, Vol. 12, pp. 343–346.

Neuber, H., 1958, *Kerbspannungslehre*, Springer-Verlag, Berlin/-Göttingen/Heidelberg.

Peach, M., and Koehler, J. S., 1950, "The Forces Exerted on Dislocations and the Stress Field Produced by Them," *Physical Review*, Vol. 80, pp. 436–439.

Rice, J. R., 1968, "A Path-Independent Integral and the Approximate Analysis of Strain Concentration by Notches and Cracks," ASME JOURNAL OF APPLIED MECHANICS, Vol. 35, pp. 379–386.

Sen, B., 1945, "Problems of Thin Plates With Circular Holes," *Bulletin of the Calcutta Mathematical Society*, Vol. 37, pp. 33–42.

Timoshenko, S., and Goodier, J. N., 1951, *Theory of Elasticity*, McGraw-Hill, New York/Toronto/London.

Volterra, V., 1907, "Sur l'équilibre des corps élastiques multiplement connexes," *Annales de l' Ecole Normale et Supérieure*, Vol. 24, pp. 401–517.

Downloaded 03 May 2010 to 171.66.16.27. Redistribution subject to ASME license or copyright; see http://www.asme.org/terms/Terms_Use.cfm

Three-Dimensional Vibration Analysis of a Truncated Quadrangular Pyramid

T. Irie
Faculty of Engineering,
Kansai University,
Suita, 564 Japan

G. Yamada

Y. Tagawa

Faculty of Engineering,
Hokkaido University,
Sapporo, 060 Japan

An analysis is presented for the three-dimensional vibration problem of determining the natural frequencies and the mode shapes of a truncated quadrangular pyramid. For this purpose, the body is transformed into a right quadrangular prism with unit edge lengths by a transformation of variables. With the displacements of the transformed prism assumed in the forms of algebraic polynomials, the dynamical energies of the prism are evaluated, and the frequency equation is derived by the Ritz method. This method is applied to quadrangular pyramids in which the base is clamped and the other sides are free, and the natural frequencies (the eigenvalues of vibration) and the mode shapes are calculated numerically, from which the vibration characteristics arising in the pyramids are studied.

1 Introduction

This paper presents an analysis of the free vibration of a truncated quadrangular pyramid in which the base is clamped and the other sides are free. Recently, these bodies have been extensively used as machine parts, electric devices, etc., and hence vibration problems of the bodies have assumed to increase practical importance.

McNiven and Perry (1962) studied the axisymmetrical vibration of circular cylinders with free bases by use of the displacements expressed in a potential function, and Rumerman and Raynor (1971) and Hutchinson (1967, 1972, 1979) applied the series-type solution using the Bessel functions to the same problem. Hutchinson (1980) also analyzed the unaxisymmetrical vibration of the cylinders by the solution of the same type. Meanwhile, Fromme and Leissa (1970) studied the free vibration of the rectangular parallelepiped by means of the method of associated periodicity, and Hutchinson and Zillmer (1983) treated the free vibration of the rectangular parallelepiped by using the series-type solution. Leissa and Zhang (1983) studied the free vibration of the cantilevered rectangular parallelepiped by the Ritz method, and Hill (1982a, 1982b, 1984) analyzed the vibrational response by a normal mode approach. Teh and Brown (1983) studied thick laminated plates by using the three-dimensional elasticity theory. However, all of them have been confined to the studies of circular cylinders or rectangular parallelepipeds, and no papers have been presented giving the results for the quadrangular pyramids reported here.

For the purpose of this study, a truncated quadrangular pyramid is transformed into a right quadrangular prism with unit edge lengths by a transformation of variables. The three-dimensional displacements of the transformed prism are expressed in the series of the product of the power functions of Cartesian coordinates. The maximum kinetic and strain energies of the prism are evaluated analytically, and the frequency equation is derived by the conditions for a stationary value of the Lagrange functional.

By these application of the method, the natural frequencies (the eigenvalues of vibration) and the mode shapes are calculated numerically up to higher modes. The results are presented in some figures and are compared with those obtained by the beam theories.

2 Frequency Equation

Leissa and Zhang have analyzed creditably the vibration problem of the cantilevered rectangular parallelepiped by the Ritz method in the above-mentioned paper (1983). Here, the analysis method by Lessia and Zhang is extended to the problem of truncated quadrangular pyramids.

Figure 1 shows a truncated quadrangular pyramid in which the base is clamped and the other sides are free. With the origin taken at the center of the clamped base, Cartesian coordinates (x, y, z) are taken as shown in the figure. A truncated quadrangular pyramid can be transformed into a right prism with unit edge lengths by the transformation of variables,

$$x=H\xi\{a-(a-a')\zeta\},\quad y=H\eta\{b-(b-b')\zeta\}$$
$$z=H\zeta,\ (a,b;a',b')=\frac{1}{H}\ (A,B;A',B') \tag{1}$$
$$J=H^3\{a-(a-a')\zeta\}\{b-(b-b')\zeta\}$$

where $A \times B$ are the edge lengths of the clamped base, $A' \times B'$ those of the free one, H is the height of the pyramid, and J

Contributed by the Applied Mechanics Division for publication in the JOURNAL OF APPLIED MECHANICS.

Discussion on this paper should be addressed to the Editorial Department, ASME, United Engineering Center, 345 East 47th Street, New York, N.Y. 10017, and will be accepted until two months after final publication of the paper itself in the JOURNAL OF APPLIED MECHANICS. Manuscript received by ASME Applied Mechanics Division, November 5, 1985; final revision September 18, 1986.

Copyright © 1987 by ASME
Downloaded 03 May 2010 to 171.66.16.27. Redistribution subject to ASME license or copyright; see http://www.asme.org/terms/Terms_Use.cfm

is the Jacobian of the transformation. The maximum kinetic energy of the prism can be expressed as

$$T=\frac{1}{2}\rho ABH\omega^2\int_{-1/2}^{1/2}\int_{-1/2}^{1/2}\int_0^1 (u^2+v^2+w^2)fgd\zeta d\eta d\xi \qquad (2)$$

in terms of the displacements u, v, and w in the x, y, z directions, respectively, where ρ is the mass density and ω is the frequency in radians/second. By applying well known equations of linear elasticity, the maximum strain energy is written as

$$\begin{aligned}V=\frac{1}{2}\frac{AB}{H}\int_{-1/2}^{1/2}\int_{-1/2}^{1/2}\int_0^1\Big[&\lambda\Big(\frac{1}{af}u_{,\xi}+\frac{1}{bg}v_{,\eta}+w_{,\zeta}\\&+\frac{1}{f'}w_{,\xi}+\frac{1}{g'}w_{,\eta}\Big)^2+G\Big\{2\Big(\frac{1}{af}u_{,\xi}\Big)^2+2\Big(\frac{1}{bg}v_{,\eta}\Big)^2\\&+2\Big(w_{,\zeta}+\frac{1}{f'}w_{,\xi}+\frac{1}{g'}w_{,\eta}\Big)^2+\Big(\frac{1}{af}v_{,\xi}+\frac{1}{bg}u_{,\eta}\Big)^2\\&+\Big(\frac{1}{af}w_{,\xi}+u_{,\zeta}+\frac{1}{f'}u_{,\xi}+\frac{1}{g'}u_{,\eta}\Big)^2+\Big(\frac{1}{bg}w_{,\eta}+v_{,\zeta}\\&+\frac{1}{f'}v_{,\xi}+\frac{1}{g'}v_{,\eta}\Big)^2\Big\}\Big]fgd\zeta d\eta d\xi \qquad (3)\end{aligned}$$

where λ and G are the Lame's constants, and f, g, f' and g' are defined as

$$f=1-(1-a'/a)\zeta, \qquad g=1-(1-b'/b)\zeta$$
$$f'=\frac{1-(1-a'/a)\zeta}{(1-a'/a)\xi}, \qquad g'=\frac{1-(1-b'/b)\zeta}{(1-b'/b)\eta} \qquad (4)$$

The subscript, attached to the displacements u, v, w denotes partial differentiation with respect to the variables following it.

The displacements of the transformed body are approximately expressed as

$$u=\sum_{i=0}^{I}\sum_{j=0}^{J}\sum_{k=1}^{K}A_{ijk}\xi^i\eta^j\zeta^k, \quad v=\sum_{l=0}^{L}\sum_{m=0}^{M}\sum_{n=1}^{N}B_{lmn}\xi^l\eta^m\zeta^n$$
$$w=\sum_{p=0}^{P}\sum_{q=0}^{Q}\sum_{r=1}^{R}C_{pqr}\xi^p\eta^q\zeta^r \qquad (5)$$

in terms of the power functions of the transformed coordinates. Substituting equations (5) into equations (2) and (3), and utilizing these equations in the conditions for a stationary value of the Lagrange functional $L=T-V$,

$$\frac{\partial L}{\partial A_{ijk}}=0, \quad \frac{\partial L}{\partial B_{lmn}}=0, \quad \frac{\partial L}{\partial C_{pqr}}=0 \qquad (6)$$

the frequency equation is derived:

$$\begin{bmatrix} U_{ijk}^{(i'j'k')}-\Omega^2T_{ijk}^{(i'j'k')} & F_{i'j'k'}^{(lmn)} & G_{i'j'k'}^{(pqr)} \\ F_{ijk}^{(l'm'n')} & V_{lmn}^{(l'm'n')}-\Omega^2T_{lmn}^{(l'm'n')} & H_{l'm'n'}^{(pqr)} \\ G_{ijk}^{(p'q'r')} & H_{lmn}^{(p'q'r')} & W_{pqr}^{(p'q'r')}-\Omega^2T_{pqr}^{(p'q'r')} \end{bmatrix}\begin{Bmatrix}A_{ijk}\\B_{lmn}\\C_{pqr}\end{Bmatrix}=0 \qquad (7)$$

where

$$\Omega^2=\frac{\rho H^2\omega^2}{G} \qquad (8)$$

is the dimensionless frequency parameter. The natural frequencies of the pyramid are determined by calculating the eigenvalues Ω which make the determinant obtained from the square matrix of (7) zero, and the mode shapes of vibration are determined by calculating the eigenvectors A_{ijk}, B_{lmn}, C_{pqr} corresponding to the eigenvalues. The elements $U_{ijk}^{(i'j'k')}$, $V_{lmn}^{(l'm'n')}$, $W_{pqr}^{(p'q'r')}$, . . . of the matrix in (7) are calculated from the expressions

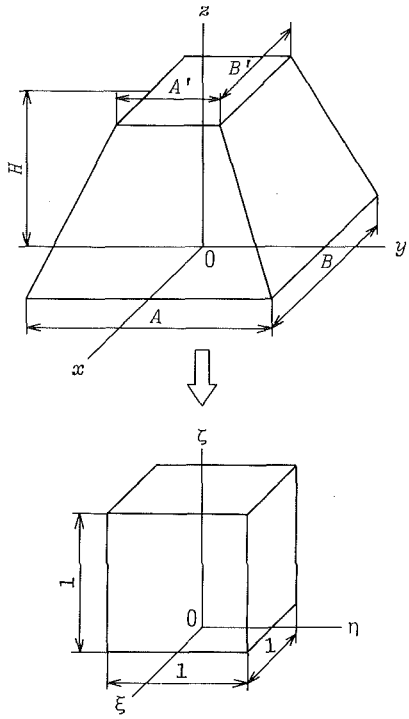


Fig. 1 Truncated quadrangular pyramid

$$\begin{aligned}U_{ijk}^{(i'j'k')}&=\int_{-1/2}^{1/2}\int_{-1/2}^{1/2}\int_0^1\Big\{(\lambda^*+2)\frac{ii'}{a^2f^2}\eta^2\zeta^2\\&+\frac{jj'}{b^2g^2}\zeta^2\xi^2+\Big(k\xi\eta+\frac{i}{f'}\eta\zeta+\frac{j}{g'}\zeta\xi\Big)\Big(k'\xi\eta+\frac{i'}{f'}\eta\zeta\\&+\frac{j'}{g'}\zeta\xi\Big)\Big\}fg\xi^{i+i'-2}\eta^{j+j'-2}\zeta^{k+k'-2}d\zeta d\eta d\xi\end{aligned}$$

$$\begin{aligned}V_{lmn}^{(l'm'n')}&=\int_{-1/2}^{1/2}\int_{-1/2}^{1/2}\int_0^1\Big\{\frac{ll'}{a^2f^2}\eta^2\zeta^2\\&+(\lambda^*+2)\frac{mm'}{b^2g^2}\zeta^2\xi^2\\&+\Big(n\xi\eta+\frac{l}{f'}\eta\zeta+\frac{m}{g'}\zeta\xi\Big)\Big(n'\xi\eta+\frac{l'}{f'}\eta\zeta+\frac{m'}{g'}\zeta\xi\Big)\\&\times fg\xi^{l+l'-2}\eta^{m+m'-2}\zeta^{n+n'-2}d\zeta d\eta d\xi\end{aligned} \qquad (9)$$

$$\begin{aligned}W_{pqr}^{(p'q'r')}&=\int_{-1/2}^{1/2}\int_{-1/2}^{1/2}\int_0^1\Big\{\frac{pp'}{a^2f^2}\eta^2\zeta^2+\frac{qq'}{b^2g^2}\zeta^2\xi^2\\&+(\lambda^*+2)\Big(r\xi\eta+\frac{p}{f'}\eta\zeta+\frac{q}{g'}\zeta\xi\Big)\Big(r'\xi\eta+\frac{p'}{f'}\eta\zeta+\frac{q'}{g'}\zeta\xi\Big)\Big\}\\&\times fg\xi^{p+p'-2}\eta^{q+q'-2}\zeta^{r+r'-2}d\zeta d\eta d\xi\end{aligned}$$

$$T_{ijk}^{(i'j'k')}=\int_{-1/2}^{1/2}\int_{-1/2}^{1/2}\int_0^1 fg\xi^{i+i'}\eta^{j+j'}\zeta^{k+k'}d\zeta d\eta d\xi$$

Downloaded 03 May 2010 to 171.66.16.27. Redistribution subject to ASME license or copyright; see http://www.asme.org/terms/Terms_Use.cfm

Table 1 Powers of series in (5) taken for the calculation

Vibration mode	u		v		w	
	i	j	l	m	p	q
SS	odd	even	even	odd	even	even
SA	even	even	odd	odd	odd	even
AS	odd	odd	even	even	even	odd
AA	even	odd	odd	even	odd	odd

Table 2 Convergence study of eigenvalues of vibration Ω^* for a truncated quadrangular pyramid: $a=b$, $a'=b'$, $a+a'=b+b'=2$, $a/a'=0.3$, $\nu=0.3$

Number of terms	SSS'S'-1	SSA'A'-1	SSS'S'-2
2×2×5	1.405	2.517	2.981
3×3×4	1.401	2.496	2.887
3×3×5	1.390	2.495	2.883
3×3×6	1.389	2.495	2.883
4×4×5	1.389	2.494	2.881
4×4×6	1.387	2.494	2.881

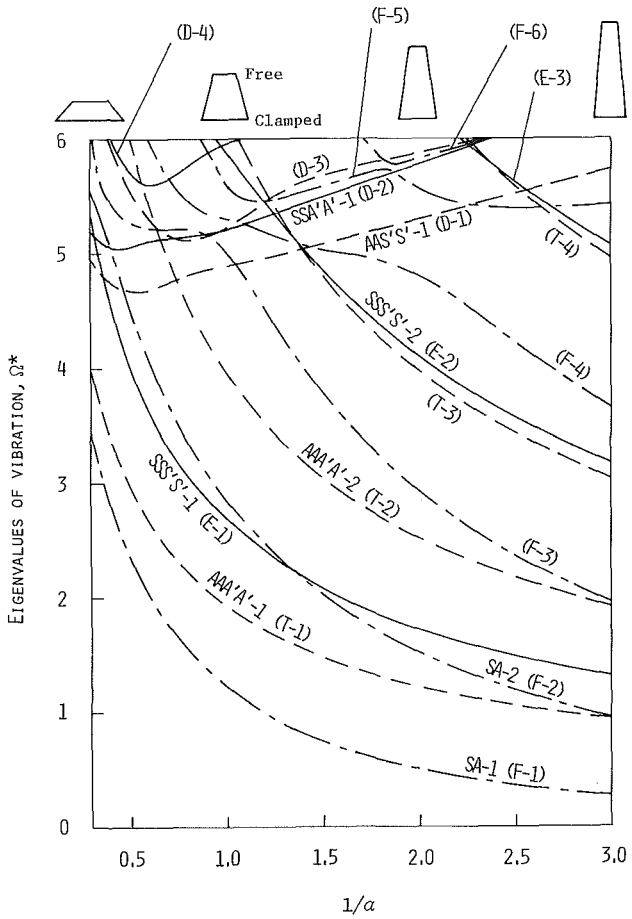


Fig. 2 Eigenvalues of vibration of truncated regular quadrangular pyramids with equal volume in which a base is free and the other clamped: $a=b$, $a'/a=b'/b=1/2$, $\nu=0.3$. (_____); SS, (- - - - -); AA, (____ - ____); SA-modes.

$$F_{ijk}^{(l'm'n')} = \int_{-1/2}^{1/2}\int_{-1/2}^{1/2}\int_0^1 \frac{1}{ab}\,(\lambda^* im' + jl')\xi^{i+l'-1}\eta^{j+m'-1}\zeta^{k+n'}\,d\zeta d\eta d\xi$$

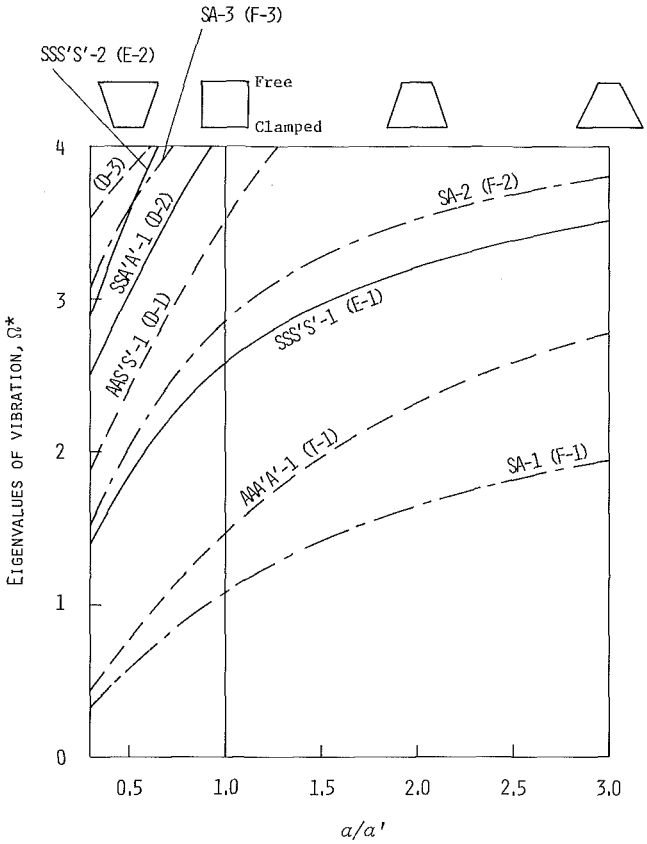


Fig. 3 Eigenvalues of vibration of truncated regular quadrangular pyramids with equal volume in which a base is free and the other clamped: $a=b$, $a'=b'$, $a+a'=b+b'=2$, $\nu=0.3$.

$$G_{ijk}^{(p'q'r')} = \int_{-1/2}^{1/2}\int_{-1/2}^{1/2}\int_0^1 \frac{1}{a}\left\{\lambda^* i\left(r'\xi\eta + \frac{p'}{f}\eta\zeta + \frac{q'}{g}\zeta\xi\right) + p'\left(k\xi\eta + \frac{i}{f'}\eta\zeta + \frac{j}{g'}\zeta\xi\right)\right\} \times g\xi^{i+p'-2}\eta^{j+q'-1}\zeta^{k+r'-1}\,d\zeta d\eta d\xi \tag{10}$$

$$H_{lmn}^{(p'q'r')} = \int_{-1/2}^{1/2}\int_{-1/2}^{1/2}\int_0^1 \frac{1}{b}\left\{\lambda^* m\left(r'\xi\eta + \frac{p'}{f}\eta\zeta + \frac{q'}{g}\zeta\xi\right) + q'\left(n\xi\eta + \frac{l}{f'}\eta\zeta + \frac{m}{g'}\zeta\xi\right)\right\} \times f\xi^{l+p'-2}\eta^{m+q'-1}\zeta^{n+r'-1}\,d\zeta d\eta d\xi$$

where λ^* is a constant expressed as $\lambda^* = 2\nu/(1-2\nu)$ in terms of Poisson's ratio ν.

3 Numerical Results and Discussion

In this section, by the application of the method, the eigenvalues of vibration and the mode shapes of the quadrangular pyramids are calculated numerically up to higher modes. Here, the eigenvalues are transformed into the values of pyramids with equal volume by the following transformation in order for clarifying the effects of the shape on the vibration:

$$\Omega^* = \frac{\sqrt[3]{V}}{H}\,\Omega, \quad V = \frac{H^3}{6}\,(2ab + ab' + a'b + 2a'b') \tag{11}$$

In a quadrangular pyramid which is symmetrical with respect to the two central planes perpendicular to the sides

Downloaded 03 May 2010 to 171.66.16.27. Redistribution subject to ASME license or copyright; see http://www.asme.org/terms/Terms_Use.cfm

(lateral faces), symmetrical (S-type) and antisymmetrical (A-type) vibrations arise with respect to the symmetry planes. For each type of vibrations, it is sufficient to take the powers in the series of (5) as shown in Table 1.

In the numerical calculation, the numbers of terms $I \times J \times K$, $L \times M \times N$, and $P \times Q \times R$ of the series in (5) may be truncated at appropriate finite numbers by considering the convergence of the numerical solution. Table 2 shows a convergence study of the eigenvalues of vibration for a truncated quadrangular pyramid when the numbers of terms increase. With an increase in numbers of terms, the eigenvalues converge within three or four significant digits. Though the numerical calculations using $4 \times 4 \times 6$ terms takes four computational times as much as that using $3 \times 3 \times 5$ terms, the difference of the eigenvalues is within only 0.2 percent. Therefore, the $3 \times 3 \times 5$ terms are employed for the present calculation. The values obtained by using $3 \times 3 \times 4$ terms for a rectangular parallelepiped ($a/a' = 1$) have been in complete agreement with the results obtained by Leissa and Zhang (1983).

Figure 2 shows the eigenvalues Ω^* versus the height ratio $1/a$ ($= H/A$) for regular quadrangular pyramids. The solid lines and the broken lines represent the SS and AA-type vibrations, respectively, and the chain lines the SA or AS-type vibration. In a regular quadrangular pyramid, symmetrical (S'-type) and antisymmetrical (A'-type) vibrations also arise with respect to the diagonal planes which bisect the right angles of the above-mentioned other symmetry planes. These types of vibration are included in the SS or AA-type vibration. There are also two groups of vibration. One of them is the extensional (E-type), flexural (F-type) and torsional (T-type) vibrations for which the eigenvalues become smaller monotonically with an increase of the ratio $1/a$. The other is the (D-type) vibration with distorted cross section which arises at higher frequencies increasing after once decreasing with an increase of the ratio $1/a$. For these regular quadrangular pyramids, the AS-type vibration has the same eigenvalues as the SA-type one.

Figure 3 shows the eigenvalues Ω^* versus the edge length ratio a/a' ($= A/A'$) for regular quadrangular pyramids with equal volume. The body with the ratio $a/a' = 1$ represents a regular quadrangular prism. With an increase of the ratio a/a' and also of the area of the clamped base, the eigenvalues become larger monotonically.

Figures 4(a) and 4(b) show the mode shapes together with

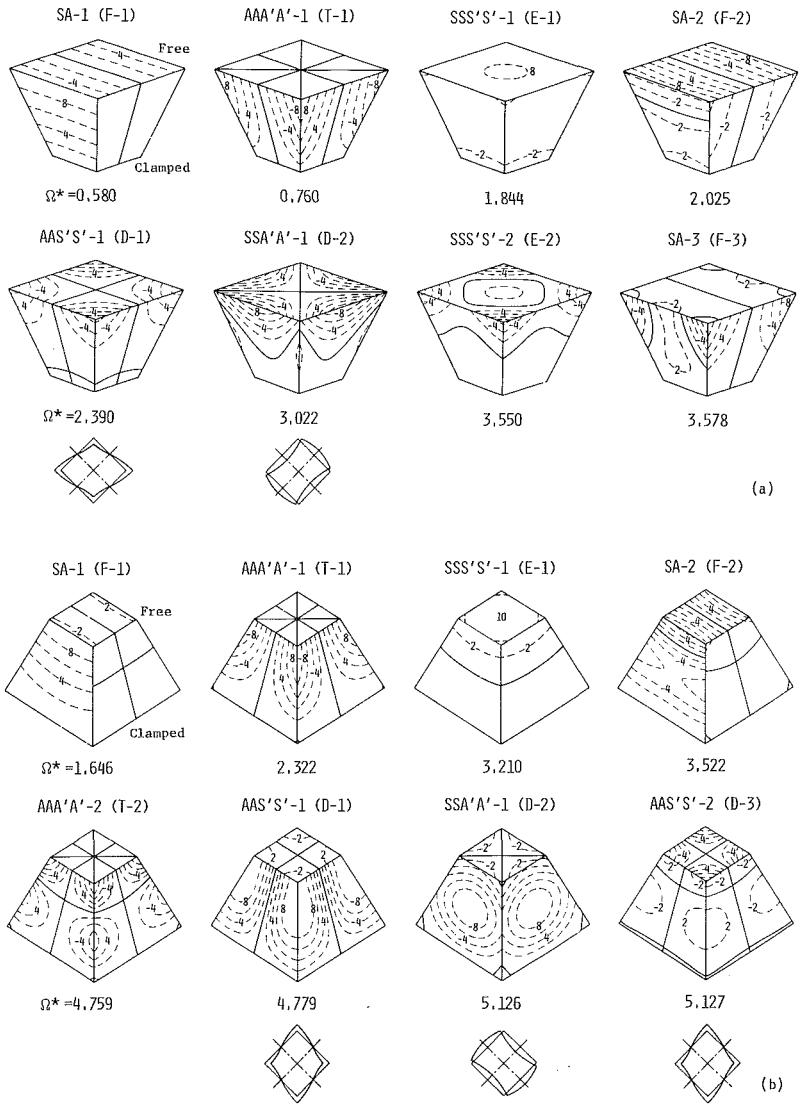


Fig. 4 Mode shapes of truncated regular quadrangular pyramids with equal volume in which a base is free and the other clamped: $a = b$, $a' = b'$, $a + a' = b + b' = 2$, $\nu = 0.3$. Fig. 4(a) $a/a' = 0.5$ and Fig. 4(b) $a/a' = 2.0$.

Downloaded 03 May 2010 to 171.66.16.27. Redistribution subject to ASME license or copyright; see http://www.asme.org/terms/Terms_Use.cfm

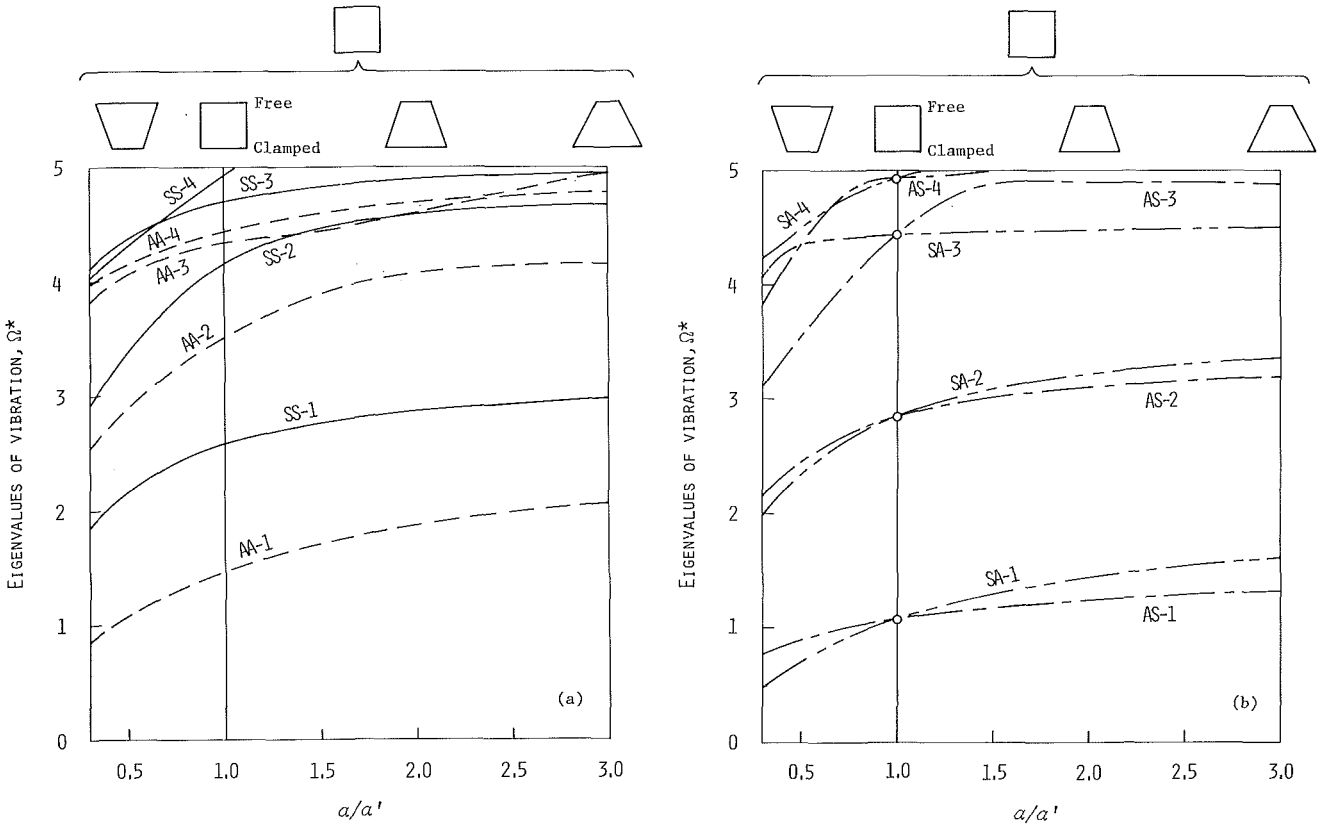


Fig. 5 Eigenvalues of vibration of truncated quadrangular pyramids with equal breadth and volume in which a base is free and the other clamped: $a+a'=2$, $b=b'=1$, $\nu=0.3$. Fig. 5(*a*) *SS* and *AA*-modes and Fig. 5(*b*) *SA* and *AS*-modes.

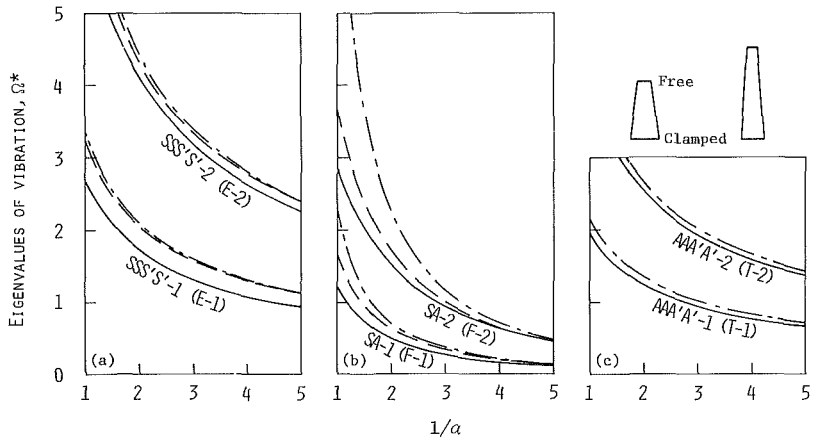


Fig. 6 Comparison of eigenvalues of vibration with the values by the beam theories for truncated regular quadrangular pyramids: $a=b$, $a'/a=b'/b=1/2$, $\nu=0.3$. (_____); three-dimensional theory, (- - - - -); modified beam theory, (___ - ___); elementary beam theory.

the eigenvalues of vibration for the regular quadrangular pyramids of the ratio $a/a' = 0.5$ and 2, respectively. The solid lines represent the nodal lines where the normal displacements of the surfaces are zero, and the dashed lines the contour lines of the displacements normal to those faces where the largest value of displacements is taken as $\pm$ 10. The $SSS'S'$-mode is the axially extensional (E-type) vibration with dominant axial displacement. The $AAA'A'$-mode is the torsional (T-type) vibration in which the torsional angle dominates. The SA or AS-mode is the flexural (F-type) vibration in which the lateral displacement is dominant. While, the $SSA'A'$ and $AAS'S'$-modes are the (D-type) vibration in which the cross section of the bodies is distored as shown in the margin of the figures.

Figures 5 show the eigenvalues Ω^* versus the edge length ratio a/a' $(= A/A')$ for the quadrangular pyramids with equal breadth and volume. With an increase of the ratio a/a', the eigenvalues become larger monotonically. In a right prism of $a/a' = 1$, the eigenvalues of the SA and AS-modes coincide with each other as shown by the circled points in Fig. 5(*b*).

Figure 6 shows a comparison of the eigenvalues with the values obtained by the beam theories for regular quadrangular

Downloaded 03 May 2010 to 171.66.16.27. Redistribution subject to ASME license or copyright; see http://www.asme.org/terms/Terms_Use.cfm

pyramids with larger axial length. The solid lines show the values obtained by the present three-dimensional theory, and the chain lines the values by the elementary beam theories. The broken lines in Fig. 6(*a*) show the eigenvalues of the extensional vibration obtained by the modified beam theory (Love, 1944) taking the radial inertia terms into account. While, the broken lines in Fig 6(*b*) show the values of the flexural vibration obtained by the Timoshenko beam theory (Irie et al., 1980) considering the effects of shear deformation and rotary inertia. In general, the values obtained by the beam theories are larger than the values by the three-dimensional theory. With an increase of the ratio $1/a$, the values by the classical beam theories gradually come close to the values by the present theory except for the extensional (*E*-type) vibration. The values of the *D*-type vibration can't be obtained by the beam theories.

The numerical computations presented here were carried out on a HITAC M-280H computer of the Hokkaido University Computing Center.

4 Conclusion

The free vibration has been studied for a truncated quadrangular pyramid in which the base is clamped and the other sides are free.

The pyramid has been transformed into a right quadrangular prism with unit edge lengths by a transformation of variables. With the displacements of the transformed prism expressed in terms of the power functions, the frequency equation has been derived by the Ritz method.

By the application of the method, the eigenvalues of vibration and the mode shapes have been calculated numerically to provide quantitative vibration characteristics. Sufficiently accurate values have been obtained by the method for quadrangular pyramids.

References

Fromme, J. R., and Leissa, A. W., 1970, "Free Vibration of the Rectangular Parallelepiped," *Journal of the Acoustical Society of America*, Vol. 48, pp. 290–298.

Hill, E. v. K., and Egle, D. M., 1982a, "The Forced Vibrational Response of a Rectangular Parallelepiped with Rigid-Lubricated Boundary," *Journal of Sound and Vibration*, Vol. 80, pp. 61–69.

Hill, E. v. K., 1982b, "Response of a Rectangular Parallelepiped to a Simulated Acoustic Emission Burst," *Journal of the Acoustical Society of America*, Vol. 71, pp. 891–901.

Hill, E. v. K., 1984, "The Vibrational Response of the Rectangular Parallelepiped with Completely Stress-Free Boundaries," *Journal of the Acoustical Society of America*, Vol. 75, pp. 442–446.

Hutchinson, J. R., 1967, "Axisymmetric Vibrations of a Solid Elastic Cylinder Encased in a Rigid Container," *Journal of the Acoustical Society of America*, Vol. 42, pp. 398–402.

Hutchinson, J. R., 1972, "Axisymmetric Vibrations of a Free Finite Length Rod," *Journal of the Acoustical Society of America*, Vol. 51, pp. 233–240.

Hutchinson, J. R., 1979, "Axisymmetric Flexural Vibrations of a Thick Free Circular Plates," ASME JOURNAL OF APPLIED MECHANICS, Vol. 46, pp. 139–144.

Hutchinson, J. R., 1980, "Vibrations of Solid Cylinders," ASME JOURNAL OF APPLIED MECHANICS, Vol. 47, pp. 907–910.

Hutchinson, J. R., and Zillmer, S. D., 1983, "Vibration of a Free Rectangular Parallelepiped," ASME JOURNAL OF APPLIED MECHANICS, Vol. 50, pp. 123–130.

Irie, T., Yamada, G., and Takahashi, I., 1980, "Vibration and Stability of a Non-Uniform Timoshenko Beam Subjected to a Follower Force," *Journal of Sound and Vibration*, Vol. 70, pp. 503–512.

Leissa, A. W., and Zhang, Z-D., 1983, "On the Three-Dimensional Vibrations of the Cantilevered Rectangular Parallelepiped," *Journal of the Acoustical Society of America*, Vol. 73, pp. 2013–2021.

Love, A. E. H., 1944, *A Treatise on the Mathematical Theory of Elasticity*, Dover, New York, pp. 428–429.

McNiven, H. D., and Perry, D., 1962, "Axially Symmetric Waves in Finite Elastic Rods," *Journal of the Acoustical Society of America*, Vol. 34, pp. 433–437.

Rumerman, M., and Raynor, S., 1971, "Natural Frequencies of Finite Circular Cylinders in Axially Symmetric Longitudinal Vibration," *Journal of Sound and Vibration*, Vol. 15, pp. 529–543.

Teh, K. K., and Brown, K. C., 1983, "On the Three-Dimensional Analysis of Thick Laminated Plates," *Journal of Sound and Vibration*, Vol. 88, pp. 213–224.

Downloaded 03 May 2010 to 171.66.16.27. Redistribution subject to ASME license or copyright; see http://www.asme.org/terms/Terms_Use.cfm

Asymmetric Wave Propagation in an Elastic Half-Space by a Method of Potentials

R. Y. S. Pak
Assistant Professor,
Department of Civil, Environmental,
and Architectural Engineering,
University of Colorado,
Boulder, CO 80309-0428
Assoc. Mem., ASME

A method of potentials is presented for the derivation of the dynamic response of an elastic half-space to an arbitrary, time-harmonic, finite, buried source. The development includes a set of transformed stress-potential and displacement-potential relations which are apt to be useful in a variety of wave propagation problems. Specific results for an embedded source of uniform distributions are also included.

1 Introduction

The dynamics of an elastic half-space under external or internal loads has long been a subject of great interest and active research because of its fundamental importance in earthquake engineering, seismology, and machine vibrations. The extensive literature dates back to the pioneering work of Lamb (1904) on waves produced by a line source. Many authors since then have considered elastic waves generated by various point and line loads acting in or on an elastic half-space, but only a few investigations were concerned with asymmetric sources. Among them may be mentioned the work of Pekeris and Longman (1955), Chao (1960), Gakenheimer and Miklowitz (1969), Johnson (1974), and Israel and Kovach (1977). However, none of these studies have considered loads or sources that are finite in extent. Of those that do, they are mostly concerned with surface loadings only, e.g., Thiruvenkatachar (1955), Arnold, Bycroft, and Warburton (1955), Thomson and Kobori (1963), Gladwell (1968), Luco and Westmann (1972), and Maiti and Mitra (1979).

In this paper, a method for the derivation of the response of an elastic half-space to an arbitrary, time-harmonic, finite, buried source is presented. The procedure is of sufficient generality to be useful in a variety of axisymmetric and asymmetric wave propagation problems. As illustrations, the results for two cases of uniform body-force fields are also included.

2 A Method of Potentials

The problem under consideration is depicted in Fig. 1. An arbitrary time-harmonic body-force field is assumed to be distributed over an open disc Π_s which is located at a depth s in a homogeneous, isotropic, linearly elastic half-space. Since the body-force field can be oriented in an arbitrary direction,

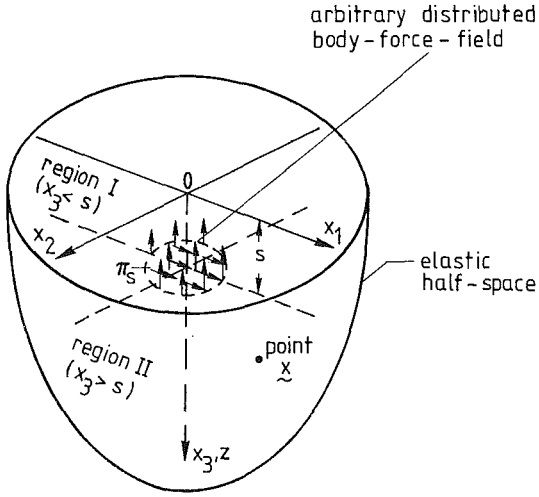


Fig. 1 A buried source in an elastic half-space

simplifications accompanying axial symmetry cannot be employed and the three-dimensional asymmetric wave propagation problem must be dealt with fully.

In elasticity, the method of potentials is a powerful tool for the treatment of complicated boundary value problems. For elastostatic problems associated with a half-space, the work of Harding and Sneddon (1945), later generalized by Muki (1960), is of classical importance as they have shown how the technique of integral transforms can be combined with the method of potentials to obtain solutions to this class of problems.

As to elastodynamic problems for a half-space, the use of Lamé potentials together with Hankel transforms has been very successful in simplifying axisymmetric cases. Similar attempts to date for general asymmetric problems have, however, not be equally attractive (Mindlin, 1963; Maiti and Mitra, 1979). One of the undesirable features of these attempts is that they do not reduce Navier's equations of motion to a set of simple real wave equations as in the axisymmetric situations. The lack of convenient transformed stress-potential and displacement-potential relations also renders the

Contributed by the Applied Mechanics Division for presentation at the 1987 Applied Mechanics, Biomechanics, and Fluids Engineering Conference, Cincinnati, OH, June 14-17, 1987, of the American Society of Mechanical Engineers.
Discussion on this paper should be addressed to the Editorial Department, ASME, United Engineering Center, 345 East 47th Street, New York, N.Y. 10017, and will be accepted until two months after final publication of the paper itself in the JOURNAL OF APPLIED MECHANICS. Manuscript received by ASME Applied Mechanics Division, December 13, 1985; final revision, April 18, 1986.
Paper No. 87-APM-4.

Copyright © 1987 by ASME
Downloaded 03 May 2010 to 171.66.16.27. Redistribution subject to ASME license or copyright; see http://www.asme.org/terms/Terms_Use.cfm

imposition of boundary and interfacial conditions difficult in buried-source problems. These are perhaps some of the reasons why many researchers, despite the complications thus incurred, still prefer to work directly with Navier's equations in tackling asymmetric problems. In what follows, a method of potentials is described which does not have the drawbacks mentioned above, and thus furnishes an efficient approach to asymmetric wave propagation problems.

2.1 Displacement Potentials. The development of the method takes as its point of departure the Helmholtz representation of a vector field. According to Helmholtz's theorem, given a suitably regular displacement vector field $\mathbf{u}$, there exists a scalar field ϕ and a vector field ψ such that

$$\mathbf{u} = \nabla\phi + \nabla \times \psi. \tag{1}$$

Lamé showed subsequently that such a representation of a displacement vector field satisfies Navier's displacement equations of motion in elasticity with zero body force fields

$$(\lambda + 2\mu)\,\nabla(\nabla \cdot \mathbf{u}) - \mu \nabla \times \nabla \times \mathbf{u} = \rho \frac{\partial^2 \mathbf{u}}{\partial t^2} \tag{2}$$

identically, provided that $\phi\,(\mathbf{x}, t)$ and $\psi\,(\mathbf{x}, t)$ are the solutions of the wave equations

$$\nabla^2\phi = \frac{1}{C_d^{\,2}} \frac{\partial^2 \phi}{\partial t^2}, \tag{3}$$

$$\nabla^2\psi = \frac{1}{C_s^{\,2}} \frac{\partial^2 \psi}{\partial t^2}, \tag{4}$$

respectively. Here, λ and μ stand for the Lamé constants of the classical theory of elasticity, while C_d and C_s are the dilatational and equivoluminal wave speeds, respectively. For the class of problems under consideration, it is sufficient to specialize the vector potential ψ to

$$\psi(\mathbf{x}) = \chi(r,\theta,z)\mathbf{e}_z + \nabla \times \eta(r,\theta,z)\mathbf{e}_z \tag{5}$$

where $\mathbf{e}_z$ is the unit vector along the z-direction of a circular cylindrical coordinate system (r, θ, z) (Morse and Feshbach, 1953). Representation (5) satisfies equation (4) identically provided

$$\nabla^2\chi = \frac{1}{C_s^{\,2}} \frac{\partial^2 \chi}{\partial t^2}, \tag{6}$$

$$\nabla^2\eta = \frac{1}{C_s^{\,2}} \frac{\partial^2 \eta}{\partial t^2}. \tag{7}$$

It can be shown that representation (5) satisfies a generalized gauge condition of the form

$$\left(\nabla^2 - \frac{1}{C_s^{\,2}} \frac{\partial^2}{\partial t^2}\right)(\nabla \cdot \psi) = 0 \tag{8}$$

which states that either $\nabla \cdot \psi = 0$ or that $\nabla \cdot \psi$ is a nonvanishing solution of equation (8) (Miklowitz, 1977). With the aid of representations (1) and (5), the wave propagation problem can thus be reduced to the determination of three scalar potentials ϕ, χ, and η, which are governed by the wave equations (3), (6), and (7), respectively. In circular cylindrical coordinates, the displacement-potential relations appear as

$$\begin{aligned} u_r &= \frac{\partial \phi}{\partial r} + \frac{1}{r}\frac{\partial \chi}{\partial \theta} + \frac{\partial^2 \eta}{\partial z \partial r}, \\ u_\theta &= \frac{1}{r}\frac{\partial \phi}{\partial \theta} - \frac{\partial \chi}{\partial r} + \frac{\partial^2 \eta}{r \partial z \partial \theta}, \\ u_z &= \frac{\partial \phi}{\partial z} - \frac{1}{r}\frac{\partial}{\partial r}\left(r\frac{\partial \eta}{\partial r}\right) - \frac{1}{r^2}\frac{\partial^2 \eta}{\partial \theta^2}, \end{aligned} \tag{9}$$

where u_r, u_θ, and u_z are the displacements in the r-, θ-, and z-directions, respectively. The strain-displacement relations are given by

$$\begin{aligned} &\epsilon_{rr} = \frac{\partial u_r}{\partial r}, \quad \epsilon_{\theta\theta} = \frac{1}{r}\left(\frac{\partial u_\theta}{\partial \theta} + u_r\right), \quad \epsilon_{zz} = \frac{\partial u_z}{\partial z}, \\ &\epsilon_{r\theta} = \frac{1}{r}\frac{\partial u_r}{\partial \theta} + r\frac{\partial}{\partial r}\left(\frac{u_\theta}{r}\right), \quad \epsilon_{z\theta} = \frac{1}{r}\frac{\partial u_z}{\partial \theta} + \frac{\partial u_\theta}{\partial z}, \\ &\epsilon_{rz} = \frac{\partial u_r}{\partial z} + \frac{\partial u_z}{\partial r}. \end{aligned} \tag{10}$$

The constitutive relations employed for the elastic medium are

$$\begin{aligned} &\tau_{rr} = \lambda\Delta + 2\mu\epsilon_{rr}, \quad \tau_{\theta\theta} = \lambda\Delta + 2\mu\epsilon_{\theta\theta}, \quad \tau_{zz} = \lambda\Delta + 2\mu\epsilon_{zz}, \\ &\tau_{r\theta} = \mu\epsilon_{r\theta}, \quad \tau_{z\theta} = \mu\epsilon_{z\theta}, \quad \tau_{rz} = \mu\epsilon_{rz}, \end{aligned} \tag{11}$$

where $\Delta = \nabla^2\phi$. The strain-potential relations can be obtained by substituting equations (9) into (10). Substitution of the resulting strain-potential relations into equations (11) leads to the stress-potential relations.

Although body-force fields have been ruled out in the formulation thus far, an examination of the momentum balance for a general plane element of infinitesimal thickness in the plane of Π_s suggests that the buried-source problem can be treated effectively as a half-space problem involving stress discontinuities across the plane $z = s$. In the mathematical treatment of this type of problem, it is convenient to view the half-space as being composed of an upper and a lower region of the same material (Regions I and II in Fig. 1) divided by the plane $z = s$, and to represent the distributed body-force field as a general discontinuity in stresses over Π_s across that plane, i.e.,

$$\begin{aligned} &\tau_{zr}(r,\theta,s^-,t) - \tau_{zr}(r,\theta,s^+,t) \\ &\qquad = \begin{cases} P(r,\theta,t), & (r,\theta,s) \in \Pi_s \\ 0, & (r,\theta,s) \notin \Pi_s \end{cases} \\ &\tau_{z\theta}(r,\theta,s^-,t) - \tau_{z\theta}(r,\theta,s^+,t) \\ &\qquad = \begin{cases} Q(r,\theta,t), & (r,\theta,s) \in \Pi_s \\ 0, & (r,\theta,s) \notin \Pi_s \end{cases} \\ &\tau_{zz}(r,\theta,s^-,t) - \tau_{zz}(r,\theta,s^+,t) \\ &\qquad = \begin{cases} R(r,\theta,t), & (r,\theta,s) \in \Pi_s \\ 0, & (r,\theta,s) \notin \Pi_s \end{cases} \end{aligned} \tag{12}$$

where $P(r, \theta, t)$, $Q(r, \theta, t)$, and $R(r, \theta, t)$ are the specified body-force distributions in the radial, angular, and axial directions, respectively. On requiring all displacements to be continuous across the plane $z = s$ and that the stresses vanish on the free surface, i.e.,

$$\tau_{zz}(r,\theta,0,t) = \tau_{zr}(r,\theta,0,t) = \tau_{z\theta}(r,\theta,0,t) = 0, \tag{13}$$

the formulation would be complete once the regularity conditions at infinity, commonly known as the "radiation conditions," are specified. A consideration of the characteristics of a half-space suggests that the solution in Region II be required to contain only outgoing waves and to be bounded as z approaches infinity. A more rigorous statement of the radiation conditions in classical elastodynamics can be found in Kupradze (1965).

2.2 Time-Harmonic Motions. For time-harmonic sources with a time factor of $e^{i\omega t}$, one may express the potentials and other quantities of interest in the form

$$\begin{aligned} &\phi(r,\theta,z,t) = \phi(r,\theta,z)e^{i\omega t}, \\ &\chi(r,\theta,z,t) = \chi(r,\theta,z)e^{i\omega t}, \\ &\eta(r,\theta,z,t) = \eta(r,\theta,z)e^{i\omega t}, \text{ etc.} \end{aligned} \tag{14}$$

Downloaded 03 May 2010 to 171.66.16.27. Redistribution subject to ASME license or copyright; see http://www.asme.org/terms/Terms_Use.cfm

With the time factor $e^{i\omega t}$ suppressed henceforth, equations (3), (6), and (7) become

$$(\nabla^2 + k_d^2)\phi = 0, \quad (\nabla^2 + k_s^2)\chi = 0, \quad (\nabla^2 + k_s^2)\eta = 0, \quad (15)$$

where $k_d = \omega/C_d$, $k_s = \omega/C_s$, and

$$\nabla^2 = \frac{\partial^2}{\partial r^2} + \frac{1}{r}\frac{\partial}{\partial r} + \frac{1}{r^2}\frac{\partial^2}{\partial \theta^2} + \frac{\partial^2}{\partial z^2}.$$

In view of the completeness of the set of angular eigenfunctions $\{e^{im\theta}\}_{m=-\infty}^{+\infty}$ for the class of solutions under consideration, one may write

$$\phi(r,\theta,z) = \sum_{m=-\infty}^{\infty} \phi_m(r,z)e^{im\theta},$$

$$\chi(r,\theta,z) = \sum_{m=-\infty}^{\infty} \chi_m(r,z)e^{im\theta}, \quad (16)$$

$$\eta(r,\theta,z) = \sum_{m=-\infty}^{\infty} \eta_m(r,z)e^{im\theta},$$

and

$$u_r(r,\theta,z) = \sum_{m=-\infty}^{\infty} u_{r_m}(r,z)e^{im\theta},$$

$$u_\theta(r,\theta,z) = \sum_{m=-\infty}^{\infty} u_{\theta_m}(r,z)e^{im\theta}, \quad (17)$$

$$u_z(r,\theta,z) = \sum_{m=-\infty}^{\infty} u_{z_m}(r,z)e^{im\theta}.$$

Likewise, one may write equations (12) as

$$\tau_{zr}(r,\theta,s^-) - \tau_{zr}(r,\theta,s^+) = \begin{cases} \sum_{m=-\infty}^{\infty} P_m(r)e^{im\theta}, & (r,\theta,s)\in\Pi_s \\ 0, & (r,\theta,s)\notin\Pi_s \end{cases}$$

$$\tau_{z\theta}(r,\theta,s^-) - \tau_{z\theta}(r,\theta,s^+) = \begin{cases} \sum_{m=-\infty}^{\infty} Q_m(r)e^{im\theta}, & (r,\theta,s)\in\Pi_s \\ 0, & (r,\theta,s)\notin\Pi_s \end{cases} \quad (18)$$

$$\tau_{zz}(r,\theta,s^-) - \tau_{zz}(r,\theta,s^+) = \begin{cases} \sum_{m=-\infty}^{\infty} R_m(r)e^{im\theta}, & (r,\theta,s)\in\Pi_s \\ 0, & (r,\theta,s)\notin\Pi_s \end{cases}$$

Substituting equations (16) into (15) and invoking the orthogonality condition of the eigenfunctions $\{e^{im\theta}\}$, one is led to the conclusion that

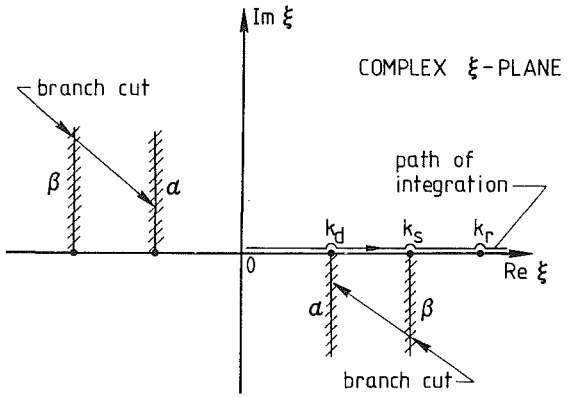


Fig. 2 Branch cuts for α and β

$$\frac{\partial^2\phi_m}{\partial r^2} + \frac{1}{r}\frac{\partial\phi_m}{\partial r} + \left(k_d^2 - \frac{m^2}{r^2}\right)\phi_m + \frac{\partial^2}{\partial z^2}\phi_m = 0,$$

$$\frac{\partial^2\chi_m}{\partial r^2} + \frac{1}{r}\frac{\partial\chi_m}{\partial r} + \left(k_s^2 - \frac{m^2}{r^2}\right)\chi_m + \frac{\partial^2}{\partial z^2}\chi_m = 0, \quad (19)$$

$$\frac{\partial^2\eta_m}{\partial r^2} + \frac{1}{r}\frac{\partial\eta_m}{\partial r} + \left(k_s^2 - \frac{m^2}{r^2}\right)\eta_m + \frac{\partial^2}{\partial z^2}\eta_m = 0,$$

$$\text{for } m = 0, \pm 1, \pm 2, \ldots .$$

In view of the geometry and the boundary conditions of the problem, it is natural to introduce the mth order Hankel transform

$$\tilde{f}^m(\xi,z) = \int_0^\infty f(r,z)rJ_m(\xi r)dr \quad (20)$$

whose inversion formula is

$$f(r,z) = \int_0^\infty \tilde{f}^m(\xi,z)\xi J_m(\xi r)d\xi. \quad (21)$$

Application of the above transform to the equations in (19) reduces them to a set of ordinary differential equations in z:

$$\frac{d^2\tilde{\phi}_m^m}{dz^2}(\xi,z) + (k_d^2 - \xi^2)\tilde{\phi}_m^m(\xi,z) = 0,$$

$$\frac{d^2\tilde{\chi}_m^m}{dz^2}(\xi,z) + (k_s^2 - \xi^2)\tilde{\chi}_m^m(\xi,z) = 0, \quad (22)$$

$$\frac{d^2\tilde{\eta}_m^m}{dz^2}(\xi,z) + (k_s^2 - \xi^2)\tilde{\eta}_m^m(\xi,z) = 0,$$

$$\text{for } m = 0, \pm 1, \pm 2, \ldots ,$$

where ξ is the transform parameter. The solutions of equations (22) can easily be found to be

$$\begin{aligned} \tilde{\phi}_m^m(\xi,z) &= A_m^I(\xi)e^{\alpha z} + B_m^I(\xi)e^{-\alpha z}, \\ \tilde{\chi}_m^m(\xi,z) &= C_m^I(\xi)e^{\beta z} + D_m^I(\xi)e^{-\beta z}, \\ \tilde{\eta}_m^m(\xi,z) &= E_m^I(\xi)e^{\beta z} + F_m^I(\xi)e^{-\beta z} \quad \text{in Region I,} \end{aligned} \quad (23)$$

and

$$\begin{aligned} \tilde{\phi}_m^m(\xi,z) &= B_m^{II}(\xi)e^{-\alpha z}, \\ \tilde{\chi}_m^m(\xi,z) &= D_m^{II}(\xi)e^{-\beta z}, \\ \tilde{\eta}_m^m(\xi,z) &= F_m^{II}(\xi)e^{-\beta z} \quad \text{in Region II,} \end{aligned} \quad (24)$$

where $\alpha = (\xi^2 - k_d^2)^{1/2}$, $\beta = (\xi^2 - k_s^2)^{1/2}$, and $A_m^I, \ldots, F_m^I$, $B_m^{II}, \ldots, F_m^{II}$ are constants of integration to be determined from the boundary conditions. The radicals α and β are made single-valued by specifying the branch cuts emanating from the branch points $\xi = \pm k_d$ and $\xi = \pm k_s$, respectively. The branches are chosen such that the real parts of α and β are

Downloaded 03 May 2010 to 171.66.16.27. Redistribution subject to ASME license or copyright; see http://www.asme.org/terms/Terms_Use.cfm

always nonnegative (see Fig. 2). Under this choice of the branches, the $e^{\alpha z}$ and $e^{\beta z}$ terms in Region II become inadmissible due to the radiation conditions and are thus omitted in equations (24).

Despite the complicated expressions for the stress-potential and displacement-potential relations in equations (11) and (9), the transformed relations, in proper combinations, are relatively simple. It can be shown that the transformed displacement-potential relations are:

$$\tilde{u}^m_{z_m} = \frac{d}{dz}\,\tilde{\phi}^m_m + \xi^2\tilde{\eta}^m_m,$$

$$\tilde{u}^{m-1}_{r_m} - i\tilde{u}^{m-1}_{\theta_m} = \xi\left(\tilde{\phi}^m_m + \frac{d}{dz}\,\tilde{\eta}^m_m + i\tilde{\chi}^m_m\right), \tag{25}$$

$$\tilde{u}^{m+1}_{r_m} + i\tilde{u}^{m+1}_{\theta_m} = -\xi\left(\tilde{\phi}^m_m + \frac{d}{dz}\,\tilde{\eta}^m_m - i\tilde{\chi}^m_m\right).$$

The transformed stress-potential relations required for the analysis take the form

$$\tilde{\tau}^m_{zz_m} = -\lambda\xi^2\tilde{\phi}^m_m + (\lambda+2\mu)\,\frac{d^2}{dz^2}\,\tilde{\phi}^m_m + 2\mu\xi^2\,\frac{d}{dz}\,\tilde{\eta}^m_m,$$

$$\tilde{\tau}^{m-1}_{zr_m} - i\tilde{\tau}^{m-1}_{z\theta_m} = \mu\xi\left(2\,\frac{d}{dz}\,\tilde{\phi}^m_m + \frac{d^2}{dz^2}\,\tilde{\eta}^m_m + \xi^2\tilde{\eta}^m_m + i\,\frac{d}{dz}\,\tilde{\chi}^m_m\right), \tag{26}$$

$$\tilde{\tau}^{m+1}_{zr_m} + i\tilde{\tau}^{m+1}_{z\theta_m} = -\mu\xi\left(2\,\frac{d}{dz}\,\tilde{\phi}^m_m + \frac{d^2}{dz^2}\,\tilde{\eta}^m_m + \xi^2\tilde{\eta}^m_m - i\,\frac{d}{dz}\,\tilde{\chi}^m_m\right).$$

For completeness, it can also be shown that

$$\tilde{\tau}^m_{rr_m} + 2\mu\left\{\left(\frac{\tilde{u_{r_m}}}{r}\right)^m + im\left(\frac{\tilde{u_{\theta_m}}}{r}\right)^m\right\} = \lambda\,\frac{d^2}{dz^2}\,\tilde{\phi}^m_m - (\lambda+2\mu)\xi^2\tilde{\phi}^m_m - 2\mu\xi^2\,\frac{d}{dz}\,\tilde{\eta}^m_m,$$

$$\tilde{\tau}^m_{\theta\theta_m} - 2\mu\left\{\left(\frac{\tilde{u_{r_m}}}{r}\right)^m + im\left(\frac{\tilde{u_{\theta_m}}}{r}\right)^m\right\} = \lambda\,\frac{d^2}{dz^2}\,\tilde{\phi}^m_m - \lambda\xi^2\tilde{\phi}^m_m, \tag{27}$$

$$\tilde{\tau}^m_{r\theta_m} + 2\mu\left\{\left(\frac{\tilde{u_{\theta_m}}}{r}\right)^m - im\left(\frac{\tilde{u_{r_m}}}{r}\right)^m\right\} = \mu\xi^2\tilde{\chi}^m_m.$$

With the aid of equations (25) and (26), the imposition of the boundary and interfacial conditions is greatly facilitated; it provides the nine equations required for the solution for the nine unknowns $A^I_m \ldots F^{II}_m$ in equations (23) and (24). This set of equations can be solved explicitly in terms of the Fourier coefficients P_m, Q_m, and R_m of the body-force field distributions. Substitution of the result into equation (25) gives the transformed Fourier components of the displacements:

$$\tilde{u}^{m-1}_{r_m} - i\tilde{u}^{m-1}_{\theta_m} = \gamma_1(z,s,\xi)\left(\frac{X_{m-}Y_m}{2\mu}\right) + \gamma_2(z,s,\xi)\left(\frac{X_{m+}Y_m}{2\mu}\right) + \gamma_3(z,s,\xi)\left(\frac{Z_m}{\mu}\right),$$

$$\tilde{u}^{m+1}_{r_m} + i\tilde{u}^{m+1}_{\theta_m} = -\gamma_1(z,s,\xi)\left(\frac{X_{m-}Y_m}{2\mu}\right) + \gamma_2(z,s,\xi)\left(\frac{X_{m+}Y_m}{2\mu}\right) - \gamma_3(z,s,\xi)\left(\frac{Z_m}{\mu}\right), \tag{28}$$

$$\tilde{u}^m_{z_m} = \Omega_1(z,s,\xi)\left(\frac{X_{m-}Y_m}{2\mu}\right) + \Omega_2(z,s,\xi)\left(\frac{Z_m}{\mu}\right),$$

where

$$\gamma_1(z,s,\xi) = \frac{1}{2}\left\{\frac{\xi^2}{\alpha k_s^2}\,e^{-\alpha|z-s|} - \frac{\beta}{k_s^2}\,e^{-\beta|z-s|} - \frac{R^+(\xi)}{k_s^2R^-(\xi)}\left(\frac{\xi^2}{\alpha}e^{-\alpha(z+s)} + \beta e^{-\beta(z+s)}\right) + \frac{4\xi^2\beta(2\xi^2-k_s^2)}{k_s^2R^-(\xi)}\left(e^{-(\beta z+\alpha s)} + e^{-(\beta s+\alpha z)}\right)\right\},$$

$$\gamma_2(z,s,\xi) = \frac{1}{2\beta}\left(e^{-\beta|z-s|} + e^{\beta(z+s)}\right),$$

$$\gamma_3(z,s,\xi) = \operatorname{sgn}(z-s)\,\frac{\xi}{2k_s^2}\left(e^{-\alpha|z-s|} - e^{-\beta|z-s|}\right) + \frac{1}{2}\,\frac{R^+(\xi)}{R^-(\xi)}\,\frac{\xi}{k_s^2}\left(e^{-\alpha(z+s)} + e^{-\beta(s+z)}\right) - \frac{2\xi(2\xi^2-k_s^2)}{R^-(\xi)k_s^2}\left(\alpha\beta e^{-(\beta z+\alpha s)} + \xi^2 e^{-(\beta s+\alpha z)}\right),$$

$$\Omega_1(z,s,\xi) = -\operatorname{sgn}(z-s)\,\frac{\xi}{2k_s^2}\left(e^{-\alpha|z-s|} - e^{-\beta|z-s|}\right) + \frac{1}{2}\,\frac{\xi}{k_s^2}\,\frac{R^+(\xi)}{R^-(\xi)}\left(e^{-\alpha(z+s)} + e^{-\beta(z+s)}\right) - \frac{2\xi(2\xi^2-k_s^2)}{R^-(\xi)k_s^2}\left(\xi^2 e^{-(\beta z+\alpha s)} + \alpha\beta e^{-(\beta s+\alpha z)}\right), \tag{29}$$

$$\Omega_2(z,s,\xi) = -\frac{\alpha}{2k_s^2}\,e^{-\alpha|z-s|} + \frac{\xi^2}{2\beta k_s^2}\,e^{-\beta|z-s|} - \frac{1}{2k_s^2}\,\frac{R^+(\xi)}{R^-(\xi)}\left(\alpha e^{-\alpha(z+s)} + \frac{\xi^2}{\beta}\,e^{-\beta(z+s)}\right) + \frac{2\xi^2\alpha(2\xi^2-k_s^2)}{k_s^2R^-(\xi)}\left(e^{-(\beta z+\alpha s)} + e^{-(\beta s+\alpha z)}\right).$$

Here,

$$X_m = \tilde{P}^{-1}_m(\xi) - i\tilde{Q}^{m-1}_m(\xi); \quad Y_m = \tilde{P}^{m+1}_m(\xi) + i\tilde{Q}^{m+1}_m(\xi);$$
$$Z_m = \tilde{R}^m_m(\xi); \quad R^{\pm}(\xi) = (2\xi^2-k_s^2)^2 \pm 4\xi^2\alpha\beta; \tag{30}$$
$$\operatorname{sgn}(z-s) = \begin{cases} +1, & z>s \\ -1, & z<s. \end{cases}$$

On substituting the inverted Fourier components of the displacements into the corresponding angular eigenfunction expansions in equations (17), the desired formal solution to the general buried-source problem under consideration can be obtained. It should, however, be noted that some of the functions defined in equations (29) have simple poles at k_r which corresponds to the root of the Rayleigh wave function $R^-(\xi)$. Moreover, there will in general be two branch points at k_s and k_d lying on the formal path of integration of the inversion integral. To be consistent with the radiation conditions and the choice of branches, the path of integration should be deformed around the singularities as shown in Fig. 2.

3 Results for Specific Source Distributions

In the preceding analysis, the open disc Π_s and the body-force field distribution have been left arbitrary. In what follows, attention will be confined to a case of common interest, where Π_s is a circular region on which the body-force field is uniformly distributed. Henceforth,

$$\Pi_s = \{(x_1,x_2,x_3)\,|\,x_1^2 + x_2^2 < a^2,\ x_3 = s\} \tag{31}$$

Downloaded 03 May 2010 to 171.66.16.27. Redistribution subject to ASME license or copyright; see http://www.asme.org/terms/Terms_Use.cfm

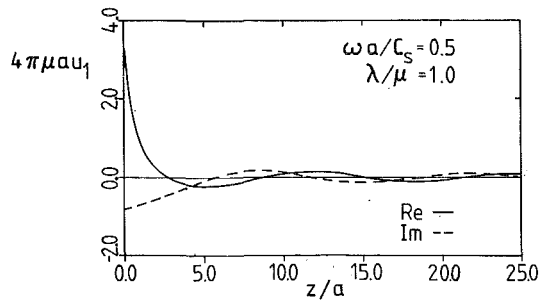


Fig. 3 Displacement u_1 under unit lateral load on Π_s ($s = 0$)

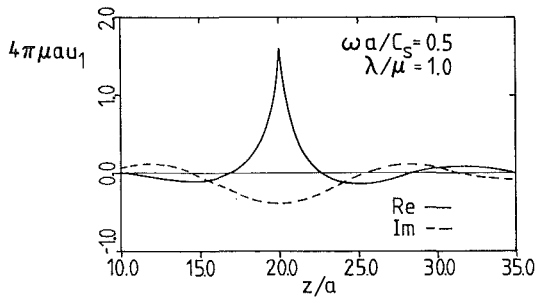


Fig. 4 Displacement u_1 under unit lateral load on Π_s ($s = 20a$)

where "a" is the radius of the circular region. Under this restriction, two cases can be examined: (*i*) a uniformly distributed horizontal body-force field of unit resultant acting in the x_1-direction, and (*ii*) a uniformly distributed vertical body-force field of unit resultant acting in the x_3-direction.

Case (*i*). For a uniformly distributed lateral force field of unit resultant acting in the x_1-direction, it can be shown that

$$P_1(r) = P_{-1}(r) = \begin{cases} \frac{1}{2\pi a^2}, & r<a \\ 0, & r\geq a \end{cases},$$

$$P_m(r) = 0 \quad \text{for} \quad m \neq \pm 1; \tag{32}$$

$$Q_1(r) = -Q_{-1}(r) = \begin{cases} i\frac{1}{2\pi a^2}, & r<a \\ 0, & r\geq a \end{cases},$$

$$Q_m(r) = 0 \quad \text{for} \quad m \neq \pm 1;$$

$$R_m(r) = 0 \text{ for all } m.$$

Combining equations (32), (30), (29), (28), and (17), one is led to the following expressions for the radial, angular, and vertical displacements:

$$u_r(r,\theta,z;\, s) = \frac{\cos\theta}{2\pi\mu a}$$

$$\left\{ \begin{array}{l} \int_0^\infty \gamma_1(z,s,\xi) J_1(\xi a)[J_0(\xi r) - J_2(\xi r)]d\xi \\ + \int_0^\infty \gamma_2(z,s,\xi) J_1(\xi a)[J_0(\xi r) + J_2(\xi r)]d\xi \end{array} \right\},$$

$$u_\theta(r,\theta,z;\, s) = \frac{-\sin\theta}{2\pi\mu a}$$

$$\left\{ \begin{array}{l} \int_0^\infty \gamma_1(z,s,\xi) J_1(\xi a)[J_0(\xi r) + J_2(\xi r)]d\xi \\ + \int_0^\infty \gamma_2(z,s,\xi) J_1(\xi a)[J_0(\xi r) - J_2(\xi r)]d\xi \end{array} \right\}, \tag{33}$$

$$u_z(r,\theta,z;\, s) = \frac{\cos\theta}{\pi\mu a}$$

$$\int_0^\infty \Omega_1(z,s,\xi) J_1(\xi a) J_1(\xi r) d\xi.$$

To provide a glimpse of the results graphically, the displacement in the x_1-direction along the z-axis (i.e., $r = 0$) is computed numerically using a method of integration by asymptotic decomposition (Pak, 1985). The results for the case of $s = 0$ (a surface source) and the case of $s = 20a$ (a buried source) at a dimensionless frequency of 0.5 are displayed in Figs. 3 and 4, respectively. Since the response and the excitation are out-of-phase in general, the displacement is represented in complex notation, with the real and the imaginary parts corresponding to the in-phase and the 90 degree out-of-phase components, respectively.

As can be seen from the figures, the responses are fairly localized functions with their significant variations being confined to the vicinity of the point $z = s$. The oscillatory nature of the functions is also quite distinct. It could be noticed from Fig. 4 that the smoothness of the real and imaginary part of $u_1(z, s)$ is quite different at the point $z = s$. While the imaginary part of $u_1(z, s)$ is very smooth at that point, the real part of $u_1(z, s)$ has a sharp cusp. This interesting feature can, however, be readily explained if the suppressed time factor $e^{i\omega t}$ in the analysis is invoked. With the time factor in place, it can be easily seen that the real part of $u_1(z, s)$ represents the response of the half-space at the instant the buried body-force field achieves its maximum strength, e.g., at $t = 0$. Since the size of the stress-discontinuity across Π_s is directly proportional to the magnitude of the force field as described by equation (12), the lack of smoothness in $u_1(z, s)$ at $z = s$ is expected. Likewise, the imaginary part of $u_1(z, s)$ can be interpreted as the response of the half-space at the instant the buried body-force field vanishes. In this case, however, equation (12) implies that the stress-discontinuity across Π_s would disappear. With the discontinuity eliminated, the observed smoothness in the response is a logical consequence.

Case (*ii*). For a uniformly distributed vertical load of unit magnitude over Π_s acting in the x_3-direction, it can be shown that

$$R_0(r) = \begin{cases} \frac{1}{\pi a^2}, & r<a \\ 0, & r\geq a \end{cases}, \quad R_m(r) = 0 \text{ for } m \neq 0; \tag{34}$$

$$P_m(r) = Q_m(r) = 0 \text{ for all } m.$$

By virtue of the general results described in equations (28) and (29), the displacements can be found as

$$\begin{aligned} u_r(r,\theta,z;\, s) &= \frac{-1}{\pi\mu a}\int_0^\infty \gamma_3(z,s,\xi) J_1(\xi a) J_1(\xi r) d\xi, \\ u_\theta(r,\theta,z;\, s) &= 0, \\ u_z(r,\theta,z;\, s) &= \frac{1}{\pi\mu a}\int_0^\infty \Omega_2(z,s,\xi) J_1(\xi a) J_0(\xi r) d\xi. \end{aligned} \tag{35}$$

This is an illustration that the current procedure is equally effective for axisymmetric problems.

Downloaded 03 May 2010 to 171.66.16.27. Redistribution subject to ASME license or copyright; see http://www.asme.org/terms/Terms_Use.cfm

4 Summary and Conclusions

In this paper, the response of an elastic half-space under the action of an arbitrary, time-harmonic, finite buried source is derived analytically by a method of potentials. Results for the specific case of embedded sources which are uniformly distributed over a circular region are also included. The procedure of derivation is of sufficient generality to be useful in a variety of axisymmetic and asymmetric wave propagation problems. With the aid of Fourier or Laplace transforms, the method can be naturally extended to the treatment of transient problems.

Acknowledgment

The support and constructive criticism offered by Professors J. K. Knowles and E. Sternberg on this work are gratefully acknowledged.

References

Arnold, R. N., Bycroft, G. N., and Warburton, G. B., 1955, "Forced Vibrations of a Body on an Infinite Elastic Solid," ASME JOURNAL OF APPLIED MECHANICS, Vol. 22, pp. 391–400.

Chao, C. C., 1960, "Dynamic Response of an Elastic Half-space to Tangential Surface Loading," ASME JOURNAL OF APPLIED MECHANICS, Vol. 27, pp. 559–567.

Eringen, A. C., and Suhubi, E. S., 1975, *Elastodynamics, Volume 2*, Academic Press, New York.

Gakenheimer, D. C., and Miklowitz, J., 1969, "Transient Excitation of an Elastic Half-Space by a Point Load Travelling on the Surface," ASME JOURNAL OF APPLIED MECHANICS, Vol. 36, pp. 505–515.

Gladwell, G. M. L., 1968, "Forced Tangential and Rotary Vibration of a Rigid Circular Disc on a Semi-infinite Solid," *International Journal of Engineering Science*, Vol. 6, pp. 591–607.

Harding, J. W., and Sneddon, I. N., 1945, "The Elastic Stresses produced by the Indentation of the Plane Surface of a Semi-Infinite Elastic Solid by a Rigid Punch," *Proc. Cambridge Phil. Soc.*, Vol. 41, pp. 16–26.

Israel, M., and Kovach, R. L., 1977, "Near-Field Motions from a Propagating Strike-Slip Fault in an Elastic Half-Space," *Bull. Seism. Soc. Am.*, Vol. 67, pp. 977–994.

Johnson, L. R., 1974, "Green's Function For Lambs Problem," *Geophys. Journal*, Vol. 37, pp. 99–131.

Kupradze, V. D., 1965, *Potential Methods in the Theory of Elasticity*, Daniel Davey and Co., New York.

Lamb, H., 1904, "On the Propagation of Tremors over the Surface of an Elastic Solid," *Phil. Trans. Royal Soc. London*, Ser. A, Vol. 203, pp. 1–42.

Luco, J. E., and Westmann, R. A., 1972, "Dynamic Response of a Rigid Footing Bonded to an Elastic Half-Space," ASME JOURNAL OF APPLIED MECHANICS, Vol. 39, pp. 527–534.

Maiti, N. C., and Mitra, M., 1979, "Wave Propagation from Extended Asymmetric Surface Sources in an Elastic Half-Space," *Bull. Seism. Soc. Am.*, Vol. 69, pp. 713–735.

Miklowitz, J., 1978, *The Theory of Elastic Waves and Waveguides*, North-Holland Publishing Company, Amsterdam.

Mindlin, I. A., 1963, "Free Elastic Waves on the Surface of a Tube of Infinite Thickness," *Appl. Math Mech.*, Vol. 27, pp. 823–828.

Morse, P. M., and Feshbach, H., 1953, *Method of Theoretical Physics, Part I and II*, McGraw-Hill, New York, pp. 1759–1767.

Muki, R., 1960, "Asymmetric Problems of the Theory of Elasticity for a Semi-Infinite Solid and a Thick Plate," *Progress in Solid Mech.*, Vol. 1, North-Holland Publishing Company, Amsterdam.

Pak, R. Y. S., 1985, "Dynamic Response of a Partially Embedded Bar Under Transverse Excitations," Ph.D. Dissertation, California Institute of Technology, Pasadena, California.

Pekeris, C. L., and Longman, I., 1955, "The Motion of the Surface of a Uniform Elastic Half-space Produced by a Buried Torque Pulse," *Geophys. Journal*, Vol. 1, pp. 146–153.

Thiruvenkatachar, V. R., 1955, "Stress Waves produced in a Semi-Infinite Elastic Solid by Impulse Applied Over a Circular Area of the Plane Face," *Proc. Congr. Theo. Appl. Mech. India*, 1st, Kharagpur, India, pp. 181–188.

Thomson, W. T., and Kobori, T., 1963, "Dynamic Compliance of Rectangular Foundations on an Elastic Half-Space," ASME JOURNAL OF APPLIED MECHANICS, Vol. 30, pp. 579–584.

Downloaded 03 May 2010 to 171.66.16.27. Redistribution subject to ASME license or copyright; see http://www.asme.org/terms/Terms_Use.cfm

An Acoustoelastic Theory for Surface Waves in Anisotropic Media

G. Thomas Mase[1]

G. C. Johnson

Department of Mechanical Engineering,
University of California,
Berkeley, CA 94720

A theory for surface waves in an anisotropic material is developed in the framework of acoustoelasticity in which the material's strain energy density is taken to be a cubic function in the strain. In order to relate the surface wave speeds to the applied stress, a configuration is introduced in which the effect of the local rotation is removed. The development shows that the surface wave speed can be determined from the eigenvalues of a particular real symmetric 2×2 matrix. Numerical results are given for uniaxial loading applied to aluminum and copper single crystals and to an ideal transversely isotropic aggregate of aluminum.

I Introduction

When a wave propagates in a homogeneously deformed elastic medium the speed of propagation depends on the state of stress. This is often called the acoustoelastic effect and is the basis for a promising nondestructive method for determining active and residual stresses in structural members. For a plane wave propagating in a principal direction of stress, an initially isotropic body transmits three bulk waves – one longitudinal and two shear waves that are polarized in the principal directions normal to the propagation direction. In the presence of stress these wave speeds are, in general, different.

It has been observed experimentally with bulk waves that most structural materials are initially anisotropic due to manufacturing processes such as rolling or drawing (Crecraft, 1967; Hsu, 1975). When the material is anisotropic the shear wave speeds differ even in the absence of stress. Early work with elastic waves superposed on finite deformations (Toupin and Bernstein, 1961; Thurston and Brugger, 1964) considered materials with arbitrary symmetry, but there have been, until recently, few usable formulations to describe the acoustoelastic response of anisotropic materials (Iwashimizu and Kubormura, 1973; Okada, 1980; Johnson and Mase, 1984).

The theory of surface waves propagating on homogeneously deformed materials is less well developed than the bulk wave theory, perhaps because the solution for the surface wave problem is more difficult to obtain. An iterative approach for solving the surface wave problem with no load in an anisotropic material has been given by Farnell (1970) where wave speeds are given by the solution of two simultaneous 3×3 determinants which arise from the equations of motion and the stress-free boundary condition. With this method there is no a priori condition which ensures the existence of surface waves and at one time it was speculated that there may be certain "forbidden directions" in which surface waves cannot propagate for a given anisotropy (Stonley, 1955; Synge, 1957; Buchwald, 1961; Lim and Farnell, 1968; Burridge, 1970).

The issue of "forbidden directions" was settled when a complete theory for surface waves was developed showing that in an unstressed, anisotropic material, surface waves may exist in all directions. The complete theory for materials with no prestress originated with Stroh (1962) who was working in the area of dislocation theory. Later, existence and uniqueness theorems for surface waves were developed (Barnett et al., 1973a, Barnett and Lothe, 1974). The results of Barnett and Lothe also provided a convenient way to calculate the surface wave speed.

The propagation of infinitesimal surface waves in a half space which is deformed was first studied by Hayes and Rivlin (1961) who looked at waves propagating in a principal direction of stretch for isotropic materials. Iwashimizu and Kobori (1978) extended this to consider propagation in any direction, not necessarily a principal direction, and introduced the second and third-order elastic constants into the strain energy function. The same assumptions used by Hayes and Rivlin were used by Hirao and Fukuoka (1981), but the condition on the initial deformation was relaxed to allow a nonuniform prestressed state. Surface wave speeds on an isotropic material were approximated as a function of stress by Martin (1974). He also discussed surface wave speeds on an anisotropic body with no stress applied, but did not look at an anisotropic material in the presence of stress. Chadwick and Jarvis (1979)

[1]Presently with the Engineering Mechanics Department, General Motors Research Laboratories, Warren, MI 48090.

Contributed by the Applied Mechanics Division for presentation at the 1987 Applied Mechanics, Biomechanics, and Fluids Engineering Conference, Cincinnati, OH, June 14–17, 1987, of the American Society of Mechanical Engineers.

Discussion of this paper should be addressed to the Editorial Department, ASME, United Engineering Center, 345 East 47th Street, New York, N.Y. 10017, and will be accepted until two months after final publication of the paper itself in the JOURNAL OF APPLIED MECHANICS. Manuscript received by ASME Applied Mechanics Division, May 17, 1985; final revision, February 10, 1986.

Paper No. 87-APM-6.

Copyright © 1987 by ASME

Downloaded 03 May 2010 to 171.66.16.27. Redistribution subject to ASME license or copyright; see http://www.asme.org/terms/Terms_Use.cfm

extended the existence and uniqueness theorems of Barnett and Lothe to the case of prestressed materials of unspecified anisotropy and then went on to study surface waves in restricted Hadamard materials.

In the present paper we discuss the response of surface waves in the usual framework of acoustoelasticity for bulk waves. We provide a fairly complete overview of the basic theory so that those in the field of acoustoelasticity who are not familiar with the work of Barnett et al. (1973a) and Chadwick and Smith (1977) will have a self-contained account of surface waves in prestressed materials. In Sections III and IV the basics of wave propagation in homogeneously deformed elastic bodies and surface waves, respectively, are covered. Acoustoelasticity is combined with the general surface wave theory of Barnett et al. (1973a) and Chadwick and Jarvis (1979) to form a six-dimensional eigenvalue problem in Section V. Our goal is to relate the surface wave speed to the applied stresses. In order to do this, we develop in Section VI the notion of a configuration in which the local rotation is removed. From the six-dimensional eigenvalue problem stated with respect to this configuration, the existence and the surface wave speed can be determined through the consideration of a real symmetric 2×2 matrix. In Section VII a numerical study of the results of Section VI is undertaken to examine the response of aluminum and copper single crystals as well as an ideal transversely isotropic aggregate of aluminum under uniaxial tension.

II Notation and Basic Relations

The purely mechanical theory of acoustoelasticity is a problem involving a small deformation, an ultrasonic wave, superposed on a finite homogeneous deformation. It is convenient to introduce three configurations for the development of the theory. Let the vectors X_A, x_i, and x_i^* denote the position of a material point of the body in the reference, homogeneously deformed, and current configurations, respectively. The reference configuration is considered to be the stress-free initial configuration, the deformed state is the configuration of the body after the homogeneous deformation, but prior to the application of the infinitesimal ultrasonic wave, and the current state is the configuration with the infinitesimal wave applied to the homogeneous deformation. Upper case Latin indices denote quantities which are referred to the reference configuration and lower case indices denote quantities which are referred to the deformed or current configuration. Quantities with lower case indices and a superscript asterisk are in the current configuration. All Latin indices range from 1 to 3 and the repeated index summation convention is assumed unless stated otherwise. The range and summation for Greek indices will be given explicitly.

The deformation gradient for the deformed configuration is defined as

$$F_{iA}=x_{i,A},\quad J=\det F_{iA}>0, \tag{1}$$

where the subscript comma denotes partial differentiation. Using the polar decomposition theorem, the deformation gradient F_{iA} can be written as the product of the right stretch tensor U_{BA}, which is symmetric and positive-definite, and the local rotation R_{iB}, which is a proper orthogonal tensor,

$$F_{iA}=R_{iB}U_{BA}. \tag{2}$$

The Cauchy-Green deformation measure C_{AB} and the Lagrange strain E_{AB} are given as

$$C_{AB}=F_{iA}F_{iB}=U_{MA}U_{MB},\quad 2E_{AB}=C_{AB}-\delta_{AB}. \tag{3}$$

Let ρ_o and ρ be the mass density in the reference and deformed configurations, respectively, and let b_i be the body force per unit mass. The equations of motion in terms of the Cauchy stress T_{ij} are written as

$$T_{ij,i}+\rho b_j=\rho\dot{v}_j, \tag{4}$$

where $\dot{v}_j$ is the material time derivative of the velocity.

Assuming the existence of a strain energy density Φ, the constitutive equation relating the symmetric (or second) Piola-Kirchhoff stress S_{AB} to the Lagrange strain is

$$S_{AB}=\rho_o\frac{\partial\Phi}{\partial E_{AB}},\quad \Phi=\Phi(E_{AB}). \tag{5}$$

The Cauchy stress is related to the symmetric Piola-Kirchhoff stress as

$$T_{ij}=(1/J)F_{iA}F_{jB}S_{AB}, \tag{6}$$

and also note that a rotated Cauchy stress can be defined as (Green and Naghdi, 1965; Johnson and Mase, 1984)

$$\sigma_{AB}=R_{iA}R_{jB}T_{ij}=(1/J)U_{AM}U_{BN}S_{MN}. \tag{7}$$

III Wave Propagation in a Homogeneously Deformed Elastic Body

The position of a material point in the current configuration is the sum of its position in the deformed configuration with the infinitesimal displacement of the ultrasonic wave u_i,

$$x_i^*=x_i+u_i(X_A,t). \tag{8}$$

The deformation gradient and the Lagrange strain in the current configuration are then given as

$$F_{iA}^*=F_{jA}(\delta_{ij}+u_{i,j}),\quad E_{AB}^*=E_{AB}+F_{iA}F_{jB}e_{ij}, \tag{9}$$

where e_{ij} is the strain due to the ultrasonic wave u_i with respect to the deformed configuration. Since u_i is an infinitesimal displacement, all quantities in the current configuration will be linearized with respect to it. Thus the linearized strain e_{ij} is given as

$$2e_{ij}=u_{i,j}+u_{j,i}. \tag{10}$$

The stresses can be linearized in u_i by expanding the derivative of the strain energy in a Taylor series about the deformed state (Johnson, 1981). The Cauchy stress in the current configuration may then be written as

$$T_{ij}^*=T_{ij}(1-u_{m,m})+T_{is}u_{j,s}+T_{kj}u_{i,k}+K_{ijks}u_{k,s}, \tag{11}$$

where

$$K_{ijks}=\rho F_{iA}F_{jB}F_{kM}F_{sN}\frac{\partial^2\Phi}{\partial E_{AB}\partial E_{MN}}. \tag{12}$$

Assuming that there are no body forces and that the deformed state is in equilibrium ($T_{ij,i}=0$), the linearized equations of motion in the current configuration may be written as

$$B_{ijks}u_{k,si}=\rho\ddot{u}_j, \tag{13}$$

where

$$B_{ijks}=K_{ijks}+T_{is}\delta_{jk}. \tag{14}$$

Assume the displacement field is of the form

$$\mathbf{u}=\mathbf{A}\exp\{ik(\mathbf{z}\cdot\mathbf{x}+p\mathbf{y}\cdot\mathbf{x}-Vt)\} \tag{15}$$

where $\mathbf{z}$ and $\mathbf{y}$ are orthogonal unit vectors. The equations of motion can then be written as

$$B'_{ijks}u_{k,is}=0, \tag{16}$$

where

$$B'_{ijks}=B_{ijks}-\rho V^2 z_i z_s\delta_{jk}. \tag{17}$$

The fourth order tensor B'_{ijks} can be thought of as the "dynamic" stiffness tensor for a wave propagating in the z_i direction (Barnett et al., 1973b).

IV Basic Equations for Surface Waves

Consider an anisotropic elastic half space with a rectangular Cartesean coordinate system x_i fixed in it with the plane $x_1=0$

Downloaded 03 May 2010 to 171.66.16.27. Redistribution subject to ASME license or copyright; see http://www.asme.org/terms/Terms_Use.cfm

defining the free surface. The coordinate system x_i can be chosen such that the stiffness tensor appears in its simplest form. Define two unit vectors, $n_i = (1, 0, 0)$ and m_i, as the inner normal to the surface and the propagation direction, respectively. The vector m_i is in the free surface and can be written as

$$m_i = (0, \cos\theta, \sin\theta), \tag{18}$$

where θ is the angle between the x_2 coordinate axis and the propagation direction.

Assume that the wave takes the form of a straight crested surface wave propagating in the $\mathbf{m} = (0, m_2, m_3)$ direction with

$$u_k = A_k \exp\{ik(px_1 + m_2x_2 + m_3x_3 - Vt)\}, \quad k = \omega/V, \tag{19}$$

where ω is the frequency, V is the propagation speed and p is a complex constant. A surface wave is assumed to be a linear combination of terms of the form of equation (19) which satisfy the equations of motion, equation (13), and the stress free boundary condition

$$T^*_{ij}n_i = 0 \text{ when } x_1 = 0. \tag{20}$$

In order for the displacements u_k to be a nontrivial solution to the equations of motion, p and V must satisfy the characteristic equation

$$\det\{B_{ijks}m_im_s + p[B_{ijks}(m_in_s + n_im_s)] + p^2B_{ijks}n_in_s - \rho V^2\delta_{jk}\} = 0. \tag{21}$$

For a given V, equation (21) is a sextic equation in p and may be solved for the six roots p_α ($\alpha = 1$ to 6) which occur in complex conjugate pairs (Barnett et al., 1973a). Roots with negative imaginary parts are inadmissible since the motion must remain bounded as $x_1 \to \infty$, and for this reason the p_α are sometimes called decay parameters. Writing the displacements as a linear combination of terms having phase velocity V, but with p equal to one of the three roots with positive imaginary parts, p_α ($\alpha = 1,2,3$), the displacement field is given as

$$u_i = \sum_{\alpha=1}^{3} A_{i\alpha}C_\alpha \exp\{ik(p_\alpha x_1 + m_2x_2 + m_3x_3 - Vt)\}, \tag{22}$$

where $A_{i\alpha}$ are the complex eigenvectors associated with the characteristic equation, equation (21), and C_α are the weighting factors for the linear combination. Given the displacements in equation (22) the weighting factors C_α must be determined by the application of the stress free boundary condition. Substituting equation (22) into (20) gives a system of three homogeneous equations in the weighting factors C_α ($\alpha = 1,2,3$). For a nontrivial solution, the determinant of the coefficients must vanish giving,

$$\det\{B_{1jks}A_{k\alpha}m_{s\alpha}\} = 0, \quad \alpha = 1,2,3, \tag{23}$$

where $m_{1\alpha} = p_\alpha$, $m_{2\alpha} = m_2$, and $m_{3\alpha} = m_3$. This determinant is, in general, complex because $m_{1\alpha}$ and $A_{k\alpha}$ are complex.

The surface wave problem thus consists of finding a phase velocity V and the corresponding p_α which satisfy the real determinant in equation (21) and the complex determinant of equation (23). Using only the tools discussed so far, an iterative approach must be used to find the surface wave speed (unless it is a special case). The usual approach is to choose a velocity V and calculate the decay constants p_α ($\alpha = 1,2,3$) with positive imaginary parts from equation (21). These are used in equation (23) to evaluate the value of the boundary condition determinant. If this value is nonzero, then another velocity is chosen until equation (23) is satisfied. Before starting the iterative calculations, there is no a priori way of determining whether or not a surface wave even exists.

The complex form of the boundary condition, equation (23), caused temporary confusion in the surface wave literature. It was proposed that there may be certain directions in anisotropic materials in which surface waves cannot propagate. Synge (1957) suggested that since equation (23) is complex, it is equivalent to two real conditions and from this assumption concluded that surface waves may only be capable of propagating only in certain discrete directions. Synge's assumption was shown to be too restrictive by Stroh (1962) who wrote the stress-free boundary condition in terms of the straight crested wave amplitude vectors $\mathbf{A}_\alpha$. Stroh pointed out that the amplitude vectors are eigenvectors which can be arbitrarily normalized, and hence the stress free boundary condition can always be written as a real determinant by choosing an appropriate normalization. The work of Stroh was posed in the form of a six-dimensional eigenvalue problem which he used to study the uniform motion of straight-line dislocations. Barnett et al. (1973a) extended the six-dimensional formalism of Stroh to derive existence and uniqueness theorems for surface waves. The only shortcoming of the theory was that for an isotropic material in the static state (zero phase velocity), the six-dimensional eigenvalue problem was nonsimply degenerate (Lothe and Barnett, 1976). This special case was remedied by considering a straight crested wave propagating in a general direction in the sagittal plane (the sagittal plane is the plane perpendicular to the free surface containing the propagation vector). By integrating certain quantities over all angles in the sagittal plane, the degenerate isotropic case was overcome (Lothe and Barnett, 1976). The complete theory of Barnett et al. (1973a) showed that in a stress-free, anisotropic elastic half space surface waves always exist and are unique. However, two types of surface waves resulted from this theory: A pure mode surface wave which is a classical surface wave with displacements decaying exponentially away from the free surface, and an exceptional surface wave which is a bulk wave that satisfies the stress-free boundary condition. Chadwick and Jarvis (1979) advanced Barnett and Lothe's work to give existence and uniqueness theorems for prestressed half spaces. They showed that the existence of surface waves is dependent on the magnitude of the applied prestress.

V Determining the Surface Wave Speed

In this section we will rederive the surface wave theory of Barnett and Lothe in a form that is convenient for determining the surface wave speeds in homogeneously deformed elastic materials. First, a straight crested wave is considered propagating in an arbitrary direction in the sagittal plane. The force per unit area parallel to a plane which is orthogonal to the sagittal plane and contains the propagation direction is introduced. Using the equations of motion (with the assumed displacements) and the force per unit area discussed above, a six-dimensional eigenvalue problem is formed whose eigenvalues are the decay parameters for the surface wave. Taking the last three equations of the six-dimensional eigenvalue problem a real second-order tensor is found that, when averaged over all angles in the sagittal plane, can be used to determine existence and type of surface wave. The vanishing of the determinant of this real tensor is equivalent to equation (23) as a condition for the satisfaction of the stress free boundary condition. The existence criterion is slightly altered when prestress is present. Once the existence and type of surface wave is determined, the surface wave speed is found by considering a real 2×2 submatrix of the aforementioned real second-order tensor.

It is desirable to replace the complex determinant of equation (23) with a real determinant as the condition needed to satisfy the stress-free boundary condition. To do this, consider a straight crested wave defined by

$$\mathbf{u} = \mathbf{A}\exp\{ik(p\mathbf{y}\cdot\mathbf{x} + \mathbf{z}\cdot\mathbf{x} - Vt)\}, \tag{24}$$

where $\mathbf{z}$ (the propagation direction) and $\mathbf{y}$ are given as

$$\mathbf{z} = \mathbf{m}\cos\chi + \mathbf{n}\sin\chi, \qquad \mathbf{y} = -\mathbf{m}\sin\chi + \mathbf{n}\cos\chi, \tag{25}$$

Downloaded 03 May 2010 to 171.66.16.27. Redistribution subject to ASME license or copyright; see http://www.asme.org/terms/Terms_Use.cfm

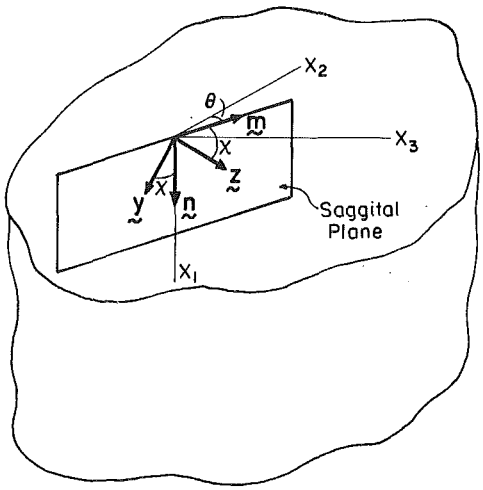


Fig. 1 Coordinate system and unit vectors for the half space considered

and χ is the angle between the vectors **m** and **z** (see Fig. 1). Notice that when $\chi = 0$, the displacements of equation (24) reduce to those in equation (19). By considering a wave propagating in the **z** direction we can eventually obtain a real determinant which can be used to satisfy the stress free boundary condition.

To incorporate the concept of a free surface, Lothe and Barnett (1976) introduced J_j as

$$J_j(\mathbf{y}) = y_i B_{ijks} u_{k,s}, \tag{26}$$

which represents the force per unit area parallel to the surface defined by the unit vector **y**. When $\chi = 0$, the vector **y** equals **n** and **J** represents the force per unit area in the free surface. Using equation (24) in (26) gives

$$\begin{aligned}\mathbf{J} &= \hat{\mathbf{J}}\exp\{ik(\mathbf{z}\cdot\mathbf{x} + p\mathbf{y}\cdot\mathbf{x} - Vt)\} \\ &= ik[\mathbf{R}(\mathbf{y},\mathbf{z}) + p\mathbf{Q}(\mathbf{y})]\mathbf{u},\end{aligned} \tag{27}$$

where $\mathbf{R}(\mathbf{y},\mathbf{z})$ and $\mathbf{Q}(\mathbf{y})$ are real tensors whose components are given by

$$\begin{aligned}Q_{jk}(\mathbf{y}) &= B'_{ijks} y_i y_s, \\ R_{jk}(\mathbf{y},\mathbf{z}) &= R_{kj}(\mathbf{z},\mathbf{y}) = B'_{ijks} y_i z_s.\end{aligned} \tag{28}$$

There exists a so-called limiting velocity which is the minimum velocity for which $\mathbf{Q}(\mathbf{y})$ becomes singular for some angle χ (Barnett et al., 1973a). For velocities less than the limiting velocity, $\mathbf{Q}(\mathbf{y})$ is invertible for all χ and thus equation (27) can be written as

$$p\mathbf{A} = -\mathbf{Q}^{-1}(\mathbf{y})\mathbf{R}(\mathbf{y},\mathbf{z})\mathbf{A} - ik^{-1}\mathbf{Q}^{-1}(\mathbf{y})\hat{\mathbf{J}}. \tag{29}$$

The equations of motion will be used along with **J** to form a six-dimensional eigenvalue problem whose eigenvalues are the decay parameters p, and whose eigenvectors are certain combinations of the amplitude vector **A** and the force vector $\hat{\mathbf{J}}$.

Using the displacements of equation (24) in the equations of motion, equation (16), yields

$$\{p^2\mathbf{Q}(\mathbf{y}) + p[\mathbf{R}(\mathbf{y},\mathbf{z}) + \mathbf{R}(\mathbf{z},\mathbf{y})] + \mathbf{Q}(\mathbf{z})\}\mathbf{A} = 0. \tag{30}$$

When $\chi = 0$ the condition for nontrivial solutions for **A** reduces to the same determinant given in equation (21). By regrouping terms in equation (30) and using the definition of **J** in equation (27) the equations of motion can be written as

$$ik^{-1}p\hat{\mathbf{J}} = [p\mathbf{R}(\mathbf{z},\mathbf{y}) + \mathbf{Q}(\mathbf{z})]\mathbf{A}. \tag{31}$$

In order to get equation (31) in a form that will facilitate the formation of a six-dimensional eigenvalue problem, with p being an eigenvalue, premultiply equation (29) by $\mathbf{R}(\mathbf{z},\mathbf{y})$ to give

$$\begin{aligned}p\mathbf{R}(\mathbf{z},\mathbf{y})\mathbf{A} = &-\mathbf{R}(\mathbf{z},\mathbf{y})\mathbf{Q}^{-1}(\mathbf{y})\mathbf{R}(\mathbf{y},\mathbf{z})\mathbf{A} \\ &- ik^{-1}\mathbf{R}(\mathbf{z},\mathbf{y})\mathbf{Q}^{-1}(\mathbf{y})\hat{\mathbf{J}}.\end{aligned} \tag{32}$$

Equation (31) may then be written as

$$\begin{aligned}ik^{-1}p\hat{\mathbf{J}} = &[\mathbf{Q}(\mathbf{z}) - \mathbf{R}(\mathbf{z},\mathbf{y})\mathbf{Q}^{-1}(\mathbf{y})\mathbf{R}(\mathbf{y},\mathbf{z})]\mathbf{A} \\ &- ik^{-1}\mathbf{R}(\mathbf{z},\mathbf{y})\mathbf{Q}^{-1}(\mathbf{y})\hat{\mathbf{J}},\end{aligned} \tag{33}$$

and defining $\mathbf{L} = ik^{-1}\hat{\mathbf{J}}$ this becomes

$$\begin{aligned}p\mathbf{L} = &[\mathbf{Q}(\mathbf{z}) - \mathbf{R}(\mathbf{z},\mathbf{y})\mathbf{Q}^{-1}(\mathbf{y})\mathbf{R}(\mathbf{y},\mathbf{z})]\mathbf{A} \\ &- \mathbf{R}(\mathbf{z},\mathbf{y})\mathbf{Q}^{-1}(\mathbf{y})\mathbf{L}.\end{aligned} \tag{34}$$

Letting ξ be a six-dimensional vector defined as

$$\xi = \begin{Bmatrix}\mathbf{A} \\ \mathbf{L}\end{Bmatrix}, \tag{35}$$

equations (29) and (34) can be combined in the form

$$(\mathbf{N} - p\mathbf{1})\xi = 0, \tag{36}$$

where **1** is the six-dimensional identity tensor and **N** is a real tensor given as

$$\mathbf{N} = \begin{bmatrix}\mathbf{S}_1 & \mathbf{S}_2 \\ \mathbf{S}_3 & \mathbf{S}_1{}^T\end{bmatrix}. \tag{37}$$

The 3×3 submatrices of **N** are

$$\begin{aligned}\mathbf{S}_1 &= -\mathbf{Q}^{-1}(\mathbf{y})\mathbf{R}(\mathbf{y},\mathbf{z}), \\ \mathbf{S}_2 &= -\mathbf{Q}^{-1}(\mathbf{y}), \\ \mathbf{S}_3 &= \mathbf{Q}(\mathbf{z}) - \mathbf{R}(\mathbf{z},\mathbf{y})\mathbf{Q}^{-1}(\mathbf{y})\mathbf{R}(\mathbf{y},\mathbf{z}).\end{aligned} \tag{38}$$

When $\chi = 0$, the eigenvalues (decay constants) of the six-dimensional problem are the same as in the three-dimensional approach (Section IV) since equation (30), used in deriving the six-dimensional equation, is the same as equation (21) in this case.

We will now show that once the decay parameters, p_α ($\alpha = 1$ to 6), are calculated, the stress-free boundary condition can be expressed in terms of a real determinant by considering the tensor $\mathbf{S}_3$. The last three equations of equation (36) can be written as

$$\mathbf{S}_3\mathbf{A}_\alpha + \mathbf{S}_1{}^T\mathbf{L}_\alpha = p_\alpha\mathbf{L}_\alpha, \tag{39}$$

where the subscript α represents quantities associated with the eigenvalue p_α. The three-dimensional eigenvectors $\mathbf{A}_\alpha$ and $\mathbf{L}_\alpha$ have the following completeness and spectral relations (Chadwick and Smith, 1977)

$$\sum_{\alpha=1}^{6} \mathbf{A}_\alpha \otimes \bar{\mathbf{L}}_\alpha = \mathbf{I}, \quad \sum_{\alpha=1}^{6} \mathbf{L}_\alpha \otimes \bar{\mathbf{L}}_\alpha = 0. \tag{40}$$

where **I** is the three-dimensional identity tensor and $\bar{\mathbf{L}}_\alpha$ is the complex conjugate of $\mathbf{L}_\alpha$. Taking the tensor product of equation (39) with the complex conjugate of $\mathbf{L}_\alpha$ and summing over all α gives

$$\mathbf{S}_3 \sum_{\alpha=1}^{6} \mathbf{A}_\alpha \otimes \bar{\mathbf{L}}_\alpha + \mathbf{S}_1{}^T \sum_{\alpha=1}^{6} \mathbf{L}_\alpha \otimes \bar{\mathbf{L}}_\alpha = \sum_{\alpha=1}^{6} p_\alpha \mathbf{L}_\alpha \otimes \bar{\mathbf{L}}_\alpha. \tag{41}$$

Using the relations in equation (40), the tensor S_3 can be written as

$$\mathbf{S}_3 = \sum_{\alpha=1}^{6} p_\alpha \mathbf{L}_\alpha \otimes \bar{\mathbf{L}}_\alpha. \tag{42}$$

To show that the real tensor $\mathbf{S}_3$ can be used in the boundary condition, we must consider the dependence of **N**, ξ_α, and p_α on χ. Chadwick and Smith (1977) have shown that

$$\frac{\partial}{\partial\chi}\mathbf{N} = -(\mathbf{1} + \mathbf{N}^2), \tag{43}$$

and

$$\frac{\partial p_\alpha}{\partial\chi} = -(1 + p_\alpha^2). \tag{44}$$

Downloaded 03 May 2010 to 171.66.16.27. Redistribution subject to ASME license or copyright; see http://www.asme.org/terms/Terms_Use.cfm

From this, the eigenvectors ξ, and thus $\mathbf{A}_\alpha$ and $\mathbf{L}_\alpha$, are found to be independent of χ. Integrating equation (44) it follows that (Chadwick and Smith, 1977)

$$\int_o^{2\pi} p_\alpha d\chi = \pm 2\pi i, \tag{45}$$

where the sign of the right-hand side of equation (45) is assigned according to whether roots p_α with positive or negative imaginary parts are chosen.

At this point it is convenient to order the eigenvalues p_α so that p_α has positive imaginary parts for $\alpha = 1, 2, 3$, and negative imaginary parts for $\alpha = 4, 5, 6$. For velocities below the limiting velocity, p_α, $\mathbf{A}_\alpha$, and $\mathbf{L}_\alpha$ ($\alpha = 4, 5, 6$) are complex conjugates of p_α, $\mathbf{A}_\alpha$, and $\mathbf{L}_\alpha$ ($\alpha = 1, 2, 3$), respectively (Barnett and Lothe, 1978). The identity

$$\sum_{\alpha=1}^{6} \mathbf{L}_\alpha \otimes \bar{\mathbf{L}}_\alpha = 0$$

now implies that for a given α, the quantity $\mathbf{L}_\alpha \otimes \bar{\mathbf{L}}_\alpha$ is purely imaginary.

In knowing how ξ and p_α depend on χ, it is possible to acquire an expression for the average of $\mathbf{S}_3$ over χ from which the stress-free boundary condition can be expressed. We introduce $\bar{\mathbf{S}}_3$ as the average value of $\mathbf{S}_3$ over all angles χ,

$$\bar{\mathbf{S}}_3 = \frac{1}{2\pi}\int_o^{2\pi} \mathbf{S}_3 d\chi = \frac{1}{2\pi}\int_o^{2\pi} \left(\sum_{\alpha=1}^{6} p_\alpha \mathbf{L}_\alpha \otimes \bar{\mathbf{L}}_\alpha \right) d\chi. \tag{46}$$

Making use of equation (45), the fact that vectors $\mathbf{L}_\alpha$ are independent of χ, and that $\mathbf{L}_\alpha \otimes \bar{\mathbf{L}}_\alpha$ ($\alpha = 1, 2, 3$) are purely imaginary conjugates of $\mathbf{L}_\alpha \otimes \bar{\mathbf{L}}_\alpha$ ($\alpha = 4, 5, 6$), $\bar{\mathbf{S}}_3$ can be written as

$$\bar{\mathbf{S}}_3 = 2i \sum_{\alpha=1}^{3} \mathbf{L}_\alpha \otimes \bar{\mathbf{L}}_\alpha, \tag{47}$$

and is seen to be real and symmetric.

The real matrix $\bar{\mathbf{S}}_3$ contains the information needed to discuss the stress-free boundary condition. For the particular half space being considered ($\mathbf{n} = (1, 0, 0)$) the force per unit area of the free surface is written as

$$J_j(\mathbf{n}) = B_{1jks} u_{k,s}. \tag{48}$$

If the displacements of equation (22) are used in equation (48), the condition for nontrivial weighting factors, C_α, can be written as $\det J_{j\alpha} = 0$, $\alpha = 1, 2, 3$ where the matrix $J_{j\alpha}$ is formed from combining the force vectors corresponding to the admissible eigenvalues p_α. Multiplying $J_{j\alpha}$ element-by-element by $ik^{-1}\exp\{-ik(\mathbf{m}\cdot\mathbf{x} + p\mathbf{n}\cdot\mathbf{x} - Vt)\}$ the condition for nontrivial C_α can be written as

$$\det L_{i\alpha} = 0, \quad \alpha = 1,2,3. \tag{49}$$

If equation (49) is satisfied then it follows that

$$[\det L_{i\alpha}]^2 = \det\left[\sum_{\alpha=1}^{3} \mathbf{L}_\alpha \otimes \bar{\mathbf{L}}_\alpha \right] = 0 \tag{50}$$

Equations (47) and (50) show that if $\det \bar{\mathbf{S}}_3 = 0$ then the stress-free boundary condition is satisfied and hence, satisfying the boundary condition is tantamount to the vanishing of the determinant of a real symmetric tensor.

The tensor $\bar{\mathbf{S}}_3$ plays a more important role in the theory of surface waves than simply replacing the complex determinant used to satisfy the stress-free boundary condition. By considering $\bar{\mathbf{S}}_3$ the existence and the surface wave speed can be determined. There are four properties of $\bar{\mathbf{S}}_3$, derived by Barnett et al. (1973a), from which existence and surface wave speed follow. These properties are:

1. The rank of $\bar{\mathbf{S}}_3$ is one at the surface wave speed.
2. The eigenvalues of $\bar{\mathbf{S}}_3$ are monotonically decreasing functions of velocity.
3. When the body is not loaded the eigenvalues of $\bar{\mathbf{S}}_3$ are all positive for $V = 0$.
4. $\bar{\mathbf{S}}_3$ is singular at the limiting velocity since $\mathbf{Q}(\mathbf{y})$ is singular at that velocity. (51)

Using the properties (51) the existence of a surface wave in a stress-free half space can be determined from the statement (after Barnett and Lothe, 1978):

> "A pure mode surface wave exists if the trace of $\bar{\mathbf{S}}_3$ is less than 0 at the limiting velocity $V = V_L$." (52)

If the above is not the case then there is a bulk wave which travels at the limiting velocity satisfying the stress-free boundary condition (Barnett and Lothe, 1974). A surface wave not satisfying (52) will be called an exceptional surface wave.

When the half space is loaded, Chadwick and Jarvis (1979) have shown that an existence statement similar to (52) can still be made. If, however, enough prestress is present to cause two of the eigenvalues of $\bar{\mathbf{S}}_3$ to be zero at $V = 0$, the homogeneous deformation and propagation direction are said to belong to the neutral set (Chadwick and Jarvis, 1979) in which a standing wave satisfies the stress-free boundary condition. More severe prestress can cause these eigenvalues to become negative at $V = 0$ and, because of the monotonicity of the eigenvalues, they will remain negative as V increases to V_L and hence no surface wave can exist. For a prestressed material the following existence criterion can be used (after Chadwick and Jarvis, 1979):

> "A pure mode or an exceptional surface wave exists in a prestressed material if all the eigenvalues of $\bar{\mathbf{S}}_3$ at $V = 0$ are positive. Whether the wave is a pure mode or an exceptional surface wave is determined from (52)." (53)

For the prestress levels that were applied in the numerical examples discussed later, the eigenvalues of $\bar{\mathbf{S}}_3$ were always positive at $V = 0$.

The fact that $\bar{\mathbf{S}}_3$ is of rank one at the surface wave speed gives a relatively simple method to calculate the surface wave speed V_R. Since two of the eigenvalues are zero at $V = V_R$ all subdeterminants of $\bar{\mathbf{S}}_3$ vanish at this velocity. Thus, one only needs to find the smallest velocity such that any 2×2 subdeterminant vanishes to determine the surface wave speed. This velocity will be the velocity for which the smallest eigenvalue of any 2×2 submatrix is zero. Choosing the upper left submatrix, the surface wave speed is the zero of the function

$$\frac{(\bar{S}_3)_{11} + (\bar{S}_3)_{22}}{2} - \left\{ \left(\frac{(\bar{S}_3)_{11} - (\bar{S}_3)_{22}}{2} \right)^2 + [(\bar{S}_3)_{12}]^2 \right\}^{1/2} = 0. \tag{54}$$

VI Calculation of Surface Wave Speeds

This section describes the scheme used for calculating the surface wave speeds from the components of the tensor $\bar{\mathbf{S}}_3$. First, an equation for $\bar{\mathbf{S}}_3$ is given which makes the numerical integration as simple as possible. From the previous section, we know that the existence and the calculation of surface wave speed are determined from the eigenvalues of $\bar{\mathbf{S}}_3$. A similarity transformation of $\bar{\mathbf{S}}_3$ yields a rotated tensor $\bar{\mathbf{S}}_3^R$ whose components are more easily calculated than those of $\bar{\mathbf{S}}_3$. Under this transformation the eigenvalues remain the same allowing $\bar{\mathbf{S}}_3^R$ to be used in checking for existence and calculating the surface wave speed. The trace of a tensor is invariant under a similarity transformation so that the type of surface wave (pure mode or exceptional) can be also determined from $\bar{\mathbf{S}}_3^R$.

To compute the components of $\bar{\mathbf{S}}_3$ equations (38) and (46) can be used to write

$$\bar{\mathbf{S}} = \frac{1}{2\pi}\int_o^{2\pi} \{\mathbf{Q}(\mathbf{z}) - \mathbf{R}(\mathbf{z},\mathbf{y})\mathbf{Q}^{-1}(\mathbf{y})\mathbf{R}(\mathbf{y},\mathbf{z})\} d\chi. \tag{55}$$

Downloaded 03 May 2010 to 171.66.16.27. Redistribution subject to ASME license or copyright; see http://www.asme.org/terms/Terms_Use.cfm

The numerical integration of equation (55) can be lengthy because of the large number of summed terms in the integrand ($\mathbf{Q}(\mathbf{y})$ and $\mathbf{R}(\mathbf{y},\mathbf{z})$ are each calculated as the sum of nine terms). It is therefore desirable to expand the integrand and move as many terms as possible outside the integral. After this is done, the components of $\bar{\mathbf{S}}_3$ are given as

$$(\bar{S}_3)_{mg} = (1/2\pi)\epsilon_{pjs}t_j B'_{nrgp}B'_{wmis}\left\{\epsilon_{vwn}t_v\int_o^\pi Q_{ir}^{-1}(\mathbf{y})d\chi + (m_w n_n + n_w m_n)\int_o^\pi Q_{ir}^{-1}(\mathbf{y})\cos(2\chi)d\chi + (n_w n_n - m_w m_n)\int_o^\pi Q_{ir}^{-1}(\mathbf{y})\sin(2\chi)d\chi\right\}, \quad (56)$$

where $\mathbf{t}=\mathbf{m}\times\mathbf{n}$, and B'_{ijks} is as defined in equation (17) with unit vector $\mathbf{z}$ replaced by $\mathbf{m}$.

In evaluating B_{ijks}, recall from equations (12) and (14) that K_{ijks} has four terms involving F_{iA} and a second derivative of the strain energy density with respect to the strain. Let the strain energy density be written as a power series in the strain and, to account for the dependence of the wave's velocity on stress, retain second and third-order terms in the expansion. The strain energy is written as

$$\rho_o\Phi = 1/2C_{ABCD}E_{AB}E_{CD} + 1/6C_{ABCDMN}E_{AB}E_{CD}E_{MN}, \quad (57)$$

where C_{ABCD} and C_{ABCDMN} are the second and third-order elastic constants, respectively. For a given prestress, there is an associated strain which can be determined. Unfortunately, from this strain the deformation gradient F_{iA} can only be determined to within an arbitrary rotation R_{iB}. For this reason, the tensor K_{ijks} cannot be directly calculated from equation (12) for a given prestress. We now introduce the tensor B^R_{IJKS} as

$$B^R_{IJKL} = K^R_{IJKL} + \sigma_{IL}\delta_{JK}, \quad (58)$$

where

$$K^R_{IJKL} = \rho U_{IA}U_{JB}U_{KC}U_{LD}\frac{\partial^2\Phi}{\partial E_{AB}\partial E_{CD}}, \quad (59)$$

and σ_{IL} is the rotated stress of equation (7). Given the strain, the right stretch tensor can be uniquely determined and hence the tensor K^R_{IJKL} can be evaluated. Using equations (14) and (58) we note that $B^R_{IJKL} = R_{iI}R_{jJ}R_{kK}R_{sL}B_{ijks}$ where R_{iI} is the local rotation tensor which is proper orthogonal. A transformation of this type is called a similarity transformation and under this kind of transformation the eigenvalues are invariant. Formally, if one uses B^R_{IJKL}, in equation (56) the resulting tensor, $\bar{\mathbf{S}}^R_3$, is obtained from a similarity transformation of $\bar{\mathbf{S}}_3$, which means that the eigenvalues of $\bar{\mathbf{S}}^R_3$ and $\bar{\mathbf{S}}_3$ are the same. The eigenvalues of $\bar{\mathbf{S}}_3$, from which surface wave speed is determined, can then be calculated using the symmetric right stretch tensor U_{BA} instead of the deformation gradient.

Knowing the components of $\bar{\mathbf{S}}^R_3$, the existence of a pure mode or an exceptional surface wave is checked by considering the eigenvalues of $\bar{\mathbf{S}}^R_3$ at $V=0$. If any of the eigenvalues are less than or equal to zero then a surface wave does not exist. Furthermore, since two of the eigenvalues will vanish simultaneously, it will suffice to look at the eigenvalues of a 2×2 submatrix. For a pure mode or an exceptional surface wave to exist it is necessary that, for $V=0$,

$$\frac{(\bar{S}^R_3)_{11}+(\bar{S}^R_3)_{22}}{2} - \left\{\left(\frac{(\bar{S}^R_3)_{11}-(\bar{S}^R_3)_{22}}{2}\right)^2 + [(\bar{S}^R_3)_{12}]^2\right\}^{1/2} > 0. \quad (60)$$

Once it has been established that equation (60) is satisfied, the limiting velocity must be found so that the distinction between a pure mode and an exceptional surface wave can be made. The limiting velocity is the minimum velocity for which $\mathbf{Q}(\mathbf{y})$ becomes singular for some angle χ. The eigenvalues of $Q_{ij}(\mathbf{y})$ are $\rho[c_i^2(\mathbf{y}) - V^2\cos^2\chi]$ where $c_i(\mathbf{y})$ are the eigenvalues of the tensor $B_{ijks}y_jy_s$ and represent the bulk wave speeds for propagation in the y_i direction. If these speeds are ordered so that $c_1(\mathbf{y}) < c_2(\mathbf{y}) < c_3(\mathbf{y})$, it follows that $\mathbf{Q}(\mathbf{y})$ becomes singular when $V^2 = c_1^2\sec^2\chi$. So the limiting velocity, V_L, can be calculated from

$$V_L = \min_{-\pi/2<\chi<\pi/2} \{c_1^2(\mathbf{y})\sec^2\chi\}. \quad (61)$$

The limiting velocity can also be geometrically defined in terms of the slowness surfaces of the material. The limiting velocity is the velocity for which a line L, parallel to the x_1 direction first touches the outermost sheet of the slowness surface (Barnett and Lothe, 1978).

When the limiting velocity is known it can be determined whether a pure mode or an exceptional surface wave is propagating. If the trace of $\bar{\mathbf{S}}^R_3$ is positive, then the wave is an exceptional wave travelling at the limiting velocity. When the trace is negative, a pure mode wave is propagating and its velocity is found to be the zero of equation (54) using $\bar{\mathbf{S}}^R_3$ in place of $\bar{\mathbf{S}}_3$.

VII Numerical Results

In this section numerical results predicted from the model of Section VI are given for single crystal aluminum, single crystal copper, and a transversely isotropic aluminum aggregate with

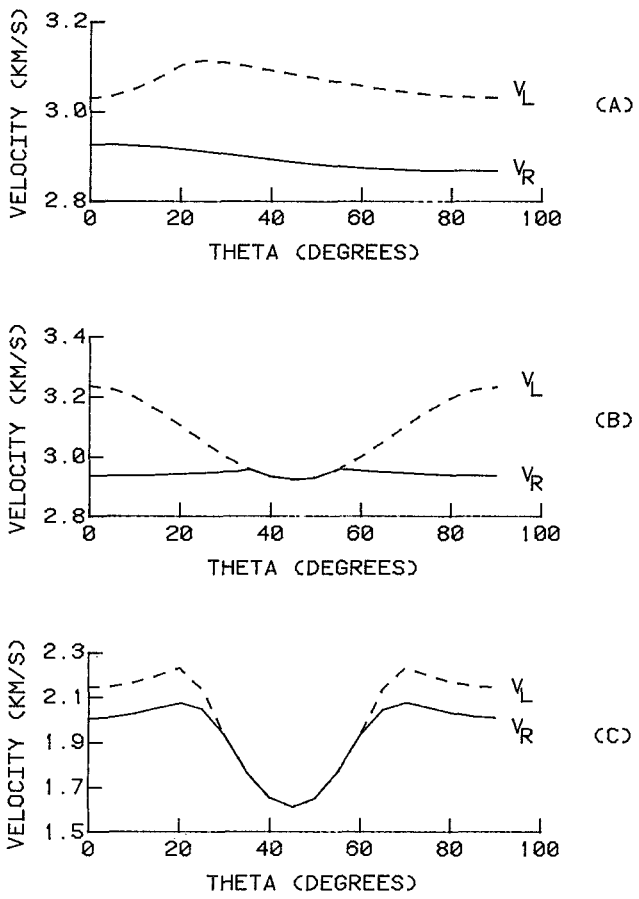


Fig. 2 The limiting velocity, V_L, and surface wave speed, V_R, for unstressed: (A) <111> textured aluminum aggregate; (B) single crystal aluminum; (C) single crystal copper

Downloaded 03 May 2010 to 171.66.16.27. Redistribution subject to ASME license or copyright; see http://www.asme.org/terms/Terms_Use.cfm

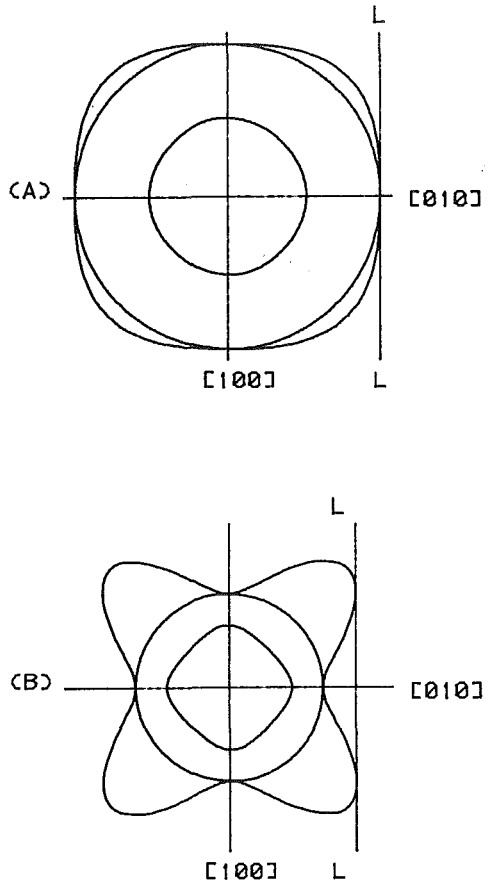


Fig. 3 Slowness surfaces for: (*A*) single crystal aluminum; (*B*) single crystal copper

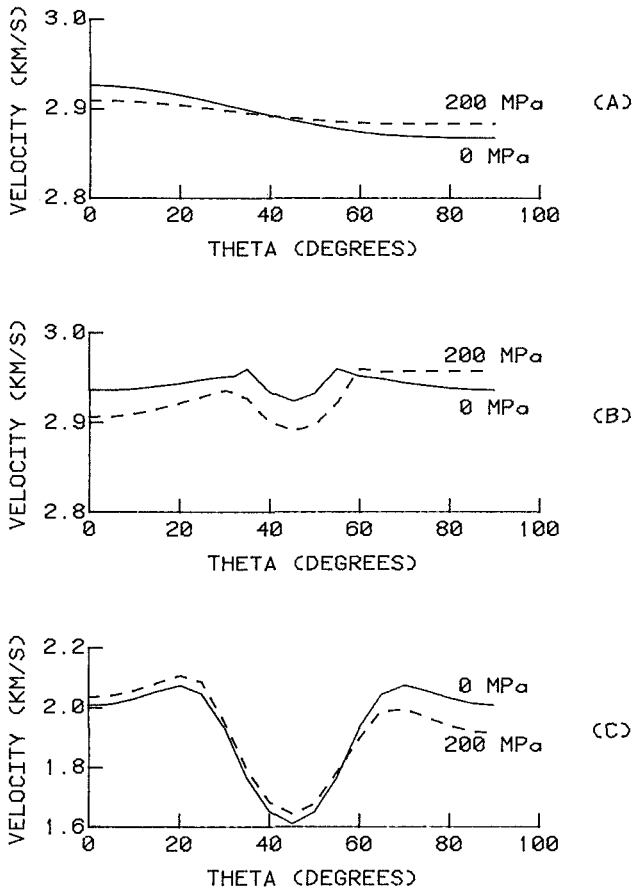


Fig. 4 Surface wave speed versus propagation direction with no stress (solid line) and with 200 MPa applied in the $\theta = 0$ direction (dashed line) for: (*A*) <111> textured aluminum aggregate; (*B*) single crystal aluminum; (*C*) single crystal copper

<111> texture whose symmetry axis is the x_3 axis. In making the numerical calculations the second and third-order elastic constants must be known. The elastic constants for the <111> textured aluminum are taken from Johnson (1982) where the second and third-order constants are derived from the elastic properties of the constituent cubic crystal and the crystalline orientation relative to the body's symmetry axis. For the single crystal aluminum and copper, the elastic constants were taken from Thomas (1968) and Hiki and Granato (1966), respectively. The elastic constants used are given in Table 1. The response of aluminum and copper was examined to study two materials whose degree of anisotropy differs considerably. If we define a measure of anisotropy as the ratio of C_{44} to $(C_{11} - C_{12})/2$ the degree of anisotropy is 1.22 for aluminum and 3.27 for copper.

All the results given here are for surface waves propagating on a half space that is defined by the inward normal $\mathbf{n} = (1,0,0)$. The direction of propagation in the surface is given by angle θ which is the angle between the x_2 axis (the [010] direction for the single crystals) and the propagation vector.

The limiting velocity and surface wave speed were examined as a function of propagation direction in the stress-free state for the three materials. For the aluminum aggregate, a pure mode surface wave exists in all directions (Fig. 2*a*). This is shown by the limiting velocity being everywhere greater than the surface wave speed. The surface wave speed varies continuously from the fast direction ($\theta = 0$ deg) to the slow direction ($\theta = 90$ deg) as would be expected. Surface wave speeds for single crystal aluminum vary continuously and exhibit symmetry with respect to $\theta = 45$ deg as can be seen from Fig. 2(*b*). However, pure mode waves are not propagated in all directions. Between $\theta = 35$ deg and $\theta = 55$ deg the surface wave speed is equal to the limiting velocity meaning an exceptional surface wave is propagating in this direction. Copper is a more severely anisotropic cubic crystal and Fig. 2(*c*) shows how much more the limiting velocity and surface wave speed vary between the x_2([010]) and x_3[001]) directions. For instance, the limiting velocity of copper varies 31 percent between $\theta = 0$ deg and $\theta = 45$ deg while for aluminum this change is 17 percent. The pure mode directions for copper were in the sectors given by $\theta = 0$ deg to 30 deg and 60 deg to 90 deg. When the surface wave speeds for single crystal aluminum and copper are normalized by the shear wave speed in the x_2 direction, the results presented agree with those of Farnell (1970).

It is of interest to note that for the aluminum single crystal with $\theta = 0$ deg, the limiting velocity is equal to the slowest shear wave speed in that direction, but for copper this is not the case. This can be explained by looking at the slowness surfaces for single crystal aluminum and copper and recalling the geometric definition of the limiting velocity. The slowness surface for single crystal aluminum is shown in Fig. 3(*a*) and the line L first becomes tangent to the the outer slowness sheet at $\chi = 0$ deg. This means the shear wave speed and the limiting velocity are equal in this direction (3234 m/s). From the slowness surface of copper, Fig. 3(*b*), we see that the line L first touches the outermost sheet at $\chi = 37.8$ deg and hence the limiting velocity (2158 m/s) is less than the shear wave speed (2911 m/s) in the x_2 direction.

The materials were then numerically subjected to a tensile stress of 200 MPa in the x_2 direction. With this tensile stress applied to the aluminum aggregate, the surface wave speed decreases 16 m/s for propagation in the direction of loading and increases 17 m/s for propagation normal to the loading

Downloaded 03 May 2010 to 171.66.16.27. Redistribution subject to ASME license or copyright; see http://www.asme.org/terms/Terms_Use.cfm

Table 1 Second and third-order elastic constants used in numerical computations

SECOND-- AND THIRD-ORDER ELASTIC CONSTANTS FOR ALUMINUM AND COPPER(GPa)

	Single Crystal Copper	Single Crystal Aluminum	<111> Texture Aluminum
C_{11}	166.1	106.75	111.8
C_{12}	119.9	60.41	58.68
C_{13}	119.9	60.41	56.97
C_{33}	166.1	106.75	113.6
C_{55}	75.6	28.34	24.87
C_{66}	75.6	28.34	26.58
C_{111}	-1271.	-1076.	-1435.
C_{112}	-814.	-315.	-254.1
C_{113}	-814.	-315.	-164.3
C_{133}	-814.	-315.	-294.9
C_{123}	-50.	36.	-36.77
C_{166}	-780.	-340.	-295.1
C_{155}	-780.	-340.	-197.3
C_{144}	-3.	-23.	-71.77
C_{456}	-95.	-30.	-62.77
C_{333}	-1271.	-1076.	-1312.
C_{366}	-3.	-23.	-63.77
C_{355}	-780.	-340.	-335.9

(Fig. 4(*a*)). Figures 4(*b*) and 4(*c*) show how the surface wave speeds in aluminum and copper vary due to the presence of the applied stress. Both aluminum and copper are cubic materials, but their response to the applied stress is quite different. In aluminum, a mildly anisotropic material, the surface wave speed decreases 18 m/s in the direction of loading and increases 16 m/s normal to the loading direction. For copper, a material whose anisotropy is more severe, the opposite is true: the surface wave speed increases 27 m/s in the direction of loading and decreases 92 m/s normal to the load.

The pure mode directions for aluminum do not change under 200 MPa tensile stress in the $\theta = 0$ deg direction. It should be noted that data points are taken every five degrees so the pure mode directions may change less than five degrees and not show up in our computations. The sectors of pure mode propagation for copper which is loaded change in the same manner. For unstressed copper, the pure mode directions are from 0–25 and 65–90 deg changing to 0–30 and 65–90 deg with the applied stress.

VIII Conclusion

The surface wave theory of Barnett et al. (1973a) has been adapted so that it can be used in acoustoelasticity, a nondestructive method for measuring stresses in structural materials. In order to do this, a configuration was introduced in which the effect of local rotation was removed so that the surface speeds could be written as a function of the applied stress. In the present paper, existence and surface wave speed were determined from a real symmetric 2×2 matrix whose components were written with respect to the rotated configuration introduced. The components of this matrix were computed by numerically integrating certain combinations of the material's second and third-order elastic constants.

A numerical study was undertaken to calculate the surface wave speeds for half spaces with and without prestress. In the absence of prestress, the results for single crystal aluminum agree with the previous work of Farnell (1970). When uniaxial tension was applied to single crystal aluminum and single crystal copper, materials whose degree of anisotropy varies considerably, their response was quite different. With 200 MPa tensile stress applied in the direction of propagation, the surface wave speed decreased for aluminum while it increased for copper. For the two single crystals studied, the pure mode directions of propagation did not appear to be very sensitive to the applied stress. The aluminum aggregate propagated pure mode waves in all directions in the free surface both in the presence and absence of prestress. For all three materials, a pure mode or an exceptional surface wave always existed in all directions for tensile loading up to 200 MPa.

Formulation of the acoustoelastic problem in the present paper is a step in the direction of obtaining a tractable explicit expression for the surface wave speed in terms of the applied stress. The advantage of this method over previous work is that the vanishing of the determinant of a real symmetric 2×2 matrix is the condition needed to satisfy the stress-free boundary condition rather than the vanishing of the determinant of a complex 3×3 matrix. While the method presented here does not offer an explicit expression for the surface wave speed in terms of applied stress for an anisotropic material, it may lead to a solution for the surface wave speed in terms of stress for a slightly anisotropic material.

Acknowledgment

This work was supported by the National Science Foundation under Grant Number MEA 8410535.

References

Barnett, D. M., and Lothe, J., 1978, "The Existence of Rayleigh (Surface) Wave Solutions in Anisotropic Linear Elastic Half Spaces," *Modern Problems in Elastic Wave Propagation*, Miklowitz, J., and Achenbach, J. D., eds., Wiley, New York, NY, pp. 445–457.

Barnett, D. M., Lothe, J., Nishioka, K., and Asaro, R. J., 1973a, "Elastic Surface Waves in Anisotropic Crystals: A Simplified Method for Calculating Rayleigh Velocities Using Dislocation Theory," *J. Phys. F: Metal Phys.*, Vol. 3, pp. 1083–1096.

Barnett, D. M., Nishioka, K., and Lothe, J., 1973b, "Surface Waves in Anisotropic Media. A Formulation for the Purpose of Rapid Numerical Calculations," *Phys. Stat. Sol. B*, Vol. 55, pp. K115–K117.

Barnett, D. M., and Lothe, J., 1974, "Consideration of the Existence of Surface Wave (Rayleigh Wave) Solutions in Anisotropic Elastic Crystals," *J. Phys. F: Metal Phys.*, Vol. 4, pp. 671–686.

Buchwald, V. T., 1961, "Rayleigh Waves in Anisotropic Media," *Quart. Journ. Mech. and Appl. Math.*, Vol. 14, pp. 461–469.

Burridge, R., 1970, "The Directions in Which Rayleigh Waves May be Propagated on Crystals," *Quart. Journ. Mech. and Appl. Math.*, Vol. 23, pp. 217–224.

Chadwick, P., and Jarvis, D. A., 1979, "Surface Waves in a Pre-Stressed Elastic Body," *Proc. R. Soc. Lond. A.*, Vol. 366, pp. 517–536.

Chadwick, P., and Smith, G. D., 1977, "Foundations of the Theory of Surface Waves in Anisotropic Elastic Materials," *Advances in Applied Mechanics*, Vol. 17, Academic Press, NY, pp. 303–376.

Crecraft, D. J., 1967, "The Measurement of Applied and Residual Stresses in Metals Using Ultrasonic Waves," *J. Sound Vib.*, Vol. 5, pp. 173–192.

Farnell, G. W., 1970, "Properties of Elastic Surface Waves," *Physical Acoustics*, Mason, W. P., and Thurston, R. N., eds., Academic Press, NY, Vol. 6, pp. 109–166.

Green, A. E., and Naghdi, P. M., 1965, "A General Theory of an Elastic-Plastic Continuum," *Arch. Rational Mech. Anal.*, Vol. 18, pp. 251–281.

Hayes, M., and Rivlin, R. S., 1961, "Surface Waves in Deformed Elastic Materials," *Arch. Rational Mech. Anal.*, Vol. 8, pp. 358–380.

Hiki, Y., and Granato, A. V., 1966, "Anharmonicity in Noble Metals; Higher Order Elastic Constants," *Phys. Rev.*, Vol. 144, pp. 411–419.

Hirao, M., and Fukuoka, H., 1981, "Acoustoelastic Effect of Rayleigh Sur-

Downloaded 03 May 2010 to 171.66.16.27. Redistribution subject to ASME license or copyright; see http://www.asme.org/terms/Terms_Use.cfm

face Waves in Isotropic Materials," ASME JOURNAL APPLIED MECHANICS, Vol. 48, pp. 119–124.

Hsu, N. N., 1974, "Acoustic Birefringence and the Use of Ultrasonic Waves for Experimental Stress Analysis," *Exper. Mech.*, Vol. 14, pp. 169–176.

Iwashimizu, Y., and Kubomura, K., 1973, "Stress-Induced Rotation of Polarization Directions of Elastic Waves in Slightly Anisotropic Materials," *Int. J. Solids Struct.*, Vol. 9, pp. 99–114.

Iwashimizu, Y., and Kobori, O., 1978, "The Rayleigh Wave in a Finitely Deformed Elastic Material," *J. Acoust. Soc. Am.*, Vol. 64, pp. 910–916.

Johnson, G. C., 1981, "Acoustoelastic Theory for Elastic-Plastic Materials," *J. Acoust. Soc. Am.*, Vol. 70, pp. 591–595.

Johnson, G. C., 1982, "Acoustoelastic Response of Polycrystalline Aggregates Exhibiting Transverse Isotropy," *J. Nondestructive Eval.*, Vol. 3, pp. 3–10.

Johnson, G. C., and Mase, G. T., 1984, "Acoustoelasticity in Transversely Isotropic Materials," *J. Acoust. Soc. Am.*, Vol. 75, pp. 1741–1747.

Lim, T. C., and Farnell, G. W., 1968, "Search for Forbidden Directions of Elastic Surface-Wave Propagation in Anisotropic Crystals," *J. Appl. Phys.*, Vol. 39, pp. 4319–4325.

Lothe, J., and Barnett, D. M., 1976, "On the Existence of Surface Wave Solutions for Anisotropic Elastic Half-Spaces with Free Surface," *J. Appl. Phys.*, Vol. 47, pp. 428–433.

Martin, B. G., 1974, "Rayleigh-Wave Velocity, Stress and Preferred Grain Orientation in Aluminum," *Non-Destructive Testing-Research and Practice*, Vol. 7, pp. 199–203.

Okada, K., 1980, "Stress-Acoustic Relations for Stress Measurement by Ultrasonic Technique," *J. Acoust. Soc. Jpn.* (*E*), Vol. 1, pp. 193–200.

Stonely, R., 1955, "The Propagation of Surface Elastic Waves in Cubic Crystals," *Proc. Roy. Soc.*, Vol. 232A, pp. 447–458.

Stroh, A. N., 1962, "Steady State Problems in Anisotropic Elasticity," *J. Math. and Phys.*, Vol. 41, pp. 77–103.

Synge, J. L., 1957, "Elastic Waves in Anisotropic Media," *J. Math. and Phys.*, Vol. 35, pp. 323–334.

Thomas, J. F., 1968, "Third-Order Elastic Constants of Aluminum," *Phys. Rev.*, Vol. 175, pp. 955–962.

Thurston, R. N., and Brugger, K., 1964, "Third-Order Elastic Constants and the Velocity of Small Amplitude Elastic Waves in Homogeneously Stressed Media," *Phys. Rev.*, Vol. 133, pp. A1604–A1610.

Toupin, R. A., and Bernstein, B., 1961, "Sound Waves in Deformed Perfectly Elastic Materials. Acoustoelastic Effect," *J. Acoust. Soc. Am.*, Vol. 33, pp. 216–225.

Downloaded 03 May 2010 to 171.66.16.27. Redistribution subject to ASME license or copyright; see http://www.asme.org/terms/Terms_Use.cfm

J. F. Doyle
Associate Professor,
School of Aeronautics and Astronautics,
Purdue University,
West Lafayette, Ind. 47907

S. Kamle
Assistant Professor,
Department of Aeronautical Engineering,
Indian Institute of Technology,
Kanpur, India 208016

An Experimental Study of the Reflection and Transmission of Flexural Waves at an Arbitrary T-Joint

Further developments of an experimental methodology for analyzing the effect of structural joints on wave propagation are presented. Experimental results for an arbitrary T-joint are discussed as well as improved ways of characterizing the incident wave.

Introduction

The analysis of the propagation of stress waves through a framed structure is complicated by the presence of joints. These joints act as both filters and sources of new waves. That is, an incident flexural wave can generate new flexural waves as well as longitudinal and torsional waves. It is desirable to have a simple approach to handling these problems in order to avoid costly detailed analyses. However, before this can be done it is necessary to understand fully the interaction of a single joint on an incident wave.

This paper presents further developments of an experimental methodology (Doyle and Kamle, 1985) for analyzing the effect of structural joints on wave propagation. First, a parametric study is performed on a model of a T-joint so as to elucidate the primary influences on the response of the joint. This is followed by introducing refinements to the scheme for experimentally characterizing an incident flexural wave. Finally, the application to an arbitrary T-joint is discussed and experimentally verified.

Analysis of an Arbitrary T-Joint

The equations of motion of the joint of Fig. 1 are

$$-F_1+\sum_2 F_m\cos\theta_m-\sum_2 V_m\sin\theta_m=m_j\ddot{u}$$

$$-V_1+\sum_2 F_m\sin\theta_m+\sum_2 V_m\cos\theta_m=m_j\ddot{v}$$

$$-M_1+\frac{L}{2}V_1+\sum_2 M_m+\frac{L}{2}\sum V_m=I_j\ddot{\phi} \tag{1}$$

where the summation is over the number of members and the right-hand side refers to centroidal values of the joint. F, V, and M are the normal force, shear force and bending moment, respectively. There is no torsion since only planar excitations are considered.

Assuming the joint to be rigid, the displacement continuity gives for each member an equation of the form

$$u_1-\left[u_m\mathrm{Cos}\theta_m-v_m\mathrm{Sin}\theta_m+\frac{L}{2}\mathrm{Sin}\theta_m\frac{dv_m}{dx_m}\right]=0$$

$$v_1-\left[u_m\mathrm{Sin}\theta_m+v_m\mathrm{Cos}\theta_m-\frac{L}{2}(1+\mathrm{Cos}\theta_m)\frac{dv_m}{dx_m}\right]=0 \tag{2}$$

and for slope continuity

$$\frac{dv_1}{dx_1}-\frac{dv_m}{dx_m}=0 \tag{3}$$

where u and v are longitudinal and transverse displacements, respectively, referred to the axis of the member. L is a parameter characterizing the size of the joint. Using these equations the centroidal values of the joint can be estimated as

$$u=u_1 \qquad m_j=\rho_j\pi L^2 w_j/4$$

$$v=v_1-\frac{L}{2}\frac{dv_1}{dx_1} \qquad I_j=m_jL^2/8$$

$$\phi=\frac{dv_1}{dx_1} \tag{4}$$

From these it is apparent that the controlling parameters of the joint are its mass (as dictated by its density ρ_j) and its physical size (as dictated by L).

The axial force, shear force, and bending moments, respectively, are related to the displacements by

$$F=EA\frac{\partial u}{\partial x}\quad V=-EI\frac{\partial^3 v}{\partial x^3}\quad M=EI\frac{\partial^2 v}{\partial x^2} \tag{5}$$

where EA and EI are the axial and bending stiffnesses. Finally, if the flexural and longitudinal displacements are expanded in the forms

Contributed by the Applied Mechanics Division for publication in the JOURNAL OF APPLIED MECHANICS.
Discussion on this paper should be addressed to the Editorial Department, ASME, United Engineering Center, 345 East 47th Street, New York, N.Y. 10017, and will be accepted until two months after final publication of the paper itself in the JOURNAL OF APPLIED MECHANICS. Manuscript received by ASME Applied Mechanics Division, June 11, 1985; final revision, June 2, 1986.

Copyright © 1987 by ASME
Downloaded 03 May 2010 to 171.66.16.27. Redistribution subject to ASME license or copyright; see http://www.asme.org/terms/Terms_Use.cfm

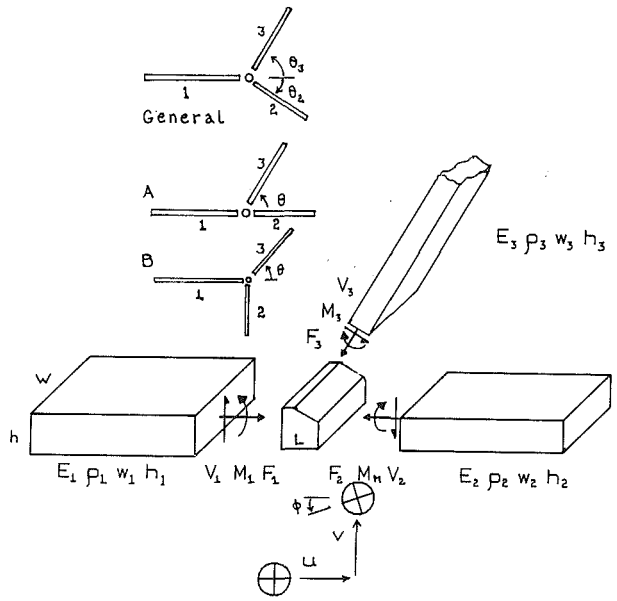


Fig. 1 Model of arbitrary T-joint and designation of joint arrangements

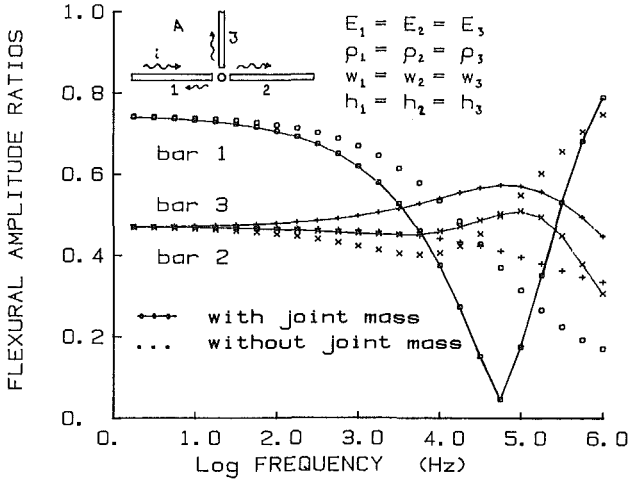


Fig. 2 The effect of frequency on the flexural coefficients

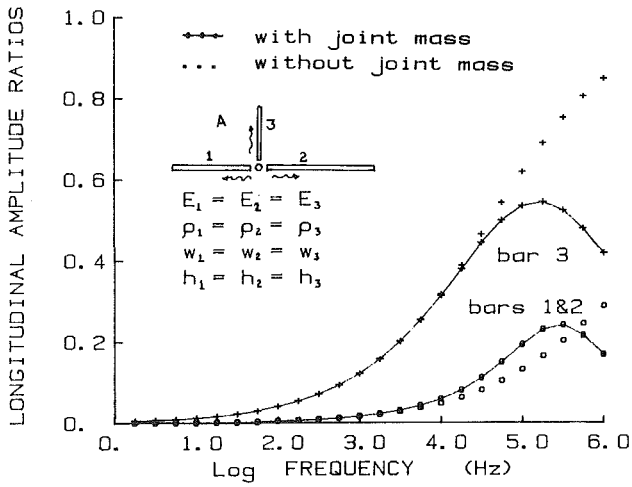


Fig. 3 The effect of frequency on the longitudinal coefficients

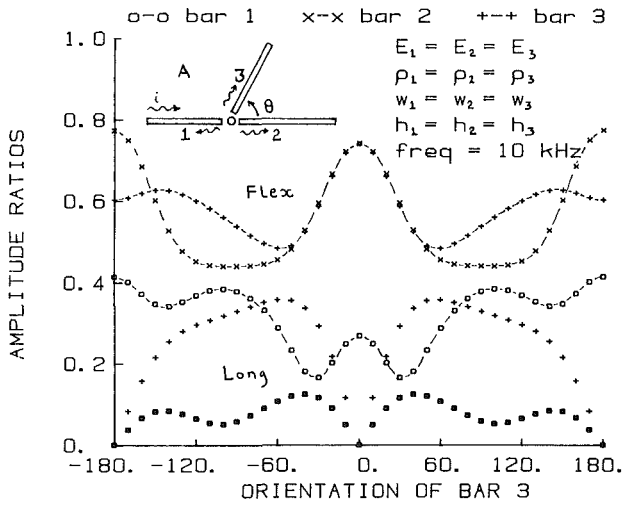


Fig. 4 The effect of orientation of bar 3 on both the flexural and longitudinal coefficients. Joint arrangement *A*.

$$v(x,t) = \sum_n [A_n e^{-iK_n x} + B_n e^{-K_n x}] e^{i\omega_n t} \qquad K_n = \sqrt{\omega_n}\left[\frac{\rho A}{EI}\right]^{\frac{1}{4}}$$

$$u(x,t) = \sum_n [P_n e^{-iK_{Ln} x}] e^{i\omega_n t} \qquad K_{Ln} = \omega_n \sqrt{\rho/E} \qquad (6)$$

where K_{Ln} is the longitudinal wave number, then a system of nine equations can be set up so as to determine the nine wave coefficients. The Appendix shows the system of equations that must be solved to obtain the wave coefficients. This must be done at each frequency. In the paper by Doyle and Kamle (1985) the corresponding equations were solved explicitly, but for more general joints it is best to solve them numerically. This is done in the present case as part of the numerical procedure for propagating and reconstructing the waves.

The system of equations as set up could be used to study the incident longitudinal wave problem treated by Desmond (1981), or the incident near-field wave problem treated by Mace (1984), as special cases. However, only incident flexural waves will be considered in this paper.

The following is a brief summary of a parametric study of the joint. For simplicity each arm is assumed to be of the same geometry and material, and member 1 carries the incident wave. The joint is modeled as a rigid cylinder with independently specified diameter and density. Desmond (1981) made an attempt to model the actual shape of the joint but a parametric study showed the structural response to be relatively insensitive to the joint parameters. It is only at very high frequencies or large joints (relative to the significant wavelengths) that the particular geometry of the joint is significant.

In nearly all the cases considered the wave coefficients are complex numbers indicating a phase change relative to the incident wave. However, in the interest of brevity only the amplitude of the waves will be reported. Figure 2 shows the variation of the flexural amplitude ratios with frequency for a T-joint with equal arms. Whether the joint is considered to have mass or not these plots show that it is has a frequency effect. This effect is most pronounced for frequencies greater than 10 kHz. The same is true for the longitudinal components as shown in Fig. 3. For this T-joint arrangement the longitudinal waves in bars 1 and 2 are the same.

Figures 4 and 5 show the effect of the orientation of bar 3. It is interesting that in comparison to Fig. 4, Fig. 5 shows less orientation effects.

It is of interest here to review the main assumptions made in modeling the joint:

Downloaded 03 May 2010 to 171.66.16.27. Redistribution subject to ASME license or copyright; see http://www.asme.org/terms/Terms_Use.cfm

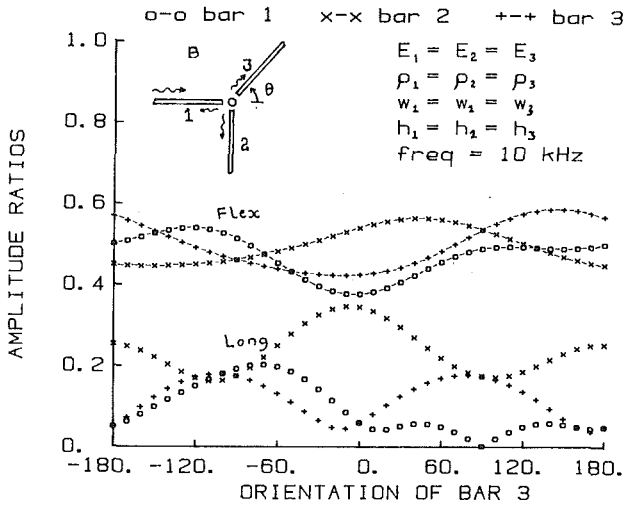


Fig. 5 The effect of orientation of bar 3 on both the flexural and longitudinal coefficients. Joint arrangement *B*.

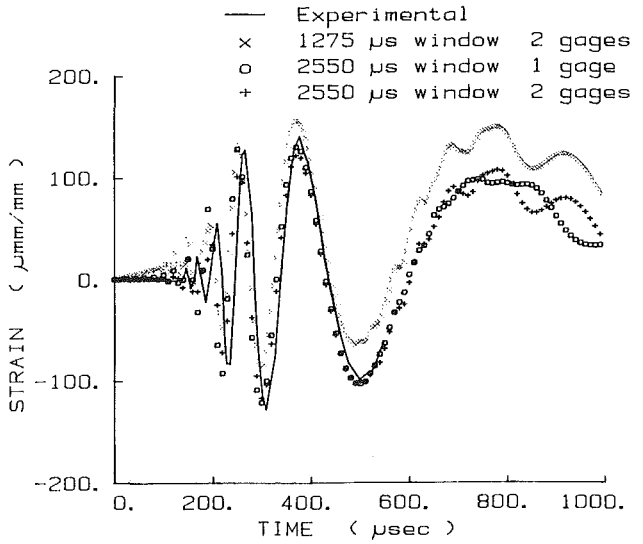


Fig. 6 The effect of sampling window on the ability to accurately propagate a wave

- The flexural waves have a Bernoulli-Euler beam dispersion relation.
- The longitudinal waves are nondispersive.
- The joint is a rigid mass.

All three assumptions are justified by the same reason, namely, the frequency content of the experimentally generated incident wave is such that there is little difference between the elementary theories and a higher order one, such as a Timoshenko beam. This is shown in Fig. 1 of the paper by Doyle and Kamle (1985). Doyle (1984) studied the impact of a beam using both the elementary theory and a modified Timoshenko beam theory. No noticeable differences in the results were observed. When the frequency content is low (< 25 kHz) the wavelengths are large. For example, the smallest wavelength in the present experiments is about 2 in. (50 mm). This is much larger than the physical size of the joint (about 0.25 in. or 6 mm) thus justifying treating the joint as a rigid mass.

Improvements in Characterizing the Incident Wave

In order to get an accurate assessment of the performance of the joint model, it is essential to have an accurate characterization of the incident wave. This characterization

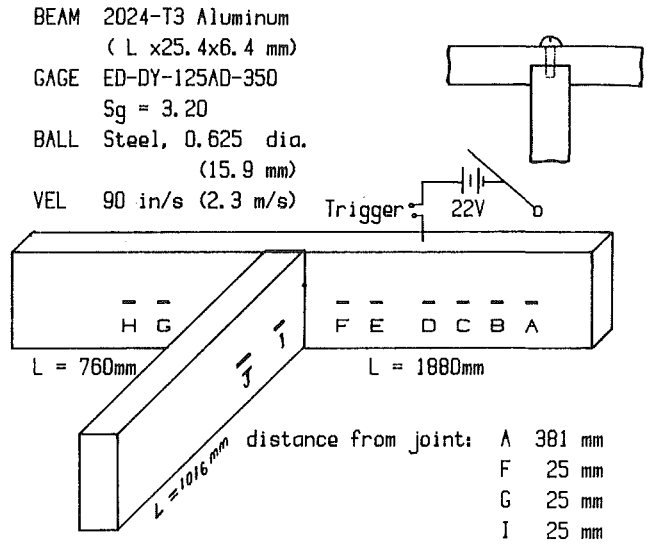


Fig. 7 Model of the T-joint experimentally tested

must be done away from the joint so as to avoid reflections. Since flexural waves are dispersive, then it is also required to be able to propagate the wave accurately. That is, it is necessary to sample away from the joint but accurately predict what the wave looks like at the joint.

The general flexural wave in a beam is of the form

$$v(x,t) = \sum_n [A_n e^{-iK_n x} + B_n e^{-K_n x}] e^{i\omega_n t}$$

A_n and B_n are two sets of unknown complex coefficients. Kamle and Doyle (1985) introduced a scheme using two strain gage samplings to obtain these coefficients. A simplification can be obtained if the waves are generated by impact since symmetry of the wave about the impact site ($x=0$) requires

$$B_n = -iA_n \tag{7}$$

Consequently, the general flexural wave can be written in terms of a single set of coefficients and a single strain gage sampling is sufficient to characterize the incident wave. This coefficient can be obtained explicitly as

$$A_n = -\frac{2}{hK_n^2}\,\hat{e}(x_s,\omega_n)/[ie^{-iK_n x_s} - e^{-K_n x_s}] \tag{8}$$

where x_s is the sampling position and $\hat{e}(x_s,\omega_n)$ is the FFT transform of the strain record.

Figure 6 shows an example of predicting the wave (analogous to Fig. 3 of the Doyle and Kamle (1985) paper) when only one gage is used. Since the propagating distance of 280 mm is so large, an extra large window (total time sample of signal) is incorporated by padding the signal with zeroes. In fact the maximum distance the wave can be propagated without components from neighboring windows drifting into view corresponds to the distance travelled by the lowest frequency component for a time equal to the zero padding. This is estimated as

$$x < 2T_{\text{pad}}\sqrt{\frac{2\pi}{T}}\left[\frac{EI}{\rho A}\right]^{\frac{1}{4}} \tag{9}$$

where T is the sampling window. The improvement in predicted response is quite pronounced when the large window is used, even though the identical strain gage signal is sampled less frequently. The single gage sampling with the larger window is even better than the two gage samplings on the smaller window.

These results show that it is possible to characterize the

Downloaded 03 May 2010 to 171.66.16.27. Redistribution subject to ASME license or copyright; see http://www.asme.org/terms/Terms_Use.cfm

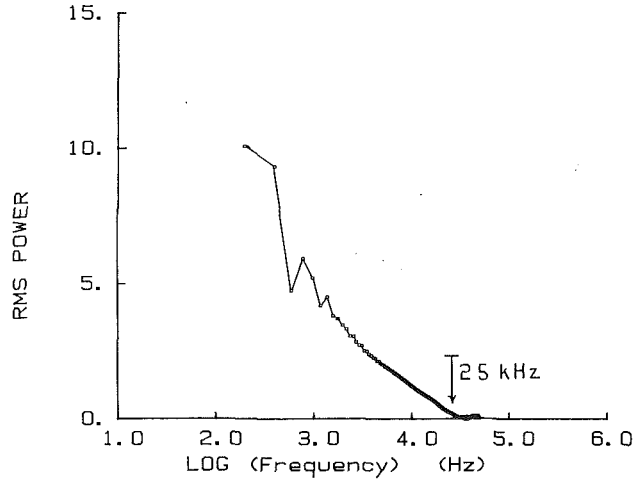


Fig. 8 The RMS power spectrum for the incident wave

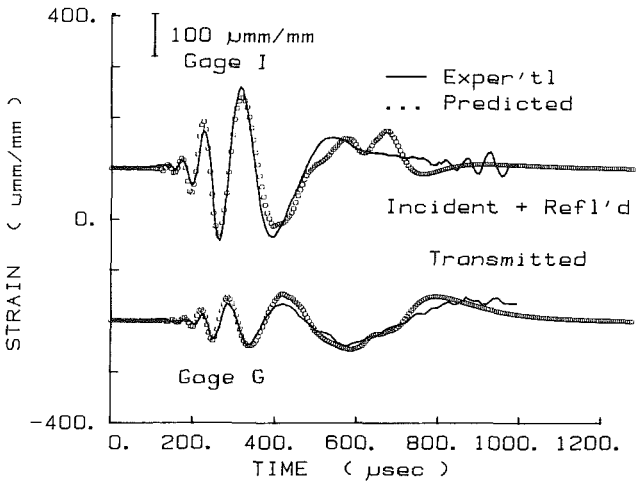


Fig. 9 Comparison of the predicted and experimental strains for a location before the joint. Joint arrangement *A*.

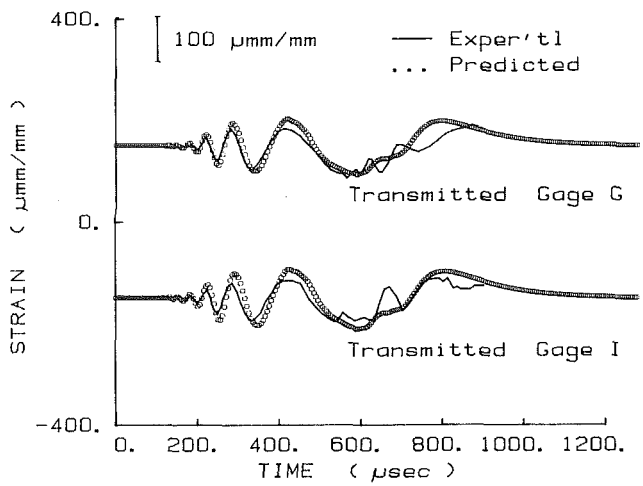


Fig. 10 Comparison of the predicted and experimental strains for two locations after the joint. Joint arrangement *A*.

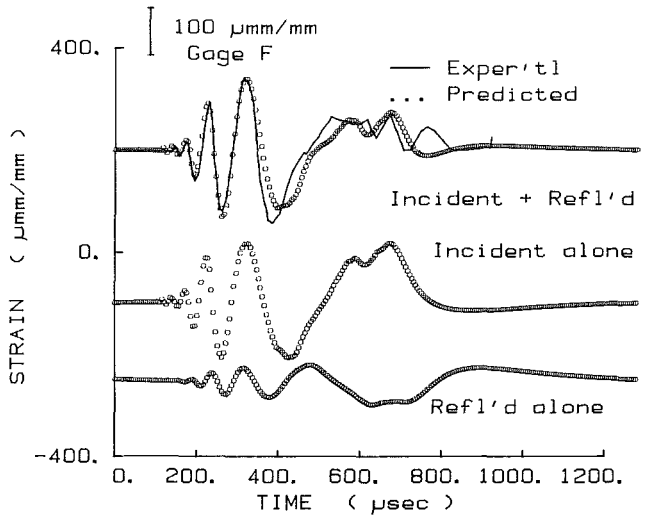


Fig. 11 Comparison of the predicted and experimental strains for locations before and after the joint. Joint arrangement *B*.

signal when it is remote from the joint and yet accurately predict what the signal looks like at the joint.

Experimental Results for a T-Joint

An aluminum jointed frame was made as shown in Fig. 7. Gages are placed on both sides so as to separate the longitudinal waves from the flexural waves. The data acquisition arrangement is similar to that used by Doyle (1984) and Doyle and Kamle (1985). Two arrangements of the joint are investigated:

A: Bar 2 is collinear with Bar 1, Bar 3 is perpendicular to Bar 1.

B: Both Bar 2 and Bar 3 are perpendicular to Bar 1.

Arrangement *A* can be checked against Figs. 2, 3, and 4 while arrangement *B* can be checked against Fig. 5.

Figure 8 shows the RMS power spectrum for the incident wave. It is apparent that most of the amplitudes are contained in the frequency range less than 25 kHz. Consequently, it is expected that the precise description of the joint mass will have little effect on the response. Figure 9 shows a comparison of the predicted response for a gage positioned before the joint with that of experiment. The agreement is very good. Figure 10 shows the results for gages positioned after the joint. The comparison is fair; there seems to be a definite decrease in the measured amplitudes compared to the predictions. It is possible that the joint has an energy loss or conversion not accounted for by the theory.

Figure 11 shows the results for gages positioned before and after the T-joint for the *B* arrangement. While the agreement is good, there is nonetheless a definite underestimation in the reflection and overestimation in the transmitted amplitudes. This again supports the contention that the joint has more flexibility than intended.

The longitudinal waves measured in both cases were negligibly small, on the order of a microstrain. This is in agreement with the predictions. A parametric study on the size of the joint (changing L within reasonable limits) showed that it had little effect on the predictions.

Conclusion

The methodology developed was shown to be quite successful in predicting the effects of an arbitrary T-joint on the propagation of flexural waves. The dynamic response is not sensitive to the particular values of the joint model, it depends primarily on the member arrangement and only secondarily on the particular shape and mass of the joint.

One of the reasons for developing this methodology is to allow the experimental characterization of actual joints in structures. That is, to allow the experimental determination of the $[A]$ coefficients in the Apendix by taking measurements of the waves before and after the joint. It appears that the

Downloaded 03 May 2010 to 171.66.16.27. Redistribution subject to ASME license or copyright; see http://www.asme.org/terms/Terms_Use.cfm

method is sensitive enough to do this. This, of course, would remove the burden of having to develop more complex joint models for the real structures and thereby allow concentration on other aspects of the problem (such as the effects of multiple joints.)

References

Desmond, T. P., 1981, "Theoretical and Experimental Investigation Stress Waves at a Junction of Three Bars," ASME JOURNAL OF APPLIED MECHANICS, Vol. 48, pp. 148–154.

Doyle, J. F., 1984, "Further Developments in Determining the Dynamic Contact Law," *Experimental Mechanics*, Vol. 24, pp. 265–270.

Doyle, J. F., and Kamle, S., 1985, "An Experimental Study of the Reflection and Transmission of Flexural Waves at Discontinuities," ASME JOURNAL OF APPLIED MECHANICS, Vol. 52, pp. 669–673.

Mace, B. R., 1984, "Wave Reflection and Transmission in Beams," *Journal of Sound and Vibration*, Vol. 97, pp. 237–246.

APPENDIX

Summary of Joint Equations

The solution of the generated waves at the joint can be written in the form

$$[A]\{Z\} = \{B\}$$

where $\{Z\}$ are the various wave coefficients represented as

$$\{Z\} = \{C_{1n}, D_{1n}, P_{1n}, A_{mn}, B_{mn}, P_{mn}, \ldots\}$$

The square matrix $[A]$ and column vector $\{B\}$ are zero except

$$A(1,3) = -i[EAK_{Ln}]_1 + m_j\omega_n^2$$

$$A(1,2+m) = i[EIK_n \text{Cos } \theta]_m = -2A(1,3+m)$$

$$A(1,4+m) = -i[EAK_{Ln} \text{Cos } \theta]_m$$

$$A(2,1) = -i[EIK_n^3]_1 + m_j\omega_n^2\left(1 - i\frac{L}{2}K_{1n}\right)$$

$$A(2,2) = [EIK_n^3]_1 + m_j\omega_n^2\left(1 - \frac{L}{2}K_{1n}\right)$$

$$A(2,2+m) = -i[EIK_n^3 \text{Cos } \theta]_m = -iA(2,3+m)$$

$$A(2,4+m) = -i[EAK_{Ln} \text{Sin } \theta]_m$$

$$A(3,1) = \left[EIK_n^2\left(1 + \frac{L}{2}K_n\right)\right]_1 + iI_j\omega_j^2K_{1n}$$

$$A(3,2) = -\left[EIK_n^2\left(1 + \frac{L}{2}K_n\right)\right]_1 + I_j\omega_n^2K_{1n}$$

$$A(3,2+m) = -\left[EIK_n^2\left(1 + \frac{L}{2}K_n\right)\right]_m = -A(3,3+m)$$

$$A(4,3) = 1$$

$$A(4,2+m) = \left[\text{Sin } \theta\left(1 + i\frac{L}{2}K_n\right)\right]_m$$

$$A(4,3+m) = \left[\text{Sin } \theta\left(1 + \frac{L}{2}K_n\right)\right]_m$$

$$A(4,4+m) = -[\text{Cos } \theta]_m$$

$$A(5,1) = 1 = A(5,2)$$

$$A(5,2+m) = -\left[\text{Cos } \theta + i\frac{L}{2}K_n(1 + \text{Cos } \theta)\right]_m$$

$$A(5,3+m) = -\left[\text{Cos } \theta + \frac{L}{2}K_n(1 + \text{Cos } \theta)\right]_m$$

$$A(5,4+m) = -[\text{Sin } \theta]_m$$

$$A(6,1) = iK_{1n} = iA(6,2)$$

$$A(6,2+m) = i[K_n]_m = iA(6,3+m) \qquad (A1)$$

When the incident wave is flexural then

$$B(2) = -i[EIK_n^3]_1 - m_j\omega_n^2\left(1 + i\frac{L}{2}K_{1n}\right)$$

$$B(3) = -\left[EIK_n^2\left(1 - i\frac{L}{2}K_n\right)\right]_1 + iI_j\omega_n^2K_{1n}$$

$$B(5) = -1$$

$$B(6) = iK_{1n} \qquad (A2)$$

and when the incident wave is longitudinal

$$B(1) = -i[EAK_{Ln}]_1 + m_j\omega_n^2$$

$$B(4) = -1 \qquad (A3)$$

The subscript m ranges from 2 to the number of members at the joint.

Downloaded 03 May 2010 to 171.66.16.27. Redistribution subject to ASME license or copyright; see http://www.asme.org/terms/Terms_Use.cfm

On the Initiation of Necking Modes in Layered Plastic Solids

P. S. Steif
Department of Mechanical Engineering,
Carnegie-Mellon University,
Pittsburgh, PA 15213
Assoc. Mem. ASME

The deformation of a solid consisting of alternating material layers with interface undulations is studied analytically. We assess the relative rate of growth or decay of these interface imperfections with straining. The analysis is based on a regular perturbation expansion of the finite strain, nonlinear field equations, the small parameter being the amplitude of the undulations relative to the layer thickness. Attention is focused on the influence of material and geometric parameters on imperfection growth-rates. It is found that significant connections exist between the growth of imperfections and the tendency for undulatory bifurcation modes to emerge from a perfect, layered solid.

1 Introduction

On the micro-level, 100 percent pearlitic steels can exhibit two rather different deformation patterns as precursors to crack nucleation. Depending on the metallurgical treatment, there can be either necking of the cementite (carbide) layers, or shear bands crossing an entire pearlite colony, the latter mode leading to noticeably less ductility (Alexander and Bernstein, 1984). Though micro-scale features not obviously incorporated into a continuum framework most likely impinge on this problem, some progress can be made by studying the mechanics of finitely strained layered solids. Particularly relevant to the pearlite problem is the recent work by Steif (1986a, 1986b) on the emergence of necking-type modes in layered, plastic solids. Attention was directed towards assessing the influence of material properties on the competition between necking and shear band modes. A loss of ellipticity in either of the two layer materials was taken to signal the possible emergence of shear bands. Depending on the material parameters, necking-type modes were found to be possible (Steif, 1986b) for different combinations of deformation regimes in the two materials; namely, elliptic-elliptic, elliptic-hyperbolic, and hyperbolic-hyperbolic. (The parabolic regime was not encountered for the constitutive law considered.) Thus, even if no elliptic-elliptic necking mode bifurcation were possible for a given combination of material parameters, the shear bands would still, in theory, have to compete with hyperbolic-regime necking modes.

Necking modes in layered solids are further studied in the present paper. Our goal is to shed somewhat more light on the shear band-necking mode competition by illustrating an important difference between hyperbolic-regime necking modes and elliptic-regime necking modes. This difference is in the deformation response of the layered solid when imperfections exist at the layer interfaces. The response in the presence of imperfections has been explored in other contexts, notably Koiter's (1945) pioneering work on elastic buckling and post-buckling behavior of structures. In the elastic buckling context, which constitutes an elliptic-regime bifurcation, imperfections in the form of the bifurcation mode are found to grow immediately upon application of the load. By way of contrast, a range of work (Anand and Spitzig, 1980; Tvergaard, Needleman, and Lo, 1981; Abeyeratne and Triantafyllidis, 1981; Tvergaard, 1982) on the role played by imperfections in stimulating shear band formation suggests that significant localized shearing begins only at loads which are relatively close to the bifurcation load. It is of interest here to study somewhat of a hybrid situation – geometric modes which appear in the hyperbolic regime – and to compare the initiation of such modes with the initiation of geometric modes in the elliptic regime.

To do this we perform a linear perturbation analysis of a layered solid possessing interface undulations (waviness). The following question is considered: Will a small interface undulation, a nascent neck or bulge, tend to grow or decay with straining? While the style of analysis given here is similar to many analyses of the initial response of solids with existing imperfections, it bears closest resemblance to studies by Hutchinson and Obrecht (1977) and Hutchinson, Neale, and Needleman (1978) of the growth and decay of surface undulations in viscous solids. However, these investigations differ from the present one insofar as their history-independent constitutive law (nonlinear creep) leads immediately to an Eulerian formulation, while a slightly more complicated Lagrangian formulation is called for here. Our analysis also differs from linear perturbation analyses in buckling which generally focus on approximate theories for structures such as shells and columns (Needleman and Tvergaard, 1982). Here, as in Abeyeratne and Triantafyllidis (1981), the perturbation analysis is within the context of the full set of finite strain field equations. To provide a direct comparison with previous bifurcation studies of layered solids, and to simplify the analysis, we assume the layers are rate-independent, nonlinear, hyperelastic solids. This constitutive model, which can be used to represent the total loading moduli at a yield sur-

Contributed by the Applied Mechanics Division for publication in the JOURNAL OF APPLIED MECHANICS.
Discussion on this paper should be addressed to the Editorial Department, ASME, United Engineering Center, 345 East 47th Street, New York, N.Y. 10017, and will be accepted until two months after final publication of the paper itself in the JOURNAL OF APPLIED MECHANICS. Manuscript received by ASME Applied Mechanics Division, March 4, 1985; final revision, September 15, 1986.

Copyright © 1987 by ASME
Downloaded 03 May 2010 to 171.66.16.27. Redistribution subject to ASME license or copyright; see http://www.asme.org/terms/Terms_Use.cfm

face vertex, implies a relatively realistic response to nonproportional stress increments, provided no unloading occurs. Specific calculations will be carried out for power-law materials.

2 Preliminaries

Field quantities will be expressed in terms of a fixed Cartesian coordinate frame x_α. Greek letters ($\alpha, \beta, \gamma, \ldots$) can take on values 1 or 2, and the Einstein summation convention on repeated indices applies. For plane strain, the deformation is described by the displacements u_α (x_1, x_2) of a material particle which resided at the point (x_1, x_2) before the deformation. Useful deformation measures are the deformation gradient $F_{\alpha\beta}$

$$F_{\alpha\beta} \equiv \delta_{\alpha\beta} + u_{\alpha,\beta}$$

the Lagrangian strain tensor

$$\eta_{\alpha\beta} \equiv \frac{1}{2}\left[u_{\alpha,\beta} + u_{\beta,\alpha} + u_{\gamma,\alpha}u_{\gamma,\beta}\right]$$

and the right Cauchy-Green tensor

$$G_{\alpha\beta} \equiv \delta_{\alpha\beta} + 2\eta_{\alpha\beta}$$

where $(\ )_{,\beta}$ denotes differentiation with respect to x_β.

The local intensity of deformation may also be described by the principal stretches λ_1 and λ_2. In terms of λ_1 and λ_2, the two invariants of $G_{\alpha\beta}$ are

$$I_1 = G_{11} + G_{22} = \lambda_1^2 + \lambda_2^2 \text{ and } I_2 = G_{11} + G_{22} = \lambda_1^2\lambda_2^2$$

When the material is incompressible $\lambda_2 = 1/\lambda_1$, and, hence, $I_2 = 1$.

It is convenient to employ the symmetric Kirchhoff stress $\tau_{\alpha\beta}$, which is conjugate to $\eta_{\alpha\beta}$. Here we concentrate on nonlinear, hyperelastic solids, characterized by a strain energy density $W(\eta_{\alpha\beta})$ per unit initial volume. In terms of W, $\tau_{\alpha\beta}$ is given by

$$\tau_{\alpha\beta} = \frac{\partial W}{\partial_{\eta\alpha\beta}}$$

For an incompressible, isotropic, hyperelastic solid, deforming in plane strain, W depends only on the invariant I_1, whence

$$\tau_{\alpha\beta} = 2W'(I_1)\delta_{\alpha\beta} - pG^{-1}_{\alpha\beta} \tag{1}$$

where a prime denotes differentiation with respect to the independent variable, a superscript -1 denotes matrix inverse, and p is the hydrostatic pressure.

Consider a surface that had unit area and a unit normal n_β in the undeformed configuration. $\tau_{\alpha\beta}$ is related to the traction T_α on such a surface by

$$T_\alpha = F_{\alpha\gamma}\tau_{\gamma\beta}n_\beta \tag{2}$$

Mechanical equilibrium in the absence of body forces requires that

$$(F_{\alpha\gamma}\tau_{\gamma\beta})_{,\beta} = 0 \tag{3}$$

We will also employ the Cauchy stress, $\sigma_{\alpha\beta}$, which relates $\bar{T}_\alpha$, the traction vector per unit deformed area, to the unit normal N_β of such a deformed element according to

$$\bar{T}_\alpha = \sigma_{\alpha\beta}N_\beta$$

3 Problem Statement

The development below makes reference to two infinite structures; one, the perfect, layered structure, is shown schematically in Fig. 1(*a*). Alternating layers of two isotropic, hyperelastic solids, labelled A and B, perfectly bonded at their interfaces, are subjected to a uniform in-plane stretch $\lambda_1 = \lambda$ parallel to their interfaces. The assumption of incompressibility implies that the strain is uniform throughout the composite, though certain stress components can be discontinuous across the interfaces. We take the loading normal to the interface to have zero force resultant.

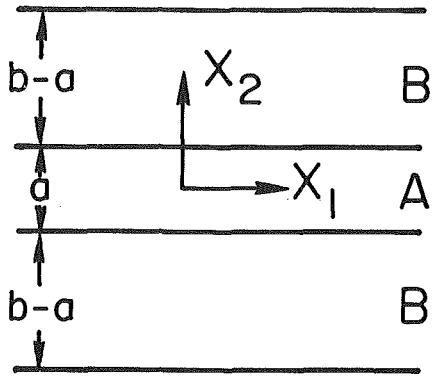


Fig. 1(*a*) Schematic of perfect, layered solid

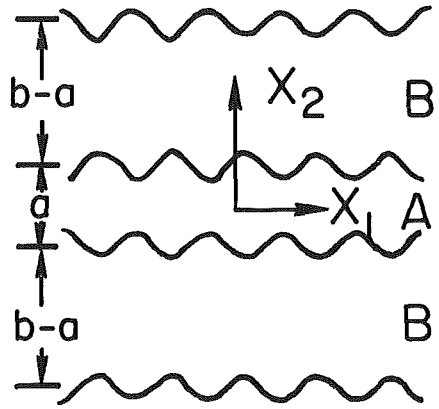


Fig. 1(*b*) Schematic of layered solid with interface undulations

One arrives at the second structure, the perturbed structure, by introducing a periodic waviness in all the interfaces, as shown schematically in Fig. 1(*b*). Consider the A layer in which the coordinate origin is situated. In the perfect structure, the interfaces are located at $x_2 = a/2$; in the perturbed structure the interfaces are located at

$$x_2 = \pm\frac{a}{2}\left[1 + \xi\ \cos\frac{2\pi x_1}{\ell}\right]$$

where ℓ is the wavelength of the perturbation, and ξ is the ratio of the perturbation amplitude to the layer A thickness. The symmetries induced by introducing periodic perturbations in all interfaces are exploited below. To the perturbed structure we apply the same overall loading as was applied to the perfect structure.

A number of features of the solution can be deduced from the periodicity of the perturbed structure. At all layer midplanes, the shear stress is zero and the normal displacement is uniform in x_1. Furthermore, for a given stretch, the displacement u_2 is equal in the perfect and perturbed structures at the layer midplanes. The shear tractions and normal displacements also vanish at the planes $x_1 = \pm n\ell$ ($n = 0, 1, 2, \ldots$).

4 Solution Procedure

We now develop an approximate solution to the above problem by means of a regular perturbation series in the parameter ξ about the perfect structure. In the interest of

Downloaded 03 May 2010 to 171.66.16.27. Redistribution subject to ASME license or copyright; see http://www.asme.org/terms/Terms_Use.cfm

brevity, mathematical details will be kept to a minimum. Extensive use is made of the methods employed in Abeyeratne and Triantafyllidis (1981).

Let quantities with a superscript $\dot{(\ )}$, e.g., $\dot{u_\alpha}$, denote field variables when the perfect structure is subjected to an inplane stretch $\lambda_1 = \lambda$. We assume the field variables in the perturbed structure can be expanded about the perfect structure in powers of ξ, for example

$$u_\alpha = \dot{u_\alpha} + \xi \tilde{u}_\alpha + O(\xi^2) \tag{4a}$$

$$\tau_{\alpha\beta} = \dot{\tau_{\alpha\beta}} + \xi \tilde{\tau}_{\alpha\beta} + O(\xi^2) \tag{4b}$$

where the deformation in the perfect structure is

$$\dot{F_{11}} = \lambda \quad \dot{F_{22}} = \frac{1}{\lambda} \quad \dot{F_{12}} = \dot{F_{21}} = 0$$

One must be careful to give equations (4) the following interpretation. The stresses in the perturbed region A ($0 < x_2 < a/2\,[1 + \xi \cos 2\pi x_1/\ell]$) are taken to be equal to the constant stresses which would prevail in the unperturbed A layers, plus an additional amount $\xi\,\tilde{\tau}_{\alpha\beta}$ which varies spatially. Similar interpretations apply to other quantities in both A and B.

The expansions (4) are substituted into (1) and (3), and only terms of order $O(\xi)$ are retained. Some intermediate steps in this procedure are found in Abeyeratne and Triantafyllidis (1981). Following Abeyeratne and Triantafyllidis (1981), we change from the variables x_1 and x_2 to

$$y_1 = \lambda x_1 \qquad y_2 = \frac{1}{\lambda} x_2$$

With this change, one finds that the incompressibility condition to order $O(\xi)$ implies the existence of a stream function ψ such that

$$\tilde{u}_1 = \psi_{;2} \qquad \tilde{u}_2 = -\psi_{;1}$$

where $(\ )_{;\alpha} \equiv \dfrac{\partial(\ )}{\partial y_\alpha}$.

In terms of the stream function ψ, the equation of equilibrium is found to be

$$\left[\mu + \frac{1}{2}(\dot{\sigma_{11}} - \dot{\sigma_{22}})\right]\psi_{;1111} + [4\mu^* - 2\mu]\psi_{;1122} + \left[\mu - \frac{1}{2}(\dot{\sigma_{11}} - \dot{\sigma_{22}})\right]\psi_{;2222} = 0 \tag{5}$$

where we have made the identifications

$$\dot{\sigma_{11}} - \dot{\sigma_{22}} = 2W'(\dot{I_1})\left(\lambda^2 - \frac{1}{\lambda^2}\right) \qquad \mu = W'(\dot{I_1})\left(\lambda^2 + \frac{1}{\lambda^2}\right)$$

$$u^* = W'(I_1)\cdot\left(\lambda^2 + \frac{1}{\lambda^2}\right) + W''(I_1)\cdot\left(\lambda^2 - \frac{1}{\lambda^2}\right)^2$$

The moduli μ^* and μ relate the Jaumman rigid-body time rates of $\sigma_{11} - \sigma_{22}$ and σ_{12} to the corresponding strain-rates (see Hill and Hutchinson, 1975). Equation (5), as well as the interface tractions derived below, are identical to the equations governing the incremental deformation of a homogeneous block (Hill and Hutchinson, 1975). Henceforth, we will take $\dot{\sigma_{22}} = 0$.

At the interface between A and B, the displacements and tractions must be continuous to order $O(\xi)$. The continuity of the $\dot{u_\alpha}$ implies that the $\tilde{u}_\alpha$ be continuous. In the undeformed configuration, the unit normal to the interface, n_α, has components

$$n_1 = \frac{\pi a}{\ell}\,\xi\,\sin\frac{2\pi x_1}{\ell} \qquad n_2 = 1$$

to order $O(\xi)$. Expanding equation (2) for the tractions T_α one finds

$$\frac{T_1}{\lambda\xi} = \dot{\sigma_{11}}\frac{\pi a}{\lambda^2\ell}\sin\frac{2\pi y_1}{\lambda\ell} + \left(\mu - \frac{1}{2}\dot{\sigma_{11}}\right)[\psi_{;22} - \psi_{;11}] \tag{6a}$$

$$\frac{1}{\xi\lambda}\frac{\partial T_2}{\partial y_1} = -\left[4\mu^* - \mu - \frac{1}{2}\dot{\sigma_{11}}\right]\psi_{;211} - \left[\mu - \frac{1}{2}\dot{\sigma_{11}}\right]\psi_{;222} \tag{6b}$$

where the pressure increment $\tilde{p}$ has been eliminated by differentiation with respect to y_1, a procedure which is valid to order $O(\xi)$. By expanding, to order $O(\xi)$, the normal N_α to the deformed interface, one can readily see that the first term on the right-hand-side of equation (6*a*) represents the shear traction per unit deformed area of interface induced by the stress $\dot{\sigma_{11}}$.

In both A and B, we look for solutions of the form $\psi = f(y_2)\sin 2\pi y_1/\lambda\ell$, insuring the proper periodicity in y_1. Symmetry conditions at $y_2 = 0$ and $b/2\lambda$ are automatically satisfied by functions $f(y_2)$ of the form

$$f_A(y_2) = \mathrm{Re}\left[c\,\sin\frac{2\lambda}{\lambda\ell}\,\alpha y_2\right] \qquad \text{in } A$$

$$f_B(y_2) = \mathrm{Re}\left[d\,\sin\frac{2\pi}{\lambda\ell}\,\beta\left(\frac{b}{2\lambda} - y_2\right)\right] \qquad \text{in } B$$

where c, d, α, and β are, in general, complex constants, and Re [ ] denotes the real part of the enclosed quantity. (Henceforth, α and β will not function as subscripts to indicate Cartesian components). Substituting the assumed forms for ψ into the equilibrium equation (5) for A and B, one finds that α and β satisfy

$$\alpha^2 = \frac{R_A - 1 \pm i\sqrt{2R_A - 1 - S_A^2}}{R_A - S_A} \qquad \beta^2 = \frac{R_B - 1 \pm i\sqrt{2R_B - 1 - S_B^2}}{R_B - S_B}$$

where $R = \dfrac{\mu}{2\mu^*}$ and $S = \dfrac{\dot{\sigma_{11}}}{4\mu^*}$ in each of A and B.

As discussed by Hill and Hutchinson (1975), the incremental field equations are elliptic, hyperbolic, or parabolic according to the values of R and S. Here we concentrate on the elliptic regime in which $R > 1$ and $S < \sqrt{2R - 1}$. In this regime, α and β are complex-valued and can be taken to lie in the first quadrant. If we define the real and imaginary parts $\alpha \equiv p_A + ir_A$ and $\beta \equiv p_B + ir_B$, then

$$p^2 + r^2 = \sqrt{\frac{R+S}{R-S}} \qquad p^2 - r^2 = \frac{R-1}{R-S}$$

holds for both A and B.

The constants c and d are determined by enforcing the displacement and traction continuity conditions. Since we are retaining only terms of order $O(\xi)$, and since the deformation associated with ψ is already of order $O(\xi)$, the continuity conditions must be evaluated at the unperturbed interface $y_2 = a/2\lambda$. Thus, we may interpret the two terms in the traction T_1 (equation (6*a*)) as due to, respectively, the unperturbed stress evaluated at the perturbed boundary, and the perturbation in the stress field evaluated at the unperturbed boundary. Evaluating the continuity conditions, one finds

$$\mathrm{Re}[c\sin\alpha q_A] = \mathrm{Re}[d\sin\beta q_B] \tag{7a}$$

$$\mathrm{Re}[c\alpha\cos\alpha q_A] = -\mathrm{Re}[d\beta\cos\beta q_B] \tag{7b}$$

$$\mathrm{Re}\{c[(R_A - S_A)\alpha^2 - (R_A + S_A - 2)]\alpha\cos\alpha q_A\} = \eta\,\mathrm{Re}\{d[-(R_B - S_B)\beta^2 + (R_B + S_B - 2)]\beta\cos\beta\, q_B\} \tag{7c}$$

$$\frac{1}{S_A}\{\mathrm{Re}[c(R_A - S_A)(1 - \alpha^2)\sin\alpha q_A] - \eta\,\mathrm{Re}[d(R_B - S_B)(1 - \beta^2)\sin\beta q_B]\} = \frac{1}{2\pi}\left[\eta\,\frac{S_B}{S_A} - 1\right] \tag{7d}$$

where $\eta = \mu_B^*/\mu_A^*$, $q_A = \dfrac{\pi a}{\lambda^2\ell}$ and $q_B = \dfrac{\pi}{\lambda^2\ell}\,[b - a]$.

Downloaded 03 May 2010 to 171.66.16.27. Redistribution subject to ASME license or copyright; see http://www.asme.org/terms/Terms_Use.cfm

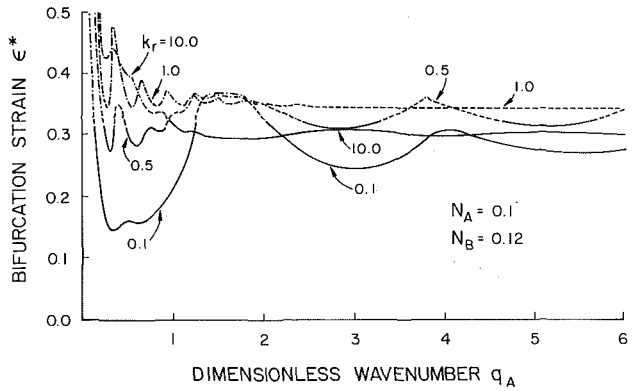


Fig. 2 Bifurcation strain as a function of wavenumber for a case of similar hardening rates. N_A = 0.1; N_B = 0.12; $(b-a)/a$ = 7.0; (——) A and B elliptic; (----) A hyperbolic, B elliptic; (-•-•) A and B hyperbolic.

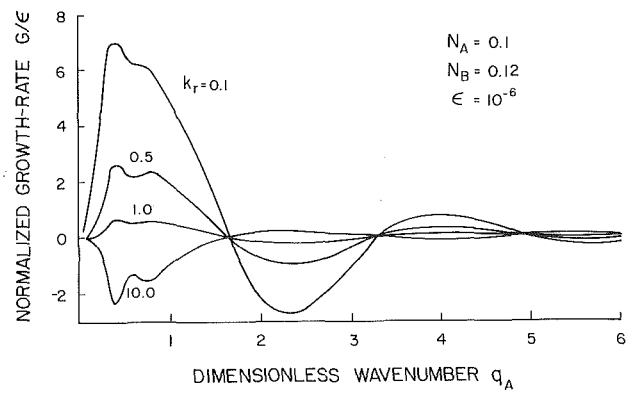


Fig. 3 Normalized growth-rate as a function of wavenumber for a case of similar hardening rates. N_A = 0.1; N_B = 0.12; $(b-a)/a$ = 7.0; ϵ = 10^{-6}.

As expected, equations (7), except for the inhomogeneous terms in (7*d*), are identical to the bifurcation equations governing the emergence of interface ripples in a perfect, layered structure (Steif, 1986b). Recall that the dimensions a and b are as measured before straining begins. Thus, the dimensionless wavenumbers q_A and q_B are the ratios of the respective layer thicknesses to the imperfection wavelength, as measured subsequent to the stretch λ. Bifurcation analyses relevant to the present work typically take the current configuration (at the instant of bifurcation) to be the reference state. Thus, direct comparisons between the present work and bifurcation studies of layered solids should be made on the basis of the q_A and q_B as defined above.

The complex constants c and d can be determined from equations (7) by separating into real and imaginary parts. One can go on to calculate displacements and stresses. Of particular interest here is whether the nonuniformity becomes more or less *severe* with overall straining. Let a_m be the maximum thickness of the perturbed A layer (measured at the crest of the ripples), and let a_p be the thickness of the A layer in a perfect structure, both measured at the same level of overall stretching. Then, we define the relative nonuniformity, t, to be

$$t=\frac{a_m-a_p}{a_p}$$

With t_u and t_d denoting, respectively, the values of the relative nonuniformity in the undeformed and deformed states, we define the relative increase, G, of this nonuniformity measure to be

$$G\equiv\frac{t_d-t_u}{t_u}=\frac{2\lambda}{a}\frac{\tilde{u}(y_2=a/2\lambda)}{\cos\dfrac{2\pi y_1}{\lambda\ell}}$$

$$=-4\pi\ \mathrm{Re}\left[\frac{c}{a\ell}\sin\alpha q_A\right]$$

Henceforth, G will be referred to as the growth-rate, even though the deformations are time dependent.

5 Results

Calculations of G have been carried out taking materials A and B to be nonlinear, hyperelastic solids which, in plane strain, have a true stress-logarithmic strain curve

$$\sigma=k\epsilon^N$$

where $\epsilon \equiv 1n\,\lambda$. In general, k and N are different in A and B, though the only independent parameters are N_A, N_B, and $k_r \equiv k_B/k_A$. With such a constitutive law,

$$S=\frac{\epsilon}{N}\quad\text{and}\quad R=\frac{\epsilon}{N}\coth(2\epsilon)$$

and, thus, the equations remain elliptic provided

$$\frac{2\epsilon}{N}\coth(2\epsilon)-1-\frac{\epsilon^2}{N^2}>0$$

When the strain is small, i.e., when it satisfies the conditions $\epsilon << 1$ and $\epsilon << N$, one can show that

$$\alpha^2=1-2N\pm i\,2N\sqrt{\frac{1}{N}-1}$$

and, thus, α^2 is equal to the parameter ξ^2 in Hutchinson et al. (1978). (Their stress exponent n is the reciprocal of our hardening rate N.) In fact, when $k_r = 0$, and the strain is small (as specified above), the entire small imperfection analysis of Hutchinson et al. (1978) is recovered, except now the material is interpreted as a small strain, power-law, elastic solid. In the small strain limit, our growth-rate G is identical to their parameter $\dot{a}/a$.

Bifurcation studies of layered solids (Steif, 1986a; Steif, 1986b) revealed a number of trends insofar as the dependence of the necking-mode bifurcation strain on material properties. Generally, if one layer is dominant (we say A is dominant if $k_r << 1$), then the first bifurcation mode of the composite tends to be dictated by the behavior of the dominant layer when it stands alone. That is, if an elliptic-regime necking mode is possible at that wavelength for the dominant layer alone, then the layered structure exhibited a similar mode while the dominant layer was still elliptic. The other layer is in the elliptic or hyperbolic regime depending on the hardening rate of that layer. On the other extreme, if the materials are identical, no internal necking mode is possible while in the elliptic regime. The overall trend is for similar hardening rates and dissimilar stiffnesses to promote elliptic-elliptic necking modes.

The results of the present analysis complement these trends. In Fig. 2 the bifurcation strain is plotted as a function of wavenumber for a case of similar hardening rates: $N_A = 0.1$ and $N_B = 0.12$. Now, we contemplate applying a small strain, $\epsilon = 10^{-6}$, to each of the layered solids represented in Fig. 2, except with undulations introduced at the interfaces. The resulting growth-rates, normalized by the strain ϵ, are plotted in Fig. 3 as a function of wavenumber q_A. It was found that virtually identical curves were found when ϵ was taken smaller than 10^{-6}; that is, $\epsilon = 10^{-6}$ essentially gives the small strain response.

Consider the curves in Figs. 2 and 3 corresponding to $k_r = 0.1$. Clearly, undulations which would appear first in a perfect, layered solid exhibit the highest growth-rate, even at this very low level of straining. It was consistently found that an elliptic-elliptic necking bifurcation signals that imperfec-

Downloaded 03 May 2010 to 171.66.16.27. Redistribution subject to ASME license or copyright; see http://www.asme.org/terms/Terms_Use.cfm

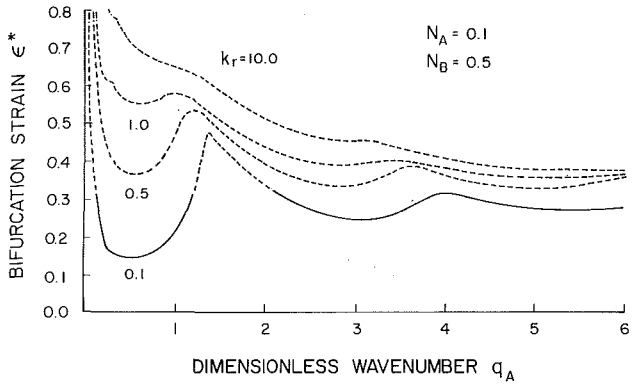


Fig. 4 Bifurcation strain as a function of wavenumber for a case of dissimilar hardening rates. $N_A = 0.1$; $N_B = 0.5$; $(b-a)/a = 7.0$; (——) A and B elliptic; (----) A hyperbolic; B elliptic; (-·-·-) A and B hyperbolic.

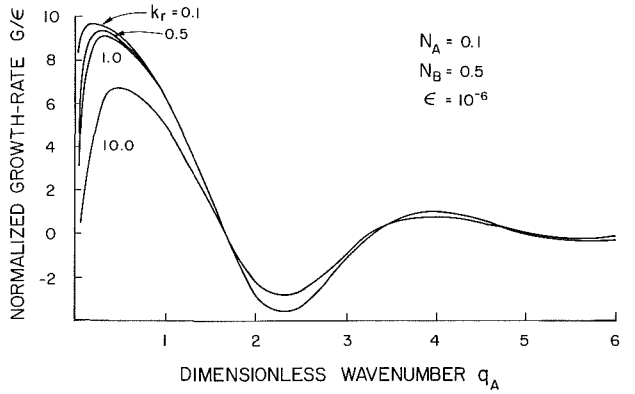


Fig. 5 Normalized growth-rate as a function of wavenumber for a case of dissimilar hardening rates. $N_A = 0.1$; $N_B = 0.5$; $(b-a)/a = 70$; $\epsilon = 10^{-6}$.

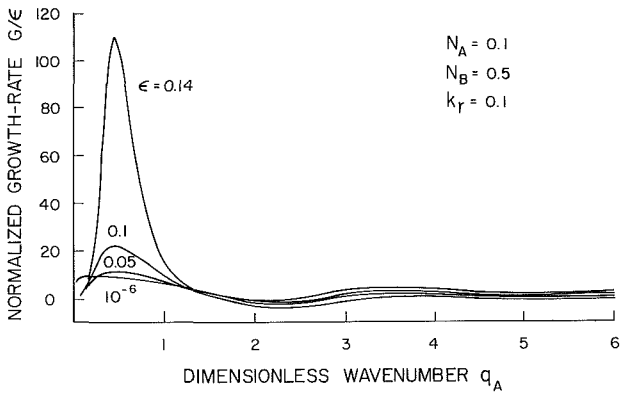


Fig. 6 Normalized growth-rate as a function of wavenumber showing increase in the growth-rate with increasing strain as an elliptic regime bifurcation is approached. $N_A = 0.1$; $N_B = 0.5$; $k_r = 0.1$; $(b-a)/a = 7.0$.

tions of similar wavelength will grow even at the very beginning of straining. This is similar to the initial response of imperfect structures to loads which would induce buckling. As k_r is increased to 0.5 and to 1.0, the necking bifurcation occurs at increasing strain for a given q_A and, eventually, no undulations appear in the elliptic regime. As can be seen from the growth-rate curves of Fig. 3, diminishing or negative growth-rates are associated with nonelliptic necking modes. When $k_r = 10.0$, layer B is dominant, and it will exhibit necking bifurcations in the elliptic regime. The peak growth-rate when B dominates (occurring near $q_A = 2.5$) is less than that when A dominates. It was previously observed (Steif, 1986b) that a relatively thin dominant layer exhibits a lower bifurcation

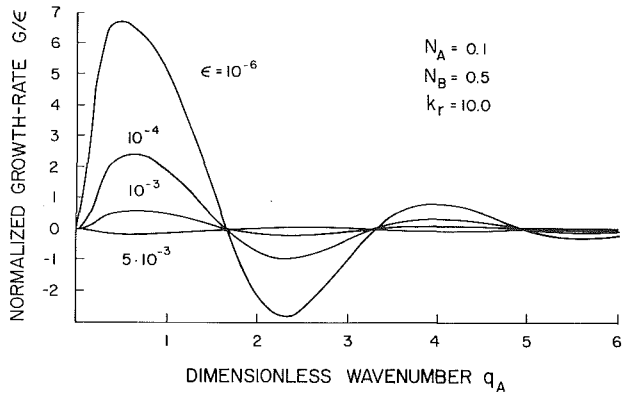


Fig. 7 Normalized growth-rate as a function of wavenumber showing a decrease in the growth-rate with increasing strain when no bifurcation occurs in the elliptic regime. $N_A = 0.1$; $N_B = 0.5$; $k_r = 10.0$; $(b-a)/a = 7.0$.

strain than a relatively thick dominant layer. The analogous observation here has the interpretation that as the less stiff layer diminishes in thickness, higher average transverse strains are required in that layer to achieve a given imperfection growth-rate.

We turn now to a case of dissimilar hardening rates to study further the growth of imperfections having the same wavelength as hyperbolic-regime necking modes. The bifurcation results are shown in Fig. 4 for the case in which $N_A = 0.1$ and $N_B = 0.5$. When A is dominant, the rectangular block bifurcations emerge (except for very long wavelengths). However, when B is dominant ($k_r = 10.0$), layer A goes hyperbolic before interface undulations can appear. The normalized growth-rates of interface imperfections for the same set of layered solids at small strains are plotted in Fig. 5. Undulations grow at nearly the same rate for all values of k_r shown. At this point it appears that some hyperbolic modes can be stimulated to grow from imperfections as readily as elliptic modes.

This tentative conclusion is explored more deeply by considering the effect of further straining. Hence, the case of $k_r = 0.1$ is reconsidered in Fig. 6 for several values of applied strain. Obviously, the growth-rate increases with straining. Because equations (7) are singular at an elliptic regime bifurcation, the growth-rate becomes arbitrarily large as the bifurcation strain is approached. Clearly, the expansions are not uniformly valid as one approaches the bifurcation strain. On the other hand, for the case of $k_r = 10.0$, plotted in Fig. 7, the imperfections begin to decay by the time the strain reaches 0.5 percent. Even at relatively small strains, the geometric and material nonlinearities have a substantial effect. Of course, one would expect that as the strain approached the bifurcation strain, the appropriate imperfection would grow rapidly. The evidence supplied by the present linear analysis is reminiscent of the observation (e.g., Abeyeratne and Triantafyllidis, 1981) that shear bands only grow significantly at loads very close to the ellipticity limit. Regarding the reliability of this conclusion, we note that the first order perturbation analysis remains valid at finite strains provided that the amplitude of the perturbation remains small compared with the layer thicknesses. In some cases, however, this restriction may mean in effect that the linear analysis is valid only for strains which are small compared with the bifurcation strain.

We note the fact, of some physical significance, that no matter what the properties of materials A and B, the imperfection growth-rate approaches zero as the wavelength becomes long compared with the layer thicknesses (provided neither k_A nor k_B is zero). Analogously, one finds no infinite wavelength undulation bifurcation. This long wavelength behavior has the remarkable consequence that there is a finite wavelength that

Downloaded 03 May 2010 to 171.66.16.27. Redistribution subject to ASME license or copyright; see http://www.asme.org/terms/Terms_Use.cfm

grows more rapidly than all others. That the imperfection growth-rate *must* be zero for incompressible layers can be seen from the following argument.

Consider the incremental deformation in the vicinity of, say, $(x_1, x_2) = (0, a/2\,(1+\xi))$. The tangential strain $\tilde{u}_{1;1}$ must be continuous across the interface; hence, by incompressibility, the normal strain $\tilde{u}_{2;2}$ is continuous. Say $\tilde{u}_{1;1}$ is positive, $\tilde{u}_{2;2}$ is, thus, negative. Furthermore, say that the imperfection is to grow, i.e., $\tilde{u}_2 > 0$. (These assumptions are immaterial to the argument.) Since $\tilde{u}_2 = 0$ at $y_2 = 0$ and $b/2\lambda$, this requires that $\tilde{u}_{2;2}$ change sign (become positive) somewhere in A ($0 < y_2 < a/2\lambda$). Now, one expects all incremental field quantities to decay as one moves away from the interface on a length of order λ. Thus, for λ/a sufficiently large, the incremental field quantities cannot change much over the thickness of A and, surely, cannot change sign. This precludes the growth or decay of interface imperfections when the wavelength is very long compared with the layer thickness.

6 Conclusions

Results from the linear analysis performed here indicate that there are significant connections between the emergence of interface undulation bifurcations and the growth of undulatory interface imperfections. If undulation bifurcations appear while both layers are still elliptic, then, roughly, the wavelengths for which bifurcation occurs first show the highest growth-rates, even at infinitesimal strains. Furthermore, the growth-rate of those wavelengths increases with strain. When bifurcations of a given wavelength do not emerge until one or both materials has entered the hyperbolic regime, imperfections of the same wavelength usually decay, either at infinitesimal strains or at relatively small strains. This suggests that shear bands in pearlite are only in competition with necking modes which involve both materials being in the elliptic regime. Because of the kinematic restrictions implied by incompressibility, imperfections of very long wavelength cannot grow: one particular wavelength must then grow faster than all others. When the stiff layer is relatively narrow, this wavelength is on the order of five to ten times the thickness of the stiff layer. Such a mode appears to be consistent with observations of carbide necking modes in fine pearlites.

While the mechanical properties of the constituent carbide and ferrite in pearlite have not been measured directly, the following scenario appears possible. The carbide layer is the dominant (harder) layer, and it is narrow compared with the ferrite. Also, carbide has the higher hardening rate. In fine pearlites, the hardening rate of the ferrite is sufficiently high to permit a necking mode to emerge while both materials are elliptic. However, the hardening rate of the ferrite in coarse pearlites is low enough that no elliptic bifurcation is possible, and shear bands initiate failure instead.

Acknowledgment

This work has been supported by the Association of American Railroads through the Affiliated Laboratory at Carnegie-Mellon University, and by the Department of Mechanical Engineering, Carnegie-Mellon University.

References

Abeyeratne, R., and Triantafyllidis, N., 1981, "The Emergence of Shear Bands in Plane Strain," *International Journal of Solids Structures*, Vol. 17, pp. 1113–1134.

Alexander, D. J., and Bernstein, I. M., 1984, "Microstructural Control of Flow and Fracture in Pearlitic Steels," in *Phase Transformations in Ferrous Alloys*, Marder, A. R., and Goldstein, J., eds., TMS, Warrendale, Pennsylvania, pp. 243–257.

Anand, L., and Spitzig, W. A., 1980, "Initiation of Localized Shear Bands in Plane Strain," *J. Mech. Phys. Solids*, Vol. 28, pp. 113–128.

Hill, R., and Hutchinson, J. W., 1975, "Bifurcation Phenomena in the Plane Tension Test," *J. Mech. Phys. Solids*, Vol. 23, pp. 239–264.

Hutchinson, J. W., Neale, K. W., and Needleman, A., 1978, "Sheet Necking – I. Validity of Plane Stress Assumptions of the Long-Wavelength Approximation," in *Mechanics of Sheet Metal Forming*, Koistinen, D. P., and Wang, N.-M., eds., Plenum Publishing Corporation, pp. 111–126.

Hutchinson, J. W., and Obrecht, H., 1977, "Tensile Instabilities in Strain-Rate Dependence Materials," *Fracture 1977*, ICF4, Taplin, D. M. R., ed., Vol. 1, pp. 101–116.

Koiter, W. T., 1945, "On the Stability of Elastic Equilibrium," in Dutch, Thesis, Delft, H. J. Paris, Amsterdam.

Needleman, A., and Tvergaard, V., 1982, "Aspects of Plastic Postbuckling Behavior," in *Mechanics of Solids, The Rodney Hill 60th Anniversary Volume*, Hopkins, H. G., and Sewell, M. J., eds., Pergamon Press, Oxford, pp. 453–498.

Steif, P. S., 1986a, "Bimaterial Interface Instabilities in Plastic Solids," *International Journal Solids Structures*, Vol. 22, pp. 195–207.

Steif, P. S., 1986b, "Periodic Necking Instabilities in Layered Plastic Composites," *International Journal Solids Structures*, to be published.

Tvergaard, T., 1982, "Influence of Void Nucleation on Ductile Shear Fracture at a Free Surface," *J. Mech. Phys. Solids*, Vol. 30, pp. 399–425.

Tvergaard, V., Needleman, A., and Lo, K. K., 1981, "Flow Localization in the Plane Strain Tensile Test," *J. Mech. Phys. Solids*, Vol. 29, pp. 115–141.

Downloaded 03 May 2010 to 171.66.16.27. Redistribution subject to ASME license or copyright; see http://www.asme.org/terms/Terms_Use.cfm

The Reverse Spaghetti Problem: Drooping Motion of an Elastica Issuing from a Horizontal Guide[1]

L. Mansfield

J. G. Simmonds

Department of Applied Mathematics,
University of Virginia,
Charlottesville, VA 22901

The nonlinear equations of motion of an elastica that moves out of a horizontal guide at a constant velocity are expressed in terms a dimensionless weight-to-stiffness ratio and a dimensionless velocity. The equations are written in horizontal-vertical directions rather than tangential-normal directions to minimize algebraic complexities. The introduction of deformation potentials allows each of the linear momentum equations to be integrated once. This simplifies the remaining equations. A series solution of the equations, useful for small motions—and perhaps useful for design—is given. To facilitate numerical solution, the triangular space-time domain of the problem is transformed into a square domain in pseudo space-time. Finally, some solutions based on the finite element method are presented for typical values of the dimensionless weight-to-stiffness and velocity parameters.

Introduction

"The spaghetti problem," named and solved by Carrier (1949), is to determine the motion of a dangling, inextensible *string* being drawn upward through a hole in a rigid wall. If the string has an initial transverse motion, the associated kinetic energy, in the linear theory employed by Carrier, does not change, so as the string moves into the hole, its kinetic energy is squeezed into an ever shrinking piece. On reaching the hole, the tail of the string must therefore have infinite transverse velocity. This explains why ingesting spaghetti improperly inevitably leads to a spot of tomato sauce on one's blouse or tie.

The reverse spaghetti problem is to find out what happens when one spits out a piece of hot spaghetti which, if undercooked, is not totally limp. Remarkably, the same analysis applies to a sheet of paper issuing from a rigid horizontal guide into a uniform gravitational field. Of particular interest to designers of copying machines are the end-orbits of the paper.

In what follows, we model the paper as an elastica, compute these orbits, and show that they depend on two parameters only, namely

$$\mu \equiv mgL^3/B \text{ and } \nu \equiv VL\sqrt{m/B}, \tag{1}$$

a dimensionless weight-to-stiffness ratio and a dimensionless velocity, respectively. In (1), m is the mass per unit area of the paper, g is the acceleration of gravity, L is the length of the paper, B is its bending stiffness, and V is the constant velocity at which the paper is assumed to issue from the guide (see Fig. 1). The easiest way to determine μ is to make static measurements with a ruler on a drooping piece of paper. Doing so, we found that $\mu \approx 50$ for paper used in ditto and copying machines. Typical values of ν range from 0 to 10.

There are two novel features in the analysis. First, by the introduction of deformation potentials, we are able to express the equations of motion in simplified forms that reduce, if the velocity is zero, to the static equations for a uniformly loaded elastica first studied by Hummel & Morton (1927). Second, by a nonlinear change of independent variables, a problem with a moving boundary and initial conditions at a point is recast as an initial/boundary value problem on a "canonical" square.

The Governing Equations

In Fig. 1, let $(\bar{X}, \bar{Y})$ denote the Cartesian coordinates of a particle at time T on the centerline of the elastica that initially had coordinates $(X, 0)$. If $0 < X < L - VT$, i.e., in the guide,

$$\bar{X} = X + VT, \ \bar{Y} = 0 \tag{2}$$

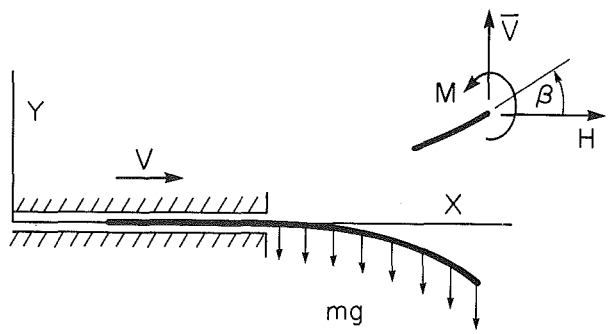


Fig. 1 Geometry, loading, and stress conventions

[1]The portion of this work dealing with paper was sponsored by the Xerox corporation.

Contributed by the Applied Mechanics Division for publication in the JOURNAL OF APPLIED MECHANICS.

Discussion on this paper should be addressed to the Editorial Department, ASME, United Engineering Center, 345 East 47th Street, New York, N.Y. 10017, and will be accepted until two months after final publication of the paper itself in the JOURNAL OF APPLIED MECHANICS. Manuscript received by ASME Applied Mechanics Division, December 11, 1985; final revision May 7, 1986.

Copyright © 1987 by ASME
Downloaded 03 May 2010 to 171.66.16.27. Redistribution subject to ASME license or copyright; see http://www.asme.org/terms/Terms_Use.cfm

whereas if $L-VT<X<L$, i.e., outside the guide, we have the equations of motion

$$H_X = m\bar{X}_{TT},\ \bar{V}_X - mg = m\bar{Y}_{TT} \tag{3}$$

$$M_X + \bar{V}\cos\beta - H\sin\beta = 0, \tag{4}$$

where we have neglected rotary inertia and denoted partial differentiation by a subscript. As indicated in Fig. 1, H, $\bar{V}$, and M denote, respectively, the horizontal and vertical forces and moment that the material to the right of a particle initially at $(X, 0)$ exerts on the material to the left and β is the angle the tangent to the deformed centerline makes with the X axis.

As constitutive relations, we assume the conventional moment-curvature relation

$$M = B\beta_X \tag{5}$$

plus *inextensionality* which implies that

$$\bar{X}_X = \cos\beta,\ \bar{Y}_X = \sin\beta. \tag{6}$$

The above equations, save for the gravity term in equations (3), may be found in Section 6 of Keller and Ting (1966). Noting that $\bar{X} = VT$ and $\bar{Y} = 0$ at the end of the guide, we may replace equations (6) by the integrated relations

$$\bar{X}(X,T) = VT + \int_{L-VT}^{X} \cos\beta(\xi,T)\,d\xi,$$

$$\bar{Y}(X,T) = \int_{L-VT}^{X} \sin\beta(\xi,T)\,d\xi. \tag{7}$$

Reduction of the Governing Equations

In static problems, each of the equations (3) can be integrated and the result, along with equation (5), substituted into equation (4) to yield an equation for β alone. To effect the analogous reduction in dynamic problems we introduce the *deformation potentials*

$$P(X,T) \equiv \int_L^X \bar{X}(\xi,T)\,d\xi,\ Q(X,T) \equiv \int_L^X \bar{Y}(\xi,t)\,d\xi. \tag{8}$$

Because the right end of the elastica is free, equations (3) can be integrated to yield

$$H = mP_{TT},\ \bar{V} = m[g(X-L) + Q_{TT}]. \tag{9}$$

Substituting these relations along with equation (5) into equation (4), we have

$$B\beta_{XX} - mg(L-X)\cos\beta = m(P_{TT}\sin\beta - Q_{TT}\cos\beta). \tag{10}$$

This equation along with

$$P_{XX} = \cos\beta,\ Q_{XX} = \sin\beta \tag{11}$$

which follow from equations (6) and (8) constitute the governing field equations outside the guide. They are to be solved subject to the boundary conditions that at the wall the velocity is horizontal and the slope is zero while at the free end the bending moment is zero. Expressed in terms of the basic field variables β, P, and Q, these boundary conditions read

$$\text{at } X = L - VT, \beta = Q_X = 0,\ P_x = L;\ \text{at } X = L, \beta_X = P = Q = 0. \tag{12}$$

Because all of the elastica is initially in the guide, the initial conditions apply at merely one point, $(L, 0)$, and may be viewed as requiring that conditions at the end of the guide $(X = L - VT)$ match those at the free end $(X = L)$ as $T \to 0$.

Nondimensionalization

Let

$$P \equiv L^2 P,\ Q \equiv L^2 q \tag{13}$$

$$X \equiv Lx \equiv L(1-s),\ T \equiv (L/V)t \tag{14}$$

Substituting these expression into equations (10) and (11) and recalling the dimensionless weight-to-stiffness ratio μ and the dimensionless velocity ν defined in (1), we obtain the dimensionless field equations

$$\beta_{ss} - \mu s\cos\beta = \nu^2(p_{tt}\sin\beta - q_{tt}\cos\beta) \tag{15}$$

$$p_{ss} = \cos\beta,\ q_{ss} = \sin\beta. \tag{16}$$

These are to be solved on the triangular domain $0<s<t$, $0<t<1$ subject to the boundary conditions

$$\beta_s(0,t) = p(0,t) = q(0,t) = 0,\ \beta(t,t) = q_s(t,t) = 0,$$

$$p_s(t,t) = -1. \tag{17}$$

It follows from equations (8), (13), and (14) that, *relative to the end of the guide*, the dimensionless Cartesian coordinates of the end of the elastica are given by

$$\bar{x}_e \equiv (\bar{X}(L,T) - L)/L = -p_s(0,t) - 1,$$

$$\bar{y}_e \equiv \bar{Y}(L,T)/L = -q_s(0,t). \tag{18}$$

Series Solutions

By direct computation, we find that the initial/boundary value problem (15)–(18) has a formal series solution in powers of s and t of the form

$$\beta = \frac{1}{6}\mu(s^3 - t^3) + \frac{\mu\nu^2}{24}(s^4 t - 6s^3 t^2 + 5t^5)$$

$$+ \frac{\mu\nu^4}{5040}(3s^7 - 875s^4 t^3 + 3885s^3 t^4 - 3013t^7) + \ldots \tag{19}$$

$$p = -s + \frac{s^2}{2} - st - \frac{\mu^2}{20160}(5s^8 - 28s^5 t^3$$

$$+ 140s^2 t^6 - 180st^7) + \ldots \tag{20}$$

$$q = \frac{\mu}{120}(s^5 - 10s^2 t^3 + 15st^4) + \frac{\mu\nu^2}{720}(s^6 t - 9s^5 t^2$$

$$+ 75s^2 t^5 - 111st^6) + \ldots \tag{21}$$

$$\bar{x}_e = t\left(1 - \frac{\mu^2 t^6}{112} + \ldots\right) \tag{22}$$

$$\bar{y}_e = -\frac{\mu t^4}{8}\left(1 - \frac{37\nu^2 t^2}{30} + \ldots\right). \tag{23}$$

In copying machines, paper is cantileverd only for relatively short distances and excessive drooping is avoided. Thus, the above series may be useful for design work. In any event, they provide a useful check on the numerical calculations to be described next.

Transformation of the Initial/Boundary Value Problem

As we have noted, the initial conditions in the above formulation occur at a *point* in the st plane. This is awkward for numerical work where it is preferable to have the initial conditions on a *line* and to work with a rectangular solution domain rather than with a triangular one. This motivates the change of variables

$$s = \sigma\tau,\ t = \tau,\ 0 \le \sigma, \tau \le 1 \tag{24}$$

that maps the triangular region in Fig. 2(*a*) onto the square in Fig. 2(*b*). It is useful to think of σ as a "pseudo" distance and τ as a "pseudo" time. By the chain rule

$$f_\sigma = f_s\tau,\ f_\tau = f_s\sigma + f_t; \tag{25}$$

hence

Downloaded 03 May 2010 to 171.66.16.27. Redistribution subject to ASME license or copyright; see http://www.asme.org/terms/Terms_Use.cfm

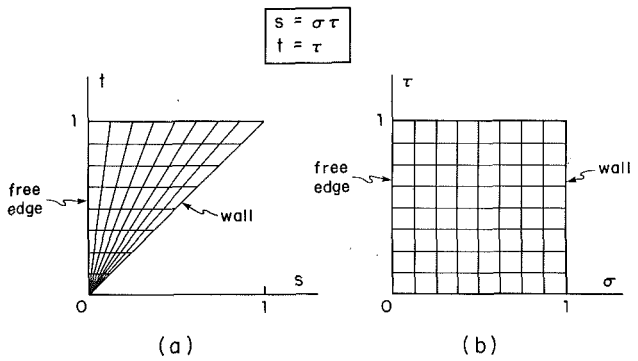


Fig. 2 Transformation from real to pseudo space-time variables

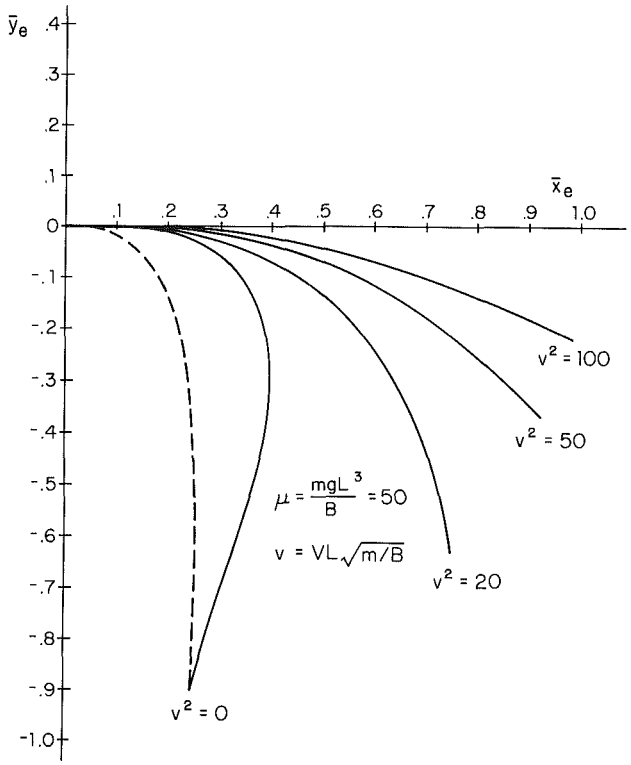


Fig. 3 End-orbits for a fixed weight-to-stiffness ratio and various dimensionless velocities

$$f_s = \tau^{-1} f_\sigma, f_t = f_\tau - (\sigma/\tau) f_\sigma. \tag{26}$$

Repeated application of equations (25) and (26) yields

$$f_{ss} = \tau^{-2} f_{\sigma\sigma} \tag{27}$$

$$f_{st} = -\tau^{-2} f_\sigma + \tau^{-1} f_{\sigma\tau} - \sigma\tau^{-2} f_{\sigma\sigma} \tag{28}$$

$$f_{tt} = f_{\tau\tau} + 2\sigma\tau^{-2} f_\sigma - 2\sigma\tau^{-1} f_{\sigma\tau} + \sigma^2\tau^{-2} f_{\sigma\sigma}. \tag{29}$$

With the above, the dimensionless equations of motion (15) and (16) take the form

$$\beta_{\sigma\sigma} - \mu\sigma\tau^3\cos\beta = \nu^2[(\tau^2 p_{\tau\tau} - 2\sigma\tau p_{\sigma\tau} + 2\sigma p_\sigma)\sin\beta - (\tau^2 q_{\tau\tau} - 2\sigma\tau q_{\sigma\tau} + 2\sigma q_\sigma)\cos\beta]. \tag{30}$$

$$p_{\sigma\sigma} = \tau^2\cos\beta,\ q_{\sigma\sigma} = \tau^2\sin\beta. \tag{31}$$

The initial and boundary conditions are, from equations (17), (25), and (26),

$$\text{at } \tau = 0: p = q = q_\tau = \beta = \beta_\tau = 0,\ p_\tau = -\sigma \tag{32}$$

$$\text{at } \sigma = 0: p = q = \beta_\sigma = 0;\ \text{at } \sigma = 1: p_\sigma = -\tau,\ q_\sigma = \beta = 0. \tag{33}$$

Numerical Solution

As several of the boundary conditions in equations (33) are imposed on derivatives rather than on values of the unknows themselves, derivatives in σ were discretized using the finite element method. In the finite element method, derivative boundary conditions are natural and therefore need not be explicitly enforced. A grid is introduced on [0, 1] and at each (pseudo) time step $\tau = \tau^n - n$ is an index, not a power-approximations are sought of the form

$$\beta^h(\sigma) = \sum_{i=1}^{N} \beta_i^n \phi_{1,i}(\sigma),\ p^h(\sigma) = \sum_{i=1}^{N} p_i^n \phi_{2,i}(\sigma),$$

$$q^h(\sigma) = \sum_{i=1}^{N} q_i{}^n \phi_{3,i}, \tag{34}$$

where the $\phi_{j,i}$ are piecewise linear polynomials which satisfy $\phi_{1,i}(1) = \phi_{2,i}(0) = \phi_{3,i}(0) = 0$. The time derivatives are discretized using backward differences. This leads to the nonlinear algebraic system

$$\begin{aligned}
&(\Delta\tau)^2 \int_0^1 \sum_{j=1}^{N} \beta_j^{n+1} \phi'_{1,j}(\sigma)\phi'_{1,i}(\sigma) \\
&+ \mu(\tau+\Delta\tau)^3 \sigma\cos\Big(\sum_{j=1}^{N} \beta_j^{n+1}\phi_{1,j}(\sigma)\Big)\phi_{1,i}(\sigma)d\sigma \\
&+ \nu^2\Big[\int_0^1 \Big\{(\tau+\Delta\tau)^2 \sum_{j=1}^{N} (p_j^{n+1} - p_j^n)\phi_{2,j}(\sigma) \\
&- \sum_{j=1}^{N} (p_j^n - p_j^{n-1})\phi_{2,j}(\sigma)\Big\}\phi_{1,i}(\sigma)d\sigma \\
&+ \int_0^1 \Big\{-2\Delta\tau\sigma(\tau+\Delta\tau)\sum_{j=1}^{N}(p_j^{n+1} - p_j^n)\phi'_{2j}(\sigma) \\
&+ 2(\Delta\tau)^2\sigma\sum_{j=1}^{N} p_j^{n+1}\phi'_{2,j}(\sigma)\Big\}\phi_{1,i}(\sigma)d\sigma \\
&- \int_0^1 \Big\{(t+\Delta\tau)^2 \sum_{j=1}^{N}(q_j^{n+1} - q_j^n)\phi'_{3,j}(\sigma) \\
&- \sum_{j=1}^{N}(q_j^n - q_j^{n-1})\phi_{3,j}(\sigma)\Big\}\phi_{1,i}(\sigma)d\sigma \\
&- \int_0^1 \Big\{-2\Delta\tau\sigma(\tau+\Delta\tau)\sum_{j=1}^{N}(q_j^{n+1} - q_j^n)\phi'_{3,j} \\
&+ 2(\Delta\tau)^2\sigma\sum_{j=1}^{N} q_j^{n+1}\phi'_{3,j}(\sigma)\Big\}\phi_{1,i}(\sigma)d\sigma\Big] = 0,
\end{aligned} \tag{35}$$

$i = 1, \ldots, N$

$$\begin{aligned}
&\int_0^1 \sum_{j=1}^{N} p_j^{n+1}\phi'_{2,j}(\sigma)\phi'_{2,i}(\sigma)d\sigma \\
&+ (\tau+\Delta\tau)^2 \int_0^1 \cos\Big(\sum_{j=1}^{N}\beta_j^{n+1}\phi_{1,j}(\sigma)\Big)\phi_{2,i}(\sigma)d\sigma \\
&= -(\tau+\Delta\tau)\phi_{2,i}(1),
\end{aligned} \tag{36}$$

$i = 1, \ldots, N$

Downloaded 03 May 2010 to 171.66.16.27. Redistribution subject to ASME license or copyright; see http://www.asme.org/terms/Terms_Use.cfm

$$\int_0^1 \sum_{j=1}^{N} q_j^{n+1}\phi'_{3,j}(\sigma)\phi'_{3,j}(\sigma)d\sigma$$

$$+(\tau+\Delta\tau)^2\int_0^1 \sin\left(\sum_{j=1}^{N}\beta_j^{n+1}\phi_{1,j}(\sigma)\right)\phi_{3,i}(\sigma)d\sigma=0, \tag{37}$$

$$i=1, \ldots, N,$$

which was solved using Newton's method.

Rather than obtain approximations for $\bar{x}_e$ and $\bar{y}_e$ by differentiating the results for $p(\sigma)$ and $q(\sigma)$, we find it more accurate to obtain them from

$$x_e=\int_0^1 \tau\cos\beta(\sigma)d\sigma,\ y_e=\int_0^1 \tau\sin\beta(\sigma)d\sigma. \tag{38}$$

For convenience, backward differences were used instead of the more accurate Crank-Nicholson or trapesoidal rule approximations. Thus, for accuracy, the time step should be smaller than the grid spacing used in the finite element discretization. We found that only three or four iterations were required at each time step for Newton's method to converge and that the entire computation from $\tau = 0$ to $\tau = 1$ required only a couple of seconds on the CDC 855.

Graphical Results

Fig. 3 shows end orbits of an elastica for a weight-stiffness ratio $\mu = 50$ (which is typical for office paper) and for various dimensionless velocities. The dashed line respresents the static shape of a fully extruded, cantilevered elastica.

References

Carrier, G. F., 1949, "The Spaghetti Problem," *Am. Math. Monthly*, Vol. 56, pp. 669–672.

Hummel, F. H., and Morton, W. B., 1927, "On the Large Bending of Thin Flexible Strips and the Measurement of their Elasticity," *Phil. Mag. 4*, Ser. 7, pp. 348–357.

Keller, J. B., and Ting, L., 1966, "Periodic Vibrations of Systems Governed by Nonlinear Partial Differential Equations," *Comm. Pure Appl. Math.*, Vol. 19, pp. 371–420.

Downloaded 03 May 2010 to 171.66.16.27. Redistribution subject to ASME license or copyright; see http://www.asme.org/terms/Terms_Use.cfm

Ray Solutions on Surfaces of Revolution

L. S. Chien
Research Assistant.

C. R. Steele
Professor.
Fellow ASME

Division of Applied Mechanics,
Department of Mechanical Engineering,
Stanford University,
Stanford, CA 94305

Our concern is the development of techniques for the analysis of wave propagation and general transient response of thin shells to local loading. In general, ray methods are useful for such problems. In the present work, the ray solutions are obtained for a shell of revolution with high prestress, for which the bending stiffness of the shell wall can be neglected. The equation is that for an inhomogeneous, anisotropic medium with a non-Euclidean metric. Of special interest in the present shell problem is the global connectivity of ray paths. For an example the conical shell is considered. The rays for uniform pressure are shown to deviate substantially from geodesics. A ray emitted from a point on the cone may make several spirals around the small end of the cone before moving toward the large end in an almost straight line. The implication is that high focusing of energy can occur from a mild impact on the side of a conical shell.

1 Introduction

Asymptotic expansions have been used to determine the static and dynamic response of elastic shells since the early 1900's by H. Reissner, O. Blummenthal, and E. Meissner. These methods are very similar to those used for solving wave mechanics problems. Whitham (1974) used the variational method to determine wave propagation through an inhomogeneous, dispersive medium. Steele (1977) indicated that this variational approach can be utilized for waves in shells. For the general surface, the asymptotic analysis leads to "geometric optics", in which the determination of "rays" and "caustics" plays an important role. The ray solution is, of course, a valid approximation when the wavelength of the solution is short in comparison with the distance over which the equation coefficients vary significantly.

Hayes (1970) introduced a symmetrical curvature tensor for solving rays on nonflat space. The Snell's law with modified wavenumber was also introduced on cylindrically and spherically symmetric media to solve for rays on a nonflat surface. By Snell's law, the ray equations become simpler whenever the dispersion relation has no explicit dependence upon certain coordinates of the propagation space. The surface of revolution provides a demonstration of this. In the present work, the general formulas for the computation of all rays for any arbitrarily prescribed axisymmetric distribution of prestress are obtained. For the special case of the conical shell (a flat space) the results are particularly simple. We consider two cases: (1) constant stress throughout the shell surface, and (2) uniform pressure applied to the surface of the shell.

2 Eikonal Equations

In the present work, the following form of the wave equation is considered:

$$\nabla \cdot (\mathbf{N} \cdot \nabla W) - \rho h \frac{\partial^2 W}{\partial t^2} = 0 \tag{1}$$

in which the density is ρ, the thickness is h, the gradient operator is defined on the surface, $\nabla = \mathbf{a}^\alpha \, \partial/\partial x^\alpha$, $\mathbf{N}$ is the stress tensor, and W is the normal displacement.

For a flat surface, this is the standard wave equation governing the response of a membrane with a static tension distribution. The same equation governs plane waves in an anisotropic medium. Our interest is in the behavior of the solutions on a curved surface. Naghdi (1972) discusses the classical and modern theories for stress and deformation in thin shells. A general asymptotic wave solution is given by Steele (1977). Equation (1) represents an approximation for the normal displacement waves in the case that the static prestress $\mathbf{N}$ provides the dominant stiffness.

The appropriate asymptotic expansion form of the displacement W is

$$W(\mathbf{r},t) \approx e^{i(\omega t - \xi(\mathbf{r};\omega))} \cdot \left\{ \Psi_0(\mathbf{r}) + \frac{1}{\omega} \Psi_1(\mathbf{r}) + \frac{1}{\omega^2} \Psi_2(\mathbf{r}) + \ldots \right\} \tag{2}$$

in which $\mathbf{r}$ is the position vector, and ω is frequency.

Considering only the leading term of (2) gives

$$W(\mathbf{r},t) \approx \Psi_0 e^{i(\omega t - \xi(\mathbf{r};\omega))} \tag{3}$$

The Lagrangian density per unit of surface area is

$$L = \frac{1}{2}(\rho h W_t^2 - \nabla W \cdot \mathbf{N} \cdot \nabla W) \tag{4}$$

where

Contributed by the Applied Mechanics Division for presentation at the 1987 Applied Mechanics, Biomechanics, and Fluids Engineering Conference, Cincinnati, OH, June 14–17, 1987, of the American Society of Mechanical Engineers.
Discussion of this paper should be addressed to the Editorial Department, ASME, United Engineering Center, 345 East 47th Street, New York, N.Y. 10017, and will be accepted until two months after final publication of the paper itself in the JOURNAL OF APPLIED MECHANICS. Manuscript received by ASME Applied Mechanics Division, December 30, 1985; final revision, July 24, 1986.
Paper No. 87-APM-13.

Copyright © 1987 by ASME
Downloaded 03 May 2010 to 171.66.16.27. Redistribution subject to ASME license or copyright; see http://www.asme.org/terms/Terms_Use.cfm

$$\nabla W \cdot \mathbf{N} \cdot \nabla W = N_x W_x^2 + N_y W_y^2$$

The displacement W is interpreted as the small displacement from the primary equilibrium state. The spatial phase change, ξ, and the amplitude of normal displacement, Ψ_0, are the unknown functions. It is now assumed, however, that these functions are of "slow" variation in comparison with that of the equation coefficients.

The remarkable feature of the approach developed by Whitham (1974) for the asymptotic analysis of waves is that no further equations are necessary.

The variational formulation is

$$U(W) = \int_{t_1}^{t_2} \int_{\Sigma} L \, d\Sigma \, dt$$

Substituting (3) into (4), and letting $\mathbf{k} = \nabla \xi$, gives the approximation

$$L = \frac{1}{2}(\rho h \omega^2 - \mathbf{k} \cdot \mathbf{N} \cdot \mathbf{k}) \Psi_0^2 \tag{5}$$

The "time-averaged" Lagrangian is calculated as

$$\mathfrak{L} = \frac{\omega}{\pi} \int_0^{\frac{2\pi}{\omega}} L \, dt$$

$$= \frac{1}{4} F \Psi_0^2 \tag{6}$$

where

$$F = (\rho h \omega^2 - \mathbf{k} \cdot \mathbf{N} \cdot \mathbf{k})$$

$$= F(\mathbf{k}, \mathbf{r}; \omega)$$

Hamilton's Principle states that the surface integral of (6) must be a stationary value

$$\delta U = \delta \left(\int_{\Sigma} \mathfrak{L} \, d\Sigma \right)$$

$$= 0 \tag{7}$$

Since $\mathfrak{L}$ depends explicitly on the unknown amplitude function, Ψ_0, and on the spatial derivatives of phase, ξ, the Euler equations of the variational problem are

$$\frac{\partial \mathfrak{L}}{\partial \Psi_0} = 0 \tag{8}$$

$$\frac{\partial}{\partial t} \frac{\partial \mathfrak{L}}{\partial W_t} + \nabla \cdot \frac{\partial \mathfrak{L}}{\partial \nabla \xi} = 0 \tag{9}$$

Solving (8) gives the eikonal equation (i.e., equation of geometric optics) for ξ

$$F(\mathbf{k}, \mathbf{r}; \omega) = 0 \tag{10}$$

i.e.,

$$F = \mathbf{k} \cdot \mathbf{N} \cdot \mathbf{k} - \rho h \omega^2 = 0 \tag{11}$$

Equation (11) gives the dispersion-phase relationship.

For constant ω, (9) becomes

$$\nabla \cdot \frac{\partial \mathfrak{L}}{\partial \nabla \xi} = 0 \tag{12}$$

Substituting (6) into (12) gives

$$\frac{\partial \mathfrak{L}}{\partial \nabla \xi} = \frac{1}{4} \frac{\partial F}{\partial \nabla \xi} \Psi_0^2$$

and

$$\nabla \cdot \left(\Psi_0^2 \frac{\partial F}{\partial \nabla \xi} \right) = 0 \tag{13}$$

Equation (13) is the transport equation of Ψ_0 and gives the amplitude of normal displacement.

The use of the "time-averaged" Lagrangian provides a clear, economical derivation of the significant relations for the asymptotic analysis. As a matter of fact, (10) through (13) apply even when $\mathbf{k}$ is complex-valued. In this case, (2) yields the solution with exponential rather than sinusoidal spatial variation.

3 Ray Solutions on Surfaces of Revolution

The eikonal equation (10) or (11) is a first-order partial differential equation for $\xi(\mathbf{r})$ which can be solved by the method of characteristics. The characteristics, or "ray paths", emitted from a given point on a surface in prescribed directions can also be determined by the variational approach.

Consider the variational problem of phase change along a curve Γ with endpoints p_1 and p_2 on a surface.

$$\xi_{12} = \int_{p_1}^{p_2} d\xi$$

$$= \int_{p_1}^{p_2} d\mathbf{r} \cdot \nabla \xi$$

$$= \int_{p_1}^{p_2} d\mathbf{r} \cdot \mathbf{k}$$

$$= \int_{p_1}^{p_2} \frac{\partial \mathbf{r}}{\partial \sigma} \cdot \mathbf{k} \, d\sigma \tag{14}$$

subjected to constraint condition (10).

By finding the extreme (stationary) value, (14) yields the following Euler equations

$$\frac{\partial \mathbf{r}}{\partial \sigma} = F_{\mathbf{k}} \tag{15}$$

$$\boldsymbol{\delta} \cdot \frac{\partial \mathbf{k}}{\partial \sigma} = -F_{\mathbf{r}} \tag{16}$$

Note that $\boldsymbol{\delta} = \mathbf{a}^{\alpha} \otimes \mathbf{a}_{\alpha}$ is the intrinsic unit dyadic, the dot product of which with a tangent vector produces the vector identically. When dotted with a general vector, as in the above case, the normal component is eliminated.

The parameter along the ray σ is related to the phase function ξ by

$$\frac{\partial \xi}{\partial \sigma} = \frac{\partial \mathbf{r}}{\partial \sigma} \cdot \nabla \xi$$

$$= \mathbf{k} \cdot F_{\mathbf{k}} \tag{17}$$

Thus the rays can be thought of as lines of minimum phase change subject to constraint condition (10). Generally, $\partial \mathbf{r}/\partial \sigma$ (which gives the direction of the tangent of the ray) and $\mathbf{k}$ are not in the same direction. If the rays emitted from a boundary curve are used as one family of coordinate lines, and those lines of constant ξ (i.e., constant phase) are used for the second set of coordinate lines, then the resulting coordinates are called "ray coordinates." The ray coordinate lines are not necessarily orthogonal to each other.

Rearranging (11) we get

$$\frac{F}{\rho h \omega^2} = \frac{\mathbf{k} \cdot \mathbf{N} \cdot \mathbf{k}}{\rho h \omega^2} - 1 = 0 \tag{18}$$

Let

Downloaded 03 May 2010 to 171.66.16.27. Redistribution subject to ASME license or copyright; see http://www.asme.org/terms/Terms_Use.cfm

$$\mathcal{F}=\frac{F}{\rho h\omega^2};\ \mathcal{K}=\frac{\mathbf{k}}{\omega};\ \text{and}\ \mathfrak{N}=\frac{\mathbf{N}}{\rho h}$$

thus (11) and (12) become

$$\mathcal{F}=\mathcal{K}\bullet\mathfrak{N}\bullet\mathcal{K}-1=0 \tag{19}$$

$$\nabla\bullet\left(\Psi_0^2\frac{\partial\mathcal{F}}{\partial\mathcal{K}}\right)=0 \tag{20}$$

Substituting (19) into (15) through (17), we get the following "condition on path."

$$\frac{\partial\mathbf{r}}{\partial\sigma}=\mathcal{F}_{\mathcal{K}}=2\,\mathfrak{N}\bullet\mathcal{K} \tag{21}$$

$$\delta\bullet\frac{\partial\mathcal{K}}{\partial\sigma}=-\mathcal{F}_{\mathbf{r}}=-\nabla\mathfrak{N}\bullet\bullet\mathcal{K}\otimes\mathcal{K}=\mathfrak{N}^{\beta\gamma}|_{\alpha}\mathcal{K}_{\gamma}\mathcal{K}_{\beta}\mathbf{a}^{\alpha} \tag{22}$$

$$\frac{\partial\xi}{\partial\sigma}=\mathcal{K}\bullet\mathcal{F}_{\mathcal{K}}=2\,\mathcal{K}\bullet\mathfrak{N}\bullet\mathcal{K}=2 \tag{23}$$

The ray equations are

$$\frac{\partial\mathbf{r}}{\partial\xi}=\mathfrak{N}\bullet\mathcal{K} \tag{24}$$

$$\delta\bullet\frac{\partial\mathcal{K}}{\partial\xi}=-\frac{1}{2}\nabla\mathfrak{N}\bullet\bullet\mathcal{K}\otimes\mathcal{K} \tag{25}$$

Using the meridional arclength ρ and the circumferential angle θ for coordinates, the metric is

$$ds^2=d\rho^2+r^2d\theta^2 \tag{26}$$

so that

$$\mathbf{r}'=\rho'\mathbf{e}_1+r\theta'\mathbf{e}_2 \tag{27}$$

where the prime denotes differentiation with respect to ξ and the prestress is

$$\mathfrak{N}=\mathfrak{N}_1\mathbf{e}_1\mathbf{e}_1+\mathfrak{N}_2\mathbf{e}_2\mathbf{e}_2 \tag{28}$$

where $\mathfrak{N}_1$ and $\mathfrak{N}_2$ are the physical components and $\mathbf{e}_1$, $\mathbf{e}_2$ are unit vectors in the meridional and circumferential directions, respectively.

The inverse of (2) gives

$$\mathcal{K}=\mathfrak{N}^{-1}\bullet\frac{\partial\mathbf{r}}{\partial\xi}=\frac{1}{\mathfrak{N}_1}\rho'\mathbf{e}_1+\frac{1}{\mathfrak{N}_2}r\theta'\mathbf{e}_2 \tag{29}$$

Therefore, the left-hand side of (25) is

$$\delta\bullet\frac{\partial\mathcal{K}}{\partial\xi}=\left[\left(\frac{\partial}{\partial\rho}\left(\frac{1}{\mathfrak{N}_1}\right)\right)\left(\frac{\partial\rho}{\partial\xi}\right)^2+\frac{1}{\mathfrak{N}_1}\frac{\partial^2\rho}{\partial\xi^2}-\left(\frac{\partial\theta}{\partial\xi}\right)^2\frac{r}{\mathfrak{N}_2}\cos\phi\right]\mathbf{e}_1+\left[\frac{\partial\theta}{\partial\xi}\frac{1}{\mathfrak{N}_1}\frac{\partial\rho}{\partial\xi}\cos\phi+\left(\frac{\partial}{\partial\rho}\left(\frac{r}{\mathfrak{N}_2}\right)\right)\frac{\partial\rho}{\partial\xi}\frac{\partial\theta}{\partial\xi}+\frac{r}{\mathfrak{N}_2}\frac{\partial^2\theta}{\partial\xi^2}\right]\mathbf{e}_2 \tag{30}$$

while the right-hand side of (25) is

$$-\frac{1}{2}\nabla\mathfrak{N}\bullet\bullet\mathcal{K}\otimes\mathcal{K}=-\frac{1}{2}\left[\frac{\partial\mathfrak{N}_1}{\partial\rho}\left(\frac{1}{\mathfrak{N}_1}\rho'\right)^2+\frac{\partial\mathfrak{N}_2}{\partial\rho}\left(\frac{r}{\mathfrak{N}_2}\theta'\right)^2\right]\mathbf{e}_1+\left[-\left(\mathfrak{N}_1-\mathfrak{N}_2\right)\frac{\cos\phi}{r}\left(\frac{r}{\mathfrak{N}_2}\theta'\right)\left(\frac{1}{\mathfrak{N}_1}\rho'\right)\right]\mathbf{e}_2 \tag{31}$$

Setting the $\mathbf{e}_2$ components equal gives a result which reduces to

$$\frac{1}{r}\frac{\partial}{\partial\xi}\left(\frac{r^2}{\mathfrak{N}_2}\theta'\right)=0 \tag{32}$$

Thus,

$$\theta=\frac{A\,\mathfrak{N}_2}{r^2} \tag{33}$$

where A is a constant. Setting the $\mathbf{e}_1$ components equal gives

$$\frac{\partial}{\partial\rho}\left(\frac{1}{\mathfrak{N}_1}\right)\left(\rho'\right)^2+\frac{1}{\mathfrak{N}_1}\rho''-\frac{r\cos\phi}{\mathfrak{N}_2}\left(\theta'\right)^2=-\frac{1}{2}\left[\frac{\partial\,\mathfrak{N}_1}{\mathfrak{N}_1^2\partial\rho}\left(\rho'\right)^2+\frac{\partial\,\mathfrak{N}_2}{\partial\rho}\left(\frac{r}{\mathfrak{N}_2}\theta'\right)^2\right] \tag{34}$$

Utilizing (32) reduces this to

$$\frac{\partial}{\partial\rho}\left(\frac{1}{\mathfrak{N}_1}\left(\rho'\right)^2\right)=-\frac{1}{2}A^2\frac{\partial}{\partial\rho}\left(\left(\mathfrak{N}_2^{-1/2}r\right)^2\right) \tag{35}$$

Integrating then yields the result

$$\rho'=\pm\left(B\,\mathfrak{N}_1-\frac{A^2}{r^2}\mathfrak{N}_1\mathfrak{N}_2\right)^{1/2} \tag{36}$$

where B is a new constant. However, from (27), (33), and (36) substituted into (19), the value $B = 1$ is found.

The angle α between the ray and the meridian is obtained from the relation

$$\sin\alpha=r\frac{d\theta}{dr}=r\frac{\theta'}{r'}=\frac{\dfrac{A\,\mathfrak{N}_2}{r}}{\left[\mathfrak{N}_1+\dfrac{A^2\mathfrak{N}_2}{r^2}\left(\mathfrak{N}_2-\mathfrak{N}_1\right)\right]^{1/2}} \tag{37}$$

In terms of ray coordinates, the amplitude function, Ψ_0, is calculated from (13)

$$\Psi_0=\frac{\text{const.}}{(a^{1/2}\mathbf{k}\bullet F_{\mathbf{k}})^{1/2}} \tag{38}$$

where $a^{1/2}$ is the determinant of the metric and can be obtained by calculating the area between two sets of adjacent ray coordinates.

The envelope of rays is a curve on which a equals zero. An improved solution is required for such a region.

The angle α between the ray and the meridian is found as

$$\sin\alpha=\frac{\dfrac{A\,\mathfrak{N}_2}{r}}{\left[\mathfrak{N}_1+\dfrac{A^2\mathfrak{N}_2}{r^2}\left(\mathfrak{N}_2-\mathfrak{N}_1\right)\right]^{1/2}} \tag{39}$$

Note, when $\mathfrak{N}_1 = \mathfrak{N}_2 = \mathfrak{N} =$ *constant* (39) reduces to

Downloaded 03 May 2010 to 171.66.16.27. Redistribution subject to ASME license or copyright; see http://www.asme.org/terms/Terms_Use.cfm

$r \sin \alpha = A\ \mathfrak{N}/\mathfrak{N}^{1/2} = constant$, which is the theorem of Clairaut [9]. The rays are then geodesics on the surface.

Equations (40) through (42) describe the wave fronts, ξ, of rays emitted from a prescribed point, (ρ_0, θ_0), the ray path, θ, along the meridian on a surface of revolution, and the ray length, S,

$$\xi = \xi_0 \pm \int_{\rho_0}^{\rho} \frac{1}{\left(\mathfrak{N}_1 - \dfrac{A^2}{r^2}\,\mathfrak{N}_1\mathfrak{N}_2\right)^{1/2}}\, d\rho \tag{40}$$

$$\theta = \theta_0 \pm \int_{\rho_0}^{\rho} \frac{\dfrac{A\,\mathfrak{N}_2}{r^2}}{\left(\mathfrak{N}_1 - \dfrac{A^2}{r^2}\,\mathfrak{N}_1\mathfrak{N}_2\right)^{1/2}}\, d\rho \tag{41}$$

$$S = S_0 \pm \int_{\rho_0}^{\rho} \left[\frac{\mathfrak{N}_1 + \dfrac{A^2}{r^2}\,\mathfrak{N}_2(\mathfrak{N}_2 - \mathfrak{N}_1)}{\mathfrak{N}_1 - \dfrac{A^2}{r^2}\,\mathfrak{N}_1\mathfrak{N}_2}\right]^{1/2} d\rho \tag{42}$$

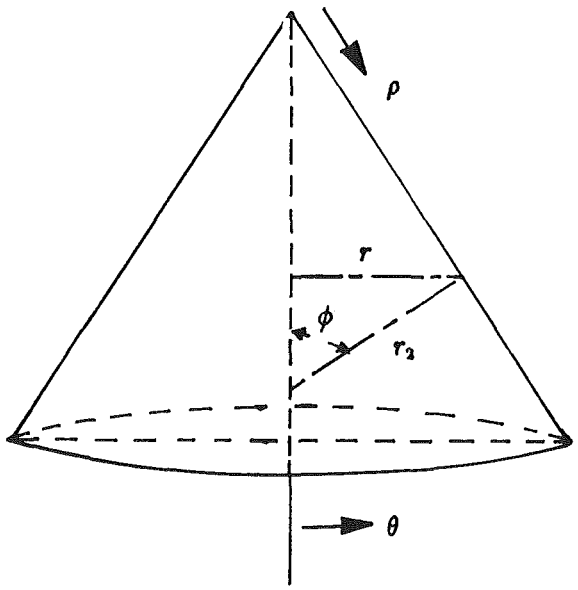
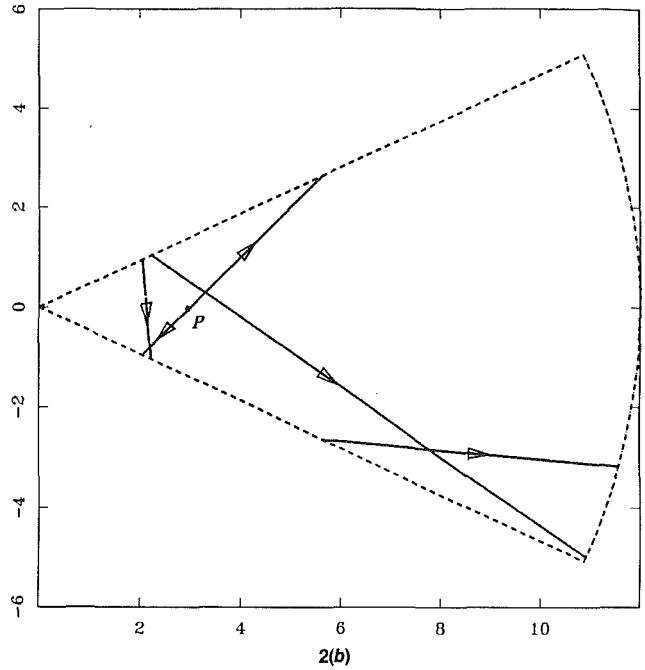
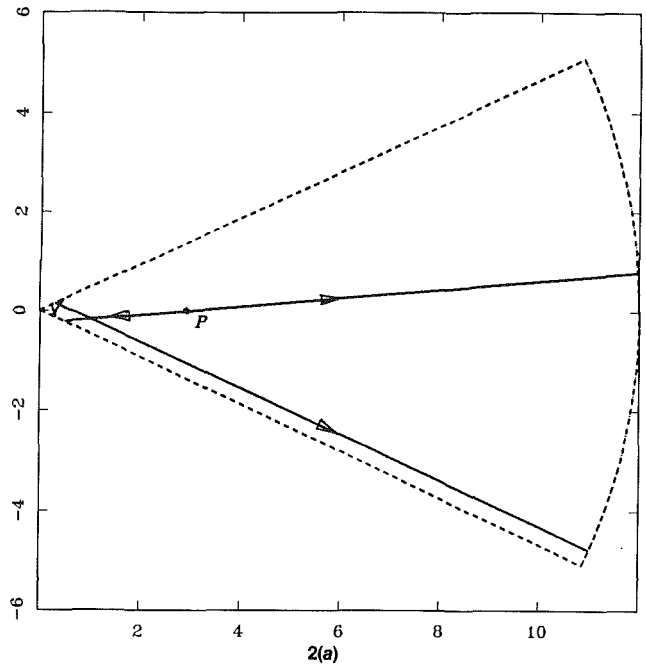


Fig. 1 The geometric features of a cone surface





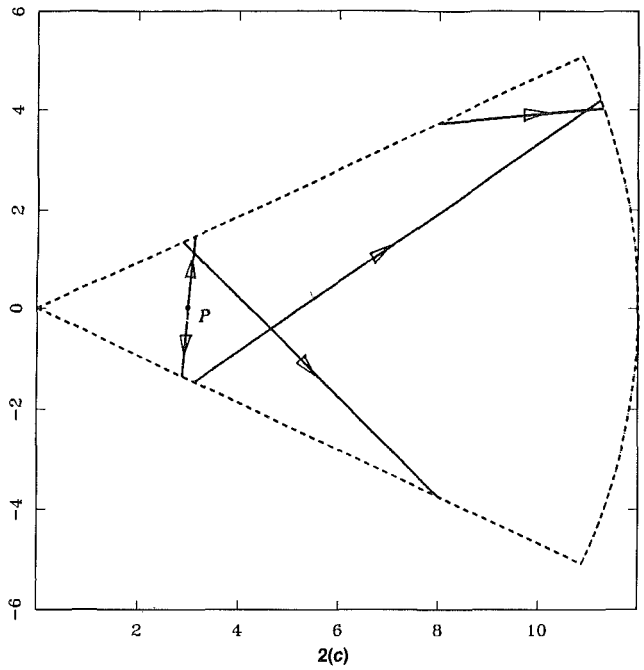


Fig. 2 Geodesics (rays for constant stress) for the cone angle of 8 deg. Forward and backward rays originate at point P with the angle: (a) α_0 = 5 deg; (b) α_0 = 45 deg; (c) α_0 = 85 deg.

Downloaded 03 May 2010 to 171.66.16.27. Redistribution subject to ASME license or copyright; see http://www.asme.org/terms/Terms_Use.cfm

where ξ_0 and S_0 are initial values determined by the ray's starting point (ρ_0, θ_0); and the constant A is

$$A = \left\{ \frac{r\,\mathfrak{N}_1^{1/2}\tan\alpha}{\mathfrak{N}_2^{1/2}(\mathfrak{N}_2 + \mathfrak{N}_1\tan^2\alpha)^{1/2}} \right\} \Bigg|_{\substack{\rho=\rho_0 \\ \theta=\theta_0 \\ \alpha=\alpha_0}} \tag{43}$$

More details of the derivation are given by Chien (1985).

4 Cone

Equations (40) through (42) describe rays on a general surface of revolution. In the present section, the equations are applied to the cone shown in Fig. 1.

$$r_1 \to \infty$$

$$r = \rho\cos\phi$$

$$r_2 = \frac{r}{\sin\phi} \tag{44}$$

The two loading conditions to be considered are: (1) constant stress throughout the cone surface, (2) uniform pressure applied to the surface of the cone.

(1) Constant Stress (Geodesics). Constant isotropic stress throughout the shell surface

$$\mathfrak{N}_1 = \mathfrak{N}_2 = \mathfrak{N} \tag{45}$$

produces rays which are the geodesics for the surface.

Substituting (44) and (45) into (41) yields

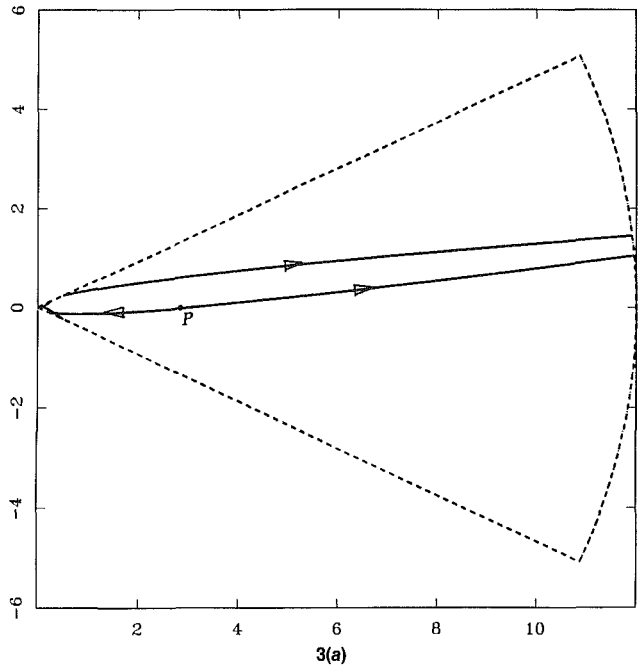
$$\theta = \theta_0 \pm \int_{\rho_0}^{\rho} \frac{\dfrac{A\,\mathfrak{N}}{r^2}}{\left(\mathfrak{N} - \dfrac{A^2}{r^2}\,\mathfrak{N}^2\right)^{1/2}} d\rho$$

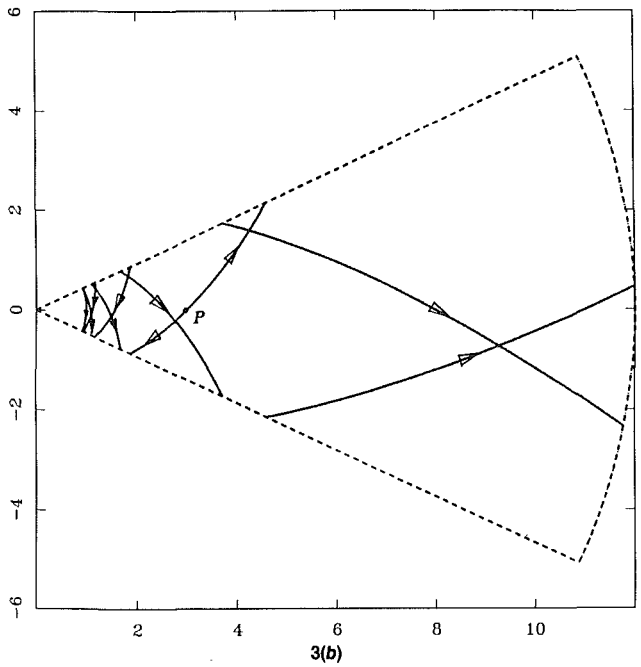
$$= \theta_0 \pm \frac{A\,\mathfrak{N}^{1/2}}{\cos\phi} \int_{\rho_0}^{\rho} \frac{1}{\rho(\rho^2\cos^2\phi - A^2\mathfrak{N})^{1/2}}\, d\rho \tag{46}$$

Hence,

$$\theta = \theta_0 \pm \frac{1}{\cos\phi}\left[\cos^{-1}\left(\frac{1}{\rho}\,\frac{A\,\mathfrak{N}^{1/2}}{\cos\phi}\right) - \cos^{-1}\left(\frac{1}{\rho_0}\,\frac{A\,\mathfrak{N}^{1/2}}{\cos\phi}\right)\right] \tag{47}$$

With the constant A written in terms of the initial point of ray (43), the expression for the circumferential angle (41) becomes





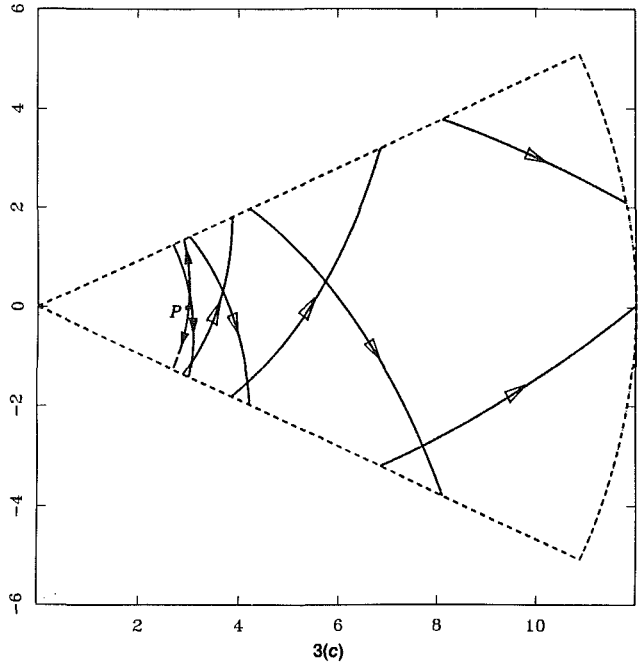


Fig. 3 Rays for uniform pressure for the cone angle of 8 deg. Forward and backward rays originate at point *P* with the angle: (*a*) α_0 = 5 deg; (*b*) α_0 = 45 deg; (*c*) α_0 = 85 deg.

Downloaded 03 May 2010 to 171.66.16.27. Redistribution subject to ASME license or copyright; see http://www.asme.org/terms/Terms_Use.cfm

$$\theta=\theta_0\pm\frac{1}{\cos\phi}\left[\cos^{-1}\left(\frac{\tan\alpha_0}{(1+\tan^2\alpha_0)^{1/2}}\frac{\rho_0}{\rho}\right)\right.$$
$$\left.-\cos^{-1}\left(\frac{\tan\alpha_0}{(1+\tan^2\alpha_0)^{1/2}}\right)\right] \tag{48}$$

The arclength along the ray (42) reduces to

$$S=S_0+\cos\phi\int_{\rho_0}^{\rho}\frac{\rho}{(\rho^2\cos^2\phi-A^2\mathfrak{N})^{1/2}}\,d\rho$$
$$=S_0+\frac{1}{\cos\phi}[(\rho^2\cos^2\phi-A^2\mathfrak{N})^{1/2}-(\rho_0^2\cos^2\phi-A^2\mathfrak{N})^{1/2}] \tag{49}$$

and the phase (40) becomes

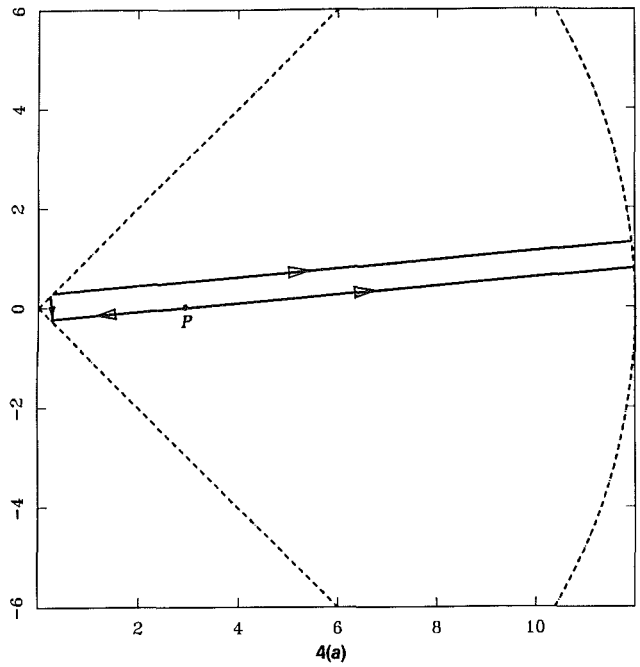
$$\xi=\xi_0+\int_{\rho_0}^{\rho}\frac{1}{\left(\mathfrak{N}-\frac{A^2}{\rho^2\cos^2\phi}\mathfrak{N}^2\right)^{1/2}}\,d\rho$$
$$=\xi_0+\frac{1}{\mathfrak{N}^{1/2}}\left[\left(\rho^2-\frac{\tan^2\alpha_0}{1+\tan^2\alpha_0}\rho_0^2\right)^{1/2}\right.$$
$$\left.-\left(\rho_0^2-\frac{\tan^2\alpha_0}{1+\tan^2\alpha_0}\rho_0^2\right)^{1/2}\right] \tag{50}$$

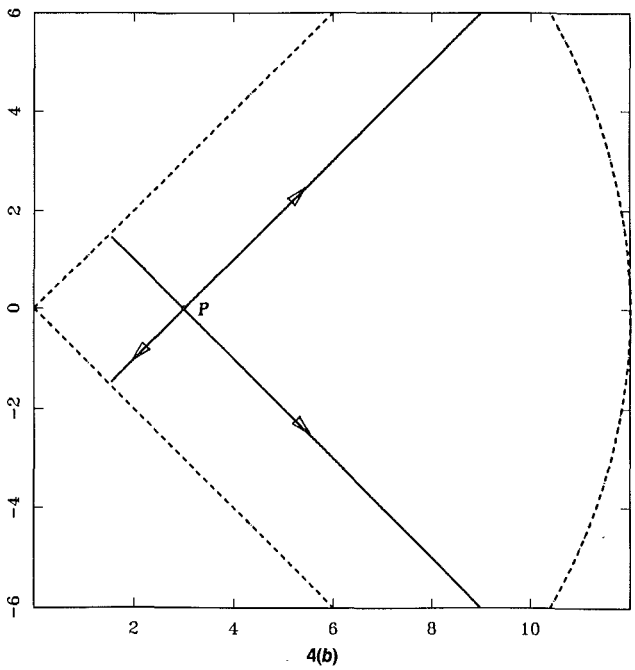
Figure 2 illustrates rays originating at point P on the wall of a conical shell (shown unrolled and flattened) with constant stress. The cone angle is 8 deg. The initial angle between the ray and the generator is (*a*) 5 deg, (*b*) 45 deg, and (*c*) 85 deg. The cone angle is changed to 15 deg in Fig. 4.

(2) Uniform Pressure. Uniformly distributed pressure p has the following stress components:

$$\mathfrak{N}_1=\mathfrak{N}_\phi=\frac{pr_2}{2}=\frac{pr}{2\sin\phi}$$
$$\mathfrak{N}_2=\mathfrak{N}_\theta=\frac{pr_2}{2}\left(2-\frac{r_2}{r_1}\right)=\frac{pr}{\sin\phi} \tag{51}$$

Substituting (44) and (51) into (41) gives





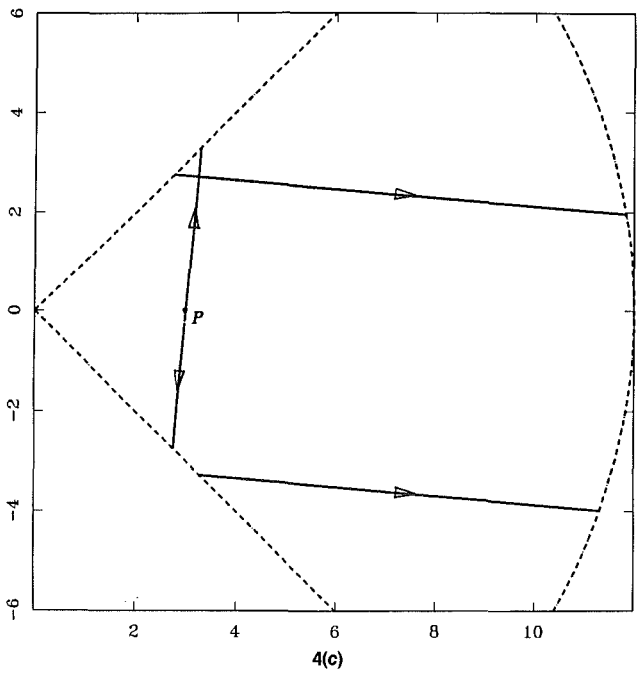


Fig. 4 Geodesics (rays for constant stress) for the cone angle of 14.48 deg. Forward and backward rays originate at point *P* with the angle: (*a*) α_0 = 5 deg; (*b*) α_0 = 45 deg; (*c*) α_0 = 85 deg.

Downloaded 03 May 2010 to 171.66.16.27. Redistribution subject to ASME license or copyright; see http://www.asme.org/terms/Terms_Use.cfm

$$\theta=\theta_0\pm\int_{\rho_0}^{\rho}\frac{\dfrac{Ap}{r\sin\phi}}{\left[\dfrac{pr}{2\sin\phi}-\dfrac{A^2p^2}{2\sin^2\phi}\right]^{1/2}}\,d\rho$$

$$=\theta_0\pm\frac{\sqrt{2}}{\cos\phi}\int_{\rho_0}^{\rho}\frac{1}{\rho\left[\dfrac{\rho\cos\phi\sin\phi}{A^2p}-1\right]^{1/2}}\,d\rho \tag{52}$$

Hence,

$$\theta=\theta_0$$
$$\pm\frac{2\sqrt{2}}{\cos\phi}\left\{\tan^{-1}\left[\left(\frac{\cos\phi\sin\phi}{A^2p}\rho-1\right)^{1/2}\right]-\tan^{-1}\left[\left(\frac{\cos\phi\sin\phi}{A^2p}\rho_0-1\right)^{1/2}\right]\right\} \tag{53}$$

With the constant A written in terms of the initial point on the ray (43), the expression for the circumferential angle (41) becomes

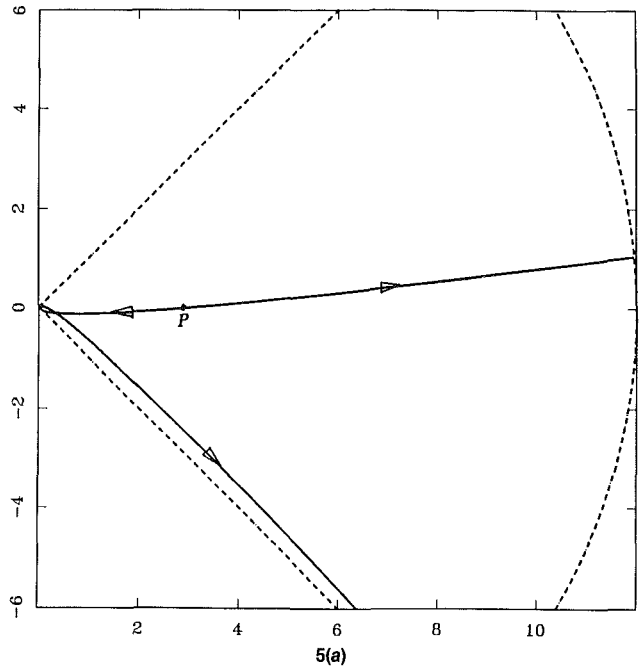
$$\theta=\theta_0$$
$$\pm\frac{2\sqrt{2}}{\cos\phi}\left\{\tan^{-1}\left[\left(\frac{2+\tan^2\alpha_0}{\tan^2\alpha_0}\frac{\rho}{\rho_0}-1\right)^{1/2}\right]-\tan^{-1}\left[\left(\frac{2+\tan^2\alpha_0}{\tan^2\alpha_0}-1\right)^{1/2}\right\}\right. \tag{54}$$

Therefore, the ray behavior is also determined by initial angle α_0, prescribed point (ρ_0, θ_0), and cone angle $(\pi/2 - \phi)$.

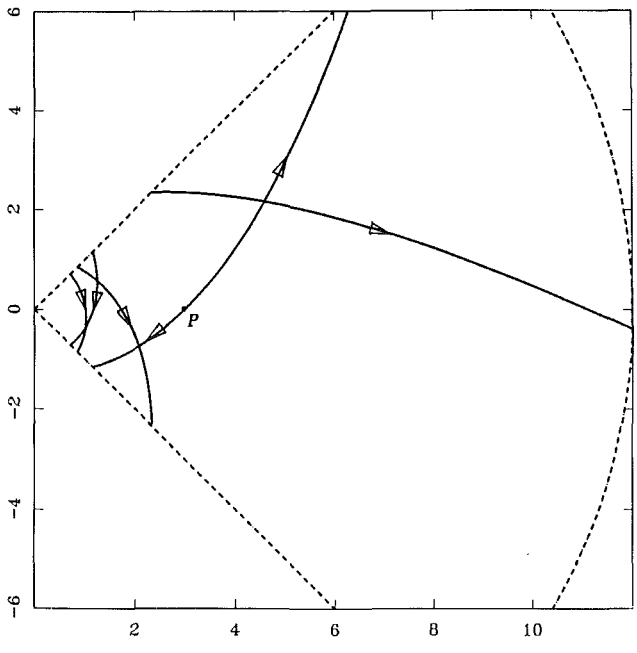
Also, substituting (44) and (51) into (42) gives the ray length.

$$S=S_0+\int_{\rho_0}^{\rho}\left[\frac{\rho+\dfrac{A^2p}{\cos\phi\sin\phi}}{\rho-\dfrac{A^2p}{\cos\phi\sin\phi}}\right]^{1/2}d\rho$$

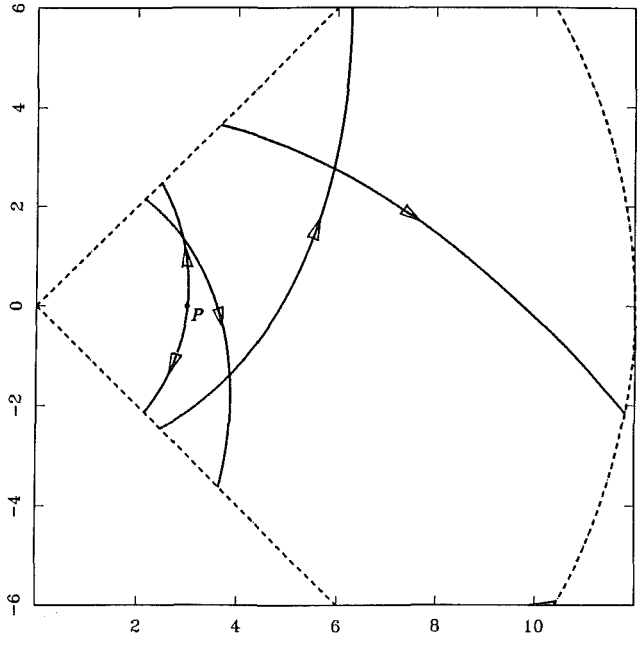
$$=S_0+\left[\rho^2-\left(\frac{A^2p}{\cos\phi\sin\phi}\right)^2\right]^{1/2}-\left[\rho_0^2-\left(\frac{A^2p}{\cos\phi\sin\phi}\right)^2\right]^{1/2}-\frac{2A^2p}{\cos\phi\sin\phi}\left[ln\left(\left(\rho+\frac{A^2p}{\cos\phi\sin\phi}\right)^{1/2}\right.\right.$$



5(a)



5(b)



5(c)

Fig. 5 Rays for uniform pressure for the cone angle of 14.48 deg. Forward and backward rays originate at point *P* with the angle: (*a*) α_0 = 5 deg; (*b*) α_0 = 45 deg; (*c*) α_0 = 85 deg.

Downloaded 03 May 2010 to 171.66.16.27. Redistribution subject to ASME license or copyright; see http://www.asme.org/terms/Terms_Use.cfm

$$+\left(\rho-\frac{A^2p}{\cos\phi\sin\phi}\right)^{1/2}\Bigg)$$

$$-ln\left(\left(\rho_0+\frac{A^2p}{\cos\phi\sin\phi}\right)^{1/2}+\left(\rho_0-\frac{A^2p}{\cos\phi\sin\phi}\right)^{1/2}\right)\Bigg] \tag{55}$$

The phase of the rays is calculated by substituting (44) and (51) into (40)

$$\xi=\xi_0+\int_{\rho_0}^{\rho}\frac{1}{\left[\frac{p\rho\cos\phi}{2\sin\phi}-\frac{A^2p^2}{2\sin^2\phi}\right]^{1/2}}d\rho$$

$$=\xi_0+\left(\frac{2\sin\phi}{p\cos\phi}\right)^{1/2}\left[2\left(\rho-\frac{\tan^2\alpha_0}{2+\tan^2\alpha_0}\rho_0\right)^{1/2}\right.$$

$$\left.-2\left(\rho_0-\frac{\tan^2\alpha_0}{2+\tan^2\alpha_0}\rho_0\right)^{1/2}\right] \tag{56}$$

Figure 3 illustrates the ray originating at point P on the wall of a conical shell (shown unrolled and flattened) with internal uniform pressure. The cone angle is 8 deg. The initial angle between the ray and the generator is (*a*) 5 deg, (*b*) 45 deg, and (*c*) 85 deg. The cone angle of 15 deg is shown in Fig. 5.

5 Conclusions

The interesting feature is that rays may have a complex form even for a surface as simple as the cone. Consider a ray initiated at a point on the wall, which is at the initial inclination $\alpha = \alpha_0 < 90$ deg with the meridian. A point moving along the ray will spiral toward the vertex, completely wrapping around the cone several times when the cone angle is small. During this motion, the angle α increases, and when $\alpha = 90$ deg, the point is at the minimum distance from the vertex. As the point continues along the ray path, moving away from the vertex, several spirals around the cone again occur. Finally, as α approaches 180 deg, the ray path is asymptotic to a meridian.

As the initial angle α_0 increases, the "top-most" point moves closer to the initial point and coincides with the initial point when $\alpha_0 = 90$ deg. The $\alpha_0 = 85$ deg case shows this behavior. On the other hand, when $\alpha_0 = 0$ deg, the ray should pass through the cone vertex, which is the top-most point in this case. The $\alpha_0 = 5$ deg case illustrates this situation.

The cone angle plays an important role in the behavior. More spiralling occurs for smaller cone angles, as shown by comparing the rays for the cone angles of 8 deg and 15 deg.

The general behavior described holds for the rays for homogeneous, isotropic wave speed in our constant stress case, and for the inhomogeneous, orthotropic wave speed in our pressure stress case. In the former case the rays are geodesics, which are straight lines in the flat mapping of the conical surface shown in Figs. 2 and 4. Pressure loading of a cone produces circumferential membrane stress twice that of the meridional. Thus, the speed of propagation in the circumferential direction is twice that in the meridional. In addition, the speed increases linearly with the distance from the vertex. This has a substantial effect on the rays, which can be seen in Figs. 3 and 5. The higher speed in the circumferential direction causes increased spiraling of the rays, while the gradient in magnitude of the speed causes a curvature of the rays.

No caustic is formed by the rays from a point on the wall. Thus, application of these results for the solution of boundary value problems can be carried out without difficulty.

References

Chien, L. S., 1985, "Ray Solutions on Surfaces of Revolution," Engineer Thesis, Dept. of Mechanical Eng., Stanford University, Stanford, CA.

Hayes, W. D., 1970, "Kinematic Wave Theory," *Proc. Roy. Soc. Lond.*, Vol. A.320, pp. 209–226.

Naghdi, P. M., 1972, "The Theory of Shells and Plates," in *Handbuch der Physik VIa/2*, Springer, Berlin.

Steele, C. R., 1971, "A Geometric Optics Solution for the Thin Shell Equation," *Int. J. Engrg. Sci.*, Vol. 9, pp. 681–704.

Steele, C. R., 1972, "An Asymptotic Fundamental Solution of the Reduced Wave Equation on a Surface," *Quart. Appl. Math.*, Vol. 29, pp. 509–524.

Steele, C. R., 1977, "Bending Wave in Shells," *Quart. of Appl. Math.*, Jan.

Ugural, A. C., 1981, *Stresses in Plates and Shells*, McGraw-Hill, New York.

Whitham, G. B., 1974, *Linear and Nonlinear Waves*, Wiley, New York.

Willmore, T. J., 1959, *Differential Geometry*, Oxford Univ. Press, London.

Downloaded 03 May 2010 to 171.66.16.27. Redistribution subject to ASME license or copyright; see http://www.asme.org/terms/Terms_Use.cfm

Crushing of an Elastic-Perfectly Plastic Ring or Tube Between Two Planes

C. Y. Wang
Professor,
Michigan State University,
East Lansing, Mich. 48824
Mem. ASME

A thin ring is crushed between two rigid planes. Due to plastic deformation the ring does not recover its original shape when the compression is removed. For an elastic–perfectly plastic flexural material, the ring undergoes two to five different stages. The mathematical problem is formulated and solved by exact numerical integration and accurate analytical approximations.

Introduction

Consider a circular ring (or tube) whose axis of symmetry is sandwiched between two rigid parallel planes. When a compressive force is applied, the ring will flatten between the planes. If the thickness of the ring is small compared to the minimum radius of curvature, the elastica approximation may be used. The large deformations of an elastica ring was first solved by Sonntag (1943) using elliptic functions. If we let $F = F'R^2/EI$ where $2F'$ is the compressive force, R is the radius of the ring, and EI is the flexural rigidity, Sonntag found that the ring collapses in two stages.

Stage I. $0 < F < 1.392$ the ring touches each plane at one point. The shape is a nodal elastica for small F but changes to an undulating elastica for larger F. This result was also obtained by Frisch-Fay (1960).

Stage II. $1.392 < F < \infty$. The ring touches each plane along a finite segment. More accurate results for this stage were obtained by Wang (1981a).

The above analyses are for perfectly elastic material, i.e., the circular shape will be recovered when the compression is removed. In practice, however, the recovery will not be complete due to plastic set at large deformations. In what follows, we shall study the crushing of a ring whose moment-curvature relation (Fig. 1) is elastic–perfectly plastic. We assume creep and strain hardening are negligible and deformations are caused mainly by bending. The moment m is equal to $EI\kappa$ when the curvature difference κ is smaller than a constant κ_0. For $\kappa > \kappa_o$ the moment remains constant at $EI\kappa_o$. But when κ decreases from the plastic range ($\kappa > \kappa_o$) the moment decreases at once with the rate EI. Fig. 1 closely resembles moment-curvature curves of inelastic materials (Timoshenko and Gere, 1961; Smith and Sidebottom, 1965).

The present analysis applies to very *thin* flexible rings or tubes, for example, a tube made of a sheet of paper. For thick inelastic rings the crushed shape consists of plastic hinges and segments of rigid arcs. In such a case a rigid-perfectly plastic constitutive equation is more appropriate (DeRuntz and Hodge, 1963; Reid and Reddy, 1978).

Formulation

Figure 2 shows a possible sequence of events when the ring is crushed. Stages I and II are the elastic deformations of previous authors. The curvature difference κ = (actual curvature − original natural curvature) is everywhere less than κ_o. If the force is removed, the ring will recover its circular geometry. However, if the force is increased until the maximum curvature difference κ is greater than κ_o, a plastic hinge will develop at that location. In Stage III the local moment remains at $EI\kappa_o$ while the configuration admits two opposite plastic corners on the plane of symmetry. When the com-

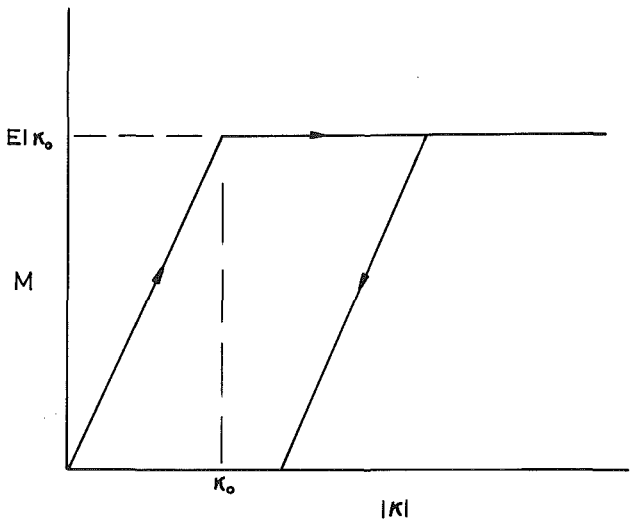


Fig. 1 Moment-curvature relation. Plastic bending occurs when $\kappa > \kappa_o$.

Contributed by the Applied Mechanics Division for presentation at the 1987 Applied Mechanics, Biomechanics, and Fluids Engineering Conference, Cincinnati, OH, June 14–17, 1987, of the American Society of Mechanical Engineers.
Discussion of this paper should be addressed to the Editorial Department, ASME, United Engineering Center, 345 East 47th Street, New York, N.Y. 10017, and will be accepted until two months after final publication of the paper itself in the JOURNAL OF APPLIED MECHANICS. Manuscript received by ASME Applied Mechanics Division, February 3, 1986; final revision, May 19, 1986.
Paper No. 87-APM-3.

Copyright © 1987 by ASME
Downloaded 03 May 2010 to 171.66.16.27. Redistribution subject to ASME license or copyright; see http://www.asme.org/terms/Terms_Use.cfm

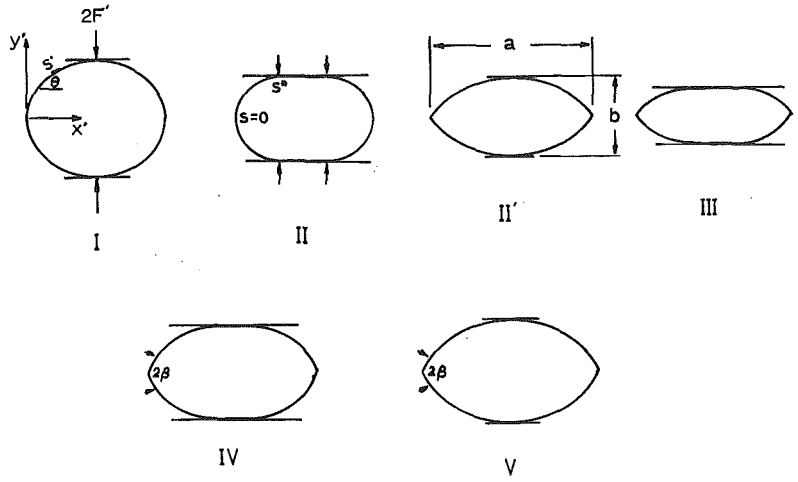


Fig. 2 The various stages in crushing a ring. Stages I and II perfectly elastic loading; Stages II′ and III elasto-plastic loading; Stages IV and V elasto-plastic unloading.

pressive force is gradually removed, due to plastic set, the angle of the two corners stays practically constant. In Stage IV the deformed ring has two segments in contact with the rigid planes and in Stage V two points are in contact. We expect the final relaxed shape to be two connected circular arcs. In some cases plastic deformation may occur during Stage I. When that happens Stage II will be supplanted by Stage II′, a plastic hinge development with two points in contact. Depending on the magnitude of the compressive force, not all five stages may be realized.

Let us place the origin of a Cartesian system (x', y') on the symmetry plane as shown in Fig. 2. Let s' be the arc length and θ be the local angle of inclination. Excluding the plastic hinge and the contact segments, the ring behaves as an elastica,

$$m = EI\kappa = EI\left(\frac{d\theta}{ds'} + \frac{1}{R_o}\right) \tag{1}$$

Here R_o, the natural radius of curvature of the wall (that when the ring is cut open say), may not be the radius of the closed ring R. Thus the governing equation is (Frisch-Fay, 1962).

$$EI\frac{d^2\theta}{ds'^2} = F' \cos\theta \tag{2}$$

Normalizing all lengths by R and dropping primes, equation (2) reduces to

$$\frac{d^2\theta}{ds^2} = F\cos\theta \tag{3}$$

For Stage I the boundary conditions are

$$\theta(0) = \frac{\pi}{2}, \quad \theta\left(\frac{\pi}{2}\right) = 0 \tag{4}$$

For Stage II, let s^* be the arc length where the cylinder begins to touch the rigid plane. Thus

$$\theta(0) = \frac{\pi}{2}, \quad \theta(s^*) = \frac{d\theta}{ds}(s^*) = 0, \quad 0 < s^* < \frac{\pi}{2} \tag{5}$$

For Stage II′

$$-\frac{d\theta}{ds}(0) = \alpha, \quad \theta\left(\frac{\pi}{2}\right) = 0 \tag{6}$$

where α, defined as $R(\kappa_o - 1/R_o)$, is the normalized difference between the plastic curvature and the natural curvature. For Stage III

$$-\frac{d\theta}{ds}(0) = \alpha, \quad \theta(s^*) = \frac{d\theta}{ds}(s^*) = 0 \tag{7}$$

For Stage IV

$$\theta(0) = \beta, \quad 0 < \beta < \frac{\pi}{2}, \quad \theta(s^*) = \frac{d\theta}{ds}(s^*) = 0 \tag{8}$$

For Stage V

$$\theta(0) = \beta, \quad \theta\left(\frac{\pi}{2}\right) = 0 \tag{9}$$

When $\theta(s)$ is obtained, the shape can be integrated from

$$\frac{dx}{ds} = \cos\theta, \quad x(0) = 0 \tag{10}$$

$$\frac{dy}{ds} = \sin\theta, \quad y(0) = 0 \tag{11}$$

The maximum dimensions a, b are from

$$a = 2x\left(\frac{\pi}{2}\right), \quad b = 2y\left(\frac{\pi}{2}\right) \text{ for point contact} \tag{12}$$

$$a = 2\left(\frac{\pi}{2} - s^* + x(s^*)\right), \; b = 2y(s^*) \text{ for line contact} \tag{13}$$

In principle, one can solve equation (3) by elliptic functions. However, that method is very inconvenient to use, since the angle θ is implicit in the elliptic integrals. In what follows we shall make full use of similarity, perturbation methods, and numerical integration for the solution.

Similarity

The deformation becomes geometrically similar when a natural length scale is absent. This situation occurs in the folding processes of [3] and also occurs in Stages II, III, and IV of the present problem. The general formulation is as follows. Let

$$t = \sqrt{F}s, \; \xi = \sqrt{F}x, \; \eta = \sqrt{F}y \tag{14}$$

Equations (3), (10) become

$$\frac{d^2\theta}{dt^2} = \cos\theta, \quad \frac{d\xi}{dt} = \cos\theta, \tag{15}$$

$$\frac{d\eta}{dt} = \sin\theta \tag{16}$$

Downloaded 03 May 2010 to 171.66.16.27. Redistribution subject to ASME license or copyright; see http://www.asme.org/terms/Terms_Use.cfm

The boundary conditions are

$$\theta(0)=\beta,\ \xi(0)=\eta(0)=0 \tag{17}$$

$$\theta(t^*)=\frac{d\theta}{dt}\,(t^*)=0 \tag{18}$$

Multiply equation (15) by $d\theta/dt$ and integrate once,

$$\frac{1}{2}\left(\frac{d\theta}{dt}\right)^2=\sin\theta+C_1 \tag{19}$$

The constant of integration C_1 is zero from equation (18). Thus

$$\frac{d\theta}{dt}\,(0)=-\sqrt{2\sin\beta} \tag{20}$$

On the other hand, equations (15), (16) give

$$\xi=\frac{d\theta}{dt}+C_2 \tag{21}$$

From equations (17), (20), $C_2=\sqrt{2\sin\beta}$. Thus at t^*

$$\xi(t^*)=\sqrt{2\sin\beta} \tag{22}$$

For the exact numerical integration of the similarity solution, one picks any angle β and integrate equations (15–17) and (20) as an initial value problem (e.g., a Runge-Kutta algorithm). The integration terminates at $\theta = 0$ and we note t^*, $\xi(t^*)$, $\eta(t^*)$. The solution depends on β only and is independent of the compression force F. Thus from equation (13) the dimensions are

$$a=2\left(\frac{\pi}{2}-\frac{t^*}{\sqrt{F}}+\frac{\sqrt{2\sin\beta}}{\sqrt{F}}\right),\ b=2\frac{\eta(t^*)}{\sqrt{F}} \tag{23}$$

The maximum curvature (at zero) is

$$\frac{d\theta}{ds}\,(0)=-\sqrt{2F\sin\beta} \tag{24}$$

For Stage II we set $\beta = \pi/2$. For Stage III α is fixed. Obtain β from

$$\beta=\sin^{-1}\left(\frac{\alpha^2}{2F}\right) \tag{25}$$

Perturbation Solution for Small β

If F is large in Stages III and IV, β and thus θ may be small compared to unity. A perturbation solution is possible. Define r^* and r

$$r^*\equiv\sqrt{\frac{F}{\beta}}\,s^*,\ r\equiv r^*-s\sqrt{\frac{F}{\beta}} \tag{26}$$

We also expand θ in a power series

$$\theta=\beta\theta_o(r)+\beta^3\theta_1(r)+\beta^5\theta_2(r)+\ldots \tag{27}$$

Upon substitution into equation (3) we obtain the successive equations

$$\frac{d^2\theta_o}{dr^2}=1,\ \frac{d^2\theta_1}{dr^2}=-\frac{1}{2}\,\theta_o^2,\ \frac{d^2\theta_2}{dr^2}=-\theta_o\theta_1+\frac{\theta_o^4}{24} \tag{28}$$

The boundary conditions are that at $r = 0$, both θ and $d\theta/dr$ are zero. The solutions are as follows

$$\theta_o=\frac{r^2}{2},\ \theta_1=-\frac{r^6}{240},\ \theta_2=\frac{r^{10}}{19200} \tag{29}$$

For the length of the curved section, we note

$$\beta=\theta(r^*)=\beta\,\frac{r^{*2}}{2}-\frac{\beta^3 r^{*6}}{240}+\frac{\beta^5 r^{*10}}{19200}+0(\beta^7) \tag{30}$$

Equation (30) can be inverted

$$r^*=\frac{1}{\sqrt{2}}\left(2+\frac{1}{30}\,\beta^2+\frac{1}{720}\,\beta^4+\ldots\right) \tag{31}$$

Thus

$$a=\pi-\sqrt{\frac{2\beta}{F}}\left[2+\frac{1}{30}\,\beta^2+\frac{1}{720}\,\beta^4+0(\beta^6)\right]+\sqrt{\frac{8\sin\beta}{F}} \tag{32}$$

For the vertical distance we set

$$y\sqrt{\frac{\beta}{F}}\,[\beta y_o(r)+\beta^3 y_1(r)+\beta^5 y_2(r)+\ldots] \tag{33}$$

together with equations (11), (27) the successive equations are

$$\frac{dy_o}{dr}=-\theta_o=-\frac{r^2}{2},\ \frac{dy_1}{dr}=-\theta_1+\frac{1}{6}\,\theta_o^3=\frac{r^6}{40} \tag{34}$$

$$\frac{dy_2}{dr}=-\theta_2+\frac{1}{2}\,\theta_o^2\theta_1-\frac{\theta_o^5}{120}=\frac{r^{10}}{1200} \tag{35}$$

Thus

$$b=2y(s^*)=2\beta\sqrt{\frac{\beta}{F}}\left(\frac{r^{*3}}{6}-\beta^2\,\frac{r^{*7}}{280}+\beta^4\,\frac{r^{*11}}{13200}+\ldots\right)$$

$$=\frac{2\beta}{3}\sqrt{\frac{2\beta}{F}}\left[1-\frac{1}{28}\,\beta^2+\frac{1}{5280}\,\beta^4+0(\beta^6)\right] \tag{36}$$

Numerical Solution

For Stages I, II′, and V, similarity does not exist since the radius R is a natural length scale. The numerical scheme is as follows. For given F and $\theta(0) = \beta$ we guess $d\theta/ds(0)$ and integrate equation (3) by the fifth order Runge-Kutta-Fehlberg algorithm until $s = \pi/2$. A solution is obtained if $\theta = 0$ there. If not $d\theta/ds(0)$ is adjusted. For given α the method is similar with a guessed $\theta(0)$. Using one-parameter shooting, the family of solutions for various F is obtained.

Perturbation Solution for Small F

When F is small in Stages I, II′, and V, the shape consists of almost circular arcs and we may expand as follows

$$\theta=\theta_o(z)+F\theta_1(z)+F^2\theta_2(z)+\ldots \tag{37}$$

where

$$\theta_o=z\equiv\beta\left(1-\frac{2s}{\pi}\right) \tag{38}$$

is a circular arc. Equation (3) gives

$$\frac{d^2\theta_1}{dz^2}=\frac{\pi^2}{4\beta^2}\cos z,\ \frac{d^2\theta_2}{dz^2}=-\frac{\pi^2}{4\beta^2}\,\theta_1\sin z \tag{39}$$

Both θ_1 and θ_2 are zero at $s = 0, \pi/2$. The solution is

$$\theta_1=\frac{\pi^2}{4\beta^2}\left[1-\cos z-\frac{(1-\cos\beta)}{\beta}\,z\right]$$

$$\theta_2=\frac{\pi^4}{16\beta^4}\left[\sin z-\frac{1}{8}\sin 2z\right.$$

$$\left.+\frac{(1-\cos\beta)}{\beta}\,(2-2\cos z-z\sin z)+C_1 z\right]$$

$$C_1=-\frac{\sin\beta}{\beta}+\frac{\sin 2\beta}{8\beta}$$

$$+\frac{(1-\cos\beta)}{\beta^2}\,(\beta\sin\beta+2\cos\beta-2) \tag{41}$$

Thus

$$\frac{d\theta}{ds}=-\frac{2\beta}{\pi}\left\{1+F\,\frac{\pi^2}{4\beta^2}\left[\sin z-\frac{(1-\cos\beta)}{\beta}\right]\right.$$

$$\left.+\frac{F^2\pi^4}{16\beta^4}\left[\cos z-\frac{1}{4}\cos 2z\right.\right.$$

Downloaded 03 May 2010 to 171.66.16.27. Redistribution subject to ASME license or copyright; see http://www.asme.org/terms/Terms_Use.cfm

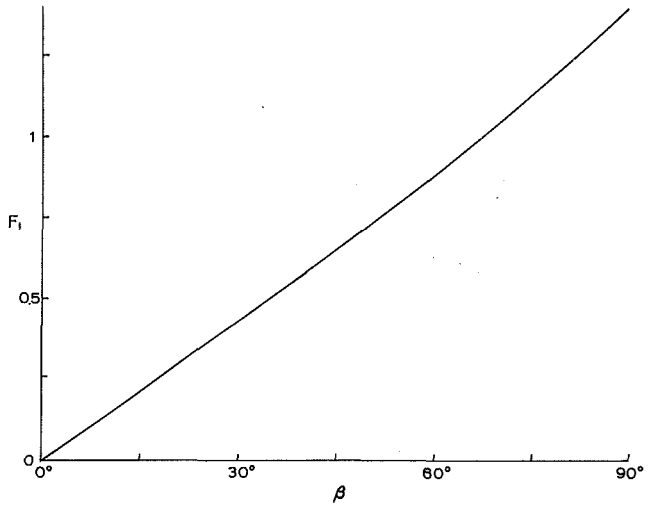


Fig. 3 The function $F_1(\beta)$

$$+\frac{(1-\cos\beta)}{\beta}(\sin z - z\cos z)+C_1\Big]+0(F^3)\Big\} \tag{42}$$

From equation (10)

$$x=\frac{1}{F}\left[\frac{d\theta}{ds}-\frac{d\theta}{ds}(0)\right] \tag{43}$$

$$a=2x\left(\frac{\pi}{2}\right)=\frac{\pi\sin\beta}{\beta}-\frac{F\pi^3}{4\beta^3}\left[\frac{1}{4}\right.$$

$$\left.-\frac{1}{4}\cos 2\beta-\frac{(1-\cos\beta)}{\beta}\sin\beta\right]+0(F^2) \tag{44}$$

For the vertical displacement we set

$$y=y_o(z)+Fy_1(z)+\ \ldots \tag{45}$$

in equation (11) to obtain

$$\frac{dy_o}{dz}=-\frac{\pi}{2\beta}\sin z,\quad \frac{dy_1}{dz}=-\frac{\pi}{2\beta}\theta_1\cos z, \tag{46}$$

The solution is

$$y_o=-\frac{\pi}{2\beta}(\cos\beta-\cos z)$$

$$y_1=-\frac{\pi^3}{8\beta^3}\left[\sin z-\frac{z}{2}-\frac{\sin 2z}{4}\right.$$

$$\left.-\frac{(1-\cos\beta)}{\beta}(z\sin z+\cos z)-C_2\right] \tag{47}$$

where

$$C_2=-\frac{(1-\cos\beta)\cos\beta}{\beta}-\frac{\beta}{2}+\frac{1}{4}\sin 2\beta \tag{48}$$

Therefore,

$$b=2y|_{z=o}=\frac{\pi}{\beta}(1-\cos\beta)+\frac{F\pi^3}{4\beta^3}\left(C_2+\frac{1-\cos\beta}{\beta}\right)+0(F^2) \tag{49}$$

For Stage I, $\beta = \pi/2$, for Stage V, β = const, for Stage II′, α is constant and β is obtained from an inversion of equation (42):

$$\beta=\frac{\alpha\pi}{2}\left\{1-\frac{F}{\alpha^2}\left[\sin\frac{\alpha\pi}{2}-\frac{2}{\alpha\pi}\left(1-\cos\frac{\alpha\pi}{2}\right)\right]\right.$$

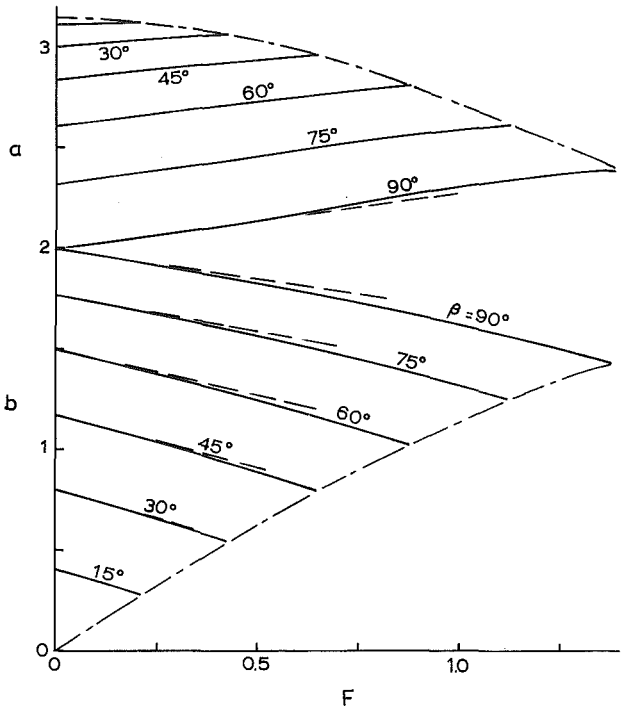


Fig. 4 Dimensions of the ring for Stage I and V. (— — —) approximations from equations (44), (49); (—•—•—) boundary of Stage V.

$$-\frac{2F^2}{\alpha^4}\left[\sin\frac{\alpha\pi}{2}-\frac{2}{\alpha\pi}\left(1-\cos\frac{\alpha\pi}{2}\right)\right]^2$$

$$-\frac{F^2}{\alpha^4}\left[\frac{1}{2}+\frac{1}{4}\cos\alpha\pi+\frac{\sin\frac{\alpha\pi}{2}}{2\alpha\pi}\left(4-7\cos\frac{\alpha\pi}{2}\right)\right.$$

$$\left.-\frac{8}{\alpha^2\pi^2}\left(1-\cos\frac{\alpha\pi}{2}\right)^2\right]+0(F^3)\Big\} \tag{50}$$

Results and Comparisons

Our exact numerical integration shows the conditions for the following compression stages:

Stage I: $0<F<1.39320$ and $\alpha\equiv R(\kappa_o-1/R_o)\geq\sqrt{2F}$

Stage II: $1.39320\leq F<\infty$ and $\alpha\geq\sqrt{2F}$ (minimum $\alpha=1.66925$)

Stage III: $0<F<1.39320$ and $\alpha<\sqrt{2F}$ (maximum $\alpha=1.66925$)

Stage III: $1.39320\leq F<\infty$ and $\alpha<\sqrt{2F}$

The boundary value of 1.39320 compares well with 1.392 obtained by Sonntag (1943) using elliptic functions. During compression F increases from 0 to a maximum $F_{\max}$. The relaxation will be perfectly elastic and reversible if $\alpha\geq\sqrt{2F_{\max}}$. The conditions for the plastic relaxation stages are:

Stage IV: $F_1<F<\infty$ and $\alpha<\sqrt{2F_{\max}}$

Stage V: $0<F\leq F_1$ and $\alpha<\sqrt{2F_{\max}}$

Figure 3 shows the value of F_1 as a function of β (the maximum angle at $F_{\max}$).

Figure 4 depicts the dimensions a, b of the crushed ring dur-

Downloaded 03 May 2010 to 171.66.16.27. Redistribution subject to ASME license or copyright; see http://www.asme.org/terms/Terms_Use.cfm

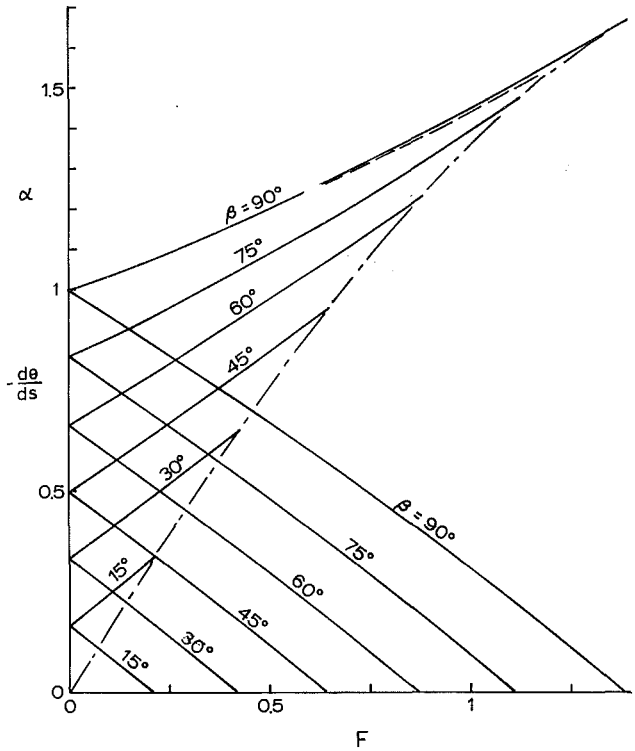


Fig. 5 Maximum and minimum curvature for Stage I and Stage V. (— — —) approximation from equation (42); (• — • —) boundary of Stage V. In Stage II′, α and F determines β.

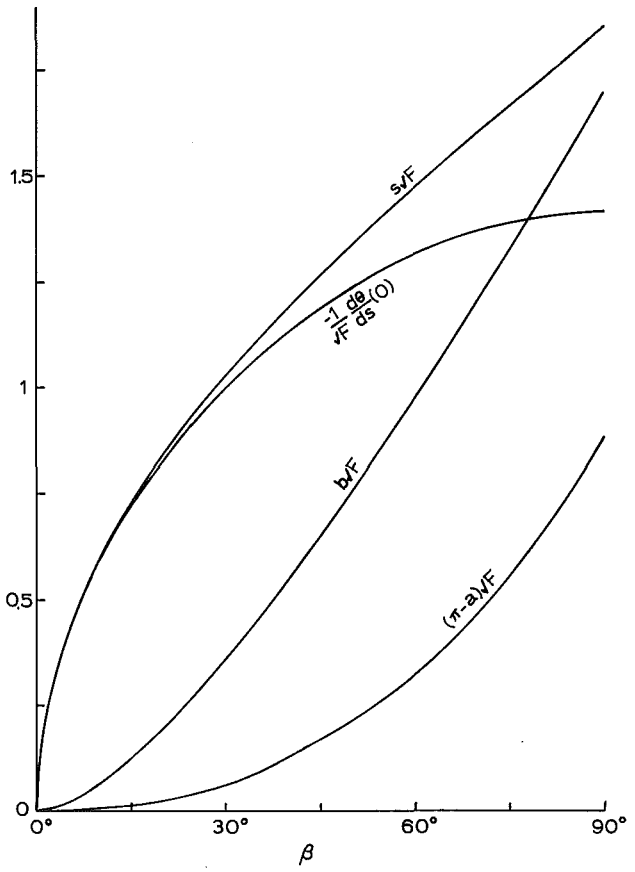


Fig. 6 Similarity solutions for Stage II and IV. Analytical solutions equations (24), (31) (32), and (36) are indistinguishable from exact numerical solutions.

Table 1 Similarity values at $\beta = \pi/2$ (Stage II)

$s^*\sqrt{F}$	1.85407	1.85284	equation (31)
$(\pi - a)\sqrt{F}$	0.879713	0.877246	equation (32)
$b\sqrt{F}$	1.69443	1.69469	equation (36)
$\left\lvert \frac{d\theta}{ds}(0) \right\rvert / \sqrt{F}$	$\sqrt{2}$	$\sqrt{2}$	equation (24)

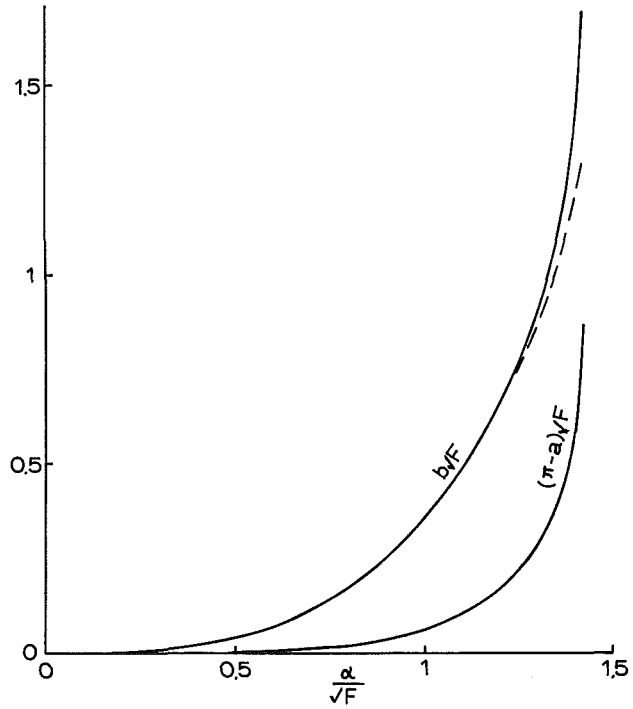


Fig. 7 Similarity solution for Stage III. Solid lines are from exact numerical integration and also from equations (25), (32), and (36). Dashed line is from equation (51).

ing Stage I (β = 90 deg) and Stage V (β = constant < 90 deg). Our linear approximations for small F, equations (44), (49) compare well with results from exact numerical integration.

Figure 5 shows the maximum curvature (at $s = 0$) and minimum curvature (at $s = \pi/2$) for Stages I and V. Our perturbation solution equation (42), although derived for small F, is surprisingly accurate (within 1 percent of exact numerical results) that only the worst case is shown. For Stage II′, α instead of β is a constant. Since $|d\theta/ds(0)| = \alpha > 1$, one obtains β from a horizontal intersecting line in the upper half of Fig. 5, then uses this value to determine the dimensions from Fig. 4.

Figure 6 shows the exact similarity solution for Stage II (at β = 90 deg) and Stage IV (β = const < 90 deg). In terms of similarity variables, one curve is sufficient to represent a family of curves. Our approximate solutions for small β, equations (31), (32), and (36) are now so accurate that they are indistinguishable from exact numerical results. Table 1 shows a comparison of the numerical values for the worst case (at $\beta = \pi/2$). For Stage III α is constant. One obtains β from the exact relation equation (25). Using this proceedure, $b\sqrt{F}$ is plotted against $\alpha/\sqrt{F}$ in Fig. 7, which also shows the high accuracy of equation (36). Now if the arc sine in equation (25) were expanded for large F and substituted into equation (36), we obtain

$$b\sqrt{F} = \frac{\alpha^3}{F\sqrt{F}}\left(\frac{1}{3} + \frac{\alpha^4}{56F^2} + \frac{3\alpha^8}{1408F^4} + \cdots\right) \tag{51}$$

Downloaded 03 May 2010 to 171.66.16.27. Redistribution subject to ASME license or copyright; see http://www.asme.org/terms/Terms_Use.cfm

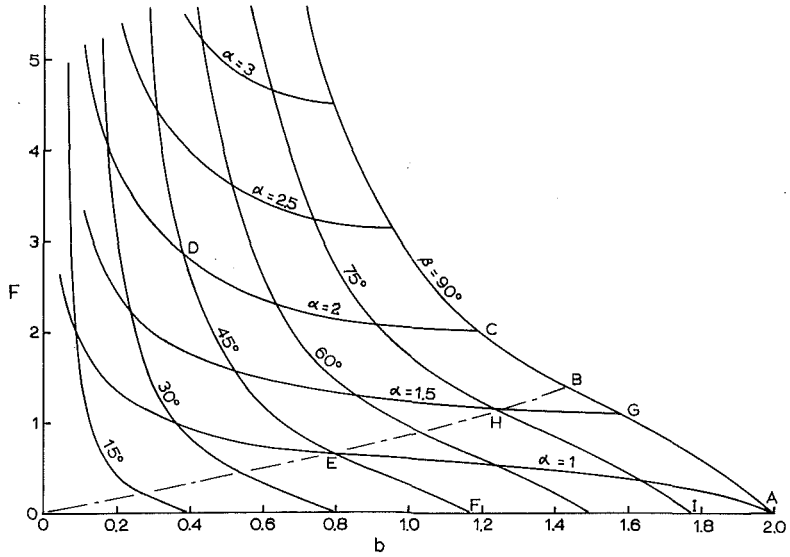


Fig. 8 The composite force-distance curves; (— — —) separates point contact stages and line contact stages

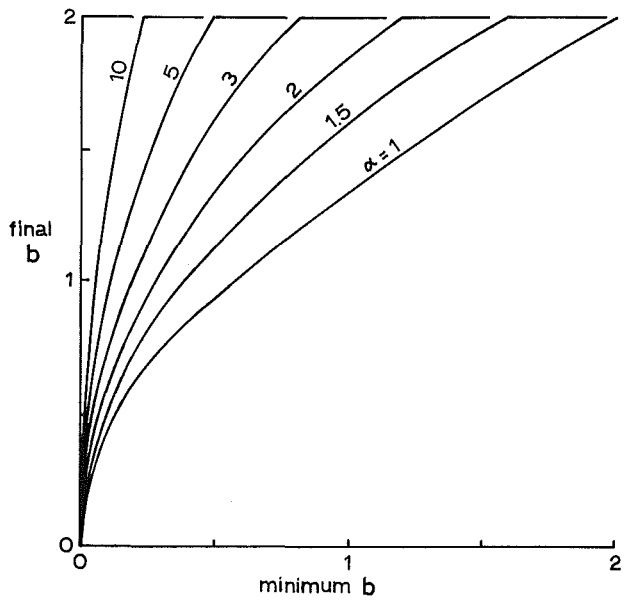


Fig. 9 The final recovered distance b as a function of minimum distance at maximum compression

This form agrees with the result obtained by the author (Wang, 1981b) when studying the related problem of unfolding a curved sheet. As shown in Fig. 7, equation (51) is less accurate in comparison with equations (25) and (36), implying the small radius of convergence of the arc sine expansion. These comparisons show the usefulness of analytic approximations, especially in view of tedious numerical integrations and elliptic integrals.

The Composite Force – Distance Curve

The force-(vertical) distance history of crushing an elastic-perfectly plastic ring can be constructed using the results obtained for the various stages. Figure 8 shows $F-b$ relation for various constant α and various constant β. For example, let us take a ring with $\alpha = 2$ and compress it between two parallel plates until the distance is 38 percent of the original radius before relaxation to zero compression. The history can be traced from Fig. 8 as follows. At point A the force is zero and the distance is 2. As compression increases the ring undergoes Stage I from A to B and Stage II from B to C. At C the maximum curvature reaches α and two plastic hinges develop. From C to D (Stage III) the ring experiences the irreversible deformation at constant α. Minimum distance $b = 0.38$ is reached at D where $F_{max} = 2.84$ and $\beta = 45$ deg. When F is decreased, the ring relaxes through Stage IV (DE) and Stage V (EF). The final, partially recovered ring is lens-shaped with a final distance of 1.175 at point F. The total work done is the area enclosed by $ABCDEFA$.

For $\alpha < 1.66925$ the compression-relaxation Stages may be fewer. For instance, at $\alpha = 1.5$, the history may be Stage I from A to G, Stage II′ from G to H and Stage V from H to I. For $\alpha = 1$, two stages may be sufficient. Note that all constant β lines are reversible and constant α lines are irreversible (towards the left only).

Figure 9 shows the final relaxed distance b as a function minimum distance at maximum compression. For example, if $\alpha = 2$ complete recovery is expected if minimum b is greater than 1.198 and partial recovery otherwise. In the limiting case of infinite F_{max} there is no recovery at all.

For real materials the constitutive relation in Fig. 1 will be replaced by a smooth continuous curve. In that case the problem can only be numerically integrated. By studying the elastic-perfectly plastic case we are able to make many analytical conclusions. It is hoped that the major features of the crushing process is not lost in the idealization.

References

DeRuntz, J. A., and Hodge, P. G., 1963, "Crushing of a Tube Between Rigid Plates," ASME JOURNAL OF APPLIED MECHANICS, Vol. 30, pp. 391–395.

Frisch-Fay, R., 1960, "The Deformation of Elastic Circular Rings," *Australian Journal of Applied Science*, Vol. 11, pp. 329–340.

Frisch-Fay, R., 1962, *Flexible Bars*, Butterworths, London.

Reid, S. R., and Reddy, T. Y., 1978, "Effect of Strain Hardening on the Lateral Compression of Tubes Between Rigid Plates," *International Journal of Solids Structures*, Vol. 14, pp. 213–225.

Smith, J. O., and Sidebottom, O. M., 1965, *Inelastic Behavior of Load-Carrying Members*, Wiley, New York, Chap. 4.

Sonntag, R., 1943, "Zur Theorie des Geschlossenen Kreisringes Mit Grosser Formanderung," *Ingenieur-Archiv*, Vol. 13, pp. 380–397.

Timoshenko, S. P., and Gere, J. M., 1961, *Theory of Elastic Stability*, 2nd Ed., McGraw-Hill, New York, Chap. 3.

Wang, C. Y., 1981a, "Folding of Elastica-Similarity Solutions," ASME JOURNAL OF APPLIED MECHANICS, Vol. 48, pp. 199–200.

Wang, C. Y., 1981b, "Unfolding a Curved Elastic Sheet," *Journal Mechanical Engineering Science*, Vol. 23, pp. 217–219.

Downloaded 03 May 2010 to 171.66.16.27. Redistribution subject to ASME license or copyright; see http://www.asme.org/terms/Terms_Use.cfm

Asymptotic Solutions for Warping and Distortion of Thin-Walled Box Beams

C. D. Balch
Mem. ASME

C. R. Steele
Fellow ASME

Division of Applied Mechanics,
Department of Mechanical Engineering,
Stanford University,
Stanford, CA 94305

The equations of conventional thin plate theory are used to formulate an eigenvalue problem for effects of self-equilibrating end loads in thin-walled rectangular cross section tubes, or box beams. The problem is analyzed by a perturbation procedure, which is based on a small parameter proportional to the square root of the ratio of wall thickness to cross section width. Solution of the unperturbed problem yields a family of membrane and inextensional end-effect eigenfunctions which are found to have decay distances on the order of the beam width or shorter. The perturbation procedure is carried out to obtain closed form asymptotically valid solutions for warping and distortional effects which decay much more slowly. These asymptotic solutions compare favorably with previous analytical and experimental results.

1 Introduction

The thin-walled rectangular closed cross section tube, or box beam, is a common structural element in the frameworks of bridges, buildings, and motor vehicles. It is typically viewed as effective and economical for carrying torsion and bending loads. In addition to torsion and beam bending, however, generalized loads which distort and warp the beam cross section can be applied. The box beam is relatively flexible with respect to these deformations, which are associated with plate bending of the thin walls.

Vlasov (1961) showed that distortional effects can be described by a fourth order ODE in a displacement quantity, analogous to the beam on elastic foundation. This "BEF" analogy was further developed by Wright et. al. (1968) as a tool for predicting warping and distortional stresses. In the BEF analogy, the beam behavior arises from in-plane bending of the box beam walls, and the elastic foundation effect is provided by the cross section's transverse bending stiffness, or resistance to distortion. Kŕístek (1970a) carried out an analysis for tapered deformable sections, representing the flexible cross section by an equivalent frame. Recently, Boswell and Zhang (1984) have presented an analytical approach for distortion of thin-walled box-spine beams, which also leads to a BEF-type equation.

In this paper, an asymptotic solution for the box beam distortion problem is developed under the assumptions of conventional thin plate theory, relying on a small perturbation parameter proportional to the square root of the ratio of wall thickness to cross section width. Distortion is examined as a special case of the more general problem of self-equilibrating end loads, the effects of which decay exponentially along the beam's length.

The present work differs from the previous contributions in that the only assumptions made are those of classical plane stress and plate bending behavior in the small displacement linear elastic regime. No other kinematic assumptions (e.g., negligible in-plane shear strain), or assumptions regarding stress distributions (e.g., linear variation along the section contour) are made. Attention is, however, restricted to closed rectangular cross sections of uniform thickness.

End effects are represented by a set of eigenfunctions of the type introduced by Papkovitsch (1940) and Fadle (1941) for the problem of a semi-infinite plate strip with prescribed loading at one end. (See also Timoshenko and Goodier, 1970). Several studies of end effects have utilized the "Papkovitsch-Fadle" eigenfunctions and related functions. For example, orthogonalization procedures and a variational approach based on the eigenfunctions are proposed by Horvay (1957) and Horvay and Born (1957). Benthem (1963) presents a related Laplace transform technique and applies it to the analysis of corner stress singularities. Biorthogonality properties are discussed by Smith (1952) and more generally by Johnson and Little (1964). A completeness proof for the Papkovitsch-Fadle eigenfunctions is provided by Gregory (1980). Generalizations of the eigenfunctions to curved plate strips (Ramachandra-Rao, 1976) and anisotropic behavior (Choi and Horgan, 1977) are also possible.

In the present work, the eigenvalue problem is formulated and solved for the box beam as an assembly of plate strips. The asymptotic distortional solution is compared with previous results, and some general observations are made regarding Saint-Venant end effects in thin-walled box beams.

Contributed by the Applied Mechanics Division for presentation at the 1987 Applied Mechanics, Biomechanics, and Fluids Engineering Conference, Cincinatti, OH, June 14-17, 1987, of the American Society of Mechanical Engineers.

Discussion of this paper should be addressed to the Editorial Department, ASME, United Engineering Center, 345 East 47th Street, New York, N.Y. 10017, and will be accepted until two months after final publication of the paper itself in the JOURNAL OF APPLIED MECHANICS. Manuscript received by ASME Applied Mechanics Division, January 22, 1986; final revision, April 26, 1986.
Paper No. 87-APM-15.

Copyright © 1987 by ASME
Downloaded 03 May 2010 to 171.66.16.27. Redistribution subject to ASME license or copyright; see http://www.asme.org/terms/Terms_Use.cfm

Table 1 Dimensionless continuity conditions along an edge of the box beam

Plane Stress Problem	Plate Bending Problem
$\frac{\partial^2\bar{\phi}^I}{\partial\xi^2}-\nu\frac{\partial^2\bar{\phi}^I}{\partial\eta^2}=\frac{\partial^2\bar{\phi}^{II}}{\partial\xi^2}-\nu\frac{\partial^2\bar{\phi}^{II}}{\partial\eta^2}$	$\frac{\partial^2\bar{w}^I}{\partial\xi^2}+\nu\frac{\partial^2\bar{w}^I}{\partial\eta^2}=\frac{\partial^2\bar{w}^{II}}{\partial\xi^2}+\nu\frac{\partial^2\bar{w}^{II}}{\partial\eta^2}$
$\frac{\partial^2\bar{\phi}^I}{\partial\xi\partial\eta}=\frac{\partial^2\bar{\phi}^{II}}{\partial\xi\partial\eta}$	$\frac{\partial^2\bar{w}^I}{\partial\xi\partial\eta}=\frac{\partial^2\bar{w}^{II}}{\partial\xi\partial\eta}$
$\frac{\partial^2\bar{\phi}^I}{\partial\eta^2}=-\epsilon^2\left[\frac{\partial^3\bar{w}^{II}}{\partial\xi^3}+(2-\nu)\frac{\partial^3\bar{w}^{II}}{\partial\xi\partial\eta^2}\right]$	$\frac{\partial^2\bar{w}^I}{\partial\eta^2}=\epsilon^2\left[\frac{\partial^3\bar{\phi}^{II}}{\partial\xi^3}+(2+\nu)\frac{\partial^3\bar{\phi}^{II}}{\partial\xi\partial\eta^2}\right]$
$\frac{\partial^2\bar{\phi}^{II}}{\partial\eta^2}=\epsilon^2\left[\frac{\partial^3\bar{w}^I}{\partial\xi^3}+(2-\nu)\frac{\partial^3\bar{w}^I}{\partial\xi\partial\eta^2}\right]$	$\frac{\partial^2\bar{w}^{II}}{\partial\eta^2}=-\epsilon^2\left[\frac{\partial^3\bar{\phi}^I}{\partial\xi^3}+(2+\nu)\frac{\partial^3\bar{\phi}^I}{\partial\xi\partial\eta^2}\right]$

2 Governing Equations and Continuity Conditions

The thin-walled box beam and coordinate system are shown in Fig. 1. The circumferential coordinate (along the midsurface of the cross section) is denoted by **x**, and the axial coordinate is denoted by **y**. The usual biharmonic equations apply to each of the beam walls (also referred to as strips):

$$\nabla^2\nabla^2\phi=0$$
$$\nabla^2\nabla^2 w=0 \tag{1}$$

where $\phi(x,y)$ is an Airy stress function, $w(x,y)$ is the outward normal displacement of the strip, and

$$\nabla^2=\frac{\partial^2}{\partial x^2}+\frac{\partial^2}{\partial y^2}.$$

The stress resultants (force/length) N_x, N_y, and N_{xy} are given by:

$$N_x=\frac{\partial^2\phi}{\partial y^2}$$
$$N_y=\frac{\partial^2\phi}{\partial x^2} \tag{2}$$
$$N_{xy}=-\frac{\partial^2\phi}{\partial x\partial y}$$

The initial analysis concerns the semi-infinite box beam with prescribed boundary tractions (or displacements) at $y=0$ and no other loads; hence equations (1) are homogeneous.

Consider the edge $x=a$ shared by strips *I* and *II* (see Fig. 1). (Symmetry conditions will obviate the need to examine any other edges.) The following kinematic continuity conditions must be satisfied along this edge:

$$\epsilon_y^I=\epsilon_y^{II}$$
$$\frac{\partial^2 w^I}{\partial x\partial y}=\frac{\partial^2 w^{II}}{\partial x\partial y}$$
$$\frac{\partial^2 w^I}{\partial y^2}=-\frac{\partial^2 u^{II}}{\partial y^2} \tag{3}$$
$$\frac{\partial^2 w^{II}}{\partial y^2}=\frac{\partial^2 u^I}{\partial y^2}$$

where ϵ_y is axial strain, and u and w are the midplane displacements in the x and normal directions. The superscript (*I, II*) indicates strip (*I, II*), and all the quantities are evaluated in the limit as the edge is approached from the indicated side. (Note that the normal is not uniquely defined on the edge.)

The following equilibrium conditions must hold also along the edge $x=a$:

$$N_{xy}^I=N_{xy}^{II}$$
$$N_x^I=V_x^{II}$$
$$N_x^{II}=-V_x^I \tag{4}$$
$$M_x^I=M_x^{II}$$

where M_x and V_x are moment and Kirchoff shear resultants.

Equations (3) and (4) can be written in terms of the stress function ϕ and normal displacement w, making use of equations (2) and the following relations:

$$\epsilon_y=\frac{1}{Et}(N_y-\nu N_x)$$

$$\frac{\partial^2 u}{\partial y^2}=-\frac{1}{Et}\left[\frac{\partial^3\phi}{\partial x^3}+(2+\nu)\frac{\partial^3\phi}{\partial x\partial y^2}\right]$$

$$M_x=-D\left(\frac{\partial^2 w}{\partial x^2}+\nu\frac{\partial^2 w}{\partial y^2}\right) \tag{5}$$

$$V_x=-D\left[\frac{\partial^3 w}{\partial x^3}+(2-\nu)\frac{\partial^3 w}{\partial x\partial y^2}\right]$$

where

$$D=Etc^2 \tag{6}$$
$$c=t/[12(1-\nu^2)]^{1/2} \tag{7}$$

are the plate bending stiffness of the walls and the "reduced thickness." To facilitate the perturbation approach, it is convenient to render the equations dimensionless by employing the coordinates:

$$\xi=x/a$$
$$\eta=y/a \tag{8}$$

the dimensionless variables:

$$\bar{\phi}=\phi/(Eta^2)$$
$$\bar{w}=wc/a^2 \tag{9}$$

and the small perturbation parameter ϵ defined by:

$$\epsilon=(c/a)^{1/2} \tag{10}$$

Relations (5–10) enable the continuity equations (3) and (4) to be cast in the dimensionless form given in Table 1. Examination of Table 1 reveals the analogous structure of the plane stress and plate bending contributions. In the limit $\epsilon\to 0$ (diminishing thickness), the eight edge continuity conditions decouple into four membrane conditions and four inextensional bending conditions.

3 Box Beam End Effects

End effects in the semi-infinite thin-walled box beam can be represented by the following solutions to equations (1) (see, e.g., Timoshenko and Goodier, 1970):

Downloaded 03 May 2010 to 171.66.16.27. Redistribution subject to ASME license or copyright; see http://www.asme.org/terms/Terms_Use.cfm

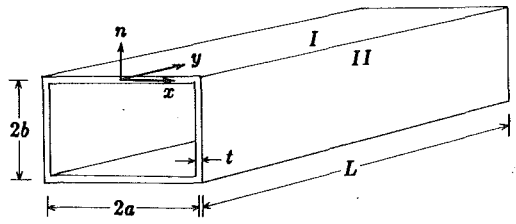


Fig. 1 The thin-walled box beam and coordinate system

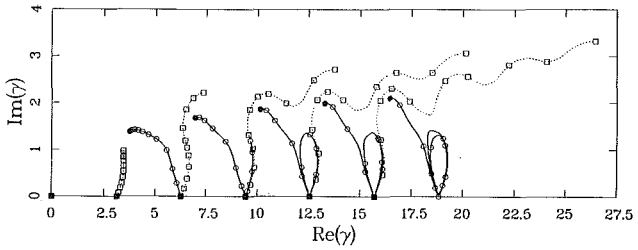


Fig. 2 Root loci of the first 11 eigenvalues γ_0 (roots of equation (21)) as a function of $\alpha = b/a$. Roots are located at dark circles and squares for $\alpha = 1$. Light circles and squares indicate root locations as α decreases to 0.5 by increments of 0.05.

$$\Phi = \begin{bmatrix} \bar{\phi}^I \\ \bar{\phi}^{II} \\ \bar{w}^I \\ \bar{w}^{II} \end{bmatrix} = e^{-\gamma\eta} \begin{bmatrix} A^I \sin\gamma\xi + B^I \gamma\xi\cos\gamma\xi \\ A^{II}\sin\gamma\xi + B^{II}\gamma\xi\cos\gamma\xi \\ C^I \sin\gamma\xi + D^I\gamma\xi\cos\gamma\xi \\ C^{II}\sin\gamma\xi + D^{II}\gamma\xi\cos\gamma\xi \end{bmatrix} \tag{11}$$

where the superscript (I, II) refers to strip (I, II), and the quantities γ, $A^{(I,II)}$, $B^{(I,II)}$, $C^{(I,II)}$, and $D^{(I,II)}$ are unknown constants to be determined. For purposes of notational simplicity, the $\xi = 0$ reference point for a given strip is taken to coincide with the x coordinate of that strip's line of symmetry.

The chosen eigenfunctions are antisymmetric, corresponding to odd symmetry about each of the beam's principle axes. Three other cases can be obtained by interchanging sines and cosines on either or both strips. For purposes of the present analysis, only the odd-odd case will be treated, because the distortional effects to be discussed possess this symmetry. The other symmetry cases are analogous, and are omitted for brevity.

Solutions of a form similar to equation (11), but with oscillating behavior in η and exponential behavior in ξ were obtained by Křístek (1970b) for the transverse loading problem. These solutions and others based on the "Elasticity Method" of folded plate theory (see, e.g., Goldberg and Leve, 1957, or DeFries-Skene and Scordelis, 1964) are not suitable for the end effect problem.

Substituting the solutions (11) into the continuity equations of Table 1 and collecting terms on the left-hand side yields the following eigenvalue problem:

$$\begin{bmatrix} & & & \\ [M]_{11} & \epsilon^2[M]_{12} & & \\ & & & \\ \epsilon^2[M]_{21} & [M]_{22} & & \end{bmatrix} \begin{bmatrix} A^I \\ B^I \\ A^{II} \\ B^{II} \\ C^I \\ D^I \\ C^{II} \\ D^{II} \end{bmatrix} = \begin{bmatrix} 0 \\ 0 \\ 0 \\ 0 \\ 0 \\ 0 \\ 0 \\ 0 \end{bmatrix} \tag{12}$$

where

$$[M_{11}(\gamma;\alpha,\nu)] = \begin{bmatrix} (1+\nu)\sin\gamma & 2\sin\gamma + (1+\nu)\gamma\cos\gamma & (1+\nu)\sin\alpha\gamma & 2\sin\alpha\gamma + (1+\nu)\alpha\gamma\cos\alpha\gamma \\ -\cos\gamma & \gamma\sin\gamma - \cos\gamma & \cos\alpha\gamma & \cos\alpha\gamma - \alpha\gamma\sin\alpha\gamma \\ \sin\gamma & \gamma\cos\gamma & 0 & 0 \\ 0 & 0 & \sin\alpha\gamma & \alpha\gamma\cos\alpha\gamma \end{bmatrix} \tag{13}$$

$$[M_{12}(\gamma;\alpha,\nu)] = \begin{bmatrix} 0 & 0 & 0 & 0 \\ 0 & 0 & 0 & 0 \\ 0 & 0 & (1-\nu)\gamma\cos\alpha\gamma & -[(1-\nu)\alpha\gamma^2\sin\alpha\gamma + (1+\nu)\gamma\cos\alpha\gamma] \\ (1-\nu)\gamma\cos\gamma & -[(1-\nu)\gamma^2\sin\gamma + (1+\nu)\gamma\cos\gamma] & 0 & 0 \end{bmatrix} \tag{14}$$

$$[M_{22}] = [M_{11}(\gamma;\alpha,-\nu)] \tag{15}$$

$$[M_{21}] = -[M_{12}(\gamma;\alpha-\nu)] \tag{16}$$

The parameter $\alpha = b/a$ is the cross section aspect ratio, and the decay coefficient γ of equation (11) is an unknown eigenvalue.

In order to proceed with the perturbation approach, the following expansions are utilized:

$$\gamma = \gamma_0 + \epsilon\gamma_1 + \epsilon^2\gamma_2 + \ldots \tag{17}$$

$$\{X\} = \{X_0\} + \epsilon\{X_1\} + \epsilon^2\{X_2\} + \ldots \tag{18}$$

$$[M] = [M_0] + \epsilon[M_1] + \epsilon^2[M_2] + \ldots \tag{19}$$

where $[M]$ and $\{X\}$ denote the 8×8 matrix and 8×1 eigenvector of equation (12).

Consider the unperturbed case $\epsilon = 0$. From equations (11), (12) it is evident that the plane stress and plate bending eigenvalue problems decouple. The characteristic equations are:

$$\begin{aligned} \det[M_{11}(\gamma_0)] &= 0 \\ \det[M_{22}(\gamma_0)] &= 0 \end{aligned} \tag{20}$$

Either of equations (20) leads to the equation:

$$\sin^2\alpha\gamma_0(2\gamma_0 - \sin 2\gamma_0) + \sin^2\gamma_0(2\alpha\gamma_0 - \sin 2\alpha\gamma_0) = 0 \tag{21}$$

Equation (21) is transcendental and possesses an infinite set of complex valued roots $\gamma_0^{(k)}$; $k = 0, 1, 2 \ldots$; which depend parametrically on α. The real and imaginary parts of the corresponding eigenfunctions $\Phi^{(k)}$ each provide an independent solution to equations (1); thus a set of basis functions for end effects is obtained.

The loci of the first 11 roots of equation (21) as a function of the parameter α are depicted in Fig. 2 for $0.5 \le \alpha \le 1$. Figure 2 shows only the first quadrant roots, but note that if γ_0 is a root of equation (21), the values $-\gamma_0$, $\bar{\gamma}_0$, and $-\bar{\gamma}_0$ are also roots. The dark circles and squares (see Fig. 2) indicate the locations of the roots for $\alpha = 1$ (square cross section), and the light circles and squares indicate new locations as α is decreased from 1 by increments of 0.05. Two types of roots are identified in Fig. 2:

(1) Roots which move asymptotically to infinity as α decreases, (loci are dotted lines marked with squares); and

(2) Roots with convoluted loci near the real axis; (loci are solid lines marked with circles).

Note that the seemingly trivial root at $\gamma_0 = 0$ is an exception

Downloaded 03 May 2010 to 171.66.16.27. Redistribution subject to ASME license or copyright; see http://www.asme.org/terms/Terms_Use.cfm

and does not depend on α. A modified Newton-Raphson procedure was employed in locating the roots of Eq. (21).

The eigenfunction coefficients A_0, B_0, C_0, and D_0 are given in Appendix A. If an eigenvalue $\gamma_0^{(k)}$ is real, the eigenfunction $\Phi^{(k)}$ has no imaginary part; thus one basis function is apparently lost. (This corresponds to the coalescing of a root with its conjugate.) It can be shown in this case that $B_0^{(I,II)} = D_0^{(I,II)} = 0$ in equation (11) and a second solution exists of the form:

$$\Phi^{(k)*} = \eta\Phi^{(k)} \tag{22}$$

which is equivalent to the Levy-type solution for the rectangular plate.

The behavior of an eigenfunction $\Phi^{(k)}$ can be deduced from the location of the eigenvalue $\gamma_0^{(k)}$. For $\mathbf{Re}(\gamma_0^{(k)}) \sim O(1)$, the end-effect eigenfunction has a decay distance of $O(a)$ along the beam axis. If $\mathbf{Re}(\gamma_0^{(k)})$ is large, the function $\Phi^{(k)}$ oscillates rapidly in the ξ direction, and decays rapidly in the η direction. Figure 2 indicates that the unperturbed eigenfunctions have decay distances $O(a)$ or shorter.

At this point, it appears as though the perturbation procedure need not be carried further, since for sufficiently thin-walled sections with $\epsilon << 1$, the membrane and inextentional bending solutions given by equation (11) (with γ determined by equation (21)) should yield a complete basis of end-effect eigenfunctions, accurate to $O(\epsilon)$.

Consider, however, the solution to equation (21) $\gamma_0^{(0)} = 0$. For $\epsilon << 1$, this root can be expressed:

$$\gamma^{(0)} = \epsilon\gamma_1^{(0)} + \epsilon^2\gamma_2^{(0)} + \ldots \tag{23}$$

This suggests a slowly decaying end effect, which becomes nondecaying as $\epsilon \to 0$. The unperturbed problem yields no nontrivial solution corresponding to this root; so the perturbation procedure is continued in order to obtain an asymptotically valid expression for this solution, which will be seen to describe cross section distortion.

4 Asymptotic Solution for γ Near Zero

From equations (12), (18), and (19), the following expansion is obtained:

$$[M]\{X\} = [M_0]\{X_0\} + \epsilon([M_0]\{X_1\} + [M_1]\{X_0\}) + \epsilon^2([M_0]\{X_2\} + [M_1]\{X_1\} + [M_2]\{X_0\}) + \ldots = \{0\} \tag{24}$$

where it is assumed that the perturbation is carried out for the case of interest $\gamma_0 = 0$, and the identifying superscript in equation (23) is dropped for simplicity. The explicit expressions for $[M_0]$, $[M_1]$, and $[M_2]$, which depend on γ, are given in Appendix B. The unknown coefficients γ_i are to be determined along with the coefficient vectors $\{X_i\}$ by examination of equation (24). The terms in each power of ϵ must vanish independently.

The zeroth order problem in ϵ is:

$$[M_0]\{X_0\} = \{0\} \tag{25}$$

and has the solution:

$$\{X_0\} = k_0 \begin{bmatrix} \alpha \\ -\alpha \\ -1 \\ 1 \\ 0 \\ 0 \\ 0 \\ 0 \end{bmatrix} + k_0' \begin{bmatrix} 0 \\ 0 \\ 0 \\ 0 \\ \alpha \\ -\alpha \\ -1 \\ 1 \end{bmatrix} \tag{26}$$

where k_0 and k_0' are (thus far) arbitrary constants. The solution (26) can be verified from the form of $[M_0]$ (see Appendix B).

The first order problem in ϵ can be written:

$$[M_0]\{X_1\} = -[M_1]\{X_0\} \tag{27}$$

The right hand side of equation (27) equals $\{0\}$ (see Appendix B), which leads to a solution for $\{X_1\}$:

$$\{X_1\} = k_1\{X_0\} \tag{28}$$

where k_1 can be chosen arbitrarily since it affects only the overall multiplicative constant as follows:

$$\{X_0\} + \epsilon\{X_1\} = (1 + k_1\epsilon)\{X_0\} \tag{29}$$

The second order problem in ϵ can be written:

$$[M_0]\{X_2\} = -[M_1]\{X_1\} - [M_2]\{X_0\} \tag{30}$$

Taking $k_1 = 0$ in equation (28) and substituting equations (26), (28) into equation (30) yields:

$$[M_0]\{X_2\} = k_0 \begin{bmatrix} -\frac{2+\nu}{3}\alpha(1-\alpha^2)\gamma_1^3 \\ \alpha(1+\alpha)\gamma_1^2 \\ -\frac{1}{3}\alpha\gamma_1^3 \\ \frac{1}{3}\alpha^3\gamma_1^3 \\ 0 \\ 0 \\ -2\gamma_1 \\ 2\alpha\gamma_1 \end{bmatrix} + k_0' \begin{bmatrix} 0 \\ 0 \\ 2\gamma_1 \\ -2\alpha\gamma_1 \\ -\frac{2-\nu}{3}\alpha(1-\alpha^2)\gamma_1^3 \\ \alpha(1+\alpha)\gamma_1^2 \\ -\frac{1}{3}\alpha\gamma_1^3 \\ \frac{1}{3}\alpha^3\gamma_1^3 \end{bmatrix} \tag{31}$$

Note, however, that $[M_0]$ is singular. In order for a solution of equation (31) to exist, the right-hand side of equation (31), denoted by $\{R_2\}$, must satisfy:

$$\{R_2\}^{\mathbf{T}}\{V_i\} = \{0\} \tag{32}$$

where $\{V_i\}$ represents the set of vectors which satisfy:

$$[M_0]^{\mathbf{T}}\{V_i\} = \{0\} \tag{33}$$

and the superscript $\mathbf{T}$ denotes transposition.

It can be verified from the form of $[M_0]$ that the $\{V_i\}$ are, up to a multiplicative constant, given by:

$$\{V_1\} = \begin{bmatrix} 0 \\ \alpha\gamma_1 \\ \alpha \\ -1 \\ 0 \\ 0 \\ 0 \\ 0 \end{bmatrix}; \quad \{V_2\} = \begin{bmatrix} 0 \\ 0 \\ 0 \\ 0 \\ 0 \\ \alpha\gamma_1 \\ \alpha \\ -1 \end{bmatrix} \tag{34}$$

Substitution of the right-hand side of equation (31) and the vectors given by equations (34) into equation (32) provides a secondary eigenvalue problem in k_0, k_0', and γ_1:

$$\begin{bmatrix} \frac{1}{3}\alpha(1+\alpha)\gamma_1^2 & 2 \\ 2 & -\frac{1}{3}\alpha(1+\alpha)\gamma_1^2 \end{bmatrix} \begin{bmatrix} k_0 \\ k_0' \end{bmatrix} = \begin{bmatrix} 0 \\ 0 \end{bmatrix} \tag{35}$$

Downloaded 03 May 2010 to 171.66.16.27. Redistribution subject to ASME license or copyright; see http://www.asme.org/terms/Terms_Use.cfm

The determinant of the 2×2 matrix of equation (35) must equal zero, which yields:

$$\gamma_1^4+\frac{36}{\alpha^2(1+\alpha)^2}=0 \tag{36}$$

Equation (36) has the four roots:

$$\gamma_1=\left[\frac{6}{\alpha(1+\alpha)}\right]^{1/2} e^{i\pi(1.+2n)/4} \tag{37}$$

where $n=0, 1, 2, 3$.

Consider the first quadrant root corresponding to $n=0$. For this root, equation (35) leads to:

$$k_0'=-ik_0 \tag{38}$$

Equations (37) and (38) can now be substituted into equation (31), and the solution for $\{X_2\}$ is obtained:

$$\{X_2\}=\begin{bmatrix} A_2^{\mathrm{I}} \\ B_2^{I} \\ A_2^{\mathrm{II}} \\ B_2^{\mathrm{II}} \\ C_2^{\mathrm{I}} \\ D_2^{\mathrm{I}} \\ C_2^{\mathrm{II}} \\ D_2^{\mathrm{II}} \end{bmatrix} =\frac{k_0}{(1+\alpha)(1+\alpha^2)}\begin{bmatrix} -i(4+\alpha+\alpha^3) \\ -i(\alpha+4\alpha^2+\alpha^3) \\ i(1+\alpha^2+4\alpha^3) \\ i(1+4\alpha+\alpha^2) \\ -(4+\alpha+\alpha^3) \\ -(\alpha+4\alpha^2+\alpha^3) \\ (1+\alpha^2+4\alpha^3) \\ (1+4\alpha+\alpha^2) \end{bmatrix} \tag{39}$$

$$+\frac{k_0\nu(1-\alpha)}{(1+\alpha^2)}\begin{bmatrix} -i \\ i \\ -i\alpha \\ i\alpha \\ 1 \\ -1 \\ \alpha \\ -\alpha \end{bmatrix} +k_2\begin{bmatrix} \alpha \\ -\alpha \\ -1 \\ 1 \\ 0 \\ 0 \\ 0 \\ 0 \end{bmatrix} +k_2'\begin{bmatrix} 0 \\ 0 \\ 0 \\ 0 \\ \alpha \\ -\alpha \\ -1 \\ 1 \end{bmatrix}$$

where k_0 is the arbitrary constant appearing in equation (26), and k_2 and k_2' (which drop out in the subsequent analysis) are additional arbitrary constants for the homogeneous contributions. The matrix algebra was carried out with the aid of the symbolic manipulation program MACSYMA (1983).

The eigenfunction corresponding to the perturbed eigenvalue can now be evaluated, utilizing the expansions:

$$\gamma=\epsilon\gamma_1+\mathbf{O}(\epsilon^2) \tag{40}$$

$$\{X\}=\{X_0\}+\epsilon^2\{X_2\}+\mathbf{O}(\epsilon^3) \tag{41}$$

where ϵ is given by equation (10), γ_1 is given by equation (37) (with $n=0$), $\{X_0\}$ is given by equations (26), (38), and $\{X_2\}$ is given by equation (39). The vector $\{X\}$ provides the eight coefficients required in the eigenfunctions (11).

For the stress function (either strip) in equation (11), equations (40), (41) lead to:

$$\bar{\phi}\cong e^{-\epsilon\gamma_1\eta}\{(A_0+\epsilon^2A_2)[\epsilon\gamma_1\xi-(\epsilon\gamma_1\xi)^3/6] +(B_0+\epsilon^2B_2)[\epsilon\gamma_1\xi-(\epsilon\gamma_1\xi)^3/2]\} \tag{42}$$

where the two-term Taylor series expansion used in ξ is uniformly convergent because $|\xi|\le 1$, and $\epsilon\gamma_1<<1$. Collecting the leading terms in ϵ, equation (42) becomes:

$$\bar{\phi}\cong\epsilon^3e^{-\epsilon\gamma_1\eta}\left[(A_2+B_2)\gamma_1\xi-\frac{1}{6}(A_0+3B_0)\gamma_1^3\xi^3\right] \tag{43}$$

Evaluating $\bar{\phi}^I$, $\bar{\phi}^{II}$, $\bar{w}^I$, and $\bar{w}^{II}$ in this manner, substituting for the coefficients from equations (26), (39), and defining a new arbitrary multiplicative constant $\bar{k}$ yields:

$$\begin{bmatrix} \bar{\phi}^I \\ \bar{\phi}^{II} \\ \bar{w}^I \\ \bar{w}^{II} \end{bmatrix} =\bar{k}e^{-\epsilon\gamma_1\eta}\begin{bmatrix} if^I(\xi) \\ if^{II}(\xi) \\ f^I(\xi) \\ f^{II}(\xi) \end{bmatrix} +O(\epsilon) \tag{44}$$

where

$$f^I(\xi)=\frac{1}{6}\xi^3-\frac{2+\alpha}{6}\xi$$

$$f^{II}(\xi)=-\frac{1}{6\alpha}\xi^3-\frac{1+2\alpha}{6}\xi \tag{45}$$

The real and imaginary parts of equation (44) provide two asymptotically valid solutions to the box beam end effect problem. These solutions decay much more slowly in the axial direction than the eigenfunctions corresponding to the nonzero roots of equation (21), but the solutions (44) are needed to complete the basis set for end effects.

5 Interpretation of the Asympototic Solution

It is convenient to define a real parameter

$$\lambda=\epsilon\left[\frac{3}{\alpha(1+\alpha)}\right]^{1/2} \tag{46}$$

so that

$$\epsilon\gamma_1=\lambda(1+i) \tag{47}$$

After substitution of equation (47) into equation (44), equations (2) are used to compute the following expressions for the axial stress and shear resultants:

$$\begin{Bmatrix} N_y^I \\ N_y^{II} \end{Bmatrix}\cong\bar{k}Ete^{-\lambda\eta}(\sin\lambda\eta+i\cos\lambda\eta)\begin{Bmatrix} \xi \\ -\xi/\alpha \end{Bmatrix} \tag{48}$$

$$\begin{Bmatrix} N_{xy}^I \\ N_{xy}^{II} \end{Bmatrix}\cong\bar{k}Et\lambda e^{-\lambda\eta}[(\cos\lambda\eta-\sin\lambda\eta) -i(\cos\lambda\eta+\sin\lambda\eta)]\begin{Bmatrix} \frac{\xi^2}{2}-\frac{2+\alpha}{6} \\ -\frac{\xi^2}{2\alpha}+\frac{1+2\alpha}{6} \end{Bmatrix} \tag{49}$$

where the superscript (*I*, *II*) refers to strip (*I*, *II*).

The axial stress resultant given by equation (48) varies linearly with ξ, reaching maximum values at the corners ($\xi=1$ for strip *I*; $\xi=-\alpha$ for strip *II*). This is the "bimoment" state discussed by Vlasov (1961). Equation (49) gives the shear resultant, which varies parabolically along the cross section contour but changes sign in the vicinity of the edge. This type of shear distribution at $\eta=0$ is a distortional end load.

Note that at the end $\eta=0$, both real and imaginary parts of the solution possess a distortional (shear) component but only the imaginary part possesses axial warping stress. It is therefore possible to construct linear combinations with arbitrary magnitudes of warping stress N_y and distortional stress N_{xy} at the end. Bending moment and transverse shear can of course be evaluated from $\bar{w}$ in equation (44).

The complex decay coefficient γ is evaluated explicitly from equations (10), (37), and (40) as:

$$\gamma=\left[\frac{3}{1-\nu^2}\right]^{1/4}\left[\frac{t}{\alpha(1+\alpha)a}\right]^{1/2} e^{i\pi/4}+O(\epsilon^2) \tag{50}$$

The analysis of Boswell and Zhang (1984) results in the following equation for γ:

Downloaded 03 May 2010 to 171.66.16.27. Redistribution subject to ASME license or copyright; see http://www.asme.org/terms/Terms_Use.cfm

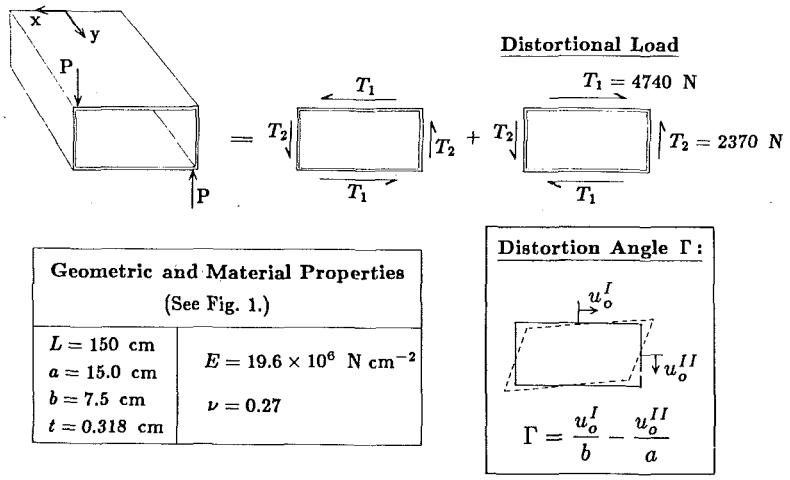


Fig. 3 Torsion and distortion of box beam with one built-in end (specifications from Boswell and Zhang, 1985)

$$\gamma^4 + \frac{a^4(1-\nu^2)k_d}{EJ} = 0 \tag{51}$$

where for the rectangular cross section under consideration,

$$k_d = \frac{12D}{(1+\alpha)a}$$
$$J = \frac{1}{3}\alpha^2(1+\alpha)a^5 t \tag{52}$$

This gives the result:

$$\gamma = 3^{1/4}\left[\frac{t}{\alpha(1+\alpha)a}\right]^{1/2} e^{i\pi/4} \tag{53}$$

which agrees with equation (50), except for a factor of $(1-\nu^2)^{1/4}$. The same expression (53) is arrived at by applying the formulas of Křístek (1970a) or Vlasov (1961). It is clear from the foregoing that the solution (44) is an asymptotically valid representation of the cross section distortion phenomenon discussed by previous investigators.

6 The Finite Box Beam: Membrane and Inextensional Solutions

For the finite box beam, the negative roots of equation (21) must be considered as well as the conjugate roots (which were included implicitly by taking the real and imaginary parts of equation (11) as independent solutions). For $\mathbf{Re}(\gamma) < 0$, the solution (11) grows exponentially with η, and represents the effects of a self-equilibrating load applied at $\eta = L/a$. For shorter beams, hyperbolic functions in η can be used in place of the exponentials, and the ends (relocated to $\eta = \pm L/2a$ for convenience) become significantly coupled.

Consider the distortional solution (44) for a finite box beam with $\sinh(\epsilon\gamma_1\eta)$ or $\cosh(\epsilon\gamma_1\eta)$ dependence in the η direction. In the limit $\epsilon \to 0$, there are four real solutions of the form:

$$\begin{bmatrix} \bar{\phi}^I \\ \bar{\phi}^{II} \\ \bar{w}^I \\ \bar{w}^{II} \end{bmatrix} = \bar{k} \begin{bmatrix} g_1(\eta) f^I(\xi) \\ g_1(\eta) f^{II}(\xi) \\ g_2(\eta) f^I(\xi) \\ g_2(\eta) f^{II}(\xi) \end{bmatrix} \tag{54}$$

where $g_1(\eta)$ and $g_2(\eta)$ are the leading terms of a Taylor series expansion in $\lambda\eta$. The limiting solutions (54) are two membrane distortion modes with:

$$g_1(\eta) \sim O(1)$$
$$g_2(\eta) \sim O(\epsilon) \tag{55}$$

and two inextensional bending modes with:

$$g_1(\eta) \sim O(\epsilon)$$
$$g_2(\eta) \sim O(1) \tag{56}$$

The explicit forms of these solutions are given in Appendix C.

For uniform convergence in the limit, it is required that:

$$\frac{\lambda L}{2a} << 1 \tag{57}$$

or

$$\frac{t}{a} << \left(\frac{1-\nu^2}{3}\right)^{1/2} 8\alpha(1+\alpha)\left(\frac{a}{L}\right)^2 \tag{58}$$

Thus a purely membrane or inextensional approximation to the distortion problem can be applied to longer box beams only if the walls are extremely thin.

7 Example: Distortional Load with Built-in End

As an example of distortional behavior, consider a box beam with a built-in end at $y = 0$, subject to torsion by two point loads at $y = L$ as shown in Fig. 3. This case has been investigated experimentally and analytically by Boswell and Zhang (1985). The load can be decomposed into torsion and distortional components (see Fig. 3), and the distortional component of the solution can be represented by the asymptotic result (44) (see equation (49)). The distortion angle is defined as follows (see Fig. 3):

$$\Gamma(y) = \frac{u_0^I}{b} - \frac{u_0^{II}}{a} \tag{59}$$

The boundary conditions for this example are taken as:

$$\text{at } y = 0 \quad \begin{cases} v = 0 \\ \Gamma = 0 \end{cases} \tag{60}$$

$$\text{at } y = L \quad \begin{cases} N_y = 0 \\ \int_{-a}^{a} N_{xy}\,dx = -T_1 \end{cases} \tag{61}$$

where v is the axial displacement (in the y direction). Standard methods of plane stress elasticity lead to a solution which is a linear combination of four asymptotic solutions of the form (44). The contributions of the rapidly decaying end effects ($\gamma_0 \neq 0$ in equation (17)) are neglected here, but are required

Downloaded 03 May 2010 to 171.66.16.27. Redistribution subject to ASME license or copyright; see http://www.asme.org/terms/Terms_Use.cfm

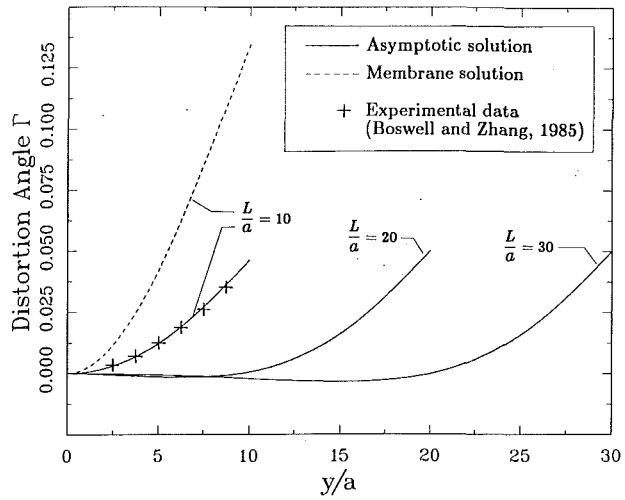


Fig. 4 Distortion angle Γ versus axial coordinate y for box beam with built-in end at $y=0$, subject to distortional loading at $y=L$

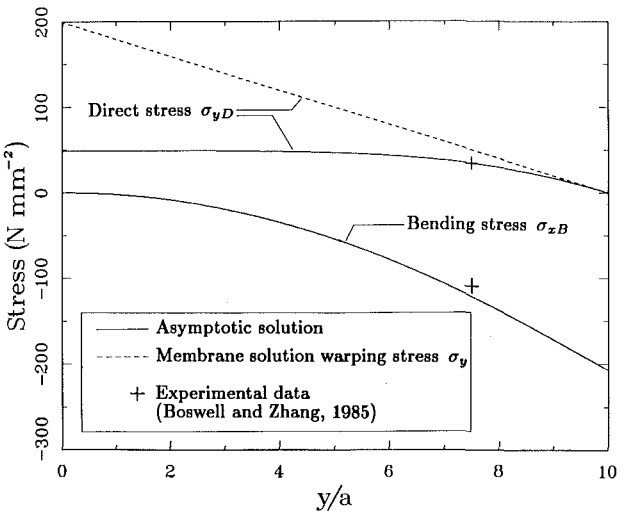


Fig. 5 Distortional stresses at edge $x=a$ versus axial coordinate y for box beam with built-in end at $y=0$, subject to distortional loading at $y=L$, ($L/a=10$)

for pointwise satisfaction of general boundary conditions and to guarantee accuracy for distances $O(a)$ or less from the ends.

Figure 4 shows the distortion angle Γ as a function of y, the distance along the beam, for the example under consideration ($L/a=10$). The asymptotic solution agrees well with the experimental values of Boswell and Zhang (1985). The numerical results of Boswell and Zhang (1985) are not shown in Fig. 4, but are also in close agreement with the experimental values and the asymptotic solution. Note that the membrane solution (limit $\epsilon\to 0$) overestimates the distortion considerably for $L/a=10$, and is a poor approximation. This follows from the inequality (57) since

$$\frac{\lambda L}{2a}\cong 0.8=O(1) \tag{62}$$

Figure 4 also shows the asymptotic solution for two other lengths: $L/a=20$ and $L/a=30$ (with other parameters held fixed). This demonstrates the axial decay distance δ of the asymptotic solution for a beam with this ratio of thickness to cross section width:

$$\delta=\frac{a}{\lambda}\cong 6.3a \tag{63}$$

Figure 5 shows the variation of the warping (direct) stress σ_{yD} and the transverse bending stress σ_{xB} on the outer surface for $L/a=10$, computed along the edge $x=a$. The maximum warping stress occurs at the root $y=0$, while the maximum bending stress occurs at the tip $y=L$. Note that the membrane solution gives axial warping stresses which increase linearly toward the root, with no decay along the beam.

8 Comparison With the Cylindrical Shell

Novoshilov (1959) demonstrated that the coupled fourth order equations for shallow shells can be conveniently formulated in terms of the complex stress function:

$$\Psi=\phi-iEtcw \tag{64}$$

Division of equation (64) by Eta^2 yields the dimensionless function $\bar{\Psi}$:

$$\bar{\Psi}=\phi/(Eta^2)-icw/a^2 \tag{65}$$

It is interesting that equation (65) provides the appropriate dimensionless quantities for the asymptotic analysis of the box beam. (See equations (9)). In the case of the box beam, however, the bending-membrane coupling which is characteristic of shell behavior arises not from the differential equations (1), but from the edge continuity conditions (3) and (4).

The asymptotic solutions (44) for the box beam can be compared with asymptotic solutions for the circular cylindrical shell subject to edge loads varying sinusoidally about the circumference. For the cylinder, the following real decay coefficient is obtained (Steele, 1965):

$$\lambda_{cyl}=n[c/(2R)]^{1/2} \tag{66}$$

where n is the Fourier harmonic index of the edge load, and R is the cylinder radius and reference length. From equations (10) and (46), the asymptotic solution for the box beam has the real decay coefficient:

$$\lambda=\left[\frac{6}{\alpha(1+\alpha)}\right]^{1/2}[c/(2a)]^{1/2} \tag{67}$$

As is apparent from equations (66) and (67), the asymptotic solutions for the cylinder and box beam have analogous exponential behavior in the axial direction; the decay coefficients depend similarly on the ratio of thickness to cross section width. In particular, the stress state corresponding to $n=2$ for the cylinder has the same circumferential periodicity as the box beam solution stresses (48) and (49), and represents analogous warping/distortion behavior.

9 Conclusions

A perturbation procedure has been presented for the solution of the end effect problem in thin-walled box beams. A family of eigenfunctions which satisfy the plane stress and plate bending biharmonic equations was obtained. These functions decay exponentially along the length of the beam in accordance with Saint-Venant's principle, and are a basis set for the representation of self-equilibrating end loads. In general, the decay distance is on the order of the cross section width or shorter, with the exception of the stress states corresponding to axial warping and transverse distortion of the cross section. These states decay relatively slowly, and approach nondecaying membrane and inextensional solutions for extremely thin-walled sections, thus demonstrating the limited validity of Saint-Venant's principle. Closed form solutions which are asymptotically valid for thin sections were obtained for the warping/distortional states. These solutions were found to agree with previous analytical and experimental results.

Acknowledgment

This work was partially supported by the General Motors

Downloaded 03 May 2010 to 171.66.16.27. Redistribution subject to ASME license or copyright; see http://www.asme.org/terms/Terms_Use.cfm

Research Laboratories, Warren, Michigan. The authors wish to thank Dr. L. J. Howell, Dr. J. A. Bennett, Dr. D. C. Chang, N. L. Johnson, and the staff of the GMR Engineering Mechanics Department for encouragement and helpful discussions.

References

Benthem, J. P., 1963, "A Laplace Transform Method for the Solution of Semi-Infinite and Finite Strip Problems in Stress Analysis," *Quart. J. Mech. Appl. Math.*, Vol. 16, pp. 413–29.

Boswell, L. F., and Zhang, S. H., 1984, "The Effect of Distortion in Thin-Walled Box-Spine Beams," *Int. J. Solids Struct.*, Vol. 20, (9/10), pp. 845–62.

Boswell, L. F., and Zhang, S. H., 1985, "An Experimental Investigation of the Behavior of Thin-Walled Box Beams," *Thin-Walled Structures*, Vol. 3, pp. 35–65.

Choi, I., and Horgan, C. O., 1977, "Saint-Venant's Principle and End Effects in Anisotropic Elasticity," ASME JOURNAL OF APPLIED MECHANICS, Vol. 44, pp. 424–30.

DeFries-Skene, A., and Scordelis, A. C., 1964, "Direct Stiffness Solution for Folded Plates," *ASCE J. Struct. Div.*, Vol. 90, (ST4), pp. 15–47.

Fadle, J., 1941, "Die Selbstspannungs-Eigenwertfunktionen der Quadratischen Scheibe," *Ingenieur-Archiv*, Vol. 11, pp. 125–49.

Goldberg, J. E., and Leve, H. L., 1957, "Theory of Prismatic Folded Plate Structures," *Int. Assoc. Bridge Struct. Eng.*, Vol. 17, pp. 59–86.

Gregory, R. D., 1980, "The Traction Boundary Value Problem for the Elastostatic Semi-Infinite Strip; Existence of Solution, and Completeness of the Papkovich-Fadle Eigenfunctions," *J. Elast.*, Vol. 10, pp. 295–327.

Horvay, G., 1957, "Biharmonic Eigenvalue Problem of the Semi-Infinite Strip," *Quart. Appl. Math.*, Vol. 15, pp. 65–81.

Horvay, G., and Born, J. S., 1957, "Some Mixed Boundary Value Problems of the Semi-Infinite Strip," ASME JOURNAL OF APPLIED MECHANICS, Vol. 24, pp. 261–8.

Johnson, M. W., Jr., and Little, R. W., 1964, "The Semi-Infinite Elastic Strip," *Quart. Appl. Math.*, Vol. 22, pp. 335–44.

Kristek, V., 1970a, "Tapered Box Girders of Deformable Cross Section," *ASCE J. Struct. Div.*, Vol. 96, (ST8), pp. 1761–93.

Kristek, V., 1970b, "Box Girders of Deformable Cross Section – Some Theory of Elasticity Solutions," *Proc. Inst. Civ. Eng.*, Vol. 47, pp. 239–53.

MACSYMA, 1983, "MACSYMA Reference Manual," Version Ten, Second Printing, The Mathlab Group, Laboratory for Computer Science, MIT, and Symbolics, Inc., Cambridge.

Novoshilov, V. V., 1959, *The Theory of Thin Shells*, P. Noordhoff Ltd., The Netherlands.

Papkovitsch, P. F., 1940, "Uber eine form der Lösung des Byharmonischen Problems für das Rechteck," *Doklady Akademiia Nauk SSSR*, Vol. 27, pp. 334–8.

Ramachandra-Rao, B. S., 1976, "End Effects in Long Curved Beam," *J. Eng. Mech. Div. ASCE*, Vol. 102, (EMI), pp. 19–29.

Smith, R. C. T., 1952, "The Bending of a Semi-Infinite Strip," *Australian J. Sci. Research*, Vol. 5, pp. 227–37.

Steele, C. R., 1965, "Shells with Edge Loads of Rapid Variation – II," ASME JOURNAL OF APPLIED MECHANICS, Vol. 32, pp. 87–98.

Timoshenko, S. P., and Goodier, J. N., 1970, *Theory of Elasticity*, Third Ed., McGraw-Hill, New York.

Vlasov, V. Z., 1961, *Thin-walled Elastic Beams*, Second Ed., published for NSF, Washington, D. C. and the U.S. Dept. of Commerce, by the Israel Program for Scientific Translations, Jerusalem.

Wright, R. N., Abdel-Samad, S. R., and Robinson, A. R., 1968, "BEF Analogy for Analysis of Box Girders," *J. Struct. Div.*, ASCE, Vol. 94, (ST7), pp. 1719–43.

APPENDIX A

Eigenfunction Coefficients

The coefficients corresponding to a given root γ_0 of equation (21) are obtained from equation (12). For the unperturbed case ($\epsilon = 0$):

$$A_0^I = 1$$

$$B_0^I = -\frac{\sin\gamma_0}{\gamma_0\cos\gamma_0}$$

$$A_0^{II} = \alpha\frac{\cos\alpha\gamma_0}{\cos\gamma_0}\left(\frac{2\gamma_0 - \sin 2\gamma_0}{2\alpha\gamma_0 - \sin 2\alpha\gamma_0}\right) \tag{A1}$$

$$B_0^{II} = -\frac{\sin\alpha\gamma_0}{\gamma_0\cos\gamma_0}\left(\frac{2\gamma_0 - \sin 2\gamma_0}{2\alpha\gamma_0 - \sin 2\alpha\gamma_0}\right)$$

For $\epsilon = 0$, the membrane and inextensional problems are equivalent and decoupled, so that:

$$C_0^{(I,II)} = A_0^{(I,II)}$$
$$\tag{A2}$$
$$D_0^{(I,II)} = B_0^{(I,II)}$$

APPENDIX B

Explicit Forms of $[M_0]$, $[M_1]$, and $[M_2]$

The 8×8 matrix $[M]$ in equation (12) can be expanded in ϵ according to equation (19). Rows 1, 3, 4, 5, 7, and 8 of $[M]$ were divided through by ϵ in order to consolidate the leading terms of each row in the matrix $[M_0]$. This algebra was carried out with the aid of the symbolic manipulation program MACSYMA (1983). The upper two 4×4 submatrices of the matrices $[M_0]$, $[M_1]$, and $[M_2]$ are given below. (The lower two 4×4 submatrices can be obtained from equations (15), (16)).

$$[M_0]_{11} = \begin{bmatrix} \gamma_1(1+\nu) & \gamma_1(3+\nu) & \alpha\gamma_1(1+\nu) & \alpha\gamma_1(3+\nu) \\ -1 & -1 & 1 & 1 \\ \gamma_1 & \gamma_1 & 0 & 0 \\ 0 & 0 & \alpha\gamma_1 & \alpha\gamma_1 \end{bmatrix} \tag{B1}$$

$$[M_0]_{12} = [0] \tag{B2}$$

$$[M_1]_{11} = \begin{bmatrix} \gamma_2(1+\nu) & \gamma_2(3+\nu) & \alpha\gamma_2(1+\nu) & \alpha\gamma_2(3+\nu) \\ 0 & 0 & 0 & 0 \\ \gamma_2 & \gamma_2 & 0 & 0 \\ 0 & 0 & \alpha\gamma_2 & \alpha\gamma_2 \end{bmatrix} \tag{B3}$$

$$[M_1]_{12} = [0] \tag{B4}$$

$$[M_2]_{11} = \begin{bmatrix} (1+\nu)\left(\gamma_3 - \frac{1}{6}\gamma_1^3\right) & (3+\nu)\gamma_3 - \frac{5+3\nu}{6}\gamma_1^3 & (1+\nu)\left(\alpha\gamma_3 - \frac{1}{6}\alpha^3\gamma_1^3\right) & \alpha(3+\nu)\gamma_3 - \frac{5+3\nu}{6}\alpha^3\gamma_1^3 \\ \frac{1}{2}\gamma_1^2 & \frac{3}{2}\gamma_1^2 & -\frac{1}{2}\alpha^2\gamma_1^2 & -\frac{3}{2}\alpha^2\gamma_1^2 \\ \gamma_3 - \frac{1}{6}\gamma_1^3 & \gamma_3 - \frac{1}{2}\gamma_1^3 & 0 & 0 \\ 0 & 0 & \alpha\gamma_3 - \frac{1}{6}\alpha^3\gamma_1^3 & \alpha\gamma_3 - \frac{1}{2}\alpha^3\gamma_1^3 \end{bmatrix} \tag{B5}$$

Downloaded 03 May 2010 to 171.66.16.27. Redistribution subject to ASME license or copyright; see http://www.asme.org/terms/Terms_Use.cfm

$$[M_2]_{12} = \begin{bmatrix} 0 & 0 & 0 & 0 \\ 0 & 0 & 0 & 0 \\ 0 & 0 & \gamma_1(1-\nu) & -\gamma_1(1+\nu) \\ \gamma_1(1-\nu) & -\gamma_1(1+\nu) & 0 & 0 \end{bmatrix} \tag{B6}$$

APPENDIX C

Distortional Solutions in Limit $\epsilon \to 0$

For the finite box beam, the distortional solutions have the form (see equations (44), (45)):

$$\begin{bmatrix} \bar{\phi}^I \\ \bar{\phi}^{II} \\ \bar{w}^I \\ \bar{w}^{II} \end{bmatrix} = \bar{k} \begin{Bmatrix} \cosh\epsilon\gamma_1\eta \\ \text{or} \\ \sinh\epsilon\gamma_1\eta \end{Bmatrix} \begin{bmatrix} if^I(\xi) \\ if^{II}(\xi) \\ f^I(\xi) \\ f^{II}(\xi) \end{bmatrix} \tag{C1}$$

Expanding the real and imaginary parts of equation (C1) for small ϵ (keeping leading terms only) yields the four real solutions:

$$\Phi_1 = \begin{bmatrix} f^I(\xi) \\ f^{II}(\xi) \\ -\lambda\eta f^I(\xi) \\ -\lambda\eta f^{II}(\xi) \end{bmatrix} \quad \Phi_2 = \begin{bmatrix} \eta f^I(\xi) \\ \eta f^{II}(\xi) \\ -\lambda\eta^2 f^I(\xi) \\ -\lambda\eta^2 f^{II}(\xi) \end{bmatrix} \tag{C2}$$

$$\Phi_3 = \begin{bmatrix} \lambda\eta f^I(\xi) \\ \lambda\eta f^{II}(\xi) \\ f^I(\xi) \\ f^{II}(\xi) \end{bmatrix} \quad \Phi_4 = \begin{bmatrix} \lambda\eta^2 f^I(\xi) \\ \lambda\eta^2 f^{II}(\xi) \\ \eta f^I(\xi) \\ \eta f^{II}(\xi) \end{bmatrix} \tag{C3}$$

where $\lambda \sim O(\epsilon)$ (see equation (46)). In the limit $\epsilon \to 0$, solutions (C2) become membrane states. Φ_1 represents pure bimoment warping stress, while Φ_2 represents warping stress accompanied by distorting shear stress. Solutions (C3) approach inextensional bending modes of cross section distortion.

Downloaded 03 May 2010 to 171.66.16.27. Redistribution subject to ASME license or copyright; see http://www.asme.org/terms/Terms_Use.cfm

Initial Postbuckling Behavior of Imperfect, Antisymmetric Cross-Ply Cylindrical Shells Under Torsion

David Hui
Assistant Professor,
Mem. ASME

I. H. Y. Du
Ph.D. Student.

The Ohio State University,
Department of Engineering Mechanics,
Columbus, Ohio 43210

This paper deals with the initial postbuckling of antisymmetric cross-ply closed cylindrical shells under torsion. Under the assumptions employed in Koiter's theory of elastic stability, the structure is imperfection-sensitive in certain intermediate ranges of the reduced-Batdorf parameter (approx. $4 \leq Z_H \leq 20.0$). Due to different material bending-stretching coupling behavior, the (0 deg inside, 90 deg outside) two-layer clamped cylinder is less imperfection sensitive than the (90 deg inside, 0 deg outside) configuration. The increase in torsional buckling load due to a higher value of Young's moduli ratio is not necessarily accompanied by a higher degree of imperfection-sensitivity. The paper is the first to consider imperfection shape to be identical to the torsional buckling mode and presents concise parameter variations involving the reduced-Batdorf paramter and Young's moduli ratio.

1 Introduction

Due to increased use of light-weight, high-strength composite materials in aerospace, mechanical, and hydrospace industries, buckling and postbuckling of laminated closed cylindrical shells has become an important research topic. One of the earliest stability analyses of orthotropic cylindrical shells under torsion was presented by March et al. (1945). Subsequently, Hayashi and Hirano (1964), Chechill and Cheng (1968), Shaw and Simitses (1982, 1984) and Simitses et al. (1985) gave further examinations of this problem. Comprehensive experimental investigations of torsional buckling of laminated cylindrical shells were presented by Marlowe et al. (1973), Wilkins and Love (1974), Booton (1976), Booton and Tennyson (1979), and Herakovich and Johnson (1981). A detailed summary of the literature on torsional buckling of laminated cylindrical shells can be found in review articles by Tennyson (1975) and Simitses (1986). In passing, comprehensive reviews on buckling of composite cylindrical shells under compression and external pressure were presented by Tennyson (1984) and Galletly and Pemsing (1985). An excellent review on buckling of laminated open cylindrical panels was reported by Leissa (1985) and three recent texts were written by Kollar and Dulacska (1984), Yamaki (1984), and Bushnell (1985).

The present work was motivated by the work of Budiansky (1967), Booton (1976), and Simitses, Shaw, and Sheinman (1985). The limitations of these works will be addressed in this paper. Budiansky (1967) presented a rigorous initial postbuckling behavior of isotropic homogeneous cylindrical shells under torsion, using Koiter's (1945) general stability theory, but he did not consider laminated cylinders. Booton (1976) considered the effects of "axisymmetric" geometric imperfections on torsional or combined-load buckling of laminated cylindrical shells, using Koiter's (1963) special stability theory, but he did not consider nonaxisymmetric imperfections or postbuckling. Simitses, Shaw, and Sheinman (1985) presented a rigorous large deflection analysis of laminated cylinders under torsion. The imperfection terms were present in the governing equations and they were solved using a generalization of Newton's method applicable to differential equations (Thurston, 1965). They employed imperfection shapes which are "similar" to the buckling modes of the geometry as well as to other shapes. They obtained these shapes by employing the methodology of Shaw and Simitses (1984). The present study attempts to examine in detail problems similar to the one examined by Simitses et al. using Koiter's well-accepted and equally rigorous alternative approach. Particular emphasis is placed on the "nonaxisymmetric" imperfection shapes which are identical to those of the buckling modes. These shapes are likely to be more realistic than the axisymmetric imperfections.

The present paper is an extension of Budiansky (1967) and Yamaki and Kodama's (1980) work to "laminated" cylindrical shells. The analysis is based on a solution of the Donnell-type nonlinear equilibrium and compatibility equations, using Koiter's (1945) general theory of elastic stability. Using a Koiter-type perturbation method, a sequence of linearized differential equations is derived. The classical

Contributed by the Applied Mechanics Division for presentation at the 1987 Applied Mechanics, Biomechanics, and Fluids Engineering Conference, Cincinnati, OH, June 14-17, 1987, of the American Society of Mechanical Engineers.
Discussion on this paper should be addressed to the Editorial Department, ASME, United Engineering Center, 345 East 47th Street, New York, N.Y. 10017, and will be accepted until two months after final publication of the paper itself in the JOURNAL OF APPLIED MECHANICS. Manuscript received by ASME Applied Mechanics Division, February 7, 1986; final revision, July 2, 1986.
Paper No. 87-APM-12.

Copyright © 1987 by ASME
Downloaded 03 May 2010 to 171.66.16.27. Redistribution subject to ASME license or copyright; see http://www.asme.org/terms/Terms_Use.cfm

buckling load and the corresponding buckling mode are obtained by discretizing the governing differential equations and boundary conditions using the central finite difference scheme. The resulting eigenvalue problem is solved using the shifted inverse power method in conjunction with the LINPACK equation solver (Dongarra et al., 1979). The cubic terms of the potential energy vanish due to symmetry considerations and computation of the quartic term (related to the postbuckling b coefficients defined by Budiansky, 1967) requires solution of the second order field equations. It should be noted that the present Koiter-type analysis is valid only for imperfection shapes identical to that of the buckling mode and for imperfection amplitudes which are sufficiently small.

The example problems are chosen for antisymmetric cross-ply cylindrical shells under torsion. The shells are either clamped or simply-supported and the in-plane boundary conditions are axially and circumferentially immovable in the buckling state and second order field solution. Due to material bending-stretching coupling, the two layer (0 deg inside, 90 deg outside) and the (90 deg, 0 deg) designs have almost identical torsional buckling load but different postbuckling stiffness. The parameter variations involving the reduced-Batdorf parameter and Young's moduli ratio are presented.

2 Governing Nonlinear Differential Equations and the Classical Buckling Load

The initial postbuckling behavior of geometrically imperfect, laminated cylindrical shells is based on a solution of the nonlinear Donnell-type equilibrium and compatibility equations, written in terms of an out-of-plane displacement W (positive outwards) and a stress function F, respectively (Hui 1985a,b).

$$L_D^*(W)+L_B^*(F)+(1/R)F_{,XX} = F_{,YY}W_{,XX}+F_{,XX}W_{,YY}-2F_{,XY}W_{,XY} \tag{1}$$

$$L_A^*(F)-L_B^*(W)-(1/R)W_{,XX} = (W_{,XY})^2-W_{,XX}W_{,YY} \tag{2}$$

In the above R is the shell radius, X and Y are the axial and circumferential coordinates, and $L_A^*(\,)$, $L_B^*(\,)$, and $L_D^*(\,)$ are the linear fourth order differential operators defined by Tennyson et al. (1971, 1980).

Consistent with Koiter's (1945) theory of elastic stability, the total displacement and the total stress fucntion can be expressed as the sum of the prebuckling state, the buckling state, and the second order field in the form (Hui et al., 1981)

$$\begin{aligned} w &= w_p+\xi w_{\mathrm{I}}+\xi^2 w_{\mathrm{II}} \\ f &= f_p+\xi f_{\mathrm{I}}+\xi^2 f_{\mathrm{II}} \end{aligned} \tag{3}$$

In the above, ξ is the amplitude of the buckling mode normalized with respect to the total laminated thickness h, $w = W/h$, $f = F/(E_2h^3)$ and E_2 is Young's modulus in the in-plane transverse direction. The nondimensional applied axial load σ, the lateral pressure p, and the nondimensional torsional load τ are related to the prebuckling stress function and the membrane stress resultants by,

$$(\sigma,p,\tau)=(f_{p,yy},f_{p,xx},-f_{p,xy}) = (|N_x|,N_y,N_{xy})[R/(E_2h^2)] \tag{4}$$

Assuming a membrane prebuckling state and introducing the following nondimensional quantities,

$$\begin{aligned} &(x,y)=(X,\ Y)/(Rh)^{1/2}, \\ &a_{ij}^*=(E_2h)A_{ij}^*,\ b_{ij}^*=B_{ij}^*/h, \\ &d_{ij}^*=D_{ij}^*/(E_2h^3) \end{aligned} \tag{5}$$

the nondimensional linearized equilibrium and compatibility equations for the buckling state becomes,

$$L_d^*(w_1)+L_b^*(f_1)+f_{1,xx}+\sigma w_{1,xx}+pw_{1,yy}-(2\tau)w_{1,xy}=0 \tag{6}$$

$$L_a^*(f_1)-L_b^*(w_1)-w_{1,xx}=0 \tag{7}$$

The nondimensional differential operators are defined as Hui (1986a),

$$L_a^*(\,)=a_{22}^*(\,)_{,xxxx}+(2a_{12}^*+a_{66}^*)(\,)_{,xxyy}+a_{11}^*(\,)_{,yyyy}-2a_{26}^*(\,)_{,xxxy}-2a_{16}^*(\,)_{,xyyy} \tag{8}$$

$$L_b^*(\,)=b_{21}^*(\,)_{,xxxx}+(b_{11}^*+b_{22}^*-2b_{66}^*)(\,)_{,xxyy}+b_{12}^*(\,)_{,yyyy}+(2b_{26}^*-b_{61}^*)(\,)_{,xxxy}+(2b_{16}^*-b_{62}^*)(\,)_{,xyyy} \tag{9}$$

$$L_d^*(\,)=d_{11}^*(\,)_{,xxxx}+(2)(d_{12}^*+2d_{66}^*)(\,)_{,xxyy}+d_{22}^*(\,)_{,yyyy}+4d_{16}^*(\,)_{,xxxy}+4d_{26}^*(\,)_{,xyyy} \tag{10}$$

The general solution for buckling of a laminated cylindrical shell under pure torsion or combined load involving torsion is,

$$\begin{aligned} w_{\mathrm{I}}(x,y) &= w_s(x)\sin(Ny)+w_c(x)\cos(Ny) \\ f_{\mathrm{I}}(x,y) &= f_s(x)\sin(Ny)+f_c(x)\cos(Ny) \end{aligned} \tag{11}$$

where $N = n(h/R)^{1/2}$. Substituting $w_1(x, y)$ and $f_1(x, y)$ into the equilibrium equation for the buckling state and collecting terms involving $\sin(Ny)$ and $\cos(Ny)$, one obtains two ordinary differential equations, respectively,

$$L_d^{**}[w_s(x)]-L_d^{***}[w_c(x)]+L_b^{**}[f_s(x)]-L_b^{***}[f_c(x)]+f_s(x)_{,xx}+\sigma w_s(x)_{,xx}-pN^2w_s(x)+(2\tau)Nw_c(x)_{,x}=0 \tag{12}$$

$$L_d^{**}[w_c(x)]+L_d^{***}[w_s(x)]+L_b^{**}[f_c(x)]+L_b^{***}[f_s(x)]+f_c(x)_{,xx}+\sigma w_c(x)_{,xx}-pN^2w_c(x)-(2\tau)Nw_s(x)_{,x}=0 \tag{13}$$

Similarly, collecting $\sin(Ny)$ and $\cos(Ny)$ from the compatibility equation for the buckling state, one obtains, respectively,

$$L_a^{**}[f_s(x)]-L_a^{***}[f_c(x)]-L_b^{**}[w_s(x)]+L_b^{***}[w_c(x)]-w_s(x)_{,xx}=0 \tag{14}$$

$$L_a^{**}[f_c(x)]+L_a^{***}[f_s(x)]-L_b^{**}[w_c(x)]-L_b^{***}[w_s(x)]-w_c(x)_{,xx}=0 \tag{15}$$

In the above equations, the ordinary differential operators are defined as

$$\begin{aligned} L_a^{**}(\,) &= a_{22}^*(\,)_{,xxxx}-N^2(2a_{12}^*+a_{66}^*)(\,)_{,xx}+N^4a_{11}^*(\,) \\ L_a^{***}(\,) &= -2a_{26}^*N(\,)_{,xxx}+2a_{16}^*N^3(\,)_{,x} \end{aligned} \tag{16a,b}$$

$$\begin{aligned} L_b^{**}(\,) &= b_{21}^*(\,)_{,xxxx}-N^2(b_{11}^*+b_{22}^*-2b_{66}^*)(\,)_{,xx}+N^4b_{12}^*(\,) \\ L_b^{***}(\,) &= (2b_{26}^*-b_{61}^*)N(\,)_{,xxx}-(2b_{16}^*-b_{62}^*)N^3(\,)_{,x} \end{aligned} \tag{17a,b}$$

$$\begin{aligned} L_d^{**}(\,) &= d_{11}^*(\,)_{,xxxx}-2N^2(d_{12}^*+2d_{66}^*)(\,)_{,xx}+N^4d_{22}^*(\,) \\ L_d^{***}(\,) &= 4d_{16}^*N(\,)_{,xxx}-4d_{26}^*N^3(\,)_{,x} \end{aligned} \tag{18a,b}$$

The boundary conditions considered in this paper are assumed to be identical at both ends of the cylindrical shells at $x = 0$ and at $x = L/(Rh)^{1/2}$ and $w(x=0) = 0$, $w(x = L/(Rh)^{1/2}) = 0$. The out-of-plane boundary conditions are either clamped $w_{,x}$ $(x = 0) = 0$ or simply-supported M_x $(x = 0) = 0$. In the mixed formulation in terms of w and f, the zero bending moment condition is (Hui, 1986a)

$$-b_{11}^*f_{,yy}(x=0)-b_{21}^*f_{,xx}(x=0)+b_{61}^*f_{,xy}(x=0)-d_{11}^*w_{,xx}(x=0)-2d_{16}^*w_{,xy}(x=0)=0 \tag{19}$$

Note that $(\,)=0$ at $x = 0$ implies $(\,)_{,y} = 0$ and $(\,)_{,yy}=0$, etc. at $x = 0$. The in-plane boundary conditions are either axially immovable or axially movable, that is, (Booton, 1976),

$$U_{,YY}(x=0)=0 \quad \text{or} \quad f_{,yy}(x=0)=0 \tag{20}$$

Further, the shell is either circumferentially immovable or circumferentially movable,

Downloaded 03 May 2010 to 171.66.16.27. Redistribution subject to ASME license or copyright; see http://www.asme.org/terms/Terms_Use.cfm

$$V,_Y(x=0)=0 \quad \text{or} \quad f,_{xy}(x=0)=0 \tag{21}$$

Using the following strain-displacement relation at $x = 0$,

$$-\epsilon_{y,X}(X=0)+\gamma_{xy,Y}(X=0) = U,_{YY}(X=0)-(1/R)W,_X(X=0) \tag{22}$$

the axially immovable boundary condition can be written in terms of w and f,

$$[a^*_{16}f,_{yyy}+2a^*_{26}f,_{xxy}-(a^*_{12}+a^*_{66})f,_{xyy} -a^*_{22}f,_{xxx}-0+(b^*_{22}-2b^*_{66})w,_{xyy} +(2b^*_{26}-b^*_{61})w,_{xxy}+b^*_{21}w,_{xxx}+w,_x]=0 \quad \text{at } x=0 \tag{23}$$

Note that $\epsilon_y = V,_{Y^+}(W/R)+(1/2)(W,_Y)^2$ and

$$\epsilon_y=(h/R)[a^*_{12}f,_{yy}+a^*_{22}f,_{xx} -a^*_{26}f,_{xy}-b^*_{21}w,_{xx}-b^*_{22}w,_{yy}-2b^*_{26}w,_{xy}] \tag{24a}$$

Using the strain-displacement condition that $\epsilon_y\ (X=0) = V,_Y(X=0)$, the circumferentially immovable boundary condition $V,_Y(X=0)=0$ becomes,

$$[a^*_{12}f,_{yy}+a^*_{22}f,_{xx}-a^*_{26}f,_{xy}-b^*_{21}w,_{xx}-2b^*_{26}w,_{xy}]=0 \quad \text{at } x=0 \tag{24b}$$

using the conditions $w(x=0)=0$, $w,_y(x=0)=0$ and $w,_{yy}(x=0)=0$.

In the present paper, the in-plane boundary conditions are $U,_{YY}(x=0)=0$ and $V,_Y(x=0)=0$ for the buckling and second order field analyses, while the prebuckling state is assumed to be a membrane one. Substituting the separable form of the buckling mode into the $U,_{YY}(X=0)=0$ boundary condition, and collecting terms involving $\sin(Ny)$ and $\cos(Ny)$, one obtains, respectively,

$$[a^*_{16}N^3f_c-2a^*_{26}Nf_{c,xx}+(a^*_{12}+a^*_{66})N^2f_{s,x} -a^*_{22}f_{s,xxx}-N^2(b^*_{22}-2b^*_{66})w_{s,x}-N(2b^*_{26} -b^*_{61})w_{c,xx}+b^*_{21}w,_{xxx}+w_{s,x}]=0 \quad \text{at } x=0 \tag{25}$$

$$[-N^3a^*_{16}f_s+2a^*_{26}Nf_{s,xx}+N^2(a^*_{12}+a^*_{66})f_{c,x} -a^*_{22}f_{c,xxx}-N^2(b^*_{22}-2b^*_{66})w_{c,x}+N(2b^*_{26} -b^*_{61})w_{s,xx}+b^*_{21}w_{c,xxx}+w_{c,x}]=0 \quad \text{at } x=0 \tag{26}$$

Similarly, collecting terms involving $\sin(Ny)$ and $\cos(Ny)$ in the $V,_Y(x=0)=0$ boundary condition, one obtains, respectively,

$$[-N^2a^*_{12}f_s+a^*_{22}f_{s,xx}+Na^*_{26}f_{c,x} -b^*_{21}w_{s,xx}+2b^*_{26}Nw_{c,x}]=0 \quad \text{at } x=0 \tag{27}$$

$$[-N^2a^*_{12}f_c+a^*_{22}f_{c,xx}+Na^*_{26}f_{s,x} -b^*_{21}w_{c,xx}-2b^*_{26}Nw_{s,x}]=0 \quad \text{at } x=0 \tag{28}$$

3 Second Order Fields and Postbuckling Coefficients

Due to the symmetry consideration that a sign change of the buckling mode represents a configuration which is identical to the original mode, the cubic term of the potential energy vanishes. In order to compute the quartic terms of the potential energy (Koiter, 1945), it is necessary to solve for the second order fields $w_{II}(x, y)$ and $f_{II}(x, y)$.

Substituting the total displacement and the total stress function (equation (3)) into the governing nonlinear equilibrium and compatibility equations and then collecting terms involving ξ^2, one obtains the two governing partial differential equations for the second order fields,

$$L_{a^*}(w_{II})+L_{b^*}(f_{II})+f_{II,xx}+\sigma w_{II,xx}+pw_{II,yy}-(2\tau)w_{II,xy} =f_{I,yy}w_{I,xx}+f_{I,xx}w_{I,yy}-2f_{I,xy}w_{I,xy} \tag{29}$$

$$L_{a^*}(f_{II})-L_{b^*}(w_{II})-w_{II,xx}=(w_{I,xy})^2-w_{I,xx}w_{I,yy} \tag{30}$$

Substituting the buckling mode $w_I(x, y)$ and $f_I(x, y)$ into the right-hand sides of equations (19) and (20), it is clear that the second order fields are of the form,

$$w_{II}(x,y)=w^*(x)+w_A(x)\cos(2Ny)+w_B(x)\sin(2Ny) \tag{31}$$

$$f_{II}(x,y)=f^*(x)+f_A(x)\cos(2Ny)+f_B(x)\sin(2Ny) \tag{32}$$

Thus, the equilibrium and compatibility equations for the second order fields may be uncoupled into two sets of ordinary differential equations. The first set involves $w^*(x)$ and $f^*(x)$ and the second set deals with $w_A(x)$, $w_B(x)$, $f_A(x)$ and $f_B(x)$. The first set is,

$$a_{22}f^*(x),_{xxxx}-b_{21}w^*(x),_{xxxx}-w^*(x),_{xx} =(N^2/4)[w_s(x)^2+w_c(x)^2],_{xx} \tag{33}$$

$$d^*_{11}w^*(x),_{xxxx}+b^*_{21}f^*(x),_{xxxx}+f^*(x),_{xx}+\sigma w^*(x),_{xx} =(-N^2/2)[w_s(x)f_s(x)+w_c(x)f_c(x)],_{xx} \tag{34}$$

It can be easily checked from equations (24a,b) that the singlevaluedness requirement of the circumferential displacement for the second order problem is precisely equation (33).

The zero-moment boundary condition at $x = 0$ for the $w^*(x)$ and $f^*(x)$ problem is (see equation (19)),

$$-b^*_{21}f^*_{xx}(x=0)-d^*_{11}w,^*_{xx}(x=0)=0 \tag{35}$$

Further, the $U,_{YY}(x=0)$ condition for the y-independent $w^*(x)$ and $f^*(x)$ problem is (see equation (23)),

$$-a^*_{22}f,^*_{xxx}(x=0)+b^*_{21}w,^*_{xxx}(x=0)+w^*_{,x}(x=0)=0 \tag{36}$$

and similarly, the $V,_Y(x=0)=0$ condition can be obtained from equation (24),

$$a^*_{22}f,^*_{xx}(x=0)-b^*_{21}w,^*_{xx}(x=0)=0 \tag{37}$$

The second set of four coupled ordinary differential equations are obtained from the compatibility equation which involved $\cos(2Ny)$ and $\sin(2Ny)$, respectively,

$$L_{a^{**}}[f_A(x)]+L_{a^{***}}[f_B(x)]-L_{b^{**}}[w_A(x)] -L_{b^{***}}[w_B(x)]-w_A(x),_{xx}=(N^2/2)[(w_{s,x})^2 -(w_{c,x})^2-w_sw_{s,xx}+w_cw_{c,xx}] \tag{38}$$

$$L_{a^{**}}[f_B(x)]-L_{a^{***}}[f_A(x)]-L_{b^{**}}[w_B(x)] +L_{b^{***}}[w_A(x)]-w_B(x),_{xx}=(N^2/2)[(-2)(w_{s,x})(w_{c,x}) +w_cw_{s,xx}+w_sw_{c,xx}] \tag{39}$$

and from the equilibrium equation which involves $\cos(2Ny)$ and $\sin(2Ny)$, respectively,

$$L_{d^{**}}[w_A(x)]+L_{d^{***}}[w_B(x)]+L_{b^{**}}[f_A(x)]+L_{b^{***}}[f_B(x)] +f_A(x),_{xx}+(\sigma)w_A(x),_{xx}-(2N)^2pw_A(x)-(4N)(\tau)w_B(x),_x =(N^2/2)[w_{s,xx}f_s-w_{c,xx}f_c+w_sf_{s,xx}-w_cf_{c,xx} -2w_{s,x}f_{s,x}+2w_{c,x}f_{c,x}] \tag{40}$$

$$L_{d^{**}}[w_B(x)]-L_{d^{***}}[w_A(x)]+L_{b^{**}}[f_B(x)]-L_{b^{***}}[f_A(x)] +f_B(x),_{xx}+(\sigma)w_B(x),_{xx}-(2N)^2pw_B(x)+(4N)(\tau)w_A(x),_x =(N^2/2)[-w_{c,xx}f_s-w_{s,xx}f_c-w_cf_{s,xx}-w_sf_{c,xx} +2w_{c,x}f_{s,x}+2w_{s,x}f_{c,x}] \tag{41}$$

It is important to note that the linear differential operators $L_{a^{**}}(\,)$, $L_{a^{***}}(\,)$, $L_{b^{**}}(\,)$, $L_{b^{***}}(\,)$, $L_{d^{**}}(\,)$, and $L_{d^{***}}(\,)$ employed in equations (38)–(41) are the same as that presented for the buckling state except that the wave number N should be replaced by $2N$ in equations (16a,b), (17a,b), and (18a,b).

Downloaded 03 May 2010 to 171.66.16.27. Redistribution subject to ASME license or copyright; see http://www.asme.org/terms/Terms_Use.cfm

Table 1 Torsional buckling load and b coefficient for Boron-epoxy cross-ply cylindrical shells

	(i) Clamped N_L = infinite			(ii) Clamped (0° out, 90° in)		(iii) Clamped (90° in, 0° out)		(iv) s.s N_L = infinite	
Z_H	N	τ_c	b	N	τ_c	N	τ_c	N	τ_c
1.0	3.82	30.51	0.476	3.62	16.53	3.66	16.79	2.42	17.90
2.0	2.28	7.619	0.392	2.02	4.157	2.12	4.183	1.68	4.183
3.0	1.50	3.492	0.114	1.44	1.975	1.42	1.980	1.10	2.301
4.0	1.22	2.143	0.0409	1.04	1.357	1.00	1.356	1.08	1.515
5.0	1.10	1.516	−0.00170	1.00	0.9713	0.98	0.9623	1.00	1.174
6.0	1.02	1.199	−0.0193	1.00	0.7599	0.98	0.7570	0.90	0.9674
7.0	0.96	0.9890	−0.0308	1.02	0.6500	0.98	0.6493	0.86	0.8653
8.0	0.92	0.8854	−0.0316	0.98	0.5863	0.96	0.5826	0.88	0.7905
9.0	0.86	0.8005	−0.0333	0.98	0.5373	0.94	0.5339	0.86 (Z_H = 8.5)	0.7548
10.0	0.84	0.7419	−0.0319	0.94	0.5027	0.92	0.4989	0.82	0.6901
12.0	0.74	0.6751	−0.0286	0.80	0.4725	0.80	0.4685	0.84	0.6356
15.0	0.86	0.6162	−0.0229	0.72	0.4440	0.72	0.4411	–	–
18.0	0.66	0.5674	−0.0184	0.68	0.4169	0.70	0.4058	0.82	0.5739
20.0	0.66	0.5400	−0.0161	0.70	0.3847	0.70	0.3832	0.82 (Z_H = 19)	0.5524
30.0	0.64	0.4732	−0.00900	0.62	0.3383			0.64	0.4695
40.0	0.58	0.4387	−0.00575	0.56	0.3116			0.58	0.4365
50.0	0.54	0.4137	−0.00397	0.54	0.2973			0.52	0.4123
70.0	0.46	0.3765	−0.00230	0.52	0.2553			0.46	0.3758
100.0	0.40	0.3372	−0.00124	0.44	0.2264			0.40	0.3369

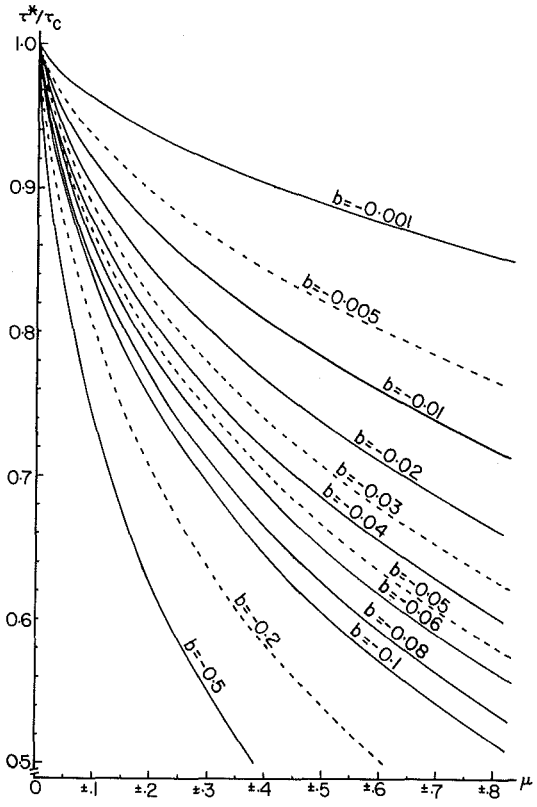


Fig. 1 Imperfection-sensitivity curves for various b coefficients

The in-plane boundary conditions for the above four coupled ODE for the second order fields can be obtained directly from equations (25)–(28) by replacing the wave number N by $2N$ and w_c, w_s, f_c, f_s by w_A, w_B, f_A, f_B, respectively.

In order to examine the stability of the single-mode symmetric system at the onset of buckling, it is necessary to compute the postbuckling b coefficient (see Hutchinson and Amazigo, 1967). The structure has stable postbuckling behavior (hence imperfection-insensitive) if b is positive and it has unstable postbuckling (imperfection-sensitive) if b is negative. The degree of imperfection sensitivity is measured by the magnitude of the postbuckling b coefficient. The equilibrium paths are specified by

$$b\xi^3 + [1-(\tau^*/\tau_c)]\xi = \mu(\tau/\tau_c) \tag{42}$$

where τ^* is the buckling load of the imperfect system, τ_c is the classical buckling load of the perfect system, and μ is the imperfection amplitude (assumed to be of the same shape as buckling mode) normalized with respect to the total thickness of the laminate. The imperfection amplitude is related to the buckling load (valid only if $b < 0$),

$$(3/2)(-3b)^{1/2}\mu(\tau/\tau_c) = [1-(\tau/\tau_c)]^{3/2} \tag{43}$$

The b coefficient is defined to be (Budiansky, 1967, and Hui, 1986b),

$$b = (C_1 + C_2)/|D_1| \tag{44}$$

where,

$$C_1 = 2\int_{y=0}^{y_o}\int_{x=0}^{Z_H} \{f_{I,yy}w_{I,x}w_{II,x} + f_{I,xx}w_{I,y}w_{II,y} - f_{I,xy}(w_{I,x}w_{II,y} + w_{I,y}w_{II,x})\}dx\,dy \tag{45}$$

$$C_2 = \int_{y=0}^{y_o}\int_{x=0}^{Z_H} \{f_{II,yy}(w_{I,x})^2 + f_{II,xx}(w_{I,y})^2 - 2f_{II,xy}w_{I,x}w_{I,y}\}dx\,dy \tag{46}$$

$$D_1 = (2\tau)\int_{y=0}^{y_o}\int_{x=0}^{Z_H} w_{I,x}w_{I,y}dx\,dy = (\tau N)y_o\int_{x=0}^{Z_H}(-w_c w_{s,x} + w_s w_{c,x})dx \tag{47}$$

In the above, $y_o = 2\pi R/(Rh)^{1/2}$ and the reduced-Batdorf parameter is defined to be the ratio of the shell length L to the characteristic length $(Rh)^{1/2}$, that is,

$$Z_H = L/(Rh)^{1/2} \quad \text{or} \quad Z_H = (L/R)(R/h)^{1/2} \tag{48}$$

so that the problem is independent of the individual values of L/R and R/h. Finally, substituting the buckling mode w_I, f_I and the second order fields w_{II} and f_{II} into C_1 and C_2, and performing the integration in the circumferential direction analytically, one obtains,

$$C_1 = (N^2 y_o)\int_{x=0}^{Z_H}\{w_x^*(-f_s w_{s,x} - f_c w_{c,x}) + (1/2)w_{A,x}(f_s w_{s,x} - f_c w_{c,x}) - (1/2)w_{B,x}(f_s w_{c,x} + f_c w_{s,x}) - w_A(f_{s,xx}w_s - f_{c,xx}w_c) + w_B(f_{s,xx}w_c + f_{c,xx}w_s) + w_A(f_{s,x}w_{s,x} - f_{c,x}w_{c,x})$$

Downloaded 03 May 2010 to 171.66.16.27. Redistribution subject to ASME license or copyright; see http://www.asme.org/terms/Terms_Use.cfm

$$- w_B(f_{s,x}w_{c,x} + f_{c,x}w_{s,x}) - [w^*_{,x}(f_{s,x}w_s + f_{c,x}w_c) + (1/2)w_{A,x}(f_{s,x}w_s - f_{c,x}w_c) + (1/2)w_{B,x}(-f_{s,x}w_c - f_{c,x}w_s)]\}dx \quad (49)$$

$$C_2 = (N^2 y_o)\int_{x=0}^{Z_H} \{-f_A[-(w_{s,x})^2 + (w_{c,x})^2] - 2f_B w_{s,x}w_{c,x} + (1/2)f^*_{,xx}(w_s^2 + w_c^2) + (1/4)f_{A,xx}(w_s^2 - w_c^2) - (1/2)f_{B,xx}w_s w_c + f_{A,x}(w_s w_{s,x} - w_c w_{c,x}) - f_{B,x}(w_c w_{s,x} + w_s w_{c,x})\}dx \quad (50)$$

4 Discussion of Results

Since it is impractical to present a complete parameter variation of the composite cylindrical shells, example problems are chosen from antisymmetric laminated cross-ply cylindrical shells made of Boron-epoxy materials. The material parameters are (Hui, 1985a,b),

$$E_1/E_2 = 10.0, \quad G_{12}/E_2 = 0.5, \quad \nu_{12} = 0.25$$

The in-plane boundary conditions in all the example problems are $U,_{YY}(X = 0) = 0$ and $V,_Y(X = 0) = 0$ with identical conditions at the other end $X = L$. The following four cases are being considered:

(*i*) Clamped, N_L = infinite,
(*ii*) Clamped, N_L = 2, 0 deg inside and 90 deg outside
(*iii*) Clamped, N_L = 2, 90 deg inside and 0 deg outside
(*iv*) Simply-supported, N_L = infinite

where N_L is the number of layers. Within the limits of where the Donnell shell theory is applicable (number of circumferential full-waves n is either 0 or greater than 5), the results presented are valid for all radius-to-thickness ratios. Thus, the geometry of the cylindrical shell can be described by the reduced-Batdorf parameter Z_H.

The coupled ordinary differential equations are discretized in the axial direction using the central finite difference scheme from $X = 0$ to $X = L$. The boundary conditions at each end of the shell are also discretized. For a given value of the circumferential wave number N, the smallest eigenvalue is obtained by using the shifted inverse power method. The classical torsional buckling load is obtained by repeating the procedure for all possible values of N. In all the present example problems, it is found that the torsional buckling load occurs in equal and opposite pairs, indicating that it is independent of the direction in which the torque is applied. This situation is quite analogous to the shear buckling of antisymmetric cross-ply rectangular plates (Hui, 1984) and cylindrical panels (Hui, 1985b). For other types of lamination, it must be noted that the direction of torque application may play an important role in laminated cylindrical shells (Marlowe et al., 1973, and Wilkins and Love, 1974) and shear buckling of laminated cylindrical panels (Zhang and Matthews, 1983). In the computation of the postbuckling b coefficient, the maximum deflection $(w_s^2 + w_c^2)^{1/2}$ is taken to be unity and it does not necessarily occur at the middle of the shell $X = L/2$. Integration in the axial direction is performed using Simpson's rule. It is important to point out that the present Koiter (1945) postbuckling analysis is valid only for imperfection shape identical to that of the buckling mode and that the imperfection amplitude should be sufficiently small.

Table 1 shows the torsional buckling data for each of the four cases of antisymmetric cross-ply cylindrical shells for various values of the reduced-Batdorf parameter Z_H. The optimal circumferential wave number N which corresponds to the classical torsional buckling load is also displayed and this decreases with increasing Z_H. It is found that the classical buckling load is not very sensitive to a slight change in the circumferential wave number, whereas the postbuckling b coefficient is quite sensitive to N. The classical buckling load decreases with increasing Z_H.

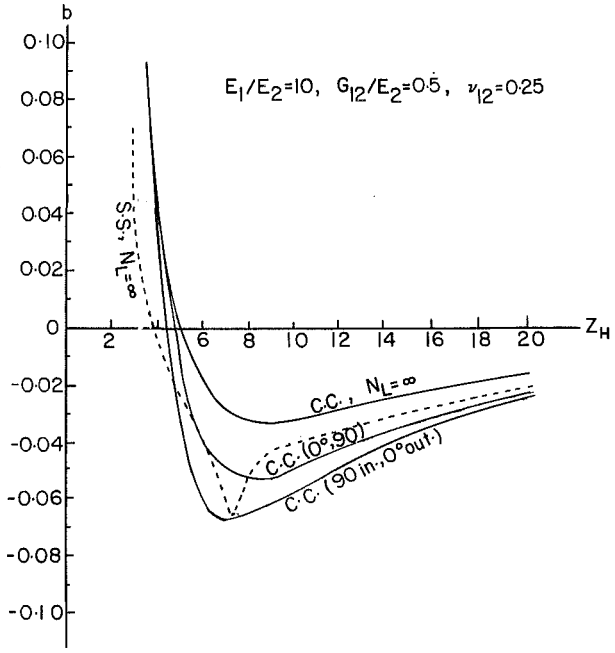


Fig. 2 Postbuckling b coefficient versus the reduced-Batdorf parameters for antisymmetric cross-ply Boron-epoxy cylinders under torsion

Figure 1 shows a graph of the buckling load (normalized with respect to the classical buckling load of the perfect system) versus the imperfection amplitude for various values of the b coefficients. The structure is imperfection-sensitive if b is negative and the degree of imperfection-sensitivity increases with increasing magnitude of the b coefficient.

Figure 2 shows a graph of the postbuckling b coefficient versus the reduced-Batdorf parameter for each of the four cases of antisymmetric cross-ply cylindrical shells. The b coefficients are positive for sufficiently small values of Z_H and the transition between positive and negative values of b occurs at Z_H between 3.0 and 5.0 for each of the four cases considered. Furthermore, the range of values of the reduced-Batdorf parameter Z_H which corresponds to the maximum imperfection-sensitivity is 4.0 to 9.0. For larger values of Z_H, the b coefficients remain negative but approach zero in all four cases. Judging from the magnitude of the b coefficients, the (0 deg inside and 90 deg outside) two-layered cylindrical shell is less imperfection-sensitive than the (90 deg, 0 deg) design due to different bending-stretching coupling behavior; however, the classical torsional buckling loads are identical for these two configurations. As a check on the analysis, the classical buckling load and the b coefficients for the special case of isotropic homogeneous cylindrical shells agree very well with the ones presented by Budiansky (1967) for all values of the Batdorf parameter.

Figure 3 shows the classical torsional buckling load of perfect orthotropic (N_L = infinite) cross-ply cylindrical shells versus Young's moduli ratio, keeping $G_{12}/E_2 = 0.5$ and $\nu_{12} = 0.25$. The torsional buckling load for the clamped cylinder with reduced-Batdorf parameter Z_H being 4 is found to be significantly higher than that for $Z_H = 10$ or 20. Moreover, as shown in Fig. 4, the b coefficients for $Z_H = 4$ are generally much more positive than that for $Z_H = 10$ or $Z_H = 20$. Thus, the $Z_H = 4$ configuration is a much better design than $Z_H = 10$ or 20. For fixed Young's moduli ratio between 1 and 40, the

Downloaded 03 May 2010 to 171.66.16.27. Redistribution subject to ASME license or copyright; see http://www.asme.org/terms/Terms_Use.cfm

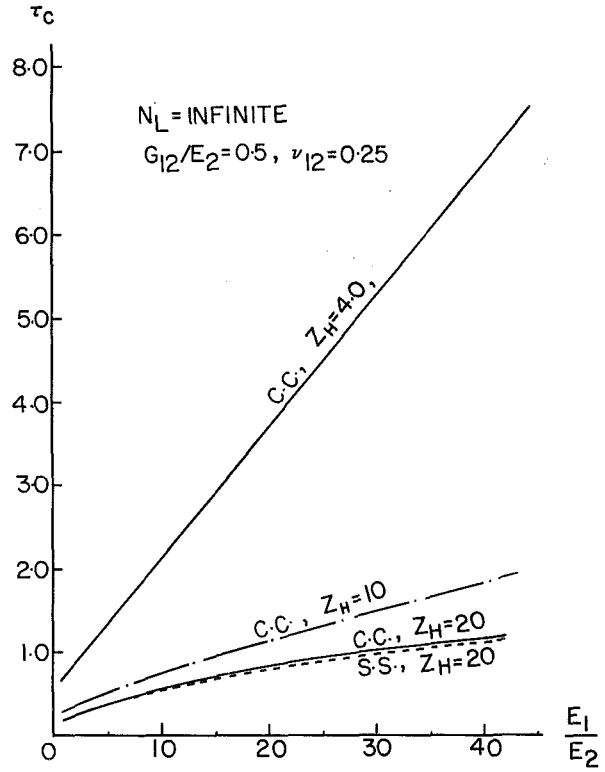


Fig. 3 Classical torsional buckling load versus Young's moduli ratio for orthotropic cross-ply cylindrical shells under torsion

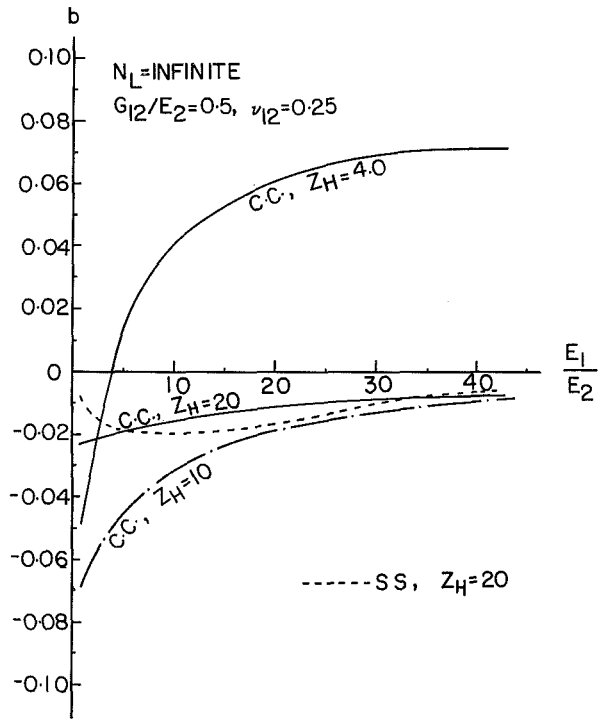


Fig. 4 Postbuckling *b* coefficient versus Young's moduli ratio for orthotropic cross-ply cylindrical shells under torsion

$Z_H = 10$ design has higher torsional buckling load than the $Z_H = 20$ configuration but at the expense of a more severe imperfection sensitivity. However, at least for fixed values of the reduced-Batdorf parameters being 4, 10, and 20, it appears that an increase in the Young's moduli ratio (causing a higher classical torsional buckling load) is not necessarily accompanied by an increase in the imperfection-sensitivity. This indicates that from the point of view of high buckling load and low imperfection-sensitivity, it is advantageous to use Graphite-epoxy ($E_1/E_2 = 40$) rather than Boron-epoxy ($E_1/E_2 = 10$) or Glass-epoxy ($E_1/E_2 = 3$) for cross-ply cylindrical shells under torsion.

Since the shape of the geometric imperfection considered by Simitses is not the same as that for the torsional buckling mode, a direct comparison between the present result with that of Simitses cannot be made. The present parameters involving the reduced-Batdorf parameter are in qualitative agreement with the imperfection sensitivity results of Simitses. However, the stronger geometries are not necessarily more sensitive to imperfection than the weaker ones as indicated by the present parameter variation involving Young's moduli ratio; this phenomenon is not supported in Simitses' findings, due to different material parameters and stacking sequences being considered.

Finally, the cross-ply cylindrical shell is most sensitive to imperfections (as indicated by relatively large negative values of b) in a rather low range of Z_H. That is, the shorter cylinders are more sensitive to imperfections than the longer ones. Since thin shell theory holds for R/h 30 (or so), the analysis is valid for sufficiently large values of Z_H. For example, if $L/R = 1$, $Z_H > 5.5$ and, similarly, if $L/R = 2$, $Z_H > 11$ and if $L/R = 10$, $Z_H > 55$.

5 Conclusions

The initial postbuckling behavior of antisymmetrically laminated cross-ply cylindrical shells under torsion has been examined. The torsional buckling loads and the associated postbuckling stiffness coefficients have been presented for Boron-epoxy cylindrical shells and concise parameter variations have been performed on the reduced-Batdorf parameter and Young's moduli ratio. Due to different bending-stretching coupling characteristics, the (0 deg inside and 90 deg outside) two-layer design is less imperfection-sensitive than the (90 deg, 0 deg) configuration. The laminated cylinders under torsion are imperfection-sensitive for the reduced-Batdorf parameter being approximately $4 \leq Z_H \leq 20$. Further, the increase in the torsional buckling load due to a higher value of Young's modulus ratio is not necessarily accompanied by a higher degree of imperfection-sensitivity.

It should be emphasized that these conclusions are valid only for certain shell configurations and boundary conditions. They are valid if at least three assumptions hold true: (*i*) The geometric imperfection is of the same shape as the torsional buckling mode (Koiter, 1945) and the imperfection amplitude is sufficiently small; (*ii*) the thin-shell theory is valid; (*iii*) membrane prebuckling state. For antisymmetric cross-ply layups, the last assumption is valid since pure shear is compatible (equation (19)) with a momentless prebuckling state with $b^*_{61} = b^*_{62} = b^*_{66} = 0$. It should be cautioned that a momentless prebuckling state is not consistent with the constitutive relations for antisymmetric "angle-ply" laminated cylindrical shells subjected to pure torsion. It is expected that angle-plies can provide greater torsional stiffness and strength and an extension of the present work to these laminates, which would involve a nonlinear prebuckling state (see Hui, 1986a), is in progress.

References

Booton, M., 1976, "Buckling of Imperfect Anisotropic Cylinders under Combined Loading," University of Toronto Institute for Aerospace Studies (UTIAS), Report No. 203.

Booton, M., and Tennyson, R. C., 1979, "Buckling of Imperfect Anisotropic Circular Cylinders Under Combined Loading," *AIAA Journal*, Vol. 17, pp. 278–287.

Budiansky, B., 1967, "Post-Buckling Behavior of Cylinders in Torsion," *Theory of Thin Shells*, IUTAM Symposium, Niordson, F. I., ed., Springer-Verlag, 1969, pp. 212–233.

Downloaded 03 May 2010 to 171.66.16.27. Redistribution subject to ASME license or copyright; see http://www.asme.org/terms/Terms_Use.cfm

Bushnell, D., 1985, *Computerized Buckling Analysis of Shells*, Martinus Nijhoff Publishers, Boston and Lancaster.

Chechill, D. S., and Cheng, S., 1968, "Elastic Buckling of Composite Cylindrical Shells Under Torsion," *Journal of Spacecraft and Rockets*, Vol. 5, pp. 973–978.

Dongarra, J. J., Bunch, J. R., Moler, C. B., and Stewart, G. W., 1979, "LINPACK User's Guide," published by Society of Industrial and Applied Mathematics (SIAM), Philadelphia; also Argonne National Lab. Report TM-313, Aug. 1977.

Galletly, G. D., and Pemsing, K., 1985, "Interactive Buckling Tests on Cylindrical Shells Subjected to Axial Compression and External Pressure – A Comparison of Experiment, Theory, and Various Codes," *Proc. of the Institution of Mechanical Engineers*, Part C, Vol. 199, No. C4, pp. 259–280.

Hayashi, T., and Hirano, Y., 1964, "Postbuckling Behavior of Orthotropic Cylinders under Torsion," *Trans. Japan Society of Aero. Space Sciences*, Vol. 7, pp. 47–54.

Herakovich, C. T., and Johnson, E. R., 1981, "Buckling of Composite Cylinders under Combined Compression and Torsion – Theoretical/Experimental Correlation," Test Methods for Fibrous Composites, American Society for Testing and Materials (ASTM), Technical Publication 734, pp. 341–360.

Hui, D., Tennyson, R. C., and Hansen, J. S., 1981, "Mode Interaction of Axially Stiffened Cylindrical Shells: Effects of Stringer Axial Stiffness, Torsional Rigidity and Eccentricity," ASME JOURNAL OF APPLIED MECHANICS, Vol. 48, No. 4, pp. 915–922.

Hui, D., 1984, "Shear Buckling of Anti-Symmetric Cross Ply Rectangular Plates," *Fibre Science and Technology*, Vol. 21, No. 4, pp. 327–340.

Hui, D., 1985a, "Axisymmetric Postbuckling of Symmetrically Laminated Short Cylindrical Panels under Compression," *Composite Structures*, Vol. 3, pp. 81–95.

Hui, D., 1985b, "Effects of Shear Loads on Vibration and Buckling of Antisymmetric Cross-Ply Cylindrical Panels," *Structural Dynamics*, Proceedings of the 1985 ASME Pressure Vessels and Piping Conference, PVP-Vol. 98-6, S. S. Chen et al., eds., pp. 205–212; *International Journal of Nonlinear Mechanics*, in press.

Hui, D., 1986a, "Imperfection Sensitivity of Axially Compressed Laminated Flat Plates due to Bending-Stretching Coupling," *International Journal of Solids and Structures*, Vol. 22, pp. 13–22.

Hui, D., 1986b, "Imperfection-Sensitivity of Elastically Supported Beams and its Relation to the Double-Cusp Instability Model," *Proceedings of the Royal Society of London*, Series A, Vol. A405, p. 143–158.

Hutchinson, J. W., and Amazigo, J. C., 1967, "Imperfection-Sensitivity of Eccentrically Stiffened Cylindrical Shells," *AIAA Journal*, Vol. 5, No. 3, pp. 392–401.

Koiter, W. T., 1945, "On the Stability of Elastic Equilibrium," Doctoral Thesis, Delft, The Netherlands, English Trans., NASA-TT-F10-833, 1967, and AFFDL-TR-70-25, 1970.

Koiter, W. T., 1963, "The Effect of Axisymmetric Imperfections on the Buckling of Cylindrical Shells under Axial Compression," *Proceedings of the Koninklijke Nederlandse Akademie Van Wetenschappen*, Series B, Vol. 66, pp. 265–279.

Kollar, L., and Dulacska, E., 1984, "Buckling of Shells for Engineers," translated from Hungarian, Wiley, New York.

Leissa, A. W., 1985, "Buckling of Laminated Composite Plates and Shell Panels," Air Force Wright Aeronautical Lab., AFWAL-TR-85-3069, pp. 454.

March, H. W., Norris, C. B., Smith, C. B., and Kuenzi, E. W., 1945, "Buckling of Thin-Walled Plywood Cylinders in Torsion," Forest Products Lab., Madison, Wis., Report 1529.

Marlowe, D. E., Sushinsky, G. F., and Dexterr, H. B., 1973, "Elastic Torsional Buckling of Thin-Walled Composite Cylinders," Composite Materials Testing and Design, Third Conference, ASTM.

Shaw, D., and Simitses, G. J., 1982, "Imperfect, Laminated, Cylindrical Shells in Torsion and Axial Compression," 33rd Congress of the International Astronautical Federation (IAF '82), Sept. 27–Oct. 2, Paris, France, Published by AIAA.

Shaw, D., and Simitses, G. J., 1984, "Instability of Laminated Cylinders in Torsion," ASME JOURNAL OF APPLIED MECHANICS, Vol. 51, pp. 188–191.

Simitses, G. J., 1986, "Buckling and Postbuckling of Imperfect Cylindrical Shells," *Proceedings of the ASME Joint PVP and Computer Engineering Division Conference*, Chicago, Hui, D., Duke, J., and Chung, H., eds., ASME PVP-119 and NDE-3, pp. 1–11.

Simitses, G. J., Shaw, D., and Sheinman, I., 1985, "Imperfection Sensitivity of Laminated Cylindrical Shells in Torsion and Axial Compression," *Composite Structures*, Vol. 4, pp. 335–360.

Tennyson, R. C., Chan, H. K., and Muggeridge, D. B., 1971, "The Effect of Axisymmetric Shaped Imperfections on the Buckling of Laminated Anisotropic Circular Cylinders," *Transactions of the Canadian Aeronautics and Space Institute* (CASI), Vol. 4, No. 2, pp. 131–139.

Tennyson, R. C., 1975, "Buckling of Laminated Composite Cylinders: A Review," *Composites*, Vol. 1, pp. 17–24.

Tennyson, R. C., Booton, M., and Hui, D., 1980, "Changes in Cylindrical Shell Buckling Behavior Resulting from System Parameter Variations," *Proceedings of the 15th International Congress of Theoretical and Applied Mechanics*, Rimrott, F. P. J., and Tabarrok, B., eds., North Holland Publishing Co., pp. 417–428, invited IUTAM paper.

Tennyson, R. C., 1984, "Thin-Walled Structures in Aerospace Design," *Developments in Thin-Walled Structures – 2*, Rhodes, J., and Walker, A. C., eds., Elsevier Applied Science Publishers, pp. 173–210.

Thurston, G. A., 1965, "Newton's Method Applied to Problems in Nonlinear Mechanics," ASME JOURNAL OF APPLIED MECHANICS, Vol. 32, pp. 383–388.

Wilkins, D. J., and Love, T. S., 1974, "Combined Compression-Torsion Buckling Tests of Laminated Composite Cylindrical Shells," *Proc. of AIAA/ASME/SAE 15th Structures, Structural Dynamics and Materials Conference*, Las Vegas, Nev., AIAA Paper No. 74-379.

Yamaki, N., and Kodama, S., 1980, "Perturbation Analyses for the Postbuckling and Imperfection Sensitivity of Circular Cylindrical Shells under Torsion," *Theory of Shells, Proceedings of the Third IUTAM Symposium on Shell Theory*, Tbilisi, U.S.S.R., Aug. 22–28, 1978, Koiter, W. T., and Mikhailov, G. K., eds., North-Holland Publishing Co., Amsterdam, 1980, pp. 635–668.

Yamaki, N., 1984, "Elastic Stability of Circular Cylindrical Shells," North-Holland Publishing Co., Amsterdam.

Zhang, Y., and Matthews, F. L., 1983, "Initial Buckling of Curved Panels of Generally Layered Composite Materials," *Composite Structures*, Vol. 1, pp. 3–30.

Downloaded 03 May 2010 to 171.66.16.27. Redistribution subject to ASME license or copyright; see http://www.asme.org/terms/Terms_Use.cfm

A Composite Plate Theory for Arbitrary Laminate Configurations

A. Toledano
Research Assistant.

H. Murakami
Associate Professor of Applied Mechanics.

Department of Applied Mechanics and Engineering Sciences,
University of California, San Diego,
La Jolla, Calif. 92093

In order to improve the accuracy of in-plane responses of shear deformable composite plate theories, a new laminated plate theory was developed for arbitrary laminate configurations based upon Reissner's (1984) new mixed variational principle. To this end, across each individual layer, piecewise linear continuous displacements and quadratic transverse shear stress distributions were assumed. The accuracy of the present theory was examined by applying it to the cylindrical bending problem of laminated plates which had been solved exactly by Pagano (1969). A comparison with the exact solutions obtained for symmetric, antisymmetric, and arbitrary laminates indicates that the present theory accurately estimates in-plane responses, even for small span-to-thickness ratios.

1 Introduction

Thick laminated plates and shells find extensive applications as structural elements. As a result, various approximate theories have been developed in an effort to properly assess their mechanical behavior under static and dynamic loads.

In a series of papers Pagano (1969, 1970, 1971, 1972) gave the exact solution for the problem of cylindrical bending and simply supported plates. He pointed out the importance of considering shear deformation effects in order to accurately predict the plate lateral deflection and the necessity of improving the thickness variation of in-plane displacements, which are assumed to be C^1-linear functions in both classical plate theory (CPT) and Reissner-Mindlin plate theory (FSD).

One of the earliest attempts in deriving an approximate theory for laminates is credited to Yu (1959). He investigated the plane strain problem of isotropic sandwich plates by assuming piecewise linear displacement distributions. Yang, Norris, and Stavsky (1966) extended Reissner-Mindlin plate theory to the case of an arbitrary number of bonded anisotropic layers. Whitney and Pagano (1970) using this latter approach, and later Whitney (1972), concluded that the introduction of shear deformations cannot improve the in-plane stress distributions as determined from classical plate theory.

As a remedy to these difficulties, higher order theories have been proposed in which the displacement assumptions are expressed in terms of power series in the thickness variable. The number of plate equations of such theories does not increase with the number of layers. Theories including quadratic variations (Whitney and Sun, 1973, and Nelson and Lorch, 1974) and cubic variations (Hildebrand, Reissner, and Thomas, 1949, Lo, Christensen, and Wu, 1977) of in-plane displacements through the plate thickness belong to this category. Reddy's (1984) high-order theory is obtained by imposing the condition of vanishing transverse shear strains on the top and bottom surfaces of the plate. Whitney (1972) derived in-plane displacements by integrating the transverse shear strains deduced by Whitney and Pagano (1970). This resulted in a higher order approximation which accurately predicted in-plane strains, but the resulting modified stresses did not necessarily satisfy the original plate equilibrium equations.

Another class of higher order theories employs the displacements to be continuous and piecewise-smooth functions, i.e., smooth within each layer (Yu, 1959). Durocher and Solecki (1975) have followed this approach to analyze transversely isotropic sandwich plates. Mau (1973), Srinivas (1973), and Seide (1980) have considered the case of an arbitrary number of layers. No shear correction factors were introduced by the last two authors. In all these theories, the number of field equations and edge boundary conditions depends on the number of layers.

Most of the theories discussed so far, which are classified as displacement-based theories, suffer from a common deficiency: constitutive equations lead to discontinuous interlaminar stresses. This shortcoming has been overcome in the theory proposed by Murakami (1985) which is based upon Reissner's (1984) new mixed variational principle. This theory is obtained by superposing a zig-zag shaped C^0-linear function to the in-plane displacements given by Reissner-Mindlin plate theory. It was later extended by including Legendre polynomials in the displacement variations across the plate thickness (Toledano and Murakami, 1986). In both these theories, the number of equilibrium equations and edge boundary conditions are independent of the number of layers. Thus, the theories have some limitations when applied to composite plates with arbitrary laminate configuration.

In order to improve the in-plane response of composite plates for arbitrary laminate configuration, a new theory which accounts for transverse shear deformations has been

Contributed by the Applied Mechanics Division for publication in the JOURNAL OF APPLIED MECHANICS.

Discussion on this paper should be addressed to the Editorial Department, ASME, United Engineering Center, 345 East 47th Street, New York, N.Y. 10017, and will be acepted until two months after final publication of the paper itself in the JOURNAL OF APPLIED MECHANICS. Manuscript received by ASME Applied Mechanics Division, February 7, 1986.

Copyright © 1987 by ASME
Downloaded 03 May 2010 to 171.66.16.27. Redistribution subject to ASME license or copyright; see http://www.asme.org/terms/Terms_Use.cfm

developed by assuming piecewise continuous in-plane displacement distributions. In order to guarantee continuity of interlaminar stresses, Reissner's (1984) new mixed variational principle has been invoked by taking the transverse stresses to be quadratic functions of a local thickness coordinate across each layer. Governing equations and consistent boundary conditions are then deduced. The advantage of using Reissner's new mixed variational principle is that it automatically yields the appropriate shear correction factors for the transverse shear constitutive equations. A comparison with Pagano's (1969) exact elasticity solution for symmetric, antisymmetric, and arbitrary laminates in cylindrical bending, shows that the proposed theory can accurately predict in-plane displacements and stresses at low span-to-thickness ratios. To further assess the range of applicability of the present theory, results previously obtained by Murakami (1985) are also presented.

2 Formulation

Consider an N-layer laminated composite plate of uniform thickness h, as shown in Fig. 1. A Cartesian coordinate system is chosen such that the middle surface of the plate occupies a domain D in the x_1, x_2 plane, the x_3 axis being normal to this plane. The following notation: $(\ )^{(k)}$, $k = 1,2, \ldots, N$ will designate quantities associated with the kth layer. The thickness of each layer is $n^{(k)}h$, in which the volume fractions $n^{(k)}$ satisfy the relation

$$\sum_{k=1}^{N} n^{(k)} = 1 \tag{1}$$

Unless otherwise specified, the usual Cartesian indicial notation is employed where Latin and Greek indices range from 1 to 3 and 1 to 2, respectively. Repeated indices imply the summation convention and $(\ )_{,i}$ is used to denote partial differentiation with respect to x_i.

With the help of the foregoing notation, the governing equations for the displacement vector $u_i^{(k)}$ and stress tensor $\sigma_{ij}^{(k)}$ associated with the kth layer are:

a) Equilibrium Equations

$$\sigma_{ji,j}^{(k)} + f_i^{(k)} = 0;\ \sigma_{ji}^{(k)} = \sigma_{ij}^{(k)} \tag{2}$$

where f_i are body forces;

b) Constitutive Equations for Monoclinic Layers

$$\begin{bmatrix} \sigma_{11} \\ \sigma_{22} \\ \sigma_{12} \end{bmatrix}^{(k)} = \begin{bmatrix} \tilde{C}_{11} & \tilde{C}_{12} & \tilde{C}_{16} \\ \tilde{C}_{12} & \tilde{C}_{22} & \tilde{C}_{26} \\ \tilde{C}_{16} & \tilde{C}_{26} & \tilde{C}_{66} \end{bmatrix}^{(k)} \begin{bmatrix} e_{11} \\ e_{22} \\ 2e_{12} \end{bmatrix}^{(k)} + \begin{bmatrix} C_{13} \\ C_{23} \\ C_{36} \end{bmatrix}^{(k)} \left(\frac{\sigma_{33}}{C_{33}}\right)^{(k)} \tag{3a}$$

$$e_{33}^{(k)} = -\left(\frac{C_{13}}{C_{33}}\right)^{(k)} e_{11}^{(k)} - \left(\frac{C_{23}}{C_{33}}\right)^{(k)} e_{22}^{(k)} - \left(\frac{C_{36}}{C_{33}}\right)^{(k)} 2e_{12}^{(k)} + \left(\frac{\sigma_{33}}{C_{33}}\right)^{(k)} \tag{3b}$$

$$\begin{bmatrix} 2e_{23} \\ 2e_{31} \end{bmatrix}^{(k)} = \begin{bmatrix} C_{44} & C_{45} \\ C_{45} & C_{55} \end{bmatrix}^{(k)-1} \begin{bmatrix} \sigma_{23} \\ \sigma_{31} \end{bmatrix}^{(k)} \equiv \begin{bmatrix} \tilde{C}_{55} & -\tilde{C}_{45} \\ -\tilde{C}_{45} & \tilde{C}_{44} \end{bmatrix}^{(k)} \begin{bmatrix} \sigma_{23} \\ \sigma_{31} \end{bmatrix}^{(k)} \tag{3c}$$

where C_{ij} are the elastic constants and $\tilde{C}_{ij}$ $(i, j = 1,2,6)$ represent the reduced stiffnesses introduced by Whitney and Pagano (1970) in the contracted notation;

c) Strain-Displacement Relations

$$e_{ij}^{(k)} = \frac{1}{2}\left(u_{i,j}^{(k)} + u_{j,i}^{(k)}\right) \tag{4}$$

d) Interface Continuity Conditions

$$u_i^{(k)} = u_i^{(k+1)} \text{ and } \sigma_{3i}^{(k)} = \sigma_{3i}^{(k+1)};\ k = 1,2, \ldots, N-1 \tag{5}$$

e) Upper and Lower Surface Stress Conditions

$$\sigma_{3i}^{(1)} = T_i^{+} \text{ on } x_3 = \frac{h}{2} \tag{6a}$$

$$\sigma_{3i}^{(N)} = T_i^{-} \text{ on } x_3 = -\frac{h}{2} \tag{6b}$$

The objectives in developing the present composite plate theory are: first, to improve the assumed variations of in-plane displacements through the plate thickness; second, to take into account the effect of transverse shear deformation and derive appropriate constitutive equations; and finally, for *arbitrary* laminate configurations, to assess and compare its range of applicability with the laminated plate theory proposed by Murakami (1985).

In order to carry out this task, Reissner's (1984) new mixed variational principle for displacements and transverse stresses was applied to the N-layer composite plate:

$$\begin{aligned} &\iint_D \left[\sum_{k=1}^{N} \int_{A^{(k)}} \left\{\delta e_{ij}^{(k)} \sigma_{ij}^{(k)} + [u_{3,\alpha}^{(k)} + u_{\alpha,3}^{(k)} - 2e_{3\alpha}^{(k)}(\cdots)]\delta\tau_{3\alpha}^{(k)} \right.\right. \\ &\left.\left. + [u_{3,3}^{(k)} - e_{33}^{(k)}(\cdots)]\delta\tau_{33}^{(k)}\right\} dx_3\right] dx_1 dx_2 \\ &= \iint_D \left[\sum_{k=1}^{N} \int_{A^{(k)}} \delta u_i^{(k)} f_i^{(k)} dx_3\right] dx_1 dx_2 \\ &+ \iint_D \left[\delta u_i^{(1)}\left(x_1, x_2, \frac{h}{2}\right) T_i^{+} \right. \\ &\left. - \delta u_i^{(N)}\left(x_1, x_2, -\frac{h}{2}\right) T_i^{-}\right] dx_1 dx_2 \\ &+ \int_{\partial D_T} \left[\sum_{k=1}^{N} \int_{A^{(k)}} \delta u_i^{(k)} {}^{\nu}T_i^{(k)} dx_3\right] ds \end{aligned} \tag{7}$$

where ∂D_T denotes the boundary of D with outward normal ν_α on which tractions ${}^{\nu}T_i$ are prescribed and $A^{(k)}$ is the x_3 domain occupied by the kth layer. Also $\tau_{3i}^{(k)}$ denote the approximate transverse stresses and $e_{3i}^{(k)}(\cdots)$ are given by equations (3*b*,*c*). Due to the nature of Reissner's mixed variational principle, equations (3*a*) are taken to be the definitions of $\sigma_{\alpha\beta}^{(k)}$ used in connection with (7).

3 Trial Displacement and Transverse Stress Fields

The present laminated plate theory which accounts for transverse shear effects is obtained by assuming a linear variation of the in-plane displacements across each individual layer, as shown in Fig. 2. Transverse displacements are taken to be constant throughout the entire thickness of the plate. Therefore, shear strains are constant within each layer, but differ from layer to layer. This approach has been previously adopted by Seide (1980) for the N-layer case. However, no mention of shear correction factors was made in his paper.

The appropriate trial functions used in connection with Reissner's mixed variational principle, equation (7), are chosen to be:

Downloaded 03 May 2010 to 171.66.16.27. Redistribution subject to ASME license or copyright; see http://www.asme.org/terms/Terms_Use.cfm

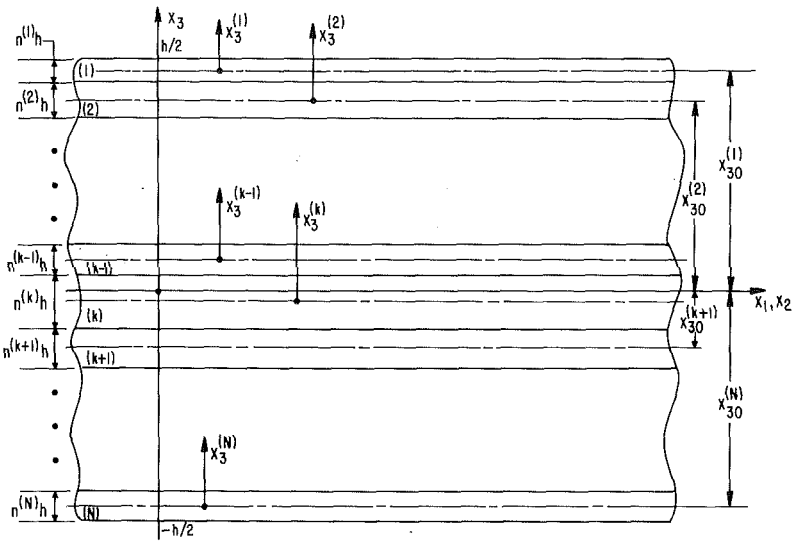


Fig. 1 Plate geometry and coordinate system

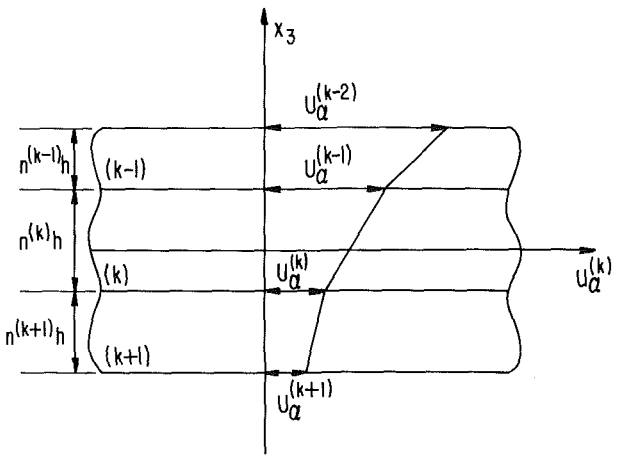


Fig. 2 Approximation of in-plane displacements

a) Trial Displacement Field

$$u_\alpha^{(k)}(x_i) = U_\alpha^{(k-1)}(x_\beta) g_1^{(k)}(x_3^{\{k\}}) + U_\alpha^{(k)}(x_\beta) g_2^{(k)}(x_3^{\{k\}}) \tag{8a}$$

$$u_3^{\{k\}}(x_i) = U_3(x_\beta) \tag{8b}$$

where $$g_\alpha^{(k)}(x_3^{\{k\}}) \equiv \frac{1}{2} + (-1)^{\alpha+1} \frac{x_3^{\{k\}}}{n^{(k)}h} \tag{9}$$

$x_3^{\{k\}}$ is a local x_3-coordinate system with its origin at the center $x_{30}^{\{k\}}$ of the kth layer, i.e.,

$$x_3^{\{k\}} \equiv x_3 - x_{30}^{\{k\}} \tag{10}$$

From equations (8*a*) and (9) it is seen that $U_\alpha^{(k)}$ ($k = 1,2, \cdots, N-1$), $U_\alpha^{(0)}$ and $U_\alpha^{(N)}$ represent the values of $u_\alpha^{(k)}$ at the interfaces, top and bottom surfaces of the plate, respectively. Also, equations (8) satisfy interface displacement continuity conditions equation (5*a*).

b) Trial Transverse Stress Field

$$\tau_{3\alpha}^{\{k\}}(x_i) = Q_\alpha^{(k)}(x_\beta) F_1(z) + T_\alpha^{(k-1)}(x_\beta) F_2(z) + T_\alpha^{(k)}(x_\beta) F_3(z) \tag{11a}$$

$$\tau_{33}^{\{k\}}(x_i) \equiv 0 \tag{11b}$$

where $$F_1(z) = \frac{3}{2n^{(k)}h}(1-z^2) \tag{12a}$$

$$F_i(z) = \frac{3}{4} z^2 + \frac{1}{2}(-1)^i z - \frac{1}{4}, \quad i = 2,3 \tag{12b}$$

and $$z \equiv \frac{2x_3^{\{k\}}}{n^{(k)}h}; \quad -1 \le z \le 1 \tag{13}$$

Also $$Q_\alpha^{(k)} \equiv \int_{A^{(k)}} \tau_{3\alpha}^{\{k\}} dx_3 \tag{14}$$

In equation (11*a*), $T_\alpha^{(k-1)}$ and $T_\alpha^{(k)}$ are the values of $\tau_{3\alpha}^{\{k\}}$ at the top and bottom surfaces of the kth layer, respectively. From equation (6) one has

$$T_i^{(0)} = T_i^+ \text{ and } T_i^{(N)} = T_i^- \tag{15}$$

Equations (11) satisfy the interface stress continuity conditions, equation (5*b*). Due to the approximation for $u_3^{\{k\}}$ which yields $e_{33}^{\{k\}} = 0$, $\sigma_{33}^{\{k\}}$ becomes a reactive stress. Consequently, $\sigma_{33}^{\{k\}}$ can be determined by integrating the third equilibrium equation.

4 Laminated Plate Equations

Substituting equations (8) and (11) into equation (7) and using Gauss's theorem, one obtains:

a) Equilibrium Equations

$$\frac{1}{2} N_{\beta\alpha,\beta}^{(1)} + \frac{1}{n^{(1)}h}\left(M_{\beta\alpha,\beta}^{(1)} - N_{3\alpha}^{(1)}\right) + \frac{1}{2} {}^N F_\alpha^{(1)} + \frac{1}{n^{(1)}h} {}^M F_\alpha^{(1)} + T_\alpha^+ = 0 \tag{16a}$$

$$\begin{aligned} &-\frac{1}{2}\left(N_{\beta\alpha,\beta}^{(k)} + N_{\beta\alpha,\beta}^{(k+1)}\right) - \frac{1}{h}\left(\frac{M_{\beta\alpha,\beta}^{(k)}}{n^{(k)}} - \frac{M_{\beta\alpha,\beta}^{(k+1)}}{n^{(k+1)}}\right) \\ &+ \frac{1}{h}\left(\frac{N_{3\alpha}^{(k)}}{n^{(k)}} - \frac{N_{3\alpha}^{(k+1)}}{n^{(k+1)}}\right) \\ &+ \frac{1}{2}\left({}^N F_\alpha^{(k)} + {}^N F_\alpha^{(k+1)}\right) - \frac{1}{h}\left(\frac{{}^M F_\alpha^{(k)}}{n^{(k)}} - \frac{{}^M F_\alpha^{(k+1)}}{n^{(k+1)}}\right) \\ &= 0; \; k = 1,2, \cdots, N-1 \end{aligned} \tag{16b}$$

$$\frac{1}{2} N_{\alpha\beta,\beta}^{(N)} - \frac{1}{n^{(N)}h}\left(M_{\beta\alpha,\beta}^{(N)} - N_{3\alpha}^{(N)}\right) + \frac{1}{2} {}^N F_\alpha^{(N)} - \frac{1}{n^{(N)}h} {}^M F_\alpha^{(N)} - T_\alpha^- = 0 \tag{16c}$$

Downloaded 03 May 2010 to 171.66.16.27. Redistribution subject to ASME license or copyright; see http://www.asme.org/terms/Terms_Use.cfm

$$\sum_{k=1}^{N} N_{3\alpha,\alpha}^{(k)} + {}^{N}F_3 + T_3^{+} - T_3^{-} = 0 \tag{16d}$$

where $\left(N_{\alpha\beta}^{(k)}, M_{\alpha\beta}^{(k)}\right) \equiv \int_{A^{(k)}} (1, x_3^{(k)}) \sigma_{\alpha\beta}^{(k)} dx_3$;

$$N_{3\alpha}^{(k)} \equiv \int_{A^{(k)}} \tau_{3\alpha}^{(k)} dx_3 \tag{17a,b}$$

$$\left({}^{N}F_{\alpha}^{(k)}, {}^{M}F_{\alpha}^{(k)}\right) \equiv \int_{A^{(k)}} (1, x_3^{(k)}) f_{\alpha}^{(k)} dx_3;$$

$${}^{N}F_3 \equiv \sum_{k=1}^{N} \int_{A^{(k)}} f_3^{(k)} dx_3 \tag{17c,d}$$

b) Boundary Conditions

Specify $U_{\alpha}^{(k)}$ or $\left[\frac{1}{2}(N_{\beta\alpha}^{(k)} + N_{\beta\alpha}^{(k+1)}) - \frac{1}{h}\left(\frac{M_{\beta\alpha}^{(k)}}{n^{(k)}} - \frac{M_{\beta\alpha}^{(k+1)}}{n^{(k+1)}}\right)\right]\nu_{\beta}$ (18*a*)

Specify U_3 or $\sum_{k=1}^{N} N_{3\alpha}^{(k)} \nu_{\alpha}$ (18*b*)

Equations (18) constitute $(2N + 3)$ conditions. It can be seen that the natural edge traction boundary conditions are coupled; i.e. force and moment resultants acting on two adjacent layers are involved.

c) Constitutive Equations for Monoclinic Layers

$$Q_1^{(k)} - \left(\frac{\tilde{C}_{45}}{\tilde{C}_{44}}\right)^{(k)} Q_2^{(k)} - \frac{n^{(k)}h}{12}\left(T_1^{(k-1)} + T_1^{(k)}\right) + \frac{n^{(k)}h}{12}\left(\frac{\tilde{C}_{45}}{\tilde{C}_{44}}\right)^{(k)}\left(T_2^{(k-1)} + T_2^{(k)}\right) = \frac{5}{6\,\tilde{C}_{44}^{(k)}}\left(U_1^{(k-1)} - U_1^{(k)} + n^{(k)}h\,U_{3,1}\right) \tag{19a}$$

$$-\left(\frac{\tilde{C}_{45}}{\tilde{C}_{55}}\right)^{(k)} Q_1^{(k)} + Q_2^{(k)} + \frac{n^{(k)}h}{12}\left(\frac{\tilde{C}_{45}}{\tilde{C}_{55}}\right)^{(k)}\left(T_1^{(k-1)} + T_1^{(k)}\right) - \frac{n^{(k)}h}{12}\left(T_2^{(k-1)} + T_2^{(k)}\right) = \frac{5}{6\,\tilde{C}_{55}^{(k)}}\left(U_2^{(k-1)} - U_2^{(k)} + n^{(k)}h\,U_{3,2}\right) \tag{19b}$$

$$\frac{1}{10}\left(\tilde{C}_{44}^{(k)} Q_1^{(k)} + \tilde{C}_{44}^{(k+1)} Q_1^{(k+1)}\right) - \frac{1}{10}\left(\tilde{C}_{45}^{(k)} Q_2^{(k)} + \tilde{C}_{45}^{(k+1)} Q_2^{(k+1)}\right) + \frac{h}{30}\left[n^{(k)}\tilde{C}_{44}^{(k)} T_1^{(k-1)} - 4\left(n^{(k)}\tilde{C}_{44}^{(k)} + n^{(k+1)}\tilde{C}_{44}^{(k+1)}\right) T_1^{(k)} + n^{(k+1)}\tilde{C}_{44}^{(k+1)} T_1^{(k+1)}\right] \tag{19c}$$

$$-\frac{h}{30}\left[n^{(k)}\tilde{C}_{45}^{(k)}\, T_2^{(k-1)} - 4\left(n^{(k)}\tilde{C}_{45}^{(k)} + n^{(k+1)}\tilde{C}_{45}^{(k+1)}\right) T_2^{(k)} + n^{(k+1)}\tilde{C}_{45}^{(k+1)} T_2^{(k+1)}\right] = 0$$

$$-\frac{1}{10}\left(\tilde{C}_{45}^{(k)}\, Q_1^{(k)} + \tilde{C}_{45}^{(k+1)} Q_1^{(k+1)}\right) + \frac{1}{10}\left(\tilde{C}_{55}^{(k)}\, Q_2^{(k)} + \tilde{C}_{55}^{(k+1)} Q_2^{(k+1)}\right) - \frac{h}{30}\left[n^{(k)}\tilde{C}_{45}^{(k)}\, T_1^{(k-1)} - 4\left(n^{(k)}\tilde{C}_{45}^{(k)} + n^{(k+1)}\tilde{C}_{45}^{(k+1)}\right) T_1^{(k)} + n^{(k+1)}\tilde{C}_{45}^{(k+1)} T_1^{(k+1)}\right] \tag{19d}$$

$$+\frac{h}{30}\left[n^{(k)}\tilde{C}_{55}^{(k)}\, T_2^{(k-1)} - 4\left(n^{(k)}\tilde{C}_{55}^{(k)} + n^{(k+1)}\tilde{C}_{55}^{(k+1)}\right) T_2^{(k)} + n^{(k+1)}\tilde{C}_{55}^{(k+1)} T_2^{(k+1)}\right] = 0$$

In equations (19*a*,*b*) k ranges from 1 to N, while in equations (19*c*,*d*) k ranges from 1 to $(N-1)$. Equations (19) can be solved for $Q_{\alpha}^{(k)}$ and $T_{\alpha}^{(k)}$ in terms of $U_{\alpha}^{(k)}$ and $U_{3,\alpha}$. As a result, the quantities $N_{3\alpha}^{(k)}$ can be determined as functions of these displacement variables. Such expressions will automatically include appropriate shear correction factors by virtue of Reissner's mixed variational principle.

The remaining constitutive equations for $N_{\alpha\beta}^{(k)}$ and $M_{\alpha\beta}^{(k)}$ are obtained by substituting equations (3*a*), (4), and (8) into (17*a*) to yield

$$\begin{bmatrix} N_{11} \\ N_{22} \\ N_{12} \end{bmatrix}^{(k)} = \frac{n^{(k)}h}{2} \begin{bmatrix} \tilde{C}_{11} & \tilde{C}_{12} & \tilde{C}_{16} \\ \tilde{C}_{12} & \tilde{C}_{22} & \tilde{C}_{26} \\ \tilde{C}_{16} & \tilde{C}_{26} & \tilde{C}_{66} \end{bmatrix}^{(k)} \begin{bmatrix} U_{1,1}^{(k-1)} + U_{1,1}^{(k)} \\ U_{2,2}^{(k-1)} + U_{2,2}^{(k)} \\ U_{1,2}^{(k-1)} + U_{2,1}^{(k-1)} + U_{1,2}^{(k)} + U_{2,1}^{(k)} \end{bmatrix} \tag{20a}$$

$$\begin{bmatrix} M_{11} \\ M_{22} \\ M_{12} \end{bmatrix}^{(k)} = \frac{(n^{(k)}h)^2}{12} \begin{bmatrix} \tilde{C}_{11} & \tilde{C}_{12} & \tilde{C}_{16} \\ \tilde{C}_{12} & \tilde{C}_{22} & \tilde{C}_{26} \\ \tilde{C}_{16} & \tilde{C}_{26} & \tilde{C}_{66} \end{bmatrix}^{(k)} \begin{bmatrix} U_{1,1}^{(k-1)} - U_{1,1}^{(k)} \\ U_{2,2}^{(k-1)} - U_{2,2}^{(k)} \\ U_{1,2}^{(k-1)} + U_{2,1}^{(k-1)} - U_{1,2}^{(k)} - U_{2,1}^{(k)} \end{bmatrix} \tag{20b}$$

5 Cylindrical Bending of Laminated Plates

In order to test the accuracy and assess the range of applicability of the present theory, cylindrical bending of composite plates under sinusoidal loading is considered. The plate is simply supported at the ends $x_1 = 0$ and l, and is infinitely long in the x_2 direction. The prescribed boundary conditions on the top and bottom surfaces of the plate are

$$T_1^{+} = 0,\ T_3^{+} = q \sin\frac{\pi x_1}{l} \qquad \text{on } x_3 = \frac{h}{2} \tag{21a}$$

$$T_1^{-} = T_3^{-} = 0 \qquad \text{on } x_3 = -\frac{h}{2} \tag{21b}$$

Downloaded 03 May 2010 to 171.66.16.27. Redistribution subject to ASME license or copyright; see http://www.asme.org/terms/Terms_Use.cfm

The boundary conditions for the simply supported ends are, from boundary conditions (18)

$$U_3 = 0 \text{ at } x_1 = 0, l \tag{22a}$$

$$\frac{1}{2}\left(N_{11}^{(k)} + N_{11}^{(k+1)}\right) - \frac{1}{h}\left(\frac{M_{11}^{(k)}}{n^{(k)}} - \frac{M_{11}^{(k+1)}}{n^{(k+1)}}\right) = 0 \text{ at } x_1 = 0, l \tag{22b}$$

For simplicity, only cylindrical bending of laminated plates consisting of *orthotropic* layers will be considered in the subsequent analysis. However, no additional restrictions are imposed on layer thicknesses, elastic moduli and stacking sequence. In this case, there holds

$$Q_2^{(k)} = T_2^{(k)} \equiv 0 \tag{23}$$

$$\tilde{C}_{45}^{(k)} = 0 \text{ and } \tilde{C}_{44}^{(k)} = 1/C_{55}^{(k)} \tag{24}$$

As a result, terms involving $Q_2^{(k)}$ and $T_2^{(k)}$ will drop out from equations (19*a*,*c*), while equations (19*b*,*d*) will not appear altogether. The remaining equations for $Q_1^{(k)}$ and $T_1^{(k)}$ can be written in matrix form as

$$\mathbf{Q}_1 - h[B_1]\mathbf{T}_1 = \mathbf{b} \tag{25a}$$

$$[D_1]\mathbf{Q}_1 + h[F_1]\mathbf{T}_1 = \mathbf{0} \tag{25b}$$

where

$$\mathbf{Q}_1 \equiv [Q_1^{(1)}, Q_1^{(2)}, \ldots, Q_1^{(N)}]^T \tag{26a}$$

$$\mathbf{T}_1 \equiv [T_1^{(1)}, T_1^{(2)}, \ldots, T_1^{(N-1)}]^T \tag{26b}$$

and $[B_1]$, $[D_1]$, and $[F_1]$ are matrices of dimensions $N \times (N-1)$, $(N-1) \times N$ and $(N-1) \times (N-1)$, respectively. These matrices are only functions of $n^{(k)}$ and $C_{55}^{(k)}$. The right-hand side of equation (25*a*) contains the displacement variables $U_1^{(k)}$ and $U_{3,1}$. Equations (25) can be solved for $Q_1^{(k)}$ and $T_1^{(k)}$ to yield

$$h\,\mathbf{T}_1 = -[F_1^{-1}][D_1]\mathbf{Q}_1 \tag{27a}$$

$$\mathbf{Q}_1 = ([I] + [B_1][F_1^{-1}][D_1])^{-1}\mathbf{b} \tag{27b}$$

where $[I]$ is the $N \times N$ identity matrix.

The remaining constitutive equations are simply, from equation (20)

$$N_{11}^{(k)} = \frac{(n^{(k)}h)}{2}\,\tilde{C}_{11}^{(k)}\left(U_{1,1}^{(k-1)} + U_{1,1}^{(k)}\right) \tag{28a}$$

$$M_{11}^{(k)} = \frac{(n^{(k)}h)^2}{12}\,\tilde{C}_{11}^{(k)}\left(U_{1,1}^{(k-1)} - U_{1,1}^{(k)}\right) \tag{28b}$$

$$N_{12}^{(k)} = N_{22}^{(k)} = M_{12}^{(k)} = M_{22}^{(k)} \equiv 0 \tag{28c}$$

Using surface boundary conditions (21), the equilibrium equations (16) for cylindrical bending in the absence of body forces reduce to

$$\frac{1}{2}N_{11,1}^{(1)} + \frac{1}{n^{(1)}h}\left(M_{11,1}^{(1)} - N_{31}^{(1)}\right) = 0 \tag{29a}$$

$$\frac{1}{2}\left(N_{11,1}^{(k)} + N_{11,1}^{(k+1)}\right) - \frac{1}{h}\left(\frac{M_{11,1}^{(k)}}{n^{(k)}} - \frac{M_{11,1}^{(k+1)}}{n^{(k+1)}}\right) + \frac{1}{h}\left(\frac{N_{31}^{(k)}}{n^{(k)}} - \frac{N_{31}^{(k+1)}}{n^{(k+1)}}\right) = 0;\ k = 1,2,\ldots,N-1 \tag{29b}$$

$$\frac{1}{2}N_{11,1}^{(N)} - \frac{1}{n^{(N)}h}\left(M_{11,1}^{(N)} - N_{31}^{(N)}\right) = 0 \tag{29c}$$

$$\sum_{k=1}^{N} N_{31,1}^{(k)} + q\sin\frac{\pi x_1}{l} = 0 \tag{29d}$$

The form of the dependence on the displacement variables $U_1^{(k)}$ and U_3 of the constitutive equations (27*b*) and (28*a*,*b*), and the nature of the applied load suggests the following expressions for the displacements

$$U_1^{(k)} = h\,\hat{U}_1^{(k)}\cos\frac{\pi x_1}{l} \text{ and } U_3 = h\,\hat{U}_3\sin\frac{\pi x_1}{l} \tag{30}$$

where $\hat{U}_1^{(k)}$ and $\hat{U}_3$ are nondimensional quantities by definition. It is easily proven that the boundary conditions (22) are satisfied when (30) are substituted therein.

Finally, inserting (30) into the constitutive equations (27*b*) and (28*a*,*b*), and these in turn into the equilibrium equations (29), yields a system of $(N+2)$ algebraic equations with the $(N+2)$ nondimensional amplitudes $\hat{U}_1^{(k)}$ and $\hat{U}_3$ as unknowns. This system is conveniently written in matrix form as

$$[X]\hat{\mathbf{U}} = \mathbf{F} \tag{31}$$

$$\text{where } \hat{\mathbf{U}} = [\hat{U}_1^{(0)}, \hat{U}_1^{(1)}, \ldots, \hat{U}_1^{(N)}, \hat{U}_3]^T \tag{32a}$$

$$\mathbf{F} = [0,0,\ldots,0,q]^T \tag{32b}$$

and $[X]$ is a $(N+2) \times (N+2)$ matrix.

6 Numerical Results and Discussion

In order to test the accuracy of the present theory, the problem of cylindrical bending of an infinitely long strip under sinusoidal loading is re-examined. The exact elasticity solution has been given by Pagano (1969), where a symmetric three layer cross-ply laminate was considered, the 0 deg layers being at the outer surfaces of the plate. The elastic properties are

$$\text{for the 0 deg layers } \frac{\tilde{C}_{11}}{E_T} = 25.062657,\ \frac{C_{55}}{E_T} = 0.5 \tag{33a}$$

$$\text{and for the 90 deg layers } \frac{\tilde{C}_{11}}{E_T} = 1.002506,\ \frac{C_{55}}{E_T} = 0.2 \tag{33b}$$

where E_T is a reference modulus.

Following Pagano's (1969) nondimensionalization, the displacements and stresses are written in the form

$$\bar{u}_1^{(k)} = \left(\frac{E_T}{q}\right)\frac{u_1^{(k)}(0,x_3)}{h},\ \bar{u}_3^{(k)} = \left(\frac{E_T}{q}\right)\frac{100\,h^3}{l^4}\,u_3^{(k)}\left(\frac{l}{2}, 0\right) \tag{34}$$

$$\bar{\sigma}_{11}^{(k)} = \frac{1}{q}\,\sigma_{11}^{(k)}\left(\frac{l}{2}, x_3\right)$$

$$\text{Also } \bar{x}_3 = \frac{x_3}{h} \text{ and } S = \frac{l}{h} \tag{35}$$

In the various curves the solid line represents the exact solution while the results of the present theory are shown by a broken line. Also shown, for comparison purposes, are the results given by the laminated plate theory proposed by Murakami (1985) which are represented by a dashed-dotted line. It is a shear deformable theory obtained by superposing to the linear variations of the Reissner-Mindlin theory a zig-zag in-plane displacement variation across the plate thickness. The displacements are then expressed by

$$u_\alpha^{(k)}(x_i) = U_\alpha(x_\beta) + \psi_\alpha(x_\beta)x_3 + S_\alpha(x_\beta)(-1)^k\,\frac{2x_3^{(k)}}{n^{(k)}h} \tag{36a}$$

$$u_3^{(k)}(x_i) = U_3(x_\beta) \tag{36b}$$

For brevity, this theory will be called here "the first-order zig-zag theory" and abbreviated as *ZZ*. The high-order model proposed by Toledano and Murakami (1986) is obtained by including in equation (36) the Legendre Polynomials of order $n = 1,2,3$ with respect to the x_3 coordinate.

Downloaded 03 May 2010 to 171.66.16.27. Redistribution subject to ASME license or copyright; see http://www.asme.org/terms/Terms_Use.cfm

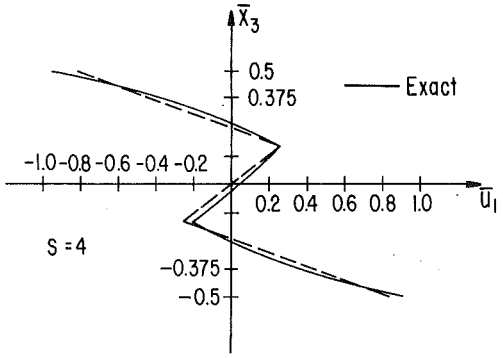


Fig. 3(*a*) Thickness variation of in-plane displacement $\bar{u}_1^{(k)}$ of a symmetric 3-layer cross-ply laminate for $S = 4$

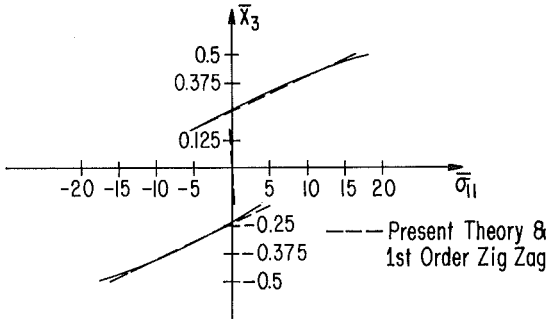


Fig. 3(*b*) Thickness variation of in-plane normal stress $\bar{\sigma}_{11}^{(k)}$ of a symmetric 3-layer cross-ply laminate for $S = 4$

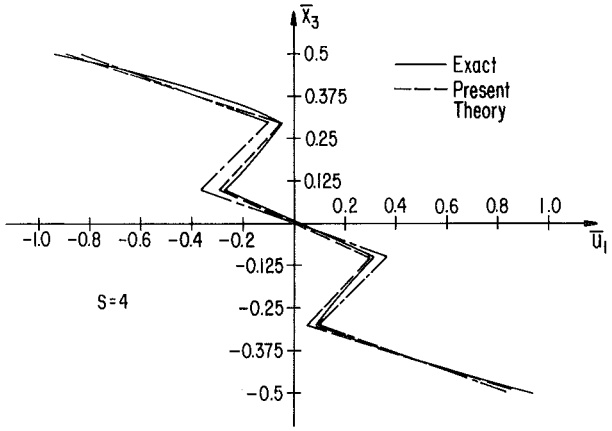


Fig. 4(*a*) Thickness variation of in-plane displacement $\bar{u}_1^{(k)}$ of a symmetric 5-layer cross-ply laminate for $S = 4$

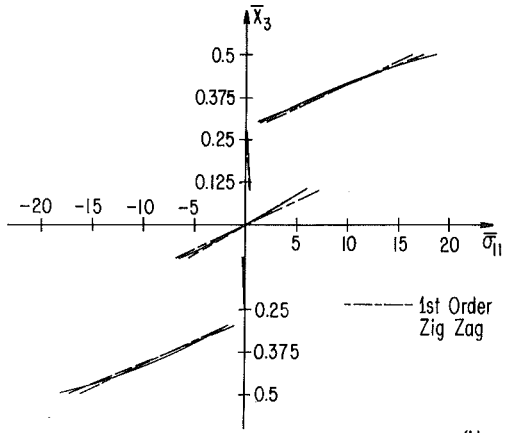


Fig. 4(*b*) Thickness variation of in-plane normal stress $\bar{\sigma}_{11}^{(k)}$ of a symmetric 5-layer cross-ply laminate for $S = 4$

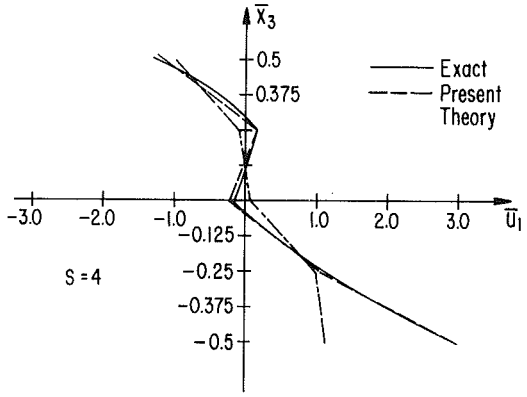


Fig. 5(*a*) Thickness variation of in-plane displacement $\bar{u}_1^{(k)}$ of an antisymmetric 4-layer cross-ply laminate for $S = 4$

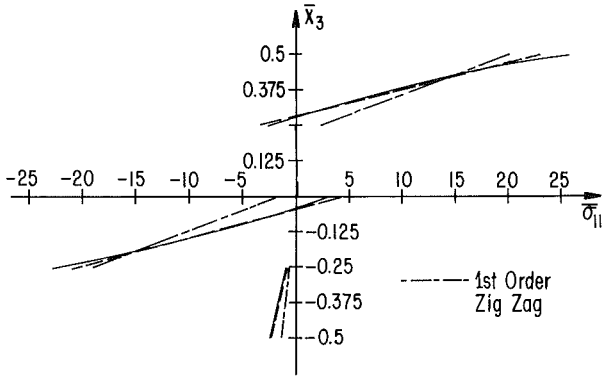


Fig. 5(*b*) Thickness variation of in-plane normal stress $\bar{\sigma}_{11}^{(k)}$ of an antisymmetric 4-layer cross-ply laminate for $S = 4$

For a symmetric 3-layer cross-ply laminate (0/90/0) with layers of equal thickness, Table 1 shows the values of the central deflection $\bar{u}_3$ obtained from the different theories for a span-to-thickness ratio $S = 4$. As observed, the present theory and the first-order zig-zag theory yield exactly the same numerical result. This is also true for the thickness variations of the in-plane displacement $\bar{u}_1^{(k)}$ and normal stress $\bar{\sigma}_{11}^{(k)}$. As shown in Figs. 3*a*,*b*, very close agreement is found between both theories and Pagano's exact solution. It should be pointed out that the numerical results obtained by Seide (1980) differ slightly from those given here since no shear correction factors were introduced by him.

The present theory was next tested for a symmetric 5-layer cross-ply laminate (0/90/0/90/0) with layers of equal thickness. The central deflection $\bar{u}_3$ for $S = 4$ is shown in Table 1, where closer agreement between the present theory and the exact solution is observed as compared to the first-order zig-zag theory. The distributions across the plate thickness of in-plane variables $\bar{u}_1^{(k)}$ and $\bar{\sigma}_{11}^{(k)}$ are compared in Figs. 4*a*,*b*. It is seen that the present theory has improved upon *ZZ*, especially in the interior layers of the plate.

As antisymmetric 4-layer cross-ply laminate (0/90/0/90) with layers of equal thickness, was also examined. In this case, the error in the central deflection between the exact solution and *ZZ* is quite large (~ 21 percent), while the present theory still gives a satisfactory value (see Table 1). The variations across the plate thickness of the in-plane displacement $\bar{u}_1^{(k)}$ and normal stress $\bar{\sigma}_1^{(k)}$ are shown in Figs. 5*a*,*b* for $S = 4$, respectively. From the curves for $\bar{u}_1^{(k)}$, it is seen that the first-order zig-zag theory deviates significantly from the exact solution at the bottom layer of the plate. On the other hand, the present theory is in very good agreement with the exact solution.

To further assess the range of applicability of both the pre-

Downloaded 03 May 2010 to 171.66.16.27. Redistribution subject to ASME license or copyright; see http://www.asme.org/terms/Terms_Use.cfm

Table 1 Central deflection $\bar{u}_3$ for symmetric 3 and 5-layer and antisymmetric 4-layer cross-ply laminates ($S = 4$)

	N=3 (0/90/0)	N=5 (0/90/0/90/0)	N=4 (0/90/0/90)
Exact Solution	2.887	3.044	4.181
Present Theory	2.907	3.059	4.202
1st-Order Zig-Zag	2.907	3.018	3.316

Table 2 Geometric and physical properties of arbitrary 3, 4, and 5-layer laminates ($S = 4$)

Number of Layers N	Layer	Volume Fraction $n^{(k)}$	Material
3	1	0.25	3
	2	0.40	1
	3	0.35	2
4	1	0.25	1
	2	0.35	3
	3	0.30	2
	4	0.10	1
5	1	0.10	1
	2	0.25	2
	3	0.15	3
	4	0.20	1
	5	0.30	3

Table 3 Central deflection $\bar{u}_3$ for arbitrary 3, 4, and 5-layer laminates ($S = 4$)

	N=3	N=4	N=5
Exact Solution	2.341	1.665	2.456
Present Theory	2.364	1.644	2.467
1st-Order Zig-Zag	1.992	1.303	1.261

sent theory and the first-order zig-zag model, arbitrary laminate configurations consisting of 3, 4, and 5 layers were tested. Three different materials were used, with the following elastic properties:

$$\text{Material 1: } \frac{\tilde{C}_{11}}{E_T} = 1.002506 \quad , \frac{C_{55}}{E_T} = 0.2 \tag{37a}$$

$$\text{Material 2: } \frac{\tilde{C}_{11}}{E_T} = 32.631 \quad , \frac{C_{55}}{E_T} = 8.21 \tag{37b}$$

$$\text{Material 3: } \frac{\tilde{C}_{11}}{E_T} = 25.062657 \quad , \frac{C_{55}}{E_T} = 0.5 \tag{37c}$$

The laminate configurations corresponding to the three cases examined are shown in Table 2. In all cases, $S = 4$.

The values of the central deflection for the three laminate configurations are given in Table 3. It can be observed that the discrepancies with the exact solution are larger in the case of the first-order zig-zag theory than in the case of the present theory. In particular, the error in $\bar{u}_3$ for $N = 5$ is as high as 49 percent. The variations across the plate thickness of the in-plane displacement $\bar{u}_1^{(k)}$ and normal stress $\bar{\sigma}_{11}^{(k)}$ are shown in Figs. 6, 7, and 8 for $N = 3$, 4, and 5, respectively. As expected, the symmetric distributions obtained by the present theory and ZZ for $N = 3$ and 5 no longer hold for arbitrary laminate configurations. In all the cases considered, the present theory is still in good agreement with the exact solution, except possibly at the top layer of the 4-ply laminate (see Fig. 7). On the other hand, it is seen that the first-order zig-zag theory deviates considerably from the exact solution.

Some important points are now discussed. The accuracy of

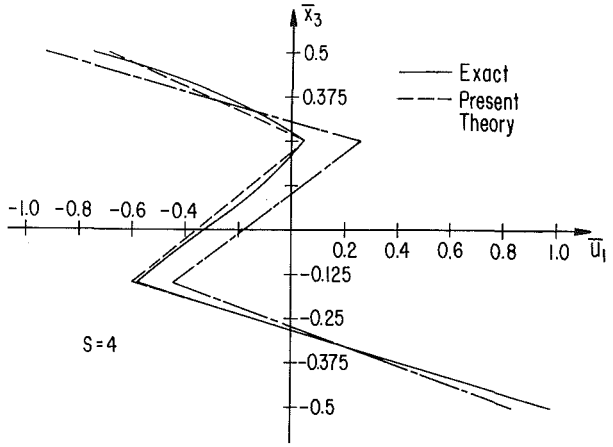


Fig. 6(a) Thickness variation of in-plane displacement $\bar{u}_1^{(k)}$ of an arbitrary 3-layer laminate for $S = 4$

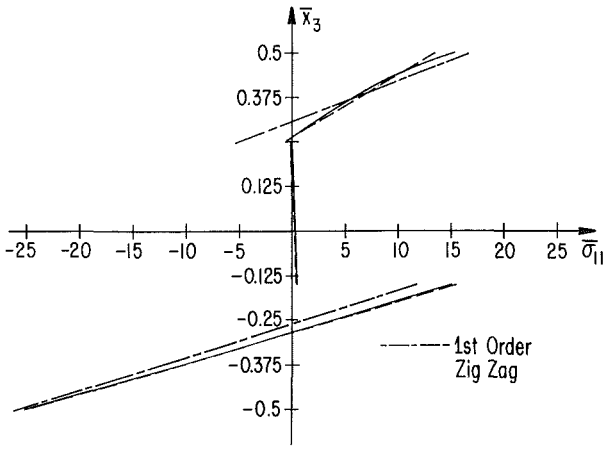


Fig. 6(b) Thickness variation of in-plane normal stress $\bar{\sigma}_{11}^{(k)}$ of an arbitrary 3-layer laminate for $S = 4$

the present theory can be improved by dividing each ply into a finite number of sub-layers, but at the expense of increasing computer storage. Also, the proposed theory possesses two main drawbacks, which are: first, the number of equilibrium equations and edge boundary conditions increases with the number of layers; and second, due to the coupling of the natural edge boundary conditions (see equation (18)), no clear physical meaning seems to be associated with them.

In the present work, results have been restricted to in-plane stresses, since they are considered primary quantities in any approximate laminated plate analysis. Once the quantitites $Q_\alpha^{(k)}$, $T_\alpha^{(k-1)}$ and $T_\alpha^{(k)}$ have been computed by solving the constitutive equations (19), a *direct* evaluation using equation (11*a*) will yield continuous transverse stresses. However, the alternate procedure of computing the transverse stresses by integrating the equilibrium equations using the in-plane stresses found directly from the displacement solution yields more accurate results. Such results are presented in the paper by Murakami (1985).

Next, as a possible explanation for the increased discrepancies in the case of arbitrary laminates between the exact solution and the first-order zig-zag theory, the following argument is proposed. The inclusion of the zig-zag shaped C^0 function was motivated by the displacement microstructure of *periodic* laminated composites (Murakami, Maewal, and Hegemier, 1981). Obviously, for arbitrary laminate configurations, this periodicity is destroyed. Therefore, the first-order zig-zag theory should be expected to break down in these particular cases.

Finally, it is worth mentioning that an advantage of the zig-zag model is that the number of equations to be solved for the

Downloaded 03 May 2010 to 171.66.16.27. Redistribution subject to ASME license or copyright; see http://www.asme.org/terms/Terms_Use.cfm

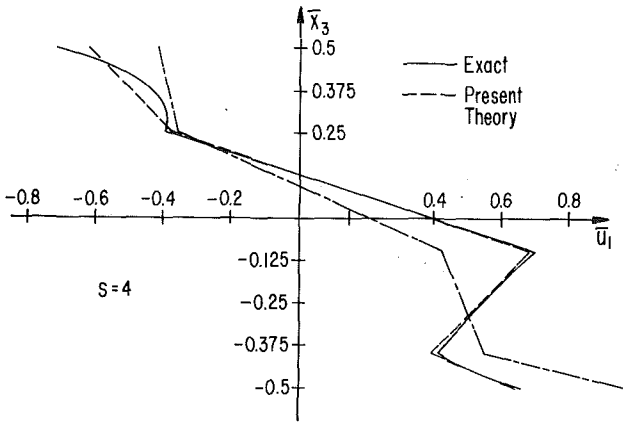


Fig. 7(a) Thickness variation of in-plane displacement $\bar{u}_1^{(k)}$ of an arbitrary 4-layer laminate for $S = 4$

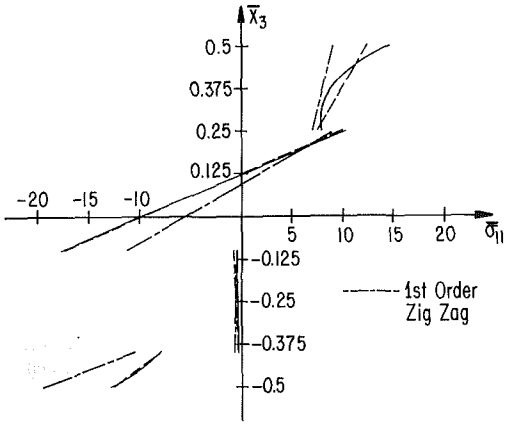


Fig. 7(b) Thickness variation of in-plane normal stress $\bar{\sigma}_{11}^{(k)}$ of an arbitrary 4-layer laminate for $S = 4$

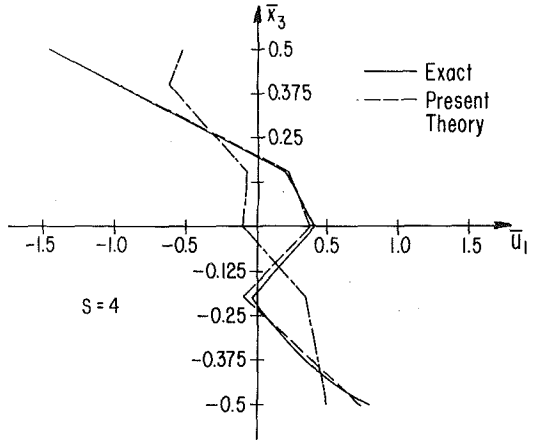


Fig. 8(a) Thickness variation of in-plane displacement $\bar{u}_1^{(k)}$ of an arbitrary 5-layer laminate for $S = 4$

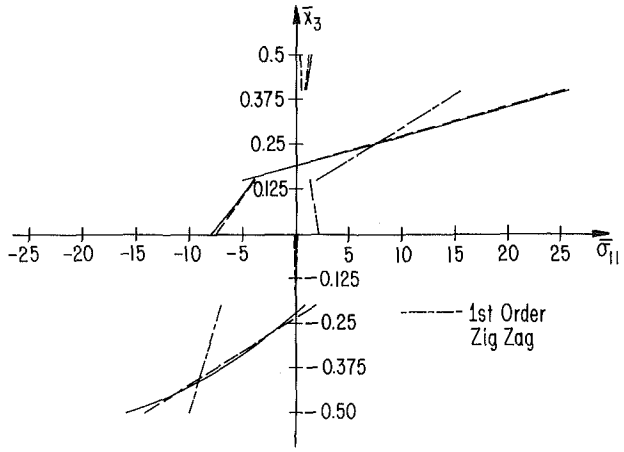


Fig. 8(b) Thickness variation of in-plane normal stress $\bar{\sigma}_{11}^{(k)}$ of an arbitrary 5-layer laminate for $S = 4$

displacement-type variables are independent of the number of layers. This is certainly not true for the present theory. In design problems involving laminates with a large number of layers, these considerations should be taken into account.

7 Conclusion

A composite plate theory, which accurately predicts in-plane responses of arbitrary laminates, was developed by assuming a linear variation of in-plane displacements and a quadratic variation of transverse stresses across each individual lamina. Transverse displacements were kept constant throughout the entire plate thickness. Governing equations and appropriate boundary conditions were then deduced from Reissner's (1984) new mixed variational principle. The accuracy of the theory was examined for the case of cylindrical bending of an infinitely long strip and compared with the exact solution given by Pagano (1969). The results obtained by the laminated plate theory proposed by Murakami (1985), and called "the first-order zig-zag theory" were also shown. Values for the central deflection and in-plane displacement and normal stress for symmetric, antisymmetric, and arbitrary laminates were presented. It was observed that the first-order zig-zag theory gave satisfactory results only for symmetric cross-ply laminates. The discrepancies between this theory and the exact solution were more pronounced for laminates of arbitrary configurations that for antisymmetric cross-ply laminates. On the other hand, in all the cases considered, the present theory was in close agreement with the exact solution. Despite certain shortcomings, the good correlation with the exact elasticity solution indicates that the proposed theory may prove useful in the investigation of the mechanical response of arbitrary laminates.

Acknowledgment

The research was supported by the Office of Naval Research under Contract N00014-84-K-0468 to the University of California at San Diego. The authors are grateful to Dr. A. Kushner for his support.

References

Durocher, L. L., and Solecki, R., 1975, "Steady-State Vibrations and Bending of Transversely Isotropic Three-Layer Plates," *Development in Mechanics*, Vol. 8, Proceedings of the 14th Midwestern Mechanics Conference, pp. 103–124.

Hildebrand, F. B., Reissner, E., and Thomas, G. B., 1949, "Notes on the Foundations of the Theory of Small Displacements of Orthotropic Shells," NACA, Technical Note No. 1833.

Lo, K. H., Christensen, R. M., and Wu, E. M., 1977, "A High-Order Theory of Plate Deformation—Part 2: Laminated Plates," ASME JOURNAL OF APPLIED MECHANICS, Vol. 44, pp. 669–676.

Mau, S. T., 1973, "A Refined Laminated Plate Theory," ASME JOURNAL OF APPLIED MECHANICS, Vol. 40, pp. 606–607.

Murakami, H., 1985, "Laminated Composite Plate Theory with Improved In-Plane Responses," *Proceeding of the 1985 PVP Conference*, PVP Vol. 98-2, ASME, pp. 257–263; also, 1986, ASME JOURNAL OF APPLIED MECHANICS, Vol. 53, pp. 661–666.

Murakami, H., Maewal, A., and Hegemier, G. A., 1981, "A Mixture Theory with a Director for Linear Elastodynamics of Periodically Laminated Media," *International Journal of Solids and Structures*, Vol. 17, pp. 155–173.

Nelson, R. B., and Lorch, D. R., 1974, "A Refined Theory of Laminated Orthotropic Plates," ASME JOURNAL OF APPLIED MECHANICS, Vol. 41, pp. 171–183.

Downloaded 03 May 2010 to 171.66.16.27. Redistribution subject to ASME license or copyright; see http://www.asme.org/terms/Terms_Use.cfm

Pagano, N. J., 1969, "Exact Solutions for Composite Laminates in Cylindrical Bending," *Journal of Composite Materials*, Vol. 3, pp. 398–411.

Pagano, N. J., 1970, "Exact Solutions for Rectangular Bidirectional Composites and Sandwich Plates," *Journal of Composite Materials*, Vol. 4, pp. 20–34.

Pagano, N. J., 1970, "Influence of Shear Coupling in Cylindrical Bending of Anisotropic Laminates," *Journal of Composite Materials*, Vol. 4, pp. 330–343.

Pagano, N. J., 1971, "Further Study of Composite Laminates Under Cylindrical Bending," *Journal of Composite Materials*, Vol. 5, pp. 521–528.

Pagano, N. J., and Hatfield, S. J., 1972, "Elastic Behavior of Multi-Layered Bidirectional Composites," *AIAA Journal*, Vol. 10, pp. 931–933.

Reddy, J. N., 1984, "A Simple Higher-Order Theory for Laminated Composite Plates," ASME JOURNAL OF APPLIED MECHANICS, Vol. 51, pp. 745–752.

Reissner, E., 1984, "On a Certain Mixed Varitional Principle and a Proposed Application," *International Journal for Numerical Methods in Engineering*, Vol. 20, pp. 1366–1368.

Seide, P., 1980, "An Improved Approximate Theory for the Bending of Laminated Plates," *Mechanics Today* (The E. Reissner Anniversary Volume), Vol. 5, Nemat-Nasser, S., ed., pp. 451–466.

Srinivas, S., 1973, "A Refined Analysis of Composite Laminates," *Journal of Sound and Vibration*, Vol. 30, No. 4, pp. 495–507.

Toledano, A., and Murakami, H., "A High-Order Laminated Plate Theory with Improved In-Plane Responses," *International Journal of Solids and Structures*, in press.

Whitney, J. M., 1972, "Stress Analysis of Thick Laminated Composite and Sandwich Plates," *Journal of Composite Materials*, Vol. 6, pp. 426–440.

Whitney, J. M., and Pagano, N. J., 1970, "Shear Deformation in Heterogeneous Anisotropic Plates," ASME JOURNAL OF APPLIED MECHANICS, Vol. 37, pp. 1031–1036.

Whitney, J. M., and Sun, C. T., 1973, "A Higher Order Theory for Extensional Motion of Laminated Composites," *Journal of Sound and Vibration*, Vol. 30, No. 1, pp. 85–97.

Yang, P. C., Norris, C. H., and Stavsky, Y., 1966, "Elastic Wave Propagation in Heterogeneous Plates," *International Journal of Solids and Structures*, Vol. 2, pp. 665–684.

Yu, Y. Y., 1959, "A New Theory of Elastic Sandwich Plates—One-Dimensional Case," ASME JOURNAL OF APPLIED MECHANICS, Vol. 26, No. 3, pp. 415–421.

Downloaded 03 May 2010 to 171.66.16.27. Redistribution subject to ASME license or copyright; see http://www.asme.org/terms/Terms_Use.cfm

Axisymmetric Motion of a Viscous Fluid Inside a Slender Surface of Revolution

D. A. Caulk
Mem. ASME
Engineering Mechanics Department,
General Motors Research Laboratories,
Warren, Mich. 48090

P. M. Naghdi
Honorary Mem. ASME
Department of Mechanical Engineering,
University of California,
Berkeley, Calif. 94720

Starting with the exact three-dimensional equations for an incompressible linear viscous fluid, an approximate system of one-dimensional nonlinear equations is derived for axisymmetric motion inside a slender surface of revolution. These equations are obtained by introducing an approximate velocity field into weighted integrals of the momentum equation over the circular cross-section of the fluid. The general equations may be specialized to reflect specific conditions on the lateral surface of the fluid, such as the presence of surface tension, a confining elastic membrane, or a rigid tube. Two specific examples are considered which involve flow in a rigid tube: (1) unsteady starting flow in a nonuniform tube, and (2) axisymmetric swirl superimposed on Poiseuille flow. In each case comparison is made with earlier, more restricted results derived by perturbation methods.

1 Introduction

Various physical problems involve the flow of a viscous fluid inside a slender surface of revolution. Depending on the conditions on the lateral surface of the fluid, however, the nature of the flow can be quite different. When the lateral surface is free, the fluid flows as a jet. This problem was considered by Goren and Wronski (1966), Tuck (1976), and Geer (1977), among others. A rigid lateral surface represents flow in a pipe. This problem was analyzed by Manton (1971) and Hall (1974). A flexible elastic boundary is representative of certain biological flows, as considered, for example, by Morgan and Keily (1954), Womersley (1955), and Rubinow and Keller (1978). Because of the difficult nature of these problems, they have been analyzed by various approximate methods, usually employing expansion of the solution in powers of a small parameter (e.g., Reynolds number, boundary displacement, or slenderness ratio). Although the geometry in each of the above problems is similar, the approach in each case has been different, depending strongly on the lateral boundary conditions.

While our overall objectives are similar to the references cited above, in this paper we adopt an approach which does not depend on the specific nature of the lateral surface. Instead of expanding the solution in powers of small parameter, we make an a priori assumption on the form of the velocity field based on the slender geometry of the region. This velocity field satisfies both the incompressibility condition and the kinematic boundary condition exactly. The momentum equation is not satisfied pointwise in the fluid, but rather in weighted integrals over the fluid cross-section. Because the momentum equation is only satisfied in this integrated sense, we would expect such an approach to be primarily useful for determining "bulk" quantities at a particular station along the axis of symmetry, e.g., flow rate or resultant surface traction, rather than detailed distributions in the cross-section itself.

We begin in Section 2 by assuming that the velocity field in the slender surface of revolution can be approximated by a general third order polynomial in the radial coordinate, with coefficient functions which depend on the axial coordinate z (see Fig. 1). Constraints are imposed on these coefficient functions by requiring the assumed velocity field to satisfy the incompressibility condition pointwise in the fluid. The assumed velocity field is also required to satisfy the kinematical condition that the lateral surface of the fluid be material. The remaining equations governing the motion are derived by integrating the momentum equation and three higher moments of the momentum equation through a normal cross section of the region. After accounting for the axial symmetry, the fluid motion is characterized by six one-dimensional scalar equations for the unknown coefficient functions in the velocity field (equations (2.33)–(2.38)), together with two constraint relations arising from incompressibility (equations (2.18*a*, *b*)), and a single equation reflecting the fact that the lateral surface is material (equation (2.16)).

The general system of equations is specialized in Section 3 for three different types of lateral surface: (1) flow of a free jet in the presence of surface tension; (2) flow inside a rigid tube of variable radius; and (3) flow inside an elastic membrane. The resulting system of equations in each case has general applicability, with the only assumptions being the representation for the velocity field and satisfaction of integrated versions of the momentum equations in the three-dimensional theory.

Contributed by the Applied Mechanics Division for presentation at the 1987 Applied Mechanics, Biomechanics, and Fluids Engineering Conference, Cincinnati, OH, June 14–17, 1987, of the American Society of Mechanical Engineers.
Discussion on this paper should be addressed to the Editorial Department, ASME, United Engineering Center, 345 East 47th Street, New York, N.Y. 10017, and will be accepted until two months after final publication of the paper itself in the JOURNAL OF APPLIED MECHANICS. Manuscript received by ASME Applied Mechanics Division, October 15, 1985; final revision, April 7, 1986.
Paper No. 87-APM-1.

Copyright © 1987 by ASME
Downloaded 03 May 2010 to 171.66.16.27. Redistribution subject to ASME license or copyright; see http://www.asme.org/terms/Terms_Use.cfm

In the rest of the paper, we consider the application of the approximate theory to examples involving flow in a rigid tube. The first of these is an explicit analytical solution in Section 4 for unsteady starting flow in a general nonuniform tube. This solution not only compares extremely well with the exact unsteady solution for the special case of a uniform tube, but it reduces exactly to the classical result for steady Poiseuille flow in the limit of large time. For steady, low Reynolds number flow in a nonuniform tube, this solution also reduces asymptotically to Manton's (1971) asymptotic solution of the full three-dimensional equations. In the second example discussed in Section 5, we examine axisymmetric swirl superposed on Poiseuille flow and consider the steady solution for the decay of the swirl with distance down the tube. This solution compares quite favorably with the experimental results of Talbot (1954), as well as the leading terms of his perturbation solution of the full Navier-Stokes equations.

Before closing this section, it may be noted that the approach used here is akin to the development of theories for elastic rods using a direct theory of a Cosserat curve (see, for example, Green et al., 1974 a, b; Naghdi, 1982, Part B). In fact, for the special case of axisymmetric motion considered here, corresponding results from each approach should be the same. But because the determination of general inertia terms in the direct formulation for fluids is more involved than the present limited context would justify (for a development in the case of a general two-dimensional fluid sheet, see Green and Naghdi, 1984), our development here proceeds by approximation from the usual three-dimensional equations.

2 Basic Equations

Let x_i $(i = 1, 2, 3)$ be rectangular Cartesian coordinates, $\mathbf{e}_i$ the associated unit base vectors, and for convenience set $x_3 = z$. Consider axisymmetric motion of an incompressible fluid inside a surface of revolution about the x_3 axis and let $\phi(z, t)$ denote the instantaneous radius of that surface at z and time t. Further, let $\mathbf{t}$ denote the stress vector on a surface whose outward unit normal is $\nu^* = \nu_i^* \mathbf{e}_i$. Then, the three-dimensional equations governing the fluid motion are

$$\mathbf{t}_{i,i} = \rho^* \left(\frac{\partial \mathbf{v}^*}{\partial t} + \mathbf{v}^*_{,i} v_i^* \right), \tag{2.1}$$

$$v^*_{i,i} = 0, \tag{2.2}$$

$$\mathbf{t}_i = -p^* \mathbf{e}_i + \sigma_{ij} \mathbf{e}_j, \quad \mathbf{t} = \nu_i^* \mathbf{t}_i, \tag{2.3}$$

where $\mathbf{t}_i$ are related to $\mathbf{t}$ and σ_{ij} by (2.3), ρ^* is the constant fluid density, and $\mathbf{v}^* = v_i^* \mathbf{e}_i$ is the velocity vector. Also, the stress is composed of an arbitrary presure p^*, which is determined by the solution of equations (2.1) and (2.2), and a deviatoric stress response σ_{ij}, which is specified by a constitutive equation. Throughout the paper, Latin indices take the values 1, 2, 3, Greek indices 1, 2, and the usual summation convention is employed over a repeated index. The boundary of the fluid is defined by

$$\phi^2 - x_\alpha x_\alpha = 0 \tag{2.4}$$

and the components of the outward unit normal to this surface are

$$\nu_\alpha^* = x_\alpha / \phi (1 + \phi_z^2)^{1/2}, \quad \nu_3^* = -\phi_z / (1 + \phi_z^2)^{1/2}, \tag{2.5}$$

where a subscripted variable denotes partial differentiation. Since equation (2.4) defines a material surface, the velocity must satisfy the condition

$$\phi \phi_t + \phi \phi_z v_3^* - x_\alpha v_\alpha^* = 0 \tag{2.6}$$

on the boundary (2.4).

We assume that the fluid velocity inside the surface of revolution (2.4) is approximated by the finite series

$$\mathbf{v}^* = \mathbf{v} + \sum_{N=1}^{K} x_{\alpha_1} \cdots x_{\alpha_N} \mathbf{w}_{\alpha_1 \ldots \alpha_N}, \tag{2.7}$$

where

$$\mathbf{v} = v_i(z,t)\mathbf{e}_i,$$

$$\mathbf{w}_{\alpha_1 \ldots \alpha_N} = w^i_{\alpha_1 \ldots \alpha_N}(z,t)\mathbf{e}_i \, (N = 1,2, \ldots, K), \tag{2.8}$$

and the vectors $\mathbf{w}_{\alpha_1 \ldots \alpha_N}$ are completely symmetric with respect to their indices. Since the motion is symmetric about the x_3 axis, the velocity components are not all independent and must transform according to

$$v_\alpha^* \to Q_{\alpha\beta} v_\beta^*, \quad v_3^* \to v_3^* \tag{2.9}$$

under the coordinate transformation

$$x_\alpha \to Q_{\alpha\beta} x_\beta, \quad x_3 \to x_3,$$

where $Q_{\alpha\beta}$ is any orthogonal two-dimensional tensor. It follows that the various component functions in equations (2.8) must satisfy

$$v_\alpha = 0, \tag{2.10}$$

$$w^\gamma_{\alpha_1 \ldots \alpha_N} = Q_{\gamma\lambda} Q_{\alpha_1\beta_1} \cdots Q_{\alpha_N\beta_N} w^\lambda_{\beta_1 \ldots \beta_N}, \tag{2.11}$$

$$w^3_{\alpha_1 \ldots \alpha_N} = Q_{\alpha_1\beta_1} \cdots Q_{\alpha_N\beta_N} w^3_{\beta_1 \ldots \beta_N}; \quad (N = 1,2, \ldots, K) \tag{2.12}$$

for all orthogonal tensors $Q_{\alpha\beta}$. Consequently, $w^\beta_{\alpha_1 \ldots \alpha_N}$ and $w^3_{\alpha_1 \ldots \alpha_N}$ must be components of two-dimensional isotropic tensors. But since these component functions must also be symmetric with respect to the indices $\alpha_1 \ldots \alpha_N$, their most general representation is (see, for example, Jeffreys 1931)[1]

$$\begin{gathered} w^\beta_\alpha = \delta_{\alpha\beta}\zeta + e_{\alpha\beta}\omega, \quad w^3_\alpha = 0, \\ w^\gamma_{\alpha\beta} = 0, \quad w^3_{\alpha\beta} = \delta_{\alpha\beta}\gamma, \\ w^\lambda_{\alpha\beta\gamma} = c_{\alpha\beta\gamma\mu}(\delta_{\mu\lambda}\sigma + e_{\mu\lambda}\eta), \quad w^3_{\alpha\beta\gamma} = 0, \end{gathered} \tag{2.13}$$

where $\delta_{\alpha\beta}$ is the two-dimensional Kronecker symbol, $e_{\alpha\beta}$ is the permutation symbol defined by $e_{11} = e_{22} = 0$, $e_{12} = -e_{21} = 1$, and

$$c_{\alpha\beta\gamma\lambda} = \frac{1}{3}(\delta_{\alpha\beta}\delta_{\gamma\lambda} + \delta_{\alpha\gamma}\delta_{\beta\lambda} + \delta_{\alpha\lambda}\delta_{\beta\gamma}). \tag{2.14}$$

The various coefficients $\zeta, \omega, \gamma, \sigma, \eta$ are scalar functions of z, t whose physical significance will be indicated presently. The expressions corresponding to equations (2.13) when $N > 3$ can be recorded in a similar manner, but they will not be needed here. In what follows, we set $K = 3$ in the representation (2.7) and with the help of equations (2.13) write the velocity $\mathbf{v}^*$ as

$$\begin{aligned} \mathbf{v}^* = [(\zeta + x_\gamma x_\gamma \sigma)\delta_{\beta\alpha} + (\omega + x_\gamma x_\gamma \eta)e_{\beta\alpha}]x_\beta \mathbf{e}_\alpha \\ + (v + x_\gamma x_\gamma \gamma)\mathbf{e}_3. \end{aligned} \tag{2.15}$$

The physical significance of the six independent velocity coefficients in equations (2.13) is now apparent: v represents the velocity along the axis of symmetry, γ is related to transverse shearing motion, ω and η are related to rotational motion about $\mathbf{e}_3$, while ζ and σ are related to transverse elongation.

With equation (2.15), the kinematic condition (2.6) on the lateral boundary reduces to

$$\phi_t + (v + \phi^2\gamma)\phi_z - (\zeta + \phi^2\sigma)\phi = 0 \tag{2.16}$$

and the incompressibility constraint (2.2) becomes

$$(v_z + 2\zeta) + x_\alpha x_\alpha (\gamma_z + 4\sigma) = 0. \tag{2.17}$$

For equation (2.17) to hold at every point in the fluid, the velocity coefficients must satisfy the separate conditions

$$v_z + 2\zeta = 0, \quad \gamma_z + 4\sigma = 0. \tag{2.18}$$

Hence the boundary condition (2.6) and the constraint (2.2)

[1] Since all vector components are referred to Cartesian base vectors in this paper, we use superscripts and subscripts interchangeably without confusion.

Downloaded 03 May 2010 to 171.66.16.27. Redistribution subject to ASME license or copyright; see http://www.asme.org/terms/Terms_Use.cfm

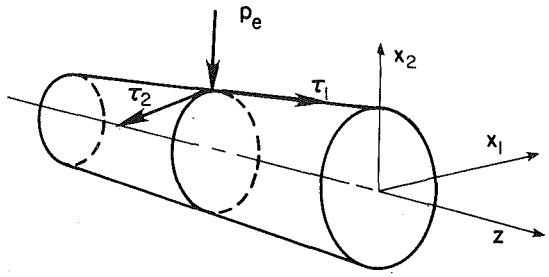


Fig. 1 Geometry of fluid region, showing components of the surface traction vector

are satisfied exactly by the velocity field (2.15), provided we impose the conditions (2.16) and (2.18). Instead of satisfying the momentum equation (2.1) pointwise in the fluid, we impose the following integral conditions:[2]

$$\int_A \left[\mathbf{t}_{i,i} - \rho^* \left(\frac{\partial \mathbf{v}^*}{\partial t} + \mathbf{v}^*_{,i} v^*_i\right)\right] da = 0, \tag{2.19}$$

$$\int_A \left[\mathbf{t}_{i,i} - \rho^* \left(\frac{\partial \mathbf{v}^*}{\partial t} + \mathbf{v}^*_{,i} v^*_i\right)\right] x_{\alpha_1} \cdots x_{\alpha_N} da = 0, \tag{2.20}$$

$$(N = 1,2,3),$$

where A is an arbitrary cross-section of the slender surface of revolution defined by z = constant and bounded by the circle (2.4). Using the divergence theorem and a form of Liebnitz' rule, equations (2.19) and (2.20) can be reduced to the four vector equations

$$\frac{\partial \mathbf{n}}{\partial z} + \mathbf{f} = \mathbf{a}, \tag{2.21}$$

$$\frac{\partial \mathbf{m}^{\alpha_1 \cdots \alpha_N}}{\partial z} + \mathbf{l}^{\alpha_1 \cdots \alpha_N} = \mathbf{k}^{\alpha_1 \cdots \alpha_N} + \mathbf{b}^{\alpha_1 \cdots \alpha_N},$$

$$(N = 1,2,3), \tag{2.22}$$

where $\mathbf{n}$, $\mathbf{k}^{\alpha_1 \cdots \alpha_N}$, $\mathbf{m}^{\alpha_1 \cdots \alpha_N}$ are force resultants defined by

$$\mathbf{n} = \int_A \mathbf{t}_3 da, \quad \mathbf{k}^\alpha = \int_A \mathbf{t}_\alpha da, \quad \mathbf{k}^{\alpha\beta} = \int_A (\mathbf{t}_\alpha x_\beta + \mathbf{t}_\beta x_\alpha) da,$$

$$\mathbf{k}^{\alpha\beta\gamma} = \int_A (\mathbf{t}_\alpha x_\beta x_\gamma + \mathbf{t}_\beta x_\alpha x_\gamma + \mathbf{t}_\gamma x_\alpha x_\beta) da, \tag{2.23}$$

$$\mathbf{m}^{\alpha_1 \cdots \alpha_N} = \int_A \mathbf{t}_3 x_{\alpha_1} \cdots x_{\alpha_N} da.$$

The quantities $\mathbf{a}$ and $\mathbf{b}^{\alpha_1 \cdots \alpha_N}$ are inertia terms defined by

$$\mathbf{a} = \int_A \rho^* \left(\frac{\partial \mathbf{v}^*}{\partial t} + \mathbf{v}^*_{,i} v^*_i\right) da,$$

$$\mathbf{b}^{\alpha_1 \cdots \alpha_N} = \int_A \rho^* \left(\frac{\partial \mathbf{v}^*}{\partial t} + \mathbf{v}^*_{,i} v^*_i\right) x_{\alpha_1} \cdots x_{\alpha_N} da \tag{2.24}$$

and $\mathbf{f}$, $\mathbf{l}^{\alpha_1 \cdots \alpha_N}$, which arise due to surface traction on the lateral boundary (2.4), are defined by

$$\mathbf{f} = \int_{\partial A} (1 + \phi_z^2)^{1/2} \mathbf{t}\, ds,$$

$$\mathbf{l}^{\alpha_1 \cdots \alpha_N} = \int_{\partial A} (1 + \phi_z^2)^{1/2} \mathbf{t}\, x_{\alpha_1} \cdots x_{\alpha_N} ds. \tag{2.25}$$

The surface conditions on the lateral boundary enter directly in the one-dimensional field equations (2.21) and (2.22) through these latter quantities. It is convenient to resolve the stress vector on the lateral surface in terms of its normal and tangential components in the form (see Fig. 1)

$$\mathbf{t} = \tau_1 \boldsymbol{\lambda} - p_e \boldsymbol{\nu}^* + \tau_2 \mathbf{e}_\theta, \tag{2.26}$$

where $\boldsymbol{\lambda}$, $\mathbf{e}_\theta$ are unit tangent vectors defined by

$$\mathbf{e}_\theta = (x_\alpha/\phi) e_{\alpha\beta} \mathbf{e}_\beta, \quad \boldsymbol{\lambda} = \boldsymbol{\nu}^* \times \mathbf{e}_\theta, \tag{2.27}$$

so that ($\boldsymbol{\lambda}$, $\boldsymbol{\nu}^*$, $\mathbf{e}_\theta$) form a right-handed triad. With the help of equations (2.5) and (2.27), the expression for the stress vector (2.26) can be rewritten in terms of its rectangular Cartesian components as

$$\mathbf{t} = \phi^{-1}[(1 + \phi_z^2)^{-1/2}(\tau_1 \phi_z - p_e) x_\alpha \delta_{\alpha\beta} + \tau_2 e_{\alpha\beta} x_\alpha] \mathbf{e}_\beta + (1 + \phi_z^2)^{-1/2}(p_e \phi_z + \tau_1) \mathbf{e}_3. \tag{2.28}$$

Substituting this expression into equation (2.25) and integrating, we obtain

$$\mathbf{f} = 2\pi\phi(p_e \phi_z + \tau_1) \mathbf{e}_3,$$
$$\mathbf{l}^\alpha = \pi\phi^2[(\tau_1 \phi_z - p_e)\delta_{\alpha\beta} + (1 + \phi_z^2)^{1/2} \tau_2 e_{\alpha\beta}] \mathbf{e}_\beta,$$
$$\mathbf{l}^{\alpha\beta} = \pi\phi^3(p_e \phi_z + \tau_1) \delta_{\alpha\beta} \mathbf{e}_3, \tag{2.29}$$
$$\mathbf{l}^{\alpha\beta\gamma} = \frac{3}{4} \pi\phi^4[(\tau_1 \phi_z - p_e)\delta_{\mu\lambda} + (1 + \phi_z^2)^{1/2} \tau_2 e_{\mu\lambda}] c_{\alpha\beta\gamma\mu} \mathbf{e}_\lambda.$$

The deviatoric stress response in a linear viscous fluid is specified by

$$\sigma_{ij} = \mu(v^*_{i,j} + v^*_{j,i}), \tag{2.30}$$

where μ is the shear viscosity of the fluid. When equations (2.15) and (2.30) are substituted into the definitions (2.23) for the force resultants, a straightforward calculation yields the explicit results

$$\mathbf{n} = -p\mathbf{e}_3 + 2\pi\mu\phi^2 \left(v_z + \frac{1}{2} \phi^2 \gamma_z\right) \mathbf{e}_3,$$
$$\mathbf{k}^\alpha = -p\mathbf{e}_\alpha + 2\pi\mu\phi^2(\zeta + \phi^2\sigma) \mathbf{e}_\alpha,$$
$$\mathbf{m}^\alpha = \frac{1}{4} \pi\mu\phi^4 \left[\left(2\gamma + \zeta_z + \frac{2}{3} \phi^2 \sigma_z\right) \delta_{\alpha\beta} + \left(\omega_z + \frac{2}{3} \phi^2 \eta_z\right) e_{\alpha\beta}\right] \mathbf{e}_\beta,$$
$$\mathbf{k}^{\alpha\beta} = \frac{1}{2} \pi\mu\phi^4 \left(2\gamma + \zeta_z + \frac{2}{3} \phi^2 \sigma_z\right) \delta_{\alpha\beta} \mathbf{e}_3, \tag{2.31}$$
$$\mathbf{m}^{\alpha\beta} = -q\delta_{\alpha\beta} \mathbf{e}_3 + \frac{1}{2} \pi\mu\phi^4 \left(v_z + \frac{2}{3} \phi^2 \gamma_z\right) \delta_{\alpha\beta} \mathbf{e}_3,$$
$$\mathbf{k}^{\alpha\beta\gamma} = -3q c_{\alpha\beta\gamma\mu} \mathbf{e}_\mu + \frac{1}{2} \pi\mu\phi^4[(3\zeta + 5\phi^2\sigma)\delta_{\mu\lambda} + \eta e_{\mu\lambda}] c_{\alpha\beta\gamma\mu} \mathbf{e}_\lambda,$$
$$\mathbf{m}^{\alpha\beta\gamma} = \frac{1}{8} \pi\mu\phi^6 \left[\left(2\gamma + \zeta_z + \frac{3}{4} \phi^2 \sigma_z\right) \delta_{\mu\lambda} + \left(\omega_z + \frac{3}{4} \phi^2 \eta_z\right) e_{\mu\lambda}\right] c_{\alpha\beta\gamma\mu} \mathbf{e}_\lambda,$$

where p and q are pressure resultants defined by

$$p = \int_A p^* da, \quad q\delta_{\alpha\beta} = \int_A p^* x_\alpha x_\beta da. \tag{2.32}$$

Finally, we can explicitly evaluate the inertia terms by substituting equation (2.15) into equations (2.24). When the results of this integration are combined with equations (2.29) and (2.31), the integrated momentum equations (2.21) and (2.22) reduce to the following six independent scalar equations:

[2] In general, we should also impose an integrated version of the angular momentum equation as in the paper of Green, Naghdi, and Wenner (1974a); but, in the present development, it happens that this equation is satisfied identically by the constitutive equations (2.31).

Downloaded 03 May 2010 to 171.66.16.27. Redistribution subject to ASME license or copyright; see http://www.asme.org/terms/Terms_Use.cfm

$$2\pi\mu\left[\phi^2\left(v_z+\frac{1}{2}\,\phi^2\gamma_z\right)\right]_z+2\pi\phi(\tau_1+\phi_z p_e)$$
$$=p_z+\pi\rho^*\phi^2\left\{v_t+v_z\left(v+\frac{1}{2}\,\phi^2\gamma\right)\right.$$
$$+\frac{1}{2}\,\phi^2\left[\gamma_t+\gamma_z\left(v+\frac{2}{3}\,\phi^2\gamma\right)\right.$$
$$\left.\left.+2\gamma\left(\zeta+\frac{2}{3}\,\phi^2\sigma\right)\right]\right\}, \tag{2.33}$$

$$\frac{1}{4}\,\pi\mu\left[\phi^4\left(\zeta_z+\frac{2}{3}\,\phi^2\sigma_z\right)\right]_z+\frac{1}{2}\,\pi\mu(\phi^4\gamma)_z$$
$$-2\pi\mu\phi^2(\zeta+\phi^2\sigma)+\pi\phi^2(\phi_z\tau_1-p_e)$$
$$=-p+\frac{1}{4}\,\pi\rho^*\phi^4\left\{\zeta_t+\zeta_z\left(v+\frac{2}{3}\,\phi^2\gamma\right)+\zeta\left(\zeta+\frac{2}{3}\,\phi^2\sigma\right)\right.$$
$$-\omega\left(\omega+\frac{2}{3}\,\phi^2\eta\right)+\frac{2}{3}\,\phi^2\left[\sigma_t+\sigma_z\left(v+\frac{3}{4}\,\phi^2\gamma\right)\right.$$
$$\left.\left.+3\sigma\left(\zeta+\frac{3}{4}\,\phi^2\sigma\right)-\eta\left(\omega+\frac{3}{4}\,\phi^2\eta\right)\right]\right\}, \tag{2.34}$$

$$\frac{1}{4}\,\mu\left[\phi^4\left(\omega_z+\frac{2}{3}\,\phi^2\eta_z\right)\right]_z+\phi^2(1+\phi_z^2)^{1/2}\tau_2$$
$$=\frac{1}{4}\,\rho^*\phi^4\left\{\omega_t+\omega_z\left(v+\frac{2}{3}\,\phi^2\gamma\right)+2\omega\left(\zeta+\frac{2}{3}\,\phi^2\sigma\right)\right.$$
$$\left.+\frac{2}{3}\,\phi^2\left[\eta_t+\eta_z\left(v+\frac{3}{4}\,\phi^2\gamma\right)+4\eta\left(\zeta+\frac{3}{4}\,\phi^2\sigma\right)\right]\right\}, \tag{2.35}$$

$$\frac{1}{2}\,\pi\mu\left[\phi^4\left(v_z+\frac{2}{3}\,\phi^2\gamma_z\right)\right]_z-\pi\mu\phi^4\gamma$$
$$-\frac{1}{2}\,\pi\mu\phi^4\left(\zeta_z+\frac{2}{3}\,\phi^2\sigma_z\right)+\pi\phi^3(\tau_1+\phi_z p_e)$$
$$=q_z+\frac{1}{4}\,\pi\rho^*\phi^4\left\{v_t+v_z\left(v+\frac{2}{3}\,\phi^2\gamma\right)\right.$$
$$\left.+\frac{2}{3}\,\phi^2\left[\gamma_t+\gamma_z\left(v+\frac{3}{4}\,\phi^2\gamma\right)+2\gamma\left(\zeta+\frac{3}{4}\,\phi^2\sigma\right)\right]\right\}, \tag{2.36}$$

$$\frac{1}{24}\,\pi\mu\left[\phi^6\left(\zeta_z+\frac{3}{4}\,\phi^2\sigma_z\right)\right]_z+\frac{1}{12}\,\pi\mu(\phi^6\gamma)_z$$
$$-\frac{1}{2}\,\pi\mu\phi^4\left(\zeta+\frac{5}{3}\,\phi^2\sigma\right)+\frac{1}{4}\,\pi\phi^4(\phi_z\tau_1-p_e)$$
$$=-q+\frac{1}{24}\,\pi\rho^*\phi^6\left\{\zeta_t+\zeta_z\left(v+\frac{3}{4}\,\phi^2\gamma\right)+\zeta\left(\zeta+\frac{3}{4}\,\phi^2\sigma\right)\right.$$
$$-\omega\left(\omega+\frac{3}{4}\,\phi^2\eta\right)+\frac{3}{4}\,\phi^2\left[\sigma_t+\sigma_z\left(v+\frac{4}{5}\,\phi^2\gamma\right)\right.$$
$$\left.\left.+3\sigma\left(\zeta+\frac{4}{5}\,\phi^2\sigma\right)-\eta\left(\omega+\frac{4}{5}\,\phi^2\eta\right)\right]\right\}, \tag{2.37}$$

$$\frac{1}{24}\,\mu\left[\phi^6\left(\omega_z+\frac{3}{4}\,\phi^2\eta_z\right)\right]_z-\frac{1}{6}\,\mu\phi^6\eta+\frac{1}{4}\,\phi^4(1+\phi_z^2)^{1/2}\tau_2$$
$$=\frac{1}{24}\,\rho^*\phi^6\left\{\omega_t+\omega_z\left(v+\frac{3}{4}\,\phi^2\gamma\right)+2\omega\left(\zeta+\frac{3}{4}\,\phi^2\sigma\right)\right.$$
$$\left.+\frac{3}{4}\,\phi^2\left[\eta_t+\eta_z\left(v+\frac{4}{5}\,\phi^2\gamma\right)+4\eta\left(\zeta+\frac{4}{5}\,\phi^2\sigma\right)\right]\right\}. \tag{2.38}$$

So far we have said nothing specific about the lateral surface of the fluid, apart from its symmetry and the fact that it is a material surface. The governing equations (2.16), (2.18), and (2.33)–(2.38) are valid for both a free jet (with or without surface tension), as well as for fluid flow inside a straight circular tube (either rigid or flexible) of variable radius. These various cases are distinguished by introducing assumptions for the surface tractions p_e, τ_1, τ_2 or by imposing further restrictions on the velocity (2.15).

3 Specific Forms for the Lateral Surface

The simplest form of the lateral surface is a free surface, corresponding to the motion of a straight circular jet in air. This case can be characterized by the specific stipulations

$$p_e-p_o=T\left[\frac{\phi_{zz}}{(1+\phi_z^2)^{3/2}}-\frac{1}{\phi(1+\phi_z^2)^{1/2}}\right], \tag{3.1}$$
$$\tau_1=\tau_2=0, \tag{3.2}$$

where p_o is a constant external pressure, T is the surface tension, and we have neglected any entrainment of the surrounding air. Without recording the explicit equations, we note that when $\gamma=\sigma=\eta=0$, the governing equations (2.16), (2.18), and (2.33)–(2.35) for a free jet reduce to those of Caulk and Naghdi (1979), which were used to examine capillary instability. The resulting dispersion relation for capillary instability (Caulk and Naghdi, 1979) indicated some improvement over an earlier result of Weber (1931) when a comparison was made with numerical calculations of Chandrasekhar (1961, p. 544) who used the exact three-dimensional equations. In this connection, it may be noted that since the present equations are based on the more general velocity assumption (2.15), they are likely to give further improved results for this problem, but we do not pursue this matter here.

On the boundary of a rigid tube, we impose a no-slip condition and require that the assumed velocity (2.15) vanish identically on the surface (2.4). It follows that

$$\zeta+\phi^2\sigma=0,\quad \omega+\phi^2\eta=0,\quad v+\phi^2\gamma=0. \tag{3.3}$$

Now since $\phi=\phi(z)$, equation (2.16) is satisfied identically and the two independent incompressibility conditions $(2.18)_{1,2}$ reduce to

$$v_z+2\zeta=0,\quad (\phi^2 v)_z=0. \tag{3.4}$$

Finally, the integrated momentum equations (2.33)–(2.38) become

$$2\pi\phi(\tau_1+\phi_z p_e)$$
$$=p_z+\frac{1}{2}\,\pi\rho^*\phi^2\left(v_t+vv_z+\frac{2}{3}\,v^2\phi_z/\phi\right), \tag{3.5}$$

$$\frac{1}{12}\,\pi\mu(\phi^4\zeta)_{zz}+\pi\phi^2(\phi_z\tau_1-p_e)$$
$$=-p+\frac{1}{12}\,\pi\rho^*\phi^4\left(\zeta_t+\frac{1}{2}\,\zeta_z v\right.$$
$$\left.-\frac{1}{2}\,\zeta^2-\frac{1}{2}\,\omega^2-\frac{1}{2}\,vv_z\phi_z/\phi\right), \tag{3.6}$$

Downloaded 03 May 2010 to 171.66.16.27. Redistribution subject to ASME license or copyright; see http://www.asme.org/terms/Terms_Use.cfm

$$\frac{1}{12}\mu(\phi^4\omega)_{zz}+\phi^2(1+\phi_z^2)^{1/2}\tau_2$$

$$=\frac{1}{12}\rho^*\phi^4\left(\omega_t+\frac{1}{2}v\omega_z+\omega v\phi_z/\phi\right), \tag{3.7}$$

$$\frac{1}{6}\pi\mu(\phi^4 v)_{zz}+\pi\mu\phi^2 v-\frac{1}{6}\pi\mu(\phi^4\zeta)_z+\pi\phi^3(\tau_1+\phi_z p_e)$$

$$=q_z+\frac{1}{12}\pi\rho^*\phi^4(v_t+vv_z+v^2\phi_z/\phi), \tag{3.8}$$

$$\frac{1}{96}\pi\mu(\phi^6\zeta)_{zz}-\frac{1}{12}\pi\mu(\phi^4 v)_z+\frac{1}{3}\pi\mu\phi^4\zeta$$

$$+\frac{1}{4}\pi\phi^4(\phi_z\tau_1-p_e)=-q+\frac{1}{96}\pi\rho^*\phi^6\left(\zeta_t+\frac{2}{5}\zeta_z v\right.$$

$$\left.-\frac{4}{5}\zeta^2-\frac{2}{5}\omega^2-\frac{3}{5}vv_z\phi_z/\phi\right), \tag{3.9}$$

$$\frac{1}{96}\mu(\phi^6\omega)_{zz}+\frac{1}{6}\mu\omega\phi^4+\frac{1}{4}\phi^4(1+\phi_z^2)^{1/2}\tau_2$$

$$=\frac{1}{96}\rho^*\phi^6\left(\omega_t+\frac{2}{5}v\omega_z-\frac{2}{5}\omega\zeta+\frac{6}{5}\omega v\phi_z/\phi\right). \tag{3.10}$$

In this case, the surface force components p_e, τ_1, τ_2 are unknown reactions which are determined as part of the solution to the momentum equations (3.5)–(3.10). The equations for peristaltic pumping can be derived in a similar manner by prescribing $\phi = \phi(z, t)$ and replacing equation $(3.3)_1$ by $\phi_t = \phi(\zeta + \phi^2\sigma)$.

A third form of the lateral surface is an isotropic elastic membrane. For simplicity we suppress the effect of rotation in this case ($\omega = \eta = 0$) and assume that the elastic membrane is unstressed when the tube has a uniform radius a. We suppose that the membrane undergoes a small displacement $\mathbf{u}$ from this state represented by

$$\mathbf{u}=u\mathbf{e}_3+(\phi-a)\mathbf{e}_r, \tag{3.11}$$

where u is a function of z and t. In terms of the components of the boundary traction in equation (2.26), the linearized equilibrium equations for the membrane are

$$p_e=\frac{Eh}{1-\bar{\nu}^2}[(\phi-a)/a^2+\bar{\nu}u_z/a], \tag{3.12}$$

$$\tau_1=\frac{Eh}{1-\bar{\nu}^2}[u_{zz}+\bar{\nu}\phi_z/a], \tag{3.13}$$

where E is the modulus of elasticity, $\bar{\nu}$ is Poisson's ratio, and h is the membrane thickness.[3] Assuming that the fluid is not allowed to slip relative to the membrane, then the axial component of the displacement vector must satisfy the kinematic boundary condition

$$u_t=v+a^2\gamma. \tag{3.14}$$

To be consistent with the assumption of small displacement, the momentum equations (2.33), (2.34), (2.36), and (2.37) must be also linearized about a state of rest.

For the flow of an inviscid fluid inside a tube, the conditions on the lateral surface are distinctly different from those for viscous fluid. Consequently, it is not possible to obtain this case by simply taking the limit $\mu \to 0$ in the momentum equations. Instead, we must set $\tau_1 = \tau_2 = 0$ at the outset and omit the no-slip conditions $(3.3)_{2,3}$ or (3.14).

[3]The use of an overbar on the symbol $\bar{\nu}$ for Poisson's ratio is to avoid confusion with the kinematic viscosity ν to be introduced in Section 4.

4 A General Unsteady Solution

Consider flow in a rigid tube without rotation ($\omega = \eta = 0$) and introduce the volume flow rate Q defined by

$$Q=\frac{1}{2}\pi\phi^2 v, \tag{4.1}$$

which, because of equation $(3.4)_2$, depends only on time. Eliminating p_e, τ_1, q, and ζ from among equations (3.4)–(3.10), we obtain

$$(p/\phi^2)_z=-\mu Q\phi^{-4}\left[8+\frac{1}{2}\phi_z^4+\frac{1}{4}\phi^2\phi_{zz}^2+2\phi\phi_z^2\phi_{zz}\right.$$

$$\left.-\frac{1}{12}\phi^3\phi_{zzzz}+\frac{8}{3}(\phi_z^2+\phi\phi_{zz})\right]$$

$$-\frac{4}{3}\rho^*\dot{Q}\phi^{-4}\left[\phi^2+\frac{1}{64}(\phi^4)_{zz}\right]$$

$$+\frac{4}{\pi}\rho^*Q^2\phi^{-4}\left[\phi_z/\phi-\frac{1}{40}(\phi\phi_{zzz}-3\phi_z\phi_{zz})\right]. \tag{4.2}$$

Integrated over a finite section of the tube $0 \le z \le L$, this expression becomes

$$G=\left(\frac{8\mu A}{\pi a^4}\right)Q+\left(\frac{4\rho^*C}{\pi^2a^5}\right)Q^2+\left(\frac{4\rho^*B}{3\pi a^2}\right)\dot{Q}, \tag{4.3}$$

where

$$A=\int_{z_1}^{z_2}\left(\frac{a}{\phi}\right)^4\left\{1+\frac{1}{3}\phi_z^2+\frac{1}{16}\phi_z^4+\frac{1}{32}\phi^2\phi_{zz}^2\right.$$

$$\left.+\frac{1}{3}\phi\phi_{zz}\left(1+\frac{3}{4}\phi_z^2\right)-\frac{1}{96}\phi^3\phi_{zzzz}\right\}\frac{dz}{L}, \tag{4.4}$$

$$B=\int_{z_1}^{z_2}\left(\frac{a}{\phi}\right)^2\left\{1+\frac{3}{16}\phi_z^2+\frac{1}{16}\phi\phi_{zz}\right\}\frac{dz}{L}, \tag{4.5}$$

$$-C=\int_{z_1}^{z_2}\left(\frac{a}{\phi}\right)^5\left\{\phi_z-\frac{1}{40}\phi^2\phi_{zzz}+\frac{3}{40}\phi\phi_z\phi_{zz}\right\}\frac{dz}{L}, \tag{4.6}$$

$$GL=P(z_1)-P(z_2),\quad P=p/\pi\phi^2, \tag{4.7}$$

$$a=\phi(0). \tag{4.8}$$

The quantities A, B, and C are nondimensional constants determined by the geometry of the tube over the finite interval, P is the average pressure at any section of the tube, and G is the mean pressure gradient over the interval $0 \le z \le L$.

Consider now the specific case when G is constant and the flow begins from rest. In this case, the solution of equation (4.3) is

$$Q(t)=\frac{\pi Ga^4}{4\mu A}\left\{1+\beta\coth\left[-\frac{3\nu}{a^2}\left(\frac{A}{B}\right)\beta t\right]\right\}^{-1}, \tag{4.9}$$

where

$$\beta^2=1+\frac{\rho^*a^3G}{4\mu^2}\left(\frac{C}{A^2}\right) \tag{4.10}$$

and $\nu = \mu/\rho^*$ is the kinematic viscosity. In the limit of long time

$$\lim_{t\to\infty}Q(t)=\frac{\pi Ga^4}{4\mu}\left[\left(A^2+\frac{\rho^*a^3G}{4\mu^2}C\right)^{1/2}+A\right]^{-1}, \tag{4.11}$$

which expresses the steady volume flow rate in terms of the mean pressure gradient, viscosity and tube geometry.

Flow separation occurs when the axial component of the surface shear traction (see Fig. 1) is in the direction of the flow or when $\tau_1 > 0$. The expression for τ_1 can be obtained from equations (3.4)–(3.10) and is given by

Downloaded 03 May 2010 to 171.66.16.27. Redistribution subject to ASME license or copyright; see http://www.asme.org/terms/Terms_Use.cfm

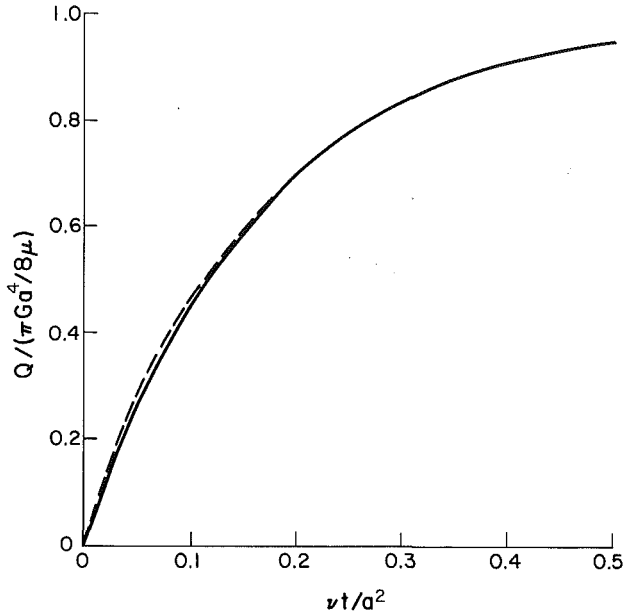


Fig. 2 Normalized volume flow rate for starting flow in a uniform tube: (——) one-dimensional solution from equation (4.14) and (----) exact three-dimensional solution from equation (4.15)

$$-2\pi\phi^2(1+\phi_z^2)\tau_1 = 8\mu Q\phi^{-1}\left[1+\frac{1}{3}\ (\phi_z^2+\phi\phi_{zz})\right.$$

$$+\frac{1}{16}\ \phi_z^4+\frac{1}{32}\ \phi^2\phi_{zz}^2+\frac{3}{8}\ \phi\phi_z^2\phi_{zz}+\frac{1}{24}\ \phi_{zzz}\phi_z\phi^2$$

$$\left.-\frac{1}{96}\ \phi^3\phi_{zzzz}\right]+\frac{4}{3\pi}\ \rho^*Q^2\phi^{-2}\left[-\phi_z+\frac{1}{2}\ \phi_z^3+\frac{3}{40}\ \phi_{zzz}\phi^2\right.$$

$$\left.-\frac{19}{40}\ \phi_{zz}\phi_z\phi\right]+\frac{1}{3}\ \rho^*\dot{Q}\phi\left[1-\frac{1}{4}\ \phi_z^2+\frac{1}{4}\ \phi_{zz}\phi\right]. \quad (4.12)$$

In the special case of a uniform tube of radius a, the nondimensional constants (4.4)–(4.6) reduce to

$$A=B=1, \quad C=0 \quad (4.13)$$

and the general expression (4.9) becomes

$$Q(t)=\frac{\pi Ga^4}{8\mu}\ [1-\exp(-6\nu t/a^2)], \quad (4.14)$$

which approaches the exact three-dimensional solution for steady Poiseuille flow as $t\to\infty$. The exact three-dimensional solution corresponding to equation (4.14) is given by (see for example Batchelor 1967):

$$Q(t)=\frac{\pi Ga^4}{8\mu}\left[1-32\sum_{n=1}^{\infty}\lambda_n^{-4}\exp\left(-\lambda_n^2\ \frac{\nu t}{a^2}\right)\right], \quad (4.15)$$

where λ_n (n = 1, 2, 3, . . .) are zeroes of the zeroth-order Bessel function. If the infinite series in equation (4.15) is approximated by just the first term, the expression for Q becomes

$$Q(t)\simeq\frac{\pi Ga^4}{8\mu}\left[1-0.96\ \exp\left(-5.78\ \frac{\nu t}{a^2}\right)\right], \quad (4.16)$$

which compares favorably with the one-dimensional result (4.14). Figure 2 represents a comparison of equation (4.14) with the exact expression (4.15). Agreement between the two results is remarkably good, even at very small values of time.

For the special case of steady flow at low Reynolds number in a tube of slowly varying radius, the results of this section can be compared to those of Manton (1971) who proceeded by asymptotic expansion of the full three-dimensional equations. To make this comparison, we introduce the nondimensional variables

$$\bar{z}=\epsilon z/a, \quad \bar{\phi}=\phi/a, \quad (4.17)$$

where a is a characteristic radius of the tube and ϵ is a small parameter. Substituting equation (4.17) into (4.2) and (4.12) and expanding these expressions in powers of ϵ, we obtain

$$-\partial P/\partial\bar{z}=\frac{8\mu Q}{\pi a^3}\ \bar{\phi}^{-4}\left[\epsilon^{-1}-\frac{1}{4}\ R(\bar{\phi}_{\bar{z}}/\bar{\phi})\right.$$

$$\left.+\frac{1}{3}\ \epsilon(\bar{\phi}_{\bar{z}}^2+\bar{\phi}\bar{\phi}_{\bar{z}\bar{z}})\right]+O(\epsilon^2), \quad (4.18)$$

$$-\tau_1=\frac{4\mu Q}{\pi a^3}\ \bar{\phi}^{-3}\left[1-\frac{1}{12}\ \epsilon R(\bar{\phi}_{\bar{z}}/\bar{\phi})\right.$$

$$\left.-\frac{1}{3}\ \epsilon^2(2\bar{\phi}_{\bar{z}}^2-\bar{\phi}\bar{\phi}_{\bar{z}\bar{z}})\right]+O(\epsilon^3), \quad (4.19)$$

where

$$R=\frac{2Q}{\pi a\nu} \quad (4.20)$$

is the Reynolds number for the flow. Expressed in the same notation, the corresponding results obtained by Manton are

$$-\partial P/\partial\bar{z}=\frac{8\mu Q}{\pi a^3}\ \bar{\phi}^{-4}\left[\epsilon^{-1}-\frac{1}{4}\ R(\bar{\phi}_{\bar{z}}/\bar{\phi})+\frac{1}{3}\ \epsilon(\bar{\phi}_{\bar{z}}^2+\bar{\phi}\bar{\phi}_{\bar{z}\bar{z}})\right.$$

$$\left.+\frac{11}{2880}\ \epsilon R^2\bar{\phi}^{-2}\left(\bar{\phi}\bar{\phi}_{\bar{z}\bar{z}}-\frac{11}{3}\ \bar{\phi}_{\bar{z}}^2\right)\right]+O(\epsilon^2), \quad (4.21)$$

$$-\tau_1=\frac{4\mu Q}{\pi a^3}\ \bar{\phi}^{-3}\left[1-\frac{1}{12}\ \epsilon R(\bar{\phi}_{\bar{z}}/\bar{\phi})-\frac{1}{3}\ \epsilon^2(2\bar{\phi}_{\bar{z}}^2-\bar{\phi}\bar{\phi}_{\bar{z}\bar{z}})\right.$$

$$\left.+\frac{1}{576}\ \epsilon^2R^2\bar{\phi}^{-2}\left(\bar{\phi}\bar{\phi}_{\bar{z}\bar{z}}-\frac{67}{15}\ \bar{\phi}_{\bar{z}}^2\right)\right]+O(\epsilon^3). \quad (4.22)$$

To the order of ϵ retained in the expressions for $\partial P/\partial\bar{z}$ and τ_1, the only difference between the two pairs of results occurs in terms multiplied by R^2, which are extremely small in the range of validity of Manton's analysis.

Although the general transient solution (4.9) for starting flow in a tube is not restricted to small Reynolds number or a uniform tube radius, it compares extremely well with both the exact solution (4.15) and the asymptotic results (4.21) and (4.22) in two special cases.

5 Swirling Flow in a Uniform Tube

In this section we consider swirling motion ($\omega\neq 0$) superposed on axial flow in a uniform tube, and from the steady state solution of the problem obtain the decay of the swirl with the distance along the axis of the tube. Let the tube radius be a, and since $v = v_o$ = constant by equation $(3.4)_2$, the momentum equations (3.7) and (3.10) become

$$\frac{1}{12}\ \mu a^2\omega_{zz}+\tau_2=\frac{1}{12}\ \rho^*a^2\left(\omega_t+\frac{1}{2}\ v_o\omega_z\right), \quad (5.1)$$

$$\frac{1}{24}\ \mu a^2\omega_{zz}+\frac{2}{3}\ \mu\omega+\tau_2=\frac{1}{24}\ \rho^*a^2\left(\omega_t+\frac{2}{5}\ v_o\omega_z\right). \quad (5.2)$$

When τ_2 is eliminated between these equations, they reduce to

$$a^2\omega_{zz}-\frac{3}{5}\ Ra\omega_z-16\omega=\frac{a^2}{\nu}\ \omega_t, \quad (5.3)$$

where ν is the kinematic viscosity introduced in equation (4.9) and the Reynolds number R is again defined by equation (4.20).

We now seek a solution of equation (5.3) for steady flows ($\omega_t = 0$) in the form

Downloaded 03 May 2010 to 171.66.16.27. Redistribution subject to ASME license or copyright; see http://www.asme.org/terms/Terms_Use.cfm

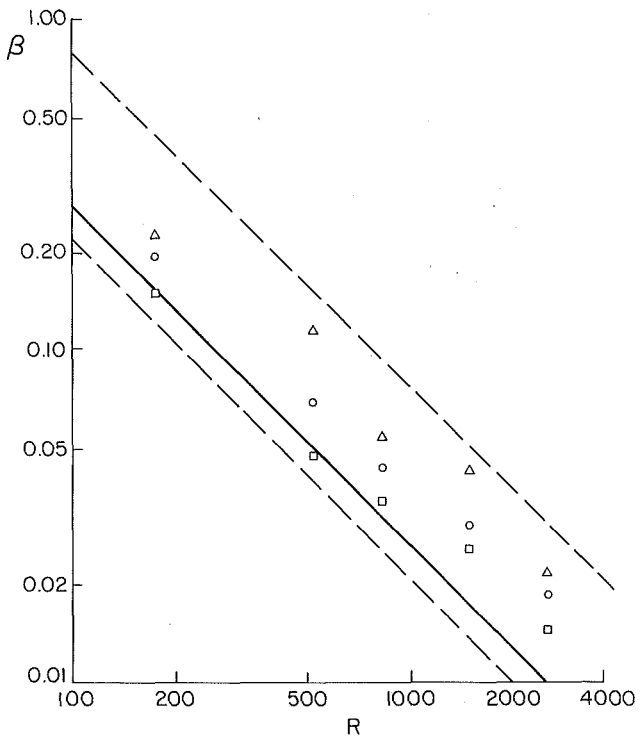


Fig. 3 Comparison of the theoretical prediction of the swirl decay β downstream in a uniform tube with experimental results of Talbot (1954) as a function of the Reynolds number R: (Δ) measured at z/a = 15; (○) measured at z/a = 25; (□) measured at z/a = 40 (from Talbot, 1954). The solid line represents the exponential decay of the present solution given by (5.4). The lower and upper dashed lines represent, respectively, the exponential decay of the first and second terms in Talbot's perturbation solution.

$$\omega = \omega_o \exp\left(-\beta \frac{z}{a}\right), \tag{5.4}$$

where ω_o is a constant and β represents the swirl decay. Substitution of equation (5.4) into equation (5.3) with its right-hand side equal to zero yields

$$\beta^2 + \frac{3}{5} R\beta - 16 = 0,$$

and the relevant root is

$$\beta = \frac{1}{2}\left\{-\frac{3}{5} R + \left[\left(\frac{3}{5} R\right)^2 + 64\right]^{1/2}\right\}. \tag{5.5}$$

The solution (5.4) with β given by equation (5.5) can be readily compared to the experimental results obtained by Talbot (1954). Figure 3 shows his measurements of the local exponential decay at three stations downstream from the beginning of swirl over a range of Reynolds numbers from 177 to 2700. The overall agreement is quite good, especially at z/a = 40 where entrance effects are completely damped out. (In this connection, it should be noted that no entrance effect can appear in the solution (5.4*a*) since the six independent velocity coefficients v, γ, ζ, σ, ω and η are completely determined by the geometry of the pipe, the flow rate Q, and the initial rotation ω_o.)

In the same paper, Talbot (1954) considered a linearized form of the Navier-Stokes equations in which he neglected the radial velocity component and deviation from Poiseuille flow in the axial direction. The solution of these equations was then obtained as a series of hypergeometric functions in the radial coordinate multiplied by a decaying exponential in z. Through a separate analysis of this solution, Talbot found that his approximation was valid only at distances well-downstream from the beginning of swirl ($z/a > 25$, see his Fig. 6). In fact, his error estimates are singular near $z = 0$. With this as background, we also show in Fig. 3 the rate of exponential decay of the first two terms in his series solution, but caution that his results cannot be *directly* compared to the experimental data as can our solution (5.4).

Acknowledgment

The work of P. M. Naghdi was supported by the Fluid Mechanics Program of the U.S. Office of Naval Research under Contract N00014-86-K-0057, Work Unit 4322534 with the University of California, Berkeley.

References

Batchelor, G. K., 1967, *An Introduction to Fluid Mechanics*, Cambridge Press.

Caulk, D. A., and Naghdi, P. M., 1979, ASME JOURNAL OF APPLIED MECHANICS, Vol. 46, pp. 291–297.

Chandrasekhar, S., 1961, *Hydrodynamic and Hydromagnetic Stability*, Clarendon Press, Oxford.

Geer, J., 1977, *The Physics of Fluids*, Vol. 20, pp. 1613–1630.

Goren, S. L., and Wronski, S., 1966, *Journal of Fluid Mechanics*, Vol. 25, pp. 185–198.

Green, A. E., and Naghdi, P. M., 1984, *Archive for Rational Mechanics and Analysis*, Vol. 86, pp. 39–63.

Green, A. E., Naghdi, P. M., and Wenner, M. L., 1974a, *Proceedings of the Royal Society of London*, Vol. A 337, pp. 451–483.

Green, A. E., Naghdi, P. M., and Wenner, M. L., 1974b, *Proceedings of the Royal Society of London*, Vol. A 337, pp. 485–507.

Hall, P., 1974, *Journal of Fluid Mechanics*, Vol. 64, pp. 209–226.

Jeffreys, H., 1931, *Cartesian Tensors*, Cambridge Press.

Manton, M. J., 1971, *Journal of Fluid Mechanics*, Vol. 49, pp. 451–459.

Morgan, G. W., and Keily, J. P., 1954, *Journal of the Acoustical Society of America*, Vol. 26, pp. 323–328.

Naghdi, P. M., 1979, *Journal of Non-Newtonian Fluid Mechanics*, Vol. 5, pp. 233–265.

Naghdi, P. M., 1982, *Proceedings of the IUTAM Symposium on Finite Elasticity*, Carlson, D. E., and Shield, R. T., eds., pp. 47–103.

Rubinow, S. T., and Keller, J. B., 1978, *Journal of Fluid Mechanics*, Vol. 88, pp. 181–203.

Talbot, L., 1954, ASME JOURNAL OF APPLIED MECHANICS, Vol. 21, pp. 1–7.

Tanner, R. T., 1966, *British Journal of Applied Physics*, Vol. 17, pp. 663–670.

Tuck, E. O., 1976, *Journal of Fluid Mechanics*, Vol. 76, pp. 625–640.

Weber, C., 1931, *Zeitschrift für angewandte Mathematik und Mechanik*, Vol. 11, pp. 136–154.

Womersley, J. R., 1955, *Philosophical Magazine.*, Vol. 46, pp. 199–221.

Downloaded 03 May 2010 to 171.66.16.27. Redistribution subject to ASME license or copyright; see http://www.asme.org/terms/Terms_Use.cfm

Turbulent Boundary Layers With Mass Transfer by the Dorodnitsyn Finite Element Method

C. A. J. Fletcher

R. W. Fleet

Department of Mechanical Engineering,
University of Sydney,
Sydney, New South Wales 2006, Australia

The Dorodnitsyn finite element formulation is extended to cover incompressible, two-dimensional turbulent boundary layers with surface mass transfer in the normal direction. The method is shown to give accurate and economical answers with only eleven points spanning the boundary layer. Good agreement is obtained when the computational solutions are compared with the experimental results of McQuaid [13] for skin friction coefficient, displacement and momentum thickness and velocity profiles. Zero and adverse pressure gradient and discontinuous injection cases have been considered.

1 Introduction

The Dorodnitsyn boundary layer formulation [1] is based on replacing independent variables x and y (in two dimensions) by x and u/u_e, where u is the velocity component in the direction, x, of boundary layer development and u_e is the known velocity component at the outer edge of the boundary layer. Also by integrating across the boundary layer with respect to u it is possible to extract a nondimensional velocity gradient as the dependent variable.

The Dorodnitsyn formulation has a number of inherent advantages. First the infinite domain in y is replaced by a finite domain in u/u_e, i.e., $0 \leq u/u_e \leq 1$. Downstream boundary layer growth is automatically captured without the need for regridding or grid stretching. A uniform grid in the u/u_e direction gives high resolution close to the wall; this is particularly important for turbulent boundary layer flow [2].

Due to the particular nature of the integral formulation it is possible to avoid the explicit appearance of the normal velocity component, v, as a dependent variable. By treating the nondimensional velocity gradient as the dependent variable the skin friction can be computed very accurately.

Originally the Dorodnitsyn formulation was developed for use with the method of integral relations [3]. However, the integral nature of the Dorodnitsyn formulation also permits the establishment of Galerkin spectral and finite element interpretations [4].

The introduction of orthonormal approximating and weight functions to replace the Dorodnitsyn functions [5] has produced a technique, the orthonormal method of integral relations, that produces solutions of high accuracy with relatively few unknowns in the approximate solution. It is this technique which is now recognized as a Galerkin spectral method [4] and will be referred to here as the Dorodnitsyn spectral method (DOROD-SPEC). This technique has been applied with considerable success to incompressible and compressible laminar [5, 6, 7] and turbulent [2, 8, 9] boundary layer flows.

The finite element interpretation of the Dorodnitsyn boundary-layer formulation has been applied previously to two-dimensional incompressible laminar boundary-layer flow [7] and to incompressible [2] and compressible [9] turbulent boundary-layer flow. The Dorodnitsyn finite element formulation has also been used to predict the behavior of swirling boundary-layer flow on the inner surface of a conical diffuser [10].

A feature of the Dorodnitsyn finite element formulation is that accurate solutions are obtained very economically. For four representative (different pressure gradients) turbulent boundary-layer flows taken from the 1968 Stanford Conference [11] the Dorodnitsyn finite element formulation (DOROD-FEM) is as accurate but *ten times as economical* [2], typically, as a representative finite difference package, STAN5 [12].

In the present paper the Dorodnitsyn finite element formulation is extended to include boundary-layer flow with surface mass transfer (blowing or suction) in Section 2. Solutions obtained with DOROD-FEM are compared with the experimental results of McQuaid [13] in Section 3.

2 Dorodnitsyn Finite Element Formulation

In this section the Dorodnitsyn boundary layer formulation is developed for two-dimensional turbulent flow with surface mass transfer in the normal direction. Subsequently the Dorodnitsyn equation is given a modified Galerkin finite element interpretation [4] and a computationally-efficient algorithm is developed.

2.1 Dorodnitsyn Boundary Layer Formulation With Surface Mass Transfer. For two-dimensional turbulent boundary layers the governing equations are

$$\partial u/\partial x + \partial v/\partial y = 0 \tag{1}$$

Contributed by the Applied Mechanics Division for publication in the JOURNAL OF APPLIED MECHANICS.

Discussion on this paper should be addressed to the Editorial Department, ASME, United Engineering Center, 345 East 47th Street, New York, N.Y. 10017, and will be accepted until two months after final publication of the paper itself in the JOURNAL OF APPLIED MECHANICS. Manuscript received by ASME Applied Mechanics Division, October 25, 1983; final revision, July 23, 1985.

Copyright © 1987 by ASME
Downloaded 03 May 2010 to 171.66.16.27. Redistribution subject to ASME license or copyright; see http://www.asme.org/terms/Terms_Use.cfm

$$u\partial u/\partial x + v\partial u/\partial y = u_e \partial u_e/\partial x + \frac{1}{\mathrm{Re}}\,\partial\{(1+\nu_T/\nu)\partial u/\partial y\}/\partial y. \quad (2)$$

In obtaining equation (2) the expression $\rho\nu_T\partial u/\partial y$ has been substituted for the Reynolds stress, $-\rho\,\overline{u'v'}$. The equation system, (1) and (2), is parabolic and requires initial conditions.

$$u(x_o,y) = u_i(y) \text{ and } v(x_o,y) = v_i(y) \quad (3)$$

and boundary conditions,

$$u(x,0) = 0,\ v(x,0) = v_w \text{ and } u(x,\infty) = u_e(x), \quad (4)$$

where v_w is the prescribed normal velocity at the wall. In equations (2) and (4), $u_e(x)$ is the velocity distribution (known) at the boundary layer outer edge. In equations (1) to (4), x and y have been nondimensionalized with a reference length, L, and u, u_e, v, and v_w have been nondimensionalized with a reference velocity, u_∞. The Reynolds number is then given by $\mathrm{Re} = u_\infty L/\nu$.

Dorodnitsyn [1] introduced the following variables,

$$\xi = \int_o^x u_e(x')dx',\ \eta = R_e^{1/2} u_e(x) y \quad (5)$$

$$u' = u/u_e,\ v' = R_e^{1/2} v/u_e \text{ and } w' = v' + \eta u'(\partial u_e/\partial\xi)/u_e. \quad (6)$$

Substitution into equations (1) to (4) gives

$$\partial u'/\partial\xi + \partial w'/\partial\eta = 0 \quad (7)$$

$$u'\partial u'/\partial\xi + w'\partial u'/\partial\eta = (1/u_e)\partial u_e/\partial\xi + \partial\{(1+\nu_T/\nu)\partial u'/\partial\eta\}/\partial\eta \quad (8)$$

with auxiliary conditions,

$$u' = 0,\ w' = R_e^{1/2} v_w/u_e \text{ at } \eta = 0 \text{ and } u' = 1 \text{ at } \eta = \infty \quad (9)$$

The following product is constructed,

$f_k x$ equation (7) + $(\partial f_k/\partial u')x$ equation (8),

where $f_k(u')$ is a general weight (test) function, whose specific form is determined by the particular computational method used, e.g., equation (16).

An integration is made over the product, with respect to η. The result is (dropping the prime $'$)

$$\frac{\partial}{\partial\xi}\int_o^\infty u f_k d\eta + [w f_k]_o^\infty = \frac{1}{u_e}\frac{du_e}{d\xi}\int_o^\infty \frac{df_k}{du}(1-u^2)d\eta + \int_o^\infty \frac{df_k}{d\eta}\frac{\partial}{\partial\eta}\left\{\left(1+\frac{\nu_T}{\nu}\right)\frac{\partial u}{\partial\eta}\right\}d\eta. \quad (10)$$

It is clear that w (and hence v) only appear as limiting values at $\eta = 0$ and ∞. The influence of the value of w at $\eta = \infty$ is removed from equation (10) by choosing $f_k(\eta = \infty) = 0$.

Finally the variable of integration is charged from η to u and following dependent variables introduced,

$$\mathfrak{I} = 1/\textcircled{H} = \partial u/\partial\eta. \quad (11)$$

Equation (10) then becomes

$$\frac{\partial}{\partial\xi}\int_o^1 u f_k \textcircled{H}\, du - \mathrm{R\acute{e}}^{1/2} F\left[f_k\right]_{u=0} = \frac{1}{u_e}\frac{du_e}{d\xi}\int_o^1 \frac{\partial f_k}{\partial u}(1-u^2)\textcircled{H}\, du + \int_o^1 \frac{\partial f_k}{\partial u}\frac{\partial}{\partial u}\left\{(1+\nu_T/\nu)\mathfrak{I}\right\}du, \quad (12)$$

where $F = v_w/u_e$.

Equation (12) is the Dorodnitsyn turbulent boundary layer formulation with prescribed mass transfer at the wall, in the normal direction.

The particular choice for the dependence of the weight function, f_k, on u and the form of the approximate solution for $\mathfrak{I}$ and $\textcircled{H}$ leads to either the method of integral relations [3], the Dorodnitsyn finite element formulation [2, 7], or the Dorodnitsyn spectral formulation [5, 6, 8, 9, 14].

In the Dorodnitsyn spectral formulation, orthonormal functions are constructed from the original Dorodnitsyn weight function, $f_k = (1-u)^k$. The orthonormal functions then replace f_k in equation (12) and are used as the trial functions in the approximate solutions for $\mathfrak{I}$ and $\textcircled{H}$. The application of the Dorodnitsyn spectral formulation to the present problem is described by Fleet and Fletcher [14].

2.2 Finite Element Formulation. In this formulation it is more convenient to replace ξ with the original longitudinal coordinate, x. Consequently equation (12) has the equivalent form,

$$\frac{\partial}{\partial x}\int_o^1 u f_k \textcircled{H}\, du - R_e^{1/2} u_e F f_k(0) = \frac{1}{u_e}\frac{du_e}{dx}\int_o^1 \frac{df_k}{du}(1-u^2)\textcircled{H}\, du + u_e\int_o^1 \frac{df_k}{du}\frac{\partial}{\partial u}\left\{(1+\nu_T/\nu)\mathfrak{I}\right\}du. \quad (13)$$

The following approximate (trial) solutions are introduced for $\textcircled{H}$ and $(1+\nu_T/\nu)\mathfrak{I}$,

$$\textcircled{H} = \sum_{j=1}^{M}\{N_j(u)/(1-u)\}\theta_j(x) \quad (14)$$

and

$$(1+\nu_T/\nu)\mathfrak{I} = \sum_{j=1}^{M}\{(1-u)N_j(u)\}\{(1+\nu_T/\nu)\tau(x)\}_j. \quad (15)$$

The terms $N_j(u)$ are one-dimensional shape functions [4], typically either linear or quadratic. The factor $(1-u)$ is necessary to ensure that $\mathfrak{I}$ and $\textcircled{H}$ demonstrate the correct behavior at the outer edge of the boundary layer.

In equation (15) the approximate solution has been deliberately introduced for the group of terms, $\{(1+\nu_T/\nu)\mathfrak{I}\}$. This leads to a group finite element formulation [15] and a significant gain in economy. This is because the eddy viscosity, ν_T, is a complicated function of the velocity component u and normal coordinate [2]. The group representation limits the evaluation of ν_T to the nodes only.

The weight function, f_k, in equation (13) is given by

$$f_k(u) = (1-u)N_k(u) \quad (16)$$

The structure of equation (16) ensures that $f_k(u) = 0$ at $u = 1.0$ as required after equation (10).

Substitution of equations (14) to (16) into equation (13) produces a modified Galerkin method [4]. Evaluation of the various integrals leads to the following system of ordinary differential equations,

$$\sum_j CC_{kj}\frac{d\theta_j}{dx} = \mathrm{R\acute{e}}^{1/2}\, u_e F\,\delta_{1k} + \frac{1}{u_e}\frac{du_e}{dx}\sum_j EF_{kj}\theta_j + u_e\sum_j AA_{kj}(1+\nu_T/\nu)_j\tau_j, \quad (17)$$

where $\delta_{1k} = 1$ if $k = 1$

$= 0$ if $k \neq 1$.

The algebraic coefficients in equation (17) are evaluated from

$$CC_{kj} = \int_o^1 N_k N_j u\, du,\ EF_{kj} = \int_o^1 N_j\left\{\frac{dN_k}{du}(1-u) - N_k\right\}(1+u)du \quad (18)$$

and $AA_{kj} = \int_o^1 \left\{\frac{dN_j}{du}(1-u) - N_j\right\}\left\{\frac{dN_k}{du}(1-u) - N_k\right\}du.$

Downloaded 03 May 2010 to 171.66.16.27. Redistribution subject to ASME license or copyright; see http://www.asme.org/terms/Terms_Use.cfm

For reasons of efficiency, an implicit algorithm is developed from equation (17) as follows. First, equation (17) is approximated by

$$\sum_j CC_{kj}\Delta\theta_j^{n+1} = \Delta x\{\omega S^{n+1} + (1-\omega)S^n\}, \tag{19}$$

where S is the right-hand side of equation (17), n denotes the downstream location, and $\Delta\theta_j^{n+1} = \theta_j^{n+1} - \theta_j^n$. The parameter ω controls the degree of implicitness; here $\omega = 0.6$ has been used. After linearization of S^{n+1} about the downstream location, $x^{(n)}$, equation (19) has the following structure,

$$\sum_j CCC_{kj}\Delta\theta_j^{n+1} = P_k \tag{20}$$

where $CCC_{kj} = CC_{kj} - \omega\,\Delta x\left[\left\{\frac{1}{u_e}\frac{du_e}{dx}\right\}^{n+1} EF_{kj} - u_e^{n+1}AA_{kj}G_j^n\right]$,

$$G_j^n = \left[(1+\nu_T/\nu)\tau^2 - \left\{\partial(\nu_T/\nu)/\partial\theta\right\}\tau\right]_j^n$$

and

$$P_k = \Delta x\left[R_e^{1/2}u_eF\,\delta_{1k} + \left\{\omega\left[\frac{1}{u_e}\frac{du_e}{dx}\right]^{n+1} + (1-\omega)\left[\frac{1}{u_e}\frac{du_e}{dx}\right]^n\right\}\sum_j EF_{kj}\theta_j^n + \left\{\omega\,u_e^{n+1} + (1-\omega)u_e^n\right\}\sum_j AA_{kj}(1+\nu_T/\nu)_j^n\tau_j^n\right].$$

The system of equations, (20), is tridiagonal for linear shape functions and pentadiagonal for quadratic shape functions so that a generalized Thomas algorithm can be used to march from $x^{(n)}$ to $x^{(n+1)}$. To achieve maximum economy no iteration is undertaken at each downstream step. Numerical convergence experiments [7] indicate that the scheme is accurate to $0(\Delta x)$. However, good agreement has been obtained with known exact solutions [7] and experimental results [2] with relatively coarse variable stepsizes, Δx. The mechanism for changing the stepsize, Δx, is described by Fletcher and Fleet [2].

The Dorodnitsyn finite element formulation uses a van Driest modified mixing-length representation for the eddy viscosity near the wall. In the outer boundary layer a Clauser eddy viscosity dependence on displacement thickness is used. Details are given by Fletcher and Fleet [2].

3 Results and Discussion

In this section DOROD-FEM solutions are compared with the experimental data of McQuaid [13] for the three cases shown in Table 1. The length scale $L = 211$ mm to match the experimental conditions. In the experiments blowing starts at $x = 125$ mm, $u_\infty = 15.24$ m/s for Cases 1 and 2 and $u_\infty = 45.72$ m/s for Case 3. In Table 1 a positive value of F implies blowing.

The DOROD-FEM solutions have been obtained with linear finite elements and 11 equally-spaced grid points across the boundary layer. For laminar boundary layer flow [7] it was found that quadratic elements were computationally more efficient. However, for turbulent boundary layer flows without injection [2] it was found that quadratic elements gave no special advantage in accuracy to offset the reduced economy, when compared with linear elements. It was also found [2] that the use of 21 points across the boundary layer gave slightly more accurate predictions of displacement thickness, δ^*, and momentum thickness, θ, but was no more accurate for the prediction of skin friction coefficient, c_f.

Table 1 Test cases

Case	Description	F	No. of steps, Δx
1	Zero pressure gradient, $\mathrm{Re} = 0.219\times10^6$	-0.0017, 0.0, 0.0017, 0.0032	58, 70 128, 151
2	Adverse pressure gradient $\mathrm{Re} = 0.242\times10^6$	0.0020	148
3	Zero pressure gradient, discontinuous injection, $\mathrm{Re} = 0.625\times10^6$	$F = 0.0034$, $1.0 \le x \le 2.096$; $F = 0.0$, $2.096 \le x < 4$	216

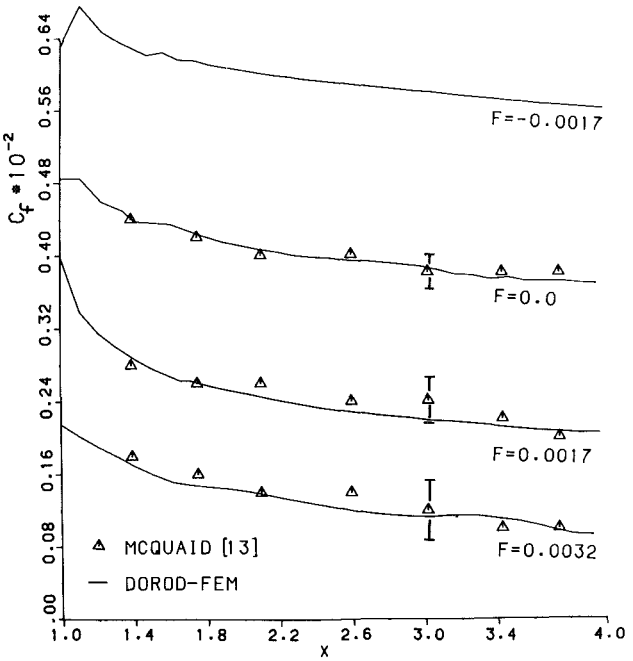


Fig. 1 Skin friction variation for Case 1

The number of steps, Δx, in the downstream direction is shown in Table 1 for the DOROD-FEM solutions. Generally an increase in the blowing parameter, F, increases the number of steps through a restriction on the maximum stepsize. The larger number of steps required for Case 3 is associated with the automatic reduction in stepsize that occurs in the region of the discontinuity in the injection ($x = 2.096$). Comparative execution times for Case 1 using a finite difference package, STAN5, indicate that DOROD-FEM is more than ten times as economical as STAN5 when blowing occurs. This is about the same level of relative economy as was found for turbulent boundary flows without injection [2].

3.1 Zero Pressure Gradient (Case 1). For Case 1 in Table 1 DOROD-FEM solutions have been obtained for both suction and blowing. However, experimental results [13] are available only for the blowing cases. The variation of skin friction coefficient with downstream location is shown in Fig. 1. It is clear that suction increases skin friction and blowing reduces skin friction. The small perturbation shown in the skin friction solution for the suction case ($F = -0.0017$) close to the starting position ($x = 1.00$) is probably due to small errors in the starting velocity profile. For this case the starting velocity profile was "constructed" from the experimental velocity profile at $x = 1$ for $F = 0$. For the three blowing cases experimental [13] velocity profiles at $x = 1.0$ are available.

Downloaded 03 May 2010 to 171.66.16.27. Redistribution subject to ASME license or copyright; see http://www.asme.org/terms/Terms_Use.cfm

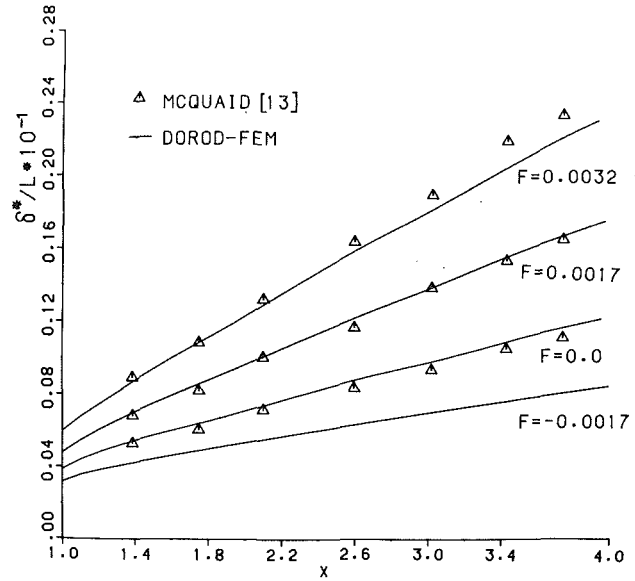


Fig. 2 Variation of displacement thickness for Case 1

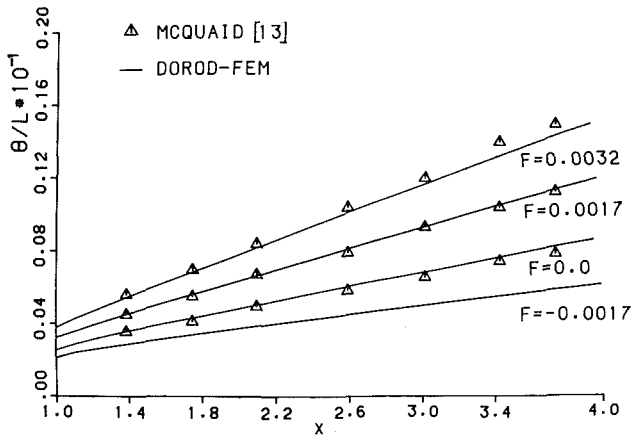


Fig. 3 Variation of momentum thickness for Case 1

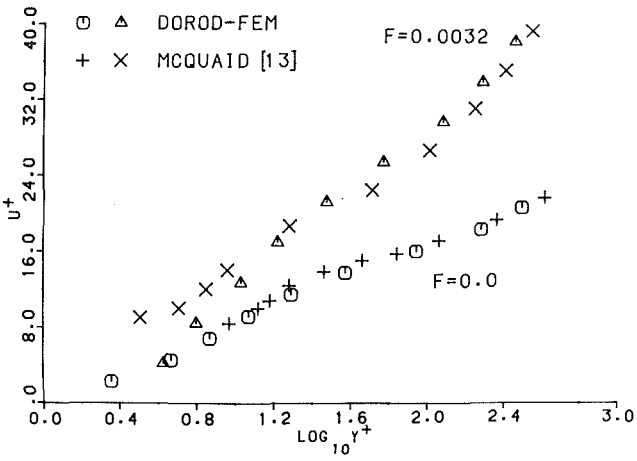


Fig. 4 Velocity distributions at $x = 3.00$ for Case 1

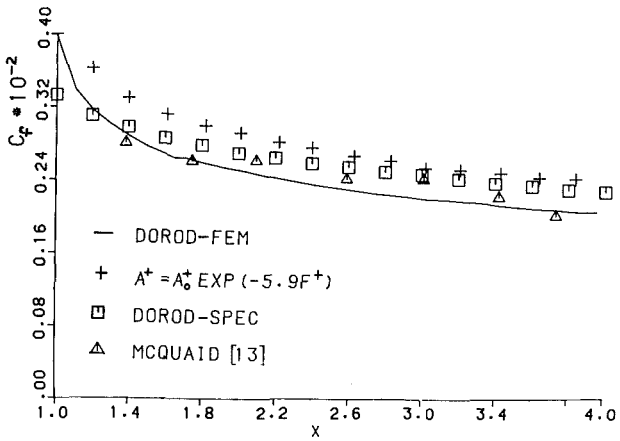


Fig. 5 Skin friction variation comparison, $F = 0.0017$

It is clear (Fig. 1) that DOROD-FEM is providing an accurate prediction of the skin friction distribution. However the experimental skin friction data were not obtained directly but from an evaluation of the two-dimensional momentum integral equation,

$$c_f = 2\left[\frac{d\theta}{dx} - F + (\theta/\delta^* + 2)\frac{\theta}{u_e}\frac{du_e}{dx}\right],$$

from the measured velocity distribution. An indication of the uncertainty in determining the experimental skin friction coefficient is indicated in Fig. 1.

The variation of displacement thickness with downstream position, for various blowing and suction conditions, is shown in Fig. 2. As can be seen suction reduces the displacement thickness and blowing increases the displacement thickness. Agreement with the experimental data of McQuaid [13] is good except for $F = 0.0032$ at far downstream locations.

The corresponding variation in momentum thickness with downstream location is shown in Fig. 3. As with the displacement thickness, the momentum thickness is reduced by suction and increased by blowing at the same downstream location. Good agreement is achieved with the experimental results of McQuaid [13] at all values of the blowing parameter, F.

For Case 1 representative velocity distributions at $x = 3.00$ are shown in Fig. 4. Agreement between the computed and measured velocity distributions are good at $F = 0$ and reasonable for $F = 0.0032$. The velocities are nondimensionalized with u_τ which is proportional to $c_f^{-0.5}$, so that a small value of c_f for $F = 0.0032$ (see Fig. 1) tends to magnify any discrepancy between the measured and computed velocities. The only major discrepancy is occurring adjacent to the innermost experimental point which is probably doubtful since the continuous velocity distribution should also go through $u^+ = 1, y^+ = 1$. The computed solution appears to be reverting to the zero-blowing solution adjacent to the wall.

For eddy viscosity representations based on a mixing length assumption it is customary to assume that the mixing length is proportional to the normal distance y with an additional exponential term to account for the local dampening effect of the wall on the turbulent fluctuations and hence on the mixing length. Thus the following formula for the mixing length is typical [2]

$$\ell^+ = \kappa y^+ (1 - \exp(-y^+/A^+)),$$

where κ is the von Karman constant ($\kappa = 0.41$) and all lengths carrying the superscript + have been nondimensionalized by $[\nu/u_e\{2/c_f\}^{1/2}]$. A^+ is a constant for a flat plate and typically $A^+ = 26$. Cebeci [16] has proposed that A^+ should vary with different blowing and suction conditions by replacing A^+ with

$$A^+ \exp(-5.9\,F^+),$$

where $F^+ = F\,(2/c_f)^{1/2}$.

The solution for $F = 0.0017$ with this adjustment to A^+ is shown in Fig. 5. It can be seen that with the adjustment to A^+, the present method overpredicts the experimental results. The effect of this modification on the displacement and momentum thickness is not as great, causing a slight reduction.

Downloaded 03 May 2010 to 171.66.16.27. Redistribution subject to ASME license or copyright; see http://www.asme.org/terms/Terms_Use.cfm

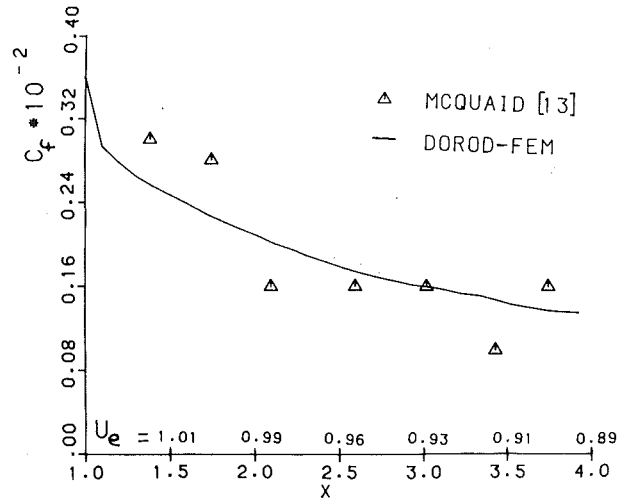


Fig. 6 Skin friction variation for Case 2; $F = 0.0020$

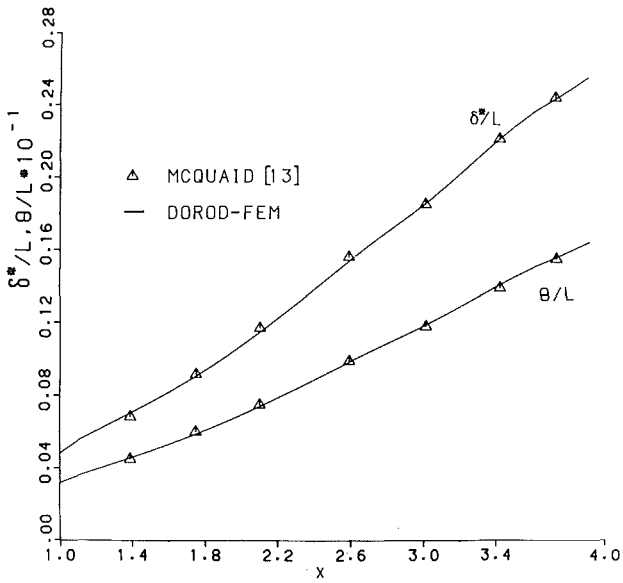


Fig. 7 Displacement and momentum thickness variation for Case 2

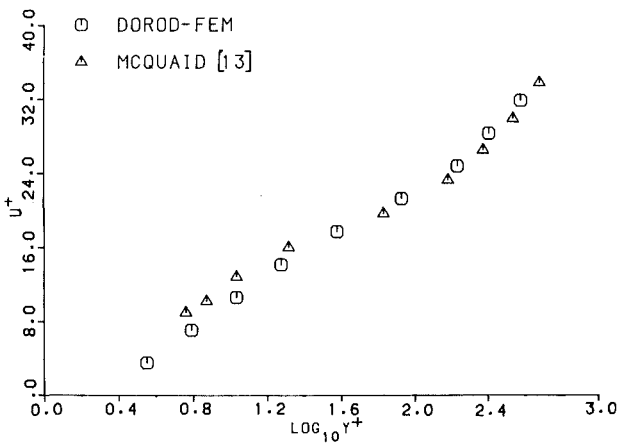


Fig. 8 Velocity distribution at $x = 3.00$ for Case 2

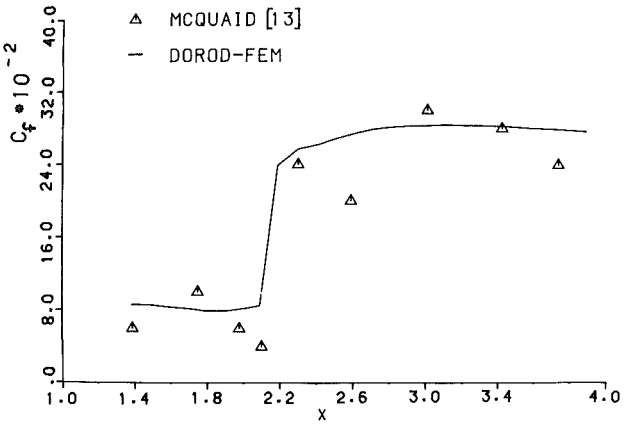


Fig. 9 Skin friction variation for discontinuous injection

However, for the larger blowing value $F = 0.0032$ (not shown) the magnitude of c_f greatly exceeded the experimental values (by 50 percent) at all downstream locations.

Also shown in Fig. 5 is a solution obtained with the spectral Dorodnitsyn formulation (DOROD-SPEC). This solution was obtained with five unknown coefficients in the equivalent of equations (14) and (15) and with various integrals, equivalent to equation (18), evaluated in two halves with six Gauss quadrature points in each. It can be seen that DOROD-SPEC predicts a slightly higher skin friction coefficient than DOROD-FEM but generally still within the error band ascribed to the experimental data.

3.2 Adverse Pressure Gradient (Case 2). For this case the velocity u_e (see Fig. 6) falls continuously in the range, $1 \leq x \leq 4.12$. The blowing parameter is $F = 0.0020$ and the Reynolds number is $\mathrm{Re} = 0.242 \times 10^6$. The variation of skin friction coefficient with downstream location is shown in Fig. 6. Comparing the magnitude of the skin friction coefficient with that for a zero pressure gradient (Fig. 1, $F = 0.0017$) at the same downstream location, it is clear that the predicted skin friction coefficient is lower under the influence of the adverse pressure gradient. The experimental values for the skin friction coefficient show a distinct lack of local smoothness so that the agreement between the computed results and experimental results is considered satisfactory.

The variation of displacement and momentum thickness with downstream location for the adverse pressure gradient case is shown in Fig. 7. The adverse pressure gradient causes a more rapid growth of both thicknesses with downstream position than does a zero pressure gradient (Figs. 2 and 3). Excellent agreement with the experimental results of McQuaid [3] is indicated in Fig. 7.

For the adverse pressure gradient case a typical velocity distribution is provided in Fig. 8. Agreement between the computed and experimetnal data is good in the outer part of the boundary layer. Close to the wall the experimental results indicate a slightly larger velocity for the same y location.

Taken collectively the results shown in Figs. 6 to 8 indicate that the Dorodnitsyn finite element method is giving accurate predictions of the boundary layer development under the combined influences of blowing and an adverse pressure gradient.

3.3 Discontinuous Injection (Case 3). For this case a constant blowing rate of $F = 0.0034$ was maintained in the interval $1.0 \leq x \leq 2.096$ and for $x > 2.096$, $F = 0$. The pressure gradient was nominally zero. However, just ahead of the injection discontinuity there was a slightly favorable pressure gradient and just downstream there was a slightly adverse pressure gradient.

The effect of the discontinuity in injection on the skin friction is substantial (Fig. 9); removal of the injection causes an immediate increase in the skin friction coefficient. The increase is seen to be accurately predicted by the present method when due account is taken of the uncertainty in the experimental values of skin friction coefficient.

Downloaded 03 May 2010 to 171.66.16.27. Redistribution subject to ASME license or copyright; see http://www.asme.org/terms/Terms_Use.cfm

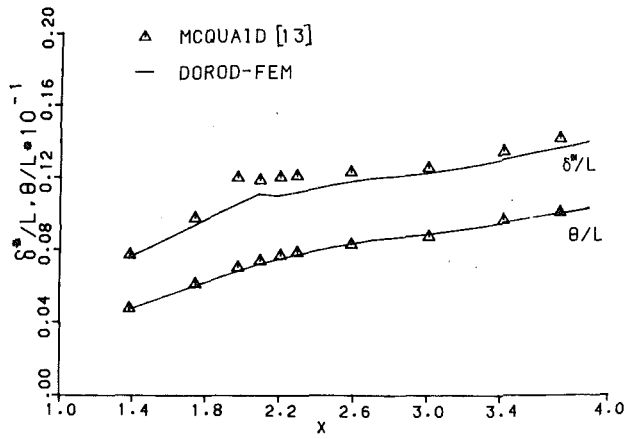


Fig. 10 Displacement and momentum thickness variation for discontinuous injection

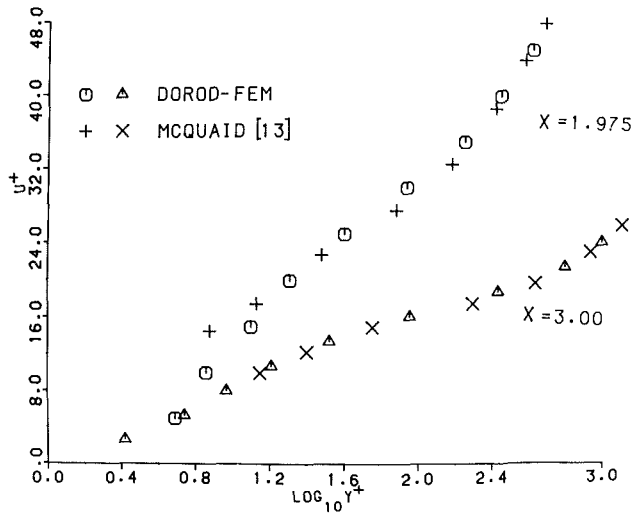


Fig. 11 Velocity distributions for discontinuous injection

For the discontinuous injection case the corresponding development of the displacement and momentum thickness is shown in Fig. 10. The gross effect of removing the injection is to cause both the displacement and momentum thickness to grow at a reduced rate with downstream location. The computational method successfully predicts this effect for both thicknesses. However, the experimental data indicate a slightly greater rise in the displacement thickness ahead of the point where the injection is discontinued than do the computational results. The reason for this is not known.

Velocity distributions both upstream and downstream of the point of injection discontinuity ($x = 2.096$) are shown in Fig. 11. For station $x = 1.975$ agreement between the predicted and measured velocities is good for locations away from the wall. Close to the wall the present method appears to underpredict the measured velocities. This same tendency is apparent for Cases 1 (Fig. 4) and 2 (Fig. 8). However, downstream of the point where the injection is discontinued the velocity profiles ($x = 3.00$) in Fig. 11 indicate close agreement between the predicted and measured results.

4 Conclusions

The Dorodnitsyn finite element formulation has been extended to include turbulent boundary layer flow with mass transfer in the normal direction at the wall. The present algorithm is very economical and accurate with only eleven points across the boundary layer.

Comparisons with the experimental data of McQuaid [13] indicate that the present method is able to predict accurately the downstream development of skin friction, displacement thickness, momentum thickness, and velocity profiles. Accurate predictions have been demonstrated for both zero and adverse pressure gradients and for flows with discontinuous injection. The only consistent discrepancy appears to be a slight underestimate of the magnitude of the velocity close to the wall when blowing is present.

Acknowledgment

The authors are grateful to Dr. K. Srinivas for his assistance in producing the figures.

References

1 Dorodnitsyn, A. A., "General Method of Integral Relations and its Application to Boundary Layer Theory," *Advances in Aeronautical Sciences*, Vol. 3, 1962, pp. 207–219.

2 Fletcher, C. A. J., and Fleet, R. W., "A Dorodnitsyn Finite Element Formulation for Turbulent Boundary Layers," *Computers and Fluids*, Vol. 12, 1984, pp. 31–45.

3 Holt, M., *Numerical Methods in Fluid Dynamics*, Springer Verlag, 1984.

4 Fletcher, C. A. J., *Computational Galerkin Methods*, Springer Verlag, 1984.

5 Fletcher, C. A. J., and Holt, M., "An Improvement to the Method of Integral Relations," *Journal of Computational Physics*, Vol. 18, 1975, pp. 154–164.

6 Fletcher, C. A. J., and Holt, M., "Supersonic Flow about Inclined Cones," *Journal of Fluid Mechanics*, Vol. 74, 1976, pp. 561–591.

7 Fletcher, C. A. J., and Fleet, R. W., "Dorodnitsyn Finite Element Formulation for Laminar Boundary Layer Flow," *Int. Journal for Numerical Methods in Fluids*, Vol. 4, 1984, pp. 399–419.

8 Yeung, W. S., and Yang, R. J., "Application of the Method of Integral Relations to the Calculation of Two-Dimensional Incompressible Turbulent Boundary Layers," ASME JOURNAL OF APPLIED MECHANICS, Vol. 48, 1981, pp. 701–706.

9 Fleet, R. W., and Fletcher, C. A. J., "Application of the Dorodnitsyn Boundary Layer Formulation to Turbulent Compressible Flow," *Proc. Eighth Australasian Fluid Mechanics Conference*, Newcastle, Australia, 1983, pp. 1C1–1C4.

10 Fletcher, C. A. J., "Application of the Dorodnitsyn Finite Element Method to Swirling Boundary Layer Flow," *Int. Journal for Numerical Methods in Fluids*, Vol. 5, 1985, pp. 443–462.

11 *Computation of Turbulent Boundary Layers—1968 AFOSR—ISP—Stanford Conference*, Coles, P., and Hirst, E., eds., Vol. 2, 1968.

12 Reynolds, W. C., "Computation of Turbulent Flows," *Annual Review of Fluid Mechanics*, Vol. 8, 1976, pp. 183–208.

13 McQuaid, J., "Experiments on Incompressible Turbulent Boundary Layers with Distributed Injection," ARC R & M No. 3549, 1967.

14 Fleet, R. W., and Fletcher, C. A. J., "Application of the Dorodnitsyn Boundary Layer Formulation to Wall Blowing," *Proc. Computational Techniques and Applications Conference-83*, Noye, J., and Fletcher, C. A. J., eds., North-Holland, 1984.

15 Fletcher, C. A. J., "The Group Finite Element Formulation," *Computer Methods in Applied Mechanics and Engineering*, Vol. 37, 1983, pp. 225–243.

16 Cebeci, T., "Variation of the van Driest Damping Parameter with Mass Transfer," *AIAA Journal*, Vol. II, 1973, pp. 237–238.

Downloaded 03 May 2010 to 171.66.16.27. Redistribution subject to ASME license or copyright; see http://www.asme.org/terms/Terms_Use.cfm

Bohou Xu[1]
Ph.D.

E. B. Hansen
Professor of Applied Mathematics.

Laboratory of Applied Mathematical Physics,
The Technical University of Denmark,
DK-2800 Lyngby, Denmark

Transient Stokes Flow in a Wedge

The transient flow in the sector region bounded by two intersecting planes and a circular cylinder is determined in the Stokes approximation. The plane boundaries are assumed to be at rest while the cylinder is rotating with a constant velocity starting at $t = 0$. *The problem is solved by means of three different methods, a finite element, a finite difference, and a boundary element method. The corresponding problem in which the constant velocity boundary condition on the cylinder is replaced by a condition of constant stress is also solved by means of the finite element method.*

1 Introduction

Moffatt (1964a) has shown that the Stokes equation for the stream function in a region between two intersecting planes admits solutions representing infinite systems of eddies, provided the angle of the fluid region between the planes is less than a certain value, approximately equal to 146 deg. The eddies decrease in size and intensity as a geometric progression as the vertex is approached. The existence of these solutions suggests that infinite systems of eddies occur in completely defined boundary value problems involving wedge shaped regions. Since Moffatt's discovery this suggestion has been confirmed in a number of exactly soluble boundary value problems for the Stokes equation. The first one was the problem of flow in an infinite wedge between two planes where a strip of finite width in each plane, with edges parallel to the line of intersection, is replaced by a sleeve moving in the plane of the boundary with a constant velocity (Moffatt, 1964b). In this case geometric progressions of eddies are found to exist near the line of intersection as well as in the region from the sleeves outwards towards infinity. Another example is the problem of flow along a plane past a circular cylinder touching a plane (Schubert, 1967). Here geometric progressions of eddies are present in the two cusp regions between the cylinder and the plane. The eddy structure of slow viscous flow in a wedge was demonstrated experimentally by Taneda (1979). He was able to observe two eddies of the infinite progression predicted by theory when the fluid in a wedge was agitated by a rotating cylinder. Since the ratio between corresponding velocities in two successive eddies is about 10^{-3} in the geometry used by Taneda it is understandable that only two eddies could be observed.

Until recently only time-independent Stokes flows in wedge shaped regions have been studied theoretically, but it seems of interest to investigate also the transient development from rest to the stationary state of such flows. A step in this direction was recently taken by Carbonaro (1985), who computed the stationary oscillating flow between two parallel planes when a sleeve of finite width in each plane is oscillating. (The same geometry but with a constant exitation rather than an oscillatory one is of course included in the work described in Moffatt (1964b) as the limiting case when the angle between the two planes vanishes.) A next step could be to study the transient development from rest to the time-independent flow considered in Moffatt (1964b) by means of Fourier transforms using Carbonaro's results.

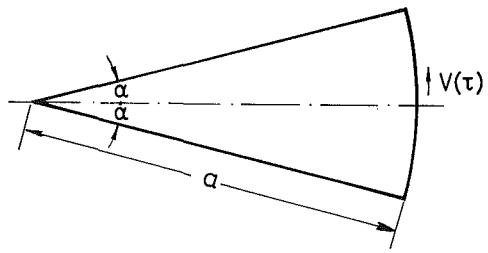


Fig. 1 A wedge with radius $r = a(=1)$ and dihedral angle 2α. The boundary condition on $r = a$ is velocity $(v) = 1$ or shear stress $(\tau) = 1$.

In this paper we investigate two transient problems. In both of them the flow region is bounded by two intersecting planes and a circular cylinder with axis on the line of intersection (see Fig. 1). The two planes are at rest while the cylinder surface is assumed to be moving. In the first problem the cylinder starts from rest at $t = 0$ and rotates around its axis with a constant angular velocity for $t > 0$. The second problem differs from the first one in that the boundary condition of constant velocity on the cylinder is replaced by that of a constant tangential stress. In both cases the fluid is assumed to be initially at rest. The first problem is solved by means of three different methods and the results are compared. These methods are a finite element, a finite difference, and a boundary integral equation method. The second problem is solved by means of a finite element method only, but that problem has recently been solved by an integral equation method also (Bohou Xu, 1986).

G. I. Taylor (1962) has shown that near the corner between two walls, of which one is moving and the other is at rest, the stresses are inversely proportional to the distance from the corner, so that the integrated forces diverge. For this reason the first problem is unrealistic in the sense that the total torque required to move the cylinder is infinite. A similar criticism can be made against the numerous treatments of steady flow

[1]Present address: Dept. of Mechanics, Zhejiang University, Hangzhou, P.R.C.

Contributed by the Applied Mechanics Division for presentation at the 1987 Applied Mechanics, Biomechanics, and Fluids Engineering Conference, Cincinnati, OH, June 14–17, 1987, of the American Society of Mechanical Engineers.

Discussion of this paper should be addressed to the Editorial Department, ASME, United Engineering Center, 345 East 47th Street, New York, N.Y. 10017, and will be accepted until two months after final publication of the paper itself in the JOURNAL OF APPLIED MECHANICS. Manuscript received by ASME Applied Mechanics Division, July 8, 1985; final revision April 11, 1986.

Paper No. 87-APM-2.

Copyright © 1987 by ASME
Downloaded 03 May 2010 to 171.66.16.27. Redistribution subject to ASME license or copyright; see http://www.asme.org/terms/Terms_Use.cfm

in a rectangular cavity with a moving lid, which have appeared in the literature.

2 A Rotating Cylinder

We consider two-dimensional Stokes flow in a sector bounded by the line sections $\theta = \pm\alpha$, $0 \leqq r \leqq a$ and the circular arc $r = a$, $-\alpha \leqq \theta \leqq \alpha$, where r and θ are polar coordinates (see Fig. 1). Then the stream function, ψ, which is defined so that the velocity components are $v_r = r^{-1}\partial\psi/\partial\theta$ and $v_\theta = -\partial\psi/\partial r$, satisfies the time-dependent Stokes equation, $\nu\Delta\Delta\psi = \Delta\psi_t$, where ν is the kinematic viscosity, Δ is Laplace's operator, and t is time. We assume that the straight parts of the boundary are at rest while the cylinder, of which the curved boundary is a part, rotates with a constant angular velocity around its axis. Then the fluid velocity vanishes on the straight parts while it is tangential and equal to the surface velocity, v_0, on the curved part. Along the boundary the stream function has a constant value, which we put equal to zero. In terms of the nondimensional variables $r_1 = r/a$, $t_1 = \nu t/a^2$, and $\psi_1 = \psi_1(r_1, \theta, t_1) = \psi(r, \theta, t)/(av_0)$ the problem is then given by the equation

$$\Delta\Delta\psi = \Delta\psi_t, \tag{1}$$

in $\Omega = \{(r,\theta) \mid 0 < r < 1, -\alpha < \theta < \alpha\}$, the boundary conditions

$$\psi(r,\theta,t) = 0, \tag{2}$$

along the entire boundary, $\partial\Omega$, and

$$\psi_\theta(r, \pm\alpha, t) = 0 \text{ for } 0 \leqq r < 1,$$
$$\psi_r(1,\theta,t) = -1 \text{ for } -\alpha \leqq \theta \leqq \alpha, \tag{3}$$

and the initial condition

$$\psi(r,\theta,0) = 0 \tag{4}$$

for $(r,\theta)\epsilon\Omega$. In equations (1) through (4) and in the sequel the index $_1$ on the nondimensional variables is omitted.

2(a) The Finite Element Method (FEM). In order to apply the finite element method to our problem we replace equation (1) by the equation

$$\int_\Omega f(\Delta\Delta\psi - \Delta\psi_t)d\Omega = 0 \tag{5}$$

where f is an arbitrary continuously differentiable function with piecewise continuous second derivatives. We then apply Green's first and second identities to obtain the formula

$$\int_\Omega (\Delta f\Delta\psi + \nabla f \cdot \nabla\psi_t)d\Omega$$
$$+ \int_{\partial\Omega} \left[f\frac{\partial\Delta\psi}{\partial N} - \frac{\partial f}{\partial N}\Delta\psi - f\frac{\partial\psi_t}{\partial N}\right]ds = 0, \tag{6}$$

where $\partial\Omega$ is the boundary of Ω, and $\partial/\partial N$ denotes differentiation in the direction of the outward normal to $\partial\Omega$.

Based on equation (6), equation (1) can be solved by Galerkin's method. To do so, we insert a continuously differentiable finite element approximation for ψ and insert the element functions successively for f. The elements are bounded by straight lines θ = constant and circles r = constant, and the element functions are sums of products of third order Hermite polynomials with the values of ψ and the derivatives ψ_r, ψ_θ, and $\psi_{r\theta}$ at the nodes as parameters. Explicit expressions for these element functions are given in Huebner (1975). At the vertex the element degenerates into a triangular sector. At $(r, \theta) = (1, \pm\alpha)$, where the derivatives are discontinuous we put $\psi_r = -1$, $\psi_\theta = 0$, and $\psi_{r\theta} = 0$. The integrals obtained after insertion in equation (6) are evaluated by means of a two-point Gauss formula in each coordinate direction. In the system of linear, first order differential equations,

$$\{M\}\{c'\} + \{K\}\{c\} = \{R\}, \tag{7}$$

for the element parameters, $\{c\}$, which is obtained in this way, the matrices $\{M\}$ and $\{K\}$ are constant, symmetric, and positive definite. The system is solved by the one-step, second order method given by the formula

$$\left(\{M\} + \frac{1}{2}\Delta t\{K\}\right)\{c_n\}$$
$$= \left(\{M\} - \frac{1}{2}\Delta t\{K\}\right)\{c_{n-1}\} + \Delta t\{R\}. \tag{8}$$

At each time step the linear algebraic system of equations (8) is solved by an LDL^t-method.

2(b) The Finite Difference Method (FDM). In the finite difference method we replace the time derivative ψ_t by a backward difference quotient and obtain the inhomogeneous Helmholtz's equation

$$h\Delta\Delta\psi_{n+1} - \Delta\psi_{n+1} = -\Delta\psi_n, \tag{9}$$

where h is the time step and $\psi_n = \psi_n(\bar{r}) = \psi(r,\theta,nh)$, $n = 0, 1, \ldots$. We express equation (9) in terms of the polar coordinates r and θ and replace the derivatives by central differences. The system of nodes is the same as the one used in the finite element method augmented with rows of nodes one space-step outside the boundaries, so that the derivative boundary conditions in equation (3) can be expressed in terms of central differences. At each time step the system of linear algebraic equations obtained in this way is solved by Gauss elimination using the IMSL-subroutine LEQT2F.

2(c) The Boundary Integral Equation Method (BIE). As in the finite difference method, we first replace the time derivative ψ_t by a backward difference quotient and obtain equation (9). In order to develop our integral equation method we then consider equation (9) together with the function

$$G(R) = \frac{1}{2\pi}(K_0(h^{-1/2}R) + \ell nR) \tag{10}$$

where $R = |\bar{r} - \bar{r}'|$ and K_0 is the modified Hankel function of order zero. The function G satisfies the equation

$$h\Delta\Delta G - \Delta G = -\delta(\bar{r} - \bar{r}'). \tag{11}$$

In order to derive an integral formula for ψ_{n+1} at an arbitrary point $\bar{r}'$ in Ω, we consider the integral

$$I = \int_\Omega [G(h\Delta\Delta\psi_{n+1} - \Delta\psi_{n+1}) - \psi_{n+1}(h\Delta\Delta G - \Delta G)]d\Omega. \tag{12}$$

Because of equations (9) and (11) this integral is equal to

$$I = -\int_\Omega G\Delta\psi_n d\Omega + \psi_{n+1}(\bar{r}'). \tag{13}$$

By using Green's second identity and the boundary conditions in equations (2) and (3), which are satisfied by ψ_n, we rewrite equation (13) as

$$I = \int_C G ds - \int_\Omega \psi_n \Delta G d\Omega + \psi_{n+1}(\bar{r}'), \tag{14}$$

where C is the arc $r = 1$, $-\alpha < \theta < \alpha$. The integral in equation (12) may also be written as

$$I = \int_\Omega \nabla \cdot [h(G\nabla\Delta\psi_{n+1} - \Delta\psi_{n+1}\nabla G + \Delta G\nabla\psi_{n+1}$$
$$- \psi_{n+1}\nabla\Delta G) - G\nabla\psi_{n+1} + \psi_{n+1}\nabla G]d\Omega. \tag{15}$$

Using Gauss' theorem and the boundary conditions for ψ we find from equation (15) that

$$I = h\int_{\partial\Omega} \left[G\frac{\partial\Delta\psi_{n+1}}{\partial N} - \frac{\partial G}{\partial N}\Delta\psi_{n+1}\right]ds - \int_C (h\Delta G - G)ds. \tag{16}$$

Downloaded 03 May 2010 to 171.66.16.27. Redistribution subject to ASME license or copyright; see http://www.asme.org/terms/Terms_Use.cfm

Here $\partial\Omega$ is the boundary of Ω and $\partial/\partial N$ denotes the derivative in the direction of the outward normal to $\partial\Omega$. Equating (14) and (16) we obtain the formula

$$\psi_{n+1}(\bar{r}') = h\int_{\partial\Omega}\left[G\frac{\partial\Delta\psi_{n+1}}{\partial N} - \frac{\partial G}{\partial N}\Delta\psi_{n+1}\right]ds$$

$$-h\int_C \Delta G ds + \int_\Omega \psi_n \Delta G d\Omega. \tag{17}$$

When we let $\bar{r}'$ in equation (17) approach a point on $\partial\Omega$ and use that ψ_{n+1} vanishes on $\partial\Omega$ we obtain an integral equation for the unknowns $\partial\Delta\psi_{n+1}/\partial N$ and $\Delta\psi_{n+1}$.

In order to derive another integral equation we operate on $\bar{r}'$ with Laplace's operator on both sides of equation (17). Since $\bar{r}'$ in equation (17) is a point in the interior of Ω, $\delta(\bar{r}-\bar{r}')$ vanishes for all points $\bar{r}\epsilon\partial\Omega$. Consequently, the Laplacian of the two last terms on the right-hand side of equation (17) is equal to

$$-\int_C \Delta G ds - h^{-1}\psi_n(\bar{r}') + h^{-1}\int_\Omega \psi_n \Delta G d\Omega. \tag{18}$$

When the last integral in (18) is expressed by means of equation (17), the formula

$$\Delta\psi_{n+1}(\bar{r}') = \frac{-1}{2\pi}\int_{\partial\Omega}\left[\ell nR\frac{\partial\Delta\psi_{n+1}}{\partial N} - \frac{\partial \ell nR}{\partial N}\Delta\psi_{n+1}\right]ds$$

$$+h^{-1}(\psi_{n+1}(\bar{r}') - \psi_n(\bar{r}')), \tag{19}$$

is obtained. Here it has been used that $h\Delta G = -(2\pi)^{-1}\ell n\, R$. By letting $\bar{r}'$ in equation (19) approach the boundary $\partial\Omega$ we obtain the integral equation

$$\beta\Delta\psi_{n+1}(\bar{r}') = -\frac{1}{2\pi}\int_{\partial\Omega}\left[\ell nR\frac{\partial\Delta\psi_{n+1}}{\partial N} - \frac{\partial \ell nR}{\partial N}\Delta\psi_{n+1}\right]ds, \tag{20}$$

where $\beta = 1/4$ if $\bar{r}' = (1, \pm\alpha)$, $\beta = \alpha/\pi$ if $r' = 0$, and $\beta = 1/2$ otherwise.

At each time step the set of two integral equations given by equation (17), with $\psi_{n+1}(\bar{r}')$ equal to zero, and equation (20) is solved by a collocation method in the following way. The two unknowns are approximated by functions which are linear between two consecutive ones of a set of nodes which are distributed evenly on the straight boundary $\theta = \alpha$, $0 < r < 1$ and on the arc $r = 1$, $0 \leqq \theta \leqq \alpha$. On the rest of the boundary $\Delta\psi_{n+1}$ and $\partial\Delta\psi_{n+1}/\partial N$ are fixed so that they are both symmetric around $\theta = 0$. The equations are then required to be satisfied at the same set of nodes on $\theta = \alpha$, $0 < r < 1$ and on $r = 1$, $0 \leqq \theta \leqq \alpha$. The integrals over the intervals between consecutive nodes, except those of which $\bar{r}'$ is an end point, are evaluated by means of a four-point Gauss formula. In the intervals where $\bar{r}'$ is an end point, the terms which diverge logarithmically as $\bar{r}'$ is approached are evaluated analytically. The set of linear algebraic equations for the unknown values of $\Delta\psi_{n+1}$ and $\partial\Delta\psi_{n+1}/\partial N$ at the nodes is solved by Gauss elimination using the IMSL-subroutine LEQT2F.

2(d) Numerical Results and Discussion. Based on the three methods described above numerical calculations were carried out on the IBM 3081 computer at the NEUCC in Lyngby, Denmark.

In order to estimate the time needed to reach the stationary state we first determined the smallest eigenvalue, $\lambda_{\min}$, of the matrix equation $\{K\}\{v\} = \lambda\{M\}\{v\}$ associated with equation (7) for different element sizes in a wedge with dihedral angle $2\alpha = 30$ deg. The results are shown in Table 1. We take the fact that the values shown are close to each other as an indication that they are also close to the smallest eigenvalue of the problem given by the equation $\Delta\Delta\psi + \lambda\Delta\psi = 0$ associated with equation (1) and the homogeneous boundary conditions corresponding to equations (2) and (3). Putting $\lambda_{\min}$ equal to the value 284.71 found with the finest mesh we define *the transient time*, T_c, as $T_c = 5/\lambda_{\min} = 0.01756$. The physical meaning of the transient time is that at time $t = T_c$ the flow deviates from the stationary one by relative amounts of the order $\exp(-5) \simeq 7\cdot10^{-3}$. In the wedge flow experiment reported in Taneda (1979) the parameters were $2\alpha = 28.5$ deg, $a \simeq 5$ cm, and $\nu = 20$ cm^2/s, so that the real time interval corresponding to T_c becomes $a^2T_c/\nu \simeq 0.022$ s if the eigenvalue $\lambda_{\min}$ corresponding to $2\alpha = 30$ deg is used as an approximation. The fact that this interval is very small agrees with a statement in Taneda (1979) that "the time taken for the steady flow to be established is negligible."

Table 1 The smallest eigenvalue of the matrix equation $[K] = \lambda[M]$ for different meshes in a wedge with $2\alpha = 30$ deg. With a mesh $m*n$ one-half of the wedge is divided into elements by m circles (including the circle $r = 1$) and $n + 1$ radii (including the radii $\theta = 0$ and $\theta = \alpha$).

Mesh	λ min
20 * 4	282.87
30 * 6	282.85
40 * 9	284.71

Table 2 The stream function ψ on $\theta = 0$ in a wedge with $2\alpha = 30$ deg found by means of the three methods. The results in the top line (marked FFEM) are found using a finer mesh and a smaller time step than in the other FEM calculations.

t	Method	cpu (sec.)	r 0.1	0.3	0.5	0.7	0.9
0.0002	FFEM	578	-4.07E-10	6.83E-6	2.27E-4	2.02E-3	9.17E-3
	FEM	10.7	1.43E-9	7.50E-6	2.30E-4	2.01E-3	9.01E-3
	BIE	71.4	-2.02E-6	5.03E-6	2.13E-4	1.96E-3	9.04E-3
	FDM	14.9	3.46E-9	7.97E-6	3.32E-4	3.37E-3	1.67E-3
0.002	FEM	107	2.19E-10	-3.15E-7	3.96E-4	6.23E-3	3.24E-2
	BIE	714	-1.29E-6	-1.15E-6	4.05E-4	6.59E-3	3.35E-2
	FDM	149	2.02E-10	-1.25E-6	3.61E-4	6.99E-3	3.85E-2
0.02	FEM	203	1.98E-11	-5.19E-6	1.28E-4	1.20E-2	4.68E-2
	BIE	1357	1.88E-5	-1.14E-6	1.65E-4	1.23E-2	4.68E-2
	FDM	284	-3.29E-11	-3.78E-6	1.01E-4	1.19E-2	5.12E-2

In order to compare the three methods we next carried out a series of computations with $2\alpha = 30$ deg. Some of the results for the stream function as a function of r on the angular bisector of the wedge ($\theta = 0$) are presented in Table 2. The results marked FFEM in the top line of the table were obtained by means of the FEM using a 40*9 mesh and a time step $\Delta t = 4\cdot10^{-5}$ (the definition of the meshes is the same as in Table 1). All the other results in the table are found using a time step $\Delta t = 2\cdot10^{-4}$ until $t = 2\cdot10^{-3}$ and $\Delta t = 2\cdot10^{-3}$ afterwards, and with meshes 30*6, 40*10, and 60*15 for the FEM, BIE, and FDM, respectively. The table shows that in the outer part of the wedge the results obtained by means of the FEM and the BIE agree well with each other at all three instants of time while those for $t = 2\cdot10^{-4}$ found from the FDM deviate considerably from the corresponding ones found by the other methods. Later, however, all the three sets of results for that region agree well with each other. Since the values, which the stream function takes on in the region near the vertex, are much smaller than those further out in the wedge, it is not surprising that the results from the three methods differ greatly as the vertex is approached. The CPU times used to obtain the various results are included in the table. It is seen that the BIE is far more time consuming than the FEM. Since the two methods appear to be equal with respect to accuracy it was therefore decided to use the FEM in all the subsequent com-

Downloaded 03 May 2010 to 171.66.16.27. Redistribution subject to ASME license or copyright; see http://www.asme.org/terms/Terms_Use.cfm

Table 3 The zeros on $\theta = 0$ of the stream function and the peak values of the velocity in the eddies at different times

Time	1st eddy		2nd eddy		3rd eddy	
	r_1	v_1	r_2	v_2	r_3	v_3
0.0002	0.1001	-0.1455				
0.002	0.3033	-0.1717	0.1067	1.234E-5		
0.02	0.4700	-0.2315	0.2170	5.112E-4	0.1000	1.149E-6

Table 4 The zeros on $\theta = 0$ of the stream function and the peak velocities in the eddies in the stationary state for different dihedral angles, 2α

2α	1st eddy		2nd eddy		3rd eddy	
	r_1	v_1	r_2	v_2	r_3	v_3
30°	0.4700	0.2315	0.2170	5.112E-4	0.1000	1.149E-6
60°	0.1998	0.2678	0.0000	3.065E-4		
120°	0.0000	0.3381				

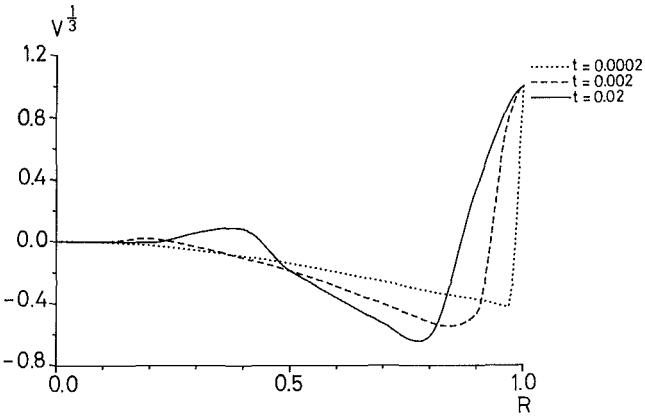


Fig. 2 The velocity distribution on the angular bisector ($\theta = 0$) in a wedge with dihedral angle $2\alpha = 30$ deg and boundary condition $v = 1$ at times $t = 2 \cdot 10^{-4}$, $2 \cdot 10^{-3}$, and $2 \cdot 10^{-2}$. Note that the figure shows $v^{1/3}$ and not the velocity v itself.

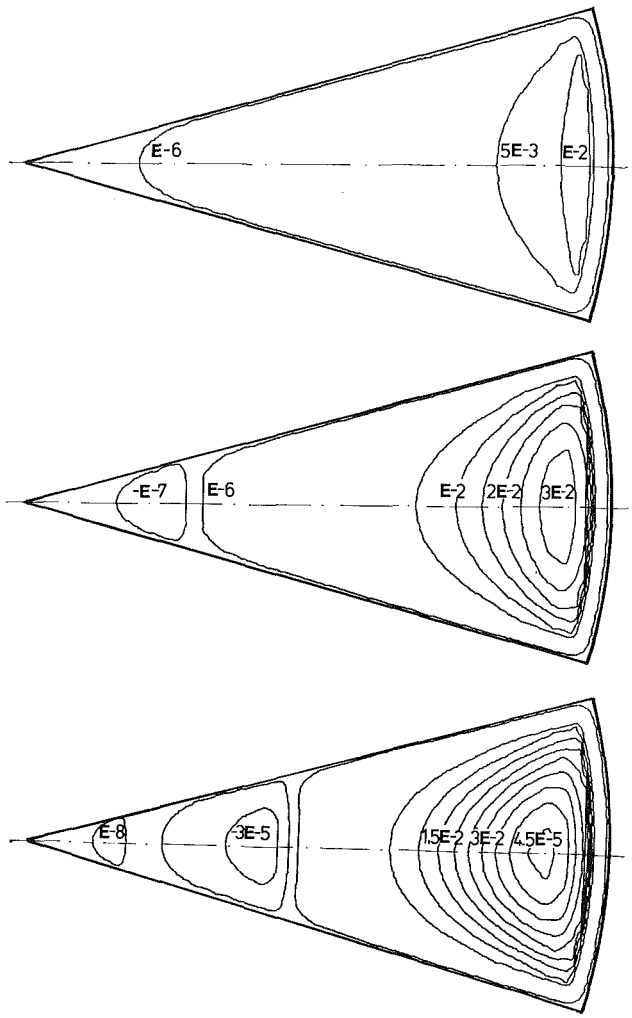


Fig. 3 Stream line plots corresponding to the distributions shown in Fig. 2: 3(*a*), $t = 0.0002$, 3(*b*), $t = 0.002$, and 3(c), $t = 0.02$. Note that the stream lines in the weaker eddies are shown with a larger density than in the strongest one.

putations. The results given in the first line of the table (FEM with time step $\Delta t = 4 \cdot 10^{-5}$ and a 40*9 mesh) and those in the second line (FEM with $\Delta t = 2 \cdot 10^{-4}$ and a 30*6 mesh) indicate that there is no need to reduce the time step below $2 \cdot 10^{-4}$ or to refine the mesh from 30*6. Therefore, we have used time steps $\Delta t = 2 \cdot 10^{-4}$ until $t = 2 \cdot 10^{-3}$ and $\Delta t = 2 \cdot 10^{-3}$ afterwards and a 30*6 mesh in all the computations described in the sequel.

The velocity distributions on the angular bisector of a wedge with dihedral angle $2\alpha = 30$ deg at $t = 2 \cdot 10^{-4}$, $t = 2 \cdot 10^{-3}$, and $2 \cdot 10^{-2}$ are illustrated in Fig. 2, and the corresponding stream line patterns in the complete wedge region are shown in Fig. 3. Since the peak velocity decreases several decades from one local maximum to the next one, we have plotted $v^{1/3}$ instead of v itself in Fig. 2, so that the details of the weaker eddies become more visible. For a similar reason the streamlines in Fig. 3 are shown with a larger density in the weaker eddies than in the strongest one.

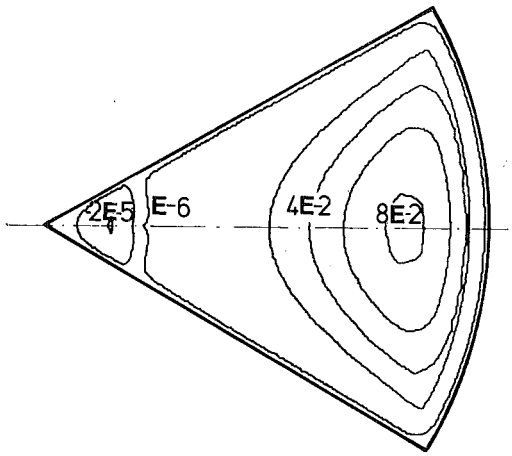
Equation (1) is parabolic. Therefore, the whole body of fluid is set into motion at $t = 0$. However, it appears that, in analogy with fields governed by the heat equation, the initial motion is only a weak precursor because, as the figures show, velocities comparable with those in the stationary motion occur later in the inner than in the outer part of the wedge. For example, Fig. 2 and Table 3 show that the ratio between the peak velocities in the outermost eddy and the next one decreases with increasing time. We also note that at $t = 0.0002$ the outermost eddy penetrates deeply into the region, but that later it shrinks and the second eddy moves outward. It seems reasonable to expect that the intensities, sizes, and positions of those eddies which are too weak to be detected in our results develop, in time, in the same way as the second one.

The eddy type solutions mentioned in the introduction are of the form $\mathrm{Re}\, R^{\lambda+1} f(\theta)$, where λ is a solution to the equation

$$\sin 2\alpha\lambda + \lambda \sin 2\alpha = 0, \tag{21}$$

if the stream function is even in θ, as is the case here. Equation (21) has an infinite number of pairs of complex conjugate roots. If we assume that the stream function ψ_∞ for the stationary flow is a superposition of solutions of this type with $\mathrm{Re}\lambda > 0$, then the contribution ψ_1 corresponding to the roots $\lambda_1 = \mu_1 + i\nu_1$ and $\lambda_1^* = \mu_1 - i\nu_1$ with the smallest positive real part is dominating for r sufficiently small while for larger values of r several of the eddy type solutions may be expected to contribute notably to ψ_∞. In the eddy type solutions the r coordinates of the zeros of the stream function on $\theta = 0$ and the peak values of the velocities in the eddies form geometrical progressions. The first several roots of equation (21) have been tabulated for various values of α by Lugt and Schwiderski (1965). From the table values of μ_1 and ν_1 for $2\alpha = 30$ deg the ratio between the r coordinates of consecutive zeros of ψ_1 on $\theta = 0$ is found to be $\gamma_r \equiv \exp(\pi / |\nu_1|) = 2.112$ and the ratio

Downloaded 03 May 2010 to 171.66.16.27. Redistribution subject to ASME license or copyright; see http://www.asme.org/terms/Terms_Use.cfm



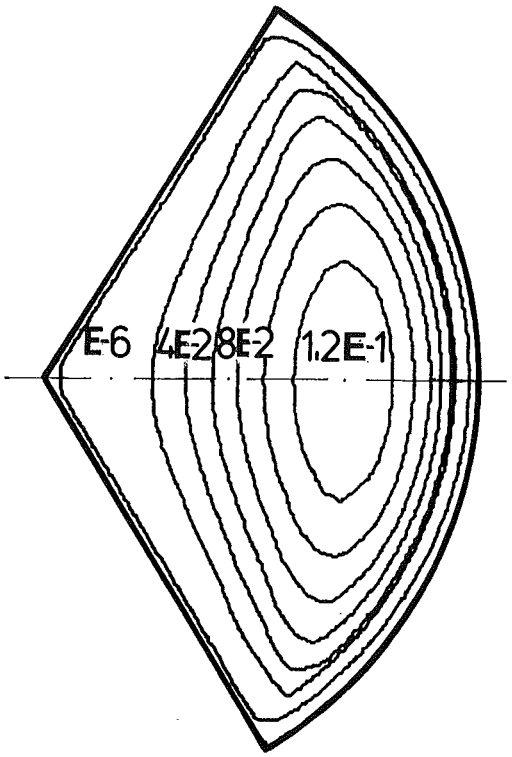


Fig. 4 Stream line plots of the stationary flow in wedges with dihedral angles 60 deg (4(*a*)) and 120 deg (4(*b*)). Other details are as in Fig. 3.

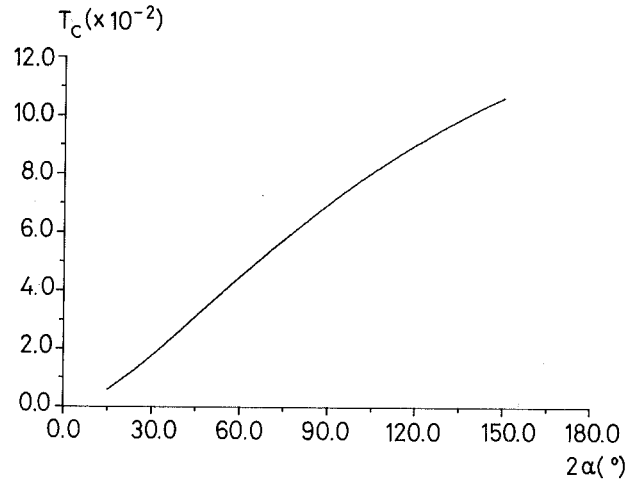


Fig. 5 The transient time T_c as a function of the dihedral angle for boundary condition $v = 1$

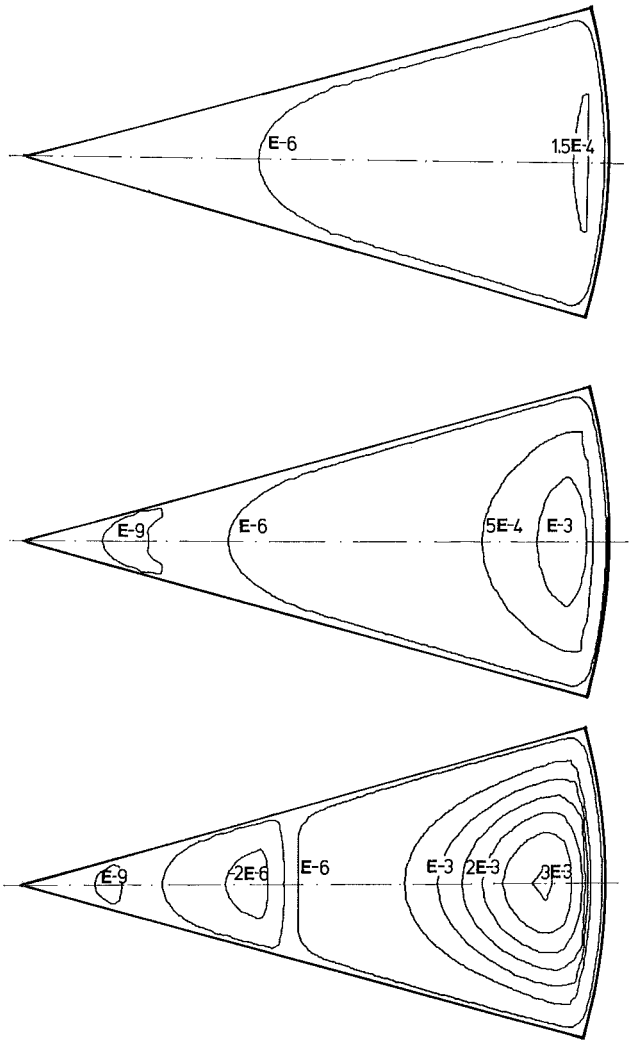


Fig. 6 Stream line plots for the boundary condition $\tau = 1$. Other details are as in Fig. 3.

between consecutive peak values of v is found to be $\gamma_v \equiv \exp(\pi/\mu_1) = 440.3$. For $2\alpha = 30$ deg, Table 3 shows the r coordinates (r_1, r_2, and r_3) of the zeros of ψ, and the velocities (v_1, v_2, and v_3) at those relative velocity maxima which we have been able to detect. For $t = 0.02$ the flow is almost identical with the stationary one and from the values in Table 3 we find that $r_1/r_2 = 2.166$, $r_2/r_3 = 2.170$, $v_1/v_2 = 452.9$, and $v_2/v_3 = 444.9$. The fact that r_1/r_2 and r_2/r_3 are close to each other and to γ_r and, similarly, that v_1/v_2 and v_2/v_3 are close to each other and to γ_v indicates that ψ_1 is the dominating contribution to ψ_∞ not only for small r but in the entire wedge region.

Computations were also carried out for wedges with dihedral angles larger than 30 deg. In Fig. 4 the stream line pattern in the stationary state is shown for $2\alpha = 60$ deg and 120 deg. In accordance with the fact that the infinite system of eddies disappears when 2α becomes larger than about 146 deg, the outermost eddy is seen to fill a larger and larger part of the wedge as the dihedral angle increases. This is also understandable from the point of view that the larger the angle is, the less are the straight walls able to impede the motion and, therefore, the velocity field can penetrate deeper into the region. The figure also shows that, as a larger fraction of the fluid takes part in the motion, the location of the center of the eddy moves inward so that the average velocity gradient in the outer part of the fluid region decreases. Thus, when the

Downloaded 03 May 2010 to 171.66.16.27. Redistribution subject to ASME license or copyright; see http://www.asme.org/terms/Terms_Use.cfm

dihedral angle is larger, more energy must be supplied to the fluid before the stationary state is reached and, furthermore, the power supplied from the cylinder to the fluid decreases since the power is proportional to the velocity gradient at the moving boundary. These two mechanisms both tend to increase the time it takes to reach the stationary state. Figure 5 shows the results of a computation of the transient time, T_c, which was defined in the beginning of this section, as a function of the dihedral angle. The figure shows that T_c is indeed an increasing function of 2α.

3 A Cylinder With a Constant Shear Stress Boundary Condition

If the boundary condition of constant velocity on the cylinder is replaced by one of constant shear stress, τ, the same equations and conditions hold except that the boundary condition $\psi_r(a,\theta,t) = v$ is replaced by

$$\Delta\psi(a,\theta,t) - \frac{2}{a}\frac{\partial\psi}{\partial r}(a,\theta,t) = -\frac{\tau}{\rho\nu}, \tag{22}$$

where ρ is the fluid density. If, in this case, we introduce dimensionless variables $\psi_2 = \rho\varphi\psi/\tau$ and, as before, $r_1 = r/a$ and $t_1 = \nu t/a^2$, the nondimensionalized problem (with indices $_1$ and $_2$ omitted) is given by equations (1) through (4) with the lower condition in equation (3) replaced by

$$\Delta\psi(1,\theta,t) - 2\psi_r(1,\theta,t) = -1 \quad \text{for} \quad -\alpha < \theta < \alpha. \tag{23}$$

This problem was solved by the FEM in a way analogous to the one described in Section 2(a). It was found that for a wedge with $2\alpha = 30$ deg the transient time, as defined in Section 2(a), is equal to $2.3 \cdot 10^{-2}$, which is somewhat larger than for the velocity boundary condition. Thus, with a constant stress on the circular boundary it takes a longer time to reach the stationary state than with a constant velocity. The stream line plots, of which some are shown in Fig. 6, are quite similar to those in Fig. 3.

References

Carbonaro, P., 1985, "Sequences of Eddies in Oscillatory Stokes Flow," *Journal de Mécanique Théorique et Appliquée*, Vol. 4, pp. 425–432.

Huebner, K. H., 1975, *The Finite Element Method for Engineers*, Wiley, New York, pp. 172–174.

Lugt, H. L., and Schwiderski, E. W., 1965, "Flows Around Dihedral Angles – I: Eigenmotion Analysis," *Proc. R. Soc.*, A.285, pp. 382–399.

Moffatt, H. K., 1964a, "Viscous and Resistive Eddies Near a Sharp Corner," *Journal of Fluid Mechanics*, Vol. 18, pp. 1–18.

Moffatt, H. K., 1964b, "Viscous Eddies Near a Sharp Corner," *Archivum Mechaniki Stosowanej*, Vol. 2, pp. 365–372.

Schubert, G., 1967, "Viscous Flow Near a Cusped Corner," *Journal of Fluid Mechanics*, Vol. 27, pp. 647–656.

Taneda, S., 1979, "Visualization of Separating Stokes Flow," *Jour. Phys. Soc., Japan*, Vol. 46, pp. 1935–1942.

Taylor, G. I., 1962, "On Scraping Viscous Fluid From a Plane Surface," *Miszellaneen der Angewandten Mechanik (Festschrift Walter Tollmien)*, Schäfer, M., ed., Akademie-Verlag, Berlin, pp. 313–315, reprinted in *The Scientific Papers of Sir Geoffrey Ingram Taylor*, Cambridge University Press, 1971, Vol. IV, pp. 410–413.

Xu, B., 1986, "Transient Stokes' Flow in a Wedge with a Stress Boundary Condition," *Zeitschrift für angew. Math. u. Mech.*, Vol. 66, T270–T272, 1986.

Downloaded 03 May 2010 to 171.66.16.27. Redistribution subject to ASME license or copyright; see http://www.asme.org/terms/Terms_Use.cfm

Frequency Response of a Nonlinear Pneumatic System

Ying-Tsai Wang[1]

Rajendra Singh
Associate Professor,
Mem. ASME

Fluid Power Laboratory,
Department of Mechanical Engineering,
The Ohio State University,
Columbus, Ohio 43210

This paper studies the dynamic behavior of a pneumatic chamber connected to a reservoir through an orifice and to a linear mechanical system. In this paper, we focus our attention mainly on the nonlinearity associated with mass flow rate through the orifice and its effect on the overall system behavior. Nonlinearities induced by the friction and gas compressibility are also considered. Using the method of harmonic balance, we reduce a difficult mathematical formulation of this nonlinear pneumatic system to a simple nonlinear governing equation and a set of algebraic equations which yield frequency response easily at the first, second, and third harmonics. An excellent agreement between the method of harmonic balance and numerical integration has been found. Results obtained using a quasi-linear model are also given.

1 Introduction

In this paper, we consider a pneumatic chamber connected to a reservoir through an orifice/valve and to a linear mechanical system as shown schematically in Fig. 1. This simple model could represent several practical applications dealing with single-sided cylinder type actuators or isolators, air suspension vehicles, gas bearings, etc. An analytical solution of such a system is not available because of the nonlinearities associated with the orifice, gas compressibility, and friction. We will apply the method of harmonic balance and validate the approximate analytical solution for frequency response by comparing results with those obtained from a quasi-linear model and with those predicted by the numerical integration of the governing equations.

2 Literature Review

For a gas bearing, similar to the system considered here, Doebelin (1980) used a linear model to demonstrate the stability considerations using the Routh criterion. Andersen (1967), Cavanaugh (1976), and Bachrach and Rivin (1983) have also treated open systems to be linear, especially the orifice or valve elements. Linear models for other pneumatic components and systems are also given by Anderson (1967), Blackburn et al. (1960), Cavanaugh (1976), and McCloy and Martin (1980). However, such linear models, while easy to use, may not be able to predict the true dynamic behavior. Furthermore, in some cases, a linearized mathematical description cannot be given or an operating point may not even exist. Hundal (1980) has also pointed out that the linear models are not suitable for shock isolation problems.

Nonlinear models of the pneumatic systems have been solved using the numerical integration techniques. For instance, Hundal (1980, 1982a, and 1982b) has analyzed pneumatic isolators and absorbers numerically. Wang et al. (1984) simulated a cushioning-type, double-acting shock-absorbing cylinder, and predicted time histories and performance indices; good correlations between simulation and experiment are reported. The numerical simulation technique is obviously very attractive and could lead to useful design information. But it could be very time consuming and difficult to implement from the computer algorithm viewpoint for complex systems; numerical convergence problems could also arise when many small control volumes are involved. It should be recognized that a numerical solution may not necessarily lead to an improved understanding of the system behavior.

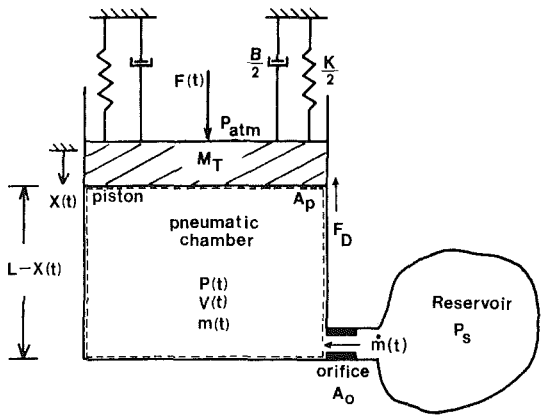


Fig. 1 Schematic of an example case: open pneumatic chamber

[1]Currently with the National Taiwan Institute of Technology, Republic of China.

Contributed by the Applied Mechanics Division for presentation at the 1987 Applied Mechanics, Biomechanics, and Fluids Engineering Conference, Cincinnati, OH, June 14–17, 1987, of the American Society of Mechanical Engineers.

Discussion of this paper should be addressed to the Editorial Department, ASME, United Engineering Center, 345 East 47th Street, New York, N.Y. 10017, and will be accepted until two months after final publication of the paper itself in the JOURNAL OF APPLIED MECHANICS. Manuscript received by ASME Applied Mechanics Division, July 24, 1985; final revision, June 18, 1986.

Paper No. 87-APM-5.

Copyright © 1987 by ASME
Downloaded 03 May 2010 to 171.66.16.27. Redistribution subject to ASME license or copyright; see http://www.asme.org/terms/Terms_Use.cfm

The feasibility of finding approximate analytical solution of pneumatic systems using perturbation techniques has not been investigated properly with the exception of closed chamber analyses by Chen (1977) and Wang (1986). (However, it should be noted that the perturbation techniques have been applied to many other physical systems – see Mickens, 1981; Nayfeh and Mook, 1979; Siljak, 1969.) Chen (1977) analyzed a closed pneumatic chamber with only the nonlinearity induced by the gas compressibility. Recently, Wang (1986) examined the dynamic behavior of a closed pneumatic chamber coupled with a linear mechanical system; nonlinearities induced by the gas compressibility, sliding, and dry friction were included. He found that the nonlinear effects are large, as these are associated with the "hard" singularity (Bota and Mickens, 1984); he also showed the difficulties associated with the analytical solution of this system. The method of harmonic balance was then applied to this problem and an excellent agreement between the method of harmonic balance and numerical integration was evident at the zeroth, first, and second harmonics.

3 Mathematical Formulation

For the gas chamber control volume V as shown in Fig. 1, we assume an ideal equation of state with gas constant R and the polytropic thermodynamic process of exponent n

$$P(t)V(t)=m(t)RT(t) \tag{1}$$

$$P(t)\left[\frac{V(t)}{m(t)}\right]^n=P(0)\left[\frac{V(0)}{m(0)}\right]^n, P(t)T(t)^{\frac{n}{1-n}}=P(0)T(0)^{\frac{n}{1-n}} \tag{2}$$

where P, m, and T are pressure, mass, and temperature, respectively. The continuity equation is then used to relate $m(t)$ and mass flow rate $\dot{m}(t)$ through the valve, assumed to be an ideal orifice of discharging coefficient C and geometric area A_o.

$$m(t)=m(0)+\int_0^t \dot{m}(\zeta)d\zeta \tag{3}$$

$$\dot{m}=CA_oP_s\left[\left(\frac{P}{P_s}\right)^{\frac{2}{\gamma}}-\left(\frac{P}{P_s}\right)^{\frac{\gamma+1}{\gamma}}\right]^{\frac{1}{2}}\left[\frac{2\gamma g}{(\gamma-1)RT_s}\right]^{\frac{1}{2}},$$

$$\text{where } \frac{P}{P_s}>\left[\frac{2}{\gamma+1}\right]^{\frac{\gamma}{\gamma+1}} \tag{4a}$$

$$\dot{m}^*=CA_oP_s\left[\frac{\gamma g}{RT_s}\right]^{\frac{1}{2}}\left[\frac{2}{\gamma+1}\right]^{\frac{\gamma+1}{2(\gamma-1)}},$$

$$\text{where } \frac{P}{P_s}\le\left[\frac{2}{\gamma+1}\right]^{\frac{\gamma}{\gamma+1}} \tag{4b}$$

where γ is the specific heat ratio, g is the gravitational constant, the subscript s is the supply condition associated with the reservoir, and the superscript * indicates the critical value associated with the choking condition; hence, $\dot{m}^*$ is the maximum mass flow rate. Now, we can combine equations (1)–(3) to obtain a single equation for the thermofluid process.

$$\dot{P}(t)V(t)+nP(t)\dot{V}(t)-n\dot{m}(t)RT(0)\left[\frac{P(t)}{P(0)}\right]^{\frac{n-1}{n}}=0 \tag{5}$$

The equation of motion for the piston is

$$M_T\ddot{X}(t)+B\dot{X}(t)+KX(t)=F(t)+M_Tg-P(t)A_p+P_{atm}A_p-F_D(t) \tag{6}$$

where M_T is the total mass, B is the linear mechanical damping coefficient, K is the linear mechanical spring stiffness, $F(t)$ is the external force, P_{atm} is the atmosphere pressure, and F_D is the total damping force which is assumed to be of the following form: $F_D=\mu_{\dot{X}}\dot{X}+\mu_pP$, where $\mu_{\dot{X}}$ is the viscous friction coefficient (in force/velocity unit) and μ_p is the scaled sliding friction coefficient (in area unit) to account for P_{atm}. Note that $\mu_{\dot{X}}$ and μ_p are unique to the physical system and must be known (Andersen, 1967; Wang, 1986).

From the initial point ($t=0$), we define the excitation $F(t)$ and responses $X(t)$ and $P(t)$ as

$$F(t)=f_o+f(t),\ P(t)=p_o+p(t),\ X(t)=x_o+x(t),$$

$$f_o=\lim_{T\to\infty}\frac{1}{T}\int_0^T F(t)dt \tag{7}$$

Now, we define response operating points x_o and p_o corresponding to f_o. From equation (5), we get $\dot{m}_o=0$; therefore, the operating point p_o is uniquely defined by the supply conditions P_s as $p_o=P_s$. And, from equation (6), we obtain

$$Kx_o=f_o+M_Tg-(A_p+\mu_p)p_o+P_{\text{atm}}A_p \tag{8}$$

For x_o, equation (8) dictates that, when $K=0$, the operating point exists only when $0=f_o+M_Tg-(A_p+\mu_p)p_o+P_{\text{atm}}A_p$. But for $K\neq0$, a unique x_o value corresponds to f_o and p_o, i.e., $x_o\equiv x_o(f_o,p_o)$. These unique operating points will now be considered as the reference conditions for dynamic analysis. We also define nondimensional parameters and variables as follows:

$$\begin{aligned}
\bar{D}_o &= D_o/D_p,\ \bar{A}_o=A_o/A_p=\bar{D}_o{}^2,\ \bar{x}=x/(L-x_o),\\
&\quad \bar{p}=p/p_o,\ \bar{f}=f/[p_oA_p],\\
\bar{K} &= K(L-x_o)/[p_oA_p],\ \omega_n=(K/M_T)^{1/2},\ \bar{\omega}=\omega/\omega_n,\\
&\quad \bar{\mu}_p=\mu_pp_o/[p_oA_p],\\
\xi &= (B+\mu_{\dot{X}})/[2(KM_T)^{1/2}],\ \alpha=C_c(M_TgRT/K)^{1/2}/(L-x_o),\\
\tau &= \gamma^{1/2}[2/(\gamma+1)]^{(\gamma+1)/2(\gamma-1)},\ \bar{m}=mRT_o/[p_oA_p(L-x_o)]
\end{aligned}$$

where ω is the excitation frequency and ω_n is the undamped natural frequency of the mechanical system.

4 Nature of Nonlinearity

To study the basic nature of nonlinearity, the governing equations, equations (5) and (6), are written in the dimensionless form as

$$\dot{\bar{p}}[1-\bar{x}]-n[1+\bar{p}]\dot{\bar{x}}=n\dot{\bar{m}}[1+\bar{p}]^{\frac{n-1}{n}} \tag{9}$$

$$\ddot{\bar{x}}+2\xi\omega_n\dot{\bar{x}}+\omega_n{}^2\bar{x}=\frac{\omega_n{}^2}{\bar{K}}[\bar{f}-(1+\bar{\mu}_p)\bar{p}] \tag{10}$$

These equations could be combined to yield a single equation, as given below, which is a third order ordinary nonlinear differential equation in the following form; here H is defined as the nonlinear function.

$$\dddot{\bar{x}}(t)+2\xi\omega_n\ddot{\bar{x}}(t)+\omega_n{}^2\dot{\bar{x}}(t)=\frac{\omega_n{}^2}{\bar{K}}\dot{\bar{f}}(t)-H(\bar{f},\dot{\bar{f}},\bar{x},\dot{\bar{x}},\ddot{\bar{x}},\dddot{\bar{x}}), \tag{11}$$

where

$$H(\bar{f},\dot{\bar{f}},\bar{x},\dot{\bar{x}},\ddot{\bar{x}},\dddot{\bar{x}})=\left[\frac{\omega_n{}^2}{\bar{K}}\dot{\bar{f}}-\dddot{\bar{x}}-2\xi\omega_n\ddot{\bar{x}}-\omega_n{}^2\dot{\bar{x}}\right]\bar{x}$$

Downloaded 03 May 2010 to 171.66.16.27. Redistribution subject to ASME license or copyright; see http://www.asme.org/terms/Terms_Use.cfm

Table 1 Order analysis of the zeroth and first five harmonics at $\bar{f}_1 = 0.4$ and $\bar{\omega} = 0.419$

Harmonic coefficient	Numerical integration		The method of harmonic balance		Quasi-linear model
	$\bar{x}_m/\bar{x}_1$	$\bar{p}_k/\bar{p}_1$	$\bar{x}_m/\bar{x}_1$	$\bar{p}_k/\bar{p}_1$	$\bar{x}_m/\bar{x}_1$, $\bar{p}_k/\bar{p}_1$
0	−0.026	−0.019	0	0	0
1	1	1	1	1	1
2	0.061	0.053	0.101	0.057	0
3	0.034	0.048	0.070	0.066	0
4	0.009	0.019	0	0	0
5	0.007	0.024	0	0	0
Reference values	$\bar{x}_1 = 0.445$	$\bar{p}_1 = 0.208$	$\bar{x}_1 = 0.507$	$\bar{p}_1 = 0.237$	$\bar{x}_1 = 0.349$ $\bar{p}_1 = 0.276$

$$+n\left[\frac{\omega_n^2}{\bar{K}}(1+\bar{\mu}_p+\bar{f})-\ddot{\bar{x}}-2\xi\omega_n\dot{\bar{x}}-\omega_n^2\bar{x}\right]\dot{\bar{x}}$$

$$+n\dot{\bar{m}}\left[\frac{\omega_n^2}{\bar{K}}(1+\bar{\mu}_p+\bar{f})-\ddot{\bar{x}}-2\xi\omega_n\dot{\bar{x}}-\omega_n^2\bar{x}\right]^{\frac{n-1}{n}}\left[\frac{\omega_n^2}{\bar{K}}(1+\bar{\mu}_p)\right]^{\frac{1}{n}}$$

First, consider the case when $\dot{\bar{m}}=0$. Equation (11) is reduced to the closed chamber case of Wang (1986) as

$$\ddot{\bar{x}}(t)+2\xi\omega_n\dot{\bar{x}}(t)+\omega_n^2\bar{x}(t)=\frac{\omega_n^2}{\bar{K}}\bar{f}(t)-H(\bar{x}), \tag{12}$$

where

$$H(\bar{x})=\frac{\omega_n^2}{\bar{K}}(1+\bar{\mu}_p)\bar{p}=\frac{\omega_n^2}{\bar{K}}(1+\bar{\mu}_p)[(1-\bar{x})^{-n}-1]$$

This equation clearly demonstrates the "hard" singularity as $H\to\infty$ when $\bar{x}\to 1$. We also note the "anharmonic" type oscillations as H is not symmetric about $\bar{x}=0$ (Mahaffey, 1976).

Second, examine the case when $\dot{\bar{m}}\neq 0$. A clear identification of the nature of nonlinearity seems very difficult as all variables and their products appear in equation (11). This is the result of adding the nonlinear orifice element to the pneumatic chamber. Since for the closed chamber, Wang (1986) found large nonlinear effects and "hard" singularity, we must assume that these are still in evidence for the open chamber case as well.

5 The Method of Harmonic Balance

We will now find an approximate solution for equation (11) using the method of harmonic balance. Our selection of this method is based on the claim by Mickens (1984) who stated that the method of harmonic balance is the only suitable technique of analyzing a system with very strong nonlinear interactions. Wang (1986) has already used this method successfully for the closed pneumatic chamber case.

A general analytical solution for equations (4)–(6) or (11) is very difficult, if not impossible. Therefore, we must simplify them in order to perform the perturbation analysis. Accordingly, we assume that (*i*) the flow is unchoked, $\dot{m}\leq\dot{m}^*$, (*ii*) the thermodynamic process is isothermal, $n=1$; and (*iii*) the discharge coefficient C is a constant, $C=C_c$. Such conditions are found in many practical situations and therefore our assumptions should be valid. Equation (4) is now simplified and generalized as

$$\dot{m}(t)=C_cA_o\left[|P_s^2-P^2(t)|\frac{g}{RT_s}\right]^{\frac{1}{2}}\text{sign}(P_s-P(t)) \tag{13}$$

where sign $(P_s-P)\begin{cases}=-1\\=0\\=1\end{cases}$ at $P_s-P\begin{cases}<0\\=0\\>0\end{cases}$

and equation (5) is reduced to

$$\dot{P}(t)V(t)+P(t)\dot{V}(t)=\dot{m}(t)RT \tag{14}$$

Therefore, the resulting equations in the nondimensional form are

$$\dot{\bar{p}}(t)[1-\bar{x}(t)]-[1+\bar{p}(t)]\dot{\bar{x}}(t)=\alpha\bar{D}_o^2\omega_n[|1-(1+\bar{p}(t))^2|]^{1/2}\text{sign}(-\bar{p}(t)) \tag{15}$$

$$\ddot{\bar{x}}(t)+2\xi\omega_n\dot{\bar{x}}(t)+\omega_n^2\bar{x}(t)=\frac{\omega_n^2}{\bar{K}}\bar{f}(t)-(1+\bar{\mu}_p)\bar{p}(t)] \tag{16}$$

Now, we apply the method of harmonic balance to predict the frequency response. According to this method, the excitation and responses are simultaneously assumed as follows:

$$\begin{aligned}\bar{f}(t) &= \bar{f}_1\cos(\omega t+\theta_{f1}),\\ \bar{p}(t) &= \sum_{k=0}^{\infty}\bar{p}_k\cos(k\omega t+\theta_{pk}),\\ \bar{x}(t) &= \sum_{m=0}^{\infty}\bar{x}_m\cos(m\omega t+\theta_{xm})\end{aligned} \tag{17}$$

Since there is some ambiguity regarding the order approximation associated with the application of the method of harmonic balance to a pneumatic system as shown by Wang (1986), we first examine the harmonic orders using the results obtained by the numerical integration of equations (4)–(6) or (11). Table 1 indicates that the zeroth harmonic is even less than the third harmonic and that the second and third harmonics are of the same order of magnitude (this table will be discussed in detail later). Furthermore, since the pneumatic system applications do not deal with very high frequencies, the interest here could be limited up to the third harmonic. Hence, $\bar{p}(t)$ and $\bar{x}(t)$ are approximated as

$$\begin{aligned}\bar{p}(t) &\simeq \bar{p}_1\cos(\omega t+\theta_{p1})+\bar{p}_2\cos(2\omega t+\theta_{p2})+\bar{p}_3\cos(3\omega t+\theta_{p3}),\\ \bar{x}(t) &\simeq \bar{x}_1\cos(\omega t+\theta_{x1})+\bar{x}_2\cos(2\omega t+\theta_{x2})+\bar{x}_3\cos(3\omega t+\theta_{x3})\end{aligned} \tag{18}$$

where

$$\bar{p}_2/\bar{p}_1=\bar{x}_2/\bar{x}_1=0(\epsilon),\ \bar{p}_3/\bar{p}_1=\bar{x}_3/\bar{x}_1=0(\epsilon^2)$$

and $\bar{p}_1=\bar{x}_1=0(\epsilon)$.

The procedure of determining response for equations (15) and (16) is: (*i*) substitute equations (17) for $\bar{f}(t)$ and (18) for $\bar{p}(t)$ and $\bar{x}(t)$ into equations (15) and (16); (*ii*) expand $|1-(1+\bar{p})^2|^{1/2}$ sign $(-\bar{p})$ to a sine and cosine series; and (*iii*) to reduce the mathematical difficulty, set θ_{p1} equal to zero, not θ_{f1}. Mathematical manipulations yield twelve coupled algebraic equations, which allow us to solve for the first, se-

Downloaded 03 May 2010 to 171.66.16.27. Redistribution subject to ASME license or copyright; see http://www.asme.org/terms/Terms_Use.cfm

cond, and third harmonic coefficients and phases, step by step, without any interference. Closed form solutions are as follows:

$$\bar{f}_1^{\,2} = \sigma_1 \bar{p}_1^{\,2} + \sigma_2 \bar{p}_1^{\,3/2} + \sigma_3 \bar{p}_1 \tag{19}$$

where

$$\sigma_1 = [1 + \bar{\mu}_p + (1-\bar{\omega}^2)\bar{K}]^2 + [2\xi\bar{\omega}\bar{K}]^2$$
$$\sigma_2 = 6.468\alpha\xi\bar{D}_o^{\,2}\bar{K}(1+\bar{\mu}_p)$$
$$\sigma_3 = [3.234\alpha\xi\bar{D}_o^{\,2}\bar{K}]^2 + [1.617\alpha\bar{D}_o^{\,2}(1-\bar{\omega}^2)\bar{K}/\bar{\omega}]^2$$

$$\bar{x}_1 = \left[\bar{p}_1^{\,2} + \left(\frac{1.617\alpha\bar{D}_o^{\,2}}{\bar{\omega}}\right)^2 \bar{p}_1\right]^{1/2} \tag{20}$$

$$\tan\theta_{x1} = \frac{-1.617\alpha\bar{D}_o^{\,2}}{\bar{\omega}\bar{p}_1^{\,1/2}} \tag{21}$$

$$\tan\theta_{f1} = \frac{(1-\bar{\omega}^2)\bar{K}\bar{x}_1\sin\theta_{x1} + 2\xi\bar{\omega}\bar{K}\bar{x}_1\cos\theta_{x1}}{(1+\bar{\mu}_p)\bar{p}_1 + (1-\bar{\omega}^2)\bar{K}\bar{x}_1\cos\theta_{x1} - 2\xi\bar{\omega}\bar{K}\bar{x}_1\sin\theta_{x1}} \tag{22}$$

$$\bar{x}_2 = \frac{(1+\bar{\mu}_p)\bar{x}_1\bar{p}_1}{2\{[1+\bar{\mu}_p + (1-4\bar{\omega}^2)\bar{K}]^2 + [4\xi\bar{\omega}\bar{K}]^2\}^{1/2}} \tag{23}$$

$$\bar{p}_2 = \frac{\bar{K}\bar{x}_2[(1-4\bar{\omega}^2)^2 + (4\xi\bar{m})^2]^{1/2}}{1+\bar{\mu}_p} \tag{24}$$

$$\tan\theta_{x2} = \frac{-\{[1+\bar{\mu}_p + (1-4\bar{\omega}^2)\bar{K}]\sin\theta_{x1} - 4\xi\bar{\omega}\bar{K}\cos\theta_{x1}\}}{-\{[1+\bar{\mu}_p + (1-4\bar{\omega}^2)\bar{K}]\cos\theta_{x1} + 4\xi\bar{\omega}\bar{K}\sin\theta_{x1}\}} \tag{25}$$

$$\tan\theta_{p2} = \frac{-\{(1-4\bar{\omega}^2)\sin\theta_{x2} + 4\xi\bar{\omega}\cos\theta_{x2}\}}{-\{(1-4\bar{\omega}^2)\cos\theta_{x2} - 4\xi\bar{\omega}\sin\theta_{x2}\}} \tag{26}$$

$$\bar{x}_3 = \left\{\frac{(1+\bar{\mu}_p)^2(\Gamma_1^{\,2} + \Gamma_2^{\,2})}{[1+\bar{\mu}_p + (1-9\bar{\omega}^2)\bar{K}]^2 + [6\xi\bar{\omega}\bar{K}]^2}\right\}^{1/2} \tag{27}$$

where

$$\Gamma_1 = 0.333[\bar{x}_1\bar{p}_2\cos(\theta_{p2} + \theta_{x1}) + \bar{x}_2\bar{p}_1\cos\theta_{x2}]$$

$$\Gamma_2 = 0.333[\bar{x}_1\bar{p}_2\sin(\theta_{p2} + \theta_{x1}) + \bar{x}_2\bar{p}_1\sin\theta_{x2}] - \frac{0.114\alpha\bar{D}_o^{\,2}\bar{p}_1^{\,1/2}}{\bar{\omega}}$$

$$\bar{p}_3 = \frac{\bar{K}\bar{x}_3[(1-9\bar{\omega}^2)^2 + (6\xi\bar{\omega})^2]^{1/2}}{1+\bar{\mu}_p} \tag{28}$$

$$\tan\theta_{x3} = \frac{-\{[1+\bar{\mu}_p + (1-9\bar{\omega}^2)\bar{K}]\Gamma_2 - [6\xi\bar{\omega}\bar{K}]\Gamma_1\}}{-\{[1+\bar{\mu}_p + (1-9\bar{\omega}^2)\bar{K}]\Gamma_1 + [6\xi\bar{\omega}\bar{K}]\Gamma_2\}} \tag{29}$$

$$\tan\theta_{p3} = \frac{-\{(1-9\bar{\omega}^2)\sin\theta_{x3} + 6\xi\bar{\omega}\cos\theta_{x3}\}}{-\{(1-9\bar{\omega}^2)\cos\theta_{x3} - 6\xi\bar{\omega}\sin\theta_{x3}\}} \tag{30}$$

To examine the uniqueness of the solution, we consider equation (19) for $\bar{p}_1$, which is a nonlinear algebraic equation. Since ξ, $\bar{K}$, and $\bar{\mu}_p$ are positive, σ_1, σ_2, and σ_3 must be definitely positive. Incidently, no negative $\bar{p}_1$ can be considered; hence $\bar{p}_1$ is unique and numerically convergent. After solving $\bar{p}_1$, other harmonic results as given by equations (2)–(30) could be uniquely solved for and all results converge numerically. Note that the uniqueness does not imply local stability of the solution as other stable motions may occur. The solution obtained here yields only the information which is presupposed by equation (18).

6 Quasi-Linear Model

Since our operating point for the nonlinear perturbation analysis is associated with $\dot{m}_o = 0$ or $p_o = P_s$, the linear system theory cannot describe equations (4) or (13). Thus, we must perform the quasi-linearization by assuming the following: (*i*) $\dot{\bar{p}}\dot{\bar{x}} \simeq 0$; (*ii*) $\bar{p}\dot{\bar{x}} \simeq 0$; and (*iii*) the orifice is modeled as a resistance of constant value R_c which is assumed to be half of the critical flow resistance, i.e.,

$$R_c = \frac{P_s - P}{\dot{m}} \simeq \frac{1}{2\left\{C_c A_o\left[\frac{\gamma g}{RT_s}\right]^{\frac{1}{2}}\left[\frac{2}{\gamma+1}\right]^{\frac{\gamma+1}{2(\gamma-1)}}\right\}} \tag{31}$$

In the nondimensional form, we define

$$\bar{R}_c = \frac{1-(1+\bar{p})}{\dot{\bar{m}}/\omega_n} \simeq \frac{1}{2\bar{D}_o^{\,2}\alpha\tau} \tag{32}$$

Hence, equation (9) is reduced to a first order differential equation

$$\dot{\bar{p}} + 2\bar{D}_o^{\,2}\alpha\tau\omega_n\bar{p} \simeq \dot{\bar{x}} \tag{33}$$

Thus the governing linear equation, a third order ordinary differential equation, is as follow

$$\dddot{\bar{x}} + [2\xi + 2\bar{D}_o^{\,2}\alpha\tau]\omega_n\ddot{\bar{x}} + \left[1 + 4\bar{D}_o^{\,2}\alpha\tau\xi + \frac{1+\bar{\mu}_p}{\bar{K}}\right]\omega_n^{\,2}\dot{\bar{x}} + 2\bar{D}_o^{\,2}\alpha\tau\omega_n^{\,3}\bar{x} = \frac{\omega_n^{\,2}}{\bar{K}}\dot{\bar{f}} + 2\bar{D}_o^{\,2}\alpha\tau\omega_n^{\,3}\bar{f} \tag{34}$$

Applying the Routh criterion to equation (34), we determine that the roots are stable.

7 Results

Now we can compare the results obtained using the method of harmonic balance as given by equations (19)–(30) with the results predicted by the numerical integration of equations (9) and (10), and with the results given by the quasi-linear model of equations (33) and (34). Numerical parameters used for the demonstration of the validity of the analytical solution are chosen as:

$$\bar{K} = 0.511,\ \xi = 0.5,\ \bar{\mu}_p = 0,\ \bar{D}_o = 0.05,\ \alpha = 95.37,$$
$$\tau = 0.685,\ \omega_n = 0.5$$

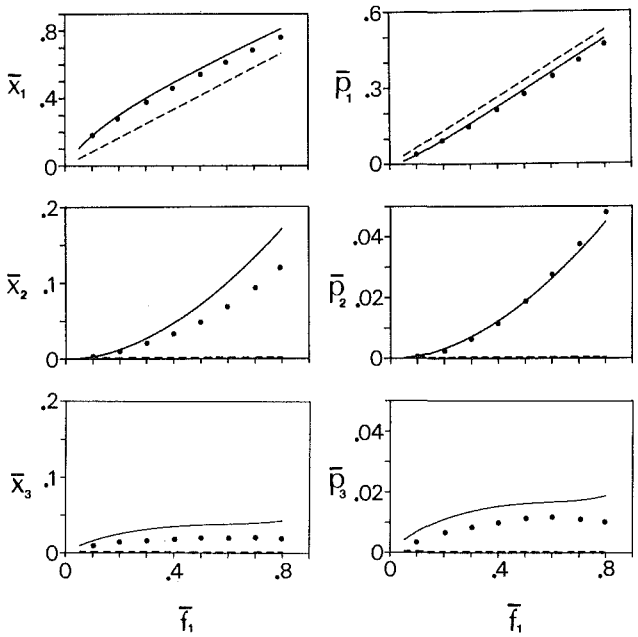


Fig. 2 Response versus excitation at $\bar{\omega} = 0.419$: (- - - -) quasi-linear model; (. .) numerical integration; (———) method of harmonic balance

Downloaded 03 May 2010 to 171.66.16.27. Redistribution subject to ASME license or copyright; see http://www.asme.org/terms/Terms_Use.cfm

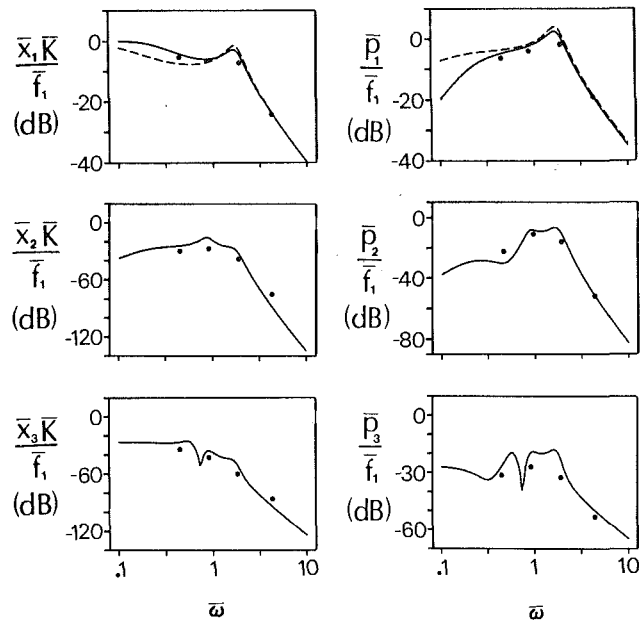


Fig. 3 Magnitude frequency response curves at $\bar{f}_1 = 0.4$: (- - - -) quasi-linear model; (. .) numerical integration; (———) method of harmonic balance

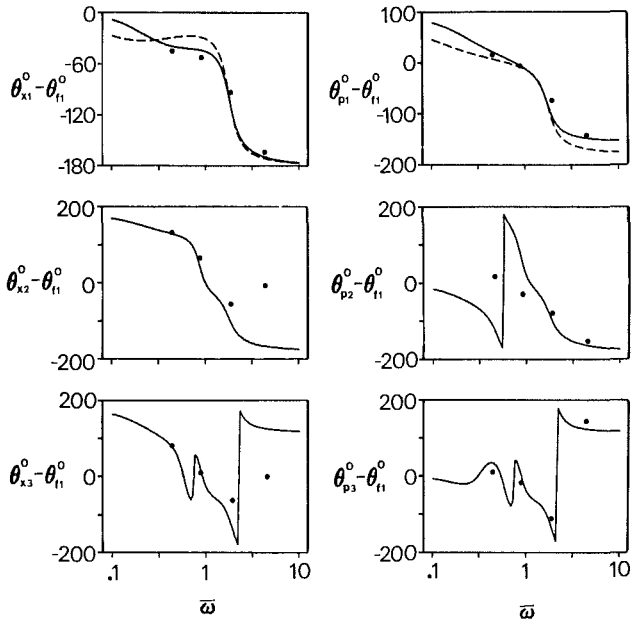


Fig. 4 Phase frequency response curves at $\bar{f}_1 = 0.4$: (- - - -) quasi-linear model; (. .) numerical integration; (———) method of harmonic balance

In Table 1, an order analysis for both $\bar{x}$ and $\bar{p}$ at the zeroth and first five harmonics has been performed using the first harmonic as the reference. Although the harmonic coefficients predicted by the numerical integration do not follow our assumption for the method of harmonic balance perfectly, we find the results to be very reasonable considering the assumptions and simplifications involved.

Frequency response curves for a linear system are given by plotting the response versus frequency as the dimensionless response (normalized by dividing it by the excitation $\bar{f}$) is not a function of the excitation $\bar{f}$. For a nonlinear system, this is obviously not true, i.e., $\bar{x} = \bar{x}(\bar{f}, \bar{\omega})$. Hence, a three-dimensional representation is required to sketch the sinusoidal response. But, since a three-dimensional graph is difficult to visualize,

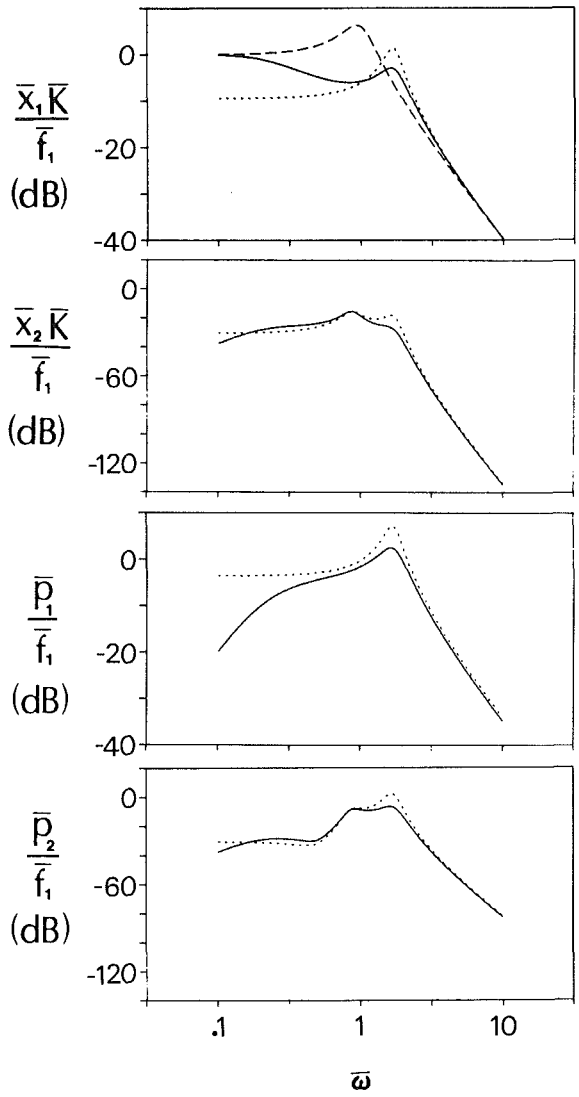


Fig. 5 Magnitude frequency response curves for various nonlinearities at $\bar{f}_1 = 0.4$: (- - - -) pure mechanical system; (. . . .) closed chamber; (———) open chamber

we will illustrate the response through two-dimensional views by taking $\bar{x} = \bar{x}(\bar{\omega})|_{\bar{f}=\text{constant}}$ and $\bar{x} = \bar{x}(\bar{f})|_{\bar{\omega}=\text{constant}}$.

We compare response $\bar{x}$ and $\bar{p}$ with excitation $\bar{f}$ levels in Fig. 2 for the first, second, and third harmonics. Even though we had noted some ambiguity earlier regarding the harmonic order, the method of harmonic balance still predicts second and third harmonic results successfully. In addition, an excellent agreement is found between the method of harmonic balance and the numerical integration at the first harmonic. We also note that the quasi-linear model, while not capable of predicting response at second and third harmonics, yields reasonable results at the first harmonic.

Figures 3 and 4 show the frequency response curves with ω_n as the reference frequency. By adding an orifice, the overall system becomes a third order system, and its "resonant" frequency is shifted to $\bar{\omega} = 1.62$. We again find excellent agreement, with the exception of results for the phase at the higher frequencies and harmonics, between the predictions by the method of harmonic balance and by the numerical integration. And, at the first harmonic, the quasi-linear model matches well with other models.

All of the frequency response results predicted by the numerical integration technique and the method of harmonic balance did not show any instability or jump phenomenon.

Downloaded 03 May 2010 to 171.66.16.27. Redistribution subject to ASME license or copyright; see http://www.asme.org/terms/Terms_Use.cfm

8 Orifice Nonlinearity

In order to determine the effect of orifice nonlinearity, we compare frequency response magnitudes at first and second harmonics for the following cases: (*i*) pure mechanical system; (*ii*) closed pneumatic system ($\bar{D}_o = 0$); and (*iii*) open pneumatic system ($\bar{D}_o = 0.05$). The results obtained using the method of harmonic balance are shown in Fig. 5. Results for the first harmonic ($\bar{x}_1$ and $\bar{p}_1$) indicate that the nonlinear orifice has strong influence at very low frequencies ($\bar{\omega} \ll 1$) and in the vicinity of the resonance ($\bar{\omega} = 1.62$). At very low frequencies, the orifice completely eliminates the pneumatic spring or cushioning effect; therefore, the $\bar{x}_1$ response of open chamber case is the same as that of the pure mechanical system. In the vicinity of resonance, magnitudes associated with the open chamber are lower compared to the closed-chamber case. This demonstrates that the orifice acts mainly as the damper since the resonant frequency for both cases is about the same. Results for the second harmonic ($\bar{x}_2$ and $\bar{p}_2$) indicate that the open and closed chambers behave approximately in the same manner except that the orifice adds slightly more damping.

The orifice also changes the order of harmonics. For example, the response at the zeroth harmonic for the open system is considerably lower than the response at the first harmonic, i.e., $\bar{x}_0/\bar{x}_1 \leq 0(\epsilon^2)$. Conversely for the closed system, $\bar{x}_0/\bar{x}_1 = 0(\epsilon^1)$ was found. This illustrates that the orifice essentially diminishes the unsymmetrical nature of the compression process which will reduce the "anharmonic" type oscillations.

9 Conclusion

The major accomplishment of this study has been in gaining a better understanding of the effect of the nonlinear orifice and in eliminating the mathematical difficulty associated with zero mean flow rate case while using the method of harmonic balance. In spite of several simplifications involved and some doubt regarding the harmonic order, our analytical solution still provides accurate predictions when compared to the numerical integration technique. Of more importance is the fact that a difficult mathematical formulation of a nonlinear pneumatic system has been reduced to a set of simple algebraic equations which are much easier to deal with; also a substantial saving in computer time is evident. Further work in this area is in progress with emphasis in the modeling of "real" world components and systems.

References

Andersen, B. W., 1967, *The Analysis and Design of Pneumatic Systems*, Wiley, New York.

Bachrach, B. I., and Rivin, E., 1983, "Analysis of a Damped Pneumatic Spring," *Journal of Sound and Vibration*, Vol. 86, No. 2, pp. 191–197.

Blackburn, J. F., Reethof, G., and Shearer, J. L., 1960, *Fluid Power Control*, M.I.T. Press, Cambridge, Mass.

Bota, K. B., and Mickens, R. E., 1984, "Approximate Analytic Solutions for Singular Nonlinear Oscillators," *Journal of Sound and Vibration*, Vol. 96, No. 2, pp. 277–279.

Cavanaugh, R. D., 1976, Chap. 33, "Air Suspension and Servo-Controlled Isolation Systems," *Shock and Vibration Handbook*, 2nd Harris, C. M., and Crede, C. E., eds., McGraw-Hill, New York.

Chen, F. Y., 1977, "Dynamic Response of a Cam-Actuated Mechanism with Pneumatic Coupling," *ASME Journal of Engineering for Industry*, Vol. 99, No. 3, pp. 598–603.

Doebelin, E. O., 1980, *System Modeling and Response*, Wiley, New York.

Hundal, M. S., 1980, "Pneumatic Shock Absorbers and Isolators," *Shock and Vibration Digest*, Vol. 12, No. 9, pp. 17–21.

Hundal, M. S., 1982a, "Response of Pneumatic Isolator to Standard Pulse Shapes," *Shock and Vibration Bulletin*, Vol. 52, No. 4, pp. 161–168.

Hundal, M. S., 1982b, "Passive Pneumatic Shock Isolator: Analysis and Design," *Journal of Sound and Vibration*, Vol. 84, No. 1, pp. 1–9.

Mahaffrey, R. A., 1976, "Anharmonic Oscillator Description of Plasma Oscillations," *Physics of Fluids*, Vol. 19, No. 9, pp. 1387–1391.

McCloy, D., and Martin, H. R., 1980, *Control of Fluid Power: Analysis and Design*, Ellis Horwood Limited, New York.

Mickens, R. E., 1984, "Comments on the Method of Harmonic Balance," *Journal of Sound and Vibration*, Vol. 94, No. 3, pp. 456–460.

Wang, Y. T., Singh, R., Yu, H. C., and Guenther, D. A., 1984, "Computer Simulation of a Shock-Absorbing Pneumatic Cylinder," *Journal of Sound and Vibration*, Vol. 93, No. 3, pp. 353–364.

Wang, Y. T., 1986, "Frequency Response of Nonlinear Pneumatic Systems," Ph.D. Dissertation, The Ohio State University, Columbus, Ohio.

Downloaded 03 May 2010 to 171.66.16.27. Redistribution subject to ASME license or copyright; see http://www.asme.org/terms/Terms_Use.cfm

L. E. Galhoud
Graduate Student.

S. F. Masri
Professor.

J. C. Anderson
Associate Professor.

Department of Civil Engineering,
University of Southern California,
Los Angeles, CA 90089-0242

Transfer Function of a Class of Nonlinear Multidegree of Freedom Oscillators

Analytical and experimental studies were made of the dynamic response of a multidegree-of-freedom system with a geometric nonlinearity, which is encountered in many practical engineering applications. An exact solution was derived for the steady-state motion of a viscously damped two-degree-of-freedom oscillator with an unsymmetric geomtric nonlinearity, under the action of harmonic excitation. Experimental measurements of a distributed-parameter mechanical model under harmonic excitation verified the analytical findings. The effect of various dimensionless parameters on the system response was determined.

1 Introduction

The forced vibration of dynamic systems with motion-limiting stops is of great concern in many practical engineering problems. For example, a simple model that is used to obtain first-order estimates of the transfer function of a nuclear power plant pipe loop that is provided with a snubber is shown in Fig. 1. Similary, some vibration isolation/transmissibility problems involving dynamic interaction between oscillating components that are interconnected by resilient elements incorporating snubbers can be adequately modeled as shown in Fig. 2.

Both of the groups of problems related to Figs. 1 and 2 are subsets of the more general class of problems depicted in Fig. 3. Each of the discrete elements g_1, g_2, and g_3 shown in Fig. 3 is linear and consists of a massless linear spring k_i and viscous dashpot c_i. Nonlinear element g_4 is piece-wise linear and has an unsymmmetric "deadspace" zone of magnitude d which causes the element resistance to vanish unless the separation between the masses m_1 and m_2 exceeds the gap size. Harmonic excitations of different amplitudes F_1 and F_2 but the same frequency Ω are applied to m_1 and m_2, respectively.

Studies of nonlinear systems with bilinear characteristics have been conducted by Klotter (1953), Caughey (1954), Watanabe (1978), Jones nad Muszynska (1979), Moon and Holmes (1979), Masri et al. (1981), Shaw (1985), and Lo (1985).

This paper reports some of the results of a comprehensive analytical and experimental investigation of the nonlinear mechanical system shown in Fig. 6, which consists of a cantilever (striker) beam carrying a concentrated mass whose motion is limited on one side by a stop (target) beam.

Contributed by the Applied Mechanics Division for publication in the JOURNAL OF APPLIED MECHANICS.

Discussion on this paper should be addressed to the Editorial Department, ASME, United Engineering Center, 345 East 47 Street, New York, N.Y. 10017, and will be accepted until two months after final publication of hte paper itself in the JOURNAL OF APPLIED MECHANICS. Manuscript received by ASME Applied Mechanics Division, August 26, 1985; final revision, August 18, 1986.

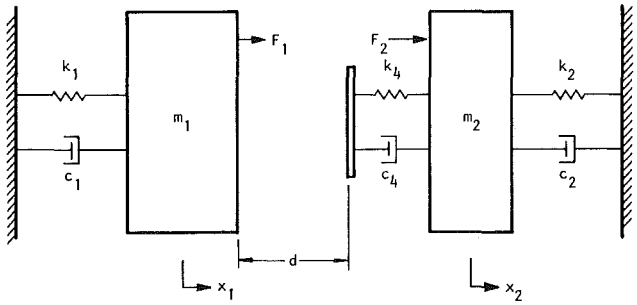


Fig. 1 Model of pipe/snubber system

An exact closed-form solution for the steady-state motion of the simplified nonlinear two-degree-of-freedom (2DOF) mathematical model shown in Fig. 3 is given in Section 2, a comparison of the analytical and experimental results is presented in Section 3, and the effects of the various system parameters are discussed in Section 4.

2 Steady-State Solution

2.1 Formulation. The equations of motion for the system in Fig. 3 are

$$m_1\ddot{x}_1 + g_1(x_1,\dot{x}_1) + g_3(y,\dot{y}) + g_4(y,\dot{y}) = f_1(t) \tag{1}$$

$$m_2\ddot{x}_2 + g_2(x_2,\dot{x}_2) - g_3(y,\dot{y}) - g_4(y,\dot{y}) = f_2(t) \tag{2}$$

where

$$g_j(u,\dot{u}) = k_j u + c_j\dot{u}, \quad j = 1,2,3 \tag{3}$$

$$g_4(u,\dot{u}) = \begin{cases} 0 & u \le d \\ k_4(u-d) + c_4\dot{u}, & u > d \end{cases} \tag{4}$$

the relative displacement

$$y = x_1 - x_2 \tag{5}$$

and the exciting forces f_1 and f_2 are harmonic and of the form

Copyright © 1987 by ASME
Downloaded 03 May 2010 to 171.66.16.27. Redistribution subject to ASME license or copyright; see http://www.asme.org/terms/Terms_Use.cfm

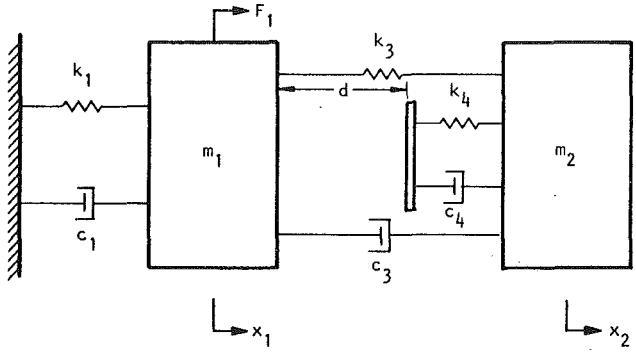


Fig. 2 Model of vibration control problem

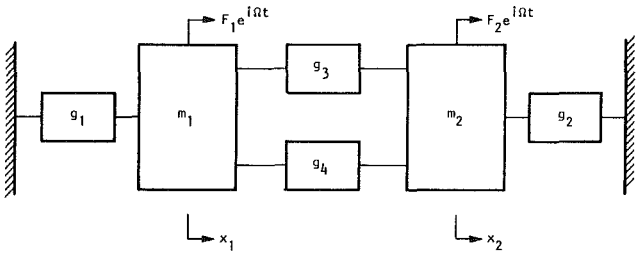


Fig. 3 Model of system

$$f_j(t) = F_j \exp(i\Omega t), \quad j = 1,2 \tag{6}$$

where $i = (-1)^{1/2}$.

An alternative form of equations (1) and (2) is

$$a_{11_n}\ddot{x}_1 + b_{11_n}\dot{x}_1 + c_{11_n}x_1 + b_{12_n}\dot{x}_2 + c_{12_n}x_2 = q_{1_n}(t) \tag{7}$$

$$a_{22_n}\ddot{x}_2 + b_{22_n}\dot{x}_2 + c_{22_n}x_2 + b_{12_n}\dot{x}_1 + c_{12_n}x_1 = q_{2_n}(t) \tag{8}$$

where

$$n = 1 \text{ if } y \le d \text{ and } n = 2 \text{ if } y > d$$

$$a_{11_1} = m_1 \qquad a_{11_2} = a_{11_1}$$

$$b_{11_1} = c_1 + c_3 \qquad b_{11_2} = c_1 + c_3 + c_4$$

$$c_{11_1} = k_1 + k_3 \qquad c_{11_2} = k_1 + k_3 + k_4$$

$$b_{12_1} = -c_3 \qquad b_{12_2} = -(c_3 + c_4)$$

$$c_{12_1} = -k_3 \qquad c_{12_2} = -(k_3 + k_4)$$

$$q_{1_1}(t) = F_1 \exp(i\Omega t) \qquad q_{1_2}(t) = F_1 \exp(i\Omega t) + k_4 d$$

$$a_{22_1} = m_2 \qquad a_{22_2} = a_{22_1}$$

$$b_{22_1} = c_2 + c_3 \qquad b_{22_2} = c_2 + c_3 + c_4$$

$$c_{22_1} = k_2 + k_3 \qquad c_{22_2} = k_2 + k_3 + k_4$$

$$q_{2_1}(t) = F_2 \exp(i\Omega t) \qquad q_{2_2}(t) = F_2 \exp(i\Omega t) - k_4 d$$

2.2 Exact Solution. Consider the steady-state motion of the system, and shift the origin of the time axis so that at $t = 0$, the relative motion $y = d$. This shift will modify the excitation forces so that they are given by

$$f_j(t) = F_j \exp[i(\Omega t + \alpha_0)]. \tag{9}$$

Letting $\alpha_1 \equiv \Omega t_1 \equiv 0$ be the time at which m_1 and m_2 terminate the contact phase of their motion, and $\alpha_2 \equiv \Omega t_2$ is the time when the next contact phase is started, and assuming on the basis of experimental evidence that the two phases of motion (element g_4 inactive in the no contact phase 1, and g_4 engaged in the contact phase 2) are repeated in an identical manner once every period of the excitation, then the exact solution of equations (7)–(9) is

$$x_{1_n}(t) = \mathbf{e}_n^T(t)\lambda_n + A_{1_n} \exp[i(\Omega t + \alpha_0)] + x_{1s_n} \tag{10}$$

$$\dot{x}_{1_n}(t) = \mathbf{e}_n^T(t)[S]_n\lambda_n + (i\Omega)A_{1_n} \exp[i(\Omega t + \alpha_0)] \tag{11}$$

$$x_{2_n}(t) = \mathbf{e}_n^T(t)[R]_n\lambda_n + A_{2_n} \exp[i(\Omega t + \alpha_0)] + x_{2s_n} \tag{12}$$

$$\dot{x}_{2_n}(t) = \mathbf{e}_n^T(t)[R]_n[S]_n\lambda_n + (i\Omega)A_{2_n} \exp[i(\Omega t + \alpha_0)] \tag{13}$$

subject to the condition $\alpha_n < \Omega t < \alpha_{n+1}$ where

$$\mathbf{e}_n(t) = \text{col.}\{\exp[s_{1n}(\Omega t - \alpha_n)/\Omega], \exp[s_{2n}(\Omega t - \alpha_n)/\Omega],$$
$$\exp[s_{3n}(\Omega t - \alpha_n)/\Omega], \exp[s_{4n}(\Omega t - \alpha_n)/\Omega]\}$$

s_{jn}, $j = 1,2,3,4$ are the roots of the characteristic equation

$$\lambda_n = \text{col.}\{\lambda_{11n}, \lambda_{21_n}, \lambda_{31_n}, \lambda_{41_n}\}$$

$$[S]_n = \text{diag.}[s_{1n}, s_{2n}, s_{3n}, s_{4n}]$$

$$[R]_n = \text{diag.}[r_{1n}, r_{2n}, r_{3n}, r_{4n}]$$

$$r_{jn} \equiv \lambda_{j1_n}/\lambda_{j2_n}; \; j = 1,2,3,4$$
$$= -(a_{22_n}s_{jn}^2 + b_{22_n}s_{j_n} + c_{22_n})/(b_{12_n}s_{j_n} + c_{12_n})$$

and where the remaining terms are as defined in the Appendix.

Introducing the following quantities

$$\mathbf{u}_n(t) \equiv \text{col.}\{x_{1n}(t), \dot{x}_{1n}(t), x_{2n}(t), \dot{x}_{2n}(t)\}$$

$$\sigma_n \equiv \text{col.}\{A_{1n}, i\Omega A_{1n}, A_{2n}, i\Omega A_{2n}\}$$

$$\beta_n \equiv \text{col.}\{x_{1s_n}, 0, x_{2s_n}, 0\}$$

$$[M_n(t)] \equiv [\mathbf{e}_n(t), [S]_n\mathbf{e}_n(t), [R]_n\mathbf{e}_n(t), [S]_n[R]_n\mathbf{e}_n(t)]^T$$

then the steady-state system response can be put concisely in the form

$$\mathbf{u}_n(t) = [M_n(t)]\lambda_n + \sigma_n \exp[i(\Omega t + \alpha_0)] + \beta_n. \tag{14}$$

Due to the nature of the steady-state motion, the solution in equation (14) must satisfy the following conditions:

$$\mathbf{u}_1(\alpha_2) = \mathbf{u}_2(\alpha_2), \tag{15}$$

$$\mathbf{u}_2(\alpha_3) = \mathbf{u}_1(\alpha_1), \tag{16}$$

$$x_{1_1}(\alpha_1) - x_{2_1}(\alpha_1) = d, \tag{17}$$

$$x_{1_2}(\alpha_2) - x_{2_2}(\alpha_2) = d. \tag{18}$$

Keeping in mind that $\alpha_1 = 0$ and $\alpha_3 = 2\pi$, then the ten unknowns of the motion needed in equation (14) are the four values of the state variable components at the start of each of the two segments that make up the solution over a full period of the excitation, and the values of α_2 and α_0. The conditions expressed in equations (15)–(18) will generate ten equations from which the unknown quantities can be determined.

With some effort (see Appendix), the use of equation (14) together with the conditions in equations (15)–(18) will eventually lead to a set of two coupled nonlinear algebraic equations of the form

$$h_1(\alpha_0, \alpha_2) = 0 \tag{19}$$

$$h_2(\alpha_0, \alpha_2) = 0 \tag{20}$$

that involve only the two unknowns α_0 and α_2.

Once the system properties are specified, equations (19) and (20) can be solved by conventional numerical techniques to yield the values of α_0 and α_2. The rest of the unknowns of the motion can then be found by back substitution.

3 Construction of Steady-State Solutions

Consider a typical problem that is modeled by the system shown in Fig. 1 with the following arbitrary set of parameters:

Downloaded 03 May 2010 to 171.66.16.27. Redistribution subject to ASME license or copyright; see http://www.asme.org/terms/Terms_Use.cfm

- Excitation frequency ratio $\Omega/\omega_1 = 1$.
- Ratio of critical damping in the primary system $\zeta_1 = 0.005$.
- Dimensionless gap size $d/(F_1/k_1) = 10$.
- Magnitude of exciting force $F_1 = 1$.
- Auxiliary mass ratio $\mu = m_2/m_1 = 0.1$.
- Excitation amplitude ratio $F_2/F_1 = \mu$.
- Auxiliary mass stiffness ratio $\omega_2/\omega_1 = 0.5$.
- Auxiliary mass ratio of critical damping $\zeta_2 = 0.01$.
- Nonlinear spring ratio of critical damping $\zeta_4 = 0.10$.
- Coupling element g_3 is absent.

The aim is to determine the steady-state motion of this system using the exact solution developed in Section 2.2. The procedure to construct such a solution is as follows:

(1) Using the values of the specified system parameters and employing standard numerial algorithms for the solutions of nonlinear algebraic equations, the initially unknown values of α_0 and α_2 can be determined from the solution of equations (19) and (20).

(2) Once α_0 and α_2 are determined, the remainder of the unknowns of the motion (i.e., the initial conditions at the beginning of the two segments of the solution) can be determined from the relationships given in the Appendix.

(3) The displacement and the velocity of the system during each of the segments ($n = 1, 2$) of the motion can be found by evaluating $x_j^{(n)}(t)$ and $\dot{x}_j^{(n)}(t)$, respectively. Note that from the definition of the segments, $x_1^{(1)}(t)$ and $x_2^{(1)}(t)$ correspond to the motion of m_1 and m_2, respectively, during the time $0 \leq \Omega t \leq \alpha_2$ where $y = (x_1 - x_2) < d$, while $x_1^{(2)}(t)$ and $x_2^{(2)}(t)$ correspond to the system motion during the remainder of the excitation period, i.e., $\alpha_2 \leq \Omega t \leq 2\pi$ where $y > d$.

(4) By appropriately adjoining the solutions for segments (1) and (2), the motion of the system over one cycle of the excitation can be completely determined. Since the solution is predicated on the assumption that the system is undergoing steady-state oscillations, the system motion in each of the succeeding periods is an exact replica of its motion during this period.

(5) The positive and negative peak values of the response can be found by numerically evaluating $x_j^{(n)}(t)$ and $\dot{x}_j^{(n)}(t)$ for differing values of t in the range $0 \leq \Omega t \leq 2\pi$, and thus determining the maximum, and minimum values of x_j and $\dot{x}_j$ during that time interval.

The construction of the steady-state solution for the set of parameters under discussion is illustrated in Fig. 4(*a*) where the displacement and velocity of m_1 and m_2 as well as the harmonic excitation are shown for one period of the excitation. The results shown in Fig. 5 are additional solutions corresponding to the same set of parameters except for the mass ratio μ which is changed to $\mu = 1$ in Fig. 5(*b,e,h*) and $\mu = 10$ in Fig. 5(*c,f,i*).

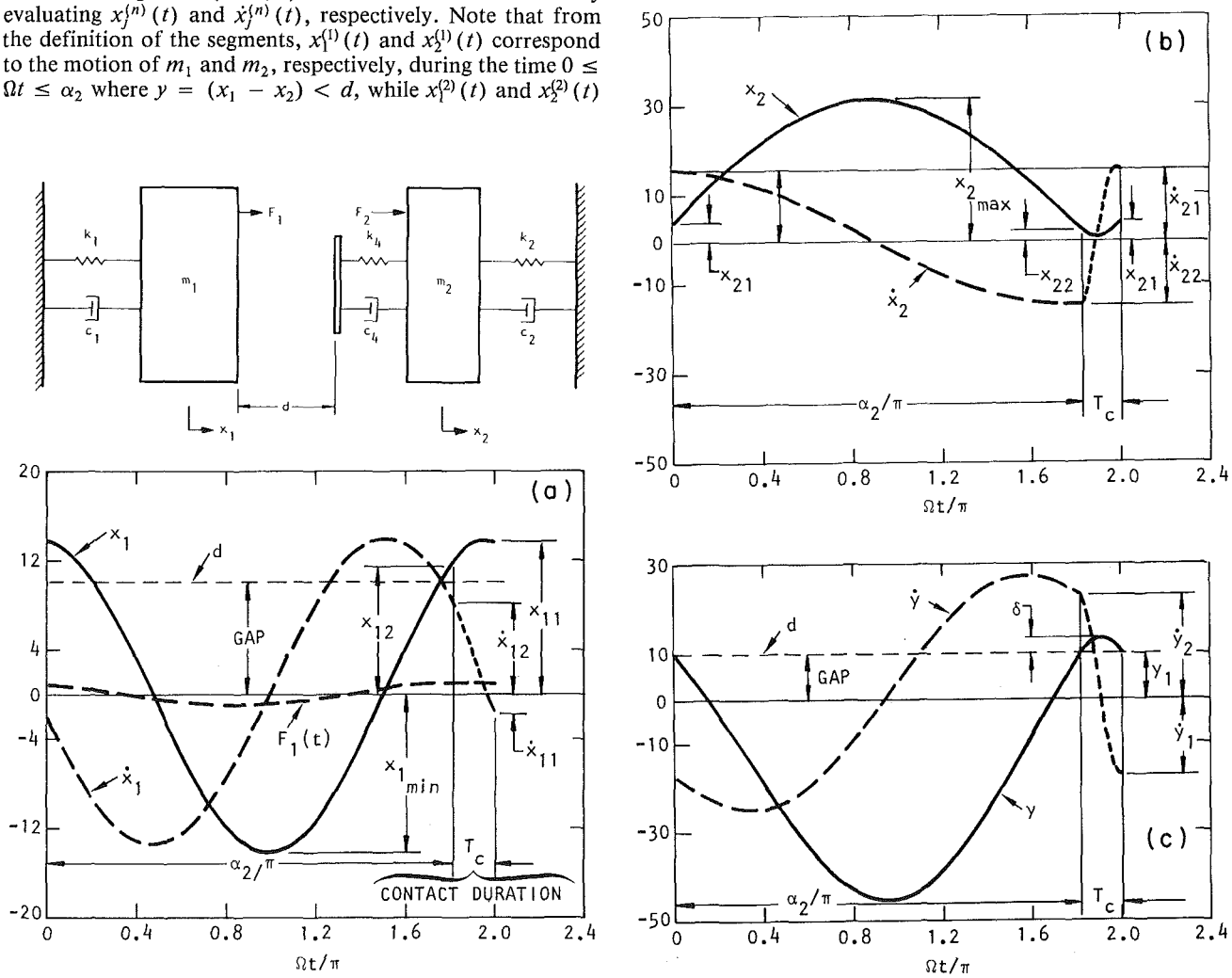


Fig. 4 *Construction of a typical steady-state solution.* Harmonic excitation acting on m_1. Mass ratio $\mu = m_2/m_1 = 0.1$; excitation frequency ratio $\Omega/\omega_1 = 1$; damping parameters $\zeta_1 = 0.005$, $\zeta_2 = 0.01$, $\zeta_4 = 0.1$; stiffness ratio $\omega_2/\omega_1 = 0.5$, $\omega_4/\omega_1 = 5$; gap ratio $d/(F_1/k_1) = 10$. (*a*) Motion of m_1; (*b*) motion of m_2; (*c*) relative motion between m_1 and m_2.

Downloaded 03 May 2010 to 171.66.16.27. Redistribution subject to ASME license or copyright; see http://www.asme.org/terms/Terms_Use.cfm

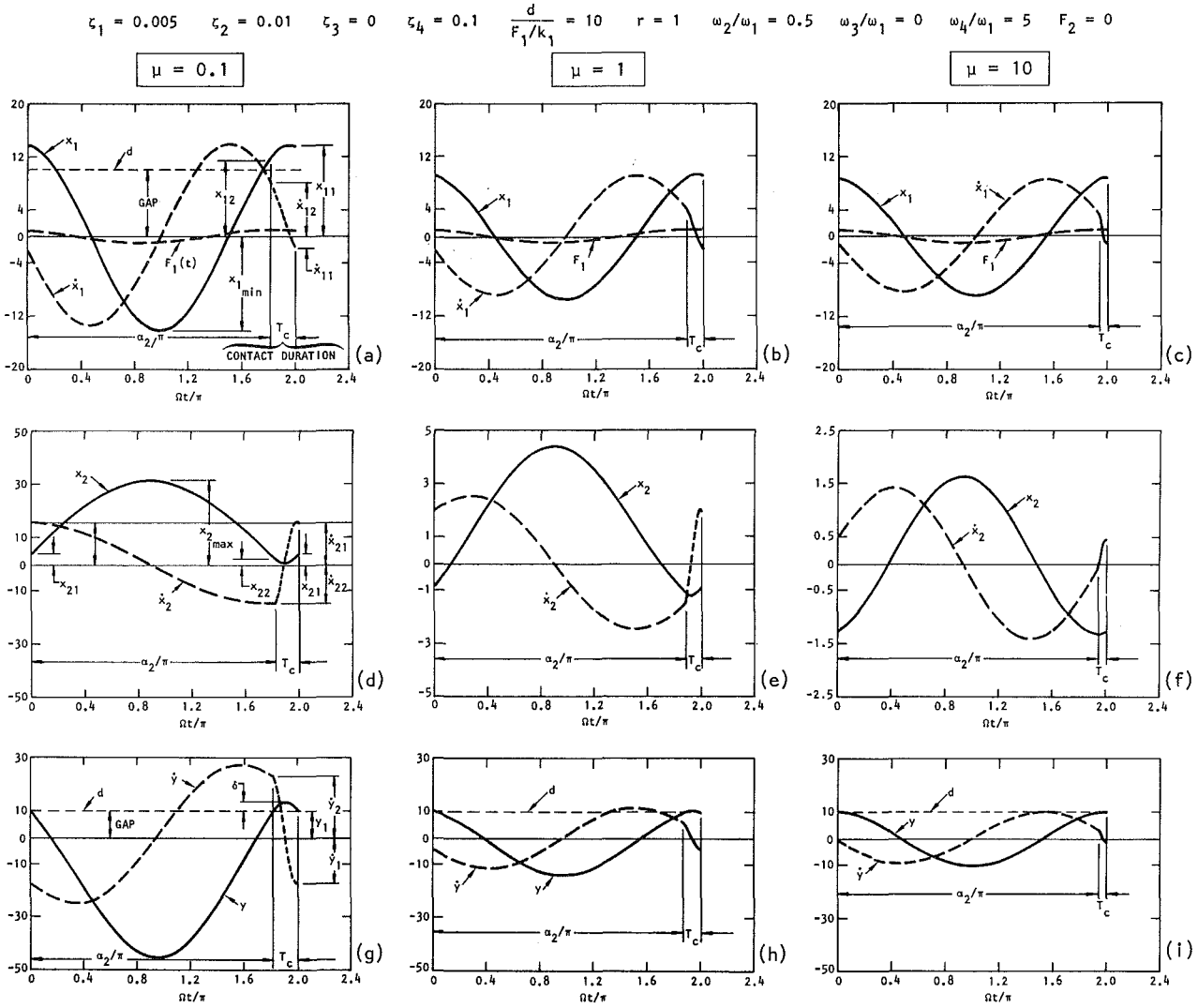


Fig. 5 Effects of the mass ratio on the exact steady-state solution of the nonlinear system in Fig 1. First column of figures corresponds to μ = 0.1; second column of figures corresponds to μ = 1.0; third column of figures corresponds to μ = 1.0; third column of figures corresponds to μ = 10.

For ease of comparison of the response curves shown in Fig. 5, the same time scale is used for all the plots, the same amplitude scale is used for the motion of the primary system m_1 (Figs. 5(*a*,*b*,*c*)), the same amplitude scale is used for the relative motion (Figs. 5(*g*,*h*,*i*)), but different amplitude scales are used for the motion of the secondary system m_2 (Figs. 5(*d*,*e*,*f*)). Noting from the definition of $\alpha_j \equiv \Omega t_j$ that, due to the shifting of the time origin, $\alpha_1 = 0$ and $\alpha_2/(2\pi)$ is the fraction of the excitation period during which $y < d$ (i.e., mass m_1 is not in contact with m_2), then the duration of the contact phase of the motion (denoted by T_c in Fig. 4*a*) is $T_c = [1 - \alpha_2/(2\pi)]T$, where $T = 2\pi/\Omega$ is the period of the excitation.

It can be seen from Fig. 4(*a*) that since, for the given set of parameters, $\alpha_2 = 1.82\pi$, then the fraction of the excitation period during which the relative displacement $y < d$ is equal to $\alpha_2/(2\pi) = 0.91$. Consequently, the duration of the contact phase of the motion is = 0.09 of the excitation period. The value of $\dot{x}_1^{(1)}$, which is the velocity of m_1 immediately after its separation from the nonlinear spring k_4, is equal to $\dot{x}_1^{(1)}(0) \equiv \dot{x}_{11} = -1.75\ (F_1/k_1)$ while the velocity of m_1 immediately before its contact with k_4 is $\dot{x}_1^{(1)}(\alpha_2) \equiv \dot{x}_{12} = 9.0\ (F_1/k_1)$. Due to the periodicity of the solution, the values of $x_j(t)$ and $\dot{x}_j(t)$ at the end of one period ($\Omega t = 2\pi$) are identical to their values at the beginning of the period ($\Omega t = 0$).

It can be seen from Figs. 4(*a*) and (*b*) that the excursion of the primary mass m_1 into the range $y > d$, which begins when $\Omega t = 1.82\pi$ and ends at $\Omega t = 2\pi$, results in a peak positive displacement of $x_{1_{max}} = 13.85\ (F_1/k_1)$ and $x_{2_{max}} = 31.34\ (F_1/k_1)$. The peak negative displacement that is seen to occur at $\Omega t \simeq 1.0$ is equal to $x_{1_{min}} = -14.21\ (F_1/k_1)$ and $x_{2_{min}} = 0.13\ (F_1/k_1)$. Note from Fig. 4(*c*) that due to the high stiffness of k_4 compared to k_1, the maximum relative displacement y is $13.39\ (F_1/k_1)$ and the minimum y is $-45.14\ (F_1/k_1)$. Thus the maximum penetration of m_1 into the nonlinear range is limited to $\simeq 0.33\ d$ (i.e., 33 percent of the gap size).

It is worth noting that while the unrestrained peak displacement of m_1 in this case would be $x_{1_{max}}/(F_1/k_1) = 1/(2\zeta_1) = 100$, the presence of the gap causes the motion of the primary system in the negative x_1 direction (where the amplitude of the motion is not restrained) to be close to its positive peak of $\simeq 14(F_1/k_1)$.

Since the duration of the contact phase of the system motion is very short in comparison to the period of the motion,

Downloaded 03 May 2010 to 171.66.16.27. Redistribution subject to ASME license or copyright; see http://www.asme.org/terms/Terms_Use.cfm

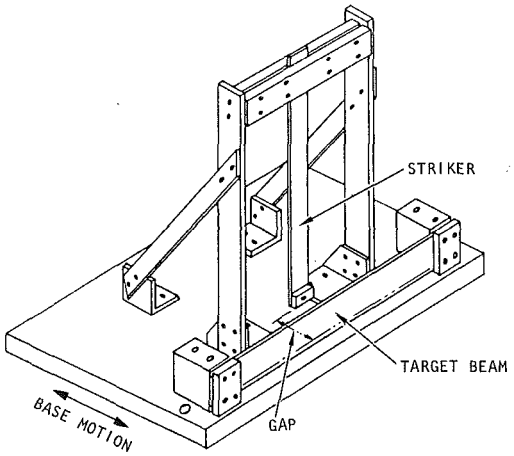


Fig. 6 Nonlinear mechanical model configuration

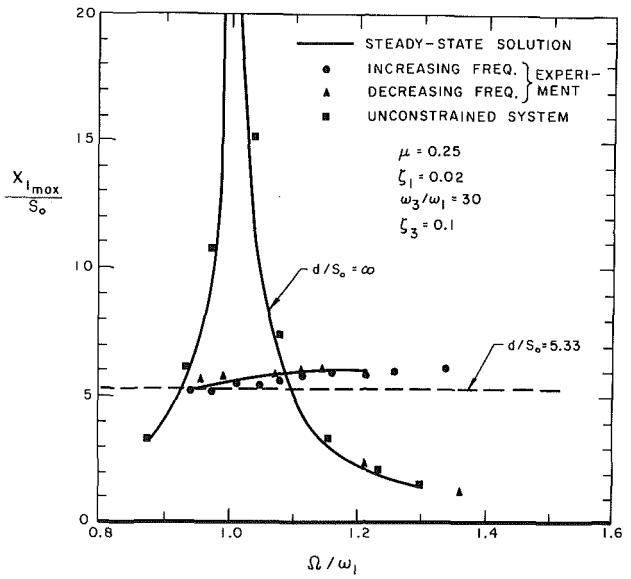


Fig. 7 Comaprison between theory and experiment of the response of the model shown in Fig. 6. $\omega_4/\omega_1 = 30$; $\zeta_4 = 0.1$. Experimental error bars are comparable in size to the diameter of the solid circles.

the concept of the coefficient of restitution e can be used to estimate the mechanical energy dissipated during the "impact" process. Thus from Fig. 4(*c*) it is evident that $e \equiv -\dot{y}_1/\dot{y}_2 = 25.23/27.80 \simeq 0.9$. This value of e is consistent with what one would expect in a nearly elastic "collision" (note that $\zeta_4 = 0.10$).

Considering the remainder of the solutions shown in Fig. 5, it is clear that with everything else being the same, an increase in the system mass ratio $\mu = m_2/m_1$ will attenuate the motion of m_2 thereby reducing the amplitude of the primary mass m_1. Note from Fig. 5(*g,h,i*) that as μ is increased from 0.1 to 1 and then to 10, the corresponding penetration ratio $\delta \simeq (y_{\max}/d - 1)$ is changed from $\delta \simeq 0.34$ to 0.05 and then to 0.01, respectively.

4 Comparison of Analytical and Experimental Results

4.1 Experimental Studies. Experimental studies were conducted to determine the steady-state motion of a nonlinear mechanical system consisting of a cantilever (striker) beam carrying a concentrated mass whose motion is limited on one side by a stop (target) beam. Details regarding the apparatus, test procedure and sample time histories of the system response under the harmonic base motion are available in Masri et al. (1981).

In the aforementioned reference, an "exact" solution was derived for the steady-state motion of a viscously damped Bernoulli-Euler beam with an unsymmetric deadspace nonlinearity under the action of harmonic excitation. The elastic beam was assumed to have uniformly distributed properties, and the geometric nonlinearity consisted of a massless elastic spring placed at some arbitrary location within the beam span and separated from the beam by a certain gap.

In using the present analytical results with the above referenced beam/stop model, the generalized mass, stiffness, and damping of the striker beam as well as the target beam were used in conjunction with the modal participation factor to convert the problem from one dealing with two impacting beams to an equivalent nonlinear problem involving two discrete components m_1 and m_2 each possessing certain inertia, stiffness, and damping properties.

4.2 Generalized Coordinate Model. In order to apply the present analytical results to the nonlinear model with distributed properties shown in Fig. 6, the generalized coordinate approach will be used to transform the model to an equivalent two-degree-of-freedom discrete nonlinear system of the type shown in Fig. 1.

Let the deflection shape $W_1(z,t)$ of the striker beam and $W_2(z,t)$ of the target beam, when the beams are not in contact, be represented by

$$W_1(z,t) = \phi_1(z)x_1(t) \tag{21}$$

and

$$W_2(z,t) = \phi_2(z)x_2(t) \tag{22}$$

where $\phi_j(t)$ and $x_j(t)$, $j=1, 2$, are the fundamental mode shapes and the corresponding generalized coordinates for the striker and target beams, respectively. For systems of the type shown in Fig. 6 containing both discrete and distributed parameters, and subjected to uniform base excitation $\ddot{S}_0(t)$, the generalized properties are

$$m_j^* = \int_0^{l_j} \mu_j(z)\phi_j^2(z)dz + \sum_k m_{jk}\phi_j^2(z_k) \tag{23}$$

$$c_j^* = \int_0^{l_j} c_j(z)\phi_j^2(z)dz, \tag{24}$$

$$k_j^* = \int_0^{l_j} E_jI_j(z)[\phi_j''(z)]^2dz, \tag{25}$$

$$p_j^*(z,t) = \int_0^{l_j} p_j(z,t)\phi_j(z)dz, \tag{26}$$

$$f_j^* = -\left(\int_0^{l_j} \mu_j(z)\phi_j^2(z)dz + \sum_k m_{jk}\phi_j^2(z_k)\right)\ddot{S}_0(t) = -\Gamma_j\ddot{S}_0(t) \tag{27}$$

where

l_j = length of beam j,
$\mu_j(z)$ = mass/unit length of beam j,
$c_j(z)$ = viscous damping/unit length of beam j,
$p_j(z,t)$ = distributed load on beam j,
$\phi_j''(z)$ = curvature of Bernoulli-Euler beam j,
Γ_j = mass participation factor for beam j,
ζ_j^* = fraction of critical damping in the fundamental mode of beam j,
$[EI(z)]_j$ = flexural stiffness of beam j,
$\ddot{S}_0(t)$ = base acceleration of the harmonically excited beams, $-S_0\Omega^2 \exp(i\Omega t)$.

Using the above listed relationships, the motion of each

Downloaded 03 May 2010 to 171.66.16.27. Redistribution subject to ASME license or copyright; see http://www.asme.org/terms/Terms_Use.cfm

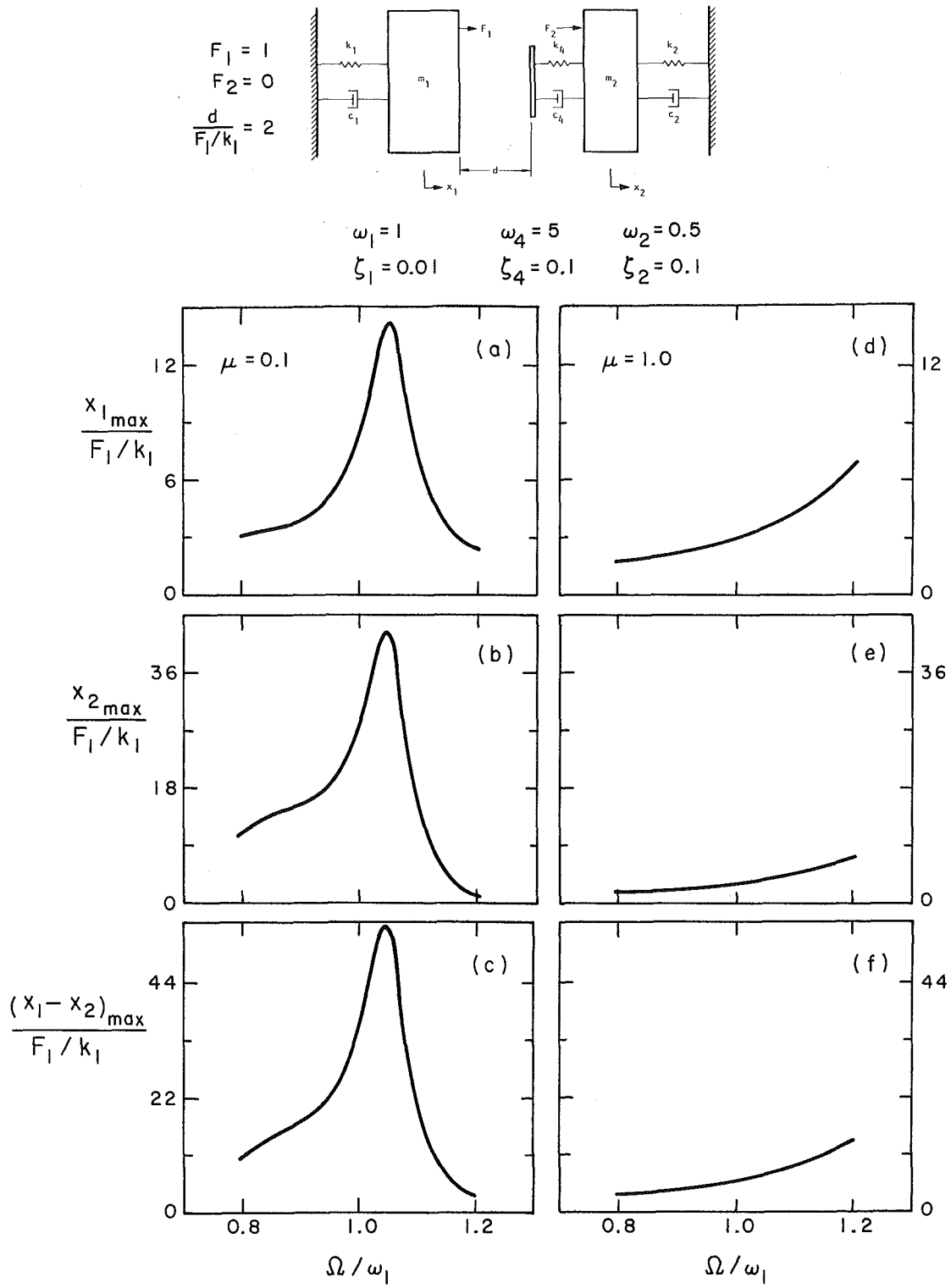


Fig. 8 Influence of the mass ratio μ on the transfer functions of the nonlinear system in Fig. 1

beam is governed during the noncontact phase of their motion by

$$m_j^* \ddot{x}_j + c_j^* \dot{x}_j + k_j^* x_j = -\Gamma_j \ddot{S}_0(t) = S_0 \Omega^2 \Gamma_j \exp(i\Omega t) \qquad (28)$$

Applying the results of the present analysis to the experiment under discussion yields the comparison shown in Fig. 7 for the transfer function of the nonlinear system. Except for the higher frequency beam modes that are not accounted for in the mathematical model in this paper, the predicted and measured response time history under steady state conditions were in good agreement (comparable in accuracy to the frequency response plots).

The difference shown in Fig. 7 between the response of the system with increasing and decreasing excitation frequency is

Downloaded 03 May 2010 to 171.66.16.27. Redistribution subject to ASME license or copyright; see http://www.asme.org/terms/Terms_Use.cfm

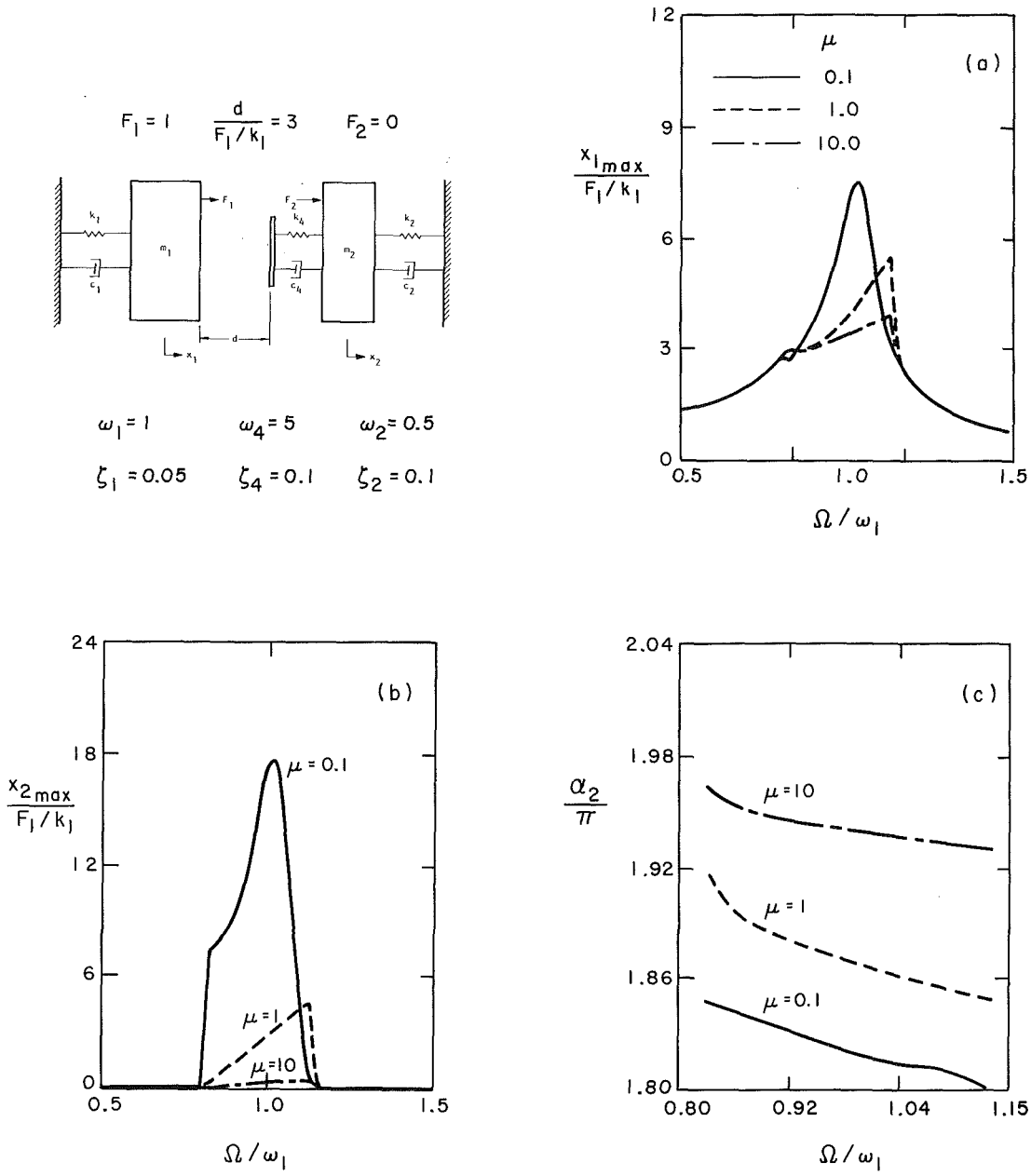


Fig. 9 Effects of the mass ratio μ on the frequency response of the nonlinear system in Fig. 1. (a) x_{1max}; (b) x_{2max}; (c) contact parameter α_2.

attributed to the jump phenomenon associated with the backbone curve related to the frequency response of the nonlinear Duffing (hardening) oscillator (Caughey, 1954).

5 Effects of System Parameters

It is of interest to note the multivalued nature of the experimentally determined frequency response curve shown in Fig. 7. This phenonmenon is evident in all the experimental results where the striker beam maintains impact with its target beam even if the increasing frequency Ω results in a linear (unconstrained) peak response $A(\Omega)$ which is less than d (i.e., insufficient to cause contact between the two beams). On the other hand, for decreasing frequency values, impacts will not be sustained until $\Omega < \Omega^*$ for which $A(\Omega) > d$.

This type of behavior (existence of multivalued response) is characteristic of systems with hardening or softening nonlinearites. This jump phenomenon (or hysteresis phenomenon), where the system response jumps abruptly from one branch of the amplification curve to another, is exhibited by systems governed, for example, by the well-known Duffing's equation (Nayfeh, 1980):

$$\ddot{x} + c\dot{x} + (ax + bx^3) = F\cos\Omega t. \tag{29}$$

Note that, due to the nature of the physical and mathematical model under consideration, the restoring forces acting on the primary system in the nonlinear range are always greater than those in the linear range. Consequently, the nonlinearity present in the system under discussion is of the hardening type.

The analytical solution predicted, and the experimental studies verified, the existence of steady-state solutions associated with the stable regions of the backbone curves of this system with a hardening nonlinearity. Some nonperiodic oscillations were observed during the experiment that may be chaotic, but further studies would have to be done to deter-

Downloaded 03 May 2010 to 171.66.16.27. Redistribution subject to ASME license or copyright; see http://www.asme.org/terms/Terms_Use.cfm

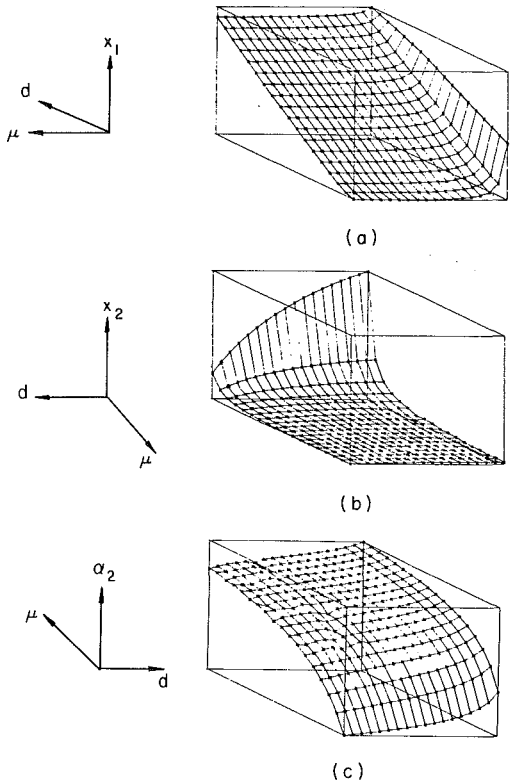


Fig. 10 A three-dimensional representation of the influence of the mass ratio μ and the gap size d on the steady-motion of the nonlinear system in Fig. 1 with a typical set of parameters. (a) x_{1max}; (b) x_{2max}; (c) contact parameter α_2.

mine if they are chaotic. The focus of the present study is periodic oscillations. However, it is worth noting that in nonlinear systems in general, and the class of strange attractor (Holmes, 1979; Moon and Holmes, 1979; Shaw 1985) in particular, periodic forcing inputs do not always lead to periodic solutions; nonperiodic, bounded, chaotic motions can occur under periodic excitation (Ueda, 1979).

The results shown in Fig. 8 indicate the influence of the mass ratio μ on the transfer functions of the nonlinear system shown in Fig. 1. The plots in Figs. 8(*a*), (*b*), and (*c*) correspond to a case where $\mu = 0.1$ while the plots in Figs. 8(*d*), (*e*), and (*f*) correspond to a case where μ is increased by an order of magnitude to 1.0. The dimensionless excitation frequency (Ω/ω_1) values covered, span a range of $\pm$ 0.20 around resonance. For ease of comparison, like quantities in the two columns of Fig. 8 are plotted to the same scale. Note that μ has a significant influence on the peak values of the absolute as well as relative motion.

The influence of μ is further clarified in the frequency response curves shown in Fig. 9 where three mass ratios are considered: $\mu = 0.1$, 1.0, and 10. Notice from Figs. 9(*a*) and (*b*) that steady-state motion with impacts occur in the range $0.82 \leq \Omega/\omega_1 \leq 1.18$. Outside this range no contact occurs between m_1 and m_2; each mass behaves as a linear SDOF system. Since m_1 is subjected to a harmonic force of magnitude F_1, its transfer function in the range of $0.82 \geq \Omega/\omega_1 \geq 1.18$ matches that of a linear oscillator. On the other hand, since m_2 in this example is not subjected to a direct driving force F_2, it does not oscillate when not contacted by m_1 (see Fig. 9(*b*).

The influence of μ on the solution parameter α_2 which governs the contact time is shown in Fig. 9(*c*). The interaction between the gap size d, the mass ratio μ, and the amplitude of x_1 and x_2 as well as α_2 is illustrated in a three-dimensional form in Fig. 10.

The results shown in Fig. 11 indicate the effects of damping parameter ζ_1 on the system shown in Fig. 9 when the mass ratio μ is 10. Notice that, if $m_2 >> m_1$, the frequency response characteristics shown in Fig. 11 are insensitive to the extent of damping in the primary system m_1.

When the general mathematical model in Fig. 3 is configured in a form corresponding to the physical model shown in Fig. 4 (i.e., coupling element g_3 missing), the effects of the key system parameters can be summarized as follows:

(1) *Mass ratio,* μ. In general, for a given set of parameters, as μ increases (i.e., as m_2 becomes more massive) the magnitude of the approach (maximum relative motion y) as well as the peak displacements of m_1 and m_2 are decreased. Also, as μ increases, the contact phase of the motion is reduced (i.e., α_2 increases). Figures 10(*a,b,c*) illustrate three-dimensional representations of the variation of some measures of the system response with the mass ratio and gap size for a typical set of parameters.

(2) *Gap size,* d. In general, the peak response of the primary system will be equal to that of an unconstrained single-degree-of-freedom system (i.e., $x_{1max} = A$) as long as $A(\Omega) < d$; otherwise, x_{1max} will depend on the snubber mass ratio and on the stiffness ratio of the nonlinear spring. In response regions where jump phenomena appear, a nonlinear response can exit even for $A(\Omega) < d$.

(3) *Stiffness ratio* ω_2/ω_1, *and* ω_4/ω_1. Both of these ratios control the duration of contact of the primary mass m_1 with the elastic stop attached to m_2, and the amount of penetration of m_1 in the nonlinear range. With increasing stiffness, both the duration of contact and the maximum penetration are decreased.

(4) *Damping ratios* ζ_1, ζ_2, *and* ζ_4. The primary system ratio of critical damping ζ_1 controls the bandwidth of the system, and hence the frequency at which impacts start (or stop) occuring. Damping parameters ζ_2 and ζ_4, which account for the mechanical energy lost during hte "impact" phase of the motion, control the amount of momentum transfer and hence the effective coefficient of restitution associated with the impact process.

As a further illustration of the application of the exact solution under discussion, consider the nonlinear model shown in Fig. 2 which represents a vibration control problem. Treating the mass m_1 in Fig. 2 as a primary system whose steady-state oscillations are to be controlled by the action of an auxiliary mass damper consisting of a mass m_2 with an unsymmetric motion-limiting stop, the frequency response characteristics indicated in Fig. 12 are obtained. For ease of comparison, like quantities in the two columns of Fig. 12 are plotted to the same scale.

The left-hand-side (LHS) column in Fig. 12 corresponds to a case where the coupling spring k_3 is relatively soft, resulting in a frequency ratio of $\omega_3/\omega_1 = 0.5$ and the stiffness of the resilient stop results in $\omega_4/\omega_1 = 5$. If all parameters are kept constant except for the coupling spring k_3 which is made stiffer so as to change ω_3/ω_1 to 1.0, the response curves shown on the RHS of Fig. 12 are obtained.

6 Summary and Conclusions

An "exact" closed-form analytical solution is derived for the steady-state motion under harmonic excitation of a two-degree-of-freedom (2DOF) lumped-parameter system incorporating an element with a geometric nonlinearity which is encounterd in many practical engineering applications.

Experimental studies with a mechanical model having distributed properties and consisting of a beam/target system were performed to verify the validity of the analytical solution

Downloaded 03 May 2010 to 171.66.16.27. Redistribution subject to ASME license or copyright; see http://www.asme.org/terms/Terms_Use.cfm

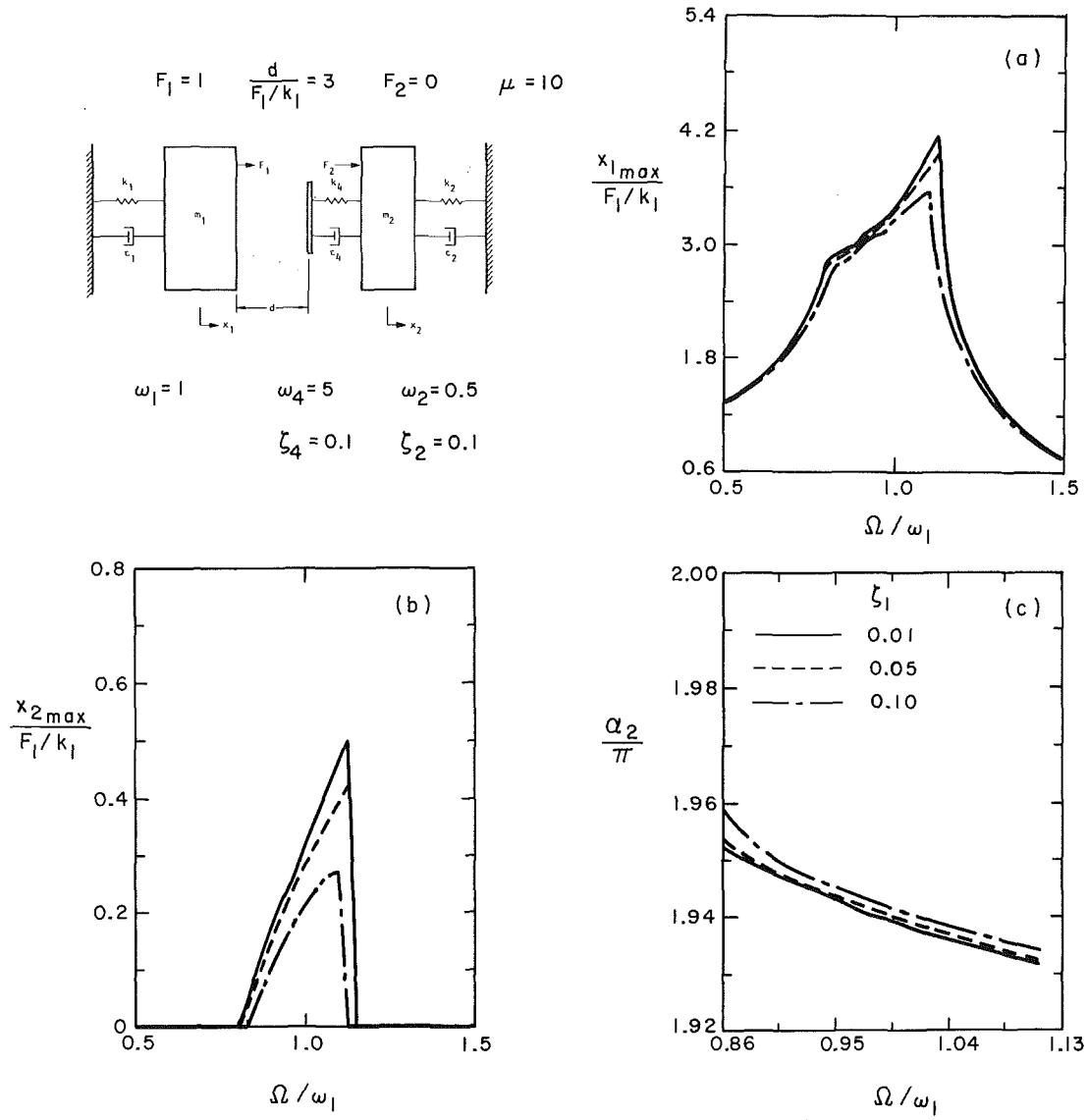


Fig. 11 Effects of the damping ζ_1 in the primary system on the frequency response of the nonlinear system in Fig 1. (a) x_{1max}; (b) x_{2max}; (c) α_2.

and also to investigate the effects of system parameters. By using the generalized coordinate approach to transform the distributed model to an equivalent nonlinear 2DOF system, good agreement was achieved between the theoretical and experimental results.

Acknowledgment

This study was supported in part by a grant from the National Science Foundation.

References

Caughey, T. K., 1954, "The Existence and Stability of Ultraharmonics and Subharmonics in Forced Nonlinear Oscillations," ASME JOURNAL OF APPLIED MECHANICS, Vol. 21, pp. 327–335.

Holmes, P. J., 1979, "A Nonlinear Oscillator With a Strange Attractor," *Philosophical Transactions of the Royal Society*, London, Vol. 292, No. 1394, pp. 419–448.

Jones, D. I. G., and Muszynska, A., 1979, "Harmonic Response of a Damped Two-Degree of Freedom System with Gaps," *Nonlinear Vibration Problems*.

Klotter, K., 1953, "Steady State Vibrations in Systems Having Arbitrary Restoring and Aribtrary Damping Forces," *Proc. Symposium on Nonlinear Circuit Analysis*, Polytechnic Institute of Brooklyn, pp. 234–245.

Lo, C. C., 1985, "A Cantilever Beam Chattering Against a Stop," *Journal of Sound and Vibration*, Vol. 69, No. 2, pp. 245–255.

Masri, S. F., Mariamy, Y. A., Anderson, J. C., 1981, "Dynamic Reponse of a Beam With a Geometric Nonlinearity," ASME JOURNAL OF APPLIED MECHANICS, Vol. 48, pp. 404–410.

Moon, F. C., and Holmes, P. J., 1979, "A Magnetoleastic Strange Attractor," *Journal of Sound and Vibration*, Vol. 65, No. 2, pp. 275–296.

Moon, F., and Shaw, S., 1983, "Chaotic Vibrations of a Beam with Nonlinear Boundary Conditions," *Int. Jrl, Nonlinear Mechanics*, Vol. 18, No. 6, pp. 465–477.

Nayfeh, A. H., and Mook, D. T., 1979, *Nonlinear Oscillations*, Wiley, New York.

Shaw, S., 1985, "Forced Vibrations of a Beam with One-Sided Amplitude Constraint—Theory and Experiments," *Journal of Sound and Vibrations*, Vol. 99, No. 2, pp. 199–212.

Shaw, S. W., "The Dynamics of a Harmonically Exited System Having Rigid Amplitude Constraints," to be published in ASME JOURNAL OF APPLIED MECHANICS.

Ueda, Y., 1979, "Randomly Transitional Phenomena in the System Governed by Duffing's Equation," *Journal of Statistical Physics*, Vol. 20, No. 2, pp. 181–196.

Watanabe, T., 1978, "Forced Vibration of Continuous System with Nonlinear Boundary Conditions," *ASME Journal of Mechanical Design*, Vol. 100, p. 487.

APPENDIX

Definition of Symbols

$$\omega_1 = (k_1/m_1)^{1/2} \qquad \omega_2 = (k_2/m_2)^{1/2}$$

Downloaded 03 May 2010 to 171.66.16.27. Redistribution subject to ASME license or copyright; see http://www.asme.org/terms/Terms_Use.cfm

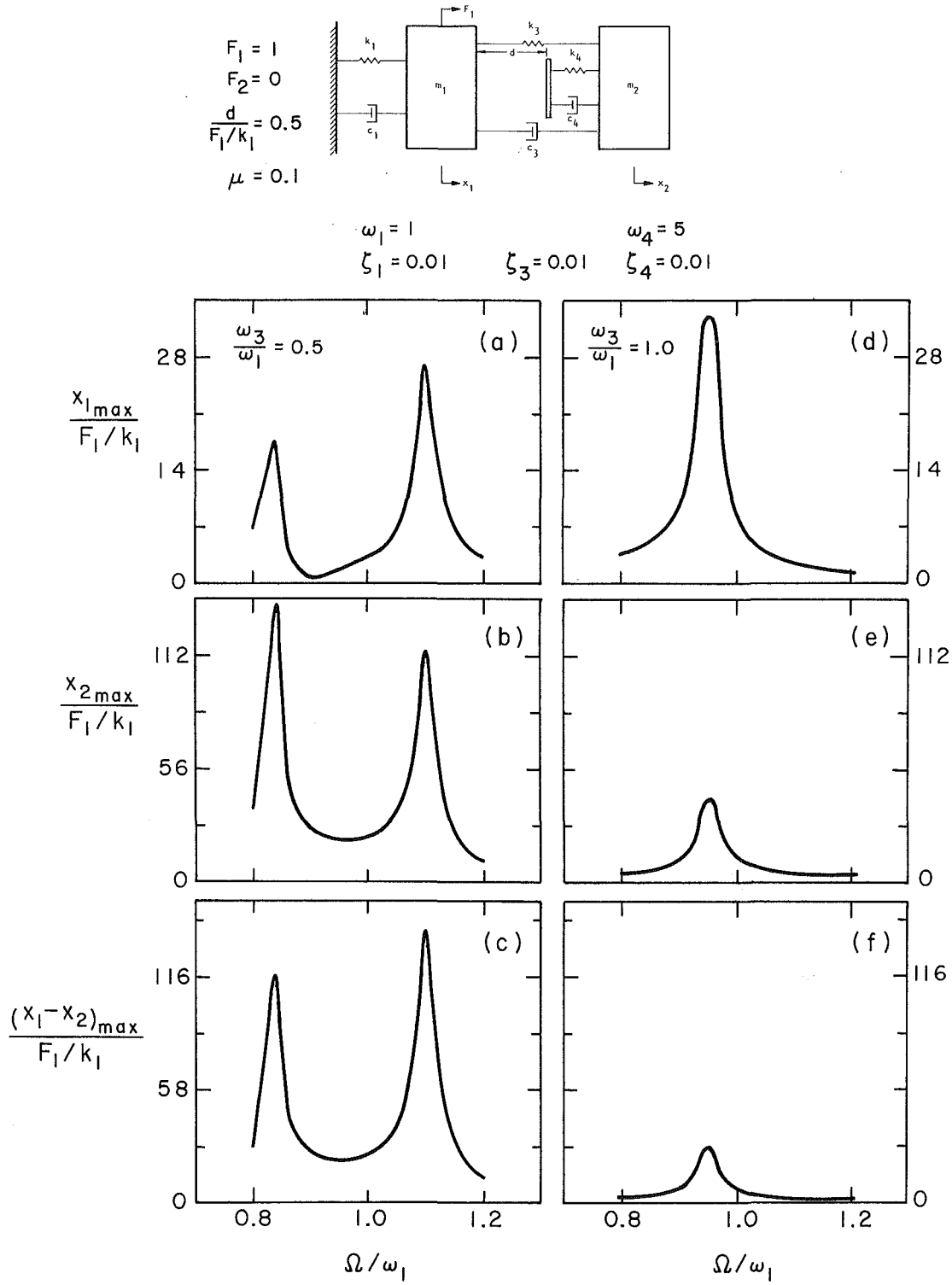


Fig. 12 Effects of the mass ratio μ on the transfer functions of the nonlinear system shown in Fig. 2

$\omega_3 = (k_3/m_1)^{1/2}$ $\quad \omega_4 = (k_4/m_2)^{1/2}$

$\zeta_1 = 0.5\ c_1(k_1 m_1)^{-1/2}$ $\quad \zeta_2 = 0.5\ c_2(k_2 m_2)^{-1/2}$

$\zeta_3 = 0.5\ c_3(k_3 m_1)^{-1/2}$ $\quad \zeta_4 = 0.5\ c_4(k_4 m_2)^{-1/2}$

$\mu = m_2/m_1$ $\quad y = x_1 - x_2$

$\alpha_i = \Omega t_j$ $\quad T = 2\pi/\Omega$

$T_c = [1 - \alpha_2/(2\pi)]T$ $\quad \delta = (y_{\max}/d - 1)$

s_{jn}, $j = 1,2,3,4$ are the roots of the characteristic equation

$$\begin{vmatrix} a_{11_n}s_n^2 + b_{11_n}s_n + c_{11_n} & b_{12_n}s_n + c_{12_n} \\ b_{12_n}s_n + c_{12_n} & a_{22_n}s_n^2 + b_{22_n}s_n + c_{22_n} \end{vmatrix}$$

$\sigma_n \equiv \text{col.}\{A_{1n}, i\Omega A_{1n}, A_{2n}, i\Omega A_{2n}\}$

$\beta_n \equiv \text{col.}\{x_{1s_n}, 0, x_{2s_n}, 0\}$

Downloaded 03 May 2010 to 171.66.16.27. Redistribution subject to ASME license or copyright; see http://www.asme.org/terms/Terms_Use.cfm

$$A_{1n} = (1/D_1)\exp(-i\alpha_0) \quad \begin{vmatrix} F_1 \exp(i\alpha_0) & i\Omega b_{12_n} + c_{12_n} \\ F_2 \exp(i\alpha_0) & -\Omega^2 a_{22_n} + i\Omega b_{22_n} + c_{22_n} \end{vmatrix}$$

$$A_{2n} = (1/D_1)\exp(-i\alpha_0) \quad \begin{vmatrix} -\Omega^2 a_{11_n} + i\Omega b_{11_n} + c_{11_n} & F_1 \exp(i\alpha_o) \\ i\alpha b_{12_n} + c_{12_n} & F_2 \exp(i\alpha_0) \end{vmatrix}$$

$$D_1 = \begin{vmatrix} -\Omega^2 a_{11_n} + i\Omega b_{11_n} + c_{11_n} & i\Omega b_{12_n} + c_{12_n} \\ i\Omega b_{12_n} + c_{12_n} & -\Omega^2 a_{22_n} + i\Omega b_{22_n} + c_{22_n} \end{vmatrix}$$

$$x_{1s_1} = 0, \qquad x_{1s_2} = +k_4 d(c_{22_2} + c_{12_2})/D_2$$

$$x_{2s_1} = 0, \qquad x_{2s_2} = -k_4 d(c_{11_2} + c_{12_2})/D_2$$

$$D_2 = c_{11_2} c_{22_2} - c_{12}^2, \; i = (-1)^{1/2}$$

$$\lambda_n \equiv \text{col.}\{\lambda_{11_n}, \mu_{21_n}, \lambda_{31_n}, \lambda_{41_n}\}$$

$$e_n(t) \equiv \text{col.}\{\exp[1/\Omega s_{1n}(\Omega t - \alpha_n)], \exp[1/\Omega s_{2n}(\Omega t - \alpha_n)], \exp[1/\Omega s_{3n}(\Omega t - \alpha_n)], \exp[1/\Omega s_{4n}(\Omega t - \alpha_n)]\}$$

$$[S]_n = \text{diag.}[s_{1n}, s_{2n}, s_{3n}, s_{4n}]$$

$$[R]_n = \text{diag.}[r_{1n}, r_{2n}, r_{3n}, r_{4n}]$$

$$\frac{\lambda_{j1_n}}{\lambda_{j2_n}} = -\frac{b_{12_n} s_j + c_{12_n}}{a_{11_n} s_j^2 + b_{11_n} s_j + c_{11_n}} = -\frac{a_{22_n} s_j^2 + b_{22_n} s_j + c_{22_n}}{b_{12_n} s_j + c_{12_n}} \equiv r_{jn}$$

$$[N]_n \equiv M_n(\alpha_{n+1}) M_n^{-1}(\alpha_n) \quad [G]_n \equiv [\mathbf{g}_n^{(1)}, \mathbf{g}_n^{(2)}]$$

$$g_n^{(1)} \equiv \text{col.}\{-[N]_n \text{Re}(\sigma_n e^{i\alpha_n}) + \text{Re}(\sigma_n e^{i\alpha_{n+1}})\}$$

$$g_n^{(2)} \equiv \text{col.}\{[N]_n Im(\sigma_n e^{i\alpha_n}) - Im(\sigma_n e^{i\alpha_{n+1}})\}$$

$$\gamma_n \equiv ([I] - [N]_n)\beta_n \qquad [I] = \text{identity matrix}$$

$$[G4] \equiv ([N]_2[N]_1 - [I])^{-1}([N]_2[G]_1 + [G]_2)$$

$$[G3] \equiv ([N]_1[N]_2 - [I])^{-1}([N]_1[G]_2 + [G]_1)$$

$$\mathbf{J1} \equiv ([N]_2[N]_1 - [I])^{-1}\gamma_2$$

$$\mathbf{J2} \equiv ([N]_1[N]_2 - [I])^{-1}[N]_1\gamma_2$$

$$(G4_{12} - G4_{32})\sin\alpha_0 + (G4_{11} - G4_{31})\cos\alpha_0 = -d + (J1_{31} - J1_{11})$$

$$(G3_{12} - G3_{32})\sin\alpha_0 + (G3_{11} - G3_{31})\cos\alpha_0 = -d + (J2_{31} - J2_{11})$$

Downloaded 03 May 2010 to 171.66.16.27. Redistribution subject to ASME license or copyright; see http://www.asme.org/terms/Terms_Use.cfm

Journal of Applied Mechanics

Brief Notes

A Brief Note is a short paper that presents a specific solution of technical interest in mechanics but which does not necessarily contain new general methods or results. A Brief Note should not exceed 1500 words *or equivalent* (a typical one-column figure or table is equivalent to 250 words; a one line equation to 30 words). Brief Notes will be subject to the usual review procedures prior to publication. After approval such Notes will be published as soon as possible. The Notes should be submitted to the Technical Editor of the JOURNAL OF APPLIED MECHANICS. Discussions on the Brief Notes should be addressed to the Editorial Department, ASME, United Engineering Center, 345 East 47th Street, New York, N. Y. 10017, or to the Technical Editor of the JOURNAL OF APPLIED MECHANICS. Discussions on Brief Notes appearing in this issue will be accepted until two months after publication. Readers who need more time to prepare a Discussion should request an extension of the deadline from the Editorial Department.

Torsion of an Elasto-Plastic Bar Via a Dislocation Method

D. A. Sotiropoulos[1] and T. Mura[1,2]

Introduction

Calculations of the elastic field caused by dislocations have been the subject of research in many areas such as seismology, materials science, and mechanics. A large number of studies considered dislocations to explain the mechanism of plastic deformation (Nabarro, 1967). The static torsion of an elasto-plastic bar in terms of dislocations has been studied by Bilby, Gardner, and Smith (1958) and by Mura (1970). Of all the possible distributions of dislocations, the distribution of screw dislocations used by Mura (1970) to solve the torsion problem seems to be the simplest one. It was assumed that the plastic zone is infinitesimal. It was subsequently shown that the sum of the dislocation stress and the linear torsion stress gives the elasto-plastic stress field. In the present study, a similar approach is employed. The straight screw dislocations are parallel to the axis of the cylinder and distributed in the annular plastic zone. However, the strength of the dislocations is not constant in the radial direction—the appropriate dependence is established—which allows the solution to be valid for a finite plastic zone.

Method of Solution

Consider a cylindrical elasto-plastic bar with a circular cross section of radius h, twisted by a constant moment M at its ends. The annular domain $c < r < h$ is in a perfectly plastic state with a yield shear stress k. It will be shown that the total stress is the sum of a dislocation stress and the applied elastic stress Mr/J ($J = \pi h^4/2$). The dislocation is made up of a continuous distribution of screw dislocations parallel to the axis of the bar (z axis) and of strength $b(r)$ in the domain $c < r < h$. Mura (1970) used this approach with $b(r)$ = constant, and his result is valid for $c \approx r \approx h$.

It is known that when the screw dislocations are distributed uniformly along a circle with radius R in an unbounded elastic material, the only nonzero dislocation stress is

$$\sigma_{\theta z} = -\frac{\mu b(R) R}{r} \quad \text{for } r > R$$
$$= 0 \quad \text{for } r < R \tag{1}$$

where μ is the shear modulus of the material.

This solution for the unbounded material can also be used for a solid cylinder since the boundary conditions at $r = h$ can be satisfied.

When the screw dislocations are distributed according to a function $b(R)$ in the domain $c < r < h$ of a solid cylinder with radius h, the stress is obtained as

$$\sigma_{\theta z} = -\frac{\mu}{r}\int_c^r b(R) R dR \quad \text{for } c \le r \le h$$
$$= 0 \quad \text{for } r \le c \tag{2}$$

If this cylindrical bar is free from tractions at the ends $z = \pm\infty$, the linear stress $\sigma_{\theta z} = M_o r/J$ must be superimposed so that the total twisting moment disappears, where

$$M_o = 2\pi\mu\int_c^h \left[r\int_c^r b(R) R dR\right] dr \tag{3}$$

When the elasto-plastic bar is twisted by the moment M and the annular domain $c < r < h$ is in a perfectly plastic state with the yield shear stress k, the total shear stress must be equal to k, that is,

$$-\frac{\mu}{r}\int_c^r b(R) R dR + \frac{M_o r}{J} + \frac{Mr}{J} = k \quad \text{for } c \le r \le h \tag{4}$$

To satisfy the above condition, the dislocation stress has to be linear, that is,

$$\frac{1}{r}\int_c^r b(R) R dR = A(r - c) \tag{5}$$

where A is a constant associated with the strength of the dislocations. Differentiation of equation (5) with respect to r gives

$$b(r) = A\left(2 - \frac{c}{r}\right) \tag{6}$$

With this, equation (4) becomes

$$-\mu A(r - c) + \frac{M_o r}{J} + \frac{Mr}{J} = k \quad \text{for } c \le r \le h \tag{7}$$

where M_o is (by substitution of equation (6) in equation (3))

[1]Department of Civil Engineering, The Technological Institute, Northwestern University, Evanston, Ill. 60201.
[2]Fellow ASME.

Manuscript received by ASME Applied Mechanics Division, February 24, 1986; final revision, September 10, 1986.

Copyright © 1987 by ASME
Downloaded 03 May 2010 to 171.66.16.27. Redistribution subject to ASME license or copyright; see http://www.asme.org/terms/Terms_Use.cfm

$$M_o = 2\pi\,\mu A\left(\frac{h^4}{4} - \frac{h^3 c}{3} + \frac{c^4}{12}\right) \tag{8}$$

Condition (7) is satisfied when

$$\begin{aligned} M_o + M &= J\,\mu\,A \\ \mu\,A\,c &= k \end{aligned} \tag{9}$$

From this, the twisting moment M, which causes the plastic state, it obtained as

$$M = \frac{\pi k(4h^3 - c^3)}{6} \tag{10}$$

which agrees with the classical value. It has therefore been established that the elasto-plastic stress field is given by the sum of the dislocation stress and the linear torsion stress. It has also been shown that the strength of the screw dislocations has to satisfy equation (6) in order for the dislocation stress to be linear in the finite domain $c \le r \le h$.

References

Bilby, B. A., Gardner, L. R. T., and Smith, E., 1958, *Acta Met.*, 6, pp. 29–33.

Mura, T., 1970, "Individual Dislocations and Continuum Mechanics," *Inelastic Behavior of Solids*, Kanninen, M. F., Adler, W. F., Rosenfield, A. R., and Jaffee, R. I., eds., McGraw-Hill, New York, pp. 211–230.

Nabarro, F. R. N., 1967, *Theory of Crystal Dislocations*, Oxford, England.

Energy Release Rate in an Idealized Nonlinear DCB Specimen

L. F. Mannion[3]

Introduction

A simple model for fiber-reinforced materials, known as the idealized theory, has been developed to analyze highly anisotropic materials while avoiding use of the Airy function; this theory is described by Pipkin (1979). The dynamic fracture of a double cantilever beam (DCB) specimen of idealized material was discussed by Mannion (1985); a kinematically identical model was presented by Freund (1977). In the references above, the shearing response is linear elastic. The present note concerns the energy release rate for a case of nonlinear shear. Fracture with nonlinear material behavior was discussed by Sih and Macdonald (1974) using essentially the Bernouilli bending theory; here, the deformation is shear rather than bending. In what follows, the problem is described, the energy release rate is calculated and is then applied to actually find the crack speed in a simple example.

Problem Formulation

A beam of length L and height $2h$ in plane stress contains a center-line crack of time-dependent length $l(t)$. The material contains two orthogonal families of straight, continuously distributed inextensible fibers parallel to the axes of a system of Cartesian coordinates (x, y). The origin is at the middle of the left-hand end and the crack is $0 < x < l(t)$, $y = 0$. The beam arms are given equal and opposite displacements at $x = 0$. The end $x = L$ is fixed so that by symmetry and inextensibility the only nonzero displacement component is $v(x, t)$ in the y direction, for $0 < x < l(t)$.

For convenient notation, the small-strain component and the velocity at a cross section are denoted, respectively, by

$$e(x,t) = v_{,x}(x,t),\ s(x,t) = v_{,t}(x,t), \tag{1}$$

where a comma followed by a subscript denotes a partial derivative. Compatibility of derivatives requires

$$e_{,t} = s_{,x}. \tag{2}$$

The stress-strain law to be used is of power-law type, giving the shear stress σ as

$$\sigma(e) = \mu|e|^{n-1}e,\ \mu, n > 0. \tag{3}$$

The form of σ in equation (3) guarantees real stress for both positive and negative shear. The relevant momentum equation is

$$\rho s_{,t} = \sigma_{,x} = \mu(|e|^{n-1}e)_{,x} \tag{4}$$

Energy Release Rate

Energy balance during fracture may be written as

$$P = \dot{T} + \dot{W} + \mathcal{F},\ (\dot{}) = d/dt, \tag{5}$$

where W and T are, respectively, the total strain and kinetic energy of the beam, P is the rate of work on the beam arms at $x = 0$ and $\mathcal{F}$ is the time rate of energy flow into the crack tip, all quantities per unit thickness. Since the energy release rate $\mathcal{G}$ is energy per unit length of new crack, we have

$$\mathcal{F} = \mathcal{G}\dot{l}. \tag{6}$$

Using equation (3), P may be written as

$$P = -2\mu h|e(0,t)|^{n-1}e(0,t)s(0,t). \tag{7}$$

The strain energy W in both beam arms is

$$W = 2\int_A \int_0^e \sigma(e)\,de\,dA = [2\mu h/(n+1)]\int_0^l |e(x,t)|^{n+1}dx, \tag{8}$$

where A is $0 < x < l(t)$, $0 < y < h$. The total kinetic energy is

$$T = \rho h\int_0^l s^2(x,t)dx. \tag{9}$$

Note that $v(l(t), t) = 0$ by symmetry; a time-derivative gives

$$e(l,t)\dot{l} + s(l,t) = 0. \tag{10}$$

Differentiating the integrals in equations (8) and (9) and using equation (10) gives

$$\dot{T} + \dot{W} = [2\mu h/(n+1)]|e(l,t)|^{n+1}\dot{l} + \rho h s^2(l,t)\dot{l} + 2h\int_0^l [\mu|e(x,t)|^{n-1}ee_{,t} + \rho s s_{,t}]dx \tag{11}$$

If equations (2) and (4) are used, the integrand in equation (11) can be written as $(\mu|e|^{n-1}es)_{,x}$; integrating, using equation (10) again and recalling equation (7) gives

$$\dot{T} + \dot{W} = h\dot{l}[\rho s^2(l,t) - (2\mu n/(n+1))|e(l,t)|^{n+1}] + P. \tag{12}$$

By comparing equations (5) and (12), $\mathcal{F}$ is obtained and then equation (6) shows that $\mathcal{G}$ is

$$\mathcal{G} = [2\mu n h/(n+1)]|e(l,t)|^{n+1} - \rho h e^2(l,t)\dot{l}^2 \tag{13}$$

As a check on the result in equation (13), let $n = 1$ in equation (3) so that the material is linear. The expression in equation (13) reduces to

$$\mathcal{G} = \mu h(1 - \dot{l}^2/c^2)e^2(l,t), \tag{14}$$

where $c = (\mu/\rho)^{1/2}$ is the usual linear elastic shear wave speed; the expression in equation (14) is that obtained directly in the linear case by Freund (1977).

Application-Wedging at Constant Speed

Consider the case where the ends at $x = 0$ are moved apart at a constant speed V, so that $v(0, t) = Vt$, and a crack begins to run from the end $x = 0$. If the crack moves at a constant

[3]Department of Mathematics and Computer Science, St. John's University, Jamaica, NY 11439.

Manuscript received by ASME Applied Mechanics Division, August 22, 1986.

Downloaded 03 May 2010 to 171.66.16.27. Redistribution subject to ASME license or copyright; see http://www.asme.org/terms/Terms_Use.cfm

$$M_o = 2\pi\ \mu A\left(\frac{h^4}{4} - \frac{h^3 c}{3} + \frac{c^4}{12}\right) \tag{8}$$

Condition (7) is satisfied when

$$\begin{aligned} M_o + M &= J\ \mu\ A \\ \mu\ A\ c &= k \end{aligned} \tag{9}$$

From this, the twisting moment M, which causes the plastic state, it obtained as

$$M = \frac{\pi k(4h^3 - c^3)}{6} \tag{10}$$

which agrees with the classical value. It has therefore been established that the elasto-plastic stress field is given by the sum of the dislocation stress and the linear torsion stress. It has also been shown that the strength of the screw dislocations has to satisfy equation (6) in order for the dislocation stress to be linear in the finite domain $c \le r \le h$.

References

Bilby, B. A., Gardner, L. R. T., and Smith, E., 1958, *Acta Met.*, 6, pp. 29–33.

Mura, T., 1970, "Individual Dislocations and Continuum Mechanics," *Inelastic Behavior of Solids*, Kanninen, M. F., Adler, W. F., Rosenfield, A. R., and Jaffee, R. I., eds., McGraw-Hill, New York, pp. 211–230.

Nabarro, F. R. N., 1967, *Theory of Crystal Dislocations*, Oxford, England.

Energy Release Rate in an Idealized Nonlinear DCB Specimen

L. F. Mannion[3]

Introduction

A simple model for fiber-reinforced materials, known as the idealized theory, has been developed to analyze highly anisotropic materials while avoiding use of the Airy function; this theory is described by Pipkin (1979). The dynamic fracture of a double cantilever beam (DCB) specimen of idealized material was discussed by Mannion (1985); a kinematically identical model was presented by Freund (1977). In the references above, the shearing response is linear elastic. The present note concerns the energy release rate for a case of nonlinear shear. Fracture with nonlinear material behavior was discussed by Sih and Macdonald (1974) using essentially the Bernouilli bending theory; here, the deformation is shear rather than bending. In what follows, the problem is described, the energy release rate is calculated and is then applied to actually find the crack speed in a simple example.

Problem Formulation

A beam of length L and height $2h$ in plane stress contains a center-line crack of time-dependent length $l(t)$. The material contains two orthogonal families of straight, continuously distributed inextensible fibers parallel to the axes of a system of Cartesian coordinates (x, y). The origin is at the middle of the left-hand end and the crack is $0 < x < l(t)$, $y = 0$. The beam arms are given equal and opposite displacements at $x = 0$. The end $x = L$ is fixed so that by symmetry and inextensibility the only nonzero displacement component is $v(x, t)$ in the y direction, for $0 < x < l(t)$.

For convenient notation, the small-strain component and the velocity at a cross section are denoted, respectively, by

$$e(x,t) = v_{,x}(x,t),\ s(x,t) = v_{,t}(x,t), \tag{1}$$

where a comma followed by a subscript denotes a partial derivative. Compatibility of derivatives requires

$$e_{,t} = s_{,x}. \tag{2}$$

The stress-strain law to be used is of power-law type, giving the shear stress σ as

$$\sigma(e) = \mu |e|^{n-1} e,\ \mu, n > 0. \tag{3}$$

The form of σ in equation (3) guarantees real stress for both positive and negative shear. The relevant momentum equation is

$$\rho s_{,t} = \sigma_{,x} = \mu(|e|^{n-1} e)_{,x} \tag{4}$$

Energy Release Rate

Energy balance during fracture may be written as

$$P = \dot{T} + \dot{W} + \mathfrak{F},\ (\dot{}) = d/dt, \tag{5}$$

where W and T are, respectively, the total strain and kinetic energy of the beam, P is the rate of work on the beam arms at $x = 0$ and $\mathfrak{F}$ is the time rate of energy flow into the crack tip, all quantities per unit thickness. Since the energy release rate $\mathcal{G}$ is energy per unit length of new crack, we have

$$\mathfrak{F} = \mathcal{G}\dot{l}. \tag{6}$$

Using equation (3), P may be written as

$$P = -2\mu h |e(0,t)|^{n-1} e(0,t) s(0,t). \tag{7}$$

The strain energy W in both beam arms is

$$W = 2\int_A \int_0^e \sigma(e)\, de\, dA = [2\mu h/(n+1)] \int_0^l |e(x,t)|^{n+1} dx, \tag{8}$$

where A is $0 < x < l(t)$, $0 < y < h$. The total kinetic energy is

$$T = \rho h \int_0^l s^2(x,t)\, dx. \tag{9}$$

Note that $v(l(t), t) = 0$ by symmetry; a time-derivative gives

$$e(l,t)\dot{l} + s(l,t) = 0. \tag{10}$$

Differentiating the integrals in equations (8) and (9) and using equation (10) gives

$$\dot{T} + \dot{W} = [2\mu h/(n+1)] |e(l,t)|^{n+1} \dot{l} + \rho h s^2(l,t)\dot{l} + 2h\int_0^l [\mu |e(x,t)|^{n-1} e e_{,t} + \rho s s_{,t}]\, dx \tag{11}$$

If equations (2) and (4) are used, the integrand in equation (11) can be written as $(\mu |e|^{n-1} e s)_{,x}$; integrating, using equation (10) again and recalling equation (7) gives

$$\dot{T} + \dot{W} = h\dot{l}[\rho s^2(l,t) - (2\mu n/(n+1))|e(l,t)|^{n+1}] + P. \tag{12}$$

By comparing equations (5) and (12), $\mathfrak{F}$ is obtained and then equation (6) shows that $\mathcal{G}$ is

$$\mathcal{G} = [2\mu n h/(n+1)] |e(l,t)|^{n+1} - \rho h e^2(l,t)\dot{l}^2 \tag{13}$$

As a check on the result in equation (13), let $n = 1$ in equation (3) so that the material is linear. The expression in equation (13) reduces to

$$\mathcal{G} = \mu h(1 - \dot{l}^2/c^2) e^2(l,t), \tag{14}$$

where $c = (\mu/\rho)^{1/2}$ is the usual linear elastic shear wave speed; the expression in equation (14) is that obtained directly in the linear case by Freund (1977).

Application-Wedging at Constant Speed

Consider the case where the ends at $x = 0$ are moved apart at a constant speed V, so that $v(0, t) = Vt$, and a crack begins to run from the end $x = 0$. If the crack moves at a constant

[3]Department of Mathematics and Computer Science, St. John's University, Jamaica, NY 11439.

Manuscript received by ASME Applied Mechanics Division, August 22, 1986.

Copyright © 1987 by ASME

Downloaded 03 May 2010 to 171.66.16.27. Redistribution subject to ASME license or copyright; see http://www.asme.org/terms/Terms_Use.cfm

speed U (to be determined), the displacement may be written as

$$v(x,t) = V(t - x/U),\ 0 < x < Ut. \tag{15}$$

From equation (15),

$$s(x,t) = V,\ e(x,t) = -V/U,\ 0 < x < Ut, \tag{16}$$

so that equation (4) is satisfied; also $v(Ut, t) = 0$, as required.

Let $\mathcal{G}_c$ be the critical value of $\mathcal{G}$ required for crack propagation. Setting $\mathcal{G} = \mathcal{G}_c$ in equation (13) while using equation (16), an algebraic equation for U is obtained which may be solved to give

$$U = V[2\mu nh/(n+1)(\mathcal{G}_c + \rho h V^2)]^{1/(n+1)}. \tag{17}$$

The fact that a constant crack speed is allowed by the fracture criterion justifies the form of $v(x, t)$ assumed in equation (15). The value of $\dot{l}$ in equation (17) is valid as long as the constant speed V is maintained at $x = 0$; in fact, equation (17) holds until such time as a stress wave carrying information about any change in $s(0, t)$ overtakes the moving crack tip.

References

Freund, L. B., 1977, "A Simple Model of the Double Cantilever Beam Crack Propagation Specimen," *Journal of Mechanics and Physics of Solids*, Vol. 25, pp. 69–79.

Mannion, L. F., 1985, "Dynamic Fracture of an Idealized Fiber-Reinforced Cantilever," ASME Journal of Applied Mechanics, Vol. 52, pp. 580–584.

Pipkin, A. C., 1979, "Stress Analysis for Fiber-Reinforced Materials," *Advances in Applied Mechanics*, Vol. 19, Academic Press, New York, pp. 1–51.

Sih, G. C., and Macdonald, B., 1974, "Effect of Material Nonlinearity on Crack Propagation," *International Journal of Engineering Science*, Vol. 12, pp. 61–77.

Dynamic Inelastic Response of Beams and Plates Under Combined Loading

S. S. Rao[4] and K. S. Raghavan[5]

Introduction

The analysis of beams and plates that carry axial loads is of practical importance. The influence of inplane loads is of greater significance when the loads are compressive. The dynamic inelastic behavior of beams and columns under axial loads is studied in this note. The analysis is based on the use of modified stiffness matrices which are functions of the inplane loads. The aim is to establish the effects of inelastic interactions between forces and displacements that are uncoupled in the small deformation elasticity theory.

For the plastic analysis of beams, the yield condition is taken as

$$|\sigma_x| > \sigma_o \tag{1}$$

for rate-independent behavior and

$$|\sigma_x| > \sigma_{YD} \tag{2}$$

for rate-sensitive behavior, where σ_x = bending stress, σ_o = yield stress, and σ_{YD} = dynamic yield stress given by

$$\sigma_{YD} = \sigma_o \left\{ 1 + \left(\frac{\dot{\epsilon}}{d} \right)^{1/n} \right\} \tag{3}$$

with $\dot{\epsilon} = \Delta\epsilon_x/\Delta t$ and d = rate sensitivity parameter. The plastic component $\Delta\epsilon_{xp}$ of the strain increment, $\Delta\epsilon_x$, is given by

$$\Delta\epsilon_{xp} = \left(1 - \frac{E_p}{E}\right)\Delta\epsilon_x \tag{4}$$

where E is the Young's modulus and E_p is the slope of the inelastic branch of the stress-strain curve [1]. The plastic work P_w of any section is given by

$$P_w = \int_o^h b(z) \cdot \sigma_o \Delta\epsilon_p \cdot dz \tag{5}$$

where $b(z)$ defines the width as a function of z. For plates, the von Mises yield criterion is used [2] and the incremental stress-strain relations are given by

$$d\vec{\sigma} = [D_{eq}]d\vec{\epsilon} \tag{6}$$

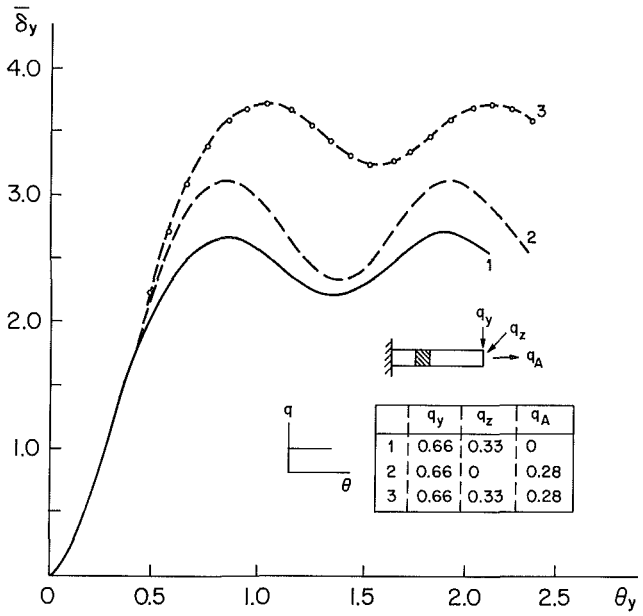


Fig. 1 Response of a cantilever in combined loading

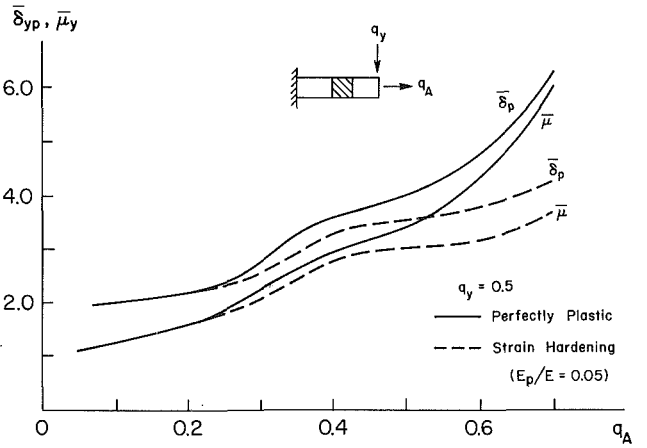


Fig. 2 Response characteristics for a cantilever beam in combined loading. (q_y and q_A are step loads. $\bar{\mu}$ = nondimensional mean displacement, $\bar{\delta}_p$ = nondimensional peak displacement. Subscript y denotes the direction.)

[4]School of Mechanical Engineering, Purdue University, West Lafayette, IN 47907.

[5]Bharat Heavy Electricals Ltd., Hyderabad, India.

Manuscript received by ASME Applied Mechanics Division, June 3, 1986; final revision, August 26, 1986.

Downloaded 03 May 2010 to 171.66.16.27. Redistribution subject to ASME license or copyright; see http://www.asme.org/terms/Terms_Use.cfm

speed U (to be determined), the displacement may be written as

$$v(x,t) = V(t - x/U),\ 0 < x < Ut. \tag{15}$$

From equation (15),

$$s(x,t) = V,\ e(x,t) = -V/U,\ 0 < x < Ut, \tag{16}$$

so that equation (4) is satisfied; also $v(Ut, t) = 0$, as required.

Let $\mathcal{G}_c$ be the critical value of $\mathcal{G}$ required for crack propagation. Setting $\mathcal{G} = \mathcal{G}_c$ in equation (13) while using equation (16), an algebraic equation for U is obtained which may be solved to give

$$U = V[2\mu nh/(n+1)(\mathcal{G}_c + \rho h V^2)]^{1/(n+1)}. \tag{17}$$

The fact that a constant crack speed is allowed by the fracture criterion justifies the form of $v(x, t)$ assumed in equation (15). The value of $\dot{l}$ in equation (17) is valid as long as the constant speed V is maintained at $x = 0$; in fact, equation (17) holds until such time as a stress wave carrying information about any change in $s(0, t)$ overtakes the moving crack tip.

References

Freund, L. B., 1977, "A Simple Model of the Double Cantilever Beam Crack Propagation Specimen," *Journal of Mechanics and Physics of Solids*, Vol. 25, pp. 69–79.

Mannion, L. F., 1985, "Dynamic Fracture of an Idealized Fiber-Reinforced Cantilever," ASME Journal of Applied Mechanics, Vol. 52, pp. 580–584.

Pipkin, A. C., 1979, "Stress Analysis for Fiber-Reinforced Materials," *Advances in Applied Mechanics*, Vol. 19, Academic Press, New York, pp. 1–51.

Sih, G. C., and Macdonald, B., 1974, "Effect of Material Nonlinearity on Crack Propagation," *International Journal of Engineering Science*, Vol. 12, pp. 61–77.

Dynamic Inelastic Response of Beams and Plates Under Combined Loading

S. S. Rao[4] and K. S. Raghavan[5]

Introduction

The analysis of beams and plates that carry axial loads is of practical importance. The influence of inplane loads is of greater significance when the loads are compressive. The dynamic inelastic behavior of beams and columns under axial loads is studied in this note. The analysis is based on the use of modified stiffness matrices which are functions of the inplane loads. The aim is to establish the effects of inelastic interactions between forces and displacements that are uncoupled in the small deformation elasticity theory.

For the plastic analysis of beams, the yield condition is taken as

$$|\sigma_x| > \sigma_o \tag{1}$$

for rate-independent behavior and

$$|\sigma_x| > \sigma_{YD} \tag{2}$$

for rate-sensitive behavior, where σ_x = bending stress, σ_o = yield stress, and σ_{YD} = dynamic yield stress given by

$$\sigma_{YD} = \sigma_o \left\{ 1 + \left(\frac{\dot{\epsilon}}{d} \right)^{1/n} \right\} \tag{3}$$

with $\dot{\epsilon} = \Delta\epsilon_x/\Delta t$ and d = rate sensitivity parameter. The plastic component $\Delta\epsilon_{xp}$ of the strain increment, $\Delta\epsilon_x$, is given by

$$\Delta\epsilon_{xp} = \left(1 - \frac{E_p}{E}\right)\Delta\epsilon_x \tag{4}$$

where E is the Young's modulus and E_p is the slope of the inelastic branch of the stress-strain curve [1]. The plastic work P_w of any section is given by

$$P_w = \int_o^h b(z) \cdot \sigma_o \Delta\epsilon_p \cdot dz \tag{5}$$

where $b(z)$ defines the width as a function of z. For plates, the von Mises yield criterion is used [2] and the incremental stress-strain relations are given by

$$d\vec{\sigma} = [D_{eq}]d\vec{\epsilon} \tag{6}$$

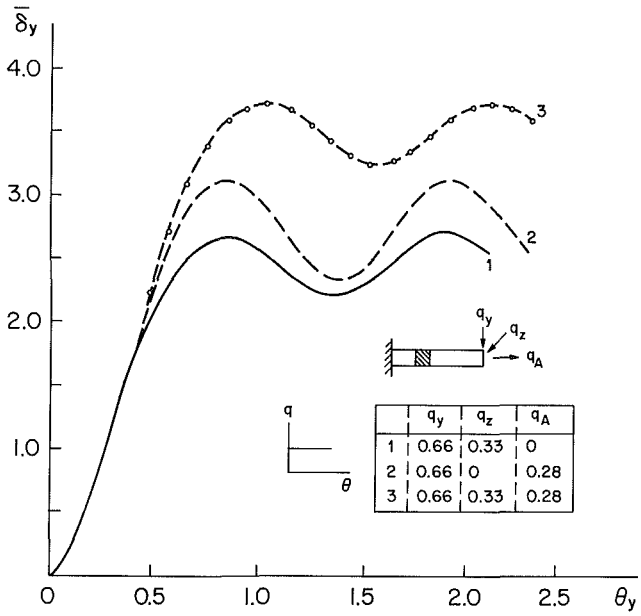


Fig. 1 Response of a cantilever in combined loading

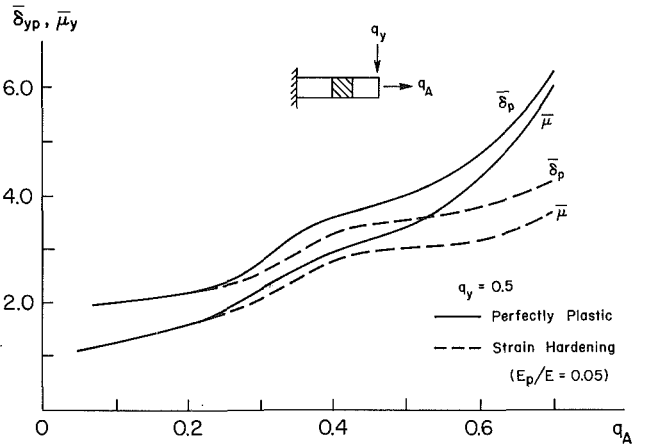


Fig. 2 Response characteristics for a cantilever beam in combined loading. (q_y and q_A are step loads. $\bar{\mu}$ = nondimensional mean displacement, $\bar{\delta}_p$ = nondimensional peak displacement. Subscript y denotes the direction.)

[4]School of Mechanical Engineering, Purdue University, West Lafayette, IN 47907.

[5]Bharat Heavy Electricals Ltd., Hyderabad, India.

Manuscript received by ASME Applied Mechanics Division, June 3, 1986; final revision, August 26, 1986.

Copyright © 1987 by ASME

Downloaded 03 May 2010 to 171.66.16.27. Redistribution subject to ASME license or copyright; see http://www.asme.org/terms/Terms_Use.cfm

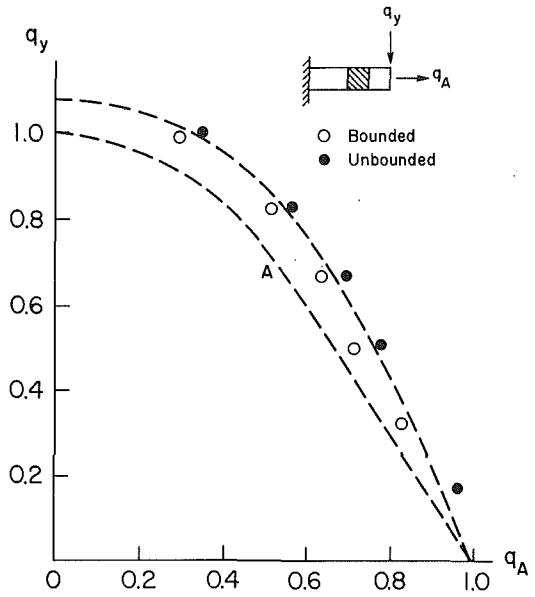


Fig. 3 Instability region for a cantilever in combined loading (q_y and q_A are step loads)

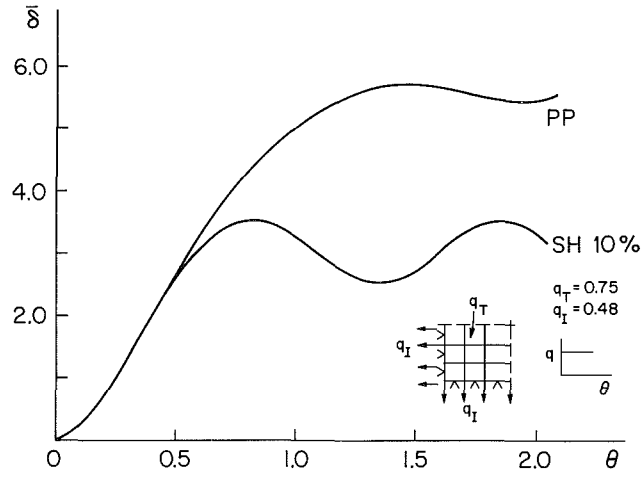


Fig. 4 Transverse response of a simply supported plate under combined loading

where the elasto-plastic matrix, $[D_{eq}]$, for bilinear stress-strain behavior is given in [1].

Finite Element Analysis

The general beam element with six degrees of freedom is used for the analysis of beams. The initial stress or geometric stiffness matrix, which modifies the transverse stiffness properties of a beam element, is derived using the geometrically nonlinear strain displacement relation. The inelastic response of beams with axial load is obtained in the usual way but for the use of the modified stiffness matrix. Only the initial condition for the axial stress σ_x is modified as

$$\sigma_{x|t=0} = \frac{P}{A} \tag{7a}$$

The strain displacement matrix and the mass matrix are not affected by the presence of the axial load. In the case of rectangular plates, the strain displacement relations for large deformation of plates based on von Karman theory, are used and the geometric stiffness matrix is derived with

$$h\frac{\partial w_x}{\partial x} = \frac{Px}{E} - \nu\frac{Py}{E},\ h\frac{\partial w_y}{\partial y} = \frac{Py}{E} - \nu\frac{Px}{E},\ \frac{\partial w_x}{\partial y} = \frac{\partial w_y}{\partial x} = 0 \tag{7b}$$

where h is the plate thickness, w_x and w_y are displacements along x and y (in plane) directions, and ν is the Poisson's ratio. The initial stress conditions are taken as

$$\sigma_{x|t=0} = \frac{Px}{h},\ \sigma_{y|t=0} = \frac{Py}{h},\ \sigma_{xy|t=0} = 0 \tag{8}$$

where Px and Py denote the distributed axial loads in x and y directions.

Nondimensional Response Parameters

The applied load p and the response δ are nondimensionalized with respect to the static yield load p_Y and the corresponding static (elastic) deflection δ_Y, respectively. The yield load is defined as the minimum load at which the moment at some point reaches the fully plastic value M_o. The time t is nondimensionalized with respect to the fundamental period T_1. Thus the nondimensionalized quantities are given by

$$q = \frac{p}{p_Y},\ \bar{\delta} = \frac{\delta}{q \cdot \delta_Y},\ \Theta = \frac{t}{T_1} \tag{9}$$

When the applied load is a uniform impulse, the initial velocity V_o is nondimensionalized with respect to a reference velocity V_r which is defined as

$$V_r = \frac{p_Y T_1}{10m} \tag{10}$$

where m is the mass per unit length of the beam. The nondimensional initial velocity λ and response $\bar{\delta}$ are then given by

$$\lambda = V_o/V_r,\ \bar{\delta} = \delta/(\lambda\delta_Y) \tag{11}$$

Numerical Results and Discussion

The response of a cantilever beam of square cross section is shown in Fig. 1. The interaction effect of the axial displacement is seen to be significantly more than that of the transverse displacement. In Fig. 2 the response characteristics showing the influence of strain hardening on the interaction effects are presented. In this case, the instability of the response was observed for $q_A = 0.8$. For any given value of q_y, there exists a certain load q_A beyond which the response would be unbounded. Complete response behavior was studied and the results are shown in Fig. 3. Here the points corresponding to stable and unstable combination of loads (numerical data) and are marked in a space defined by the corresponding loads and the curve that separates them is drawn. It is of interest to note that the corresponding interaction curve, in a space defined by the nondimensionalized generalized stresses, obtained from the maximum normal stress theory, is similar to the curve shown. The inner curve of Fig. 3 is drawn so as to closely correspond to the collapse loads given by the rigid plastic theory.

The transverse response of a square simply supported plate under the simultaneous action of uniform pressure and uniform biaxial edge loads is shown in Fig. 4. For the perfectly plastic case the peak response is seen to be almost equal to the mean response. This particular combination of transverse and inplane loads is, thus, very close to a combination that would cause instability. Referring to Fig. 3, it is seen that the point A on the inner curve corresponds closely to the nondimensional loads considered in this case. (q_y and q_A in Fig. 3 correspond to q_T and q_I of Fig. 4 with point A denoting the values $q_y = q_T = 0.75$ and $q_A = q_I = 0.48$).

Downloaded 03 May 2010 to 171.66.16.27. Redistribution subject to ASME license or copyright; see http://www.asme.org/terms/Terms_Use.cfm

References

1 Owen, D. R. J., and Hinton, E., 1980, "Finite Elements in Plasticity," Pineridge Press, Swansea.

2 Rao, S. S., and Raghavan, K. S., 1979, "Dynamic Inelastic Analysis of Thick Plates," *AIAA Journal*, Vol. 17, pp. 85–90.

Perforation of Aluminum Plates With Conical-Nosed Rods[6]

M. J. Forrestal,[7] Z. Rosenberg,[8] V. K. Luk,[9] S. J. Bless[8]

Introduction

Zukas et al. (1982) discuss many recently developed analytical and experimental methods used to study the broad field of penetration mechanics. For metal perforation, Backman and Goldsmith (1978) show eight possible perforation mechanisms that depend on the geometry and material of the targets and penetrators. Because many perforation mechanisms are possible, observations from laboratory-scale experiments usually precede and guide engineering models. We studied the mechanism shown in Fig. 1, a post-test photograph of a sectioned, aluminum target. As shown, the target experienced ductile hole-growth, and post-perforation, x-ray photographs showed that the penetrator remained undeformed.

Studies on projectile perforation of metal plates usually focus on the measurement and prediction of residual velocity and ballistic limit. Residual velocity is the post-perforation penetrator velocity, and the ballistic limit is the incident velocity below which the penetrator fails to perforate the target. Theoretical models use solution techniques that may be grouped into three categories: empirical equations fit to test data, engineering models that approximate experimental observations (Recht and Ipson, 1963), and wave-code analyses (Wilkins, 1978). For this study, we developed an engineering model based partially on the dynamic, elastic-plastic expansion of a cylindrical cavity by a rigid penetrator.

As discussed by Longcope and Forrestal (1983), the cylindrical, cavity-expansion approximation idealizes the target as thin, independent layers normal to the penetration direction. Thus, the analysis is simplified to one-dimensional motion in the radial direction. The perforation model of this study was derived from a kinetic energy-work balance and used this cavity-expansion analysis as one ingredient.

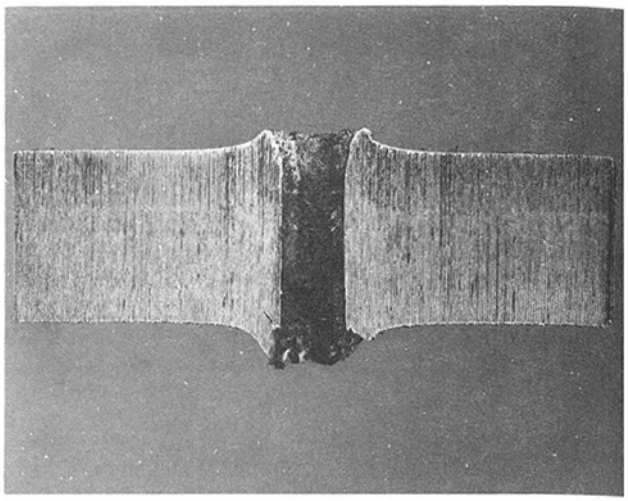


Fig. 1 Post-test photograph of a sectioned, aluminum target from a reverse-ballistic experiment at an incident velocity of 906 m/s. Penetrator entered from above.

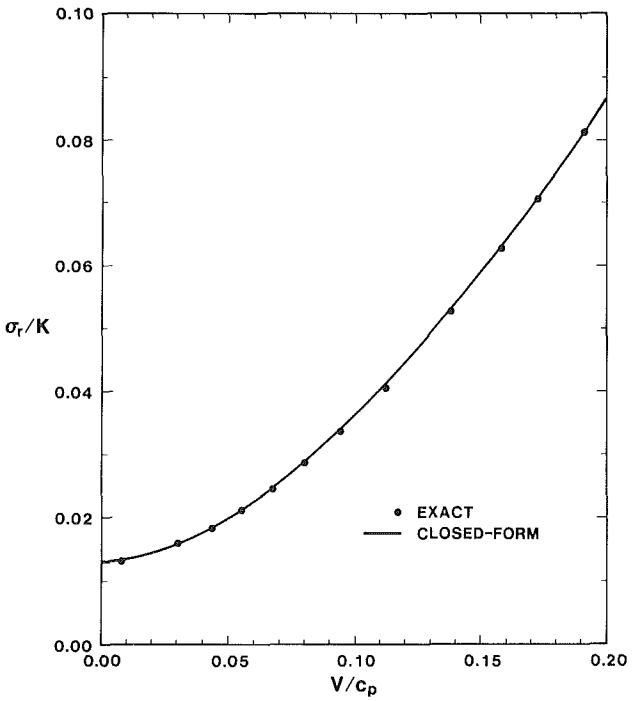


Fig. 2 Radial stress on the conical nose for an aluminum target with $Y/K = 0.0045$ and $\nu = 1/3$

Perforation Model

A rigid, conical-nosed rod penetrates an infinite plate at normal incidence. The problem is axisymmetric and further simplified by using the cylindrical, cavity-expansion approximation. The conical nose with apical angle 2ϕ and diameter $2a$ radially expands a layer of target material and opens a cavity at constant radial velocity V, where $V = V_z \tan\phi$ and V_z is the axial velocity. This expansion produces two response regions in a hypothetical layer—a plastic region (where the material has reached its flow stress) next to the penetrator nose, and an elastic region. Radial stress at the cavity wall produced by cavity-expansion is derived by Forrestal (1986) and used in the development of this perforation model.

There are three phases of penetration for a nose length ℓ that is less than plate thickness h. First, the nose enters the plate; second, the nose is fully embedded; and finally, the nose exits the plate. This model only includes forces from radial cavity-expansion and neglects sliding, frictional resistance. We start the derivation with a kinetic energy-work balance for the rigid penetrator. Thus

$$(m/2)[V_i^2 - V_r^2] = W_1 + W_2 + W_3 \tag{1}$$

where m is the rod mass; V_i, V_r are incident and residual velocities. W_1, W_2, and W_3 are the work done for each of the three penetration phases.

$$W_1 = \pi a^2 \ell \sigma_r/3;\ W_2 = \pi a^2 (h-\ell)\sigma_r;\ W_3 = 2\pi a^2 \ell \sigma_r/3 \tag{2a}$$

and

[6]This work was supported by the US Department of Energy and is a shortened version of the report, SAND86-0292J.

[7]Sandia National Laboratories, Albuquerque, NM 87185. Fellow, ASME

[8]University of Dayton Research Institute, Dayton, OH 45469.

[9]Sandia National Laboratories, Albuquerque, NM 87185. Member, ASME

Manuscript received by ASME Applied Mechanics Division, April 7, 1986; final revision, September 22, 1986.

Downloaded 03 May 2010 to 171.66.16.27. Redistribution subject to ASME license or copyright; see http://www.asme.org/terms/Terms_Use.cfm

References

1 Owen, D. R. J., and Hinton, E., 1980, "Finite Elements in Plasticity," Pineridge Press, Swansea.

2 Rao, S. S., and Raghavan, K. S., 1979, "Dynamic Inelastic Analysis of Thick Plates," *AIAA Journal*, Vol. 17, pp. 85–90.

Perforation of Aluminum Plates With Conical-Nosed Rods[6]

M. J. Forrestal,[7] Z. Rosenberg,[8] V. K. Luk,[9] S. J. Bless[8]

Introduction

Zukas et al. (1982) discuss many recently developed analytical and experimental methods used to study the broad field of penetration mechanics. For metal perforation, Backman and Goldsmith (1978) show eight possible perforation mechanisms that depend on the geometry and material of the targets and penetrators. Because many perforation mechanisms are possible, observations from laboratory-scale experiments usually precede and guide engineering models. We studied the mechanism shown in Fig. 1, a post-test photograph of a sectioned, aluminum target. As shown, the target experienced ductile hole-growth, and post-perforation, x-ray photographs showed that the penetrator remained undeformed.

Studies on projectile perforation of metal plates usually focus on the measurement and prediction of residual velocity and ballistic limit. Residual velocity is the post-perforation penetrator velocity, and the ballistic limit is the incident velocity below which the penetrator fails to perforate the target. Theoretical models use solution techniques that may be grouped into three categories: empirical equations fit to test data, engineering models that approximate experimental observations (Recht and Ipson, 1963), and wave-code analyses (Wilkins, 1978). For this study, we developed an engineering model based partially on the dynamic, elastic-plastic expansion of a cylindrical cavity by a rigid penetrator.

As discussed by Longcope and Forrestal (1983), the cylindrical, cavity-expansion approximation idealizes the target as thin, independent layers normal to the penetration direction. Thus, the analysis is simplified to one-dimensional motion in the radial direction. The perforation model of this study was derived from a kinetic energy-work balance and used this cavity-expansion analysis as one ingredient.

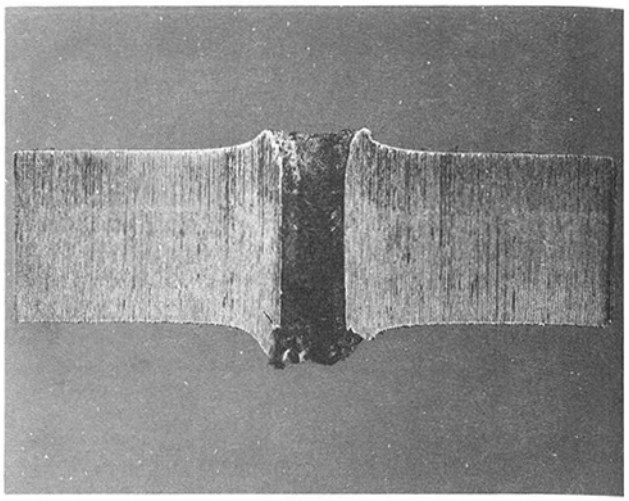


Fig. 1 Post-test photograph of a sectioned, aluminum target from a reverse-ballistic experiment at an incident velocity of 906 m/s. Penetrator entered from above.

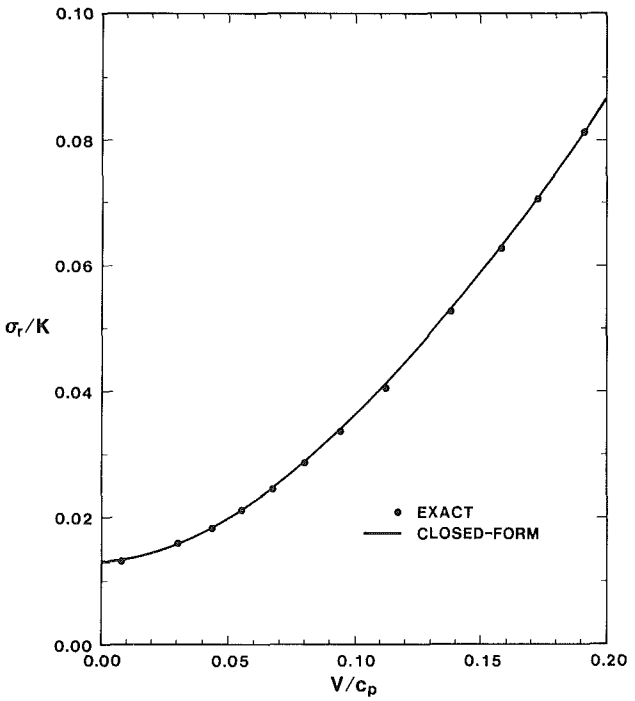


Fig. 2 Radial stress on the conical nose for an aluminum target with $Y/K = 0.0045$ and $\nu = 1/3$

Perforation Model

A rigid, conical-nosed rod penetrates an infinite plate at normal incidence. The problem is axisymmetric and further simplified by using the cylindrical, cavity-expansion approximation. The conical nose with apical angle 2ϕ and diameter $2a$ radially expands a layer of target material and opens a cavity at constant radial velocity V, where $V = V_z \tan\phi$ and V_z is the axial velocity. This expansion produces two response regions in a hypothetical layer—a plastic region (where the material has reached its flow stress) next to the penetrator nose, and an elastic region. Radial stress at the cavity wall produced by cavity-expansion is derived by Forrestal (1986) and used in the development of this perforation model.

There are three phases of penetration for a nose length ℓ that is less than plate thickness h. First, the nose enters the plate; second, the nose is fully embedded; and finally, the nose exits the plate. This model only includes forces from radial cavity-expansion and neglects sliding, frictional resistance. We start the derivation with a kinetic energy-work balance for the rigid penetrator. Thus

$$(m/2)[V_i^2 - V_r^2] = W_1 + W_2 + W_3 \tag{1}$$

where m is the rod mass; V_i, V_r are incident and residual velocities. W_1, W_2, and W_3 are the work done for each of the three penetration phases.

$$W_1 = \pi a^2 \ell \sigma_r/3;\ W_2 = \pi a^2 (h-\ell)\sigma_r;\ W_3 = 2\pi a^2 \ell \sigma_r/3 \tag{2a}$$

and

[6]This work was supported by the US Department of Energy and is a shortened version of the report, SAND86-0292J.

[7]Sandia National Laboratories, Albuquerque, NM 87185. Fellow, ASME

[8]University of Dayton Research Institute, Dayton, OH 45469.

[9]Sandia National Laboratories, Albuquerque, NM 87185. Member, ASME

Manuscript received by ASME Applied Mechanics Division, April 7, 1986; final revision, September 22, 1986.

Copyright © 1987 by ASME

Downloaded 03 May 2010 to 171.66.16.27. Redistribution subject to ASME license or copyright; see http://www.asme.org/terms/Terms_Use.cfm

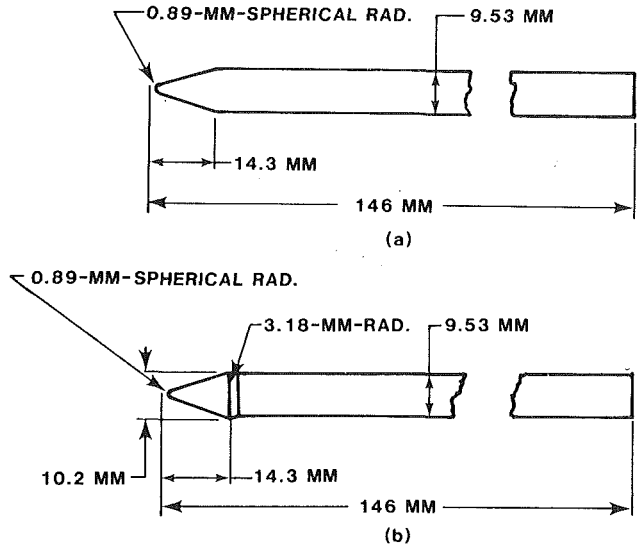


Fig. 3 Penetrator geometries

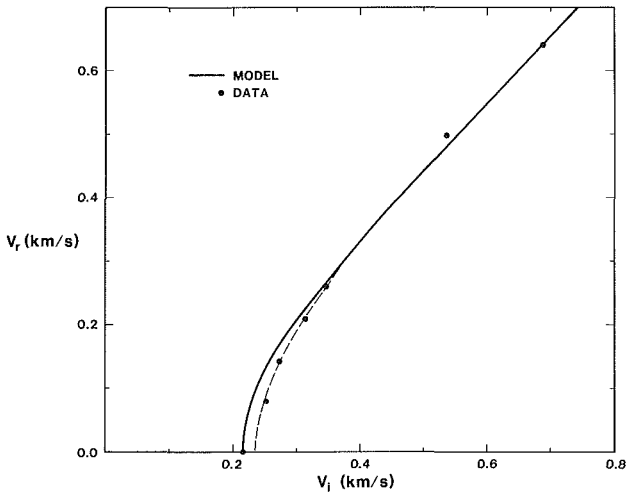


Fig. 4 Comparison of predicted and measured residual velocity

$$W_1 + W_2 + W_3 = \pi a^2 h \sigma_r \tag{2b}$$

Radial stress varies slightly during perforation; but, as will be shown later, an average value of σ_r is used in the perforation model. Thus, σ_r was taken as constant for the derivations of (2*a*, *b*). From (1) and (2*b*)

$$(m/2)[V_i^2 - V_r^2] = \pi a^2 h \sigma_r \tag{3}$$

where σ_r is the radial stress on the conical nose determined from an elastic-plastic, cavity-expansion analysis. With σ_r determined, we can calculate V_r.

Longcope and Forrestal (1983) develop cylindrical, cavity-expansion models to predict forces on conical-nosed penetrators. Target response is calculated by solving the nonlinear, wave-propagation problem with a similarity transformation and numerical evaluation of nonlinear, ordinary, differential equations. In a more recent paper, Forrestal (1986) presents accurate, closed-form solutions derived by an iterative technique. Figure 2 presents dimensionless, radial stress on the cavity wall σ_r/K versus dimensionless, cavity-expansion velocity V/c_p for an aluminum target from both the nonlinear and closed-form solutions. In these plots, K, ρ_o, ν, and Y are bulk modulus, density, Poisson's ratio, and flow stress, respectively, and $c_p = (K/\rho_o)^{1/2}$.

Equation (3) and σ_r, obtained from the cavity-expansion analysis, can now be used to estimate the residual velocity V_r. Post-analysis evaluation showed that velocity-dependent σ_r did not change significantly during penetration. Equation (3) is written as

$$V_r = V_i - \left(\frac{\pi a^2 h}{m}\right)\left[\frac{\sigma_r}{(V_i + V_r)/2}\right] \tag{4}$$

and V_r is calculated with an iterative procedure. First, substitute $V_r = V_i$ in the right side of equation (4); obtain σ_r from Fig. 2 (Recall V is radial, cavity expansion velocity; $V = V_i \tan\phi$), and calculate V_r. Second, calculate the estimated average velocity during penetration $(V_i + V_r)/2$ using the first value of V_r; obtain σ_r using the average penetration velocity, and calculate a corrected value of V_r. This procedure can be repeated if necessary; but for our applications, the second iteration was always adequate.

As mentioned, the ballistic limit is the incident velocity below which the penetrator fails to perforate the target. The ballistic limit is obtained from equation (3) with $V_r = 0$ and the quasi-static, radial stress σ_s (the value of σ_r for V approaching zero). Thus, an estimate for the ballistic limit is

$$V_{bl} = (2\pi a^2 h \sigma_s/m)^{1/2} \tag{5a}$$

$$\sigma_s = \frac{Y}{2}\left\{1 + \ell n\left[\frac{6(1-2\nu)K}{(5-4\nu)Y}\right]\right\} \tag{5b}$$

where σ_s was derived by Bishop, Hill, and Mott (1945) and Forrestal (1986). Equations (5*a*, *b*) encompass the ideas of Bethe (1941).

Experiments

Briefly,[10] a powder gun launched conical-nosed, steel rods at aluminum plates. Incident velocity was determined by the penetrator interrupting two continuously monitored laser beams. Flash x-ray photography measured residual velocity and yaw angles.

Targets. The square targets were 0.304-m-wide (12 in.), 25.4-mm-thick, 6061-T6 aluminum plates. Samples in the plane of the plates were machined for dynamic, stress-strain tests. Three tension and three compression tests were conducted at strain rates of 10^{-2} and 10° s^{-1}. Data showed negligible flow-stress variation over these twelve tests. Average flow-stress at 0.2 percent strain was 288 MPa (42.3 ksi) and the average, maximum flow-stress was 313 MPa (45.9 ksi). Our perforation model assumed an elastic-perfectly plastic material; so, for our numerical predictions, we used the average flow-stress, $Y = 300$ MPa (44.1 ksi).

Penetrators. Forrestal and Jenrette (1986) conducted reverse-ballistic experiments with the concial-nosed rod shown in Fig. 3(*a*). For incident velocities below about 500 m/s, the cavity wall rebounded after nose entry and created a friction drag on the shank. Since our model predicts only forces on the conical nose, we avoided shank drag by using the arrowhead penetrator shown in Fig. 3(*b*) for V_i less than 500 m/s. For V_i greater than 500 m/s, we used the straight penetrators shown in Fig. 6(*a*).

Penetrators were machined from T-200 maraging steel[11] and had a nominal mass of 0.078 kg. As previously mentioned, penetrators remained undeformed after perforation for incident velocities to 700 m/s.

Terminal-Ballistic Experiments. A 20-mm, rifled-bore

[10] Additional detail on the experimental program is contained in the report, SAND86-0292J.

[11] Vasco Pacific, 707 West Olympic Blvd., Montebello, CA 90640.

Downloaded 03 May 2010 to 171.66.16.27. Redistribution subject to ASME license or copyright; see http://www.asme.org/terms/Terms_Use.cfm

powder gun launched the 0.078-kg rods shown in Fig. 3 to incident velocities between 210–700 m/s. The rods were encased in two-piece, serrated, plastic sabots. Pusher plates were 15.7-mm-dia., 6.35-mm-long, titanium discs, and the obturator was made from the same material as the sabot. The sabot fit snugly in the gun barrel, while the slightly oversized obturator was forced into the barrel so as to provide a gas seal. Centrifugal force and air drag stripped the sabot, pusher plate, and obturator from the rod prior to impact.

Incident velocity was determined within one-percent accuracy by the penetrator interrupting two continuously monitored laser beams, and incident yaw was measured with an orthogonal pair of flash x-rays. Two pairs of orthogonal, flash x-rays determined residual velocity within two-percent accuracy. Incident yaw angles were less than one degree, and yaw angles after perforation were less than two degrees.

Experimental Results and Comparison with the Model

Figure 4 shows the prediction for conical-nosed rods and 25.4-mm-thick (1.0 in.), 6061-T6 aluminum targets. The data are in good agreement with the model over the tested velocity range. Calculated ballistic limit is 0.215 km/s, and the ballistic limit determined by curve fitting the data is 0.235 km/s.

Acknowledgments

The authors thank Mark Laber for assisting with the terminal-ballistic experiments and Paul Hatch for conducting the dynamic, stress-strain tests.

References

Backman, M. E., and Goldsmith, W., 1978, "The Mechanics of Penetration of Projectiles into Targets," *International Journal of Engineering Science*, Vol. 16, pp. 1–99.

Bethe, H. A., 1941, "Attempt of a Theory of Armor Penetration," Frankford Arsenal, Philadelphia, PA.

Bishop, R. F., Hill, R., and Mott, N. F., 1945, "The Theory of Indentation and Hardness Tests," *The Proceedings of the Physical Society*, Vol. 53, Part 3, pp. 147–155.

Forrestal, M. J., 1986, "Penetration into Dry Porous Rock," *International Journal of Solids and Structures*, to appear.

Forrestal, M. J., and Jenrette, B. D., 1986, Work in progress.

Longcope, D. B., and Forrestal, M. J., 1983, "Penetration of Targets Described by a Mohr-Coulomb Failure Criterion with a Tension Cutoff," *Journal of Applied Mechanics*, Vol. 50, June 1983, pp. 327–333.

Recht, R. F., and Ipson, T. W., 1963, "Ballistic Perforation Dynamics, ASME Journal of Applied Mechanics, Sept. 1963, pp. 384–390.

Wilkins, M. L., 1978, "Mechanics of Penetration and Perforation," *International Journal of Engineering Science*, Vol. 16, pp. 793–807.

Zukas, J. A., et al., 1982, *Impact Dynamics*, Wiley, New York.

Approximate Solution of Differential Equations Governing the Orientation of a Rigid Body in a Reference Frame

T. R. Kane[12] and D. A. Levinson[13]

Introduction

The orientation of a rigid body B in a reference frame A is related to the angular velocity of B in A through first-order differential equations that can be solved in closed form only under special circumstances, such as when B is constrained to rotate about an axis fixed in both A and B. Hence, given the angular velocity of B in A, one must, in general, resort to numerical integration to obtain a description of the orientation of B in A as a function of time. But such integration may be unacceptably time-consuming or may require more computing power than is readily available. For example, this can occur when the computations must be performed rapidly aboard a spacecraft or in connection with certain operations of a robotic device. In that event, it may be possible to obtain the required information from an *approximate* solution that can be generated with minimal computational effort. The present Note, like that by Kane (1973), provides such a solution.

In the next section, the quantities in terms of which the analysis is carried out are defined, and a step-by-step procedure for the determination of the orientation of a rigid body in a reference frame is set forth. Thereafter, an illustrative example is worked out. A brief derivation of the procedure appears in the last section of the note.

Procedure

Let $\mathbf{a}_i$ $(i=1,2,3)$ be a dextral set of mutually perpendicular unit vectors fixed in a reference frame A, $\mathbf{b}_i$ $(i=1,2,3)$ a similar set fixed in a rigid body B, and $C_{ij}(t)$ $(i,j=1,2,3)$ direction cosine elements defined as

$$C_{ij}(t)=\mathbf{a}_i\cdot\mathbf{b}_j \quad (i,j=1,2,3) \tag{1}$$

Introduce Euler parameters $E_k(t)$ $(k=1,\ldots,4)$ as (see Kane et al., (1983))

$$E_4(t)=0.5(1+C_{11}+C_{22}+C_{33})^{1/2} \tag{2}$$

$$E_1(t)=(C_{32}-C_{23})/(4E_4) \tag{3}$$

$$E_2(t)=(C_{13}-C_{31})/(4E_4) \tag{4}$$

$$E_3(t)=(C_{21}-C_{12})/(4E_4) \tag{5}$$

and let $x_i(t)$ $(i=1,2,3)$ be angular velocity measure numbers defined in terms of ${}^A\mathbf{x}^B$, the angular velocity of B in A, as

$$x_i(t)={}^A\mathbf{x}^B\cdot\mathbf{b}_i \quad (i=1,2,3) \tag{6}$$

Moreover, suppose that $x_i(t)$ $(i=1,2,3)$ can be expressed as

$$x_i(t)=y_i+sz_i(t) \quad (i=1,2,3) \tag{7}$$

where y_i $(i=1,2,3)$ are known *constants*, s is a "small" parameter (more about this later), and $z_i(t)$ $(i=1,2,3)$ are known functions of time t. Then, to find an approximation to $E_k(t)$ $(k=1,\ldots,4)$, proceed as follows:

1. Form m as

$$m=0.5(y_1^2+y_2^2+y_3^2)^{1/2} \tag{8}$$

2. Evaluate $P_i(t)$ $(i=1,2,3)$, defined as

$$P_i(t)=0.5\int_0^t z_i(u)\,du \quad (i=1,2,3) \tag{9}$$

3. Let

$$v(t)=\cos(mt),\ w(t)=(0.5/m)\sin(mt) \tag{10}$$

4. Form $S_k(t)$ $(k=1,\ldots,4)$ as

$$S_1(t)=y_1w+s[P_1v+(P_2y_3-P_3y_2)w] \tag{11}$$

$$S_2(t)=y_2w+s[P_2v+(P_3y_1-P_1y_3)w] \tag{12}$$

$$S_3(t)=y_3w+s[P_3v+(P_1y_2-P_2y_1)w] \tag{13}$$

$$S_4(t)=v-sw(P_1y_1+P_2y_2+P_3y_3) \tag{14}$$

[12]Professor of Applied Mechanics, Stanford University, Stanford, CA 94305. Fellow ASME.

[13]Research Scientist, Lockheed Palo Alto Research Laboratory, Palo Alto, CA 94304. Mem. ASME.

Manuscript received by ASME Applied Mechanics Division, September 3, 1986; final revision, October 6, 1986.

Downloaded 03 May 2010 to 171.66.16.27. Redistribution subject to ASME license or copyright; see http://www.asme.org/terms/Terms_Use.cfm

powder gun launched the 0.078-kg rods shown in Fig. 3 to incident velocities between 210–700 m/s. The rods were encased in two-piece, serrated, plastic sabots. Pusher plates were 15.7-mm-dia., 6.35-mm-long, titanium discs, and the obturator was made from the same material as the sabot. The sabot fit snugly in the gun barrel, while the slightly oversized obturator was forced into the barrel so as to provide a gas seal. Centrifugal force and air drag stripped the sabot, pusher plate, and obturator from the rod prior to impact.

Incident velocity was determined within one-percent accuracy by the penetrator interrupting two continuously monitored laser beams, and incident yaw was measured with an orthogonal pair of flash x-rays. Two pairs of orthogonal, flash x-rays determined residual velocity within two-percent accuracy. Incident yaw angles were less than one degree, and yaw angles after perforation were less than two degrees.

Experimental Results and Comparison with the Model

Figure 4 shows the prediction for conical-nosed rods and 25.4-mm-thick (1.0 in.), 6061-T6 aluminum targets. The data are in good agreement with the model over the tested velocity range. Calculated ballistic limit is 0.215 km/s, and the ballistic limit determined by curve fitting the data is 0.235 km/s.

Acknowledgments

The authors thank Mark Laber for assisting with the terminal-ballistic experiments and Paul Hatch for conducting the dynamic, stress-strain tests.

References

Backman, M. E., and Goldsmith, W., 1978, "The Mechanics of Penetration of Projectiles into Targets," *International Journal of Engineering Science*, Vol. 16, pp. 1–99.

Bethe, H. A., 1941, "Attempt of a Theory of Armor Penetration," Frankford Arsenal, Philadelphia, PA.

Bishop, R. F., Hill, R., and Mott, N. F., 1945, "The Theory of Indentation and Hardness Tests," *The Proceedings of the Physical Society*, Vol. 53, Part 3, pp. 147–155.

Forrestal, M. J., 1986, "Penetration into Dry Porous Rock," *International Journal of Solids and Structures*, to appear.

Forrestal, M. J., and Jenrette, B. D., 1986, Work in progress.

Longcope, D. B., and Forrestal, M. J., 1983, "Penetration of Targets Described by a Mohr-Coulomb Failure Criterion with a Tension Cutoff," *Journal of Applied Mechanics*, Vol. 50, June 1983, pp. 327–333.

Recht, R. F., and Ipson, T. W., 1963, "Ballistic Perforation Dynamics, ASME Journal of Applied Mechanics, Sept. 1963, pp. 384–390.

Wilkins, M. L., 1978, "Mechanics of Penetration and Perforation," *International Journal of Engineering Science*, Vol. 16, pp. 793–807.

Zukas, J. A., et al., 1982, *Impact Dynamics*, Wiley, New York.

Approximate Solution of Differential Equations Governing the Orientation of a Rigid Body in a Reference Frame

T. R. Kane[12] and D. A. Levinson[13]

Introduction

The orientation of a rigid body B in a reference frame A is related to the angular velocity of B in A through first-order differential equations that can be solved in closed form only under special circumstances, such as when B is constrained to rotate about an axis fixed in both A and B. Hence, given the angular velocity of B in A, one must, in general, resort to numerical integration to obtain a description of the orientation of B in A as a function of time. But such integration may be unacceptably time-consuming or may require more computing power than is readily available. For example, this can occur when the computations must be performed rapidly aboard a spacecraft or in connection with certain operations of a robotic device. In that event, it may be possible to obtain the required information from an *approximate* solution that can be generated with minimal computational effort. The present Note, like that by Kane (1973), provides such a solution.

In the next section, the quantities in terms of which the analysis is carried out are defined, and a step-by-step procedure for the determination of the orientation of a rigid body in a reference frame is set forth. Thereafter, an illustrative example is worked out. A brief derivation of the procedure appears in the last section of the note.

Procedure

Let $\mathbf{a}_i$ $(i=1,2,3)$ be a dextral set of mutually perpendicular unit vectors fixed in a reference frame A, $\mathbf{b}_i$ $(i=1,2,3)$ a similar set fixed in a rigid body B, and $C_{ij}(t)$ $(i,j=1,2,3)$ direction cosine elements defined as

$$C_{ij}(t)=\mathbf{a}_i\cdot\mathbf{b}_j \quad (i,j=1,2,3) \tag{1}$$

Introduce Euler parameters $E_k(t)$ $(k=1,\ldots,4)$ as (see Kane et al., (1983))

$$E_4(t)=0.5(1+C_{11}+C_{22}+C_{33})^{1/2} \tag{2}$$

$$E_1(t)=(C_{32}-C_{23})/(4E_4) \tag{3}$$

$$E_2(t)=(C_{13}-C_{31})/(4E_4) \tag{4}$$

$$E_3(t)=(C_{21}-C_{12})/(4E_4) \tag{5}$$

and let $x_i(t)$ $(i=1,2,3)$ be angular velocity measure numbers defined in terms of ${}^A\mathbf{x}^B$, the angular velocity of B in A, as

$$x_i(t)={}^A\mathbf{x}^B\cdot\mathbf{b}_i \quad (i=1,2,3) \tag{6}$$

Moreover, suppose that $x_i(t)$ $(i=1,2,3)$ can be expressed as

$$x_i(t)=y_i+sz_i(t) \quad (i=1,2,3) \tag{7}$$

where y_i $(i=1,2,3)$ are known *constants*, s is a "small" parameter (more about this later), and $z_i(t)$ $(i=1,2,3)$ are known functions of time t. Then, to find an approximation to $E_k(t)$ $(k=1,\ldots,4)$, proceed as follows:

1. Form m as

$$m=0.5(y_1^2+y_2^2+y_3^2)^{1/2} \tag{8}$$

2. Evaluate $P_i(t)$ $(i=1,2,3)$, defined as

$$P_i(t)=0.5\int_0^t z_i(u)\,du \quad (i=1,2,3) \tag{9}$$

3. Let

$$v(t)=\cos(mt),\ w(t)=(0.5/m)\sin(mt) \tag{10}$$

4. Form $S_k(t)$ $(k=1,\ldots,4)$ as

$$S_1(t)=y_1w+s[P_1v+(P_2y_3-P_3y_2)w] \tag{11}$$

$$S_2(t)=y_2w+s[P_2v+(P_3y_1-P_1y_3)w] \tag{12}$$

$$S_3(t)=y_3w+s[P_3v+(P_1y_2-P_2y_1)w] \tag{13}$$

$$S_4(t)=v-sw(P_1y_1+P_2y_2+P_3y_3) \tag{14}$$

[12]Professor of Applied Mechanics, Stanford University, Stanford, CA 94305. Fellow ASME.

[13]Research Scientist, Lockheed Palo Alto Research Laboratory, Palo Alto, CA 94304. Mem. ASME.

Manuscript received by ASME Applied Mechanics Division, September 3, 1986; final revision, October 6, 1986.

Copyright © 1987 by ASME
Downloaded 03 May 2010 to 171.66.16.27. Redistribution subject to ASME license or copyright; see http://www.asme.org/terms/Terms_Use.cfm

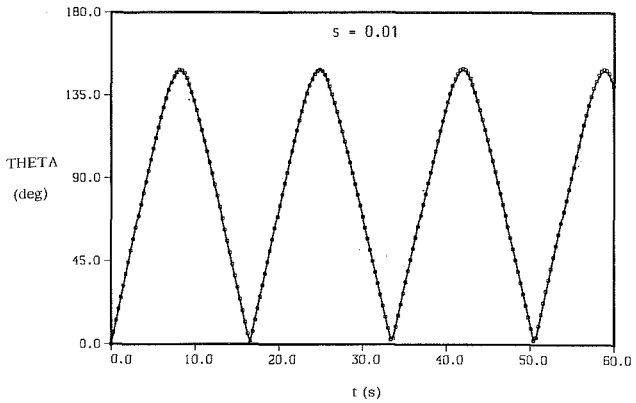


Fig. 1 THETA as a function of t

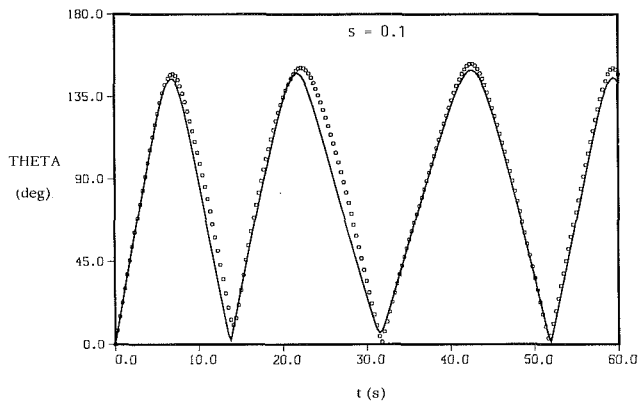


Fig. 2 THETA as a function of t

5. Finally, take

$$E_1(t) = E_1(0)S_4 + E_2(0)S_3 - E_3(0)S_2 + E_4(0)S_1 \tag{15}$$

$$E_2(t) = -E_1(0)S_3 + E_2(0)S_4 + E_3(0)S_1 + E_4(0)S_2 \tag{16}$$

$$E_3(t) = E_1(0)S_2 - E_2(0)S_1 + E_3(0)S_4 + E_4(0)S_3 \tag{17}$$

$$E_4(t) = -E_1(0)S_1 - E_2(0)S_2 - E_3(0)S_3 + E_4(0)S_4 \tag{18}$$

Example

If a rigid body B is moving in a reference frame A in such a way that the angular velocity measure numbers x_i $(i=1,2,3)$ (see equation (6)) are given by equation (7) with

$$z_i = A_i \sin(pt) + B_i \cos(pt) \quad (i=1,2,3) \tag{19}$$

where A_i, B_i $(i=1,2,3)$, and p are constants, then, performing the integration required by equation (9), one obtains

$$P_i(t) = 0.5\{A_i[1-\cos(pt)] + B_i \sin(pt)\}/p \quad (i=1,2,3) \tag{20}$$

and, as soon as numerical values for y_i (see equation (7)), A_i, B_i $(i=1,2,3)$, and p have been specified, one can use equations (10)–(18) to evaluate v, w, S_k, and E_k $(k=1, \ldots, 4)$ for any desired value of t. Before reporting the results of such computations, we note that the angle THETA between a line fixed in A, say a line parallel to the unit vector $\mathbf{a}_1$, and a line fixed in B, say parallel to the unit vector $\mathbf{b}_1$, depends on all four of E_k $(k=1, \ldots, 4)$ and thus furnishes the means for an efficient assessment of the accuracy of the approximate solution under consideration. The determination of THETA is accomplished as follows.

Written in terms of $\mathbf{b}_i$ $(i=1,2,3)$, the unit vector $\mathbf{a}_1$ is given by

$$\mathbf{a}_1 = C_{11}\mathbf{b}_1 + C_{12}\mathbf{b}_2 + C_{13}\mathbf{b}_3 \tag{21}$$

and the direction cosine elements appearing in this equation can be expressed in terms of Euler parameters as

$$C_{11} = 1 - 2(E_2^2 + E_3^2) \tag{22}$$

$$C_{12} = 2(E_1E_2 - E_3E_4) \tag{23}$$

$$C_{13} = 2(E_3E_1 + E_2E_4) \tag{24}$$

Now, if approximate values of E_k $(k=1, \ldots, 4)$ are used in equations (22)–(24), and the resulting values of C_{1j} $(j=1,2,3)$ are substituted into equation (21), the vector obtained, say $\mathbf{q}$, is an approximation to $\mathbf{a}_1$, and may have a magnitude differing from unity; but a unit vector parallel to $\mathbf{q}$, say $\mathbf{r}$, can be formed as

$$\mathbf{r} = \mathbf{q}/|\mathbf{q}| \tag{25}$$

with (see equation (21))

$$\mathbf{q} = C_{11}\mathbf{b}_1 + C_{12}\mathbf{b}_2 + C_{13}\mathbf{b}_3 \tag{26}$$

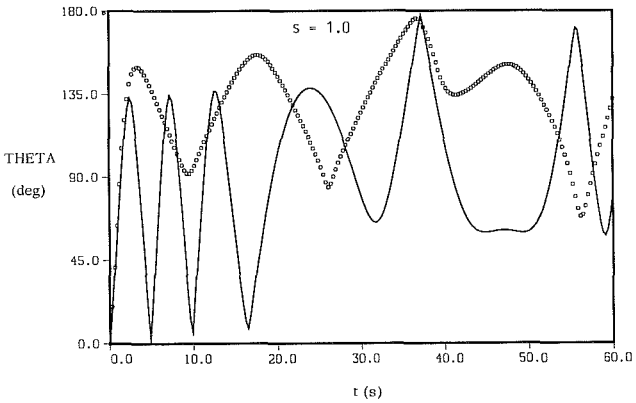


Fig. 3 THETA as a function of t

And THETA then can be expressed as

$$\text{THETA} = \cos^{-1}(\mathbf{r} \cdot \mathbf{b}_1) \tag{27}$$

or, in view of equations (25) and (26), as

$$\text{THETA} = \cos^{-1}[C_{11}(C_{11}^2 + C_{12}^2 + C_{13}^2)^{-1/2}] \tag{28}$$

Throughout what follows, we set $E_i(0) = 0$ $(i=1,2,3)$ and $E_4(0) = 1$, so that THETA vanishes at $t = 0$, and assign to y_i (see equation (7)), A_i, B_i $(i=1,2,3)$, and p (see equation (19)) the values

$$y_1 = 0.1 \quad y_2 = 0.2 \quad y_3 = 0.3 \text{ rad/s} \tag{29}$$

$$A_1 = 0.1 \quad A_2 = 0.2 \quad A_3 = 0.3 \text{ rad/s} \tag{30}$$

$$B_1 = 0.4 \quad B_2 = 0.5 \quad B_3 = 0.6 \text{ rad/s} \tag{31}$$

and $p = 0.1$ rad/s. But we consider various values of the parameter s (see equation (7)), and, for each such value, find *two* sets of the Euler parameters as functions of t, the first by numerically solving the differential equations governing the Euler parameters (see equation (34)), and the second by using the procedure set forth in the present Note. The associated values of THETA are then determined by using equation (28) in conjunction with equations (22)–(24), and results are reported in graphical form, a solid curve representing exact values, and circles representing approximate ones.

Figure 1, which deals with the case $s = 0.01$, shows that the procedure under consideration can lead to very good results, for the circles corresponding to approximate values fall right on the curve representing exact values. A tenfold increase in s, to $s = 0.1$, leads to Fig. 2, in which a difference between exact and approximate values is clearly discernible, but the qualitative agreement that manifests itself may be sufficiently great so that the approximate solution can still be regarded as useful for certain practical purposes. Finally, for $s = 1.0$, a pronounced difference between exact and approximate results

Downloaded 03 May 2010 to 171.66.16.27. Redistribution subject to ASME license or copyright; see http://www.asme.org/terms/Terms_Use.cfm

comes into evidence (Fig. 3). As was to be expected, the approximate solution is thus seen to become ever better as s becomes ever smaller. Exactly how small s must be in order for results to be acceptable in a given context always can be determined by performing a numerical integration of the differential equations governing E_k $(k=1, \ldots, 4)$.

Derivation

If $E(t)$ and $x(t)$ are the matrices

$$E=[E_1\ E_2\ E_3\ E_4] \tag{32}$$

and

$$x=0.5\begin{bmatrix} 0 & -x_3 & x_2 & -x_1 \\ x_3 & 0 & -x_1 & -x_2 \\ -x_2 & x_1 & 0 & -x_3 \\ x_1 & x_2 & x_3 & 0 \end{bmatrix} \tag{33}$$

with E_k $(k=1, \ldots, 4)$ and x_i $(i=1,2,3)$ defined as in equations (2)–(5) and (6), respectively, then the kinematical differential equations governing E_k $(k=1, \ldots, 4)$ are equivalent to

$$\dot{E}=Ex \tag{34}$$

Moreover, a matrix equation equivalent to equation (7) can be written

$$x=y+sz \tag{35}$$

where y and z are the 4×4 matrices obtained by replacing x with y and z, respectively, in equation (33). Substituting from equation (35) into equation (34), one thus finds that E must be a solution of the equation

$$\dot{E}=E(y+sz) \tag{36}$$

To solve equation (36), let $F(t)$ be a 1×4 matrix, write

$$E=E(0)e^{yt}+sF \tag{37}$$

and, after substituting from equation (37) into equation (36), linearize in s, obtaining the following equation that F must satisfy in order for equation (37) to furnish a "first order" solution of equation (36):

$$\dot{F}=Fy+E(0)e^{yt}z \tag{38}$$

Now attempt to find a 1×4 matrix $G(t)$ such that equation (38) is satisfied with F given by

$$F=Ge^{yt} \tag{39}$$

Substitution from equation (39) into equation (38) shows that this requirement is met if G satisfies the equation

$$\dot{G}=E(0)z \tag{40}$$

which it does for

$$G=E(0)\int_0^t z(u)\,du \tag{41}$$

Returning to equation (39), one can thus write

$$F=E(0)\int_0^t z(u)\,du\ e^{yt} \tag{42}$$

whereupon equation (37) yields

$$E=E(0)\left[U+s\int_0^t z(u)\,du\right]e^{yt} \tag{43}$$

where U is the 4×4 unit matrix. Moreover, in accordance with a lemma established earlier (Kane, 1973), and with m as in equation (8),

$$e^{yt}=U\cos(mt)+(y/m)\sin(mt) \tag{44}$$

and, substituting from equation (44) into equation (43), one arrives at

$$E=E(0)\left[U+s\int_0^t z(u)\,du\right][U\cos(mt)+(y/m)\sin(mt)] \tag{45}$$

This equation can be seen to be equivalent to equations (15)–(18) when equations (9)–(14) are taken into account.

References

Kane, T. R., 1973, "Solution of Kinematical Differential Equations for a Rigid Body," ASME JOURNAL OF APPLIED MECHANICS, Vol. 40, No. 1, 1973, pp. 109–113.

Kane, T. R., Likins, P. W., and Levinson, D. A., 1983, *Spacecraft Dynamics*, McGraw-Hill, New York, pp. 12–16, pp. 58–62, pp. 345–349, p. 352.

The Cracked Semi-Infinite Cylinder Under Internal Pressure

J. A. Alabi[14]

Formulas for the axial displacement and the "opening area" of a circumferential crack at the fixed end of a semi-infinite cylinder under internal pressure are given herein. The problem of a circumferential crack at the fixed end of a pipe subjected to axial tension and bending has been analyzed (Alabi, 1984; Alabi and Sanders, 1985) by thin shell theory. It seems reasonable to suppose that the analytical expression obtained in Alabi and Sanders (1985) for the energy-release rate associated with a cracked pipe under axial tension applies to a similar pipe under internal pressure since the hoop stress due to the pressure does not have any effect on the circumferential crack. This is actually borne out by an exact analysis carried out along the lines of the investigation in Alabi and Sander (1985). The effects of constraint against radial displacement turn out to be negligible.

Let the dimensional crack axial displacement $\bar{u}$ and the opening area $\bar{\Pi}$ be related to the dimensionless quantities by

$$\bar{u}=\frac{PR^2}{Eh}\,u \text{ and } \bar{\Pi}=\frac{PR^3}{Eh}\,\Pi \tag{1}$$

where p is the internal pressure, E is Young's Modulus, and h and R are, respectively, the shell thickness and radius. Then

$$4\sqrt{2}\epsilon u=\mu_1\left(\frac{\cos\theta}{\cos\alpha}-1\right)+\alpha^2-\theta^2 \tag{2}$$

$$2\sqrt{2}\epsilon\Pi=\mu_1(\tan\alpha-\alpha)+\frac{2}{3}\,\alpha^3 \tag{3}$$

where

$$\mu_1=2+\frac{\tan\alpha-\alpha}{\sqrt{2}\tan\dfrac{\alpha}{\sqrt{2}}-\tan\alpha}-\frac{\tan\alpha-\alpha}{\sqrt{2}\tan\dfrac{\pi-\alpha}{\sqrt{2}}+\tan\alpha}. \tag{4}$$

Here ϵ is given by

$$\epsilon^2=\frac{h}{R}\,[12(1-\nu^2)]^{-1/2} \tag{5}$$

ν is Poisson's ratio and 2α is the angle subtended by the crack.

[14]Mechanical Engineering Department, University of Science and Technology, Port Harcourt, Nigeria.

Manuscript received by ASME Applied Mechanics Division, January 22, 1986.

Downloaded 03 May 2010 to 171.66.16.27. Redistribution subject to ASME license or copyright; see http://www.asme.org/terms/Terms_Use.cfm

comes into evidence (Fig. 3). As was to be expected, the approximate solution is thus seen to become ever better as s becomes ever smaller. Exactly how small s must be in order for results to be acceptable in a given context always can be determined by performing a numerical integration of the differential equations governing E_k $(k=1, \ldots, 4)$.

Derivation

If $E(t)$ and $x(t)$ are the matrices

$$E=[E_1\ E_2\ E_3\ E_4] \tag{32}$$

and

$$x=0.5\begin{bmatrix} 0 & -x_3 & x_2 & -x_1 \\ x_3 & 0 & -x_1 & -x_2 \\ -x_2 & x_1 & 0 & -x_3 \\ x_1 & x_2 & x_3 & 0 \end{bmatrix} \tag{33}$$

with E_k $(k=1, \ldots, 4)$ and x_i $(i=1,2,3)$ defined as in equations (2)–(5) and (6), respectively, then the kinematical differential equations governing E_k $(k=1, \ldots, 4)$ are equivalent to

$$\dot{E}=Ex \tag{34}$$

Moreover, a matrix equation equivalent to equation (7) can be written

$$x=y+sz \tag{35}$$

where y and z are the 4×4 matrices obtained by replacing x with y and z, respectively, in equation (33). Substituting from equation (35) into equation (34), one thus finds that E must be a solution of the equation

$$\dot{E}=E(y+sz) \tag{36}$$

To solve equation (36), let $F(t)$ be a 1×4 matrix, write

$$E=E(0)e^{yt}+sF \tag{37}$$

and, after substituting from equation (37) into equation (36), linearize in s, obtaining the following equation that F must satisfy in order for equation (37) to furnish a "first order" solution of equation (36):

$$\dot{F}=Fy+E(0)e^{yt}z \tag{38}$$

Now attempt to find a 1×4 matrix $G(t)$ such that equation (38) is satisfied with F given by

$$F=Ge^{yt} \tag{39}$$

Substitution from equation (39) into equation (38) shows that this requirement is met if G satisfies the equation

$$\dot{G}=E(0)z \tag{40}$$

which it does for

$$G=E(0)\int_0^t z(u)\,du \tag{41}$$

Returning to equation (39), one can thus write

$$F=E(0)\int_0^t z(u)\,du\ e^{yt} \tag{42}$$

whereupon equation (37) yields

$$E=E(0)\left[U+s\int_0^t z(u)\,du\right]e^{yt} \tag{43}$$

where U is the 4×4 unit matrix. Moreover, in accordance with a lemma established earlier (Kane, 1973), and with m as in equation (8),

$$e^{yt}=U\cos(mt)+(y/m)\sin(mt) \tag{44}$$

and, substituting from equation (44) into equation (43), one arrives at

$$E=E(0)\left[U+s\int_0^t z(u)\,du\right][U\cos(mt)+(y/m)\sin(mt)] \tag{45}$$

This equation can be seen to be equivalent to equations (15)–(18) when equations (9)–(14) are taken into account.

References

Kane, T. R., 1973, "Solution of Kinematical Differential Equations for a Rigid Body," ASME Journal of Applied Mechanics, Vol. 40, No. 1, 1973, pp. 109–113.

Kane, T. R., Likins, P. W., and Levinson, D. A., 1983, *Spacecraft Dynamics*, McGraw-Hill, New York, pp. 12–16, pp. 58–62, pp. 345–349, p. 352.

The Cracked Semi-Infinite Cylinder Under Internal Pressure

J. A. Alabi[14]

Formulas for the axial displacement and the "opening area" of a circumferential crack at the fixed end of a semi-infinite cylinder under internal pressure are given herein. The problem of a circumferential crack at the fixed end of a pipe subjected to axial tension and bending has been analyzed (Alabi, 1984; Alabi and Sanders, 1985) by thin shell theory. It seems reasonable to suppose that the analytical expression obtained in Alabi and Sanders (1985) for the energy-release rate associated with a cracked pipe under axial tension applies to a similar pipe under internal pressure since the hoop stress due to the pressure does not have any effect on the circumferential crack. This is actually borne out by an exact analysis carried out along the lines of the investigation in Alabi and Sander (1985). The effects of constraint against radial displacement turn out to be negligible.

Let the dimensional crack axial displacement $\bar{u}$ and the opening area $\bar{\Pi}$ be related to the dimensionless quantities by

$$\bar{u}=\frac{PR^2}{Eh}\,u \text{ and } \bar{\Pi}=\frac{PR^3}{Eh}\,\Pi \tag{1}$$

where p is the internal pressure, E is Young's Modulus, and h and R are, respectively, the shell thickness and radius. Then

$$4\sqrt{2}\epsilon u=\mu_1\left(\frac{\cos\theta}{\cos\alpha}-1\right)+\alpha^2-\theta^2 \tag{2}$$

$$2\sqrt{2}\epsilon\Pi=\mu_1(\tan\alpha-\alpha)+\frac{2}{3}\,\alpha^3 \tag{3}$$

where

$$\mu_1=2+\frac{\tan\alpha-\alpha}{\sqrt{2}\tan\dfrac{\alpha}{\sqrt{2}}-\tan\alpha}-\frac{\tan\alpha-\alpha}{\sqrt{2}\tan\dfrac{\pi-\alpha}{\sqrt{2}}+\tan\alpha}. \tag{4}$$

Here ϵ is given by

$$\epsilon^2=\frac{h}{R}\,[12(1-\nu^2)]^{-1/2} \tag{5}$$

ν is Poisson's ratio and 2α is the angle subtended by the crack.

[14]Mechanical Engineering Department, University of Science and Technology, Port Harcourt, Nigeria.

Manuscript received by ASME Applied Mechanics Division, January 22, 1986.

Copyright © 1987 by ASME
Downloaded 03 May 2010 to 171.66.16.27. Redistribution subject to ASME license or copyright; see http://www.asme.org/terms/Terms_Use.cfm

The application of these formulas requires some explanation. The formulas also apply to a cracked pipe loaded by axial tension since, as has been remarked, the hoop stress due to internal pressure does not influence a circumferential crack. The formulas are applicable to a thin-walled pipe containing a sufficiently long crack. The analytical expression for the axial displacement is not accurate in the neighborhood of the crack tips. Finally, note that equations (2) and (3) are not independent since $\Pi = \int_{-\alpha}^{\alpha} ud\theta$ and that for $\alpha = \pi/2$ the right-hand-side of equations (2) and (3) are finite.

References

Alabi, J. A., 1984, "Circumferential Cracks in Cylindrical Shells," Ph.D., Thesis, Division of Applied Sciences, Harvard University.

Alabi, J. A., and Sanders, Jr., J. L., 1985, "Circumferential Crack at the fixed end of a Pipe," Engineering Fracture Mechanics, Vol. 22, No. 4, pp. 609–616.

A Method of Eliminating Lagrangian Multipliers from the Equation of Motion of Interconnected Mechanical Systems

S. Vlase[15]

Introduction

In the case of a mechanical system of rigid bodies (or more generally elastic ones), it is sometimes necessary to determine the reactions produced by the constraints. In this situation the most comfortable and used way to write motion equations and to determine reactions is the Lagrangian multipliers method. After writing the motion equations, there remain two problems: first, their solution, and second, the determination of the Lagrangian multipliers which occur linearly in the equations. The practical modality of solving all these problems is dealt with in many papers and is excellently synthesized by Paul, 1975. All of these suppose a rather great volume of computational efforts. The purpose of the present note is to show a new, simple, and "natural" method of eliminating the Lagrangian multipliers.

Kinematics

Suppose a system with M Lagrangian coordinates $(q_1, q_2, \ldots, q_M)$ subject to N explicit equations of constraint:

$$\sum_{j=1}^{M} c_{ij}\dot{q}_j = 0,\ i = 1,2,\ldots,N, \tag{1}$$

where c_{ij} depend on q_k, $k = 1,2 \ldots M$, or in matrix form:

$$[C]\{\dot{q}\} = 0 \tag{1'}$$

This system has $M-N$ degrees of freedom and $M-N$ generalized coordinates, $q_{N+1}, q_{N+2}, \ldots, q_M$. We shall denote:

$$\{\dot{q}_n\} = [\dot{q}_1 \quad \dot{q}_2 \ldots \dot{q}_N]^T;$$
$$\{\dot{q}_c\} = [\dot{q}_{N+1} \quad \ldots \quad \dot{q}_M]^T.$$

We partition $[C]$ according to the vectors $\{\dot{q}_n\}$, $\{\dot{q}_c\}$:

$$[C] = [A \vdots B].$$

Relation (1') becomes:

$$[A]\{\dot{q}_n\} + [B]\{\dot{q}_c\} = 0. \tag{2}$$

We can now compute the velocities $\{\dot{q}_n\}$ depending on the independent velocities $\{\dot{q}_c\}$:

$$\{\dot{q}_n\} = -[A]^{-1}[B]\{\dot{q}_c\} = [K]\{\dot{q}_c\} \tag{3}$$

and:

$$\{\dot{q}\} = \begin{Bmatrix} \dot{q}_n \\ \dot{q}_c \end{Bmatrix} \equiv \begin{bmatrix} K \\ E \end{bmatrix}\{\dot{q}_c\} = [P]\{\dot{q}_c\}, \tag{4}$$

where: $[K] = -[A]^{-1}[B]$, $[E]$ is a unit matrix, and

$$[P] = \begin{bmatrix} K \\ E \end{bmatrix}.$$

Relation (4) may be written:

$$\dot{q}_i = \sum_{\ell=N+1}^{M} p_{i,\ell-N}\dot{q}_\ell, i = 1,2,\ldots,M \tag{4'}$$

where p_{ij}, $i = 1, 2, \ldots, M$; $j = 1,2, \ldots, M-N$ are the elements of the matrix $[P]$.

We shall have:

$$\dot{q}_i\dot{q}_j = \left(\sum_{\ell=N+1}^{M} p_{i,\ell-N}\dot{q}_\ell\right)\left(\sum_{m=N+1}^{M} p_{j,m-N}\dot{q}_m\right) =$$

$$= \sum_{m=N+1}^{M}\sum_{\ell=N+1}^{M} p_{i,\ell-N}p_{j,m-N}\dot{q}_\ell\dot{q}_m \tag{5}$$

If we denote:

$$\{\dot{q}\}_2 = [\dot{q}_1^2 \quad \dot{q}_1\dot{q}_2\ \dot{q}_1\dot{q}_3 \ldots\ldots \dot{q}_{M-1}\dot{q}_M\ \dot{q}_M^2]^T$$
$$\{\dot{q}_c\}_2 = [\dot{q}_{N+1}^2 \ldots \quad \ldots \dot{q}_{M-1}\dot{q}_M\ \dot{q}_M^2]^T$$
$$d^{ij}_{\ell-N,m-M} = p_{i,\ell-N}p_{j,m-N};$$

$$[D] = \begin{bmatrix} d^{11}_{N+1,N+1} & d^{11}_{N+1,N+2} \ldots & \ldots d^{11}_{M-1,M} & d^{11}_{M,M} \\ d^{12}_{N+1,N+1} & d^{12}_{N+1,N+2} \ldots & \ldots & d^{12}_{M,M} \\ \vdots & & & \\ d^{M,M}_{N+1,N+1} \ldots & & \ldots & d^{M,M}_{M,M} \end{bmatrix},$$

relation (5) may be written in matrix form:

$$\{\dot{q}\}_2 = [D]\{\dot{q}_c\}_2 \tag{5'}$$

By differentiating relation (4') we obtain:

$$\ddot{q}_i = \sum_{\ell=N+1}^{M} p_{i,\ell-N}\ddot{q}_\ell + \sum_{\ell=N+1}^{M}\sum_{m=1}^{M}\frac{\partial p_{i,\ell-N}}{\partial q_m}\dot{q}_\ell\dot{q}_m =$$

$$= \sum_{\ell=N+1}^{M} p_{i,\ell-N}\ddot{q}_\ell + \sum_{\ell=N+1}^{M}\sum_{m=1}^{M}\sum_{n=N+1}^{M}\frac{\partial p_{i,\ell-N}}{\partial q_m}p_{m,n-N}\dot{q}_\ell\dot{q}_n. \tag{6}$$

If we denote:

$$f^{\,i}_{\ell n} = \sum_{m=1}^{M}\frac{\partial p_{i,\ell-N}}{\partial q_m}p_{m,n-N};$$

$$[F] = \begin{bmatrix} f^{\,1}_{N+1,N+1} & f^{\,1}_{N+1,N+2} \ldots & \ldots f^{\,1}_{M-1,M} & f^{\,1}_{M,M} \\ f^{\,2}_{N+1,N+1} & f^{\,2}_{N+1,N+2} \ldots & \ldots & f^{\,2}_{M,M} \\ \vdots & & & \\ f^{\,M}_{N+1,N+1} \ldots & & & f^{\,M}_{M,M} \end{bmatrix}$$

relation (6) is written:

$$\ddot{q}_i = \sum_{\ell=N+1}^{M} p_{i,\ell-N}\ddot{q}_\ell + \sum_{\ell=N+1}^{M}\sum_{n=N+1}^{M} f^{\,i}_{\ell n}\dot{q}_\ell\dot{q}_n \tag{7}$$

[15] Associate Professor, University of Brasov, Romania.

Manuscript received by ASME Applied Mechanics Division, March 15, 1985; final revision, July 31, 1986.

Downloaded 03 May 2010 to 171.66.16.27. Redistribution subject to ASME license or copyright; see http://www.asme.org/terms/Terms_Use.cfm

The application of these formulas requires some explanation. The formulas also apply to a cracked pipe loaded by axial tension since, as has been remarked, the hoop stress due to internal pressure does not influence a circumferential crack. The formulas are applicable to a thin-walled pipe containing a sufficiently long crack. The analytical expression for the axial displacement is not accurate in the neighborhood of the crack tips. Finally, note that equations (2) and (3) are not independent since $\Pi = \int_{-\alpha}^{\alpha} ud\theta$ and that for $\alpha = \pi/2$ the right-hand-side of equations (2) and (3) are finite.

References

Alabi, J. A., 1984, "Circumferential Cracks in Cylindrical Shells," Ph.D., Thesis, Division of Applied Sciences, Harvard University.

Alabi, J. A., and Sanders, Jr., J. L., 1985, "Circumferential Crack at the fixed end of a Pipe," Engineering Fracture Mechanics, Vol. 22, No. 4, pp. 609–616.

A Method of Eliminating Lagrangian Multipliers from the Equation of Motion of Interconnected Mechanical Systems

S. Vlase[15]

Introduction

In the case of a mechanical system of rigid bodies (or more generally elastic ones), it is sometimes necessary to determine the reactions produced by the constraints. In this situation the most comfortable and used way to write motion equations and to determine reactions is the Lagrangian multipliers method. After writing the motion equations, there remain two problems: first, their solution, and second, the determination of the Lagrangian multipliers which occur linearly in the equations. The practical modality of solving all these problems is dealt with in many papers and is excellently synthesized by Paul, 1975. All of these suppose a rather great volume of computational efforts. The purpose of the present note is to show a new, simple, and "natural" method of eliminating the Lagrangian multipliers.

Kinematics

Suppose a system with M Lagrangian coordinates $(q_1, q_2, \ldots, q_M)$ subject to N explicit equations of constraint:

$$\sum_{j=1}^{M} c_{ij}\dot{q}_j = 0,\ i = 1,2,\ldots,N, \tag{1}$$

where c_{ij} depend on q_k, $k = 1,2 \ldots M$, or in matrix form:

$$[C]\{\dot{q}\} = 0 \tag{1'}$$

This system has $M-N$ degrees of freedom and $M-N$ generalized coordinates, $q_{N+1}, q_{N+2}, \ldots, q_M$. We shall denote:

$$\{\dot{q}_n\} = [\dot{q}_1 \quad \dot{q}_2 \ldots \dot{q}_N]^T;$$
$$\{\dot{q}_c\} = [\dot{q}_{N+1} \quad \ldots \quad \dot{q}_M]^T.$$

We partition $[C]$ according to the vectors $\{\dot{q}_n\}$, $\{\dot{q}_c\}$:

$$[C] = [A \vdots B].$$

Relation (1') becomes:

$$[A]\{\dot{q}_n\} + [B]\{\dot{q}_c\} = 0. \tag{2}$$

We can now compute the velocities $\{\dot{q}_n\}$ depending on the independent velocities $\{\dot{q}_c\}$:

$$\{\dot{q}_n\} = -[A]^{-1}[B]\{\dot{q}_c\} = [K]\{\dot{q}_c\} \tag{3}$$

and:

$$\{\dot{q}\} = \begin{Bmatrix} \dot{q}_n \\ \dot{q}_c \end{Bmatrix} \equiv \begin{bmatrix} K \\ E \end{bmatrix}\{\dot{q}_c\} = [P]\{\dot{q}_c\}, \tag{4}$$

where: $[K] = -[A]^{-1}[B]$, $[E]$ is a unit matrix, and

$$[P] = \begin{bmatrix} K \\ E \end{bmatrix}.$$

Relation (4) may be written:

$$\dot{q}_i = \sum_{\ell=N+1}^{M} p_{i,\ell-N}\dot{q}_\ell, i = 1,2,\ldots,M \tag{4'}$$

where p_{ij}, $i = 1, 2, \ldots, M$; $j = 1,2, \ldots, M-N$ are the elements of the matrix $[P]$.

We shall have:

$$\dot{q}_i\dot{q}_j = \left(\sum_{\ell=N+1}^{M} p_{i,\ell-N}\dot{q}_\ell\right)\left(\sum_{m=N+1}^{M} p_{j,m-N}\dot{q}_m\right) =$$

$$= \sum_{m=N+1}^{M}\sum_{\ell=N+1}^{M} p_{i,\ell-N}p_{j,m-N}\dot{q}_\ell\dot{q}_m \tag{5}$$

If we denote:

$$\{\dot{q}\}_2 = [\dot{q}_1^2 \quad \dot{q}_1\dot{q}_2\ \dot{q}_1\dot{q}_3 \ldots\ldots \dot{q}_{M-1}\dot{q}_M\ \dot{q}_M^2]^T$$
$$\{\dot{q}_c\}_2 = [\dot{q}_{N+1}^2 \ldots \quad \ldots \dot{q}_{M-1}\dot{q}_M\ \dot{q}_M^2]^T$$
$$d^{ij}_{\ell-N,m-M} = p_{i,\ell-N}p_{j,m-N};$$

$$[D] = \begin{bmatrix} d^{11}_{N+1,N+1} & d^{11}_{N+1,N+2} \ldots & \ldots d^{11}_{M-1,M} & d^{11}_{M,M} \\ d^{12}_{N+1,N+1} & d^{12}_{N+1,N+2} \ldots & \ldots & d^{12}_{M,M} \\ \vdots & & & \\ d^{M,M}_{N+1,N+1} \ldots & & \ldots & d^{M,M}_{M,M} \end{bmatrix},$$

relation (5) may be written in matrix form:

$$\{\dot{q}\}_2 = [D]\{\dot{q}_c\}_2 \tag{5'}$$

By differentiating relation (4') we obtain:

$$\ddot{q}_i = \sum_{\ell=N+1}^{M} p_{i,\ell-N}\ddot{q}_\ell + \sum_{\ell=N+1}^{M}\sum_{m=1}^{M}\frac{\partial p_{i,\ell-N}}{\partial q_m}\dot{q}_\ell\dot{q}_m =$$

$$= \sum_{\ell=N+1}^{M} p_{i,\ell-N}\ddot{q}_\ell + \sum_{\ell=N+1}^{M}\sum_{m=1}^{M}\sum_{n=N+1}^{M}\frac{\partial p_{i,\ell-N}}{\partial q_m}p_{m,n-N}\dot{q}_\ell\dot{q}_n. \tag{6}$$

If we denote:

$$f^{\,i}_{\ell n} = \sum_{m=1}^{M}\frac{\partial p_{i,\ell-N}}{\partial q_m}p_{m,n-N};$$

$$[F] = \begin{bmatrix} f^{\,1}_{N+1,N+1} & f^{\,1}_{N+1,N+2} \ldots & \ldots f^{\,1}_{M-1,M} & f^{\,1}_{M,M} \\ f^{\,2}_{N+1,N+1} & f^{\,2}_{N+1,N+2} \ldots & \ldots & f^{\,2}_{M,M} \\ \vdots & & & \\ f^{\,M}_{N+1,N+1} \ldots & & & f^{\,M}_{M,M} \end{bmatrix}$$

relation (6) is written:

$$\ddot{q}_i = \sum_{\ell=N+1}^{M} p_{i,\ell-N}\ddot{q}_\ell + \sum_{\ell=N+1}^{M}\sum_{n=N+1}^{M} f^{\,i}_{\ell n}\dot{q}_\ell\dot{q}_n \tag{7}$$

[15] Associate Professor, University of Brasov, Romania.

Manuscript received by ASME Applied Mechanics Division, March 15, 1985; final revision, July 31, 1986.

Copyright © 1987 by ASME
Downloaded 03 May 2010 to 171.66.16.27. Redistribution subject to ASME license or copyright; see http://www.asme.org/terms/Terms_Use.cfm

or in matrix form:

$$\{\ddot{q}\} = [P]\{\ddot{q}_c\} + [F]\{\dot{q}_c\}_2 \tag{7'}$$

Equations of Motion

Since the reactions in an ideal system produce no work for any displacement compatible with the constraints, it is necessary that the supplemental forces, Q_i', associated with the reaction satisfy the condition:

$$\sum_{j=1}^{M} Q_j' \dot{q}_j = 0.$$

It may be shown that it is necessary that (e.g., Lanczos, 1966):

$$Q_j' = \sum_{i=1}^{N} \lambda_i c_{ij} \tag{8}$$

where λ_i are Lagrangian multipliers. Or in matrix form:

$$\{Q'\} = [C]^T\{\lambda\} = \begin{bmatrix} A^T \\ B^T \end{bmatrix}\{\lambda\} \tag{8'}$$

The kinetic energy can be expressed by the relation:

$$E_k = \sum_{i=1}^{M}\sum_{j=1}^{M} \frac{m^{ij}\dot{q}_i\dot{q}_j}{2} \tag{9}$$

If we apply the Lagrangian equations in the form:

$$\frac{d}{dt}\left(\frac{\partial E_k}{\partial \dot{q}_r}\right) - \frac{\partial E_k}{\partial q_r} = Q_r + \sum_{i=1}^{N} \lambda_i c_{ir}$$

we obtain:

$$\sum_{j=1}^{M} m^{rj}\ddot{q}_j + \sum_{i=1}^{M}\sum_{j=1}^{M} s^{r,ij}\dot{q}_i\dot{q}_j = Q_r + \sum_{i=1}^{N} \lambda_i c_{ir} \tag{10}$$

$$r = 1,2,\ldots,M$$

where Q_r represents the generalized force coresponding to the generalized coordinate q_r and:

$$s^{r,ij} = \frac{1}{2}\left(\frac{\partial m^{ri}}{\partial q_i} + \frac{\partial m^{rj}}{\partial q_j} - \frac{\partial m^{ij}}{\partial q_r}\right).$$

If we write:

$$[I] = \begin{bmatrix} m^{11} & m^{12} & \ldots & m^{1M} \\ m^{21} & m^{22} & \ldots & m^{2M} \\ \vdots & & & \\ m^{M1} & \ldots & & m^{MM} \end{bmatrix}$$

$$[I'] = \begin{bmatrix} s^{1,11} & s^{1,12} & \ldots & s^{1,M-1,M} \\ s^{2,11} & s^{2,12} & \ldots & s^{2,M-1,M} \\ \vdots & & & \\ s & & & \\ \vdots & & & \\ s^{M,11} & s^{M,12} & \ldots & s^{M,M-1,M} \end{bmatrix}$$

relation (9) may be written in matrix form:

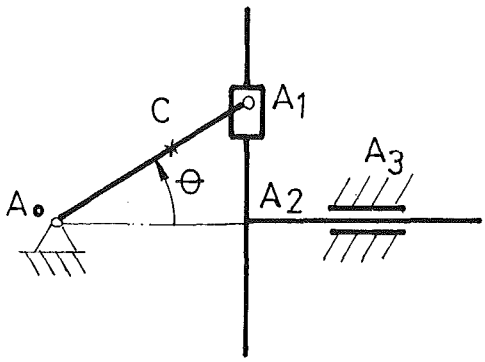


Fig. 1

$$[I]\{\ddot{q}\} + [I']\{\dot{q}\}_2 = \{Q\} + \begin{bmatrix} A^T \\ B^T \end{bmatrix}\{\lambda\} \tag{10'}$$

Description of the Method

If we multiply equations (10′) by the transposed matrix $[K^T|E]$ we obtain:

$$[K^T|E][I]\{\ddot{q}\} + [K^T|E][I']\{\dot{q}\}_2 = [K^T|E]\{Q\} + [K^T|E]\begin{bmatrix} A^T \\ B^T \end{bmatrix}\{\lambda\} \tag{11}$$

But:

$$[K^T|E]\begin{bmatrix} A^T \\ B^T \end{bmatrix} = [K^TA^T + B^T] = [-(A^{-1}B)^TA^T + B^T] = 0 \tag{12}$$

Relation (10) becomes:

$$[K^T|E][I]\{\ddot{q}\} + [K^T|E][I']\{\dot{q}\}_2 = [K^T|E]\{Q\} \tag{13}$$

Considering also (5′) and (7′) we can write as well:

$$[\tilde{I}]\{\ddot{q}_c\} + [\tilde{I}']\{\dot{q}_c\}_2 = \{\tilde{Q}\}, \tag{14}$$

where:

$$[\tilde{I}] = [K^T|E][I]\begin{bmatrix} K \\ E \end{bmatrix};$$

$$[\tilde{I}'] = [K^T|E][I][F] + [K^T|E][I'][D].$$

The equations (14) are a differential system with $M-N$ unknowns $q_{N+1}, q_{N+2}, \ldots, q_M$. These equations no longer contain Lagrangian multipliers. It follows that the elimination of Lagrangian multipliers consists mainly of the premultiplication of the system of equations by $[K^T|E]$, a simple matrix multiplication.

This extremely simple method of eliminating Lagrangian multipliers is a natural and direct solution to that problem.

Example

The mechanism in Fig. 1 is considered, for which the length of the bar A_0A_1 is known, and for which the bar's gravitation center lies in its middle. The mass of the bar A_0A_1 will be denoted with m_1, the mass of the body A_1 with m_2, the mass of the body $A_1A_2A_3$ with m_2, and the inertia moment of the bar A_0A_1 with J. In the coordinate system chosen we have $C(x_c,y_c)A_1(x_1,y_1),A_2(x_2,0)$.

The kinetic energy of the mechanism is:

Downloaded 03 May 2010 to 171.66.16.27. Redistribution subject to ASME license or copyright; see http://www.asme.org/terms/Terms_Use.cfm

$$E_k = \frac{1}{2} m_1(\dot{x}_c^2 + \dot{y}_c^2) + \frac{1}{2} J\dot{\theta}^2 + \frac{1}{2} m_2(\dot{x}_1^2 + \dot{y}_1^2) + \frac{1}{2} m_3 \dot{x}_2^2$$

where $\dot{\theta}$ represents the angular velocity of the bar A_0A_1. Since the mechanism has one degree of freedom, five kinetic conditions are required to connect the six kinetic parameters $\dot{x}_c$, $\dot{y}_c$, $\dot{\theta}$, $\dot{x}_1$, $\dot{y}_1$, $\dot{x}_2$.

The following relations may be written between the independent coordinates:

$$\begin{aligned} &x_c - \frac{\ell}{2}\cos\theta = 0 \\ &y_c - \frac{\ell}{2}\sin\theta = 0 \\ &x_c + \frac{\ell}{2}\cos\theta - x_1 = 0 \\ &y_c + \frac{\ell}{2}\sin\theta - y_1 = 0 \\ &x_1 - x_2 = 0 \end{aligned} \tag{15}$$

From equations (15), by differentiating twice and grouping the terms properly, we obtain:

$$\begin{Bmatrix} \ddot{x}_c \\ \ddot{y}_c \\ \ddot{x}_1 \\ \ddot{y}_1 \\ \ddot{x}_2 \\ \ddot{\theta} \end{Bmatrix} = \begin{Bmatrix} -\frac{\ell}{2}\sin\theta \\ \frac{\ell}{2}\cos\theta \\ -\ell\sin\theta \\ \ell\cos\theta \\ -\ell\sin\theta \\ 1 \end{Bmatrix} \ddot{\theta} + \begin{Bmatrix} -\frac{\ell}{2}\cos\theta \\ \frac{\ell}{2}\sin\theta \\ -\ell\cos\theta \\ -\ell\sin\theta \\ -\ell\cos\theta \\ 0 \end{Bmatrix} \dot{\theta}^2 \tag{16}$$

By applying the Lagrangian equations we obtain:

$$\begin{bmatrix} m_1 & & & & & \\ & m_1 & & 0 & & \\ & & m_2 & & & \\ & & & m_2 & & \\ & 0 & & & m_3 & \\ & & & & & J \end{bmatrix} \begin{Bmatrix} \ddot{x}_c \\ \ddot{y}_c \\ \ddot{x}_1 \\ \ddot{y}_1 \\ \ddot{x}_2 \\ \ddot{\theta} \end{Bmatrix}$$

$$= \begin{bmatrix} 1 & 0 & 1 & 0 & 0 \\ 0 & 1 & 0 & 1 & 0 \\ 0 & 0 & -1 & 0 & 1 \\ 0 & 0 & 0 & -1 & 0 \\ 0 & 0 & 0 & 0 & -1 \\ \frac{\ell}{2}\sin\theta & -\frac{\ell}{2}\cos\theta & -\frac{\ell}{2}\sin\theta & \frac{\ell}{2}\sin\theta & 0 \end{bmatrix} \begin{Bmatrix} \lambda_1 \\ \lambda_2 \\ \lambda_3 \\ \lambda_4 \\ \lambda_5 \end{Bmatrix} \tag{17}$$

The term $[I']$ are lacking for this example.

By using the equations (16) and (17) and by premultiplying (17) by:

$$\left[-\frac{\ell}{2}\sin\theta \quad \frac{\ell}{2}\cos\theta \quad -\ell\sin\theta \quad \ell\cos\theta \quad -\ell\sin\theta \quad 1 \right],$$

after performing the calculations, the differential equation is obtained:

$$\alpha\ddot{\theta} + \beta\dot{\theta}^2 = 0, \tag{18}$$

where:

$$\alpha = m_1\frac{\ell^2}{4} + m_2\ell^2 + m_3\ell^2\sin^2\theta + J;$$

$$\beta = m_3\ell^2\sin\theta\cos\theta.$$

Assuming equation (18) is solved, returning to the system (17) and dispensing with one equation, for example the last, the values λ_i, $i = 1,2,\ldots,5$ are easily obtained.

$$\begin{Bmatrix} \lambda_1 \\ \lambda_2 \\ \lambda_3 \\ \lambda_4 \\ \lambda_5 \end{Bmatrix} = \begin{Bmatrix} -\frac{m_1}{2}\sin\theta - m_2\sin\theta \\ \frac{m_1}{2}\cos\theta + m_2\cos\theta \\ m_2\sin\theta + m_3\sin\theta \\ m_2\cos\theta \\ -m_3\sin\theta \end{Bmatrix} \ell\ddot{\theta}$$

$$+ \begin{Bmatrix} -\frac{m_1}{2}\cos\theta - m_2\cos\theta \\ -\frac{m_1}{2}\sin\theta - m_2\sin\theta \\ m_2\cos\theta + m_3\cos\theta \\ -m_2\sin\theta \\ -m_3\cos\theta \end{Bmatrix} \ell\dot{\theta}^2.$$

It should be noted that in the case under consideration, λ_1, λ_2 represent the reaction components on point A_o, λ_3, λ_4 the reaction components on point A_1 and λ_5 the normal force on the bar $A_1A_2A_3$.

References

Lanczos, C., 1966, *The Variational Principles of Mechanics*, 3rd Edn., University of Toronto, Toronto, Canada.

Paul, B., 1975, "Analytical Dynamics of Mechanisms–A Computer Oriented Overview," *Mechanism and Machine Theory*, Vol. 10, p. 481–507.

Surface Microextensometry by Means of Moire Interferometry With a Scanning Electron Microscope

Marc-Henri Ambroise,[16] T. Bretheau,[16] P. Viaris de Lesegno[16]

1 Introduction

Microextensometry grids, made by microlithography techniques (Attwood and Hazzeldine, 1976; Bretheau and Caldemaison, 1981) allow to obtain a partial knowledge, at a very low scale, of the surface displacement field of microheterogeneous samples (polycrystals, single or

[16]Laboratoire PMTM, CNRS, Université Paris-Nord, 93430 Villetaneuse, France.

Manuscript received by ASME Applied Mechanics Division, October 10, 1985; final revision, August 12, 1986.

Downloaded 03 May 2010 to 171.66.16.27. Redistribution subject to ASME license or copyright; see http://www.asme.org/terms/Terms_Use.cfm

$$E_k = \frac{1}{2} m_1(\dot{x}_c^2 + \dot{y}_c^2) + \frac{1}{2} J\dot{\theta}^2 + \frac{1}{2} m_2(\dot{x}_1^2 + \dot{y}_1^2) + \frac{1}{2} m_3 \dot{x}_2^2$$

where $\dot{\theta}$ represents the angular velocity of the bar A_0A_1. Since the mechanism has one degree of freedom, five kinetic conditions are required to connect the six kinetic parameters $\dot{x}_c$, $\dot{y}_c$, $\dot{\theta}$, $\dot{x}_1$, $\dot{y}_1$, $\dot{x}_2$.

The following relations may be written between the independent coordinates:

$$\begin{aligned} &x_c - \frac{\ell}{2}\cos\theta = 0 \\ &y_c - \frac{\ell}{2}\sin\theta = 0 \\ &x_c + \frac{\ell}{2}\cos\theta - x_1 = 0 \\ &y_c + \frac{\ell}{2}\sin\theta - y_1 = 0 \\ &x_1 - x_2 = 0 \end{aligned} \tag{15}$$

From equations (15), by differentiating twice and grouping the terms properly, we obtain:

$$\begin{Bmatrix} \ddot{x}_c \\ \ddot{y}_c \\ \ddot{x}_1 \\ \ddot{y}_1 \\ \ddot{x}_2 \\ \ddot{\theta} \end{Bmatrix} = \begin{Bmatrix} -\frac{\ell}{2}\sin\theta \\ \frac{\ell}{2}\cos\theta \\ -\ell\sin\theta \\ \ell\cos\theta \\ -\ell\sin\theta \\ 1 \end{Bmatrix} \ddot{\theta} + \begin{Bmatrix} -\frac{\ell}{2}\cos\theta \\ \frac{\ell}{2}\sin\theta \\ -\ell\cos\theta \\ -\ell\sin\theta \\ -\ell\cos\theta \\ 0 \end{Bmatrix} \dot{\theta}^2 \tag{16}$$

By applying the Lagrangian equations we obtain:

$$\begin{bmatrix} m_1 & & & & & \\ & m_1 & & 0 & & \\ & & m_2 & & & \\ & & & m_2 & & \\ & 0 & & & m_3 & \\ & & & & & J \end{bmatrix} \begin{Bmatrix} \ddot{x}_c \\ \ddot{y}_c \\ \ddot{x}_1 \\ \ddot{y}_1 \\ \ddot{x}_2 \\ \ddot{\theta} \end{Bmatrix}$$

$$= \begin{bmatrix} 1 & 0 & 1 & 0 & 0 \\ 0 & 1 & 0 & 1 & 0 \\ 0 & 0 & -1 & 0 & 1 \\ 0 & 0 & 0 & -1 & 0 \\ 0 & 0 & 0 & 0 & -1 \\ \frac{\ell}{2}\sin\theta & -\frac{\ell}{2}\cos\theta & -\frac{\ell}{2}\sin\theta & \frac{\ell}{2}\sin\theta & 0 \end{bmatrix} \begin{Bmatrix} \lambda_1 \\ \lambda_2 \\ \lambda_3 \\ \lambda_4 \\ \lambda_5 \end{Bmatrix} \tag{17}$$

The term $[I']$ are lacking for this example.

By using the equations (16) and (17) and by premultiplying (17) by:

$$\left[-\frac{\ell}{2}\sin\theta \;\; \frac{\ell}{2}\cos\theta \;\; -\ell\sin\theta \;\; \ell\cos\theta \;\; -\ell\sin\theta \;\; 1 \right],$$

after performing the calculations, the differential equation is obtained:

$$\alpha\ddot{\theta} + \beta\dot{\theta}^2 = 0, \tag{18}$$

where:

$$\alpha = m_1\frac{\ell^2}{4} + m_2\ell^2 + m_3\ell^2\sin^2\theta + J;$$

$$\beta = m_3\ell^2\sin\theta\cos\theta.$$

Assuming equation (18) is solved, returning to the system (17) and dispensing with one equation, for example the last, the values λ_i, $i = 1,2,\ldots,5$ are easily obtained.

$$\begin{Bmatrix} \lambda_1 \\ \lambda_2 \\ \lambda_3 \\ \lambda_4 \\ \lambda_5 \end{Bmatrix} = \begin{Bmatrix} -\frac{m_1}{2}\sin\theta - m_2\sin\theta \\ \frac{m_1}{2}\cos\theta + m_2\cos\theta \\ m_2\sin\theta + m_3\sin\theta \\ m_2\cos\theta \\ -m_3\sin\theta \end{Bmatrix} \ell\ddot{\theta}$$

$$+ \begin{Bmatrix} -\frac{m_1}{2}\cos\theta - m_2\cos\theta \\ -\frac{m_1}{2}\sin\theta - m_2\sin\theta \\ m_2\cos\theta + m_3\cos\theta \\ -m_2\sin\theta \\ -m_3\cos\theta \end{Bmatrix} \ell\dot{\theta}^2.$$

It should be noted that in the case under consideration, λ_1, λ_2 represent the reaction components on point A_o, λ_3, λ_4 the reaction components on point A_1 and λ_5 the normal force on the bar $A_1A_2A_3$.

References

Lanczos, C., 1966, *The Variational Principles of Mechanics*, 3rd Edn., University of Toronto, Toronto, Canada.

Paul, B., 1975, "Analytical Dynamics of Mechanisms–A Computer Oriented Overview," *Mechanism and Machine Theory*, Vol. 10, p. 481–507.

Surface Microextensometry by Means of Moire Interferometry With a Scanning Electron Microscope

Marc-Henri Ambroise,[16] T. Bretheau,[16] P. Viaris de Lesegno[16]

1 Introduction

Microextensometry grids, made by microlithography techniques (Attwood and Hazzeldine, 1976; Bretheau and Caldemaison, 1981) allow to obtain a partial knowledge, at a very low scale, of the surface displacement field of microheterogeneous samples (polycrystals, single or

[16]Laboratoire PMTM, CNRS, Université Paris-Nord, 93430 Villetaneuse, France.

Manuscript received by ASME Applied Mechanics Division, October 10, 1985; final revision, August 12, 1986.

Copyright © 1987 by ASME

Downloaded 03 May 2010 to 171.66.16.27. Redistribution subject to ASME license or copyright; see http://www.asme.org/terms/Terms_Use.cfm

multiphase materials etc. . .); the local strain field can then be deduced (Bretheau and Caldemaison 1983). This powerful method has the advantage of not hiding the surface, and allows observation of the appearance of defects due to deformation (slip lines, cracks, interface decohesions etc. . .). However, more global information could be very useful even if in a more averaged way. To this end, the moiré method (Daniel, 1983) can be used in order to evaluate quickly the information contained within the specimen grating deposited on the surface to be studied. The surface displacement field can be determined by superposing a second grating or master grating, producing patterns of moiré interferometry fringes. These patterns depict the in-plane displacements of every point on the specimen surface as maps of equal displacement fringes, the displacement being considered perpendicularly to the master grating (Dantu, 1957). The fringe spacing is inversely proportional to the displacement gradient; the precise knowledge of the master grating pitch allows one to deduce the strain field.

We propose here a technique based upon the use of a scanning electron microscope (SEM), for producing gratings as well as for producing the moiré patterns; an application is then reported and finally we discuss the performance of and improvement in this technique.

2 Experimental

In order to completely control the electron scanning, the SEM is interfaced with a fast microprocessor that plays the role of a scan generator and a microcomputer for the data processing by means of two 12 bits digital/analog converters. Moreover, this device allows image processing.

Up to now the displacement fields are deduced from measurements on photographs of the grids taken at different stages of the deformation by means of a digitizer coupled with a microcomputer.

Square microgrids are realized by an electromicrolithographic technique (Ambroise, 1986). We obtain 1 mm^2 gold grids with a 2 μm minimum pitch and a line width thinner than 0.4 μm (Fig. 1). Under the grid, the material substructure is clearly visible.

A moiré pattern can be formed with the SEM by making an image of a microgrid by means of a line-pattern of e beam scan consistent with the one used to make the grid. When the specimen is deformed, the local displacement field at the surface of the specimen can be visualized through the resulting moiré pattern. Thus, the grid is the specimen grating and the scanning plays the role of the master grating. If the pitch of the master grating is a given ratio of the specimen grating (in the initial state), the fringe number is divided by this ratio: this allows the technique to be made more or less sensitive (Hartong, 1981).

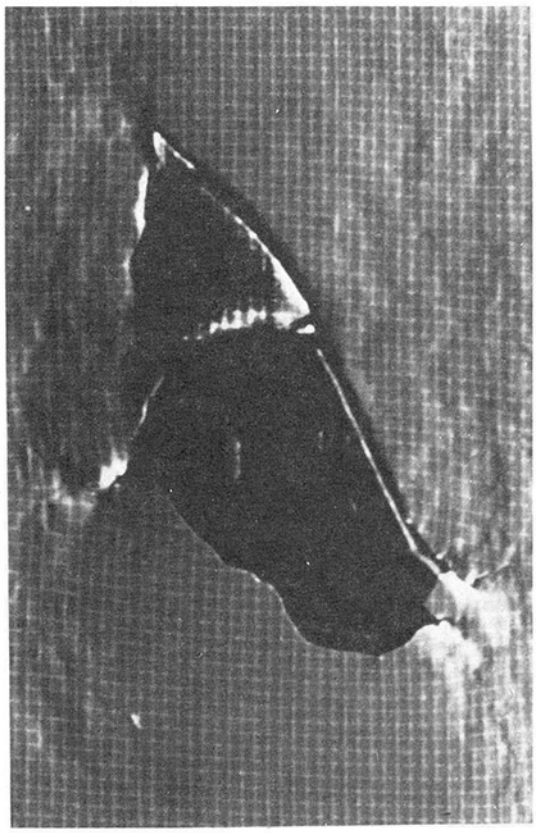


Fig. 1 Square micro-grid around a superficial inclusion (back scattered electron image) (grid pitch—3.5 μm; macroscopical strain = 0.06, vertical tensile axis). Crack initiation, interfacial decohesion and inclusion fracture are visible. Sample surface becomes strongly rough in the heavily deformed regions. Two weakly deformed regions are visible at the top and the bottom of the picture.

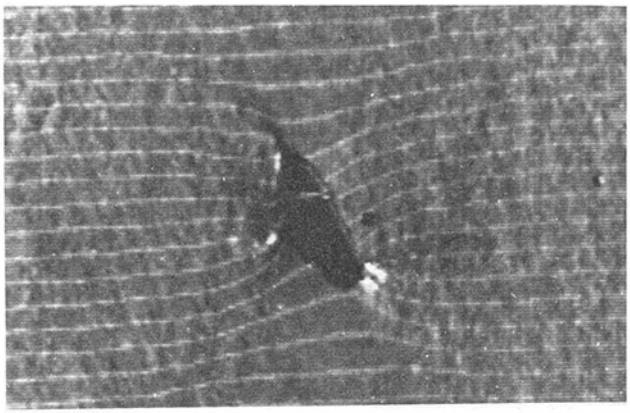


Fig. 2 Fringe moiré patterns (same inclusion as in Fig. 1). Vertical displacements for a tensile strain of about 0.06 (master grid pitch – 3.2 μm).

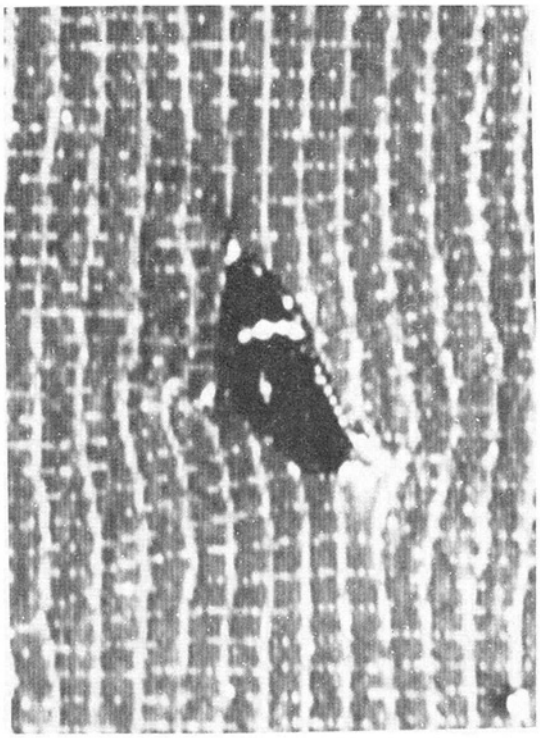


Fig. 3(*a*) Cellular moiré pattern (same inclusion as in Fig. 1). The microscope effect of the moiré method is obvious on this example: the moiré cells have the structure of the microscopical motif with its quasi periodic characteristics and defects (master grid pitch—3.2 μm).

Downloaded 03 May 2010 to 171.66.16.27. Redistribution subject to ASME license or copyright; see http://www.asme.org/terms/Terms_Use.cfm

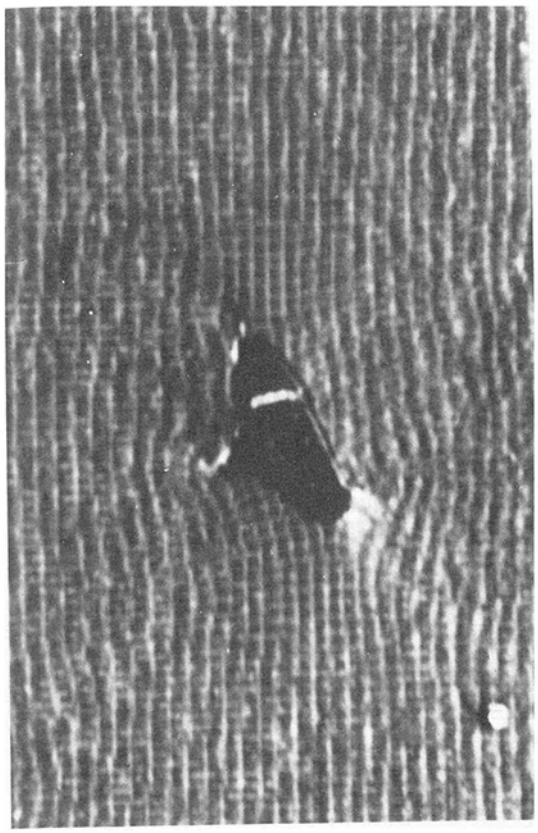


Fig. 3(*b*) Cell multiplication (× 4) (same inclusion as in Fig. 1) (master grid pitch—1.6 μm).

3 Applications

Two scales of analysis of the deformed microgrids are at our disposal:

(1) At a microscopic scale a direct measurement of the coordinates of peculiar points of the grid (e.g., line junctions) before and after deformation allows one to deduce, by finite differences, the in-plane components of relative displacements with an accuracy equal to the line-width of the grid (Bretheau and Caldemaison, 1983).

(2) At a "mesoscopic" scale a moiré pattern allows a direct visualization of the displacement field components in the projection plane. This second method displays rapidly the areas of interest for a more local and precise analysis by means of the first one (Figs. 2, 3). At present, the moiré technique remains qualitative because of the strong effects of the SEM aberrations.

At present we use the microgrid technique for the study of matrix/inclusion interactions (Bretheau and Caldemaison, 1981; Ambroise, 1986); it allows the measurement of disturbances in the surface strain field due to surface inclusions.

Figure 1 clearly shows microscopical features such as the decohesion at some inclusion/matrix interfaces, the fracture of the inclusion, the formation of some strongly strained zones near cuspidal points and, for the highest macroscopical strain, the nucleation of microcracks. On the other hand, the moiré method shows (Figs. 2, 3), for the same macroscopical strains, that the local strain is stronger at those surfaces which are nearly parallel to the tensile axis but weaker at the interfaces nearly orthogonal to the tensile axis; this is consistent with a decohesion at these interfaces. Moreover, the area affected by the presence of the inclusion is clearly visible and can be estimated as 4 times the inclusion size.

4 Improvements of the Technique

In his theory of moiré interferometry, J. Hartong (1981) shows that moiré patterns are obtained through the superposition of two grid patterns with a microscopical characteristic which repeats itself periodically on the surface and changes only on the macroscopical scale. Then the moiré pattern formed in this manner has a cellular aspect; the moiré cells that replace the fringes have the same geometry as the microscopical motif and allow the measurement of the displacement components along any direction in the surface of interest.

It is not possible, at the moment, to generate a square grid with a unique scanning; if one tries to obtain a cellular moiré pattern with two master grids made up of perpendicular lines, weak contrast results. In order to enhance the signal/noise ratio, a master grid of points is used: thus one needs only one scanning to get a cellular moiré pattern like that in Fig. 3. It is possible, by the way, to multiply the moiré cells, as it is done for moiré patterns of fringes (Fig. 2). The same result can be achieved with two superposed grids of points. Now, we are able to make grids of points with a 1 μm pitch and 0.2 μm in diameter. Moreover, when the master grid pitch is reduced, the moiré pattern pitch is reduced as well, and it becomes possible, under certain conditions, to produce moiré patterns by superposition of two moiré patterns and to exhibit thus the deformation fields directly (Hartong, 1981).

References

Ambroise, M. H., 1986, "Etude de la Nocivité d'Inclusions Superficielles: Amorçage de Fissures dans les Superalliages Préparés par Métallurgie des Poudres," Thèse de Doctorat, Université Paris XIII.

Attwood, D. G., and Hazzeldine, P. M., 1976, "A Fiducial Grid for High Resolution Metallography," *Metallography*, Vol. 9, pp. 483–501.

Bretheau, T., and Caldemaison, D., 1981, "Deformation of Polycrystals: Mechanisms and Microstructures," 2nd Risø Int. Symp., pp. 157–161.

Bretheau, T., and Caldemaison, D., 1983, "Study of Inclusion Matrix Interaction by Means of Local Strain Measurements," 4th Risø Int. Symp., pp. 173–178.

Daniel, I. M., 1983, "Experimental Methods in Applied Mechanics," ASME Journal of Applied Mechanics, Vol. 50, pp. 963–976.

Dantu, P., 1957, "Etude des Réseaux Pour l'Étude des Déformations," Publication 56-6-11 du Laboratoire des Ponts et Chaussées, Paris, pp. 26–46.

Hartong, J., 1981, "Le Moiré," *Advances in Applied Mathematics*, Vol. 2, pp. 24–75.

Impact With an Impulsive Frictional Moment

Joseph B. Keller[17]

Recently we showed how to include an impulsive frictional force in the analysis of the impact or collision of two bodies (Keller, 1986). Now we shall show how to include in addition an impulsive moment or torque which is wholly or partially frictional. For the sake of brevity, wherever possible we shall refer to the equations of Keller (1986) by their numbers and indicate how to modify them.

Let us suppose that the contact moment $[(-1)^j/t_c]G(t't_c)$ is exerted on body j by the other body during the collision. This moment must be added to the right side of equation (2.2). As a consequence we must add $(-1)^j G(t)$ to the right sides of equations (2.4) and (2.6), and $(-1)^j J_j^{-1}\Gamma$ to the right sides of equations (2.10) and (3.10). Here Γ is the impulsive angular moment defined by

$$\Gamma = \int_0^1 G(t)dt. \qquad (2.11a)$$

To find $G(t)$ we will need the relative angular velocity $\omega(t)$ of the two bodies,

[17]Departments of Mathematics and Mechanical Engineering, Stanford University, Stanford, CA 94305.

Manuscript received by ASME Applied Mechanics Division, February 3, 1986; final revision, March 3, 1986.

Downloaded 03 May 2010 to 171.66.16.27. Redistribution subject to ASME license or copyright; see http://www.asme.org/terms/Terms_Use.cfm

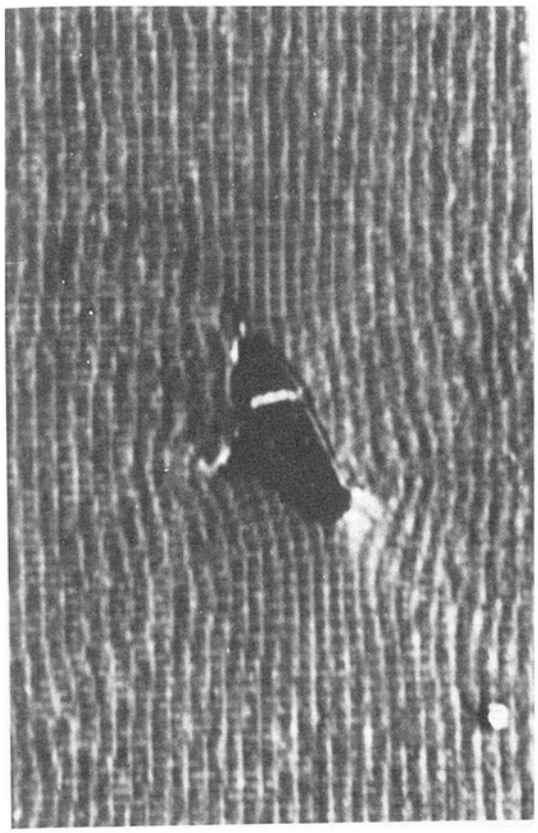


Fig. 3(*b*) Cell multiplication (× 4) (same inclusion as in Fig. 1) (master grid pitch—1.6 μm).

3 Applications

Two scales of analysis of the deformed microgrids are at our disposal:

(1) At a microscopic scale a direct measurement of the coordinates of peculiar points of the grid (e.g., line junctions) before and after deformation allows one to deduce, by finite differences, the in-plane components of relative displacements with an accuracy equal to the line-width of the grid (Bretheau and Caldemaison, 1983).

(2) At a "mesoscopic" scale a moiré pattern allows a direct visualization of the displacement field components in the projection plane. This second method displays rapidly the areas of interest for a more local and precise analysis by means of the first one (Figs. 2, 3). At present, the moiré technique remains qualitative because of the strong effects of the SEM aberrations.

At present we use the microgrid technique for the study of matrix/inclusion interactions (Bretheau and Caldemaison, 1981; Ambroise, 1986); it allows the measurement of disturbances in the surface strain field due to surface inclusions.

Figure 1 clearly shows microscopical features such as the decohesion at some inclusion/matrix interfaces, the fracture of the inclusion, the formation of some strongly strained zones near cuspidal points and, for the highest macroscopical strain, the nucleation of microcracks. On the other hand, the moiré method shows (Figs. 2, 3), for the same macroscopical strains, that the local strain is stronger at those surfaces which are nearly parallel to the tensile axis but weaker at the interfaces nearly orthogonal to the tensile axis; this is consistent with a decohesion at these interfaces. Moreover, the area affected by the presence of the inclusion is clearly visible and can be estimated as 4 times the inclusion size.

4 Improvements of the Technique

In his theory of moiré interferometry, J. Hartong (1981) shows that moiré patterns are obtained through the superposition of two grid patterns with a microscopical characteristic which repeats itself periodically on the surface and changes only on the macroscopical scale. Then the moiré pattern formed in this manner has a cellular aspect; the moiré cells that replace the fringes have the same geometry as the microscopical motif and allow the measurement of the displacement components along any direction in the surface of interest.

It is not possible, at the moment, to generate a square grid with a unique scanning; if one tries to obtain a cellular moiré pattern with two master grids made up of perpendicular lines, weak contrast results. In order to enhance the signal/noise ratio, a master grid of points is used: thus one needs only one scanning to get a cellular moiré pattern like that in Fig. 3. It is possible, by the way, to multiply the moiré cells, as it is done for moiré patterns of fringes (Fig. 2). The same result can be achieved with two superposed grids of points. Now, we are able to make grids of points with a 1 μm pitch and 0.2 μm in diameter. Moreover, when the master grid pitch is reduced, the moiré pattern pitch is reduced as well, and it becomes possible, under certain conditions, to produce moiré patterns by superposition of two moiré patterns and to exhibit thus the deformation fields directly (Hartong, 1981).

References

Ambroise, M. H., 1986, "Etude de la Nocivité d'Inclusions Superficielles: Amorçage de Fissures dans les Superalliages Préparés par Métallurgie des Poudres," Thèse de Doctorat, Université Paris XIII.

Attwood, D. G., and Hazzeldine, P. M., 1976, "A Fiducial Grid for High Resolution Metallography," *Metallography*, Vol. 9, pp. 483–501.

Bretheau, T., and Caldemaison, D., 1981, "Deformation of Polycrystals: Mechanisms and Microstructures," 2nd Risø Int. Symp., pp. 157–161.

Bretheau, T., and Caldemaison, D., 1983, "Study of Inclusion Matrix Interaction by Means of Local Strain Measurements," 4th Risø Int. Symp., pp. 173–178.

Daniel, I. M., 1983, "Experimental Methods in Applied Mechanics," ASME Journal of Applied Mechanics, Vol. 50, pp. 963–976.

Dantu, P., 1957, "Etude des Réseaux Pour l'Étude des Déformations," Publication 56-6-11 du Laboratoire des Ponts et Chaussées, Paris, pp. 26–46.

Hartong, J., 1981, "Le Moiré," *Advances in Applied Mathematics*, Vol. 2, pp. 24–75.

Impact With an Impulsive Frictional Moment

Joseph B. Keller[17]

Recently we showed how to include an impulsive frictional force in the analysis of the impact or collision of two bodies (Keller, 1986). Now we shall show how to include in addition an impulsive moment or torque which is wholly or partially frictional. For the sake of brevity, wherever possible we shall refer to the equations of Keller (1986) by their numbers and indicate how to modify them.

Let us suppose that the contact moment $[(-1)^j/t_c]G(t't_c)$ is exerted on body j by the other body during the collision. This moment must be added to the right side of equation (2.2). As a consequence we must add $(-1)^j G(t)$ to the right sides of equations (2.4) and (2.6), and $(-1)^j J_j^{-1}\Gamma$ to the right sides of equations (2.10) and (3.10). Here Γ is the impulsive angular moment defined by

$$\Gamma = \int_0^1 G(t)dt. \qquad (2.11a)$$

To find $G(t)$ we will need the relative angular velocity $\omega(t)$ of the two bodies,

[17]Departments of Mathematics and Mechanical Engineering, Stanford University, Stanford, CA 94305.

Manuscript received by ASME Applied Mechanics Division, February 3, 1986; final revision, March 3, 1986.

Copyright © 1987 by ASME
Downloaded 03 May 2010 to 171.66.16.27. Redistribution subject to ASME license or copyright; see http://www.asme.org/terms/Terms_Use.cfm

$$\omega(t)=\Omega_2-\Omega_1. \tag{3.2a}$$

We now write $G(t)$ in the form

$$G(t)=N(t)[ng_f(t)+g_T(t)],\ n\cdot g_T(t)=0. \tag{3.5a}$$

Here $N(t)$ is the normal force, $N\,ng_f$ is the frictional moment which is normal to the surface, and $N\,g_T$ is the nonfrictional moment which is tangential. We assume that g_f is given by a law of angular friction of the following form, in which $\omega_n=\omega\cdot n$:

$$g_f=-\nu\,\mathrm{sgn}\ \omega_n \text{ if } \omega_n\neq 0, \tag{3.6a}$$

$$|g_f|\leq\nu \text{ if } \omega_n=0.$$

The quantity ν is a coefficient of angular sliding friction with the dimensions of length. In principle it can be determined by analyzing the deformation of the surfaces during impact and using the usual law of friction. It ought to be proportional to μ and should depend upon $N(t)$.

When we use equations (3.5*a*) in (2.11*a*), and write g_f and g_T as functions of τ, we get

$$\Gamma=\int_0^{(1+e)\tau_0}[ng_f(\tau)+g_T(\tau)]d\tau. \tag{3.8a}$$

Then equation (3.8*a*) is used in equation (3.10) with the extra term $(-1)^j J_j^{-1}\Gamma$ on the right side, and equation (3.10) becomes

$$[\Omega_j]=(-1)^j J_j^{-1}\left(R_j\times\left\{(1+e)\tau_0 n-\mu\int_0^{(1+e)\tau_0}\hat{u}_T(\tau)d\tau\right\}\right.$$

$$\left.+\int_0^{(1+e)\tau_0}[ng_f(\tau)+g_T(\tau)]d\tau\right). \tag{3.10a}$$

Next we must add $(J_j^{-1}G)\times R_j$ to the summand in equation (4.1) and add ng_f+g_T to $R_j\times(n+f)$ in equations (4.2), (4.3), (4.4), (4.6), and (4.9). We must also add $n\cdot[J_j^{-1}\int_0^\tau(ng_f+g_T)d\tau']\times R_j$ to the summands in equations (4.7) and (4.8) with $\tau=\tau_0$ in (4.8).

To determine $\omega(\tau)$, which occurs in equation (3.6*a*), we differentiate equation (3.2*a*) and use equation (2.6) to get

$$\frac{d\omega}{dt}=\sum_{j=1}^{2}J_j^{-1}[G+R_j\times F]. \tag{4.1a}$$

Now we use equation (3.5) for F and equation (3.5*a*) for G in equation (4.1*a*) and write $N^{-1}d/dt=d/d\tau$ to obtain

$$\frac{d\omega}{d\tau}=\sum_{j=1}^{2}J_j^{-1}[ng_f+g_T+R_j\times(n+f)]. \tag{4.3a}$$

From equation (3.2*a*) the initial value of ω is

$$\omega(0)=\Omega_2^-\,-\Omega_1^-. \tag{4.4a}$$

Finally we take the inner product of n with equations (4.3*a*) and (4.4*a*) to get

$$\frac{d\omega_n}{d\tau}=\sum_{j=1}^{2}n\cdot J_j^{-1}[ng_f+g_T+R_j\times(n+f)], \tag{4.9a}$$

$$\omega_n(0)=n\cdot(\Omega_2^-\,-\Omega_1^-). \tag{4.10a}$$

We have now derived equations for the determination of $\omega_n(\tau)$ and $u_T(\tau)$. They are equations (4.9*a*), (4.10*a*), (4.9) with the extra term $(J_j^{-1}\cdot[ng_f+g_T])\times R_j$ inside the braces, and equation (4.10). In these equations the nonfrictional contact moment $g_T(\tau)$ occurs. When $g_T=0$ and ν is constant these equations can be solved as in the case without any contact moment. However, it is necessary to determine if ω_n vanishes during the collision, and if so whether it remains zero. It will remain zero if g_f satisfies the inequality in equation (3.6*a*). To find g_f one must solve equation (3.5*a*) with G determined from equation (4.1*a*) with $\omega_n=0$.

As an example let us consider a collision in which the last two terms in equation (4.9*a*) vanish. Then if $\omega_n(\tau)\neq 0$, (4.9*a*) reduces to

$$\frac{d\omega_n}{d\tau}=-\nu n\cdot(J_1^{-1}+J_2^{-1})n\,\mathrm{sgn}\ \omega_n. \tag{1}$$

The solution of equation (1) is

$$\omega_n(\tau)=\omega_n(0)-\nu\tau n\cdot(J_1^{-1}+J_2^{-1})n\,\mathrm{sgn}\ \omega_n(0). \tag{2}$$

The right side of equation (2) vanishes at

$$\tau^{**}=|\omega_n(0)|[\nu n\cdot(J_1^{-1}+J_2^{-1})n]^{-1}. \tag{3}$$

If $\tau^{**}\geq(1+e)\tau_0$, equation (2) holds throughout the collision. However, if $\tau^{**}<(1+e)\tau_0$ then $\omega_n(\tau)=0$ for $\tau\geq\tau^{**}$. This is so because equation (4.9*a*) with $\omega_n(\tau)=0$ yields $g_f=0$, and this satisfies the inequality in (3.6*a*). Thus ω_n at the end of the collision is given by equation (2) with $\tau=(1+e)\tau_0$, or by $\omega_n=0$ according as τ^{**} is greater or smaller than $(1+e)\tau_0$. Finally equation (3.8*a*) yields

$$\Gamma=-\nu\ \mathrm{sgn}\ \omega_n(0)\cdot\min[\tau^{**},(1+e)\tau_0]. \tag{4}$$

This example applies in particular to the normal collision of two spheres with $g_T=0$, including the special case of a sphere and a plane. Then $J_j=2/5\ m_j r_j^2 I$, so equations (2)–(4) become

$$\omega_n(\tau)=\omega_n(0)-\frac{5\nu\tau}{2}\left(\frac{1}{m_1r_1^2}+\frac{1}{m_2r_2^2}\right)\mathrm{sgn}\ \omega_n(0), \tag{5}$$

$$\tau^{**}=\frac{2}{5\nu}\left(\frac{1}{m_1r_1^2}+\frac{1}{m_2r_2^2}\right)^{-1}|\omega_n(0)|, \tag{6}$$

$$\Gamma\begin{cases}=-\nu(1+e)\tau_0\ \mathrm{sgn}\ \omega_n(0) & \text{if } \tau^{**}\geq(1+e)\tau_0\\ =-\dfrac{2}{5}\left(\dfrac{1}{m_1r_1^2}+\dfrac{1}{m_2r_2^2}\right)^{-1}\omega_n(0) & \text{if } \tau^{**}\leq(1+e)\tau_0.\end{cases} \tag{7}$$

Finally since $R_1=nr_1$ and $R_2=-nr_2$, equation (3.10*a*) becomes

$$[\Omega_j]=(-1)^j\frac{5}{2m_jr_j^2}\left(\mu r_j n\times\int_0^{(1+e)\tau_0}\hat{u}_T(\tau)d\tau+\Gamma\right). \tag{8}$$

Acknowledgment

Research supported by the Office of Naval Research, the Air Force Office of Scientific Reserch, the Army Research Office, and the National Science Foundation.

Reference

Keller, J. B., 1986, "Impact with Friction," ASME Journal of Applied Mechanics, Vol. 53, pp. 1–4.

Perturbation Solutions on *J*-Integral for Nonlinear Crack Problems

Ming-Yuan He[18]

A crack of length $2a$ in an infinite two-dimensional body occupies $-a\leq x_1\leq a$, $x_2=0$ and the following load systems are

[18]Institute of Mechanics, Chinese Academy of Sciences, Beijing, People's Republic of China.

Manuscript received by ASME Applied Mechanics Division, July 30, 1985; final revision, June 3, 1986.

Downloaded 03 May 2010 to 171.66.16.27. Redistribution subject to ASME license or copyright; see http://www.asme.org/terms/Terms_Use.cfm

$$\omega(t)=\Omega_2-\Omega_1. \tag{3.2a}$$

We now write $G(t)$ in the form

$$G(t)=N(t)[ng_f(t)+g_T(t)],\ n\cdot g_T(t)=0. \tag{3.5a}$$

Here $N(t)$ is the normal force, $N\,ng_f$ is the frictional moment which is normal to the surface, and $N\,g_T$ is the nonfrictional moment which is tangential. We assume that g_f is given by a law of angular friction of the following form, in which $\omega_n=\omega\cdot n$:

$$g_f=-\nu\,\mathrm{sgn}\ \omega_n \text{ if } \omega_n\neq 0, \tag{3.6a}$$

$$|g_f|\leq\nu \text{ if } \omega_n=0.$$

The quantity ν is a coefficient of angular sliding friction with the dimensions of length. In principle it can be determined by analyzing the deformation of the surfaces during impact and using the usual law of friction. It ought to be proportional to μ and should depend upon $N(t)$.

When we use equations (3.5*a*) in (2.11*a*), and write g_f and g_T as functions of τ, we get

$$\Gamma=\int_0^{(1+e)\tau_0}[ng_f(\tau)+g_T(\tau)]d\tau. \tag{3.8a}$$

Then equation (3.8*a*) is used in equation (3.10) with the extra term $(-1)^j J_j^{-1}\Gamma$ on the right side, and equation (3.10) becomes

$$[\Omega_j]=(-1)^j J_j^{-1}\left(R_j\times\left\{(1+e)\tau_0 n-\mu\int_0^{(1+e)\tau_0}\hat{u}_T(\tau)d\tau\right\}\right.$$

$$\left.+\int_0^{(1+e)\tau_0}[ng_f(\tau)+g_T(\tau)]d\tau\right). \tag{3.10a}$$

Next we must add $(J_j^{-1}G)\times R_j$ to the summand in equation (4.1) and add ng_f+g_T to $R_j\times(n+f)$ in equations (4.2), (4.3), (4.4), (4.6), and (4.9). We must also add $n\cdot[J_j^{-1}\int_0^{\tau}(ng_f+g_T)d\tau']\times R_j$ to the summands in equations (4.7) and (4.8) with $\tau=\tau_0$ in (4.8).

To determine $\omega(\tau)$, which occurs in equation (3.6*a*), we differentiate equation (3.2*a*) and use equation (2.6) to get

$$\frac{d\omega}{dt}=\sum_{j=1}^{2}J_j^{-1}[G+R_j\times F]. \tag{4.1a}$$

Now we use equation (3.5) for F and equation (3.5*a*) for G in equation (4.1*a*) and write $N^{-1}d/dt=d/d\tau$ to obtain

$$\frac{d\omega}{d\tau}=\sum_{j=1}^{2}J_j^{-1}[ng_f+g_T+R_j\times(n+f)]. \tag{4.3a}$$

From equation (3.2*a*) the initial value of ω is

$$\omega(0)=\Omega_2^-\,-\Omega_1^-. \tag{4.4a}$$

Finally we take the inner product of n with equations (4.3*a*) and (4.4*a*) to get

$$\frac{d\omega_n}{d\tau}=\sum_{j=1}^{2}n\cdot J_j^{-1}[ng_f+g_T+R_j\times(n+f)], \tag{4.9a}$$

$$\omega_n(0)=n\cdot(\Omega_2^-\,-\Omega_1^-). \tag{4.10a}$$

We have now derived equations for the determination of $\omega_n(\tau)$ and $u_T(\tau)$. They are equations (4.9*a*), (4.10*a*), (4.9) with the extra term $(J_j^{-1}\cdot[ng_f+g_T])\times R_j$ inside the braces, and equation (4.10). In these equations the nonfrictional contact moment $g_T(\tau)$ occurs. When $g_T=0$ and ν is constant these equations can be solved as in the case without any contact moment. However, it is necessary to determine if ω_n vanishes during the collision, and if so whether it remains zero. It will remain zero if g_f satisfies the inequality in equation (3.6*a*). To find g_f one must solve equation (3.5*a*) with G determined from equation (4.1*a*) with $\omega_n=0$.

As an example let us consider a collision in which the last two terms in equation (4.9*a*) vanish. Then if $\omega_n(\tau)\neq 0$, (4.9*a*) reduces to

$$\frac{d\omega_n}{d\tau}=-\nu n\cdot(J_1^{-1}+J_2^{-1})n\,\mathrm{sgn}\ \omega_n. \tag{1}$$

The solution of equation (1) is

$$\omega_n(\tau)=\omega_n(0)-\nu\tau n\cdot(J_1^{-1}+J_2^{-1})n\,\mathrm{sgn}\ \omega_n(0). \tag{2}$$

The right side of equation (2) vanishes at

$$\tau^{**}=|\omega_n(0)|[\nu n\cdot(J_1^{-1}+J_2^{-1})n]^{-1}. \tag{3}$$

If $\tau^{**}\geq(1+e)\tau_0$, equation (2) holds throughout the collision. However, if $\tau^{**}<(1+e)\tau_0$ then $\omega_n(\tau)=0$ for $\tau\geq\tau^{**}$. This is so because equation (4.9*a*) with $\omega_n(\tau)=0$ yields $g_f=0$, and this satisfies the inequality in (3.6*a*). Thus ω_n at the end of the collision is given by equation (2) with $\tau=(1+e)\tau_0$, or by $\omega_n=0$ according as τ^{**} is greater or smaller than $(1+e)\tau_0$. Finally equation (3.8*a*) yields

$$\Gamma=-\nu\ \mathrm{sgn}\ \omega_n(0)\cdot\min[\tau^{**},(1+e)\tau_0]. \tag{4}$$

This example applies in particular to the normal collision of two spheres with $g_T=0$, including the special case of a sphere and a plane. Then $J_j=2/5\ m_j r_j^2 I$, so equations (2)–(4) become

$$\omega_n(\tau)=\omega_n(0)-\frac{5\nu\tau}{2}\left(\frac{1}{m_1r_1^2}+\frac{1}{m_2r_2^2}\right)\mathrm{sgn}\ \omega_n(0), \tag{5}$$

$$\tau^{**}=\frac{2}{5\nu}\left(\frac{1}{m_1r_1^2}+\frac{1}{m_2r_2^2}\right)^{-1}|\omega_n(0)|, \tag{6}$$

$$\Gamma\begin{cases}=-\nu(1+e)\tau_0\ \mathrm{sgn}\ \omega_n(0) & \text{if } \tau^{**}\geq(1+e)\tau_0\\ =-\dfrac{2}{5}\left(\dfrac{1}{m_1r_1^2}+\dfrac{1}{m_2r_2^2}\right)^{-1}\omega_n(0) & \text{if } \tau^{**}\leq(1+e)\tau_0.\end{cases} \tag{7}$$

Finally since $R_1=nr_1$ and $R_2=-nr_2$, equation (3.10*a*) becomes

$$[\Omega_j]=(-1)^j\frac{5}{2m_jr_j^2}\left(\mu r_j n\times\int_0^{(1+e)\tau_0}\hat{u}_T(\tau)d\tau+\Gamma\right). \tag{8}$$

Acknowledgment

Research supported by the Office of Naval Research, the Air Force Office of Scientific Reserch, the Army Research Office, and the National Science Foundation.

Reference

Keller, J. B., 1986, "Impact with Friction," ASME Journal of Applied Mechanics, Vol. 53, pp. 1–4.

Perturbation Solutions on *J*-Integral for Nonlinear Crack Problems

Ming-Yuan He[18]

A crack of length $2a$ in an infinite two-dimensional body occupies $-a\leq x_1\leq a$, $x_2=0$ and the following load systems are

[18]Institute of Mechanics, Chinese Academy of Sciences, Beijing, People's Republic of China.

Manuscript received by ASME Applied Mechanics Division, July 30, 1985; final revision, June 3, 1986.

Copyright © 1987 by ASME
Downloaded 03 May 2010 to 171.66.16.27. Redistribution subject to ASME license or copyright; see http://www.asme.org/terms/Terms_Use.cfm

Table 1 Comparison between the perturbation solutions (13) and numerical results for plane strain crack with $T=0$

			$n=1$	$n=2$	$n=3$	$n=4$	$n=5$	$n=7$	$n=10$
Mode II $\frac{S}{Q}=0$	$\frac{J}{a\epsilon_e^\infty\sigma_e^\infty}$	from (13)	0.785	1.120	1.387	1.611	1.804	2.112	2.439
		from He (1983)	0.785	1.111	1.360	1.571	1.756	2.078	2.483
		% difference	*	0.8	1.95	2.48	2.65	1.61	1.83
Mode I–II $\frac{S}{Q}=0.5$	$\frac{J}{a\epsilon_e^\infty\sigma_e^\infty}$	from (13)	0.929	1.327	1.650	1.932	2.181	2.603	3.068
		from He (1983)	0.929	1.314	1.609	1.858	2.077	2.458	2.938
		% difference	*	0.98	2.48	3.83	4.77	5.57	4.24
Mode I–II $\frac{S}{Q}=1.96$	$\frac{J}{a\epsilon_e^\infty\sigma_e^\infty}$	from (13)	1.941	2.746	3.341	3.807	4.139	4.744	5.248
		from He (1983)	1.941	2.745	3.362	3.882	4.341	5.136	6.139
		% difference	*	0.004	0.06	1.97	4.88	8.26	17.0
Mode I $\frac{S}{Q}=0$	$\frac{J}{a\epsilon_e^\infty\sigma_e^\infty}$	from (13)	3.142	4.470	5.511	6.390	7.152	8.421	9.870
		from He (1983)	3.142	4.443	5.441	6.283	7.025	8.312	9.935
		% difference	*	0.60	1.27	1.67	1.78	1.16	0.66

Table 2 Comparison between the perturbation solution (15) and numerical results for Mode III crack ($\tau=0$)

		$n=1.0$	$n=1.5$	$n=2.0$	$n=3.0$	$n=5.0$	$n=10$
$\frac{J}{a\epsilon_e^\infty\sigma_e^\infty}$	from Amazigo (1974)	1.571	1.939	2.271	2.864	3.865	5.788
	from (15)	1.571	1.924	2.222	2.721	3.513	4.968
	% difference	0	0.76	2.17	4.99	9.11	14.17

considered: (1) remote uniform shear stress $\sigma_{12}=Q$ (Mode II); (2) remote uniform tensile stress $\sigma_{11}=T$, $\sigma_{22}=S$ and shear stress $\sigma_{12}=Q$ (mixed Mode I and II); (3) remote antiplane shear stress $\sigma_{23}=R$ (Mode III). We consider an incompressible solid under small strain deformation and characterized in simple tension by

$$\epsilon/\epsilon_o=\alpha(\sigma/\sigma_o)^n \tag{1}$$

where ϵ_o and σ_o are a reference strain and stress, α and n are material constants. The tensile relation is generalized to multiaxial states by the J_2 deformation theory according to

$$\frac{\epsilon_{ij}}{\epsilon_o}=\frac{3}{2}\alpha\left(\frac{\sigma_e}{\sigma_o}\right)^{n-1}\frac{s_{ij}}{\sigma_o} \tag{2}$$

where s_{ij} is the stress deviator and σ_e is the effective stress defined by

$$\sigma_e=\left(\frac{3}{2}s_{ij}s_{ij}\right)^{1/2} \tag{3}$$

Following procedures developed by He and Hutchinson (1981) and Abeyaratne (1983), we produce solutions for the relation between the J-integral and the remote stresses. The method is based on a perturbation about a specially selected uniform trivial state. With that state specified by σ and ϵ, the increments in deviatoric stress and strain satisfy

$$\dot{s}_{ij}=2\mu\left\{\frac{1}{2}(\delta_{ik}\delta_{j\ell}+\delta_{i\ell}\delta_{jk})-\frac{1}{3}\delta_{ij}\delta_{k\ell}+\frac{2}{3}\frac{1-n}{n}\epsilon_{ij}\epsilon_{k\ell}\epsilon_e^{-2}\right\}\dot{\epsilon}_{k\ell} \tag{4}$$

where

$$\mu=\frac{\sigma_e}{3\epsilon_e} \tag{5}$$

and

$$\epsilon_e=(2\epsilon_{ij}\epsilon_{ij}/3)^{1/2}.$$

Mode II Crack

The trivial state is taken as $\sigma_{11}=T<0$, $\sigma_{22}=0$. We consider the plane strain problem, so that $\sigma_{33}=T/2$ and $\sigma_e=(\sqrt{3}/2)|T|$. In this uniform trivial state the crack remains closed, J is zero and the nonzero strain components from equation (2) are

$$\epsilon_{22}=-\epsilon_{11}=\frac{\sqrt{3}}{2}\epsilon_e \tag{6}$$

Onto this trivial state we superimpose an increment of remote inplane shear stress Q so that

$$\sigma_{11}^\infty=T,\quad \sigma_{22}^\infty=0,\quad \sigma_{33}^\infty=\frac{T}{2},\quad \dot{\sigma}_{12}^\infty=Q \tag{7}$$

Following procedures which closely parallel those mentioned above, we have solved the linear incremental problem for a crack in a body with uniform incremental moduli specified by equation (4) where the strains in the trival state are given by equation (6). The result is a relation between the J-integral and Q which is exact to lowest order in Q. The result so obtained is

$$\frac{J}{a\sigma_e^\infty\epsilon_e^\infty}=\frac{3\pi\sqrt{n}}{4}\left(\frac{Q}{\sigma_e^\infty}\right)^2 \tag{8}$$

where we have taken

$$\sigma_e^\infty=\left\{\frac{3}{4}(T^2+4Q^2)\right\}^{1/2} \tag{9}$$

and

$$\epsilon_e^\infty/\epsilon_o=\alpha(\sigma_e^\infty/\sigma_o)^n \tag{10}$$

This formula is exact for $n=1$, but at this point we can only argue for its accuracy for $n>1$ when $|Q|$ is small compared to $|T|$. The accuracy at arbitrary Q will be assessed below.

Mode I–II Crack

For the crack subjected to a general plane loading, the same trivial state $\sigma_{11}=T<0$, $\sigma_{22}=0$, and $\sigma_{33}=T/2$ is used. Onto this trivial state we superimpose an increment of remote tensile stress S perpendicular to the crack and an increment of remote inplane shear stress Q parallel to the crack, so that

$$\sigma_{11}^\infty=T,\quad \dot{\sigma}_{22}^\infty=S,\quad \dot{\sigma}_{12}^\infty=Q \tag{11}$$

The incremental problem is again a linear problem. The two

Downloaded 03 May 2010 to 171.66.16.27. Redistribution subject to ASME license or copyright; see http://www.asme.org/terms/Terms_Use.cfm

incremental problems ($\dot{\sigma}_{22}^{\infty}=S$, $\dot{\sigma}_{12}^{\infty}=0$ and $\dot{\sigma}_{22}^{\infty}=0$, $\dot{\sigma}_{12}^{\infty}=Q$) therefore can be solved respectively, and the final solution is simply given by superimposing the two incremental solutions.

From He and Hutchinson (1981), for $\dot{\sigma}_{22}^{\infty}=S$, $\dot{\sigma}_{12}^{\infty}=0$, the incremental solution is

$$\frac{J}{a\epsilon_e^{\infty}\sigma_e^{\infty}}=\frac{3\pi\sqrt{n}}{4}\left(\frac{S}{\sigma_e^{\infty}}\right)^2 \tag{12}$$

The incremental solution for $\dot{\sigma}_{22}^{\infty}=0$, $\dot{\sigma}_{12}^{\infty}=Q$ is given by equation (8). Because the two incremental solutions are purely symmetric and antisymmetric, respectively, with respect to the crack, the resulting expression for J for the combined increments of S and Q is obtained by the sum of equations (12) and (8) as

$$\frac{J}{a\epsilon_e^{\infty}\sigma_e^{\infty}}=\frac{3\pi\sqrt{n}(S^2+Q^2)}{4(\sigma_e^{\infty})^2} \tag{13}$$

where now

$$\sigma_e^{\infty}=\left[\frac{3}{4}((S-T)^2+4Q^2)\right]^{1/2} \tag{14}$$

Formula (13) includes equation (8) as a special case. It is exact for $n=1$ and it is consistent with the requirement that J be homogeneous of degree $n+1$ in σ^{∞}. For $Q=0$ it reduces to the result of He and Hutchinson (1981), which has been shown to be highly accurate for arbitrary combinations of S and T except those for which $S\approx T$. Table 1 compares the prediction from formula (13) with numerical results for $J/(a\epsilon_e^{\infty}\sigma_e^{\infty})$ based on a lower bound modified energy principle which was presented by He and Hutchinson (1983) and He (1983). It is seen that the predictions from formula (13) are in close agreement with the numerical results for pure Mode II ($S=T=0$) and in pure Mode I. The greatest discrepancy is for the mixed-mode case with $S/Q=1.96$ where for $n=10$ the result from formula (13) is 17 percent above the numerical lower bound. It is very possible that part of this discrepancy may stem from the difference between the bound and the actual result.

Mode III Crack

The same procedures can be applied to the Mode III problem. In this case the trivial reference state is $\sigma_{13}=\tau$ and an increment of remote stress $\dot{\sigma}_{23}^{\infty}=R$ is applied. The resulting relation between J and R which is exact to the lowest order in R is

$$\frac{J}{a\epsilon_e^{\infty}\sigma_e^{\infty}}=\frac{3\pi\sqrt{n}}{4}\left(\frac{R}{\sigma_e^{\infty}}\right)^2 \tag{15}$$

where

$$\sigma_e^{\infty}=[3(\tau^2+R^2)]^{1/2} \tag{16}$$

This result agrees with that of Abeyaratne (1983) with $\tau=0$. As noted by that author, the result with $\tau=0$ is in excellent agreement with the exact results computed by Amazigo (1974), as can be seen in Table 2.

References

Abeyaratne, R., 1983, "On the Estimation of Energy Release Rates," *Journal of Mechanics*, Vol. 50, pp. 19–23.

Amazigo, J. C., 1974, "Fully Plastic Crack in an Infinite Body under Anti-Plane Shear," *International Journal of Solids and Structures*, Vol. 10, pp. 1003–1015.

He, M.-Y., 1983, "Fully Plastic Analysis of Mixed Mode Plane Strain Crack Problems," in *Proceedings of ICF International Symposium on Fracture Mechanics* (Beijing), Science Press, Beijing, People's Republic of China, pp. 31–41.

He, M.-Y., and Hutchinson, J. W., 1981, "The Penny Shaped Crack and the Plane Strain Crack in an Infinite Body of Power Law Material," ASME JOURNAL OF APPLIED MECHANICS, Vol. 48, pp. 830–840.

He, M.-Y., and Hutchinson, J. W., 1983, "Bounds for Fully Plastic Crack Problems for Infinite Bodies," in *Elastic-Plastic Fracture*, ASTM STP 803, Vol. I, pp. 277–290.

Downloaded 03 May 2010 to 171.66.16.27. Redistribution subject to ASME license or copyright; see http://www.asme.org/terms/Terms_Use.cfm

Journal of Applied Mechanics

Discussion

Linear Analysis of Uniformly Stressed, Orthotropic Cylindrical Shells[1]

C. W. Bert.[2] The authors are to be congratulated for presenting some interesting quantitative results on the linear behavior of thin-walled anisotropic cylindrical shells of infinite length. I have used the term *membrane* behavior since the geometry was assumed to be thin-walled and the loadings considered produce only membrane stretching and shearing action as opposed to bending and transverse shearing action. Also, I have use the term *anisotropic*, since the net effect of orthotropic material at an arbitrary orientation with respect to the cylindrical coordinate system is anisotropic material relative to the latter. Such material is sometimes called planar anisotropic (in the thin-walled case) or monoclinic in the general case. Unfortunately there is no uniformity in terminology for anisotropic materials. For instance, the present authors used the term orthotropic, while Reissner and Tsai (1972)[3] used the term anisotropic. In contrast, Pipes and Whitney (1979) have used the term anisotropic and yet gave numerical results only for the "specially orthotropic" case. One solution to this terminology dilemma would be to use the term "generally orthotropic" for the present class of material, as opposed to "specially orthotropic."

In the introductory paragraph, the authors refer to fire hoses as being helically reinforced. This is somewhat misleading, since fire hoses, as well all commercially available reinforced hoses, are bihelically reinforced, i.e., there are two families of reinforcements, one at $+\theta$ and the other at $-\theta$ with respect to the cylinder axis. This $\pm\theta$ configuration results in what is known as balanced construction in which there is no shear-normal coupling, i.e., in the tangential plane the material behaves orthotropically not anisotropically. This bihelical situation also occurs in filament-wound products such as pressure vessels, rocket motor casings, piping, etc.

Also in the introductory paragraph are mentioned axially corrugated (fluted) and helically corrugated (bellows) shells. Although it is a first approximation to "smear" the corrugations, as was done by Feodosiev (1945), Andreeva (1955), and Akasaka and Takagishi (1958) for circumferentially-corrugated diaphragms, extreme care must be exercised in obtaining the equivalent orthotropic elastic constants, since the nature of corrugations include excessive local bending action. A previous analysis of such a shell structure was presented by Franklin (1967).

Previous work on static loading of helically reinforced cylindrical shells was done by Padovan and Lestingi (1972) using the anisotropic version of Flügge's thin-shell theory. The discussor (Vanderpool and Bert, 1981) has conducted analytical and experimental investigations of helically (not bihelically) reinforced thick-walled cylinders. The analysis was based on the monoclinic version of Mirsky's thick-shell theory with exact solution for a finite-length, free-free cylinder using the Flügge-Forsberg method. The experimental specimen was specially made by hand-wrapping unidirectional S-glass/epoxy tape at 30 deg to the cylinder axis.

Finally the discussor would like to point out that there are typographical errors in equations (44) and (45) in that σ_{zz} and $\sigma_{\theta\theta}$ should be interchanged.

References

Akasaka, T., and Takagishi, T., 1958, "Vibration of Corrugated Diaphragms," *Bulletin of Japan Society of Mechanical Engineers*, Vol. 1, No. 3, pp. 215–221.

Andreeva, L. E., 1955, "Calculations Concerning Corrugated Diaphragms, Considering Them as Anisotropic Plates," in Russian, *Inzhenernii Sbornik*, Akademii Nauk SSSR, Vol. 21, pp. 128–141.

Feodosiev, V. I., 1945, "Large Displacements and Stability of a Circular Membrane with Fine Corrugations," in Russian, *Prikladnaia Matematika i Mekhanika*, Vol. 9, pp. 389–141.

Franklin, H. G., 1967, "Membrane Solution of Fiber-Reinforced Corrugated Shells of Revolution," *Journal of Composite Materials*, Vol. 1, No. 4, pp. 382–388.

Padovan, J., and Lestingi, J., 1972, "Mechanical Behavior of Fiber Reinforced Cylindrical Shells," *AIAA Journal*, Vol. 10, No. 9, pp. 1239–1241.

Pipes, R. B., and Whitney, J. M., 1979, "Analysis of the Anisotropic Cylinder of Finite Length," *Fibre Science and Technology*, Vol. 12, No. 5, pp. 327–339.

Reissner, E., and Tsai, W. T., 1972, "Pure Bending, Stretching, and Twisting of Anisotropic Cylindrical Shells," ASME Journal of Applied Mechanics, Vol. 39, No. 1, pp. 148–154.

Vanderpool, M. E., and Bert, C. W., 1981, "Vibration of a Materially Monoclinic, Thick-Wall Circular Cylindrical Shell," *AIAA Journal*, Vol. 19, No. 5, pp. 634–641.

Laminar Start-Up Flow in a Pipe[3]

G. S. Patience[4] **and A. K. Mehrotra.**[4] In his interesting paper on start-up flow, the author has introduced a parameter, M, which accounts for the head that must be devoted to the acceleration of the flow. The expression for M, equation (14), is incorrectly reported in his paper. Instead it should read as follows,

$$M \equiv (G_o D^4 / 2048 \nu^2 \rho L)$$

[1] By J. F. Wilson and G. Orgill, and published in the June, 1986, issue of the Journal of Applied Mechanics, Vol. 53, pp. 249–256.

[2] Perkinson Chair Professor of Engineering, The University of Oklahoma, Norman, OK 73019. Fellow, ASME.

[3] The date, volume, and pages of this reference were incorrectly cited in the authors' paper.

[3] By D. R. Otis, and published in the September, 1985, issue of the ASME Journal of Applied Mechanics, Vol. 52, pp. 706–711.

[4] Department of Chemical and Petroleum Engineering, The University of Calgary, Calgary, Alberta, Canada, T2N 1N4.

Copyright © 1987 by ASME
Downloaded 03 May 2010 to 171.66.16.27. Redistribution subject to ASME license or copyright; see http://www.asme.org/terms/Terms_Use.cfm

This expression can be reduced to,

$$M=\frac{\mathrm{Re}D}{64L} \tag{1}$$

We would like to point out an important limitation of the analysis presented in the paper. For the flow system considered in the paper, the effect of the hydrodynamic developing region cannot be overlooked. Neither Szymanski's (1932) solution nor the present author's solution is capable of including this effect. A parameter, ξ, is used to describe the hydrodynamic entry length in pipe flow. The parameter, ξ, is defined as,

$$\xi=\frac{L}{\mathrm{Re}D} \tag{2}$$

For values of $\xi \leq 0.05$, the fluid flow will be totally in the hydrodynamic developing region, provided a flat velocity profile can be assumed as the inlet condition (Fargie and Martin, 1971). Combining equations (1) and (2), M and ξ are related as follows:

$$M=\frac{1}{64\xi} \tag{3}$$

In order for the velocity profile to develop completely, the value of ξ must be greater than 0.05 (Fargie and Martin, 1971). In other words, the value of M should be less than 0.3125 to achieve fully developed flow. The values of M in Tables 2 to 4 of the paper are all greater than 0.3125. This indicates that the flow is not fully developed in these cases. We find it surprising that the author has ignored the effect of the developing region in his calculations. The solution method presented in the paper, which is a modification of Szymanski's solution, is not valid for cases where the effect of the developing region is significant, i.e., for low L/D ratios.

References

Fargie, D., and Martin, B. W., 1971, "Developing Laminar Flow in a Pipe of Circular Cross-Section," *Proc. Roy. Soc. Lond.*, Series A. Vol. 321, pp. 461–476.

Szymanski, P., 1932, "Quelques Solutions Exactes des Equations de l'Hydrodynamique du Fluide Visquex Dans le Case d'un Tube Cylindrique," *J. de Math. Pures et Appliquees*, Series 9, No. 11, pp. 67–107.

Author's Closure

The author appreciates the attention called to a rather unfortunate error in the definition of M where, as pointed out by Patience and Mehrotra the numerical 8 should be replaced by 2048 in equation (14). It should be noted that the correct value was used in all calculations reported in the paper, and the value 2048 is correctly shown in the example on p. 711.

It is true that I have given no attention to the entry, or developing region of the pipe flow. Yet it does not seem fair to utilize an entry length criterion based upon a steady state analysis to limit my transient solution. In fact, for small times, the flow begins identically along its entire length with viscous effects confined to a thin layer at the wall. I would suggest that the length of the entry section is initially zero and grows with time, finally reaching the criterion suggested by Patience and Mehrotra (as reported by Fargie and Martin). So it would be correct to say that each value of M should have a validity up to a certain time. Since the appropriate boundary condition for the entry into the pipe is somewhat unrealistic in most calculations (e.g., velocity constant across entrance section), I believe the most trustworthy limits to my analysis will come from experimental data.

One further point. I feel that an important feature of the entry section is in a certain sense already included in my analysis, namely, the allowance of head to provide for the acceleration of reservoir fluid from zero velocity to a velocity distribution corresponding to the pipe exit flow.

Linear Analysis of Uniformly Stressed, Orthotropic Cylindrical Shells[5]

M. W. Hyer.[6] The authors should be complimented on their meticulous analysis of an interesting problem. The study of the behavior of single and multiple-layer tubes with the principal material directions of the layers oriented off-axis results in interesting conclusions. It appears that the authors arrived at their conclusions starting with what they felt were good first approximations to the stress fields. Since their approximate stresses were independent of the spatial coordinates, the stresses automatically satisfied the equations of equilibrium. Accordingly, the resulting strains automatically satisfied the equations of compatibility. Only the strain-displacement equations provided additional information. The comments contained herein are to provide an alternative view on the functional form of the stress fields. Also, the comments here serve to point out that with orthotropic materials, an a priori assumption about the independence of the stresses on the spatial coordinates can be an inaccurate oversimplification which is based on experience with isotropic materials.

Assuming, as the authors did, that the problem is axisymmetric and that the majority of the response is due to the large portion of the tube not influenced by end effects, it can be assumed that the stresses (and hence strains) are independent of z and θ. The displacements are assumed to be independent of θ. Two of the three equilibrium equations in cylindrical coordinates immediately lead to:

$$\sigma_{zr}=\frac{C_1}{r} \text{ and } \sigma_{\theta r}=\frac{C_2}{r^2}. \tag{1}$$

For traction-free surfaces at the inner and outer radii, $C_1=C_2=0$. Hence σ_{zr} and $\sigma_{\theta r}$ are identically zero throughout the tube wall. The authors state that ". . . the shear stresses $\sigma_{\theta r}$ and σ_{zr} may be approximated as zero. . . " As can be seen, this approximation is not required. The stresses are exactly zero for this problem.

Because of the assumed independence of the response from z and θ, the strain-displacement relations simplify and three of the six compatibility equations are satisfied automatically. Those that are not lead to

$$\epsilon_{zz}=\epsilon^\circ \quad \gamma_{\theta z}=\gamma^\circ r+\frac{C_3}{r}, \tag{2}$$

the quantities ϵ°, γ°, and C_3 being constants of integration. In the above ϵ° is interpreted as the overall axial strain in the tube and γ° is related to the overall twist in the tube. Using the strain-displacement relations as the authors did leads to expressions for the axial and tangential displacements of the form

$$u(r,z)=\epsilon^\circ z+f(r);\ v(r,z)=\gamma^\circ rz+\frac{C_3 z}{r}+g(r). \tag{3}$$

Further use of the strain-displacement relations leads to the fact that

$$f(r)=C_4 \text{ and } g(r)=C_5 r, \tag{4}$$

C_4 and C_5 being constants. Finally, the remaining equilibrium equation leads to an ordinary differential equation that can be solved for the radial displacement component. The radial component is given by

[5] by J. F. Wilson and G. Orgill, and published in the June, 1986, issue of the ASME Journal of Applied Mechanics, Vol. 53, pp. 249–256.

[6] Professor, Department of Mechanical Engineering, University of Maryland, College Park, MD 20742. Mem. ASME.

Copyright © 1987 by ASME
Downloaded 03 May 2010 to 171.66.16.27. Redistribution subject to ASME license or copyright; see http://www.asme.org/terms/Terms_Use.cfm

$$w(r) = C_6 r^{\lambda} + C_7 r^{-\lambda} + \left(\frac{C_{12} - C_{13}}{C_{33} - C_{22}}\right)\epsilon^{\circ} r + \left(\frac{C_{26} - 2C_{36}}{4C_{33} - C_{22}}\right)\gamma^{\circ} r^2. \quad (5)$$

The constants C_{ij} are stiffness components which are the inverse of the authors' a'_{ij} compliance matrix. The exponent λ is given by

$$\lambda = \sqrt{\frac{C_{22}}{C_{33}}},$$

and C_6 and C_7 are constants.

Using the above displacements, expressions for the remaining nonzero stresses can be determined. They are dependent on the radial coordinate. By applying boundary conditions at the inner and outer radii, and applying integrated force and moment conditions on the cross section, the applied pressure p, applied longitudinal load P, and applied torque T enter the problem. Graphical relations between p, P, T, twist, axial expansion, etc., can be plotted. A spot check for several values of the parameters indicates that agreement between the theory in the paper and the theory here is quite close. Where the theory in the paper will deviate from the approach here is in the dependence of the stresses on the radial coordinate. For orthotropic materials the stresses at the inner radius can differ considerably from the stresses at the outer radius, even for thin-walled tubes. For example, for an orthotropic tube with a modulus ratio of 20, a mean radius to wall thickness ratio of 20, and $\theta = 45°$, the shear stress $\sigma_{\theta z}$ on the inner radius is 40 percent lower than the shear stress on the outer radius. For failure studies this difference is very important. While Wilson and Orgill are not solving for the response of an actual orthotropic material, it is important that the reader of their paper be aware that assuming the stresses are independent of the radial coordinate in the analysis of an orthotropic material can be a serious error, even for what could be considered a thin-walled tube.

As a final note, it should be mentioned that equations (44) and (45) are not correct. The right-hand sides have been interchanged.

Transient Response of an Interface-Crack in a Layered Plate[7]

An-Yu Kuo.[8] The author should be commended for providing a semianalytical solution to the Mode III fracture problem of an interface-crack in a layered plate under transient loading conditions. However, I found the numerical solutions of the two example problems in this paper questionable.

Solutions presented in Figs. 6–8 of this paper indicate that, at steady-state, the transient response at the crack region would eventually be damped out and converge to a constant value. Such a decay phenomenon has been widely observed for crack problems in an infinite space but does not seem physically feasible for a finite-thickenss, linear elastic plate. Instead, the steady-state solution is expected to oscillate with a constant amplitude around the static solution at a constant frequency.

Conceptually, the problem can be treated as the superposition of a flawless case (Cannonical Problem 1 in the paper) and a scattered field case. As indicated by equation (2.1) of the paper, solutions to the flawless case oscillate, without decay, at a constant frequency and amplitude when reaching steady-state. Therefore, at steady-state, the applied stresses at the crack surfaces in the scattered field case would oscillate without decay, so do the resulting COD and K. Also, since both the plate and the out-of-plane loads extend to inifnity, once a transient load is applied, the composite plate will oscillate forever at infinity. It does not seem right to have a plate oscillating at infinity but remaining static at the crack region.

The author might have introduced a numerical damping by solving the problem in the frequency domain and converting the solution to time domain. One possible source of the numerical damping is that the numerical solutions in the frequency domain are finite (Figs. 6–8 of the paper) even at the natural frequencies of the composite plate. Truncation of the infinite response at the natural frequencies has been known to cause numerical damping.

It would make the paper more informative if the author can either find a way to avoid this numerical damping or indicate this numerical damping phenomenon as a shortcoming of the solution scheme used.

Author's Closure

The author is thankful to Dr. Kuo for his interest in Dr. Kundu's paper and for giving him an opportunity to explain the cause of the gradual decay of COD and K in Figs. 6, 7, and 8 in that paper. The decay in the crack opening displacement (COD) doesn't necessarily mean the decay of the plate movement as well in the crack region. Under steady-state condition the plate oscillates and the two crack surfaces move with it without causing any crack opening.

The phenomenon of plate movement without any crack opening can be seen from the basic formulation of this problem. The total response is a superposition of two fields, the undisturbed field of the flawless plate (cannonical problem 1 in the paper) and the scattered field. The crack opening displacement is produced only by the scattered field which is generated by the negative of the incident stress field applied at the two surfaces of the crack. For impact or step loading, the time-dependent disturbances are carried away from the crack region by elastic waves generated by the scattered field and, hence, no oscillations in COD and K are observed after some time; then the two crack surfaces move together.

The numerical damping introduces small errors in the time history plots as can be seen from the small nonzero displacements before 0.43 microseconds (the first wave arrival time). However, it doesn't affect the major peaks in the time history plots and it is not the cause of the decay of COD or K.

Whirl Instabilities in Pressure Step Bearings[9]

J. C. Nicholas[10] **and P. E. Allaire.**[11] Have the authors attempted to calculate the typial magnitude of the pressure drop created by the step? While the authors' reference [6] shows large pressure drops compared to peak hydrodynamic

[7] By T. Kundu and published in the September, 1986, issue of the ASME JOURNAL OF APPLIED MECHANICS, Vol. 53, pp. 579–586.

[8] Senior Engineer, Structural Integrity Associates, Inc., San Jose, CA 95118.

[9] By J. Brindley, L. Elliott, and J. T. McKay and published in the June, 1986, issue of the ASME JOURNAL OF APPLIED MECHANICS, Vol. 53, pp. 430–435.

[10] Head, Rotordynamics Group, Turbodyne Division, Dresser Industries, Wellsville, NY 14895.

[11] Professor, Department of Mechanical and Aerospace Engineering, University of Virginia, Charlottesville, VA 22901.

Downloaded 03 May 2010 to 171.66.16.27. Redistribution subject to ASME license or copyright; see http://www.asme.org/terms/Terms_Use.cfm

$$w(r) = C_6 r^{\lambda} + C_7 r^{-\lambda} + \left(\frac{C_{12} - C_{13}}{C_{33} - C_{22}}\right)\epsilon^{\circ} r + \left(\frac{C_{26} - 2C_{36}}{4C_{33} - C_{22}}\right)\gamma^{\circ} r^2. \quad (5)$$

The constants C_{ij} are stiffness components which are the inverse of the authors' a'_{ij} compliance matrix. The exponent λ is given by

$$\lambda = \sqrt{\frac{C_{22}}{C_{33}}},$$

and C_6 and C_7 are constants.

Using the above displacements, expressions for the remaining nonzero stresses can be determined. They are dependent on the radial coordinate. By applying boundary conditions at the inner and outer radii, and applying integrated force and moment conditions on the cross section, the applied pressure p, applied longitudinal load P, and applied torque T enter the problem. Graphical relations between p, P, T, twist, axial expansion, etc., can be plotted. A spot check for several values of the parameters indicates that agreement between the theory in the paper and the theory here is quite close. Where the theory in the paper will deviate from the approach here is in the dependence of the stresses on the radial coordinate. For orthotropic materials the stresses at the inner radius can differ considerably from the stresses at the outer radius, even for thin-walled tubes. For example, for an orthotropic tube with a modulus ratio of 20, a mean radius to wall thickness ratio of 20, and $\theta = 45°$, the shear stress $\sigma_{\theta z}$ on the inner radius is 40 percent lower than the shear stress on the outer radius. For failure studies this difference is very important. While Wilson and Orgill are not solving for the response of an actual orthotropic material, it is important that the reader of their paper be aware that assuming the stresses are independent of the radial coordinate in the analysis of an orthotropic material can be a serious error, even for what could be considered a thin-walled tube.

As a final note, it should be mentioned that equations (44) and (45) are not correct. The right-hand sides have been interchanged.

Transient Response of an Interface-Crack in a Layered Plate[7]

An-Yu Kuo.[8] The author should be commended for providing a semianalytical solution to the Mode III fracture problem of an interface-crack in a layered plate under transient loading conditions. However, I found the numerical solutions of the two example problems in this paper questionable.

Solutions presented in Figs. 6–8 of this paper indicate that, at steady-state, the transient response at the crack region would eventually be damped out and converge to a constant value. Such a decay phenomenon has been widely observed for crack problems in an infinite space but does not seem physically feasible for a finite-thickenss, linear elastic plate. Instead, the steady-state solution is expected to oscillate with a constant amplitude around the static solution at a constant frequency.

Conceptually, the problem can be treated as the superposition of a flawless case (Cannonical Problem 1 in the paper) and a scattered field case. As indicated by equation (2.1) of the paper, solutions to the flawless case oscillate, without decay, at a constant frequency and amplitude when reaching steady-state. Therefore, at steady-state, the applied stresses at the crack surfaces in the scattered field case would oscillate without decay, so do the resulting COD and K. Also, since both the plate and the out-of-plane loads extend to inifnity, once a transient load is applied, the composite plate will oscillate forever at infinity. It does not seem right to have a plate oscillating at infinity but remaining static at the crack region.

The author might have introduced a numerical damping by solving the problem in the frequency domain and converting the solution to time domain. One possible source of the numerical damping is that the numerical solutions in the frequency domain are finite (Figs. 6–8 of the paper) even at the natural frequencies of the composite plate. Truncation of the infinite response at the natural frequencies has been known to cause numerical damping.

It would make the paper more informative if the author can either find a way to avoid this numerical damping or indicate this numerical damping phenomenon as a shortcoming of the solution scheme used.

Author's Closure

The author is thankful to Dr. Kuo for his interest in Dr. Kundu's paper and for giving him an opportunity to explain the cause of the gradual decay of COD and K in Figs. 6, 7, and 8 in that paper. The decay in the crack opening displacement (COD) doesn't necessarily mean the decay of the plate movement as well in the crack region. Under steady-state condition the plate oscillates and the two crack surfaces move with it without causing any crack opening.

The phenomenon of plate movement without any crack opening can be seen from the basic formulation of this problem. The total response is a superposition of two fields, the undisturbed field of the flawless plate (cannonical problem 1 in the paper) and the scattered field. The crack opening displacement is produced only by the scattered field which is generated by the negative of the incident stress field applied at the two surfaces of the crack. For impact or step loading, the time-dependent disturbances are carried away from the crack region by elastic waves generated by the scattered field and, hence, no oscillations in COD and K are observed after some time; then the two crack surfaces move together.

The numerical damping introduces small errors in the time history plots as can be seen from the small nonzero displacements before 0.43 microseconds (the first wave arrival time). However, it doesn't affect the major peaks in the time history plots and it is not the cause of the decay of COD or K.

Whirl Instabilities in Pressure Step Bearings[9]

J. C. Nicholas[10] **and P. E. Allaire.**[11] Have the authors attempted to calculate the typial magnitude of the pressure drop created by the step? While the authors' reference [6] shows large pressure drops compared to peak hydrodynamic

[7] By T. Kundu and published in the September, 1986, issue of the ASME JOURNAL OF APPLIED MECHANICS, Vol. 53, pp. 579–586.

[8] Senior Engineer, Structural Integrity Associates, Inc., San Jose, CA 95118.

[9] By J. Brindley, L. Elliott, and J. T. McKay and published in the June, 1986, issue of the ASME JOURNAL OF APPLIED MECHANICS, Vol. 53, pp. 430–435.

[10] Head, Rotordynamics Group, Turbodyne Division, Dresser Industries, Wellsville, NY 14895.

[11] Professor, Department of Mechanical and Aerospace Engineering, University of Virginia, Charlottesville, VA 22901.

Copyright © 1987 by ASME
Downloaded 03 May 2010 to 171.66.16.27. Redistribution subject to ASME license or copyright; see http://www.asme.org/terms/Terms_Use.cfm

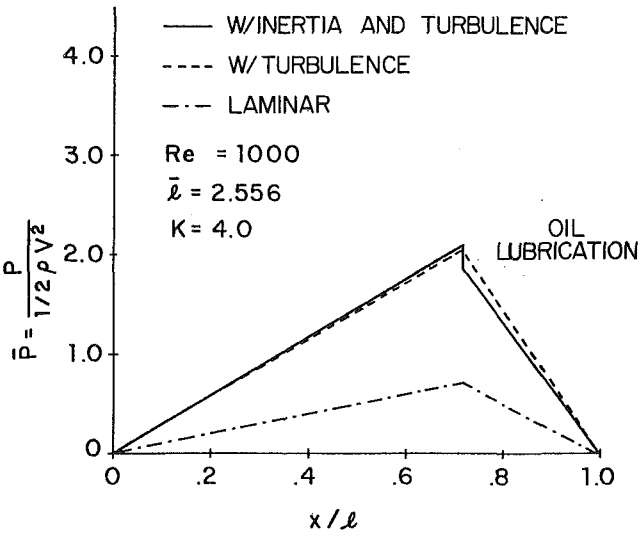


Fig. 10 Comparison of the hydrodynamic pressure profile for an oil lubricated step bearing [14]

pressures, Constantinesca and Galatense used air as a lubricant. In additional reference [14], Allaire, Nicholas, and Barrett used an infinite length finite element model to show that the magnitude of the pressure drop for step bearings with a constant load is of the order of 10 percent of peak pressures for oil lubrication and Reynolds numbers below 1500. Reference [14] also concludes that the inclusion of turbulence inside the pocket area is necessary to accurately predict the load produced by the step.

These points are illustrated in Fig. 10 which is taken from reference [14]. Including inertia effects and turbulence produces the solid line curve with a pressure discontinuity at the step (inertia theory). The pressure drop is small compared to the peak pressure as oil is used as a lubricant and the Reynolds number is 1000. Neglecting the inertia effects at the step but including turbulence is a very good approximation while pure laminar theory greatly underestimates the load. Can the authors comment on these points?

References

14 Allaire, P. E., Nicholas, J. C., and Barrett, L. E., "Analysis of Step Journal Bearings—Infinite Length, Inertia Effects," ASLE, Vol. 22, No. 4, Oct. 1979, pp. 333-341.

Authors' Closure

Our model does not permit us to calculate the actual pressure drop created by a geometrical step. It was our intention to use the observed fact of steep pressure changes at steps to motivate an exploration in our model of the effects of a pressure *discontinuity*, Δp, on the stability characteristics of the rotor orbits.

The magnitudes of Δp were in a sense arbitrarily chose, but of a magnitude suggested to us by the results of Constantinescu and Galateuse (1976), and also by unpublished results of Ruddy (1979) which we quoted. The numerical results of Allaire et al. indicate that substantially smaller pressure jumps might be expected in oil lubricated bearings, which perhaps strengthens our main conclusion that the position and extent of cavitation is of greater importance as a stability influence than a step-induced pressure jump. Finally, we are unable to comment usefully on the question of laminar/turbulent difference raised in the Discussion. As stressed earlier, we took a pressure discontinuity as given, and examined the effects in our (laminar) model.

References

Constantinescu, V. N., and Galateuse, S., 1976, "Pressure Drop Due to Inertia Forces in Step Bearings," *ASME Journal of Lubrication Technology*, Vol. 98 (i), pp. 167-174.

Ruddy, A. V., 1979, "The Dynamics of Rotor Bearing Systems with Particular Reference to the Infleunce of Fluid Film Journal Bearings and the Modelling of Flexible Rotors," Ph.D. thesis, Leeds University, England.

A Finite Element Approach to Interface Cracks[12]

M. Comninou.[13] I welcome a finite element analysis of the interface crack, but I believe it cannot clarify questions related to crack-tip behavior, and it is more suited to exploring large scale characteristics of the problem, such as the extent of the large contact zone under shear load. Nevertheless, such analysis does not have to be wrong as this one is in connection with K_I at the left tip in presence of shear. One may take exception regarding the meaning and presence of the contact zones near the crack tips, but once these zones are postulated, asymptotic analysis demands that

$$K_{\mathrm{I}}(a) = -\beta K_{\mathrm{II}}(a)$$

$$K_{\mathrm{I}}(-a) = \beta K_{\mathrm{II}}(-a)$$

where K_{I} is the stress intensity factor of the contact stress adjacent to the crack tips. This means that the algebraic signs of K_{II} at the two tips are opposite, since K_{I} must be negative at both tips. Moreover, the algebraic signs of $K_{\mathrm{II}}(a)$ and $K_{\mathrm{II}}(-a)$ do not change if the applied shear is reversed, although their magnitudes are exchanged. A detailed discussion of this behavior was published by M. Comninou and J. Dundurs in *Res Mechanica*, Vol. 1, 1980.

It is clear that the statements made by the authors regarding the stress intensity factors under shear load cannot be correct: positive $K_{\mathrm{II}}(-a)$ is inconsistent with closed tip at $-a$.

Author's Closure

The authors thank Professor M. Comninou for drawing attention to the inconsistent positive value of the stress intensity factor K_{II} at the left cracktip when postulating a closed left cracktip under shear load. The extreme large slope of the gap near the left cracktip, as has been pointed out by Comninou (1978, 1979), could be attributed to this. The main aim of the paper was to compare a Finite Element analysis with results from the literature, emphasizing differences with the theoretical model and obtaining results where the theoretical model gave no results.

References

Comninou, M., 1978, "The Interface Crack in a Shear Field," ASME Journal of Applied Mechanics, Vol. 45, pp. 287-290.

Comninou, M., 1979, "The Interface Crack in a Combined Tension-Compression and Shear Field," ASME Journal of Applied Mechanics, Vol. 46, pp. 345-348.

[12] By. H. D. van der Zande and J. H. Grootenboer and published in the September, 1986, issue of the ASME Journal of Applied Mechanics, Vol. 53, pp. 573-578.

[13] Department of Mechanical Engineering and Applied Mechanics, University of Michigan, Ann Arbor, MI 48109.

Copyright © 1987 by ASME
Downloaded 03 May 2010 to 171.66.16.27. Redistribution subject to ASME license or copyright; see http://www.asme.org/terms/Terms_Use.cfm

Invariance Considerations in Large Strain Elasto-Plasticity[14]

J. Casey.[15] Dashner is incorrect in his conclusion that the presence of microstructural anisotropy in crystalline media conflicts with the demand that intermediate stress-free configurations be subject to invariance requirements under arbitrary superposed rotations.

One should distinguish between two types of theories of plasticity: *Type A*, those in which no explicit account is taken of microstructure; and *Type B*, those in which microstructural concepts play an essential role. In both types of theories, a decomposition $\mathbf{F} = \mathbf{F}_e \mathbf{F}_p$ of the deformation gradient $\mathbf{F}$ into an elastic part $\mathbf{F}_e$ and a plastic part $\mathbf{F}_p$ can be effected through the use of intermediate stress-free local configurations. But, in theories of *Type B* the continuum is augmented with additional fields intended to represent microstructural properties.

The full invariance requirements advocated by Naghdi and coworkers (see Dashner's Ref. 2 and *its* list of references) are based on the transformations

$$\mathbf{F}^+ = \mathbf{Q}\,\mathbf{F},\ \mathbf{F}_p^+ = \bar{\mathbf{Q}}\,\mathbf{F}_p,\ \mathbf{F}_e^+ = \mathbf{Q}\,\mathbf{F}_e\bar{\mathbf{Q}}^T, \tag{1}$$

where $\mathbf{Q}$ and $\bar{\mathbf{Q}}$ are proper orthogonal. In theories of *Type A*, response functions, such as that for the symmetric Piola-Kirchhoff stress $\mathbf{S}$ for example, may be assumed to depend on $\mathbf{F}$, $\mathbf{F}_p$.[16] The full invariance requirements then imply that

$$\mathbf{S} = \tilde{\mathbf{S}}(\mathbf{E},\ \mathbf{E}_p). \tag{2}$$

Dashner's paper, being concerned with microstructural effects in metal crystals, contains a theory of *Type B*. Consider crystals for which the mechanism of plasticity is crystallographic shearing on a single slip system. The orientation of the crystal lattice is maintained during this process, so that account must be taken of the separate deformations of the lattice and the material.[17] Let the vector fields $\mathbf{n}$ and $\mathbf{s}$ represent the normal to a slip plane, and the slip direction, respectively. Let $\mathbf{n}_o$, $\mathbf{s}_o$ and $\mathbf{n}_p$, $\mathbf{s}_p$ be the values of $\mathbf{n}$, $\mathbf{s}$ in the reference and intermediate configurations, with $\{\mathbf{n}_o,\ \mathbf{s}_o\}$ orthonormal. The deformation of the augmented continuum can be broken into two steps: its deformation into the intermediate configuration, and it subsequent deformation into the present configuration. In the first step, $\mathbf{F}_p$ acts on material line elements, but not on the vectors $\mathbf{n}_o$ and $\mathbf{s}_o$. It is assumed that the latter can only rotate:

$$\mathbf{n}_p = \mathbf{\Lambda}_p\mathbf{n}_o,\ \mathbf{s}_p = \mathbf{\Lambda}_p\mathbf{s}_o, \tag{3}$$

where $\mathbf{\Lambda}_p$ is a proper orthogonal tensor. The following transformation laws may be adopted:

$$\mathbf{n}_p^+ = \bar{\mathbf{Q}}\,\mathbf{n}_p,\ \mathbf{s}_p^+ = \bar{\mathbf{Q}}\,\mathbf{s}_p, \tag{4}$$

$$\mathbf{n}^+ = \mathbf{Q}\,\mathbf{n},\ \mathbf{s}^+ = \mathbf{Q}\,\mathbf{s},\ \mathbf{\Lambda}_p^+ = \bar{\mathbf{Q}}\,\mathbf{\Lambda}_p.$$

It is consistent with the foregoing to introduce relations of the type

$$\mathbf{F}_p = \mathbf{\Lambda}_p\hat{\mathbf{F}}_p,\ \hat{\mathbf{F}}_p = \mathbf{I} + \gamma\,\mathbf{s}_o \otimes \mathbf{n}_o,$$
$$\mathbf{n} = (\det\mathbf{F}_e)\,(\mathbf{F}_e^{-1})^{\mathrm{T}}\mathbf{n}_p,\ \mathbf{s} = \mathbf{F}_e\mathbf{s}_p, \tag{5}$$

where $\otimes$ denotes tensor product and γ is a scalar-valued function. Thus, in the first step of the deformation, material line elements are subjected to a shear-slip deformation $\hat{\mathbf{F}}_p$ after which a corotation $\mathbf{\Lambda}_p$ of lattice and material line elements occurs; in the second step, material line elements and $\mathbf{s}_p$ are acted upon by $\mathbf{F}_e$, while $\mathbf{n}_p$ deforms as a normal to a material plane. Evidently,

$$\mathbf{F} = \mathbf{F}_e\mathbf{\Lambda}_p\hat{\mathbf{F}}_p,\ \hat{\mathbf{F}}_p^+ = \hat{\mathbf{F}}_p, \tag{6}$$

the latter of which should be clearly distinguished from equation $(1)_2$.

In formulating constitutive equations for the augmented continuum, one may assume that $\mathbf{S}$ depends on $\mathbf{F}$, $\mathbf{F}_p$, $\mathbf{\Lambda}_p$. Then, applying full invariance requirements, one is led to reduced properly invariant constitutive equations of the form[18]

$$\mathbf{S} = \tilde{\mathbf{S}}(\mathbf{E},\ \hat{\mathbf{F}}_p) = \bar{\mathbf{S}}(\mathbf{\Lambda}_p^T\mathbf{E}_e\mathbf{\Lambda}_p,\ \hat{\mathbf{F}}_p), \tag{7}$$

where $\mathbf{E}_e$ is the Lagrangian elastic strain tensor. Therefore, because of the additional kinematical structure of the continuum, the full invariance requirements no longer lead to equation (2) but rather to equation $(7)_1$. This disproves Dashner's assertion.

It is worth noting that if $\mathbf{\Lambda}_p$ is taken to coincide with the plastic rotation $\mathbf{R}_p$, then $\hat{\mathbf{F}}_p$ becomes equal to the plastic stretch $\mathbf{M}_p$, and a theory of *Type A* is obtained, with equation $(7)_1$ yielding equation (2).[19]

Finally, regarding Dashner's "counter-example", the configuration (κ_4, say) which results from the sequence of four slip-shear deformations of a crystal does *not* differ from the reference configuration κ_o by a purely rigid motion: material line-elements have undergone a net counterclockwise rotation, whereas the directors have retained their reference directions. Thus, the full invariance requirements do not assert that the configuration κ_4 is equivalent to κ_o. It is not the constitutive equation (2), but rather equation $(7)_1$ that applies to Dashner's example, and the physical difference between the configurations κ_4 and κ_o can be accounted for through $\hat{\mathbf{F}}_p$.

References

Asaro, R. J., 1983, "Micromechanics of Crystals and Polycrystals," *Advances in Applied Mechanics*, Vol. 23, pp. 1–115.

Mandel, J., 1973, "Thermodynamics and Plasticity," *Foundations of Continuum Thermodynamics*, Domingos, J. J. Delgado., Nina, M. N. R., and Whitelaw, J. H., eds., Wiley, New York.

Naghdi, P. M., and Trapp, J. A., 1974, "On Finite Elastic-Plastic Deformation of Metal," ASME JOURNAL OF APPLIED MECHANICS, Vol. 41, pp. 254–260.

Author's Closure

In responding to Professor Casey I must first reject his characterization of my "conclusion," which I regard as being accurately stated in the paragraph containing equation (10)[20] in the section entitled "The Difficulty." Indeed, he chooses to ignore this entire section of the paper in which an attempt is made to frame the discussion in light of the underlying principles of "determinism" and "invariance of frame." I submit that these issues are crucial and hold the key to the ultimate resolution of this ongoing debate.

Casey continues to insist on the introduction of a state

[14] By P. A. Dashner, and published in the March, 1986, issue of the ASME JOURNAL OF APPLIED MECHANICS, Vol. 53, pp. 55–60.

[15] Department of Mechanical Engineering, University of Houston—University Park, Houston, Texas 77004. Mem. ASME

[16] The dependence on hardening parameters is suppressed in this Discussion.

[17] For a review of the large body of work utilizing this concept, see Asaro (1983).

[18] An equation of the type $(7)_1$ was obtained by Mandel (1973, p. 292). The availability of the decomposition $(6)_1$ now allows one to identify Mandel's *isoclinic configuration* unambiguously as the image of the reference configuration under the mapping $\hat{\mathbf{F}}_p$. An alternative interpretation of the concept was discussed by Casey and Naghdi (Ref. 2 of Dashner[1]).

[19] The corresponding reduced form of equation $(7)_2$ was explicitly utilized by Naghdi and Trapp (1974).

[20] Equation numbers in this closure refer to those appearing in "Invariance Considerations in Large Strain Elasto-Plasticity."

Copyright © 1987 by ASME
Downloaded 03 May 2010 to 171.66.16.27. Redistribution subject to ASME license or copyright; see http://www.asme.org/terms/Terms_Use.cfm

variable, $\mathbf{F}_p$, only part of which is causually significant (i.e., determined by and reflective of past deformation history). He regards the rotational component $\mathbf{R}_p$ of $\mathbf{F}_p$ as having no significance beyond that of defining the orientation of the material element after some "imaginary" elastic unloading process. There seems to be no argument that functional dependence on such a variable must be suppressed. I choose to eliminate it by appealing to the principle of determinism for stress while Casey achieves the same end by appealing to a curious variation on the principle of invariance of frame.

Casey goes on to acknowledge that when modelling materials of "Type B" the continuum must be ". . . augmented with additional fields intended to represent microstructural properties." I cannot help but interject that this must come as quite a surprise to those who saw the standard Green-Naghdi forms (sans additional variables) as being "valid for a material which is anisotropic in the reference configuration." In any case, it seems that for materials of this type, Casey would add a proper orthogonal structure tensor $\mathbf{\Lambda}_p$ to the existing set ($\mathbf{F}_e$, $\mathbf{F}_p$, κ). While I agree that the addition of such a variable will restore the desired measure of generality to the Green-Naghdi theory, I also regard the resulting theoretical forms as being unnecessarily cumbersome.

In this regard, and owing to the admitted causal insignificance of the rotational component of $\mathbf{F}_p$, it seems reasonable (if for no other reason than economy) to combine the significant parts of the variables $\mathbf{F}_p$ and $\mathbf{\Lambda}_p$ to form a single variable. This is essentially what is done in the section entitled "Additional Considerations." This new $\mathbf{F}_p$, the equivalent of Casey's $\hat{\mathbf{F}}_p$, contains all of the relevant information contained in Casey's $\mathbf{F}_p$ and $\mathbf{\Lambda}_p$. Moreover, since its instantaneous value (based on this new definition) is determined entirely from the initial choice of a fixed "reference cell" and the microstructural "condition" of the material in its present deformed configuration, it is completely insensitive to "superposed rotations of an intermediate stress-free configuration." Indeed, $\mathbf{F}$ places the deformed material element relative to a preselected material reference, $\mathbf{F}_e$ places the underlying characteristic lattice structure (in the deformed configuration) relative to a preselected reference lattice (or cell), and $\mathbf{F}_p = \mathbf{F}_e^{-1}\mathbf{F}$. In fact, none of the stress or deformation measures contained in the proposed constitutive forms (18) have any connection to the orientation of the associated unstressed element. As a consequence, the invariance requirement advocated by Casey is rendered superfluous. I further submit that this would necessarily follow for any theory which does not stand in violation of the fundamental principle of determinism.

Finally, it is disingenuous for Professor Casey to suggest, as he does, that I have merely misunderstood and/or misinterpreted the work of Naghdi, Trapp, Casey, et al. In this regard, I know of no previous work by these authors (and Casey cites none) which contains an equation which is equivalent to Casey's equation (7). For that matter, I can find no reference to the structure tensor $\mathbf{\Lambda}_p$ or any prior discussion of materials of "Type B." Moreover, for Casey to cite the work of Mandel as if it were somehow supportive of his position is completely unwarranted. This in view of the fact that Naghdi and Casey categorically reject the ideas of Mandel in the closing paragraphs of "A Remark on the Use of the Decomposition $\mathbf{F} = \mathbf{F}_e\mathbf{F}_p$ in Plasticity." It was precisely these remarks that inspired my own participation in this debate. Indeed, if Casey now accepts the notion that material microstructure provides a legitimate basis for the definition of a unique (to within the limits of structural symmetry) intermediate unstressed configuration, then this issue is essentially resolved. I note, however, that Casey does not address the additional issues associated with the concept of "replacement invariance" or my assertions relating to the "advisability" of a Lagrangian or reference state formulation in large deformation inelasticity.

Downloaded 03 May 2010 to 171.66.16.27. Redistribution subject to ASME license or copyright; see http://www.asme.org/terms/Terms_Use.cfm

Journal of Applied Mechanics

Book Reviews

The Behavior of Structures Composed of Composite Materials, by J. R. Vinson and R. L. Sierakowski. Martinus Nijhoff Publishers, The Netherlands, 1986. 323 pages. Price: $59.50.

REVIEWED BY C. W. BERT[1]

As the field of composite materials and structures matures, there is a continuing demand for both text and reference books to keep astride of the ever advancing technology. Thus, *Mechanics of Composite Materials* (McGraw-Hill, New York, 1975) by R. M. Jones covered basic mechanics aspects, *Mechanics of Composite Materials* (Wiley, New York, 1979) by R. M. Christensen had a very rigorous yet lucid treatment of micromechanics, *Analysis and Performance of Fiber Composites* (Wiley, New York, 1980) by B. D. Agarwal and L. J. Broutman covered short-fiber composites, damage and failure, and experimental characterization in depth. Professors Vinson and Sierakowski have drawn from their wealth of industrial, research, and pedagogical experience to write an especially well-balanced treatment emphasizing the structural aspects of the field.

Chapter 1 is an introduction to the whole field of composite materials and is distinguished by its brief but extremely lucid discussion of the numerous manufacturing techniques in use, requirements for various classes of applications, and an extensive bibliography. Chapter 2 covers both anisotropic elasticity and laminate mechanics. Structural behavior of plates is covered in a very extensive Chapter 3, including bending, vibration, and buckling of thin laminated plates, transverse shear deformation effects, and sandwich panels with composite-material facings. Chapter 4 examines beam-type structures, including vibration and bending due to mechanical, thermal, and moisture loading. Chapter 5 discusses thin composite shells with emphasis on the circular cylindrical configuration, while Chapter 6 develops the use of energy methods for analysis of bending and buckling of laminated beams, plates, and circular cylindrical shells. Various strength/failure theories are described in Chapter 7, while Chapter 8 presents an in-depth review of the technology of both adhesively bonded and mechanically fastened joints, with 100 references. The book concludes with appendices on micromechanics and mechanical property characterization, including tabular data on eight fiber-reinforced composites of recent or current interest.

The book is very well written and is also well illustrated. There are exercises at the end of each chapter which should enhance the book's usefulness as a course text. This book is distinguished from other general books in the field in that it has in-depth coverage of these topics:

Sandwich plates with composite-material facings;
Circular cylindrical shells;
Adhesive and mechanical joints.

This book is highly recommended both as a text for courses in structural aspects of composites, as well as for practicing structures engineers and researchers involved with composites. In fact, a copy of it should be in the library of every composite structures designer, analyst, and researcher.

Dynamic Fracture, edited by M. L. Williams and W. G. Knauss. Martinus Nijhoff Publishers, The Netherlands, 1985. 312 pages. Price: $49.00.

REVIEWED BY F. ERDOGAN[2]

In most studies dealing with the fracture phenomenon in engineering materials, the process is assumed to take place under quasi-static conditions and the material is assumed to be rate-independent. This is due largely to the preponderance of fracture phenomena occurring in practice that may be classified as such and partly to the relative simplicity of the underlying mechanics problems. However, there are many applications in which, because of the rate-dependent behavior of the material or the dynamic effects resulting from stress waves, the time-dependence of the fracture process may be quite significant. Particularly in dealing with the problems relating to crack propagation and arrest in highly critical components such as nuclear pressure vessels or natural gas pipelines, it is essential that dynamic effects be taken into consideration in analyzing the problem and in determining the fracture properties of the material.

This book is the hardcover version of the special issue of *International Journal of Fracture* (Vol. 27, 1985, pp. 127–132) that was devoted to topics dealing with the theory and applications of dynamic fracture. The volume consists of 12 invited papers reviewing the recent progress in various aspects of the process in which inertia effects play a key role. The first paper (Knauss and Ravi-Chandar) describes the results of dynamic fracture experiments on Homalite and PMMA obtained by using the shadow optical method of caustics. Problems discussed include secondary cracking, limiting velocity, crack branching and crack arrest. A statistical fracture approach on a microscopic scale is described in the second paper (Shockey, Seaman, and Curran). The specific problem discussed is the shock wave induced spall fracture. The work on a solely material-dependent crack velocity versus fracture resistance

[1] Benjamin H. Perkinson Chair Professor, School of Aerospace, Mechanical, and Nuclear Engineering, University of Oklahoma, Norman, OK 73019. Fellow ASME.

[2] Professor and Chairman, Department of Mechanical Engineering and Mechanics, Lehigh University, Bethlehem, PA 18015.

Copyright © 1987 by ASME
Downloaded 03 May 2010 to 171.66.16.27. Redistribution subject to ASME license or copyright; see http://www.asme.org/terms/Terms_Use.cfm

relationship is reviewed in the paper by Dally, Fourney, and Irwin. The paper by Rosakis and Zehnder describes the dynamic crack propagation results in steels. The results of dynamic photoelastic experiments dealing with crack curving and branching are reviewed by Ramula and Kobayashi. The next four papers are concerned with the analytical and computational aspects of the process. The analytical work on the dynamic crack branching is described in the paper by Dempsey and Burgers. The steady-state Mode III moving crack problem for a nonlinear elastic and an elastic-perfectly plastic material is discussed by Achenbach, Li, and Nishimura. The paper by Nakamura, Shih, and Freund reviews the application of energy integrals to compute the crack driving force. The finite element results obtained by using a moving mesh to calculate the dynamic stress intensity factor are described by Atluri and Nishioka. The application of dynamic fracture concepts to the earthquake faulting process is discussed by Das. The paper by Kalthoff reviews the experimental work on the measurement of crack arrest toughness and impact fracture toughness. The final paper in the volume (by Kanninen) describes the applications of dynamic fracture concepts to the crack arrest problem in engineering structures. All in all, the collection of papers contained in this volume presentes an excellent and up-to-date review of the field and provides a long list of relevant references.

Hydrodynamic Stability Theory, by A. Georgescu. Martinus Nijhoff Publishers, The Netherlands, 1985. 307 pages. Price: $58.00.

REVIEWED BY J. T. STUART[3]

This book, which was first published in the Romanian language in 1976, was revised and enlarged in 1981 and has now been translated by the author into English, with Professor David Sattinger acting as a translation editor. The translation is good, apart from occasional infelicities of spelling.

There are five chapters, of which the first deals with classical concepts of hydrodynamic stability, namely the way in which laminar fluid flows develop instabilities which evolve into the complexity which we recognise as turbulence. Chapter 2 is concerned with function spaces and their role in the derivation of rigorous theorems for, for example, (*i*) completeness of sets of normal modes, (*ii*) proofs of a "principle of exchange of stabilities" (reality of the eigenvalue), and (*iii*) the derivation of stability criteria for particular flows, such as plane Couette flow, and for general classes of flows.

Chapter 3 is about bifurcations, branching, and stability of solutions of the Navier-Stokes equations, and treats such problems by the methods of Leray and Schauder, of Liapounov and Schmidt and of Joseph and Sattinger (for Hopf bifurcation). Chapter 4 was written in 1981 and discusses various ideas on the nature of turbulence from a theoretical and mathematical point of view, citing famous papers of Leray, Landau, Hopf, Ruelle and Takens, and Lorenz and more recent papers of Sattinger and others on symmetry-breaking bifurcations. Chapter 5 treats instability of flows in a porous media, which is of particular interest to the author.

Finally there is a set of eight appendices, six of which date from 1981, dealing with a variety of topics, including analytical and numerical methods and the stability of unsteady flows. An "Afterword" refers to some work then currently being undertaken by a variety of scientists and mathematicians in 1980 and 1981.

How does this book compare with those of Lin, Chandrasekhar, Betchov and Criminale, Drazin and Reid, and Joseph? For the first four of these books comparison is only really appropriate on the more classical and linear aspects of the problem, as discussed mainly in Chapter 1. The present treatment is rather brief with, I believe, to much attention to obsolescent methods and too few new insights into the problems and methods of solution. A "proof" by Romanov of the linearized stability of plane Couette flow is discussed, with reference to his rigorous bounds, asymptotics and numerical studies, but the present reviewer is not convinced that we yet have a rigorous proof of stability. On the classical, but nonlinear, aspects of the problem, moreover, there is no reference to the famous papers of Davey and of Malkus and Veronis on bifurcations in circular Couette flow and Bénard convection, respectively. Thus the present volume adds little on the classical side, and is of less general value than the book of Drazin and Reid.

Comparison is perhaps best made with Joseph's treatise, which is longer and far more detailed, especially in the use and description of energy methods. The major virtue of the present book is that it does put before the reader a rigorous mathematical framework, particularly analytical, which can be of use in treatments of bifurcations and, one hopes, in the study of evolution towards turbulence, or chaos, or both. The book is less original in spirit than Joseph's book, and is devoted rather more towards exposition of the points of view of the original authors. There are few novel insights here, I find.

In spite of my reservations, however, I believe that many will find this a useful reference to mathematical techniques which have been found to be of value in the theory of hydrodynamic stability in recent years.

Nonlinear Oscillations in Physical Systems, by Chihiro Hayashi. Princeton University Press, Princeton, N.J., 1985. 392 pages. Price: $19.95.

REVIEWED BY D. T. MOOK[4]

The present text is an enlarged version of the previously published text *Forced Oscillations in Nonlinear Systems*, which was published in 1953. Almost entirely, these books treat one-degree-of-freedom systems and forced oscillations. The new book presents many comparisons between analysis and experiment, perhaps more than any other book in print.

The book is divided into four parts. Part I covers "Principal Methods of Nonlinear Analysis." In Chapter One, analytical methods are discussed. These include the "Perturbation Method" (often referred to as the Lindsteadt-Poincaré Method), the "Iteration Method," the "Averaging Method," and the "Principal of Harmonic Balance." The discussions of these methods are very well constructed. Although it was the author's intention to give an account *of the basic techniques* for finding approximate solutions of nonlinear ordinary differential equations, the treatment is rather limited. The chapter does not contain any discussion of the method of multiple scales.

In Chapter Two, topological methods and graphical solu-

[3]Professor, Department of Mathematics, Imperial College, London, England, SW7.

[4]Professor, Department of Engineering Science and Mechanics, Virginia Polytechnic Institute and State University, Blacksburg, VA 24061.

Copyright © 1987 by ASME
Downloaded 03 May 2010 to 171.66.16.27. Redistribution subject to ASME license or copyright; see http://www.asme.org/terms/Terms_Use.cfm

tions are discussed. The discussion is excellent, covering the basic concepts of integral curves and singular points, the "Isocline Method," "Liénard's Method," the "Delta Method," and the "Slope-line Method."

In Chapter Three, the stability of nonlinear systems is discussed. The discussion introduces the reader to the concept of stability, the "Routh-Hurwitz Criterion for Nonlinear Systems," and the "Liaponov Criterion for Stability." Moreover, this chapter contains a discussion of the "Stability of Periodic Solutions." This leads naturally to a discussion of Floquet's theory, which is quite brief, and the application of Floquet's theory to the study of the stability of the approximations to the periodic solutions of nonlinear equations.

Part II covers "Forced Oscillations in Steady State." In Chapter Four, the stability of periodic oscillations in second-order systems is discussed. In Chapter Five, harmonic oscillations with both symmetric (only odd powers in the polynomials representing the nonlinear terms) and unsymmetric (both odd and even powers in the polynomials) characteristics are considered. The stability of the various equilibrium (steady) states is determined by the analysis of Chapter Four. The author provides examples of electrical (LRC) circuits whose responses are governed by the equations analyzed here and some experimental results for these systems.

In Chapter Six, series-resonance and parallel-resonance circuits are analyzed. For the former, the governing equation has the form

$$\ddot{v} + k\,\dot{v} + v^3 = B\cos t$$

The results are for large B. The approximate equilibrium (steady) states are found by the method of harmonic balance. For the latter, the stability analysis leads to the Mathieu equation. Higher (superharmonic) harmonics are prominent in both cases, and there are accompanying experimental investigations for both cases.

In Chapter Seven, subharmonic resonances are considered. Governing equations having quadratic, cubic, and quintic terms are analyzed. As in the other chapters, there are accompanying experimental investigations.

Part III covers "Forced Oscillations in Transient States." In Chapter Eight, harmonic oscillations are considered. The discussion covers integral curves, domains of attraction, and the various types of singular points in the state space. Both conservative and non-conservative systems are covered. There is also a section on experimental investigations.

In Chapter Nine, subharmonic oscillations are considered. Subharmonic resonances of order 1/2, 1/3, and 1/5 are covered. In addition, experimental results are presented.

In Chapter Ten, domains of attraction are considered in more detail for harmonic and subharmonic resonances. Additional experimental results are presented. In Chapter Eleven, quasi-periodic responses to harmonic disturbances are covered. This is an interesting phenomenon—a system having damping never develops a periodic response to a periodic excitation. Here is the only place in the book where the discussion involves two-degree-of-freedom systems. There are numerical and experimental results to illustrate some of the characteristics.

Part IV covers "Self-Oscillatory Systems with External Force." In Chapter Twelve the concept of entrainment is discussed. The examples involve van der Pol's equation and a modification that includes a nonlinear restoring term. In all cases there is a simple harmonic excitation. Harmonic and subharmonic responses are considered. There are numerical and experimental results to support the discussion. In Chapter Thirteen, quasi-periodic oscillations of self-exciting systems are discussed.

The book also contains six appendices which discuss expansions of the Mathieu functions, unstable solutions of Hill's equation, a stability criterion, integral curves and singular points, and an electronic synchronous switch.

In addition there is a total of 45 problems covering material in each of the 13 chapters. There are 114 references, the most recent were published in 1962, and several are in Japanese, Russian, German, and French.

The book provides well-written discussions of many nonlinear phenomena. It concentrates on single-degree-of-freedom electrical systems. More than any other text on nonlinear oscillations, this text discusses experimental results. The major weaknesses of the text are the analytical methods used (which are questionable in places), the almost total concentration on single-degree-of-freedom systems, and the lack of any discussion of such modern topics as chaos and internal resonance. Nevertheless, it is a valuable reference for all researchers and students in the field.

Sound and Structural Vibration: Radiation, Transmission and Response, by Frank Fahy. Academic Press, Inc., Publishers, Orlando, Florida, 1985. 309 pages. Price: $60.00.

REVIEWED BY D. G. CRIGHTON[5]

The technological area addressed by this book is undoubtedly one of importance, with obvious applications in aerospace, marine, and nuclear engineering and increasing importance in industrial and domestic noise control. It is also very much a scientific field to be regarded as a branch of applied mechanics. The coupled wave fields or modes in complex elastic structures exposed to fluid loading pose serious problems of physical understanding, mathematical modelling, numerical treatment and practical control—not least because an approach via either modes or waves provides at best only a partial view of phenomena that often are not really efficiently described by either. Little of this emerges from the existing literature, either in book or review form. Ad hoc assumptions—undeniably necessary for practical noise control—tend to be blurred in with rational physical argument in a way that this reviewer finds thoroughly unsatisfactory. Structural acoustics as a discipline and noise control engineering would, arguably, both benefit from a clear separation here—as elsewhere—between a physical principle expressed in mathematical form, and a prediction scheme.

Dr. Fahy's book does not make the distinction. In his preface he says that he attempts "a unified qualitative and quantitative account of the physical mechanisms and characteristics of linear interaction between audio-frequency vibrational motion in compressible fluids and structures with which they are in contact. The primary purpose is to instruct the reader in theoretical approaches. . . , while simultaneously providing physical explanations of their dependence upon the parameters of the coupled systems. It is primarily to the engineering student that the book is addressed. . .". He goes on to justify the sacrifice of "a certain amount of mathematical rigour for the sake of qualitative clarity"; as an applied mathematician I concur completely—but what I frequently miss is rigour of scientific description that surely is not out of place. Some of Dr. Fahy's aims I applaud; his emphasis on a wave rather than mode view of structural vibration must aid incorporation of fluid loading effects and help to get away from the lumped parameter descriptions that are thought too

[5]Professor, Department of Applied Mathematics and Theoretical Physics, University of Cambridge, Cambridge, United Kingdom CB3 9EW.

Copyright © 1987 by ASME
Downloaded 03 May 2010 to 171.66.16.27. Redistribution subject to ASME license or copyright; see http://www.asme.org/terms/Terms_Use.cfm

often to convey all necessary physical insight; the overall scope of the book seems appropriate; and the extensive discussion (Chapter 4) of "Transmission of Sound through Partitions" is justified by Dr. Fahy's authority here and the general didactic value of the problems discussed.

Other chapter headings are:

(1) Waves in Fluids and Solid Structures,
(2) Sound Radiation by Vibrating Structures,
(3) Fluid Loading of Vibrating Structures,
(5) Acoustically Induced Vibration of Structures,
(6) Acoustic Coupling between Structures and Enclosed Volumes of Fluid,
(7) Introduction to Numerically Based Analyses of Fluid-Structure Interaction.

Most of the coverage is descriptive, as the author admits. He expects his audience to have developed previously "the facility for performing formal analyses of fundamental vibration and acoustic problems"—and the aim of the description is, presumably, to inculcate in the already proficient reader that judgement and feel necessary for reliable predictions, attributes tested in examples of the ends of the chapters (the "challenges" ("why?", etc.,) issued at various places in the text strike me as curiously uneven in level, but Dr. Fahy's teaching experience in this field may indicate otherwise). This reviewer was not confident in tackling many of the examples – though numerical or formula answers are given, some with useful hints.

Much could be criticized at a detailed level. In Chapter 1 the acoustic wave equation is stated and followed by the linear momentum and mass conservation equations, with no mention of an equation of state. This chapter is very long on reflection, reverberant build-up, forced and resonant response, and very short indeed on ideas related to dispersion (especially in shells), despite an expressed intention to show how the dispersion relation categorizes wave interactions. In Chapter 2 the radiation field of a baffled piston—an important canonical problem—deserves more detail, as does the procedure of calculating radiation fields from an assumed vacuum-normal-mode description of surface vibration (it is stated several times that fluid loading has little effect on mode shapes, but no justification is offered or reference given). Chapter 3 has a long discussion of one fluid loading problem that can be examined in detail with elementary mathematics—the one dimensional problem of a mass-spring blockage of a gas column driven at the other end. This reveals some features, but misses what is perhaps the essential aspect of fluid-structure coupling, that between transverse structural vibration and compressive fluid motion, leading to long range effects not simply expressible in local added mass and damping terms. Some statements are misleading; for example (p. 198) "below its cut-off frequency a (duct) mode cannot effectively propagate wave energy"; others are jargon-laden, as on p. 160 where we have "the ratio of the mass-controlled field-incidence, infinite-partition transmission coefficient to the average bounded-plate resonant-mode transmission coefficient." And throughout there is, as might be expected from my earlier remarks, an odd mixture of analysis and sheer empiricism. I have absolutely no idea as to what lies behind some of the formulae presented.

These remarks may seem ungrateful, and there are in fact many good things in the book—as, for example, in much of Chapter 4, which is a good attempt to bring some science into a notoriously unscientific area. The reader is also helped by the more than 100 well reproduced figures (it is not Dr. Fahy's fault that rather curious units were used in the original publications of some of these).

In sum, a mixed reception, at least from the viewpoint of an applied mathematician, to a book which is fairly expensive in England. While improving on many books in this area, Dr. Fahy's book still leaves Junger and Feit ("Sound, Structures and their Interaction," MIT Press, 1972, long out of print, but shortly to appear in second edition) as my preferred text on structural acoustics.

Downloaded 03 May 2010 to 171.66.16.27. Redistribution subject to ASME license or copyright; see http://www.asme.org/terms/Terms_Use.cfm